62nd INTERNATIONAL CONFERENCE FOR STUDENTS OF PHYSICS AND NATURAL SCIENCES

# OPEN READINGS 2019

March 19-22
Vilnius, Lithuania

## Abstract Book

ISBN 978-609-07-0137-9

“Open Readings” – an excellent and unique event for everyone who has a genuine interest in science and the world. The conference has long traditions and brings together the brightest minds from the Europe, allowing excellent early stage networking opportunities. In the recent few years the level of invited speakers has increased from local stars to global superstars in the academia including Nobel Prize laureates. “Open Readings” might be a chance of a lifetime to meet such people face-to-face.

*Discover fresh insights into Physics and Natural Sciences,*

*Reveal encouraging routes to Innovations,*

*Enrich culture of collaboration and*

*Feel the brief of the newest scientific tendencies!*

Remember - first scientific conferences you attend always make a profound impression that stays for a long time. “Open Readings” is exactly a venue to make unforgettable memories!

Yours sincerely,

“Open Readings” Organizing Team

**Conference Chair:**

- Edvinas Skliutas, Faculty of Physics, Vilnius University & SPIE Chapter of Vilnius University

**Organising Committee:**

- Bernadeta Balčiukynaitė, *Faculty of Physics, Vilnius University & SPIE Chapter of Vilnius University*
- Živilė Čerškutė, *Faculty of Physics, Vilnius University & SPIE Chapter of Vilnius University*
- Lukas Krivickas, *Faculty of Physics, Vilnius University*
- Gintarė Kuksėnaitė, *Faculty of Physics, Vilnius University & SPIE Chapter of Vilnius University*
- Dovilė Lengvinaitė, *Faculty of Physics, Vilnius University & SPIE Chapter of Vilnius University*
- Mažena Mackoit Sinkevičienė, *Center for Physical Sciences and Technology & EPS YM Vilnius*
- Vaida Marčiulionytė, *Faculty of Physics, Vilnius University*
- Giedrius Pakalka, *Faculty of Physics, Vilnius University & SPIE Chapter of Vilnius University*
- Rasa Platakytė, *Faculty of Physics, Vilnius University*
- Simona Pūkienė, *Center for Physical Sciences and Technology*
- Edvinas Skliutas, *Faculty of Physics, Vilnius University & SPIE Chapter of Vilnius University*
- Gabrielė Stanionytė, *Faculty of Physics, Vilnius University & SPIE Chapter of Vilnius University*
- Kotryna Šiškauskaitė, *Faculty of Physics, Vilnius University*
- Laura Tauraitė, *Faculty of Physics, Vilnius University & SPIE Chapter of Vilnius University*
- Milita Užgirytė, *Faculty of Physics, Vilnius University*
- Martynas Velička, *Faculty of Physics, Vilnius University*

**Programme Committee:**

- Prof. Vilmantė Borutaitė, *Neurosciences Institute, Lithuanian University of Health Sciences*
- Dr. Kastytis Zubovas, *Fundamental Research Department, Center for Physical Sciences and Technology*
- Dr. Aurimas Vyšniauskas, *Department of Molecular Compound Physics, Center for Physical Sciences and Technology*
- Paulius Baronas, *Institute of Photonics and Nanotechnology, Faculty of Physics, Vilnius University*
- Dr. Danielis Rutkauskas, *Department of Molecular Compound Physics, Center for Physical Sciences and Technology*
- Dr. Renata Karpicz, *Department of Molecular Compound Physics, Center for Physical Sciences and Technology*
- Dr. Simona Strazdaitė, *Department of Organic Chemistry, Center for Physical Sciences and Technology*
- Dr. Ramūnas Aleksiejūnas, *Institute of Photonics and Nanotechnology, Faculty of Physics, Vilnius University*
- Dr. Akvilė Zabiliūtė – Karaliūnė, *Institute of Photonics and Nanotechnology, Faculty of Physics, Vilnius University*
- Dr. Julius Vengelis, *Laser Research Center, Faculty of Physics, Vilnius University*
- Dr. Marius Franckevičius, *Department of Molecular Compound Physics, Center for Physical Sciences and Technology*
- Dr. Viktorija Nargelienė, *Department of Physical Technologies, Center for Physical Sciences and Technology*
- Dr. Renata Butkutė, *Department of Optoelectronics, Center for Physical Sciences and Technology*
- Dr. Rasa Pauliukaitė, *Department of Nanoengineering, Center for Physical Sciences and Technology*
- Dr. Linas Minkevičius, *Department of Optoelectronics, Center for Physical Sciences and Technology*
- Dr. Tadas Paulauskas, *Department of Optoelectronics, Center for Physical Sciences and Technology*
- Dr. Andrius Gelžinis, *Institute of Chemical Physics, Faculty of Physics, Vilnius University*
- Dr. Jurga Juodkazytė, *Department of Electrochemical Materials Science, Center for Physical Sciences and Technology*

**Chairmen:**

- Prof. Saulius Juršėnas, *Institute of Photonics and Nanotechnology, Faculty of Physics, Vilnius University*
- Prof. Gintaras Valinčius, *Department of Bioelectrochemistry and Biospectroscopy, Life Sciences Center, Vilnius University*
- Dr. Kastytis Zubovas, *Fundamental Research Department, Center for Physical Sciences and Technology*
- Prof. Gintaras Valušis, *Department of Optoelectronics, Center for Physical Sciences and Technology*
- Prof. Mikas Vengris, *Laser Research Center, Faculty of Physics, Vilnius University*
- Dr. Urtė Neniškytė, *Department of Neurobiology and Biophysics, Life Sciences Center, Vilnius University*
- Prof. Vidmantas Gulbinas, *Department of Molecular Compound Physics, Center for Physical Sciences and Technoplogy*
- Dr. Kristijonas Vizbaras, *Head of Epitaxy Technology at Brolis Semiconductors*

*This conference was partially funded by a grant (No. S-MOR-19-53/(1.78)SU-396) from the Research Council of Lithuania.*

**Karl Anker Jørgensen**

**Department of Chemistry, Aarhus University, Denmark**

**ORGANOCATALYSIS - MOVING THE CATALYSIS OF LIFE FROM LAB TO INDUSTRY**

Life is a fantastic journey of chemical reaction catalyzed by enzymes and the role of catalysis cannot be overestimated; ca 70% of the nitrogen atoms in our body originates from one catalytic process – the Haber-Bosch process, ca 70% of man-made products involve catalysis and ca 25% of the world economy is directly or indirectly related to catalysis.

Asymmetric catalysis is field of catalysis for the synthesis of chiral organic molecules and organocatalysis is the new concept for achieving this goal.

The lecture will introduce the importance of asymmetric catalysis and demonstrate how this new field of asymmetric catalysis has developed from reaction in lab-scale to processes in tons-scale in industry.

**Gérard Mourou**

**Ecole Polytechnique, Palaiseau, France**

**PASSION FOR EXTREME LIGHT**

Extreme-light laser is a universal source providing a vast range of high energy radiations and particles along with the highest field, highest pressure, temperature and acceleration. It offers the possibility to shed light on some of the remaining unanswered questions in fundamental physics like the genesis of cosmic rays with energies in excess of 1020 eV or the loss of information in black-holes. Using wake-field acceleration some of these fundamental questions could be studied in the laboratory. In addition extreme-light makes possible the study of the structure of vacuum and particle production in "empty" space which is one of the field's ultimate goal, reaching into the fundamental QED and possibly QCD regimes.

Looking beyond today's intensity horizon, we will introduce a new concept that could make possible the generation of attosecond-zeptosecond high energy coherent pulse, de facto in x-ray domain, opening at the Schwinger level, the zettawatt, and PeV regime; the next chapter of laser-matter interaction.

*Prof. Mourou's visit is sponsored by "Light Conversion" and "Ekspla".*

**Anders Hagfeldt**

**École polytechnique fédérale de Lausanne, Switzerland**

**BAKING YOUR OWN SOLAR CELLS**

The breakthrough of using a dye-sensitized mesoporous oxide electrode with a very high surface area in the early 1990's created a paradigm shift in the way of being able to design molecular and nanomaterials for efficient solar cells. As an educational solar cell kit one can use white paint (titanium dioxide) and natural dyes (from blueberries, tea, wine... - find them in your grocery store!) to "bake" your own solar cell. The dye-sensitized solar cell (DSSC) is also a multidisciplinary research area including several fields of chemistry and physics. At present DSSCs are being commercialized in applications such as consumer electronics, recharging headsets, iPads, etc, and in building integration, for example as facade windows. A spin-off to DSSCs that have attracted enormous interest the last five years is the so-called perovskite solar cell (PSC). This solar cell has seen an unprecedented development and in a short time efficiency above 23% have been reached, being commensurate with conventional photovoltaics such as thin film and silicon solar cells. Intense efforts are at present taking place to stabilize, scale-up and industrialize PSCs. The talk will cover some of the historical background, describe how you can make your solar cell in the kitchen, as well as reviewing the recent developments in DSSCs and PSCs.

**Kishan Dholakia**

**University of St Andrews, United Kingdom**

**LIGHT: A FORCE TO BE RECKONED WITH**

In science fiction, one is quite familiar with the idea of moving objects using laser beams, evoking concepts such as a "tractor beam". In the laboratory science fiction turns into science fact: a powerful technique known as "optical tweezers" (OT) shows that micrometre-sized particles (and even biological material and atoms) can be grabbed, moved and generally manipulated without any physical contact using optical forces. This is a powerful demonstration of the optical dipole or gradient force in action and was recognised in the Nobel Prize in 2018. Such "optical tweezers", based primarily on Newton's laws and fundamental optics have enabled unprecedented insight about biological molecules such as DNA and molecular motors. In the microscopic world of optical tweezers, researchers are now harnessing these systems to study a host of science.

This talk will give a perspective of emergent studies in manipulation for both biomedical and fundamental science. This includes the use of particles with specific properties for new studies. This can include the rotation of particles in liquid and vacuum using vaterite [1] and nanovaterite particles [2]. These particles exhibit a birefringence that allows them to spin when using circularly polarised trapping beams. This work may be extended to study the rotation of two particles in vacuum in co- and counter-rotating geometries [3]. The use of these latter types of particles can lead to new studies in optomechanics [4].

[1] Y. Arita, M. Mazilu, and K. Dholakia, Nat Commun 4, 2374 (2013)

[2] Yoshihiko Arita, Joseph M. Richards, Michael Mazilu, Gabriel C. Spalding, Susan E. Skelton Spesyvtseva, Derek Craig, and Kishan Dholakia, ACS Nano, 2016, 10 (12), 11505 (2016)

[3] Yoshihiko Arita, Michael Mazilu, Tom Vettenburg, Ewan M. Wright, and Kishan Dholakia, Optics Letters 40(20), 4751-4754 (2015)

[4] Yoshihiko Arita, Ewan M. Wright and Kishan Dholakia, Optica 5, 910 (2018)

**Jocelyn Bell Burnell**

**University of Oxford, United Kingdom**

**BURSTS, BANGS AND THINGS THAT GO BUMP IN THE NIGHT; TRANSIENT ASTRONOMY**

Developments in CCDs and in computing now allow astronomers to make (and, if needed, add) many short exposure observations. So very faint objects can still be detected, but now we can also see things that change (in position or in brightness) on short timescales. This is opening up a whole new area of astrophysics, some of which will be described in this talk.

**Fedor Jelezko**

**Universität Ulm, Germany**

**QUANTUM SENSING WITH DIAMONDS**

Electron and nuclear spin resonance is a spectroscopic technique that provides very detailed information on almost every possible substance but also as very insensitive. This may be contrasted to the excellent sensitivity of optical single molecule spectroscopy which is able to demonstrate the detection of single molecules in condensed matter. A recent development is a combination of these techniques making it possible to detect magnetic resonance transitions of single quantum systems.

While first experiments were done with aromatic molecules at low temperatures, recently single spin magnetic resonance techniques were also applied to the study of defect centers in diamond allowing coherent single spin control and readout under ambient conditions. This new approach opened a number of interesting applications, such as quantum information processing and communication, secure quantum communication and sensing with nanometer resolution. A particularly interesting application of diamond based quantum sensing is the detection of nuclear magnetic resonance on nanometer scales, including the detection of individual nuclear spins or small ensembles of external nuclear spins. Single nitrogen vacancy (NV) color centers in diamond currently have sufficient sensitivity for detecting single external nuclear spins and resolve their position within a few angstroms. The ability to bring the sensor close to biomolecules by implantation of single NV centers and attachment of proteins to the surface of diamond enabled the first proof of principle demonstration of proteins labeled by paramagnetic markers and label-free detection of the signal from a single protein. Single-molecule nuclear magnetic resonance (NMR) experiments open the way towards unraveling dynamics and structure of single biomolecules. However, for that purpose, NV magnetometers must reach spectral resolutions comparable to that of conventional solution state NMR. New techniques were proposed for this purpose and realized recently including technique that employs quantum entanglement. The ability to sense nuclear spins by NV centers also enables the transfer of polarization from optically polarized spins of NV centers to external nuclear spins. Such diamond based techniques for dynamic nuclear spin polarization are very promising for the enhancement of sensitivity of conventional MRI imaging. Most of mentioned above results obtained so far with diamond centers are based on optical detection of single NV color centers. Recently it was shown that photoelectrical detection of NV centers base on spin selective photoionization can provide robust and efficient access to spin state of individual color centers.

# Conference programme

## 19 March, TUESDAY

| | | | |
|---|---|---|---|
| **08:45** | INTRODUCTION | | |
| **09:00** | Ifor David William Samuel<br>ORGANIC SEMICONDUCTORS: LIGHTING UP THE FUTURE | | |
| | **ORAL SESSION O1** | | |
| **10:00** | Dovydas Banevičius, Gediminas Kreiza, Dalius Gudeika, Juozas Vidas Gražulevičius, Dmytro Volyniuk, Saulius Juršėnas, Karolis Kazlauskas<br>HIGH EFFICIENCY SKY-BLUE TADF OLEDS BASED ON PENTACARBAZOLYL-SUBSTITUTED BENZENE DERIVATIVES | O1-1 | 25 |
| **10:15** | Marta Wrońska, Arkadiusz Leniart, Andrzej Sitkiewicz, Paweł W. Majewski<br>ORGANIZATION OF LIQUID CRYSTAL ON BLOCK COPOLYMER THIN FILMS | O1-2 | 26 |
| **10:30** | Agata Golebiewska, Tomasz K. Pietrzak, Jakub Plachta, Michal Jarczewski, Jacek Ryl, Marek Wasiucionek<br>PHOTOLUMINESCENCE OF PARTIALLY REDUCED Eu2+/Eu3+ ACTIVE CENTERS IN NaF-Al2O3-P2O5 GLASSY MATRIX | O1-3 | 27 |
| **10:45** | Artiom Magomedov, Amran Al-Ashouri, Ernestas Kasparavicius, Simona Strazdaite, Gediminas Niaura, Tadas Malinauskas, Steve Albrecht, Vytautas Getautis<br>MONOLAYER AS A HOLE-SELECTIVE CONTACT FOR EFFICIENT PEROVSKITE SOLAR CELLS | O1-4 | 28 |
| **11:00** | COFFEE BREAK | | |
| | **ORAL SESSION O2** | | |
| **11:30** | Milda Jakutavičiūtė, Paulius Ruzgys, Saulius Šatkauskas<br>THE INFLUENCE OF SPHEROID CELL DEFORMATIONS ON ELECTRIC FIELD INDUCED TRANSMEMBRANE POTENTIAL AND ELECTROPORATION EFFICIENCY | O2-1 | 29 |
| **11:45** | Martynas Talaikis, Maria Valldeperas, Ieva Matulaitienė, Jekaterina Latynis Borzova, Justas Barauskas, Gediminas Niaura, Tommy Nylander<br>ON THE MOLECULAR INTERACTIONS IN LIPID BILAYER-WATER ASSEMBLIES OF DIFFERENT CURVATURE | O2-2 | 30 |
| **12:00** | ~~Halina Falfushynska, Oksana Horyn, Piotr Rzymski~~<br>~~EVALUATION OF TOXICOLOGICAL RISK OF CENTRAL EUROPEAN RAPHIDIOPSIS RACIBORSKII STRAINS USING COMMON CARP CELLS~~ | O2-3 | 31 |
| **12:15** | Juste Rozene, Inga Morkvenaite-Vilkonciene, Antanas Zinovicius, Vytautas Zutautas, Vytautas Bucinskas, Arunas Ramanavicius<br>IMPROVEMENT OF ELECTRON TRANSFER IN MICROBIAL FUEL CELL USING TWO REDOX MEDIATORS BASED SYSTEM | O2-4 | 32 |
| **12:30** | Renata Sadretdinova, Alexander Dovgan, Jeffrey Viviano, Jingyi Zhang, Venkat Venkataraman, Pavel Belan<br>ROLE OF NEUROCALCIN δ DIMERIZATION IN TRANSLOCATION OF THE PROTEIN IN HIPPOCAMPAL NEURONS | O2-5 | 33 |
| **12:45** | Monika Kirsnytė, Augustas Šukys, Paulius Ragulis, Rimantas Simniškis, Žilvinas Kancleris, Karolis Požela, Arūnas Stirkė<br>DOPED POLYPYRROLE TEXTILE COMPOSITES TERMOELECTRIC ANALYSIS AND CHARACTERIZATION FOR ENERGY STORING MATERIALS | 02-6 | 34 |
| **13:00** | BREAK | | |
| | **ORAL SESSION O3** | | |
| **13:15** | Yakov Braver, Jevgenij Chmeliov, Andrius Gelzinis, Leonas Valkunas<br>MATHEMATICAL ANALYSIS OF TIME-RESOLVED FLUORESCENCE SPECTRA OF MOLECULAR SYSTEMS | O3-1 | 35 |
| **13:30** | Augustina Jozeliunaite, Edvinas Orentas, Giuseppe Sforazzini<br>LIGHT-RESPONSIVE PI-CONJUGATED MACROCYCLES COMPRISING PHOTOCHROMIC UNITS | O3-2 | 36 |
| **13:45** | Wiktoria Dołębska Tomasz Jaroń<br>SYNTHESIS OF THE POTENTIAL SOLID STATE ION CONDUCTORS CONTAINING WEAKLY COORDINATING ANIONS. | O3-3 | 37 |
| **14:00** | Andrius Pakalniskis, Aivaras Kareiva, Gediminas Niaura, Dmitry Karpinsky, Siarhei Latushka, Ramunas Skaudzius,<br>PREPARATION AND CHARACTERIZATION OF BISMUTH FERRITE - BARIUM TITANATE SOLID SOLUTION CERAMICS | O3-4 | 38 |
| **14:15** | Greta Inkrataite, Justina Aglinskaite, Pranciskus Vitta, Ramunas Skaudzius<br>INVESTIGATION OF GARNET AND POLYMER COMPOSITES | O3-5 | 39 |
| **14:30** | BREAK | | |
| **14:45** | Karl Anker Jørgansen<br>ORGANOCATALYSIS – MOVING THE CATALYSIS OF LIFE FROM LAB TO INDUSTRY | | |
| **15:45** | COFFEE BREAK | | |
| **15:45-17:00** | **POSTER SESSION P1** | | |
| **17:00** | CONFERENCE OPENING<br>Gérard Mourou<br>PASSION FOR EXTREME LIGHT | | |

## 20 March, WEDNESDAY

| | | | |
|---|---|---|---|
| **09:00** | Anders Hagfeldt<br>BAKING YOUR OWN SOLAR CELLS | | |
| | **ORAL SESSION O4** | | |

| | | | |
|---|---|---|---|
| **10:00** | Vytautas Žalandauskas, Audrius Alkauskas<br>MODELLING THE INTERACTIONS BETWEEN POINT AND LINE DEFECTS IN HEXAGONAL BORON NITRIDE USING FORCE FIELDS | O4-1 | 40 |
| **10:15** | Erica Ciotta, Luca Burratti, Paolo Prosposito, Roberto Pizzoferrato<br>FLUORESCENT GRAPHENE-OXIDE QUANTUM DOTS FOR HEAVY METAL DETECTION SYNTHESIZED BY A NEW ACID OXIDATION OF C60 FULLERENE | O4-2 | 41 |
| **10:30** | Julia Szymczak, Alexander Korneluk, Tomasz Stefaniuk<br>NUMERICALL MODELING OF LIGHT PROPAGATION IN ELECTRICALLY TUNABLE MULTILAYER HYPERBOLIC METAMATERIAL | O4-3 | 42 |
| **10:45** | Luca Burratti, Erica Ciotta, Roberto Pizzoferrato, Paolo Prosposito.<br>FLUORESCENT SILVER NANOCLUSTERS: SYNTHESIS AND POTENTIAL ENVIRONMENTAL MONITORING APPLICATIONS | O4-4 | 43 |
| **11:00** | COFFEE BREAK | | |
| | **ORAL SESSION O5** | | |
| **11:30** | Agnė Butkutė<br>LASER INDUCED DAMAGE THRESHOLD OF MULTI-PHOTON LITHOGRAPHY MADE POLYMERIC 3D MICRO-STRUCTURES | O5-1 | 44 |
| **11:45** | Dominykas Gustas, Aline Vernier, Diego Guénot, Marie Ouillé, Frederik Böhle, Stefan Hässler, Rordrigo Lopez-Martens, Agusting Lifschitz, Jérôme Faure<br>HIGH-REPETITION-RATE RELATIVISTIC ELECTRON ACCELERATION IN PLASMA WAKEFIELDS DRIVEN BY SINGLE-CYCLE LASER PULSES | O5-2 | 45 |
| **12:00** | Jokubas Pipiras, Juozas Dudutis, Simon Schwarz, Stefan Rung, Ralf Hellmann, Paulius Gečys<br>GLASS CUTTING BY OBLATE-TIP AXICON-GENERATED BESSEL-GAUSSIAN BEAMS | O5-3 | 46 |
| **12:15** | Paulius Mackonis, Augustinas Petrulenas, Vytenis Girdauskas, Aleksej M. Rodin<br>IR-SIDE OF MULTI-OCTAVE SUPERCONTINUUM GENERATION IN YAG PUMPED BY PICOSECOND PULSES | O5-4 | 47 |
| **12:30** | Marcin Suski, Anna Zygmunt, Justyna Stachera, Danuta Stefańska, Bogusław Furmann<br>TUNABLE SINGLE-MODE CW ENERGY-TRANSFER DYE LASER DIRECTLY OPTICALLY PUMPED BY A DIODE LASER | O5-5 | 48 |
| **12:45** | Maciej Chomski, Gustaw Szawioła, Bogusław Furmann<br>LAGUERRE – GAUSSIAN BEAM CONVERSION BY INTERACTION OF TWO OPTICAL VORTICES WITH Λ ATOMIC SYSTEM, INDUCED BY MICROWAVE TRANSITION | 05-6 | 49 |
| **13:00** | LUNCH BREAK | | |
| | **ORAL SESSION O6** | | |
| **13:30** | Ričardas Norkus, Sandra Stanionytė, Bronislovas Čechavičius , Renata Butkutė, Vytautas Karpus, Arūnas Krotkus<br>THZ-EXCITATION SPECTROSCOPY TECHNIQUE FOR BAND-OFFSET DETERMINATION | O6-1 | 50 |
| **13:45** | Simona Pūkienė, Bronislovas Čechavičius, Jan Devenson, Renata Butkutė<br>DIFFERENT QW STRUCTURES WITH Bi FOR INFRARED-EMITTING SEMICONDUCTOR LASERS | O6-2 | 51 |
| **14:00** | Julia Kucharek, Wojciech Pacuski<br>OPTICAL PROPERTIES OF MOLECULAR BEAM EPITAXY GROWN (Mo,Mn)Se2 , MoSe2, AND MnSe | O6-3 | 52 |
| **14:15** | Laisvydas Giriūnas, Mantas Šimėnas, Mirosław Mączka, Jūras Banys<br>EPR STUDY OF STRUCTURAL PHASE TRANSITION IN MANGANESE-DOPED [(CH3)2NH2][Cd(N3)3] HYBRID PEROVSKITE | O6-4 | 53 |
| **14:30** | Justas Pagalys, Evelina Pozingytė, Simona Pūkienė, Vytautas Jakštas, Mindaugas Karaliūnas<br>TERAHERTZ FREQUENCY RANGE TRANSMITTANCE OF GaAs/AlGaAs NANOSTRUCTURES WITH PARABOLIC QUANTUM WELLS | O6-5 | 54 |
| **14:45** | BREAK | | |
| **15:00** | Kishan Dholakia<br>LIGHT: A FORCE TO BE RECKONED WITH | | |
| **16:00** | COFFEE BREAK | | |
| **16:00-17:30** | **POSTER SESSION P2** | | |
| **17:30** | **DISCUSSION** | | |

# 21 March, THURSDAY

| | | | |
|---|---|---|---|
| **09:00** | Jocelyn Bell Burnell<br>BURSTS, BANGS AND THINGS THAT GO BUMP IN THE NIGHT; TRANSIENT ASTRONOMY | | |
| | **ORAL SESSION O7** | | |
| **10:00** | Algita Stankevičiūtė, Łukasz Wyrzykowski<br>INVESTIGATION OF INTERMEDIATE MASS BLACK HOLES VIA GRAVITATIONAL MICROLENSING | O7-1 | 55 |
| **10:15** | Matas Tartėnas, Kastytis Zubovas<br>MODELLING OF BLACK HOLE ACCRETION INDUCED BY DYNAMICAL PERTURBATIONS | O7-2 | 56 |
| **10:30** | Stanislav Komarov, Alexander Gorbatsievich<br>PARAMETERS OF RELATIVE MOTION OF A BINARY STAR MOVING IN EXTERNAL GRAVITATIONAL FIELD OF A BLACK HOLE FROM IT'S REDSHIFT | O7-3 | 57 |
| **10:45** | Anton Kuncinas, Per Osland<br>IN SEARCH OF THE S3 EXTENDED STANDARD MODEL HIGGS SECTOR DARK MATTER: FROM THEORY TO NUMERICAL ANALYSIS | O7-4 | 58 |
| **11:00** | COFFEE BREAK | | |
| | **ORAL SESSION O8** | | |

| | | | |
|---|---|---|---|
| **11:30** | Daryna Pesina<br>EPS YOUNG MINDS PROJECT: BENEFITS AND PERSPECTIVES | | |
| **11:45** | Domas Jokubauskis, Renata Butkutė, Linas Minkevičius<br>INFLUENCE OF MOLECULAR BEAM EPITAXY GROWTH CONDITIONS ON TERAHERTZ DETECTION FOR InGaAs DIODES | O8-2 | 59 |
| **12:00** | Paulina Kruk-Fura, Mateusz Jaszek, Tomasz K. Pietrzak, Marek Wasiucionek, Jerzy E. Garbarczyk<br>STABILISATION OF DELTA BI2O3 PHASE IN NANOCOMPOSITES DOWN TO ROOM TEMPERATURE BY TWIN-ROLLERS TECHNIQUE | O8-3 | 60 |
| **12:15** | Greta Merkininkaitė, Viktorija Padolskytė, Darius Gailevičius, Mangirdas Malinauskas and Simas Šakirzanovas<br>PREPARATION AND CHARACTERIZATION OF METALORGANIC PRECURSORS FOR LASER FABRICATION OF 3D MICRO-/NANO-STRUCTURES | O8-4 | 61 |
| **12:30** | Jakub Otrebski, Przemyslaw Michalski, Tomasz Pietrzak, Jerzy Garbarczyk<br>SYNTHESIS OF VANADIUM DOPED LITHIUM IRON SILICATE USING SOL-GEL METHOD | O8-5 | 62 |
| **12:45** | Aliaksei Bakavets, Yauhen Aniskevich, Genady Ragoisha, Henrikas Cesiulis, Natalia Tsyntsaru, Eugene Streltsov<br>ELECTROCHEMICALLY PULSE DEPOSITED BISMUTH - BISMUTH TELLURIDE SUPERLATTICES OF (BI2)M(BI2TE3)N SERIES. | 08-6 | 63 |
| **13:00** | LUNCH BREAK | | |
| | **ORAL SESSION O9** | | |
| **13:30** | ~~Elena Petrova, Yana Shavshukova, Dzimitry Ivashenka, Vladimir Pankov~~<br>~~MAGNETIC FERRITE NANOPARTICLES WITH INCREASED MAGNETIZATION AND CRYSTALLINITY BY SPRAY-DRYING WITH NACL AND SUBSEQUENT THERMOLYSIS~~ | O9-1 | 64 |
| **13:45** | Kumar Anubhav Tiwari, Olgirdas Tumsys, Renaldas Raisutis<br>APPLICABILITY OF WAVELET TRANSFORM FOR THE DEFECT ESTIMATIONS IN GLASS FIBER-BASED COMPOSITE STRUCTURES BY ULTRASONIC NON-DESTRUCTIVE TESTING | O9-2 | 65 |
| **14:00** | Paulius Čepulionis, Renaldas Raišutis<br>ESTIMATION OF ACOUSTIC IMPEDANCE FOR MEDICAL ULTRASOUND IMAGES | O9-3 | 66 |
| **14:15** | Rokas Jasiūnas, Huotian Zhang, Feng Gao, Vidmantas Gulbinas<br>ULTRAFAST PROCESSES IN HIGHLY EFFICIENT ORGANIC SOLAR CELLS BASED ON NOVEL NONFULLERENE ACCEPTORS | O9-4 | 67 |
| **14:30** | Tadas Lenkutis, Andrius Dzedziskis, Oleksii Balitskyi , Liudas Petrauskas, Rimgaudas Urbonas, Vytautas Bučinskas, Donatas Valiulis, Inga Morkvėnaitė-Vilkončienė<br>RESEARCH OF KUKA YOUBOT DYNAMICS | O9-5 | 68 |
| **14:45** | BREAK | | |
| **15:00** | Saulius Juodkazis<br>3D FABRICATION CHALLENGES: METHODS AND MATERIALS | | |
| **16:00** | COFFEE BREAK | | |
| **16:00-17:30** | **POSTER SESSION P3** | | |

## 22 March, FRIDAY

| | | | |
|---|---|---|---|
| **09:00** | Fedor Jelezko<br>QUANTUM SENSING WITH DIAMONDS | | |
| | **ORAL SESSION O10** | | |
| **10:00** | Janis Smits, Joshua Damron, Pauli Kehayias, Andrew McDowell, Nazanin Mosavian, Ilja Fescenko, Nathaniel Ristoff, Abdelghani Laraoui, Andrey Jarmola, Victor Acosta<br>PICOLITER SCALE SOLUTION NUCLEAR MAGNETIC RESONANCE SPECTROSCOPY USING NITROGEN-VACANCY CENTRES IN A DIAMOND CHIP | O10-1 | 69 |
| **10:15** | Tadas Matijošius, Svajus Asadauskas, Gedvidas Bikulčius, Ilja Ignatjev<br>CHARACTERIZATION OF DYES DURING COATING PROCESS OF ANODIZED ALUMINA USING RAMAN SPECTROSCOPY | O10-2 | 70 |
| **10:30** | Vytenis Barkauskas, Guillaume Pedehontaa-Hiaa, Kristina Stenstrom<br>DEVELOPMENT OF MODELING AND MEASUREMENT TECHNIQUES FOR EUROPEAN SPALLATION SOURCE SPECIFIC RADIONUCLIDES | O10-3 | 71 |
| **10:45** | Jekaterina Borzova, Gediminas Niaura<br>HYDRATION MECHANISM OF DEGRADABLE STARCH MICROSPHERES STUDIED USING VIBRATIONAL SPECTROSCOPY | O10-4 | 72 |
| **11:00** | COFFEE BREAK | | |
| | **ORAL SESSION O11** | | |
| **11:30** | Monika Toleikienė, dr. Žydrė Kadžiulienė, dr. Lina Šarūnaitė<br>SOYBEAN, LENTIL, CHICKPEA: NON-TRADITIONAL LEGUMES FOR AGRICULTURAL SUSTAINABILITY IN LITHUANIA | O11-1 | 73 |
| **11:45** | Veronika Vozniuk, Natalia Filimonova, Mykola Makarchuk, Ihor Zyma, Oleh Horbunov, Valentyn Kalnysh<br>FEATURES OF HEART RATE REGULATION AND BRAIN ACTIVITY DURING CHOICE-REACTION IN MILITARY MEN WITH TRAUMATIC BRAIN INJURY AND POSTTRAUMATIC STRESS DISORDER | O11-2 | 74 |

| | | | |
|---|---|---|---|
| **12:00** | Tautvydas Žalnierius, Dalia Koryznienė, Sigita Jurkonienė<br>HERACLEUM SOSNOWSKYI MANDEN. DRY-FRUIT DEVELOPMENT UNDER EXOGENOUS GA3 AND TIBA APPLICATION | O11-3 | 75 |
| **12:15** | Anete Kristiana Jekabsone<br>TYPE OF DIABETES – A FACTOR DETERMINING THE RESULTS OF INTRAVITREAL BEVACIZUMAB INJECTIONS IN CASE OF DIABETIC RETINOPATHY | O11-4 | 76 |
| **12:30** | Vilmantas Pupkis, Indrė Lapeikaitė, Vilma Kisnierienė<br>Cs+ AS A PLANT ION CHANNEL BLOCKER: IS IT THAT SIMPLE? | O11-5 | 77 |
| **12:45** | Laurynas Klimavičius<br>EVALUATION OF VEGETATION CONDITIONS IN DIFFERENT TYPES OF LAND USE USING SATTELITE MEASURED DATA | 011-6 | 78 |
| **13:00** | LUNCH BREAK | | |
| **13:30-14:45** | **POSTER SESSION P4** | | |
| **14:45** | COFFEE BREAK | | |
| **15:00** | Nick Goldman | | |
| **19:00** | **CLOSING PARTY and AWARDS CEREMONY** | | |

# List of poster presentations

## 19 March, TUESDAY

**15:45-17:00** **POSTER SESSION P1**

| | | |
|---|---|---|
| Agata Wróbel, Katarzyna Polak, Damian Trzybiński, Elżbieta Megiel, Krzysztof Woźniak.<br>CRYSTAL STRUCTURE AND HIRSHFELD SURFACE ANALYSIS OF 2-ETHYL-4-METHYL-6-(4-NITRO- PHENYL)-1,4-DIHYDRO-2H-[1,2,4,5]TETRAZIN-3-ONE RADICAL | P1-1 | 79 |
| Agnė Kizalaitė, Lauryna Sinušaitė, Aivaras Kareiva, Aleksėj Žarkov<br>EFFECT OF Mn DOPING ON HYDROLYSIS RATE AND DISSOLUTION OF ALPHA-TRICALCIUM PHOSPHATE | P1-2 | 80 |
| Aiste Ilciukaite, Maryte Daskeviciene, Egidijus Kamarauskas, Vygintas Jankauskas, Vytautas Getautis<br>SYNTHESIS AND PROPERTIES OF ENAMINE BASED HOLE TRANSPORTING MATERIALS CONTAINING OXYGROUPS | P1-3 | 81 |
| Aistė Kunciūtė, Remigijus Ivanauskas<br>INCORPORATION OF COPPER INTO TIN SELENIDE THIN FILMS | P1-4 | 82 |
| Andrej Akmanov, Dalius Gudeika<br>ROOM TEMPERATURE PHOSPHORESCENCE OF THIANTHRENE DERIVATIVES | P1-5 | 83 |
| Andrius Pakalniskis, Ramunas Skaudzius<br>SYNTHESIS AND INVESTGATION OF MULTIFUNCTIONAL GdPO4/Eu/Yb-Tm NANOPARTRICLES | P1-6 | 84 |
| Andrius Žilionis<br>NITROGEN-CONTAINING CYCLIC COMPOUNDS AS DERIVATIZATION REAGENTS IN TANDEM MASS SPECTROMETRY | P1-7 | 85 |
| ~~Anton Kozma~~<br>~~EQUATIONS OF TEMPERATURE DEPENDENCE OF AN ENTHALPY AND AVERAGE HEAT CAPACITY FOR EuCl3•6H2O~~ | P1-8 | 86 |
| Arminas Jurys, Tomas Javorskis, Edvinas Orentas<br>SYNTHESIS AND APPLICATIONS OF DITHIADIAZOCANES | P1-9 | 87 |
| Augustas Šukys, Monika Kirsnytė, Paulius Ragulis, Rimantas Simniškis, Žilvinas Kancleris, Raimonda Celiešiūtė-Germanienė, Arūnas Stirkė<br>INVESTIGATION OF DOPANT EFFECT ON POLYPYRROLE TEXTILE COMPOSITES | P1-10 | 88 |
| Austeja Mikalciute, Linas Vilciauskas<br>MOLECULAR DYNAMICS STUDY OF HYDROGEN BONDING IN H3PO4-H2O SYSTEMS | P1-11 | 89 |
| Daiva Tavgenienė, Saulius Grigalevičius, Gintarė Kručaitė, Raimonda Grinienė, Dovydas Blaževičius, Marius Eidimtas, Yen-Po Wang, Shang-Ru Tsai, Chih-Hao Chang<br>(BI)PHENYL SUBSTITUTED 9-(2,2-DIPHENYLVINYL)CARBAZOLES AS LOW COST HOLE TRANSPORTING MATERIALS FOR EFFICIENT RED PHOLEDS | P1-12 | 90 |
| Darya Kuzmina, Nataliia Kariaka, Viktoriya Dyakonenko, Sergii Smola, Vladyslav Lavrenchuk, Victor Trush<br>LANTHANIDE COMPLEXES BASED ON TWO TYPES PHOSPHORYLCONTAINING "ANTENNA" LIGANDS | P1-13 | 91 |
| Darya Kisurina, Vladimir Sapeshko, Ekaterina Kozlovskaya, George Pitsevich, Vytautas Balevicius<br>CONFORMATIONAL STRUCTURE AND IR SPECTRUM OF THE METHYL HYDROPEROXIDE | P1-14 | 92 |
| Deimantė Narauskaitė, Odeta Baniukaitienė<br>CALCIUM ALGINATE-BASED DRESSINGS FOR CONTROLLED DRUG DELIVERY | P1-15 | 93 |
| Deimante Simanaviciute, Vesta Navikaite-Snipaitiene, Ramune Rutkaite, Liudas Ivanauskas, Valdas Jakstas, Véronique Coma<br>INVESTIGATION OF INTERACTIONS BETWEEN CHITOSAN AND CAFFEOYLQUINIC ACID DERIVATIVES OF GREEN COFFEE BEAN EXTRACT | P1-16 | 94 |
| Deimantė Vaitukaitytė, Giedrė Bubnienė, Artiom Magomedov, Egidijus Kamarauskas, Vygintas Jankauskas, Vytautas Getautis<br>EFFICIENT CROSS-LINKABLE FLUORENE-BASED ENAMINES AS HOLE TRANSPORTING LAYERS | P1-17 | 95 |
| Domante Niuniavaite, Tadas Dambrauskas, Kestutis Baltakys<br>THE INFLUENCE OF GRANITE DUST ADDITIVE ON THE PROPERTIES OF CEMENT MORTAR | P1-18 | 96 |
| Domas Balčiūnas<br>STUDY OF GHYPHOSATE ADSORBTION ON THIN POLYPYRROLE LAYER AND ON 11-(1H-PYRROL-1-YL)UNDECANE-1-THIOL MONOLAYER FORMED POLYPYRROLE AND COMPARISION | P1-19 | 97 |
| Dovilė Lengvinaitė, Kęstutis Aidas<br>NMR SPECTRA OF WATER-IONIC LIQUID MIXTURES: LARGE-SCALE MOLECULAR DYNAMICS AND QUANTUM MECHANICS/MOLECULAR MECHANICS MODELING | P1-20 | 98 |
| Saulius Grigalevicius, Daiva Tavgeniene, Dovydas Blazevicius, Baohua Zhang, Simona Sutkuviene<br>PHENOXAZINES HAVING VARIOUS AROMATIC SUBSTITUENTS AS NEW HOST MATERIALS FOR GREEN PHOSPHORESCENT OLEDS | P1-21 | 99 |
| Dovydas Karoblis, Aivaras Kareiva, Aleksej Zarkov<br>LANTHANUM SUBSTITUTED BiMnO3 SYNTHESIS AND CHARACTERIZATION | P1-22 | 100 |
| Edvinas Staisiunas, Gytis Baranovas, Jurgis Pilipavicius<br>YTTRIA-STABILIZED ZIRCONIA MODIFIED WITH CALCIUM AND MAGNESIUM IONS BIOCOMPATIBLE COATINGS PRODUCED BY SOL-GEL APPROACH FOR DENTISTRY USES | P1-23 | 101 |
| Elena Dauksaite, Almira Ramanaviciene, Asta Kausaite-Minkstimiene<br>COMPARATIVE STUDY OF ANTI-HGH ANTIBODY IMMOBILIZATION STRATEGIES FOR HGH IMMUNOASSAY | P1-24 | 102 |
| Ernestas Kasparavičius, Tadas Malinauskas, Vytautas Getautis<br>STABILITY INVESTIGATION OF OXIDIZED SPIRO-MEOTAD | P1-25 | 103 |
| Gediminas Maskeliūnas, Mindaugas Mačernis<br>QUANTUM CHEMISTRY CALCULATIONS WITH QUNATUM COMPUTER PERFORMANCE STUDY | P1-26 | 104 |
| Giedrė Gaidamavičienė, Edvardas Kazakevičius, Artūras Žalga<br>SYNTHESIS AND CHARACTERIZATION OF ALKALINE EARTH METALS DOPED La2Mo2O9 CERAMICS | P1-27 | 105 |
| Giedrė Gaidamavičienė, Jūris Bogdanas, Gytautas Janulevičius, Artūras Žalga<br>SYNTHESIS AND CHARACTERIZATION OF CALCIUM MOLYBDATE VIA CO-PRECIPITATION AND SOL-GEL TECHNIQUES: A COMPARATIVE STUDY ON THE PROPERTIES OF OBTAINED PRODUCTS | P1-28 | 106 |

# 20 March, WEDNESDAY

**16:00-17:30** **POSTER SESSION P2**

| | | |
|---|---|---|
| Naveen Masimukku, Dalius Gudeika, Dmytro Volyniuk, Juozas Vidas Grazulevicius<br>SYNTHESIS AND INVESTIGATION OF AMBIPOLAR 1,8-NAPHTHALIMIDE-BASED DERIVATIVES | P2-88 | 268 |
| Vaida Marčiulionytė, Augustas Vaitkevičius, Mikhail Korjik, Gintautas Tamulaitis<br>PHOTOLUMINESCENCE PROPERTIES OF DOPED AND UNDOPED BISMUTH GERMANATE SCINTILLATION CRYSTALS | P2-89 | 269 |
| Mingaudas Karevičius, Ieva Beleckaitė, Andrejus Geižutis, Ramūnas Adomavičius<br>ELECTRON MOMENTUM RELAXATION TIME INFLUENCE ON THE TERAHERTZ EMISSION ENHANCEMENT IN MAGNETIC FIELD | P2-90 | 270 |
| Olena Bondar, Igor V. Fesich, Vasyl V. Lendel, Anatolii P. Bukivskii, Petro M. Bukivskii<br>OPTICAL PROPERTIES OF (Pb, Cd) IODIDE FILMS | P2-91 | 271 |
| Tomas Jurgutis, Saulius Nargelas<br>INVESTIGATION OF LUMINESCENCE QUANTUM YIELD IN GAGG:Ce and LYSO:Ce SCINTILLATION CRYSTALS | P2-92 | 272 |
| Laimonas Deveikis, Tomas Čeponis, Eugenijus Gaubas<br>SPECTRAL CHARACTERISATION OF GALLIUM NITRIDE MATERIALS APPLICABLE FOR RADIATION DETECTORS | P2-93 | 273 |
| Maksimas Anbinderis, Algirdas Sužiedėlis<br>MEASUREMENTS OF HIGH FREQUENCY PARAMETERS OF MICROWAVE DIODES IN Ka FREQUENCY RANGE USING AUTOMATED PROBE STATION SETUP | P2-94 | 274 |
| ~~Eugene Petrenko, Andrei Solovjov, Lyudmila Omelchenko, Ruslan Vovk~~<br>~~EFFECT OF ANNEALING ON A PSEUDOGAP STATE IN UNTWINNED YBa2Cu3O7-δ SINGLE CRYSTALS~~ | P2-95 | 275 |
| Ignatij Mackevic, Arturas Katelnikovas<br>SYNTHESIS AND OPTICAL INVESTIGATIONS OF CARBON QUANTUM DOTS | P2-96 | 276 |

# 21 March, THURSDAY

**16:00-17:30** **POSTER SESSION P3**

| | | |
|---|---|---|
| Tomas Vaitkūnas, Audrius Jutas<br>LATTICE DISTORTION MODEL. MODELING OF ELASTIC CONSTANTS ON CRYSTALLINE MATERIALS OF BCC-LATTICES | P3-1 | 277 |
| Domantas Berenis, Virginijus Ruibys, Ona Adomėnienė, Povilas Adomėnas, Gediminas Kreiza, Saulius Juršėnas, Karolis Kazlauskas<br>NEW BENZOYLPYRIDINE COMPOUNDS FOR APPLICATION IN TADF OLEDS | P3-2 | 278 |
| Eleonora Bolli, Alessio Mezzi, Saulius Kaciulis , Rasuole Lukose, Nerija Zurauskiene, Voitech Stankevic, Milita Vagner, Valentina Plausinaitiene, Skirmantas Kersulis, Gediminas Niaura, Saulius Balevicius<br>Co-DOPED MANGANITE/GRAPHENE AS NEW PROTOTYPE FOR MAGNETIC FIELD SENSOR APPLICATION | P3-3 | 279 |
| Simona Breidokaite, Gediminas Stankunas, Andrius Tidikas<br>MONTE CARLO METHOD APPLICATION FOR NEUTRON TRANSPORT CALCULATIONS IN IFMIF-DONES NUCLEAR SAFETY ASSESSMENT | P3-4 | 280 |
| Asta Bronušienė, Ingrida Ancutienė<br>PREPARATION OF SnS FILMS ON THE FTO GLASS BY SILAR METHOD | P3-5 | 281 |
| ~~Michał Janik, Paweł Dąbczyński, Olaf Stefańczyk, Anna M. Majcher~~<br>~~SELECTIVE COBALT (II) SALT ADSORPTION TO THIN FILMS OF POLYMER BLENDS - OBTAINING MAGNETIC DOMAINS IN NON-MAGNETIC MEDIUM~~ | P3-6 | 282 |
| Maksim Kravchenko, Tamara Korbut, Eduard Rudak, Andrey Petrovski<br>FOCK'S QUASI-STATIONARY STATES THEOREM FOR A BINOMIAL DISTRIBUTION DERIVATION TO DESCRIBE REACTOR CORE NUCLEI RADIOACTIVE DECAY | P3-7 | 283 |
| Edvinas Skliutas, Miglė Lebedevaitė, Jolita Ostrauskaitė, Mangirdas Malinauskas<br>THREE-DIMENSIONAL PHOTOSTRUCTURING OF ACRYLATED EPOXIDIZED SOYBEAN OIL | P3-8 | 284 |
| Giedrė Grigalevičiūtė, Linas Jonušauskas, Mangirdas Malinauskas<br>FEMTOSECOND LASER 3D MICROFABRICATION OF ELASTOMERIC RESIN | P3-9 | 285 |
| Nijolė Buškuvienė, Vaidas Bivainis, Indrė Danisevičienė<br>PEEL BEHAVIOUR OF HOT MELT PRESSURE SENSITIVE ADHESIVES | P3-10 | 286 |
| ~~Ekaterina Korotkith, Irina Polyakova, Ludmila Borovikova, Albert Kipper, Oleg Pisarev~~<br>~~SYNTHESIS IN PICKERING EMULSIONS OF BISMUTH-CONTAINING SORBENTS~~ | P3-11 | 287 |
| Ernesta Buzavaite-Verteliene, Tomas Tolenis, Audrius Valavicius, Marija Narkauskaite, Zigmas Balevicius<br>EXCITATION OF BLOCH SURFACE WAVES IN PERIODIC STRUCTURES USING SPECTROSCOPIC ELLIPSOMETRY | P3-12 | 288 |
| Paulius Časas, Sergejus Balčiūnas, Jūras Banys, Satoshi Wada<br>DIELECTRIC PROPERTIES OF LEAD-FREE BaTiO3-Bi(Mg1/2Ti1/2)O3-BiFeO3 CERAMICS | P3-13 | 289 |
| Vladislovas Čižas, Pranciškus Vitta<br>MULTISTANDARD POWER-LINE COMMUNICATION MODULE PROTOTYPE CREATION FOR SMART LIGHTING APPLICATIONS | P3-14 | 290 |
| Rimvydas Aleksiejunas, Albert Cesiul, Kestutis Svirskas<br>STATISTICAL LOS/NLOS CHANNEL MODEL FOR SIMULATIONS OF NEXT GENERATION 3GPP NETWORKS | P3-15 | 291 |
| Adrianna Chamryga, Tymoteusz Ciuk, Wawrzyniec Kaszub, Kinga Kościewicz, Paweł Piotr Michałowski, Artur Dobrowolski, Jakub Jagiełło, Paweł Ciepielewski, Dominika Teklińska, Małgorzata Możdżonek, Paweł Kamiński<br>WHY DO WE NEED SHOTTKY DIODES BASED ON SILICON CARBIDE? | P3-16 | 292 |
| Ignas Čiplys, Irena Kulszewicz-Bajer, Renata Karpicz<br>INVESTIGATION OF DIMETHILDIHYDROPYRENES PHOTOPHYSICAL PROPERTIES | P3-17 | 293 |
| Egle Ezerskyte, Arturas Katelnikovas<br>LUMINESCENCE OF K2(Cs/Rb)Y(VO4)2:Eu3+ PHOSPHORS WITH TRIGONAL CRYSTAL STRUCTURE | P3-18 | 294 |
| Vaiva Gribauskaite, Edita Palaimiene, Juras Banys, Anatoli V. Pushkarev, Yury V. Radyush, Nikolai M. Olekhnovich<br>DIELECTRIC INVESTIGATIONS OF THE BiFe1-xCrxO3 CERAMICS | P3-19 | 295 |
| Julija Grigorjevaite, Arturas Katelnikovas<br>RARE-EARTH IONS DOPED PHOSPHORS FOR SECURITY PIGMENTS APPLICATIONS | P3-20 | 296 |
| Algirdas Jasinskas, Sandra Stanionytė, Martynas Skapas, Bronislovas Čechavičius, Evelina Pozingytė, Renata Butkutė<br>GaAsBi MQW STRUCTURES FOR NIR LASERS | P3-21 | 297 |
| Augustas Karpavičius, Sergėjus Balčiūnas, Maksim Ivanov, Satoshi Wada, Jūras Banys<br>DIELECTRIC PROPERTIES OF BT-BT AND BF-BT COMPOSITES | P3-22 | 298 |
| Saulė Kemėraitė, Pranciškus Vitta<br>INVESTIGATION OF THE FREQUENCY-DOMAIN TECHNIQUE FOR RESEARCH OF ORGANIC SOLAR CELLS | P3-23 | 299 |

# 22 March, FRIDAY

**13:30-14:45** **POSTER SESSION P4**

# HIGH EFFICIENCY SKY-BLUE TADF OLEDs BASED ON PENTACARBAZOLYL-SUBSTITUTED BENZENE DERIVATIVES

Dovydas Banevičius[1], Gediminas Kreiza[1], Dalius Gudeika[2], Juozas Vidas Gražulevičius[2], Dmytro Volyniuk[2], Saulius Juršėnas[1], Karolis Kazlauskas[1]

[1]Institute of Photonics and Nanotechnology, Vilnius University, Vilnius (Lithuania)
[2]Department of Polymer Chemistry and Technology, Kaunas University of Technology, Kaunas (Lithuania)
dovydas.banevicius@ff.vu.lt

Thermally activated delayed fluorescent (TADF) emitters attracted great interest due to the ability to harvests all the triplet excitons via reverse intersystem crossing process into the singlet manifold thereby ensuring 100% internal quantum efficiency [1]. TADF emitters based on pentacarbazolyl-benzene were recently reported to demonstrate high efficiencies and stabilities in a blue-emitting OLED [2]. In this work, we report on new sky-blue-emitting pentacarbazolyl-substituted benzene derivatives as TADF emitters (Fig. 1) featuring phenyl ketone acceptors and sterically shielding tert-butyl groups for reduced concentration quenching as well as for better processability.

The emitters exhibited up to 50%, 60% and 80% fluorescence quantum yields in toluene solution, neat film and DPEPO host (doped at 20 wt%), respectively. Owing to deep emitter HOMO (Highest Occupied Molecular Orbital) level (-5.9 eV) and high triplet exciton energy (2.9 eV) OLEDs were fabricated using CzSi and DPEPO exciton blocking layers on different sides of the emissive layer [3]. Vacuum-processed OLEDs with doped emissive layer exhibited up to 24.6% external quantum efficiency (EQE), very high luminous efficacy and power efficiency of 121 cd/A and 100 lm/W, respectively, at the turn on voltage of 3.8 V (Fig. 1). Even though vacuum- and solution-processed non-doped OLEDs expressed lower EQE, they demonstrated severely reduced efficiency roll-off. These results indicate that new pentacarbazolyl-substituted benzene TADF emitters are promising for the application in OLED displays and solid-state lighting.

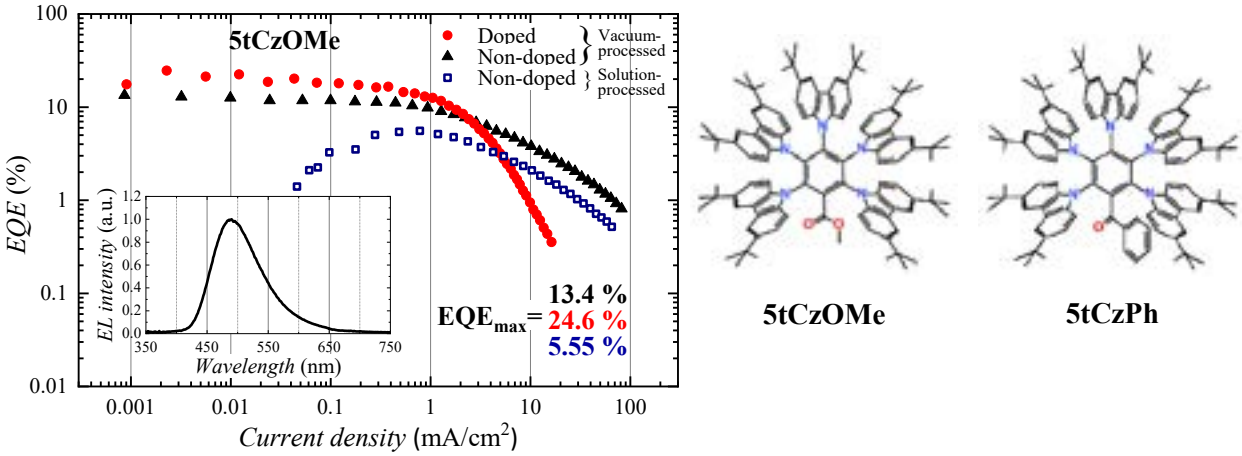


Fig 1. External quantum efficiency vs current density of vacuum-processed (doped and non-doped) and solution-processed (non-doped) OLEDs featuring **5tCzOMe** TADF emitter. Inset: electroluminescence spectra of those OLEDs. Molecular structure of derivatives **5tCzOMe** and **5tCzPh**.

[1] H. Uoyama, K. Goushi, C. Adachi et al., Highly efficient organic light-emitting diodes from delayed fluorescence, Nature **492**, 234-238 (2012).
[2] D. Zhang, M. Cai, Y. Zhang et al., Sterically shielded blue thermally activated delayed fluorescence emitters with improved efficiency and stability, Materials Horizons **3** 145-151 (2016).
[3] Q. Zhang, B. Li, C. Adachi et al., Efficient blue organic light-emitting diodes employing thermally activated delayed fluorescence', Nature Photonics **8** 326-332 (2014).

# ORGANIZATION OF LIQUID CRYSTAL ON BLOCK COPOLYMER THIN FILMS

Marta Wrońska[1], Arkadiusz Leniart[2], Andrzej Sitkiewicz[2], Paweł W. Majewski[2]

[1] Department of Physics, University of Warsaw, Poland
[2] Department of Chemistry, University of Warsaw, Poland
m.wronska5@student.uw.edu.pl

Liquid crystals (LC) and thin polymer films might seem to be an unusual pair. It may however pave the way for methods allowing to obtain new organized structures. Assembled liquid crystalline structures have been used for example to create photodiodes, but they can be also exploited as smart functional materials, such as switchable membranes for ion conduction or filtration or sensors.

The LC compound used for this research was 9ZBL[1], which exhibits the chiral- twist grain boundary – smectic A phase sequence (Ch-TGBA-SmA*) and a blue phase (SmC*) on cooling. Additionally, when applied from solution it folds into rod-like liquid crystalline compounds (LC nanotubes) in solvent vapor, as shown in Fig. 1.

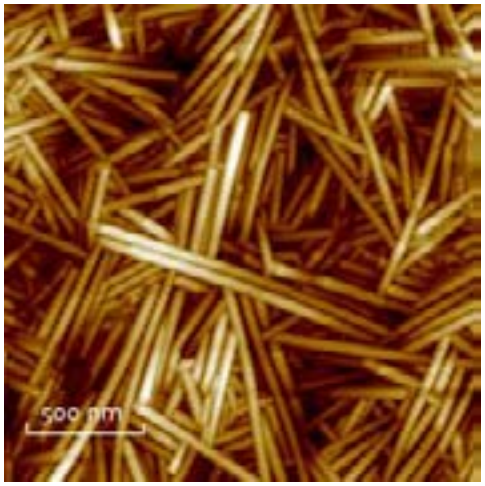


Fig. 1. Folded nanotubes of liquid crystal (9ZBL). Picture form atomic force microscope.

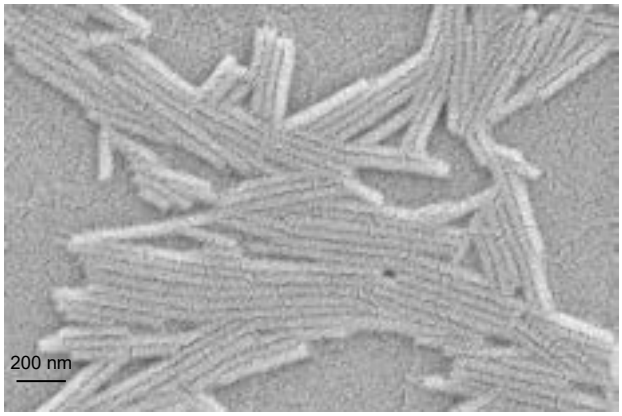


Fig. 2. Assembled liquid crystalline nanotubes (9ZBL). Picture from scanning election microscope.

The aim of the research is to use the self-assembled thin polymer films and apply block copolymer arranging techniques to assemble thin crystals, in this case the 9ZBL nanotubes. Thin block copolymer films may constitute a template[2] for arranging the applied layer of LC. Highly ordered block copolymer films transferred into inorganic matrices to provide grphoepitaxialy driven self-assembly of LC. We performed multiple method of directed self-assembly of BCP, including laser zone annealing technique[3]. The polymer used (P2VP) can be transferred either into $Al_2O_3$ or Pt nanowires.

A similar effect is possible to obtain through arranging methods for thin block copolymers, e.g. shearing force method. We used poly(sodium 4-styrenesulfonate) films on silica wafer with thin layer of 9ZBL to receive parallel nanotubes. Then we put on it polydimethylsiloxane layer, which was shifted at a constant speed under constant pressure above the temperature of crystallization.

We verified the efficiency of experiments using atomic force microscopy AFM and scanning election microscope SEM. Also, we tried to observe mechanism of folding liquid crystalline nanotubes using AFM in the solvent flow.

I should like to present the efficiency of the applied techniques with regard to LC nanotubes organisation.

**Acknowledgements:**

This research was financially supported by Foundation for Polish Science, Poland (research Grant 501/56-456326).

[1] V. Novotná, V. Hamplová et.al., *Chiral liquid crystalline compounds with a re-entrant SmA* phase*, J.Mater.Chem., 21, 14807-14814 (2011)

[2] Hu, H., Gopinadhan, M., & Osuji, C. O. *Directed self-assembly of block copolymers: a tutorial review of strategies for enabling nanotechnology with soft matter*., Soft Matter, 10(22), 3867–89 (2014).

[3] P.W. Majewski, K.G. Yager, *Rapid ordering of block copolymer thin films*, J. Physics: Condens. Matter 28 403002 (2016)

# PHOTOLUMINESCENCE OF PARTIALLY REDUCED $Eu^{2+}/Eu^{3+}$ ACTIVE CENTERS IN $NaF–Al_2O_3–P_2O_5$ GLASSY MATRIX

Agata Gołębiewska[1], Tomasz K. Pietrzak[1], Jakub Płachta[2], Michał Jarczewski[1], Jacek Ryl[3], Marek Wasiucionek[1]

[1] Faculty of Physics, Warsaw University of Technology, Koszykowa 75, 00-662 Warsaw, Poland
[2] Institute of Physics, Polish Academy of Sciences, Lotników 32/46, 02-668 Warsaw, Poland
[3] Faculty of Chemistry, Gdańsk University of Technology, Narutowicza 11/12, 80-233 Gdańsk, Poland
agata.golebiewska@fizyka.pw.edu.pl

Over the past years, the unprecedented progress in technology has shaken many industries including lighting industry. Energy-inefficient conventional lamps has been rapidly replaced by the energy efficient and prolonged lifetime LEDs. However, spectra of most of today's commercial white LEDs substantially deviate from natural light. In particular, they have a strong blue component, which is unhealthy for human vision and can even lead to serious irreversible health damages [1]. These shortcomings leave a room for considerable improvements and development of new phosphor materials with photoluminescence resembling natural light.

The most common materials used as phosphors are based on matrices doped with different rare-earth elements (REE) and, especially, lanthanides ions which have remarkable optical properties. They are characterized by [Xe] core, partially filled 4*f* shell and outer shells that screen 4*f* shell from the external field. Such an electronic structure leads, in most cases, to optical spectra of those elements consisting of sharp lines characteristic for transitions within the 4*f* shell, which basically are forbidden [2]. One should, however, be aware that the actual emission spectrum of a given REE center can also depend on a matrix composition.

Recently, the research carried out by our group [3] has proven that it is possible to synthesize REE-doped glassy materials whose photoluminescence is much more continuous, smoother and better resembling white light in visual impression. What is more, it has been shown that the synthesis conditions have a strong effect on photoluminescence spectrum. Additionally, one can control the relative $Eu^{3+}$ and $Eu^{2+}$ ions concentration and therefore manipulate photoluminescence spectrum.

In this research, $Na_3Al_2(PO_4)_2F_3$ glassy matrix doped with 1 wt% of $Eu_2O_3$ was successfully synthesized by a melt-quenching process and additional use of a double crucible method [4] in order to provide reducing atmosphere during melting. Three obtained samples with different synthesis parameters (see Fig. 1) were carefully investigated using X-ray diffractometry (XRD), differential thermal analysis (DTA), photoluminescence spectroscopy (PL), X-ray photoemission spectroscopy (XPS), absorption spectroscopy and time-resolved photoluminescence.

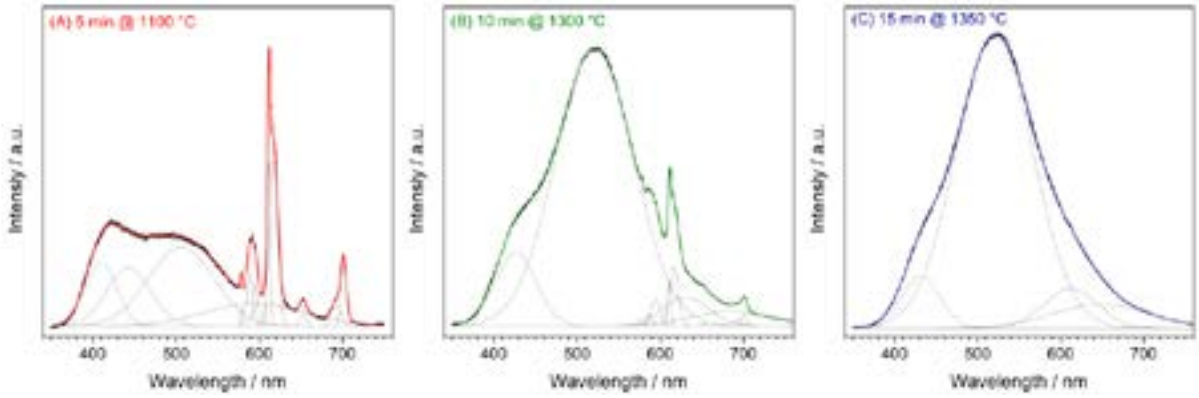


Fig. 1. Room temperature photoluminescence spectra for 3 glassy samples $Na_3Al_2(PO_4)_2F_3$ doped with $Eu_2O_3$ excited with 325 nm laser. Different synthesis parameters (time and temperature) are given in the plots [3].

[1] E. Chamorro, C. Bonnin-Arias, M.J. Pérez-Carrasco, J. Muñoz de Luna, D. Vázquez, C. Sánchez-Ramos*: Effects of Light-emitting Diode Radiations on Human Retinal Pigment Epithelial Cells In Vitro.* Photochemistry and Photobiology, 89 (2013) 468–473.

[2] B. M. Walsh: *Advances in Spectroscopy for Lasers and Sensing. Judd-ofelt theory: principles and practices*. [red.] Baldassare Di Bartolo, Ottavio Forte. Erice Italy, Springer, 2005.

[3] T.K. Pietrzak, A. Gołębiewska, J. Płachta, M. Jarczewski, J. Ryl, M. Wasiucionek, J.E. Garbarczyk: *Photoluminescence of partially reduced $Eu^{2+}/Eu^{3+}$ active centers in a $NaF–Al_2O_3–P_2O_5$ glassy matrix with tunable smooth spectra.* Journal of Luminescence 208 (2019) 322–326.

[4] K. Hirose, T. Honma, Y. Benino, T. Komatsu: *Glass-ceramics with $LiFePO_4$ crystals and crystal line patterning in glass by YAG laser irradiation*, Solid State Ionics, 178 (2007) 801–807.

# MONOLAYER AS A HOLE-SELECTIVE CONTACT FOR EFFICIENT PEROVSKITE SOLAR CELLS

Artiom Magomedov[1*], Amran Al-Ashouri[2], Ernestas Kasparavicius[1], Simona Strazdaite[3], Gediminas Niaura[3], Tadas Malinauskas[1], Steve Albrecht[2], Vytautas Getautis[1]

[1] Department of Organic Chemistry, Kaunas University of Technology, Lithuania
[2] Institute for Silicon Photovoltaics, Helmholtz-Zentrum Berlin, Germany
[3] Department of Organic Chemistry, Center for Physical Sciences and Technology, Lithuania
artiom.magomedov@ktu.lt

Currently, the fastest growing technology in the field of solar energy harvesting is perovskite solar cells (PSCs). With the efficiencies already surpassing 23% and coming closer to the Si-based solar cells, it is very important to ensure competitive price and stability of the perovskite-based devices. Stability of the final devices is not only dependent on the perovskite absorber material, but also on the selective layers, as well as all the interfaces.

In most of the best-performing PSCs organic materials, deposited by spin-coating, are used for the hole-selective layer formation. To ensure good charge transport they are usually used in a doped, partially oxidized state. However, the presence of the cation-radicals could lead to a reduces stability of the devices. In addition, morphological instability of the films, formed from the small-molecule hole transporting materials (HTMs) introduces additional issues for the devices under operational conditions [1].

To avoid problems associated with the doping, we are proposing an alternative approach for the formation of the hole-selective layer. In particular, by using a one-molecule-thick layer, transport is not anymore limited by the bulk of the organic semiconductor. In addition, use of such films would reduce the required amount of material to the minimum, thus contributing to the lower price of the final device. To achieve this goal, new carbazole-based HTM, functionalized with anchoring phosphonic acid group (**V1036**) was synthesized (Fig. 1). Organic phosphonic acids are known to bind to the surface of indium tin oxide (ITO), while substituted carbazole fragment is known to be used in a several efficient organic HTMs. Using **V1036** as a model compound, deposition method for the formation of the hole-selective monolayer on ITO was developed.

PSCs with **V1036** demonstrated the power conversion efficiency of 17.8% [2], which was close to that of the standard devices with PTAA (19.2%). Initial stability assessment showed good shelf life-time of the monolayer HTM-based devices, with the drop in performance of less than 3% after more than 4000 h. After the initial success, the concept was further developed by means of molecular engineering. A new generation of the monolayer HTMs (**V1193**, **V1194**) ensured high open-circuit voltage values of up to 1.19 V, which in a combination with over 80% fill factors resulted in a highest power conversion efficiency of 21.2%. This value surpassed the one obtained with PTAA, and is on par with the state-of-the-art inverted PSCs (21.5%) [3], without any interlayers and/or perovskite post-treatments.

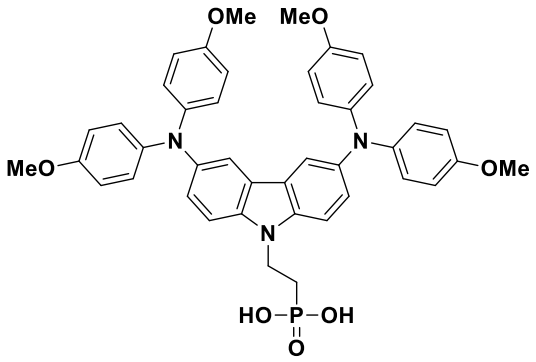


Fig. 1. Structure of the first-generation material **V1036**, used for the monolayer formation

In conclusion, we were able to show the great promise of the monolayers as a hole-selective contact in PSCs. Our work lays a foundation for the further exploration of the possible molecular structures, in particular by using molecules with additional functionalities. One more possible advantage is a conformal monolayer formation on a textured surface, which is important for the tandem solar cell application. More detailed study of the influence of the monolayer contact layer on the degradation of the device is currently undergoing.

[1] T. Malinauskas, D. Tomkute-Luksiene et al., Enhancing Thermal Stability and Lifetime of Solid-State Dye-Sensitized Solar Cells via Molecular Engineering of the Hole-Transporting Material Spiro-OMeTAD ACS Appl. Mater. Interfaces, **7**(21), 11107 (2015).
[2] A. Magomedov, A. Al-Ashouri et al., Self-Assembled Hole Transporting Monolayer for Highly Efficient Perovskite Solar Cells, Advanced Energy Materials, **8**(32), 1801892 (2018).
[3] D. Luo, W. Yang et al., Enhanced photovoltage for inverted planar heterojunction perovskite solar cells, Science, **360**(6396), 1442 (2018).

# THE INFLUENCE OF SPHEROID CELL DEFORMATIONS ON ELECTRIC FIELD INDUCED TRANSMEMBRANE POTENTIAL AND ELECTROPORATION EFFICIENCY

Milda Jakutavičiūtė, Paulius Ruzgys[1], Saulius Šatkauskas[1]

[1] Department of Biology, Vytautas Magnus University, Lithuania
milda.jakutaviciute@vdu.lt

Electroporation is a method in which short duration, high amplitude electric pulses are employed to transiently permeabilize the cell membrane, which allows the unhindered delivery of small molecules (e.g., chemotherapeutic drugs) or nucleic acids into the cell. The efficiency of the electroporation depends on many parameters, including the parameters of electric pulses applied and the parameters of cell and the surrounding medium. One of these parameters is the conductivity of electroporation medium.

As shown in [1], under electric field, lipid vesicles deform according to the conductivity ratio of the solution inside and outside of the vesicle. Therefore, it is reasonable to assume that eukaryotic cells would also deform in the electric field, assuming the form of a prolate (elongated) spheroid when the external conductivity is lower than the internal conductivity, and the form of an oblate (squashed) spheroid when the external conductivity is higher than the internal conductivity.

We modelled the effect prolate and oblate deformations would have on the transmembrane potential induced by external electric field. For this model, we assumed that the cell at rest (without external electric field) is a sphere with 9.7 μm radius, which is true for the Chinese Hamster Ovary cells in suspension. Constant cell volume during the electrodeformations was assumed. The cross section of the resulting spheroid on a plane parallel to the electrodes (perpendicular to the electric field) is a circle, and the cross section parallel to the electric field is an ellipsis. Using the formulas derived in [2] and [3], we calculated the changes in cell transmembrane potential for cell deformations when the ratio of cell radius parallel to the electric field and perpendicular to the electric field ranged from 1.5/1 to 5/1 for prolate deformations, and 1/1.5 to 1/5 for oblate deformations. Electric field voltage of 1400 V/cm was used for the model.

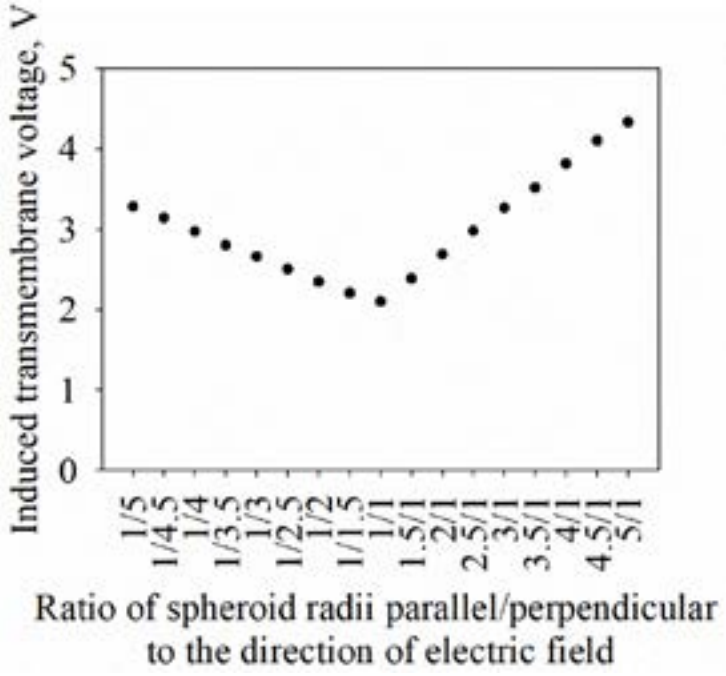


Fig. 1. The influence of spheroid deformation degree on the maximum induced transmembrane potential at the cell poles.

Fig. 1 shows the maximum induced transmembrane potential at the deformed cell poles. It can be seen that, while both oblate and prolate deformations increase the maximum induced transmembrane potential, the rise is steeper in the case of prolate deformation. Therefore, a higher increase in electroporation efficiency is expected when electroporation is performed in solutions with conductivity that is lower than intracellular conductivity.

[1] Riske, K. A., Dimova, R. Electric pulses induce cylindrical deformations on giant vesicles in salt solutions, Biophys. J. **91**(5), 1778-1786 (2006).
[2] Kotkik, T., Miklavčič, D. Analytical description on transmembrane voltage induced by electric fields on spheroidal cells. Biophys. J. **79**(2), 670-679 (2000).
[3] Gimsa, J., Wachner, D. On the analytical description of transmembrane voltage induced on spheroidal cells with zero membrane conductance. Eur. Biophys. J. **30**(6), 463-466.

# ON THE MOLECULAR INTERACTIONS IN LIPID BILAYER-WATER ASSEMBLIES OF DIFFERENT CURVATURE

Martynas Talaikis[1], Maria Valldeperas[2,3], Ieva Matulaitienė[4], Jekaterina Latynis Borzova[1], Justas Barauskas[5], Gediminas Niaura[1], and Tommy Nylander[2,3]

[1] Department of Bioelectrochemistry and Biospectroscopy, Life Sciences Center, Vilnius University, Lithuania
[2] Department of Physical Chemistry, Lund University, Sweden
[3] NanoLund, Lund University, Sweden.
[4] Department of Organic Chemistry, Center for Physical Sciences and Technology, Lithuania
[5] Camurus AB, Sweden.
martynas.talaikis@gmc.vu.lt

Amphiphilic molecules such as polar lipids self-aggregate in a variety of different morphological structures known as lipid liquid crystalline (LLC) phases. LLCs have been extensively investigated due to their possible applications in multiple fields such as drug delivery systems, biosensors, protein crystallization and immobilization, and model systems that mimic biomembranes. LLCs with an inverse bicontinuous cubic (Q) and sponge ($L_3$) phases attract most of the attention due to their ability to entrap both hydrophobic and hydrophilic compounds. It can also form water pores that are large enough to accommodate macromolecules such as proteins [1]. While the inverse bicontinuous cubic phases are well studied, there is a lack of knowledge on the structure and molecular interactions of the sponge phase.

This study [2] was carried out using molecular-level sensitive Raman spectroscopy and small-angle X-ray scattering (SAXS) methods in order to understand structure, phase behavior and molecular interactions within self-assembled lipid structures. The evolution of self-assembly of diglycerolmonooleate (DGMO) and Capmul glycerolmonooleate (GMO-50) lipid mixture with surfactant Polysorbate 80 along the dilution line allowed us to follow curvature transformation from lamellar ($L_\alpha$) to bicontinuous cubic and to the sponge LLC phases. Also, we inspected the temperature effect on LLCs curvature and related the changes observed by Raman spectroscopy to molecular interactions within the lipid bilayer.

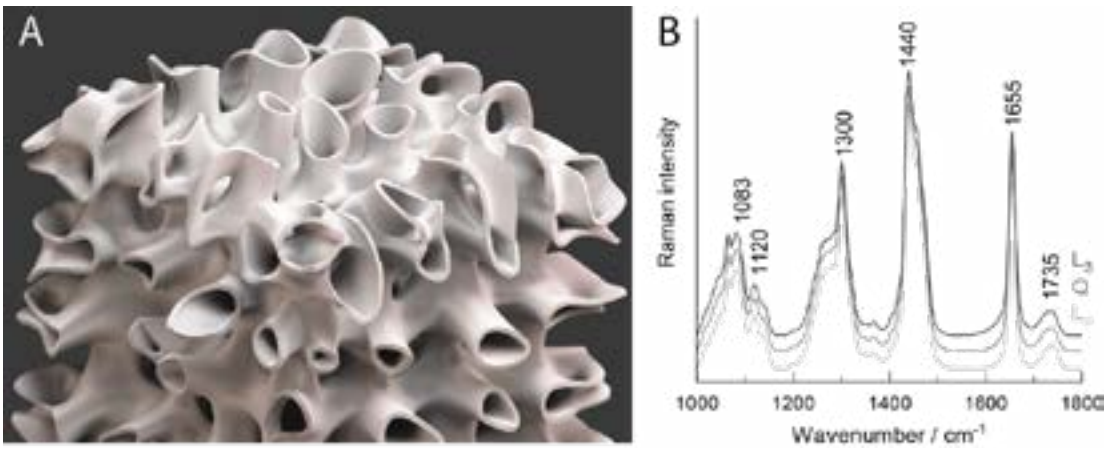


Fig. 1. The sponge phase model (A) and Raman spectra of lamellar ($L_\alpha$), cubic (Q) and sponge ($L_3$) LLCs (B).

Raman data reveal only a minute changes between different LLC samples (figure 1B), which confirm that they are all composed of a lipid bilayer although with different curvature as indicated by SAXS. However, the difference spectra point to key spectroscopic markers, which appear to be faint, but nonetheless, give profound information. Our study demonstrates that the lamellar phase presents less fluid hydrocarbon chains compared to inverse bicontinuous Q and $L_3$ phases. In addition, the disappearance of acyl-chain clusters of more ordered structures in the $L_3$ phase was also observed. Raman scattering and SAXS data suggest, that increasing temperature induces the acyl chain motion and decoupling, which in turn favors the formation of structures with larger negative curvature and bigger water pores.

These findings support the fact that the sponge phase is structurally similar to the cubic and lamellar phases. However, it displays the highest bilayer flexibility and ability to uptake large amounts of water, which is essential for encapsulation of macromolecules.

[1] Valldeperas, M. *et al.* Sponge Phases and Nanoparticle Dispersions in Aqueous Mixtures of Mono- and Diglycerides. *Langmuir* **32,** 8650–8659 (2016).
[2] Talaikis, M. *et. al.* (accepted). On the Molecular Interactions in Lipid Bilayer-Water Assemblies of Different Curvature. *Journal of Physical Chemistry,* (2019)

# EVALUATION OF TOXICOLOGICAL RISK OF CENTRAL EUROPEAN *RAPHIDIOPSIS RACIBORSKII* STRAINS USING COMMON CARP CELLS

Halina Falfushynska[1], Oksana Horyn[1], Piotr Rzymski[2]

[1] Department of Human Health, Physical Rehabilitation and Vital Activity, Ternopil Volodymyr Hnatiuk National Pedagogical University, Ukraine
[2] Department of Environmental Medicine, Poznan University of Medical Sciences, Poland
falfushynska@tnpu.edu.ua

The adverse effects of biological active compounds produced by cyanobacteria in aquatic biota have been a subject to numerous studies. Particular attention has been paid to microcystins, anatoxin-a, saxitoxin analogues, and cylindrospermopsin (CYN). The latter compound and its two natural analogues, 7-epi-CYN and 7-deoxy-CYN are known to be produced by filamentous species belonging to *Nostocales* and *Oscillatoriales* orders. Up to date no European strain of *R. (Cylindrospermopsis) raciborskii* has been reported to produce any known cyanotoxin despite a substantial research in this regard on both analytical and molecular level. However, exudates of some of *R. raciborskii* strains isolated in Europe have been reported to reveal an *in vitro* cytotoxicity in human lymphocytes and neutrophils (Polish strains) [1].

The present study investigated whether Central European *R. raciborskii* strains can affect fish cells *in vitro*. Four strains of *R. raciborskii* isolated from freshwater lakes located in Western Poland (PL1-PL4) and three strains isolated from artificial water reservoirs in Western Ukraine (UA1-UA3) were selected for the study. The Ukrainian strains were previously shown not to produce known cyanotoxins and to reveal no in vitro toxicity in human platelets [2]. Polish strains studied in this study did not produce cylindrospermopsin, microcystins and anatoxin-a. All isolates were morphologically similar. The potential toxicity of cyanobacterial extracts was evaluated in common carp (*Cyprinus carpio*) hepatocytes, red blood cells (RBC), and brain homogenate. In all tests two final concentrations, 0.1% (1 µL $mL^{-1}$; corresponding to 6 individual per mL) and 1.0% (10 µL $mL^{-1}$; corresponding to 62 individual per mL) of each *R. raciborskii* extract were used. Carp hepatocytes were exposed for 2h to both concentrations of each extract. Fish RBC were exposed for 1 h to the same cyanobacterial extract concentrations to study whether a lysosomal membrane stability, a common marker of cellular well-being, is affected.



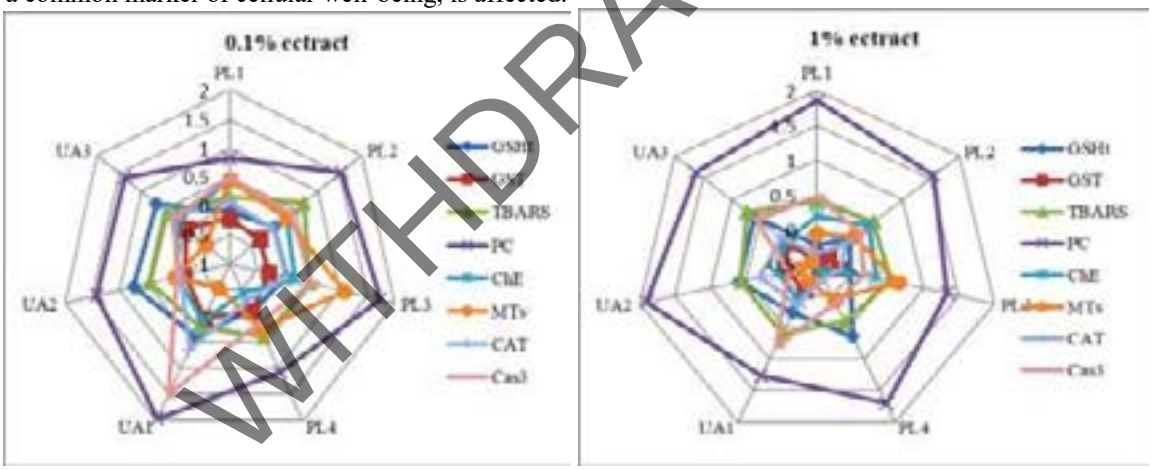


Fig. 1. Integral response index of studied biological traits of *Cyprinus carpio* cells exposed to *R. raciborskii* strains.

Studied extracts evoked different responses of catalase activity in hepatocytes with both increase and decrease observed under low and high concentrations. Cellular thiol pool was also altered with most of extracts inducing decrease in activity of glutathione-S-transferase, and Ukrainian strains leading to increase in glutathione level and decrease in metallothionein content. All studied extracts induced comparable reactive oxygen species formation, lipid peroxidation, protein carbonylation and DNA fragmentation in hepatocytes, and all but one increased activity of caspase-3. Only one extract caused lysosomal membrane destabilization as measured by neutral red retention in RBC. In contrast to extracts of Ukrainian isolates, exposure of brain homogenates to extracts of Polish strains induced increase in acetylcholinesterase activity suggesting neurotoxic action of their exudates. The results indicate that both Polish and Ukrainian strains of *R. raciborskii* may pose a toxicological risk to freshwater fish, and further that Polish strains may produce compound(s) evoking neurotoxic effects.

This work was supported by the Ministry of Education and Science of Ukraine (research grant for young fellows MV-1)

[1] B. Poniedziałek, P. Rzymski, J. Karczewski, The role of the enzymatic antioxidant system in cylindrospermopsin-induced toxicity in human lymphocytes, Toxicol In Vitro **29,** 926–932 (2015).
[2] P. Rzymski, O. Horyn, A. Budzyńska, et al., A report of *Cylindrospermopsis raciborskii* and other cyanobacteria in the water reservoirs of power plants in Ukraine, Environ Sci Pollut Res, **25**, 15245-15252 (2018).

# IMPROVEMENT OF ELECTRON TRANSFER IN MICROBIAL FUEL CELL USING TWO REDOX MEDIATORS BASED SYSTEM

Juste Rozene[1], Inga Morkvenaite-Vilkonciene[1,2], Antanas Zinovicius[3], Vytautas Zutautas[1], Vytautas Bucinskas[1], Arunas Ramanavicius[3]

[1]Department of Mechatronics, Robotics and Digital Manufacturing, Faculty of Mechanics, Vilnius Gediminas Technical University, J. Basanaviciaus g. 28, LT-03224 Vilnius, Lithuania
[2]Department of Electrochemical Materials Science, State Research Institute Centre for Physical Sciences and Technology, Sauletekio g. 3, Vilnius, Lithuania
[3]Department of Physical Chemistry, Faculty of Chemistry and Geosciences, Vilnius University, Naugarduko 24, Vilnius, Lithuania
juste.rozene@vgtu.lt

While every year the global energy demand is growing and the consequences are visible, an alternative, which is less wasteful and cleaner [1] is essential. A fuel cell is an electrochemical device that continuously converts chemical energy to electrical energy for as long as fuel and oxidant are supplied to it. Biological fuel cells operate under mild reaction conditions, namely ambient operating temperature and pressure [1]. Biological fuel cells convert the chemical energy of carbohydrates, such as sugars and alcohols, directly into electric energy. Enzymatic biofuel cells (EFC) and Microbial Biofuel Cells (MFC) recently emerge as very attractive sources of electrical energy that can convert chemical energy into electrical one and to generate electricity even from diluted solutions of biofuels [2].

Several different microorganisms, such as Actinobacillus succinogenes, Escherichia coli and Gluconobacter oxydans could be used as the catalyst in MFCs. In this research, baker's yeast (Saccharomyces cerevisiae) [3] is used because the yeast is a nonpathogenic, inexpensive, easy mass cultivation and easy to prepare. Also, yeasts can be maintained for a long time in the dried state and the relatively high power can be generated in the system.

We designed MFC, in which the yeast cells were immobilized on the anode and used as a biocatalyst. A two-redox mediator-based system was applied, one of them was menadione (vitamin K3), and another one – potassium ferricyanide ($K_3[Fe(CN)_6]$). Menadione is known as the compound, which is able to penetrate the cell wall, while the potassium ferricyanide transfer electrons to the electrode.

Experiments were performed in three-electrode based electrochemical cell, were graphite electrode (Ø3mm) with immobilized yeasts was connected as working electrode, a platinum electrode as a counter electrode, and Ag/AgCl as a reference electrode. We measured cyclic voltammetry with different concentrations of glucose and mediators (Fig. 1). It was found that the highest MFC-generated current density is 4,2m A/cm$^2$.

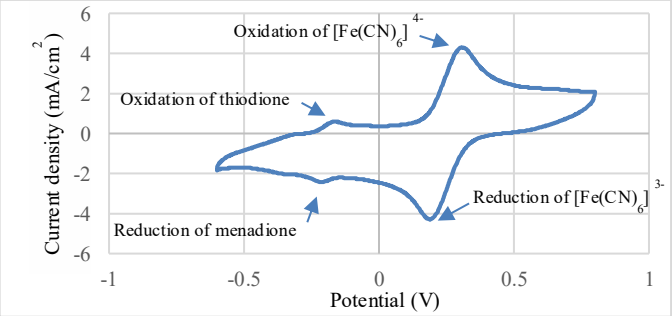


Fig. 1. The cyclic voltamperogram measured with a carbon electrode modified by yeast in phosphate-acetate buffer solution with 4.21 mM potassium ferricyanide, 80.5mM glucose and 512 µM menadione. Scan rate 0.1 V/s and the potential range from –0.6 V to 0.6 V. Reduction and oxidation peaks of menadione appears at -0.2 V and - 0.16 V; oxidation and reduction peaks of $K_3[Fe(CN)_6]$ appears at 0.2 V and 0.3 V, respectively.

In further researches, the MFC efficiency will be improved by applying different mediators and determining the generated power using several different loads.

**Acknowledgements**

This research was funded by the European Social Fund according to the activity "Development of Competences of Scientists, other Researchers and Students through Practical Research Activities" of Measure No. 09.3.3-LMT-K-712. Project No 09.3.3-LMT-K-712-02-0137.

[1] A. K. Shukla, P. Suresh, S. Berchmans, A.Rajendran, Biological fuel cells and their applications, Curr. Sci 87.4, 455-468 (2004).
[2] A. Kisieliute, A. Popov, R. M. Apetrei, G. Cârâc, I. Morkvenaite-Vilkonciene, A. Ramanaviciene, A. Ramanavicius, Towards microbial biofuel cells: Improvement of charge transfer by self-modification of microoganisms with conducting polymer–Polypyrrole. Chemical Engineering Journal, 356, 1014-1021 (2019).
[3] A. Ramanavicius, I. Morkvenaite-Vilkonciene, A. Kisieliute, J. Petroniene, A. Ramanaviciene, Scanning electrochemical microscopy based evaluation of influence of pH on bioelectrochemical activity of yeast cells− Saccharomyces cerevisiae. Colloids and Surfaces B: Biointerfaces, 149, 1-6. (2017).
[4] C. M. Martinez, L. H. Alvarez, Application of redox mediators in bioelectrochemical systems. Biotechnology advances, (2018).

# ROLE OF NEUROCALCIN δ DIMERIZATION IN TRANSLOCATION OF THE PROTEIN IN HIPPOCAMPAL NEURONS

Renata Sadretdinova[1], Alexander Dovgan[2], Jeffrey Viviano[3], Jingyi Zhang[3], Venkat Venkataraman[3], Pavel Belan[2]

[1] Kyiv Academy University, Kyiv, Ukraine;
[2] Department of Molecular Biophysics, Bogomoletz Institute of Physiology, Kyiv, Ukraine;
[3] Department of Cell Biology, Graduate School of Biomedical Sciences,
Rowan University School of Osteopathic Medicine, Stratford, NJ 08084, USA;
renata.sadretdinova@gmail.com

Neuronal $Ca^{2+}$ sensor (NCS) proteins, Neurocalcin δ (NCALD) and Hippocalcin (HPCA) control many neuronal functions via their differential $Ca^{2+}$-dependent translocation from the cytosol to the plasma membrane. In spite of the fact that both proteins have highly similar amino acid (AA) sequences, they demonstrate a great difference in $Ca^{2+}$ affinity and kinetic properties of translocation to the plasma membrane. It has been suggested that these differences between the proteins are due to $Ca^{2+}$-dependent dimerization of Neurocalcin δ, which is not observed for Hippocalcin.

To test this hypothesis, Neurocalcin δ mutant (SKA Mut) revealing no dimerization *in vitro*, was used. The mutant and wild type NCALD were tagged by fluorescent proteins and co-expressed paired wise in cultured rat hippocampal neurons. To induce $Ca^{2+}$-dependent translocations of proteins, we applied depolarizations of different duration using a patch clamp technique.

Surprisingly, disruption of $Ca^{2+}$-dependent dimerization of NCALD had only a minor influence on $Ca^{2+}$-sensitivity without a significant effect on decay time of translocation. $Ca^{2+}$-dependent NCALD insertion into the plasma membrane occurring before $Ca^{2+}$-dependent dimerization may explain this result. According to estimations conducted using our experimental results, characteristic diffusion time for NCALD insertion into the plasma membrane is about 3-fold lower than characteristic diffusion time for interaction of two NCALD in the dendritic tree of hippocampal neurons. In summary, $Ca^{2+}$-dependent dimerization of Neurocalcin δ in the cytosol does not play a significant role in determination of biophysical properties of this protein.

# DOPED POLYPYRROLE TEXTILE COMPOSITES TERMOELECTRIC ANALYSIS AND CHARACTERIZATION FOR ENERGY STORING MATERIALS

Monika Kirsnytė[1], Augustas Šukys[1], Paulius Ragulis[2], Rimantas Simniškis[2], Žilvinas Kancleris[2], Karolis Požela[1], Arūnas Stirkė[1]

[1] Department of Material Science and Electrical Engineering, Center for Physical Sciences and Technology, Lithuania
[2] Department of Physical Technologies, Center for Physical Sciences and Technology, Lithuania
monika.kirsnyte@ftmc.lt

The knowledge available on the structure-charge transport relationship acquired during the last decades on conducting polymers (CP) for organic electronics, constitutes a strong basis for the development of polymer-based thermoelectrics[1]. Conductive materials have a huge potecial as electroactive storage materials based on their π-conjugated structure, tunable condutivity properties and inexpensive manufacturing techniques, since CP can be processed from solutions at low temperatures. Polypyrrole is one of the most researched conductive polymers owing to it's inherent properties such as good conductivity, environmental stability, redox properties and biocompatability. The investigations of PPy textile composites as possible fabric energy storage materials[2] has only started and requires a systematic understanding of the influence of morphology, chemical and electronic structure on all principal thermoelectric parameters. The aim of this study was to examine and characterize doped PPy textile fabric composites as thermoelectric materials.

5 different dopants were chosen for PPy composite modification: sodium dodecyl sulfate (SDS), sodium polystyrene sulfonate (PSSNa), sodium dodecylbenzene sulfonate (DBSNa), dioctyl sodium sulfosuccinate (DOSS) and 3% multi walled carbon nanotubes (MWCNT). Doped PPy composites formation were achieved by patented *in situ* polymerization process on woven wool as dielectric substrate. Woven wool/PPy/dopant composites were synthesized in variation of dopant injection a) in adhesive polyvinyl alcohol (PVA) and $FeCl_3$ matrix, or b) in aqueous monomer pyrrole solution. PVA matrix were transferred via screen printing with particular 20 x 30 cm square pattern. Coated specimens were dried at 100 °C for 5 to 10 minutes, spray-coated with aqueous monomer solution and after quick polymerization reaction dried again respectively.

Thermoelectric sample analysis performed using infrared thermography (IRT), by thermal imaging in an anechoic chamber at ambient temperatures. Doped woven wool/PPy composites were radiated with electromagnetic wave source of 4 GHz. Thermal imaging resuls were collected during heating for 60s every 5s and cooling for 100s every 10s. Surface conductivity and shielding effectiveness measurements were carried out in an anechoic chamber in 1-20 freguency range. Composites morphology was analyzed using scanning electron microscope.

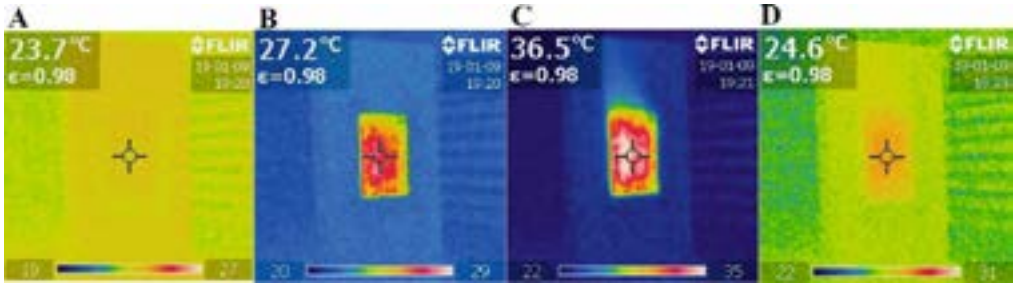


Fig. 1. Thermoelectric properties analysis of woven wool/PPy/MWCNT composites during 4 GHz electromagnetic radiation after: A – 0s, B – 5s, C – 60s, D – 160s.

Experimental investigation of IRT led to conclutions that conductive polymer distribution throughout all active composite surface was homogeneous. Termoelectric analysis showed a tendency of temperature dependence from particular dopant with respect to higher dopant concentrations. To conclude doped PPy textiles using *in situ* polymerization process could be potentially used as a frame material for energy-storing device fabrication.

[1] Bubnova, O.; Crispin, X., Towards polymer-based organic thermoelectric generators. *Energy & Environmental Science* **2012,** *5* (11), 9345-9362.
[2] Dubal, D. P.; Caban-Huertas, Z.; Holze, R.; Gomez-Romero, P., Growth of polypyrrole nanostructures through reactive templates for energy storage applications. *Electrochimica Acta* **2016,** *191*, 346-354.

# MATHEMATICAL ANALYSIS OF TIME-RESOLVED FLUORESCENCE SPECTRA OF MOLECULAR SYSTEMS

Yakov Braver[1,2], Jevgenij Chmeliov[1,2], Andrius Gelzinis[1,2], Leonas Valkunas[1,2]

[1]Department of Molecular Compound Physics, Centre for Physical Sciences and Technology, Saulėtekio 3, 10257 Vilnius, Lithuania

[2]Institute of Chemical Physics, Faculty of Physics, Vilnius University, Saulėtekio 9, 10222 Vilnius, Lithuania

jakov.braver@ff.stud.vu.lt

Time-resolved spectroscopy is particularly useful for studying properties of molecular systems since it allows to examine the *processes* taking place in the system and not just static system parameters. Using modern experimental setups we can study the ultrafast femto- and picosecond processes as well as the slower millisecond processes. However, to extract valuable information from the two-dimensional (time vs. wavelength) arrays of experimental data, its mathematical analysis is needed.

The Decay-Associated Spectra (DAS) and the Evolution-Associated Spectra (EAS) models are often incorporated [1]. By applying these models to the fluorescence data, one tries to describe the system using a number of exponentially decaying components (compartments) with their spectra and decay kinetics. The compartments used for describing the system within the DAS model are taken to be decaying independently after the initial excitation with intrinsic decay time constants $\tau_i$ (see Fig. 1). The EAS model treats the system differently, with only one component being initially excited. Its decay causes the excitation to descend sequentially to the next compartments causing them to fluoresce. After obtaining the solutions of the equations that correspond to the chosen model, we find the $\tau_i$ constants using a minimisation routine [2].

The aim of this study is to numerically simulate the time-resolved fluorescence spectra of various molecular systems and examine them using the DAS and EAS models to see whether the correct conclusions about the structure of the system can be drawn from the results of the analysis.

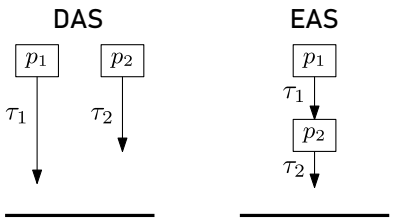


Fig. 1. Schemes depicting the decay paths of the complexes of the two-compartmental DAS and EAS models.

First, we discovered that the EAS model is suitable for identifying with certainty the time-dependent spectral shift [3] that might occur in the system (see Fig. 2). This finding later allowed us to distinguish two visually similar fluorescence maps produced by different systems, one of which exhibits a spectral shift. Next, we focused on a couple of systems that are composed of ensembles of monomers and dimers with randomly distributed parameters and found that the decay- and evolution-associated spectra match the spectra of the system's fluorescence sources (and thus provide a correct picture of the system) only in the simplest case of an ensemble of *monomers*. Finally, we studied the fluorescence spectra of an ensemble of the inter-connected monomers randomly arranged into a square lattice and concluded that the DAS and EAS models correctly hint at the presence of energy transfer in the system and allow us to evaluate the timescale of this process, but fail to indicate the numbers of different types of monomers found in the system.

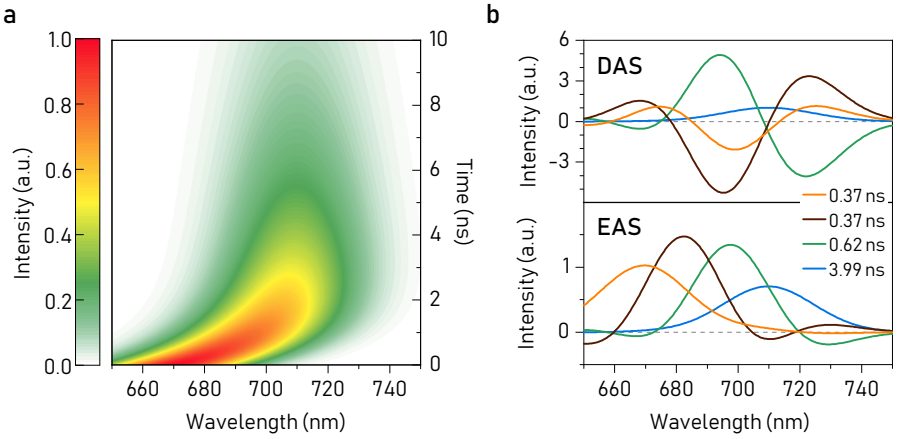


Fig. 2. Analysis of the fluorescence of a monomer with a shifting spectrum. (**a**) Modelled time-resolved fluorescence spectrum. (**b**) The spectra of the components of the system obtained using the four-compartmental DAS and EAS model.

[1] I. H. M. van Stokkum et al., Global and target analysis of time-resolved spectra, Biochim. Biophys. Acta **1657**, 82–104 (2004).

[2] V. I. Prokhorenko, Global analysis of multi-dimensional experimental data, Eur. Photochem. Assoc. Newsletter, 2012, 21–23.

[3] H. Marciniak and S. Lochbrunner, On the interpretation of decay associated spectra in the presence of time dependent spectral shifts, Chem. Phys. Lett. **609**, 184–188 (2014).

# LIGHT-RESPONSIVE π-CONJUGATED MACROCYCLES COMPRISING PHOTOCHROMIC UNITS

Augustina Jozeliūnaitė[1,2], Edvinas Orentas[1], Giuseppe Sforazzini[2*]

[1] Department of Organic Chemistry, Vilnius University, Lithuania
[2] Institute of Material Science and Engineering, Ecole Polytechnique Federale de Lausanne, Switzerland
augustina.jozeliunaite@chgf.vu.lt

The tremendous effort has been made to develop photoresponsive molecular actuators applicable as active components in the various electronic devices ranging from computer circuits, optical memory storage devices to solar cells and field effect transistors [1,2]. Hitherto there are a few attempts in developing photochromic switches capable of alternating the length of π-conjugation in its backbone by changing its geometric conformation in response to light. Thus, it allows to modulate the optical properties by controlling the HOMO – LUMO gap. However, their photo-switching efficiency suffers due to the extension of π-conjugation in the system [2].

Herein we present Photochromic Torsional Switch (PTS) comprising azobenzene chromophores, which can reversibly undergo light-induced trans – cis isomerization. When connected to polythiophene scaffold, the switching event is accompanied by the conformational change of the macrocycle resulting in a planarized polythiophene moiety with an enhanced conjugation in the backbone. In order to switch it back to the initial state, either exposure to 254 nm light or thermal relaxation in the dark can be used, the latter being significantly slower. Such architectures are ought to permit the modulation of HOMO – LUMO gap to high extent [3]. Hence, various length π-conjugated photochromic switches obtained by regioselective palladium catalysed cross-coupling reactions allowed us to validate the concept of HOMO – LUMO gap reduction upon extension of conjugated system. In the future, this specific photochromic torsional switch may allow the development of novel optoelectronic devices.

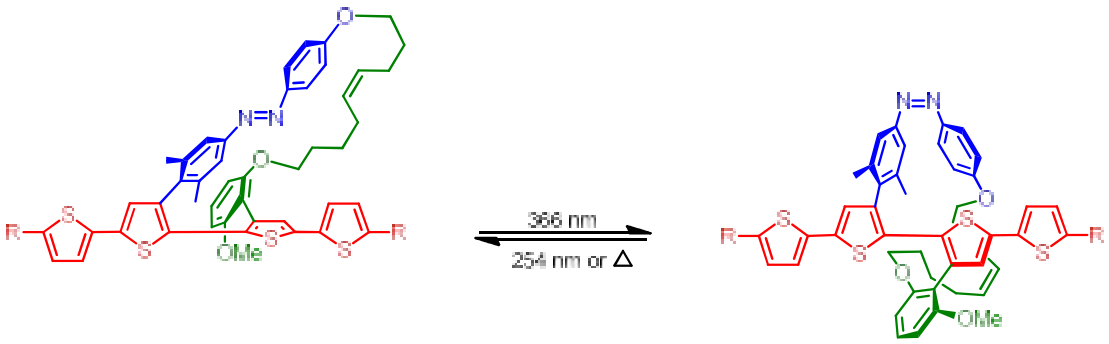


[1] Castellanos S., Grubert L., Stößer R., Hecht S., *J. Phys. Chem. C*, 2013, 117, 23529 – 23538;
[2] Stellacci F., Bertarelli C., Toscano F., Gallazzi M. C., Zotti G., Zerbi G., *Adv. Mater.*, 1999, 11, 292 – 295;
[3] Maciejewski J., Sobczuk A., Claveau A., Nicolai A. G., Petraglia R., Cervini L., Baudat E., Mieville P., Fazzi D., Corminboeuf C., Sforazzini G., *Chem. Sci.*, 2017, 8, 361 – 365.

# SYNTHESIS OF THE POTENTIAL SOLID STATE ION CONDUCTORS CONTAINING WEAKLY COORDINATING ANIONS.

Wiktoria Dołębska[1], Tomasz Jaroń[2]

[1] Department of Physics, University of Warsaw, Poland
[2] Centre of New Technologies, University of Warsaw, Poland
w.dolebska@cent.uw.edu.pl

In the project we are exploring new materials that could be used as potential energy storage materials. We target magnesium salts with weakly-coordinating anions (WCA): $Al[OC(CF_3)_3]_4^-$, $B_{12}H_{12}^{2-}$ and $B_{12}F_{12}^{2-}$. Due to weak attraction forces between relatively small cation and big WCAs such salts could be potential solid state ion conductors. They could replace currently used electrolytes in electrochemical energy storage devices - they would have better capacity thanks to magnesium charge and as solids they would also be more stable. So far we obtained some new structures of solvated salts (as shown in Fig.1) and we are working on crystallization procedures in order to obtain solvent-free salts.

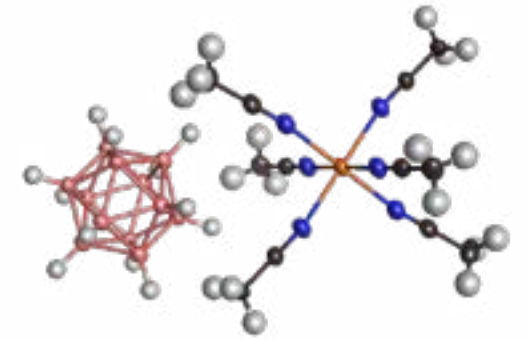

Fig. 1. One of the synthesized salts – $Mg(ANC)_6B_{12}H_{12}$.

To characterize our compounds we usually use X-ray diffraction (powder and monocrystal), FTIR spectroscopy and TGA analysis. In the nearest future we also want to perform electrochemical measurements and examine conductivity of obtained compounds. Moreover, such salts are soluble in weakly-solvating solvents. Thus want to use them as substrates in ion-exchange reactions in these solvents targeting new hydrogen-rich compounds (e.g mixed-metal borohydrides) that could be potential hydrogen storage materials. [1]

[1] T. Jaroń, P. A. Orłowski, W. Wegner, K. J. Fijałkowski, P. J. Leszczyński, W. Grochala, Angew. Chem. Int. Ed., 54 (2015) 1236–1239.

# PREPARATION AND CHARACTERIZATION OF BISMUTH FERRITE - BARIUM TITANATE SOLID SOLUTION CERAMICS

Andrius Pakalniškis[1], Aivaras Kareiva[1], Gediminas Niaura[2], Dmitry Karpinsky[3], Siarhei Latushka[3], Ramūnas Skaudžius[1]

[1]Institute of Chemistry, Vilnius University, Naugarduko 24, LT-03225 Vilnius, Lithuania
[2]Institute of Chemical Physics, Faculty of Physics, Vilnius University, Sauletekio Ave. 9, LT-10222, Vilnius Lithuania
[3]Scientific-Practical Materials Research Centre of NAS of Belarus, 220072 Minsk, Belarus
andrius.pakalniskis@chgf.vu.lt

Piezoelectricity is the ability of a material to generate a charge when mechanical stress is applied or to experience internal mechanical strain resulting from electric fields. This phenomenon was discovered in 1880 by French physicists Pierre and Jacques Currie in single-crystal quartz. Even so, the first practical applications of piezoelectric ceramics began in around world war I and have been widely used in the industries ever since. Nowadays piezoelectric materials are used in actuators, transducers for energy harvesting and so on [1, 2]. Most of these materials are lead-based and have dominated the field of application and research because of their superior properties, their tunability, and formation of the phase boundary. The main lead-based material is lead zirconate titanate $Pb(Zr_xTi_{1-x})O_3$. However due to rising environmental concerns from lead in current materials and fast mechanical decay accompanied by its ability to be only applied in relatively low temperature the alternatives are needed [3]. For these reasons, new lead-free piezoelectric ceramics are being developed. In lead- free piezoelectric compounds construction of phase boundaries is a very effective way of increasing piezoelectrical properties. However, phase boundaries of lead-free materials often sensitive to temperature and composition. Recently $BiFeO_3$ solid solutions have shown to have high piezoelectricity due to the formation of the phase boundary [4]. Because of their high Currie temperature bismuth ferrite, solid solutions could also be used at elevated temperatures. But due to the leakage of current and not clearly defined phase boundaries, further research is needed.

In this work bismuth ferrite – barium titanate ($XBiFeO_3 – (1-X)BaTiO_3$) solid solutions with different ratios are prepared by ethylene glycol and citric acid assisted sol–gel method. Obtained samples were characterized by X-ray diffraction, scanning electron microscopy, Raman spectroscopy. Electrical and magnetic properties were also measured.

**Acknowledgements.** The work has been done in frame of the project TransFerr. This project has received funding from the European Union's Horizon 2020 research and innovation programme under the Marie Sklodowska-Curie grant agreement No. 778070.

---

[1].Katzir, S., *Who knew piezoelectricity? Rutherford and Langevin on submarine detection and the invention of sonar.* Notes and Records of the Royal Society, 2012. **66**(2): p. 141-157.
[2].Zhu, X., *Piezoelectric ceramic materials: Processing, properties, characterization, and applications*. 2010. 1-36.
[3].Sahoo, B., *PZT to Lead Free Piezo Ceramics: A Review AU - Panda, P. K.* Ferroelectrics, 2015. **474**(1): p. 128-143.
[4].Wu, J., et al., *Multiferroic bismuth ferrite-based materials for multifunctional applications: Ceramic bulks, thin films and nanostructures.* 2016.**84**: p. 335-402.

# INVESTIGATION OF GARNET AND POLYMER COMPOSITES

Greta Inkrataitė[1], Justina Aglinskaitė[2], Pranciškus Vitta[2], Ramūnas Skaudžius[1]

[1]Institute of Chemistry, Faculty of Chemistry and Geosciences, Vilnius University, Naugarduko 24, LT-03225 Vilnius, Lithuania

[2]Institute of Photonics and Nanotechnology, Faculty of Physics, Vilnius University, Saulėtekio av. 3, LT-10257 Vilnius, Lithuania

greta.inkrataite@chgf.vu.lt

Over the last decades energy conservation has become a major issue. Conventional light sources such as simple wolfram lamps consume a large amount of electricity. A lot of energy can be saved by using LED lights instead of conventional ones. Cerium doped yttrium aluminium garnet is one of the most important luminescent materials that can be used in light emitting diodes (LED) to improve the quality of lighting [1]. LED lamps exhibit good energy and quantum efficiency, high color stability and are ecological. However, light emitting diodes have problems, such as short life span and reliability. One of the main causes for these problems is epoxy resin, whose small resistance to high temperature leads to failure of the diode [2]. To remove this flaw polymer is added. Polymer can also raise luminescence intensity which in turn would allow to use smaller ammount of garnet and influence other luminescence properties [3]. By selective adition of polymers different consistency composite tablets can be obtained. Ranging from glass to rubber like for various applications [4].

For this project different composites were prepared, which could be used in LED in order to improve their longevity and reliability. For the reason, YAG:Ce phosphor powder was synthesized by sol-gel method and then mixed together with either M600, M280 or EGDMA monomer which was polymerized under UV light into tablets. Composite powders were also prepared. Composites were analyzed by x-ray diffraction (XRD), scanning electron microscopy (SEM) and differential scanning calorimetry (DSC). Moreover, quantum efficiency, decay times, emission spectrum have also been investigate.

**ACKNOWLEDGEMENTS:**
This research is funded by the European Social Fund under the No 09.3.3- LMT K-712 " Development of Competences of Scientists, other Researchers and Students through Practical Research Activities" measure.

---

[1] M. Veith,, et al., Low temperature synthesis of nanocrystalline Y3Al5O12 (YAG) and Ce-doped Y3Al5O12 via different sol-gel methods. Journal of Materials Chemistry, **9(12)**: 3069-3079 (1999)

[2] R. Zhang, et al., A new-generation color converter for high-power white LED: transparent Ce3+:YAG phosphor-in-glass. Laser & Photonics Reviews, **8(1)**: 158-164 (2014)

[3] X. Wang.,et al., Effect of Boron Nitride (BN) on Luminescent Properties of Y3Al5O12:Ce Phosphors and their White Light-Emitting Diode Characteristics. International Journal of Applied Ceramic Technology, **10(4)**: 610-616 (2012)

[4] T.M. Demkiv,, et al., Luminescence properties of CsPbBr3 nanocrystals dispersed in a polymer matrix. Journal of Luminescence, **198**: 103-107 (2018)

# MODELLING THE INTERACTIONS BETWEEN POINT AND LINE DEFECTS IN HEXAGONAL BORON NITRIDE USING FORCE FIELDS

Vytautas Žalandauskas[1,2], Audrius Alkauskas[1]

[1] Department of Fundamental Research, State research institute Center for Physical Sciences and Technology, Lithuania
[2]Faculty of Physics, Vilnius University, Lithuania
vytautas.zalandauskas@ftmc.lt

Layered van der Waals crystals are attracting increasing attention due to their unique chemical and physical properties. The discovery of quantum emission in hexagonal boron nitride (*h*-BN) in 2016 opens up applications in quantum computing, quantum communication, and nanoscale sensing [1]. The exact mechanism of the measured quantum emission from defects in *h*-BN remains unclear.

Native point defects and impurities have been extensively studied using quantum chemistry calculations to determine the potential candidates of observed quantum emission [2]. Some experiments indicate that the observed luminescence may actually come from point defects located near line defects like grain boundaries and dislocations. These line defects are common in CVD-grown *h*-BN crystals. Using quantum chemistry calculations is too computationally expensive to model such large-scale systems. Therefore, the goal of the present work is to use force field (FF) methods to model these systems. In this study we have used the newest extended Tersoff potential for covalently bonded boron nitride systems and interlayer potential to model large-scale point defects and line defects in monolayer and bulk *h*-BN [3][4].

Various types of point and line defects have been created in monolayer and bulk *h*-BN crystals and we have performed energy minimization calculations to obtain optimized geometries. We have shown that crystal perturbations induced by line defects in 2D materials extend to very long distances. These crystal perturbations lead to variations of local defect geometries and thus also possibly to their optical signatures. These results will be later used in *ab-initio* calculations in our future works.

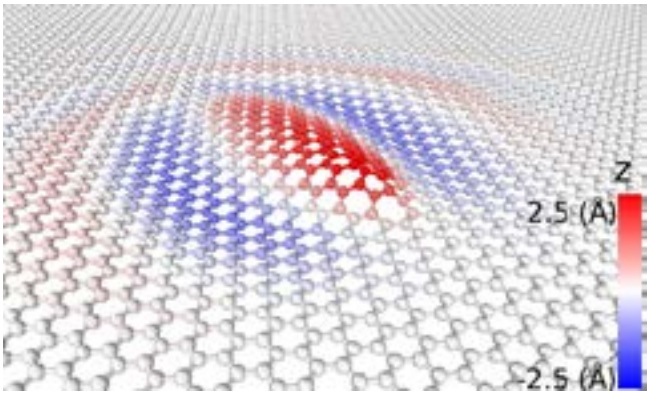


Fig. 1. Dislocation core buckling map in h-BN monolayer.

**Acknowledgement:** The research funding was financed by Research Council of Lithuania project No. 09.3.3-LMT-K-712-10-0254

[1] T. T. Tran, K. Bray, M. J. Ford et al. Boron nitride substrates for high-quality graphene electronics. *Nature Nanotechnology* **11**, 37-41 (2016).
[2] L. Weston, D. Wickramaratne, M. Mackoit, A. Alkauskas and C. Van de Walle, C. G. Native point defects and impurities in hexagonal boron nitride. *Physical Review B*, **97**(21), 214104 (2018).
[3] J. H. Los, J. M. H. Kroes, K. Albe, R. M. Gordillo, M. I. Katsnelson, and A. Fasolino *Phys. Rev. B* **96**, 184108 (2017).
[4] W. Ouyang, D. Mandelli, M. Urbakh and O. Hod. Nanoserpents: Graphene Nanoribbon Motion on Two-Dimensional Hexagonal Materials. *Nano Lett.* **18**, 6009-6016 (2018).

# FLUORESCENT GRAPHENE-OXIDE QUANTUM DOTS FOR HEAVY METAL DETECTION SYNTHESIZED BY A NEW ACID OXIDATION OF $C_{60}$ FULLERENE

Erica Ciotta[1], Luca Burratti[1], Paolo Prosposito[1,2] and Roberto Pizzoferrato[1]

[1] Department of Industrial Engineering University of Rome Tor Vergata, Via del Politecnico 1, 00133 Rome, Italy
[2] Center for Regenerative Medicine, University of Rome Tor Vergata, Via Montpellier 1, 00133 Rome, Italy
erica.ciotta@uniroma2.it

Graphene-oxide quantum dots (GOQDs) are nanomaterials with interesting and unique optical properties. Due to the small lateral dimensions, (less than 10 nm) and thanks to the luminescence properties, these materials can be exploited in many fields, such as organic light-emitting diodes, bioimaging and optical sensors [1]. Starting by different carbon allotropes, *e.g.* graphite, nanotubes, nanoflakes, it is possible to obtain GOQDs with different dimensions and oxidation degrees by chemical or physical oxidation. These reactions produce oxygen-containing functional groups, *i.e.* hydroxyl (–OH), carboxylic (–COOH) and epoxy groups, located on the carbon basal plane and at the edges of the nanosheets. As a consequence, a large number of sp3 carbon atoms and lattice defects is available in the GO structure . The result is the opening of the graphene optical bandgap with a consequent blue emission that could be exploited for many applications.

We have synthesized a new type of GOQDs in water solution starting by $C_{60}$ Buckminster fullerene using concentrated sulphuric acid ($H_2SO_4$) and nitric acid ($HNO_3$). Compared to the previous oxidation method [2], this strategy reduces the number of involved chemicals and requires a simple and direct procedure. The GOQDs photoluminescence (after excitation at 300 nm) and the absorption spectra are shown in the figure 1.

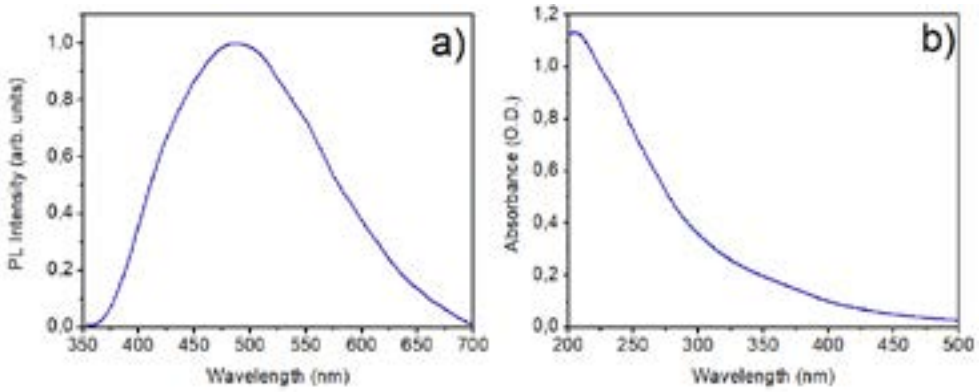


Fig. 1. Photoluminescence (a) and Absorption (b) spectra of GOQDs water solution.

Heavy metal ions in water interacting with the oxygen functional groups of the GOQDs structure can produce a variation of the photoluminescence spectrum with a quenching or an enhancement of the emission intensity [3-5]. Thanks to the change of the photoluminescence intensity is therefore possible to detect the presence of heavy metal ions in water and, in some cases, even to distinguish the type of ions. [6]. Heavy metals, in fact, can be very dangereous for the environment and for human health [7], for this reason it is necessary to monitor their presence in water and soil. In comparison to other systems, optical sensors are very promising for their stability, selectivity and absence of electrical noise. In conclusion, with an easy and low cost synthesis of luminescent GOQDs in water, a simple system to detect heavy metalions in water can obtained based on optical methods.

[1] Dong, Y., Shao, J., Chen, C., Li, H., Wang, R., Chi, Y., ... & Chen, G. Blue luminescent graphene quantum dots and graphene oxide prepared by tuning the carbonization degree of citric acid. *Carbon*, *50*(12), 4738-4743 (2012).
[2] Chua, C. K., Sofer, Z., Simek, P., Jankovsky, O., Klimova, K., Bakardjieva, S. & Pumera, MSynthesis of strongly fluorescent graphene quantum dots by cage-opening buckminsterfullerene. Acs Nano, 9(3), 2548-2555. . (2015).
[3] Ciotta, E., Prosposito, P., Tagliatesta, P., Lorecchio, C., Stella, L., Kaciulis, S., ... & Pizzoferrato, R. Discriminating between Different Heavy Metal Ions with Fullerene-Derived Nanoparticles. Sensors, 18(5), 1496 (2018).
[4] Ciotta, E., Paoloni, S., Richetta, M., Prosposito, P., Tagliatesta, P., Lorecchio, C., ... & Pizzoferrato, R. Sensitivity to heavy-metal ions of unfolded fullerene quantum dots. Sensors, 17(11), 2614 (2017).
[5] Carestia, M., Pizzoferrato, R., Gelfusa, M., Cenciarelli, O., Ludovici, G. M., Gabriele, J., ... & Gaudio, P. Development of a rapid method for the automatic classification of biological agents' fluorescence spectral signatures. Optical Engineering, 54(11), 114105 (2015).
[6] Pietrantoni, S., Francini, R., Pizzoferrato, R., Penna, S., Paolesse, R., & Mandoj, F. Energy transfer and excitation processes in thin films of rare-earth organic complexes for NIR emission. Physica status solidi c, 4(3), 1048 (2007).
[7] Jaishankar, M.; Tseten, T.; Anbalagan, N.; Mathew, B.B.; Beeregowda, K.N. Toxicity, mechanism and health effects of some heavy metals. Interdiscip. Toxicol., 7, 60–72 (2014)

# NUMERICALL MODELING OF LIGHT PROPAGATION IN ELECTRICALLY TUNABLE MULTILAYER HYPERBOLIC METAMATERIAL

Julia Szymczak[1], Alexander Korneluk[1], Tomasz Stefaniuk[1]

[1] Faculty of Physics, University of Warsaw, Pasteura 5, 02-093 Warsaw, Poland
jkuszymczak@gmail.com

Passive metal-dielectric multilayer metamaterials have been investigated by the researchers for many years. It has been shown that such structures can be used for imaging with sub-wavelength resolution, efficient light absorption, subwavelength focusing, switching, sensing, as well as spatial or temporal frequency filtering [1-3]. Here, we want to go one step further. We report on numerical modelling of light propagation in electrically tuned multilayer hyperbolic metamaterial. The considered heterostructure consists out of subsequent metal-oxide-semiconductor thin films (see Fig. 1a). As active material we use indium-tin-oxide, a highly doped n-type semiconductor with high electrical conductivity and transparency in the visible spectral range. As it was demonstrated earlier it is possible to control the carrier concentrations and thus the refractive index at the dielectric/semiconductor interface by applied external electric field [4]. We exploit this mechanism in order to tune the optical response of the hyperbolic metamaterial structure.

Two different techniques were used in order to model light propagation in studied multilayered systems. The first one is a Transfer Matrix Method (TMM), a very computationally efficient algorithm, which allows to calculate transmission refection, and absorption of planar waves through/from and in 1D multilayer stack. The second technique is a finite-difference time-domain method (FDTD), which is a fully vectorial algorithm for solving the Maxwell's equations in electrodynamic problems. We use it for calculating imaging performance of the heterostructure. To estimate the isofrequency contours associated with the metamaterial, and thus to verify dispersion operation regimes we use the effective medium theory.

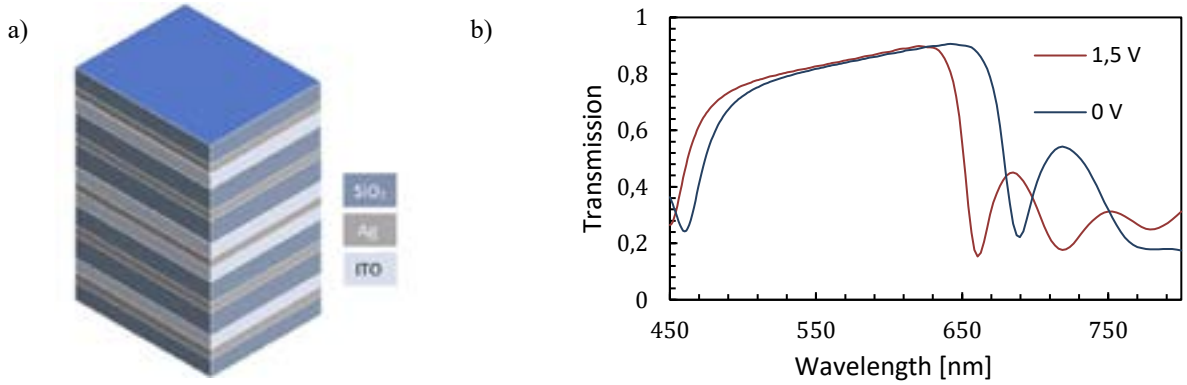


Fig. 1. (a) Schematic of considered multilayer metamaterial structure. (b) Transmission of the structure with and without applied voltage

In Fig. 1b we show one of the effects resulting from the impact of the applied voltage on the optical properties of optimised multilayer metamaterial. Without external field the structure has a broad transmission window ranging from 470 nm up to 670 nm with transmissivity reaching 85% for 650 nm. When the voltage is applied the increased carrier concentrations at the $SiO_2$/ITO interfaces leads to a significant shift in the transmission window. We believe that this effect can be utilized in ultrafast modulation or spectral filtration of metamaterial-based devices of the future.

[1] Kotyński, R., Stefaniuk, T., Comparison of imaging with sub-wavelength resolution in the canalization and resonant tunnelling regimes. Journal of Optics A: Pure and Applied Optics 11 (2009).

[2] Sreekanth, K. V. et al., Extreme sensitivity biosensing platform based on hyperbolic metamaterials. Nat. Mater. 15, 621 (2016).

[3] Guclu, C., Campione, S., Capolino, F., Hyperbolic metamaterial as super absorber for scattered fields generated at its surface. Phys. Rev. B 86, 205130 (2012).

[4] Feigenbaum, E., K. Diest, and H.A. Atwater, Unity-Order Index Change in Transparent Conducting Oxides at Visible Frequencies. Nano Letters, 10(6): p. 2111-2116 (2010).

# FLUORESCENT SILVER NANOCLUSTERS: SYNTHESIS AND POTENTIAL ENVIRONMENTAL MONITORING APPLICATIONS

Luca Burratti[1], Erica Ciotta[1], Roberto Pizzoferrato[1], Paolo Prosposito[1,2].

[1]Department of Industrial Engineering and INSTM, University of Rome Tor Vergata, Via del Politecnico 1, Rome, 00133, Italy.
[2]Center for Regenerative Medicine, University of Rome Tor Vergata, Via Montpellier 1, Rome, 00133, Italy.
luca.burratti@uniroma2.it

Fluorescent nanomaterials have attracted the interest of researchers in many science fields such as sensing [1], photonics [2] and biological applications [3]. In particular, noble metal nanoclusters (MNCs) have very bright fluorescence emission depending mainly on the dimension of the clusters. This optical feature, not present for metal nanoparticles with diameter larger than few nanometers is due to quantum confinement of electrons within of discrete energy levels in the molecular-like density of states (DOS) of the MNCs [4].

The environmental poisoning is an important and strategic topic for all the human kind. In particular heavy meal ions contamination is very dangerous since they are not biodegradable and can be accumulated in the soil and in the water, coming up to us directly by food and water. The exposure to heavy metal ions can create disease and pathology [5]. For these reasons, simple investigation methods such as the optical ones based on the change of optical characteristics (absorption or fluorescence) in presence of heavy metal ions are highly desirable.

In the present study, we synthesized two different silver nanoclusters (AgNCs) systems in water solution. AgNCs stabilized with lipoic acid (LA) and AgNCs capped with Poly (methacrylic) acid (PMAA). Concerning the synthesis, in both cases, we mixed the aqueous solution of the capping agent with the solution of $Ag^+$ (precursor salt $AgNO_3$). We used chemical reduction to convert $Ag^+$ to Ag(0) using sodium borohydride ($NaBH_4$) for the first system and photochemical approach, using an intense UV radiation, to promote the reduction of $Ag^+$ in the second case. Both AgNCs systems were characterized using absorption and fluorescence spectroscopy. Figure 1(a) shows the absorption spectrum in the UV-Vis range of AgNCs stabilized with LA (solid line) and photoluminescence emission (dotted curve) of the same solution. The inserts are photographs of the solution under white light (left side) and UV light (right side). The red fluorescence is clearly visible by naked eye. We also observed the shape and the dimensionality of the two systems through Transmission Electron Microscopy (TEM). Finally, we tested the sensitivity of both AgNCs systems to several heavy metal ions, monitoring the fluorescence emission with and without heavy metal ions. The final aim is to produce a set of different optical devices able to determine the presence of heavy metal ions in an unambiguously way. The Figure 1(b) shows a photograph of the fluorescence of two cuvettes under UV lamp. The left side cuvette contains AgNCs capped with PMAA solution without any contaminants, while the right side cuvette contains the cluster solution with Pb(II) as contaminant, in the latter case an enhancement of the fluorescence intensity is clearly visible.

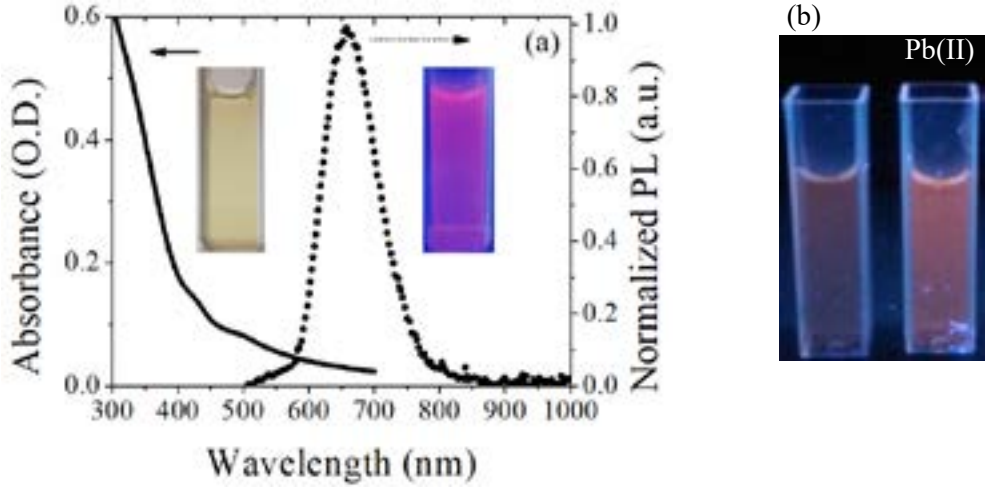


Fig. 1. (a) UV-Vis spectrum (solid line) and emission spectrum (dotted line) of AgNCs capped with LA; (b) photograph of AgNCs capped with PMAA, left side without contaminant and right side with Pb(II) ions.

[1] Ciotta, E.; Paoloni, S.; Richetta, M.; Prosposito, P.; Tagliatesta, P.; Lorecchio, C.; Venditti, I.; Fratoddi, I.; Casciardi, S.; Pizzoferrato, R. Sensitivity to heavy-metal ions of unfolded fullerene quantum dots. Sensors (Switzerland) **17**, 1–15, (2017).
[2] Zhang, Q.; Wang, C.-F.; Ling, L.-T.; Chen, S. Fluorescent nanomaterial-derived white light-emitting diodes: what's going on. J. Mater. Chem. C **2**, 4358–4373, (2004).
[3] Yahia-Ammar, A.; Sierra, D.; Mérola, F.; Hildebrandt, N.; Le Guével, X. Self-Assembled Gold Nanoclusters for Bright Fluorescence Imaging and Enhanced Drug Delivery. ACS Nano **10**, 2591–2599, (2016).
[4] Zheng, J.; Nicovich, P. R.; Dickson, R. M. Highly Fluorescent Noble-Metal Quantum Dots. Annu. Rev. Phys. Chem. **58**, 409–431, (2007).
[5] Järup, L. Hazards of heavy metal contamination. Br. Med. Bull. **68**, 167–182 (2003).

# LASER INDUCED DAMAGE THRESHOLD OF MULTI-PHOTON LITHOGRAPHY MADE POLYMERIC 3D MICRO-STRUCTURES

Agnė Butkutė[1,2], Laurynas Čekanavičius[1], Darius Gailevičius[1,2], Linas Jonušauskas[1, 2], Mangirdas Malinauskas[1]

[1]Laser Research Center, Vilnius University, Lithuania
[2]Femtika Ltd., Lithuania
agne.butkute@ff.stud.vu.lt

One of the most rapidly developed laser material processing techniques is 3D laser lithography (3DLL) [1]. This technology is based on nonlinear light-material interaction processes. This gives the possibility to make true 3D structures with sub-diffractive resolution. One of the key areas where 3DLL shows huge potential is micro-optics and photonics. In literature we can find lots of examples of functional micro-lenses and photonic crystals made by 3DLL technique [2, 3]. However, before they will become wide spread solution it is important to determine laser induced damage threshold (LIDT) of these elements.

This work is dedicated to 3DLL fabrication and LIDT characterization of polymeric bulk and woodpile structures. Various polymers and components of different internal geometries (bulk and woodpile structures) were investigated according S-on-1 measurement technique [4] as described in ISO standard [5]. The materials tested in bulk configuration were SZ2080, SZ2080 + 1% Irgacure 369 photoinitiator, PEG, SU8, Ember Clear, and Ormo Clear. Also, LIDT experiments of SZ2080 and SZ2080 +1 % IRG woodpile structures were performed. Moreover, different porosity SZ2080 woodpiles were tested. After experiments it was noticed that the most resilient material for optical components was SZ2080. The same material woodpile structures have smaller LIDT value than the bulk ones. Also, depending on the porosity of mentioned structures, the empirically examined woodpiles acted as photonic crystals with specific photonic properties that influenced the observed LIDT. It implies that LIDT of photonic crystals are caused and determined by several mechanisms. An FDTD model [6] was used to test formed woodpiles functionality. Thus, it is important to compare LIDT of photonic crystals with the same reflection/transmission characteristics in order to get accurate dependency on its porosity. Consequently, we investigated woodpiles LIDT relation with its porosity without changing its functionality, but meaningful dependency was not noticed. After evaluating all the LIDT results SZ2080 without photoinitiator was clearly more superior to any other tested material for both bulks and woodpiles, reaching LIDT of up to 160 mJ/cm$^2$ in bulk, which is around one order of magnitude lower than fused silica [7].

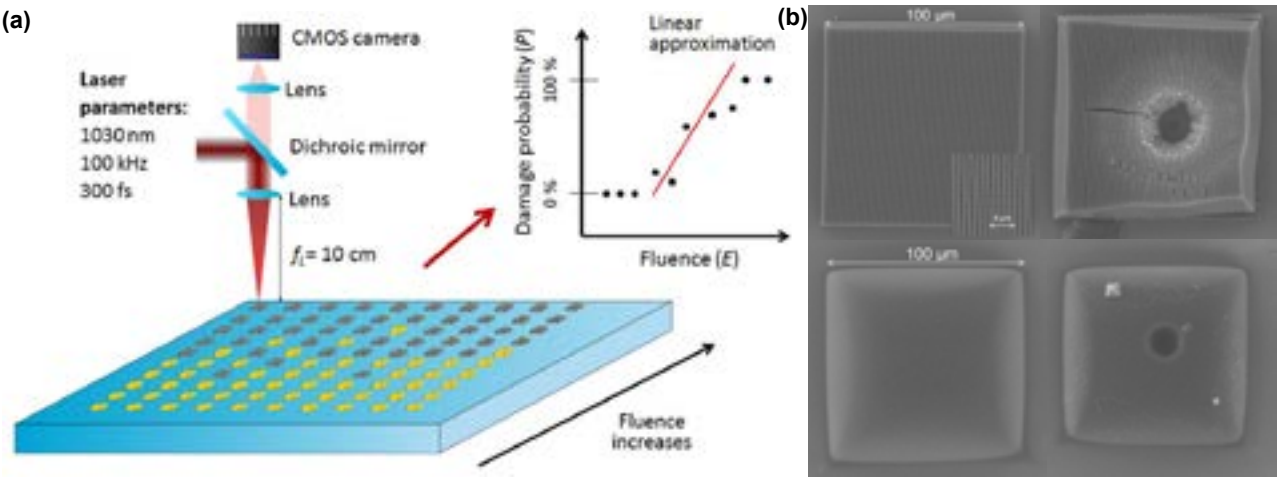


**Fig. 1. (a)** Scheme of LIDT measurement experiment. **(b)** Formed polymeric bulk and woodpile structures before and after LIDT experiment. Top left woodpile before LIDT testing, top right woodpile after LIDT testing, bottom left bulk before LIDT experiment, bottom right bulk after LIDT experiment.

[1] L. Jonušauskas, S. Juodkazis, M. Malinauskas, Optical 3D printing: bridging the gaps in the mesoscale, J. Opt. **20**(5) , 053001(2018).
[2] M. Malinauskas, H. Gilbergs, V. Purlys et al., Femtosecond laser-induced two-photon photopolymerization for structuring of micro-optical and photonic devices, SPIE **7366**, 7366 (2009).
[3] L. Maigytė, V. Purlys, J. Trull et al., Flat lensing in the visible frequency range by woodpile photonic crystals, Opt. Lett. **38**(14), 2376(2013).
[4] G. Batavičiutė, P. Grigas, L. Smalakys et al., Revision of laser-induced damage threshold evaluation from damage probability data, Rev. Sci. Instrum. **84**(4), 045108 (2013).
[5] A. Melninkaitis, D. Miksys, T. Balčiūnas et al., Automated test station for laser-induced damage threshold measurements according to ISO 11254-2 standard, SPIE **6101**, 6101 (2006).
[6] M. Mizeikis, V. Purlys, R. Buividas et al., Realization of structural color by direct laser write technique in photoresist, J. Laser. Micro. Nanoeng. **9**(1), 42 (2014).
[7] B. C. Stuart, M. D. Feit, S. Herman et al., Nanosecond-to-femtosecond laser-induced breakdown in dielectrics, Phys. Rev. **53**(4), 1749 (1995).

# HIGH-REPETITION-RATE RELATIVISTIC ELECTRON ACCELERATION IN PLASMA WAKEFIELDS DRIVEN BY SINGLE-CYCLE LASER PULSES

Dominykas Gustas, Aline Vernier, Diego Guénot, Marie Ouillé, Frederik Böhle, Stefan Hässler, Rodrigo Lopez-Martens, Agustin Lifschitz, Jérôme Faure

Laboratoire d'Optique Appliquée, Ecole Polytechnique, Université Paris-Saclay
Palaiseau, France
dominykas.gustas@ensta-paristech.fr

Continuing progress in laser technology has enabled dramatic advances in laser wakefield acceleration (LWFA), an electron acceleration technique that permits accelerating gradients three orders of magnitude higher than conventional radio-frequency methods. Due to significantly reduced space charge and velocity dispersion effects, relativistic electron bunches accelerated by laser wakefields have also been identified as a candidate tool to achieve unprecedented sub-10 fs temporal resolution in ultrafast electron diffraction (UED) experiments [1], [2]. High repetition rate operation is desirable to improve data collection statistics and wash out shot-to-shot charge fluctuations inherent to plasma accelerators. It is well known that high-quality electron beams with narrow energy spreads and small divergences can be achieved in the blowout, or "bubble" regime [3], which is at present regularly accessed with ~30 fs Joule-class lasers that can perform up to few shots per second. Our group on the contrary employed a cutting edge laser system producing few-mJ pulses compressed nearly to a single optical cycle (3.4 fs) [4] to demonstrate for the first time that, consistently with the scaling laws [5], relativistic electron beams with properties characteristic to the blowout regime and peaked at 4-6 MeV energy can also be achieved at kilohertz repetition rate [6]. We further investigate the plasma density profile effects on the accelerated charge and electron energy and show that using certain structured gas jets several tens of pC/shot can be achieved [7]. We expect this technique to lead to a highly accessible and robust instrument for the scientific community to conduct UED experiments or use it for other applications.

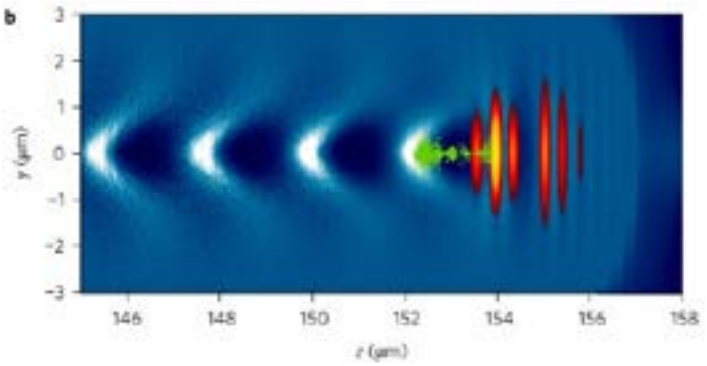


[1] J. Faure et al., Phys. Rev. Accel. Beams 19, 021302 (2016)
[2] Z.-H. He et al., Sci. Rep. 6, 36224 (2016)
[3] A. Pukhov and J. Meyer-ter-Vehn, Appl. Phys. B 74, 355-361 (2002)
[4] F. Böhle et al., Laser Phys. Lett. 11, 095401 (2014)
[5] W. Lu et al., Phys. Rev. Accel. Beams 10, 061301 (2007)
[6] D. Guénot et al., Nat. Photon. 11, 293-296 (2017)
[7] D. Gustas et al., Phys. Rev. Accel. Beams 21, 013401 (2018)

# GLASS CUTTING BY OBLATE-TIP AXICON-GENERATED BESSEL-GAUSSIAN BEAMS

Jokūbas Pipiras[1], Juozas Dudutis[1], Simon Schwarz[2], Paulius Gečys[1]

[1] Center for Physical Sciences and Technology, Savanoriu ave. 231, LT-02300, Vilnius, Lithuania
[2] Applied Laser and Photonics Group, University of Applied Sciences Aschaffenburg, 63743 Aschaffenburg, Germany
Jokubas.pipiras@ff.stud.vu.lt

With glass cutting technology advancing each decade, the laser industry is in search of efficient ways to dice glass. Bessel-Gaussian beam, due to its non-diffractive and self-healing properties, gained a particular interest in laser micromachining and, especially, in processing of transparent materials. A conical lens is the most efficient way to generate such beams, however, due to inaccuracies during fabrication, these optical elements often deviates from an ideal shape. It was recently shown that the oblate-tip axicon with an elliptical cross-section generates asymmetrical intensity pattern which induce asymmetrical modifications in glass [1]. These modifications locally weaken the sample and assure the sample separation along the cutting path, when cracks are aligned parallel [2]. It was also shown that the orientation of transverse cracks can be controlled by axicon tilt operation [3]. In this report we have investigated the Bessel-Gaussian beams, generated by axicons, which were fabricated by all laser-based technology [4], and applied for glass cutting.

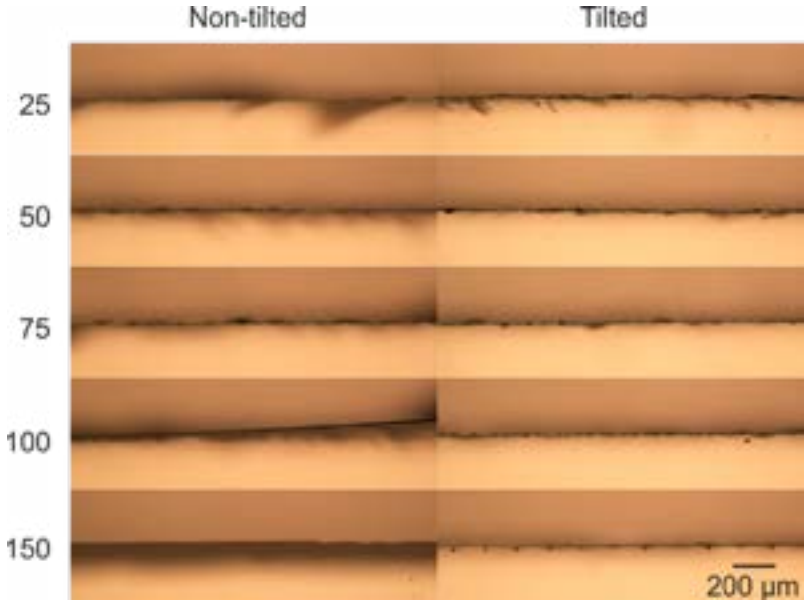


Fig. 1. Optical microscope images of the diced and separated glass sheets. Non-tilted and tilted axicon configurations were used. The intra-distance between modifications is given on the right side (in µm).

The axicons with an apex angle of 170 deg were investigated. Experiments were conducted by use of the Atlantic HE (from Ekspla) sub-nanosecond laser, which generated 300 ps pulses of 2 mJ energy at 1 kHz repetition rate. The modified soda-lime glass sheets with the thickness of 1 mm were mechanically separated by use of the 4 point bending setup with a dynamometer, which enabled to measure the flexural strength of the material. Samples were locally weakened by single-shot modifications using non-tilted and tilted axicon-generated Bessel-Gaussian beams.

The axicon tilt operation allowed to induce the directional transverse cracks in the bulk of glass, while non-tilted axicon-generated beam induced randomly orientated cracks. The optical microscope images of the diced and separated glass sheets are presented in Fig. 1. Although in both cases it was possible to dice and separate glass sheets, the tilt operation allowed to achieve higher dicing speeds, lower flexural strength and better cutting quality.

[1] J. Dudutis, P. Gečys, G. Račiukaitis, Non-ideal axicon-generated Bessel beam application for intra-volume glass modification, Opt. Express **24**, 28433–28443 (2016).
[2] J. Dudutis, R. Stonys, G. Račiukaitis, P. Gečys, Glass dicing with elliptical Bessel beam, Optics & Laser Technology **111**, 331-337 (2019).
[3] J. Dudutis, R. Stonys, P. Gečys, G. Račiukaitis, Aberration-controlled Bessel beam processing of glass, Opt. Express **26**, 3627-3637 (2018).
[4] S. Schwarz, S. Rung, C. Esen, R. Hellmann, Fabrication of a high-quality axicon by femtosecond laser ablation and CO2 laser polishing for quasi-Bessel beam generation, Opt. Express **26**, 23287-23294 (2018).

# IR-SIDE OF MULTI-OCTAVE SUPERCONTINUUM GENERATION IN YAG PUMPED BY PICOSECOND PULSES

Paulius Mackonis [1], Augustinas Petrulenas [1], Vytenis Girdauskas [1] and Aleksej M. Rodin [1,2]

[1] Solid State Laser laboratory, Department of Laser Technologies, Center for Physical Sciences and Technology, Savanoriu 231, LT-02300 Vilnius, Lithuania

[2] Ekspla Ltd, Savanoriu 237, LT-02300 Vilnius, Lithuania
mac.paulius@gmail.com

The generation of a supercontinuum (SC) in a bulk material is an inexpensive and effective method for substantially expanding the spectrum of laser pulses. Accordingly, the broad spectrum of SC makes it ideal for seeding an Optical Parametric Chirped Pulse Amplifier (OPCPA). Stable SC in the wavelength range from ~ 500 nm to ~ 1000 nm in a YAG crystal pumped with picosecond pulses [1] simplifies TW-class laser architecture [2] due to the inherent signal and pump synchronization in OPCPA. Moreover, a stable SC in the range up to 2.5 µm would eliminate the idler generation and pave the way for the development a more reliable and compact OPCPA in the IR spectral range.

Besides the stable SC in the range ~ 500 nm to ~ 1000 nm, we observed single-filament SC spanning from ~ 1100 nm to more than 2400 nm with pulse energy stability and beam pointing stability exceeding the Chirped Pulse Amplifier (CPA) - compressor [2] used as a pumping source. Such a highly stable source of broadband seed pulses together with an inexpensive CPA-compressor based on Yb:YAG rods [2] significantly simplifies the development of compact high-intensity OPCPA systems around the 2 µm spectral range.

Compressed pulses with energies up to 16 µJ, pulse width of 1.15 ps and excellent beam quality $M^2 < 1.1$ at a wavelength of 1030 nm were chipped off from a two-cascaded double-pass CPA-compressor based on Yb:YAG rods. These pulses were used to generate SC in YAG rods 15 mm and 130 mm long. We optimized the energy of the incident pulses, the focal length, numerical aperture and position to achieve the best spectral envelope and energy stability of SC, an excellent beam quality and reduced beam pointing fluctuations.

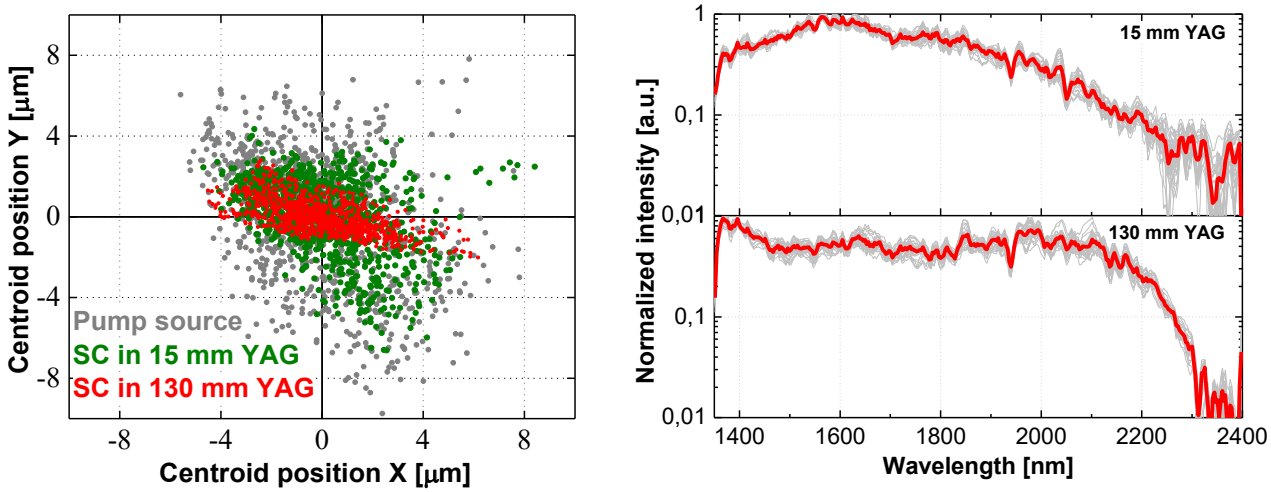


Fig. 1. The beam pointing stability of the pump source (gray dots), SC with YAG rods 15 mm long (green dots) and 130 mm (red dots) – left. The measured averaged SC spectra (red) for more than 1 hour with deviations (grey area) under optimal conditions with YAG rods 15 mm long (top) and 130 mm (bottom) – right.

Under optimal conditions, the energy stability of the SC, measured in the wavelength range from 1050 to 2500 nm, is 2 times better than the stability of the incident pulses for a YAG rod with a length of 130 mm, and for a 15 mm rod – 30 % better. Beam pointing stability of SC exceeds the source by a factor of 2.3 for a YAG rod 130 mm long and 2.7 times for a rod 15 mm (Fig. 1, left). Collimated SC has a Gaussian spatial distribution. Moreover, under optimal conditions, we did not observe any deterioration in the beam quality or the spectral envelope when tested for stability for 1 hour (Fig. 1, right) at a repetition rates of 100 Hz (over 360 thousand shots).

[1] L. Indra, F. Batysta, P. Hribek, J. Novak, Z. Hubka, J.T. Green, R. Antipenkov, R. Boge, J.A. Naylon, P. Bakule, and B. Rus, Picosecond pulse generated supercontinuum as a stable seed for OPCPA, Vol. 42, N 4, Optics letters (2017). https://doi.org/10.1364/OL.42.000843

[2] A.M. Rodin and P. Mackonis, 1 TW-Class OPCPA pumped with fiber laser seeded two-cascaded Yb:YAG rod amplifier-compressor, Papers of International Conference on Lasers and Electro-Optics Pacific Rim (CLEO-PR), Hong Kong (2018). https://doi.org/10.1364/CLEOPR.2018.Th2D.3

# TUNABLE SINGLE-MODE CW ENERGY-TRANSFER DYE LASER DIRECTLY OPTICALLY PUMPED BY A DIODE LASER

Marcin Suski[1], Anna Zygmunt[1], Justyna Stachera[1], Danuta Stefańska[1], Bogusław Furmann[1]

[1] Faculty of Technical Physics, Poznan University of Technology, Poland
marcin.j.suski@doctorate.put.poznan.pl

Energy Transfer Dye Lasers (ETDL) exploit the excitation energy transfer between the molecules in various dye mixtures in order to obtain lasing in spectral range, inaccessible by direct optical pumping, as well as to increase the lasing efficiency [1]. The dye that absorbs the pump radiation and transfers the excitation energy is referred to as a donor, whereas the dye excited indirectly is called an acceptor. In certain cases the acceptor absorbs some part of the incident pump radiation and the excitation energy transfer increases the overall lasing efficiency. Though, it is also possible to achieve laser generation of the acceptor only by means of energy transfer from the donor.

In preliminary research carried out, the absorption and fluorescence measurements of binary dye mixture were performed. Coumarin 540 was used as a donor and Rhodamine 110 as an acceptor. The measurements were performed for different acceptor concentrations. The examined dyes were selected on the basis of the work [2], where such mixture was pumped by argon laser.

On the basis of the obtained data, examination of lasing efficiency of the stated mixture in a dye laser optically pumped by a diode laser (with output power of 4 W at 445 nm) was carried out. The output power of tens of milliwatts in the single-mode regime was obtained.

Since the performance of this mixture was not satisfactory for our purposes, due to the relatively low quantum yield of both dyes a mixture of other dyes: Coumarin 498 (donor) and Pyrromethene 556 (acceptor) was introduced. The lasing efficiency of Coumarin 498 under the conditions of diode laser pumping was already comprehensively determined by the authors [3], whereas the selection of the acceptor was based on the reported literature data [4].

Fairly efficient laser generation under identical pumping conditions as previously stated was achieved, obtaining a few hundreds of milliwatts of output power. A tunable single-mode regime, suitable for high resolution spectroscopy, was also achieved and tested [5]. The fluorescence and absorption properties of the exploited mixture are still under examination.

The research within this work was financially supported by the Ministry of Science and Higher Education within the project realized at Faculty of Technical Physics, Poznan University of Technology (formerly: 06/65/DSPB/5183).

[1] G. A. Kumar and N. V. Unnikrishnan, Energy transfer and optical gain studies of FDS: Rh B dye mixture investigated under cw laser excitation, Journal of Photochemistry and Photobiology A: Chemistry 144, 107–117 (2001).
[2] M. A. Rauf and M. J. Iqbal, Coumarin-540 and Rhodamine-560 as energy transfer dye laser, Physical Chemistry 11, 61–66 (1992).
[3] D. Stefanska, M. Suski, and B. Furmann, Tunable continuous wave single-mode dye laser directly pumped by a diode laser, Laser Physics Letters 14, 045 701 (7pp) (2017).
[4] S. C. Guggenheimer et al., Efficient laser action from two cw laser-pumped pyrromethene-$BF_2$ complexes, Applied Optics 32, 3942-3943 (1993).
[5] D. Stefanska, M. Suski, A. Zygmunt, J. Stachera and B. Furmann, Tunable single-mode cw energy-transfer dye laser directly optically pumped by a diode laser, submitted to Optics and Laser Technology.

# LAGUERRE – GAUSSIAN BEAM CONVERSION BY INTERACTION OF TWO OPTICAL VORTICES WITH Λ ATOMIC SYSTEM, INDUCED BY MICROWAVE TRANSITION

Maciej Chomski[1], Gustaw Szwioła[1], Bogusław Furmann[1]

[1] *Institute of Materials Research and Quantum Engineering , Faculty of Technical Physics, Poznan University of Technology, Poland*
*maciej.s.chomski@ doctorate.put.poznan.pl*

Optical vortices are the states of light with non-zero value of Orbital Angular Momentum (OAM) which can be used in experiments based on trapped atoms by putting them in rotation or allow breaking the classic spectroscopic selection rules [1, 2]. One of the most recent application of Laguerre – Gaussian beams (LG modes) is performing optical quantum memories based on OAM transfer from photons to matter [3].

This speech is related to controlled mapping of atomic gases quantum states on states of light with OAM and the issue of the LG mode's intensity profile conversion caused by interaction with gallium atoms, whose state is controlled by simultaneous excitation by another optical vortex or Gaussian beam. In addition, the fixed microwave field is used to control this process. Presented research is a development of previously published works [4]. The analysis and numerical simulations carried out allow for considering the presented case when changing such experimental parameters as microwave field intensity or detuning light frequencies form resonant dipole transitions in gallium Λ system ($3d^{10}4s^24p^2P_{1/2}$ (F = 2) → $4s^25s^2S_{1/2}$ and $3d^{10}4s^24p^2P_{3/2}$ (F = 3) → $4s^25s^2S_{1/2}$).

The factor that distinguishes the analysis presented in this speech from previously published works was the modelling of processes occurring in the considered stationary system based on the master equation, in the form of Lindblad. The obtained results show the conversion of optical vortices resulting from their interaction with a three-level atomic system and are consistent with the results obtained for calculations performed using a different theoretical model [5]. Presented simulations predict interesting effect which has not been shown in alternative model. The ring-shaped intensity profile of LG mode is deformed to the shape of regular polygons which number of sides is directly related to the value of topological charge *l* of optical vortex (related to its OAM).

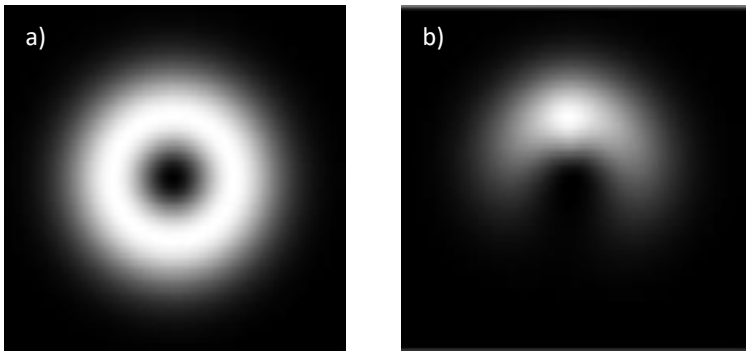


Fig. 1. Intensity profile of Laguerre – Gaussian beam: a) in free space, b) after interaction with gallium atoms cloud

Ultimately, the planned experiment, after preliminary tests on neutral atoms, will be carried out on a cloud of ions trapped in the Paul's trap, where the experiments with the double optic-microwave resonance technique were carried out as standard. This work is aimed at extending earlier techniques of manipulating quantum states of atoms and light.

The research within this work was financially supported by the Ministry of Science and Higher Education within the project realized at Faculty of Technical Physics, Poznan University of Technology (formerly: 06/65/DSPB/5183).

[1] S. M. Barnett, M. Babiker, M. J. Padgett , Optical orbital angular momentum, Phil. Trans. R. Soc. A 375: 20150444 (2017).
[2] S. Franke-Arnold, Optical angular momentum and atoms, Phil. Trans. R. Soc. A 375: 20150435, 1-6 (2017).
[3] L. Veissier, A. Nicolas, L. Giner, D. Maxein, A. S. Sheremet, E. Giacobino, J. Laurat, Reversible optical memory for twisted photons, Opt. Lett. 38, 712-714 (2013).
[4] I. Han, M. Cao, R. Liu, H. Liu, W. Guo, D. Wei, S. Gao, P. Zhang, H. Gao, F. Li, Identifying the orbital angular momentum of light based on atomic ensembles, Europhysics Letters 99: 34003 (2012).
[5] N. Radwell, T. W. Clark, B. Piccirillo, S. M. Barnett, S. Franke-Arnold, Spatially Dependent Electromagnetically Induced Transparency, Phys. Rev. Lett. 114, 123603 (2015).

# THZ-EXCITATION SPECTROSCOPY TECHNIQUE FOR BAND-OFFSET DETERMINATION

Ričardas Norkus[1], Sandra Stanionytė[1], Bronislovas Čechavičius[1] , Renata Butkutė[1], Vytautas Karpus[1], Arūnas Krotkus[1]

[1] *Centre for Physical Sciences and Technology, 10222, Saulėtekio av. 3, Vilnius, Lithuania*
ricardas.norkus@ftmc.lt

GaAsBi and related III–V alloys are referred to as bismides. They hold promise for use in laser diodes due to reduced Auger recombination and weaker emission wavelength sensitivity on temperature; also in multi-junction solar cells, and photoconductive THz range components activated by long wavelength laser pulses. To realise such applications good knowledge of band structure parameters is needed. Terahertz emission spectroscopy (TES) is novel technique for subsidiary valley and conduction band offset determination.

Terahertz radiation (THz) emission from semiconductor surfaces was demonstrated by Auston group[1]. Since the surface THz emission is a universal phenomenon in semiconductors, THz time domain spectroscopy can also be used as a characterization tool of these materials. Two main mechanisms of THz emission from femtosecond laser excited semiconductor surfaces are the photocurrent surge in the surface electric field and the spatial separation of more mobile photoexcited electrons and less mobile holes at the surface (the photo-Dember effect). The photocurrent surge effect provides the information on the energy band-bending at the crystal surface, whereas nearly monoenergetic electron bunches excited by femtosecond laser pulse and ballistically propagating towards the bulk can be exploited for studying the details of the electron energy band structure. Characteristic features on TES spectra are peaks at a semiconductor band gap, due to electric field, and peaks, due to inter-valley scattering [2].

In this work, we determined GaAs1-xBix/GaAs heterojunction offsets by varying Bi content from 3 to 12 % in measured samples. 100 nm GaAsBi samples were grown on semi-insulating GaAs by molecular beam epitaxy. Thin layers are chosen so there is uniform carrier distribution. Because of it there is no THz generation until electrons can pass through conduction band barrier. When that threshold is reached electrons are separated from holes to the GaAs substrate and THz emission occurs [3]. This effect is clearly seen in TES spectras (fig. 1) where THz emission is starting at higher photon energy than bandgap energy determined from photoluminescence measurements. Theoretical THz emission onset was fitted to the measured spectra. Conduction band and valence band offset ratio did not change with Bi content and was ~0.45.

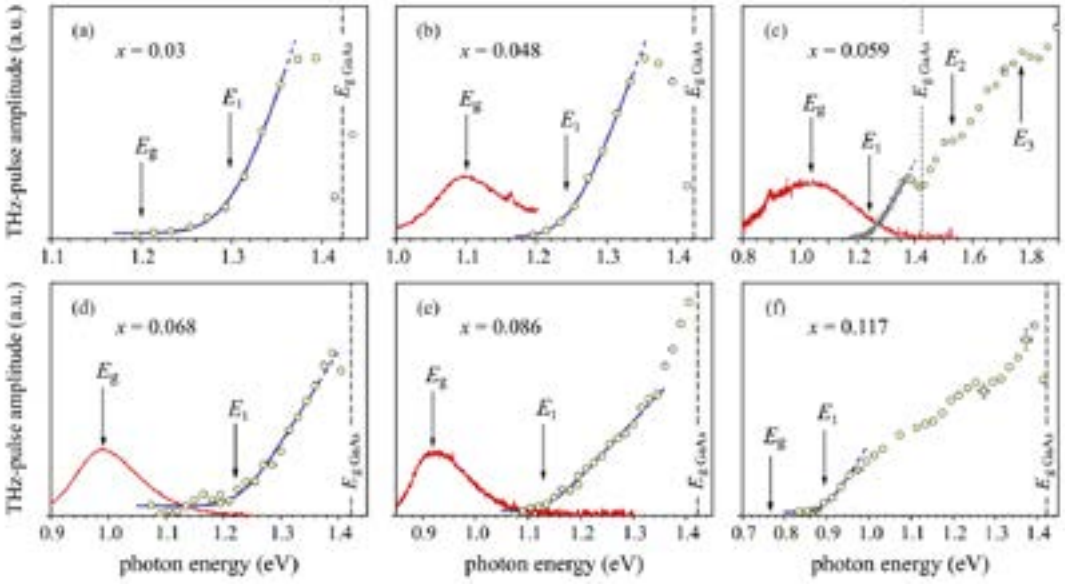


Fig. 1. TES spectra for different Bi content samples (dots), fitted theoretical shape of THz onset (solid lines) and photoluminescence curves (solid lines)

Main advantage of this technique is a direct relation between the offset values and features in TES spectra. Also it is a contactless method which does not require complicated sample structures. Resolution is limited by exciting laser bandwidth and sensitivity of THz emission setup.

[1] X.C. Zhang, B.B Hu, J.T. Darrow and D.H. Auston, Zhang X-C, Generation of femtosecond electromagnetic pulses from semiconductor surfaces Appl. Phys. Lett., 56, 1011. (1990)
[2] R. Norkus, A. Arlauskas and A. Krotkus, Terahertz excitation spectra of InP single crystals, Semicond. Sci. Technol. 33 07501 (2018).
[3] V. Karpus, R. Norkus, R. Butkutė, S. Stanionytė, B. Čechavičius, and A. Krotkus, "THz-excitation spectroscopy technique for band-offset determination" Opt. Express 26, 33807-33817 (2018)

# DIFFERENT QW STRUCTURES WITH Bi FOR INFRARED-EMITTING SEMICONDUCTOR LASERS

Simona Pūkienė, Bronislovas Čechavičius, Jan Devenson, Renata Butkutė

Center for Physical Sciences and Technology, Saulėtekio av. 3, LT-10257, Vilnius, Lithuania
simona.pukiene@ftmc.lt

Development of semiconductor laser diodes with temperature-insensitive oscillation wavelengths is expected to open up a new era of widespread application in telecommunication network. There have been strong efforts over many years to improve threshold current and temperature stability of commercial 1.3–1.55 μm wavelength InGa(Al)As(P)/InP with quantum well (QW) lasers. In recent years, the promising results were achieved developing the growth technology of GaAsBi quantum structures for optoelectronic applications including lasers. The first successful operation of an electrically injected $GaAs_{0.978}Bi_{0.022}$ single quantum well laser employing $Al_{0.2}Ga_{0.8}As$ barriers deposited by MOCVD was proposed by Ludewig *et al* in 2013, meanwhile electrically driven lasing from GaAsBi MQW diode grown by MBE with 6% of Bi at room temperature was reported by Butkute *et al* in 2014. By incorporating a small amount of Bi in a III–V semiconductor, such as GaAs, a strong bandgap reduction and increased spin–orbit splitting energy, ΔSO, occur, what reduces Auger recombination in IR wavelength range [1].

In this work series of different QWs structures with Bi were epitaxially grown by molecular beam epitaxy (MBE) on semi-insulating GaAs(100) substrates using GaAs buffer under stoichiometric conditions. The surface morphology of the structures was examined using atomic force microscopy. The lattice parameters of GaAsBi and Bi concentration have been evaluated from high resolution X-ray diffraction (XRD) spectra. Optical measurements showed the photoluminescence peak attributed to the GaAsBi QWs in the energy interval from 1 to 1.5 μm depending on different Bi concentration (Fig. 1).

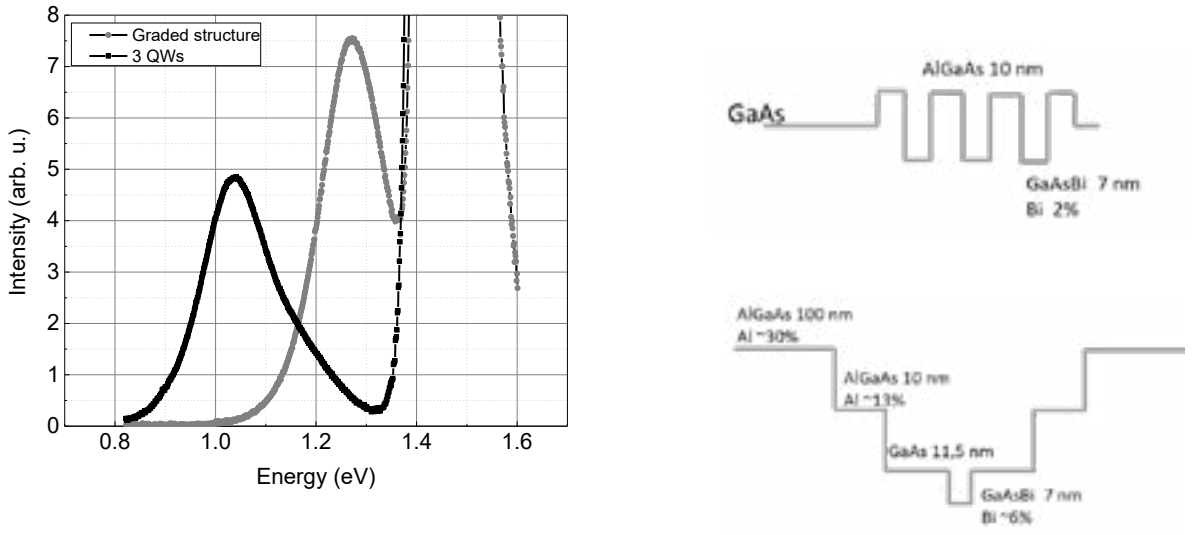


Fig. 1. RT photoluminescence measurements of different QWs structures with the different concentration of Bi. Peaks at 1.05 and 1.26 eV are attributed to 3 QW and graded QW structure, respectively.

After optimization of growth condition, the laser diode structures with a bismide QW in active area were grown on n-GaAs substrate. Laser diodes were fabricated by a UV photolithography. As-cleaved diodes were investigated.

[1] K. Alberi, J. Wu, W. Walukiewicz, K. M. Yu, O. D. Dubon, S. P. Watkins, C. X. Wang, X. Liu, Y.-J. Cho, and J. Furdyna. Valence-band anticrossing in mismatched III-V semiconductor alloys. Phys. Rev. B, 75:045203, Jan 2007

# OPTICAL PROPERTIES OF MOLECULAR BEAM EPITAXY GROWN $(Mo,Mn)Se_2$, $MoSe_2$, AND MnSe

Julia Kucharek, Wojciech Pacuski

Institute of Experimental Physics, Faculty of Physics, University of Warsaw,
Pasteura 5, PL-02-093 Warszawa, Poland
E-mail adress: j.kucharek2@student.uw.edu.pl

Doping non-magnetic semiconductors with magnetic ions such as Mn leads to formation of diluted magnetic semiconductors (DMS) e.g. (Cd,Mn)Te or (Ga,Mn)As. DMS exhibit enhanced magnetooptical properties and fascinating magnetic phenomena as for example carrier mediated ferromagnetism. Aim of this work is to answer if above concept can be applied to layered graphene-like two dimensinal (2D) materials, such as tranistion matal dichalcogenides (TMD). To study imapct of Mn ions on properties of TMD we have grown in the same conditions: undoped molybdenum diselenide ($MoSe_2$), molybdenum diselenide doped with manganese ($(Mo,Mn)Se_2$), and manganese selenide (MnSe) - as a reference. We used molecular beam epitaxy and two kinds of substrates: Si with polycrystalline $SiO_2$ buffer and $Al_2O_3$.

On $Si/SiO_2$ substrate we have grown a series of samples with various amount of deposited Mn, while amount of Mo and Se were kept constant (optimized for 1 monolayer of $MoSe_2$). Next, we investigated all samples using room temperature optical spectroscopy: Raman scattering and photoluminescence. We observe that characteristic Raman line of $MoSe_2$ at 241 $cm^{-1}$ only weakly evolved with increasing amount of Mn, but other spectral lines appears in the Raman spectrum of $(Mo,Mn)Se_2$. Also, we found that the addition of manganese have not significantly altered the result of photoluminescence. There are only very weak effects of photoluminescence quenching. It is in contrary to most of diluted magnetic semiconductors, where Mn ions are known to induce effect of total photoluminescence quenching. What is new, for high amount of Mn, new photoluminescence bands appears. We have found that Si substrate with 90 nm thick $SiO_2$ buffer is very convenient for optical study of $(Mo,Mn)Se_2$, because of constructive optical interferences. On the other hand, such kind of polycrystalline buffer gives no hope for growth of large monocrystalline layers. This is why we decided to start work on $Al_2O_3$ substrates also.

Samples grown on c-plane $Al_2O_3$ were analyzed in situ using Reflection High Energy Electron Diffraction (RHEED). This technique confirmed that in particular conditions growth of well oriented crystals is possible. Further optical microscopy analysis showed that crystals have typical sizes of 1 micrometer, so structure is not a monocrystal. Thanks to transparency of $Al_2O_3$, transmittance measurements were performed on obtained layers.

# EPR STUDY OF STRUCTURAL PHASE TRANSITION IN MANGANESE-DOPED $[(CH_3)_2NH_2][Cd(N_3)_3]$ HYBRID PEROVSKITE

Laisvydas Giriūnas[1], Mantas Šimėnas[1], Mirosław Mączka[2] and Jūras Banys[1]

[1]Faculty of Physics, Vilnius University, Saulėtekio 9, LT-10222 Vilnius, Lithuania
[2]Institute of Low Temperature and Structure Research, Polish Academy of Sciences, P.O. Box-1410, PL-50-950 Wroclaw, Poland
laisvydas.giriunas@ff.vu.lt

Hybrid perovskite frameworks are an emerging family of materials with interesting dielectric, ferroelectric and magnetic properties which could be useful in such applications as charge storage and optoelectronic devices. In general, these materials are composed of metallic centers joined together by organic or inorganic linkers forming a porous framework. Each pore confines a single molecular cation. The majority of such hybrid perovskites exhibit structural phase transitions followed by the cation ordering and framework deformation [1].

A powerful method to study local structural changes and dynamic effects in hybrid perovskites is the electron paramagnetic resonance (EPR) spectroscopy. In this study we employ continuous-wave (CW) X-band (9.37 GHz) EPR to study the structural phase transition of a recently reported [2] $[(CH_3)_2NH_2][Cd(N_3)_3]$ (DMACd) hybrid perovskite doped with a small amount of paramagnetic $Mn^{2+}$ ions.

The obtained temperature dependent EPR spectra of DMACd:$Mn^{2+}$ powder shows typical patterns of $Mn^{2+}$ ions in the $3d^5$ electronic configuration, which means that these ions have successfully replaced $Cd^{2+}$ centers and formed $MnN_6$ octahedra. Upon cooling, CW EPR spectra exhibit a drastic change at the phase transition temperature of 178 K demonstrating that $Mn^{2+}$ centers are also susceptible to the phase transition. A sudden anomalous increase of the EPR linewidth at 178 K followed by a maximum at 174 K, shown in Figure 1a, indicates a first-order character of the phase transition.

To further characterize $Mn^{2+}$ centers in DMACd, we performed simulations of the experimental CW EPR spectra using the following spin Hamiltonian [3]:

$$\mathbf{H} = \mathbf{H}_{EZ} + \mathbf{H}_{HF} + \mathbf{H}_{FS}, \tag{1}$$

where the first and second terms describe the electron Zeeman and hyperfine interactions, respectively. The last term describes the fine-structure of the spectrum which is usually characterised by the axial $D$ and orthorhombic $E$ zero-field splitting parameters. In our case, these two parameters measure the distortion of the $MnN_6$ octahedra which is directly influenced by the $DMA^+$ cation motion. The temperature dependences of $D$ and $E$ parameters, obtained from simulations, of $Mn^{2+}$ probe ions in DMACd are presented in Figure 1b. A sharp increase of these parameters at 178 K confirms a strong first-order character of the structural phase transition in DMACd.

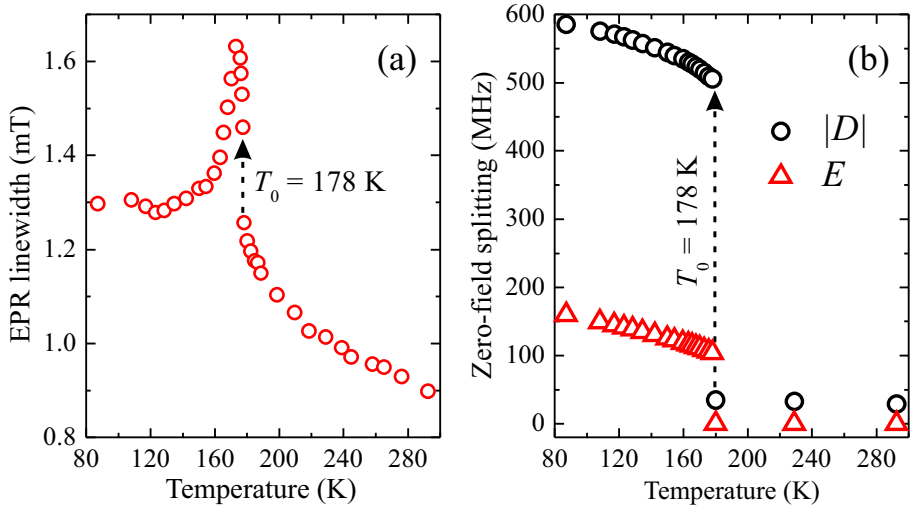


Fig. 1. Temperature dependences of (a) the peak-to-peak CW EPR linewidth and (b) $D$ and $E$ zero-field splitting parameters of $Mn^{2+}$ ions in DMACd.

[1] K. Asadi, M. A. van der Veen, Ferroelectricity in Metal–Organic Frameworks: Characterization and Mechanisms. European Journal of Inorganic Chemistry **27**, 4332-4344 (2016).
[2] Z.-Y. Du, et al., Switchable Guest Molecular Dynamics in a Perovskite-Like Coordination Polymer toward Sensitive Thermoresponsive Dielectric Materials. Angewandte Chemie **127**, 928-932 (2015).
[3] V. K. Jain, G. Lehmann, Electron paramagnetic resonance of $Mn^{2+}$ in orthorhombic and higher symmetry crystals. physica status solidi (b) **159**, 495-544 (1990)

# TERAHERTZ FREQUENCY RANGE TRANSMITTANCE OF GaAs/AlGaAs NANOSTRUCTURES WITH PARABOLIC QUANTUM WELLS

Justas Pagalys[1,2], Evelina Pozingytė[1], Simona Pūkienė[1], Vytautas Jakštas[1], Mindaugas Karaliūnas[1]

[1]Department of Optoelectronics, Center for Physical Sciences and Technology, Sauletekio Ave. 3, 10257 Vilnius, Lithuania

[2]Faculty of Physics, Vilnius University, Sauletekio Ave. 9, 10222 Vilnius, Lithuania

justas.p12@gmail.com

Terahertz (THz) frequency range electromagnetic waves interaction with matter is a significant research field in the presence. It is possible to study weak bond oscillators, such as electromagnetic charge dipoles or molecular bonds, with characteristic time in picosecond range due to the low THz photon energy [1]. On the other hand, THz waves do not interact with strong bond oscillators, therefore materials, such as plastic, paper and textile, are transparent to THz radiation. It allows the THz imaging through such opaque materials and perform the spectroscopy of covered and sealed objects and substances. For the THz technology application the more compact, more efficient and cheaper THz emitters are desirible [2, 3]. THz spectral range is between radio waves and infrared radiation, therefore THz generation is a chalanging task. For optoelectronic methods THz photon energy is rather low and for radio-electronic methods THz frequency is rather high. There are several physics phenomena which can be exploited for THz emission. In this work, the responce of GaAs/AlGaAs parabolic quantum well (PQW) nanostructures to THz radiation is studied.

Samples were grown using molecular beam epitaxy technique. The schema of deposited layers stack and the corresponding energy band diagram of one of the samples are shown in the Fig. 1 a) and b), respectively. Sample consists of 350 $\mu$m thick si-GaAs substrate, 100 nm thick GaAs buffer layer, 200 nm thick $Al_{0.3}Ga_{0.7}As$, 50 nm thick PQW layer followed by 100 nm thick $Al_{0.3}Ga_{0.7}As$ and 20 nm thick GaAs capping layer. The PQW was designed for equidistant energy subbands structure to meet the difference between the subbands of 29 meV what correspnds to 7 THz frequency.

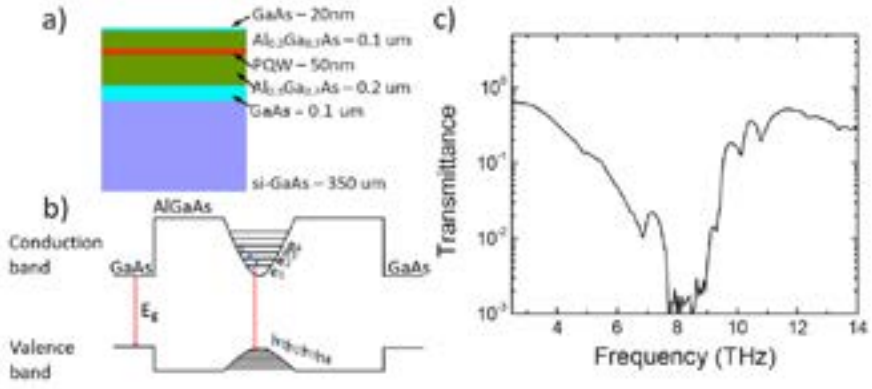


Fig. 1. a) Schema of the MBE grown layers stack; (b) corresponding energy band diagram; (c) transmittance spectrum of the sample with GaAs/AlGaAs PQW in THz spectral range.

Fuorier transform spectroscopy (FTS) in the THz frequency range was used to measure transmittance spectra of the sample. The FTS set-up was based on Michelson interferometer which consisted of a 6 $\mu$m thick HDPE beam spilter and two mirrors. One of the mirrors was fixed and the other was moved back and forth for the collimated beam modulation. The beam was generated by the Hg arc lamp, modulated by the optical chopper, transmitted through the FTS set-up as well as the sample and registered by the Golay cell. The experimental conditions allowed to reach the spectral resolution better than 60 GHz. The sample was attached to the cold finger of liquid-nitrogen-cooled cryostat allowing to stabilize the temperature of the sample at 84 K. The measurements were carried out in 0.23 mbar vacuum environment.

Prior to FTS experiment the low temperature photoluminescence (PL) spectroscopy at 3 K temperature was carried out for the sample containing PQW. It showed that the structure of energy subbands in the PQW is nearly the designed one. THz range transmittance spectra shown in Fig. 1 c) revealed the reststrahlen band of GaAs between 7.6 THz and 9 THz and AlAs transverse optical phonon spectral line at 10.86 THz frequency. Detailed analysis of transmittance spectra around 7 THz of the samples with GaAs/AlGaAs PQW nanostructures by comparison with the GaAs/AlGaAs epitaxial layers have not showed explicit differences. It is expected that the use of additional excitation source to populate the PQW subbands with carriers can lead to the noticable spectral responce to the THz radiation around the 7 THz frequency.

[1] A. Bonvalet, J. Nagle, V. Berger, A. Migus, J.-L. Martin, M. Joffre, Femtosecond infrared emission resulting from coherent charge oscillations in quantum wells, Phys. Rev. Lett. **76**, 4392–4395 (1996).

[2] A. Tzimis, A. V. Trifonov, G. Christmann, S. I. Tsintzos, Z. Hatzopoulos, I. V. Ignatiev, A. V. Kavokin, P. G. Savvidis, Strong coupling and stimulated emission in single parabolic quantum well microcavity for terahertz cascade, Applied Physics Letters **107**(10), 101101 (2015).

[3] B. Paulillo, J.-M. Manceau, L. H. Li, A. G. Davies, E. H. Linfield, R. Colombelli, Room temperature strong light-matter coupling in three dimensional terahertz meta-atoms, Applied Physics Letters **108**(10), 101101 (2016).

# INVESTIGATION OF INTERMEDIATE MASS BLACK HOLES VIA GRAVITATIONAL MICROLENSING

Algita Stankevičiūtė[1], Łukasz Wyrzykowski[1]

[1] Astronomical Observatory, University of Warsaw, Poland
algita@astrouw.edu.pl, atigla@gmail.com

In recent years, Intermediate Mass Black Holes (IMBHs) (with masses between 100 – $10^5$ $M_\odot$) attracted wide attention due to importance in understanding how the black holes at various masses are formed, in particular the super-massive ones seen in quasars [1]. It is presumed that they can be formed by various occurring phenomena, including direct collapse of unpolluted gas in very massive stars [2], from compact stellar clusters [3] and some can even originate from the mysterious dark matter and potentially be partially responsible for the dark matter content of the Universe. So far, there has been no robust detection of IMBH, with only a couple of candidates suggested [4].

One of the most novel techniques to detect and characterise IMBHs is gravitational microlensing phenomenon [5, 6], which is presented in Fig. 1.

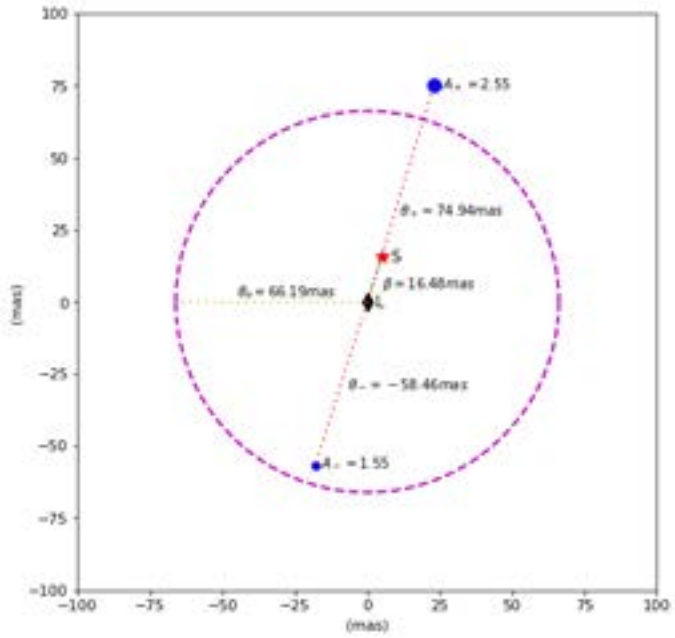


Fig. 1. Gravitational microlensing phenomenon by the IMBHs with a mass of 2000 $M_\odot$

In this research, we are analysing ultra-precise astrometric data from Gaia space mission and from VLTI. If a black hole acts as a gravitational lens, it creates two images of the background source (Fig. 1), in the Milky Way these will be just stars of our Galaxy. Separation of the images depends on the mass of the lens, but even for an IMBH, they are unresolvable if observed with typical instruments (separations up to 100 milli-arcseconds). ESA's mission Gaia is the best of them since it also observes the entire sky, hence can provide candidates from all over the sky [7, 8]. The observations can be followed-up with ESO's VLTI optical interferometer GRAVITY that provides milli-arcsecond angular resolution in near infrared wavelengths. An interferometric instrument GRAVITY is used for interferometric imaging, as well as for astrometry [9]. Two independent systems: fringe tracking (FT) and infrared wavefront sensing system (CIAO) help to correct automatically the residual optical path difference between the beams [9]. This concept will be presented for optical interferometry, regarding to VLTI.

We hope to discover first cases of IMBHs in the Milky Way by using gravitational microlensing phenomenon.

[1] Jenna M. Cann, et al. The Hunt for Intermediate Mass Black Holes in the JWST Era. The Astrophysicsal Journal **861**, 1-11 (2018).
[2] Bin Yue, et al. The brief era of direct collapse black hole formation. Monthly Notices of the Royal Astronomical Society **440**, 1263-1273 (2014).
[3] Clovis Hopman and Simon Portegies Zwart. Gravitational waves from remnants of ultraluminous X-ray sources. Monthly Notices of the Royal Astronomical Society: Letters **363**, L56-L60 (2005).
[4] Mar Mezcua. Observational evidence for intermediate-mass black holes. International Journal of Modern Physics D **26**, 1730021-1-25 (2017).
[5] B. Paczynski. Gravitational Microlensing: Black Holes, Planets; OGLE, VLTI, HST and Space Probes. arXiv: 0306564 [astro-ph/] 26 Jun 2003
[6] Sjur Refsdal and H. Bondi. The Gravitational Lens Effect. Monthly Notices of the Royal Astronomical Society **128**, 295-306 (1964).
[7] Cameron A. Lemon, et al. Gravitationally lensed quasars in Gaia: I. Resolving small-separation lenses. Monthly Notices of the Royal Astronomical Society **472**, 5023-5032 (2017).
[8] A. Lindegren, et al. Gaia Data Release 2: The astrometric solution. Astronomy and Astrophysics **616**, 1-25 (2018).
[9] S. Gillessen, et al. GRAVITY: a four-telescope beam combiner instrument for the VLTI. Proceedings Volume 7734, Optical and Infrared Interferometry II (2010).

# MODELLING OF BLACK HOLE ACCRETION INDUCED BY DYNAMICAL PERTURBATIONS

Matas Tartėnas[1], Kastytis Zubovas[1,2]

[1]Faculty of Physics, Vilnius University, Lithuania
[2]Department of Fundamental Research, Center for Physical Sciences and Technology, Vilnius, Lithuania
matas.tartenas@gmail.com

Currently, the black hole at the center of the Milky Way is inactive, but there are reasons to believe it was not always so and there were at least two activity periods in the recent past [1]. The first of these, happening a few million years ago, could be responsible for the formation of the Fermi bubbles [2]. It is suggested that such an event could be initiated by a perturbation of the molecular gas ring that surrounds the black hole by an infalling molecular cloud.

We aim to reproduce the activity period with a pair of models: a hydrodynamical Gadget-3 model of the several-parsec-wide region of the Galactic centre and a thin $\alpha$ accretion disc around the central black hole. The hydrodynamical model consists of three main components: the central black hole ($M_{\rm bh} = 4\times10^6\,{\rm M}_\odot$), the CNR-like toroidal gas ring ($M_{\rm r} = 10^4\,{\rm M}_\odot$, $R_{\rm in} = 1.5\,{\rm pc}$, $R_2 = 4\,{\rm pc}$) and the infalling molecular cloud ($M_{\rm mc} = 10^4\,{\rm M}_\odot$, $R_{\rm mc} = 1\,{\rm pc}$). The accretion disc is fed by the particles that cross a sink boundary ($r_{\rm sink} = 0.01\,{\rm pc}$) in the hydrodynamical model. Our accretion disc extends from $3R_{\rm s}$ to $26107R_{\rm s}$ and consists of 151 rings.

By varying the initial inclination angle ($\gamma$) of the orbit of the molecular cloud we change the outcome of the encounter, including the feeding rate of the central accretion disc and the morphology of resulting structures. After the accretion disc feeding rates are determined in each simulation, we use them as input parameters in the corresponding accretion disc simulations. We feed the accretion disc at five different feeding radii to investigate the effects of feeding by gas carrying different angular momenta.

We find that the feeding rate of the central accretion disc is dependent on the initial angle and reaches up to $\sim \dot{M}_{\rm Edd}$. The $\log(M_{\rm total})$ transferred to the central accretion disc (Fig. 1) can be approximated by a linear function:

$$\log M/M_0 \approx 2.34^{+0.14}_{-0.15}\times10^{-2}\gamma - 4.34^{+0.22}_{-0.19}.$$

Also the morphology of the system is affected by the change in $\gamma$: systems with initial infall angle $\gamma \geq 60^\circ$ produce a central disk and more highly inclined initial orbits lead to a more compact and less massive resulting ring. After the most extreme collision, the energy liberated during the nuclear activity period is equal to about 4.5% of the energy required for Fermi bubble formation ($E_{\rm Fermi} \approx 3.2\times10^{58}\,{\rm erg}$) with initial ring mass $\sim 10^4{\rm M}_\odot$. The highest possible ring mass ($\sim 10^6{\rm M}_\odot$), combined with an equivalent cloud mass, would produce the required energy.

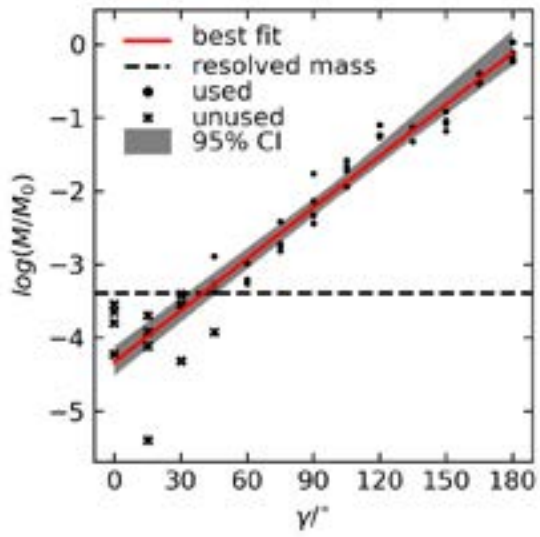


Fig. 1. The total mass transferred to the central accretion disc during the activity period ($\sim 0.5$ Myr) with different initial collision angles $\gamma$

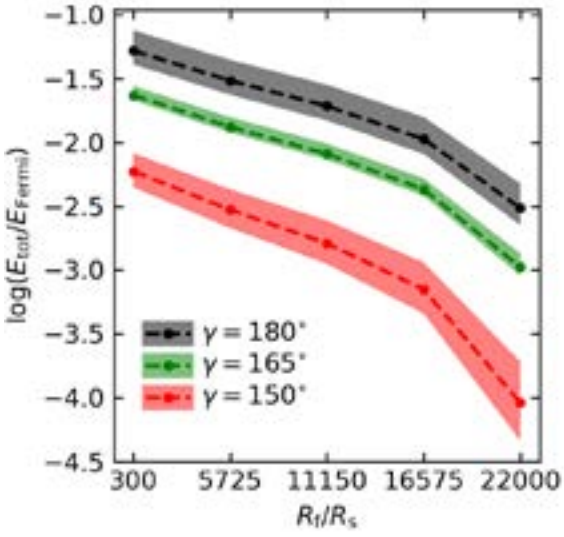


Fig. 2. The total energy released during the activity period at with different feeding radii $R_{\rm f}$ in the units of $E_{\rm Fermi}$

[1] Ponti G., Morris M. R., Terrier R., Goldwurm A., 2013, in Cosmic Rays in Star-forming Environments, edited by D. F. Torres, O. Reimer, vol. 34 of Astrophysics and Space Science Proceedings, 331.
[2] Zubovas K., Nayakshin S., 2012, MNRAS, 424, 666.

# PARAMETERS OF RELATIVE MOTION OF A BINARY STAR MOVING IN EXTERNAL GRAVITATIONAL FIELD OF A BLACK HOLE FROM IT'S REDSHIFT

Stanislav Komarov[1], Alexander Gorbatsievich[1]

[1]Department of Theoretical Physics and Astrophysics, Belarusian State University, Nezavisimosti av., 4, 220030 Minsk, Belarus.
staskomarov@tut.by

The various approaches for studying the time evolution of the redshift of light of star in external gravitational field are presented in many papers (see, e. g., [1, 2, 3, 4]). They investigate the influence of trajectory of motion of the source on redshift, that can be used for future tests of various theories of gravity, for example, by applying the results to sources in the vicinity of the Galactic Center. Certain of the cited papers provide approaches for solution of inverse problem: calculating of the parameters of motion of the source using observable characteristics of radiation, such as redshift and intensity (see, e. g., [3, 1, 4]).

In the present work we describe a method that allows to solve inverse problem for the source in binary star that moves in external gravitational field of supermassive Kerr black hole using the redshift data only. With contrast to the case binary motion in absence of strong external gravitational field the results of our investigation show that presence of the field gives possibility to find all parameters of the orbit of relative motion of the stars in binary.

The presented method is illustrated on the example of mathematical model of the system that compose point masses $m_1$ and $m_2$, moving in external Kerr gravitational field. The mass of the emitter is $m_1$. The world lines for propagation of electromagnetic radiation of emitter are calculated as isotropic geodesics in Kerr metric in certain approximation (linear to Kerr parameter $a/M$, where $a$ is the angular momentum of the black hole and $M$ it's mass). Then the redshift can be found from [5]:

$$z(\tau) = (1+z_0(\tau))\left(1-\frac{1}{c}\frac{\mathrm{d}}{\mathrm{d}\tau}\left(n_{(\alpha)}X_1^{(\alpha)}\right)\right) - 1 + O\left(\frac{\rho^2}{M^2}, \frac{v^2}{c^2}\right), \tag{1}$$

Here $z(\tau)$ is the redshift of received light as function of proper time of the source $\tau$. $X^{(\alpha)}$ is Fermi coordinates of the source star in the frame of the center of mass of the system, $n^{(\alpha)}$ is components of the unit vector of the light ray in Fermi coordinates, $c$ is speed of light, $\rho \sim X^{(\alpha)}$, $v$ is the relative velocity of the stars. $z_0(\tau)$ is redshift of the imagine source in the center of mass of the binary.

| Parameter | Model value | Calculating value |
|---|---|---|
| Eccentricity, $e$ | 0.68 | 0.58 |
| Period of relative motion, $T$ | 20.268 $Mc^{-1}$ | 20.264 $Mc^{-1}$ |
| Mass function, $M_2$ | 0.0062 $M^{1/3}$ | 0.0066 $M^{1/3}$ |
| Pericenter longitude, $\omega_r$ | 1.56 rad | 1.32 rad |
| Orbital inclination, $i$ | 1.55 rad | 1.31 rad |
| Position angle, $\zeta$ | 1.72 rad | 3.05 rad |

Table 1. The model parameters characterising relative motion of the components of the binary and the calculating ones from the solution of inverse problem.

The numerical results for the solution of inverse problem are presented in Table 1. Mass function in the presented data is defined by $M_2 = \sin(i)m_2/(m_1+m_2)^{2/3}$.

[1] Youjun Lu Fupeng Zhang and Qingjuan Yu. On testing the Kerr metric of the massive black hole in the galactic center via stellar orbital motion: full general relativistic treatment. Astrophys. J., 809:27, 2015.

[2] T. Paumard M. Grould, F. H. Vincent and G. Perrin. General relativistic effects on the orbit of the s2 star with gravity. Astronomy and Astrophysics, 608:A60, 1–22, 2017.

[3] Alexander Tarasenko. Reconstruction of a compact object motion in the vicinity of a black hole by its electromagnetic radiation. Phys. rev. D, 81:123005, 2010.

[4] A. Herrera-Aguilar and Ulises Nucamendi. Kerr black hole parameters in terms of the redshift/blueshift of the photons emited by geodesic particles. Phys. Rev. D, 92:045024, 2015.

[5] Komarov S., Gorbatsievich A., Tarasenko A. Redshift of a compact binary star in the neighborhood of a supermassive black hole. General Relativity and Gravitation, 50:132, 2018.

# IN SEARCH OF THE $S_3$ EXTENDED STANDARD MODEL HIGGS SECTOR DARK MATTER: FROM THEORY TO NUMERICAL ANALYSIS

Anton Kuncinas, Per Osland

Department of Physics and Technology, University of Bergen, Norway
Anton.Kuncinas@protonmail.com

The Standard Model (SM) of particle physics has been extensively tested for a few decades. The last missing piece, the Higgs boson, was discovered in 2012 with a combined mass of $m_h = 125.09 \pm 0.21(\text{stat.}) \pm 0.11(\text{syst.})$ GeV [1] based on data from the ATLAS and CMS experiments. Properties of the observed scalar particles are in agreement with those of the SM Higgs boson, nevertheless there is still no experimental verification that it is the only Higgs boson. Acknowledging the fact that the SM is the theory, which describes an approximate observable world it is worth taking a note that there is physics beyond the SM. One of the physical phenomena, which does not fit the frame of the SM is the absence of the Dark Matter (DM) candidate and thus SM fails to describe nearly 85% of matter. An extension of the Higgs sector would solve some of the issues. Thus we propose and are motivated that such extension could potentially solve several problems.

We study an extension of the SM in which there are two additional copies of the Higgs $SU(2)$ doublets added to the scalar potential. The extension of the SM Higgs sector we are interested in is the so-called three-Higgs-doublet model (3HDM). Such extension leads to eight additional scalar fields with respect to the SM. In general all scalar fields of the same electrical charge mix to form physical Higgs states. Based on mixing this can lead to some interesting properties. We are interested in a specific case of the 3HDM, i.e. the $S_3$-symmetric 3HDM [2], which is a permutation group of the three Higgs $SU(2)$ doublets. We take a look at the specific $S_3$ vacuum configuration C-III-c-$v^2$ [3], i.e. a softly broken C-III-c vacuum configuration: $\{\hat{w}e^{i\sigma}, \hat{w}, 0\}$. Although a complex phase is present in vacuum it does not lead to spontaneous CP violation. By introducing an additional $\mathbb{Z}_2$ symmetry we prevent decay of the lightest scalar particle associated with the inert $SU(2)$ doublets to scalar particles associated with active $SU(2)$ doublets. Therefore the lightest inert scalar is presumably a DM candidate.

Dozens of new quantum field theory models are presented these days and new particles are proposed as a solution to current problems in particle physics. Therefore, for a viable model a study should be conducted along with comparing plausible data with the available experimental one. There are several possible ways to check particle physics model, which involves but is not limited by the scalar potential stability, tree-level unitarity, electorweak oblique parameters [4]. Precise calculations are needed in order to test theoretical expectations at decent accuracy. An indisputable contribution to the development of physics was made by a computer as a tool. There is an abundance of available computation tools and therefore we focus on some of them. For this reason, we want to introduce to basic computation tools and what it takes to start from a theoretical model and develop it to produce viable theoretical and experimental data. In our study we use `Mathematica` for spectrum generator and perform an additional check using `SARAH` [5], and for experimental constraints we consider `CalcHEP` [6] package to check relic density using `micrOMEGAs` [7] and compare decay rates with `HiggsBounds` [8]. We present preliminary results of the 3HDM $S_3$ C-III-c-$v^2$ DM candidate by taking a look at experimental and theoretical constraints.

[1] G. Aad *et al.* [ATLAS and CMS Collaborations], Phys. Rev. Lett. **114** (2015) 191803 doi:10.1103/PhysRevLett.114.191803.
[2] S. Pakvasa and H. Sugawara, Phys. Lett. **73B** (1978) 61. doi:10.1016/0370-2693(78)90172-7
E. Derman, Phys. Rev. D **19** (1979) 317. doi:10.1103/PhysRevD.19.317
J. Kubo, H. Okada and F. Sakamaki, Phys. Rev. D **70** (2004) 036007 doi:10.1103/PhysRevD.70.036007.
[3] D. Emmanuel-Costa, O. M. Ogreid, P. Osland and M. N. Rebelo, JHEP **1602** (2016) 154 Erratum: [JHEP **1608** (2016) 169] doi:10.1007/JHEP08(2016)169, 10.1007/JHEP02(2016)154
[4] W. Grimus, L. Lavoura, O. M. Ogreid and P. Osland, Nucl. Phys. B **801** (2008) 81 doi:10.1016/j.nuclphysb.2008.04.019.
D. Das and U. K. Dey, Phys. Rev. D **89** (2014) no.9, 095025 Erratum: [Phys. Rev. D **91** (2015) no.3, 039905] doi:10.1103/PhysRevD.91.039905, 10.1103/PhysRevD.89.095025.
J. Haller, A. Hoecker, R. Kogler, K. Mönig, T. Peiffer and J. Stelzer, Eur. Phys. J. C **78** (2018) no.8, 675 doi:10.1140/epjc/s10052-018-6131-3.
[5] F. Staub, Comput. Phys. Commun. **185** (2014) 1773 doi:10.1016/j.cpc.2014.02.018.
[6] A. Belyaev, N. D. Christensen and A. Pukhov, Comput. Phys. Commun. **184** (2013) 1729 doi:10.1016/j.cpc.2013.01.014.
[7] G. Belanger, F. Boudjema, A. Pukhov and A. Semenov, Comput. Phys. Commun. **185** (2014) 960 doi:10.1016/j.cpc.2013.10.016.
[8] P. Bechtle, O. Brein, S. Heinemeyer, O. Stål, T. Stefaniak, G. Weiglein and K. E. Williams, Eur. Phys. J. C **74** (2014) no.3, 2693 doi:10.1140/epjc/s10052-013-2693-2.

# INFLUENCE OF MOLECULAR BEAM EPITAXY GROWTH CONDITIONS ON TERAHERTZ DETECTION FOR InGaAs DIODES

Domas Jokubauskis, Renata Butkutė, Linas Minkevičius

Department of Optoelectronics, Center for Physical Sciences and Technology, Lithuania
domas.jokubauskis@ftmc.lt

InGaAs-based bow-tie diodes for terahertz (THz) range are found to be well-suited for development of compact THz imaging systems [1]. To further optimize design for sensitive and broadband THz detection, one of the major challenges remains to understand influence of growth conditions and role of defects for device operation. We present detailed study of photoreflectance and THz sensitivity of InGaAs bow-tie diodes. The diodes are fabricated from InGaAs wafers grown by molecular beam epitaxy (MBE) on semi-insulating InP substrate under different technological conditions. Photoreflectance spectra indicated presence of strong built-in electric fields reaching up to 49 kV/cm. Furthermore, varying bias current, we evaluated fabricated devices for optimal room temperature operation in THz range with respect to signal-to-noise ratio.

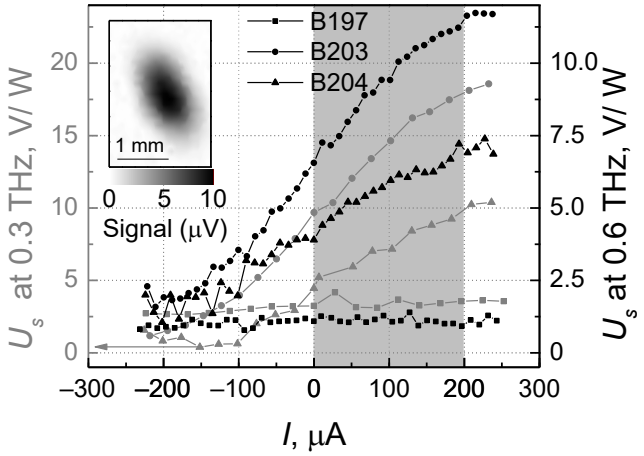


Fig. 1. Voltage sensitivity of the InGaAs diode detector with different In/Ga ratios at 0.3 THz and 0.6 THz frequency with modulation frequency of 1 kHz. Inset indicates the raster scan of the 0.6 THz beam profile at the focal plane obtained with detector B203. Shadowed area indicates optimal working regime of the detector.

Figure 1 depicts the sensitivity as a function of current for all types of the studied samples at frequencies of 0.3 THz and 0.6 THz. As it is seen, sensitivity of InGaAs bow-tie diodes fabricated from the wafers B203 and B204 increases while raising the current and reaches 17.5 V/W and 10 V/W at 0.3 THz and 12.5 V/W and 7 V/W at 0.6 THz, respectively, at the bias current of 0.2 mA. Higher voltage sensitivity of the detector B203 is caused by the larger asymmetry in the IV curves and stronger built-in electric fields in comparison to other studied samples. Raster scan of THz beam profile at 0.6 THz (inset in Figure 1) illustrates the suitability of the diode for THz imaging aims.

To conclude, the THz detectors layers grown with beam equivalent pressure In/Ga ratio equal to 2.06 are found to be well suited for fabrication of room temperature bow-tie THz detectors enabling sensitivity of 13 V/W and noise equivalent power (NEP) of 200 pW/√Hz at 0.6 THz due to strong built-in electric field effects [2].

This research was funded by Lietuvos Mokslo Taryba (LAT 04/2016)—project KITKAS.

[1] G. Valušis et al., "Compact solutions for spectroscopic solid-state-based terahertz imaging systems," in Terahertz Emitters, Receivers, and Applications VIII, 2017, p. 27.
[2] V. Palenskis et al., "InGaAs Diodes for Terahertz Sensing—Effect of Molecular Beam Epitaxy Growth Conditions," Sensors, vol. 18, no. 11, p. 3760, Nov. 2018.

# STABILISATION OF DELTA $BI_2O_3$ PHASE IN NANOCOMPOSITES DOWN TO ROOM TEMPERATURE BY TWIN–ROLLERS TECHNIQUE

Paulina Kruk–Fura, Mateusz Jaszek, Tomasz K. Pietrzak,
Marek Wasiucionek, Jerzy E. Garbarczyk

Faculty of Physics, Warsaw University of Technology, Poland
paulina.kruk-fura@fizyka.pw.edu.pl

Polycrystalline bismuth (III) oxide is very well known for its occurrence in $\alpha$, $\beta$, $\gamma$ and $\delta$ phases (Fig. 1), which is widely reported in the literature. Furthermore, $Bi_2O_3$ seems to exhibit different properties, according to its crystalline phase, which makes it an exceptionally interesting material from the perspective of science path for solid state matter, along with possible practical applications. In particular, the $\delta$phase of $Bi_2O_3$ exhibits the highest conductivity in high temperature range (1 S/cm at 750 °C) from among all known oxygene ion conductors. However, it is stable only in a narrow temperature range from 730 to 825 °C [1].

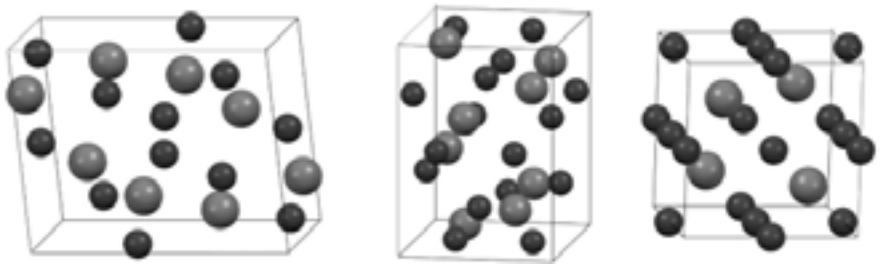

Fig. 1. Unit cells of the most important phases of bismuth (III) oxide (from left to right): ($P2_1/C$) monoclinic ($\alpha$); ($P42_{1C}$) tetragonal ($\beta$); (Pn-3m) fluorite-type fcc ($\delta$), generated by Mercury software [2] from CIFs no. 1010004, 1545547, 1010311, respectively.

Its very high ionic conductivity has motivated many researchers to look for a method to stabilise this fluorite-type structure to lower temperature. So far the successful strategies to achieve the stabilisation of the delta phase have included doping (e.g. by rare-earth elements [3]) or synthesis in form of thin layers [4]. Our approach to reach the same goal is significantly different. Previous experience with studies on $V_2O_5$ has shown that via twin–rollers technique one may obtain this material directly as a nanocomposite. Moreover, different cooling rates applied upon synthesis can significantly alter the properties of the samples [5].

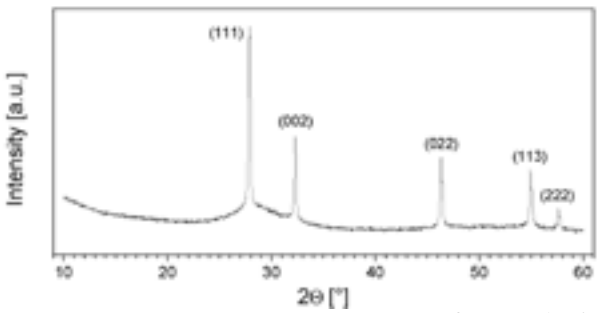


Fig. 2. Room temperature XRD pattern of as-synthesized material. Miller indexes of $\delta$–$Bi_2O_3$ phase, assigned to experimental diffraction lines, prove that the fcc phase was obtained.

Similarly to $V_2O_5$, $Bi_2O_3$ remains amoderate glass former. Therefore our idea, presented in this work, is to apply twin–rollers technique in order to obtain bismuth oxide nanocomposites. An additional investigation path was to examine, how parameters of the synthesis (e.g. cooling rate) affect thermal stability of as-received materials. X-ray diffraction measurements (XRD) have shown that via twin–rollers technique we succeeded in synthesising nanocomposites in the desired $\delta$–phase, which remained stable at room temperature (Fig. 2). Moreover, studies executed by X-ray diffraction in function of temperature (HT–XRD) revealed that this phase remains stable up to ca. 550 °C, depending on parameters of the synthesis.

This work is supported by National Science Centre, Poland, Grant Preludium–14 no. 2017/27/N/ST5/01943.

[1] H. A. Harwig, On the structure of bismuthsesquioxide: the $\alpha$, $\beta$, $\gamma$, and $\delta$ phase, Journal of Inorganic and General Chemistry, **444**, 151–166 (1978).
[2] http://www.ccdc.cam.ac.uk/mercury/
[3] M. Leszczynska, X. Liu, W. Wrobel et al., Oxide ion distribution, vacancy ordering and electrical behaviour in the $Bi_3NbO_7Bi_3YbO_6$ pseudo-binary system, Journal of Materials Chemistry **A2**, 18624–18634 (2014).
[4] H. T. Fan, S. S. Pan, X. M. Teng et al., $\delta$–$Bi_2O_3$ thin films prepared by reactive sputtering: Fabrication and characterization, Thin Solid Films **513**, 142–147 (2006).
[5] T.K. Pietrzak, M. Maciaszek, J.L. Nowiski et al., Electrical properties of $V_2O_5$ nanomaterials prepared by twin rollers technique, Solid State Ionics **225**, 658–662 (2012).

# PREPARATION AND CHARACTERIZATION OF METALORGANIC PRECURSORS FOR LASER FABRICATION OF 3D MICRO-/NANO-STRUCTURES

Greta Merkininkaitė[1,2], Viktorija Padolskytė[2,3], Darius Gailevičius[2,3],

Mangirdas Malinauskas[3], and Simas Šakirzanovas[1]

[1] Faculty of Chemistry and Geosciences, Vilnius University, Lithuania
[2] Femtika Ltd., Lithuania
[3] Laser Research Center at Vilnius University, Lithuania
greta.merkininkaite@chgf.vu.lt

Direct laser writing using multi-photon polymerization has become a powerful technique for the fabrication of fullythree-dimensional micro- and nano-structures for diverse applications in microfluidic, micro mechanic and electronic, biomedical, metamaterial as well as nano-photonic research fields [1, 2]. Such numerous applications require precursors with different chemical, physical and optical properties. Development of new chemical composition materials suitable for both laser 3D polymerization and optimized for applications remains an urgent and timely task.

The aim of this work was to synthesize a series of organic-inorganic polymer precursors [3] and investigate the prospects of 3D formation of these materials as well as to evaluate the diffusion of polymerization reactions in both absence and presence of an inhibitor in the starting mixture. The following steps have been accomplished to achieve this goal. First silicon and zirconium hybrid compounds were synthesized *via* sol-gel method varying the molar ratio of silicon (Si) and zirconium (Zr) complexes (Si:Zr, where Si=9; 8; 7; 6; 5 and Zr=1; 2; 3; 4; 5). Secondly, the influence of polymerization inhibitor concentration on structure resolution was experimentally evaluated. Differences in chemical composition of synthesized sols, gels and polymers were determined using Fourier transform infrared spectroscopy (FTIR). Measurements of absorption spectra and refractive indices were performed for determination of differences in optical properties. Scanning electron microscopy (SEM) images of fabricated 3D structures (periodic lattices and resolution bridges) revealed the suitability of precursors for laser lithography.

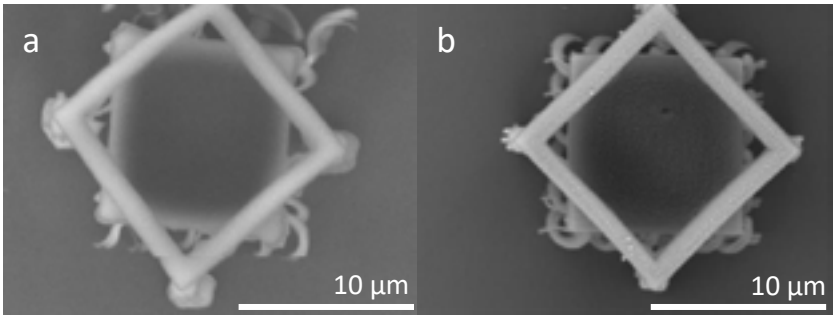


**Fig. 1** SEM micrographs of cube structure in absence (a) and presence (b) of an inhibitor in the starting mixture.

The study shows that silicon and zirconium hybrid organic-inorganic compounds synthesized by the sol-gel method are suitable for 3D laser lithography and the inhibitor has an effect on structure resolution (Fig. 1). Qualitative and quantitative analysis of the inhibitor influence on the diffusion of polymerization reactions will be presented and discussed.

1. Gailevičius, D., et al., Additive-manufacturing of 3D glass-ceramics down to nanoscale resolution. Nanoscale Horizons; DOI: 10.1039/C8NH00293B; (2019)
2. Sakellari, I., et al., Diffusion-Assisted High-Resolution Direct Femtosecond Laser Writing. ACS Nano; **6**(3), 2302-2311; (2012)
3. Ovsianikov, A., et al., Ultra-Low Shrinkage Hybrid Photosensitive Material for Two-Photon Polymerization Microfabrication. ACS Nano; **2**(11), 2257-2262; (2008)

# SYNTHESIS OF VANADIUM DOPED LITHIUM IRON SILICATE USING SOL-GEL METHOD

Jakub S. Otrębski, Przemysław P. Michalski, Tomasz K. Pietrzak, Jerzy E. Garbarczyk

Faculty of Physics, Warsaw University of Technology, Poland
jakub1@wp.eu

Notwithstanding the increasing energy efficiency of modern electronic devices, the batteries are still the relevant part and determine the usefulness of the entire device. Nowadays, the majority of used methods for cathode materials production in Li-ion batteries industry require a high temperature (usually a few hundreds of °C) synthesis process [1]. This might significantly increase the cost and complexity of the whole battery production. One of the solution for mentioned disadvantage is applying sol-gel as a low temperature synthesis method. Sol-gel method allows to execute the proper synthesis part at temperatures in the range of 60–80 °C. Moreover, the porosity as well as surface area might be strictly controlled by conducting the process at very specific conditons (e.g. pressure, temperature, concentrations) [2].

Proposed material – lithium iron silicate ($Li_2FeSiO_4$) achieves theoretical gravimetric capacity of 332 $mAhg^{-1}$, what makes it the potential candidate as a cathode material in the batteries. Nevertheless, the material suffers from low value of electronic conductivity. The solution might be well-known method of increasing the conductivity by vanadium doping [3].

Precursors – $LiCH_3COO$ (Aldrich 99.95%), $Fe(NO_3)_3$ (Aldrich 99.99%), $NH_4VO_3$ (Aldrich 99%) were dissolved in water in stoichiometric proportions, then ethanolic solution of TEOS (Aldrich 99%) was added and aqueous solution of citric acid (Aldrich 99%) was added dropwise. The solution was heated up to 80 °C and under continuous magnetic stirring was left until obtaining hydrogel (dense, high viscosity material). The hydrogel was dried in 80 °C for 48 h to remove water. In this step xerogel was received. The xerogel was grinded in mortar, a part of it was mixed with different carbon sources (sucrose, active carbon) and pelletized. The last step was calcination of the pellets at high temperature in neutral atmosphere of argon flow.

An influence of pH value in precursors solution, calcination temperature and source of added carbon on phase composition of final samples was investigated. Characterization was carried out by X-ray diffractometry (XRD), differential thermal analysis (DTA) and impedance spectroscopy (IS).

(a) Samples synthesis. Precursors solutions in the magnetic stirrer.

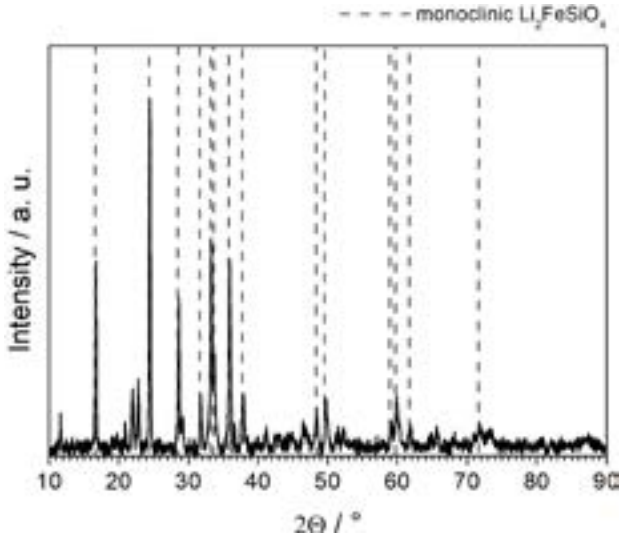


(b) X-ray diffractogram of $Li_2FeSiO_4$ sample calcinated at 825 °C. Red dashed lines indicate m-$Li_2FeSiO_4$ phase.

Samples after drying were almost fully amorphous besides small content of $LiNO_3$ phase. Determined optimal conditions were argon atmosphere and calcination temperature equal to 825 °C. Samples annealed at this temperature revealed the highest content of the expected $Li_2FeSiO_4$ phase. Calcinations at lower temperatures caused appearring of iron oxides phases in the sample, whereas higher temperatures calcinations ended up with $Fe_2SiO_4$ phase in the composition. Processes of calcination conducted in the air (non-neutral atmosphere) were conducive to $Li_2SiO_3$ phase crystallization. Furthermore, investigated were calcination in highly reducing atmosphere deriving from active carbon and sucrose. However, such atmosphere caused strong iron reduction in the material. Thermal analysis proved weight loss in a few steps, which had maximums at 215 °C, 337 °C and 584 °C. First two might be attributed to gelating agents (e. g. citric acid) decomposition, whereas the last one is connected with lithium nitrate decay.

[1] S. YANG, P. Y. ZAVALIJ, M. S. WHITTINGHAM: *Hydrothermal synthesis of lithium iron phosphate cathodes*. Electrochemistry Communications **3** (2001) 505 – 508.

[2] S. C. PILLAI, S. HEHIR: *Sol-Gel Materials for Energy, Environment and Electronic Applications*. Springer 2017.

[3] J. HONG, C. S. WANG, X.CHEN, S. UPRETI, M. S. WHITTINGHAM: *Vanadium Modified $LiFePO_4$ for Li-ion Batteries*. Electrochemical and Solid-State Letters **12** (2009) 33 – 38.

# ELECTROCHEMICALLY PULSE DEPOSITED BISMUTH - BISMUTH TELLURIDE SUPERLATTICES OF $(Bi_2)_m(Bi_2Te_3)_n$ SERIES

Aliaksei Bakavets[1,2,*], Yauhen Aniskevich[1,2], Genady Ragoisha[1], Henrikas Cesiulis[3], Natalia Tsyntsaru[3], Eugene Streltsov[2]

[1]Research Institute for Physical Chemical Problems, Belarusian State University, Minsk, 220006, Belarus
[2]Chemistry Department, Belarusian State University, Minsk, 220030, Belarus
[3]Department of Physical Chemistry, Faculty of Chemistry, Vilnius University, Vilnius, Lithuania
*e-mail: alexeibokovets@gmail.com

Bismuth telluride is one of the best thermoelectric materials performing at room temperature. Layered crystal structure of bismuth telluride provides possibility of Bi layers insertion and results in formation of $(Bi_2)_m(Bi_2Te_3)_n$ superlattices with low lattice thermal conductivity.

Solid state synthesis of $(Bi_2)_m(Bi_2Te_3)_n$ was reported in [1,2]. Here we present our results on the electrodeposition of the similar superlattices. Cyclic voltammetry profile of $(Bi_2)_m(Bi_2Te_3)_n$ electrodeposited onto stainless steel in acidic $Bi^{3+}$ and $TeO_2$ containing aqueous solution shows two anodic peaks; the first one was attributed to selective $(Bi_2)_m$ oxidation (Figure 1) and the other one to oxidation of the remaining $Bi_2Te_3$. We have found that electrochemical pulse deposition onto stainless steel from acidic $Bi^{3+}$ and $TeO_2$ solutions of different $Bi^{3+}/TeO_2$ ratio below $(Bi_2)_m$ anodic oxidation potential can give layered compounds. The bismuth mole fraction in the deposits varies from 0.41 to 0.7; this is in agreement with the phase diagram for Bi/Te binary system that shows the possibility of binary compounds formation in the range from $Bi_2Te_3$ to $Bi_7Te_3$. The layered structure of the deposits was proved using XRD analysis, XPS analysis, and TEM. Rietveld refinement of XRD profiles has shown that all the deposits corresponded to the subcell of the same symmetry as $Bi_2Te_3$ (*R-3m*) and lattice parameters $a \approx 4.0$ Å, and $c \approx 6.0$ Å. Refined *a* and *c* show clear dependences on bismuth mole fraction (Figure 2) in the films similar to those reported for superlattices obtained by solid state synthesis [1]. Moreover, based on our data, bismuth bilayers can be selectively removed by applying the electrode potential in the range between the $(Bi_2)_m$ anodic oxidation peak and the anodic peak attributed to $Bi_2Te_3$ oxidation. The anodic removal of bismuth bilayers was accompanied by lattice parameters change to those characteristic of bismuth telluride. We observed this electrochemically stimulated structural change only on samples with initially high bismuth content.

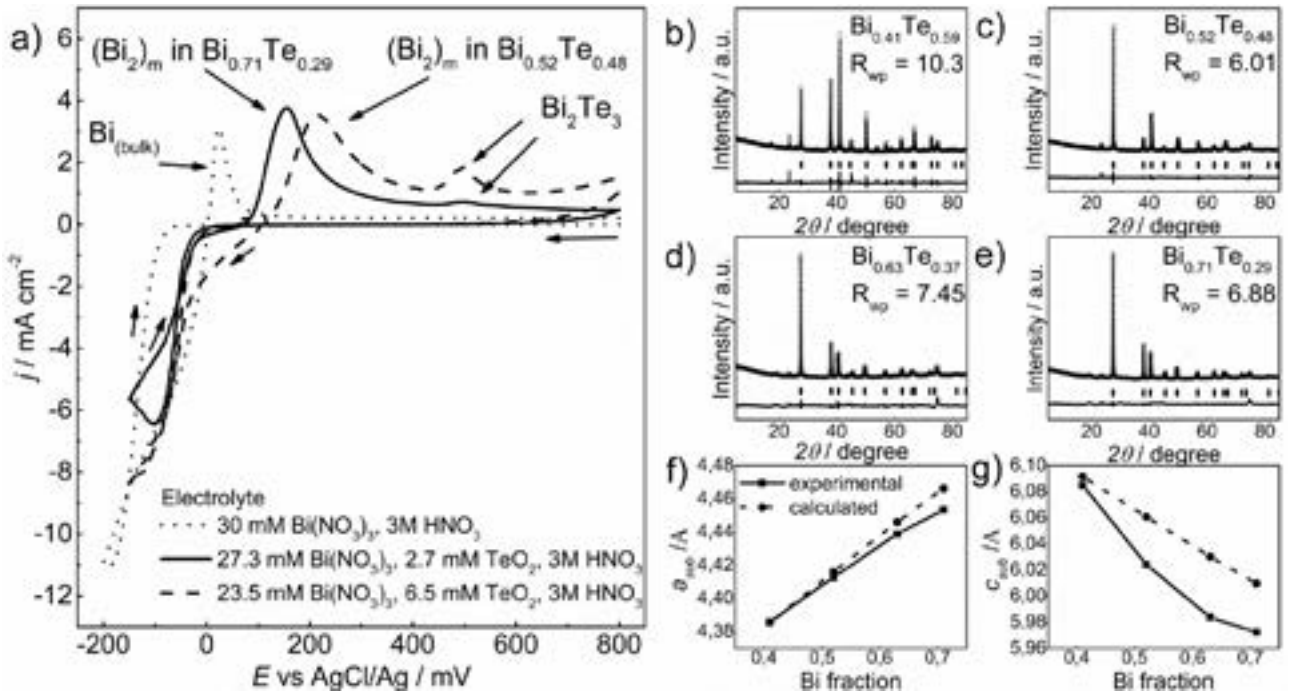


Fig. 1. (a) Anodic oxidation potentials of Bi in superlattices vs. bulk Bi and bismuth telluride, (b-e) XRD experimental data and refinement parameters for various superlattices in $(Bi_2)_m(Bi_2Te_3)n$ series, (f-g) dependence of the refined lattice parameters a and c on the bismuth mole fraction in the synthesized films.

Acknowledgment: This research has received funding from Horizon 2020 research and innovation programme under MSCA-RISE-2017 grant agreement No. 778357.

[1]. J.W.G. Bos, F.P. Faucheux et al., Phase stability,structures and properties of the $(Bi_2)_m(Bi_2Te_3)_n$ natural superlattices, Solid State Chem. 193 13-18 (2012).
[2]. J.W.G. Bos, H.W. Zandbergen er al., Structures and thermoelectric properties of the infinitely adaptive series $(Bi_2)_m(Bi_2Te_3)_n$, Phys. Rev. B 75, 195203 (2007).

# MAGNETIC FERRITE NANOPARTICLES WITH INCREASED MAGNETIZATION AND CRYSTALLINITY BY SPRAY-DRYING WITH NaCl AND SUBSEQUENT THERMOLYSIS

Elena Petrova[1], Yana Shavshukova[1], Dzimitry Ivashenka[1], Vladimir Pankov[1]

[1] Department of Physical Chemistry, Belarusian State University, Belarus
petrovaeg@bsu.by

Nanosized magnetic particles based on iron oxides are of great importance for a wide area of applications: sensors, catalysts, sorbents, magnetic dug delivery, magnetic resonancy imaging, etc. Lots of these applications require non-agglomerated particles with a large surface area and average diameter below 50 nm. However, such particles exhibit quite low specific magnetization as compared to bulk materials due to the surface spin disorder of surface atoms [1]. Many conventional methods of magnetic nanoparticle synthesis, such as coprecipitation, spray pyrolysis and reverse micelle synthesis, require additional thermal treatment to increase crystallinity and specific magnetization of the particles [2]. The main problem of this approach is a significant increase of particle size as a result of annealing.

In this work, zinc-substituted cobalt and magnesium ferrite nanoparticles were prepared by coprecipitation from water solution of corresponding nitrates. The resulting suspensions were mixed with NaCl and then spray-dried at 200 °C using Labultima–222 ADVANCED Laboratory Spray Dryer. The powders obtained were then annealed at 300-900 °C to increase specific magnetization of nanoferrites. The isolating layer of NaCl formed between the particles during spray-drying prevented them form aggregation and sintering during annealing. After the annealing, NaCl matrix was removed by washing with deionised water. The difference between this approach and spray pyrolysis in presence of NaCl is lower spraying temperature (200 °C for spray-drying vs. 500-700 °C for pyrolysis), which makes it easier and more cost-efficient [3].

Structural, morphological and magnetic properties of the resulting nanoparticles were investigated by XRD, SEM, TEM, FT-IR spectroscopy and SQUID magnetometry. After spray-drying, ferrite nanoparticles and NaCl form hollow spheres with an average diameter of 1-5 μm, while the size of single nanoparticles is ~5-10 nm. Average crystallite size calculated from XRD data, as well as particle diameter measured from SEM, does not increase significantly up to 700 °C and does not exceed 10 nm. Further raise of annealing temperature to 900 °C leads to intense recrystallization and therefore increase of particle size to 40-60 nm (major fraction). Specific magnetization of the ferrites was found to increase with the increase of annealing temperature – from 31.5 to 91.3 emu/g for $Co_{0,65}Zn_{0,35}Fe_2O_4$ and from 4.69 to 22.31 for $Mg_{0,5}Zn_{0,5}Fe_2O_4$ annealed at 300 and 900 °C, respectively. This might be caused by cation redistribution between spinel sublattices of ferrites, which is proved by changes in lattice parameter *a* (Table 1). Another reason is the structure ordering, decrease of defect concentration and increase of crystallinity of nanoparticles with the increase of temperature due to recrystallization.



Table 1. Structural and magnetic properties of the ferrite nanoparticles annealed at different temperatures: lattice parameter a, average crystallite size $d_{XRD}$, specific magnetization M (measured at 0.86 T) and crystallinity degree

| T, °C | $Co_{0,65}Zn_{0,35}Fe_2O_4$ | | | | $Mg_{0,5}Zn_{0,5}Fe_2O_4$ | | | |
|---|---|---|---|---|---|---|---|---|
| | *a*, Å | $d_{XRD}$, nm | M, emu/g | Crystallinity degree, % | *a*, Å | $d_{XRD}$, nm | M, emu/g | Crystallinity degree, % |
| 300 | 8.344 | 5.54 | 31.5 | 87.20 | 8.429 | 3.73 | 4.69 | 66.17 |
| 500 | 8.355 | 6.74 | 44.2 | 90.39 | 8.408 | 4.46 | 17.76 | 82.05 |
| 700 | 8.406 | 8.01 | 58.9 | 91.73 | 8.437 | 10.60 | - | 72.92 |
| 900 | 8.406 | 30.91 | 91.3 | 98,76 | 8.420 | 34.23 | 22.31 | 89.62 |

All the particles exhibit superparamagnetic behavior with no coercivity at room temperature, and their average size does not exceed 100 nm even after annealing at 900 °C. This proves the method described to be effective for producing non-agglomerated nanosized ferrites with increased magnetization and crystallinity.

[1] H.M. El-Sayed, I.A. Ali, A. Azzam, A.A. Sattar. Influence of the magnetic dead layer thickness of Mg-Zn ferrites nanoparticle on their magnetic properties. Journal of Magnetism and Magnetic Materials. Vol. 424, 226-232 (2017).

[2] K. Nadeem, S. Rahman, M. Mumtaz. Effect of annealing on properties of Mg doped Zn-ferrite nanoparticles. Progress in Natural Science: Materials International. Vol. 25, 111-116 (2015)

[3] E. Petrova, M. Roschchina, V. Pankov. Non-agglomerated $MgFe_2O_4$ nanoparticles with increased saturation magnetization value via annealing in NaCl matrix. 60th International Conference for Students of Physics and Natural sciences Open Readings 2017. ISSN 2029-4425. Vilnius, Lithuania. P.297 (2017)

# APPLICABILITY OF WAVELET TRANSFORM FOR THE DEFECT ESTIMATIONS IN GLASS FIBER-BASED COMPOSITE STRUCTURES BY ULTRASONIC NON-DESTRUCTIVE TESTING

Kumar Anubhav Tiwari[1], Olgirdas Tumsys[2], Renaldas Raisutis[3]

[1,2,3] Ultrasound Research Institute, Kaunas University of Technology, Lithuania
k.tiwari@ktu.lt

Glass fiber-based composite materials are widely used for the construction of various structures of industrial and household applications. The most common applications are wind turbine blade (WTB) and aircraft wings which operates under cyclic loads and fiber-reinforced plastic pipes [1, 2]. Ultrasonic non-destructive testing (NDT) due to its deep penetration feature, high sensitivity, availability of wide range of transducers producing different types of waves (*e.g.* longitudinal, shear, Lamb waves etc.) and ability to extract the defect features from only one side access, is widely used for the detection and estimation of defects, flaws and delamination in the composite structures. However, the interaction of ultrasound with multi-layered composite materials causes complex mechanism such as scattering, attenuation, reflection, refraction of propagating waves and mode conversion etc. which in turn reducing the signal to noise ratio (SNR) by producing nonstationary correlated noise. Therefore, the signal processing of the received ultrasonic signals is necessary for the identification and estimation of size and location of defects.

The objective of this work is to develop the signal processing approach based on discrete wavelet transform (DWT) for the estimation of size and location of the defects located on composite structures by denoising and processing the received ultrasonic signals after an experimental investigation. The DWT is one of the most promising signal processing techniques for noise removal from the non-stationary signals [3, 4]. The ultrasonic signals are decomposed into a sum of elementary signals called as wavelets. By manipulating the wavelet coefficients with the utilization of proper thresholding techniques enable the reduction of noise and distortions from the signal.

Two different objects: a segment of WTB containing two artificially constructed disbond-type defects (15 mm and 25 mm diameters) by milling process on its trailing edge and a multi-layered pipe containing three side-drilled holes (6.3, 5.1 and 4.4 mm lengths respectively each having diameter of 0.7 mm) are considered for the investigation. Both objects contained the glass fiber reinforced layer in its structure. Apart from the attenuation, dispersion of propagating waves, the biggest problem in order to locate and estimate the size of defects in both objects (WTB and multi-layered pipe) under investigation is the nonstationary structure noise caused by scattering of ultrasonic waves by the fibers. In both cases, the DWT based algorithm is developed and applied on the received ultrasonic signals to extract the defect features with significant accuracy.

In the case of WTB, a pair of contact-type piezoceramic transducers (center frequency of 190 kHz and -6 dB bandwidth up to 300 kHz) fixed on moving panel with 50 mm separation, operating in a pitch-catch mode (one transducer as a transmitter and other as a receiver), generating/receiving ultrasonic guided Lamb waves are used to scan up to 500 mm over the defect-free and defective regions with a scanning step of 1mm. In order to proceed the contact-type ultrasonic testing, a conical-shaped protection layer of 2 mm diameter is attached to the bottom of each transducer. The transmitter was excited by 150 kHz, 3-period rectangular burst signal and receiver recorded the signals with a sampling frequency of 100 MHz. The low-frequency ultrasonic system "*Ultralab*" developed by Ultrasound Research Institute of the Kaunas University of Technology was used for the experimental analysis and data acquisition. The disbond-type defects of 15 mm and 25 mm diameters located on WTB were accurately detected after applying DWT on experimental B-scan following with amplitude detection technique which was not possible without processing.

In the case of plastic pipes, a pulse-echo immersion technique is used for the detection of defects. The ultrasonic longitudinal wave generated by the piezoelectric transducer (the aperture 19 mm and the resonant frequency of 5 MHz) propagates through a three-layer pipe structure. The transducer was excited by 140 V pulse of 80 ns duration and A-scans and B-scans are recorded by scanning the transducer along the length of pipe. The reflection of waves occurs by layer boundaries, discontinuities, front and back surfaces of layers. Moreover, the wave shape and spectral components were significantly altered by the inhomogeneous middle layer (Glass fiber-reinforced layer). The experiment was performed by using the imaging system "*Izograf*" developed by Ultrasound Research Institute of the Kaunas University of Technology. In the case of multi-layered fiber-reinforced pipe, the measurement error did not exceed ±1 mm.

Hence, the signal processing technique based on DWT is useful for the identification of defects in all composite structures producing complexity in characteristics of received ultrasonic waves due to multi-layered and fiber reinforced structure.

[1] K. A. Tiwari, R. Raisutis, Identification and characterization of defects in glass fiber reinforced plastic by refining the guided Lamb waves, Materials 11, 1-23 (2018).

[2] R. Kazys, O. Tumsys, D. Pagodinas, A new ultrasonic technique for detection and location of defects in three-layer plastic pipes with a reinforced layer, Ultrasgarsas 63, 19-27 (2008).

[3] M. A. Rodriguez et. al., Ultrasonic flaw detection in NDE of highly scattering materials using wavelet transform and Wigner-ville transform processing, Ultrasonics 42, 847-851 (2004)

[4] K. A. Tiwari, R. Raisutis, Post-processing of ultrasonic signals for the analysis of defects in wind turbine blade using guided waves, Journal of strain analysis for engineering design, 1-10 (2018).

# ESTIMATION OF ACOUSTIC IMPEDANCE FOR MEDICAL ULTRASOUND IMAGES

Paulius Čepulionis[1], Renaldas Raišutis[1]

[1] Prof. Kazimieras Baršauskas Ultrasound Research Institute, Kaunas University of Technology
paulius.cepulionis@ktu.lt

Study proposes a new method for tow-dimensional acoustic impedance imaging for medical ultrasound B-scan images that can be performed without slicing the specimen or material as a reference. Over the last decade, there has been significant improvement in ultrasonic systems. Acoustic impedance calculation was one of the significant discoveries and uses, but no one was able to calculate it using a traditional single-element focused medical ultrasound devices. [1]

In most of optical observation of biological tissue, the specimen is sliced into several micrometers in thickness, and fixed on a glass substrate. On the other hand, acoustic impedance imaging can be performed without non-destructive process. The proposed method is the conversion of a B-mode image into an acoustic impedance image. The time domain reflectometry theory and transmission line model were used as reference in the calculation. Significant scatter, refraction, and attenuation were assumed not to take place during the propagation of an ultrasonic wave. Hence, they were ignored in calculations.

Two Aquaflex Ultrasound Gel Pad has been used with different characteristics were employed as the specimens to be observed. All studies have been conducted at the Department of Skin and Venereal Diseases of the Lithuanian University of Health Sciences by using Commercial DUB-USB (Taberna pro medicum, Lueneburg, Germany) single-element focused ultrasonic transducer (fundamental frequency, 22 MHz; bandwidth, 12–28 MHz, focused, focal distance – 11 mm). The radiofrequency data were analyzed in the time-frequency domain to make boundaries more noticeable. The study had been approved by regional ethics committee (Nr. P3-BE-2-25/2009).

In order to calibrate the accuracy of acoustic impedance, both of phantoms with different characteristics were prepared. Their acoustic impedance was measured using density and acoustic resistance. The intensity of the reflected signal was lower with higher acoustic impedance, as the acoustic impedance of the phantoms was lower than that of the substrate. The lower signal intensity was subsequently converted into higher acoustic impedance. An example of real phantoms can be given in the figures: the first example (Fig. 1) shows an example of a transition from a lower acoustic impedance medium to a high, and a second example (Fig. 2) shows a reverse example – from a higher acoustic impedance medium goes to lower acoustic impedance medium.

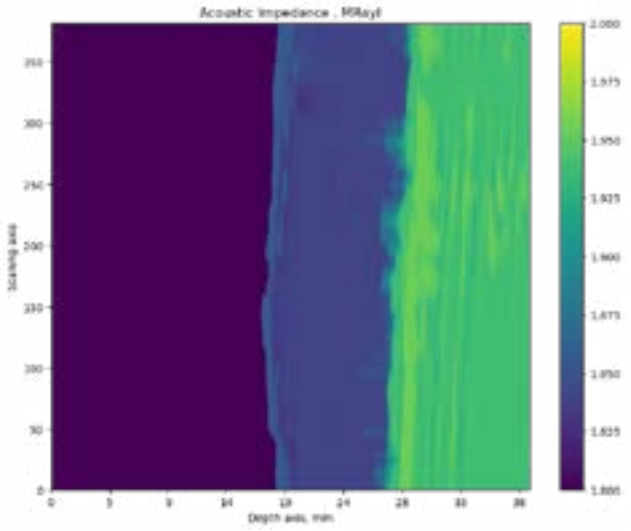


Fig. 1. Phantom from two different Aquaflex Gel Pads

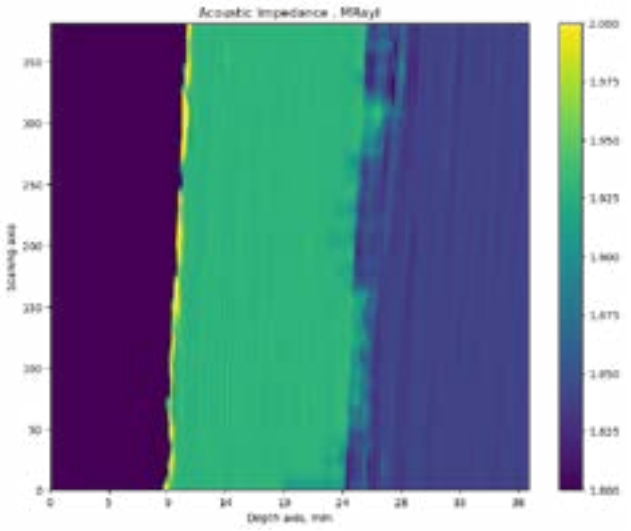


Fig. 2. Phantom from two different Aquaflex Gel Pads reversed

The tow-dimensional acoustic impedance imaging for medical ultrasound B-scan images technique is believed to be a powerful tool for biological tissue characterization, as neither staining nor slicing is required. Some good results are obtained and hence method showed their possible applications in the study of acoustic properties of B-mode images.

[1] A Nakano, T. Uemura, N. Hozum et al., Non-contact Observation of Cultured Cells by Acoustic Impedance Microscope, 2008 IEEE Ultrasonics Symposium (2008).

# ULTRAFAST PROCESSES IN HIGHLY EFFICIENT ORGANIC SOLAR CELLS BASED ON NOVEL NONFULLERENE ACCEPTORS

Rokas Jasiūnas[1], Huotian Zhang[2], Feng Gao[2], Vidmantas Gulbinas[1]

[1] Center for Physical Sciences and Technology, Saulėtekio av. 3, LT-10257, Vilnius, Lithuania
[2] Biomolecular and Organic Electronics, Department of Physics, Chemistry and Biology (IFM), Linköping University, 58183 Linköping, Sweden
rokas.jasiunas@ftmc.lt

The ever growing demand for carbon-neutral energy source has led photovoltaic (PV) technologies to become fastest-grow ing form of renewable energy. Among many different PV technologies, organic photovoltaic (OPV), being based on earth-abundant materials and showing short energy payback times, has been exclusively attractive. Donor:acceptor bulk-heterojunction structure has enabled efficient photon – electron conversion mechanism and is by far most widespread structure for OPV. For almost two decades highest power conversion efficiencies (PCE) were obtain with fullerene type acceptors. Fullerene owning to its ball-like fully conjugated structure, which enables high electron accepting and isotropic electron transport capabilities was believed to be crucial part of efficient OPV technology. Other acceptor molecules, generally named nonfullerene (NF) molecules, usually shows low PCE's, mostly due to difficult morphological control. However, NF acceptor resurgence was witnessed in the last three years, with power conversion efficiency sky rocketing to record braking >13.5% values, exceeding those reached by fullerene based systems.

Today there are >100 different acceptor molecules displaying high efficiencies. Most of them are so called A-D-A type molecules, distinct by its two symmetrical electron accepting complexes connected via conjugated electron donating backbone, which itself is surrounded by non-conjugated tails. Most striking feature of such molecules is efficient exciton splitting at low, or even negligible, driving forces made by HOMO/LUMO level mismatch at D/A interface. It enables energy loss minimization and results in high $V_{OC}$ values. Nevertheless, fundamental question on how exciton split into charge carrier in these NF OSC at low driving forces remains open.

To address this problem we have performed conventional transient absorption measurements with 4 different donor:acceptor material combinations (PBDB-T:Y1; PBDB-T-2Cl:ITIC; PDCBT-2F:ITIC; PBDB-T: PCBM) each with few different D/A mass ratios. Ten samples in total were investigated with PCE ranging from 3.2% to 11.1%. Excitation wavelength was chosen to excite either donor or acceptor specifically, thus electron transfer both from donor to acceptor and from acceptor to donor could be observed.

As expected, after exciting acceptor extremely fast (<10ps) hole transfer from acceptors HOMO to donor HOMO orbital was observed, for all the samples with A-D-A type acceptor, which is one of already known distinct feature of NF molecules. However, less expected result manifested after donor's excitation took place. In this case, ground state bleaching of an acceptor was extremely low, especially in case of best performing PBDB-T:Y1 sample. This could mean that either excited state of the donor does not produce a free charge carrier pair (which could not be compatible with high PCE of these samples), or that acceptor's absorption spectra does not change after receiving electron. We hypothesize that electron received in delocalized HOMO orbital might swiftly localize at the electron accepting part of A-D-A complexes, whereas absorption spectra could be mostly determined by the middle part. This would explain no absorption bleaching after receiving electron, and more important, this two-level system, with the localized electron decreasing HOMO level, might also explain high electron transfer efficiency at a negligible HOMO level mismatch.

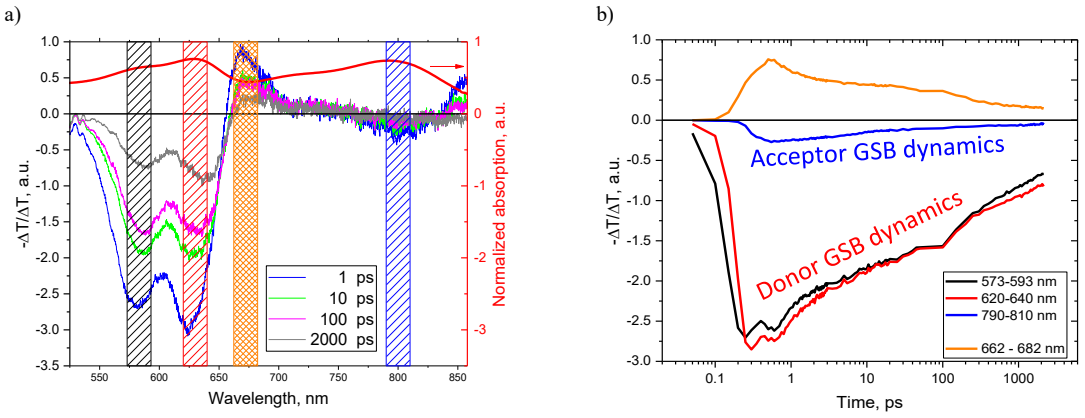


Fig 1. Transient absorption spectra (a) and dynamics (b) recorded after 515nm pump excitation for PBDB-T:Y1 sample.

# RESEARCH OF KUKA YOUBOT DYNAMICS

Tadas Lenkutis[1], Andrius Dzedziskis[1], Oleksii Balitskyi[2] , Liudas Petrauskas[1], Rimgaudas Urbonas[1], Vytautas Bučinskas[1], Donatas Valiulis[1], Inga Morkvėnaitė-Vilkončienė[1,2]

[1] Department of Mechatronics, robotikcs and digital manufaturing, University of Vilnius Gediminas technical university
[2]Department of Electrochemical Materials Science, State Research Institute Centre for Physical Sciences and Technology, Sauletekio g. 3, Vilnius, Lithuania
tadas.lenkutis@vgtu.lt (corresponding author)

Robots are used in a variety of processes, including manufacturing, entertainment, services, and scientific research. To maintain a technical edge and thereby remain competitive, more and more businesses are applying advanced technical solutions in their operational processes. Such a wide application encourages the development of universal robotic systems and research into their capabilities and performance characteristics. Kuka-Youbot is one of the best known and widely distributed examples of universal robotic systems [1]. This modular robotic system was developed by KUKA as open source project for education and research. This system consists of two main modules: i) a robotic arm with 5 degrees of freedom, and ii) a omni-directional mobile platform. It can be assembled in various configurations, such as a stationary robotic arm, a mobile platform, a robotic arm mounted on a mobile platform and two robotic arms mounted on one mobile platform. Due to its design features and configuration possibilities, it is often used by researchers as a tool or as an object [2]. Using a robot for a specific task is dependent on its positioning accuracy (positioning error between stated and real position of arm end effector) and repeatability (positioning error between real positions of arm end effector performing repeating movements) and other parameters, which are considered to be a unique characteristics of the particular machine [3]. Modern industrial robots demonstrate high-level accuracy, yet they must be closely monitored and maintained to ensure that they continue to meet the conditions for which they have been programmed and in which they operate [4].

In our research, KUKA YouBot vibrations were measured and dynamics of this robot was evaluated. Vibrations of gripper were measured in tree perpendicular directions with accelerometers “Ini 603C01”. Experiments were performed in two different positions of robot arm. Experimental setup is shown in figure 1.

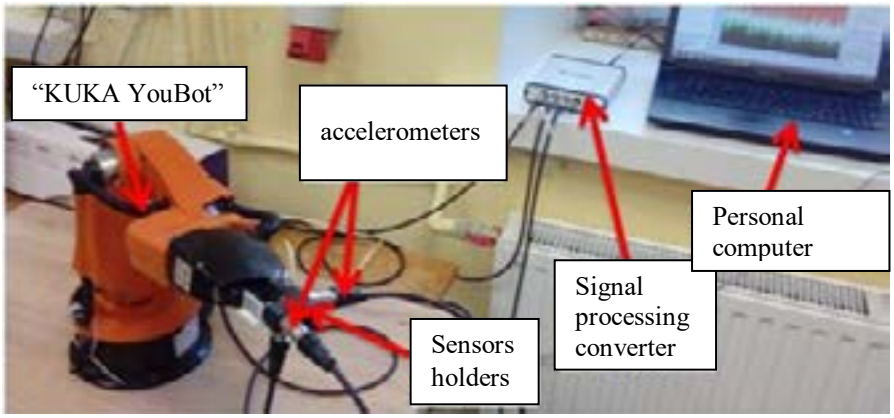


Fig. 1. Experimental setup

KUKA YouBot vibrations were measured with accelerometers “Ini 603C01” and signal was transferred to personal computer through signal processing converter “USB-4432” produced by “National Instruments” company. Later data was processed with “Origin 9.0” software package.

[1] V. Abry, Kuka Youbot: the Open Source arm, 2010.
[2] G. De Maria, P. Falco, C. Natale, S. Pirozzi, Integrated force/tactile sensing: The enabling technology for slipping detection and avoidance, Robotics and Automation (ICRA), 2015 IEEE International Conference on, IEEE2015, pp. 3883-9.
[3] Bhangale, P. P., V. P. Agrawal, and S. K. Saha. "Attribute based specification, comparison and selection of a robot." Mechanism and Machine Theory 39.12 (2004): 1345-1366.
[4] Y. Jin, I.M. Chen, G. Yang, Kinematic design of a family of 6-DOF partially decoupled parallel manipulators, Mechanism and Machine Theory, 44(2009) 912-22.

# PICOLITER SCALE SOLUTION NUCLEAR MAGNETIC RESONANCE SPECTROSCOPY USING NITROGEN-VACANCY CENTRES IN A DIAMOND CHIP

Janis Smits[1,2], Joshua Damron[1], Pauli Kehayias[1,3],Andrew McDowell[4], Nazanin Mosavian[1], Ilja Fescenko[1], Nathaniel Ristoff[1],Abdelghani Laraoui[1],Andrey Jarmola[5,6], Victor Acosta[1]

[1]Center for High Technology Materials and Department of Physics and Astronomy, University of New Mexico, Albuquerque, NM, 87106, USA
[2]Laser Centre of the University of Latvia, Riga, LV-1586, Latvia
[3]Sandia National Laboratories, Albuquerque, NM, 87123, USA
[4]NuevoMR LLC, Albuquerque, NM, 87106, USA
[5]Department of Physics, University of California, Berkeley, CA, 94720, USA
[6]ODMR Technologies Inc., El Cerrito, CA, 94530, USA
janis.smits@lu.lv

Nuclear magnetic resonance spectroscopy is a powerful way of probing chemical composition and structure of matter. Typically implementations are based on inductive acquisition which scales poorly with small sample volumes (∼nL). Quantum sensors based on nitrogen-vacancy (NV) centres in diamond are a promising alternative owing to their non-inductive detection method.

Most implementations up to now have relied on the stochastic polarization naturally emerging at small sensing volumes ($\sim$ 1 pL) to achieve reasonable sensitivity, however this puts a lower bound on the achievable spectral resolution due to spin diffusion of about $\sim$ 100 Hz [2]. Glenn et. al. [3] addressed the resolution issue by substantially increasing the effective sensing volume and detecting the thermal equilibrium magnetization. This resulted in an order of magnitude improvement in resolution ($\sim 9 \pm 1$ Hz) and a molar sensitivity of $\sim$ 370 M (defined as the minimum proton spin concentration necessary to obtain a signal-to-noise ratio of 3:1 in 1 second of averaging time).

We report [1] a further order of magnitude improvement in resolution and sensitivity, realizing a spectral resolution of $0.65 \pm 0.05$ Hz and a molar sensitivity of $\sim$ 27 M, by spatially separating the pre-polarization and detection phases of the measurement. This is achieved by embedding a $35 \times 1000 \times 1000$ µm thick diamond membrane into a microfluidic chip (see Figure 1(a)) and employing precise spatial and temporal magnetic field compensation. We use the developed

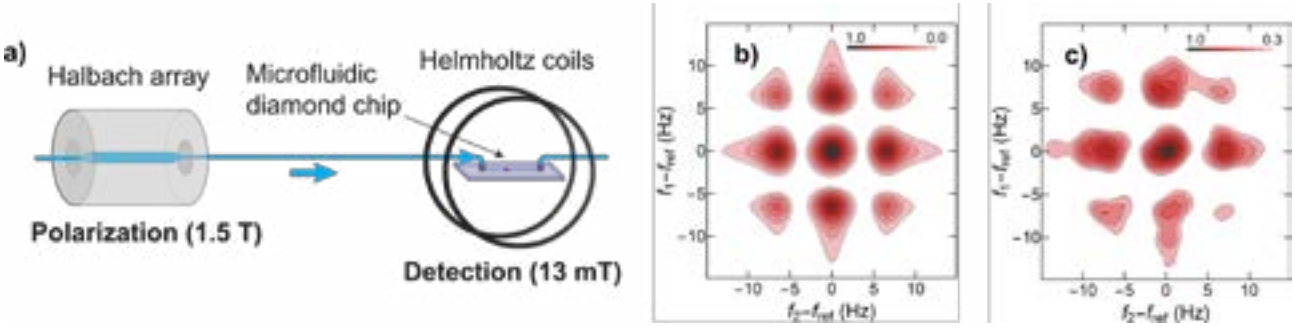


Fig. 1. a) A schematic of the measurement process. The analyte spins are polarized in the Halbach array and then quickly shuttled to the detection region. b) Simulated 2D NMR spectra of 1,4-difluorobenzene developed using the simulation package SPINACH [4]. c) Measured NV NMR spectra of 1,4-difluorobenzene.

platform to measure the first (to the best of our knowledge) experimental 2D NMR spectra obtained using NVs (see Figure 1 (b,c)).

The results represent a significant step towards applications such as mass-limited spectroscopy and single-cell biology. A remaining challenge is the limited sensitivity of our technique which could be further improved using external polarizing agents [5] or polarization transfer from NVs themselves.

[1] Smits, J., Damron, J., Kehayias, P., McDowell, A.F., Mosavian, N., Fescenko, I., Ristoff, N., Laraoui, A., Jarmola, A. and Acosta, V.M., 2019. Two-dimensional nuclear magnetic resonance spectroscopy with a microfluidic diamond quantum sensor. arXiv:1901.02952 (2019).
[2] Aslam, Nabeel, Matthias Pfender, Philipp Neumann, Rolf Reuter, Andrea Zappe, Felipe Fvaro de Oliveira, Andrej Denisenko et al. "Nanoscale nuclear magnetic resonance with chemical resolution." *Science* 357(6346), 67-71, (2017).
[3] Glenn, David R., Dominik B. Bucher, Junghyun Lee, Mikhail D. Lukin, Hongkun Park, and Ronald L. Walsworth. "High-resolution magnetic resonance spectroscopy using a solid-state spin sensor." *Nature* 555(7696), 351, (2018).
[4] Hogben, H. J., M. Krzystyniak, G. T. P. Charnock, P. J. Hore, and Ilya Kuprov. "Spinach - a software library for simulation of spin dynamics in large spin systems." *Journal of Magnetic Resonance* 208(2), 179-194, (2011).
[5] Bucher, Dominik B., David R. Glenn, Hongkun Park, Mikhail D. Lukin, and Ronald L. Walsworth. "Hyperpolarization-enhanced NMR spectroscopy with femtomole sensitivity using quantum defects in diamond." arXiv:1810.02408 (2018).

# CHARACTERIZATION OF DYES DURING COATING PROCESS OF ANODIZED ALUMINA USING RAMAN SPECTROSCOPY

Tadas Matijošius, Svajus Asadauskas, Gedvidas Bikulčius, Ilja Ignatjev

Institute of Chemistry, Center for Physical Sciences and Technology (FTMC), Vilnius, Lithuania
tadas.matijosius@ftmc.lt

Alumina ($Al_2O_3$) coatings are often produced by electrochemical oxidation (anodization) to obtain good mechanical properties, improved surface hardness, paintability, corrosion resistance and other desirable characteristics for robotics, aerospace, medicine and other high-tech areas. Porous $Al_2O_3$ coatings up to 100 μm in thickness, which can be obtained by anodization, are highly beneficial for industrial purposes (i.e. painting), because anodic coating easily adsorbs dyes due to capillary action [1]. In this study, a non-destructive analysis method, based on Raman spectroscopy, was developed to monitor penetration rates of organic dyes into fully anodized Al foil.

Al foil of 99.95% purity (0.03% Fe, 0.02% Si) with a sheet thickness of 50 μm was anodized in $H_2SO_4$ / oxalic acid electrolyte at 15 °C and 200 A/m² anodic current density according to previous procedure [2]. The process was stopped when anodizing current dropped to 0A in order to retain ~20 nm barrier layer, which assured foil integrity. Two types of commercially available chromium-complexed anionic azo dyes Sanodal Deep Black MLW™ and Sanodure Green LWN™ (Clariant, Switzerland) referred to as the "black dye" and "green dye" respectively, were chosen for the detection of penetration rates throughout fully anodized Al foil. A droplet of 5 μL with a dye concentration of 2 g/L in water was deposited onto the anodized foil for Raman spectroscopy analysis.

Echelle type spectrometer RamanFlex 400 (PerkinElmer, Inc.) used a diode laser of 785 nm beam as an excitation source. A fiber optic cable with working distance of 7 mm and a thermoelectrically cooled CCD detector were used for spectra collection at room temperature. The beam was focused into a ~200 μm diameter spot on surface of Al foil with laser power of 30 mW. Before dye deposition the beam was advanced into the inside of anodized Al pores from the bottom until the intensity of background photoluminescence (PL) achieved the maximum value. Periodically, Raman spectra were collected within 30 min after the dye deposition. Each spectrum accumulated 3 scans with an integration time of 10 seconds, which were divided by the total accumulation time followed by subtraction of background. The polystyrene standard (ASTM E1840) spectrum was used for calibration. Spectral analysis was obtained with Grams/AI 8 software (Galactic Industries Co, USA).

PL phenomena that have negative effect for Raman scattering was negligible for fully anodized Al foil. Therefore, Raman spectroscopy was used to determine the penetration rate of commercially available anionic azo dyes throughout fully anodized Al foil. Most intensive vibrational modes of 1285 $cm^{-1}$ for black dye and 1264 $cm^{-1}$ for green dye were assigned to endocyclic CN and exocyclic CN functional groups respectively, Fig. 1.

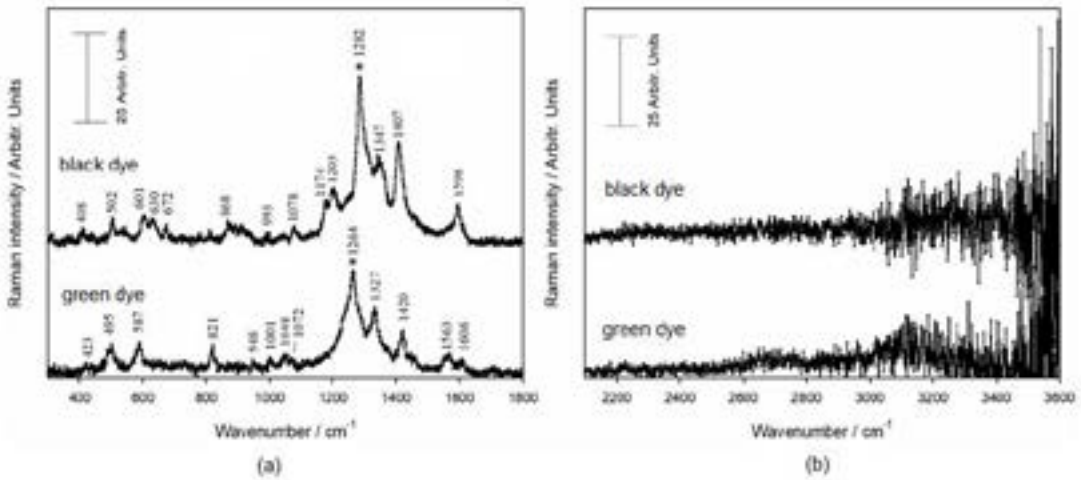


Fig. 1. Near-field (a) and far-field (b) Raman spectra of both dyes after 30 min of drop deposition on anodized Al foil (upper curve – black dye, lower curve – green dye)

It was observed that after 30 minutes the most intensive vibrational modes of each dye showed a small but distinct shift to lower frequencies. According to higher frequency shift of C-N vibrational mode (1285 $cm^{-1}$ to 1282 $cm^{-1}$ vs 1265 $cm^{-1}$ to 1263.6 $cm^{-1}$) the interaction of the black dye with the anodized Al foil was much stronger than that of the green dye.

Raman spectroscopy successfully monitored the penetration rate and the behavior of azo dyes in the anodized coating. This method could be applied to characterize newly developed organic dyes for Al coloring.

[1] R. O. Al-Kaysi, T. H. Ghaddar, G. Guirado, Fabrication of One-Dimensional Organic Nanostructures Using Anodic Aluminum Oxide Templates, Journal of Nanomaterials **7**, 1-14 (2009).
[2] T. Matijošius, A. Ručinskienė, A. Selskis, G. Stalnionis, K. Leinartas, S. J. Asadauskas, Friction reduction by nanothin titanium layers on anodized alumina, Surface and Coatings Technology **307**, 610-621 (2016).

# DEVELOPMENT OF MODELING AND MEASUREMENT TECHNIQUES FOR EUROPEAN SPALLATION SOURCE SPECIFIC RADIONUCLIDES

Vytenis Barkauskas[1], Guillaume Pedehontaa-Hiaa[1], Kristina Stenström[1]

[1] Division of Nuclear Physics, Lund University, Sweden
vytenis.barkauskas@nuclear.lu.se

The European Spallation Source (ESS) is a state-of-the-art neutron source being built in Lund, Sweden. This large-scale user facility will be used for studies of the structure and dynamics of the materials using neutrons [1]. The worldwide experience from operation of spallation sources is very limited. An inevitable side effect of the neutron generation is the production of various radionuclides, resulting from spallation in the proton accelerator and target, as well as from neutron activation of surrounding structures, soil, and air. A fraction of the radionuclides formed in ESS may be released to the environment during normal operation, as well as in potential accidents. Quantitative evaluation of these radionuclides is vital ensuring the radiological safety of the workers, general public and environment.

We are using the existing competence at Lund University and developing it further regarding modeling of radionuclide production and measurement for ESS-specific radionuclides. In 2017-2018, natural and man-made radionuclides were assessed in the Lund area, including gamma-emitters as well as the pure beta-emitters $^{3}$H and $^{14}$C [2].

In current experimental work we are focusing on difficult-to-measure radionuclides (alpha and beta emitters), requiring radiochemical sample pre-treatment before activity measurements. Radiochemistry methods are being developed related to separation of ESS-specific radionuclides prior to measurement. Two basic techniques - liquid scintillation counting (LSC) and alpha spectrometry – are employed for detection of the relevant radionuclides. LSC was successfully used for evaluation of tritium of the background samples of e.g. air, precipitation, ground and surface water, bioindicators, crops, fruits, milk and sewage sludge. Results of current environmental tritium activity in the ESS site measured using LSC technique show natural levels of tritium only – less than than 5 Bq/l. We aim to make the most of the LSC technique, not only for tritium, but also for other radionuclides that are expected to be formed in the ESS facility, e.g. $^{14}$C, $^{22}$Na, $^{55}$Fe, $^{90}$Sr. Alpha spectrometry is planned to be used for the detection of actinides, polonium and alpha-emitting rare-earth metals ($^{148, 150}$Gd, $^{146}$Sm, $^{154}$Dy).

A review of publications which radionuclides are expected to be formed in the ESS and the independent Monte Carlo modeling of ESS components provides basis for our preparation for further measurements after the start of ESS operation. The review of available publications allowed us to identify 234 most important radionuclides, with half-life longer than 10 hours.

In order to perform independent analysis, a simplified model of ESS target and main surrounding structures was created for target composition modeling using FLUKA code (see Fig. 1a). The preliminary radionuclide production results given by the model are mapped in the Fig. 1b. Our preliminary model evaluation results show that content of tritium (the most mobile radionuclide) generated in the target is in the same orders of magnitude as in other publications [3]. The same correspondence is noticed for $^{148}$Gd, the alpha emitter which has the highest effective dose coefficient for inhalation among the radionuclides generated in the target.

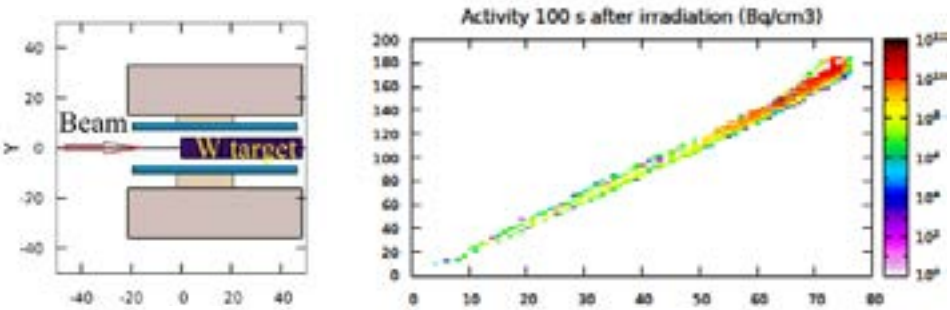


Fig. 1. a) ESS target model, b) Preliminary results of the radionuclide production in ESS target.

Further analysis of the results and model development is planned to be performed in the near future, also using other modeling tools (e. g. MCNP code).

This work is supported by Swedish Radiation Safety Authority (SSM), grant No. SSM2018-1636-1.

[1] R. Garoby, et al., The European Spallation Source Design, Physica Scripta, **93**, 014001 (2017).
[2] Ch. Bernhardsson, et al., *Assessment of "Zero Point" radiation around the ESS facility*, LU Report MA RADFYS 2018:01 (BAR-2018-04), 2018.
[3] Z. Kókai, et al., Comparison of different target material options for the European Spallation Source based on certain aspects related to the final disposal, Nucl Instrum Methods Phys Res B, **416**, 1-8 (2018).

# HYDRATION MECHANISM OF DEGRADABLE STARCH MICROSPHERES STUDIED USING VIBRATIONAL SPECTROSCOPY

Jekaterina Borzova, Gediminas Niaura

Department of Bioelectrochemistry and Biospectroscopy, Institute of Biochemistry, Life Sciences Center, Vilnius University, Vilnius, Lithuania
Jekaterina.Borzova@gmc.vu.lt

Degradable starch micro spheres (DSM) is polymerised maltodextrin with additional crosslinks that form a porous starch network. In addition to an active substance it becomes an innovative delivery system. Loaded DSM applied to amylase containing area gradually break down the three dimensional network of starch releasing encapsulated substance with the end product of glucose making DSM safe and pure drug delivery system. In 2016 Vitaly Kocherbitov and his team explored thermodynamic features of DSM during the gradual hydration using DSC, Sorption calorimetry, SEM, Optical microscopy, gravimetric swelling studies, rheology, and SAXS [1]. They established water quantity limits when DSM undergoes phase transitions (glass transition at 18 wt% of $H_2O$ at room temperature), swelling capacity etc. However, the hydration mechanism at molecular level is still not fully understood. In this study, Raman spectroscopy was used as an ideal probe method for that purpose.

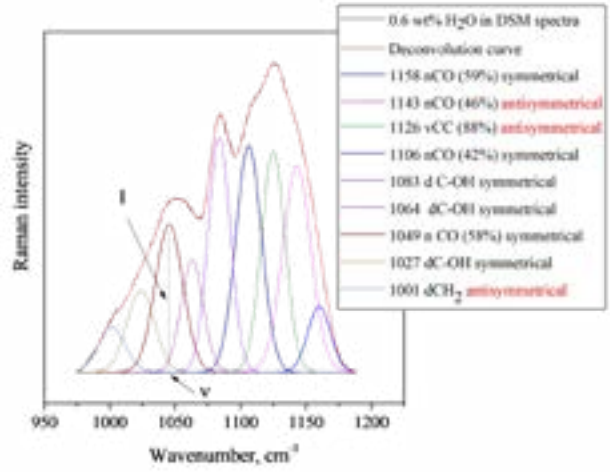


Fig. 1. Raman 975-1195 $cm^{-1}$ area deconvolution to Gaussian/Lorentzian peaks.

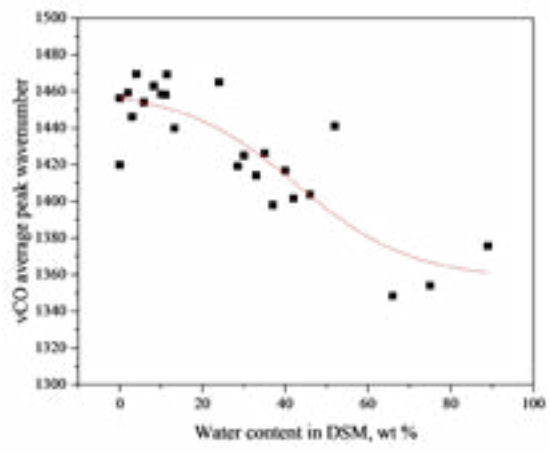


Fig.2. Stretching CO band vibration average peak wavenumber dependency on a water content, wt%.

Symmetry of each vibration band was gained from the depolarisation ratio analysis [2]. C-O, C-C, C-$H_2$, C-OH region occurring at 975-1195 $cm^{-1}$ of mixed stretching and bending vibrations [3-5] and mixed symmetry was chosen for the detailed study (Fig.1). Analysis of stretching C-O mode wavenumber average dependency on water content in DSM-water system showed the shift to lower wavenumber values starting from the glass transition (Fig 2). This shift shows the C-O stretching vibration bond strength decrement due to the formation of hydrogen bonding. Another changes were observed in bending C-OH vibration range during the hydration; namely, the shift to higher wavenumbers and an increase of Gaussian/Lorentzian peak area value. These changes were due to DSM expansion from 18 wt% (glass transition) and the level of freedom increase inside the molecule. Finally, the shift to lower wavenumbers of stretching asymmetric C-C vibrational band and decrease of Gaussian/Lorentzian peak intensity showed the decrease of C-C bonding strength due to the tension inside the molecule during the hydration.

In conclusion, it was demonstrated that the glass transition (18wt% of $H_2O$) is an onset point for molecule expansion and monolayer of water formation outside the molecule.

[1] J. Wojtasz et al., Hydration and swelling of amorphous cross-linked starch microspheres, Carbohyd. Polym. **135**, 225-233 (2016).
[2] C.D. Allemand, Depolarization ratio measurements in Raman spectroscopy, Appl. Spectrosc. **24**, 348-353 (1970).
[3] J.J. Cael et al., Infrared and Raman spectroscopy of carbohydrates. Part III: Raman spectra of the polymorphic forms of amylose, Carbohyd. Res. **29**, 123-134 (1973).
[4] J.J. Cael et al., Infrared and Raman spectroscopy of carbohydrates. Part IV: Normal coordinate analysis of V-amylose, Biopolymers **14**, 1885-1903 (1975).
[5] R. Kizil et al., Characterization of irradiated starches by using FT-Raman and FTIR spectroscopy, J. Agrocult. Food Chem. **50**, 3912-3918 (2002).

# SOYBEAN, LENTIL, CHICKPEA: NON-TRADITIONAL LEGUMES FOR AGRICULTURAL SUSTAINABILITY IN LITHUANIA

Monika Toleikienė, dr. Žydrė Kadžiulienė, dr. Lina Šarūnaitė

Institute of Agriculture, LAMMC, Lithuania
toleikiene.monika@lammc.lt

Grain legumes form root nodules which contain symbiotic bacteria fixing atmospheric nitrogen, which is a significant economic and ecological advantage for a sustainable crop rotation. In the European Union (EU), the demand for protein-rich crops greatly exceeds the level of home production. Field pea and faba bean are the main protein crops cultivated in Lithuania, while soybean, lentil and chickpea are common in the tropical climate countries. Attempts are made to reduce the reliance on the imports of these non-traditional crops by investigating novel cultivars adapted to the cultivation environments of temperate agro-climatic region.

Experiments with soybean, lentil and chickpea were conducted in Lithuania, which lies above the northern boundary of typical distribution regions of these species. The experimental plots were established in Dotnuva at Institute of Agriculture, LAMMC, on the organically managed sites in 2015 for soybean and in 2018 for lentil and chickpea. The main objective of this study was to evaluate management practices for the cultivation of the non-traditional legume species. Factors investigated: inoculation (inoculated; not inoculated), rows spacing (12.5, 25, 37.5, 50 and 75cm), three sowing dates and seed rates differing between the species and years, weed control methods (natural crop-weed competition, harrowing, manual weeding and inter-row cultivation). Yield components, maturity and nodulation were assessed during the growing seasons of 2015 and 2016.

A four-year investigation of soybean cultivation generated relevant results based on which cultivation recommendations were prepared. The yield of soybean varied from 836 to 2978 kg $ha^{-1}$ under the influence of the crop and soil management practices. Sowing date was the most important factor for soybean germination. In 2015, sowing date May 25 was more favorable than May 12. In 2016, late sowing date, June 3, resulted in 25 - 48 % yield reduction compared with May 20. Row spacing had a significant effect on the plant population density and consequently on the yield. Plants grown with a 50 cm row spacing tended to accumulate higher aboveground biomass, higher number of seeds per plant and higher seed weight compared with the plants grown with a 25 cm row spacing. Nevertheless, the plots sown at a 25 cm row spacing had 1.3 - 2.6 times higher plant population density which resulted in significantly higher grain yield.

In the variety testing trials we examined seven soybean varieties (Merlin, Violetta, Bohemians, Silesia, Brunensis, De-013-130660, H-15-007-0072) and two B. japonicum strains (‘AGF78’ and ‘2490’). Soybean yield significantly correlated with the biomass of B. japonicum nodules. Inoculated soybean accumulated 98 % higher grain yield, 7 % higher seed weight and 6 % higher protein content compared with not inoculated. Of the two B. japonicum strains, 16 % more effective nodulation was observed for ‘AGF78’ than for ‘2490’. In northeastern European climatic conditions, significantly greater N content and %Ndfa was shown by the soybean variety Merlin in symbiosis with ‘AGF78’ strain. Not-inoculated soybean could not establish symbiosis with native rhizobium bacteria, therefore soybean biomass and productivity declined due to nitrogen shortage in the organically managed agro-system.

Experiments with lentils were set up in 2018, when dry weather conditions prevailed. We investigated the effect of seed rate and sowing time on lentil development and productivity. The highest productivity was achieved when sowing lentil early in spring on April 30. Also, a seed rate of 240 kg $ha^{-1}$ was optimal and gave the highest yield increase to 1298 kg $ha^{-1}$. The most effective row spacing for weed decrease was 12.5 cm. Manual weeding was effective weed control practice, while harrowing did not differ significantly from natural crop-weed competition. Lentils were able to form symbiosis with local rhizobium bacteria and did not suffer from shortage of nitrogen derived from the atmosphere.

In the first year of chickpea investigation, it produced a low yield ranging between 391 – 809 kg $ha^{-1}$ depending on the seed rate and sowing time. The highest productivity was demonstrated by sowing chickpea at the earliest date, April 30, and at the highest seed rate of 190 kg $ha^{-1}$. Chickpea exhibited high competitive ability against weeds, while harrowing decreased crop plant density and consequently the yield. The best row spacing was 25 cm. Chickpea also requires special rhizobium bacteria, but even after inoculation, it failed to form nodules for nitrogen fixation this year.

These data show that soybean, lentil and chickpea have the potential to be cultivated under Lithuanian conditions in organic agro-ecosystems. However, the preliminary findings of the first experimental year show better performance and therefore better prospects for lentils than chickpea. Yet, in order to draw more valid conclusions the study needs to be continued for a longer period.

# FEATURES OF HEART RATE REGULATION AND BRAIN ACTIVITY DURING CHOICE REACTION IN MILITARY MEN WITH TRAUMATIC BRAIN INJURY AND POSTTRAUMATIC STRESS DISORDER

Veronika Vozniuk[1], Natalia Filimonova[1], Mykola Makarchuk[1], Ihor Zyma[1], Oleh Horbunov[2], Valentyn Kalnysh[3]

[1] Department of physiology and anatomy, ESC Institute of biology and medicine, Taras Shevchenko National University of Kyiv, Ukraine
[2] Faculty of computer science and cybernetics, Taras Shevchenko National University of Kyiv, Ukraine
[3] Kundiiev Institute of Occupational Health of the NAMS of Ukraine, Ukraine
veronicavozniuk@gmail.com

Traumatic brain injury (TBI) is the most common brain injury among military personnel who took part in armed conflicts [1] (War in Afganistan, Iraq conflict, Israel-Palestinian conflict, War in eastern Ukraine and etc.). Also military personnel suffers from post-traumatic stress disorder (PTSD) [2]. As far as TBI disrupts brain structure and its functions [3], consequences of TBI are long-term and have a huge impact on cognitive processes and control of behavior [4]. PTSD affects normal execution of cognitive processes as well [5]. Decision making implies execution of basic cognitive processes which are based on choice reaction. Disrupting of information processes during execution of choice reaction can result in inadequate outcome. Development of efficient rehabilitation methods for patients with TBI and PTSD requires additional information about features of brain activity of these people.

The study involved 33 male volunteers, right-handed, 18-28 y.o., without health complaints – students of Taras Shevchenko National University of Kyiv (control group); 14 male volunteers, right-handed, 22-52 y.o., military men of Armed Forces of Ukraine with mild TBI (mTBI), who took part in armed conflict in the East of Ukraine, later – military men with mTBI – the patients of Kundiiev Institute of Occupational Health of the NAMS of Ukraine, Kyiv; and 31 volunteers, right-handed, 20-54 y.o.: 18 military men of Armed Forces of Ukraine with mTBI and 13 with PTSD, both groups also took part in armed conflict in the East of Ukraine, – patients of Center for Medical Rehabilitation and Health Centre of the Ministry of Defence of Ukraine "Pushcha Voditsa".

In the study simple reaction time (SRT) and choice reaction time (CRT) of responses made by right and left hand were measured. EEG and ECG were recorded before patients got tested and during simple reaction and choice reaction tasks. Brain structures engaged in choice reaction and corresponding dipoles of brain activity were indentified with analyzing of EEG records in low resolution electromagnetic tomography LORETA. Activation levels of parasympathetic and sympathetic divisions of autonomic nervous system (ANS) were rated due to the mode of R-R intervals and the mode amplitude of R-R intervals.

CRT of responses made by right and left hand for the military men with mTBI was significantly longer compared to control group (454 [436; 552] ms vs. 402 [392; 435] ms (p=0,002) for right hand and 486 [460; 576] ms vs. 414 [390; 430] ms (p=0,002) for left hand), while there was no statistically significant difference between the response time made by right and left hand between the military men with PTSD and control group (447 [394; 486] ms vs. 402 [392; 435] ms (p=0,116) for right hand and 430 [416; 477] ms vs. 414 [390; 430] ms (p=0,06) for left hand). Increased activity of the parasympathetic division of ANS was revealed only in the military men with mTBI, comparing the mode of R-R intervals during simple reaction task and choice reaction task (0,710 [0,658; 0,909] s vs. 0,740 [0,664; 0,940] s (p=0,002)), while there were no changes in mode amplitude value (54,75 [48,8; 71,4] % vs. 53,5 [46,4; 62,8] % (p=0,584)). EEG analysis by LORETA showed that control group executed choice reaction primarily engaging fronto-parieto-occipital regions. The group with mTBI showed more activity of fronto-temporo-occipital regions. The group with PTSD had mostly right lateralized brain activity with activation of fronto-temporal regions and insula. Furthermore, there was revealed that mTBI had statistically significantly greater activation of parahippocampal gyrus, temporal and occipital lobes regions, insula and posterior cingulate gyrus during choice reaction task compared to control group (p=0,018).

In conclusion, obtained results require further researches for eventual establishment of association between features of parasympathetic nervous system activation and brain activity in the military men with mTBI during choice reaction task. Also additional approach is needed to clarify the difference between engaged in choice reaction brain regions of the military personnel with mTBI and PTSD.

[1] Faul M, Coronado V. Epidemiology of traumatic brain injury. Handb Clin Neurol. 2015;127:3-13. doi: 10.1016/B978-0-444-52892-6.00001-5
[2] Gates MA, Holowka DW, Rosen RC. Posttraumatic stress disorder in veterans and military personnel: epidemiology, screening and case recognition. Psychol Serv. 2012:9(4):361-382. doi: 10.1037/a0027649
[3] Cristofori I, Harvey SL. Traumatic brain injury and cognition. Handb Clin Neurol. 2015;128:579-61. doi: 10.1016/B978-0-444-63521-1.00037-6
[4] Dikmen SS, Corrigan JD, Levin HS, Machamer J, Stiers W, Weisskopf MG. Cognitive outcome following traumatic brain injury. J Head Trauma Rehabil. 2009:24(6):430-438. doi: 10.1097/htr.0b013e3181c133e9
[5] Scott JC, et al. A quantitative meta-analysis of neurocognitive functioning in posttraumatic stress disorder. Psychol Bull. 2015;141(1):105-140. doi: 10.1037/a0038039.

# *HERACLEUM SOSNOWSKYI* MANDEN. DRY-FRUIT DEVELOPMENT UNDER EXOGENOUS $GA_3$ AND TIBA APPLICATION

Tautvydas Žalnierius, Dalia Koryznienė, Sigita Jurkonienė

Nature Research Centre, Institute of Botany, Laboratory of Plant Physiology, Lithuania
t.zalnierius@gmail.com

Sosnowsky's hogweed (*Heracleum sosnowskyi* Manden.) is invasive plant entered into list of Invasive Alien Species of Union concern [1]. It is highly toxic plant to humans and well established in seven EU countries where transforms the landscape. Sosnowsky's hogweed propagates only by dry-fruits i.e. seeds and produce them once in lifetime. Well known the important role of gibberellins and auxins on seed development of fleshy fruits [2,3]. To figure out the role of gibberellic acid ($GA_3$) in dry-fruit i.e. seed development, we applied Sosnowsky's hogweed's unpollinated ovaries in satellite and stem branch umbels by different concentrations (0.07 mM, 0.14 mM, 0.28 mM, 0.43 mM) of exogenous $GA_3$. $GA_3$ treatment didn't have a significant effect on size of *H. sosnowskyi* seeds, however it caused changes in shape. Longitudinal sections of mericarps and SEM micrographs of embryos revealed that embryos after $GA_3$ (0.43 mM) treatment were at torpedo stage, whilst mature embryos in control seeds had been observed (Fig. 1).

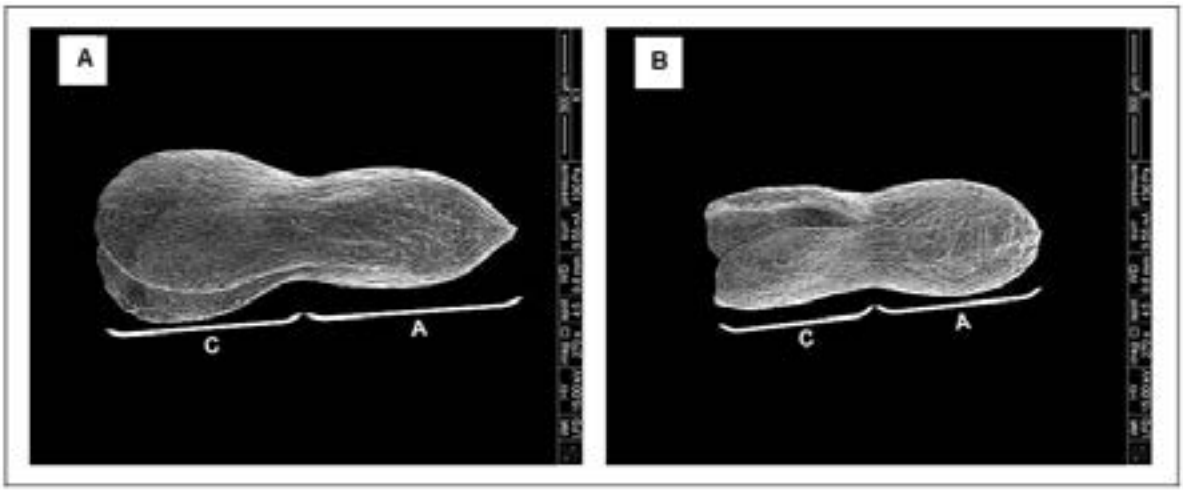


Fig. 1. Scanning micrographs of embryos received from mericarps of *H. sosnowskyi*. Untreated (A) and treated with $GA_3$ at concentration of 0.43 mM (B) plants. Abbreviations: A – axis; C – cotyledons. Scale bar, 300µm.

Furthermore, we disclosed that $GA_3$ treatment significantly reduced the germination rate *in situ* conditions of *H. sosnowskyi* mericarps from 98.0% to 16.5% in control and $GA_3$ (0.43 mM) treatments respectively. Auxin transport inhibitor (1,3,5-triiodobenzoic acid, TIBA) was used to affect auxin and gibberellin crosstalk in fruit development. [3]. Inhibition of auxin transport from the apical shoot by TIBA decreased seed germination rate in field conditions (98.1% and 29.8%; control and TIBA), the auxin effect on seeds' sufficient development was negated by indoleacetic acid (IAA) application on unpollinated ovaries right after the TIBA treatment (germination rate 96.1%). All these results suggest that exogenous $GA_3$ application has influence on dry Sosnowsky's hogweed seeds development and affects germination rate. Thus, it could be assumed that $GA_3$ could be used to inhibit the spread of this invasive plant.

[1] European Union, List of Invasive Alien Species of Union concern, – http://ec.europa.eu/environment/nature/invasivealien/list/index_en.htm [accessed 2019-01-28].
[2] J.C. Serrani, M. Fos, A. Atares et al., Effect of gibberellin and auxin on parthenocarpic fruit growth induction in the cv. Micro-Tom of tomato, Journal of Plant Growth Regulation **26**, 211-221 (2007).
[3] J.C. Serrani, E. Carrera, O. Ruiz-Rivero et al., Inhibition of auxin transport from the ovary or from the apical shoot induces parthenocarpic fruit-set in tomato mediated by gibberellins, Journal of Plant Physiology **153**, 851-862 (2010).

# TYPE OF DIABETES – A FACTOR DETERMINING THE RESULTS OF INTRAVITREAL BEVACIZUMAB INJECTIONS IN CASE OF DIABETIC RETINOPATHY

Anete Kristiana Jekabsone[1], Prof. Guna Laganovska[1,2]

[1] Faculty of Medicine, Riga Stradins University, Latvia
[2] Ophtalmology clinic, Pauls Stradins Clinical University Hospital, Latvia
anete.jek@gmail.com

**Introduction.**

Diabetes mellitus is a growing health issue in modern society. In Latvia the prevalence in 2017 was 4734/100'000. Of these patients 5,5% had retinopathy, 3,2% - maculopathy, and 0,2% were legally blind[1]**.** It is important to know the factors and their force of affecting the therapeutic effect of intravitreal (IVT) Bevacizumab injections as they are a frequently used therapy in case of macular oedema and diabetic retinopathy.

**Aim.**

The aim of the study is to evaluate diabetes type and therapy influence on visual acuity (VA) and intraocular pressure (IOP) changes before and after IVT injections of Bevacizumab.

**Materials and Methods.**

The retrospective study was conducted in Pauls Stradins Clinical University Hospitals Ophthalmology clinic in 2018. 120 ambulatory patient cards, VA (Early Treatment of Diabetic Retinopathy Study visual acuity chart) and IOP (iCare) changes were gathered and the type of diabetes and recieved diabetes therapy was registered. Patients who had other forms of retinopathy (for example Age related Macular Degeneration) were excluded. The obtained data were analysed using the statistical software IBM SPSS Statistics version 22.0. and Microsoft Excel.

**Results.**

In the study participated 15 patients with type I diabetes and 105 with type II diabetes. A statistically significant difference was found in VA before (type I - Mdn=0,4 with IQR[0,20 to 0,60] vs type II – Mdn=0,2 with IQR[0,10 to 0,30])($p<0,01$), VA at the end of therapy (type I – Mdn=0,5 with IQR[0,40 to 0,80] vs type II – Mdn=0,2 with IQR[0,10 to 0,40]) ($p<0,01$) and IOP at the end (type I – Mdn=16 with IQR[14 to 20] vs type II – Mdn=15 with IQR[12 to 17])($p<0,05$).

There were 74 patients who were recieving insulin therapy and 46 who were not. An important difference was found also in patients who were (yes) and were not (no) recieving insulin therapy in IOP at the end (yes Mdn=15 with IQR[13 to 18] vs no Mdn=13,5 with IQR[11 to 16])($p<0,05$), VA at the end (yes Mdn=0,31 with IQR[0,19 to 0,5] vs no Mdn=0,16 with IQR[0,09 to 0,33])($p<0,05$), the IOP difference from beginning to the end of therapy (yes Mdn=0 with IQR[-2 to 2] vs no Mdn=-2 with IQR[-4 to 0])($p<0,01$).

**Conclusions.**

The type of diabetes is an important factor influencing the outcome of IVT Bevacizumab injections in case of diabetic retinopathy. The VA was significantly better before and after therapy in type I diabetes group, the IOP was lower in type II group. The IOP and VA at the end was higher in insuling recieving group. This might be due to a higher level of blood glucose level control or a younger patient age which might be an interesting topic for another research. IOP difference was greater in non insulin recieving group. It would be interesting to continue a research like this to determine if there are any other mixing factors that were not taken into consideration this time, for example, other eye diseases, refraction errors etc.

[1] Slimību profilakses un kontroles centrs. *Statistikas dati par cukura diabēta pacientiem.* Table 1 and Table 11.

# $CS^+$ AS A PLANT ION CHANNEL BLOCKER: IS IT THAT SIMPLE?

Vilmantas Pupkis, Indrė Lapeikaitė, Vilma Kisnierienė

Institute of Biosciences, Life Sciences Center, Vilnius University, Lithuania
vilmantas.pupkis@gmc.vu.lt

Giant internodal cells of macroalgae *Characeae* have a long history of being used as a model system for electrophysiological investigations such as ion channel research [1]. Characeaen intermodal cells can survive after being cut out of the thallus and function as single organisms. Their large size (up to 25 cm in length, ~1 mm in diameter) enables easy access via microelectrode techniques. Recent publication of another Characeaen *Chara braunii* genome [2] encourages functional research (for example electrophysiological investigation of ion channels) that in the future could be combined with the structural data.

Plant action potentials are transient excitations of plasmalemma and tonoplast (vacuolar membrane) that transduce information about various external stimuli, including salt stress, mechanical excitation and temperature change. Action potentials are generated when cell membrane potential depolarizes (becomes less negative) to a threshold value and activates voltage-dependent $Ca^{2+}$ ion channels. Activated ion channels produce an inflow of $Ca^{2+}$ ions into the cytoplasm where they activate $Ca^{2+}$-dependent $Cl^-$ ion channels. Influx of $Ca^{2+}$ ions and efflux of $Cl^-$ ions produce a rapid membrane depolarization. Plasmalemma is repolarized to its resting potential (in *Nitellopsis* <-200 mV) by the activation of $H^+$-ATPase as well as depolarization-activated $K^+$ ion channels' produced efflux of $K^+$ ions.

$Cs^+$ ions are frequently used as $K^+$ ion channel blockers [3] and our data using patch clamp technique confirm that. $Cs^+$ effects on actions potentials of *Nitellopsis obtusa* cells using current clamp technique (Fig. 1) and effects of membrane currents during excitation using voltage clamp technique were evaluated. However, the effects of $Cs^+$ cannot always be explained as only being caused by $K^+$ ion channel blockage.

Our future aims include investigating the effects of other $Cs^+$ salts (such as $CsSO_4$) and HCl in order to isolate the effect on actions potentials and membrane currents during excitation of $Cs^+$ ions with anion component eliminated.

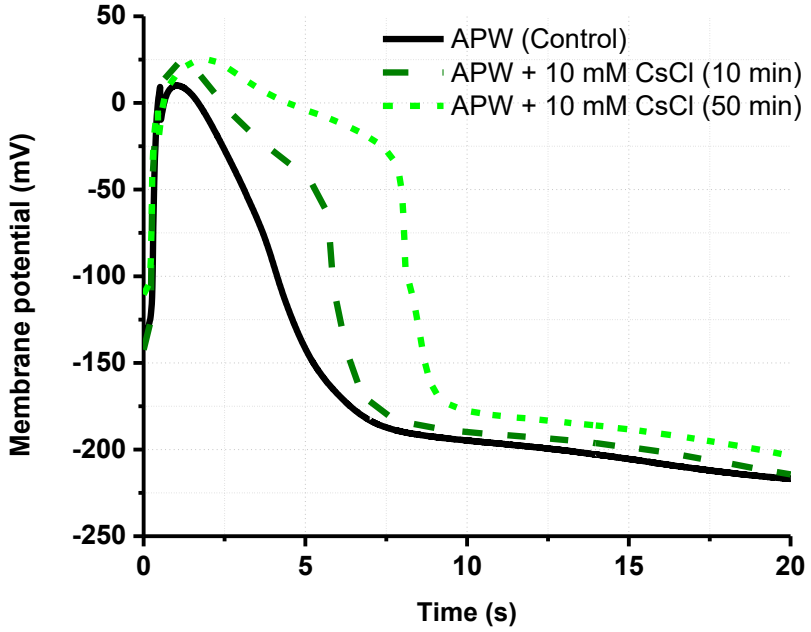


Fig. 1. Recordings of repolarization phases of 3 action potentials of *Nitellopsis obtusa*, showing effects of 10 min and 50 min exposure of 10 mM CsCl. Longer exposure time increases duration of action potential.

[1] M. J. Beilby, M. T. Casanova. *The physiology of characean cells* (Springer Science & Business Media, 2014).
[2] T. Nishiyama, H. Sakayama, J. de Vries, H. Buschmann, D. Saint-Marcoux, K.K. Ullrich, F.B. Haas, L. Vanderstraeten, D. Becker, D. Lang, S. Vosolsobě. The Chara genome: secondary complexity and implications for plant terrestrialization. Cell, **174**(2), 448-464 (2018).
[3] L.P. Zanello, F.J. Barrantes. Blockade of the $K^+$ channel of Chara contraria by $Cs^+$ and tetraethylammonium resembles that of $K^+$ channels in animal cells. Plant Science, **86**(1) (1992).

# EVALUATION OF VEGETATION CONDITIONS IN DIFFERENT TYPES OF LAND USE USING SATTELITE MEASURED DATA

Laurynas Klimavičius

Institute of GeoSciences, Vilnius University, Vilnius, Lithuania
laurynas.klimavicius@gf.stud.vu.lt

At the end of 20th century advanced remote sensing system, which is based on satellite measured data, has allowed to use new methods for vegetation conditions researches. Satellite measured data nowadays is not only more accurate, but, unlike older methods, shows vegetation conditions in a particular area, not a specific place and covers the whole Earth [1].

In this study, a sufficiently long data sequence (from 1982 till 2015) was analyzed, so the results can be used to determine the connection between meteorological factors and vegetation conditions as well as to assess impact of climate change. The research area covers a rather large area from 53º N to 59º N. The distance from the Baltic Sea and the terrain in this area is quite diverse, so different landscapes and different types of land use are covered in the study. Also, an impact of meteorological conditions on vegetation using remote sensing data in the eastern part of Baltic Sea region is little studied [2].

The main objectives of this study are to assess:

- monthly NDVI changes from 1982 till 2015 in the eastern part of Baltic Sea region.
- air temperature and precipitation impact on vegetation conditions in the whole study area (2622 cells) and in five different types of land use (pastures, wetlands, broad leaved forests, coniferous forests and arable land) (322 cells)
- impact of extreme meteorological conditions on vegetation.

In order to do that, monthly Normalized Vegetation Difference Index (NDVI) values were used. This index is calculated using near infrared (NIR) and visible (VIS) light Eq. (1) [3]

$$NDVI = (NIR-VIS)/(NIR+VIS) \quad (1)$$

NDVI is an appropriate index for this research as it has strong connection with air temperature, especially at the beginning and the end of vegetation period [4]. Precipitation has an impact on NDVI as well and it depends on the type of vegetation and the growth phase [5].

In this study, monthly NDVI data (cell size 0.144×0.144°) were obtained from NOAA STAR – NESDIS system. Different types of land use were distinguished using CORINE land cover data. Monthly precipitation and air temperature data were obtained from CRU TS v. 4.01 database (cell size 0.5×0.5°).

[1] Kogan F. N. 1997. Global drought watch from space. *Bulletin of the American Meteorological Society.* 78: 621-636.
[2] Rimkus E., Stonevičius E., Kilpys J., Mačiulytė V., Valiukas D. 2017. Drought identification in the Eastern Baltic region using NDVI. *Earth System Dynamics.* 8: 627-637. doi: 10.5194/esd-8-627-2017.
[3] Kogan F. N. 2002. World Droughts in the New Millennium from AVHRR-based Vegetation Health Indices. *EOS Transaction of American Geophysical Union*. 83: 562–563.
[4] Zhang X., Friedl M. A., Schaaf C. B. 2006. Global vegetation phenology from Moderate Resolution Imaging Spectroradiometer (MODIS): Evaluation of global patterns and comparison with in situ measurements. *Journal of Geophysical Research.* doi: 10.1029/2006JG000217.
[5] Piao S., Fang J., Zhou L., Ciais P., Zhu B. 2006. Variations in satellite-derived phenology in China's temperate vegetation. *Global Change Biology.* 12: 672-685. doi: 10.1111/j.1365-2486.2006.01123.x.

# CRYSTALLOGRAPHIC STUDIES OF TEMPO RADICAL AND ITS NOVEL DERIVATIVES

Katarzyna Polak[1], Agata Wróbel[1], Damian Trzybiński[1], Elżbieta Megiel[1], Krzysztof Woźniak[1]

[1] Department of Chemistry, Biological and Chemical Research Centre, University of Warsaw, Poland
ka.polak2@student.uw.edu.pl

2,2,6,6-Tetramethylpiperidine-1-oxyl radical (TEMPO) and its derivatives have gained significant interest due to their functionality in organic synthesis as catalysts [1]. It was reported that they exhibit both ferromagnetism and antiferromagnetism at low temperatures [2]. Furthermore, the TEMPO-related radicals might be also interesting object of crystallographic research.

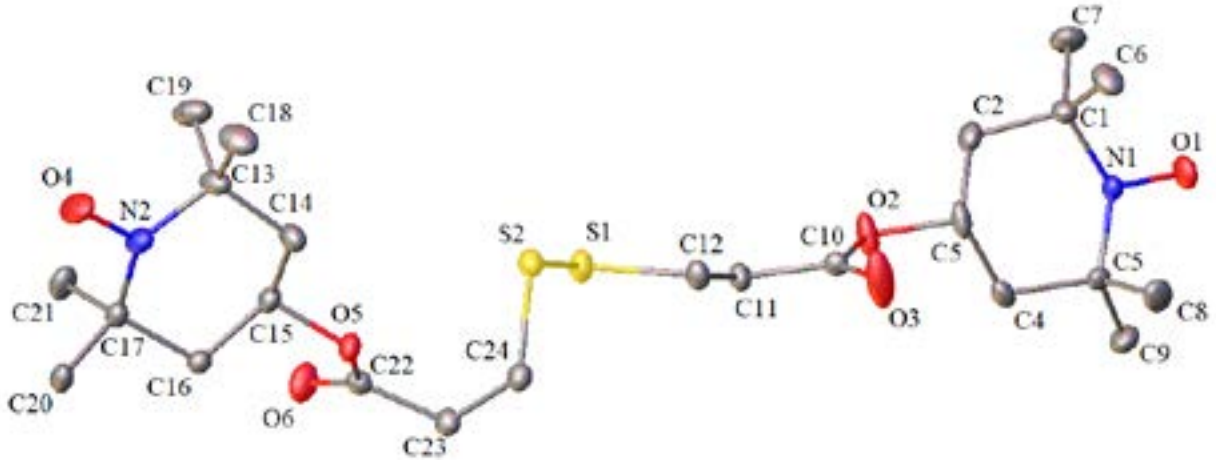


**Fig.1.** The asymmetric unit of the crystal lattice of DISSPK showing the atom numbering scheme. Displacement ellipsoids are drawn at the 50% probability level. The H-atoms were omitted for clarity.

In this work we focused on TEMPO radical and its novel derivative DISSPK. Both of the compounds' crystals were measured using Agilent Technologies SuperNova Dual Source diffractometer. Diffractometric measurements were performed with CuKα radiation at 100 K.

Although the crystal structure of TEMPO radical is known since 1974 the DISSPK compound have not been characterized yet. In case of both investigated systems the piperidine rings adopt chair conformation with two methyl substituents on each side. Crystallographic analysis revealed that their supramolecular architecture in crystal exhibit different structural features. In this presentation those differences will be discussed in details along with characterization of the significant intermolecular interactions (e.g. hydrogen bonds) occurring in their crystal networks.

*„This research was carried out at the Biological and Chemical Research Centre, University of Warsaw, established within the project co-financed by European Union from the European Regional Development Fund under the Operational Programme Innovative Economy, 2007 – 2013. The data collection was accomplished at the Core Facility for Crystallographic and Biophysical research to support the development of medicinal products sponsored by the Foundation for Polish Science (FNP)."*

[1] Soegiarto, A. C., Yan,W., Kent, A. D. &Ward, M. D. (2011). J. Mater. Chem. 21, 2204–2219.
[2] Togashi, K., Imachi, R., Tomioka, K., Tsuboi, H., Ishida, T., Nogami, T., Takeda, N. & Ishikawa, M. (1996). Bull. Chem. Soc. Jpn, 69, 2821–2830.
[3] D. Bordeaux, A. Capiomont, J. Lajzérowicz-Bonneteau, M. Jouve et M. Thomas (1974) Acta Cryst. B30, 2156-2160

# EFFECT OF Mn DOPING ON HYDROLYSIS RATE AND DISSOLUTION OF ALPHA-TRICALCIUM PHOSPHATE

Agne Kizalaite, Lauryna Sinusaite, Aivaras Kareiva, Aleksej Zarkov

*Institute of Chemistry, Vilnius University, Naugarduko g. 24, LT-03225, Vilnius, Lithuania*
*agne.kizalaite@chgf.stud.vu.lt*

Calcium phosphates (CPs) are the main constituents of bones and teeth and play an essential role in human life. Due to the similarity to the mineral phase of bones and excellent biocompatibility, different synthetic CPs have been widely applied as biomaterials for bone repair [1]. α-Tricalcium phosphate ($Ca_3(PO_4)_2$, α-TCP) is one of the representative biomaterials, which finds an application in bone cements due to its excellent resorbability and osteoconductivity [2]. α-TCP crystallizes in the monoclinic crystal system with the space group $P2_1/a$ and lattice parameters a = 12.887 Å, b = 27.280 Å, c = 15.219 Å, and β = 126.20°. The unit cell contains 312 atoms, where the number of crystallographically inequivalent sites is 18 for Ca, 12 for P, and 48 for O [3; 4]. The solubility of α-TCP is intermediate between orthophosphates, however it is much more reactive in aqueous solutions and easily hydrolyzes with a formation of calcium deficient hydroxyapatite ($Ca_{10-x}(PO_4)_{6-x}(HPO_4)_x(OH)_{2-x}$), which is similar to bone hydroxyapatite ($Ca_{10}(PO_4)_6(OH)_2$, HA) [5].

It is well known that doping at even very low levels can drastically affect physical and morphological properties of different materials, including TCP [6; 7]. At the same time surface properties such as microporosity, grain size and therewith-related surface area have been shown to play a determinant role in the process of osteoinduction of biomaterials [8]. Therefore, partial substitution of $Ca^{2+}$ ions in CP matrix by biologically active inorganic ions is a promising strategy to improve bone defect healing.

In the present work we report on the influence of Mn doping on hydrolysis rate and dissolution of α-TCP. α-TCP samples with Mn doping level from 0 to 1 mol% were synthesized by wet precipitation method. The phase purity and structure of synthesized compounds were evaluated using X-ray diffraction (XRD) analysis and Fourier-transform infrared spectroscopy (FTIR). Scanning electron microscopy (SEM) was used for the characterization of morphological features of initial powders and hydrolized products. Chemical composition of the synthesized compounds and ion release were analyzed by inductively coupled plasma optical emission spectrometry (ICP-OES).

**Acknowledgements**

This research was funded by the European Social Fund under the No. 09.3.3-LMTK-712 "Development of Competences of Scientists, other Researchers and Students through Practical Research Activities" measure (grant No. 09.3.3.-LMT-K-712-10-0066).

[1] Bouler, J. M.; Pilet, P.; Gauthier, O. ir kt. *Biphasic calcium phosphate ceramics for bone reconstruction: A review of biological response.* Acta Biomaterialia, **2017**, nr. 53, p. 1-12.
[2] Dorozhkin, Sergey V. *Calcium orthophosphates.* Journal of Materials Science, **2007**, nr. 42 (4), p. 1061-1095.
[3] Matsunaga, Katsuyuki; Kubota, Tomonori; Toyoura, Kazuaki ir kt. *First-principles calculations of divalent substitution of $Ca^{2+}$ in tricalcium phosphates.* Acta Biomaterialia, **2015**, nr. 23, p. 329-337.
[4] Yin, Xilin; Stott, M. J.; Rubio, A. *Alpha- and beta-tricalcium phosphate: A density functional study.* Physical Review B, **2003**, nr. 68 (20), p. 205205.
[5] Boanini, E.; Gazzano, M.; Bigi, A. *Ionic substitutions in calcium phosphates synthesized at low temperature.* Acta Biomaterialia, **2010**, nr. 6 (6), p. 1882-1894.
[6] Tkachenko, Serhii; Horynová, Miroslava; Casas-Luna, Mariano ir kt. *Strength and fracture mechanism of iron reinforced tricalcium phosphate cermet fabricated by spark plasma sintering.* Journal of the Mechanical Behavior of Biomedical Materials, **2018**, nr. 81, p. 16-25.
[7] Motisuke, Mariana; Mestres, Gemma; Renó, Caroline O. ir kt. *Influence of Si substitution on the reactivity of α-tricalcium phosphate.* Materials Science and Engineering: C, **2017**, nr. 75, p. 816-821.
[8] Habraken, Wouter; Habibovic, Pamela; Epple, Matthias ir kt. *Calcium phosphates in biomedical applications: materials for the future?* Materials Today, **2016**, nr. 19 (2), p. 69-87.

# SYNTHESIS AND PROPERTIES OF ENAMINE BASED HOLE TRANSPORTING MATERIALS CONTAINING OXYGROUPS

Aistė Ilčiukaitė[1], Marytė Daškevičienė[1], Egidijus Kamarauskas[2], Vygintas Jankauskas[2], Vytautas Getautis[1]

[1] Department of Organic Chemistry, Kaunas University of Technology, Lithuania
[2] Institute of Chemical Physics Vilnius University, Lithuania
aiste.ilciukaite@ktu.edu

Recently, as the world's population is growing, energy consumption is growing rapidly too. Most energy sources (oil, natural gas) pollute the environment, and we should look for ways to improve the efficiency of renewable energy sources. One of the most promising, environmentally friendly types of energy is the solar radiation [1]. In order to convert solar radiation to electricity solar cells were constructed. One of the main components of solar cells is the hole transporting material [2]. The aim of this work is to synthesize 3,4-methylenedioxy aniline-based semiconductors, that could be used as a hole transporting material in solar cells, and estimate the influence of oxy and methoxy groups on the properties of these enamines.

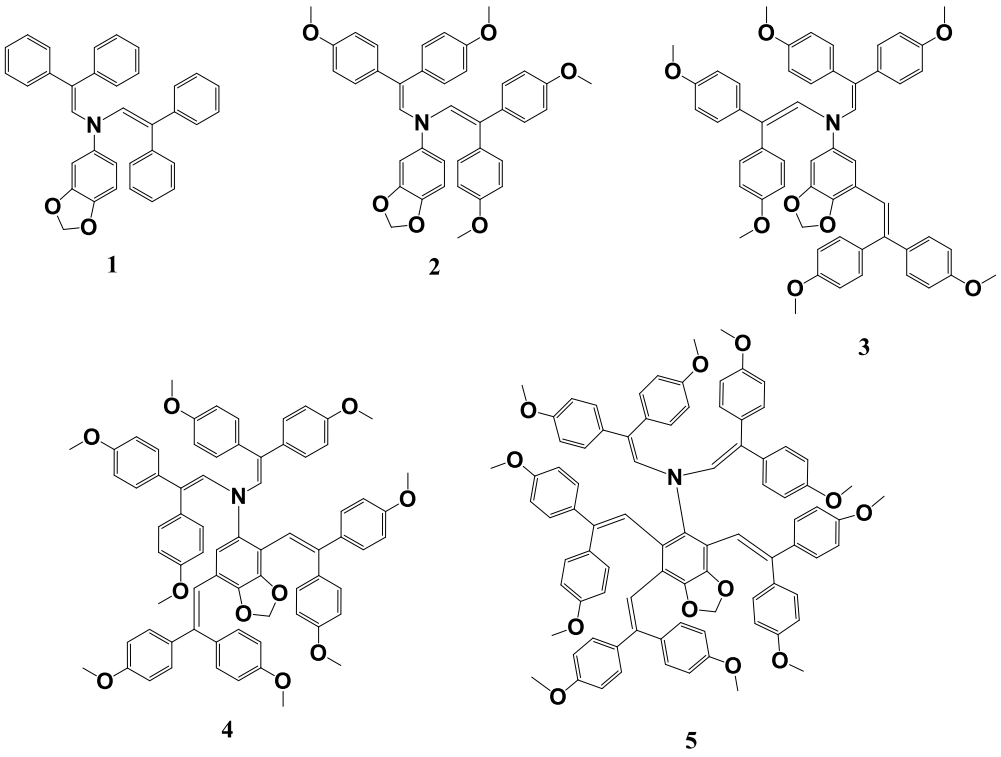


**Fig. 1**. Structures of new enamine derivatives.

During this work new enamine class compounds were synthesized **1-5**. From investigated optical properties, it is evident that all compounds have three maximum absorption peaks between 246 and 395 nm, which location depends on the number and position of methoxy groups. The synthesized compounds exhibit amorphous nature with a high glass transition temperature, a good solubility, and decent thermal stability (greater than 280 °C). It has been observed that ionization potential (5,19 – 5,31 eV) and hole drift mobility values (up to $3{,}63 \cdot 10^{-5}$ $cm^2/V \cdot s$) of all compounds (except enamine without methoxy groups) is favorable for the use in solar cells as positive charge carriers. However more than three 2,2-bis(4-methoxyphenyl)ethenyl groups in compounds **4**, **5** does not make any possitive influence on photoelectric properties.

[1] H. S. Rauschenbach, Solar Cell Array Design Handbook : The Principles and Technology of Photovoltaic Energy Conversion, ISBN 978-94-011-7915-7, (1980).
[2] L. Calio et al. Hole-Transport Materials for Perovskite Solar Cells. *Angewande Chemie International Edition* 55, 14522–14545 (2016).

# INCORPORATION OF COPPER INTO TIN SELENIDE THIN FILMS

Aiste Kunciute[1], Remigijus Ivanauskas[1]

[1] Department of Physical and Inorganic Chemistry, Kaunas University of Technology, Kaunas, Lithuania
aiste.kunciute@ktu.edu

Nowadays great attention is given to ecological problems such as global warming. Population growth increases energy demand and most of this energy comes from fossil fuels. This energy source causes carbon dioxide emission, which leads to climate change [1]. Due to this, it is very important to search alternative energy sources or develop such power station, which use wind power plants or solar cells [2].

Semiconducting materials are used for solar cells and it is very important to synthesize compounds with good electrical properties and high efficiency. These days a good characteristics shows ternary semiconductor layers such as $Cu_2SnS_3$, $Cu_3SnS_4$, $CuInSe_2$ or $CuGaSe_2$. $CuInSe_2$ layers have a great absorption coefficient but indium is rather expensive in case of this it is more economical to use copper [3, 4]. There is many deposition techniques, which let to deposit such binary or ternary layers (thermal crystallization of evaporated, chemical bath deposition, atomic layer deposition). Furthermore, composed layers can be modified by other element incorporation, for example copper could be chemically incorporate into thin films of indium selenide. This process allow to change properties of primary film [5].

In this work tin selenide layers with incorporated copper were formed on hydrophilic polymer polyamide 6 surface by simple and economic sorption-diffusion method. For the selenization polymer was immersed in 0.1 mol/L selenotrithyonate ($K_2SeS_2O_6$) in HCl 0.1 mol/L solution for 120 minutes at 60 ºC temperature. In the second stages, samples were treated with tin (II), copper (II/I) and copper (I) precursor solutions at different conditions (Fig. 1). Structural and elemental composition of the obtained layers were investigated by X-ray diffraction (XRD) analysis.

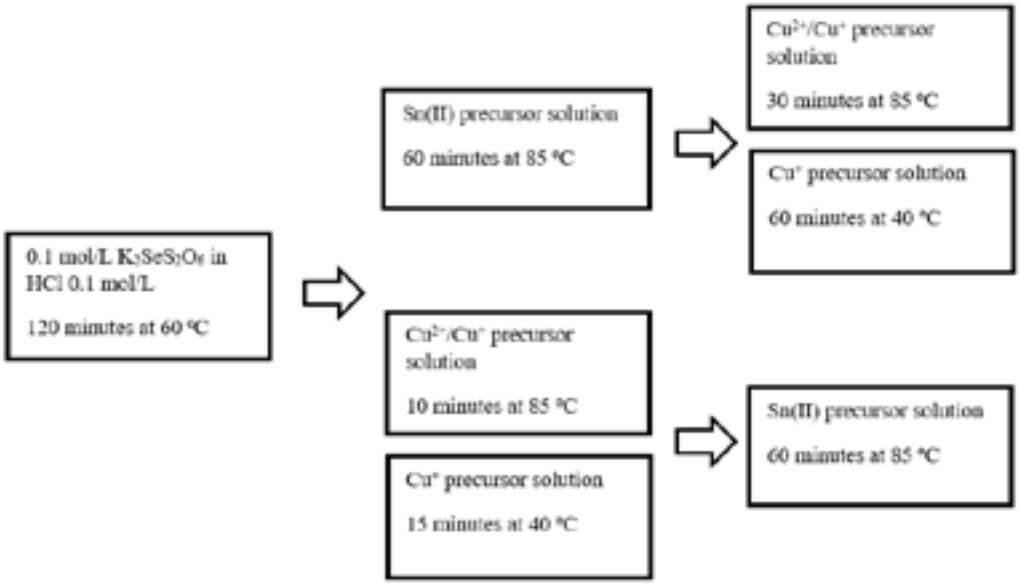


Fig. 1. Scheme of semiconductor layers formation

**Acknowledgements.**

This research is funded by the European Social Fund under the No 09.3.3-LMT-K-712-10-0230 "Development of Competences of Scientists, other Researchers and Students through Practical Research Activities" measure.

[1] B. K. Bose, Global Warming: Energy, Environmental Pollution, and the Impact of Power Electronics,Industrial Electronics Magazine **4**, 6-17 (2010).
[2] R. Simsa, H. Rognerb,K. Gregory, Carbon emission and mitigation cost comparisons between fossil fuel, nuclear and renewable energy resources for electricity generation, Energy Policy **31**, 1315–1326 (2003).
[3] M. Nakashima, T. Yamaguchi, H. Itani, $Cu_2SnS_3$ thin film solar cells prepared by thermal crystallization of evaporated Cu/Sn precursors in sulfur and tin atmosphere, Phys. Status Solidi **6**, 761–764 (2015).
[4] Sh. Ishizuka, A. Yamada, P. J. Fons, Impact of a binary $Ga_2Se_3$ precursor on ternary $CuGaSe_2$ thin-film and solar cell device properties, Applied physics letters **103**, 143903 (2013).
[5] C. J. Hibberd, K. Ernits, M. Kaelin, Chemical incorporation of copper into indium selenide thin-films for processing of $CuInSe_2$ solar cells, Progress in Photovoltaics: Research and Applications **16**, 585-593 (2008)

# ROOM TEMPERATURE PHOSPHORESCENCE OF THIANTHRENE DERIVATIVES

Andrej Akmanov, Dalius Gudeika
[1] Department of Polymer Chemistry and Technology, Kaunas University of Technology, Lithuania
Andrej.akmanov@ktu.edu

Room-temperature phosphorescence (RTP) has attracted a great deal of attention in the fields of optoelectonric devices [1], high contrast bio-imaging [2], photodynamic therapy [3], photocatalytic reactions [4], and oxygen indicators [5]. Heavy-metal complexes such as iridium complex are commonly used for room temperature phosphorescence but their potential toxicity and instability particularly in case of blue phosphors still remain to be solved. Room temperature phosphorescence from metal-free organic phosphors has attracted much attention in recent years since metal-free phosphors were presented as bright as organometallic compounds, quantum dots, and fluorescent molecules at room temperature [6].

Thianthrene being an electron-donor with a stable mono- and bicationic forms [7,8] has been used in several materials, including small molecules [8,9,10-13]. In particular, phosphorescent properties of thianthrene crystals have already been demonstrated [14], but no study has been performed on its derivatives. Of particular interest are the room temperature phosphorescent (RTP) properties of thianthrene, which suggests this group can be used to promote dual fluorescence-phosphorescence at room temperature in its derivatives.

In this study we present the synthesis of thianthrene derivatives (figure 1) examining the effect of the type of substituent on their RTP properties. The aim of the study is to understand structural and electronic effects, such as produced steric hindrance properties of benzoyl chloride substituents on thianthrene.

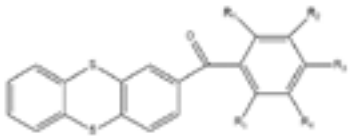

| Compound | 1 | 2 | 3 | 4 | 5 | 6 | 7 | 8 | 9 | 10 | 11 | 12 | 13 | 14 | 15 |
|---|---|---|---|---|---|---|---|---|---|---|---|---|---|---|---|
| R1 | H | F | H | H | Br | H | Cl | Cl | Cl | H | F | F | F | H | H |
| R2 | H | H | F | H | H | H | Cl | H | H | Cl | H | H | H | F | F |
| R3 | H | H | H | F | H | Br | H | F | H | F | F | H | H | F | H |
| R4 | H | H | H | H | H | H | H | H | H | H | H | F | H | H | F |
| R5 | H | H | H | H | H | H | H | H | F | H | H | H | F | H | H |

**Figure 1.** Thianthrene molecular structures studied in this work.

**[1]** D. Chaudhuri, E. Sigmund., A. Meyer et al, MetalFree OLED Triplet Emitters by Side-Stepping Kasha's Rule, *Angew. Chem. Int. Ed*., 52, 13449-13452 (**2013)**

**[2]** X. Zhen, Y. Tao, Z. An et al, Ultralong Phosphorescence of Water-soluble Organic Nanoparticles for in vivo Afterglow Imaging. *Adv. Mater.*, 29, 1606665 (**2017)**

**[3]** H.J. Sterenborg, J.W. de Wolf, M. Koning et al, Phosphorescence-fluorescence Ratio Imaging for Monitoring the Oxygen Status During Photodynamic Therapy. *Opt. Express.*, 12, 1873-1878. (**2004)**

**[4]** a) S. Telitel, F. Dumur, S. Telitel, et al, Photoredox Catalysis Using a New Iridium Complex as an Efficient Toolbox for Radical, Cationic and Controlled Polymerizations under Soft Blue to Green Lights. *Polym. Chem.*, 6, 613-624 (**2015)**; b) M.A. Garcia-Garibay, Advances at the Frontiers of Photochemical Sciences, *J. Am. Chem. Soc.*, 134, 8289-8292 (**2012)**

**[5]** a) A.S. Mathew, C.A. DeRosa, J.N. Demas et al, Difluoroboron β- diketonate Materials with Long-lived Phosphorescence Enable Lifetime based Oxygen Imaging with a Portable Cost Effective Camera. *Anal. Methods*, 8, 3109-3114 (**2016)**; b) Y. Yu, M.S. Kwon et al, Room-temperature-phosphorescence-based Dissolved Oxygen Detection by Core-shell Polymer Nanoparticles Containing Metal-free Organic Phosphors. *Angew. Chem. Int. Ed*., 56, 162071-16211 (**2017)**

**[6]** a) R.E. Andrews, K.M. Shah, J.M. Wilkinson et al, Effects of Cobalt and Chromium Ions at Clinically Equivalent Concentrations after Metal-on-metal Hip Replacement on Human Osteoblasts and Osteoclasts: Implications for Skeletal Health. *Bone,* 49**,** 717-723 (**2011)**; b) S.M. Plaza, The Safety and Efficacy of High-dose Chromium. *Altern. Med. Rev.*, 7, 218-235 (**2002)**

**[7]** L.A. Tinker, A.J. Bard, Electrochemistry in liquid sulfur dioxide. 1. Oxidation of thianthrene, phenothiazine, and 9,10-diphenylanthracene. J Am Chem Soc;101(9):2316-9. (**1979**)

**[8]** O. Hammerich, V.D. Parker, The reversible oxidation of aromatic cation radicals to dications. Solvents of low nucleophilicity. Electrochim Acta;18: 537- 41. (**1973**)

**[9]** S. Ogawa, H. Muraoka, R. Sato, Design of reversible organiceorganometallic multi-redox systems using thianthrene having ferrocene fragments. Tetrahedron Lett; 47:2479-83 (**2006**)

**[10]** J.M. Lovell, R.L. Beddoes, J.A. Joule, Synthesis of 4,6-disubstituted thianthrenes; Xray crystal structures of 4,6-diphenylthianthrene and 1-tetrathiafulvalenylnaphthalene. Tetrahedron; 52(13):4745- 56 (**1996**)

**[11]** K. Sato, M. Hyodo, M. Aoki et al, Oxidation of sulfides to sulfoxides and sulfones with 30% hydrogen peroxide under organic solventand halogen-free conditions. Tetrahedron; 57:2469-76 (**2001**)

**[12]** K. Sun, W. Jiang, X Ban et al, Novel aggregationinduced emission and thermally activated delayed fluorescence materials based on thianthrene-9,9',10,10'-tetraoxide derivatives. RSC Adv; 6: 22137- 43 (**2016**)

**[13]** M. Wroblowska, A. Kudelko, N. Kuznik et al, Synthesis of extended 1,3,4-oxadiazole and 1,3,4-thiadiazole derivatives in the Suzuki cross-coupling reactions. J Heterocycl Chem (**2016**)

**[14]** A. Arena, S. Campagna, A.M. Mezzasalma et al, Analysis of the phosphorescence of thianthren crystals. Il Nuovo Cimento;15(12): 1521-32 (**1993**)

# SYNTHESIS AND INVESTGATION OF MULTIFUNCTIONAL $GdPO_4$/Eu/Yb-Tm NANOPARTRICLES

Andrius Pakalniškis[1], Ramūnas Skaudžius[1]

[1]Institute of Chemistry, Vilnius University, Naugarduko 24, LT-03225 Vilnius, Lithuania
andrius.pakalniskis@chgf.vu.lt

Over the last couple of decades, biocompatible multifunctional magnetic and luminescent nanoparticles have received a lot of attention. Due to their possible applications in magnetic resonance and luminescent imaging, as possible drug carriers etc [1]. Most of these inorganic nanoparticles are rare-earth based materials due to their excellent magnetic and optical properties. Also, some of them are good host materials for dopant ions. One such material is $GdPO_4$ because of the phosphate groups on its surface that make it biocompatible and stable [2]. $Gd^{3+}$ ions have 7 unpaired 4f electrons resulting strong paramagnetic properties. Thus, the samples containing $Gd^{3+}$ ions are potential candidates for magnetic resonance imaging. Further gadolinium phosphate can be easily doped with other rare earth elements to make it a luminescent material as well. Europium is commonly used as a dopant because of its long decay times, narrow emission bands and orange-red light emission [3]. Other elements or even a combination of several dopants can be also used to make an upconverting system [4]. However the particles for bio applications have to be smaller than 100 nm in size, not agglomerated, and must be stable and have high luminescence intensity. Ions from the compounds must not leech into the organism. The small size of particles usually leads to low luminescence intensity but it can be increased by forming a core-shell system [5]. Also $GdPO_4$ particles of different size, shape and even of several crystal structures can be prepared. All of these factors influence the stability, as well as magnetic and luminescence properties. They can also affect the toxicity of the compound to the cells. For this reason a lot of research is still required.

In this work, rare-earth doped gadolinium phosphate was prepared using citric acid assisted hydrothermal synthesis. Effects of synthesis conditions and dopants were investigated. X-ray diffraction analysis was used to determine thermal stability and purity of obtained samples. Scanning electron microscopy and transmission electron microscopy were used to determine the shape and size of particles. Luminescence measurements of particles and their solutions were performed. Thermal gravimetric measurements were used in order to find the amount in the crystal hydrate.

**Acknowledgements.** This research is funded by the European Social Fund under the No 09.3.3- LMT K-712 "Development of Competences of Scientists, other Researchers and Students through Practical Research Activities" measure.

[1]Bohara, R.A., N.D. Thorat, and S.H. Pawar, *Role of functionalization: strategies to explore potential nano-bio applications of magnetic nanoparticles.* RSC Advances, 2016. **6**(50): p. 43989-44012.
[2]Dumont, M.F., et al., *DNA Surface Modified Gadolinium Phosphate Nanoparticles as MRI Contrast Agents.* Bioconjugate Chemistry, 2012. **23**(5): p. 951-957.
[3]Patra, C.R., et al., *Inorganic phosphate nanorods are a novel fluorescent label in cell biology.* Journal of Nanobiotechnology, 2006. **4**(1): p. 11.
[4]Ren, W., et al., *Lanthanide ion-doped GdPO4 nanorods with dual-modal bio-optical and magnetic resonance imaging properties.* Nanoscale, 2012. **4**(12): p. 3754-3760.
[5]Ansari, A.A., *Facile Synthesis Method for the Preparation of Large-scale Ultra-small GdPO4:Tb and GdPO4:Tb@LaPO4 Nanowires.* Journal of the Chinese Chemical Society, 2018. **65**(4): p. 490-496.

# NITROGEN-CONTAINING CYCLIC COMPOUNDS AS DERIVATIZATION REAGENTS IN TANDEM MASS SPECTROMETRY

Andrius Žilionis[1]

[1] Faculty of Chemistry and Geosciences, Vilnius University, Lithuania
andrius.zilionis@chf.vu.lt

Liquid chromatography – tandem mass spectrometry is one of the most powerful tools for determination of trace amounts of biological compounds. In comparison with scanning mass spectrometry measurements, a very high signal-to-noise ratio is achieved with selected reaction monitoring (SRM) detection, because the two levels of mass selection with narrow mass windows result in a very effective reduction in chemical noise [1]. As a result, an expected increase in sensitivity of one to two orders of magnitude over conventional mass spectrometry based approaches can be achieved [2]. While the first and the third quadrupoles act as mass filters to select a molecular ion of the analyte and a specific fragment ion of the analyte, the second quadrupole acts as collision cell where fragmentation takes place [1]. Since some compounds cannot be fragmented successfully because of their specific structure or the desired dissociation pathway giving the product ion of interest is only one of many dissociation pathways (thus limiting the abundance of desired product ion) [3], sensitive SRM detection of these analytes requires a specific derivatization.

In this work we present a comparison of five nitrogen-containing cyclic compounds as derivatization reagents for tandem mass spectrometric analysis of amino group-containing analytes. Five carboxylic acids were prepared by the reactions of commercially available starting materials (pyrrolidine, piperidine, 2,6-dimethylpiperidine, 1-methylpiperazine and morpholine) with bromoacetic acid as described elsewhere [4]. The carboxyl group of synthesized derivatization reagent was activated with 1-(3-dimethylaminopropyl)-3-ethylcarbodiimide/N-hydroxysuccinimide (EDC/NHS) followed by covalent attachment of the model analyte tryptamine by its primary amino group, thus forming an amide bond [5]. Reversed phase ultra-performance liquid chromatography (RP-UPLC) with gradient elution was used for separation of derivatized tryptamine and mass spectrometric detection was performed in both SRM and selected ion monitoring (SIM) modes. During SRM, amide bond cleaves and a proton remains associated with the basic nitrogen of derivatization reagent moiety while the carbonyl group undergoes neutral loss [6]. As a result, the product ion is produced. The release and stability of these product ions during collision induced dissociation process are of critical importance for the detection sensitivity and were investigated by increasing collision energy and measuring peak areas of corresponding product ions in SRM mode, while SIM mode was required for the normalization of SRM data of all five different product ions originated from five different molecular ions.

Our results demonstrate that the yields of corresponding product ions generated from pyrrolidine, morpholine and piperidine moieties are similar and they are significantly higher in comparison with the yields of corresponding product ions generated from 2,6-dimethylpiperidine and 1-methylpiperazine moieties. However, the total amount of product ion depends not only on the fragmentation process, but also on the molecular ion yield in an electrospray ionization (ESI) source. Since basic groups can be ionized easily during positive ESI and 1-methylpiperazine moiety contains more basic nitrogen atoms than any other moiety investigated, the highest molecular ion yield could be expected. Taking this into account, an additional experiment was performed in order to compare the effects of morpholine and 1-methylpiperazine moieties on positive ESI of derivatized tryptamine. RP-UPLC with isocratic elution was performed in order to assure the same ionization conditions for both derivatized compounds. EDC/NHS strategy could result in a variety of side products [7]. Since baseline separation of desired derivatization products was not achieved, active NHS esters of (4-methyl-1-piperazinyl)acetic acid and 4-morpholinylacetic acid were synthesized as described elsewhere [4]. Because NHS esters react with primary amino groups, the products of interest were the same as synthesized employing EDC/NHS strategy, but no ultraviolet (UV) absorbing side products were determined suggesting that all consumed tryptamine was converted to the desired products. Taking this into account, the areas of UV peaks were used for SIM and SRM data normalization. Surprisingly, morpholine moiety demonstrated higher ESI efficiency.

Considering both ionization of derivatized tryptamine and fragmentation of molecular ions processes, approximately two times higher product ion yield was obtained using morpholine moiety in comparison with 1-methylpiperazine moiety. Consequently, morpholine moiety was shown being a promising product ion source for the SRM detection of analytes which cannot be fragmented successfully without derivatization.

[1] V. Lange, P. Picotti, B. Domon et al., Selected reaction monitoring for quantitative proteomics: a tutorial, Molecular Systems Biology **4**, 1-14 (2008).
[2] X. Zhou, Y. Lu, W. Wang et al., "Fixed charge" chemical derivatization and data dependant multistage tandem mass spectrometry for mapping protein surface residue accessibility, Journal of the American Society for Mass Spectrometry **21**, 1339-1351 (2010).
[3] G. E. Reid, K. D. Roberts, R. J. Simpson et al., Selective identification and quantitative analysis of methionine containing peptides by charge derivatization and tandem mass spectrometry, Journal of the American Society for Mass Spectrometry **16**, 1131-1150 (2005).
[4] D. J. C. Pappin, S. Purkayastha, J. M. Coull, Isobarically labeled analytes and fragment ions derived therefrom, United States Patent No.: US 8,273,706 B2 (2012).
[5] N. J. de Mol, M. J. E. Fischer, *Surface Plasmon Resonance. Methods in Molecular Biology (Methods and Protocols)* (Humana Press, USA, 2010).
[6] S. Wiese, K. A. Reidegeld, H. E. Meyer et al., Protein labeling by iTRAQ: a new tool for quantitative mass spectrometry in proteome research, Proteomics **7**, 340-350 (2007).
[7] K. A. Totaro, X. Liao, K. Bhattacharya et al., Systematic investigation of EDC/sNHS-mediated bioconjugation reactions for carboxylated peptide substrates, Bioconjugate Chemistry **27**, 994-1004 (2016).

# EQUATIONS OF TEMPERATURE DEPENDENCE OF AN ENTHALPY AND AVERAGE HEAT CAPACITY FOR $EuCl_3 \cdot 6H_2O$

Anton Kozma

Department of Physical and Colloid Chemistry, Uzhhorod National University, Uzhhorod, Ukraine
Anton_Kozma@yahoo.com

In this work for europium chloride hexahydrate $EuCl_3 \cdot 6H_2O$ the equations of dependence of a molar enthalpy $H_T - H_{298.15}$ and average isobaric molar heat capacity $\overline{C_p}$ from absolute temperature $T$ are offered.

Now in literature [1] there are only of $EuCl_3 \cdot 6H_2O$ in temperature range 298.15–600.00 K given for true isobaric molar heat capacity $C_p$, but there are no equations for the description it $H_T - H_{298.15}$ and $\overline{C_p}$. In article [2] it is shown that $C_p$ and $\overline{C_p}$ are connected by a ratio:

$$C_p = \overline{C_p} + (T - 298.15)\frac{d\overline{C_p}}{dT} \quad (1)$$

It is also $\overline{C_p}$ possible to define from molar values of enthalpies [2]:

$$\overline{C_p} = (H_T - H_{298.15})/(T - 298.15) \quad (2)$$

From the publication [3] it is known, that the dependence $H_T - H_{298.15}$ on absolute temperature $T$ can be presented in the form $H_T - H_{298.15} = aT + bT^2 + cT^{-1} + d$, where *a, b, c, d* – coefficients. In this work, in view of results [2-4], the corresponding equations for $EuCl_3 \cdot 6H_2O$ are offered:

$$H_T - H_{298.15} = 366.909T + 0.007T^2 + 0.037 \cdot 10^7 T^{-1} - 111.257 \cdot 10^3 \quad (3)$$

$$H_T - H_{298.15} = 362T + 7 \cdot 10^{-3}T^2 + 37 \cdot 10^4 T^{-1} - 109794 \quad (4)$$

The equation (3) well describes data from the book I. Barin [1] (the maximum deviation does not exceed 0.13 %). To expression (4) we come on the basis of results [4]. Its maximum deviation is slightly higher (-1.36 %), if to compare with [1]. Additional examples are given in the table.

**Table.** Comparison of enthalpies of $EuCl_3 \cdot 6H_2O$ in the range 298.15–600.00 K, received at different approaches

| T, K | $H_T - H_{298.15}$, kJ/mol | $H_T - H_{298.15}$, kJ/mol | $\Delta(H_T - H_{298.15})$, % | $H_T - H_{298.15}$, kJ/mol | $\Delta(H_T - H_{298.15})$, % |
|---|---|---|---|---|---|
| | data [1] | by the equation (3) | | by the equation (4) | |
| 300.00 | 0.679 | 0.679 | 0.00 | 0.670 | -1.36 |
| 400.00 | 37.505 | 37.551 | 0.12 | 37.051 | -1.21 |
| 500.00 | 74.593 | 74.687 | 0.13 | 73.696 | -1.20 |
| 600.00 | 111.943 | 112.025 | 0.07 | 110.543 | -1.25 |

Note. In all considered cases at a temperature of 298.15 K an enthalpy $H_T - H_{298.15} = 0.000$ kJ/mol.



On the basis of the equations (3) and (4), having applied recommendations from [2, 3] and some results from [4], for $EuCl_3 \cdot 6H_2O$ formulas (5) and (6) describing the temperature course $\overline{C_p}$ is offered:

$$\overline{C_p} = 368.996 + 0.007T - 1240.986T^{-1} \quad (5)$$

$$\overline{C_p} = 364.087 + 0.007T - 1240.986T^{-1} \quad (6)$$

The maximum difference between the values, received when calculating behind the equations (5) and (6), does not exceed 1.34 %.

In conclusion we will note, that equation (4) and (6), received by means of a method [4], are perhaps less exact. However approach from [4] can be more universal. Likely with its help it is possible to predict heat capacity for many compounds $LnCl_3 \cdot 6H_2O$, where Ln – rare-earth metals.

[1] I. Barin (in collab. with G. Platzki). Thermochemical Data of Pure Substances. Weinheim: VCH (Germany), 3 ed., 1885 (1995).
[2] D. Sh. Tsagareishvili, G. G. Gvelesiani, V. P. Orlovsky, T. V. Belyavskaya, Enthalpy and thermal capacity of scandium and europium orthophosphates at high temperatures, Inorg. Mater. **11**, 491-493 (1975).
[3] D. Sh. Tsagareishvili, G. G. Gvelisiani, V. P. Orlovsky, T. V. Belyaevskaya, V. P. Repko, Enthalpy and thermal capacity of lanthanum, noedymium and yttrium orthophosphates under high temperatures, Inorg. Mater. **8**, 1790-1793 (1972).
[4] А.А. Козьма, Оцінка ізобарної теплоємності $EuCl_3 \cdot 6H_2O$ при температурах 298–600 К та її порівняння з відомими даними, IXth International scientific conference «Relaxed, nonlinear and acoustic optical processes and materials» – RNAOPM'2018, The first Volyn-Pomerania Interdisciplinary Summer School on «Art-Science Technology» – VPISSAST'2018, ISBN 978-966-940-159-5, Lutsk–Lake «Svityaz'», Ukraine, 64 (2018).

# SYNTHESIS AND APPLICATIONS OF DITHIADIAZOCANES

Arminas Jurys[1], Tomas Javorskis[2], Edvinas Orentas[1*]

[1] Department of Organic Chemistry, Vilnius University, Lithuania
[2] Department of Nanoengineering, Center for Physical Sciences and Technology, Vilnius, Lithuania
arminas.jurys@chgf.vu.lt

Saturated heterocyclic compounds containing two heteroatoms are privileged scaffolds for various pharmaceuticals. Among them, *S*,*N*-heterocyclic molecular scaffolds appear to be useful in designing potent antipsychotic (e.g. Quetiapine), antiarrhythmic (e.g. Diltiazem), anti-tumor (e.g. Prinomastat) and other biologically active agents [1]. Therefore, they remain to be important synthetic targets.

A collection of valuable (un)substituted *N*-protected cyclic eight-membered $C_2$-symmetric sulfenamides, 1,5,2,6-dithiadiazocanes, has been prepared in few steps from cheap and affordable starting materials. The synthetic utility of these ambipolar derivatives was demonstrated in a variety of synthetic transformations affording different *S*,*N*-heterocycles of pharmaceutical relevance (Fig.1).

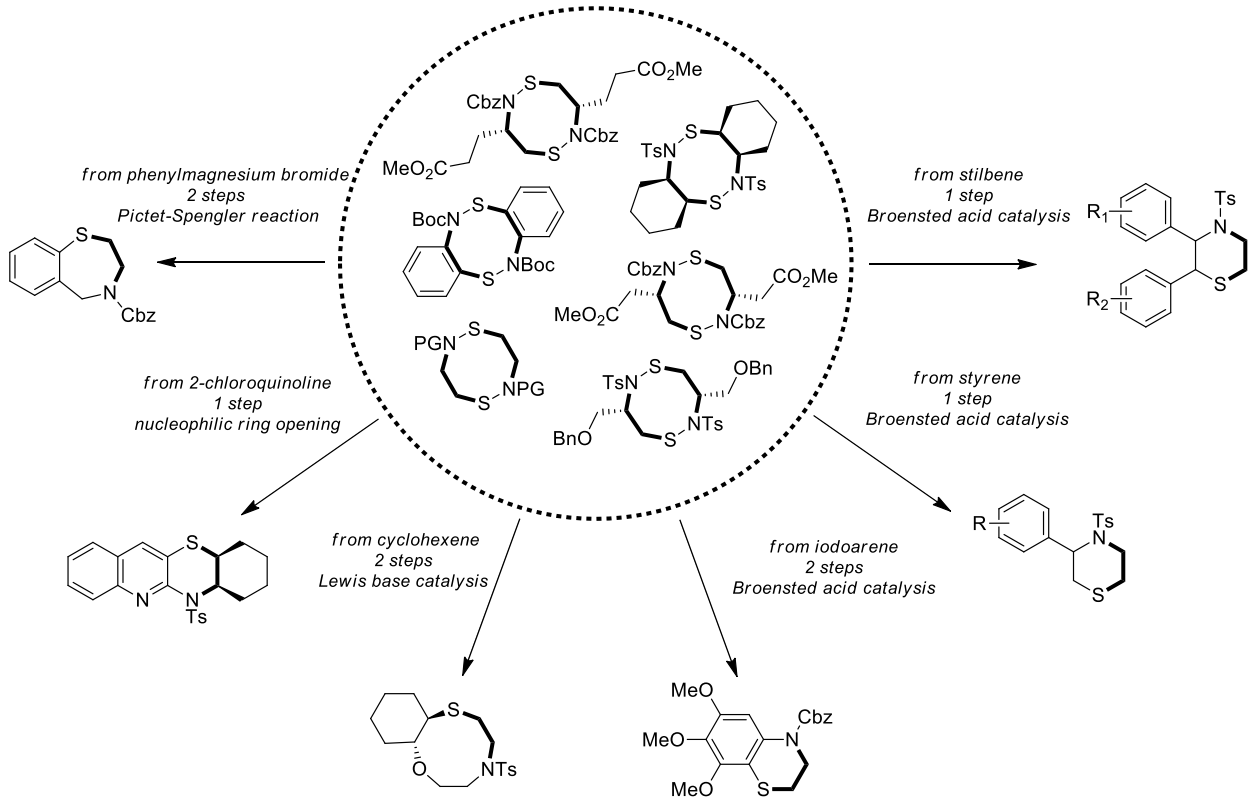


Fig. 1. 1,5,2,6-Dithiadiazocanes and some products available from them.

This research is funded by the European Social Fund under the No 09.3.3-LMTK-712 “Development of Competences of Scientists, other Researchers and Students through Practical Research Activities” measure.

[1] R. Fringuelli, L. Milanese, F. Schiaffela, Role of 1,4-Benzothiazine Derivatives in Medicinal Chemistry, Mini-Reviews in Medicinal Chemistry **5**, 1061 (2005).

# INVESTIGATION OF DOPANT EFFECT ON POLYPYRROLE TEXTILE COMPOSITES

Augustas Šukys[1], Monika Kirsnytė[1], Paulius Ragulis[2], Rimantas Simniškis[2], Žilvinas Kancleris[2], Raimonda Celiešiūtė-Germanienė[1], Arūnas Stirkė[1]

[1] Department of Material Science and Electrical Engineering, Center for Physical Sciences and Technology, Lithuania
[2] Department of Physical Technologies, Center for Physical Sciences and Technology, Lithuania,
augustas.sukys@chf.stud.vu.lt

Due to increased importance of information technology in communication field a huge attention has been focused on electromagnetic radiation (EMR) absorbers. Among well researched conjugated polymers, polypyrrole (PPy) is a cheap and tunable organic semiconductor which can be incorporated into fabrics to create flexible electronics or EMR shielding materials [1]. The aim of this work is to enhance conductivity of PPy by adding anionic dopants to create promising electrically conductive composite films for smart textile industry [2].

Two types of experiments were carried out: when dopant is in matrix and catalyst polymer solution or when dopant is in pyrrole (Py) monomer solution. 4 different dopants were used: sodium dodecyl sulfate (SDS), sodium polystyrene sulfonate (PSSNa), sodium dodecylbenzene sulfonate (DBSNa) and dioctyl sodium sulfosuccinate (DOSS). Composites were synthesized with only one dopant and on a dielectric woven wool substrate coated with polymerization reaction catalyst $FeCl_3$ evenly distributed throughout PVA (polyvinyl alcohol) adhesive polymeric matrix using screen printing with particular 3 x 3 cm square pattern. Coated specimens were dried at 60 °C then spray-coated with monomer Py and water solution and after quick polymerization reaction dried again at 60 °C.

Experimental investigations of manufactured samples have been performed using an analytical model of electromagnetic wave shielding effectiveness calculations in 8-40 GHz frequency range. Composites were characterized using scanning electronic microscopy and Fourier-transform infrared spectroscopy.

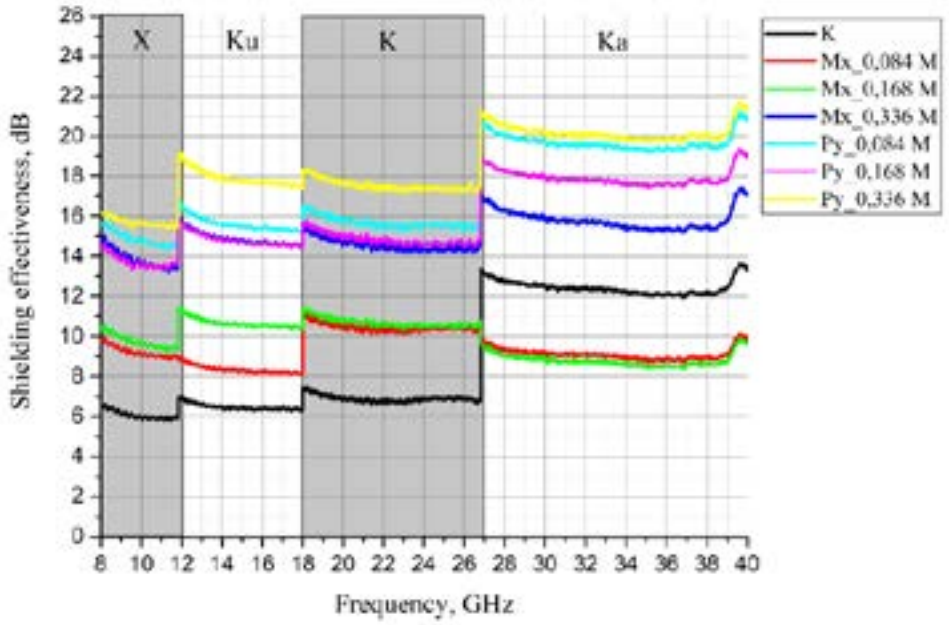


Fig. 1. Shielding effectiveness of PPy doped with SDS respectively 0,084 M; 0,168 M; 0,336 M, on woven wool in 8-40 GHz frequency range. K – no dopants; Mx – dopant is in the matrix solution; Py – dopant is in the Py monomer solution.

In conclusion, the most promising composite was achieved using SDS dopant with 0,336 M concentration, when dopant was in Py monomer solution. Comparing this composite with sample with no dopants, shielding effectiveness was improved approximately by ~9 dB. These results give a bedrock for doped polymer composites use in smart textile industry which can be used to develop commercially available flexible electronics.

[1] Takamatsu, S., et al., *Wearable Keyboard Using Conducting Polymer Electrodes on Textiles.* Adv Mater, 2016. **28**(22): p. 4485-8.
[2] Hazarika, J. and A. Kumar, *Controllable synthesis and characterization of polypyrrole nanoparticles in sodium dodecylsulphate (SDS) micellar solutions.* Synthetic Metals, 2013. **175**: p. 155-162.

# MOLECULAR DYNAMICS STUDY OF HYDROGEN BONDING IN $H_3PO_4$-$H_2O$ SYSTEMS

Austėja Mikalčiūtė, Linas Vilčiauskas

Institute of Chemistry, Faculty of Chemistry and Geosciences, Vilnius Univesity, Lithuania
austeja.mikalciute@chf.stud.vu.lt

Phosphoric acid ($H_3PO_4$) and water ($H_2O$) are well-known inorganic compounds, which have caught scientists' attention for their proton transfer mechanisms. Liquid $H_3PO_4$ has the highest intrinsic proton conductivity of all materials and $H_2O$ is the most important substance in nature and environment. Therefore, molecular studies of these compounds and their mixtures provide important insights into their structures and dynamics. We present a molecular dynamics study of hydrogen bonding in liquid $H_3PO_4$-$H_2O$ systems at different concentrations using GROMACS software package. A number of different generic force fields such as OPLS, GAFF, GROMOS 54, GROMOS 87, GROMOS 96 are tested and benchmarked for suitability in terms of agreement between various static and dynamical simulated and experimental properties: liquid densities, radial distribution functions (RDF), diffusion constants [1,2]. The most promising results for the description of hydrogen bonding have been achieved using the GAFF force field: density is determined with 3.15% relative error and the covalent bond peak (1.00Å) and hydrogen bond peak (1.58Å) in $g_{HX(X=O,\ P)}(r)$ close to experimental values of 0.98Å and 1.58Å, respectively. SPC/EF model is used for modeling water. A number of systems having 1:0, 3:1, 1:1, 1:3, 1:6 and 0:1 $H_3PO_4$-$H_2O$ ratios have been constructed and compared in terms of RDF, diffusivity and its activation energy. The RDF analysis shows that first and second solvation shells in 3:1, 1:1 and 1:3 $H_3PO_4$-$H_2O$ mixtures are almost identical to those of pure $H_3PO_4$ rather than $H_2O$, with maximums slowly but gradually shifting from those of pure $H_3PO_4$ towards the ones' accordingly seen in $H_2O$. A special analysis tool written in C++ for the hydrogen bonding in terms of bond lengths and angles for different hydrogen bonded species in these systems is developed and used for a more sophisticated analysis.

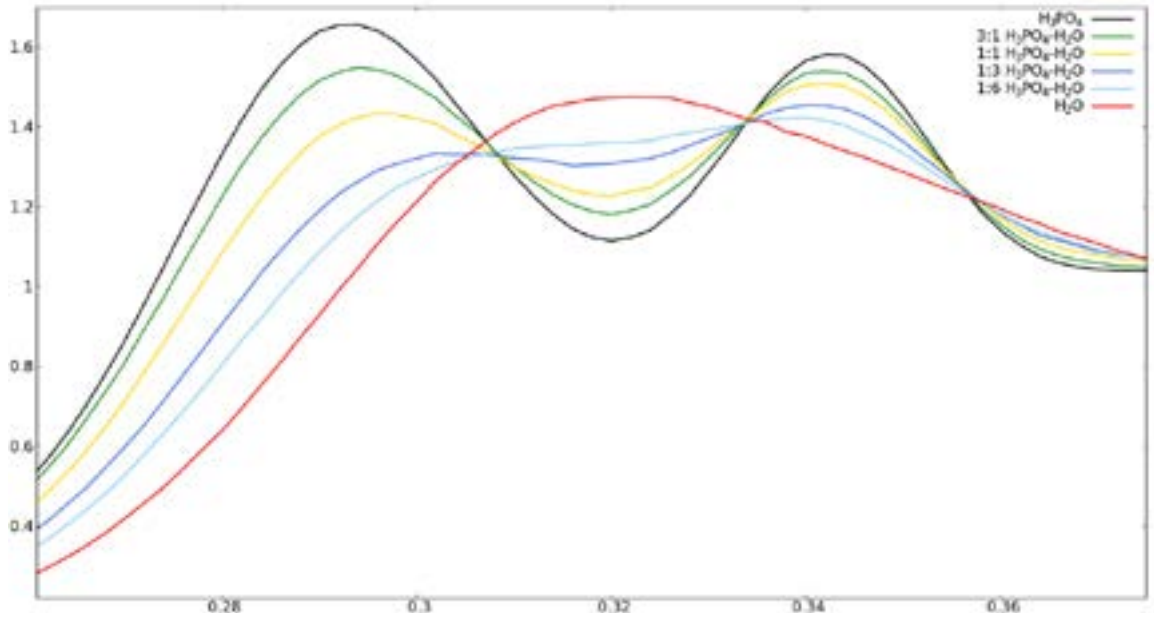


Fig 1. Second solvation shell in $g(r)_{HO}$ comparison of various $H_3PO_4$-$H_2O$ systems based on molecular dynamics simulations.

[1] Vilčiauskas, L. *Proton Transport Mechanisms of Phosphoric Acid and Related Phosphorus Oxoacid Systems: A First Principles Molecular Dynamics Study* (Doctoral dissertation, Universit¨at Stuttgart, Stuttgart, Germany), 46 (2012). Retrieved from https://d-nb.info/1021923397/34.

[2] Egan, E.P. & Luff, B.B., Measurements at 15° to 80° C. - Density of Aqueous Solutions of Phosphoric Acid, *Ind. Eng. Chem., 47(6)*, 1280—1281 (1955).

# (BI)PHENYL SUBSTITUTED 9-(2,2-DIPHENYLVINYL)CARBAZOLES AS LOW COST HOLE TRANSPORTING MATERIALS FOR EFFICIENT RED PHOLEDS

Daiva Tavgenienė[1], Saulius Grigalevičius[1], Gintarė Kručaitė[1], Raimonda Grinienė[1], Dovydas Blaževičius[1], Marius Eidimtas[1], Yen-Po Wang[2], Shang-Ru Tsai[2], Chih-Hao Chang[2]

[1] Department of Polymer Chemistry and Technology, Kaunas University of Technology, Lithuania
[2] Department of Photonics Engineering, Yuan Ze University, Taiwan
daiva.tavgeniene@ktu.lt

Phosphorescent organic light emitting diodes (PhOLEDs) have attracted much attention because they use both singlet and triplet excitons for generation of light, making 100% internal quantum efficiency possible. Achieving the high level internal quantum efficiency depends on several factors, including high quantum yield emitters, exothermic energy transfer from host to emitter, effective exciton confinement as well as balanced carrier transport [1, 2]. It is well known that carrier transporting materials are crucial to enable a balance carrier transport from cathode and anode [3]. Considerable exertion is needed for the development of efficient red PhOLED devices, because the lower gap of red phosphors usually induces serious carrier trapping, leading to higher operation voltages and carrier imbalance [4]. Accordingly, it is desirable to exploit new hole transport materials to create red PhOLEDs with reduced power consumption and improved efficiency.

In this study, the new low cost 9-(2,2-diphenylvinyl)carbazole-based derivatives with aryl substitutions were synthesized and investigated. Our previous study found that introducing the diphenylvinyl fragment in carbazole ring could increase spatial hindrance of the moiety and the derivatives could be used for the preparation of thin and stable amorphous layers on substrates [5]. The synthesis of phenyl or 4-biphenyl substituted 9-(2,2-diphenylvinyl)carbazole based derivatives (6 and 7) was carried out by synthetic route, which is shown in Scheme 1.

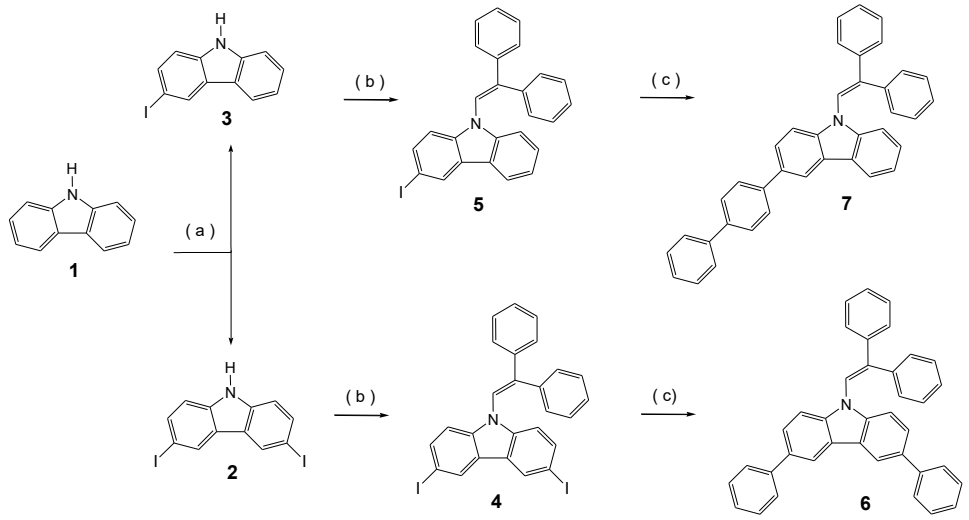


Scheme 1. a) KI, $KIO_3$, acetic acid; b) 2,2-diphenylacetaldehyde, (±)-camphor-10-sulfonic acid, toluene; c) $Pd(PPh_3)_2Cl_2$, KOH, THF, phenyl boronic acid for compound 6 or 4-biphenyl boronic acid for compound 7.

We have examined the novel hole transporting materials in the fabrication of red PhOLEDs. The respective peak efficiencies were recorded at 8.7 % (5.6 cd/A and 3.9 lm/W) and at 8.7 % (5.4 cd/A and 3.8 lm/W), correspondingly, for the devices using 3,6-diphenyl-9-(2,2-diphenylvinyl)carbazole (6) and 3-(4-biphenyl)-9-(2,2-diphenylvinyl)carbazole (7) as hole transporting materials. The high efficiencies of the red PhOLEDs suggest great potential of the new (2,2-diphenylvinyl)carbazole based electroactive materials for applications in OLED devices.

[1] C.-H Chang, C.-L. Ho, Y.-S. Chang et al., Blue-emitting Ir(III) phosphors with 2-pyridyl triazolate chromophores and fabrication of sky blue- and white-emitting OLEDs, Journal of Materials Chemistry C **1**, 2639-2647 (2013).
[2] J. Huang, B. Xu, J. H. Su et al., Efficient blue lighting materials based on truxene-cored anthracene derivatives for electroluminescent devices, Tetrahedron **66**, 7577-7582 (2010).
[3] J. Huang, J. H. Su, H. Tian. The development of anthracene derivatives for organic light-emitting diodes, Journal of Materials Chemistry **22**, 10977-10989 (2012).
[4] C.-H Chang, Y.-H. Lin, C.-C. Wu et al., Efficient phosphorescent white organic light-emitting devices incorporating blue iridium complex and multifunctional orange–red osmium complex, Organic Electronics **10**, 1235-1240 (2009).
[5] R. Griniene, J. V. Grazulevicius, K. Y. Tseng et al. Aryl substituted 9-(2,2-diphenylvinyl)carbazoles as efficient materials for hole transporting layers of OLEDs, Synthetic Metals **161**, 2466-2470 (2011).

# LANTHANIDE COMPLEXES BASED ON TWO TYPES OF PHOSPHORYLCONTAINING "ANTENNA" LIGANDS

Darya Kuzmina[1], Nataliia Kariaka[1], Viktoriya Dyakonenko[2], Sergii Smola[3], Vladyslav Lavrenchuk[1], Victor Trush[1].

[1]Department of Chemistry, Taras Shevchenko National University of Kyiv, Ukraine
[2]SSI "Institute for Single Crystals", National Academy of Sciences of Ukraine, Ukraine
[3]A.V. Bogatsky Physicochemical Institute, National Academy of Sciences of Ukraine, Ukraine
kuzmina_darya@knu.ua

Carbacylamidophosphates (CAPh) are well known class of powerful chelating ligands which can be considered as structural analogues of β diketones. They can serve as an "antenna" for enhancing of Ln(III) luminescence by providing efficient absorption of energy and its transfer to the lanthanide ion [1]. The lanthanide complexes are intensively investigated as components of luminescent materials [2]. Besides the coordination to the metal ion and sensitization of the lanthanide *4f*luminescence CAPh compounds are also known due to their wide range of biological activity [1].

The present study aimed synthesis and investigation of new luminescent mixed ligand lanthanide(III) complexes containing CAPh type ligand - dimethyl-N-benzoylamidophosphate (HL) - and the monodentate ligand triphenylphosphine oxide (TPPO) as an additional antenna. The coordination compounds under consideration were synthesized by the exchange-accession reactions from non-aqueous solutions according to the following scheme:

$$Ln(NO_3)_3 \cdot nH_2O + 3NaL + TPPO \rightarrow LnL_3TPPO + 3NaNO_3 + nH_2O$$

The obtained complexes of the general formula $LnL_3TPPO$ ( $Ln^{3+}$ = $Pr^{3+}$, $Nd^{3+}$, $Eu^{3+}$, $Gd^{3+}$, $Tb^{3+}$, $Lu^{3+}$) were characterized by X-ray and TG analysis, IR, $^1$H NMR, UV-Vis absorption and luminescent spectroscopy. By means of X-ray diffraction method for the complex $TbL_3TPPO$ (Fig. 1) it was found, that lanthanide(III) ion is bonded to three bidentate chelate CAPh-ligands through oxygen atoms of the carbonyl and phosphoryl groups and to the oxygen atom of one TPPO ligand completing coordination number of terbium ion to seven. The coordination environment of the central ion can be described as a distorted pentagonal bipyramid. The compound $TbL_3TPPO$ crystallizes in triclinic space group P-1, each unit cell contains two molecules of the complex. In crystal packing, there are numerous short contacts between neighboring molecules of the complex.

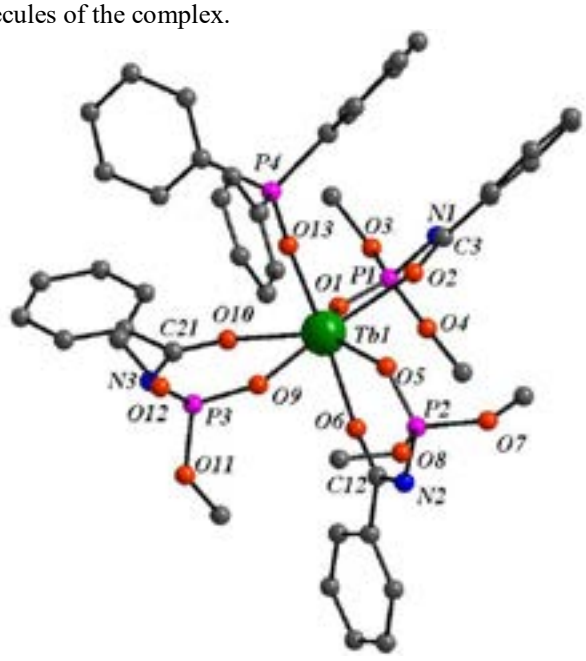


Fig. 1. Molecular structure of $TbL_3TPPO$ complex (H atoms are omitted for clarity).

[1] P. Gawryszewska and P. Smolenski, *Ligands synthethis, characterisation and role in biotechnology* (Nova Science Publishers, New York, 2014).
[2] K. Binnemans, Lanthanide-based luminescent hybrid materials, Chem. Rev., **109**, 4283-4374 (2009).

# CONFORMATIONAL STRUCTURE AND IR SPECTRUM OF THE METHYL HYDROPEROXIDE

Darya Kisurina[1], Vladimir Sapeshko[2], Ekaterina Kozlovskaya[1], George Pitsevich[1], Vytautas Balevicius[3]

[1] Belarusian State University, Minsk, Belarus
[2]University of Illinois at Chicago, Chicago, USA
[3]Vilnius University, Vilnius, Lithuania
kisurinadasha@gmail.com

Methyl hydroperoxid ($CH_3OOH$) belongs to the class of non-rigid molecules. During the rotation of the hydroxyl group in relation to the peroxide bond, two equivalent configurations of the molecule are formed. Plane, that is formed by the three heavy atoms (COO), is occurs to be the symmetry plane for the trans- (Fig.1) and cis- configurations, which are the transition states of the molecule.

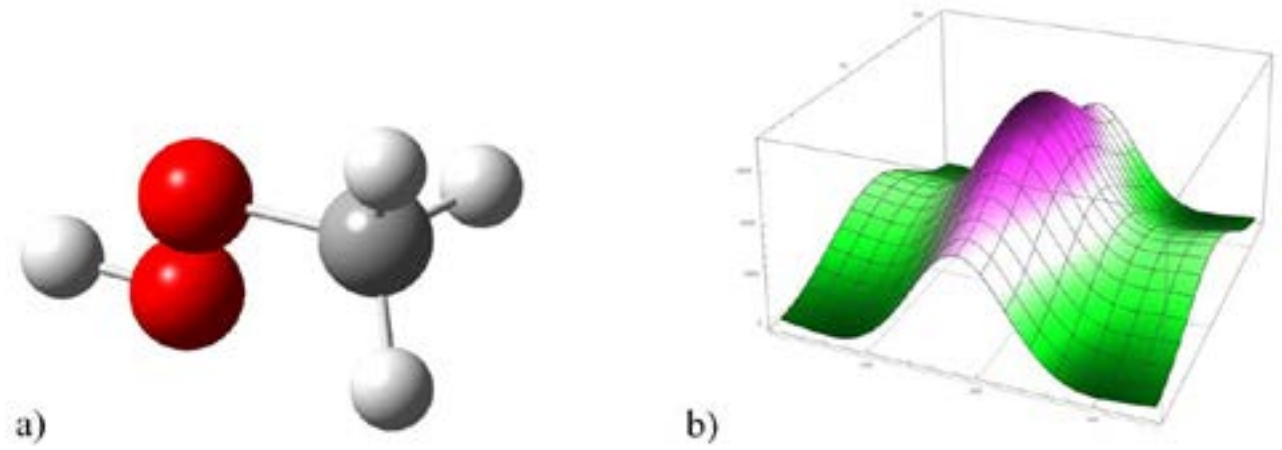


Fig.1. Trans-conformation of the methyl hydroperoxide molecule (a) and 2D PES, constructed during the variation of two torsion angles (b).

Two equivalent equilibrium configurations of the molecule are gosh-conformers. The molecule is characterized by the internal rotation of hydroxyl and methyl groups. Equilibrium configuration of $CH_3OOH$ was calculated at the MP2/acc-pVTZ level of theory. Value of C-O-O-H dihedral angle occurred to be close to 120°, and length of the peroxide O-O bond occurred to be equal to 1.456 Å. With this, methyl group loses the $C_{3V}$ symmetry. In particular, values of three O-C-H angles occur to be equal to 110, 109 и 104°, and the difference between the C-H bonds – approximately 0.001 Å. These lead to vanishing of degeneracy of the antisymmetric stretching C-H bonds vibrations, which frequencies occur to be equal to 3151 and 3178 $cm^{-1}$. Calculated in the harmonic approximation frequency values of the torsion vibrations are 170 and 261 $cm^{-1}$ for hydroxyl and methyl groups correspondingly. For more accurate evaluation of the torsion vibrations frequencies of methyl hydroperoxide molecule, calculations of 2D potential energy surface, caused by variation of two torsion coordinates, were performed (see Fig. 1b). As can be seen from Fig. 1b, trans-barrier is significantly lower than cis-barrier. Their values, according to calculations, are 102 and 2001 $cm^{-1}$. Height of the potential barrier of methyl group rotation is around 1000 $cm^{-1}$. Calculations of the torsion vibrations frequencies were performed.

# CALCIUM ALGINATE-BASED DRESSINGS FOR CONTROLLED DRUG DELIVERY

Deimantė Narauskaitė, Odeta Baniukaitienė

Department of Polymer Chemistry and Technology, Kaunas University of Technology, Lithuania
deimante.narauskaite@ktu.edu

Sodium alginate (AL) is a salt of alginic acid, a linear polysaccharide composed of 1,4-linked β-D-mannuronic acid and α-L-guluronic acid residues. Due to its gelling properties, biocompatibility, non-toxicity, biodegradability, AL is the most extensively studied material for the preparation of polymeric membrane dressings.

In this study, calcium alginate with immobilized lidocaine hydrochloride (Ca-AL-LiDHCl) and hybrid membranes with hyaluronic acid (Ca-AL-HA-LiDHCl) were prepared. Polymeric membranes were plasticized by glycerol and further cross-linked with divalent ions using calcium lactate as a source of calcium ions.

The thickness of the membranes was measured with a micrometer (293 MDC-MX, Mitutoyo Co., Kawasaki, Japan). The results showed that HA affected the thickness of the prepared membrane dressings. Ca-AL-HA-LiDHCl membranes were slightly thicker due to HA ability to absorb and hold water, as supposed. The thickness of prepared Ca-AL-HA-LiDHCl and Ca-AL-LiDHCl membranes was 0.38 mm and 0.35 mm, respectively.

The mechanical properties were determined using a universal material testing machine Zwick/Roell BDO-FB O.5 TH (Zwick, GmbH & Co, Ulm, Germany). The strips of the films had a length of 7 cm and a width of 2 cm. Computer Software V11.02 TestXpert provided the percentage elongation at break (EB, %) and tensile strength (TS, MPa) values. The results showed that HA considerably increased elongation at break values, as compared with Ca-AL-LiDHCl (Fig. 1.).

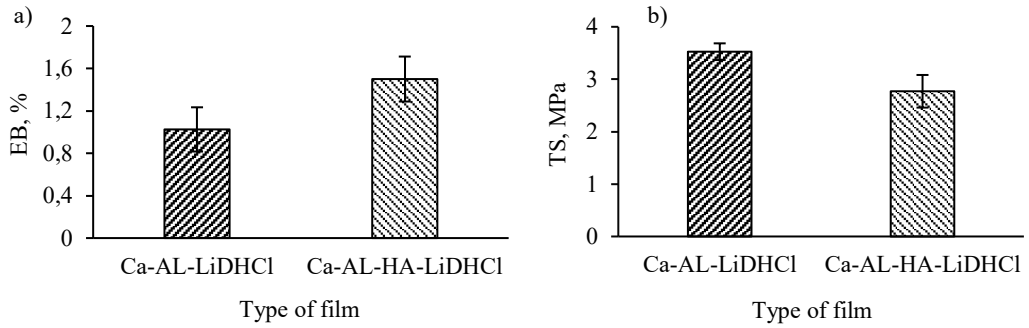


Fig. 1. Mechanical properties of membrane a) EB, % b) TS, MPa

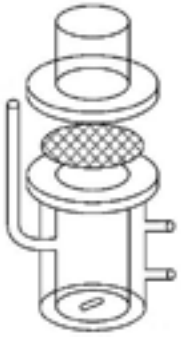

Fig. 2. Franz cell

LiDHCl release kinetics from hybrid membranes was carried out using Franz cell (Fig. 2.). The amount of released drug was determined spectrophotometrically (Cary 50 UV–VIS, Varian, Inc., Netherlands). The release profile of LiDHCl from Ca-AL-HA-LiDHCl and Ca-AL-LiDHCl hybrid membranes in a 0.9 % NaCl solution at 37 °C showed that 50 % of total LiDHCl was released after 6 h.

# INVESTIGATION OF INTERACTIONS BETWEEN CHITOSAN AND CAFFEOYLQUINIC ACID DERIVATIVES OF GREEN COFFEE BEAN EXTRACT

Deimante Simanaviciute[1], Vesta Navikaite-Snipaitiene[1], Ramune Rutkaite[1], Liudas Ivanauskas[2], Valdas Jakstas[3], Véronique Coma[4]

[1] Department of Polymer Chemistry and Technology, Kaunas University of Technology, Lithuania
[2] Department of Analytical and Toxicological Chemistry, Lithuanian University of Health Sciences, Lithuania
[3] Department of Pharmacognosy, Lithuanian University of Health Sciences, Lithuania
[4]University of Bordeaux, UMR 5629, CNRS, LCPO, France
deimante.simanaviciute@ktu.lt

Polyphenols are abundant secondary metabolites in plants and are known to prevent diseases associated with oxidative stress and its related complications. Chlorogenic acid is the main phenolic compound in green coffee bean extract (GCBE) (approximately 60%). It can exist in the form of three different isomers, namely, i.e. 3-*O*-caffeoylquinic acid, 5-*O*-caffeoylquinic acid and 4-*O*-caffeoylquinic acid [1, 2]. The effectiveness of caffeoylquinic acid derivatives (CQ) depends on preserving their stability, bioactivity and bioavailability. One of the ways to protect those anionic phenolics could be their immobilization on cationic polymers such as chitosan (ChS).

In the present study, the formation of water insoluble complexes between ChS and phenolic compounds such as CQ, present in the green coffee bean extract (GCBE) has been investigated and the adsorption of GCBE on ChS has been studied. The Langmuir adsorption model has been used to describe the equilibrium adsorption of GCBE components from the initial aqueous solution on ChS at different temperatures (Fig. 1a).

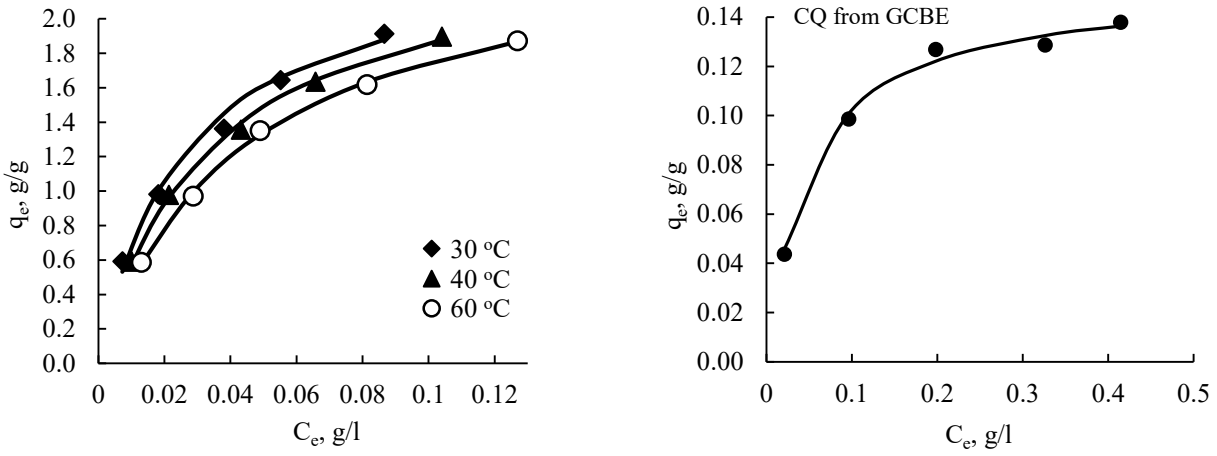


(a) (b)

Fig. 1. Adsorption isotherms of: (a) – GCBE on ChS at different temperatures, (b) – CQ adsorbed from GCBE on ChS at temperature of 30 °C. Symbols represent experimental data and lines represent fitted curves of the Langmuir adsorption model.

The UPLC and HPLC procedures were used to determine the composition of GCBE as well as to estimate the amounts of CQ adsorbed on ChS (Fig. 1b). The chromatographic analysis results clearly proved that not only CQ, but also various other phenolic compounds were adsorbed on ChS.

The antioxidant activity of the formed GCBE/ChS complexes was studied. It was demonstrated that the immobilization of active components of the natural extract effectively prevented the rapid loss of antioxidant activity over the time.

Acknowledgement. The financial support of the Research Council of Lithuania for the Lithuanian-French programme "Gilibert" project No. S-LZ-19-6 is highly acknowledged.

[1] D. Bagdas, N. Cinkilic, H.Y. Ozboluk, M.O. Ozyigit, M.S. Gurun, Antihyperalgesic activity of chlorogenic acid in experimental neuropathic pain, Journal of Natural Medicines **67** 698-704 (2013).
[2] N. Nakatani, S.I. Kayano, H. Kikuzaki, K. Sumino, K. Katagiri, T. Mitani, Identification, quantitative determination, and antioxidative activities of chlorogenic acid isomers in prune (*Prunus domestica L.*), Journal of Agricultural and Food Chemistry **48** 5512-5516 (2000).

# EFFICIENT CROSS-LINKABLE FLUORENE-BASED ENAMINES AS HOLE TRANSPORTING LAYERS

Deimantė Vaitukaitytė[1], Giedrė Bubnienė[1], Artiom Magomedov[1], Egidijus Kamarauskas[2], Vygintas Jankauskas[2], Vytautas Getautis[1]

[1] Department of Organic Chemistry, Kaunas University of Technology, Lithuania
[2] Institute of Chemical Physics, Vilnius University, Lithuania
d.vaitukaityte@gmail.com

During the past several years perovskite solar cell (PSC) technology has evolved from a scientific curiosity to a major research subject in the field of photovoltaics. In that short period of time they have gained recognition as one of the most promising photovoltaic technologies and managed to demonstrate remarkable achievements in the power conversion efficiency (PCE) exceeding 20% [1]. These results have been obtained by using 2,2′,7,7′-tetrakis(N,N-di-p-methoxy-phenylamine)-9-9′-spirobifluorene (Spiro-OMeTAD) as hole transporting material (HTM). However, it is not only quite expensive but also shows unsatisfactory long-term stability due to oxidative doping process and slow morphological degradation. In addition, it cannot effectively protect the underlying perovskite layer from the moisture penetration [2]. Formation of the cross-linkable HTM layers by a spin-coating process may serve as a promising concept to avoid several issues, associated with the use of the Spiro-OMeTAD.

In this work, fluorene-based enamines functionalized with two vinylbenzyl ether groups, named **HTM1** and **HTM2**, are presented as the building block for the cross-linkable hole transporting layers (Figure 1). Synthesis of the investigated materials was performed by a simple two-step synthetic procedure from commercially available 2-aminofluorene and 2,7-diaminofluorene providing target products in high yield. The isolated materials demonstrate good thermal stability: the 5% weight loss temperature ($T_{dec}$) of 382 °C is observed for compound **HTM1** and 393 °C for **HTM2**.

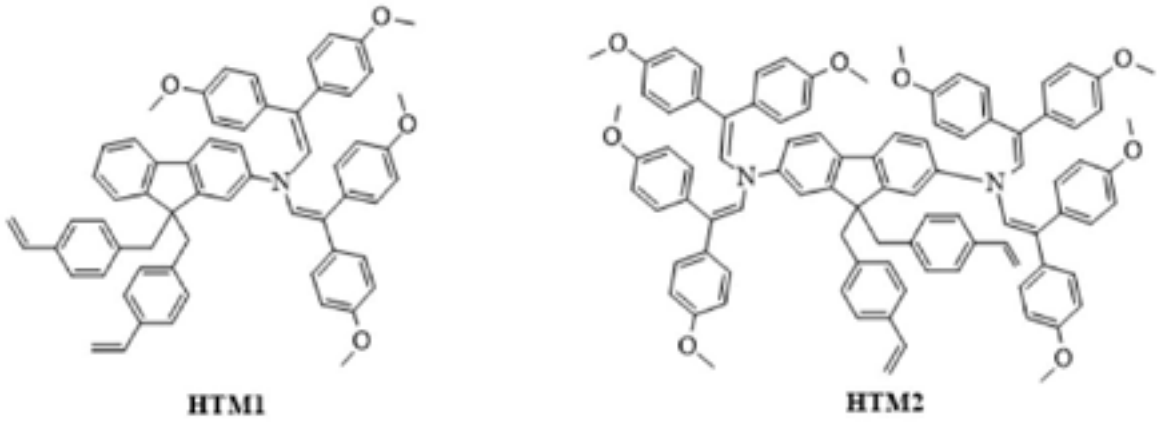


**Figure 1**. Structures of cross-linkable fluorene-based enamines **HTM1** and **HTM2**.

To investigate photoelectrical properties of synthesized HTMs hole drift mobility and ionization potential were measured. Photoelectron spectroscopy in air method was used to measure ionization energy ($I_p$). **HTM1** demonstrates higher ionization energy (5.26 eV). Additional electron donating enamine groups (**HTM2**) lower $I_p$ by 0.15 eV. $I_p$ of both compounds is suitable for the application in the PSCs. Charge transport properties of the investigated HTMs were measured using xerographic time-of-flight technique. **HTM1** has demonstrated comparable hole mobility with Spiro-OMeTAD, while **HTM2** showed significantly higher hole drift mobility ($10^{-3}$ $cm^2/Vs$) at strong electric fields.

The cross-linking of **HTM2** was investigated using differential scanning calorimetry analysis (DSC). The first heating curve shows the cross-linking process starting at 190 °C and ending at 239 °C. There are no transitions observed during the cooling or second heating cycle of **HTM2**, from which it can be concluded that the cross-linking reaction was complete during the first heating cycle. However, the thermal cross-linking condition for vinyl groups requires a relatively high temperature, which already exceeds the temperature limit that perovskite can tolerate [2]. In order to lower the cross-linking temperature an aliphatic cross-linker containing four thiol groups, pentaerythritol tetrakis(3-mercaptopropionate) (PETMP), was used. DSC was employed to study the cross-linking between **HTM2** and PETMP. The cross-linking temperature was observed from 122 to 141 °C during the first scan. These results imply the fast and complete thermal cross-linking occurs due to the facile thiol-ene reaction.

Thus, synthesized fluorene-based HTMs have potential to become useful materials for protecting the effective underlying perovskite layer in the PSCs.

[1] W. S. Yang, B. W. Park, E. H. Jung et al., Iodide management in formamidinium-lead-halide-based perovskite layers for efficient solar cells, Science **356**, 1376-1379 (2017). https://doi.org/10.1126/science.aan2301.
[2] Z. Li, Z. Zhu, C. C. Chueh et al., Facile Thiol-Ene Thermal Crosslinking Reaction Facilitated Hole-Transporting Layer for Highly Efficient and Stable Perovskite Solar Cells, Adv. Energy Mater. **1601165** (2016). https://doi.org/10.1002/aenm.201601165.

# THE INFLUENCE OF GRANITE DUST ADDITIVE ON THE PROPERTIES OF CEMENT MORTAR

Domante Niuniavaite, Tadas Dambrauskas, Kestutis Baltakys
Department of Silicate Technology, Kaunas University of Technology, Lithuania
domante.niuniavaite@ktu.edu

Recycling of construction and industrial waste in the production of building materials is considered to be one of the most alternative and promising ways of waste management. Waste, such as concrete rubble, bricks, tiles, construction dust, bulk aggregates, etc., account for about 80-85% of all construction waste and can be reused, especially if the waste itself contains accumulated waste energy. Recycling of construction waste not only reduces the area of occupied land but also reduces the consumption of natural resources [1-2]. One of the construction reusing materials is granite cutting waste. The granite stone preparation process generates a large amount of waste (about 30% of total global production) such as granite rubble of varying sizes, cuts and dust. Due to the enormous amount of waste, environmental hazards and high-performance characteristics, the use of granite stone waste in the cement mortar industry is an excellent alternative to dealing with waste reusing [3-5]. Thus the aim of this work was to determine the of granite cutting waste on the strength properties of concrete and on the formation of hydration products.

The mixtures of modified cement mortals were formed of ordinary Portland cement, three different fractions of sand, granite cutting waste and plasticizer additive (Table 1).

**Table 1.** The composition of the mixture of modified cement mortar

| Mixture | wt. % of components in the mixture | | | | | |
|---|---|---|---|---|---|---|
| | CEM I 42.5 N | Fraction of sand | | | Plasticizer | Granite cutting waste |
| | | 0/0.5 | 0.5/1 | 1/4 | | |
| GCW0 | 15 | 20.0 | 30.0 | 34.9 | 0.1 | 0 |
| GCW 2 | | 19.0 | 29.0 | | | 2 |
| GCW 5 | | 17.5 | 27.5 | | | 5 |
| GCW 7 | | 16.5 | 26.5 | | | 7 |
| GCW 10 | | 15.0 | 25.0 | | | 10 |
| GCW 12 | | 14.0 | 24.0 | | | 12 |
| GCW 15 | | 12.5 | 22.5 | | | 15 |
| GCW 20 | | 10.0 | 20.0 | | | 20 |
| GCW 25 | | 7.5 | 17.5 | | | 25 |
| GCW 30 | | 5.0 | 15.0 | | | 30 |

It was determined, that the highest compressive strength after 28 days of hydration was achieved sample with 12 % granite dust (24.65 MPa). It is worth mentioning that obtained values match requirements of the EN 13813 standard and samples can be assigned to C25 strength class. The hydration products were characterized by XRD and STA analysis.

1. Kaminskas A., Kaminskas R. Statybinės medžiagos iš technogeninių žaliavų. Mokslo monografija. Technologija, Kaunas, 2010, 386p.
2. Naujokaitis A. Statybinės medžiagos. Sausieji statybiniai mišiniai. Technika, Vilnius, 2010, 364 p.
3. Arulraj G. P., Adin A., Kannan T. S. Granite powder concrete. IRACST – Engineering Science and Technology: An International Journal (ESTIJ), 2013, vol.3, p. 193–198.
4. Felixkala T., Partheeban P. Granite powder concrete. Indian Journal of Science and Technology, 2010, vol. 3, p 311–317.
5. Arulraj G. P., Adin A., Kannan T. S. Granite powder concrete. IRACST – Engineering Science and Technology: An International Journal (ESTIJ), 2013, vol.3, p. 193–198.

# STUDY OF GHYPHOSATE ADSORBTION ON THIN POLYPYRROLE LAYER AND ON 11-(1H-PYRROL-1-YL)UNDECANE-1-THIOL MONOLAYER FORMED POLYPYRROLE AND COMPARISON

Domas Balčiūnas[1], Deivis Plaušinaitis[1]

[1]Vilnius University, Faculty of Chemistry and Geosciences, Institute of Chemistry, Department of Physical Chemistry, 24 Naugarduko, LT-03225 Vilnius, Lithuania
domas.balciunas@chf.stud.vu.lt

The interest in conducting polymers has proportioned a growing interest on the surface plasmon resonance (SPR) technique due to its high sensitivity, in situ and real time measurements in characterizing films [1]. The combination of SPR with electrochemical measurements (ESPR) has been demonstrated as a powerful technique for the simultaneous characterization and manipulation of electrode/electrolyte interfaces [2].

The surface functionalization by molecular assembling in the applications of organic electronics has attracted enormous interest during the past decades. Self-assembled monolayers (SAMs) are promising approach for the molecular assembling down to nanoscale [3], so it is extremely useful for sensitivity investigation then trying to discover relevant biosensor.

Glyphosate-based formulations (the most common being Roundup or N-(phosphonomethyl)glycine) are the most widely sold and used herbicide globally. They are used on food crops during cultivation, also used in gardens, along roads and railway tracks. After 40 years of ignorance policy on glyphosate's secondary side effects, many studies in recent years have suggested that glyphosate has worrying health effects at levels regularly detected in food and tap water. In order of such global issue many scientists are trying to discover the best analytical solutions and one of the most popular – research of suitable biosensors.

A biosensor is a device that incorporates a biological recognition (sensing) element in close proximity to, or integrated with the signal transducer, to give a reagentless sensing system specific to a target compound (analyte).

Main objectives of this study are to reveal biosensor on the basis of polypyrrole (PPy) which would be sensitive to glyphosate (Glyp) by using ESPR method. In order of that we studied glyphosate adsorption on PPy formed on SPR gold disk and compared it with glyphosate adsorption on polypyrrole thin layer formed on 11-(1H-pyrrol-1-yl)undecane-1-thiol (PUT) monolayer which was assembled on SPR gold disk.

The use of SPR and electrochemical impedance spectroscopy methods revealed that Glyp adsorbs from PBS solutions on PPy coated gold surface (Fig. 1), also as adsorbs on PPy formed on PUT monolayer which was assembled on gold surface. For next step we are going to study Glyp behavior on PPy surface, investigating non-imprinted polymer (NIP) and molecularly imprinted polymer (MIP) PPy sensitivity on Glyp.

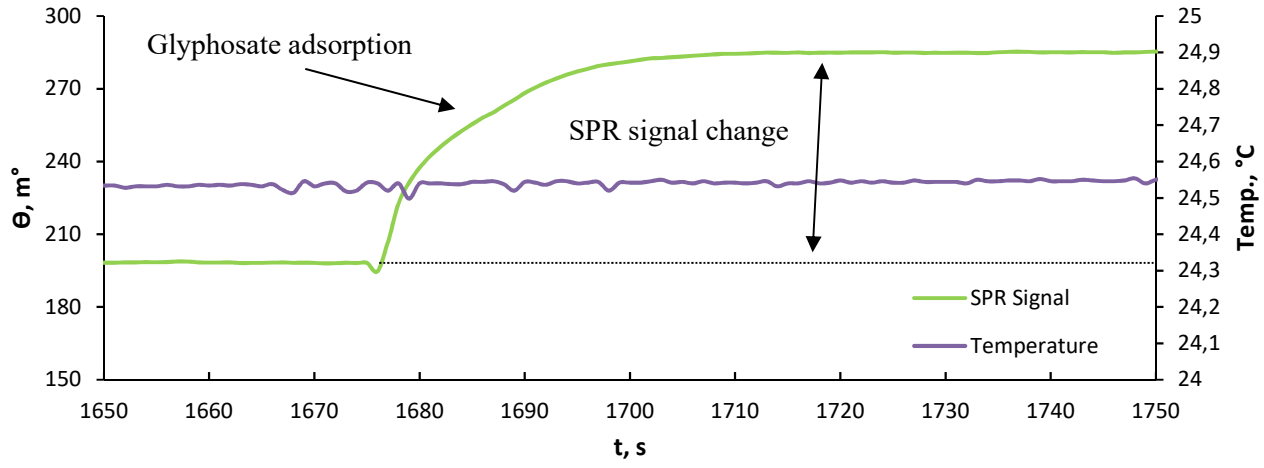


Fig. 1. Surface plasmon resonance angle vs. time curve recorded during Glyphosate adsorption on PPy layer formed from 10mM Py in PBS on Gold surface (pH=7.0). Glyphosate injection time 1676 second.

[1] Flavio S. Damos, Rita C.S. et al. *Electrochimica Acta 51*, p. 1304 (2006).
[2] Akira Baba, Shengjun Tian et al. *Journal of Electroanalytical Chemistry 562*, p. 95 (2004).
[3] M. Jalal Uddin, M. Khalid Hossain et al. *Results in Physics* 7, p. 2289 (2017).

# NMR SPECTRA OF WATER-IONIC LIQUID MIXTURES: LARGE-SCALE MOLECULAR DYNAMICS AND QUANTUM MECHANICS/MOLECULAR MECHANICS MODELING

Dovilė Lengvinaitė[1], Kęstutis Aidas[1]

[1] Institute of Chemical Physics, Faculty of Physics, Vilnius University, Lithuania
dovile.lengvinaite@ff.vu.lt

Ionic liquids are salts that have a melting point below 100 ºC. Many ionic liquids remain liquid at or near room temperature and are called room-temperature ionic liquids. Ionic liquids are typically composed of organic cations and mostly inorganic anions, and these liquids have many potential applications in separations, organic synthesis, catalysis and electrochemical devices. These liquids are considered as environmentally friendly solvents because they are nonvolatile, thermally stable and recyclable [1]. Besides many useful features of RTIL, they are known to be highly hygroscopic. RTIL will absorb water from the atmosphere as soon as they are exposed to it, and this is virtually unavoidable for any real-life application of these liquids. On one hand, even small amounts of water can change the properties of the RTIL considerably, on the other hand, the mixtures of water and IL can exhibit new unexpected properties [2].

The imidazolium based IL are in fact among the most widely studied RTIL. Imidazolium cations are composed of polar imidazolium ring with the apolar alkylic chain attached to it. Polar domains are composed of imidazolium rings and anions whereas alkylic chains assemble into nonpolar domains. Classical MD simulations predict that if water is dissolved in an IL, heterogeneous structure of the IL is maintained and water molecules tend to form the so-called water pockets [3]. Interestingly, the existence of water pockets has been recently confirmed experimentally using small-angle X-ray scattering and neutron scattering [4].

Very interesting NMR measurements of water mixtures with some imidazolium based IL have been very recently carried out by the NMR spectroscopy group of Vilnius University. RTIL of 1-butyl-3methyl-imidazolium, C4Mim, and anions such as halides, Cl-/Br-/I-, tetrafluoroborate, BF4-, and nitrate, NO3-, were considered. Interestingly, the H-1 NMR chemical shift of water was found to evolve non-monotonically with the changing concentration of the binary solution IL and water. When molar fraction of IL is increased, the H-1 NMR chemical shift of water first goes down. However, this chemical shift starts to increase starting from certain concentration of the ionic liquid, thus exhibiting a pronounced minimum. This kind of behavior is observed for all IL composed of C4Mim and cosmotropic anions, - that is, nitrate and halides. On the other hand, the H-1 NMR chemical shift of water was always found to decrease with the rising concentration of the [C4Mim][BF4] IL. Similarly, the chemical shift of the H2 proton in the imidazolium ring was found increase considerably with increasing concentration of [C4Mim][Cl]/[Br]/[I]/[NO3], but it was seen to be insensitive to the concentration of [C4Mim][BF4]. Clearly, these experimental findings reflect the structural changes of the samples with changing concentration of IL and water.

The aim of project is to model the H-1 NMR spectra of [C4Mim][Cl] and [C4Mim][BF4] RTIL mixtures with water of various concentrations (see Fig. 1). Large-scale classical molecular dynamics (MD) simulations of the IL/water systems have been carried out in order to sample the phase space and record the trajectories. These have been used in the subsequent calculations of NMR shielding constants using linear response quantum mechanics/molecular mechanics approaches. The theoretical results would certainly shed light on the early stages of water pocket formation within the IL and give valuable theoretical interpretation for the experimental findings just discussed.

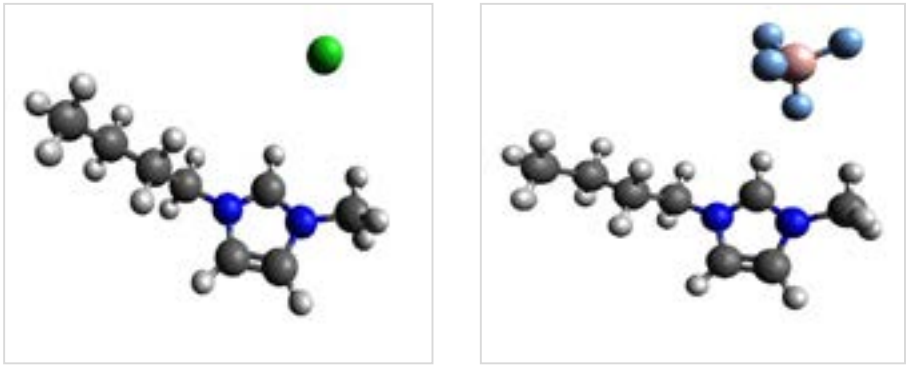

Fig. 1. 1-Butyl-3-methylimidazolium chloride (on the left side) and 1-Butyl-3-methylimidazolium tetrafluoroborate (on the right side).

[1] Welton, Chem. Rev. **99**, 2071 (1999).
[2] Nanda, Phys. Chem. Chem. Phys., **18**, 25801 (2016).
[3] Moreno et al., J. Phys. Chem. B, **112**, 7826 (2008).
[4] Saihara et al., Sci. Rep., **5**, 10619 (2015).

# THE IMPROVEMENT OF MICROPROPAGATION TECHNIQUES OF CHANDLER WALNUT.

Kayumov Abdurashid Abdujalilovich[1].

[1]Academy of Science of Uzbekistan, Scientific-Research Institute of Horticulture, Viticulture named after academician M.Mirzayev, Uzbekistan.
abdurashidmail@mail.ru

The implementation of in vitro technology in large-scale production of walnut seedlings presents superiority. The micropropagation techniques of explants obtained from walnut nodal segments of Chandler variety have advantages in early plant ripening, development of the root system, and compatibility of rootstock and scion in grafted plants [1].

The development of the root system and the acclimatization of walnut explants exhibit complicated behavior during micropropagation. The conventional micropropagation approaches for in vitro rooting of walnut explants is not effective, therefore, the improvement of tissue culture protocols is required. The establishment of new technologies is a key for coming through these issues.

The young walnut stems of 0,5-0,8 cm width with leaf buds of Chandler walnut are cutted and treated with fungicidal solutions (Penconazole and copper oxychloride) for 20 minutes. After, they are washed with distilled water 3 times and dried on filter paper in a laminar flow cabinet. The stems are placed in flasks with water and the flask bottleneck is covered with a transparent plastic film. After bud growth, the leaf explants of a 3 cm length are cut in a laminar flow cabinet, treated with sodium hypochlorite solution for 10 minutes, and washed with distilled water 3 times.

A ready-made nutrient medium DKW [2] was used and solidified with 3.5 g / l phytogel (Gelzan ®). Before sterilization, the pH of the all nutrient solutions were adjusted to 5,9. The media sterilization is hold at a temperature of 121°C and a pressure of 105 KPa for 20 minutes. The leaf buds of Chandler walnut are transferred into DKW multiplication medium with the addition of benzyl aminopurine - BAP (1 mg / l), indole butyric acid - IBA (0,01 mg / l), and phytogel (2,5 g / l). They are kept in growth chambers, programmed to 16 hours light / 8 hours dark photoperiodic and 25°C temperature mode. After 40 days, the explants are transferred to the new nutrient medium.

The modified WPM (Woody Plant Medium) is used for in vitro rooting of Chandler walnut explants. The root system is induced by adding 10 mg/l IBA to nutrient medium and etiolating for a week. The auxin free nutrient medium supplemented with vermiculite is used for subsequent root development in 16 hours light / 8 hours dark photoperiodic condition. The rooted walnut seedlings are washed gently in order to eliminating nutrient medium residues. Subsequently, they are placed into polystyrene trays containing peat and vermiculite, and acclimatized. The high relative humidity is provided during the first week of acclimatization. After the appearance of the new leaves, the humidity is reduced and ventilation is increased. Young seedlings are transferred to nursery after sufficient accumulation of lignin and hardening.

Figure 1. The in vitro cultured Chandler walnut explants in multiplication nutrient media.

1-5 microshoots are formed from each Chandler walnut explant in DKW fortified with BAP (1 mg / l) and IBA (0,01 mg / l). The mean number of microshoots is 2,38; and the mean length is 3,15 cm. The root system of Chandler walnut explants is induced with etiolating and adding 10 mg/l IBA. Subsequent development of root system is observed in a hormone free modified WPM supplemented with vermiculite. The walnut seedlings successfully acclimatized at high humidity. The improvement of micropropagation techniques of Chandler walnut provides development of plant production for commercial use.

[1] Hasey, J.K., Westerdahl, B.B., Micke, W.C., Ramos, D.E. &Yeater, J.T. (2001) Yield performance of own-rooted “Chandler” walnut versus “Chandler” walnut on Paradox Rootstock. Acta Hort. 544, 489–493.

[2] Driver, J.A. & Kuniyuki, A.N. (1984) In vitro propagation of Paradox Walnut roostock. HortSci. 19, 507–509.

# Lanthanum substituded $BiMnO_3$ synthesis and characterization

Dovydas Karoblis[1], Aivaras Kareiva[1], Aleksej Zarkov[1]

[1] Faculty of Chemistry and Geosciences, Vilnius University, Lithuania
Dovydas.Karoblis@chgf.vu.lt

Manganites are mixed oxides of manganese which crystalizes in perovskite structure, and whose broad stoichiometric formula is ABO(3±δ) ; where A is a lanthanide element and B is manganese, which also includes the ability to generate an exact or not oxygen stoichiometry. [1] Multiferroic bismuth manganite ($BiMnO_3$) is known as a material that exhibits both ferromagnetic and ferroelectric properties [2]. Multiferroic materials offer new range of applications like microwave resonators, gyrators, data storage and etc [3]. It is well known, that pure $BiMnO_3$ cannot be synthesized under ambient conditions. On the other hand, substituting part of bismuth with other elements, like lanthanum, can be done and those materials exhibit structural, magnetic phase transitions at different ratios of cations [4].

In this study, lanthanum doped bismuth manganites $La_{1-x}Bi_xMnO_3$ (x = 0.0-0.65) were prepared by sol-gel combustion synthesis method. The precursors were mixed and stirred for 1 h at 80 °C temperature. After the formation of sol, solvent was evaporated at 120 °C. Combustion reaction occurs when the temperature reaches 250 °C. Final annealing temperature (1000 °C) were chosen according to previously obtained results. For the characterization of obtained samples X-ray diffraction (XRD) analysis, scanning electron microscopy (SEM), Fourier transform infrared spectroscopy (FTIR) and other methods were used.

The obtained results showed that sol-gel combustion synthesis route is suitable for the fabrication of $La_{1-x}Bi_xMnO_3$. With this method the maximum concentration of bismuth can be 65%, which is biggest reported so far, when material is synthesized under ambient conditions. Also not only one structural phase transition can be observed, but also another one at that maximum concentration.

[1] E. Hernandez et al., Revista Mexicana de F´ısica 61 (2015) 166–169
[2] H. G. Zhang et al., J. Phys.: Conf. Ser. 430 (2013) 012072.
[3] Melvin M. Vopson Fundamentals of Multiferroic Materials and Their Possible Applications, Critical Reviews in Solid State and Materials Sciences, 0:1–28, 2014
[4] Y.D. Zhao et al., Structure, magnetic and transport properties of $La_{1-x}Bi_xMnO_3$, Journal of Magnetism and Magnetic Materials 280 (2004) 404–411

# YTTRIA-STABILIZED ZIRCONIA MODIFIED WITH CALCIUM AND MAGNESIUM IONS BIOCOMPATIBLE COATINGS PRODUCED BY SOL-GEL APPROACH FOR DENTISTRY USES

Edvinas Staisiunas[1], Gytis Baranovas[1], Jurgis Pilipavicius[1]

[1] Department of Inorganic Chemistry, Faculty of Chemistry and Geosciences, Vilnius University, Lithuania
edvinas.staisiunas@gmail.com

One of the most commonly employed implant materials in odontology is titanium or its alloys. Nonetheless, the surface of titanium is prone to mechanical abrasion. This is the consequence of increased surface roughness and easier facilitation of bacteria. In some scarce occasions this can be the cause of peri-implantitis [1]. In order to solve this problem, some surface modifications of titanium are necessary to enhance its abrasion resistance. Yttria-stabilized zirconia (YSZ) ceramics are already used in dentistry for dental crowns and partial fixed dental prostheses as it exhibits exceptional mechanical properties, chemical stability and biocompatibility as well as having esthetic properties [2]. Coatings of modified YSZ by calcium or magnesium ions might be a promising approach as the ions can improve the biocompatibility and possibly limit cracking of YSZ coatings.

The purpose of this research was to obtain monophase, uniform, crackless YSZ modified by calcium and magnesium ions coatings via sol-gel process for later studies in characterizing high biocompatibility and low bacterial activity.

A stable YSZ-Ca and YSZ-Mg sols were prepared via alkoxide hydrolysis route [3]: yttrium nitrate was mixed with a) calcium nitrate tetrahydrate b) magnesium nitrate hexahydrate, diluted, acetylacetone diluted in isopropanol was added as a chelating agent, water was added as hydrolysis agent, finally adding zirconium propoxide. Sols having concentration of $Ca^{2+}$ or $Mg^{2+}$ ion of 1%, 4%, 7%, 10%, 15% and 20% were tried to be synthesized. The concentration of modified YSZ in isopropanol for homogenous coatings was set to 5%. Afterwards, sols that had chemical stability and stable tetragonal YSZ phase were coated on titanium substrate by spin-coating method. X-Ray Diffraction (XRD) was used to characterize the YSZ phase by analyzing powder, which was obtained by heating the sol, which was in turn heated at 650 °C for 4 hours and grinded for homogeneity of the sample. Coatings were annealed at 650 °C for one hour to obtain homogenous monophase coatings (the heating temperature was set in accord to TGA analysis data). The coatings were characterized by scanning electron microscopy (SEM). The annealed coatings showed cracked surfaces in both $Y_{0,06}\,Zr_{0,93}\,Ca_{0,01}\,O_{1,96}$ (figure 1) and $Y_{0,06}\,Zr_{0,93}\,Mg_{0,01}\,O_{1,96}$ (figure 2) systems.

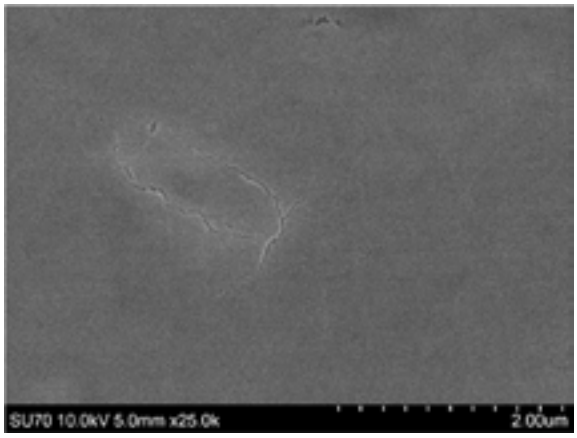


**Figure 1.** $Y_{0,06}\,Zr_{0,93}\,Ca_{0,01}\,O_{1,96}$ coating on titanium substrate

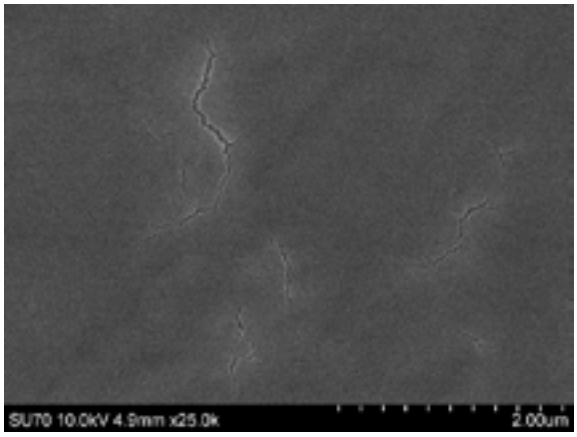


**Figure 2.** $Y_{0,06}\,Zr_{0,93}\,Mg_{0,01}\,O_{1,96}$ coating on titanium substrate

**Acknowledgement:** This research was funded by the European Social Fund under the No 09.3.3-LMT-K-712 "Development of Competences of Scientists, other Researchers and Students through Practical Research Activities" measure.

[1] Shi, X., et al. Hydrothermal treatment for TiN as abrasion resistant dental implant coating and its fibroblast response. Materials Science and Engineering: C **49**, 1-6 (2015).

[2] Aragón-Duarte, M. C., et al. Nanomechanical properties of zirconia- yttria and alumina zirconia- yttria biomedical ceramics, subjected to low temperature aging. Ceramics International **43**, 3931-3939 (2017).

[3] Xia, S., et al. Sol-gel synthesis of yttria stabilized zirconia membranes through controlled hydrolysis of zirconium alkoxide. Journal of Membrane Science **162**, 181–188 (1999).

# COMPARATIVE STUDY OF ANTI-HGH ANTIBODY IMMOBILIZATION STRATEGIES FOR HGH IMMUNOASSAY

Elena Dauksaite, Almira Ramanaviciene, Asta Kausaite-Minkstimiene

NanoTechnas – Centre of Nanotechnology and Material Science, Institute of Chemistry, Faculty of Chemistry and Geosciences, Vilnius University, Naugarduko str. 24, LT-03225 Vilnius, Lithuania
elle.dau@gmail.com

Human Growth Hormone (HGH) is a peptide hormone involved in many physiological processes, so both of its deficiency and excess can cause various disorders for people of different ages. In adults, an excess of the HGH produces a disorder known as acromegaly, whose initial symptom is typical enlargement of the hands and feet. Complications of the disorder may include type II diabetes, sleep apnea and high blood pressure. In children, increased HGH levels can lead to excessive growth of long bones, resulting in the child being abnormally tall. This disorder is commonly known as gigantism. The available data suggest that an excess of the HGH in more than 95 % is due to a benign tumor, known as a pituitary adenoma [1]. The HGH can also be secreted by endometrial, breast, liver, prostate or colon cancer cells. A deficiency of the HGH may cause hypoglycemia in newborn infants, growth failure in later infancy and childhood. In adults, the HGH deficiency causes loss of body weight and bone density and leads to a number of physical and psychological symptoms, including poor memory, social withdrawal, and even depression [2]. Hence, determination of the HGH concentration is undoubtedly important in diagnosis both its deficiency and its excess. There are many HGH immunoassays used in practice [3]. Although they can provide the desired sensitivity, specificity and selectivity, most of them are highly disadvantageous, because they are time consuming, require specialized labels and in many cases they require complex sample preparation. Therefore, new methods for the determination of HGH are still required. An excellent alternative to them is surface plasmon resonance (SPR) immunosensors, which offer several significant advantages including real-time and label-free detection of analytes. This is achieved by measuring changes in the refractive index caused by the antigen-antibody interaction taking place at a surface of SPR sensor chip. SPR immunosensors allow detection of very low analyte concentrations in a relatively small volume of the sample. Moreover, an ability to detect and quantify biospecific interactions in the complex solutions makes SPR immunosensors capable of identifying specific analytes without time-consuming sample preparations. An analysis with SPR immunosensor can be performed within a few minutes and very often it is possible multiple analysis, if proper regeneration of the SPR sensor surface is performed [4]. Due to these advantages, SPR immunosensors are powerful tool for bioanalytical and biomedical investigations.

Efficient immobilization of antibodies on a surface of the SPR sensor chip is an essential step in the preparation of the SPR immunosensor [5], since the choice of the immobilization technique greatly affects antibody-antigen interactions efficiency. This is due to asymmetric structure of antibody molecule, which determines that it can be immobilized in a random or oriented manner. Meanwhile, sensitivity of the SPR immunosensor depends on orientation and surface concentration of immobilized antibodies [6]. A great variety of methods suitable for immobilization of antibodies have been developed and described in the literature, but this area of research is still very relevant. Therefore, the objective of this study was to compare the effect of different immobilization techniques on the surface concentration of monoclonal mouse antibodies against human growth hormone (anti-HGH) on SPR sensor chip and estimate binding capacity of the immobilized anti-HGH with HGH. In the present study, anti-HGH antibodies were immobilized using five different methods. First immobilization method was random immobilization of intact anti-HGH (intact-anti-HGH) via 11-mercaptoundecanoic acid (MUA) self-assembled monolayer (SAM). For this purpose, SPR sensor chips for some time were incubated in 11-mercaptoundecanoic acid (MUA) in methanol. Then carboxyl functional groups of MUA were activated with a mixture of N-(3-dimethylaminopropyl)-N′-ethylcarbodiimide hydrochloride (EDC) and N-hydroxysuccinimide (NHS). After activation anti-HGH antibodies were immobilized covalently through their primary amine functional groups. Second, random immobilization of intact anti-HGH within carboxymethyl dextran hydrogel by direct covalent amide coupling with a mixture of EDC and NHS technique. Third immobilization method was oriented coupling of intact-anti-HGH to Protein-G layer assembled on MUA SAM via Fc-fragment of antibodies. Fourth immobilization method was oriented immobilization of fragmented anti-HGH antibodies (frag-anti-HGH) via their native thiol-groups directly coupled to the gold. To liberate these thiol groups, the intact-anti-HGH was chemically "divided" into two frag-anti-HGH fragments by chemical reduction with 2-mercaptoethylamine. And finally fifth immobilization method was oriented coupling of intact-anti-HGH to 3-aminophenylboronic acid (BA), which was assembled on MUA or MUA and 3,3'-dithiodipropionic acid mixed SAM, via cis-diols in the oligosaccharide chains of antibodies.

[1] L. Rostomyan, A. F. Daly, P. Petrossians et al., Clinical and genetic characterization of pituitary gigantism: an international collaborative study in 208 patients, Endocrine-Related Cancer **22**, 745-757 (2015).
[2] A. Kausaite-Minkstimiene, A. Ramanaviciene, A. Ramanavicius, Surface plasmon resonance biosensor for direct detection of antibodies against human growth hormone, Analyst **134**, 2051-2057 (2009).
[3] M. Bidlingmaier, C. J. Strasburger, Growth hormone assays: current methodologies and their limitations, Pituitary **10**, 115-119 (2007).
[4] A. Kausaite-Minkstimiene, A. Ramanavicius, J. Ruksnaite et al., A surface plasmon resonance immunosensor for human growth hormone based on fragmented antibodies, Analytical Methods **5**, 4757-4763 (2013).
[5] J. M. Lee, H. K. Park, Y. Jung et al., Direct immobilization of protein G variants with various numbers of cysteine residues on a gold surface, Analytical Chemistry **79**, 2680-2687 (2007).
[6] A. A. Karyakin, G. V. Presnova, M. Y. Rubtsova, Oriented immobilization of antibodies onto the gold surfaces via their native thiol groups, Analytical Chemistry **15**, 3805-3811 (2000).

# STABILITY INVESTIGATION OF OXIDIZED spiro-MeOTAD

E. Kasparavičius*[1], T. Malinauskas[1], V. Getautis[1]

[1] Department of Organic Chemistry, Kaunas University of Technology, Lithuania
ernestas.kasparavicius@ktu.lt

Population growth and ever-increasing energy consumption prompts new search for cleaner and safer alternatives to fossil fuels and nuclear energy. One of the most attractive alternatives is photovoltaic systems. Because of simple manufacturing and good performance prospects perovskite solar cells received growing interest from research community. As a result of rapid development in this field, perovskite photovoltaic systems have reached 23.7% [1] efficiency.

Charge-transporting materials has been developed for use in perovskite solar cells and vast majority of them require the use of chemical doping as an essential step for preparation of efficient devices.[2] Oxidized 2,2′,7,7′-tetrakis(N,N-di-p-methoxyphenylamine)-9-9′-spirobifluorene (Spiro-MeOTAD) could be one of the potential weak links in the perovskite solar cell composition. Interestingly, very little investigation is done concerning the oxidized HTMs applied in the PSC and their properties.[3]

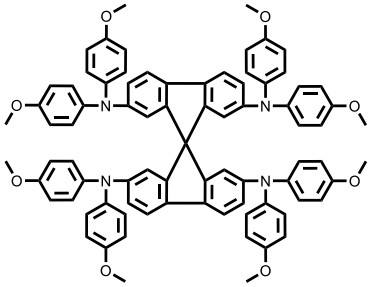

**Spiro-MeO-TAD**

Despite relatively high performance of perovskite solar cells, there is still a long list of things to do before requirements for commercialization are met. One of them is long term stability of the devices. Lead halide perovskite itself is moisture sensitive material and degrades rapidly when exposed to the ambient conditions. This problem is well-known and considerable amount of research is dedicated towards solving or mitigating it. Another possible weak link is dopant-containing hole transporting materials, containing considerable amounts of oxidized HTM.

In this work hole-transporting material spiro-MeOTAD, has been investigated under various conditions in order to estimate overall lifetime and influence of different additives. Interestingly, that a significant number of samples containing films of oxidized spiro-MeOTAD, started to crystallize at elevated temperatures. It is known that oxidized HTM, formed during doping, is responsible for the increased conductivity and ultimately for better efficiency of hole extraction process in the PSC device; therefore, observed instability of the oxidized HTMs in the thin films at elevated temperatures could be one of the causes of drop in conductivity reported for the doped spiro-MeOTAD. It could also potentially be one of the reasons why perovskite solar cells lose their efficiency under prolonged thermal stress. Possible solution to this problem could be use of HTMs that do not require doping and therefore do not rely on oxidized materials to improve conductivity. Development of the efficient technique to regenerate oxidized species in situ in the functioning device could be another albeit more complicated alternative

[1] H.-S. Kim, A. Hagfeldt and N-G. Park, Morphological and compositional progress in halide perovskite solar cells, Chem. Commun., 2019,55, 1192-1200

[2] H. Kim, K.-G. Lim, T.-W. Lee, Energy Environ. Sci. 2016, 9, 12–30.

[3] J.-P. Correa-Baena, W. Tress, K. Domanski, E. H. Anaraki, S.-H. Turren-Cruz, B. Roose, P. P. Boix, M. Gratzel, M. Saliba, A. Abate, A. Hagfeldt, Energy Environ. Sci. 2017, 10, 1207–1212.

# QUANTUM CHEMISTRY CALCULATIONS WITH QUNATUM COMPUTER PERFORMANCE STUDY

Gediminas Maskeliūnas, Mindaugas Mačernis

Institute of Chemical Physics, Vilnius University, Lithuania
gediminas.maskeliunas@ff.stud.vu.lt

In photosynthesis the energy of light is being absorbed by the LH2 complexes where bacteria-chlorophyll and carotenoid systems are responsible for this phenomena. β-Carotene molecule is the typical model used for researching carotenoid properties, which systems contains polyene chains [1, 2]. Thus, various quantum chemistry methods are required in order to model carotenoids. All carotenoid molecule calculations are very long and complex even for modern HPC (supercomputers). Quantum computers are expected to have a breakthrough in this field but its possibilities are not yet understood. There is a possibility to access the IBM quantum computers and various quantum computer simulators. The simulators can be run on supercomputers which creates a good development environment for quantum type algorithms. The new breakthrough is expected in Couple Cluster (CC) class quantum chemistry calculation where the problem complexity grows exponentially when increasing molecular calculation size. CC methods are based on Hartree-Fock (HF) calculations. Specialized calculation libraries, such as "Qiskit Aqua Chemistry" are being developed for the IBM quantum computer and the quantum simulators [3]. There are already demonstrated quantum algorithm applications for the small molecules [4]. The library use mixed calculations by combining quantum algorithms with well know packages such as PSI4, PySCF, PyQuante, which are based on objective oriented Python programming.

In order to perform quantum computer simulations it is necessary to have the needed Python libraries and supercomputing facilities. The one used is the "HPC Saulėtekis" supercomputer Fizika2000 (www.supercomputing.ff.vu.lt). The results must be compared with the traditional computing algorithms which are in the PySCF package. The main research object is the β-Carotene molecule and different length polyene chains. However, in order to perform such task there is a need to do quantum computing simulator performance study with various qubits and its parameters. Thus the primary molecule was used $H_2$ molecule for initial performance analysis.

There were successfully installed Qiskit aqua chemistry libraries and the PySCF package into supercomputer "Fizika 2000". The ground state energy of the $H_2$ molecule was calculated with the quantum simulators using two different algorithms: Quantum Phase Estimation (QPE) and Variational Quantum Eigensolver (VQE). The QPE algorithm has a limited number of the changeable parameters, but enough for it to be sophisticated. The changed variable parameters were ancillary qubits (*num_ancillae*), the number of time slices (*num_time_slices)* and expansion mode (*expansion_mode*). There were several hundred runs of various modifications of the $H_2$ molecule ground state energy problem changing all the available parameters in order to find the optimal energy value and the execution time we have sorted out the results (see some examples in Table 1).

**Table 1.** Example of $H_2$ problem results (expansion mode: suzuki, number of time slices: 50, variable: ancillary qubits)

| num | time, s | Energy, Hartrees |
|---|---|---|
| 1 | 4.890022755 | -1.320490405 |
| 2 | 6.591337919 | -1.320490405 |
| 3 | 8.608515263 | -0.810375555 |
| 4 | 11.24328351 | -1.320490405 |
| 5 | 13.53698087 | -1.192961693 |
| 6 | 16.06198859 | -1.129197336 |
| 7 | 18.35524225 | -1.129197336 |
| 8 | 20.9236033 | -1.097315158 |
| 9 | 23.63072705 | -1.15310897 |
| 10 | 28.32836843 | -1.11724152 |
| 11 | 31.93432903 | 1.133182609 |
| 12 | 38.39482903 | -1.134178927 |

The QPE algorithm give out randomized results no matter how the parameters are changed. The VQE algorithm has more added variable parameters which is essential to our work in finding out the optimal parameters to run the problem with consistent results. The VQE algorithm is better predictable and comparable with classical algorithms.

[1] M. Macernis, D. Galzerano, J. Sulskus, E. Kish, YH. Kim, S. Koo, L. Valkunas, B. Robert Resonance Rama Spectra of Carotenoid Molecules: Influence of Methyl Substitutions, J. Phys. Chem. A, 2015, 119 (1), 56-66.

[2] M. Macernis, J. Sulskus, Malickaja S Ruban A, L. Valkunas Resonance Raman Spectra and Electronic Transitions in Carotenoids: A Density Functional Theory Study, J. Phys. Chem. A., 2014, 118(10), 1817-1825.

[3] IBM Q Experience, https://quantumexperience.ng.bluemix.net/

[4] A. Kandala, A. Mezzacapo, K. Temme, M. Takita, M. Brink, JM Chow, JM Gambetta Hardware-efficient variational quantum eigensolver for small molecules and quantum magnets, Nature 2017, 549, 242

[5] Qiskit AQUA Chemistry, https://www.qiskit.org/aqua/

# SYNTHESIS AND CHARACTERIZATION OF ALKALINE EARTH METALS DOPED $La_2Mo_2O_9$ CERAMICS

Giedrė Gaidamavičienė[1], Edvardas Kazakevičius[2], Artūras Žalga[1]

[1] Faculty of Chemistry and Geosciences, Vilnius University, Naugarduko Str. 24, LT-03225 Vilnius, Lithuania
[2] Faculty of Physics, Vilnius University, Sauletekio av. 9/3, LT-10222 Vilnius, Lithuania
giedre.prievelyte@chf.vu.lt

Oxide-ion conductors have attracted considerable interest due to their potential applications as components of solid oxide fuel cells (SOFCs), oxygen sensors, oxygen pumps and oxygen-permeable membrane catalysts [1]. SOFCs are characterized as devices with high energy-conversion efficiency and a positive environmental impact. However, electrolyte materials for SOFCs have to meet some requirements: exhibit high ion conductivity, which in turn implies very specific structural features only met by a restricted number of solid oxides [2]. Nowadays, most widely used materials for SOFC electrolyte are gadolinium-doped ceria (GDC) and yttria-stabilized zirconia (YSZ). However, these ceramic materials require high-operating temperatures (~1273 K) to obtain high oxide-ion conductivity. Such conditions have some disadvantages like as seal in high temperature, interface reaction between components of SOFC, the sintering of the electrodes and more [3]. Moreover, in recent years, the $La_2Mo_2O_9$-type compounds, known as the LAMOX family, which was originally reported by Lacorre et al., have also attracted great interest due to their high oxygen-ion conductivity at medium temperatures. $La_2Mo_2O_9$ undergoes a reversible transition from monoclinic α to cubic β structure at ~ 853 K, leading to an increase in the ionic conductivity up to two orders of magnitude and reaching values higher than those corresponding to YSZ (0.06 S/m at 1073 K). Besides, YSZ or GDC generate oxygen vacancies by doping other metal cations, while lanthanum molybdate possesses intrinsic oxygen vacancies, and the vacant intrinsic oxygen sites allow accommodation of oxygen excess in the structure thus resulting the high-ionic conductivity [3, 4]. Nevertheless, the phase transition between these structures clearly limits their potential application in SOFCs. The stabilization of cubic β phase at room temperature was a hard task of many scientists, nevertheless, it was found that the doping of different elements in the La, Mo and O sites stabilizes the high-temperature crystal phase indefinitely. It was observed that La site substitution with lower valence cations such as $Ca^{2+}$, $Sr^{2+}$, $Ba^{2+}$ and another could stabilize cubic phase and increase oxygen-vacancy concentration [5, 6]. In such case, the obtained transport properties of $La_2Mo_2O_9$ strongly depend on preparation technique of final ceramic. Usually, unfavorable effect could be caused by impurities, porosity and low connectivity between the grains. To avoid such problems there is possible to use so called sol-gel synthesis, which provides both a good homogenization between starting materials and a high purity of the final ceramic.

This is the main reason why in this paper we report environmentally friendly and simple aqueous sol-gel synthesis of La–M–Mo–O tartrate gel precursors (M= $Ca^{2+}$, $Sr^{2+}$ and $Ba^{2+}$) for $La_{2-x}M_xMo_2O_{9-\delta}$ ceramics. Herein is important to note that the use of tartaric acid in the sol-gel processing makes a possibility to reduce interactions between the individual components avoiding the formation of precipitates during the evaporation stage from the reaction mixture. Moreover, using this method there is possible to synthesize $La_2Mo_2O_9$ compound homogeneously substituted by $Ca^{2+}$, $Sr^{2+}$ and $Ba^{2+}$ ions, controlling their amount and the crystallinity of the final ceramics. In order to obtain dense and fully crystalline ternary oxide the as-prepared gels were heat-treated at 1273 K for 5 hours. Next to that, the obtained powders were additionally pelletized and sintered in air at 1473 K for 5 h. In order to investigate the crystallization and thermal decomposition mechanism of La–M–Mo–O tartrate gel precursors, the thermogravimetry and differential scanning calorimetry (TG–DSC) analysis was applied. Besides, in order to confirm the phasic transition between room-temperature α-$La_2Mo_2O_9$ and high-temperature β-$La_2Mo_2O_9$ phases, the investigation of as-prepared powders using DSC and XRD methods was performed. Additionally, all samples sintered at 1427 K temperature were investigated by scanning electron microscopy (SEM) in case to see whether there is a dense surface of sintered ceramics and how dopant amount can affect their surface morphology.

[1] X. P. Wang and Q. F. Fang, Low-frequency internal friction study of oxide-ion conductor $La_2Mo_2O_9$, Journal of Physics-Condensed Matter **13**, 1641-1651 (2001).
[2] D. Marrero-Lopez, D. Perez-Coll, J. C. Ruiz-Morales et al., Synthesis and transport properties in $La_{2-x}A_xMo_2O_{9-\delta}$ (A=$Ca^{2+}$, $Sr^{2+}$, $Ba^{2+}$, $K^{+}$) series, Electrochimica Acta **52**, 5219-5231 (2007).
[3] X. Gao, T. He and Y. Shen, Structures, electrical and thermal expansion properties of Sr-doped $La_2Mo_2O_9$ oxide-ion conductors, Journal of Alloys and Compounds **464**, 461-466 (2008).
[4] P. Lacorre, F. Goutenoire, O. Bohnke, R. Retoux and Y. Laligant, Designing fast oxide-ion conductors based on $La_2Mo_2O_9$, Nature, **404**, 856-858 (2000).
[5] A. Kežionis, D. Petrulionis, E. Kazakevičius, S. Kazlauskas, A. Žalga, R. Juškėnas, Charge carrier relaxation phenomena and phase transition in $La_2Mo_2O_9$ ceramics investigated by broadband impedance spectroscopy, Electrochimica Acta, **213**, 306-313 (2016).
[6] A. Žalga, G. Gaidamavičienė, Ž. Gricius et al., Aqueous sol-gel synthesis, thermoanalytical study and electrical properties of $La_2Mo_2O_9$, Journal of Thermal Analysis and Calorimetry **132**, 1499-1511 (2018).

# SYNTHESIS AND CHARACTERIZATION OF CALCIUM MOLYBDATE VIA CO-PRECIPITATION AND SOL-GEL TECHNIQUES: A COMPARATIVE STUDY ON THE PROPERTIES OF OBTAINED PRODUCTS

Giedrė Gaidamavičienė[1], Jūris Bogdanas[2], Gytautas Janulevičius[1], Artūras Žalga[1,2]

[1] Department of Applied Chemistry, Institute of Chemistry, Faculty of Chemistry and Geosciences, Vilnius University, Naugarduko Str. 24, 03225 Vilnius, Lithuania
[2] Vilniaus Fabijoniškių Secondary School, P. Žadeikos Str. 2, 06318, Vilnius, Lithuania
giedrė.gaidamaviciene@gmail.com

Metal molybdates of the general formula $AMoO_4$ (A = Mg, Ca, Sr, Ba, Cd, Zn, Pb, etc.) have been studied extensively for decades, owing to their technological importance in a variety of applications such as phosphors, scintillation materials, microwave devices, catalysts, or optoelectronic devices. Many different preparation techniques have been used for the preparation of $AMoO_4$ (A = Mg, Ca, Sr, and Ba) ceramics. The choice of synthesis technique usually depends on variety factors that can shorten, facilitate, and reduce the preparation way [1]. Below, in the Fig. 1, there is possible to see the differences that occur after the annealing at the same temperature but using different heat-treatment ways of the same double oxide [2].

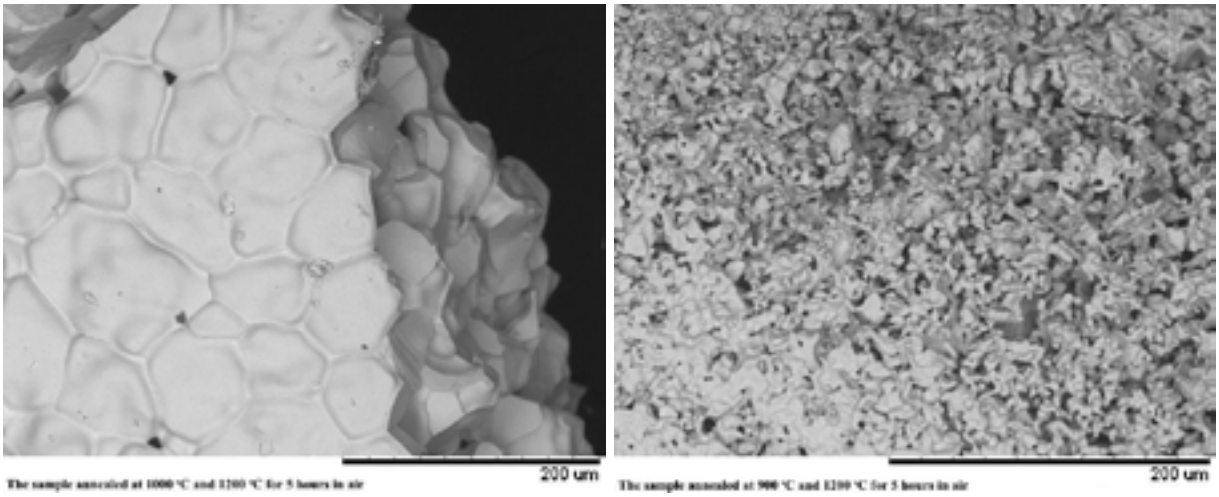


Fig. 1. SEM images of $La_2Mo_2O_9$ ceramic using different heat-treatment proceeding ways [2].

This is the reason why, in this work both the aqueous sol–gel synthesis method and co-precipitation technique were successfully used for the preparation of $CaMoO_4$ ceramic material. Moreover, in order to show the peculiarities of the final compounds, the SEM, XRD and TGA–DTA characterization techniques were additionally also applied, which clearly revealed all differences of obtained products that was mainly provided by the uniqueness of the synthesis method.

[1] G. Braziulis, G. Janulevičius, R. Stankeviciute, A. Žalga, Aqueous sol–gel synthesis and thermoanalytical study of the alkaline earth molybdate precursors, Journal of Thermal Analysis and Calorimetry **118** 613–621 (2014).
[2] A. Žalga, G. Gaidamavičienė, Ž. Gricius, E. Užpurvytė, J. Gadeikis, A. Diktanaitė, M. Barre, T. Šalkus, A. Kežionis, E. Kazakevičius, Aqueous sol–gel synthesis, thermoanalytical study and electrical properties of $La_2Mo_2O_9$, Journal of Thermal Analysis and Calorimetry **132** 1499–1511 (2018).

# NAPHTYL SUBSTITUTED TRIPHENYLAMINE DERIVATIVES AS HOLE TRANSPORTING MATERIALS FOR EFFICIENT RED PHOLED

Gintare Krucaite [1], Dovydas Blazevicius [1], Marius Eidimtas [1], Dmytro Volyniuk [1], Jurate Simokaitiene [1], Saulius Grigalevicius [1], Chun-Han Lin[2], Chang-Min Shao[2], Chih-Hao Chang[2]

[1] Department of Polymer Chemistry and Technology, Kaunas University of Technology, Radvilenu plentas 19, LT50254, Kaunas, Lithuania

[2] Department of Electrical Engineering, Yuan Ze University, Chung-Li 32003, Taiwan

gintare.krucaite@ktu.lt

Phosphorescent organic light emitting diodes (PhOLEDs) have drawn much attention because they use both singlet and triplet excitons for the emission of light and 100% internal quantum efficiency is possible in this case. The high internal quantum efficiency depends on several factors such as high quantum yield emitters, exothermic energy transfer from host to emitter, effective exciton confinement as well as balanced carrier transport [1, 2]. It is well demonstrated that carrier transporting materials are very important to enable a balanced carrier transport from cathode and anode [3, 4].

The synthesis of naphthyl substituted triphenylamine compounds (**1NTPA-3NTPA**) was carried out by two step synthetic route as shown in Scheme 1. Tris(4-bromophenyl)amine (**2**) as a key material was obtained by bromination reaction of triphenylamine (**1**) with *N*-bromosuccinimide in DMF. 1-Naphthyl substituted derivatives **1NTPA-3NTPA** were obtained by the Suzuki reaction of the tris(4-bromophenyl)amine (**2**) with 1-naphthalene boronic acid.

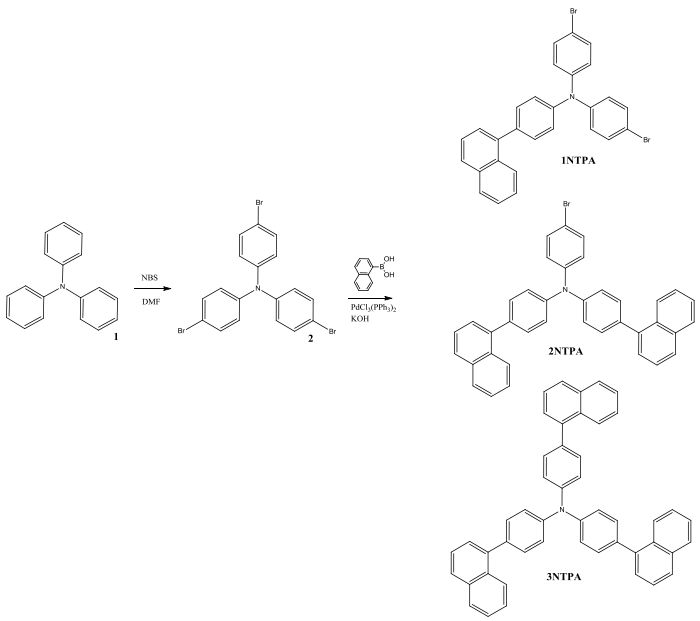


Fig. 1. Synthetic route to 1NTPA-3NTPA .

Naphthyl substituted triphenylamine and its derivatives with bromine atoms were synthesized and investigated. The respective glass transition temperatures of the materials were estimated to be in a range 65-137 ℃, which can provide morphologically-stable amorphous films for applications in organic light emitting diodes. The compounds possess adequate ionization potentials (5.5-5.75 eV), high hole drift mobilities ($>10^{-3}$ $cm^2/ V·s$) and suitable triplet energies (~ 2.4 eV), which make them suitable hole transporting materials for use in red phosphorescent organic light-emitting diodes. A superior peak efficiency of 17.9% (31.4 cd/A and 26.9 lm/W) was achieved in a device having hole transporting layer of tris[4-(1-naphthyl)phenyl]amine. Furthermore, the device gave efficiencies of 17.7% and 16.6% recorded at luminance levels of $10^2$ and $10^3$ $cd/m^2$. The efficiency drop from the maximum to the value recorded at the luminance of $10^3$ $cd/m^2$ for the device was only 7%.

**Acknowledgements.** This research was funded by a grant No. S-MIP-17-64 from the Research Council of Lithuania.

[1] C.-H. Chang, C.-L. Ho, Y.-S. Chang et al., Blue-emitting Ir(III) phosphors with 2-pyridyl triazolate chromophores and fabrication of sky blue- and whiteemitting OLEDs, J. Mater. Chem. C, **1** 2639-2647 (2013).

[2] J. Huang, B. Xu, J.H. Su, et al., Efficient blue lighting materials based on truxene-cored anthracene derivatives for electroluminescent devices, Tetrahedron **66** 7577-7585 (2010).

[3] J. Huang, J.H. Su and H. Tian, The development of anthracene derivatives for organic light-emitting diodes, J. Mater. Chem. **22** 10977-10989 (2012).

[4] C. W. Lee, J. Y. Lee, A hole transport material with ortho- linked terphenyl core structure for high power efficiency in blue phosphorescent organic light-emitting diodes, Org. Electron. **15** 399-404 (2014).

# ELECTROPOLYMERIZATION OF INDOLE DERIVATIVES AND THEIR ELECTROCHROMIC PROPERTIES

Delianas Palinauskas[1],Šarūnas Žukauskas[1], Gintautas Bagdžiūnas[1,2*]

[1] Department of Physical Chemistry, Vilnius University, Faculty of Chemistry and Geosciences, Naugarduko str. 24, Vilnius, Lithuania
[2] Department of Material Science and Electrical Engineering, Center for Physical Sciences and Technology, Sauletekio av. 3, Lithuania
gintautas.bagdziunas@ftmc.lt

The electrochemical synthesis of electrically conducting organic polymers has proven important in allowing development of new polymeric materials with electrochemical and/or electrical properties [1]. According to this approach, semiconducting polymers have been obtained from a wide variety of monomers which include thiophene [2], aniline [3], carbazole [4] and etc. For the discovery and study of conducting polymers, the chemistry Nobel Prize in 2000 was awarded These conducting polymers have received much attention in both fundamental and practical studies because they have electrical and electrochemical properties similar to those of both traditional semiconductors and metals. Moreover, these polymers have been successfully used in biosensors as conducting mediator between enzyme and electrode [1,4], LED lighting and electrical supercapacitors and in other applications [5].

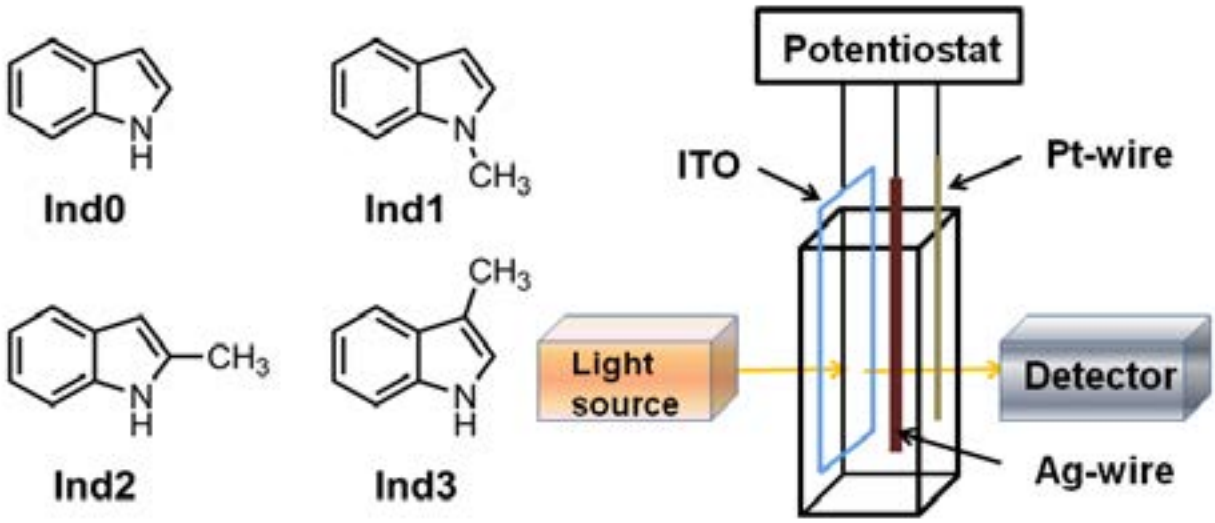


Fig. 1. Structures of the starting methyl substituted indole derivatives and schematic view of the electrochemical cell for the electrochemical investigations.

In this work, substituent effects in the electropolymerization of the methyl substituted indole derivatives on a transparent indium tin oxide (ITO) electrode were investigated (Fig. 1). These prepared polymers were studied by using the cyclo voltamperometry (CV), Raman spectrometry, scanning electron microscopy (SEM) methods. Moreover, for a study of electrochromic properties, most stable conducting polymer based on a nonsubstituted indole was used and evaluated. We hope that this work will be useful for further research of conductive polymers.

**Acknowledgments**: Financial support from the Research Council of Lithuania a grant No. 09.3.3-LMT-K-712-02-0186 is gratefully acknowledged.

[1] Nezakati, T.; Seifalian, A.; Tan, A.; Seifalian, A. M. Conductive Polymers: Opportunities and Challenges in Biomedical Applications. *Chem. Rev.* **2018**, 118 (14), 6766–6843.
[2] Gicevicius, M.; Bagdziunas, G.; Abduloglu, Y.; Ramanaviciene, A.; Gumusay, O.; Ak, M.; Soganci, T.; Ramanavicius, A. Experimental and Theoretical Investigations of an Electrochromic Azobenzene and 3,4-Ethylenedioxythiophene-Based Electrochemically Formed Polymeric Semiconductor. *ChemPhysChem* **2018**, 19 (20), 2735–2740.
[3] Gicevicius, M.; Celiesiute, R.; Kucinski, J.; Ramanaviciene, A.; Bagdziunas, G.; Ramanavicius, A. Analytical Evaluation of Optical PH-Sensitivity of Polyaniline Layer Electrochemically Deposited on ITO Electrode. *J. Electrochem. Soc*. **2018**, 165 (14), H903–H907.
[4] Bagdžiūnas, G.; Žukauskas, Š.; Ramanavičius, A. Insights into a Hole Transfer Mechanism between Glucose Oxidase and a P-Type Organic Semiconductor. Biosensors and Bioelectronics **2018**, 102, 449–455.
[5] Le, T.-H.; Kim, Y.; Yoon, H. Electrical and Electrochemical Properties of Conducting Polymers. *Polymers* **2017**, 9 (4), 150.

# EFFECTS OF BORON ON LUMINESCENCE PROPERTIES OF YTTRIUM/LUTETIUM ALUMINIUM GARNETS SCINTILLATORS

Greta Inkrataitė[1], Anatoli Popov[2], Ramūnas Skaudžius[1]

[1]Institute of Chemistry, Faculty of Chemistry and Geosciences, Vilnius University,
Naugarduko 24, LT-03225 Vilnius, Lithuania

[2]Institute of Solid State Physics, University of Latvia, 8 Kengaraga street, LV-1063, Riga, Latvia

greta.inkrataite@chgf.vu.lt

Nowadays light based technology is very popular and can be used in different aspects of life. One of the areas, where light based technologies can be used is scintillators, which are made from luminescent materials. That is the base for devices, which are used for detecting and measuring radioactive contamination, monitoring nuclear materials and computed tomography. The most common scintillators are usually made from inorganic compounds. Materials for this case are variuos alkali-metal halides, alkali earth halides, lanthanide halides, transition metal, post–transition metal, rare-earth oxyorthosilicates or elpasolites [1]. Recently, garnets are one of the most popular materials applied as scintillators. In this work presented garnets are cerium doped yttrium aluminium garnet (YAG:Ce) and lutetium aluminium garnet (LuAG:Ce). Cerium activated scintillators have been investigated for thermal neutron and high energy radiation (X-ray, γ ray) detection [2]. In order to get wide spread application and fast scintillators it is very important to improve their light yield, self-absorption and decay time. These properties could be enhanced by co-doping garnets with boron. It is important that absolute light output is increased due to improved energy migration when garnets are doped with boron, which leads to better performance of scintillators [3]. One of the biggest drawbacks of these phosphors is long decay time. When it is too long, one image could be superimposed on another and this problem may also be solved by incorporation of boron into the garnet structure. Fast response time can allow detection of rare events in particle physics [4].

For this project different compounds were prepared, which could be used in scintillators in order to increase their light yield and self-absorption, also reduce phosphor decay time. The chosen compounds were, YAG:Ce and LuAG:Ce co-doped with boron. Phosphor powder was synthesized by sol-gel method and heated under different atmospheres. Samples were analyzed by x-ray diffraction (XRD), scanning electron microscopy (SEM) and high energy radiation detection was measured. Of course, quantum efficiency, decay times, emission spectrum have also been investigated.

---

[1] D. S. McGregor, Materials for Gamma-Ray Spectrometers: Inorganic Scintillators. Annual Review of Materials Research, **48**: 13.1–13.33 (2018)
[2] A.D. Sontakke, et al., A Comparison on Ce3+ Luminescence in Borate Glass and YAG Ceramic – Understanding the Role of Host's Characteristics. The Journal of Physical Chemistry C: 1-41 (2016)
[3] C. Foster, et al., oron Codoping of Czochralski Grown Lutetium Aluminum Garnet and the Effect on Scintillation Properties. Journal of Crystal Growth, **486**: 126-129 (2018)
[4] H. S. Yoo, et. al., Preparation and photoluminescence properties of YAl3(BO3)4:Tb3+, Bi3+ phosphor under VUV/UV excitation. Optical Materials, **31**: 131-135 (2008)

# QUANTUM CHEMICAL MODELLING OF AQUEOUS ACIDITY AND TAUTOMERIC EQUILIBRIUM CONSTANTS OF SECONDARY BENZENESULFONAMIDES

Greta Majauskaitė[1], Kęstutis Aidas[2]

[1]Faculty of Chemistry and Geosciences, Vilnius University, Lithuania
[2]Institute of Chemical Physics, Faculty of Physics, Vilnius University, Lithuania
greta.majauskaite@chf.stud.vu.lt

An acid dissociation constant $pK_a$ is one of the key parameters of a chemical compound. This constant determines the protonation state of the compound for a given acidity of the solution, and this has profound ramifications in drug discovery and design. For example, biological activity of a drug can be greatly affected by the pH of the cell environment. Moreover, many organic compounds undergo reactions of tautomerisation, and have two or more different tatomeric forms, and therefore the control of drug efficiency can be an arduous task. Different tautomeric forms and protonation states affect overall bio-specificy of a compound in question. Experimental measurements of aqueous acidities of different tautomeric species is challenging and in many cases impossible. For this reason, the development of computational schemes for reliable prediction of these thermodynamic properties based on quantum chemical methods is of utmost importance.

The aim of this study is to assess the effect of tautomerisation on aqueous acidities by using quantum chemical methods rooted in density functional theory. A set of secondary benzenesulfonamides (Fig. 1.), including 4-amino-N-(1,3-oxazol-2-yl)benzenesulfonamide, 4-amino-N-cyanobenzenesulfonamide, N-[(4-aminophenyl)sulfonyl]acetamide, N-[(4-Aminophenyl)sulfonyl]benzamide, N-[(4-Aminophenyl)sulfonyl]-2-chloroacetamide, has been selected for analysis, the experimnental acidities of these compounds are taken from Ref. [1]. We have performed a comprehensive conformational analysis of all the compounds in different tautomeric and protonation states. All calculations were performed using M0-52X functional and cc-pVTZ basis set, and the SMD model was applied to account for solvation. Aqueous acidity and tautomeric equilibrium constants were calculated according to the direct thermodynamic cycle. Apparent constants have been evaluated to allow for direct comparison between experimental and computational results.

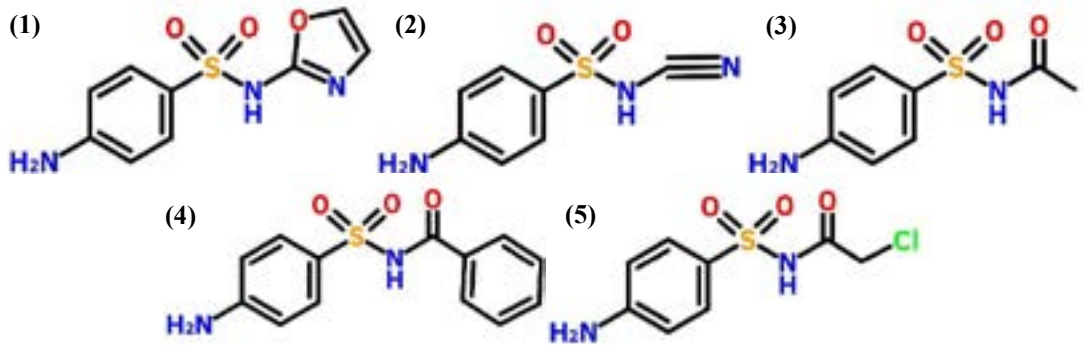


Fig. 1. Secondary benzenesulfonamides: 4-amino-N-(1,3-oxazol-2-yl)benzenesulfonamide **(1)**, 4-amino-N-cyanobenzenesulfonamide **(2)**, N-[(4-aminophenyl)sulfonyl]acetamide **(3)**, N-[(4-Aminophenyl)sulfonyl]benzamide **(4)**, N-[(4-Aminophenyl)sulfonyl]-2-chloroacetamide **(5)**

Our calculations show that amide-imidic acid tautomerism has negligible impact on the apparent acidity constants, as amide tautomer was in all cases found to be the dominating tautomeric form of N-[(4-aminophenyl)sulfonyl]acetamide, N-[(4-Aminophenyl)sulfonyl]benzamide, N-[(4-Aminophenyl)sulfonyl]-2-chloroacetamide compounds. On the other hand, we have found the canonical nitrile tautomer to be not the most stable form of 4-amino-N-cyanobenzenesulfonamide where imine tautomers are more stable. Our results thus show that a possible nitrile-imine and amine-imine tautomerism can not be ignored when aqueous acidities of benzensulfonamides are concerned.

Authors are thankful to the High Performance Computing Center “HPC Saulėtekis” for computational recourses.

[1] P.H. Bell, R.O. Roblin. J. Am. Chem. Soc. 64 (1942), 2905

# SYNTHESIS AND INVESTIGATION OF NEW ORGANIC SEMICONDUCTORS WITH AMIDE AND STYRENE FUNCTIONAL GROUPS

Greta Plančiūnaitė, Tadas Malinauskas

Department of Organic Chemistry, Kaunas University of Technology, Lithuania
greta.planciunaite@ktu.lt

The growing consumption of fossil fuel cause the increasing pollution and greenhouse gas emissions. To resolve this issue, subsequent studies focused on finding environmental friendly ways to produce energy from renewable sources are being conducted. One of the possible solutions could be Solar energy which is converted into electricity *via* solar cells. During the last decade, perovskite solar cells (PSC) have received considerable attention as promising photovoltaic devices for efficient light to power conversion. In PSCs hole transporting layer plays an important role in increasing power conversion efficiency (PCE). Currently spiro-MeOTAD is the most efficient small organic molecule hole transporting material (HTM) which allows reaching PCE up to 22%. [1] However this molecule is characterized by low conductivity of carriers and requires oxidative additives to boost performance in the devices, however, using additives results in PSC long-term stability problems. [2]

Many researchers investigate new organic HTMs which could be used in PSC construction without any additives enabling high PCE without the loss in device stability. For this purpose N.Giuseppone *et al*. studied triphenylamine derivatives containing amide moiety. The chemical structure of these derivatives allow the molecule to self-assemble into ordered supramolecular architectures under light irradiation which enhance conductivity. [3] The weak Van der Wals forces, hydrogen bonds and π-stacking found in these particular supramolecular structures are sufficient to hold the structure together in solution or under gentle film deposition conditions, but break when manufcturing films using spin-coating technique. S. Y. Kim group have reported work on triphenylamines containing diacetylene moieties allow photoinduced self-assembly of the molecules into aggregates by visable light and subsequent covalent fixation *via* polymerization by UV irradiation. [4]

The aim of this this work was to synthesize and investigate new organic HTMs containing triphenylamine-core, amide and styrene moieties. These molecules have a tendency to self-assemble into orderly structures under exposure to light in the chlorinated solvents.

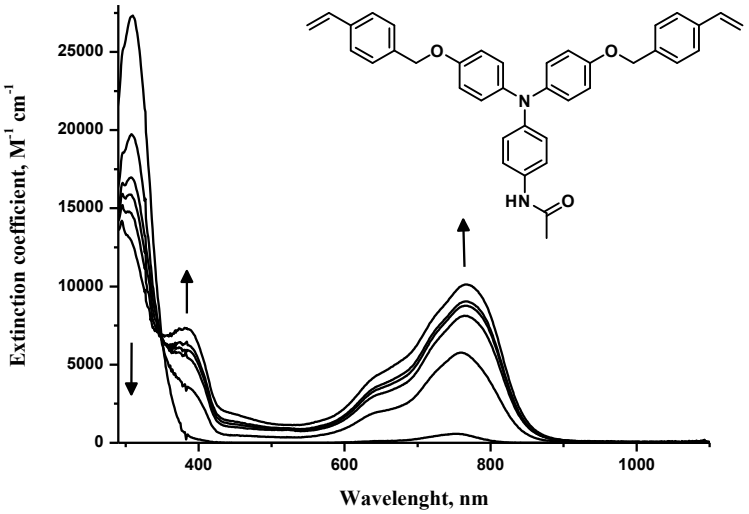


Fig. 1. UV/Vis/NIR absorption spectra of HTM1 under visible light irradiation

The self-assembly process of HTM1 can be observed in UV/Vis/NIR spectroscopy where new absorption bands appear: 770 nm and 384 nm, while absorption band 308 nm decreases in 1,1,2,2- tetrachloroethane solution under visible light irradiation. To photopolymerization of HTM1 was initiated using photoinitiators and UV irradiation. The molecules synthesized in this work are thermally stable and possess suitable ionization potential for application in PSC.

This research was funded by the European Social Fund under the No 09.3.3.-LMT-K-712-10-0253 "Development of Competences of Scientists, other Researchers and Students through Practical Research Activities" measure.

[1] Z. H. Luis, K. Ono, Y Qi. Recent advances in Spiro-MeOTAD hole transport material and its applications in organic–inorganic halide Perovskite solar cells, Advanced Materials Interfaces, **5**, 1-22 (2017)

[2] G. Niu, X. Guo, L. Wang. Review of recent progress in chemical stability of perovskite solar cells, Journal of Material Chemistry A, **3**, 8970-8980 (2015)

[3] E. Muolin, F. Niess, M. Maaloum, E Buhler., I. Nyrkova, N. Giuseppone, The Hierarchical Self-Assembly of Charge Nanocarriers: A Highly Cooperative Process Promoted by Visible Light. Angewandte Chemie, **49**, 6974 –6978 (2010)

[4] J. Kim, J. Lee, W. Y. Kim, H. Kim, S. Lee, H. C. Lee, Y. S. Lee, M. Seo, S. Y. Kim. Induction and control of supramolecular chirality by light in self-assembled helical nanostructures, Nature Communications, **6**, 1-8 (2015)

# SELECTIVE PROTECTION OF GLYCEROL

Greta Olimpija Remeikytė[1], Rytis Deržinauskas[1], Tatjana Charkova[2]

[1] Faculty of Chemistry and Geosciences, Vilnius University, Lithuania
[2] Department of Organic Chemistry, Center for Physical Sciences and Technology, Lithuania
greta.remeikyte@gmail.com

A simple, economic glycerol is an abundant source for a great variety of glycerol ethers with useful biological and physical properties such as immunostimulatory, anti-inflammatory, antimicrobial, antibacterial, antifungal, antitumor activity etc. The similarity of hydroxyl groups remains a main problem in glycerol etherification reactions – isomeric mono-, di- and triproducts are synthesized under similar conditions [1]. Many hydroxyl protecting groups have been reported to resolve this problem, but only not many of them are in common use [2, 3].

In our ongoing project of developing glycerol-based molecular systems, we have chosen to protect hydroxyl group by using p-methoxybenzyl (PMB) alcohol. PMB group can be selectively removed under acidic or mildly oxidizing conditions that do not affect alkenes, benzyl ethers, ketones, tosylates and some others derivatives [2, 3]. This open alternative way to use PMB glycerols in the synthesis of functionally complex compounds, where extensive selective protection-deprotection protocols are required.

We successfully found a new synthesis route of primary PMB monoprotected glycerol (Scheme 1, compound 4). Firstly, we protect commercial glycerol by using PMB alcohol. The primary product is isolated from produced mixture of isomers (90% and 10% respectively) by two simple steps: selective coupling with cyclohexanone and acidic hydrolysis of new synthesized cyclohexylidene-1-(4-methoxybenzyl)glycerol (compound 3). Hereby, we suggest inexpensive reagents and safely low temperature regimes for all protection-deprotection steps. All used resins and inorganic reagents are simply removed by filtration, neutralization and extraction procedures; this also makes isolation of products easier and more convenient. Then, monoprotected PMB glycerol is tritylated (synthesis of compound 5) and used for synthesis of monoalkyl glycerol ether (compound 6). Two selective deprotection methods have been shown: with p-toluenesulfonic acid (PTSA) and with 2,3-dichloro-5,6-dicyano-1,4-benzoquinone (DDQ) reagent. Undoubtedly, it will be used for the synthesis of more complex structures in the near future.

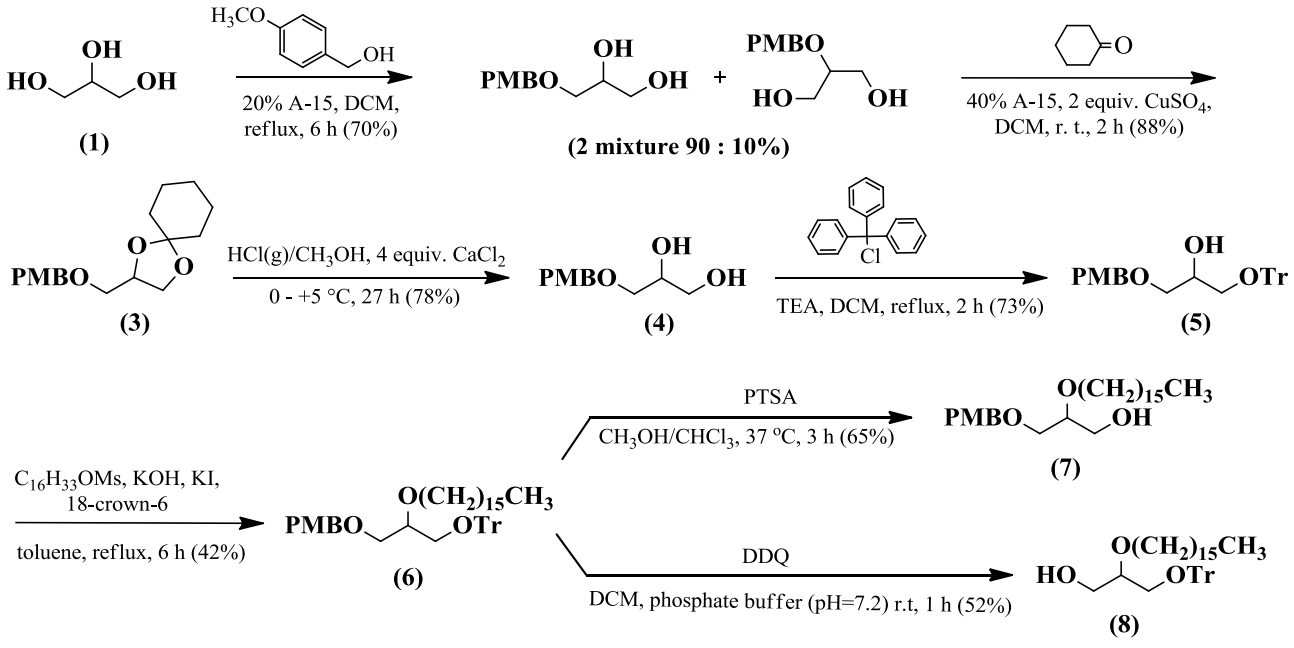


Scheme 1. Selective protection-deprotection of glycerol.

[1] M. Sutter, E. Da Silva, N. Duguet, Y. Raoul, E. Métay, M. Lemaire, Glycerol ether synthesis: a bench test for green chemistry concepts and technologies, Chemical Reviews **115**, 8609-8651 (2015).
[2] P. J. Kocieński, *Protecting groups*, (3rd edition, Thieme, New York, 2003).
[3] T. W. Greene and P. G. Wuts, *Protective groups in organic synthesis*, (3rd edition, Wiley, New York 1999).

# EXPLORING REACTION PATHWAYS AND EXPLAINING SITE-SELECTIVITY OF 1,3-DIPOLAR CYCLOADDITIONS TO PORPHOLACTONES FROM THE FIRST PRINCIPLES

Gustautas Snarskis[1], Jonas Žurauskas[2], Augusto Costa Tomé[3]

[1] Department of Applied Chemistry, Vilnius University, Lithuania
[2] Department of Organic Chemistry, Vilnius University, Lithuania
[3] Department of Chemistry and QOPNA, University of Aveiro, Aveiro, Portugal
gustautas.snarskis@chf.stud.vu.lt

In recent years much interest is attracted by various modifications of porphyrins in order to obtain desired chemical photophysical properties. This enables various applications ranging from pigments to photodynamic therapy [1].

Nonetheless, synthesis of porphyrin derivatives is often challenging, low yielding and poorly selective. Therefore, extensive understanding of mechanisms and thermodynamics of these reactions is crucial for planning efficient synthesis.

In this communication we present mechanistic insights on selective azomethine ylide and nitrone additions to *meso*-tetrakis(pentafluorophenyl)porpholactone, based on density functional theory (DFT). Calculations for minimum energy pathways were performed at IEF-PCM/B3LYP/6-31G(d) level of theory, together with deliberate analysis of frontier molecular orbitals (FMO) carried out at IEF-PCM/B3LYP/6-311G(d,p) level of theory.

Gibbs free energy calculations (fig. 1) correctly predicts the outcome of both reactions and suggests that additions are controlled differently: kinetic control in case of addition with azomethine ylide and thermodynamic when nitrone is used. To shine some intuition on seemingly controversial stabilities of transition states we applied FMO theory, which has been known to be decent in explaining selectivity 1,3-dipolar cycloadditions for a long time [2,3]. Careful examination of FMO's geometries and their atomic contributions indicates to be reasonable and intuitive tool in foreseeing selectivity for this type of reactions.

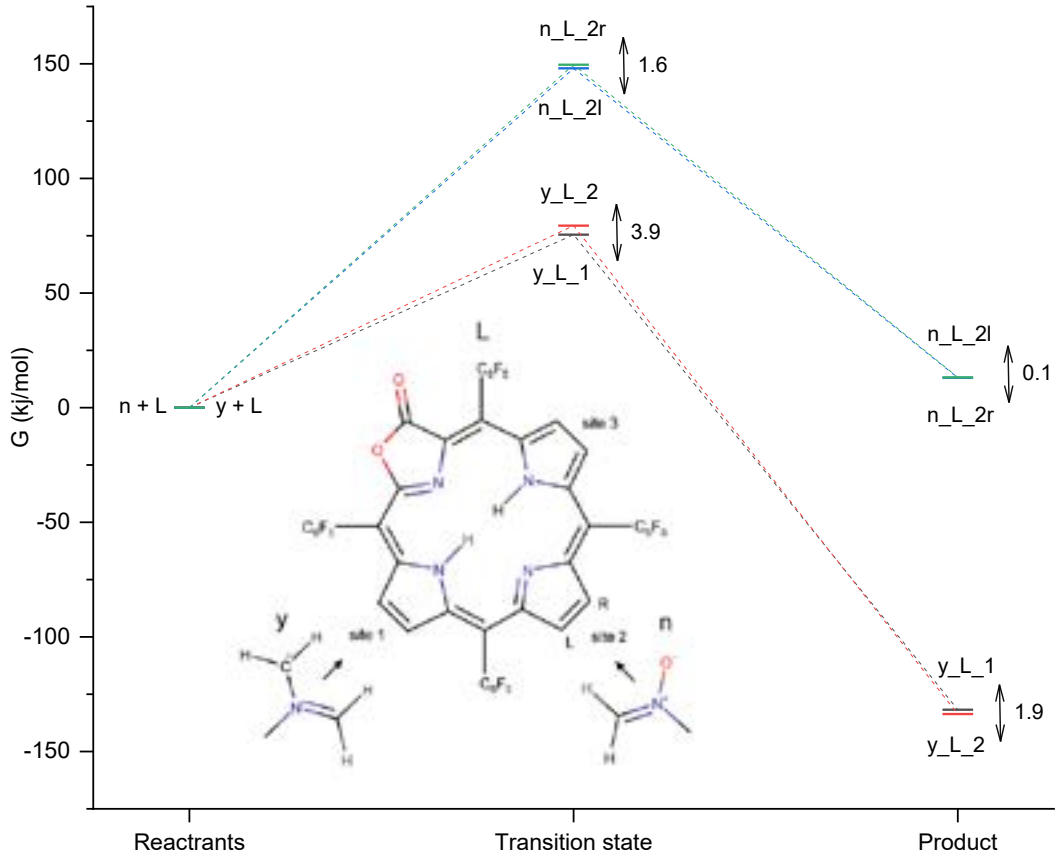


Fig. 1. Minimum energy pathway diagram for azomethine ylide (y) and nitrone (n) 1,3-dipolar cyclodditions to *meso*-tetrakis(pentafluorophenyl)porpholactone (L).

[1] Huang, Haoyuan; Song, Wentao; Rieffel, James; Lovell, Jonathan F. (2015) Front. Phys. 3: 23.
[2] Caramella, Pierluigi; Houk, K.N. (1976). J. Am. Chem. Soc. 98: 6397–6399.
[3] Caramella, Pierluigi; Gandour, Ruth W.; Hall, Janet A.; Deville, Cynthia G.; Houk, K. N. (1977). J. Am. Chem. Soc. 99: 385–392.

# LITHIUM DISILICATE MODIFIED WITH CALCIUM AND MAGNESIUM IONS BIOCERAMIC COATINGS PREPARED VIA SOL-GEL METHOD FOR ODONTOLOGICAL USES

Gytis Baranovas[1], Edvinas Staisiunas[1], Jurgis Pilipavicius[1], Zivile Stankeviciute[2]

[1] Department of Inorganic Chemistry, Faculty of Chemistry and Geosciences, Vilnius University, Lithuania
[2] Department of Applied Chemistry, Faculty of Chemistry and Geosciences, Vilnius University, Lithuania
gytisba7@gmail.com

Both titanium and its alloys are utilized as a dental implant material and yield high success rate in restoring lost teeth function. Nevertheless, inflammation of the soft tissues due to allergic reaction to Ti and V ions and possible meager soft tissue formation in the immediate proximity of the implant that leads to bacteria induced dental plaque still remain as the predominant problems of titanium implants [1]. Alteration of the surface of the implants is required to make the surface more biocompatible for the tissues whilst restricting possible bacterial activity. Lithium disilicate ceramics are already used as a material for single crowns and partial fixed dental prostheses because of its esthetic and functional properties [2]. Inclusion of calcium and magnesium into lithium disilicate system has a potential to further enhance its antibacterial properties as lithium calcium silicate ceramics have shown potential to improve growth of tissue material [3].

The objective of this work is to obtain crack-free modified lithium disilicate ceramic coatings via sol-gel method while not obtaining any impurities caused by added calcium and magnesium ions as well as displaying higher biocompatibility and low bacterial activity than pure lithium disilicate.

Pure lithium disilicate $Li_2Si_2O_5$ was obtained by mixing lithium methoxide with tetramethyl orthosilicate in dehydrated methanol, then adding water and complexing agent acetylacetone. For modification with calcium and magnesium same synthesis was used, only difference being the dissolvement of $Ca(NO_3)_2 \cdot 4H_2O$ and $Mg(NO_3)_2 \cdot 6\ H_2O$ in dehydrated methanol beforehand. Sols with varying quantities of Ca and Mg were produced, dried into powder, heat treated in 600°C and characterized by x-ray diffraction (XRD). $Li_2Si_2O_5$ modified with Ca increasing quantity of modifications led to increased development of lithium metasilicate (figure 1), while $Li_2Si_2O_5$ altered with Mg displayed no impurities whilst modified with similar amount of material (figure 2). Nevertheless, both $Li_2Si_2O_5$ systems have shown promising results and coatings from modified $Li_2Si_2O_5$ sols are going to be produced to examine their uniformity and biocompatibility.

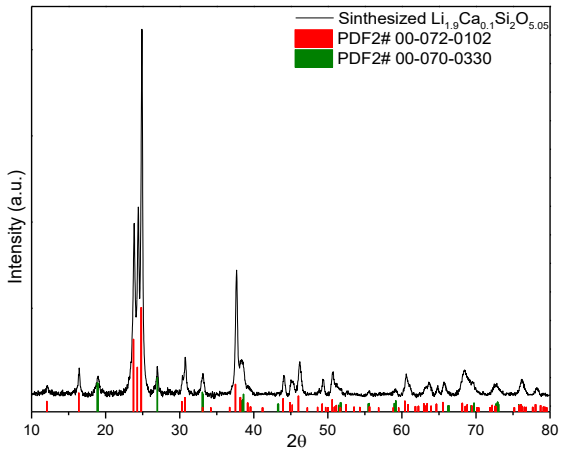


Fig. 1. XRD graph of lithium disilicate modified with 5% calcium

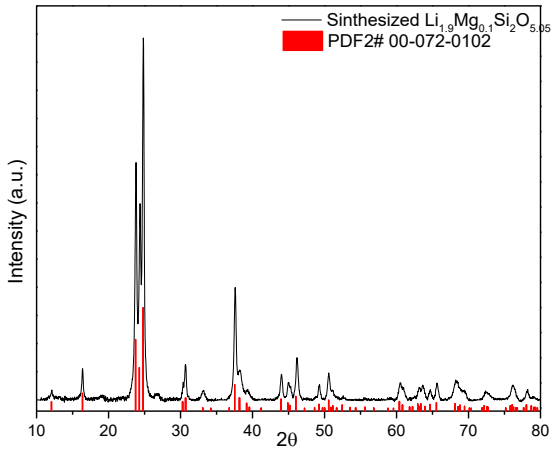


Fig. 2. XRD graph of lithium disilicate modified with 5% magnesium

[1] Shi, X., et al. Hydrothermal treatment for TiN as abrasion resistant dental implant coating and its fibroblast response. Materials Science and Engineering: C **49**, 1-6 (2015).
[2] Pieger, S., et al. Clinical outcomes of lithium disilicate single crowns and partial fixed dental prostheses: a systematic review. J Prosthet Dent **112**, 22-30 (2014).
[3] Chen, L., et al. 3D printing of a lithium-calcium-silicate crystal bioscaffold with dual bioactivities for osteochondral interface reconstruction. Biomaterials (2018).

**Acknowledgement:** This research was funded by the European Social Fund under the No 09.3.3-LMT-K-712 "Development of Competences of Scientists, other Researchers and Students through Practical Research Activities" measure.

# ELECTROCHROMIC PROPERTIES OF CONDUCTIVE POLYMER AND TEXTILE COMPOSITES

Ieva Agne Cechanaviciute, Mindaugas Gicevicius, Arunas Ramanavicius

Faculty of Chemistry and Geosciences, Vilnius University, Naugarduko str. 24, Vilnius, Lithuania
ievaagne@gmail.com

While color is an integral part of everyday life and can be used to reflect emotions, identify or alert, a change in color is even more powerful tool in terms of expression and communication. A promising way to produce color changing flexible displays is combining textiles with electrochromic electrically conductive polymers. There is a great potential provided by the conductive polymers due to the color manipulation possibilities [1], comparative ease of preparation [2] and rapid response times. This study investigates the combinations of electrochemically polymerized polyaniline and poly(3,4-ethylenedioxythiophene) (PEDOT) with two different textile substrates and explores its possible applications.

Electrochemical polymerization was carried out using three electrode system, where platinum wire served as counter electrode, silver wire as reference electrode and textile as working electrode. Polyester (PES) fabric with stainless steel fibers and copper-nickel coated PES (PES-Cu-Ni) textiles were used. Electrochemical depositions of polyaniline and PEDOT were performed by potential cycling, using 0.1 M aniline solution in 0.5 M sulfuric acid and 20 mM EDOT solution in acetonitrile with 0.1 M $LiClO_4$.

Electrochromic color change of polyaniline and PEDOT textile composites was investigated using video image analysis software ImageJ. By using an appropriate combination of red (R), green (G), and blue (B) intensities, many colors can be displayed. Using ImageJ it is possible to measure RGB channels' intensity changes. Measurements are based on analyzing separate pixels [3]. To ensure same lightning conditions all videos were filmed in special photography box (24x24x24 cm) with LED lights (Fig.1).

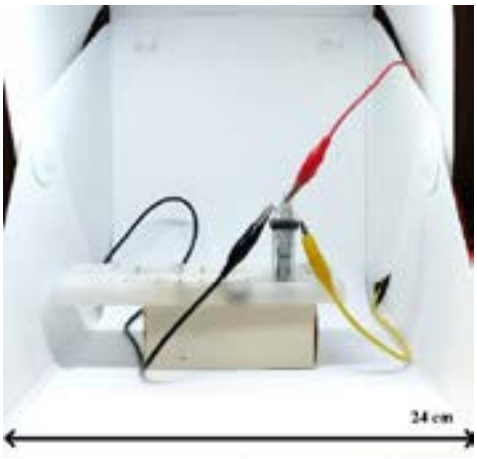


Fig. 1. Photography box with LED lights


Fig. 2 Electrochromic color change of polyaniline

Both PES-Stainless steel and PES-Cu-Ni textiles demonstrated reversable electrochromic color change with aforementioned conductive polymers. For polyaniline observed color change was dark green-blue (Fig. 2.), for PEDOT from transparent to dark blue. This leads to a promising expectation that conductive polymers and textiles can be combined for further application developing communicative flexible devices.

[1] Gaupp CL, Reynolds JR, Multichromic copolymers based on 3,6-bis(2-(3,4-ethylene- dioxythiophene))-N-alkyl carbazole derivatives, Macromolecules 36, 6305–6315 (2003).
[2] Dirk Schawaller, Michael Voss, Volker Bauch, Erik Frank, Michael R. Buchmeiser; Flexible, switchable electrochromic textiles, Macromol. Mater. Eng.p. 330–335 (2013)
[3] Abramoff, M.D.; Magalhães, Paulo J.; Ram, Sunanda J., Image processing with ImageJ, Biophotonics international, 11, 36 – 42 (2004)

# INVESTIGATION OF ELECTROPHILIC CYCLIZATION REACTIONS OF 2-(3-SUBSTITUTED 2-PROPYNYLTHIO) METHYL-1H-BENZIMIDAZOLES

Indrė Misiūnaitė, Rita Bukšnaitienė, Ieva Karpavičienė

Faculty of Chemistry and Geosciences, Vilnius University, Naugarduko 24, LT-03225, Vilnius, Lithuania
Indre.Misiunaite@gmail.com

Derivatives containing imidazo[2,1-c][1,4]thiazine fragment can be potential anti HSV-1 suppressor[1], β-lactamase inhibitor [2], anti trypanosomatid agents[3] and shows cytotoxic properties [4]. However, only several synthetic ways are used for this type of heterocycle [5]. One of the new routes to imidazothiazine could be through electrophile initiated heteroatom cyclization reaction of alkynes which is used in synthesis of other types of heterocycles [6]. In the literature there is no information about formation of imidazo[2,1-c][1,4]thiazine using propargylic substrates in any cyclization reactions. Hence, this is a new potential investigation field in organic chemistry. Keeping in mind that benzimidazoles and a lot of their derivatives are interesting due to their biological properties [7], we decided to synthesize various 2-(3-substituted 2-propynylthio) methyl-1H-benzimidazoles **1** and investigate their intramolecular electophilic cyclization.

The starting materials **1** were prepared from 2-bromo-1-arylpropynes and (1H-benzo[d]imidazol-2-yl)methanethiol, with sodium hydroxide. Then the electrophile initiated cyclization reactions of propynythiomethylbenzimidazoles **1** were investigated. It was found that electrophile has a significant effect on the reaction results. Depending on electophile it is possible to obtain thiazinobenzimidazole **2** derivatives or addition products **3** without cyclization. The scope and limitations of this reaction will be enlarged in presentation.

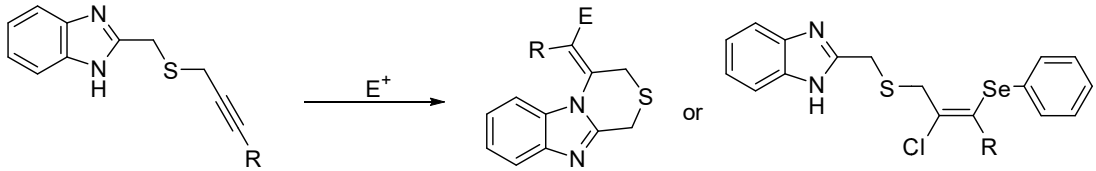


**1** **2** **3**

R= p-$MeC_6H_4$, p-$OMeC_6H_4$, $C_6H_5$, $C_2H_5$
$E^+$=$I^+$, $Br^+$, $PhSe^+$, p-OMe-$C_6H_4$-$C^+$OMe

$E^+$=$PhSe^+$

*This research is funded by the European Social Fund under the No 09.3.3-LMT-K-712"Development of Competences of Scientists, other Researchers and Students through Practical Research Activities" measure.*

[1] S.A. Galal, S.I. El-Naem, A.O.H El-Nezhaway, M.A. Ali, H.I. El-Diwani, Arch. Pharm. Chem. Life Sci., 11, 2011, 255-263
[2] T.S. Mansour, P.A. Bradford, A.M. Venkatesan, Annual reports in medicinal chemistry 43, 2008 247 - 267
[3] M. Boiani, L. Boiani, A. Denicola, S.T.de Ortiz, E.Serna, N. Vera de Bilbao, L. Sanabria, G. Yaluff, H. Nakayama, A.Rojas de Arias, C. Vega, M. Rolan, A. Gomez Barrio, H. Cerecetto, M. Gonza´lez, J. Med. Chem. 49, 2006, 3215-3224
[4] M.E. Suh, M.J. Kang, S.Y. Park, Bioorg. Med. Chem., 9, 2001, 2987-2991
[5] A. Chimirri, A.M. Monforte, P. Monforte, F. Nicolò, A. Rao, M. Zappalàa, Heterocycles, 53, 2000, 613-620
[6] B. Godoi, R.F. Schumacher, G. Zeni, Chem. Rev. 111, 2011, 2937-2980
[7] F.A.S. Alasmary, A.M. Snelling, M.E. Zain, Ah.M. Alafeefy, A.S. Awaad, N. Karodia, Molecules, 20, 2015, 15206-15223

# SYNTHESIS AND PHOTOPHYSICAL PROPERTIES OF PYRIMIDINE-CARBAZOLE BASED FLUOROPHORES

Irina Fiodorova[1], Rokas Skaisgiris[2], Vytautas Steckis[1], Jelena Dodonova[1], Tomas Serevičius[2], Saulius Juršėnas[2], Sigitas Tumkevičius[1]

[1] Department of Organic Chemistry, Faculty of Chemistry and Geosciences, Vilnius University, Naugarduko Str. 24, LT-03225 Vilnius, Lithuania

[2] Institute of Photonics and Nanotechnology, Faculty of Physics, Vilnius University, Sauletekio 3, LT-10257 Vilnius, Lithuania.

irina.fiodorova@chgf.vu.lt

OLEDs are considered as one of the most promising green technologies for future displays and lighting resources owing to their low power consumption and their being ultra-thin, lightweight, and flexible. Recently, thermally activated delayed fluorescent (TADF) emitters consisting of pure organic materials have been developed as a new generation of emitters to harvest all the molecular excitons [1]. The main requirement for efficient TADF is thought to be a negligible energy difference between the lowest singlet and triplet states ($\Delta E_{ST}$), which is obtained in the compounds possessing donor–acceptor fragments with strong intermolecular charge transfer (ICT) [2]. One of the promising design strategies for TADF materials is to use a highly twisted structures between the donor and acceptor moieties. The twisted structure has rather small overlap of the highest occupied molecular orbital (HOMO) and the lowest unoccupied molecular orbital (LUMO) and thus results in small singlet−triplet energy gap [3]. Compounds bearing pyrimidine heterocycle as an electron withdrawing unit were demonstrated to be promising for TADF applications [4, 5a]. In this connection and continuing our work aimed to the search of efficient fluorescent materials among the pyrimidine-based heterocycles [5] we present herein results on the synthesis and photophysical properties of a series of novel 4,6-bis(3,6-disubstituted 9-carbazolyl)pyrimidines (**I**) (Fig. 1).

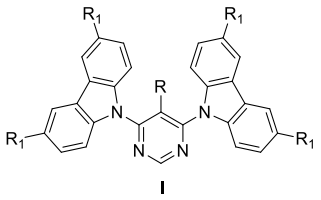


**I**

Fig. 1. General structure of pyrimidine-carbazole based fluorophores.

The target compounds **I** were synthesized starting from an easily accessible 4,6-dihydroxypyrimidine modifying it to appropriate 4,6-dichloro derivatives and performing substitution reactions of chlorine groups with corresponding carbazole derivatives. Aryl groups into the 5th position of pyrimidine ring were introduced by using palladium-catalyzed Suzuki cross-coupling reaction of corresponding 5-bromopyrimidines with selected arylboronic acids.

Optical properties of the synthesized conjugates were assessed by DFT calculations and investigated by absorption, time integrated and time-resolved fluorescence spectroscopies and fluorescence quantum yield measurements. The obtained data revealed that bare pyrimidine – carbazole molecule exhibits near-UV fluorescence (360 nm) with a large $\Delta E_{ST}$ gap of about 700 meV, thus only room temperature phosphorescence (RTP) with no TADF was observed. By introducing larger substituents R and/or $R_1$ we were able to red-shift fluorescence up to blue emission (440 nm) without changing triplet energy much, therefore reducing $\Delta E_{ST}$ value to 300 meV, in the process enabling TADF and turning off RTP emissions.

In this work we showed that single-bonded pyrimidine-carbazole molecules are promising as blue TADF emitters and their $\Delta E_{ST}$ value can be tuned by different substituents in positions R or $R_1$.

**Acknowledgements**

This research was funded by a grant (no. S-MIP-17-73) from the Research Council of Lithuania.

[1] H. Uoyama, K. Goushi et al., Highly Efficient Organic Light-emitting Diodes from Delayed Fluorescence, Nature, **492**, 234-238 (2012).

[2] (a) F. B. Dias, T. J. Penfold, et al. Photophysics of Thermally Activated Delayed Fluorescence, Molecules. Methods Appl. Fluoresc., **5**, 012001 (2017); (b) Y. Tao, K. Yuan et al., Thermally Activated Delayed Fluorescence Materials Towards the Breakthrough of Organoelectronics. Adv. Mater., **26**, 7931–7958 (2014).

[3] (a) K. Goushi, K. Yoshida et al., Organic Light-emitting Diodes Employing Efficient Reverse Intersystem Crossing for Triplet-to-Singlet State Conversion, Nature Photonics, **6**, 253-258 (2012); (b) Q. Zhang, J. Li, J. et al., Design of Efficient Thermally Activated Delayed Fluorescence Materials for Pure Blue Organic Light Emitting Diodes, J. Am. Chem. Soc., **134**, 14706-14709 (2012).

[4] R. Komatsu, H. Sasabe, J. Kido, Recent progress of pyrimidine derivatives for high-performance organic light-emitting devices, J. Photon. Energy, **8**, 032108 (2018).

[5] (a) T. Serevicius, T. Buciunas et al., Room temperature phosphorescence vs. thermally activated delayed fluorescence in carbazole–pyrimidine cored compounds, J. Mater. Chem. C, **6**, 11128-11136 (2018); (b) L. Skardziute, J. Dodonova et al., Synthesis and Optical Properties of the Isomeric Pyrimidine and Carbazole Derivatives: Effects of Polar Substituents and Linking Topology, Dyes Pigm., **118**, 118–128 (2015): (c) J. Bucevicius, L. Skardziute, et al., 2,4-Bis(4-aryl-1,2,3-triazol-1-yl)pyrrolo[2,3-*d*]pyrimidines: Synthesis and Tuning of Optical Properties by Polar Substituents, RSC Adv, **5**, 38610-38622 (2015);

# SELECTIVE SYNTHESIS OF 12,13- AND 17,18-DIHYDROPORPHOLACTONES

Jonas Zurauskas[1], Gustautas Snarskis[1], Ana F.R. Cerqueira[2], Samuel Guieu[2], Filipe A. Almeida[2] Paz, Augusto C. Tome[2]

[1] Department of Chemistry, Vilnius University, Vilnius, Lithuania
[2] Department of Chemistry, University of Aveiro, Portugal
jonas.zurauskas@chf.stud.vu.lt

Porpholactones are a class of pyrrole-modified porphyrins in which a pyrrolic unit is formally replaced by one oxazolone unit. These compounds have a very rich chemistry and may be converted into a number of other pyrrole-modified porphyrins [1,2]. However, the participation of porpholactones in cycloaddition reactions has never been reported. In this communication we report the reaction of *meso*-tetrakis(pentafluorophenyl)porpholactone with azomethine ylides and nitrones. Pyrrolidine-fused and isoxazolidine-fused dihydroporpholactones are formed site-selectively in these reactions.

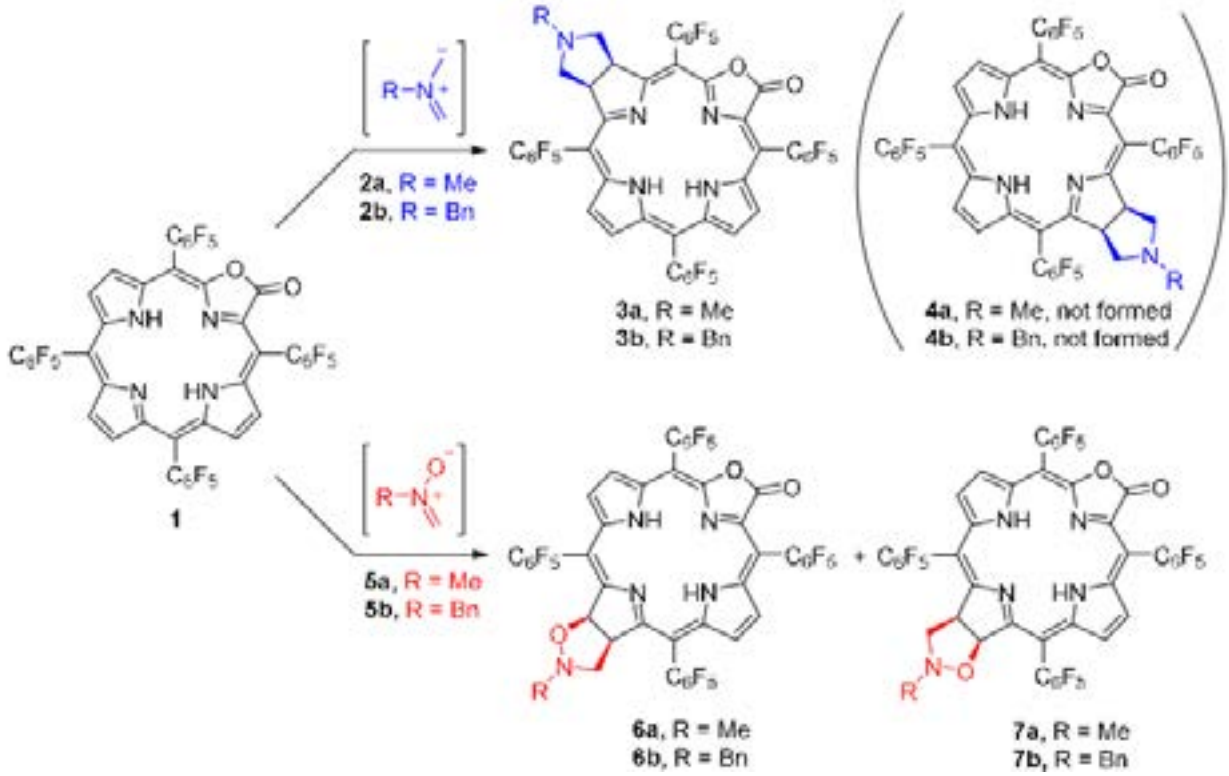


Fig. 1. Synthesis of corresponding porpholactone cycloadducts

[1] C. Brückner, *Acc. Chem. Res*. **2016**, *49*, 1080.
[2] L.D. Costa, J.I.T. Costa, A.C. Tomé, *Molecules* **2016**, *21*, 320.

# OPTICAL PROPERTIES OF FOG INTERSTITIAL AEROSOL PARTICLES IN THE PO VALLEY (ITALY)

Julija Pauraite[1], Stefania Gilardoni[2], Francesca Costabile[2], Luca Diliberto[2], Gianpaolo Gobbi[2], Francesca Barnaba[2], Matteo Rinaldi[2], Marco Paglione[2], Stefano Decesari[2], Maria Cristina Facchini[2], Giulia Pavese[3], Vidmantas Ulevicius[1]

[1] Center for Physical Sciences and Technology, Savanoriu 231, Vilnius, Lithuania
[2] Institute of Atmospheric Sciences and Climate (ISAC) of the National Research Council of Italy (CNR), Bologna, 40129, Italy
[3] Institute of Methodologies for Environmental Analysis of the National Research Council of Italy (CNR), Tito Scalo, 85050, Italy
julija.pauraite@ftmc.lt

The interaction between aerosol and atmospheric water (such as fog) can affect microphysical and chemical properties of atmospheric particles [1]. Nevertheless, there is lack of knowledge about changes in chemical composition and optical properties due to the fog. Several studies have proved the influence of fog on aerosol size and chemical composition [2]. The increasing frequency of fog in rising economy countries, characterized by high aerosol emissions, urges a better knowledge of aerosol-fog interaction.

We investigated aerosol optical properties in fall-wintertime in San Pietro Capofiume (rural background site) in the Po Valley. During experiments in November-December 2015, we deployed an Aerosol Mass Spectrometer (HR-ToF-AMS), a 7-wavelength Aethalometer, and an integrating Nephelometer (TSI). Ancillary measurements included liquid water content and the meteorological parameters (relative humidity, temperature and wind speed). We used Positive matrix factorization (PMF) of AMS organic aerosol mass spectra to further characterize the sources of ambient organic aerosol (OA). Furthermore, absorption Angström exponent (AAE), scattering Angström exponent (SAE) and single scattering albedo (SSA) were calculated.

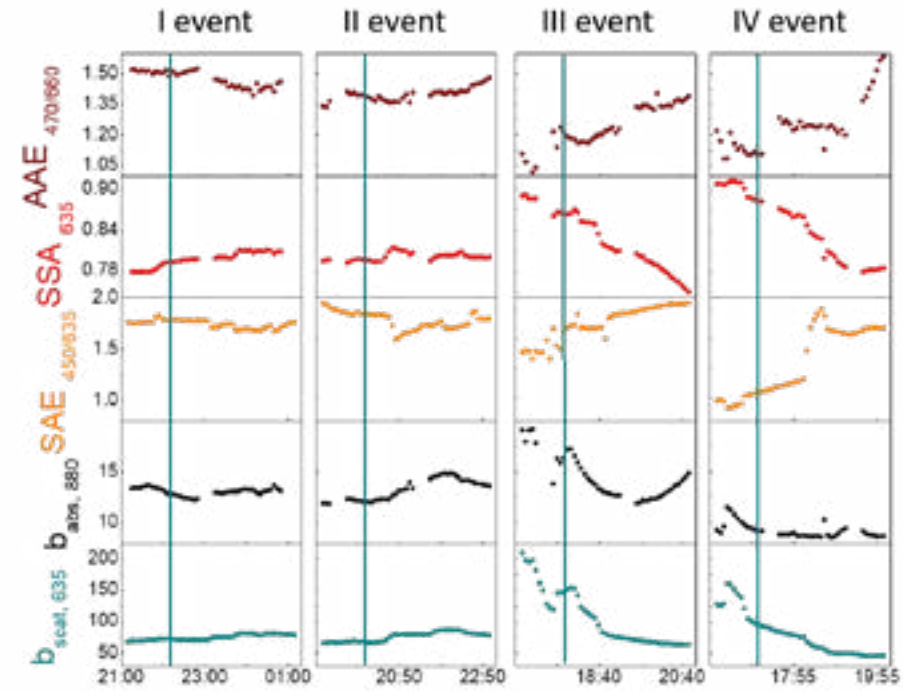


Fig 1. Time trend of AAE (brown), SSA (red), SAE (orange), babs (black) and bscat (blue) one hour before and three hours after the beginning of each fog event. Light-blue vertical lines indicate the formation of each fog.

Three types of OA were observed: hydrocarbon-like organic aerosol (HOA), biomass burning organic aerosol (BBOA) and oxygenated organic aerosol (OOA). During 4 fog events the scavenging efficiency of OOA was the highest and varied between 37% and 57%. The changes in aerosol optical properties 1 h before and during the fog formation were observed (Fig 1). During all fog events, AAE followed changes of BBOA. Based on AAE and SAE values different mixed states were characterised. Main changes due to the fog appeared in SSA, followed by decrement by 0.07 unit during first 3 h after the fog formation. Identified changes in atmosphere due to the fog estimated by this study can be used to forecast the air quality at highly polluted areas with increasing fog frequency.

[1] S. Gilardoni et al., (2014). Atmospheric Chemistry and Physics, 14, 6967–6981.
[2] M. Sasakawa et al., (2003). Journal of Geophysical Research. Atmospheres, 108.

# ELECTROCHEMICAL IMPEDANCE SPECTROSCOPY AS A TOOL FOR THE INVESTIGATION OF REDOX ACTIVITY OF LIVING CELLS

Jurate Petroniene[1], Inga Morkvenaite-Vilkonciene[2], Juste Rozene[2], Arunas Ramanavicius[1,3]

[1] Department of Physical Chemistry, Faculty of Chemistry and Geoscience, Vilnius University, Vilnius, Lithuania;
[2] Department of Mechatronics and Robotics, Faculty of Mechanics, Vilnius Gediminas Technical University, J.Basanaviciaus 28, 03224 Vilnius, Lithuania;
[3] Laboratory of NanoTechnology, Institute of Semiconductor Physics, State Research Institute Centre for Physical and Technological Sciences, Sauletekio av. 3, LT-10222 Vilnius, Lithuania;
arunas.ramanavicius@chf.vu.lt

Electrochemical impedance spectroscopy (EIS) is widely used in various bioelectrochemical researches. Conventional EIS techniques gives only average response of the whole system. In order to observe localized EIS, the working electrode has to be moved in close to the surface of interest. In this case, scanning electrochemical microscopy (SECM) [1] and EIS could be merged, and this system is called scanning electrochemical impedance microscopy (SEIM). However, measurements by this technique are complicated due to very long experiment time, for example, in the 1mHz-100kHz frequency range measurement of EIS at one point will take 20 min. To take care of this problem, SECM can be combined with Fast Fourier transformation (FFT) electrochemical impedance technique, which measures electrochemical impedance in early mentioned range of frequencies in seconds. Thus, we have three techniques for the EIS measurements, each of them has its own advantages/disadvantages. The idea of our research was to compare these three techniques in order to find out the differences of results when biological samples are investigated. We choose yeast Saccaromyces cerevisiae [2], diluted in suspension (non-immobilized) [3]. We used two redox mediators-based system, one of them was lipophilic redox mediator 2-Methyl-1,4-naphthoquinone (Menadione), and another - hydrophilic mediator sodium 1,4–naphthoquinone–2–sulfonate. We measured EIS with all three techniques. It was found that the response depends on time, therefore, EIS-FFT technique in living cells investigation is a very promising candidate (Fig. 1). On the other hand, the yeast reaches steady-state after some time. Therefore, conventional EIS has the same advantage then one is interested in the final result of processes, occurred in the cells. Using SEIM, the volume of solution is small, and working electrode is ultramicroelectrode (UME), thus, the steady-state current on UME can be achieved very fast. This tool could be used to detect yeasts redox activity in industry using small volumes of yeast suspensions.

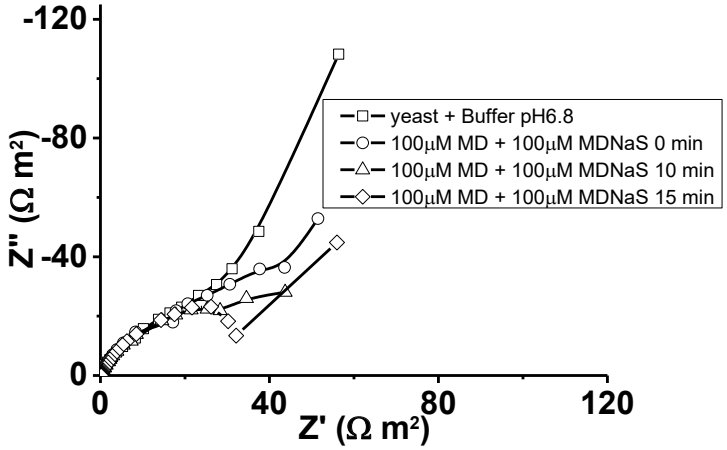


Fig. 1. EIS registered in SEIM mode at different time intervals. Yeasts was dissolved and measured in PBS, pH 6.8, at -0,5V *vs* Ag|AgCl|$KCl_{(sat.)}$

**Acknowledgements** This research was funded by the European Social Fund according to the activity "Development of Competences of Scientists, other Researchers and Students through Practical Research Activities" of Measure No. 09.3.3-LMT-K-712. Project No 09.3.3-LMT-K-712-02-0137

**Keywords** Electrochemical impedance microscopy, *Saccharomyces cerevisiae*, two redox mediators-based system, menadione

[1] Morkvenaite-Vilkonciene, I., A. Ramanaviciene, and A. Ramanavicius, 9,10-Phenanthrenequinone as a redox mediator for the imaging of yeast cells by scanning electrochemical microscopy. Sensors and Actuators B: Chemical, 2016. 228: p. 200-206.

[2] A.Ramanavicius, I. Morkvenaite-Vilkonciene, A. Kisieliute, J.Petroniene, A.Ramanaviciene. Scanning electrochemical microscopy based evaluation of influence of pH on bioelectrochemical activity of yeast cells − Saccharomyces cerevisiae Colloids and Surfaces B: Biointerfaces. Amsterdam : Elsevier Science BV Vol. 149 (2017). p. 1-6. ISSN: 0927-7765; DOI: 10.1016/j.colsurfb.2016.09.039

[3] Sh. Yamashoji Different characteristics between menadione and menadione sodium bisulfite mediator in yeast suspension. Biochemistry and Biophysics Reports. Volume 6, July 2016, Pages 88-93; https://doi.org/10.1016/j.bbrep.2016.03.007

# SYNTHESIS OF CATIONIC STARCH USING 3-CHLORO-2-HYDROXYPROPYL TRIMETHYLAMONIUM CHLORIDE

Karolina Almonaityte[1], Joana Bendoraitiene[1], Ramune Rutkaite[1], Greta Cizauskaite[1], Véronique Coma[2]

[1]Department of Polymer Chemistry and Technology, Kaunas University of Technology, Lithuania
[2]University of Bordeaux, UMR 5629, CNRS, LCPO, France
karolina.almonaityte@ktu.edu

Recently modified biopolymers as cheap and effective sorbents are widely investigated. Among these, starch is biodegradable, renewable and relatively inexpensive biopolymer, which makes it attractive as an environmentally friendly material for industrial use [1]. The properties of chemically modified starches are very different from those of native starch. Cationic starch with positively charged functional groups can be used in the wastewater treatment processes in order to remove negatively charged organic and inorganic impurities.

Cationic starches of different DS were obtained by etherification of native potato starch (S) with 3-chloro-2-hydroxypropyl trimethylammonium chloride (CHPTAC) using NaOH and adding CaO. Molar ratios of reagents in the reaction mixture S : CHPTAC: NaOH: CaO are shown in Table 1. Reactions were carried out at 45 °C for 44-48 h and obtained cationic starches powders were purified by washing with isopropanol and water mixture and when followed by the Soxhlet extraction with methanol.

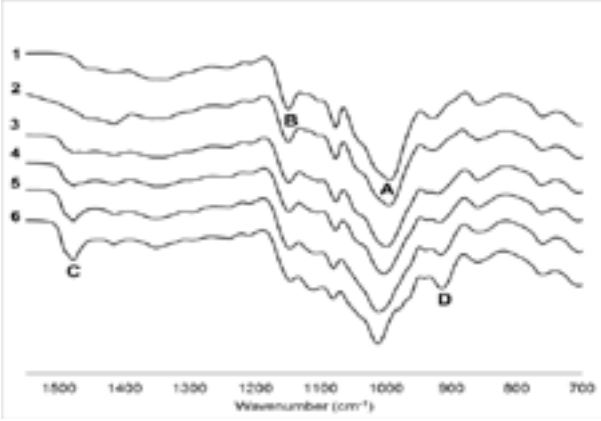


Fig. 1. FT-IR spectra of potato starch (1) and cationic starches with different DS: 2 – 0.05; 3 – 0.25; 4 – 0.40; 5 – 0.56; 6 – 0.84

Table 1. Influence of reagents molar ratio in reaction mixture on DS of cationic starches

| Molar ratio of reagents S : CHPTAC : NaOH : CaO | Degree of substitution (DS) | Reaction yield, % |
|---|---|---|
| 1 : 0.05 : 0.09 : 0.04 | 0.05 | 100 |
| 1 : 0.25 : 0.29 : 0.04 | 0.25 | 100 |
| 1 : 0.40 : 0.44 : 0.04 | 0.40 | 100 |
| 1 : 0.60 : 0.64 : 0.04 | 0.56 | 93 |
| 1 : 1.00 : 1.04 : 0.04 | 0.84 | 84 |

FT-IR spectra (Fig. 1) showed characteristic peaks of native starch and cationic starches. The strong band at 1008 $cm^{-1}$ (peak A) is attributed to CH2–O–CH2 stretching vibrations, peak around 1152 $cm^{-1}$ (peak B) is assigned to C–O stretching vibrations, and peak around 1480 $cm^{-1}$ ( peak C) is characteristic of C–N bonds of quaternary ammonium groups. Peak D at 944 $cm^{-1}$ corresponds to the stretching vibrations of quaternary ammonium group.

Furthermore, the physical properties of CHPTAC modified starches were very much different from those of native starch. X-ray diffraction analysis revealed that degree of crystallization in synthesized cationic starches was lower than that in native starch. Moreover, the gelatinization of modified starches proceeded at higher temperatures than that of starch and maximum viscosity of paste during the gelatinization was significantly lower.

Acknowledgment. The financial support of the Research Council of Lithuania for the Lithuanian-French programme “Gilibert” project No. S-LZ-19-6 is highly acknowledged.

[1] X. Guo-xiu, Z. Shu-fen, J. Ben-zhi, Y. Jin-zong, Study on adsorption behavior of crosslinked cationic starch maleate for chromium (VI), Carbohydrate Polymers: **66**, 246–251(2006).

# THE INFLUENCE OF CRYSTALLITE SIZE ON MAGNETORESISTIVITY OF NANOSTRUCTURED $La_{1-x}Sr_xMn_yO_{3\pm\delta}$ THIN FILMS

Karolis Motiejuitis[1], Rasuolė Lukošė[2], Valentina Plaušinaitienė[1]

[1]Institute of Chemistry, Faculty of Chemistry and Geosciences, Vilnius University, Naugarduko st. 24, LT- 03225 Vilnius, Lithuania

[2]Department of Material Science and Electrical Engineering, Center for Physical Sciences and Technology, Sauletekio av. 3, LT-10257 Vilnius, Lithuania

Karolis.motiejuitis@chgf.stud.vu.lt

$La_{1-x}Sr_xMn_yO_{3\pm\delta}$ (LSMO) is an interesting material for its magnetoresistive (MR) properties where the resistance of the substance is changing under the influence of magnetic field. Due to this effect polycrystalline LSMO films are already used as scalar magnetic field sensors [1]. Currently used magnetic field sensors based on LSMO are operating at relatively high magnetic fields (>10 T), while at lower magnetic fields the magnetoresistance anisotropy (MRA) becomes a main problem. Therefore, to enable the usage of LSMO films as magnetic field sensors at average and low magnetic fields, the control and reduction of MRA should be achieved.

In the present study LSMO films were grown by pulsed injection metal organic chemical vapor deposition (PI-MOCVD) method. Two types of experiments were performed to grow LSMO films: 1) by using a single injector with precursor solution; 2) by using two injectors, one with precursor solution and the second one with pure solvent. The used technological changes, with certain supply of the precursor and/or solvent solution, enabled the dilution of the precursors in the vapor phase and to control the growth of LSMO films at early growth stage. The surface morphology of the grown LSMO films was characterized by Scanning Electron Microscopy (SEM), elemental composition by Inductively Coupled Plasma – Mass Spectrometry (ICP-MS), crystallographic properties by X-ray Diffractometry (XRD), and magnetoresistance magnitude was measured under permanent magnetic field up to 0.7 T using an electromagnet.

Chemical composition of LSMO films remained the same independent of differences in deposition process. However, larger crystallites were observed for second deposition series resulting in higher MR and nearly two times lower MRA, leading to improved possibility of LSMO films as magnetic field sensors at low and intermediate magnetic fields.

[1] Balevičius, S.; Žurauskienė, N.; Stankevič, V. ir kt. *Nanostructured thin manganite films in megagauss magnetic field.* Applied Physics Letters, **2012**, nr. 101 (9), p. 407-411.

# OPTICAL PROPERTIES OF $CaAlBO_3F_2$ GLASSY MATRIX DOPED WITH RARE-EARTH ELEMENTS (Eu, Sm, Pr)

Dominika Wąs[1], Agata Gołębiewska[1], Jakub Płachta[2], Tomasz K. Pietrzak[1]

[1] Faculty of Physics, Warsaw University of Technology, Koszykowa 75, 00-662 Warsaw, Poland
[2] Institute of Physics, Polish Academy of Sciences, Lotników 32/46, 02-668 Warsaw, Poland
dominika.was.96@gmail.com

Rare-earth elements (REE) are extremely important components of many technology fields, such as lasers in military and medicine, telecomunication and for LED lamps production. Currently, the most common LED's phosphors are made of materials doped with REE. Futhermore, luminescent materials doped with europium have been used in lighting and displays. For instance, the famous phosphor $Y_2O_2S:Eu^{3+}$ (red emission) has been used in high efficiency flourescent lamps, field emission displays and plasma display panels [1]. The colour emitted by phosphors can be altered by doping with different rare-earth ions [2]. Lanthanides (REE subgroup that includes europium, samarium and praseodymium) are characterised by specific electronic configuration where *4f* shell is not fully filled with electrons and screened by external shells. Therefore, opticaly active *4f* shell electrons are preserved from the influence of the surrounding. This is why mentioned spectacular phenomenon has found various applications including LED lamps phosphors, the most significant from this research point of view.

Latest studies have shown very attractive luminescence properties of materials doped with trivalent rare-earth ions. Many consider europium to be one of the most important activator to produce intense pure red emission [3].

Recently, Solid State Ionic Divison's research showed that the ratio of $Eu^{2+}/Eu^{3+}$ can be controlled by altering synthesis conditions during melt-quenching process [4]. In such action one can obtain glass with continuous photoluminescence spectrum close to visible light spectrum. This leads to the purpose of this research which is investigating another glassy matrix doped with europium and other REE, samarium and praseodymium.

Therefore, $CaF_2$-$Al_2O_3$-$B_2O_3$ glassy matrix doped with 1 wt% of REE oxide ($Eu_2O_3$, $Pr_6O_{11}$, $Sm_2O_3$) was obtained by melt-quenching method. Substrates were melted for 15 min in 1300 °C. In Fig. 1 one can see photographs of samples with visible photoluminescence effect after excitation with 405 nm laser.

Figure 1. Matrix doped with: left - $Sm_2O_3$, right: $Eu_2O_3$.

Obtained materials were investigated using X-ray diffractometry (XRD), differential thermal analysis (DTA) and photoluminescence spectrum measurements (PL). Therefore, aim of this research is to investigate and compare properties of glassy matrix doped with different REE.

[1] Jianwei Qiao, Lei Wang, Yongfu Liu, Ping Huang, Qiufeng Shi, Yue Tian, Cai'e Cui, *Preparation, photoluminescence and thermally stable luminescence of high brightness red $LiY_5P_2O_{13}:Eu^{3+}$ phosphor for white LEDs,* Journal of Alloys and Compounds 686 (2016) 601e607.

[2] Xiulan Wu, Yehui Jiao, Qiang Ren, Ou Hai, Fei Lin, Huanhuan Li, Wenni Bai, *Photoluminescence and energy transfer in $Sr_3La(BO_3)_3$:Ce, Sm and $Sr_2TiO_4$:Sm, Eu phosphors*, Optics and Laser Technology 108 (2018) 456–465.

[3] Heng Guo, Liangling Sun, Jia Liang, Bin Li, Xiaoyong Huang, *High-efficiency and thermal-stable $Eu^{3+}$-activated $Ca_3Y(AlO)_3(BO_3)_4$ redemitting phosphors for near-UV-excited white LEDs,* Journal of Luminescence 205 (2019) 115–121.

[4] Tomasz K. Pietrzak, Agata Gołębiewska, Jakub Płachta, Michał Jarczewski, Jacek Ryl, Marek Wasiucionek, Jerzy E. Garbarczyk, *Photoluminescence of partially reduced $Eu^{2+}/Eu^{3+}$ active centers in a $NaF–Al_2O_3–P_2O_5$ glassy matrix with tunable smooth spectra,* Journal of Luminescence 208 (2019) 322–326.

# DETECTION OF C4 PLANT SUGAR IN ADULTERATED HONEY USING IRMS AND UHPLC

Krišs Dāvids Labsvārds[1], Lauma Buša[1], Kristīne Meile[2], Arturs Vīksna[1]

[1] Department of Chemistry, University of Latvia, Latvia
[2] Latvian State Institute of Wood Chemistry, Latvia
[3]The Institute of Food Safety, Animal Health and Environment "BIOR", Latvia
kriss.labsvards@gmail.com

Honey is a sweet, viscous food substance produced by bees from floral nectar. Natural bee honey is a unique sweetening agent that can be used by humans without processing. However, honey can easily be adulterated with various cheaper sweeteners, resulting in higher commercial profits [1]. Commonly used adulterants include high fructose corn syrup, maltose syrup, refined beet and cane sugar etc. Stable isotope ratio mass spectrometry (SIRMS) can be used to determine the adulteration of honey with C4 plant (corn or cane) sugar since its $\delta^{13}C$ values are around -10‰ to -20‰ but bees use floral nectar from C3 plants which $\delta^{13}C$ values are about -22‰ to -33‰. Significant $\delta^{13}C$ value difference between honey and its protein provide valuable information of honey authenticity [2,3].

Five adulterated honey samples were made adding different amounts of sugarcane sucrose syrup (3%, 6%, 9%, 12%, 15%) to pure honey. The protein from the honey was extracted using dialysis membrane with MWCO 12 kDa. Determination of $\delta^{13}C$ ratios in protein and honey was carried out with Nu Horizon SIRMS at the University of Latvia, using certified organic reference materials USGS-40 and USGS-41 (L-Glutamic acid). The $\delta^{13}C$ values are expressed relative to VPDB. Waters Acquity UHPLC system with Waters Acquity UHPLC BEH Amide column (100 mm × 2.1 mm, ⌀ 1.7 μm) combined with Waters ELSD detector were used to determine weight fraction of sucrose in pure and adulterated honeys

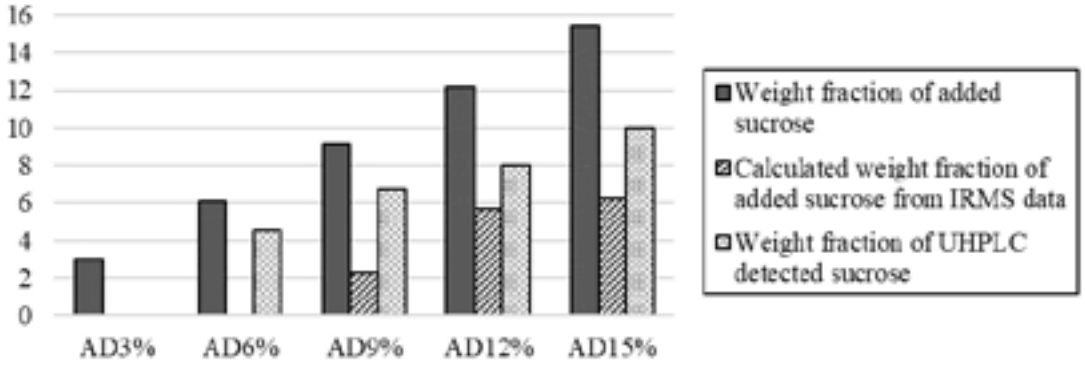


Fig. 1. Weight fraction of sucrose in adulterated honey.

Despite dissimilar results of calculated and detected weight fraction of sucrose to actually added weight fraction, results show expected increase in $\delta^{13}C$ values as C4 plant adulterant concentration increases to honey. Only adulterated honeys with added sucrose content higher than 6% weight fraction have high enough $\delta^{13}C$ value difference between honey and protein to calculate amount of added sucrose. UHPLC method did not provide exact quantitative information to components which weight fraction is lower than 5%.

[1] M. Oroian, S. Ropciuc, S. Paduret, Honey adulteration detection: voltammetric e-tongue versus official methods for physicochemical parameter determination, Journal of The Science of Food and Agriculture **98**, 4304-4311 (2018).
[2] L. S. Chua, J.Y. Lee, G.F. Chan, Honey protein extraction and determination by mass spectrometry, Analytical and Bioanalytical Chemistry **405**, 3063-3074 (2013).
[3] L. Wu, B. Du, Y. V. Heyden, L. Chen, L. Zhao, M. Wang, X. Xue, Recent advancements in detecting sugar-based adulterants in honey – A challange. Trends in Analitical Chemistry **86** 25-38 (2017).

# STRUCTURAL ASPECTS OF FORMATION OF SOLID SOLUTIONS IN DIFFERENT BENPERIDOL - DROPERIDOL PHASES

Kristaps Saršūns, Agris Bērziņš, Elīna Sala

Faculty of Chemistry, University of Latvia, Jelgavas street 1, Riga, Latvia
kristapssarsuns@inbox.lv

Benperidol and droperidol are neuroleptic pharmaceuticals used as antipsychotics. Both compounds have very similar molecular structures - the two are only different by the order of C-C bond in the central ring (see. Figure.1 - piperidine ring in benperidol, tetrahydropyridine in droperidol).

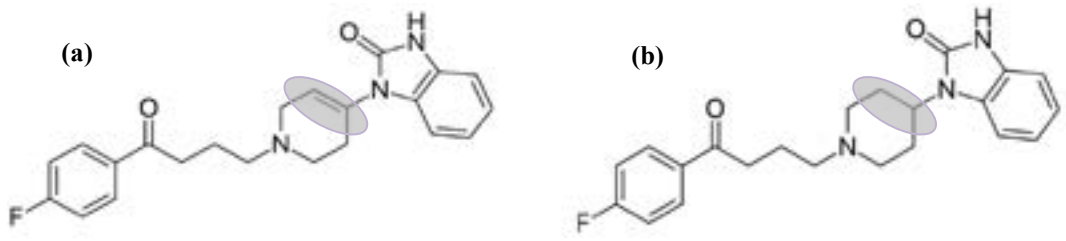


**Figure 1. Molecular structure of (a) droperidol and (b) benperidol**

It is known that benperidol forms five polymorphs ($^{B}$I – $^{B}$V) and eleven solvates (the most stable being $^{B}S_{Me}$, $^{B}S_{Et}$, $^{B}S_{ACN}$, $^{B}$DH), but droperidol forms four polymorphs ($^{D}$I – $^{D}$IV) and eleven solvates (the most stable being $^{D}S_{Me}$, $^{D}S_{Et}$, $^{D}S_{ACN}$, $^{D}$DH) [1,2]. In previous research in cross-seeding experiments it was observed that it is possible to obtain droperidol phases isostructural to the benperidol phases, which suggest on solid solution formation between both compounds [3].

In this research mixtures of both compounds were crystallized to test the solid solution formation (see Table 1) while computational calculations were carried out to identify structural aspects responsible for differences observed in solid solution formation in different phases.

**Table 1. Experimentally obtained crystalline phases in benperidol – droperidol mixtures**

| Benperidol – droperidol proportion, % | Phase | | | | |
|---|---|---|---|---|---|
| | Methanol solvate | Acetonitrile solvate | Ethanol solvate | Ansolvate | Dihydrate |
| 0:100 | $^{D}S_{Me}$ | $^{D}S_{ACN}$ | $^{D}S_{Et}$ | $^{D}$II | $^{D}$DH |
| 5:95 | ***SS$^{D}S_{Me}$*** | ***SS$^{D}S_{ACN}$*** | $SS^{D}S_{Et}$+$SS^{B}S_{Et}$ | $SS^{D}$II+$SS^{B}$II | ***SS$^{D}$DH*** |
| 10:90 | ***SS$^{D}S_{Me}$*** | ***SS$^{D}S_{ACN}$*** | ***SS$^{B}S_{Et}$*** | $SS^{D}$II+$SS^{B}$II | ***SS$^{D}$DH*** |
| 20:80 | $SS^{D}S_{Me}$+$SS^{B}S_{Me}$ | ***SS$^{D}S_{ACN}$*** | ***SS$^{B}S_{Et}$*** | ***SS$^{B}$II*** | $SS^{D}$DH+$SS^{B}$DH |
| 30:70 | $SS^{D}S_{Me}$+$SS^{B}S_{Me}$ | $SS^{D}S_{ACN}$+$SS^{B}S_{ACN}$ | ***SS$^{B}S_{Et}$*** | ***SS$^{B}$II*** | $SS^{D}$DH+$SS^{B}$DH |
| 40:60 | $SS^{D}S_{Me}$+$SS^{B}S_{Me}$ | $SS^{D}S_{ACN}$+$SS^{B}S_{ACN}$ | ***SS$^{B}S_{Et}$*** | ***SS$^{B}$II*** | $SS^{D}$DH+$SS^{B}$DH |
| 50:50 | ***SS$^{B}S_{Me}$*** | $SS^{D}S_{ACN}$+$SS^{B}S_{ACN}$ | ***SS$^{B}S_{Et}$*** | ***SS$^{B}$II*** | $SS^{D}$DH+$SS^{B}$DH |
| 60:40 | ***SS$^{B}S_{Me}$*** | $SS^{D}S_{ACN}$+$SS^{B}S_{ACN}$ | ***SS$^{B}S_{Et}$*** | ***SS$^{B}$II*** | $SS^{D}$DH+$SS^{B}$DH |
| 70:30 | ***SS$^{B}S_{Me}$*** | ***SS$^{B}S_{ACN}$*** | ***SS$^{B}S_{Et}$*** | ***SS$^{B}$II*** | ***SS$^{B}$DH*** |
| 80:20 | ***SS$^{B}S_{Me}$*** | ***SS$^{B}S_{ACN}$*** | ***SS$^{B}S_{Et}$*** | ***SS$^{B}$II*** | ***SS$^{B}$DH*** |
| 90:10 | ***SS$^{B}S_{Me}$*** | ***SS$^{B}S_{ACN}$*** | ***SS$^{B}S_{Et}$*** | ***SS$^{B}$II*** | ***SS$^{B}$DH*** |
| 95:5 | – | – | – | ***SS$^{B}$I*** | – |
| 100:0 | $^{B}S_{Me}$ | $^{B}S_{ACN}$ | $^{B}S_{Et}$ | $^{B}$I | $^{B}$DH |

D – droperidol phase, B – benperidol phase, $S_{Me}$ – methanol solvate, $S_{Et}$ – ethanol solvate, $S_{ACN}$ – acetonitrile solvate, DH – dihydrate, I, II – polymorphs, SS – solid solution.

[1] Bērziņš, A.; Skarbulis, E.; Rēķis, T.; Actiņš, A. On the Formation of Droperidol Solvates: Characterization of Structure and Properties. *Crystal Growth & Design*. **2014**, *14*, 2654-2664.p.

[2] Bērziņš, A.; Skarbulis, E.; Actiņš, A. Structural Characterization and Rationalization of Formation, Stability, and Transformations of Benperidol Solvates. *Crystal Growth & Design*. **2015**, *15*, 2337-2351.p.

[3] Bērziņš, A.; Actiņš, A. Why Do Chemically Similar Pharmaceutical Molecules Crystallize in Different Structures: A Case of Droperidol and Benperidol. *Crystal Growth & Design*. **2016**, *16*, 1643-1653.p.

# FRACTIONATION OF STABLE CARBON ISOTOPE ($\delta^{13}C$) IN AUTOMOTIVE PARTICULATE MATTER EMISSIONS

Laurynas Bučinskas[1,2], Andrius Garbaras[1,2], Jonas Matijošius[3]

[1] Department of Nuclear Research, Center for Physical Sciences and Technology, Lithuania
[2] Faculty of Physics, Vilnius University, Lithuania
[3] Faculty of Transport Engineering, Vilnius Gediminas Technical University, Lithuania
laurynas.bucinskas@ftmc.lt

It is well known that excessive automotive engine exhaust emissions of gases (carbon monoxide, hydrocarbons, nitrogen oxide) and particulate matter (PM) pose a threat to public health and urban air quality. Human exposure to polluted air containing PM can cause numerous health problems, such as cardiovascular, cerebrovascular and respiratory diseases [1]. In an effort to reduce automotive emissions modern cars use a variety of engine modifications, catalytic systems and filters which in turn alter the isotopic ratio of carbonaceous particles (isotopic fractionation effect). Diesel engines are of particular interest due to higher production of particulates (soot) in comparison to gasoline engines [2].

The aim of this work was to examine particulate matter fractionation in automotive emissions using $\delta^{13}C$ and $^{14}C$ measurements. Experiments were performed in a specialized dynamometer laboratory to ensure reproducibility and accuracy of the results. Four light passenger vehicles with different fuels (diesel, 95 RON gasoline, 98 RON gasoline) were tested using simulated transient cycles in urban and rural areas. Additionally, driving modes of 30, 60, 90 km/h and at maximum power were tested. Engine exhaust particulate matter was collected on quartz filters. Later, isotopic ratio $\delta^{13}C$ values of fuel and exhaust carbonaceous particulates were measured using stable isotope ratio mass spectrometer. $\delta^{13}C$ values were then compared and level of isotopic fractionation determined, as shown in Fig 1. Finally, biofuel fraction was evaluated using accelerator mass spectrometer which required additional intermediate sample graphitization step.

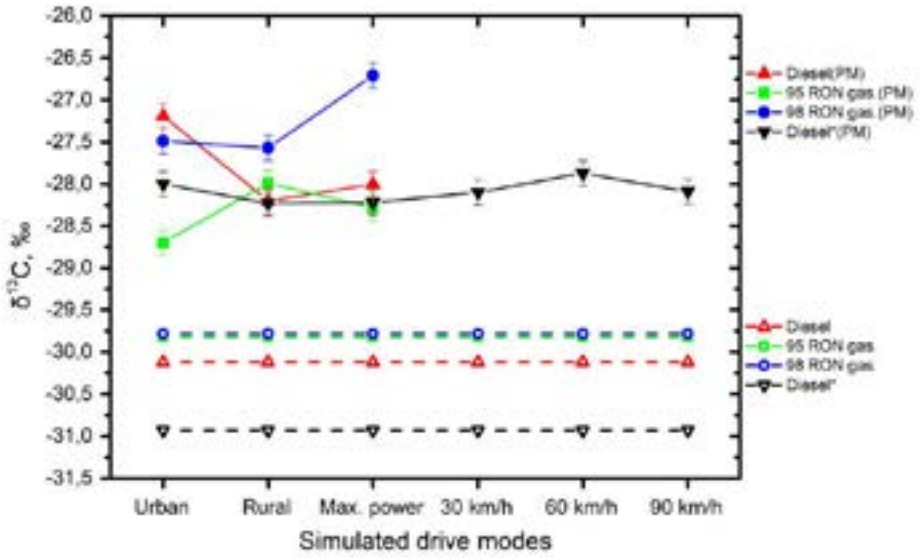


Fig. 1. $\delta^{13}C$ values of particulate matter and fuel in liquid phase during separate simulated drive modes.

The obtained results show particulate matter $\delta^{13}C$ values ranging from -28.7 ‰ to -26.7 ‰ during separate driving modes. Most significant fractionation was observed when using diesel fuel. Average $\delta^{13}C$ value was found to be equal to -27.9 ‰ in automotive emissions and fractionation $\Delta^{13}C$ (particulates-fuel) equal to 2.1 ‰. Finally, it was determined that biofuel fraction in fuels differed considerably and ranged from 6.1 % to 13.5 %.

[1] J. O. Anderson, J. G. Thundiyil, and A. Stolbach, "Clearing the Air: A Review of the Effects of Particulate Matter Air Pollution on Human Health," *Journal of Medical Toxicology*. 2012.
[2] M. V. Twigg, "Progress and future challenges in controlling automotive exhaust gas emissions," *Appl. Catal. B Environ.*, 2007.

# TRACING ANTHROPOGENIC 14C REDISTRIBUTION IN THE IGNALINA NUCLEAR POWER PLANT COOLING POND

Laurynas Butkus[1], Rūta Barisevičiūtė[1], Žilvinas Ežerinskis[1], Justina Šapolaitė[1], Evaldas Maceika[1], Algirdas Pabedinskas[1], Andrius Garbaras[1], Jonas Mažeika[2], Rūta Druteikienė[1], Vidmantas Remeikis[1]

[1] Center for Physical Sciences and Technology, Vilnius, Lithuania
[2] Nature Research Centre, Vilnius, Lithuania
laurynas.butkus@ftmc.lt

Radiocarbon ($^{14}C$) is a long-lived carbon isotope that has a half-life of 5730 ± 40 years. $^{14}C$ is produced naturally by cosmic radiation in the upper atmosphere. Nuclear power plants are one of the main producers of anthropogenic $^{14}C$. In nuclear reactors, the formation of radiocarbon takes place in the coolant, the cooling system of the control and safety rod channels, fuel elements and graphite brickwork [1]. Anthropogenic radiocarbon can be released into the environment in gaseous forms, with liquid releases or with spent nuclear fuel.

During photosynthesis radiocarbon can be easily assimilated into the plants. As a result, $^{14}C$ can be transported through the food chain and accumulate in a human body. Therefore, radiocarbon is considered a primary source of increased human radiation dose from industrial nuclear activities [2].

The aim of this research was to evaluate the impact of anthropogenic $^{14}C$ contamination from Ignalina NPP (INPP) on the Lake Drūkšiai (the Ignalina Nuclear Power Plant cooling pond) system. The lake sediment and vendace (*Coregonus albula*) scale samples were collected from the Drūkšiai lake. The ages of sediment layers were estimated using $^{137}Cs$ and $^{210}Pb$ dating methods. ABA (acid-base-acid) chemical pretreatment procedure was used to extract humin (HM) and humic acid (HA) fractions from the sediments. Chemically pretreated samples were graphitized with the Automated Graphitization Equipment AGE 3 (IonPlus AG). Radiocarbon measurements in prepared samples were performed using the single stage accelerator mass spectrometer (SSAMS, NEC, USA).

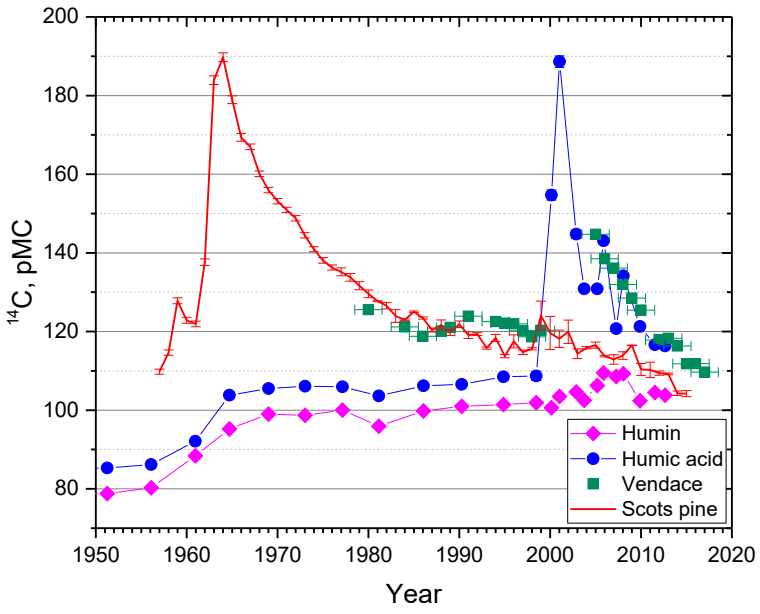


Fig. 1. Temporal $^{14}C$ variations in the INPP cooling pond and the tree rings of Scots pine

$^{14}C$ measurements in HM and HA fractions showed that after the start of the operation of the INPP in 1983, the radiocarbon concentration in these organic fractions increased by 3.86 pMC and 2.6 pMC, respectively (Fig. 1). Furthermore, $^{14}C$ content in vendace scales increased from 121.2 pMC (in 1984) to 123.9 pMC (in 1991).

In 1999s, there is a sharp increase of $^{14}C$ concentration (by 79.89 pMC) in HA fraction. In the same year, an increase of radiocarbon content in the Scots pine (*Pinus sylvestris*) near the INPP was also observed [3]. Since 2001, $^{14}C$ activities in vendace scales are similar to those in HA. The $^{14}C$ enriched organic matter that was released from the INPP in 1999s was incorporated into the food chain and then accumulated both in sediments and fish.

[1] V. B. Gaiko et al., Discharge of 14C by nuclear power stations with RBMK-1000 reactors, Sov. At. Energy 59, 703–705 (1985).
[2] IAEA, Generic Models for Use in Assessing the Impact of Discharges of Radioactive Substances to the Environment., (2001).
[3] Ž. Ežerinskis et al., Annual Variations of 14 C Concentration in the Tree Rings in the Vicinity of Ignalina Nuclear Power Plant, Radiocarbon 60, 1227–1236 (2018).

# SYNTHESIS OF SODIUM YTTRIUM FLUORIDE VIA HYDROTHERMAL METHOD AND CHARACTERIZATION

Lukas Bereiša, Simas Šakirzanovas

Institute of Chemistry, Department of Applied Chemistry, Vilnius University, Vilnius, Lithuania
lukas.bereisa@chf.stud.vu.lt

Various rare-earth doped fluorides caught scientist attention recently as promising luminescent materials. One of those is sodium yttrium fluoride, which is interesting host to be doped with rare-earth ions as it possess appropriate optical properties, is thermally stable and biologically inert material [1].

Not only size of the particles but shape as well is responsible for various physicochemical properties of material, including luminescence. Rare earth doped fluorides can be applied as phosphors in light emitting diodes (LEDs), solid-state lasers, displays, solar cells, as anti-counterfeiting agents and so on [2]. $NaYF_4$ can also be applied in biomedical field as well - as bio-imaging/theranostic particles or as drug delivery probes [3].

Herein we report synthesis route to obtain single-phase $NaYF_4$ particles under hydrothermal conditions. Desired morphology (spheres, rods) can be obtained by altering pH value and amount of coordinating agent (malonic acid) within reaction mixture. Obtained particles were analyzed by means of using X-Ray diffraction (XRD), scanning electron microscopy (SEM).

Further plans are to improve this synthesis route in order to obtain monodisperse particles and to dope them with rare-earth ions.

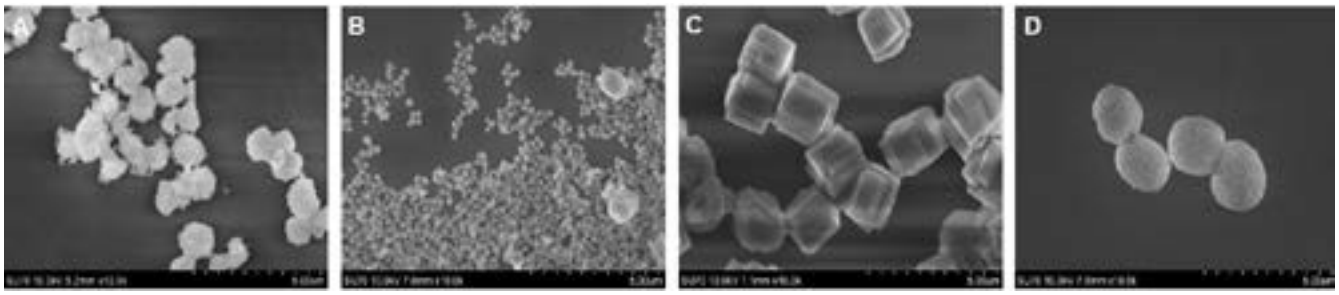


Figure 1. SEM images of $NaYF_4$ particles synthesized via hydrothermal method using different pH: a) 1; b) 5; c) 7; d) 10.

[1] Runowski, M. and Lis, S., *Nanocrystalline rare earth fluorides doped with $Pr3^+$ ions.* Applied Surface Science, 2014. **320**(0): p. 742-745.
[2] Wang, Z., et al., *Synthesis and enhancement of red UC luminescence properties of ordered hexagonal $NaYF_4$:$Yb^{3+}$/$Er^{3+}$ nanowire arrays.* Journal of Fluorine Chemistry, 2011. **132**(12): p. 1012-1039.
[3] Liang. X., et al., *Synthesis of hollow and mesoporous structured $NaYF_4$:Yb,Er upconversion luminescent nanoparticles for targeted drug delivery*. Journal of Rare Earths, 2017. **35**(5): p. 419-429.

# ELABORATION OF THE NEW METHOD OF SYNTHEESIS OF MxB(CF3)4 SALTS, M=Li, Na, Mg – POTENTIAL SOLID ELECTROLYTES

Magdalena Grochowska [1], Tomasz Jaroń [2]
[1] Faculty of Chemistry, University of Warsaw, Poland
[2] Centre of New Technologies, University of Warsaw, Poland
mm.grochowska3@student.uw.edu.pl

Solid state ionic conductors are interesting alternatives to the solutions of metal salts in organic solvents, which are typically used as electrolytes in electrochemical batteries. One of the groups of potential ionic conductors are the salts of weakly coordinating anions – characterized by very weak cation-anion interactions and high redox and thermal stability. Tetrakistrifluoromethyl borate, [B(CF3 )4]- , is an example of such anion. Although a few of its salts were mentioned in the literature, only the crystal structure of K[B(CF3)4] and Cs[B(CF3)4] were reported, and no electrochemical characterization of such salts has been conducted. The currently known methods of synthesis of the M[B(CF3)4] x salts are either inefficient or hazardous, involving such precursors as fluorine or chlorine monofluoride[1]. Here we present our effort to develop a more convenient synthetic approach, which could be carried out in a typical laboratory. We report a series of the methods tested and present the obtained chemical compounds, characterized by their crystal structures and spectroscopically.

[1] Eduard Bernhardt, Gerald Henkel et al., Synthesis and Properties of the Tetrakis(trifluoromethyl)borate Anion, [B(CF3)4]ÿ: Structure Determination of Cs[B(CF3)4] by Single-Crystal X-ray Diffraction, Chem. Eur. J. 2001, 7, No. 21

# PHENOXAZINES HAVING VARIOUS AROMATIC SUBSTITUENTS AS NEW HOST MATERIALS FOR GREEN PHOSPHORESCENT OLEDS

Saulius Grigalevicius [1], Daiva Tavgeniene [1], Dovydas Blazevicius [1], Baohua Zhang [2], Simona Sutkuviene [3]

[1] Department of Polymer Chemistry and Technology, Kaunas University of Technology, Radvilenu plentas 19, LT50254, Kaunas, Lithuania

[2] Center for Advanced Analytical Science, c/o School of Chemistry and Chemical Engineering, Guangzhou University, Guangzhou 510006, P.R. China

[3] Department of Biochemistry, Faculty of Medicine, Lithuanian University of Health Sciences, Tilzes str. 18, LT47181, Kaunas, Lithuania

dovbla@ktu.lt

In the phosphorescent devices, to reduce quenching associated with relatively long excited-state lifetimes of triplet emitters and triplet-triplet annihilation, triplet emitters are normally used as emitting guests in a host material, and thus suitable hosts are widely investigated for the phosphorescent devices [1, 2]. For electrophosphorescence from triplet guests, it is important that the triplet level of the host would be larger than that of the triplet emitter to prevent reverse energy transfer from the guest back to the host [3]. Another essential requirement is the ability of the material to form stable amorphous films. This property guarantees that the guest stays uniformly diluted in the host to minimize the effect of concentration quenching [4].

The structures of phenoxazine-based host materials **1-3** is shown in Fig. 1. 10-Hexylphenoxazine was firstly synthesized by reaction of 10H-phenoxazine with an excess 1-bromohexane under basic conditions in acetone. 3-Formyl-10-hexylphenoxazine was then prepared from the 10-hexylphenoxazine by the Vilsmeier formylation procedure. The objective material 10-hexyl-3-(1,3-dioxoindan-2-ylmethylene)phenoxazine (**1**) was prepared by the reaction of 3-formyl-10-hexylphenoxazine with an excess of indan-1,3-dione in 1,4-dioxane. 2-(10-Hexylphenoxazin-3-yl)-1-phenylphenanthro[9,10-d]imidazole (**2**) was synthesized by rection of 3-formyl-10-hexylphenoxazine with phenanthrene-9,10-dione, ammonium acetate and aniline in acetic acid. 3-[Bis(9-ethylcarbazol-3-yl)methyl)-10-hexylphenoxazine (**3**) was prepared in rection of 3-formyl-10-hexylphenoxazine with an excess 9-ethylcarbazole.

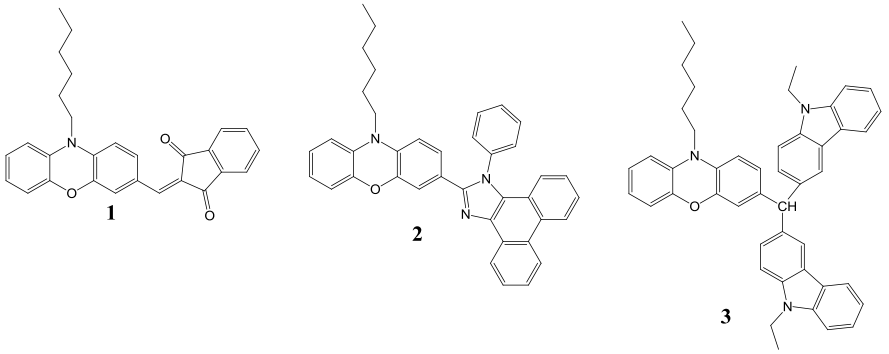


Fig. 1. Phenoxazine - based host materials

Materials **2** and **3** formed homogeneous solid amorphous films with glass transition temperatures of 75 -93 $^{o}$C. Layers of the synthesized compounds showed ionization potentials of 5.24-5.56 eV. Compounds **2** and **3** were tested as host materials for green phosphorescent OLEDs by using green triplet emitter of bis[2-(2-pyridinyl-N)phenyl-C](acetylacetonato)iridium(III) as the guests. The device with the host of material **3** exhibited the best overall performance. The efficient green OLED using the host demonstrated low turn-on voltage of 3.1 V, a maximum brightness of 5366 cd/m$^2$, and maximum current efficiency of 18.3 cd/A. For the technically important brightness of 1000 cd/m$^2$ an efficiency above 15.7 cd/A was detected in the device.

**Acknowledgements.** The OLED materials were develop in the frame of project funded by a grant No. S-MIP-17-64 from the Research Council of Lithuania. Dr. D. Volyniuk is acknowledged for measurements of ionization potentials.

[1] K. S. Yook, J. Y. Lee, Small molecule host materials for solution processed phosphorescent organic light-emitting diodes, Adv. Mater. 26 (2014) 4218.

[2] Y. Tao, Q. Wang, C. Yang, Q. Wang, Z. Zhang, T. Zou, J. Qin, D. Ma, A simple carbazole/oxadiazole hybrid molecule: an excellent bipolar host for green and red phosphorescent OLEDs, Angew. Chem. Int. Ed. 47 (2008) 8104.

[3] C. Adachi, R.C. Kwong, P. Djurovich, V. Adamovich, M. A. Baldo, M.E. Thompson S.R. Forrest, Efficient, deep-blue organic electrophosphorescence by guest charge trapping, Appl. Phys. Lett., 79 (2001) 2082.

[4] J.H. Jou, S. Sahoo, S. Kumar, H.H. Yu, P.H. Fang, M. Singh, G. Krucaite, D. Volyniuk, J.V. Grazulevicius, S. Grigalevicius, A wet- and dry-process feasible carbazole type host for highly efficient phosphorescent OLEDs, J. Mater. Chem. C, 3 (2015) 12297.

# SILICA WITH CHEMICALLY IMMOBILIZED METHYL RED FOR REMOVAL OF DYE POLLUTANTS FROM DILUTED SOLUTIONS

Volodymyr Tkachuk, Nadiia Roik, Lyudmila Belyakova

Chuiko Institute of Surface Chemistry of NAS of Ukraine, 17 General Naumov Str., Kyiv, 03164, Ukraine
tkachuk.1996@ukr.net

The use of organic dyes in the textile, printing, leather, paper, pharmaceutical and other industries results in the release of considerable amounts of dye-containing effluents into the environment. Among them azo dyes belong to the most numerous (60–70 % of all dyes) and hazardous class of pollutants. Potential danger for human arises from toxic, carcinogenic, mutagenic, and teratogenic effects of azo dyes and their biotransformation products, aromatic amines. Therefore, development of affordable, effective and simple techniques for removal of azo dyes from wastewaters is of great interest.

Our research was focused on the design of effective silica sorbent for industrial azo dyes removal from wastewaters. For this, silica with chemically immobilized methyl red (MR) moieties (MR-$NH_2$-MCM-41) was synthesized by base catalyzed sol–gel condensation of tetraethoxysilane and MR-silane as silica source, and quaternary ammonium salt as structure directing agent. The influence of MR-containing groups on mesoporous structure of resulting material was elucidated by low-temperature adsorption-desorption of nitrogen as well as x-ray powder diffraction analysis and compared with corresponding parameters for control silica ($NH_2$-MCM-41) with surface 3-aminopropyl groups (Table). Composition of surface layer of prepared silica sorbents was established by potentiometric titration of 3-aminopropyl groups (Table).

Table. Structural parameters of MCM-41-type silica materials.

| Silica | S, $m^2/g$ | V, $cm^3/g$ | D, nm | [3-aminopropyl groups], mmol/g |
|---|---|---|---|---|
| $NH_2$-MCM-41 | 515 | 0.91 | 3.93; 5.09 | 0.28 |
| MR-$NH_2$-MCM-41 | 828 | 0.72 | 3.54; 5.29 | 0.18 |

Sorption of MR on synthesized silica materials was studied in dependence of acidity of solution and contact time. In accordance with the obtained results, effective removal of MR from diluted aqueous solutions by $NH_2$-MCM-41 takes place at pH values from 2.5 to 5. Introduction of MR-containing groups in surface layer of silica sorbent causes substantial increase of MR uptake over pH range from 1 to 7. Obviously, in addition to the hydrogen bonding, hydrophobic interactions of adsorbate with MR-$NH_2$-MCM-41 surface play a key role in sorption. In accordance with the kinetic studies, process of MR sorption on synthesized materials follows the pseudo-second order kinetic model. Analysis of Weber-Morris plots indicates that the intraparticle diffusion is not the only one mechanism controlling the rate of MR sorption removal.

In order to evaluate the influence of chosen synthetic strategy on the affinity of resulting mesoporous materials to the various dye pollutants, comparative sorption of different dyes (MR, alizarin yellow (AY), dimethyl yellow (DMY), methyl orange (MO), m-cresol purple (MCP), alizarin red S (AR), and eriochrome black R (ECB)) on synthesized silicas was studied from phosphate buffer solutions with pH 4.8 (Fig.).

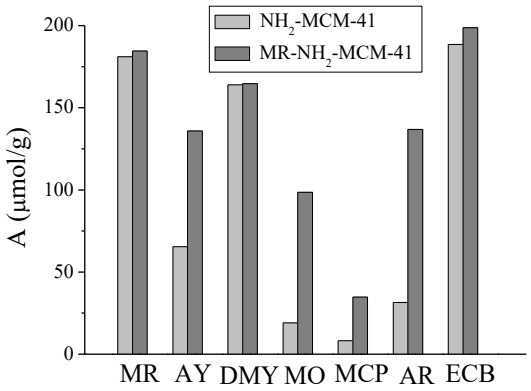


Fig. Removal of dye pollutants by $NH_2$-MCM-41 (light gray) and MR-$NH_2$-MCM-41 (dark gray) from phosphate buffer solutions (pH 4.8) with initial concentrations of dyes equal to 0.2 mmol/l.

Obtained results can be useful in creation of new organosilica materials for effective dye pollutants removal from wastewaters.

# DEVELOPING OF RECYCLING METHODS OF THE SALTS OF WEAKLY COORDINATING ANIONS

**Małgorzata Domańska[1], Tomasz Jaroń[2]**

[1]*Department of Physics, University of Warsaw, Poland*
[2]*Laboratory of Chemical Energy Carriers, Centre of New Technologies, University of Warsaw, Poland*
m.domanska@cent.uw.edu.pl

Weakly Coordinating Anions (shortly: *WCA*) are large anions with the negative charge dissipated over several electronegative atoms and often shielded by bulky organic groups. Due to such construction, they have relatively weak interaction with the cations and are extremely resistant chemically, electrochemically and thermally, which can be utilized in extremely oxidizing environments. Another property of metal salts containing these anions is the solubility of many of them in moderately polar and very weakly solvating solvents, e.g. dichloromethane. This allows the use of these substances as precursors in synthesis of various solvent-free metal ionic compounds, which is often impossible to carry out with other methods. Borohydrides (Fig. 1) or the derivatives of metal amidoboranes are among the compounds prepared utilizing WCAs[1,2].

The main goal of the current work is to close the synthetic process and to re-synthesize Li[An] salt from the usual by-product, [Cat][An], where [Cat] = [$Bu_4N$] and [An] = [$Al(O(CF_3)_3)_4$]. We aim at development of preferably one-step, high yield method. During the study we use moisture-free environment (Schlenk line and glovebox), wide range of solvents as well as ultrasounds and vibrational mill as the mixing factors. The products are characterized by a range of methods such as powder and single crystal X-ray diffraction, FTIR and NMR spectroscopy, and thermogravimetric analysis.

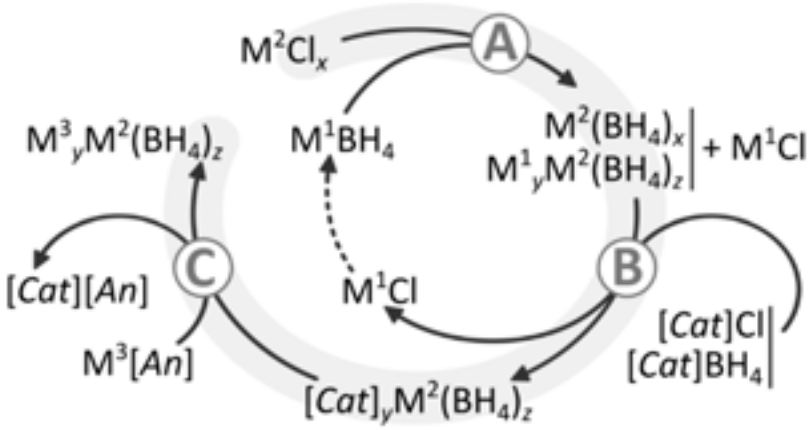


Fig.1 Synthesis of mixed-metal borohydrides, $M^3_y[M^2(BH_4)_z]$,
z= x+ y. For zinc compounds prepared this way: M1=Li, M2= Zn,
$M_3$=Li, Na, K, [Cat]= [$Ph_4P$] or [$n Bu_4N$], [An]=[$Al\{OC(CF_3)_3\}_4$] or [$B\{3,5\text{-}(CF_3)_2C_6H_3\}_4$]

[1] T. Jaroń, P. A. Orłowski, W. Wegner, K. J. Fijałkowski, P. J. Leszczyński, W. Grochala, *Angew. Chem. Int. Ed.*, **54** (2015) 1236–1239.
[2] R. Owarzany, K. J. Fijałkowski, T. Jaroń, P. J. Leszczyński, Ł. Dobrzycki, M. K. Cyrański, W. Grochala, *Inorg. Chem.*, **55** (2016) 37–45

# PHOTOELECTROCHEMICAL ACTIVITY OF SOL-GEL DERIVED $WO_3$ FILMS IN ARTIFICIAL PHOTOSYNTHESIS

Maliha Parvin, Milda Petrulevičienė, Irena Savickaja, Benjaminas Šebeka, Arnas Naujokaitis, Vidas Pakštas, Jurga Juodkazytė

Center for Physical Sciences and Technology, Saulėtelio av. 3, Vilnius 10257, Lithuania
maliha.parvin@ftmc.lt

Artificial photosynthesis is a process, which converts solar energy to chemical energy stored in small molecules or compounds, for instance, $H_2$, $H_2O_2$, HCOOH, $CH_3OH$, etc. by using a manmade device that mimics the structure that can run the natural photosynthesis [1]. Tungsten (VI) oxide is a promising n-type transition metal oxide semiconductor with a band gap of about 2.5 – 2.8 eV which can absorb approximately 12% of solar light with maximum ~ 6.3% energy conversion efficiency and therefore has received a lot of attention. Photoelectrocatalytic properties of $WO_3$ are of particular interest because the energy of photoinduced holes in the valence band of $WO_3$ is sufficient to oxidize $H_2O$, $Cl^-$ $SO_4^{2-}$, etc., and that is why the outcome of the photoanodic reaction depends greatly on the electrolyte composition [2].

In this work, $WO_3$ thin films on conducting glass (fluorine doped tin oxide - FTO) substrate were prepared by sol-gel method in aqueous solution by dip-coating technique. Firstly, peroxytungsten acid (PTA) was synthesized as precursor using sodium tungstate dehydrate ($Na_2WO_4$ x $2H_2O$), nitric acid and hydrogen peroxide. Next PTA was dissolved in ethanol obtaining PTA sol-gel, which was deposited on FTO substrate by dip-coating technique. After coating procedure samples were annealed at 500 °C for 2 h with heating rate of 5 °C/min. The coatings were characterized using X-ray diffraction (XRD) analysis, scanning electron microscopy (SEM) and photoelectrochemical measurements in sulphate and chloride solutions.

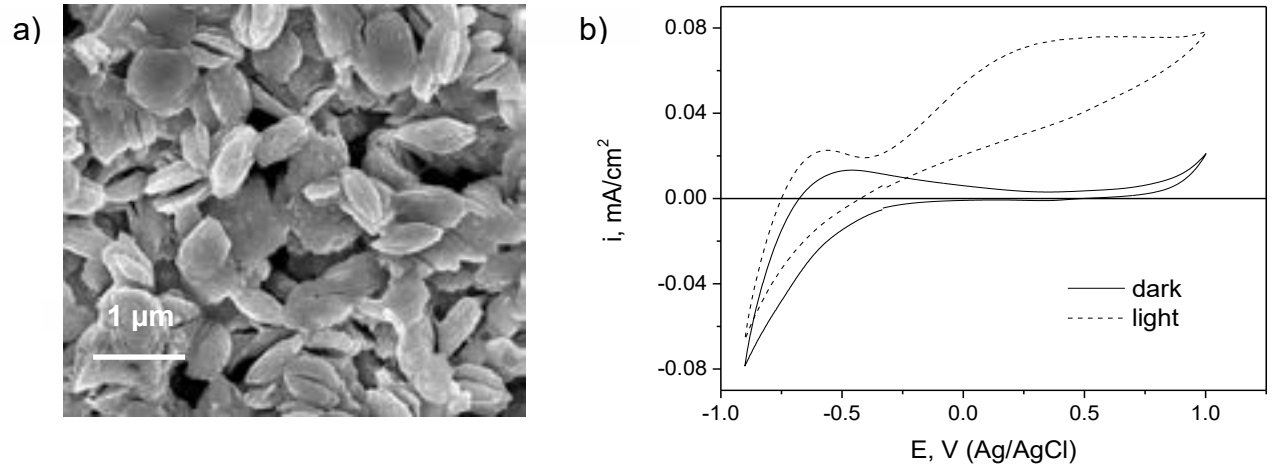


Fig. 1. a) SEM image of sol-gel derived $WO_3$ film, b) cyclic voltammograms of FTO/$WO_3$ photoelectrode in 0.5 M NaCl + 1.0 M KOH solution in dark and under illumination (100 mW $cm^{-2}$) run at 50 mV/s

SEM images revealed that sol-gel derived $WO_3$ films are composed of tiny plates with dimensions of several hundreds nanometers (Fig. 1a). Structure of the coatings was analyzed using XRD technique. The results showed crystalline structure of the films annealed at 500°C. Obviously patterns at 2θ= 23.13°, 23.56°, 24.33°, 41.67°, 44.38°, 45.74°,47.24°, 48.35°, 49.89°, 50.62°, 51.83°, 53.63°, 54.25°, 54.88°, 55.86° corresponded to monoclinic $WO_3$ structure in accordance with ICDD 01-083-0950. Also $Na_2W_4O_{13}$ and FTO crystalline phases were observed. According to literature [3], the structure of bulk tungsten oxide annealed at 500°C should be orthorhombic (β -$WO_3$, 330 °C to 740 °C), whereas annealed at lower temperatures should be monoclinic (γ-$WO_3$, 170 °C to 330 °C). In this study structure of tungsten oxide was found to be monoclinic, implying that substrate also influences phase structure of the coating.

Cyclic voltammograms of FTO/$WO_3$ photoanodes recorded in alkaline chloride solution in dark and under illumination revealed remarkable photoelectrochemical activity with almost 8-fold increase in anodic photocurrent at E = 0.5 V (Ag/AgCl) (Fig. 2b). The dependence of photoelectrochemical performance of sol-gel derived $WO_3$ films on the anionic composition and pH of the electrolytes along with stability of the photoactive material were investigated and the results will be presented at the conference.

[1] K. Sayama, Production of high-value-added chemicals on oxide semiconductor photoanodes under visible light for solar chemical-conversion processes, ACS Energy Letters **3,** 1093-1101 (2018).
[2] J. C. Hill, K. Sh. Choi, Efffect of electrolytes on the selectivity and stability of n-type $WO_3$ photoelectrodes for use in solar water oxidation, J. Phys. Chem C **116,** 7612-7620 (2012)
[3] H. Zheng, J.Z. Ou, M.S. Strano, R.B. Kaner, A. Mitchell, K. Kalantar-Zadeh, Nanostructured tungsten oxide - Properties, synthesis, and applications, Adv. Funct. Mater. 21 (2011) 2175–2196. doi:10.1002/adfm.201002477.

# SYNTHESIS AND INVESTIGATION OF ORGANOMETALLIC PRECURSORS USED FOR LAYERS FORMATION OF INORGANIC SEMICONDUCTORS

Mantas Marčinskas, Tadas Malinauskas

Faculty of Chemical Technology, Kaunas University of Technology, Lithuania
mantas.marcinskas@ktu.edu

Nowadays, usage of fossil fuel supplies about 85% of world's electricity power demands. The products of fossil fuel burning, such as carbon, nitrogen and sulfur oxides, negatively affect human's health and cause change of climate [1]. Therefore, more and more attention is payed to development and use of renewable energy sources. One of the most attractive alternatives is photovoltaic systems, which use sun as free and endless source of energy [2].

Current silicon based solar cells, reach efficiencies as high as 25%, but requires complicated production technology and especially pure silicon [3]. In recent years perovskite solar cells (PSC) attract more and more attention, during just few years efficiency of energy conversion was improved from 3.9% to 22.1%. These devices are based on perovskite, which benefits from simple synthesis, inexpensive precursors, sufficiently high conductivity and intensive, wide range light absorption [4]. Hole transporting materials (HTM) play important role in perovskite solar cells and directly affect both energy conversion efficiency and stability. At this moment, the best results have been achieved using organic HTMs (for example spiro-OMeTAD), however, due to necessity to use additives, such as *tert*-butylpyridine or LiTFSI salt, these devices suffer from degradation and offer relatively poor thermal and UV stability [5]. Additionally, organic HTMs usually require expensive and complex synthesis as well as use of aggressive or sensitive reagents [6].

Inorganic hole transporting materials usually offer better thermal stability, superior conductivity, can be used without dopants and generally are cheaper than organic analogues. Copper (I) thiocyanate demonstrate great potential, high hole mobility, good thermal stability and low price. Recently, perovskite solar cells, with CuSCN as HTM, exceeded 20% energy conversion efficiency. On the other hand, CuSCN is insoluble in most common organic solvents, used for solar cell's layers formation, therefore fabrication of PSCs becomes more complicated [7].

In this work organometallic CuSCN complexes were synthesized using different organic ligands. These organometallic precursors have relatively low thermal stability and thermally decompose to CuSCN and volatile organic ligand which evaporates during the layer formation step (**Fig. 1**).

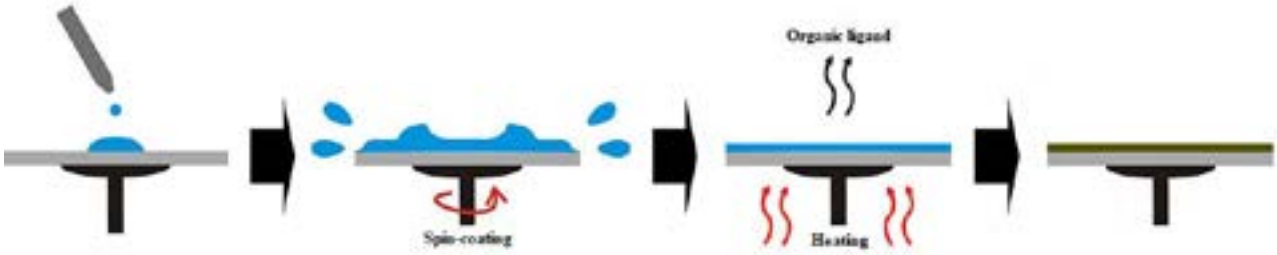


**Fig. 1.** The formation of CuSCN layer by spin-coating and heating

The solution of organometallic complex is deposited on the substrate via spin-coating. Afterwards, the complex decomposes under heating, organic part slowly evaporates and pure CuSCN layer is received.

This research was funded by the European Social Fund under the No 09.3.3-LMT-K-712-10-0237 "Development of Competences of Scientists, other Researchers and Students through Practical Research Activities" measure.

[1] Nazeeruddin MK. In retrospect: twenty-five years of low-cost solar cells. *Nature* 2016, 538 (7626), 463-464.
[2] Green MA. Third generation photovoltaics: ultra-high conversion efficiency at low cost. *Prog Photovoltaics Res Appl.* 2001, 9(2), 123–135.
[3] Smith DD, Cousins PJ, Masad A, Waldhauer A, et.al. Generation III high efficiency lower cost technology: Transition to full scale manufacturing. *Proc. 38th IEEE Photovoltaic Specialists Conf.* (PVSC) 2012, 001594-001597.
[4] Yang WS, Park BW, Jung EH, Jeon NJ, Kim YC, et.al. Iodide management in formamidinium-lead-halide–based perovskite layers for efficient solar cells. *Science*. 2017, 356 (6345), 1376-1379.
[5] Chen J, Park NG. Inorganic Hole Transporting Materials for Stable and High Efficiency Perovskite Solar Cells. *J. Phys. Chem. C*. 2018, 122 (25), 14039−14063.
[6] Krüger J, Plass R, Cevey L, Piccirelli M, Grätzel M, Hach U. High efficiency solid-state photovoltaic device due to inhibition of interface charge recombination. *Appl. Phys. Lett.* 2001, 79, 2085–2087.
[7] Arora N, Dar MI, Hinderhofer A, Pellet N, Schreiber F, et.al. Perovskite solar cells with CuSCN hole extraction layers yield stabilized efficiencies greater than 20%. *Science* 2017, 358 (6364), 768-771.

# IR SPECTRA OF THE WATER DIMER ISOLATED IN ARGON MATRIX BY ANALYZING MICROSOLVATION EFFECTS IN $(H_2O)_2+Ar_N$ (N=1-4) COMPLEXES AND USING POLARIZABLE CONTINUUM MODEL

Maria Safonova[1], Ekaterina Kozlovskaya[1], George Pitsevich[1]

[1]Belarusian State University, Minsk, Belarus
e-mail: marusyasaf@gmail.com

Water clusters are of interest as an intermediate between single molecule and the liquid medium. Water dimer is the simplest water cluster but experimental investigation of this object is a difficult task. At the moment, there are two experimental methods to analyze IR spectra of the water dimer. First is IR vibrational predissociation spectra taken in a super-sonic molecular beam [1]. The second method is matrix isolation [2]. Comparing data of these two methods one can see that the most interesting stretching vibration of the donor hydroxyl group has a higher frequency in case of free water dimer than in case of matrix isolation. To analyze the matrix effect on structure and vibrational spectra of the water dimer, we have found the equilibrium geometry of the $(H_2O)_2+Ar_N$, where N=1-4. The calculations were carry out using wB97DX/acc-pVTZ and B3LYP-D3/acc-pVTZ levels of theory. Equilibrium structure of the water dimer was also found using polarizable continuum model (PCM) at the same levels of theory. Some of the considered $(H_2O)_2+Ar_N$ structures are presented in Fig.1.

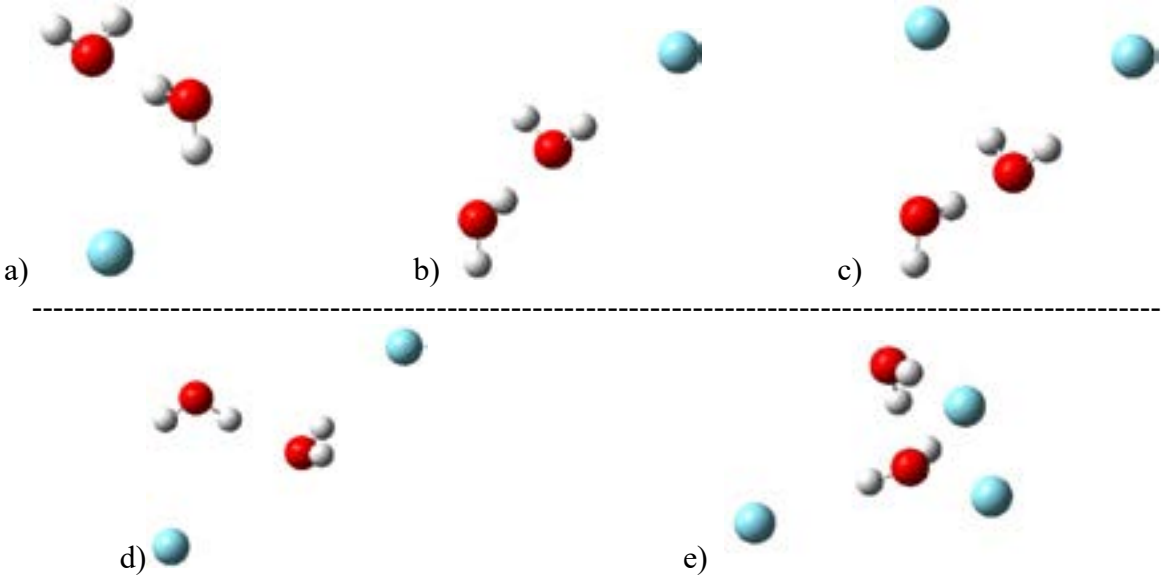


Fig. 1. Equilibrium configurations of the water dimer complex with one (a,b), two (c,d) and three (e) Argon atoms, calculated at wB97XD/acc-pVTZ level of theory.

According to calculated data, single Ar atom does not effect the geometric parameters of the water dimer. But addition of the next one Ar atom leads to decreasing of the hydrogen bridge length. This tendency is more clearly seen in case of the appearance of three argon atoms near the water dimer. Results of the calculations in frame of PCM one can consider like limit when number of the Ar atoms became very large. In this limit the length of the hydrogen bridge is decreased by 0.005 Å. Tendency of the hydrogen bond strengthening is also confirmed by decreasing of the frequency of stretching donor O-H vibrations with increasing number of argon atoms.

[1] R.H. Page, G.F. Jeremy, Y.R. Shen, Y.T. Lee, Chem.Phys.Lett., **106** (1984) 373.
[2] Y. Bouteiller, B. Tremblay, J.P. Perchard, Chem.Phys., **386** (2011) 29.

# INVESTIGATION OF WATER SOLUBLE CONJUGATED POLYMER MPS-PPV

Marijus Jurkūnas[1,2*], Arūnas Stirkė[1], Aušvydas Vareikis[2]

[1] Department of Material Science and Electrical Engineering, Center for Physical Sciences and Technology, Lithuania
[2] Faculty of Chemistry and Geoscience, Vilnius University, Lithuania
marijus.jurkunas@chf.stud.vu.lt

Conjugated polyelectrolytes (CPEs) are organic semiconductors that are characterized by a π-π conjugated backbone and ionic side groups, which exhibit high solubility in polar media, such as alcohol and water. CPEs have attracted increasing attention for their various potential applications in optoelectronic devices, optical sensors (chemo- and biosensors) [1] and biological imaging [2, 3]. Also, π-π conjugated polyelectrolytes have been extensively studied due to their use in organic light emitting diodes (OLEDs), organic solar cells and organic photovoltaic cells (OPVCs) [3]. One of CPEs is poly(p-phenylenevinylene) (PPV) derivative anionic Poly[5-methoxy-2-(3-sulfopropoxy)-1,4-phenylenevinylene] (MPS-PPV) contains all listed properties thus making it unique due to its versatility. Knowing that MPS-PPV can be used in wide spectrum of application fields ranging from chemical and biological sensors to polymer light-emitting diodes, we concentrate into all basic properties of MPS-PPV that some of them are poorly or even not discussed and suggest new methods for useful applications.

Based on Gilch dehalogenation reaction [1], the MPS-PPV has been synthesized and fully characterized. The structure of polymer and its precursors were confirmed by $H^1$NMR, $C^{13}$NMR and Fourier transformation IR (FT-IR) absorption spectroscopy. TGA analysis showed 2-step degradation of MPS-PPV which usually contains about 7-8 % wt humidity. Knowing that MPS-PPV is negatively charged polyelectrolyte and fluorescent in UV light a new method for MPS-PPV molar mass determination was developed by using 0.8% TAE buffer and agarose as matrix. Molar mass was described by polymer mobility in agarose gel comparing with Gene Ruler, 1 kb plus DNA ladder mobility. Electrophoresis was performed applying 6.18 V/cm for ~30 min. According to the electrophoresis test results 20-60 kDa polymer molar mass appeared to be most dominant with long tail until 240 kDa. In the other hand, centrifugal filtration test with 5 different molecular weight cuttoffs showed most concentrated MPS-PPV fraction of 100-300 kDa meaning that MPS-PPV mobility in agarose is higher than DNA ladder standard. Fluorescence of MPS-PPV in DMSO appeared to be 20 times greater comparing with queues solution. Most intense fluorescence obtained at concentration ~$10^{-4}$ M (by monomer units) in both solutions. Reabsorption effect of MPS-PPV can be observed only in DMSO solution diluting from $10^{-3}$ to $10^{-4}$ M (by monomer units). Fluorescence kinetics experiment showed 3-step decay mechanism for water solution and 2-step for DMSO solution. Quantum efficiency of MPS-PPV grows form ~7% to ~16% when concentration reduces. MPS-PPV HOMO and LUMO energy levels were measured that are ~5.2 eV and ~3.0 eV, respectively, which is suitable for PLED.

We build FTO/TPD/MPS-PPV/$Alq_3$/Al polymer LED which showed weak red-orange glow, while improved structure ITO/TPD/MPS-PPV/$Alq_3$/LiF/Al showed only $Alq_3$ electroluminescence spectra. Another future application for MPS-PPV could be a new dopant for polypyrrole (PPy) according to application for patent [5]. MPS-PPV could be incorporated in the matrix of PVA and initiator with idea of making the composite layer more conductive and possibly electrically stable (Fig. 1). Also, the deposed polypyrrole using cyclic voltammetry technique (0V to +0.8 V, 100 cycles at 50 mV/s) by addition of MPS-PPV in pyrrole solution appeared 200 times thinner, flatter and mechanically more attached to ITO electrode than PPy layer performed in absence of MPS-PPV (Fig. 1.) in same conditions. This application has tremendous potential to solve adhesiveness problems of electrochemically deposited conjugated polymers and requires more investigation in this phenomenon.


Fig. 1. MPS-PPV application ideas for PPy composite layer and electrochemically synthesized PPy on ITO.

[1] Dalvi-Malhotra, J. and L. Chen, *Enhanced Conjugated Polymer Fluorescence Quenching by Dipyridinium-Based Quenchers in the Presence of Surfactant.* The Journal of Physical Chemistry B, 2005. **109**(9): p. 3873-3878.

[2] Kahveci, Z., et al., *New Red-Emitting Conjugated Polyelectrolyte: Stabilization by Interaction with Biomolecules and Potential Use as Drug Carriers and Bioimaging Probes.* ACS Applied Materials & Interfaces, 2016. **8**(3): p. 1958-1969.

[3] Chen, L., et al., *Highly sensitive biological and chemical sensors based on reversible fluorescence quenching in a conjugated polymer.* Proceedings of the National Academy of Sciences, 1999. **96**(22): p. 12287-12292.

[4] Chang, S.-C., et al., *Dual-color polymer light-emitting pixels processed by hybrid inkjet printing.* Applied Physics Letters, 1998. **73**(18): p. 2561-2563.

[5] M. Kirsnytė, M. Jurkūnas, P. Ragulis, R. Simniškis, A. Stirkė., *A method of PPy in situ polymerization in adhesive polymer matrix with embedded catalyst*, Lietuvos valstybinis patentų biuras, 2018. Patent No. 2018001

# STRUCTURE AND SPECTRAL PROPERTIES OF CATIONIC LANTHANIDE(III) COMPLEXES WITH CARBOCYLAMIDOPHOSPHATE (CAPH) LIGAND AND TETRAPHENYLBORATE-ION AS COUNTERION

Mariya Strugatska[1], Igor Holovij[1], Iryna Olyshevets[1], Viktoriya Dyakonenko[2], Vladimir Ovchynnikov[1]

[1] Taras Shevchenko National University of Kyiv, 12, Lva Tolstogo Str., Kyiv, 01033, Ukraine
[2] SSI "Institute for Single Crystals", National Academy of Science of Ukraine, Kharkiv 61001, Ukraine
mariya.strugatskaya@gmail.com

Experimental and theoretical studies of polyfunctional ampolydentate ligands is one of the most interesting directions in modern coordination chemistry. The study of their properties and structure allows us to obtain metal complexes having valuable optical, magnetic, catalytic, biological, etc. properties.

Due to the attractive photophysical properties of some lanthanide complexes, these compounds are promising for the broad range of possible applications, from luminescent labels up to the materials used in electroluminescent diodes (LEDs).

Among the polydentate ligands, a particular place is occupied by the carbacylamidophosphates (CAPh) - compounds having a functional fragment -C(O)N(H)P(O)-. Presence of phosphoryl group in the composition of CAPh ligands determine to them a high affinity for the majority of metal ions, and especially for rare-earth elements. The ampolydentate character of the CAPh ligands allows to obtain different bi- and polynuclear homo- and heterometal coordination compounds.

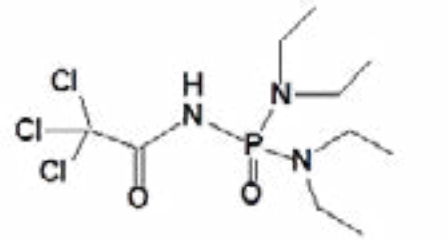


Fig.1. HL = bis(N,N'-diethylamido)(N''-trichloroacetyl)triamidophosphate

Cationic lanthanide(III) complexes with general formula $[Ln(L)_2Dipy_2]BPh_4$, (where Ln = La, Eu, Tb, Nd, Gd, Lu; $L^-$ = bis(N,N'-diethylamido)(N``-trichloroacetyl)triamidophosphate ion (Fig. 1); Dipy = α,α'– dipyridyl), were synthesized and characterized by means of elemental, IR, $^1H$ NMR, luminescence and UV-Vis spectroscopy.

The single crystal structure of Europium complex was determined by X-ray diffraction method. It was found, that the complex has an ionic structure and tetraphenylborate-ion acts as an anion. The deprotonated form of the ligand is coordinated to the europium ion in a bidentate manner via the oxygen atoms of the phosphoryl and the carbonyl groups with formation of six-membered metallocycles. The α,α'– dipyridyl molecules are coordinated to the metal in a bidentate manner via the nitrogen atoms completing the coordination number of europium to eight.

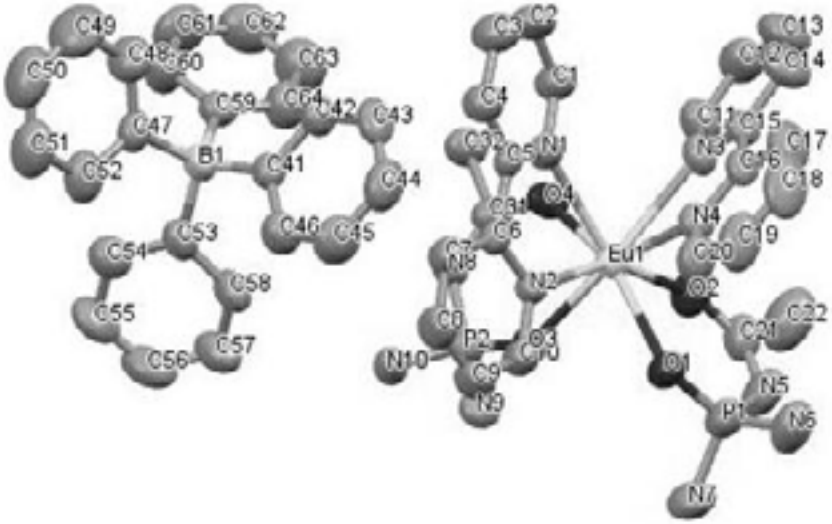


Fig.2. The crystal structure of $[Eu(L)_2Dipy_2]BPh_4$ with $C_2H_5$ groups of diethylamide fragments at the phosphorus atoms as well as hydrogen and chlorine atoms being omitted for clarity

# SYNTHESIS AND PROPERTIES OF AMPHOTERIC HYDROXYETHYL STARCH DERIVATIVES

Miglė Babelytė, Joana Bendoraitienė, Ramunė Rutkaitė

Department of Polymer Chemistry and Technology, Kaunas University of Technology, Lithuania
migle.babelyte@ktu.edu

Amphoteric starch contains both cationic and anionic groups in the same molecule. Generally, cationic starch derivatives are starch ethers prepared by using tertiary amino or quaternary ammonium groups containing reagents. Meanwhile, anionic starches can be synthesized by introducing phosphate, phosphonate, sulfate, sulfonate or carboxyl groups into starch molecules. The synthesis of amphoteric starches might be achieved by applying two different approaches, namely, firstly anionic modification and thereafter cationic modification or firstly introduction of positively charged groups and then anionic modification. The main applications of amphoteric starches are in the paper industry as wet-end additives and viscosity modifiers in construction industry [1]. In addition, amphoteric starches can be used in cosmetic industry as thickeners or emulsion stabilizers.

The aim of the present work to prepare amphoteric hydroxyethyl starches (CHES/AHES) of different composition and to investigate their polyelectrolyte complexes formation in water by using natural green coffee bean extract.

Preparation of CHES/AHES has been achieved by using cationic and anionic modifying reagents by two - step reaction as demonstrated in the synthesis scheme in Fig. 1.

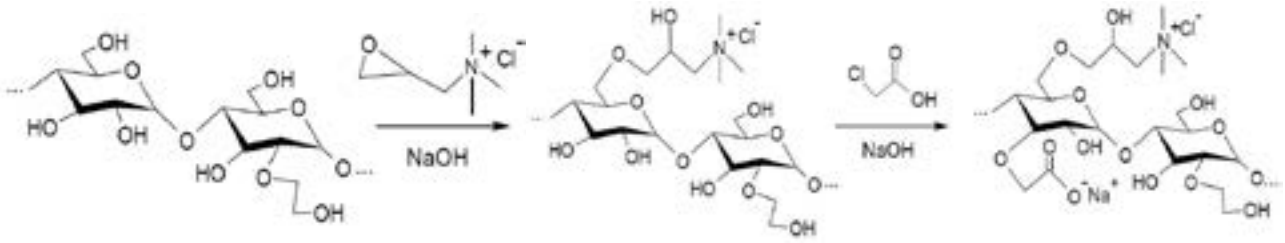


Fig. 1. Two – step synthesis scheme for preparation of amphoteric starches

Firstly, cationic hydroxyethyl starch (CHES) was prepared by the reaction of hydroxyethyl starch (HES) with (2,3-epoxypropyl)trimethylammonium chloride (EPTMAC) in the presence of sodium hydroxide at 45°C for 24 h [1]. The molar ratio of the HES : EPTMAC : NaOH : $H_2O$ was 1 : 0.35 : 0.04 : 3 aiming to obtain CHES with a degree of substitution (DS) of 0.29. Synthesized CHES then were reacted with monochloroacetic acid (mClAA) in alkaline solution at 55 °C for 48 h. By using molar ratio of the CHES : mClAA : NaOH : $H_2O$ equal to 1 : 1-1.5 : 2.4-3.6 : 90, the CHES/AHES with the degree of substitution (DS) of anionic groups equal to 0.27 and 0.55 were obtained (Table 1).

Table 1. Characteristics of amphoteric hydroxyethyl starch derivatives

| **Amphoteric hydroxyethyl starch derivative** | **Molar ratio** | | | | **DS of CHES** | **DS of AHES** |
|---|---|---|---|---|---|---|
| | **CHES** | **mClAA** | **NaOH** | **$H_2O$** | | |
| $CHES_{0.29}$/ $AHES_{0.27}$ | 1 | 1 | 2.4 | 90 | 0.29 | 0.27 |
| $CHES_{0.29}$/ $AHES_{0.55}$ | 1 | 1.5 | 3.6 | 90 | 0.29 | 0.55 |

Water soluble amphoteric hydroxyethyl starch derivatives can form polyelectrolyte complexes with cationic or anionic compounds due to the presence of anionic and cationic groups in the same molecule. The polyelectrolyte complex formation in water between water soluble amphoteric hydroxyethyl starches and components of green coffee bean extract have been investigated. By changing pH and concentration of amphoteric hydroxyethyl starch and green coffee bean extract in water the complex particles were obtained and characterized thereinafter.

**Acknowledgement.** This research was funded by the European Social Fund under the measure No 09.3.3-LMT-K-712-10-0296 “Development of Competences of Scientists, other Researchers and Students through Practical Research Activities”.

[1] R. Rutkaitė, J. Bendoraitienė, R. Klimavičiūtė, E. Lekniutė, I. Narmontaitė, V. Šinkūnaitė (2012). Charged starch nanoparticles prepared by polyelectrolyte complex formation, Chemija, Vol. 23. No. 4, 328 – 335.

# Fabrication of porous Co-Pt nanowires and their magnetic properties

Modestas Vainoris[1], Natalia Tsyntsaru[1,2], Elisabeth Podlaha-Murphy[3], Jordi Sort[4], Henrikas Cesiulis[1]

[1]Dept. of Physical Chemistry, Vilnius University, Vilnius, Lithuania
[2]Institute of Applied Physics, Chisinau, Moldova
[3]Dept. of Chemical & Biomolecular Engineering, Clarkson University, Potsdam, NY, USA
[4]Physics Dep., Science Faculty, Autonomous University of Barcelona, Barcelona, Spain
m.vainoris@chgf.vu.lt

Lately Co-Pt alloy has received considerable attention, because of its unique magnetic properties. – ability to not be affected by superparamagnetism at grain sizes even below 6 nm [1]. These alloys are great candidates for miniaturization of magnetic materials and implementation into magnetic recording devices, micro-electromechanical systems (MEMS). Several techniques have been developed to obtain films, nanowires and other structures of Co-Pt alloy with perpendicular anisotropy. Many techniques focus only on the fabrication of magnetic nanowires – lithography, molecular-beam epitaxy, vapor-liquid-solid growth etc. However, utilization of electrodeposition into nanoporous membranes still is the most widely used technique to fabricate versatile and textured nanowires [2-3].

The aim of this work was to manufacture self-supported Co-Pt porous nanowires using double template method, and investigate their magnetic properties. First of the templates used were anodized aluminum (AAO) membranes with pore diameter of 0.2 μm to form cylindrical nanowires. Second template applied during electrodeposition, which makes growing nanowires porous, was dynamic hydrogen bubble template, when reduction of metal ions occurs in between the hydrogen bubbles. Pulse deposition technique was applied for nanowires fabrication. The influence of cathodic current density, pulse time and its length on the growth of Co-Pt nanowires was investigated. Influence on porosity of three different hydrogen bubbles coalescence suppressant has been investigated, namely ammonium chloride, magnesium sulfate and acetic acid. Effects on nanowires porosity of a surfactant that reduces surface tension, specifically isopropanol, have also been investigated. Obtained nanowires have been studied using XRD, SEM equipped with EDS module, XRF techniques. Magnetic properties of Co-Pt nanowires have been assessed in and out of AAO membranes using VSM magnetometer.

**Acknowledgments**. This research has received funding from H2020, under MSCA-RISE-2017 grant agreement No. 778357 and Research Council of Lithuania project No 09.3.3-LMT-K-712-08-0003.

[1] D. Weller, A. Moser, L. Folks, M. E. Best, W. Lee, M. F. Toney, M. Schwickert, J. U. Thiele, and M. F. Doerner, IEEE Trans. Magn. 36,10 2000.

[2] G.D. Sulka, A. Brzózka, L. Liu, Fabrication of diameter-modulated and ultrathin porous nanowires in anodic aluminum oxide templates, Electrochim. Acta. 56 (2011) 4972–4979.

[3] J. Yu, F. Wang, Y. Wang, H. Gao, J. Li, K. Wu, Interfacial reaction growth approach to preparing patterned nanomaterials and beyond, Chem. Soc. Rev. 39 (2010) 1513–1525.

# SYNTHESIS AND STUDIES OF TETRASUBSTITUTED CARBAZOLE DERIVATIVES

Monika Piasliakaite, Ruta Minickaite, Dalius Gudeika

Department of Polymer Chemistry and Technology, Kaunas University of Technology, Lithuania
monika.piesliakaite@ktu.edu

Carbazoles are prevalent as structural motifs in various synthetic materials. As is well known, the properties of carbazole derivatives are closely related to their molecular structures [1]. In the previous papers, the derivatives of carbazole unit as central core were commonly prepared by functionalizing at its 3,6- [2], 2,7- [3] or 9- [4] positions. The as-prepared compounds with thermally and morphologically stable properties can expand the application of carbazole in organic light-emitting devices (OLEDs). Due to their thermal stability, good film-forming properties and high luminescence, the starburst molecules have attracted much more attention to the application in OLEDs, photovoltaics and field effect transistors [5].

In this study, we report a carbazole derivative by using carbazole as the central core and functionalizing at its 1,3,6,8-positions with ethenylaryl moieties and investigation of their thermal, optical, photophysical and electrochemical properties of the synthesized compounds.

The synthesized compound exhibit thermal stability with 5% weight loss temperature exceeding 412 °C. The ionization potential, electron affinity values were estimated by cyclic voltammetry. The analysis revealed that compound with 2-ethenylnaphthalenyl substituents exhibited higher thermal stability than compounds with 1-ethenyl-2,3,4,5,6-pentafluorophenyl and 4-ethenylpyridinyl moieties. The synthesized compounds form glasses with glass transition temperatures of 59-134 ºC. The dilute solutions of the synthesized derivatives exhibit absorption maxima in the range of 355-380 nm, and fluorescence intensity maxima in the range of 400-470 nm. The ionization potential values of the synthesized materials range from 5.27 to 5.58 eV.

[1] W. Jiang, Z.J. Ge, P.Y. Cai, B. Huang, Y.Q. Dai, Y.M. Sun, J. Qiao, L.D. Wang, L. Duan, Y. Qiu, Star-Shaped Dendritic Hosts Based on Carbazole Moieties for Highly Efficient Blue Phosphorescent OLEDs, Journal of Materials Chemistry **22**, 12016-12022 (2012).
[2] W.Y. Hung, L.C. Chi, W.J. Chen, Y.M. Chen, S.H. Chou, K.T. Wong, A new benzimidazole/carbazole hybrid bipolar material for highly efficient deep-blue electrofluorescence, yellow–green electrophosphorescence, and two-color-based white OLEDs, Journal of Materials Chemistry **20**, 10113-10119 (2010).
[3] J.Y. Shen, X.L. Yang, T.H. Huang, J.T. Lin, T.H. Ke, L.Y. Chen, C.C. Wu, M.C.P. Yeh, Advanced Functional Materials, Ambipolar Conductive 2,7-Carbazole Derivatives for Electroluminescent Devices **17**, 983-995 (2007).
[4] K. E. Linton, A. L. Fisher, C. Pearson, M. A. Fox, L. O. Palsson, M. R. Bryce, M. C. Petty, Colour tuning of blue electroluminescence using bipolar carbazole–oxadiazole molecules in single-active-layer organic light emitting devices (OLEDs), Journal of Materials Chemistry **22**, 11816-11825 (2012).
[5] F. Niu, H. Niu, Y. Liu, J. Lian, P. Zeng, Synthesis, characterization and application of starburst 9-alkyl-1,3,6,8-tetraaryl-carbazole derivatives for blue-violet to UV OLEDs, RSC Advances **1**, 415-423 (2011).

# SYNTHESIS AND MAGNETIC PROPERTIES OF $Co_{0.65}Zn_{0.35}Fe_2O_4$ MAGNETIC NANOPARTICLES WITH HIGH CRYSTALLINITY BY ULTRASONIC SPRAY PYROLYSIS METHOD

Dzimitry Ivashenka[1], Elena Petrova[1], Vladimir Pankov[1]

[1]Department of Physical Chemistry, Belarusian State University, Belarus
che.ivashenkDV@bsu.by

Over the past decades, the production of spinel ferrite nanoparticles has been intensively studied due to their promising magnetic properties. Cobalt ferrite ($CoFe_2O_4$) is especially attractive because of its high coercivity and moderate saturation magnetization. It was shown that substitution of $Co^{2+}$ with $Zn^{2+}$ leads to enhanced magnetic properties of nanocrystalline ferrites [1]. Zinc substituted cobalt ferrites are considered to be suitable magnetic materials for such applications as magnetic drug delivery [2], magnetic resonance imaging, information storage system, ferrofluids [3], etc.

Our study is devoted to improvement of ultrasonic spray pyrolysis (USP) technique in order to enhance magnetic properties of ferrite nanoparticles. It's generally known that increasing crystallinity of magnetic nanoparticles leads to the increase of saturation magnetization. Therefore, the main aim of this research is to increase nanoparticle's crystallinity by calcination at high temperatures. At first, cobalt-zinc ferrite suspension was prepared by co-precipitation from a solution of metal nitrates taken in stoichiometric amount. Sodium chloride (wt. concentration 5: 1 with respect to ferrite) was added to the suspension to prevent aggregation and sintering during calcination. Magnetic nanoparticles were obtained from as-prepared suspension by USP method at 600°C. Thus, cobalt-zinc ferrite nanoparticles in inert matrix were synthesized. Finally, calcination was carried out within temperature range from 300 to 900 °C in order to improve crystallinity.

The phase composition and structure of ferrites were studied by XRD and FT-IR spectroscopy. The size and morphology of the particles were examined by SEM, saturation magnetization of samples was measured by SQUID magnetometry. The average size of nanoparticles annealed at 300°C is about 7 nm (Fig.1). It was found that significant growth of those occurs during annealing process at 900°C. Nevertheless, major fraction of the particles remained within nanoscale range (about 80 nm) although recrystallization process caused formation of the larger particles fraction (200 nm and higher). The calculations of the crystallite size based on the diffraction reflection broadening correlate to average size data obtained from SEM. The average crystallite size was found to be 53 nm for annealing at 900°C, 7 nm –at 300°C. With increasing annealing temperature from 300°C to 900°C saturation magnetization increased from 45.0 emu/g to 78.6 emu/g. (Table.1)



Table 1. Magnetic properties of the ferrite nanoparticles annealed at different temperatures

| T, °C | 900 | 700 | 500 | 300 |
|---|---|---|---|---|
| $M_s$, emu/g | 78,6 | 54,7 | 45,6 | 45,0 |

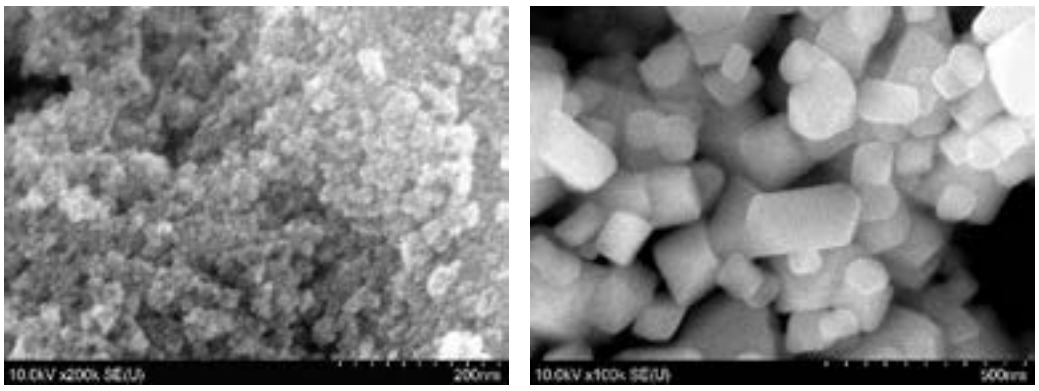

a b

Fig.1. SEM images of CoZnFe2O4 nanoparticles annealed at 300°C (a), 900°C (b)

[1] S. Dey, J. Ghose, Synthesis, characterisation and magnetic studies on nanocrystalline $Co_{0.2}Zn_{0.8}Fe_2O_4$, Materials Research Bulletin 38.11-12, 1653-1660 (2003):

[2] W. Pon-On, N. Charoenphandhun et al., Encapsulation of magnetic $CoFe_2O_4$ in $SiO_2$ nanocomposites using hydroxyapatite as templates: A drug delivery system, Materials Chemistry and Physics 131(1-2), 485-494 (2011).

[3] K. Raj, B. Moskowitz, R. Casciari, Advances in ferrofluid technology, Journal of magnetism and magnetic materials 149.1-2, 174-180 (1995):

# SPECTROSCOPIC AND COMPUTATIONAL STUDIES OF ZINC PORPHYRINS AND THEIR HOST-GUEST SUPRAMOLCULAR COMPLEXES WITH TAKEMOTO ORGANOCATALYST

Nele Konrad[1], Darya Meniailava[2], Irina Osadchuk[1,3] and Dzmitry G. Kananovich[1]

[1] Department of Chemistry and Biotechnology, Tallinn University of Technology, Estonia
[2] Faculty of Physics, Belarusian State University, Belarus
[3] Physical Chemistry Department, Institute Charles Gerhardt, University of Montpellier, France
nele.konrad@taltech.ee

Metalloporphyrins are widely used chromophores, which possess unique absorption properties. In strong supramolecular complexes between achiral metalloporphyrin as a host and chiral substrate as a guest chirality transfer occurs. It is also known, that in chlorinated solvents like chloroform and dichloromethane porphyrins bind strongly primary amines. [1] The cooperation of experimental facilities for measuring optical spectra and performing quantum-chemical calculations allows to get reliable information about the mechanism of chirogenesis.

In this work we present comprehensive experimental and computational study of host-guest supramolecular interactions of Takemoto organocatalyst [2] and zinc porphyrins complexes (Fig. 1). For the determination of the strength of the intermolecular binding between host and guest UV/Vis titration method was used. For monitoring the chirality transfer CD spectroscopy was applied. High level quantum-chemical calculations were performed in the framework of DFT and TDDFT approximations.

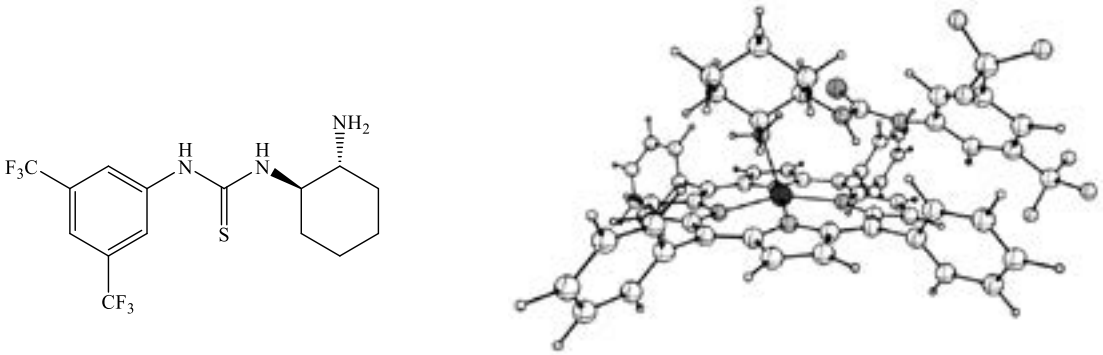


Fig. 1. Takemoto organocatalyst and calculated equilibrium structure of supramolecular complex of zinc tetraphenylporphyrin and Takemoto organocatalyst.

UV titrations showed that achiral hosts, zinc porphyrins, and chiral guest Takemoto organocatalyst form supramolecular complexes. Furthermore, in the complexes due to the strong binding a chirality induction was observed using CD spectroscopy. All this has been supported by extensive computational studies, which included conformation analysis, geometry optimisation, UV/Vis and CD spectra calculations in solvent (Fig. 2).

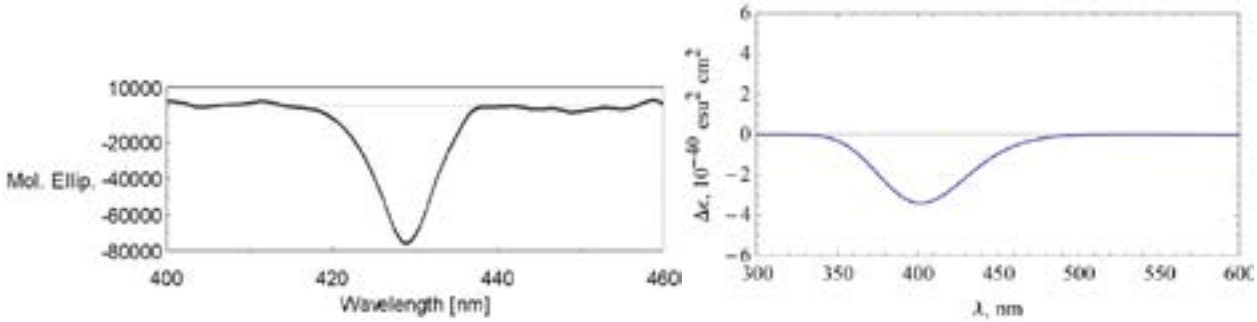


Fig. 2. Experimental CD (left) and calculated CD (right) of supramolecular complex of zinc tetraphenylporphyrin and Takemoto organocatalyst.

The results of the work could be applied in asymmetric catalysis and chirality sensors, which are based on combination of metal catalysis, organocatalysis, supramolecular chemistry and computational design.

This work was supported by Tallinn University of Technology (grant number B58 and PUTJD749) and Dora Plus program.

[1] G. A. Hembury, V. V. Borovkov, Y. Inoue, Chirality-Sensing Supramolecular Systems, Chem. Rev. **108**, 1-73 (2008).
[2] T. Okino, Y. Hoashi, Y. Takemoto, Enantioselective Michael Reaction of Malonates to Nitroolefins Catalyzed by Bifunctional Organocatalysts, J. Am. Chem. Soc. **125**, 12672-12673 (2003).

# DEVELOPMENT OF MIXED-MODE POLYMERIC SORBENT FOR THE DETERMINATION OF MEDICINE DRUG IN BIOLOGICAL MATRICES

Nerijus Karlonas

The State Forensic Medicine Service, Toxicology Laboratory, Didlaukio 86E, LT-08303 Vilnius, Lithuania
nerijuskarlonas@yahoo.com

Zopiclone is nonbenzodiazepine hypnotic drug that is used for the treatment of insomnia. This drug was developed with the intent to overcome some disadvantages of benzodiazepines, such as dependence and next day sedation [1,2]. Several analytical methods based on chromatographic and electrophoretic techniques for the determination of zopiclone have been reported [3]. However, it is essential to develop a fast and sensitive method for the determination of zopiclone in the biological matrix.

In order to perform analyte determination in the extract by gas chromatography with negative ion chemical ionization mass spectrometry the selection of solid phase extraction (SPE) sorbent as well as washing and eluting solvents is particularly important. Zopiclone in the sample at the acidic pH has a positive charge, thus cation exchange sorbent such as mixed-mode Oasis MCX could be appropriate. This sorbent is capable to interact with analyte by hydrophilic-lipophilic and ion-exchange interactions [4,5] and therefore it is suitable for achieving an efficient extraction of zopiclone.

The retention and elution of zopiclone could be affected by the pH of the sample solution, which was varied from pH 1 to pH 10. Special attention was paid for to the selection of washing and eluting solvent in the SPE procedure, resulting in very pure and free from moisture extract, which can successfully be applied for gas chromatography-mass spectrometry. Different solvents or mixtures of solvents for elution of the adsorbed analyte, and washing step eliminating interferences in the column were tested.

The acidic solution at pH 4.0 was used during the sample loading step. Column with adsorbed zopiclone ($pK_a$ 6.79 ± 0.42) via ion-exchange interactions, could be washed with a pure organic solvent (1-propanol) in order to remove acidic and neutral interfering compounds. Then analyte was eluted with acetonitrile containing 4 % of $NH_4OH$. After these steps visibly cleaner extracts were obtained in comparison with those obtained using reversed-phase interactions.

The developed method for zopiclone determination in biological matrices was validated following the recommendation for new methods [6,7,8]. The linear relationships with the correlation coefficients ($r^2$) better than 0.9960, LOD and LOQ values equal to 0.60 ng $mL^{-1}$ and 2.00 ng $mL^{-1}$ were evaluated. It was determined that extraction efficiency ranged from 82.9 (±6.2) % to 94.6 (±3.4) %. The precision (RSD) for zopiclone was between 4.08 - 9.52 %, while the accuracy was in the range of 93.0 - 106.3 %. The presented method has several advantages over other methods: elimination of interferences and low-volume of samples (0.2 mL). Effective sample preparation as well as relatively short time of analyses proved a great applicability of presented method in clinical laboratories.

[1] A. C. Moffat, M. D. Osselton. Clarke's analysis of drugs and poisons, fourth ed., Pharmaceutical Press, London, UK, pp. 2257-2259 (2011).
[2] M. R. Pressman. Sleep Med. Rev. **15**, 285-292 (2011).
[3] M. A. Tonon, P. S. Bonato. Bioanalysis **4**, 291-304 (2012).
[4] N. Karlonas, A. Padarauskas, A. Ramanavicius, A. Ramanaviciene. Journal of Separation Science **36**, 1437-1445 (2013).
[5] N. Fontanals, P. A. G. Cormack, R. M. Marce, F. Borrull. Trends Anal. Chem. **29**, 765-779 (2010).
[6] F. T. Peters, O. H. Drummer, F. Musshoff. Forensic Science International **165**, 216-224 (2007).
[7] N. Karlonas, A. Padarauskas, A. Ramanavicius, Z. Minkuviene, A. Ramanaviciene. Chemija **23**, 91-99 (2012).
[8] N. Karlonas, A. Ramanavicius, A. Ramanaviciene. Journal of Separation Science **37**, 551-557 (2014).

# NOVEL ISOSTRUCTURAL HETEROPOLY SALTS WITH PEACOCK-WEAKLEY TYPE ANION $Na_9[Ln(W_5O_{18})_2]\cdot 35H_2O$ AND THULIUM OR YTTERBIUM HETEROATOMS

Mariichak Oleksandra Yu.[1], Kaabel Sandra[2], Karpichev Yevgen A.[2,3], Kapitanov Illia V.[2,3], Rozantsev Georgiy M.[1], Radio Serhii V.[1]

[1]Vasyl' Stus Donetsk National University, Ukraine
[2]Tallinn University of Technology, Estonia
[3]L.M. Litvinenko Institute of Physical Organic Chemistry & Coal Chemistry NAS of Ukraine
o.marijchak@donnu.edu.ua

Isostructural neutral sodium heteropoly decatungstolanthanidates(III) $Na_9[Ln(W_5O_{18})_2]\cdot 35H_2O$ (Ln = Tm (**SI**), Yb (**SII**)) with Peacock-Weakley type anion and Tm, and Yb as heteroatoms were synthesized using procedure, described in [1]. The compounds were obtained as colorless crystals from the aqueous solutions acidified up to Z=0.8 ($Z=\nu(H^+)/\nu(WO_4^{2-})$) from $Ln(NO_3)_3 – Na_2WO_4 – HNO_3 – H_2O$ systems. The formation of the salts is going according to the reaction:

$$Ln^{3+} + 10\ WO_4^{2-} + 8\ H^+ = [Ln(W_5O_{18})_2]^{9-} + 4H_2O.$$

The salts were characterized by elemental analysis, FT-IR spectroscopy, and single crystal X-ray diffraction analysis. The latter confirmed that the compounds have Peacock-Weakley type anion, and they are isostructural. There is one case of isostructurality of acidic double salts $K_3Na_4H_2[Ln(W_5O_{18})_2]\cdot(21\text{-}22)H_2O$ (Ln = Pr, Nd, Sm, Gd, Tb, Dy), which crystallize in a monoclinic crystal system, in space group $P2_1/n$ [2]. Isolated salts with Tm and Yb heteroatoms belong to the second group represented by neutral salts $Na_9[Ln(W_5O_{18})_2]\cdot 35H_2O$ (Ln = Y, Nd, Eu [3], Tb, Dy, Ho, Er [4]), which crystallize in a triclinic space group $P–1$.

$Na_9[Ln(W_5O_{18})_2]\cdot 35H_2O$ (Ln = Tm, Yb) consists of decatungstolanthanidate(III) anion, eight octahedrally coordinated $Na^+$ cations, one tetragonal-pyramidal $Na^+$ cation, and 35 $H_2O$ molecules. The decatungstolanthanidate(III) anion is comprised of two $[W_5O_{18}]^{6-}$ lacunary units, which coordinate to a central $Tm^{3+}$ or $Yb^{3+}$ cation in the form of square antiprism.

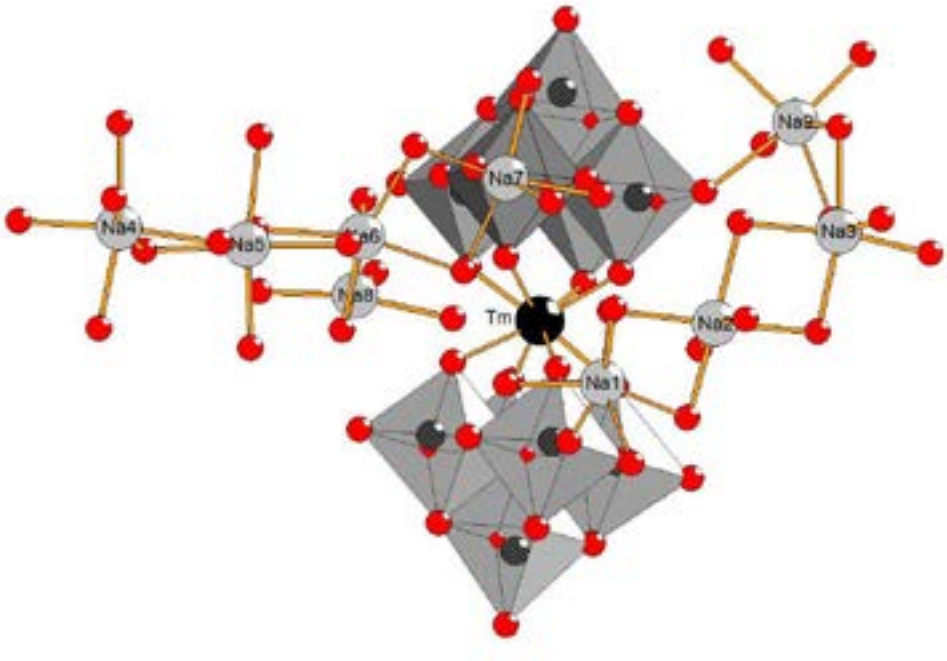


Fig. 1. Crystal structure of $Na_9[Tm(W_5O_{18})_2]\cdot 35H_2O$ (**SI**) (in (**SII**) position of Tm is occupied by an Yb atom)

Acknowledgements. The study was carried out within the Fundamental Research Programme funded by the Ministry of Education and Science of Ukraine (Project No. 0119U100025).

[1] O.Yu. Mariichak, E.S. Ivantsova, G.M. Rozantsev et al., Thulium-containing heteropoly tungstate with Peacock–Weakley anion: synthesis, properties, and surface micromorphology, Voprosy Khimii i Khimicheskoi Technologii, **3**, 38 (2015).
[2] T. Ozeki, T. Yamase, Effect of Lanthanide Contraction on the Structures of the Decatungstolanthanoate Anions in $K_3Na_4H_2[LnW_{10}O_{36}]\cdot nH_2O$ (Ln= Pr, Nd, Sm, Gd, Tb, Dy), Crystals Acta Cryst., **B50**, 128 (1994).
[3] Y. Yan, B. Li, W. Li et al., Controllable vesicular structure and reversal of a surfactant-encapsulated polyoxometalate complex, Soft Matter **5**(20): 4047 (2009).
[4] M. Vonci, M.J. Giansiracusa, W. Van den Heuvel et al., Magnetic excitations in polyoxotungstate-supported lanthanoid single-molecule magnets: An inelastic neutron scattering and ab initio study, Inorg. Chem., **56**, 378 (2017).

# SYNTHESIS OF 4,6-DISUBSTITUTED BENZENE-1,3-DIOLES CONTAINING HYDROXAMIC ACIDS

Paulina Kaziukonytė, Algirdas Brukštus

Department of Chemistry and Geosciences, Vilnius University, Lithuania
paulina.kaziukonyte@chgf.vu.lt

Inhibition of histone deacetylases (HDACs) is a proven way to treat cancer, as four drugs are already approved by the United States Food and Drug Administration [1]. Meanwhile, compounds inhibiting HSP90 (Heat Shock Protein) shows promising anti-tumor properties as well, acting as a single agent or in combination with additional drugs [2]. We propose that it is possible to combine active fragments of inhibition to yield small-molecule drugs with improved therapeutic and side effect profile [3]. We chose known pharmacophores for the task - resorcinol moiety was selected to target HSP90 and hydroxamic acid functional group to target HDAC. Some of the created and fulfilled syntheses of designed molecules are given below.

Syntheses of 5-chloro- and 5-isopropyl-2,4-dihidroxyphenylcarbohydroxamic acids (figure 1) were started with commercially available compound **1**. Esterification reaction was carried out to give compound **2**, which in the following reaction were substituted in the 5th position to give compounds **3**. Lastly, hydroxamic acid functional group was introduced.

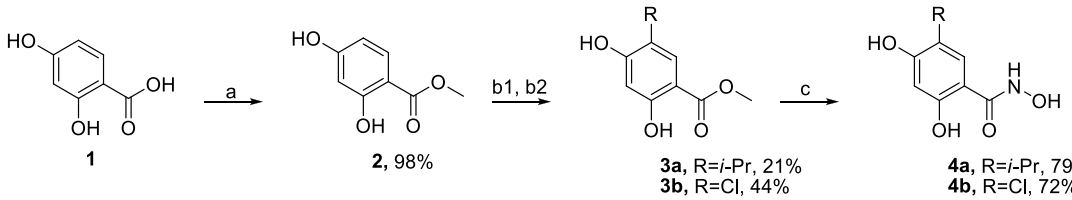


Figure 1. Syntheses of 5-substituted-2,4-dihydroxyphenylcarbohydroxamic acids. Reagents and conditions: a) $H_2SO_4$, MeOH, 30h, reflux, b1) i-PrBr, $AlCl_3$, DCM, reflux, b2) $SO_2Cl_2$, DCM, 2h 0°C, 20h 20°C, c) $NH_2OH{\cdot}HCl$, NaOH, $H_2O$, 3h 0°C, 12h 20°C.

Further syntheses to benzimidazole derivatives (figure 2) were started from compounds **5** and **6**. Vilsmeier–Haack reaction was carried out to give compound **7a** and substitution reaction gave product **7b**. Combination of compounds **7** and **8** gave compounds **9**, which were converted to hydroxamic acids.

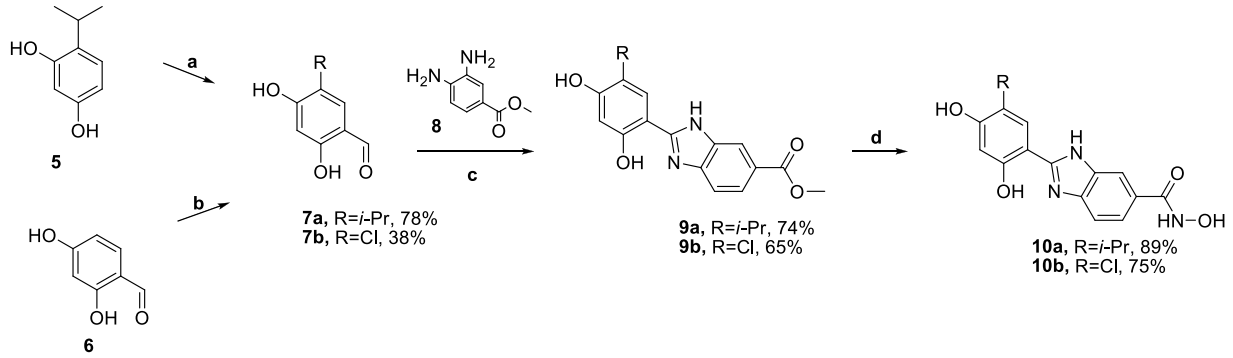


Figure 2. Syntheses of 2-arylbenzimidazo-5-carbohydroxamic acids. Reagents and conditions: a) $POCl_3$, DMF, 1h 0°C, 1h 20°C, 1h 50°C, b) NCS, HCl, $CHCl_3$, 4h, reflux, c) $Na_2S_2O_5$, DMF, 4h 80°C, d) $NH_2OH{\cdot}HCl$, NaOH, $H_2O$, 3h 0°C, 12h 20°C

Inhibition activities of compounds **4** and **10** are yet to be analyzed.

[1] T. Eckschlager, J. Plch, M. Stiborova, J. Hrabeta, Histone Deacetylase Inhibitors as Anticancer Drugs, International Journal of Molecular Sciences **18**, 1414 (2017);
[2] Y. Li, T. Zhanga, S. J. Schwartz, D. Suna, New Developments in Hsp90 Inhibitors as Anti-cancer Therapeutics: Mechanisms, Clinical Perspective and More Potential, Drug Resistance Updates **12**, 17-27 (2009);
[3] N. Dessalew, W. Mikre, On the Paradigm Shift Towards Multitarget Selective Drug Design, Current Computer-Aided Drug Design **4**, 76-90 (2008).

# SYNTHESIS AND CHARACTERISTICS OF NEW ORGANIC SEMICONDUCTOR WITH FOUR CARBAZOLYL CHROMOPHORES

Povilas Luižys[1], dr. Marytė Daškevičienė[1]

[1]Department of Organic Chemistry, Kaunas University of Technology, Lithuania
povilas.luizys@ktu.lt

There is a growing focus on renewable energy sources in the world and one of the most promising is solar energy. Converting it into electricity can theoretically satisfy the energy needs of mankind. Therefore, in many countries, development of technologies utilizing solar energy is stimulated in various ways. Over the last few years, perovskite solar cells (PSCs) have become a subject of great interest in the development of next generation solar cells (SCs) that have already exceeded 22% efficiency [1]. These elements are characterized by simplicity of construction and cheap raw materials compared to common (commercial) silicon SCs. Faster commercialization of the PSCs technology is hindered by drawbacks that need to be resolved. Firstly, hole transporting organic semiconductor spiro-OMeTAD, crystallizes in the device over time, thus reducing its efficiency [2]; secondly, additives are needed to increase the conductivity of semiconductor, which are the cause of rapid device degradation. Therefore, the search for new efficient organic semiconductors remains highly relevant.

In this work a new organic p-type semiconductor with four carbazolyl chromophores (Fig.1), which would be suitable for use in constructing PSCs was synthesized.

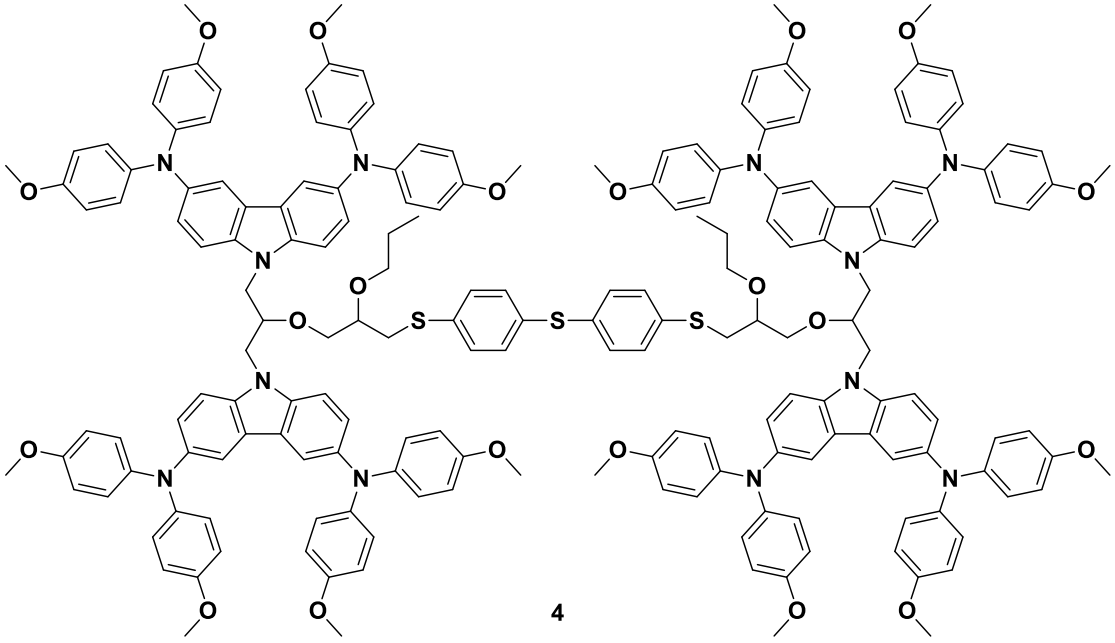


Fig. 1. Structure of organic semiconductor with four carbazolyl chromophores.

In order to obtain the target product from 3,6-dibromocarbazole, a glycidyl ether reacted with 4,4'-thiobisbenzenethiol and an intermediate tetramer was isolated. Then, during the alkylation, its analogue with alkoxy groups was obtained. The target product from tetramer and 4,4′-dimethoxydiphenylamine wasn't obtained during the Buchwald reaction. The goal product was isolated in an alternative way. The glycidyl ether with four diphenylamine fragments was synthesized and then tetramer was obtained during reaction with 4,4'-thiobisbenzenethiol. The final alkylation step yielded the target compound **4**.

The structure of the newly synthesized organic semiconductor was confirmed by $^{1}$H NMR, $^{13}$C NMR, IR spectroscopy. The thermal, optical, and electrical properties of the compound, which will allow to judge its suitability for PSCs, are currently being investigated.

[1] M. Saliba, J. Correa-Baena, M. Grätzel et al., Perovskite solar cells: from the atomic level to film quality and device performance, Angew. Chem. Int. Ed. 57, 2554-2569 (2018)
[2] Tobat P. I. Saragi, T. Spehr, A. Siebert et al., Spiro compounds for organic optoelectronics, Chem. Rev. 107, 1011-1065 (2007)

# MODIFICATION OF ELECTRODEPOSITED $MoS_{2-x}$ WITH Se TO FORM MOLYBDENUM SULFOSELENIDES

Ramunas Levinas[1], Natalia Tsyntsaru[1,2], Henrikas Cesiulis[1]

[1] Vilnius University, Naugarduko st. 24, Vilnius, Lithuania
[2] Institute of Applied Physics of ASM, 5 Academy st., Chisinau, Moldova
ramunas.levinas@chf.vu.lt

Molybdenum disulfide ($MoS_2$) is a material that belongs to a class of chemical compounds called transition metal dichalcogenides. It has a graphene-like layered structure due to the strong bonds between metal and chalcogenide ligands, but relatively weak Van der Waals interactions between layers. These peculiarities lead to a wide use of $MoS_2$ as a solid lubricant in machinery. From an academic point of view, it has been under research for its semicondutor, electro- and photocatalytic properties. $MoS_2$ is considered as a promising alternative to a platinum cathode for hydrogen evolution reaction (HER) catalysis in acidic media. Recent research in the field has revealed the influence of the polymeric structure of amorphous $MoS_2$ [1], as well as the several different active sites [2] on HER catalysis. The limiting step of the hydrogen evolution reaction on these materials is the Volmer adsorption step on the active sites of the cathode. The majority of these active sites in amorphous $MoS_2$ are likely to be sulfur vacancies, i.e. unsaturated Mo sites. As one favorable way to form catalytically active $MoS_2$, electrodeposition can be considered. It results in amorphous film growth with a large number of defects – sulfur vacancies. However, an amorphous structure hinders charge transfer, and thus has a negative impact on the electrochemical stability of the material. In order to improve the stability of $MoS_2$ films, some sulfur atoms can be substituted with the similar selenium atoms, which are more conductive.

The electrodeposition of molybdenum sulfoselenides was carried out using a one-step deposition process from a common Mo, S, and Se ion precursors, which were synthesized from $MoO_4^{2-}$, $Na_2S$, and $Na_2Se$. Chemical analysis confirmed that both S and Se were electrodeposited alongside with Mo. However, a large amount of oxygen is also present in the coating, which may indicate the formation of some oxides. The surface morphology of $MoS_{2-n}Se_n$ films reveals the scattered micrometer-sized crystallites (Fig. 1). The obtained films were also investigated for their HER electrocatalytic and photocatalytic properties.

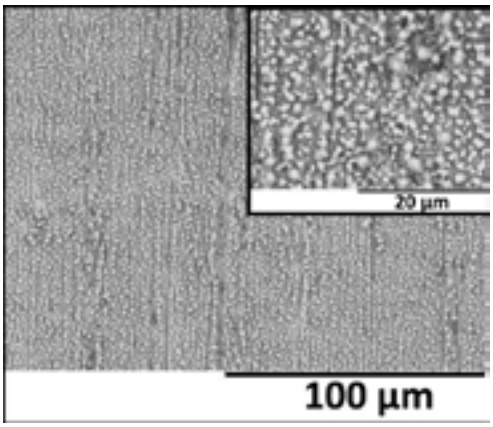


Fig. 1. SEM image of $MoS_{2-n}Se_n$ film (inset is a high magnification image), electrodeposited at -1.0 V vs Ag/AgCl for 600 s from the electrolyte containing 25 mM of $MoS_3Se$.

**Acknowledgements.** Authors acknowledge funding from H2020 project SMARTELECTRODES (No.778357) and by Research Council of Lithuania No 09.3.3-LMT-K-712-08-0003.

[1] P.D. Tran, T. V. Tran, M. Orio, S. Torelli, Q.D. Truong, K. Nayuki, Y. Sasaki, S.Y. Chiam, R. Yi, I. Honma, J. Barber, V. Artero, Coordination polymer structure and revisited hydrogen evolution catalytic mechanism for amorphous molybdenum sulfide, Nat. Mater. **15** (2016).
[2]G. Li, D. Zhang, Q. Qiao, Y. Yu, D. Peterson, A. Zafar, R. Kumar, S. Curtarolo, F. Hunte, S. Shannon, Y. Zhu, W. Yang, L. Cao, All The Catalytic Active Sites of $MoS_2$ for Hydrogen Evolution, J. Am. Chem. Soc. 138 (2016) 16632–1663

# THERMAL REDUCTION OF GRAPHITE OXIDE IN THE PRESENCE OF MALONIC ACID

Rūta Aukštakojytė[1], Justina Gaidukevič[1], Jurgis Barkauskas[1]

[1] Institute of Chemistry, Faculty of Chemistry and Geosciences, Vilnius University,
Naugarduko 24, LT-03225 Vilnius, Lithuania
*ruta.aukstakojyte@chgf.vu.lt*

Graphene is a plane sheet of $sp^2$ hybridized carbon atoms arranged into a honeycomb lattice. In recent decades it has drawn wide attention due to its unique physicochemical characteristics such as a high specific surface area (2630 $m^2\ g^{-1}$), large Young's modulus (1.0 TPa), excellent thermal conductivity (~5000 $W\ m^{-1}\ K^{-1}$) and high electron mobility ($2.5 \cdot 10^5$ $cm^2\ V^{-1}\ s^{-1}$). These properties of graphene lattice are important in many applications including lithium-ion batteries, solar cells, photocatalysts, biosensors, transistors, water purification systems, super capacitors and etc. [1].

Chemical reduction of graphite oxide (GO) is the one of most facile ways for low-cost, high yield and rapid production of graphene. However, the most popular chemical reducing agents, such as hydrazine, hydroquinone, sodium borohydride, lithium aluminium hydride, are hazardous and corrosive. The product obtained using these reagents has poor electrical conductivity, due to the defects remaining in crystal lattice and have negative impact on bio-related applications, too [2,3]. Therefore, effective and environmentally-friendly reducers for GO are still in focus.

In this work, we present the thermal reduction of GO in the presence of malonic acid, which is a green and inexpensive reducer decomposing thermally at 135 ℃. Graphite oxide was prepared from the natural graphite by the synthesis protocol reported by Yan et al. [4]. In a typical experiment, graphite powder was treated with conc. $H_2SO_4$, $K_2S_2O_8$ and $P_2O_5$. Later, this pre-oxidized graphite was subjected to oxidation by Hummers method using $NaNO_3$, $H_2SO_4$ and $KMnO_4$ [5]. The obtained GO was reduced by adding malonic acid with molar ratio of 1:3 or 1:5 and thermal annealing under Ar gas atmosphere for 30 min at different temperatures 200 ºC, 300 ºC, 600 ºC, 800 ºC. Reduced GO products were analyzed by Fourier Transform infrared (FTIR), Raman spectroscopy and X-ray diffraction (XRD) analysis.

The results show that the level of GO reduction to graphene phase depends on the reduction conditions. Reduction of GO at low temperatures results formation of an amorphous product. XRD analysis of GO-MA-600 and GO-MA-800 shows a similar ‘d’ spacing of 0.350 nm with a hexagonal structure, indicating the formation of a more ordered graphitic structure after annealing. Moreover, IR analysis of these sample exhibits a significant reduction of oxygen functionalities.

[1] M. T. H. Aunkor, I. M. Mahbubul, R. Saidur and H. S. C. Metselaar, The green reduction of graphene oxide, RSC Adv. **6**, 27807 (2016).
[2] A. Kumar and M. Khandelwal, A novel synthesis of ultra thin graphene sheets for energy storage applications using malonic acid as a reducing agent, J. Mater. Chem. A **2,** 20345-20357 (2014).
[3] Dandan Hou, Qinfu Liu, Hongfei Cheng, Hao Zhang, Sen Wang, Green reduction of graphene oxide via Lycium barbarum extract, Journal of Solid State Chemistry **246**, 351–356 (2017).
[4] X. Yan, J. Chen, J. Yang, Q. Xue, P. Miele, Fabrication of Free-Standing, Electrochemically Active, and Biocompatible Graphene Oxide−Polyaniline and Graphene−Polyaniline Hybrid Papers, App. Mater. **9**, 2521-2529 (2010).
[5] W. S. Hummers, and R. E. Offeman, Preparation of Graphitic Oxide, J. Am. Chem. Soc., **80,** 1339 (1958).

# FLUORENE-BASED HOLE TRANSPORTING MATERIALS FOR EFFICIENT AND STABLE PEROVSKITE SOLAR CELLS

Šarūnė Daškevičiūtė[1], Nobuya Sakai[2], Marius Franckevičius[3], Marytė Daškevičienė[1], Artiom Magomedov[1], Egidijus Kamarauskas[4], Vygintas Jankauskas[4], Henry Snaith[2], Vytautas Getautis[1]

[1] Department of Organic Chemistry, Kaunas University of Technology, Lithuania
[2] Clarendon Laboratory, Department of Physics, Oxford University, United Kingdom
[3] Center for Physical Sciences and Technology, Lithuania
[4] Institute of Chemical Physics Vilnius University, Lithuania
sarune.daskeviciute@ktu.lt

Solid-state organic hole transporting materials (HTMs) are one of the important components of the perovskite solar cells (PSCs), ensuring stability of the perovskite absorber layer, good charge separation, and as a consequence high performance of the devices. Currently, Spiro-OMeTAD is the most popular choice for the HTM layer, and is used for the majority of the state-of-the-art PSC devices. However, due to the complicated multi-step synthetic procedure, price of the Spiro-OMeTAD remains at a very high level. However, it is not only quite expensive but also shows unsatisfactory long-term stability due to oxidative doping process and slow morphological degradation [1].

In this work, novel small-molecule HTMs **V1050** and **V1061** were designed and synthesized (Fig.1). Synthesis was performed using a facile three-step synthetic route, starting from simple fluorene derivatives. The coplanar central core was chosen in order to improve the efficiency of HTM, as was previously shown by Li and co-workers [2]. As a hole transporting fragment, 4,4′-dimethoxydiphenylamine 3,6-disubstituted carbazole was used, due to its good performance in PSCs [3]. The synthesized compounds exhibit amorphous nature with a high glass transition temperature, a good solubility, and decent thermal stability.

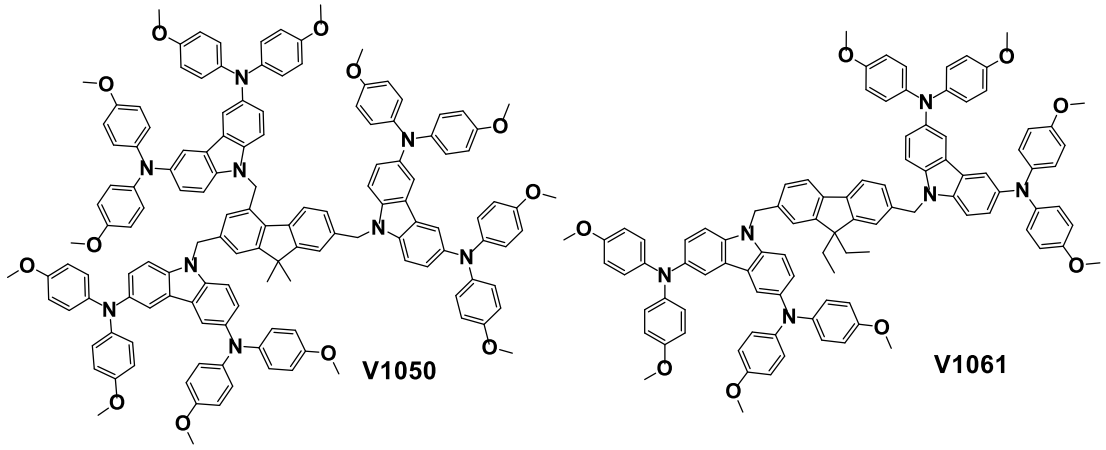


**Figure 1**. Structures of fluorene-based HTMs **V1050** and **V1061**.

PSCs of planar configuration, employing **V1050** HTM showed a high power conversion efficiency of 18.3%, which is comparable to the 18.9% efficiency, obtained in the same device configuration, only using Spiro-OMeTAD as a HTM. In addition, devices with **V1050** and **V1061** showed better stability in comparison to Spiro-OMeTAD based devices. Aging test was performed on a non-encapsulated devices under uncontrolled humidity conditions (relative humidity around 60%) in the dark and under continuous full sun illumination. Overall, we believe that the **V1050** can be a usefull alternative HTM to Spiro-OMeTAD for perovskite solar cells, thus bringing PSCs closer to commercial production.

[1] Z. Li, Z. Zhu, C. C. Chueh et al., Facile Thiol-Ene Thermal Crosslinking Reaction Facilitated Hole-Transporting Layer for Highly Efficient and Stable Perovskite Solar Cells, Adv. Energy Mater. **1601165** (2016).
[2] W.-J. Chi, P.-P. Sun, Z.-S. Li, A Strategy to Improve the Efficiency of Hole Transporting Materials: Introduction of a Highly Symmetrical Core, Nanoscale **8**, 17752-17756 (2016).
[3] A. Magomedov, S. Paek et.al., Diphenylamine-Substituted Carbazole-Based Hole Transporting Materials for Perovskite Solar Cells: Influence of Isomeric Derivatives, Adv. Funct. Mater. 2**8**, 17043511 (2018).

# SYNTHESIS AND STUDIES OF THIOXANTHONE BASED DERIVATIVES EXHIBITING TADF, AGGREGATION INDUCED EMISSION ENHANCEMENT AND RTP

Simas Macionis, Nasiri Sohrab, Dalius Gudeika, Dmytro Volyniuk, Juozas V. Grazulevicius

Kaunas University of Technology, Department of Polymer Chemistry and Technology, Lithuania
Radvilėnų plentas 19, LT-50254, Kaunas, Lithuania
simas.macionis@ktu.edu

For the past few decades organic light emitting diodes (OLEDs) have been a widely researched field in organic optoelectronics. A great deal of research has been made in effort to achieve highly efficient materials for various high-resolution OLED displays and lightning devices [1]. Thermally activated delayed fluorescence (TADF) emitters have been recently attracting much attention due to their ability to push the internal quantum efficiency of OLEDs up to 100% of their theoretical value [2]. TADF enables the possibility of harvesting both singlet and triplet excitons due to very low energy gap ($\Delta E_{ST}$) in most cases <100 meV.

Recently, two different thioxanthone based emitters were reported showing good thermal stability, high external quantum efficiency of OLEDs (up to 21,5%) and aggregation-induced emission enhancement (AIEE) and TADF capabilities [3]. OLEDs containing thioxanthone-based material characterized by efficient TADF showed external quantum efficiencies ranging from 11 to 13.6% [4].

In this work, four thioxanthone based derivatives with different donor fragments were synthesized and their thermal, electrochemical, photophysical properties were investigated. It was discovered that some of the aforementioned materials not only exhibited TADF and AIEE effects, but also showed room temperature phosphorescence. OLEDs with maximum external quantum efficiencies up to 8% were fabricated using thioxanthone-based derivatives.

[1] O'Brien D. F, Baldo M. A, Thompson M. E, Improved Energy Transfer in Electrophosphorescent Devices, Appl. Phys. Lett **74**, 442 (1999).
[2] C. Bizzarri, F. Hundemer, J. Busch, Triplet emitters versus TADF emitters in OLEDs: A comparative study, Polyhedron **140**, 51-66 (2018).
[3] Hui Wang, Lisha Xie, Qian Peng, Novel Thermally Activated Delayed Fluorescence Materials–Thioxanthone Derivatives and Their Applications for Highly Efficient OLEDs, Advanced Materials **26**, 5198-5204 (2014).
[4] Zhiheng Wang, Yunchuan Li, Xinyi Cai, Structure−Performance Investigation of Thioxanthone Derivatives for Developing Color Tunable Highly Efficient Thermally Activated Delayed Fluorescence Emitters, Applied Materials & Interfaces **8**, 8627-8636 (2016).

# SYNTHESIS AND INVESTIGATION OF FILMS FROM POLYESTERS MODIFIED WITH α,ω -DIHYDROXY-POLY(DIMETHYLSILOXANE)

Sonata Gailiūnaitė, Saulutė Budrienė

Faculty of Chemistry and Geosciences, Department of Polymer Chemistry, Vilnius University, Vilnius, Lithuania
sonata.gailiunaite@chgf.stud.vu.lt

Tissue engineering is a fast-growing field of science that enables the creation of biological tissues. The tissues are grown on a synthetic artificial carcass which is created using 3D printing technology (Fig. 1). It is very important to choose the right materials for the frame, it must be biocompatible, so that the cells could reproduce and functionalize, it must have mechanical strength, be flexible, biodegradable and non-toxic [1]. Poly(dimethylsiloxane) (PDMS) elastomer is one of those biocompatible polymers which is widely used in medicine due to it‘s properties such as: biocompatibility, gas permeability, non-toxicity, chemical and biological inertness, transparency, and because of it’s low cost. However, its use is limited by hydrophobicity which can cause cellular adhesion on the surface to be short-lived, and low mechanical resistance. By improving these features, the ability to use PDMS is significantly enhanced. That’s why many strategies have been suggested to enhance hydrophilicity of PDMS [2].

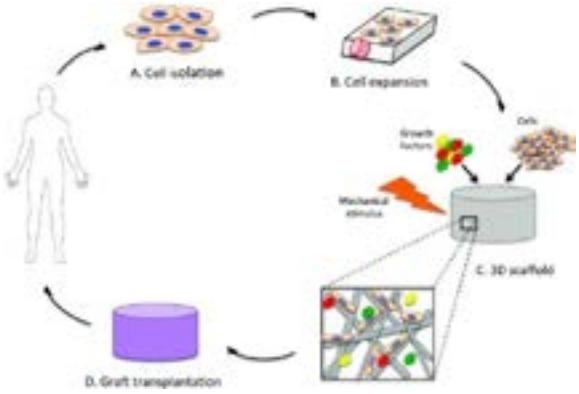


Fig.1. Schematic depicting the principles of tissue engineering [3].

The aim of this work was to obtain biocompatible films from polyesters modified with hydroxyl terminated PDMS. Polyester films were synthesized from azelaic acid, maleic anhydride, diethylene glycol and were chemically modified with hydroxyl terminated PDMS, at various initial molar ratios. Glycidyl methacrylate, (hydroxyethyl)methacrylate and/or buthyl methacrylate were attached to obtained copolymers to form UV-curable product. Crosslinking was initiated by photoinitiator Irgacure 651 and UV light. The films were tested for swelling and solubility in hexane, ethanol and water. To investigate the hydrophilicity of films, a study of humidification angle was performed. The strength of the films was also measured by tensile test.

---

[1] C. Yu et. al., *Scanningless and continuous 3D bioprinting of human tissues with decellularized extracellular matrix.* Biomaterials **194,** 1-13 (2019).
[2] B.Y. Yoo et. al., *Dual surface modification of PDMS-based silicone implants to suppress capsular contracture.* Acta Biomaterialia **76**, 56-70 (2018).
[3] J.V. Serbo, S. Gerecht, *Vascular tissue engineering: biodegradable scaffold platforms to promote angiogenesis.* Stem Cell Research & Therapy **4**, 8 (2013)

# OVERALL AND SPECIFIC MIGRATION FROM COMMERCIAL POLYETHYLENE PACKAGES

Toma Petrulionienė[1], Grėta Grakauskaitė[2], Evaldas Naujalis[1]

[1] Department of Metrology, State research institute Center for Physical Sciences and Technology, Lithuania
[2] Department of Polymer Chemistry, Vilnius University, Lithuania
toma.petrulioniene@ftmc.lt

Polyethylene is one of the most widely used plastics for food packaging due to its uncomplicated modification. It exhibits outstanding chemical resistance, high tensile strength and low density. But in order to get the package that we need, additives must be used during manufacturing processes. All these additives can migrate through the functional barrier in to food and contaminate it as the potential migrants might be dangerous chemical substances. All the migrated substances can cause human health problems such as disrupting thyroid systems or allergies [1,2].

The aim of this work was to identify if overall migration of substances from commercially available food packages made from polyethylene occurs. Also, to verify if the migration limits agree with the legislation. According to Commission Regulation (EU) No 10/2011 of 14 January 2011 on plastic materials and articles intended to come into contact with food, plastic materials and articles shall not transfer their constituents to food simulants in quantities exceeding 10 milligrams of total constituents released per $dm^2$ of food contact surface ($mg/dm^2$). What is more, specific migration of barium, cobalt, copper, iron, lithium, manganese and zinc were tested. The results were evaluated according to the same Commission Regulation (EU) No 10/2011 of 14 January 2011, where the limits of metals are 1 mg/kg for barium, 0.05 mg/kg for cobalt, 5 mg/kg for iron, 0.6 mg/kg for lithium and manganese, 25 mg/kg for zinc. In addition, the content of cadmium, chromium, lead and mercury was tested in order to verify if there are any commercially available packages where the content of the metals mentioned exceeds limits according to European Parliament and Council Directive 94/62/EC of 20 December 1994 on packaging and packaging wastes where the sum of concentration levels of cadmium, lead, chromium and mercury present in packaging or packaging components shall not exceed 100 ppm by weight.

For this reason, overall migration tests were held in different food simulants (ethanol, acetic acid and isooctane) and testing conditions of contact using food simulants which were chosen according to the Commission Regulation (EU) No 10/2011 of 14 January 2011. Furthermore, the determination of metals was carried out by atomic absorption spectrophotometry (AAS). Fig.1 shows the schematic overview of the analytical strategy that was applied. The results revealed the presence of constituents and metals which can migrate to food from polyethylene packaging. The interpretation of the origin of the metals is discussed in the latest work done by the group of scientists who published a huge database called “Chemicals associated with plastic packaging” [3].

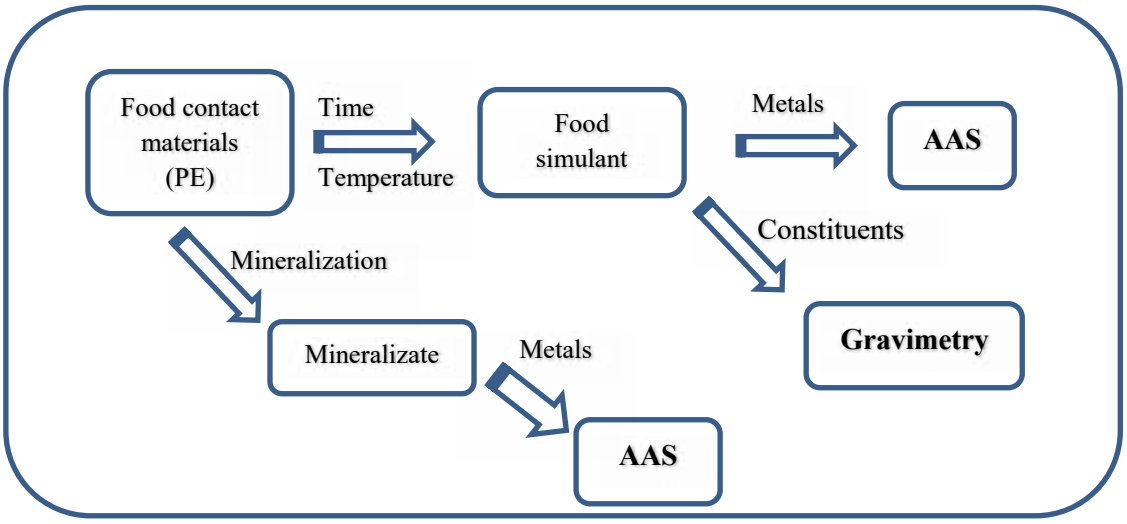


Fig. 1. Schematic overview of the analytical strategy applied to study PE food packaging materials.

[1] Nerlis Pajaro-Castro, Karina Caballero-Gallardo, Jesus Olivero-Verbel, 2014. Identification of volatile organic compounds (VOCs) in plastic products using gas chromatography and mass spectrometry (GC/MS). Rev. Ambient. Agua vol. 9 n. 4 n. Taubate - Oct./Dec. https://doi.org/10.4136/ambi-agua.1435.

[2] Mandana Ghisari, Eva Cecilie Bonefeld-Jorgensen, 2009. Effects of plasticizers and their mixtures on oestrogen receptor and thyroid hormone functions. J. Tox. Let. 189, 67-77. https://doi.org/10.1016/j.toxlet.2009.05.004.

[3] Groh KJ, Backhaus T, Carney-Almroth B, Geueke B, Inostroza PA, Lennquist A, Maffini M, Leslie HA, Slunge D, Trasande L, Warhurst M, Muncke J., 2018. Chemicals associated with plastic packaging: Inventory and hazards. PeerJ Preprints 6:e27036v1. https://doi.org/10.7287/peerj.preprints.27036.

# OPTICAL PROPERTIES OF $Cu_xS$ THIN FILMS DEPOSITED BY CHEMICAL BATH TECHNIQUE

Tomas Petrašauskas[1], Neringa Petrašauskienė[2], Rasa Alaburdaitė[2], Edita Paluckienė[2]

[1] Faculty of Physics, Vilnius University, Lithuania
[2] Department of Physical and Inorganic Chemistry, Kaunas University of Technology, Lithuania
tomas.petrasauskas@ff.stud.vu.lt

Copper sulfide ($Cu_xS$) is wide-band-gap *p*-type semiconductor material with modern applications ranging from industrial to biomedical. Various polymers, modified by copper sulfides, represent a new class of materials – composites with novel properties. $Cu_xS$ is an interesting material for its metal–like electrical conductivity, chemical–sensing capability and ideal characteristics for solar energy absorption. Consequently, polymers modified by $Cu_xS$ are used: as the conductive substrates for deposition of metal and semiconductors; as gas sensors functioning at temperatures tending to room temperature; as polarizer of infrared radiation; and as active absorbents of radio waves.

Electrically conductive $Cu_xS$ films can be prepared by the chemical bath technique or sorption-diffusion methods [1-3]. Polyamide (PA) as semi-hydrophilic polymer is capable to absorb ions or molecules of various electrolytes from aqueous and non aqueous solutions.

$Cu_xS$ thin films were deposited on PA (Tecamid 6, density 1.13 g·cm$^{-3}$, 500 μm thick) using $CuCl_2$ and $Na_2S_2O_3$ mixture for 16 h. The deposition process was carried out by repeating such deposition cycles till 3 times.

The aim of this work was to obtain $Cu_xS$ thin films by the chemical bath deposition method and determine the effect of variation of number of cycles of deposition on the optical properties with a view to ascertaining the possible applications. The UV-Visible absorption spectroscopy is a powerful tool for the investigation of optical properties of material. Absorbance of the films was characterized using PerkinElmer Lambda 35 UV/VIS spectrometer. The absorption spectrum for copper sulfide thin films was recorded in the wavelength region from 200 nm to 1100 nm.

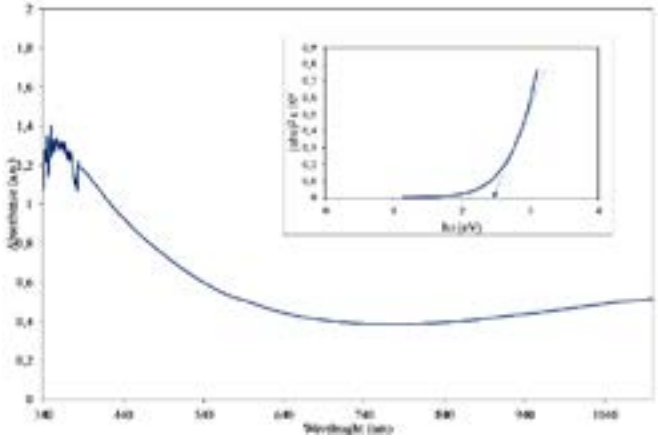

Fig. 1. UV-VIS absorption spectra of $Cu_xS$ thin films after. The optical band gaps of the $Cu_xS$ thin films are plotted in the inset.

Fig.1 shows that absorbance of $Cu_xS$ films (after 3 cycles of deposition) is generally high in the UV region (300-400 nm) and low absorbance in the visible spectrum (400-765 nm). This makes the films suitable for coating of eye glasses to prevent UV radiation from getting to the eyes. It is also useful for coating of windows to prevent UV radiation and aid visibility since absorption in the visible region is low. Low absorption in the visible region makes it a veritable material for buffer layer in solar cell. The absorbance of the films is directly proportional to number of cycles of deposition.

The optical bandgap of the $Cu_xS$ thin films was determined from the absorption spectra using Tauc's relation

$$\alpha h\upsilon = A(h\upsilon - E_g)^n \qquad (1)$$

where $h\nu$ is the photon energy, α – optical absorption coefficient, $E_g$ – the optical energy bandgap, $A$ – the optical transition dependent constant, and $n$ – characterizes the transition. For allowed direct transitions, $n$ = 2 and allowed indirect transitions, $n$ = 1/2. Fig. 1 shows the plot of $(\alpha h\nu)^2$ against $h\nu$. The variation of $(\alpha h\nu)^2$ with $h\nu$ is linear which indicates that the direct transition is present. Extrapolating the straight line portion of the plot of $(\alpha h\nu)^2$ against $h\nu$ to energy axis for zero absorption coefficient give optical bandgap energy value as 2.5 eV. The films were found to have average transmittance of about 40 % in the UV-VIS regions while exhibiting average reflectance of about 20 % in the same regions. Some of the films could be effective for solar control, eyeglasses, and as well good materials for solar cell fabrication.

[1] V. Janickis, N. Petrašauskienė, S. Žalenkienė, I. Morkvėnaitė-Vilkončienė, A. Ramanavičius, *Journal of nanoscience and nanotechnology,* **18(1)**, 604-613 (2018).
[2] V. Janickis, N. Petrašauskienė, *Chemija*, **28(4)**, 214-225 (2017).
[3] R. Alaburdaitė, E. Paluckienė, S. Grevys, Chalcogenide Lett, **13(12)**, 529-536 (2016).

# SYNTHESIS OF ALKENE-STRAPPED NAPHTHALENE DIIMIDES AS MODEL SYSTEMS TO PROBE ALKENE π –AROMATIC π INTERACTIONS

Ugnė Rimkaitė, Ieva Karpavičienė, Edvinas Orentas

[1]Vilnius University, Faculty of Chemistry and Geosciences, Naugarduko 24, LT-03225, Vilnius, Lithuania
ugnerimkaite@gmail.com

Derivatives, that contain naphthalene diimide (NDI) frameworks are considered to be the strongest organic π -acids. [1] This unique property, together with their ability to self-assemble into multilayered structures, render NDI derivatives promising materials for new molecular optoelectronic and electronic devices [2], bioactivatable cross-linking agents [3], anion sensors, and π – acid organocatalysts [4]. In our research, we sought to explore the highly electron defficient aromatic system of NDIs for the modulation of the electron density of alkene double bonds, located on top of the NDI's π -acidic surface. Toward this goal, a collection of symmetric preorganized NDI derivatives, possesing cyclic alkene motifs, was synthesized and characterized.

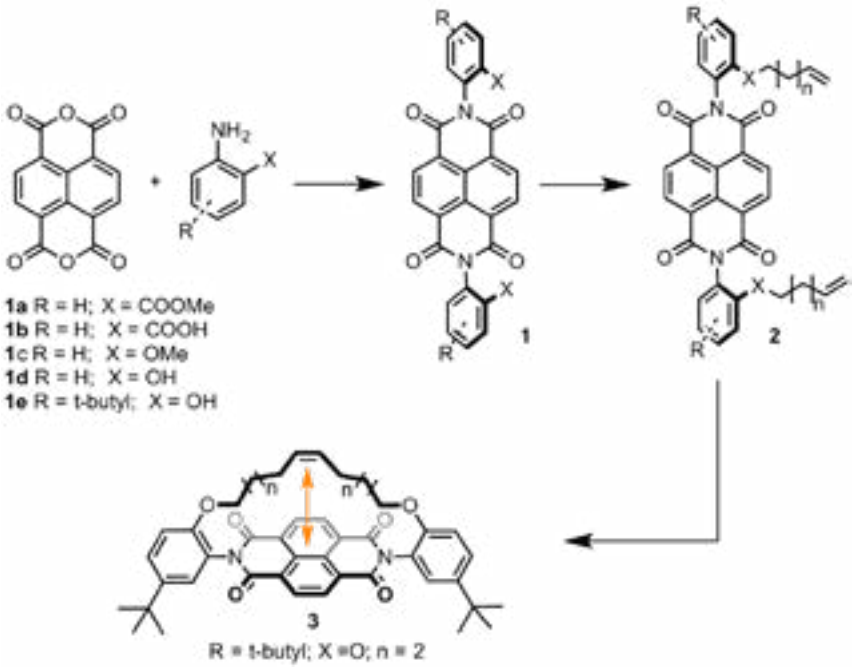


The starting NDIs were obtained from corresponding aniline derivatives and commercially available 1,4,5,8-naphthalenetetracarboxylic dianhydride. The synthetic procedure was initially optimized for 2-amino-*tert*-butyl-phenol derived intermediate **1d**, which was then utilized for the synthesis of bis-alkene **2**. The latter was subjected to olefin metathesis reaction to provide model compound **3** in good yield.

[1] Y. Zhao, N. Sakai, S. Matile, *Nature Commun*., **5**, 3911 (2014)
[2] Y. Ofir, A.Zelichenok, S. Yitzchaik, *J. Mater. Chem*., **16**, 2142–2149 (2006)
[3] M. Di Antonio, F. Doria, M. Mella, D. Merli, A. Profumo, M. Freccero, *J. Org. Chem*., **72**, 8354-8360 (2007)
[4] H. Ke, L. Wang, Y. Chen, M. J. Lin, J. Z. Chen, J. Molec. Catalys. A: Chem., **385**, 26–30 (2014)

# THE INFLUENCE OF TIME AND STIRRING OF EXTRACTION AND DIFFERENT SOLVENT ON CONCENTRATION OF FLAVONOIDS

Vaida Vaškelienė, Rasa Šlinkšienė

Department of Physical and Inorganic Chemistry, Kaunas University of Technology
vaida.vaskeliene@ktu.lt

In the last decade, a healthy lifestyle has become popular in the world so people are increasingly willing to use products made from natural plant materials. Scientists carry out a variety of research to find out which plant material is rich in vitamins, antioxidants and other useful active substances necessary for the human body. Most often studied and analysed are medicinal plants, which abound in Lithuania. Rowan, Sorbus aucuparia L., that is widespread in Lithuania attributed to medicinal plants and that have medicinal characteristic [1].

On the data basis of various, scientific articles [2–3] there are carotenoids, flavonoids, and organic acids (succinic, malic and citric), various vitamins (C, E, K, P), essential oils, leaven, carbohydrates, minerals (Zn, Fe, Mg and Mn compounds) in rowan berries. In O. Ragažinskienė [4] and in other literature sources are indicated the concentrations of the various active substances in fresh rowan berries which are identified during the investigation such as: carotenoids up to 65.0 mg / 100 ml; vitamin C 44.5–72.5 mg / 100 ml; iodine 1.5–2.4 mg / 100 ml; vitamin E 0.6–1.6 mg / 100 ml; saccharides 4.0–7.0%; flavonoids 0.13–2.1 %; sorbic acid and sorbitol up to 3.0 %; other organic acids 1.9–2.6 %; yeast to 0.45 %.

In this experiment, the dried minced rowan berries were poured out with various concentrations of ethanol solutions, ratio 1:10. To evaluate different factors influencing the concentration of flavonoids, extracts were produced not only by changing the ethanol concentration, but by also using different stirring techniques. Stirring with a magnetic and propeller stirrers (the same stirring speed is maintained) and changing the stirring time (30 minutes and 1 hour). The results of this experiment are presented in Table 1.

Table. 1. The influence of time and stirring of extraction and different solvent on concentration of flavonoids

| Concentration of ethanon | Duration | | | | | | | | | | | |
|---|---|---|---|---|---|---|---|---|---|---|---|---|
| | 0,5 h | | | | | | 1 h | | | | | |
| | Stirrer | | | | | | Stirrer | | | | | |
| | Magnetic | | | Propeller | | | Magnetic | | | Propeller | | |
| | $\bar{X}^*$ | $S^2_x \cdot 10^{6\,**}$ | $S_x \cdot 10^{6\,***}$ | $\bar{X}^*$ | $S^2_x \cdot 10^{6\,**}$ | $S_x \cdot 10^{6\,***}$ | $\bar{X}^*$ | $S^2_x \cdot 10^{6\,**}$ | $S_x \cdot 10^{6\,***}$ | $\bar{X}^*$ | $S^2_x \cdot 10^{6\,**}$ | $S_x \cdot 10^{6\,***}$ |
| | Average concentration of flavonoids, % | | | | | | | | | | | |
| 50% | 0,043 | 1,53 | 0,77 | 0,040 | 0,43 | 0,21 | 0,074 | 3,31 | 1,66 | 0,071 | 0,57 | 0,28 |
| 60% | 0,050 | 2,71 | 1,35 | 0,048 | 0,04 | 0,02 | 0,091 | 0,68 | 0,34 | 0,084 | 3,24 | 1,62 |
| 70% | 0,069 | 2,60 | 1,30 | 0,062 | 2,28 | 1,14 | 0,126 | 1,53 | 0,77 | 0,118 | 0,32 | 0,16 |
| 80% | 0,155 | 0,10 | 0,01 | 0,151 | 0,32 | 0,16 | 0,250 | 0,04 | 0,08 | 0,219 | 1,74 | 0,09 |
| 96% | 0,304 | 0,60 | 0,30 | 0,286 | 2,81 | 1,40 | 0,492 | 1,32 | 0,66 | 0,488 | 1,39 | 0,69 |

* – $\bar{X}$ – Average concentration of carotenoids, %
** –$S^2_x$– Variance
*** – $S_x$ – Standard deviation

The table shows the data, that when ethanol concentration increases the concentration of flavonoids increases too. During extraction using a magnetic stirrer we receive a higher concentration of flavonoids than stirring with propeller stirrer. The highest concentration of flavonoids was found, as an extract produced using 96 % ethanol, stirring for 1 hour with a magnetic stirrer (0.492 %), lowest – using 50 % ethanol and stirring for 0.5 hour with propeller stirrer (0.040 %). Stirring extract for 1 hour concentration of flavonoids is almost twice as high on average as stirring for 30 minutes. It can be concluded that stirring accelerates extraction, but by extraction with stirring 1 hour maximum concentration of flavonoids was not reached and in order to get optimal results, the experiment should be continued with a longer stirring time.

Preparation of extraction by stirring is not the only way to produce extraction, to find out which extraction method is optimal taking in to account flavonoid concentration, extraction time, temperature, berries processing ways and extractor concentration. Extraction with a Soxhlet apparatus has also been tested, but the experiment has not been completed therefore, no results can be provided.

[1] Z. Gudžinskas, Žalioji sveikatos versmė: vaistinių augalų vadovas, Kaunas: Brentus, ISBN 978–609–95303–3–8, (2012).
[2] M. Olszewska. et al., 2008. Separation of quercetin, sexangularetin, kaempferol and isorhamnetin for simultaneous HPLC determination of flavonoid aglycones in inflorescences, leaves and fruits of three Sorbus species. Journal of Pharmaceutical and Biomedical Analysis, vol. 48, p. 629–635. Prieiga per internetą: https://doi.org/10.1016/j.jpba.2008.06.004.
[3] O. Raspea, C. A. Findlay, L. Jacquemart, Sorbus aucuparia, Journal of Ecology, Vol. 88, no. 5, p. 910–930 (2000). DOI: 10.1046/j.1365-2745.2000.00502.x.
[4] O. Ragažinskienė, S. Rimkienė, V. Sasnauskas, Vaistinių augalų enciklopedija, Kaunas: Lututė, ISBN 9955–575–73–5 2005.

# Co(II) AND Cu(II) COMPLEXES BASED ON CAPh TYPE LIGAND N, N`-DIBENZYL –N``-TRICHLORACETYLPHOSPHORTRIAMIDE

Valeriia Zozulia[1], Julia Shatrava[1], Viktoriya Dyakonenko [2], Tatyana Sliva[1], Vladimir Ovchynnikov[1]

[1] Department of Chemistry, Taras Shevchenko National University of Kyiv, Ukraine
[2] SSI "Institute for Single Crystals", National Academy of Science of Ukraine, Kharkiv 61001, Ukraine
valeriiaz@bigmir.net

Carbacylamidophosphates (CAPh) – compounds containing the functional fragment -C(O)N(H)P(O)= belong to the broad class of the powerfull ampolydentate ligands. Due to the presence of phosphoryl group in the composition of CAPh ligands they have high affinity for the majority of metal ions. The possibility to be involved in the coordination sphere both in molecular and acidic forms, makes the coordination chemistry of these ligands extremely diverse and interesting [1].

On the basis of one representative of CAPh ligands - N, N'-dibenzyl-N "- trichloroacetylphosphortriamide (HL), di- and tetrameric complexes of the composition $Co_2L_4(CH_3OH)_2$ and $Cu_4L_4(OCH_3)_4$ were synthesized and obtained in the crystalline state. Obtained compounds were investigated by means of IR spectroscopy, thermogravimetric, magnentochemical and X-ray diffraction analysis.

The bidentate-cyclic coordination of CAPh ligand through oxygen atoms of the phosphoryl and carbonyl groups was established for both complexes under consideration.

In the $Co_2L_4(CH_3OH)_2$ structure cobalt ions are connected in the centrosymmetric dimers due to the bridging function of the phosphoryl groups (Fig. 1). The coordination sphere of each cobalt ions includes also methanol molecule, coordinated by oxygen atom and additionally linked to the carbonyl group by hydrogen bond. Last one can be considered as an additional stabilizing factor in the formation of the dimeric structure.

Complex $Cu_4L_4(OCH_3)_4$ contents methylate ions which due to $\mu^3$-bridging function connect four copper ions in the tetramer (Fig. 1). According to results of thermogravimetric investigations, the first mass loss for the cobalt complex corresponds to missing of two methanol molecules (the range temperature from 80°C to 150°C). This process combines with the process of oxidative degradation of organic ligands.

Unlike the compound of cobalt, the tetrameric copper complex contains methylate ions, therefore it is resistant to the temperature of 110°C. Further rising of temperature leads to the destruction of the organic part of copper complex.

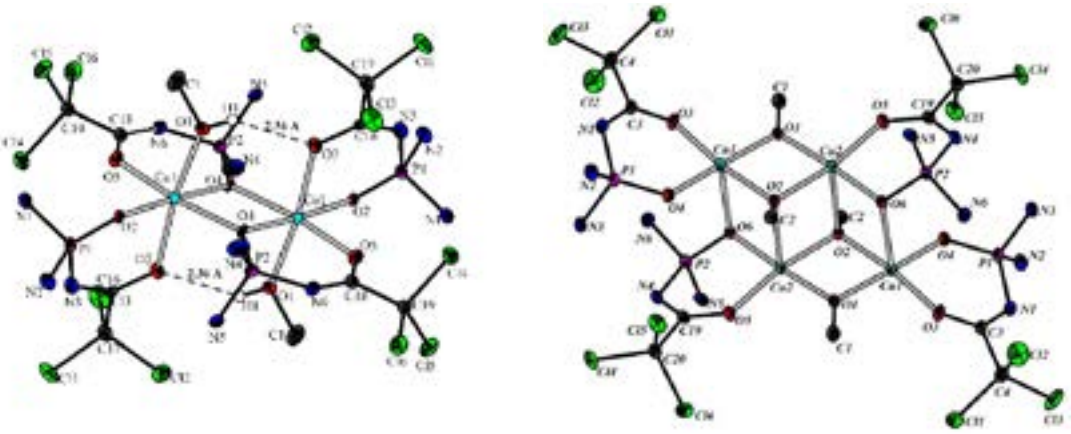

(A) (B)

Fig. 1. The molecular structure of the dimer $Co_2L_4(CH_3OH)_2$ (A) and the tetramer complex $Cu_4L_4(OCH_3)_4$ (B) (protons and benzyl substituents are omitted for clarity).

[1] Powerful new ligand systems: carbacylamidophosphates (CAPh) and sulfonylamidophosphates (SAPh). Ligands. Synthesis, characterization and role in biotechnology. Amirkhanov V., Ovchynnikov V., Trush V., Gawryszewska P., Jerzykiewicz L.B., Nova Science Publishers Inc. 2014 – P. 199-248.

# THE EFFECT OF THE USE OF WOOD ASH ON METALLIC ELEMENTS CONTENT IN THE FOREST FLOOR, SOIL AND BLUEBERRIES *(VACCINIUM MYRTILLUS)*

Vitālijs Lazarenko[1], Vita Rudoviča[1], Arturs Vīksna[1], Zaiga Anna Zvaigzne[2], Modris Okmanis[2]

[1]University of Latvia, Faculty of Chemistry, Jelgavas iela 1, Riga, Latvia
[2]Latvian State Forest Research Institute "Silava", Rīgas iela 111, Salaspils, Latvia
vitalijs.lazarenko@lu.lv

The aim of our research was to analyze the influence of wood ash on metallic elements content in the forest floor, soil and blueberries.

Samples of blueberries, soil and forest floor for quantifying the chemical content of metallic elements were collected from three different sampling plots. The first sampling plot was fertilized with bottom ash in February 2018, but the second and third plots were fertilized with fly ash in February 2017. Three tons of wood ash were used for the area of one hectare.

Blueberry *(Vaccinium myrtillus)* samples were collected at the end of August and in early September 2018. The samples of soil and forest ground were collected at the end of October 2018. Soil samples were collected in two depth layers: 0-10 cm and 10-20 cm. After collecting, the samples of soil and forest floor were air-dried.

The unwashed blueberries were dried at 50°C and mineralized in the mixture $HNO_3$:$H_2O_2$ (6:2) using the closed microwave digestion system. The concentration of the elements in the sample solutions was determined by ICP-MS.

The air-dried and sieved soil samples were extracted in 1M $HNO_3$ solution. The concentration of metallic elements was determined by TXRF and as the internal standard was used gallium standard solution. The ash was dissolved in conc. $HNO_3$ and the forest floor samples were ashed in muffle at 550°C. The concentration of metallic elements was determined by TXRF.

The results show that the cadmium content in the first sampling plot fertilized with bottom ash is about 1.5 times higher values than in the second and third sampling plot cases fertilized with fly ash. The content of other metallic elements in blueberries from controlled and fertilized plots is similar.

The content of determined elements in the soil samples has no noticeable differences between the controlled and fertilized sampling plots.

In the first plot, the concentration of manganese in blueberries and soil samples was higher than in other sampling plots. The peaty soil collected in the first plot had similar content of nickel, zinc, strontium and lead in different depth levels. The content of copper was higher in the layer of depth 10-20 cm. In the second sapling plot, it was determined that the content of manganese, nickel, and lead is higher on all levels of depth in comparison with other plots.

*This work was supported by Short term scientific mission organized in scope of project "Research program on improve of forest growth conditions 2016-2021".*

# DEVELOPMENT OF TXRF METHOD FOR DETERMINATION OF CALCIUM AND PHOSPHORUS MOLAR RATIO IN HYDROXYAPATITES

Vladlens Grebņevs[1,2], Arturs Vīksna[1], Oskars Purmalis[3], Māris Klaviņš[3], Kārlis-Agris Gross[2]

[1] Department of Analytical Chemistry, University of Latvia, Jelgavas street 1, Riga, Latvia
[2]Biomaterials Research Laboratory, Riga Technical University, Paula Valdena street 3/7, Riga, Latvia
[3] Faculty of Geography and Earth Sciences, University of Latvia, Jelgavas street 1, Riga, Latvia

vladlens.grebnevs@lu.lv

Hydroxyapatites (HAp) and other calcium phosphates, being similar to a chemical composition of human's bone inorganic fraction, nowadays are mostly recognized and widely used biomaterials for bone and teeth renewal. Performing quality control, Ca and P molar ratio (Ca/P) serves as an underlying analytical parameter indicating HAp properties and suitability for implant production. Nowadays used methods for Ca/P determination (photometry [1], ICP-OES, gravimetry [2] and other), being well-established and easily accessible, still have some essential limitations. Accordingly, elaboration of a new simple and low-cost analytical procedure for quick and precise Ca/P ratio measuring is required.

Data gathered during continuous investigation of different Ca/P determination methods showed that TXRF (Total Reflection X-ray Spectrometry) is the most applicable tool for this aim due to simple sample preparation procedure (see Fig. 1), relatively short one analysis time, multi-element analysis possibility and low hardware maintenance costs. Unlike classical WD/ED-XRF, TXRF is arranged in a special geometry - an incident beam impinges upon a sample below critical angle, making it much more sensitive technique. Until now TXRF method has been successfully applied to a great variety of different biological samples [3].

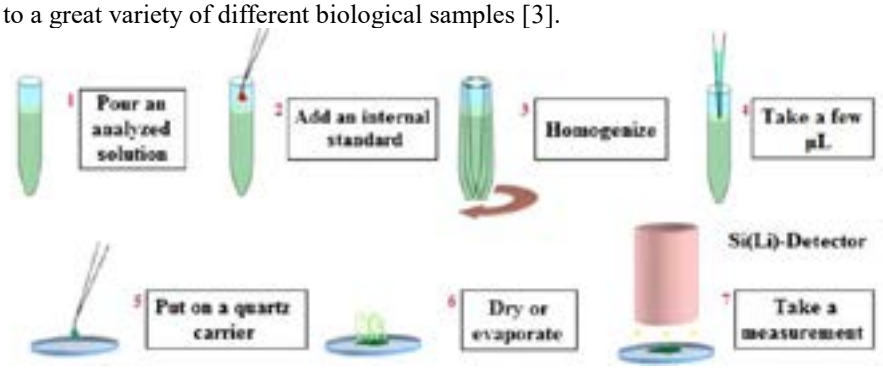


Fig. 1. Step-by-step instruction for analyzed solution preparation for TXRF analysis.

A key problem of TXRF is a small sensitivity of P analysis due to its relatively low Kα line intensity. Other major drawback is difficulty in achieving uniform crystallization and distribution of sample containing elements putting analyzed solution on a quartz carrier and drying the droplet. Besides solving these problems, research also includes a suitable standard element for both element quantification and HAp solubility studies plus some validation basics (see Fig. 2) to make sure that TXRF method shows accurate calcium and phosphorus quantification results.

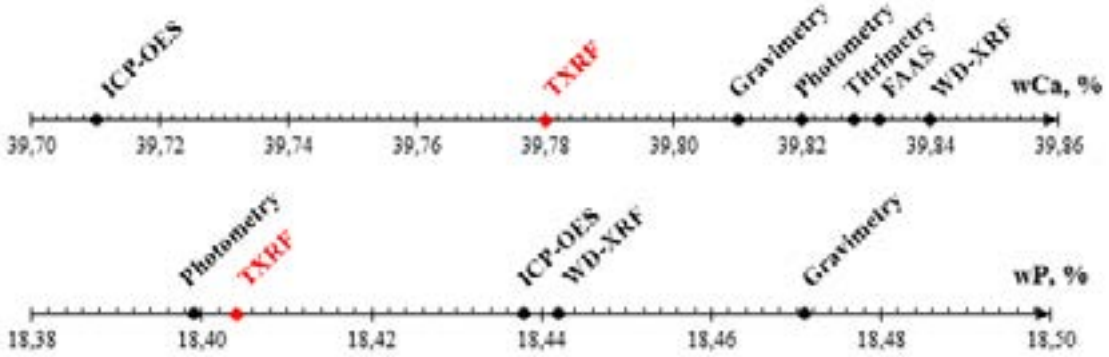


Fig. 2. Comparison of calcium and phosphorus quantification results by different methods in a HAp sample.

[1] G.L. Vogel, L.C. Chow et. al., A Microanalytical Procedure for the Determination of Calcium, Phosphate and Fluoride in Enamel Biopsy Samples, Caries Research **17**, 23-31 (1983).
[2] N.S. Chikerur, T.S. Narasaju, Quantitative Separation of Calcium, Strontium and Phosphate, Analyst **93**, 344 (1968).
[3] A. Viksna, E.S. Lindgren et al., Analysis of Whole Blood and Placenta - A Case Study of Mothers and their Babies, Journal of Trace and Microprobe Techniques **14**, 553-564 (2002).

# EXCITON ANNIHILATION IN CYLINDRICAL MOLECULAR AGGREGATES

Vytautas Bubilaitis[1], Darius Abramavičius[1]

[1]Institute of Chemical Physics, Faculty of Physics, Vilnius University, Lithuania
vytautasbubilaitis@gmail.com

Spectroscopic methods are extremely important in physics. The information obtained by multi-pulse spectroscopy methods that allow to observe fast processes in molecular aggregates, often depend on intensity of the impulse with which they are probed.

Exciton-exciton annihilation process is one of the processes that can be observed at higher pulses intensities. The annihilation is the process when two nearby excitations occupy the same site and create a short lived double excited state, which quickly relaxes non radiationally to a single excited state. Thus effectively it is a processes in which two excitation quickly decay to a single excitation.

The exciton annihilation can be observed in pump-probe spectra. To calculate these spectra we will use nonlinear exciton equations(NEE)[1, 2]. Unlike in other method these equations do not require solving eigenvalue equations, equations can be written in site basis. A system of differential equations is numerically propagated for creation and annihilation operators. This allows an arbitrary processes be easily included into these equations. Often methods electric field is assumed to be weak and a perturbation series is made according to it. In NEE equations electric field is included explicitly. This allows to simulate experiments where excitation field has an arbitrary envelope.

NEE equations were applied to model a cylindrical aggregate. There are plenty of measured spectra[3]for these type of aggregates. Two models for cylindrical aggregate were studied which differ in transition dipole moments orientations. Calculated Pump-probe spectra are shown in figure 1. The first model is similar to H type aggregate and second to J type, the general shape is similar to measured spectra of these type of aggregate. Inclusion of nonlinear terms into equations produces a non exponential decay in calculated spectra, which reflects the exciton annihilation process.

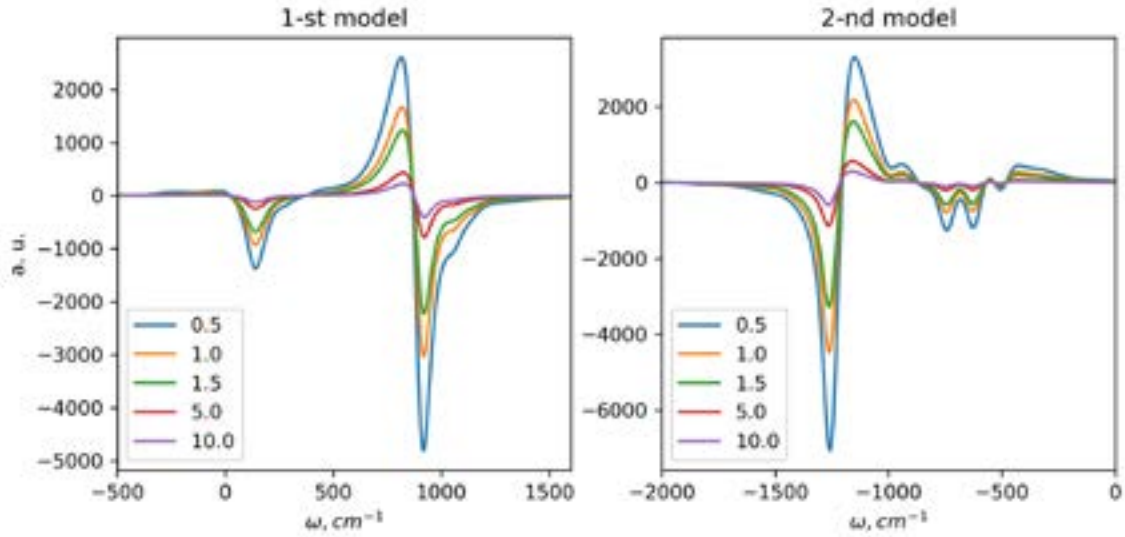


Fig. 1. Calculated pump-probe spectra at different time delays in ps for two different cylindrical aggregate models.

[1] D. Abramavicius, B. Palmieri, D. V. Voronine, F. Sanda, and S. Mukamel, Coherent multidimensional optical spectroscopy of excitons in molecular aggregates: Quasiparticle versus supermolecule perspectives, Chem. Rev., jun 2009, 109, 2350–2408.

[2] S. Mukamel and D. Abramavicius, Many-body approaches for simulating coherent nonlinear spectroscopies of electronic and vibrational excitons, Chem. Rev., jun 2004, 35.

[3] H. v. Berlepsch and C. Böttcher, Supramolecular structure of TTBC j-aggregates in solution and on surface, Langmuir, apr 2013, 29, 4948–4958.

# EQUILIBRIA OF INDIVIDUAL ISOPOLY TUNGSTATE ANIONS FORMATION IN PHYSIOLOGICAL SOLUTIONS

Oleksii Yuliia A.[1], Mishchanchuk Karyna V.[2], Mariichak Oleksandra Yu.[1], Rozantsev Georgiy M.[1], Radio Serhii V.[1]

[1] Educational and Scientific Institute of Chemistry, Vasyl' Stus Donetsk National University, Vinnytsia, UKRAINE
[2] University College London, London, UNITED KINGDOM
radio@donnu.edu.ua

By means of continuous pH-metric titration the state of the individual isopoly tungstate anions in the «$Na_2WO_4$ – HCl – PS» systems (PS – physiological solution; PS = Ringer's solution, Ringer-Locke's solution, Trisol solution; $C_W$ = 0.01 mol $L^{-1}$) at different temperatures (25 and 36.6$^0$C) in the range of acidity $Z=\nu(H^+)/\nu(WO_4^{2-})$ = 0.0–2.5 was studied and herein reported.

The results of pH-potentiometry were used as a background for subsequent mathematical modeling of equilibria processes in the investigated solutions and for calculation of logarithms of concentration constants ($lgK_C$) of isopoly tungstate anions formation (quasi-Newton procedure, CLINP 2.1 software [1]). Thus, mathematical models describing complexation processes were built and checked for excessiveness and sufficiency. Calculation of formation constants allowed us to build the diagrams of distribution of different ionic forms related to acidity Z and were used to define areas of existence for individual isopoly tungstate anions in physiological solutions (see Fig. 1).

It was found out that in the «$Na_2WO_4$ – HCl – PS» systems like in the «$Na_2WO_4$ – HCl – $H_2O$» [2] or aqueous-organic solutions [3] hexatungstate ($[W_6O_{20}(OH)_2]^{6-}$), paratungstate B ($H_x[W_{12}O_{40}(OH)_2]^{(10-x)-}$, x = 0–3), heptatungstate ($H[W_7O_{24}]^{5-}$), metatungstate ($H_2[W_{12}O_{40}(OH)_2]^{(4-x)-}$, x = 0–2) anions are formed. And processes of protonation and deprotonation of $HCO_3^-$ also are occurred.

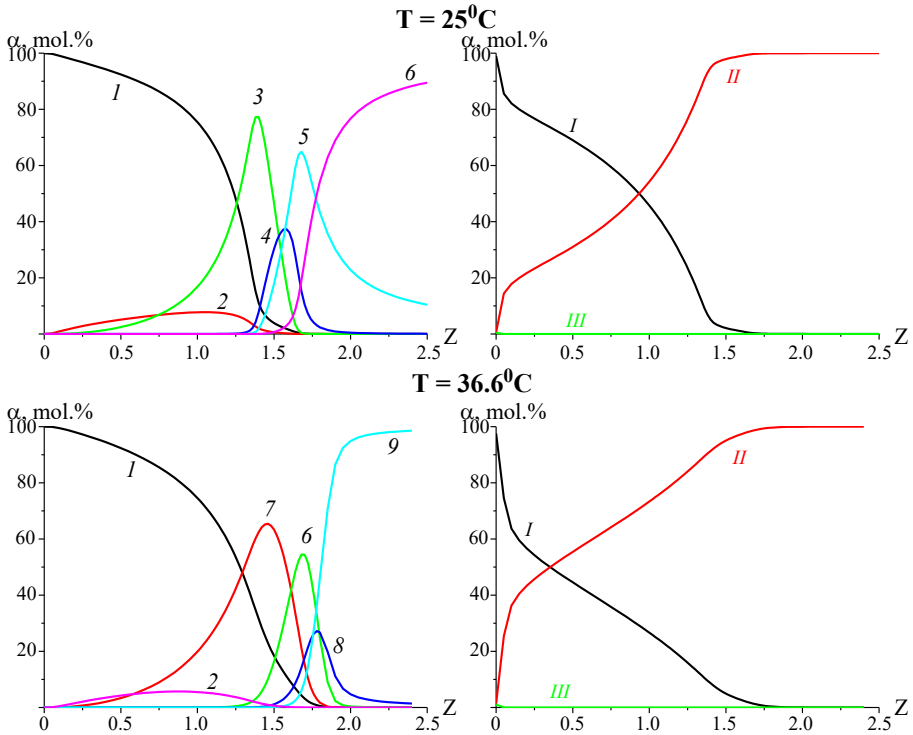


Figure 1. Calculated diagrams of isopoly tungstate anions distribution $\alpha$, mol.% = $\varphi(Z)$ in the system «$Na_2WO_4$ – HCl – Ringer's solution» at 25 and 36.6$^0$C: *1* – $WO_4^{2-}$; *2* – $W_6O_{20}(OH)_2^{6-}$; *3* – $W_{12}O_{40}(OH)_2^{10-}$; 4 – $H_2W_{12}O_{40}(OH)_2^{8-}$; *5* – $H_3W_{12}O_{40}(OH)_2^{7-}$; *6* – $W_{12}O_{38}(OH)_2^{6-}$; *7* – $HW_7O_{24}^{5-}$; *8* – $HW_{12}O_{38}(OH)_2^{5-}$; *9* – $H_2W_{12}O_{40}(OH)_2^{4-}$; *I* – $HCO_3^-$; *II* – $CO_2 \cdot H_2O$; *III* – $CO_3^{2-}$.

Acknowledgements. The study was carried out within the Fundamental Research Programme funded by the Ministry of Education and Science of Ukraine (Project No. 0119U100025).

[1] Yu. V. Kholin, *Quantitative physicochemical Analysis of Complex Formation in Solutions and on Chemically Modified Silicas: Content Models, Mathematical Methods, and Their Applications* (Folio, Kharkov, 2000) (in Russian).
[2] S.V. Radio, M.A. Kryuchkov, E.G. Zavialova et al., Equilibrium in the acidified aqueous solutions of tungstate anion: synthesis of Co(II) isopolytungstates. Crystal structure of Co(II) paratungstate B $Co_5[W_{12}O_{40}(OH)_2]\cdot 37H_2O$, J. Coord.Chem., **63**, 1678-1689 (2010).
[3] E.Yu. Poimanova, S.V. Radio, E.E. Belousova et al., Isopoly tungstate anions in water–dimethyl sulfoxide solutions, Russ. J. Inorg. Chem., **63**, 1243-1250 (2018).

# SIZE AND LIGAND EFFECTS IN Cd UNDERPOTENTIAL DEPOSITION AND PHOTOELECTROCHEMISTRY ON CdSe QD FILMS

Yauhen Aniskevich[1,2], Artsiom Antanovich[1], Mikalai Malashchonak[2], Anatol Prudnikau[1], Mikhail Artemyev[1], Genady Ragoisha[1], Eugene Streltsov[2]

[1]Research Institute for Physical Chemical Problems of the Belarusian State University, Minsk, 220006, Belarus
[2]Chemistry Department, Belarusian State University, Minsk, 220030, Belarus
aniskevich.y.m@gmail.com

Quantum dots (QDs) are attractive materials for use in photovoltaic systems, sensors, photocatalysts and as luminescent labels due to tunability of their properties by size, shape and surface chemistry [1]. Electrochemical methods provide efficient way to study charge transfer across QD/electrolyte interface in dark or under illumination and determine potentials of interfacial transfer which can be further related with electronic structure of QDs [2], [3].

We have studied peculiarities of charge transfer on electrophoretically deposited films of CdSe QDs of variable size and capping ligand (oleate and sulfide) using Cd underpotential deposition (upd) as a probe reaction and studied their photoelectrochemical response in $Na_2SO_3$ solution. The Cd upd potential shows strong dependence on QD size (Fig. 1a). Oleate ligand replacement by sulfide enhances significantly efficiency of the charge transfer with this probe reaction on CdSe QDs.

Unlike bulk semiconductors, the QD film electrodes exhibit photocurrent switching phenomenon in potentiodynamic experiment with modulated illumination (Fig. 1b). The photocurrent switching consists in the transition between anodic and cathodic photocurrents controlled by the electrode potential. Both the oleate and sulfide-capped CdSe QDs show photocurrent switching (Fig. 1c) but quantum efficiency of the photocurrent was higher for QDs with sulfide capping.

The discovered effects are of interest as means of QDs characterization and quantification of the quantum confinement effect via electrochemistry.

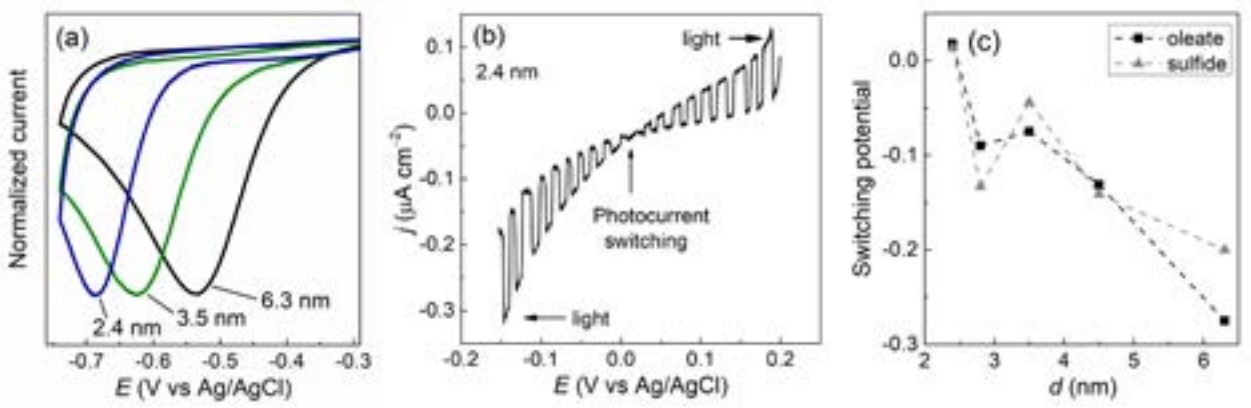


Fig. 1. (a) Size-dependent response in cyclic voltammetry of Cd upd on CdSe QD films in electrolyte containing $Cd^{2+}$ (labels correspond to QD diameter). (b) Current-potential curve for CdSe QD film in 0.1 M $Na_2SO_3$ under modulated illumination. (c) Photocurrent switching potentials of CdSe QD films at variable QD diameter.

Acknowledgment: This research has received funding from Horizon 2020 research and innovation programme under MSCA-RISE-2017 grant agreement No. 778357.

[1] Semiconductor Nanocrystal Quantum Dots: Synthesis, Assembly, Spectroscopy and Applications; Rogach, A. L., Ed.; Springer, 2008.

[2] Y.M. Aniskevich et al., Underpotential Deposition of Cadmium on Colloidal CdSe Quantum Dots: Effect of Particle Size and Surface Ligands, J. Phys. Chem. C 123, 931-939 (2019)

[3] M.E. Kazyrevich et al., Photocurrent Switching Effect on platelet-like BiOI Electrodes: Influence of Redox System, Light Wavelength and Thermal Treatment, Electrochimica Acta 190, 612-619 (2016).

# DOPED BIFLUORENE CRYSTALS FOR LASER APPLICATIONS: THE ROLE OF ULTRAFAST ENERGY TRANSFER

Paulius Baronas[1], Gediminas Kreiza[1], Patrik Scajev[1], Povilas Adomėnas[1], Karolis Kazlauskas[1], Chihaya Adachi[2], and Saulius Juršėnas[1]

[1] Institute of Photonics and Nanotechnology, Vilnius University, Vilnius (Lithuania)
[2] Center for Organic Photonics and Electronics Research (OPERA), Kyushu University, Nishi (Japan)
paulius.baronas@ff.vu.lt

Organic single crystals with long-range molecular order ensure high carrier mobility, enhanced photochemical and thermal stability as well as negligible light-scattering, what makes them attractive as an optical gain medium for electrically-pumped organic lasers [1]. Unfortunately, amplified spontaneous emission (ASE) thresholds of the crystals are typically more than one order of magnitude higher as compared to those of amorphous neat or doped films. In our previous works we have been able to significantly reduce ASE threshold of organic crystals by employing rational design of bifluorene-based compounds that has enabled a control of intermolecular coupling realizing high radiative rates and high fluorescence quantum yield ($QY_{PL}$ > 0.8) in the sublimation-grown single crystals [2]. In depth investigation of intermolecular coupling revealed strongly anisotropic and exceptionally high exciton diffusion (D = 1 $cm^2/s$) in crystal direction referring to the highest dipole coupling [3]. Considering the pronounced exciton diffusion in bifluorene crystals our further work was focused on crystal doping (see fig. 1), which allowed an even further reduction of ASE threshold to a record value (400 $W/cm^2$ or 2 $\mu J/cm^2$) [4]. Finally, our most recent work addresses triplet formation and ASE threshold as a function of doping concentration, which would be important for continuous wave laser applications.

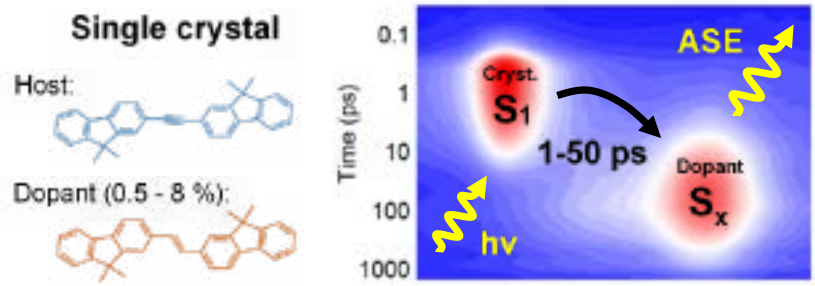


Fig. 1. Molecular composition of doped bifluorene crystals and transient absorption data depicting fast energy transfer from host to dopant molecules in a crystal.

[1] A. J. C. Kuehne, M. C. Gather, Chem. Rev. 116, 13823 (2016).
[2] G. Kreiza, et al., Adv. Optical Mater. 5, 1600823 (2016).
[3] P. Baronas, et al., Appl. Phys. Lett. 112, 033302 (2018).
[4] P. Baronas, et al., ACS Appl. Mater. Interfaces 10, 2768 (2018).

# SYNERGY EFFECTS IN EPOXY RESIN COMPOSITES FILLED WITH CARBON NANOTUBES AND MAGNESIUM OXIDE NANOPARTICLES

Povilas Bertašius[1], Darya Meisak[1,2], Jan Macutkevič[1], Jūras Banys[1]

[1]Faculty of Physics, Vilnius University, Lithuania
[2]Institute for Nuclear Problems, Belarusian State University, Minsk, Belarus
pov.bertasius@gmail.com

Polymeric composites are widely used as materials which not only have desired properties of polymers such as the flexibility, ease of manufacture, lightness, resistance to fractures, but can also be given additional ones like the electrical conductivity. Huge electrical conductivity in composites can be achieved with only a small addition of carbon nanotubes (CNT) [1]. Reducing the required amount of CNT to achieve such properties is very desirable since currently CNTs are expensive and take a long time to be produced. Using dielectric spectroscopy in this work were investigated hybrid epoxy resin composites filled with CNT and the electrically insulating and thermally conductive [2] MgO nanoparticles (mean diameter 40 nm) in order to find the synergetic effects and possible positive enhancement of dielectric properties.

The epoxy resin composite samples were of constant 0.46 % CNT volume (vol.) concentration, while MgO concentrations were: 0, 0.5, 1, 2 vol. %. The selected CNT concentration is slightly above the percolation threshold required for the CNT to connect into a pathway for electrical current. The measurements were performed in the 20 Hz – 1 MHz frequency and 33 – 500 K temperature ranges.

Composites with 0.46 % CNT in addition to any amount of MgO nanoparticles showed increased values of the dielectric permittivity, DC conductivity and critical frequency. The highest conductivity values were observed for samples with the lowest 0.5 vol. % concentration of MgO, while increasing MgO content above this value showed the conductivity together with dielectric permittivity decreasing.

These results imply that during the preparation of composites a low concentration (about 0.5 vol. %) of MgO works as an agent which promotes better dispersion of CNT inside epoxy resin, which overall has a strong positive effect on the formation of an electrical percolation network.

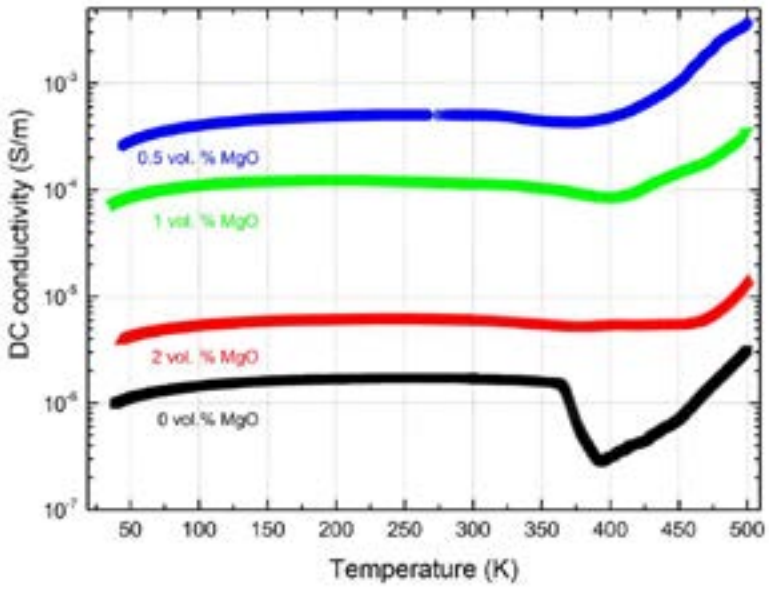


Figure 1. DC conductivity of the epoxy resin hybrid composites with 0.46 vol. % CNT and 0-2 vol. % MgO inclusions in a 33 – 500 K temperature range.

[1] Michael F. L. De Volder, Sameh H. Tawfick, Ray H. Baughman, John Hart, Carbon Nanotubes: Present and Future Commercial Applications, *Science vol.* 337, 535-537 (2013).
[2] Amir Masound Pourrahimi, Love K. H. Pallon, Dongming Liu, Tuan Anh Hoang, Stanislaw Gubanski, Mikael S. Hedenqvist, Richard T. Olsson, Ulf W. Gedde, Polyethylene Nanocomposites for the Next generation Ultralow-Transmision-Loss HVDC Cables Insulation Containing Moisture-Resistant MgO Nanoparticles, *ACS Appl. Mater. Interfaces 2016, 8,* 14824-14833 (2016).

# CHITOSAN FILMS WITH INCORPORATED CHITOSAN AND ROSMARINIC ACID COMPLEXES

Dovilė Liudvinavičiūtė[1], Rima Klimavičiūtė[1], Ramunė Rutkaitė[1], Vèronique Coma[2]

[1] Department of Polymer Chemistry and Technology, Kaunas University of Technology, Lithuania
[2] University of Bordeaux, UMR 5629, CNRS, LCPO, France
dovile.liudvinaviciute@ktu.edu

There has been a growing interest in recent years to develop biodegradable, edible packaging films from biopolymers to improve food safety and shelf life. Chitosan (CH) is a biodegradable, non-toxic, biocompatible, inexpensive natural polymer that has a good film-forming ability but weak antioxidant ant antimicrobial properties. Incorporation of antioxidant and/or antimicrobial agents into CH films is a good way to improve physical and biological properties of CH films [1]. Phenolic compounds can be selected as additives for CH films because of their abundancy in the plant kingdom, antioxidant, antimicrobial, anti-inflammatory properties [2].

The aim of present study was to incorporate insoluble rosmarinic acid (RA) and CH complexes having different RA to CH molar ratio (further referred as CR) into CH films, and to investigate their mechanical and chemical properties.

CR powders with the molar ratio of RA to CH equal to 0.22. 0.39, 0.6 and 0.88 were obtained by using multistep adsorption process [3]. 1 % CH solution was prepared in 1 % acetic acid, and 20 % (v/w) of glycerol was added as a plasticizer. Then 5 % (w/w) of CR powders was added into CH solution, after homogenization mixture was poured into Petri dishes, and kept at 25 $^{o}$C for 48 h. Finally, films were collected form Petri dishes and stored for further analysis.

Mechanical properties of CH and CH/CR films were evaluated according to ASTM D882 by using Universal testing machine BDO-FBO.5TH (Zwick GmbH, Germany), and are shown in Table. As it could be seen from the presented data, the values of tensile strength, elongation at break and the Young's module depended on the molar ratio of CR added into the film forming solution. CH films with CR having RA to CH molar ratio of 0.22 had the highest value of tensile strength and the Young's module.

Solubility and moisture sorption of films was also evaluated, and obtained data is presented in Table. Both CH and CH/CR films were soluble in water. Moisture sorption of films also depended on the CR molar ratio, and rapidly decreased with the increased amount of RA in complex added to CH films. This could be explained by increased hydrophobicity of CR powders with higher amount of adsorbed RA [3].

**Table.** Mechanical properties, water solubility, moisture sorption of CH and CH/CR films

| Film | Tensile strength (MPa) | Elongation at break (%) | Young's modulus (MPa) | Water solubility* (%) | Moisture sorption** (%) |
|---|---|---|---|---|---|
| CH | 45.6 ± 5.3 | 19.0 ± 5.8 | 1327 ± 127 | 97.4 ± 0.2 | 44.7 ± 0.4 |
| CH/CR(0.22) | 54.4 ± 2.1 | 13.1 ± 3.2 | 2037 ± 96 | 97.7 ± 0.2 | 40.1 ± 1.5 |
| CH/CR(0.39) | 47.2 ± 4.9 | 23.7 ± 2.4 | 1585 ± 79 | 97.4 ± 0.2 | 32.5 ± 2.1 |
| CH/CR(0.6) | 44.9 ± 2.8 | 15.2 ± 2.1 | 1609 ± 273 | 97.3 ± 0.2 | 29.7 ± 1.0 |
| CH/CR(0.88) | 45.3 ± 3.9 | 15.4 ± 5.9 | 1724 ± 181 | 96.9 ± 0.2 | 27.7 ± 0.5 |

* After 24 h
** After 24 h in desiccator with RH = 95 %.

Acknowledgement. The financial support of the Research Council of Lithuania for the Lithuanian-French programme "Gilibert" project No. S-LZ-19-6 is highly acknowledged.

[1] G. Kerch, Chitosan films and coatings prevent losses of fresh fruit nutritional quality: A review, Trends in Food Science & Technology 46, 159-166 (2015).
[2] F. Shahidi, P. Ambigaipalan, Phenolics and polyphenolics in foods, beverages and spices: Antioxidant activity and health effects – A review, Journal of Functional Foods 18, 820-897 (2015).
[3] D. Liudvinaviciute, K. Almonaityte, R. Rutkaite, J. Bendoraitiene, R. Klimaviciute, Adsorption of rosmarinic acid from aqueous solution on chitosan powder, International Journal of Biological Macromolecules 118, 1013–1020 (2018).

# DEVELOPMENTS OF GREEN SOLUTION-PROCESSED ORGANIC LIGHT EMITTING DIODES EXPLOITING EXCIPLEX-FORMING HOSTS AND TADF EMITTERS

Matas Gužauskas[1], Dmytro Volyniuk[2], Aušra Tomkevičienė[2], Juozas Vidas Gražulevičius[2]

[1] Department of Physics, Kaunas University of Technology, Lithuania
[2] Department of Polymer Chemistry and Technology, Kaunas University of Technology, Lithuania
matas.guzauskas@ktu.edu

Since advantages of organic light emitting diodes (OLEDs) such as a wide viewing angle, fast response, high brightness, low turn-on voltage, etc., they are great candidates for flexible large area lightings and displays. To reach high external quantum efficiencies of OLEDs, emitters exhibiting thermally activated delayed fluorescence (TADF) were incorporated in device structures [1]. These TADF emitters are characterized by ability of light-emitting harvesting of singlet and triplet excitons allowing to reach internal quantum efficiency of 100 % in the best cases. That is practically not possible without appropriate hosts for the chosen emitters. It was recently shown that exciplex-forming solid-state mixtures of donating and accepting organic semiconductors are efficient hosts for the TADF emitters resulting in extremely low turn-on voltages (~2.1 V) and high power efficiency of TADF OLEDs [2]. However, number of efficient exciplex-forming hosts is very limited.

In this work, highly efficient host-guest systems were developed and tested in solution-processed OLEDs. Variety exciplex-forming hosts and TADF emitter (guest) systems were investigated by steady-stay and time-resolved spectroscopy. Among them, the best system included TADF host TCz1:PO-T2T [3] and TADF emitter DAcIPN [4] where TCz1 and PO-T2T are electron-donating 3,6-bis(carbazol-9-yl)-9-(2-ethyl-hexyl)-9H-carbazole and electron-accepting 2,4,6-tris[3-(diphenylphosphinyl) phenyl]-1,3,5-triazine compounds while DAcIPN is 4,6-Di(9,9-dimethylacridan-10-yl) isophthalonitrile, respectively. Electroluminescent properties of this system TCz1:PO-T2T:DAcIPN were tested in OLEDs having structure ITO/PEDOT:PSS/TCz1:PO-T2T:DAcIPN/TSPO1/TBPi/LiF/Al where the hole injection layer is poly(2,3-dihydrothieno-1,4-dioxin)-poly(styrenesulfonate) (PEDOT:PSS), hole blocking and electron transporting layers are diphenyl[4-(triphenylsilyl) phenyl]phosphine oxide (TSPO1) and 2,2′,2"-(1,3,5-benzinetriyl)-tris(1-phenyl-1-H-benzimidazole) (TPBi), respectively. Light-emitting layer TCz1:PO-T2T:DAcIPN were spin-coated consisting the ratio of 1:1 of donor TCz1 – acceptor PO-T2T exciplex and 10 wt % of TADF emitter DAcIPN. The fabricated device was characterized by green emission with stable electroluminescence (538 nm) at different voltages (Figure 1). Commision Internationale l'Eclairage (CIE 1931) chromaticity coordinates (x, y) of the green devices was found to be (0.33, 0.58). Proving efficiency of the developed host-guest systems TCz1:PO-T2T:DAcIPN, high maximum brightness of 10500 cd/m$^2$ were obtained for the fabricated solution-processed devices.

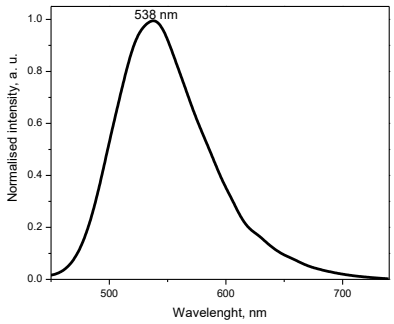


Fig. 1. EL spectrum of the fabricated devices at 9 V.

[1] Chan, C.-Y., Tanaka, M., Nakanotani, H. & Adachi, C. Efficient and stable sky-blue delayed fluorescence organic light-emitting diodes with CIEy below 0.4. *Nat. Commun.* **9**, 5036 (2018).
[2] Peng, J., Xu, X., Feng, X. J. & Li, L. Fabrication of solution-processed pure blue fluorescent OLED using exciplex host. *J. Lumin.* **198**, 19–23 (2018).
[3] Guzauskas, M. *et al.* Dual nature of exciplexes: exciplex-forming properties of carbazole and fluorene hybrid trimers. *J. Mater. Chem. C* **7**, 25–32 (2019).
[4] Skuodis, E. *et al.* Aggregation, thermal annealing, and hosting effects on performances of an acridan-based TADF emitter. *Org. Electron. physics, Mater. Appl.* **63**, 29–40 (2018).

# INFLUENCE OF CONDUCTIVE LAYER ON FANO RESONANCE IN A MIRRORED ARRAY OF SPLIT RING RESONATORS

Andrius Kamarauskas[1,2], Gediminas Šlekas[1], Dalius Seliuta[1], Žilvinas Kancleris[1]

[1] Department of Physical Technologies, Center for Physical Sciences and Technology, Lithuania
[2] Faculty of Electronics, Vilnius Gediminas' Technical University, Lithuania
andrius.kamarauskas@ftmc.lt

Recently it was found [1] that in a mirrored array of split ring resonators (SRR) (Fig. 1) Fano resonance arises due to direct interaction of the 3rd order plasmonic mode and the lattice mode. Investigated metasurface consisting of SRRs was formed on a thin polytetrafluoroethylene (PTFE) layer (125 μm, $\varepsilon = 2.2$). It was shown that the resonance appears when the specific resonance mode is excited, which is weakly coupled with external electromagnetic field. This specific mode is known as a dark mode contrary to a usual light mode, which has large radiation losses.

In the present paper we numerically investigate the influence of the surface conductivity of 2D coating that covers the metasurface on Fano resonance amplitude. As an example of such a surface might be the graphene layer that is now widely investigated. The surface resistivity of it can be changed by increasing a number of layers in a coating, or by changing the Fermi energy of the graphene by applying external DC electric field [2].

The custom-made program based on a finite-difference time-domain method was used. For the simulation of the SRR array, the unit cell shown in Fig. 1 is modelled with periodic boundary conditions at the lateral edges. The differentiated Gaussian pulse is generated using total-field-scattered-field plane wave source. The incident wave falls perpendicularly to the SRR array surface. The modelling domain is truncated by the uniaxial perfectly matched layers to introduce the absorption of waves without reflection. To calculate the transmittance spectra, a method based on the generalized Goertzel algorithm is used [3].

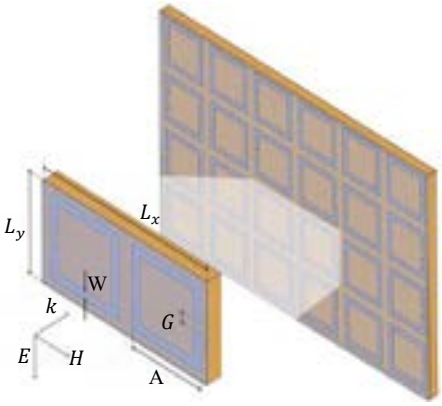


Fig. 1. Investigated structure with SRRs on PTFE and conductive layer on the top. Electric field is perpendicular to the resonator gap, $L_x$=2·$L_y$.

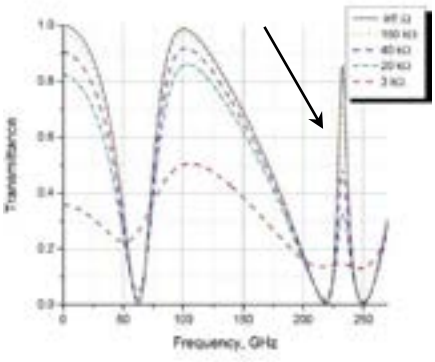


Fig. 2. Transmittance spectrum versus frequency for different surface resistivities of the top layer: $W$=$G$ =50 μm, $A$=500 μm, $L_y$ =600 μm. Arrow indicates Fano resonance at 223.4 GHz.

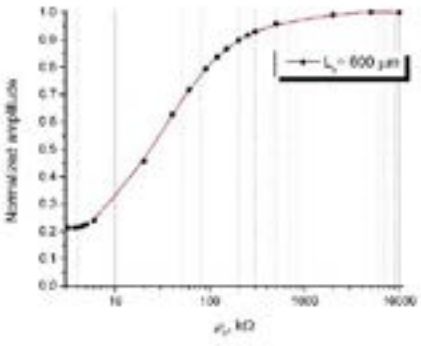


Fig. 3. Dependence of normalized Fano resonance amplitude on the surface resistivity of the top layer.

Calculation results of transmittance spectra versus frequency for different values of the surface resistivity of the 2D layer are shown in Fig. 2. Values of the surface resistivity is indicated in the figure. It is seen that by decreasing the surface resistivity Fano resonance amplitude (marked in the figure by arrow) strongly decreases, whereas its influence on plasmonic resonances is less pronounced. When the surface resistivity exceeds 10 MΩ per square Fano resonance amplitude reaches uttermost value, which was calculated [1] without the conductive layer. In the opposite case, when the surface resistivity approaches to 3 kΩ per square Fano resonance totally disappears and conductive layer by itself manly governs the transmittance through the investigated structure. Dependence of the Fano resonance amplitude normalized to its maximum amplitude at $\rho_s = \infty$ is shown in Fig. 3. It is seen that in the intermediate range of the surface resistivity the maximum influence of it to the Fano resonance amplitude is observed which might be used for sensing applications.

[1] D. Seliuta, G. Šlekas, G. Valušis, Ž. Kancleris, Fano resonance arising due to direct interaction of plasmonic and lattice modes in a mirrored array of split ring resonators, Optics letters (accepted).
[2] S. Xiao, T. Wang, Xiaoyun Jiang, Strong interaction between graphene layer and Fano resonance in terahertz metamaterials, Journal of Physics D, Vol. 50, No 19, 195101 (2017).
[3] G. Šlekas, P. Ragulis, D. Seliuta, and Ž. Kancleris, Using of Generalized Goertzel Algorithm for FDTD Calculation of the Transmission and Reflection Spectra of Periodic Structures, IEEE Trans. Electromagn. Compat. 59, 2038 (2017).

# SYNTHESIS AND PROPERTIES OF PHENOTHIAZINE AND CARBAZOLE-BASED DERIVATIVES FOR OPTOELECTRONIC APPLICATIONS

Liveta Lapienyte[1], Rasa Keruckiene, Matas Guzauskas, Dmytro Volyniuk, Simona Vekteryte, Juozas Vidas Grazulevicius

Department of Polymer Chemistry and Technology, Kaunas University of Technology, K. Barsausko St. 59-A-539, LT-51423
Kaunas, Lithuania
liveta.lapienyte@gmail.com

Electroactive organic compounds are used as light-emitting materials for optoelectronic devices such as light-emitting diodes, solar cells and electrophotographic photoreceptors [1, 2]. Phenothiazine and carbazole-based compounds have advantageous characteristics such as thermal and electrochemical stability, high electron/hole conductivity and efficient luminescence [3, 4]. Due to these properties phenothiazine and carbazole fragments were chosen for this study. The synthesis and properties of phenothiazine and carbazole derivatives bearing trifluorophenyl-acceptor group **1-5** are presented (Fig 1). The materials **1-5** were synthesized by Ullman-coupling and Suzuki-coupling methods.

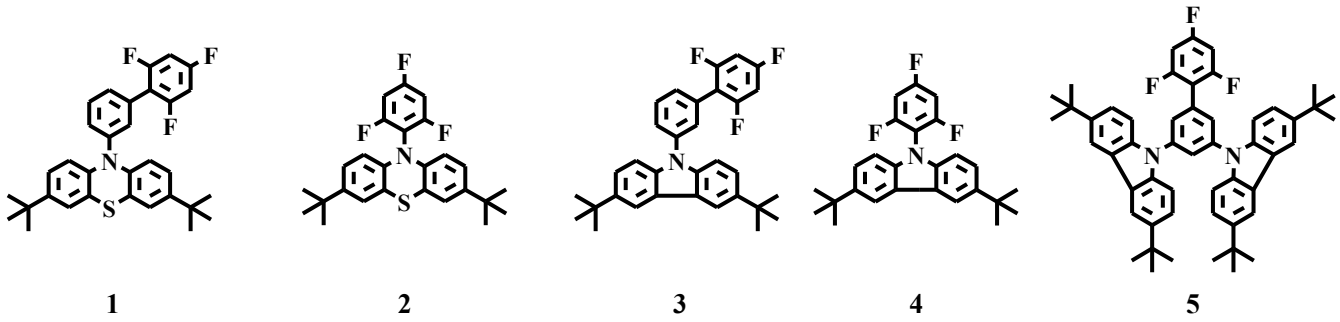


Fig. 1. Structures of **1-5**.

The structures of the synthesized compounds were proved by $^{1}H$ and $^{13}C$ NMR spectroscopy and mass spectrometry.

The behavior on heating of compounds **1-5** was studied by differential scanning calorimetry (DSC) and thermogravimetric analysis (TGA) under a nitrogen atmosphere. A temperature ranging from 201°C to 369 °C of compounds **1-5**. Compound **5** demonstrates the highest thermal stability (369 °C).

The ionization potentials of the derivatives were estimated by cyclic voltammetry (CV). They were found to be comparable and ranged from 4.85-5.25 eV. The electron photoemission spectra of layers of the derivatives showed the ionization potentials of 5.84-6.19 eV.

The fluorescence emission wavelength of compounds is in the region of green-blue light. Triplet energy values ranging from 2.58 eV to 2.88 eV were determined from phosphorescence spectra. Because of that the materials can be used as matrix for blue emitters [5].

**Acknowledgment**. This research was funded by the European Social Fund under the No 09.3.3-LMT-K-712 "Development of Competences of Scientists, other Researchers and Students through Practical Research Activities" measure.

[1] Forrest, S. R.; Thompson, M. E. Eds. Organic Electronics and Optoelectronics. Chem. Rev. **2007**, 107, 923-1386.
[2] Shirota, Y.; Kageyama, H. Charge Carrier Transporting Molecular Materials and Their Applications in Devices. Chem. Rev. **2007**, 107, 953−1010.
[3] Gruzdeva M. S.; Chervonovaa U. V.; Venediktova E. A.; Rozhkovaa E. P.; Kolkera A. M.; Mazaevb E. A.; Dudinaa N. A. and Domrachevac N. E. Synthesis and Photochemical Properties of 3,6-Di-tert-butyl-9H-carbazole Derivatives. Russian Journal of General Chemistry, **2015**, Vol. 85, No. 6, pp. 1431–1439.
[4] Jen-Hsien Huang and Kuen-Chan Lee. Highly Stable, Solution-Processable Phenothiazine Derivative as Hole Collection Material for Organic Solar Cells. ACS Applied Materials & Interfaces **2014** 6 (10), 7680-7685.
[5] G. Grybauskaite-Kaminskiene, D. Volyniuk, V. Mimaite, O. Bezvikonnyi, A. Bucinskas, G. Bagdziunas, J.V. Grazulevicius. Aggregation-Enhanced Emission and Thermally Activated Delayed Fluorescence of Derivatives of 9-Phenyl-9H -Carbazole: Effects of Methoxy and tert-Butyl Substituents. Chem. Eur. J., **2018**, 24, 9581-9591.

# METAL-FREE ROOM TEMPERATURE PHOSPHORESCENT ORGANIC MATERIALS

Karolis Leitonas[1], Aušra Tomkevičienė[1], Juozas Vidas Gražulevičius[1]

[1] Department of Polymer Chemistry and Technology, Kaunas University of Technology, Barsausko g. 59, Kaunas, Lithuania
karolis.leitonas@ktu.edu

Metal-free organic materials that show room-temperature phosphorescence (RTP) are attractive alternatives to organometallic phosphors because of their low cost, abundant and environmentally friendly properties, flexible synthesis, and good stability. In particular, metal-free organic molecules showing efficient RTP have great potential in diverse optoelectronic and photonic applications, such as luminescent labels, imaging and sensing, and even organic light-emitting diodes [1].

Here we report on a series of metal- and halogen-free molecules based on thianthrene and phenothiazine units. Photophysical properties of thianthrene derivatives have not been extensively studied so far while phenothiazine is a unit in many luminescent materials [2] and emits phosphorescence at room temperature in solid *Zeonex*® films. By varying the number of phenothiazine units, it was intended to study the impact of these substituents on the emissive and photoelectrical properties of the synthesized compounds.

Emission spectra of the solutions of all the studied compounds in low-polarity toluene were found to be of structureless shape. While in solutions phosphorescence is completely quenched by oxygen and collision between solvent and solute molecules, in the solid state these quenching factors are omitted, thus promotion of intersystem crossing rate ($k_{ISC}$) can occur. Upon degassing the solid samples of molecular dispersions of the compounds in *Zeonex*®, emissive bands peaking at 510 nm showed up (Fig. 1). In case of solution of GB8 compound the contribution of phosphorescence was found to be high at room temperature. The ratio of integrated areas of photoluminescence (PL) spectra of the solution of GB8 compound acquired with and without oxygen reached 35.

To give insight into electron properties of studied molecules the cyclic voltammetry, photoelectron spectroscopy and charge transporting properties have been performed.

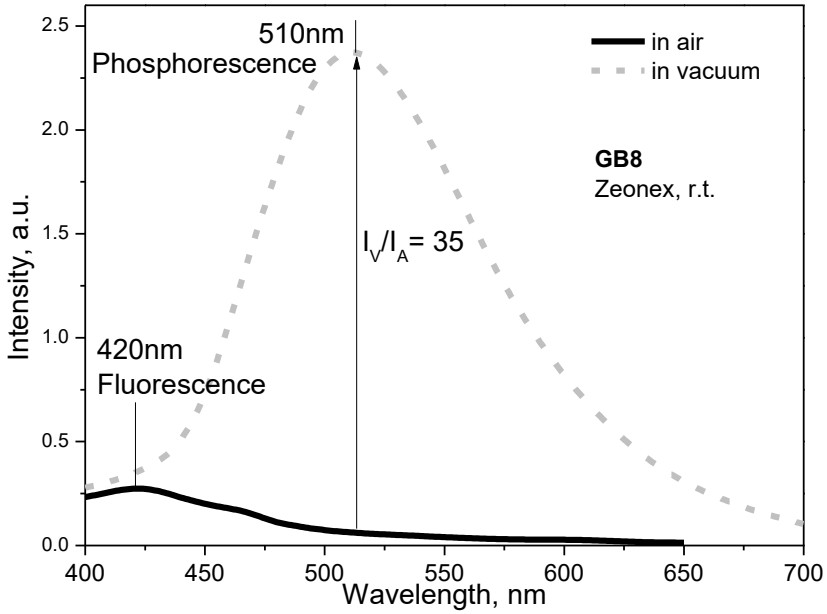


Fig. 1. PL spectra of the solid solutions of the synthesized compound GB8 in *Zeonex*® (1 wt.%) recorded in air and vacuum

[1] Liu Y, Zhan G, Liu ZW, Bian ZQ, Huang CH. *Room-temperature phosphorescence from purely organic materials*. Chin Chem Lett 2016;27(8):1231-1240.

[2] S. Gan, W. Luo, B. He, L. Chen, H. Nie, R. Hu, A. Qin, Z. Zhao and B. Z. Tang, *Integration of aggregation-induced emission and delayed fluorescence into electronic donor-acceptor conjugates* J. Mater. Chem. C, 2016, 4, 3705-3708.

# NANOCRYSTALLISED $NA_3M_2(PO_4)_2F_3$ GLASSES WITH NASICON-LIKE STRUCTURE (M = V, TI)

Paulina Kruk–Fura, Piotr J. Mikoajczuk, Tomasz K. Pietrzak, Jerzy E. Garbarczyk

Faculty of Physics, Warsaw University of Technology, Poland
paulina.kruk-fura@fizyka.pw.edu.pl

Materials of the following composition $Na_3M_2(PO_4)_2F_3$, where M = V, Ti, are investigated as prospective cathode materials for sodium-ion batteries. For instance, cathodes based on polycrystalline $Na_3V_2(PO_4)_2F_3$ exhibits a reasonably good gravimetric capacity (equal at least 128 mAh/g) with an average voltage ca. 3.75 V [1]. Recent studies revealed that the gravimetric capacity value is rather structural than redox limited [2]. This issue may be overcome by substituting vanadium by another transitions metals, e.g. titanium and synthesis of this materials in nanocrystalline form via thermal nanocrystallisation of glassy analogues [3, 4].

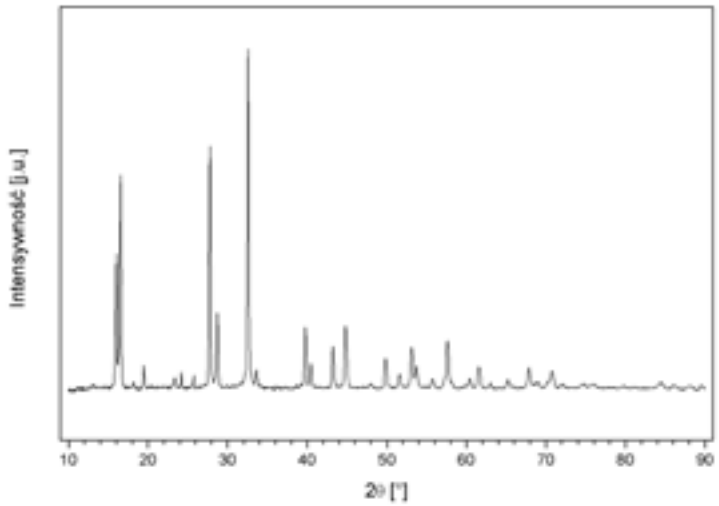


Fig. 1. XRD pattern of $Na_3V_2(PO_4)_2F_3$ nanomaterial with NASICON–like structure (ICDD nr 000660150).

Nanograins obtained during this process are characterised by an average diameter from 5 to 50 nm, which results not exclusively in growth of gravimetric capacity value, but higher electronic conductivity as well. Synthesis of glass from calculated amounts of properly chosen compounds is a two step method, described in detail in [5]. The batch is melted in a furnace at ca. 1300 °C and subsequently is rapidly cooled via melt-quenching technique. Thermal events occurring in the obtained materials were investigated by differential thermal analysis (DTA) method.

The amorphousness of initial samples along with observation of thermal nanocrystallization process were executed by X-ray diffraction in function of temperature (HT–XRD). Samples crystallized in pure NASICON-like structure (Fig. 1) and what is important, an average dimension of grains was below 100 nm. Measurements of electrical conductivity in function of temperature were performed using impedance spectroscopy method and proved that thermal nanocrystalisation of glassy analogues of $Na_3M_2(PO_4)_2F_3$ systems may improve total conductivity of as-received materials.

[1] R. A. Shakoor, Dong-Hwa Seo, Hyungsub Kim et. al., A combined first principles and experimental study on $Na_3V_2(PO_4)_2F_3$ for rechargeable Na batteries, Journal of Material Chemistry, **22**, 20535–20541 (2012).
[2] I. L. Matts, S. Dacek, T. K. Pietrzak et al., Explaining Performance-Limiting Mechanisms in Fluorophosphate Na-Ion Battery Cathodes through Inactive Transition-Metal Mixing and First-Principles Mobility Calculations, Chemistry of materials, **27**, 6008–6015 (2015).
[3] T.K. Pietrzak, J.E. Garbarczyk, I. Gorzkowska et al., Electrical properties vs. microstructure of nanocrystallized $V_2O_5$-$P_2O_5$ glasses, Journal of Power Sources, **194**, 73–80 (2009).
[4] J.E. Garbarczyk, T.K. Pietrzak, M. Wasiucionek et al., High electronic conductivity in nanostructured materials based on lithium-iron-vanadate-phosphate glasses, Solid State Ionics **272**, 53–59 (2015).
[5] T.K. Pietrzak, P.P. Michalski, M. Wasiucionek et al., Synthesis of nanostructured $Li_3M_2(PO_4)_2F_3$ glass-ceramics (Me = V, Fe, Ti), Solid State Ionics, **288**, 193-198 (2016).

# CARBAZOLE OR TERT-BUTYL ACRIDINE-BASED DERIVATIVES CONTAINING DIFFERENT PHENYLETHYLENE MOIETIES AS AGGREGATION-INDUCED EMISSION-ACTIVE LUMINOGENS

Aina Petrauskaite, Monika Cekaviciute, Jurate Simokaitiene, Juozas Vidas Grazulevicius

Departament of Polymer Chemistry and Technology, Kaunas University of Technology, Lithuania
aina.petrauskaite@ktu.edu

Development of inexpensive, reliable and effective organic fluorophores is one of the most intense research field in recent years due to their valuable applications in organic light-emitting diodes (OLEDs), light emitting organic field effect transistors and other optical devices. Many organic materials exhibit very high luminescence efficiency in dilute solutions, but become non-emissive or weakly emissive in the aggregate state, owing to the aggregation caused quenching [1]. Organic emissive materials are normally used in the form of thin solid films. Materials exhibiting aggregation-induced emission enhancement (AIEE) enable to develop high-performance OLEDs without the need of doping [2]. Despite significant progress of AIEE materials over the last decades, new fluorophores with good charge-transporting properties, high thermal and electrochemical stability are still in high demand.

In this work we report on new effective AIEE molecules synthesized via Buchwald-Hartwig coupling of carbazole or tert-butyl acridine and arylethylene moieties. The synthesized compounds were identified by IR, $^{1}$H NMR, $^{13}$C NMR spectroscopies and mass spectrometry. The thermal, photophysical and electrochemical properties of the compounds were studied. THF/water systems of various ratios were used to investigate aggregation effect on emission properties. Compounds were well soluble in THF but not soluble in water which led to the formation of molecular aggregates resulting in enhancement of the fluorescence intensity with increasing water fraction in the systems. For all the compounds except compound **2** fluorescence intensity started to grow dramatically when the content of water reached ca. 90%. This observation indicates the effect of AIEE. The synthesized fluorophores exhibit efficient emission in solid state with fluorescence intensity in the range of 445 – 724 nm and photoluminescence quantum yields reaching 86%. The compounds were found to possess high thermal stabilities with 5% weight loss temperatures exceeding 310°C. Compounds **1**, **3** and **4** form glasses with glass transition temperatures at 188, 105 and 53°C respectively.

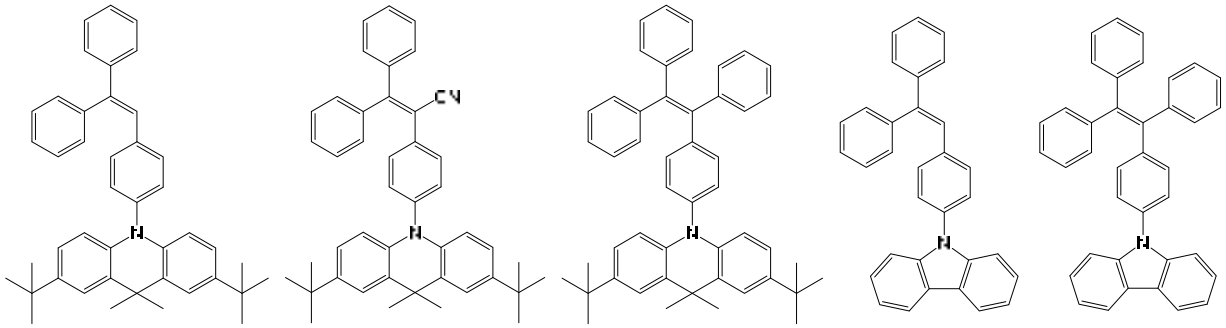


**1** **2** **3** **4** **5**

Fig. 1. Chemical structures of the synthesized compounds.

Acknowledgement:
This research is/was funded by the European Social Fund under the No 09.3.3- LMT-K-712 “Development of Competences of Scientists, other Researchers and Students through Practical Research Activities” measure.

[1] Y. Hong, J. W. Y. Lama, B. Z., Tang, Aggregation-induced emission: phenomenon, mechanism and applications, Chem. Commun, 4332–4353 (2009).
[2] A. Tomkeviciene, J. Sutaite, D. Volyniuk, N. Kostiv, G. Simkus, V. Mimaite, J.V. Grazulevicius, Aggregation-induced emission enhancement in charge-transporting derivatives of carbazole and tetra(tri)phenylethylene, Dyes and Pigments **140,** 363-374 (2017).

# HIGHLY ORDERED BLOCK COPOLYMER THIN FILMS AS CONVERTIBLE TEMPLATES FOR METAL-SEMICONDUCTOR NANOMESHES

Przemysław Puła[1,2*], Arkadiusz Leniart[1], Andrzej Sitkiewicz[1], Paweł W. Majewski[1]

[1]Faculty of Chemistry, University of Warsaw, Warsaw, Poland
[2] Faculty of Physics, University of Warsaw, Warsaw, Poland
p.pula@student.uw.edu.pl

Block copolymers (BCPs) usually consist of a few blocks, that are covalently bonded. They are a class of self-assembling materials, that drew much attention thanks to its unusual properties. Worth mentioning is the self-assembly phenomenon. It is a powerful motif, in which BCP tries to minimize energy and thus forms diverse structures such as lamellaes, cylinders or spheres. Also, parameters of obtained nanostructures can be easily tailored by changing composition and molecular weight of BCP, which affects the periodicity of BCP thin films. When one combines it with large scalability, it makes BCPs great candidates to become widespread in the semiconductor industry as organic matrices for fabricating metal-semiconductor nanostructures.

In order to achieve that, the use of a method to control its ordering parameters, that comes together with the reasonable time of a process is essential. An easy and cheap technique is thermal annealing, but the long time of a process limits its wider application in industry. Another option, that shows better quality along with the shorter process time is Laser Zone Annealing (LZA) method. In this technique very high temperature gradients are induced, while the focused laser beam locally heats the substrate with the polymer ontop [1]. As a result, uniaxially aligned BCP films are obtained.

There are many ways to deposit metal or semiconductor compounds. To obtain metal nanostructures Aqueous Metal Reduction (AMR) method is utilized. A BCP film is immersed in a solution of complex metal salt (e.g. $K_2PtCl_4$ for Pt) dissolved in an acidic environment. Via electrostatic interaction anion bounds with a favourable functional group in BCPs [2]. Oxide semiconductors might be deposited by the Sequential Infiltration Synthesis (SIS) technique. Sequential Infiltration Synthesis (SIS) is a variation of an Atomic Layer Deposition (ALD) method, where two gaseous precursors are introduced to the reaction chamber separately and homogenously saturate the surface. During exposure time each precursor infiltrates the bulk of polymer material and reacts with functional groups (e.g. carbonyls). Consequently, the inorganic nanomaterial precursor is embedded in a polymer matrix [3].

Combining these methods allows one to fabricate multilayered metal-semiconductor nanomeshes. In our work, we were able to successfully obtain double-layered heterostructures, that were examined by Scanning Electron Microscopy (SEM) and Atomic Force Microscopy (AFM) measurements. These investigations may pave the way in the development of more efficient miniaturized chemical sensor with higher sensitivity and lower power consumption, comparing to the currently sold devices.

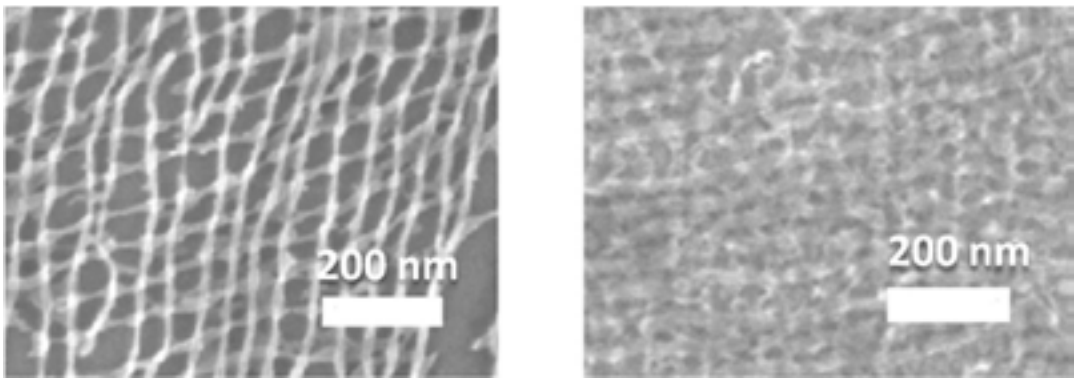


Fig. 1. SEM images of metal-semiconductor nanomeshes.

[1] Majewski, P. W., Rahman, A., Black, C. T., & Yager, K. G. (2015). Arbitrary lattice symmetries via block copolymer nanomeshes. *Nature communications*, *6*.

[2] Chai, J., & Buriak, J. M. (2008). Using cylindrical domains of block copolymers to self-assemble and align metallic nanowires. *Acs nano*, *2*(3), 489-501.

[3] Peng, Q., Tseng, Y. C., Darling, S. B., & Elam, J. W. (2011). A route to nanoscopic materials via sequential infiltration synthesis on block copolymer templates. *Acs Nano*, *5*(6), 4600-4606

# IMPROVEMENT OF THE FIBROUS SORBENTS PROPERTIES FOR WASTE WATER TREATMENT FROM IRON IONS

Nataliia Tarasenko[1], Viktoriia Plavan[2], Maksym Koliada[2]

[1] Department of General and Inorganic Chemistry, National Technical University of Ukraine Igor Sikorsky Kyiv polytechnic institute, Ukraine
[2] Department of Applied Ecology, Technology of Polymers and Chemical Fibers, Kyiv National University of Technologies and Design, Ukraine
xtf.fdp@gmail.com

Pollution of waste water with heavy metal ions is an environmental problem and it takes place in many industries. Sorption sequestration of metals from waste water has become quite widespread due to the high efficiency and the absence of secondary pollution. Polymeric and textile waste can be a raw material for the production of fibrous sorption-active materials [1,2].

The aim of the study is the determination of the sorption properties improvement of the fibrous sorbents in relation to the iron compounds by the solutions of different nature plant polyphenols.

Fibrous textile wastes containing 70% polyurethane fibers 162C (linear density 4.4 tex) and 30% polyamide fibers 6.6 f20/1 (linear density 3.3 tex) were used to obtain a polymeric composite material with sorption properties. The efficiency of the sorbent depends on the presence of active functional groups capable of binding ions of heavy metals irreversibly. Polyurethane fibers are similar to polyamides due to their chemical properties, as they also contain amide groups -NH-CO-. However, the additional oxygen atom included in the polyurethane chain -NH-CO-O- gives it more flexibility. It is of a very high interest to determine the effective method of modifying chemical fibers to increase the activity of their functional groups, in particular by the method of controlled chemical destruction with breakdown of C-N bonds [3].

For chemical fibers modification the processing of the fibrous sorbent was carried out with a solution of plant poly phenols (PP) for 24 hours at a temperature of 20 and 40°C. The degree of absorption of PP by fibrous sorbent was controlled by changing the optical density of the solution. During this time, the optical density decreased by more than 30%, which indicates the absorption of PP sorbent, and at a treatment temperature of 40ºC, the absorption rate is higher than at 20ºC.

The saturated PP sorbent was subsequently used to study its effectiveness in relation to iron salts. Treatment with iron salts was carried out at a temperature of 20 and 40ºC for 24 hours. The content of iron compounds after applying of fibrous sorbent into solutions decreases mainly during the first 2 hours, and at 40ºC the process of sorption is more intense, although the degree of absorption of iron compounds from solutions is generally not high and is about 30%.

To clarify the experimental data on $Fe^{3+}$ content in solutions after processing by fiber-based sorbents, we introduced the X-ray fluorescence analysis.

The interaction features of iron compounds with fibrous sorbent were determined by the method of IR spectroscopy. In particular, was confirmed the involvement of carboxyl groups of modified polyamide and polyurethane fibers, which form the basis of the sorption material, in interaction with iron ions.

Thus, fibrous textile waste can be used to produce environmentally safe polymeric composite materials for wastewater treatment from heavy metal ions. The degree of absorption of iron compounds from solutions can be increased by optimizing the modification process of the chemical fibers that are part of the sorbent, using the pre-regulated destruction of chemical fibers in order to activate surface functional groups, etc.

[1] Hoang, A. T., Bui, X. L., & Pham, X. D. A novel investigation of oil and heavy metal adsorption capacity from as-fabricated adsorbent based on agricultural by-product and porous polymer. Energy Sources, Part A: Recovery, Utilization, and Environmental Effects, **40**(8), 929–939 (2018).
[2] Adam, M. R.; Hubadillah, S. K.; Esham, M. I. M.; Othman, M. H. D.; Rahman, M. A.; Ismail, A. F.; Jaafar, J. Adsorptive Membranes for Heavy Metals Removal From Water. Membrane Separation Principles and Applications. In *Membrane Separation Principles and Applications: From Material Selection to Mechanisms and Industrial Uses*; Ahmad, F. I.; Mukhlis, A. R.; Mohd Hafiz, D. O.; Takeshi M.; Elsevier: New York, 2019; pp 361-400.
[3] W.E. Nelson. *Nylon Plastics Technology*, London-Boston: Published for the Plastics and Rubber Institute [by] Newnes-Butterworths, 1976. 230 p.

# FORMATION AND INVESTIGATION OF SILVER-INDIUM SELENIDE LAYERS ON ARCHITECTURAL TEXTILE SURFACE

Lina Jatautė, Valentina Krylova

Department of Physical and Inorganic Chemistry, Kaunas University of Technology, Lithuania
lina.sciupakovaite@ktu.edu

Architectural textile (AT) consists of different layers combined with the matrix. The matrix can be made with yarns of natural or synthetic fibres. PVC (polyvinylchloride) coated polyester (PES) fabric is one of the most commonly used material in many modern architecture projects because of its excellent synergy of functionality and aesthetics [1]. The coating and fillers can protect the yarns against UV, abrasion, atmosphere, rainwater and moisture. $CaCO_3$ and $TiO_2$ are the dominant fillers in the PVC based AT production [2].

Polymers modified with the inorganic materials combine the functionalities of polymer matrices, such as a low weight and easy formability, with the unique features of inorganic materials. The inorganic materials improve its optical, mechanical, electrical, magnetic and rheological properties [3]. There is currently a great interest in $A^{I}B^{III}C^{VI}_2$ semiconductor particles, for their importance as light harvesting materials [4]. The new structure could improve the efficiency of solar tracking made by photovoltaic panels.

In present investigation, we have tried to synthesize Ag-In-Se layers on AT (PES/PVC) surface. The surface properties of AT are important to silver-indium selenide layers adhesion and growth. Various surface properties as type and the density of surface charge, balance between the hydrophilicity and the hydrophobicity on surface, the chemical structure and functional groups, surface topography and roughness, the interfacial free energy could affect particles attachment and film growth.

AT-Ag-In-Se composites obtained by three-step assembly synthesis route. Firstly, for change physical surface properties the AT mechanical roughened and treated with etching solution [5]. Second, a chemical bath deposition method employed for preparation of AT-Se precursors at room temperature using $H_2SeO_3$ and $Na_2SO_3$ solutions. Third, this AT-Se further serves as proxies for silver-indium selenide formation. The formations of silver-indium selenide were attained by exposing the AT-Se into an $AgNO_3$ and $In(NO_3)_3$ solutions at room temperature. The reaction system depends on the heterogeneous reaction between $Ag^+$ and $In^{3+}$ ions and Se on AT surface. The obtained composites characterized by optical microscopy, mass fraction change of the deposited elements measurements, wettability measurements and X-ray diffraction analysis (XRD).

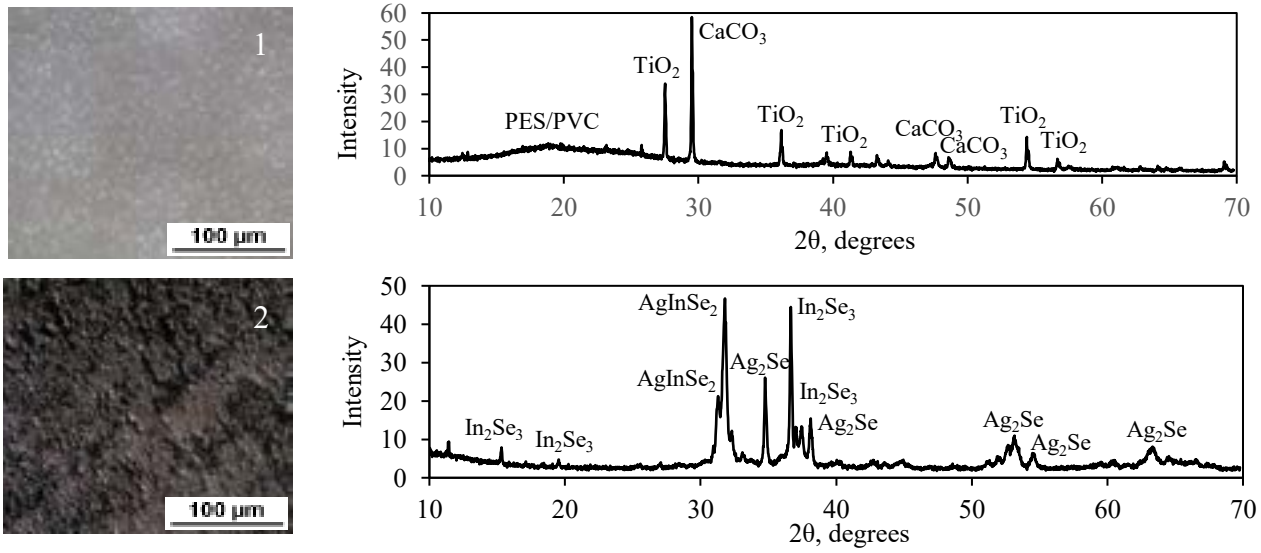


Fig. 1. Optical micrographs image and XRD: 1 – virgin AT, 2– AT-Ag-In-Se composite.

The prepared AT-Ag-In-Se composites are reproducible, uniformity of the surfaces increases with increasing immersions time in precursor's solutions. XRD analysis showed the formation of silver-indium selenide layers (Fig. 1).

[1] C. Paech, Structural membranes used in modern building facades, Procedia Engineering, **155**, 61-70 (2016).
[2] H. Wiebking, Fillers in PVC: A review of the basics, Specialty Minerals Inc. 640 N. 13 St., Easton, PA 18042, 1998.
[3] M. Z. Rong, M. Q. Zhang, H Liu, et al., Microstructure and tribological behaviour of polymeric nanocomposites, Industrial Lubrication and Tribology, **53**, 72-77 (2001).
[4] S. Ozaki, S. Adachi, Optical absorption and photoluminescence in the ternary chalcopyrite semiconductor $AgInSe_2$, Journal of Applied Physics, **100**, 113526 (2006).
[5] M. Rudzinskaja, V. Krylova. Architectural textile etching and investigation of its suitability for $Ag_2Se$ semiconductor film deposition, XVI student's scientific conference Mathematics and natural sciences: theory and applications 2018, ISBN 9786090214534, Kaunas University of Technology, 34-35 (2018).

# BARIUM STANATE: PI-MOCVD THIN FILM DEPOSITION AND NONSTOICHIOMETRY ISSUES

Tomas Murauskas[1], Valentina Plaušinaitienė[1], Virgaudas Kubilius[1]

[1] Department of Inorganic Chemistry, Vilnius University, Lithuania
tomas.murauskas@chf.vu.lt

Cost-effective transparent conductive oxide (TCO) material composed of cheap and abundant elements is highly desired in nowadays optoelectronics. Recently a wide-bandgap La-doped barium stannate (LBSO) n-type semiconductor has been discovered. LBSO single crystal conductive properties rival those of Sn-doped $In_2O_3$ (ITO)[1]. Additionally, $BaSnO_3$ is of perovskite type lattice which allowing this material to be incorporated in various heterostructures as a lattice-matched electrode[2]. Although, achieving desirable thin film properties for optoelectronic applications is still challenging due to nonstoichiometry and various defects as well as substrate-films interaction – understanding of these factors is crucial for BSO applications. Therefore, in this work thin undoped $BaSnO_3$ films have been deposited using pulsed injection metal organic chemical vapor deposition (PI-MOCVD) method allowing easier compositional control and simultaneous deposition on multiple substrates. In order to achieve low and high film/substrate lattice mismatch, pseudocubic $LaAlO_3$, $SrTiO_3$ and hexagonal $Al_2O_3$ substrates were selected respectively. $Sn(thd)_2$ and $Ba(thd)_2$ precursor solution with various ratios in dimethoxyethane was used for thin film deposition. Depositions were carried out in $Ar:O_2$ (8:2 v/v) atmosphere. Layer composition was determined using ICP-MS and Energy Dispersive X-ray (EDX) spectroscopy techniques. Surface morphology and film structure were characterized using Scanning Electron Microscopy (SEM) and X-ray diffractometry. Optical properties were investigated using variable angle spectroscopic ellipsometry and UV-Vis spectrophotometry in transmission mode.

Thin BSO films deposited on (100) $LaAlO_3$, (100) $SrTiO_3$ substrates were highly epitaxial. While polycrystalline films were obtained on Sapphire C substrate. It was determined that a surplus amount of $Ba(thd)_2$ is required to produce stoichiometric films. Interestingly, slight deviation form stoichiometric ratio resulted in significant structural and optical changes while a cubic symmetry was maintained. Also, no additional phases were detected even with a drastic increase of Ba/Sn ratio. Strong lattice parameter correlation with the Ba/Sn ratio in the films suggests a defect-forming mechanism related to oxygen, barium atom vacancies and $(BaO)_2$ Ruddlesden-Popper crystallographic shear faults.

[1] Hanjong Paik, Zhen Chen et al., Adsorption-controlled growth of La-doped $BaSnO_3$ by molecular-beam epitaxy, APL Materials, **5**, 116107 (2017).

[2] Useong Kim, Chulkwon Park et al., All-perovskite transparent high mobility field effect using epitaxial $BaSnO_3$ and $LaInO_3$, APL Materials **, 3**, 036101 (2015).

# ZINC STANNATE THIN FILM DEPOSITION BY PI-MOCVD METHOD AND INVESTIGATION OF THEIR PROPERTIES

Eglė Rinkevičiūtė[1], Tomas Murauskas[1], Valentina Plaušinaitienė[1]

[1] Department of Inorganic Chemistry, Faculty of Chemistry and Geosciences, Vilnius University, Lithuania
egle.rinkeviciute@chf.stud.vu.lt

Indium tin oxide (ITO) is a tin-doped $In_2O_3$. It is a n-type wide-bandgap semiconductor, widely used as transparent conducting oxide (TCO). However, due to indium shortcomings and toxicity issues, rapid research for new type TCOs began.

Recently, ternary semiconducting oxides $A^{II}_2B^{IV}O_4$ attracted tremendous interest and $Zn_2SnO_4$ (also known as zinc tin oxide or ZTO) is considered to be one of the most perspective TCO. According to Kawazoe *et al.* [1], linear chains of edge sharing octahedra running along the <110> direction leads to formation of an extended conduction band, therefore higher electron conductivity is expected, not to mention good transparency, low cost and non-toxicity.

Nevertheless, obtaining thin ZTO film without any residual zinc or tin oxide is quite challenging. Currently used growth methods for ZTO films encounter this problem or the growth conditions are inflexible due to limitations of the method itself. MOCVD method has pliable deposition conditions, which can be optimized to grow pure ZTO films and change their properties relatively easily.

The aim of this work was to find the optimal conditions for the growth of single phase ZTO thin films by Pulse-Injection Metalorganic Chemical Vapour Deposition (PI-MOCVD) method. Additionally, ZTO films were grown on differently cut sapphire substrates and their optical and electrical properties were investigated.

For the deposition of thin ZTO films $Zn(thd)_2$ and $Sn(thd)_2$ (thd - 2,2,6,6-tetramethyl-3,5-heptandionate) precursors were dissolved in 1,2-dimethoxyethane and injected to the reaction chamber in micro doses. Impact of deposition conditions (such as concentration of oxygen in gas flow, volume of gas flow, pressure during the deposition, etc.) to the properties of the films was explored. The composition of thin ZTO films was determined by Energy Dispersive X-ray Spectroscopy (EDX). Film phase composition was examined with X-ray Diffraction (XRD) and morphology - with Atomic Force Microscope (AFM) and Scanning electron Microscope (SEM).

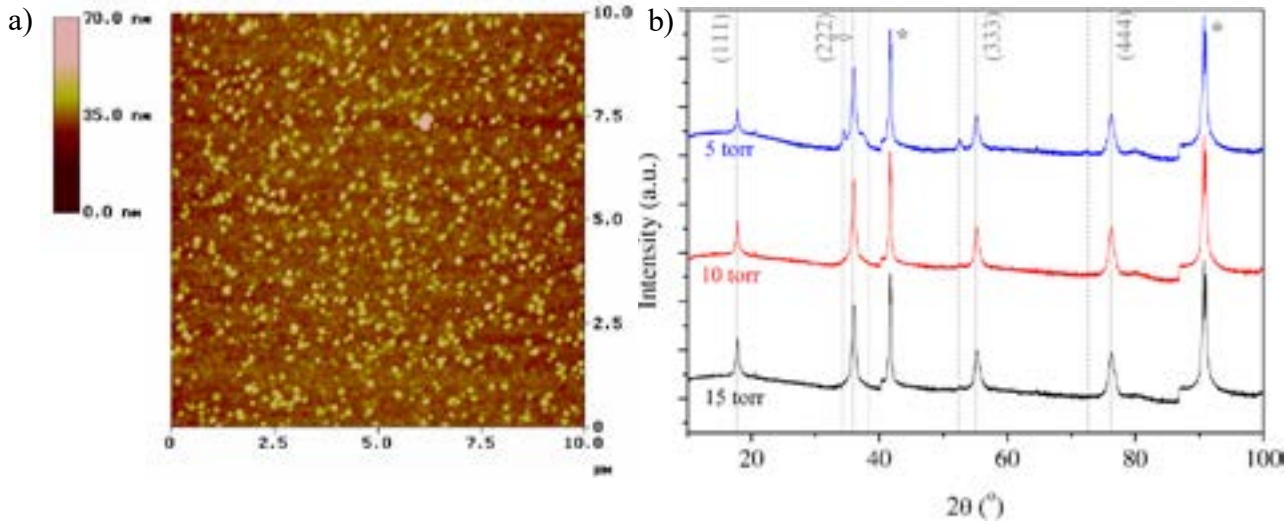


Fig. 1 a) Atomic force micrograph of ZTO film, b) X-ray diffractograms of ZTO films grown under different deposition pressures

To our knowledge, single phase thin $Zn_2SnO_4$ films were grown on sapphire substrates by PI-MOCVD for the first time (Fig. 1). In order to obtain a pure crystal phase of $Zn_2SnO_4$ (without any other crystal phases), zinc surplus in film was necessary. Additionally, the transparency and conductivity of the films were measured and band gap ($E_g$) was calculated.

1[1] H. Kawazoe, K. Ueda, Transparent Conducting Oxides Based on the Spinel Structure, J. Am. Ceram. Soc. **82,** 3330-3336 (1999).

# EPR OF FERROELECTRIC PHASE TRANSITION IN $[NH_4][Zn(HCOO)_3]$ FORMATE FRAMEWORK

Marius Navickas[1], Mirosław Mączka[2], Andreas Pöppl[3], Jūras Banys[1], Mantas Šimėnas[1]

[1]Faculty of Physics, Vilnius University, Sauletekio 9, LT-10222 Vilnius, Lithuania
[2]Institute of Low Temperature and Structure Research, Polish Academy of Sciences,
P.O. Box-1410, PL-50-950 Wroclaw 2, Poland
[3]Faculty of Physics and Earth sciences, Leipzig University, Linnestrasse 5, Leipzig, Germany D-04103
marius.navickas@ff.stud.vu.lt

Metal-organic frameworks (MOFs) are hybrid coordination polymers with an open pore system [1]. These coordination networks are formed from the various organic linker molecules and metal centers. The application areas of these highly porous compounds range from the biology to gas storage and separation [2,3]. The pore system in some of MOFs is already occupied by the guest molecules. The most popular class of such dense MOFs is metal-formate frameworks, which exhibit interesting ferroelectric and ferromagnetic (multiferroic) properties [4].

In this work, we present X- and Q-band continuous wave (CW) EPR study of $[NH_4][Zn(HCOO)_3]$ framework doped with a tiny amount of paramagnetic $Mn^{2+}$ ions. Extremely low concentration of these probe ions (0.1 mol%) allows us to resolve hyperfine and fine structure in the CW EPR spectrum. The latter interaction proved to be susceptible to the ferroelectric phase transition in $[NH_4][Zn(HCOO)_3]$ framework. From the CW EPR spectra obtained at different temperature (Fig. 1), we observed structural order-disorder phase transition to the ferroelectric phase at 190 K related to the $NH_4$ cation ordering and zinc-formate framework deformation.

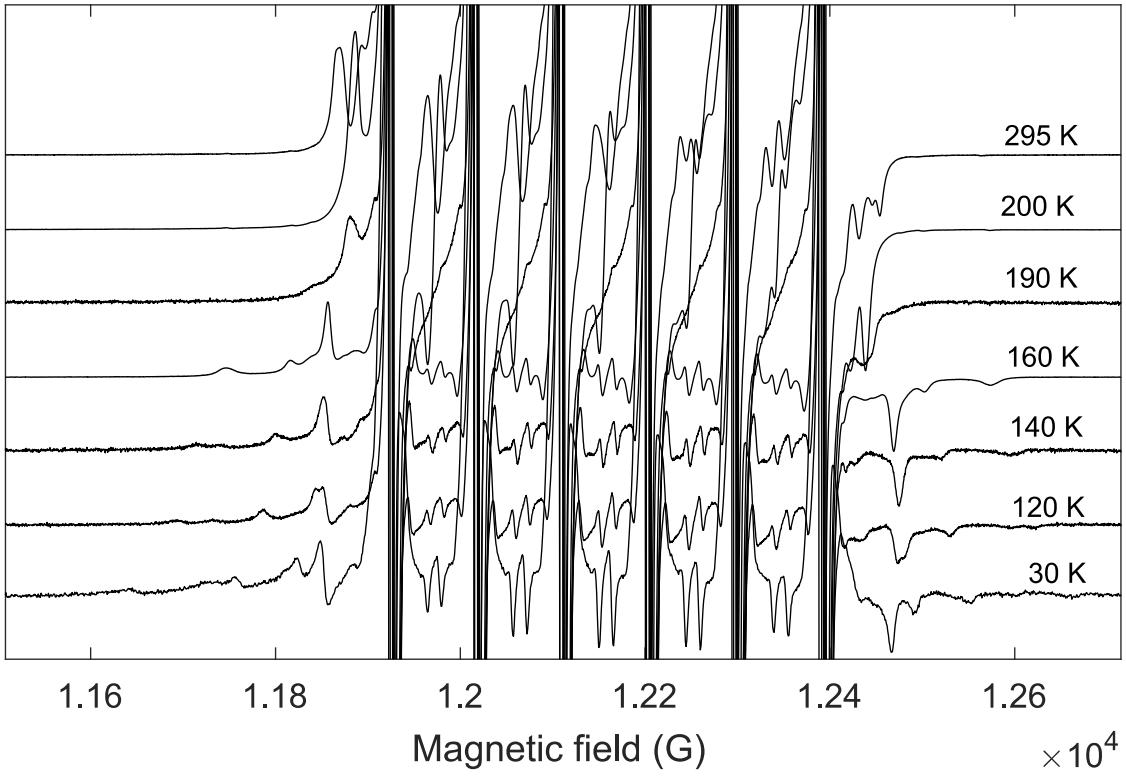


Fig. 1. Temperature dependence of the Q-band CW EPR spectra of $Mn^{2+}$ doped $[NH_4][Zn(HCOO)_3]$.

[1] *Coordination Polymers and Metal Organic Frameworks: Terminology and Nomenclature Guidelines* (IUPAC, 2010, January–February, 23).
[2] Jian-Rong Li, Julian Sculley, Hong-Cai Zhou, Metal−Organic Frameworks for Separations, Chem. Rev. **112**, 869−932 (2012).
[3] Youn-Sang Bae, Omar K. Farha, Alexander M. Spokoyny, et al., Carborane-based metal-organic frameworks as highly selective sorbents for $CO_2$ over methane, Chem. Commun. **35**, 4135–4137 (2008).
[4] Prashant Jain, Vasanth Ramachandran, Ronald J. Clark et al., Multiferroic Behavior Associated with an Order-Disorder Hydrogen Bonding transition in metal-organic Frameworks (MOFs) with the Perovskite $ABX_3$ Architecture, J. Am. Chem. Soc. **131**, 13625–13627 (2009).

# AMPHIPHILIC SORBENTS FOR SELECTIVE SORPTION OF CHOLESTEROL

Osipenko A.A.[1], Polyakova I.V.[1], Borovikova L.N. [1], Pisarev O.A. [1,2]

[1] Institute of Macromolecular Compounds, Russian Academy of Sciences, St. Petersburg, Russia
[2] Department of Medical Physics, Peter the Great St. Petersburg Polytechnic University, St. Petersburg, Russia
osipeno4kalexa@mail.ru

The accumulation of cholesterol (CS) in an organism and its level in human blood exceeding 6 mM/L promotes development of atherosclerosis, which is one of the main causes of morbidity and mortality in developed countries. A high level of triglycerides, very low-density lipoproteins, and low-density lipoproteins (LDLs), known as atherogenic lipoproteins, as well as a low level of antiatherogenic high-density lipoproteins, is attributed, together with cholesterol, to main atherosclerosis factors. The level of cholesterol in blood can be substantially reduced by diet and pharmacotherapy with hypolipidemic preparations (e.g., statins). However, there exists a particular category of medical cases with a homozygotic form of familiar hyperlipoproteidemia or hyper cholesterolemia, in which an extremely high level of cholesterol and LDLs is preserved in blood even after a special-purpose medicinal therapy. In these cases, the most efficient methods are those of efferent therapy, in which cholesterol and LDLs are selectively removed from the blood of an ill person in the extracorporeal mode. The method of LDL-apheresis on expensive immunoaffine sorbents is the most widely used [1, 2]. A possible alternative to these sorbents are those simulating the natural receptors, the so-called molecularly imprinted polymers (MIPs) synthesized in the presence of a biologically active target molecule serving as a template [3]. Simultaneously, the development of MIPs will solve the problem of biocompatibility of hemosorbents because the contact of blood with animal antibodies serving as affine ligands in immunosorbents is unsafe for humans [4].

Molecularly imprinted polymers (MIPs) are crosslinked polymers obtained in the presence of a target molecule as a template. After the template is removed by washing, cavities with molecular recognition sites that can bind selectively to the original template are stored in the polymer networks. MIPs are highly selective to capture the target analyte as the antibody. But as artificial receptors, MIPs are easy and rapid to prepare, very stable in harsh conditions, and allow the usage of a great variety of binding/eluting conditions without the risk of losing binding activity.

The aim of our study was to prepare cholestrol-imprinted polymers (Ch-MIPs) by the block and emulsion copolymerization. The block Ch-MIPs were prepared by the Ch-imprinting in copolymerized hydroxyethyl methacrylate (HEMA) as an amphiphilic monomer and ethyleneglycol dimethacrylate (EGDMA) as a crosslinker in *n*-propanol. The Ch-imprinted core–shell particles were prepared by emulsion copolymerization. In this method, imprint-cavities were formed in the HEMA-EGDMA copolymer layer at the surface of nanocomposites (NCs) of selen(Se) stabilzed with polyvinylpyrrolidone (PVP). An excess amount of Se/PVP-NCs in processes, which involved contact of comonomers and water, and then contact of water and butanol resulted in the formation of stabilized Pickering emulsions of oil/water/oil type. It is remarkable that the copolymerization was carried out in aqueous microdroplets in conditions close to bioseparation medium. More over, PVP made the hybrid polymer prominantly amphiphilic [5].

The size and surface morphologies of the formed block and hybrid polymer particles were studied using the scanning electron microscopy (SEM). The block sorbents had the dense homogeneous porous structure with meso- and micropores, whereas the surface of the hybrid particles consisted of microglobules ranging from 0,5 to 1 μm cross-linked together. It is obvious that in that case, the obtained composite microparticles acquired a well-defined spherical shape indicative of a successful emulsification using Se/PVP-NCs as a Pickering stabilizer.

In the process of plasma sorption *in vitro*, it was shown that the sorption selectivty increased on the Ch-imprinted polymers if compare with the corresponding non-imprinted polymers. At the same time, hydrodynamics of sorption on the hybrid polymers were better than on the bulk polymers due to more prominent amphiphilicity and narrow surface sorption layer in the hybrid networks.

The study was supported by the Russian Foundation for Basic Research (project no. 18-33-00710 mol_a).

[1] Seidel D., Armstrong V.W., Schuff-Werner P. // Eur. J. Clin. Invest. 1991. V. 21. N. 4, P. 375.
[2] Whitcombe M.J., Rodriguez, M.E., Villar, P., et al. // J. Am. Chem. Soc. 1995. V. 117. N. 24. P. 7105.
[3] Piletska, E.V., Guerreiro, A.R., Whitcombe, M.J., et al. // Macromolecules. 2009. V. 42. N. 29, P. 4921.
[4] Altynova, E.V., Afanas'eva, O.I., Boldyrev, A.G., et al. //Efferent. Ter. 2006. V. 12. N. 4. P. 3.
[5] Polyakova, I., Borovikova, L., Osipenko, A., Vlasova, E., Volchek, B., Pisarev, O. Surface molecularly imprinted organic-inorganic polymers having affinity sites for cholesterol // Reactive and Functional Polymers. 2016. V.109. P. 88.

# BROADBAND ELECTROMAGNETIC PROPERTIES OF CHLOROPRENE RUBBER AFTER LONG-TERM ULTRAVIOLET AGEING AND THERMAL DEGRADATION

Yaraslau Padrez[1,3], Dzmitry Bychanok[1, 2], Vitaly Ksenevich[3], Dzmitry Adamchuk[3], Naum Naveh[4], Reut Sela[4] and Polina Kuzhir[1, 2]

[1] Research Institute for Nuclear Problems Belarusian State University, Republic of Belarus
[2] Tomsk State University, Russian Federation
[3] Belarusian State University, Republic of Belarus
[4] Polymers and Plastics Engineering Dept., Shenkar College of Engineering and Design, Israel
yaraslaupadrez@gmail.com

Chloroprene rubber (CR) is one of the most important synthetic rubber resins widely used in industry. Its excellent characteristics such as weather and ozone resistance, good resistance to open fire, adhesion to fabrics and metals, fuel resistance make it a requisite source material for the mass production of mechanical rubber goods. Useful properties of CR may be effectively extended by using them in composite materials, and many recent investigations have proven CR as an effective dielectric matrix in composites production [1-4].

The present work is focused on ultra-broadband experimental characterization of electromagnetic (EM) properties of neat chloroprene rubber materials as is and after various types of their degradation. Particularly, the complex dielectric permittivity of investigated materials was experimentally measured in low-frequency range 20 Hz-2 MHz using an impedance meter. The electromagnetic response was also measured in Ka-band (26-37 GHz) using scalar network analyzer and waveguide transmission line. Finally, the samples under study were investigated in 0.1-0.9 THz range using a THz time-domain spectrometer.

The well-defined correlation between degradation of CR and the change of its dielectric permittivity was observed. Within the frequency range of 1 kHz - 0.9 THz we found out that the thermal degradation together with the immersion of oil leads to a decrease of both real and imaginary parts of dielectric permittivity. Ultraviolet aging leading vice-versa to increase of dielectric permittivity of samples under study. Additionally, the influence of graphene inclusions on long-term ultraviolet aging and thermal degradation was investigated.

[1] D. Ponnamma, K. K. Sadasivuni, C. Wan, S. Thomas, and M. A.-A. AlMa'adeed, "Flexible and stretchable electronic com posites" (Springer, 2015)
[2] H. Kuwahara, S. Sudo, M. Iijima, and S. Ohya, "Dielectric properties of thermally degraded chloroprene rubber" Polymer Degradation and Stability 95, 2461-2466 (2010).
[3] A. Das, A. Ghosh, and D. Basu, "Evaluation of physical and electrical properties of chloroprene rubber and natural rubber blends" KGK-Kautschuk Gummi Kunststoffe 58, 230-238 (2005).
[4] R.Sela, D. Bychanok, Y. Padrez, D. Adamchuk, V. Ksenevich, N. Naveh and P. Kuzhir, "Electromagnetic properties of chloroprene rubber after long-term ultraviolet ageing, oil immersion and thermal degradation" submitted for publication in Material express journal.

.

# LOW FREQUENCY DIELECTRIC P ROPERTIES AND ATMOSFERIC EFFECTS OF ZIF-90 METAL-ORGANIC FRAMEWORK

Diana Pavlovaitė[1], Sergejus Balčiūnas[1], Mantas Šimėnas[1], Martynas Kinka[1], Fa-Kuen S[2], Kevin C.-W Wu[3,4], Jūras Banys[1] and Robertas Grigalaitis[1]

[1] Faculty of Physics, Vilnius University, Sauletekio av. 9, LT-10222 Vilnius, Lithuania

[2]Department of Chemistry, National Central University, Chung-Li 32001, Taiwan

[3]Department of Chemical Engineering, National Taiwan University, Taipei 10617, Taiwan

[4]Center of Atomic Initiative for New Materials (AI-MAT), National Taiwan University, No. 1, Sec. 4, Roosevelt Rd., Taipei 10617, Taiwan

diana.pavlovaite@ff.stud.vu.lt

Metal-organic frameworks (MOFs) have emerged in the recent years as promising materials as their properties suggest variety of potential applications in gas adsorption and storage, microreactors, etc.[1] due to their porous structure. Gas adsorption properties of zeolitic imidazolate frameworks (ZIFs) are believed to be tightly related to a flexible nature of organic linkers in these compounds. In this research ZIF-90 compound was studied in different atmospheres: vacuum, $N_2$, $CO_2$ and air, in 150-400K temperature range and 100 Hz – 1 MHz region.

Performed dielectric spectroscopy experiments with dehydrated sample in vacuum, $N_2$ and $CO_2$ conditions compared to the results of hydrated sample studies in air allowed us to reveal the differences in activation energy, that we suppose, is due to the different dynamics of ICA linker. As noted in Fig.1 the activation energy of linker movement in vacuum ($E_a$ = 0.23 eV) is significantly lower compared to dynamics in gas atmospheres ($E_a$ = 0.36 eV).

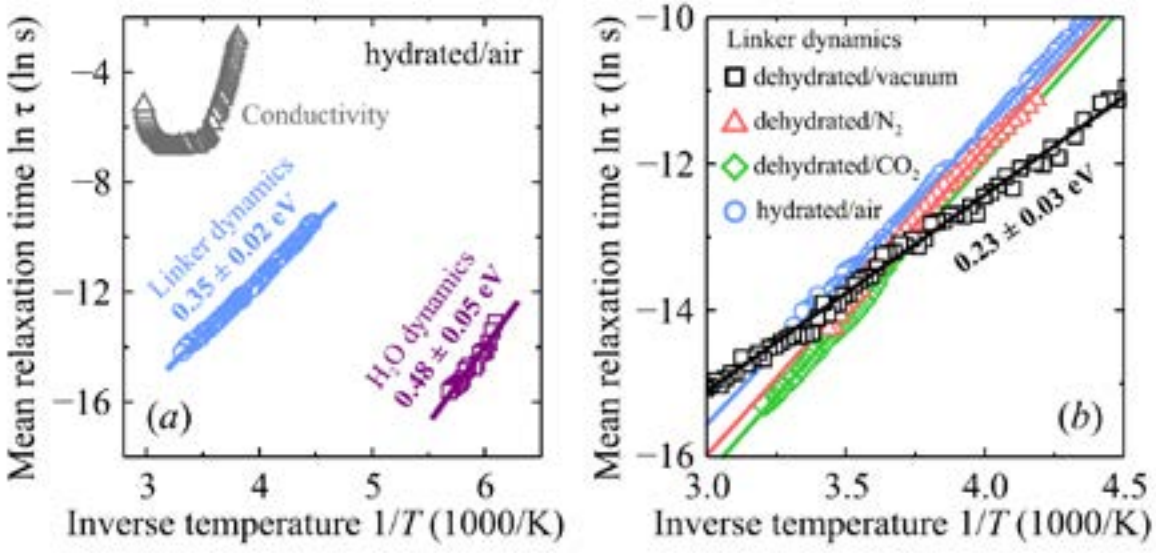


Fig.1 Inverse temperature dependence of the mean relaxation time of (a) different dipolar processes in hydrated ZIF-90 and (b) linker dynamics for ZIF-90 in different atmospheres. The lines are linear fits indicating Arrhenius processes.

---

[1] I. Ahmed, S.H. Jhung, Composites of metal–organic frameworks: Preparation and application in adsorption, Mater. Today. 17 (2014) 136–146. doi:10.1016/j.mattod.2014.03.002.

[2]Sergejus Balčiūnas, Mantas Šimėnas, Diana Pavlovaitė, Martynas Kinka, Fa-Kuen Shieh, Kevin C.-W Wu, Jūras Banys, and Robertas Grigalaitis, Low-Frequency Dipolar Dynamics and Atmospheric Effects in ZIF-90 Metal–Organic Framework**, . J. Phys. Chem. C** 2019 *123* (1), 631-636 **9**

# INFLUENCE OF Co-DOPING ON THE STRUCTURAL AND MAGNETORESISTIVE PROPERTIES of La-Sr-Mn-Co-O THIN FILMS

Milita Vagner[1], Rasuolė Lukošė[2], Valentina Plaušinaitienė[1]

[1] Institute of Chemistry, Faculty of Chemistry and Geosciences, Vilnius University, LT- 03225 Vilnius, Lithuania
[2] Department of Material Science and Electrical Engineering, Center for Physical Sciences and Technology, LT-10257 Vilnius, Lithuania
milita.vagner@chgf.vu.lt

Thin nanostructured manganite-cobaltite films can be applied as room temperature B-scalar magnetic field sensors. Undoped $La_{1-x}Sr_xMnO_3$ films have high metal-insulator transition temperatures ($T_m$), the substitution of Co for Mn in $La_{1-x}Sr_xMn_{1-y}Co_yO_3$ (LSMCO) lowers $T_m$, increases the resistivity and gives expectively higher values of magnetoresistance at the room temperature [1].

Pulsed-injection metalorganic chemical vapor deposition (PI-MOCVD) method was used for the deposition of thin nanostructured (on $Al_2O_3$ substrate) and textured (on $LaAlO_3$ substrate) $La_{1-x}Sr_x(Mn_{1-y}Co_y)_zO_3$ (x=0.18, z=1.15) films. The novelty of the research is not only the certain doping level of Co, but also the nonstoichiometry of Mn leading to the change of structural, transport and magnetic properties of the LSMCO films

In present study, it was determined that with the increase of Co content (up to 0.16) results in the decrease of metal-insulator transition temperature ($T_m$) (Figure 1a). The metal-insulator transition temperature $T_m$ is related to the transfer integral between the manganese ions and thus to the angle of the $Mn^{3+}$-$O^{2-}$-$Mn^{4+}$ bonds. The substitution of Co for Mn presumably destroys these bonds and thus weakens the double-exchange interaction [2]. However, the increase of Co improves the magnetoresistive properties of the LSMCO films: increase of magnetoresistance with Co content up to magnetic fields of 60 T.

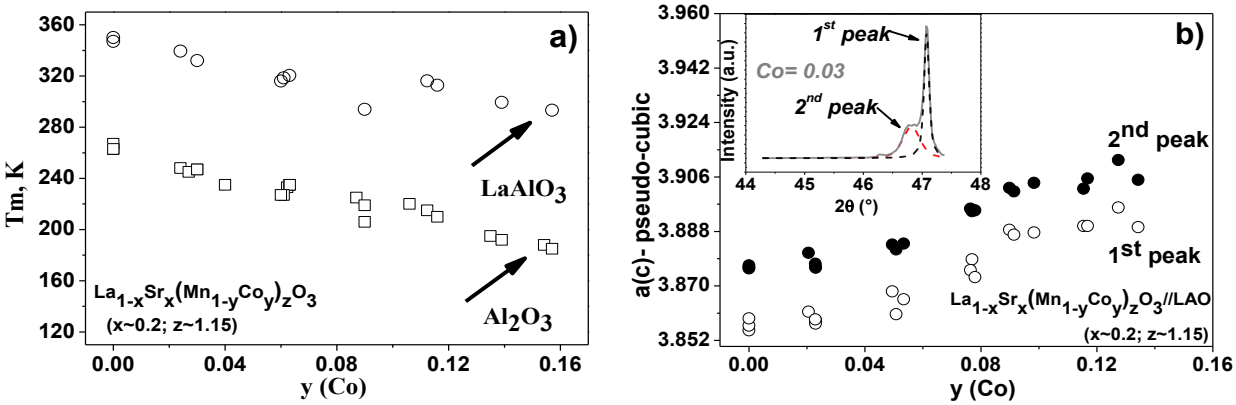


Fig. 1. a) Metal-insulator transition temperature $T_m$ dependence on Co content of nanostructured (squares) and textured (dots) LSMCO films; b) Lattice parameters dependence on Co content of textured LSMCO films.

X-ray diffraction (XRD) data revealed that all samples are single-phase. The lattice parameters were determined by the XRD patterns (Figure 1b). Substitution of Mn by Co results in systematic increase in lattice parameters of textured films with the increase of Co content. This dependence may be explained by epitaxial strain or/and oxygen vacancies.

The composition of the films and exact doping level of Co was determined by inductively coupled plasma mass spectrometry (ICP-MS). Electrical and magnetic properties of LSMCO films were investigated by using a low dc electric field and pulsed magnetic fields up to 60T. Structural analysis was determined by X-ray diffraction (XRD). Surface morphology was studied by scanning electron microscopy (SEM).

The possibility to apply the manganite-cobaltite films for the development of B-scalar magnetic field sensors is considered.

[1] J. Hu, H. Qin, J. Chen, and R. K.Zheng, "Room temperature magnetoresistance in $La_{0.67}Sr_{0.33}Mn_{1-x}Co_xO_3$"J. Appl. Phys., **91**, 8912–8914, (2002).

[2] X. G. Chen et al., "Magnetic and transport properties of cobalt doped $La_{0.7}Sr_{0.3}MnO_3$,"J. Appl. Phys., **116**, 103907-1–103907-10, (2014).

# FORMATION OF SELF-REORGANIZED RIPPLE NANO-STRUCTURES ON TITANIUM METAL SURFACE

Giedrius Balčas[1], Antanas Urbas[1, 2], Sergejus Orlovas[1]

[1] Center of Physical Sciences and Technology, Industrial Laboratory for Photonic Technologies, Lithuania
[2] Altechna R&D Ltd, Lithuania
giedrius.balcas@ff.stud.vu.lt

The interest in the formation of ultra-short laser micro/nano machining of self-organizing surface structures has grown significantly in the last decade, due to its promising applications in various fields. Textured materials, that undergo femtosecond laser treatment, have shown to possess altered mechanical, chemical, tribological, and wetting properties [1, 2, 3].

Periodic structures of the nano scale, also known as ripple, were selected for the study. Laser-induced periodic surface structures, further LIPSS, were first investigated in 1965 [5]. Observed LIPSS nano structures exhibit a surface geometry of long periodic grooves and bumps. The low spatial frequency LIPSS periodicity is close to the central frequency of the laser radiation if the beam used is perpendicular to the sample's surface, and the orientation of the structures is perpendicular to the incident laser radiation electric field direction. The mechanism that drives the formation of low spatial frequency structures is generally accepted to be due the interference between incident laser beam and scattered optical surface waves [6].

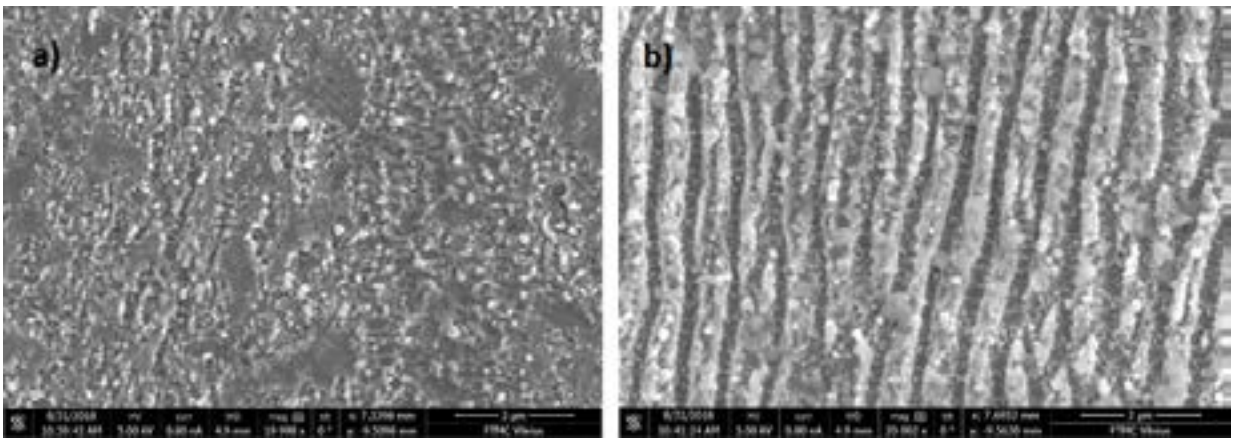


Fig. 1. Generated surface structures on polished titanium Ti-6Al-4V sample, using 20 kHz pulse repetition rate with scanning speed and average power: a) 0,48 mm/s and 80 mW b) 0,24 mm/s and 160 mW.

In this study self-reorganizing surface structures on Titanium Ti-6Al-4V sample and its dependence on laser parameters was observed, exclusively focusing on ripple morphology induced changes in drag reduction of the material. As shown in figure 1. periodicity and other characteristics of LIPSS can be altered by variation of irradiation parameters [7]. In fig. 1 a) a chaotic morphological structure is observed, whereas in fig. 1 b) a non-random ripple structure appears.

[1] Kietzig, A.M.; Hatzikiriakos, S.G.; Englezos, P. Ice friction: The effects of surface roughness, structure, and hydrophobicity. J. Appl. Phys. 2009, 106, 024303.
[2] Vorobyev, A.Y.; Guo, C.L. Metal pumps liquid uphill. Appl. Phys. Lett. 2009, 94, 224102.
[3] O. Raimbault, S. Benayoun, K. Anselme, C. Mauclair, T. Bourgade, A.-M. Kietzig, P.-L. Girard-Lauriault, S. Valette, C. Donnet. The effects of femtosecond laser-textured Ti-6Al-4V on wettability and cell response. Mater. Sci. Eng. C, 69 (2016), pp. 311-320).
[5] Birnbaum, M. Semiconductor surface damage produced by ruby lasers. J. Appl. Phys. 1965, 36, 3688–3689.
[6] J. Bonse, S. Höhm, S. V. Kirner, A. Rosenfeld, and J. Krüger, "Laserinduced periodic surface structures—A scientific evergreen," IEEE J. Sel. Topics Quantum Electron., vol. 23, no. 3, May 2017, Art. no. 9000615.
[7] W. L. Barnes, A. Dereux, and T. W. Ebbesen, "Surface plasmon subwavelength optics," Nature, vol. 424, pp. 824–830, 2003.

# INVESTIGATION OF PHOSPHOR MATRICES WITH HIGH THERMAL CONDUCTIVITY FILLERS

Justina Aglinskaitė, Akvilė Zabiliūtė-Karaliūnė, Pranciškus Vitta

Institute of Photonics and Nanotechnology, Faculty of Physics, Vilnius University
justina.aglinskaite@ff.stud.vu.lt

Solid-state lighting recently has become one of the main light sources. While light-emitting diodes are used in many different fields of illumination, they suffer efficiency droop effect. Droop-free laser diodes based white lighting starts to be used in specific cases where lighting of high directionality and power density is desired [1]. In these luminaries blue laser diode is coupled with yellow phosphor to gain white light. Phosphor powder is dispersed in matrix, which is heating due to high laser diode power density. High temperatures cause photoluminescence thermal quenching and degradation of matrices. In order to reduce temperature of phosphor, matrix must have good thermal properties. This problem usually is solved using phosphor in glass, phosphor ceramics and monocrystalline phosphors [2, 3, 4]. Here we present simple and commercially attractive method to increase thermal conductivity of phosphors with polymer matrices. In this work organic matrices used in commercial luminaries are presented with additionally added high thermal conductivity material.

Firstly, samples with three different fillers and three different holding matrices and phosphor were made and their thermal conductivity and photoluminecsence properties were measured. Composite with most suitable properties was chosen for following experiments. In the second part of experiment samples with yellow and green phosphors, one of the holding matrices and different concentrations of high conductivity powder were prepared. Relative thermal conductivity, photoluminescence decay time, intensity and quantum yield of samples were measured. In addition, samples temperature and photoluminescence intensity dependencies on incident excitation power density were evaluated.

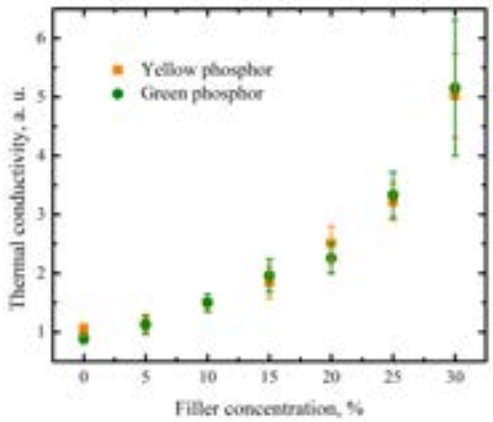


Fig. 1. Thermal conductivity dependence on filler concentration for samples with yellow and green phosphors.

It was found out, that investigated composite is suitable for holding matrices of phosphors. The introduction of high thermal conductivity filler in holding matrices increase thermal conductivity of samples few times (Fig. 1), does not absorb photoluminescence excitation or emission radiation and does not diminish quantum yield. Inclusion of fillers results in higher reflection of excitation radiation but on the other hand helps to decrease losses based on photoluminescence thermal quenching. Therefore, it is important to find optimal concentration of high thermal conductivity powder to reach maximum photoluminescence intensity.

[1] George, Anthony F., et al., Laser-driven phosphor-converted white light source for solid-state illumination, Applied optics **55.8**, 1899-1905 (2016).
[2] Song, Young Hyun, et al., High power laser-driven ceramic phosphor plate for outstanding efficient white light conversion in application of automotive lighting, Scientific reports **6**, 31206 (2016).
[3] Zhu, Qiang-Qiang, et al., A robust red-emitting phosphor-in-glass (PiG) for use in white lighting sources pumped by blue laser diodes, Journal of Alloys and Compounds **702**, 193-198 (2017).
[4] Cantore, Michael, et al., High luminous flux from single crystal phosphor-converted laser-based white lighting system, Optics Express **24.2**, A215-A221 (2016).

# COMPARISON OF METHODS FOR THE GROUND THERMOGRAPHIC MEASUREMENTS: THE CASE OF COAL-WASTE DUMPS

Anna Abramowicz

Department of Fundamental Geology, University of Silesia in Katowice, Poland

abramowiczanna@gmail.com

Ground thermography measurements are currently used for many environmental expertises, which are related to the land management or threats counteracting. The ground is measured in various areas - more and more often at the waste disposal sites. Coal-waste dumps are the objects, on which thermal monitoring is carried out with the highest care. The uncontrolled spontaneous self-ignition of stored material is a huge hazard to the environment and local residents. The prevention of hazard relies primarily on regular and complex monitoring, but there is no flawless method, so it is very difficult to predict the direction and strength of fire development [1].

It was decided to choose the effective way of measurement of the temperature distribution on the surface of coal-waste dumps. We consider three methods currently used for the thermography measurements: digital pyrometer with one meter probe and laser, handheld IR thermal camera and unmanned aerial vehicle with IR thermal camera. They are all common, easy to carry out, non-invasive and do not require a large financial outlay [2].

The aim of this presentation is comparison of thermal measurements' methods using digital pyrometer, handheld IR thermal camera and drone with IR thermal camera. Tests were executed on a small 25-year-old coal-waste dump in Ruda Śląska (Czarny Las district) in Upper Silesian Coal Basin, which has been burning since 1995. In the area of 6 hectares, 30 measuring points were placed (everyone received accurate coordinates). The temperature was measured there by a pyrometer and a thermal imaging IR camera. At a height of 50 meters, a drone with a thermal imaging camera made a flight and took almost 300 photos which then created a mosaic. Obtained measurements ranged from -10 to almost 500 Celsius degrees. The collected measurements were calibrated with each other and with the current environmental conditions. The data from the pyrometer was obtained in a vector format, while the data from the cameras were rasters. All data has been carefully analyzed for the location of hot spots and temperature values in the ArcGIS software.

The final aim of the analysis is choice of more reliable method which is less affected by error. The advantages and disadvantages of each method were noticed, proving that none of them is perfect.

[1] G.B. Stracher, A. Prakash, E.V. Sokol., Coal and Peat Fires: A Global Perspective: Volume 3: Case Studies – Coal Fires, ISBN 0444595112 (2014).

[2] J. Korski, Termowizja w monitoringu i zwalczaniu pożarów składowisk pogórniczych, Górnictwo i geologia, 5, 91-103 (2010).

# FEMTOSECOND LASER ABLATION OF METAL OXIDE FILMS FOR PRODUCTION OF PHOTOMASKS – RESOLUTION TEST

Augusto Jesus Hernandez Lombardini[1], Mindaugas Juodėnas[2], Tomas Tamulevičius[1,2]
[1]Department of Physics, Kaunas University of Technology, Studentų St. 50,
Kaunas, Lithuania, LT- 51368
[2]Institute of Materials Science, Kaunas University of Technology, K. Baršausko St. 59, Kaunas, Lithuania,
LT-51423
E-mail: augusto.hernandez@ktu.edu

Optical mask lithography is a technique based on the behavior of some substances, like thin photoresist layers, under illumination with ultraviolet light. The integration density and properties of microelectronic devices depends on their linear dimensions. During the lithographic fabrications process they are defined by the opaque or transparent patterns of the microstructures that are imposed on the photomask and used for the photolithographic exposure. The UV light illuminating the lithographic masks projects the patterns on the sample with light sensitive layer. The resolution of the mask-based lithography methods is mostly determined by the quality of the mask. Laser writing technique is an attractive alternative for the photomask fabrication [1].

In this work a UV mask was produced employing a femtosecond laser micromachining utilizing FemtoLAB workstation and third harmonic of Yb:KGW femtosecond laser Pharos. Ablation resolution tests in metal oxide films on glass substrates were organized with SCA v2.6 software. Owing for optimal microstructure resolution the pulse density, pulse energy, attainable translation speeds and other related laser processing parameters were varied. Resulting structures and their quality were analyzed under optical microscope. Typical geometrical shapes, namely lines and circles of micrometer range dimensions ablated in metal oxide film are depicted in Fig. 1.

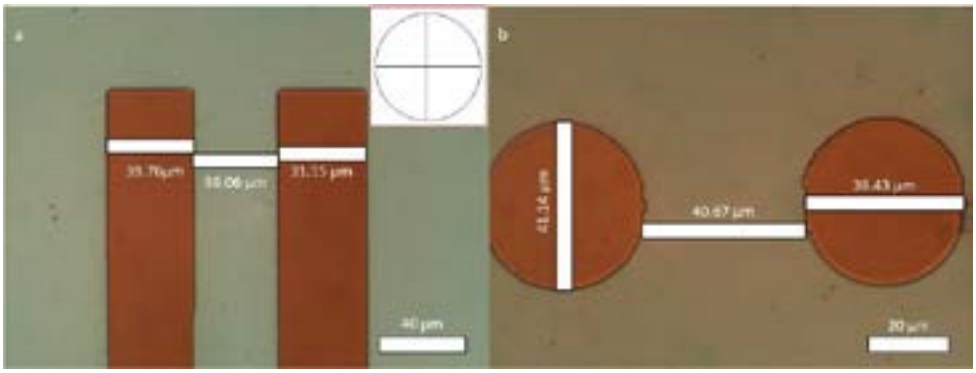


*Figure 1. Optical microscope micrographs of femtosecond laser ablated lines (a) and circles (b) in metal oxide films. The parameters of the ablation were: 343 nm wavelength, 9 mW power; 200 kHz frequency. Inset in (a) depicts the test pattern used for the ablation optimization.*

Optimization of the ablation procedure was carried out employing a test pattern consisting of straight and curved intersecting lines indicated in the inset of Fig. 1 a. Preliminary ablation experiments enabled us to produce a lithography masks depicted in Fig 1 a and b with a mark speed of 0.5 mm/s a jump speed of 10 mm/s and a pulse density of 6000 pulses/mm. The optimization of the patterning speed is still in progress.

This research was funded by the European Social Fund under the No. 09.3.3-LMT-K-712 "Development of Competences of Scientists, other Researchers and Students through Practical Research Activities" measure, grant No. 09.3.3.-LMT-K-712-10-0214.

[1] Venkatakrishnan, K., Ngoi, B., Stanley, P. et al. Appl Phys A (2002) 74: 493. https://doi.org/10.1007/s003390101030.

# THIN WATER FILM ASSISTED GLASS ABLATION WITH A HIGH PULSE REPETITION RATE LASER

Laimis Zubauskas, Edgaras Markauskas

Center for Physical Sciences and Technology, Savanoriu Ave. 231, LT-02300, Vilnius, Lithuania
laimis.zubauskas@gmail.com

Medical, electronic, and photonic industries demand fast and high-quality processing of glasses. Modern ultra-short pulsed lasers offer high average power at high-pulse repetition rates allowing fast production of high-quality parts. However, full laser potential is rarely used during the glass cutting applications. Laser parameters, such as scanning speed, pulse energy and pulse repetition rate are limited to avoid glass overheating and generation of cracks. In extreme cases, excessive laser power can even lead to a fracture of the workpiece.

Rear side drilling [1], crack generation in the bulk of the glass material [2], and direct ablation [3] are the main laser processing technologies used for glass cutting. The fastest ones are the rear side drilling and the crack-generation in the bulk of the glass material. However, these two have limitations, such as low capability in the manufacturing of small and complex shape parts, and low processing quality. Therefore, the most versatile technology seems to be the direct ablation of glasses. However, direct ablation frequently suffers from the low processing speeds due to the channel clogging with laser generated debris.

Studies have shown that the water layer introduced onto the surface of the workpiece could improve both the process quality and the laser cutting speed [4, 5]. Therefore, water-assisted processing attracted much attention in laser drilling, grooving, scribing, and cutting applications [5].

In this research, picosecond laser working at 1064 nm and 532 nm wavelengths was used to evaluate the direct laser ablation efficiency and process quality of soda-lime glass samples in ambient air and water-assisted environments. Ablated grooves and complete cutting of glass plates were investigated. A water spray was used to introduce a thin flowing water layer in the laser ablation zone.

Results showed that the applied water layer improved the ablation efficiency of grooves deeper than 250 µm or narrower than 150 µm (see Figure 1). At optimal conditions, water improved the glass ablation efficiency 11 times compared to the ablation in ambient air, reaching 0.19 $mm^3$/min/W. Finally, applied water layer improved the cut-line sharpness and reduced the chipping of glass material at the edges of the groove.

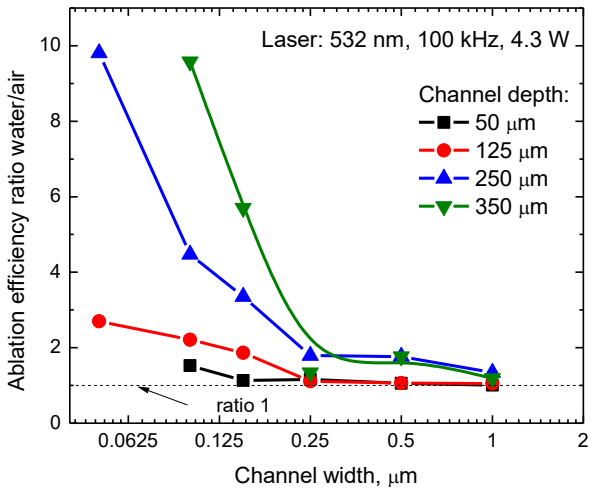


Figure 1 Glass ablation efficiency ratio between water-assisted and ambient air conditions versus ablated channel width. Cases for different channel depths presented.

[1] P. Gečys, J. Dudutis, and G. Račiukaitis, *Nanosecond Laser Processing of Soda-Lime Glass.* Journal of Laser Micro/Nanoengineering, 2015. **10**(3): p. 254-258.

[2] ] J. Dudutis, P. Gečys, and G. Račiukaitis. *Modification of glass using an axicon-generated non-symmetrical Bessel-Gaussian beam*. in *SPIE LASE*. 2017. SPIE.

[3] M. Sun, U. Eppelt, C. Hartmann, W. Schulz, J. Zhu, and Z. Lin. *Towards crack-free ablation cutting of thin glass sheets with picosecond pulsed lasers*. in *Pacific Rim Laser Damage 2017: Optical Materials for High Power Lasers*. 2017. SPIE.

[4] N. Krstulović, S. Shannon, R. Stefanuik, and C. Fanara, *Underwater-laser drilling of aluminum.* The International Journal of Advanced Manufacturing Technology, 2013. **69**(5): p. 1765-1773.

[5] W. Charee and V. Tangwarodomnukun, *Dynamic features of bubble induced by a nanosecond pulse laser in still and flowing water.* Optics & Laser Technology, 2018. **100**: p. 230-243.

# RADIATION OF CHARGE MOVING BETWEEN TWO PLANAR PERIODIC WIRE STRUCTURES

Ilia Moroz[1,2], Evgeny Gurnevich[1]

[1]Institute for Nuclear Problems, Belarussian State University, Belarus
[2]Department of Nuclear Physics, Belarussian State University, Belarus
miwa-holod@yandex.ru

Electromagnetic radiation sources for wide spectral ranges, from microwave and THz to optical and X-ray, are developed and explored very intensely in last decades. This is due to the fact that such sources can be used both for research and practical purposes in many areas, for example in biology and chemistry, non-ionization diagnostic and medicine, ultra-fast communication technology, space research, etc. [1-2]

The development of free electron lasers (FEL) and its different realizations is one of the promising directions for the creation of tunable and high efficiency radiation sources. In particular, a volume FEL (VFEL) was proposed in [3-6], which implements a volume distributed feedback allowing to reduce size of the device and threshold currents necessary to start the generation. In the first experimental prototype of VFEL [7-8], the radiation was generated by an electron beam passing near one diffraction grating (Smith-Purcell radiation), and other diffraction grating with a different period was used to form the distributed feedback.

In this paper, we consider theoretically the spontaneous radiation of a charged particle (electron) moving in a system that is very similar to the VFEL resonator from [7-8] (Fig. 1). Two planar diffraction gratings with different periods are formed by parallel metal wires. A charged particle moving between them can generate Smith-Purcell radiation. It is assumed that particle moves perpendicular to wire axes.

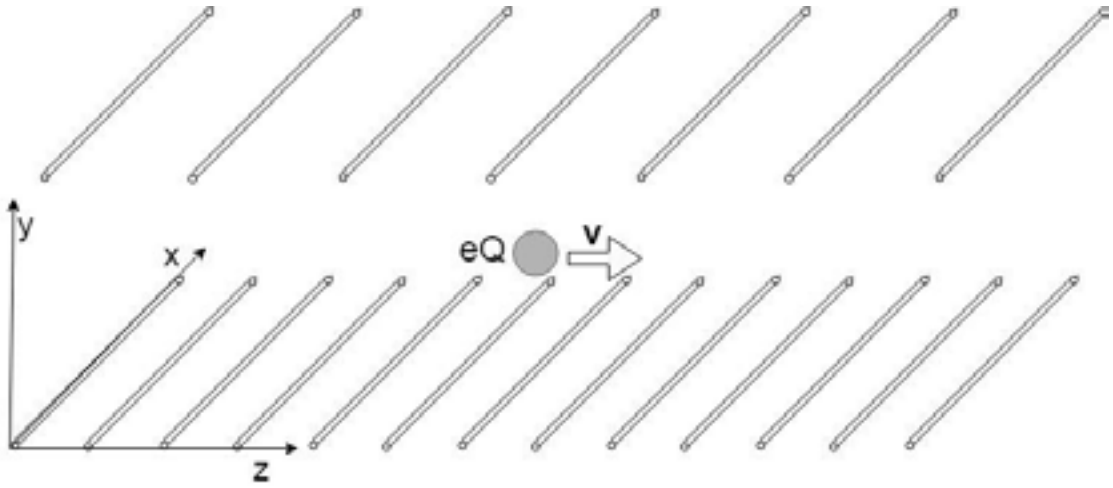


Fig. 1. Geometry of the problem.

The analytical expression for the spectral-angular distribution of radiation was obtained. It is shown that radiation intensity is sensitive to distance between particle and gratings and decreases exponentially with the growth of it. Also radiation intensity can be changed by parallel relative shift of gratings and by selecting the appropriate shift it can be made several times larger than the corresponding value for one grating.

[1] H. A. Hafez et al, Intense terahertz radiation and their applications, J. Opt. 18 (2016) 093004 (48pp), doi:10.1088/2040-8978/18/9/093004
[2] R. A. Lewis, A review of terahertz sources, J. Phys. D: Appl. Phys. 47 (2014) 374001 (11pp), doi:10.1088/0022-3727/47/37/374001
[3] V.G. Baryshevsky, I.D. Feranchuk, Parametric beam instability of relativistic charged particles in a crystal, Phys. Lett. A, 102, 14, 1984.
[4] V.G. Baryshevsky, Surface parametric radiation of charged particles, Doklady of USSR Akademy of Science, 299, 6, 1988.
[5] V.G. Baryshevsky, K.G. Batrakov, and I.Y. Dubovskaya, Parametric (quasi-cerenkov) x-ray free electron lasers, Journal of Physics D., 24, 1250, 1991.
[6] V.G. Baryshevsky, Volume free electron lasers, Nuclear Inst. and Meth. A, 445, 281, 2000.
[7] V.G. Baryshevsky et al, First lasing of a volume FEL (VFEL) at a wavelength range λ~4–6 mm. Nuclear Instruments and Methods in Physics Research A 483 (2002) 21–23
[8] V.G. Baryshevsky et al, Experimental observation of radiation frequency tuning in "OLSE-10" prototype of volume free electron laser. Nuclear Instruments and Methods in Physics Research Section B: Beam Interactions with Materials and Atoms, 252(1), 86–91

# INJECTION CURRENT EFFECT ON VCSELS STATISTICAL PARAMETERS

Labatsevich Pavel[1]

[1]Department of Physics, Belarusian State University, Belarus
pavel.lobatsevich@mail.ru

Vertical cavity surface-emitting lasers (VCSEL) provide single-mode operation in threshold. They are very attractive for optoelectronical applications, but they have polarization switching effect (PS) when injection current increase. We can eliminate this effect by changing technological operations, but PS could use in in polarization sensitive applications. Fluctuations lead to polarization switching in polarization instability area. VCSEL have three fluctuation source: the spontaneous emission intensity fluctuations, the current injection density fluctuations and nonequilibrium carriers concentration fluctuations.

In previous research papers [1] it has been shown that the spontaneous emission intensity fluctuations cannot are dominated factor (Fig 1a). The analysis of the statistical modeling results for the VCSELs in polarization instability area has shown that the numerical value of the distribution function dispersion is substantially lower than experimentally observed, especially for the intensity providing the distribution function for the intensity and degree of polarization are qualitatively similar to those observed experimental data.

This work presents the analysis of statistical simulation of output radiation in instability area with current injection density fluctuations and nonequilibrium carriers concentration fluctuations. In works [2] it has been shown that the nonequilibrium carriers concentration fluctuations can be present throw the current injection density fluctuations.


a b

Fig.1.The polarization degree histogram at the PS point with the spontaneous emission intensity fluctuations (a) and the current injection density fluctuations (b). All other parameters stay the same.

Within the framework of the earlier proposed approach to lasing dynamics inside semiconductor laser cavity the investigations of affect different fluctuation sources on statistical parameters of VCSELs in polarization switching region have been full filled. The numerical simulation results showed that pattern series obtained for the spontaneous emission intensity fluctuations remain constant for the current injection density fluctuations. This suggest radiation formation mechanism of our mathematical model does not contain internal contradictions.

The detailed analysis of the statistical simulations showed increasing gain anisotropy leads to decreasing dispersion of polarization degree and intensity distributions. Increasing spontaneous emission factor leads to increasing dispersion of polarization degree and intensity distributions. All obtained patterns have a transparent and natural interpretation based on our model [3].

The main result of our investigation is the current injection density fluctuations can initiate transitions between states with the values of the polarization degree limited by (± 1) (the effects of "mode hopping" or "stochastic resonance") (Fig.2). This effect is known enough in works [2]. Many times the similar results were observed in experimental researches. The current injection density fluctuations and nonequilibrium carriers concentration fluctuations affect gain medium. For multi-passage operation the fluctuations in the concentration of nonequilibrium carriers and injection current are more meaningful than the spontaneous emission intensity fluctuations

Based on obtained results we can assume that the spontaneous emission fluctuations are an important, but not dominated source of fluctuations. However, fluctuations in the concentration of nonequilibrium carriers and injection current are more significant in terms of the statistical parameters formation of the output radiation.

[1] P.M.Labatsevich, Spontaneous emission factor influence on output parameters of the vertical-cavity surface-emitting lasers. 60ND international conference for students of physics and natural sciences “OpenReadings-2017”. Lietuva, Vilnius, March 13-17rd, P.177.
[2] M. B. Willemsen, M. U. F. Khalid, M. P. van Exter, and J. P. Woerdman. Polarization switching of a vertical-cavity semiconductor laser as a Kramers hopping problem. Phys. Rev. Lett. – 1999 – Vol.82, – P.4815–4818.
[3] M.Jadan, J.S.Addasi, L.I.Burov, A.S.Gorbatsevich, P.M.Lobatsevich. Polarization switchimg mechanism in surface-emitting semiconductor lasers. Optik – international Journal for Light and Electron Optics, Volume 158, April 2018. P.118-126

# THE INFLUENCE OF THE SURFACE FUNCTIONAL GROUP COMPOSITION ON THE SEDIMENTATION STABILITY OF NANODIAMONDS IN AQUEOUS SUSPENSIONS

Anastasia Tabolich [1*], Michael Samtsov[2] Belko Nikita[2]

[1] Department of laser physics and spectroscopy, Belarus State University, Minsk.Belarus
[2]A.N.Sevchenko Institute of Applied Physical problems of Belarus State University, Minsk, Belarus
nastya.tabolich@mail.ru

Detonation nanodiamonds are scientifically interesting for several reasons: 1) in the recent years, interest has grown toward the problem of synthesizing diamond nanoparticles retaining a constant size in aqueous suspensions; 2) there is no single comprehensive study that would explain the aggregation mechanism of ultradispersed diamonds (UDD) in aqueous environment, although there are several versions; 3) With the accelerated growth of technological progress, it is important to use various modern methods to control and analyze particle size in order to obtain a stable aqueous suspension.

We present on the influence of the functional group composition of the nanodiamond surface on the stability of their aqueous suspensions.

It is known that the primary particles of UDD (4-6 nmin size) tend to form aggregates with particle sizes from 10 nm to several microns. The nature of these aggregates is still not completely clear. The aggregation of diamond nanoparticles can be due to the formation of hydrogen bonds, dipole-dipole or weak van-der-Waals interactions between the functional groups of adjacent UDD particles.

The aggregation of particles can occur in the process of their separation from the diamond batch. The formation of aggregates depends on many factors, including various conditions of the UDD synthesis, purification, and processing methods. In order to determine the aggregation of the UDD powder, new original techniques are being developed.

It is known from the literature that in the widely distributed laboratory studies of nanodiamonds, mechanical, physical, and chemical methods are used to deaggregate them based on existing ideas about the UDD structure [1].

As the object of this study industrial detonation nanodiamonds of the UDA-SP brand in aqueous suspensions were used. The functional group modification on the UDD surface was achieved by the vacuum annealing in the temperature range of 500-1100$^0$ C, as well as air annealing at 430$^0$C.

It was shown that all types of temperature treatment studied affect the behavior of UDD in aqueous environment. From the IR absorption spectra, it follows that carboxyl groups are removed from the nanodiamond surface by vacuum annealing, while air annealing promotes formation of cyclic anhydrides by oxidizing carboxyl groups.

Carboxyl groups form hydrogen bonds responsible for UDD agglomeration; therefore, for more efficient dispersion in an aqueous medium, preliminary vacuum or air annealing can be applied, since it inhibits formation of the hydrogen bonds between nanodiamond particles.

[1] R.U.Yakovlev, Detonation nanodiamond as a perspective medium biological active substances (Ryazan,2016)

# INVESTIGATION OF RESONANCE EFFECTS IN POCKELS CELLS WITH BBO CRYSTALS

Jonas Banys[2], Rimantas Grigonis[2], Giedrius Sinkevičius[1], Julius Vengelis[2]

[1]"Optolita", Mokslininkų str. 11, Vilnius, Lithuania
[2]Laser Research Center, Faculty of Physics, Vilnius University, Lithuania
jonas.banys.2@ff.stud.vu.lt

Many applications such as laser-induced damage testing, laser microfabrication and modification of materials sometimes require a train of defined number of ultrashort pulses with special shape energy envelopes [1]. Such pulse trains could be obtained using pulse picker systems based on electro-optical Pockels elements. Pockels cells are devices that create a phase delay in a crystal which can be modulated by applying a variable electric voltage [2]. Beta barium borate (BBO) crystals are a suitable material for Pockels cells due to their wide transmission range, high optical damage threshold and thermal stability [3, 4]. However, unwanted resonance effects can occur in Pockels elements which depolarize passing laser radiation and thus significantly reduce the efficiency of pulse picker device by reducing the contrast ratio. Knowledge of resonance conditions and optical contrast ratio dependence on high voltage control signal characteristics are relevant factors to ensure a stable selected laser pulse train.

In this work resonance effects were investigated in a special pulse picker "MP1" which was designed and made by Lithuanian company "Optolita" and used various BBO Pockels cells. Pulse picker "MP1" can output 100 ns – 1 ms duration synchronized selected laser pulse trains with repetition rate of 10 Hz – 250 kHz. The dependence of the contrast ratio of various BBO Pockels cells on the high-voltage control signal frequency and duration was investigated in this study. An Yb:KGW oscillator "Flint" generating 1033 nm wavelength, 76 MHz repetition rate and 110 fs pulses was used as a laser source. Four different BBO Pockels cells were measured; two of them had technological improvements, which aimed to reduce piezoelectric oscillations.

All of the measured BBO elements suffered from piezoelectric oscillations and piezoelectric resonances. It was determined that resonance effects – inverse piezoelectric effect, acoustic wave propagation in the crystal and photoelastic effect, cause high amplitude piezoelectric oscillations which reduce Pockels cell optical contrast ratio by 6 – 70 times at resonance frequencies. By comparing different BBO Pockels cells we showed that optical contrast ratio is 1.5 – 5 times greater with Pockels cells that use different glue and special electrodes with a notch (Fig. 1). Finally it was determined that at low high-voltage control pulse repetition frequencies (up to 10 Hz), BBO Pockels cells are free of high amplitude piezoelectric oscillations and resonances when high-voltage control pulse duration is from 100 ns to 1 ms. In such case optical contrast ratio is stable and higher than 1:1000 (Fig. 2).

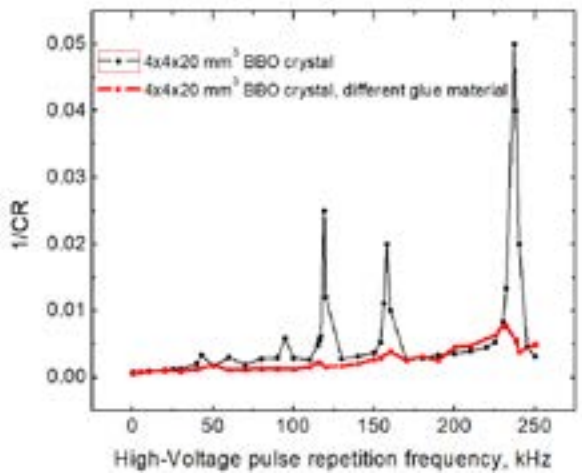


Fig. 1. Inverse contrast ratio (1/CR) dependence of same size BBO Pockels cells with different glue material on high-voltage control pulse repetition frequency.

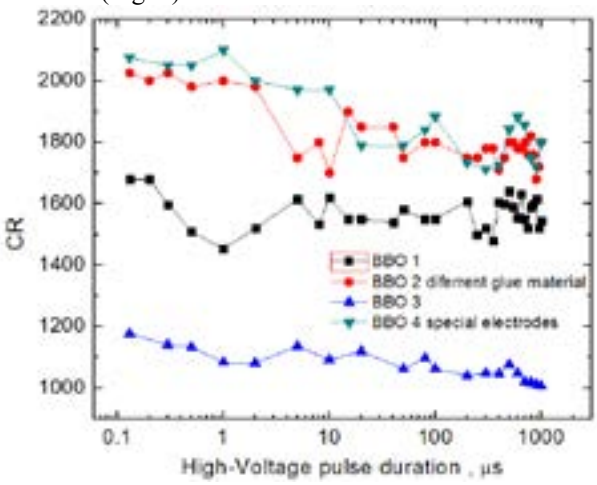


Fig. 2. Contrast ratio (1/CR) dependence of BBO Pockels cells on high-voltage control pulse duration.

This study was supported by Lithuanian agency of science, innovation and technology (MITA) and performed with the partnership of "Optolita" company.

[1] C. Kerse, et al, Ablation-cooled material removal with ultrafast bursts of pulses, Nature, 537(7618), 84, (2016).
[2] V.Sirutkaitis, E.Gaižauskas, Kietojo kūno lazeriai. (Vilniaus universiteto leidykla, Vilnius 2008).
[3] M. Roth, M. Tseitlin and N. Angert, Oxide crystals for electro-optic Q-switching of lasers, Glass physics and chemistry, 31(1), 86-95, (2005).
[4] D. Eimerl, L. Davis, S. Velsko, E.K. Graham and A. Zalkin, Optical, mechanical, and thermal properties of barium borate, Journal of applied physics, 62(5), 1968-1983, (1987).

# INVESTIGATION OF THE PROPERTIES OF DIFFERENT CONSTRUCTION DKDP POCKELS CELLS

Laimonas Masiulis[2], Giedrius Sinkevičius[1], Julius Vengelis[2]

[1]"Optolita", Mokslininkų str. 11, Vilnius, Lithuania
[2]Laser Research Center, Faculty of Physics, Vilnius University, Lithuania
laimonas.masiulis@ff.stud.vu.lt

Pockels effect is applied in electrooptic modulators which are used in laser systems, pulse pickers and production of lasers [1, 2]. One of the most commonly used and cheapest Pockels cell crystals is DKDP. It half-wave voltage is low compared with other materials. However, piezoelectric oscillations in Pockels cell crystals tend to depolarize the passing beam and reduce the efficiency of the device. Therefore, these oscillations need to be suppressed or the Pockels cell has to be operated at conditions with minimum piezoelectric oscillations.

In this study we investigated piezoelectric oscillations in different DKDP Pockels cells of a prototype pulse picker created by UAB „Optolita" which uses a novel regenerative control signal sequence technique to pick pulse trains up to 1 ms duration. The main parameter for piezoelectric oscillation estimation was measurement of pulse picker contrast ratio. This was performed using an optical setup consisting of femtosecond Yb:KGW laser oscillator generating 1033 nm wavelength, 76 MHz repetition rate and 110 fs duration pulses, two crossed Glan-Taylor polarizers, the aforementioned pulse picker and photodiode. During the first measurement we tested how the contrast ratio of pulse picker with different DKDP crystals depends on Pockels cell high voltage control signal frequency while control signal duration is fixed (Fig. 1). Further on, we measured how the contrast ratio of pulse picker with different DKDP crystals depends on Pockels cell control signal regenerative sequence duration while the control signal frequency is fixed.

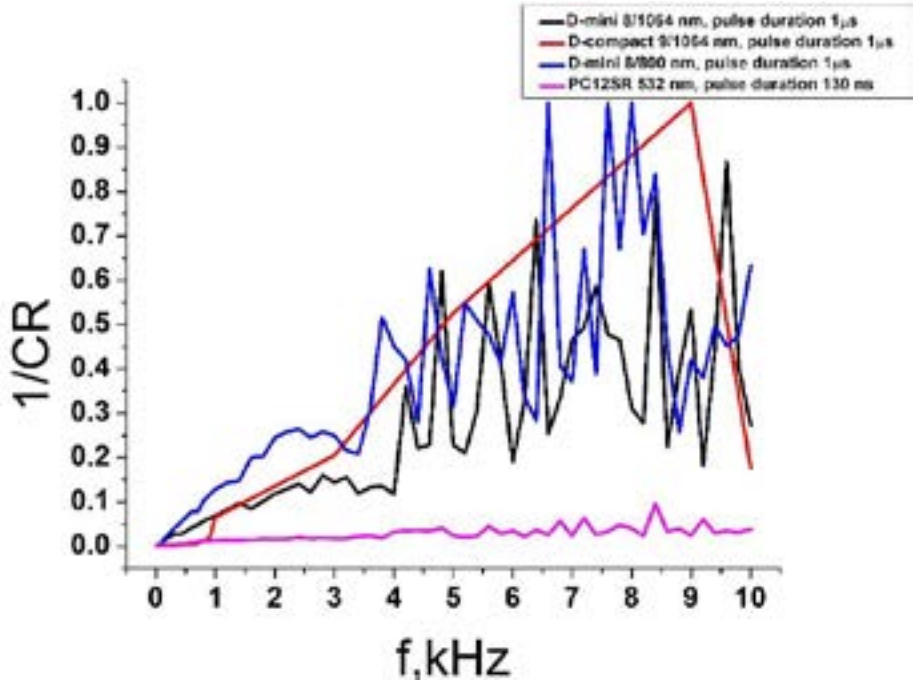


Fig. 1. Inverse contrast ratio dependence on high voltage control signal frequency.

Results showed obvious differences between different construction DKDP Pockels cells. Furthermore, in all investigated Pockels cell we determined control signal duration when piezoelectric oscillations are suppressed: it ranged from 6.6 μs to 9.9 μs.

This study was supported by Lithuanian agency of science, innovation and technology (MITA).

[1] https://www.alphalas.com.
[2] Akiko Kumada, Kunihiko Hidaka, Directly High-Voltage Measuring System Based on Pockels Effect, IEEE Trans. Power Del. **28**(3), 2013.

# MULTILAYER-DIELECTRIC REFLECTION GRATING DIFFRACTION EFFICIENCY SIMULATIONS FOR 1030 NM WAVELENGTH LASER

Andrius Žutautas[1], Lukas Stankevičius[1], Tomas Tamulevičius[1,2], Sigitas Tamulevičius[1,2]

[1]Kaunas University of Technology Department of Physics, Studentų Str. 50, LT- 51368, Kaunas, Lithuania
[2]Institute of Materials Science of Kaunas University of Technology, K. Baršausko Str. 59, LT-51423, Kaunas, Lithuania
andrius.zutautas@ktu.edu

Component damage thresholds and optical losses of ultra-short pulse lasers are prime reasons of laser power cap. Development of diffraction gratings that are essential for chirped pulse amplification (CPA) systems are the main course for achieving exawatt ($10^{18}$) peak powers [1]. Optical damage threshold above the used intensities, nearly 100% diffraction efficiencies (DE) for a broad spectral range of the ultra-short laser are the primary parameters characterizing high-diffraction efficiency periodic gratings [2]. Main optical loses of ultrashort pulse lasers occur because of the difficulty of achieving >99.9% diffraction efficiencies. A course for DE optimization using multilayer-dielectric diffraction gratings based on a 1064 nm laser line high reflectivity dielectric mirror was proposed. Simulations showed that DE of nearly 100% can be obtained by varying the thickness of the top low refractive index $SiO_2$ layer ($d_L^T$) and the grating depth ($d_{tr}$). During these numerical simulations three different structures with >0.99 DE were found (see figure 1).

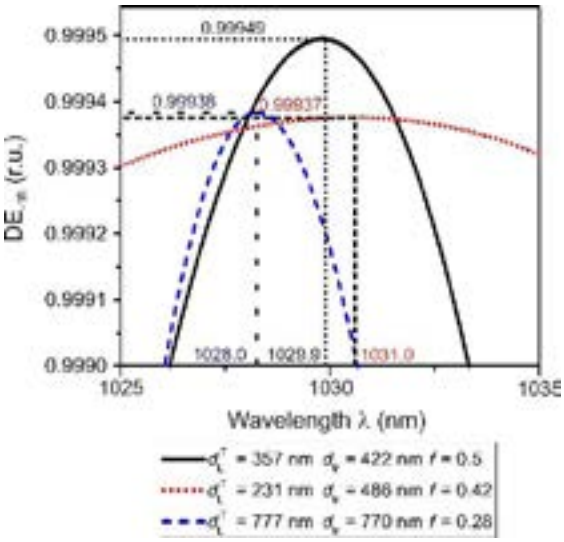


Fig. 1. Spectral DE dependence of three investigated diffraction gratings (*f* – fill factor)

[1] BONOD, Nicolas; NEAUPORT, Jérôme. Diffraction gratings: from principles to applications in high-intensity lasers. *Advances in Optics and Photonics*, 2016, 8.1: 156-199.
[2] VÁRALLYAY, Zoltán; DOMBI, Péter. Design of high-efficiency ultrabroadband dielectric gratings. *Applied optics*, 2014, 53.25: 5769-5774.

# INVESTIGATION OF TRANSMITTANCE OF LASER ABLATED SILICON IN 0.2 – 3.0 THz FREQUENCY RANGE

Evaldas Svirplys[1, 2], Simonas Indrišiūnas[1], Irmantas Kašalynas[2]

[1] Department of Laser Technologies, Center for Physical Sciences and Technology, Lithuania
[2] Department of Optoelectronics, Center for Physical Sciences and Technology, Lithuania
evaldas.svirplys@ff.stud.vu.lt

THz imaging is a promising technology for applications in security, medicine or pharmacy [1]. Improvement of optical elements for THz frequency radiation is important for minimizing the size and cost of imaging systems. One way to make THz optical systems more compact is to use diffractive optical elements – Multilevel Phase Fresnel Lenses (MPFLs). One way to produce MPFL elements is direct laser ablation [2]. Laser processing allows producing the desired elements in a relatively simple one-step fabrication without the use of auxiliary masks or materials.

In order to make MPFL production cost-effective it is important to have a sufficiently short fabrication time. Material removal rate in direct laser ablation process depends on the irradiation parameters such as laser fluence at the center of the focused laser spot ($F_0$) and laser spot overlap. At the same time fabrication quality such as roughness of the ablated surface ($R_a$) also depend on these parameters [3].

In this work, influence of various laser processing parameters on the transmission of THz radiation was investigated. Using 1064 nm wavelength picosecond and nanosecond laser pulses and 100 kHz pulse repetition rate, 6 x 6 mm$^2$ craters on a monocrystalline silicon (100) wafer were ablated varying laser fluence and spot overlap. Thus, silicon samples with different surface roughness and ablation efficiencies were prepared (Fig. 1).

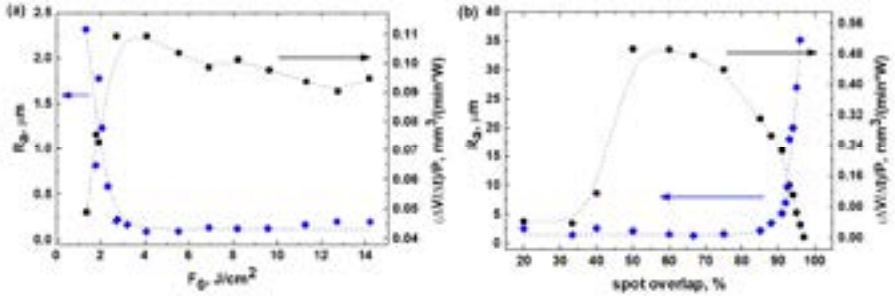


Fig. 1. (a) – picosecond laser ablation rate and surface roughness dependence on beam fluence, (b) – nanosecond laser ablation rate and surface roughness dependence on spot overlap.

Transmittance (T) of the ablated silicon plates in THz radiation frequencies were compared with theoretical model which predicts transmittance losses due to surface scattering:

$$T = (1 - R_0)\exp\left[-\left(\frac{4\pi R_a}{\lambda}\right)^2\right], \quad (1)$$

here $R_0$ is reflectance of non-ablated silicon, $\lambda$ – wavelength of scattered light. Theoretical predictions and measured transmittances using time-domain spectrometer for samples with various surface roughness are shown in Fig. 2.

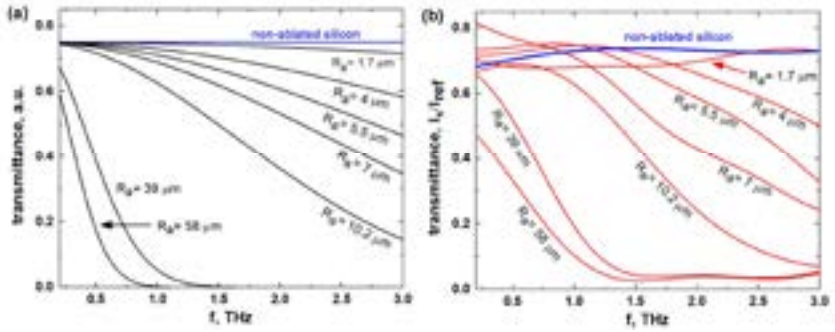


Fig. 2. Transmittance of nanosecond laser ablated silicon with various surface roughness in 0.2 – 3.0 THz frequency range (b), compared with theoretical scattering model (a).

[1] S. S. Dhillon, M. S. Vitiello, E. H. Linfield, A. G. Davies, M. C. Hoffmann, J. Booske, et al., The 2017 terahertz science and technology roadmap, J. Phys. D. Appl. Phys., p. 043001, 2017.
[2] L. Minkevičius, S. Indrišiūnas, R. Šniaukas, B. Voisiat, V. Janonis, V. Tamošiūnas, et al., Terahertz multilevel phase Fresnel lenses fabricated by laser patterning of silicon, Opt. Lett., t. 42, nr. 10, p. 1875, 2017.
[3] M. Domke, G. Piredda, J. Zehetner, ir S. Stroj, Minimizing the surface roughness for silicon ablation with ultrashort laser pulses.

# FABRICATION OF BIPOLYMERIC MICROSTRUCTURES USING THREE-DIMENSIONAL LASER LITHOGRAPHY AND INVESTIGATION OF THEIR DEFORMATIONS IN VARIOUS SOLVENTS

Emantas Tamulaitis, Darius Gailevičius, Sima Rekštytė

Laser Research Center, Vilnius University, Saulėtekio Ave. 10, Vilnius LT-10223, Lithuania
emantas.tamulaitis@ff.stud.vu.lt

Three-dimensional laser lithography (3DLL), based on multiphoton absorption in the polymer precursor volume, enables the formation of three-dimensional polymeric microstructures with high spatial resolution and accuracy out of various polymeric materials [1,2]. It has been demonstrated that structures fabricated by 3DLL undergo reversible deformations – shrinking or swelling – in different solvents [3]. Also, the type and degree of deformations differs depending on the polymeric material that is used [4]. By employing these unique features as well as, the possibility to fabricate different parts of the same object out of different polymer precursors, an opportunity for novel bipolymeric microstructures suitable for various applications arises.

During this experimental work, two polymeric substances were used for bipolymeric microstructure fabrication: hybrid organic-inorganic SZ2080 and hydrogel PEG-DA-575 (Fig. 1 a)). Structures were exposed to five different solvents and their behavior was monitored. To determine the magnitude of the bipolymeric wall deformations, the angle of bending $\Delta\alpha$ was calculated for every solvent each time the structure was submerged in it.

We show that the angle of bipolymeric wall bending depends on the solvent to which the structure is exposed. Changing the formation parameters also changes the size of this angle and the amplitude of the deformation (Fig. 1 b)). Bending in these structures results from the fact that different materials either swell or shrink to a different degree in the same solvent. The change of 3DLL formation parameters also changes the force of interaction between walls made of different polymer precursors, therefore impacting the angle of bending. The maximum amplitude of the bend angle is 50 degrees (water – 2-propanol). It has been observed that the amount of bends does not have a significant effect on the properties of bipolymeric microstructures: during the cycles of substitution of different liquids in the same solvents, the change in the size of the bend angle varies within 3 degrees. Because of these features it would be possible to use such bipolymeric elements for various microfluidic applications. We suggest that it would be feasible to integrate these structures into microchannels and use them as valves that would open or close depending on the solvent that is passing through.

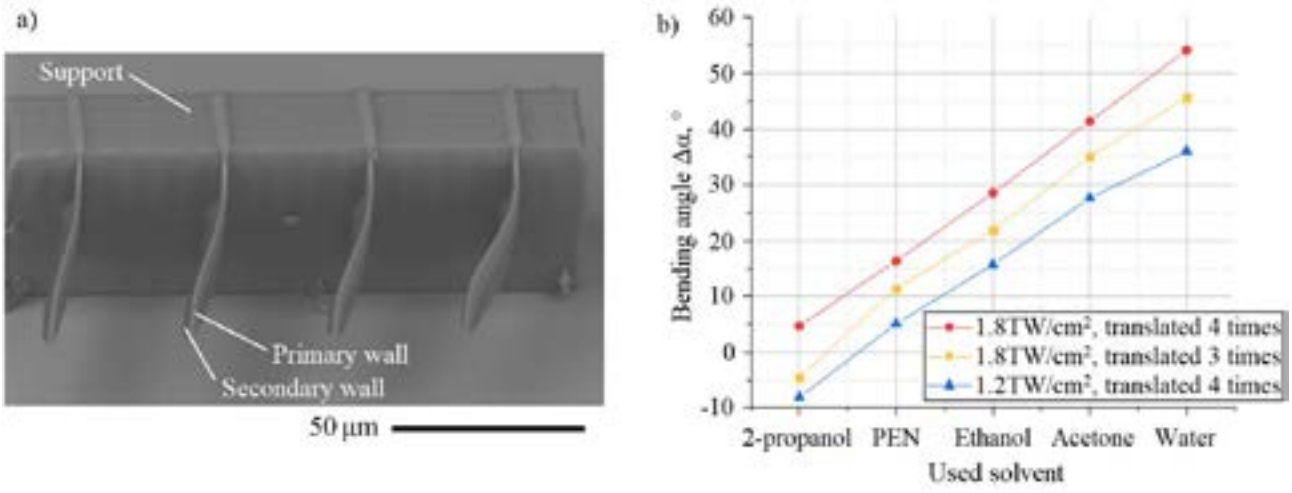


Fig. 1. SEM image of a structure with bipolymeric walls. Support and primary walls are fabricated out of SZ2080, secondary walls – out of PEG-DA-575 (a). Bending angle dependence on secondary walls fabrication parameters and solvent (b). (PEN - 4-methyl-2-pentanone)

[1] M. Malinauskas, G. Kiršanskė, S. Rekštytė, T. Jonavičius, E. Kaziulionytė, L. Jonušauskas, A. Žukauskas, R. Gadonas, and A. Piskarskas, Nanophotonic lithography: a versatile tool for manufacturing functional three-dimensional micro-/nano-objects, Lith. J. Phys. **52**, 312-326 (2012).

[2] M. Malinauskas, A. Žukauskas, S. Hasegawa, Y. Hayasaki, V. Mizeikis, R. Buividas, and S. Juodkazis, Ultrafast laser processing of materials: from science to industry, Light Sci. Appl. **5**, e16133 (2016).

[3] Y. Tian, Y.-L. Zhang, H. Xia, L. Guo, J.-F. Ku, Y. He, R. Zhang, B.-Z. Xu, Q.-D. Chena, and H.-B. Sun, Solvent response of polymers for micromachine manipulation, Phys. Chem. Chem. Phys. **13**, 4835-4838 (2011).

[4] S. Rekštytė, D. Paipulas, M. Malinauskas, and V. Mizeikis, Microactuation and sensing using reversible deformations of laser-written polymeric structures, Nanotechnology **28**, 124001 (2017).

# NONLINEAR REFRACTIVE INDEX MEASUREMENT IN THE INFRARED USING FEMTOSECOND LASER PULSES

Jurgita Strakšytė[1], Rytis Butkus[1], Gaudenis Jansonas[1]

[1]Laser Research Center, Faculty of Physics, Vilnius University, Lithuania
jurgita.straksyte@ff.stud.vu.lt

Nowadays the scientific research and experiments in the infrared (IR) attract a lot of interest as it is a promising area of high intensity laser physics, e.g. attosecond pulses generation [1]. However, even some parameters of optical materials used in the IR, are not well known. One of the most important parameters facilitating nonlinear phenomena is nonlinear refractive index or $n_2$.

In this work, determination of nonlinear refractive index using a standard z-scan [2] technique for various samples - fused silica, sapphire, BK7 and KGW are presented. The z-scan experiment was carried-out using femtosecond laser sources at infrared wavelengths.

The z-scan technique allows to easily determine nonlinear refractive index (NLR) sign and magnitude as well as the impact of nonlinear absorption (NLA). The z-scan measurements are performed by translating the sample along the beam propagation axis and measuring the phase variation behind the aperture with a detector. A typical closed aperture z-scan shows characteristic valley-peak curve which indicates positive $n_2$ sign. Nonlinear refractive index is determined from phase change ($|\Delta\varphi|$) which is calculated from normalized transmittance curve difference between valley and peak. ($\Delta T_{p-v}$) (Eq. (1,2)).

$$|\Delta\varphi| = \frac{\Delta T_{p-v}}{0{,}406(1-S)^{0{,}25}} \tag{1}$$

$$n_2 = \frac{k\Delta\varphi_0}{I_0 L_{eff}} = \left(\frac{\lambda}{2\pi}\right)\frac{\Delta\varphi_0}{I_0 L_{eff}} \tag{2}$$

Here S is linear transmission of an aperture, $I_0$ - peak intensity, $L_{eff}$ is effective sample length. The z-scan experimental setup for evaluation of the $n_2$ was developed, see Fig. 1. Here S - sample, $\lambda/2$ - half wave-plate, P1, P2 - Brewster type polarizers, L1, L2 - focusing lenses, BS - beam splitter, M - metal mirror, A - aperture, D1, D2 - detectors, F1, F2 - neutral density filters.

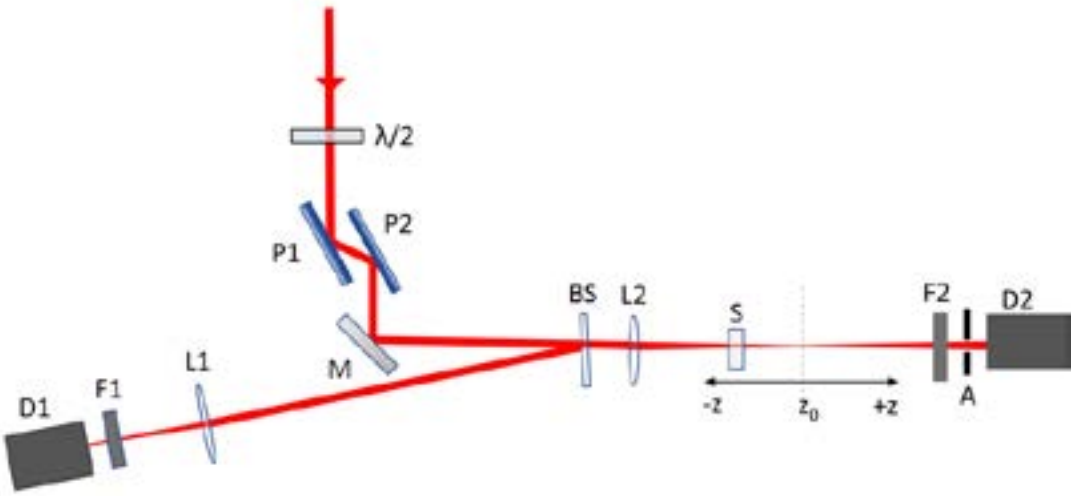


1 Fig.. Experimental scheme

The investigated optical materials were translated using a motorized delay line and the whole process of signal acquisition was automated and controlled via a LabView based program. From the closed and open aperture z-scan measurements, the nonlinear refractive index for fused silica, sapphire, BK7, KGW and AGS were determined and compared.

[1] S. Driever, K. B. Holzner, J.-C. Delagnes, N. Fedorov, M. Arnold, D. Bigourd, F. Burgy, D. Descamps, E. Cormier, R. Guichard, E. Constant, and A. Zaır, Near infrared few-cycle pulses for high harmonic generation, J. Phys. B - At. Mol. Opt. Phys., **47**(20), 204013 (2014).

[2] M. Sheik-Bahae, A. A. Said, T. Wei, D. J. Hagan, E. V. Stryland, Sensitive measurement of optical nonlinearities using a single beam, IEEE J. Quantum Electron., **26**(4), 760-769 (1990).

# OUTPUT OPTIMIZATION OF X-RAY EMISSION INDUCED BY FEMTOSECOND BESSEL BEAM PULSES

Ernestas Nacius, Anton Koroliov, Artūras Plukis

Center for Physical Sciences and Technology, Industrial laboratory for photonic technologies,
Saulėtekio av. 3, Vilnius, Lithuania
*Ernestas.nacius@ftmc.lt*

Ultrashort laser pulses are able to produce emission of high energy photons by interacting with electrons of matter atoms [1]. Due to huge amounts of energy disposed in ultrashort pulse, radiation of X-rays with pulse duration as same as invoking pulse can be generated. This way is alternative method of generation of X-rays instead of using high power synchrotrons [2]. High energy and low repetition rate Gaussian beam pulses are usually used. However, with high pulse energies, saturation of X-ray radiation is observed. This is due to plasma screening effects [3]. Saturation problem might be reduced by forming Bessel beam pulses, which have larger axial focus plane thus making same energy distribution spread in bigger volume. This method provides with X-ray emission in whole focus volume.

In this work we investigate X-ray emission output optimization, both theoretically and experimentally. Focusing conditions of Gaussian and Bessel beams are compared. Experimental part is carried out by focusing ultrashort pulses in chamber filled with noble gases and generated X-ray emission spectra is registered with spectrometer. Also the best pulse parameters are experimentally found and chosen to give best results. Additionally VIS spectra is also registered showing difference between comparing beams (Fig. 1).

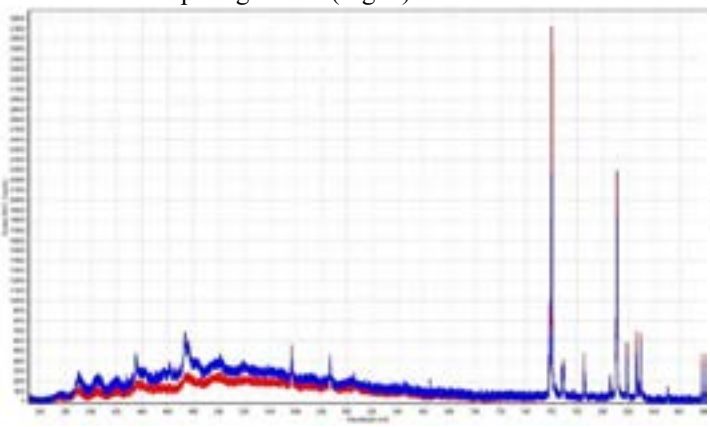

Fig. 1 VIS spectrum of Krypton gases using Gaussian (red) and Bessel (blue) beam focusing.

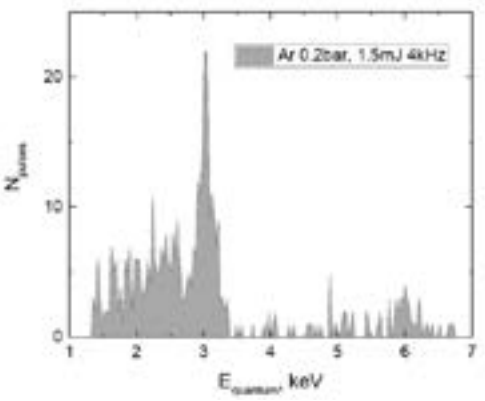


Fig. 2 X-ray spectrum of generated plasma in Argon gases using Gaussian beam. $K_\alpha$ emission peak is at 2.96 keV.

[1] T. Tajima and J. M. Dawson. Laser Electron Accelerator, Physical Review Letters, 1979, 43, 267–270
[2] E. Esarey, C. B. Schroeder, W. P. Leemans, Physics ofblaser-driven plasma-based electron accelerators, Reviews of Modern Physics 81 (3) (2009) 1229-1285
[3] U. Inan and M. Golkowski, Principles of Plasma Physics for Engineers and Scientists. Cambridge: Cambridge University Press, 2011.

# WIDE-BANDWIDTH NOPCPA PUMPED WITH "M"-SHAPED PICOSECOND PULSES

Augustinas Petrulenas[1], Paulius Mackonis[1], Vytenis Girdauskas[1], Aleksej M. Rodin[1,2]

1. Solid State Laser laboratory, Department of Laser Technologies, Center for Physical Sciences and Technology, Savanoriu 231, LT-02300 Vilnius, Lithuania

2. Ekspla Ltd, Savanoriu 237, LT-02300 Vilnius, Lithuania

augustinas.petrulenas@gmail.com

Since the first Optical Parametrical Chirped Pulse Amplifier (OPCPA) [1] was demonstrated in 1992, many different architectures of high–intensity OPCPA systems have been developed. Supercontinuum generation (SC) in the wavelength range from ~ 500 nm to ~ 1000 nm with picosecond pump pulses [2] simplifies the OPCPA architecture [3] due to the inherent signal and pump synchronization. The temporal shape of the pump pulse determines the spectral bandwidth of amplified pulses. We demonstrate a compact TW-class VIS-IR wavelength range NOPCPA with an almost lossless spectral bandwidth due to the formation of "M"-shaped ps pumping pulses after the SHG-conversion. Moreover, the reuse of depleted pulses after the 1st SHG stage increases the overall efficiency.

Compressed pulses with an energy up to 21 mJ, pulse width of 1.15 ps and excellent beam quality $M^2$ ~ 1.1 at a wavelength of 1030 nm were obtained from a two-cascaded double-pass CPA-compressor based on Yb:YAG rods [3]. A small fraction of this output was used to generate SC in a 15 mm YAG rod**.** Under optimal excitation conditions, the stability of SC pulse energy and beam pointing in the wavelength range from 600 to 1000 nm is several times greater than the source stability [4]. The second harmonic was generated in two successive cascades based on LBO and BBO crystals with a conversion of 62% and 70% respectively (Fig. 1, left), their overall efficiency reached 90%. The picosecond "M"-shaped pulses (Fig 1,right – left inset) were formed after the 1st SHG cascade due to the strong depletion of fundamental radiation.

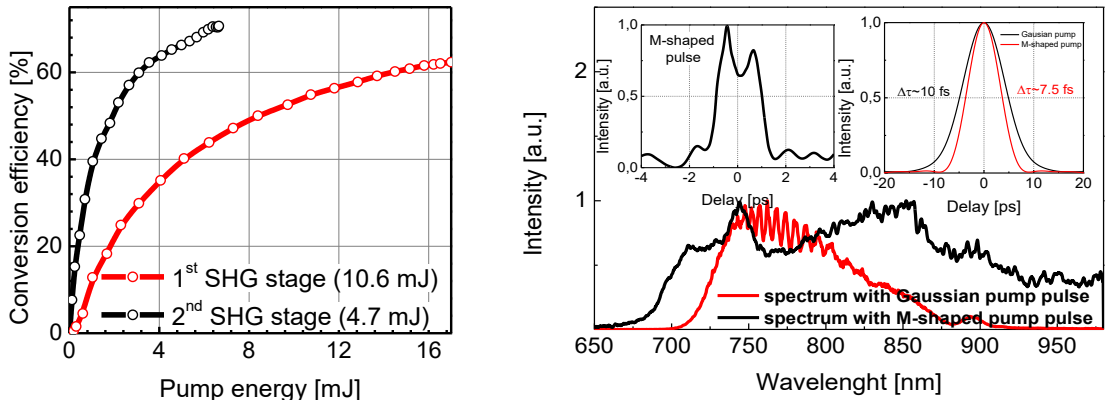


**Fig. 1.** SHG conversion efficiency for the 1st (red) and 2nd (black) SHG cascades – left. The spectra of NOPA output with Gaussian (red) and "M"-shaped (black) pumping pulse – right. Cross-correlation of the "M"-shaped pumping pulse – left inset and the Fourier transform of experimentally obtained output specrtra with Gaussian (red) and "M"-shaped pump pulses (black) -right inset.

The M-shaped ps pulses were used to pump the first two NOPA stages based on BBO crystals. A significantly wider spectral bandwidth (Fig. 1, right) is achieved, while the energy recycling after SHG stage also increases the overall NOPCPA conversion efficiency. The output energy after the first two NOPA stages exceeds 0.2 mJ. Our calculations demonstrate a significant decrease in the output pulse width (Fig. 1, right – right inset) from 10 fs (black) to 7.5 fs (red) due to the "M"-shaping of picosecond pump pulses.

[1] A.Dubietis, G. Jonušauskas and A.Piskarskas. "Powerful femtosecond pulse generation by chirped and stretched pulse parametric amplification in BBO crystal." *Optics Communications*88.4-6 (1992): 437-440. https://doi.org/10.1016/0030-4018(92)90070-8

[2] L.Indra, F.Batysta, P.Hribek, J.Novak, Z.Hubka, J.T.Green, R.Antipenkov, R.Boge, J.A.Naylon, P.Bakule, and B.Rus, Picosecond pulse generated supercontinuum as a stable seed for OPCPA, Optics Letters Vol.42, N4, pp.843-846 (2017). https://doi.org/10.1364/OL.42.000843

[3] A.M. Rodin and P. Mackonis, 1 TW-Class OPCPA pumped with fiber laser seeded two-cascaded Yb:YAG rod amplifier-compressor, Papers of International Conference on Lasers and Electro-Optics Pacific Rim "CLEO-PR'2018", Hong Kong, paper Th2D.3, 29 July – 3 August 2018. https://doi.org/10.1364/CLEOPR.2018.Th2D.3

[4] P. Mackonis, A. Petrulenas, V. Girdauskas, A. Rodin, Observation of a stable supercontinuum from 1100 nm to 2400 nm in YAG pumped with 1.2 ps pulses for a cost-effective 1 TW-class OPCPA, 8th EPS-QEOD Europhoton Conference, paper TuPD4, Barcelona, 2–7 September 2018.

# INVESTIGATION OF SUPERCONTINUUM GENERATION IN PHOTONIC CRYSTAL FIBER USING BURSTS OF TWO FEMTOSECOND PULSES

Miglė Kuliešaitė, Julius Vengelis

Laser Research Center, Faculty of Physics, Vilnius University, Lithuania
migle.kuliesaite@ff.vu.lt

Supercontinuum generation is a phenomenon, when spectrum of a short pulse expands hundreds or thousands of times. The spectrum broadening is usually achieved by launching optical pulses through a nonlinear medium. Photonic crystal fibers (PCFs) can be used as a nonlinear medium for generation of supercontinuum. The use of PCFs for supercontinuum generation enabled its use in many applications such as spectroscopy, optical coherence tomography, frequency metrology, etc. [1-2]. Usually a train of ultrashort pulses is used as pump for supercontinuum generation.

In this study we present experimental results of our investigation of supercontinuum generation in photonic crystal fiber using bursts of two femtosecond pulses. The pump source for supercontinuum generation was a femtosecond Yb:KGW laser oscillator generating 1030 nm wavelength 76 MHz repetition rate and 90 fs duration pulses. A burst of two pulses was created using a setup consisting of a beamsplitter and Brewster-type polarizer. Due to the use of a polarizer, the burst consisted of two orthogonal polarization pulses which were directed to the PCF. For supercontinuum generation, we used a 27.6 cm long polarization-maintaining highly nonlinear PCF. The PCF had core diameter of 1.8 $\pm$ 0.3 μm and average pitch of 1.19$\pm$ 0.3 μm. The PCF zero group velocity dispersion wavelengths for slow polarization mode are at 807$\pm$ 2 nm and 1040 $\pm$ 7 nm, whereas for fast polarization mode they are at 838 $\pm$ 2 nm and 1059 $\pm$ 9 nm. During the experiment, the energy ratio between the horizontal and vertical polarization beams was adjusted. While changing the temporal delay of the vertical polarization pulse in the burst with respect to the horizontal polarization pulse in the burst, the aggregated spectra of the generated supercontinuum of both orthogonal polarization modes were measured.

The generated supercontinuum spectrum extended from roughly 510 nm to 1300 nm. Supercontinuum spectra created by orthogonal polarization modes are slightly different due to somewhat different PCF dispersion for orthogonal polarization modes, so the observed spectrum is actually an aggregated spectrum of two supercontinua corresponding to orthogonal polarization modes. We determined that when temporal delay between the pulses in the burst is small, interaction between the pulses in the burst and/or the generated supercontinua corresponding to orthogonal polarization modes occurs resulting in broader aggregated supercontinuum spectrum. When temporal delay between pulses in the burst is zero, the aggregated supercontinuum spectrum is widest (Fig. 2).

This study is partially supported by the Lithuanian Research Council (LMT).

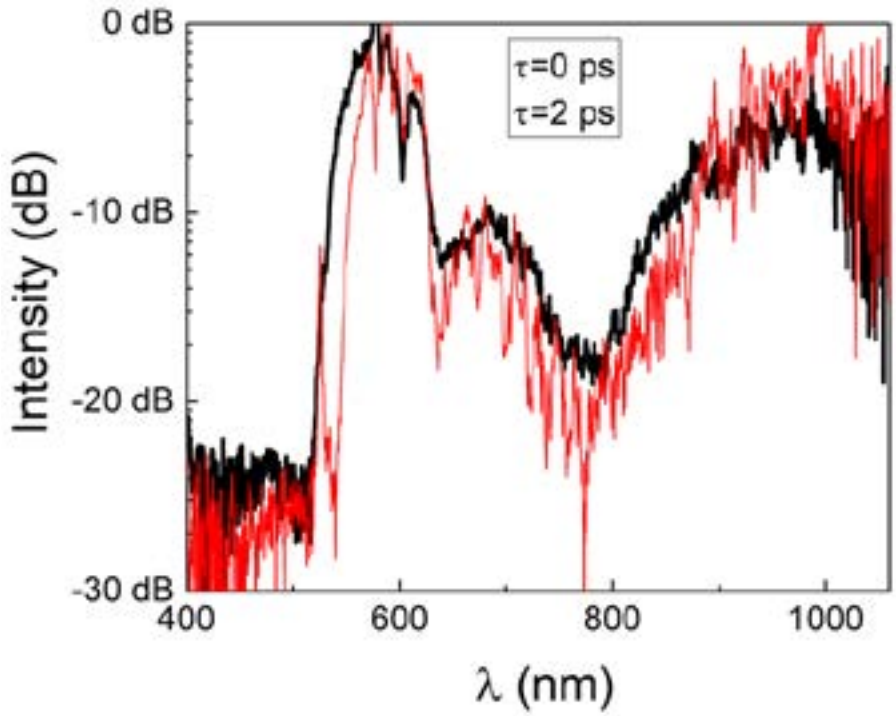


Fig. 1. Supercontinuum spectra: black curve − temporal delay between pulses in the burst is zero; red curve − two picoseconds.

[1] J. M. Dudley, G. Genty, S. Coen, Supercontinuum generation in photonic crystal fiber, Reviews of modern physics **78**, 1135–1183 (2006).
[2] G. Gentry, S. Coen and J. Dudley, Fiber supercontinuum sources, J. Opt. Soc. Am. B **24** (8), 1771-1785 (2007).

# RECONSTRUCTION OF DOT-MATRIX HOLOGRAM PARAMETERS ACCORDING TO HOLOGRAM IMAGE

Tomas Klinavičius[1], Mindaugas Juodėnas[1], Tomas Tamulevičius[1,2]

[1] Institute of Material Science of Kaunas University of Technology, K. Baršausko St. 59, LT-51423, Kaunas, Lithuania
[2] Department of Physics, Kaunas University of Technology, Studentų St. 50, Kaunas LT-51368, Lithuania
tomas.klinavicius@ktu.edu

Holographic security labels create colorful images when illuminated and are widely used for anti-counterfeiting applications. One widespread technology to realize such labels is dot-matrix holograms [1]. A dot-matrix hologram typically consists of a two dimensional array of spots that contain diffraction gratings with selected pitch and orientation imposed on a reflective surface. When the holograms are viewed by the observer under arbitrary illumination the off plane light diffraction from the hologram is actually seen and it can be described employing conical diffraction formalism [2]. Due to the complex nature of diffraction description it is difficult to determine the hologram parameters (each pixel diffraction grating pitch and orientation) before beginning their lengthy production procedures.

The problem of hologram diffraction image rendering on known hologram parameters and illumination conditions has already been solved [3]. This work explores the reverse – determination of parameters necessary to ensure that the produced hologram would look exactly as the selected colored target image under known illumination and observation conditions. Such an algorithm has a range of practical applications in the fields of dot-matrix hologram design and authorization.

The proposed algorithm considers the parameters of the target hologram image itself such as CIE 1931 colour coordinate of each pixel from a selected digital image as well as the hologram illumination conditions such as the angle of incidence and spectrum of incident light along with observation conditions of the hologram like the position of the observer and the observers' aperture diameter.

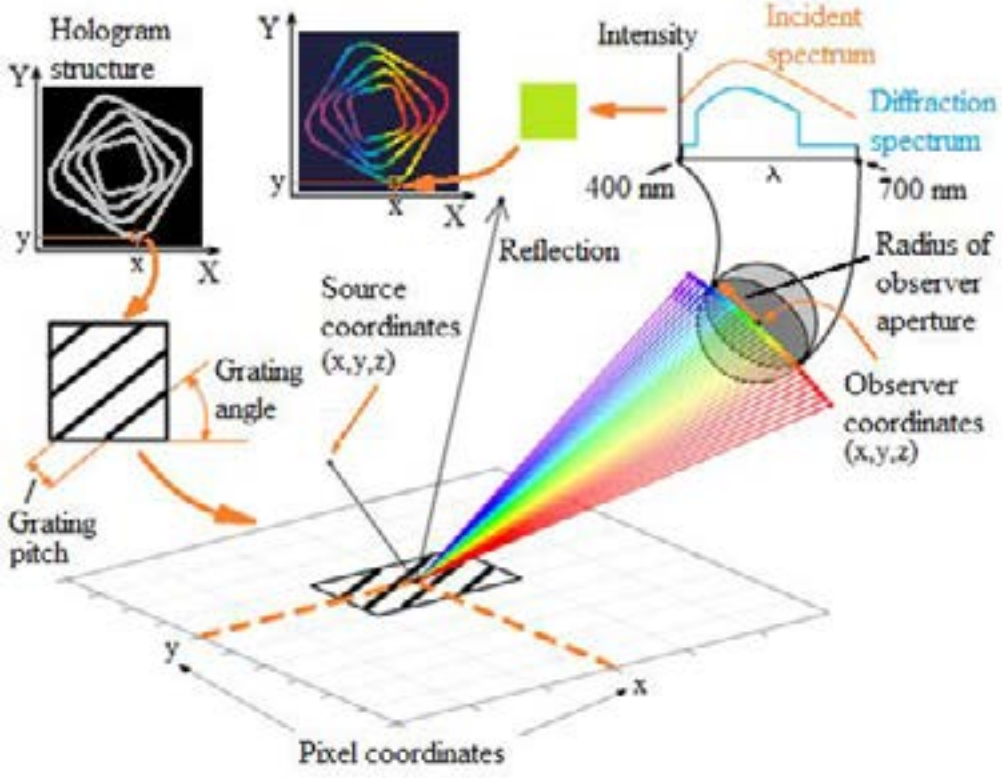


Fig. 1. The basic algorithm of rendering hologram images from their project file

[1] C. Braig, et al., *An EUV beamsplitter based on conical grazing incidence diffraction*, Optics Express 20, 1825-1838 (2012).
[2] D. Pizzanelly, *The development of direct-write digital holography,* Technical review, Holographer.org.
[3] T. Tamulevičius, M. Juodėnas, T. Klinavičius, et al. *Dot-matrix hologram rendering algorithm and its validation through direct laser interference patterning.* Scientific Reports 8, 2018. DOI: https://doi.org/10.1038/s41598-018-32294-5

# ASTIGMATISM MITIGATION IN OFF-AXIS TWO MIRROR TELESCOPE

Ramūnas Logminas[1], Arūnas Varanavičius[1]

[1] Laser Research Center, Vilnius University, Lithuania
ramunas.logminas@gmail.com

In ultrashort pulse laser systems, the dispersion free off-axis mirror telescopes are used for manipulating of beams sizes. The tilting of mirrors gives rise to geometrical beam aberrations and the astigmatism arising in off-axis mirror telescopes usually is more pronounced aberration affecting the focal spot size of the beam. The astigmatisms of optical systems lead to formation of two-line foci in vicinity of beam waist and the distance between these two foci can be used for evaluation of amount of beam astigmatism [1]. Strehl ratio is another parameter that is used for characterization of aberrated beams. Strehl ratio includes all aberrations impact on a beam quality (Strehl ratio=1, means no aberrations in a beam; the lower Strehl ratio the bigger aberrations impact and worse beam quality) [2].

It is already has been shown that a two-spherical mirror telescope can be used for the purpose of magnification or reducing of a laser beam with limited distortion that is due to aberrations [3]. The astigmatism in mirror telescope made of convex and concave mirrors can be avoided by choosing proper mirror misalignment angles. For collimated beams:

$$\theta_2 = \sqrt{-\frac{f_2}{f_1}\frac{\theta_1}{\left|1-\frac{d}{f_1}\right|}}\ , \qquad (1)$$

here $\theta_1$ – beam incidence angle to mirror telescope; $\theta_2$ – beam incidence angle to second telescope mirror; $f_1$, $f_2$ – first and telescope mirrors focal length points; d – distance between mirrors.

In this presentation we are reporting on the results of computer modeling and experimental investigations of astigmatism compensation in simple two spherical mirror telescopes.

Main components of experimental scheme were two mirror telescopes. First mirror telescope was set for low angles, so it had no contribution for astigmatism in a beam, its purpose was to expand beam in a compact way and to control beam collimation. Second mirror telescope was built by using convex and concave mirrors and rotational stages for each telescope mirror that during experiment He-Ne laser beam incidence angle to first and second mirror telescope could be changed.

Experimental results for collimated beam at different incidence angles to mirror telescope, when telescope magnification is 2.5 times, are shown in Fig. 1.

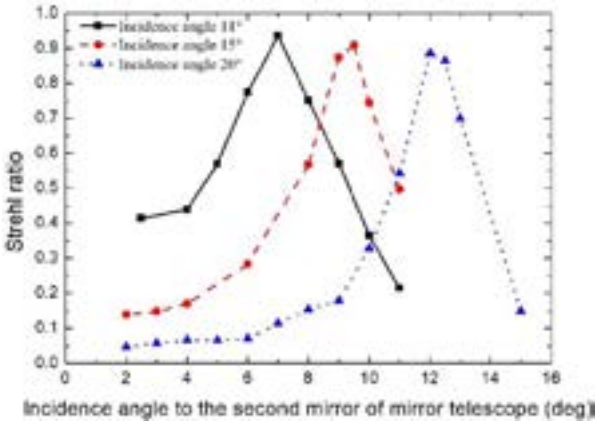


Fig. 1. Beam Strehl ratio dependence on incidence angle to second telescope mirror for different incidence angles to mirror telescope

The results presented in Fig.1 show that there is an incidence angle to second telescope mirror at which astigmatism, created by mirror telescope, is removed/greatly reduced. The astigmatism compensation was observed at particular mirror misalignment angles when increasing beam incidence angle to telescope up to 20 degrees.

Experimental results show that when the telescope magnification was increased to 5 times, the astigmatism, caused by off- axis mirror telescope, can be reduced in same efficiency as for telescope with magnification of 2.5.

In case when incident beam to mirror telescope is non-collimated, mirror telescope caused astigmatism also can be greatly reduced but less efficient compared to collimated beam at same incidence angle to mirror telescope.

The results of computer modeling of light beam propagation through off-axis misaligned mirror telescope qualitatively corresponds to our experimental findings.

[1] E. Hecht, *Optics* (Addison Wesley, San Francisco, 2002).
[2] Michael J. Kidger, *Intermediate Optical Design* (SPIE, Bellinham, Washington USA, 2004).
[3] P. Hello and C. N. Man, Design of a low-loss off-axis beam expander, Applied Optics **35**, 2534-2536 (1996).

# INVESTIGATION OF DAMAGE MECHANISMS OF TRANSPARENT MEDIA AND DIELECTRIC COATING BY ULTRFAST SPECTROSCOPY

Aivaras Pečiulis, Mikas Vengris

Laser Research Center, Vilnius University, Lithuania
aivaras.peciulis@ff.stud.vu.lt

Laser induced damage of optical components is one of the factor slowing down the development of laser technologies. As lasers' pulse peak power and radiation frequency grows, optical elements execute more functions, determining not only their laser induced damage threshold (LIDT), but understanding the whole mechanism that causes the damage would allow to seek even higher achievements in laser technologies. In this investigation, ultrafast spectroscopy methods are used to observe and analyze damage and aging processes of borosilicate glass bulk and titanium dioxide ($TiO_2$) dielectric coating.

Measurements of both transparent media bulk and dielectric coating were made using a "single-shot" method where one pump pulse shots to one sample point at which the difference transmittance spectra is being detected. Exclusion of a single pulse and moving of the sample is necessary because the object might get damaged after the first pulse. The absorption spectra is measured at the same moment (*During*), 1ms after (*After*) and from 1ms to 1s after (*Long after*) the pump pulse – this allows us to track the kinetics of induced damage in the sample.

The main results of borosilicate glass (thickness 0.17mm) bulk and titanium dioxide coating are show in Fig 1(a) and (b), respectively. Difference transmittance dependence on pump pulse energy density shows LIDT of both samples (~1.91J/cm$^2$ for glass and ~2.20J/cm$^2$ for coating) and the difference between damage observation points in time, which shows the versatility of used measuring technique and the advantage over usual LIDT testing methods.

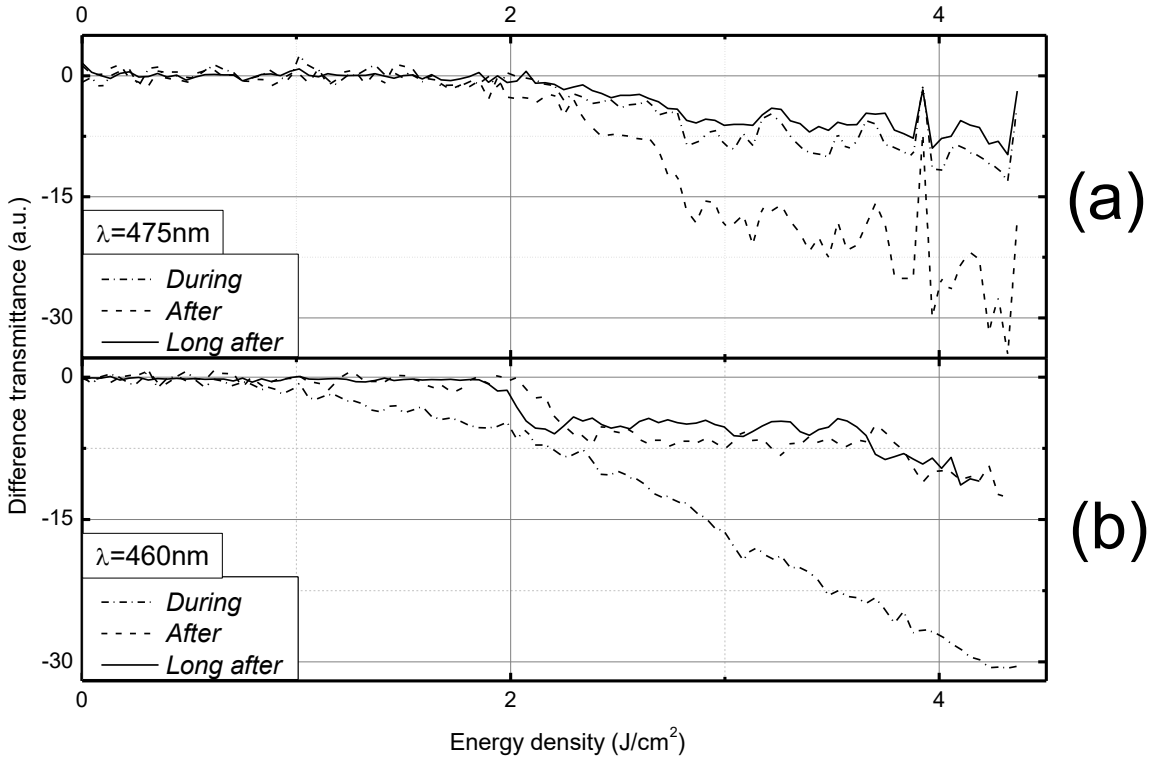


Fig. 1. Difference transmittance dependence on energy density of (a) borosilicate glass at 475nm; (b) titanium dioxide dielectric coating at 460nm.

The whole laser induced damage measuring system was assembled and tested with these primary measurements. As now we can record difference transmittance and absorption spectra in femtosecond resolution, more measurements are going to be made to inspect various materials and dielectric coatings for their LIDT and to determine damage mechanisms. Observing spectral similarities between different materials and coatings will help to understand the physical properties of the damage itself and to offer solutions how the damage can be controlled.

# OPTICAL FILAMENT INDUCED LUMINESCENCE IN LASER MEDIA

Akvilė Bunkevičiūtė, Balys Momgaudis, Mikas Vengris

Laser Reasearch center, Vilnius University, Saulėtekio Ave. 10, LT-10223 Vilnius, Lithuania
akvile.bunkeviciute@ff.stud.vu.lt

Luminescence – light emitting process when electron jumps from excited to a ground state. In order to observe this process within transparent medium a very strong electromagnetic field is required. Such intensities could be reached during experiments as cathodoluminescence, X-ray luminescence, photoluminescence, etc. In this work we are offering to use filaments of light in order to investigate luminescence spectrum and associated decay of excited states. This method is more convenient compared to cathodoluminescence or X-ray luminescence because specimen is excited by laser beam. In this way, we have system which is easily adjustable and has cheap, simple optics. Use of filaments in luminescence spectroscopy is a nondestructive way to examine transparent solid material in order to determine laser media quality.

Filament occurs when femtosecond laser pulses are focused onto transparent medium and generates wide spectrum coherent radiation – white light continuum. When light self-action occurs laser beam shrinks to micro-meter size and pulse spectrum spreads over several octaves. Filament excites impurities and charge carriers within medium. In this experiment luminescence is observed and registered from the side of the filament. In order to compare the optical quality of popular laser media crystals such as YAG, $A_2O_3$ and KGW, provided by different manufacturers spectra and luminescence decay characteristics were measured. By analyzing spectrum induced by light filament, it was possible to identify undesirable impurities and their amount in crystals. Luminescence decay measurements exposes the lifetime of states and reveals correlation between them.

In conclusion, filament luminescence is suitable way for medium quality investigation because different manufacturer specimens create specific luminescence spectra, varying in distribution of intensity and characteristic peaks.

Spectrum of YAG crystals reveals that intensive luminescence could be generated by lattice defects and transition metals. The spectra reveal a trace amount of Chromium ions. Non-homogeneous decay in short wavelength range was observed, possibly due to higher energy electron transition to lower energy states, within the band.

Luminescence in Sapphire could be generated by $F^+$ center defects and transition metal ions. The decay of the peak in UV region is correlated to peak in IR, which could indicate a transition between two distinct energy states (Fig. 1).

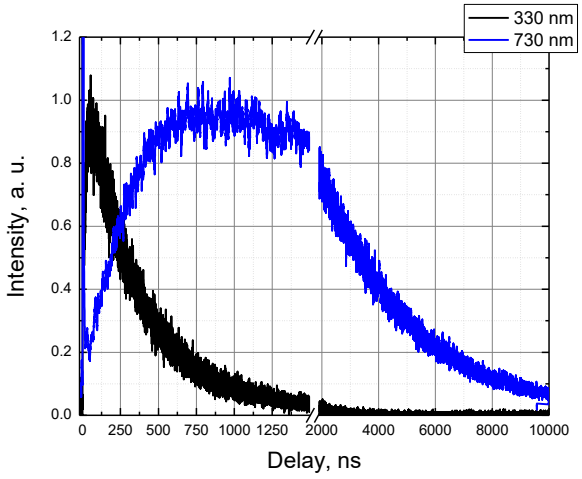


Fig. 1. UV region luminescence decay correlation with IR region in Sapphire crystal.

Luminescence peaks in KGW crystals could be created by rare earth and transition metal ions. KGW spectra hints that there is Europium and Terbium ions. The associated decay reveals that these ions creates long-lasting phosphorescence states, with possible impact on high repetition rate applications.

# STUDIES OF THE NV CENTERS $^{14}$N NUCLEAR SPIN ORIENTATION AND ALIGNMENT USING THE METHOD OF ODMR

Marcis Auzinsh[1], Andris Berzins[1], Dmitry Budker[2,3], Laima Busaite[1], Ruvin Ferber[1], Florian Gahbauer[1], Reinis Lazda[1], Arne Wickenbrock[2], Huijie Zheng[2]

[1]Laser Centre, University of Latvia
[2]Helmholtz Institute Mainz, Johannes Gutenberg University
[3]Department of Physics, University of California at Berkeley, USA
reinis.lazda@lu.lv

This work probes the energy levels of the NV centers in diamond using the ODMR spectroscopy method [1] at an axial magnetic field around 102.4 mT (GSLAC). At this magnetic field region the mixing of the hyperfine levels (of the ground state $m_s = 0 \longrightarrow m_s = \pm 1$ transitions) in the magnetic field can be studied (see Fig. 1).

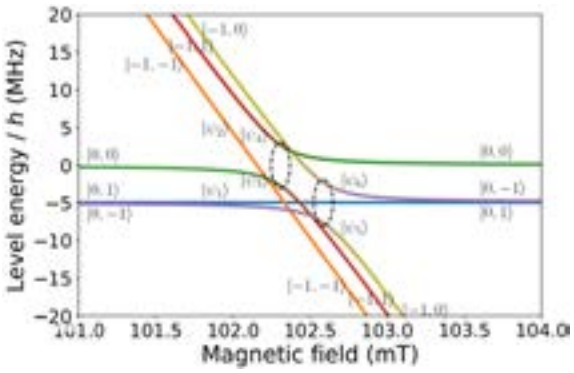


Fig. 1. Hyperfine level mixing near the GSLAC denoted by the dashed ellipses.

A theoretical model (using a Hamiltonian method [2]) that estimates the transition energies, transition probabilities between the ground-state sublevels and the hyperfine level mixing was developed. The model includes coupling to the nuclear spin of the NV center's $^{14}$N nucleus and coupling to $^{13}$C atoms as well.

Calculations from the model were combined with the measured results using a fitting procedure giving information about the polarization of the nuclear spin of the NV centers (see Fig. 2).

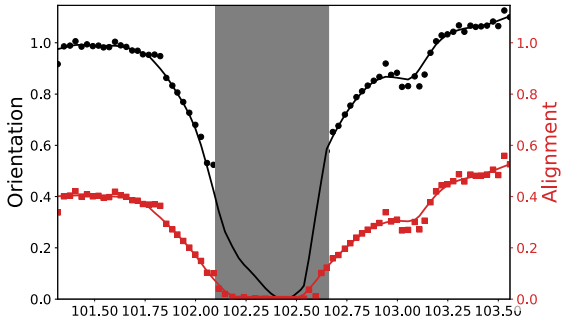


Fig. 2. Nuclear $^{14}$N spin orientation (black dots) and alignment (red squares) obtained for the ground state $m_S = 0 \longrightarrow m_S = +1$ transition from the fitted transition peak amplitudes.

**Acknowledgements**

The Riga group gratefully acknowledges the financial support from the M-ERA.NET project Metrology at the Nanoscale with Diamonds (MyND) and from the Laserlab-Europe Project (EU-H2020 654148), and from the Base/Performance Funding Project Nr. AAP2016/B013, ZD2010/AZ27. A. Berzins acknowledges support from the PostDoc Latvia Project Nr. 1.1.1.2/VIAA/1/16/024 "Two-way research of thin-films and NV centres in diamond crystal". The Mainz group acknowledges support by the German Federal Ministry of Education and Research (BMBF) within the Quantumtechnologien program (FKZ 13N14439) and the DFG through the DIP program (FO 703/2-1). H. Zheng acknowledges support from the GRK Symmetry Breaking (DFG/GRK 1581) program.

[1] M. Negyedi, J. Palots, B. Gyre, S. Dzsaber, S. Kollarics, P. Rohringer, T. Pichler and F. Simon, Rev. Sci. Instrum. **88**, 013902 (2017).
[2] J. D. A. Wood, D. A. Broadway, L. T. Hall, A. Stacey, D. A. Simpson, J.-P. Tetienne and L. C. L. Hollenberg, Phys. Rev. B **94**, 155402 (2016).

# ETCHING EFFECT ON LASER IRRADIATED ALKALI ALUMINOSILICATE GLASS

Kamilė Kasačiūnaitė[1], Antanas Urbas[1, 2], Sergejus Orlovas[1], Jurga Juodkazytė[1], Irena Savickaja[1], Vitalija Jasulaitienė[1]

[1] Center of Physical Sciences and Technology, Industrial Laboratory for Photonic Technologies, Lithuania
[2] Altechna R&D Ltd, Lithuania
kamile.kasaciunait@ftmc.lt

Femtosecond laser-induced chemical etching (FLICE) technology is a method consisting of two steps: 1) modification of the sample with a femtosecond laser and 2) chemical etching of modified sample [1]. FLICE method is being used to obtain various microstructures in glassy materials for micro-/nanofluidics and biofiltering.

This technology has been and still is very promising in the processing of different glasses. Therefore, there is a need for a better understanding of the process itself at a molecular level. The X-ray photoelectron spectroscopy (XPS) is an analytical technique that is widely used for chemical characterization of solids. In the case of glasses, XPS provides information about the surface composition, surface chemical state and ratio of non-bridging oxygen (NBO) to bridging oxygen (BO) amount. Figure 1 illustrates the difference between the O 1s spectra of unaffected aluminum silicate sample (a) and the one after laser irradiation (b). There is an obvious decrease in bridging oxygen BO2, which corresponds to Si-O-Al bonds and increase in non-bridging oxygen peak after the laser treatment [2].

It is proved that laser modified areas are etched by base or acid solutions much faster than unmodified ones. The femtosecond laser pulses tear the bonds between silicon and aluminum atoms, which are connected by bridging oxygen atoms, increasing the amount of non-bridging oxygen in the structure of alkali glasses. These reactive oxygen species are most likely readily attacked by OH- ions in KOH etching solution. Therefore, the unchained oxygen is supposed to be the main reason for accelerated etching in the laser modified regions. Nevertheless, the parameters of the laser are very important as well, the pulse energy dictates the number of non-bridging oxygens created in the glassy structure.

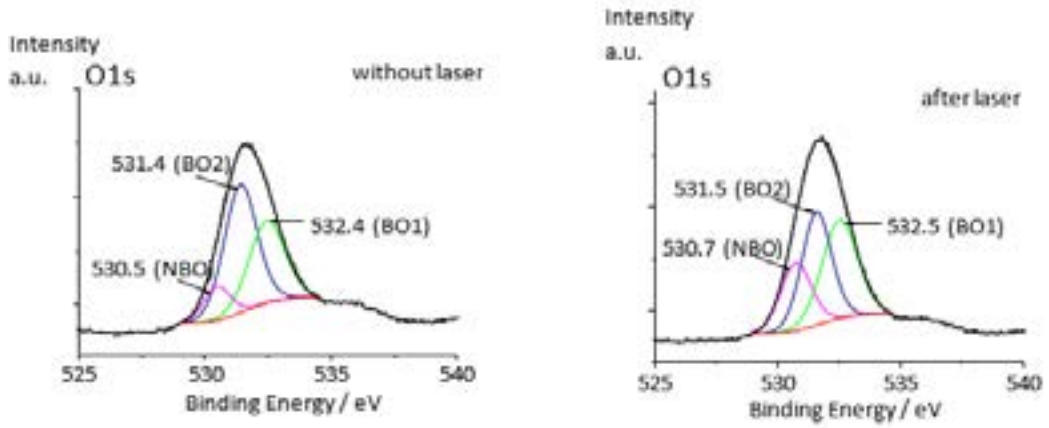


a) b)

Fig. 1. Core level O 1s spectra of (a) the unirradiated glass and (b) the irradiated sample (1028 nm, 80μJ, 20kHz, 7 J/cm$^2$) with deconvolution of NBO and BO1 (Si-O-Si) and BO2 (Si-O-Al) peaks by the least squares fitting routine of two Gaussian–Lorentzian peaks.

**Acknowledgement:** The research has been supported by the grant No. 09.3.3-LMT-K-712-10-0085 of Research Council of Lithuania.

[1] V. Stankevič, Formation and characterization of micro- opto-mechanical 3D devices for sensor application in transparent materials, doctoral thesis, Vilnius University, 2017.
[2] G.W. Tasker, D.R. Uhlmann, P.I.K. Onorato, M.N. Alexander and C.W. struck, Structure of Sodium Aluminosilicate Glasses : x-ray Photoelectron Spectroskcopy, Journal de Physique, 273 (1985).

# FOCUSING PROPERTIES SIMULATION OF COMPACT DIFFRACTIVE ELEMENT COMBINED WITH META-MATERIALS

Augustinas Karvelis[1], Linas Minkevičius[2]

[1] Faculty of Physics, Vilnius University, Lithuania
[2] Department of Optoelectronics, Center for Physical Sciences and Technology, Lithuania
augustinas.karvelis@ff.stud.vu.lt

Nowadays Terahertz (THz) radiation is actively used for imaging applications medical diagnostics, security inspection [1] or food and pharmaceutical industry [2]. Components of optical system should be compact and high efficiency. Diffractive components such as a metal zone plates and phase zone plates reduce the size of the optical systems [3] while meta-materials increase the efficiency of individual components and allow to control the parameters of the radiation.

The main goal of this work was to define the best meta-material design for focusing the 0.6 THz radiation. Dependency of focus efficiency and phase quantization level was also determined. Simulations were done using CST microwave studio program.

To achieve the focusing functionality, the split ring metasurface with various opening angles $\theta$ ware used. We have created two different designs (see Fig. 1) to identify the maximum transmission coefficient at 0.6 THz.

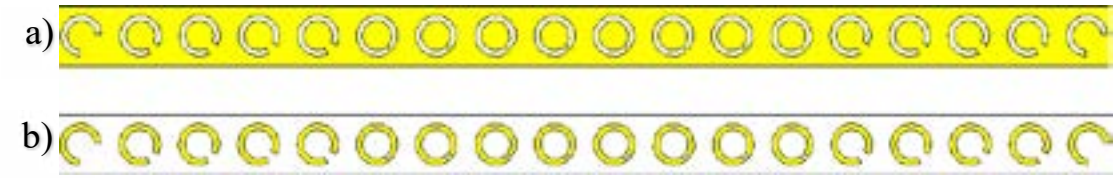


Fig. 1. 100-nm thick gold film on a silicon wafer with cutouts (a) and 100-nm split ring gold film matasurface on a silicon wafer (b).

Different opening angles $\theta$ were used in order to achieve the phase shift covering $2\pi$ range and nearly constant transmission amplitude simultaneously. The required phase distribution at the appropriate place in diffractive elements was obtained by cylindrical lens formula. Both designs of the diffractive element let to focus 0.6 THz radiation in the focal point of 4 mm is shown in Fig. 2.

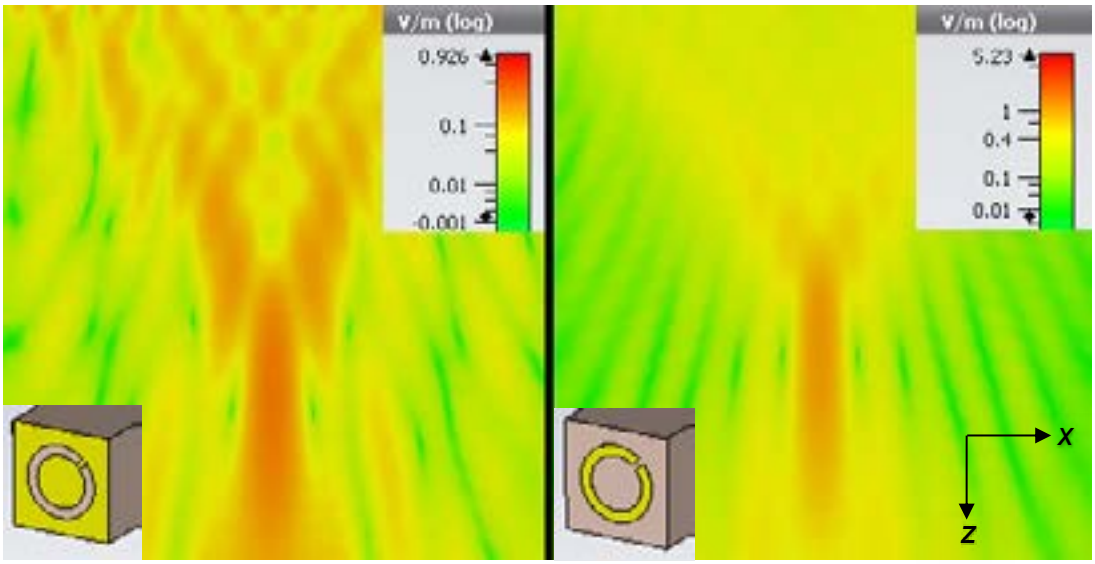


Fig. 2. Simulation result of different diffractive elements combined with split ring meta-materials.

To conclude, the focusing characteristics of the diffractive element consisting of ring-shaped metamaterials were theoretically evaluated and optimized design was estimated.

[1] V. Tamošiūnas, S. Indrišiūnas, M.Tamošiūnaitė ir kt., Focusing of Terahertz Radiation with Laser-Ablated Antireflective Structures, IEEE Transactions on Terahertz Science and Technology **8**(5), 541-548 (2018)
[2] L. Minkevičius, S. Indrišiūnas, R. Šniaukas ir kt., Compact diffractive optics for THz imaging, Lithuanian Journal of Physics **58**(1), 99-107 (2018).
[3] L. Minkevičius, K. Madeikis, B, Voisiat ir kt., Focusing Performance of Terahertz Zone Plates with Plates with Integrated Cross-Shape Apertures, Journal of infrared, millimeter and terahertz waves **35**(9), 699-702 (2014).

# FORMATION OF MICROLENSES ON FUSED SILICA‘S SURFACE BY EMTOSECOND LASER PULSES

Jonas Karosas, Valdemar Stankevič

The Center of Physical Sciences and Technology, Savanoriu Ave. 231, LT-02300, Vilnius, Lithuania
ELAS LTD, Savanoriu Ave. 235, LT-02300, Vilnius, Lithuania
jonas.k@e-lasers.com

It is possible to form micro lenses on fused silica’s surface by using femtosecond laser pulses, which can be used in fiber optics. Such formation of lenses is based on fabricating nanogratings modifications in transparent material and material elimination of modificated areas [1]. For making lenses it is necessary to reach quite good roughness, so they are etching in HF acid.

To define roughness the structures with different marking parameters, with 110 µm focusing depth, are fabricated in fused silica. Energy must be selected so that the sample through the entire depth of the structure could be made from nanogratings [2]. Fabricated structures are etched in HF 10% acid for 30 minutes, then the etching depth and the roughness are measured with profilometer. In the last step the structure is melted by hot concentrated flame and measured again to compare differences of the structure shape and roughness.

Using the results obtained before, spherical lenses on fused silica‘s surface is formed with radius of 1 mm and depth of 100 µm. Such formation of lens is based on concentric circles with different radius fabrication, except the circles are hatched with lines. After the fabrication the sample is etched in acid. Later the sample is measured with a profilometer and melted with hot flame. In the results the radiuses and focal lengths of lenses are calculated by formula:

$$\frac{1}{f} = (n-1)\left[\frac{1}{R_1} - \frac{1}{R_2} + \frac{(n-1)d}{nR_1R_2}\right]. \quad (1)$$

Micro lenses array is made from 7 lenses. Here lenses are formed so that after reaching 100 µm all circles are touching themselves forming one common area. The sample is also etched in acid and melted with flame. Such type of sample is characterized by certain wavelength because the area is wide enough for laser beam radius.

Tab 1. Parameters of structure.

| Focusing depth, µm | *f*, kHz | *E*, nJ |
|---|---|---|
| 100 | 500 | 100–150 |
| Pulse density, mm/s | *dy*, µm | *dz*, µm |
| 500-2000 | 1-5 | 5 |

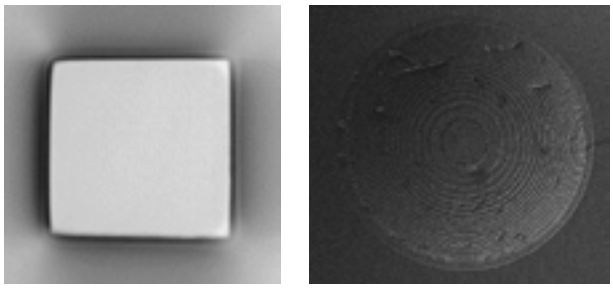

a) b)

Fig. 1. a) The view of square structure from its bottom, after 60 min of etching and 2 second of melting. b) The view of spherical lens after etching and melting. ($E$ = 200 nJ, $dy$ = 2,5 µm, $v$ = 5 mm/s).

Tab. 2. Spherical lenses radiuses and focal leghts after last machining.

| Nr. | 1 | 2 | 3 | 4 |
|---|---|---|---|---|
| *R* (mm) | 1,08 | 1,05 | 1,12 | 1,07 |
| *F* (mm) | 2,34 | 2,29 | 2,44 | 2,31 |

- The best surface roughness after etching is reached with 1000 imp/µm and distance of 2,5 µm between lines.
- In order to repeat the same micro lenses, melting should be more stable.
- In comparison of radius before and after last machining the result is 10% error.

[1] C. A. Ross, D. G. MacLachlan, D. Choudhury, R. R. Thomson, Optimization of ultrafast laser assisted etching in fused silica, Optics Express, **26**(19), 2018.
[2] V. Stankevič, *Formation and characterization of micro-opto-mechanical 3D devices for sensor application in transparent materials* (Doctoral dissertation, Technology Science, Material Engineering (08T), Vilnius, 2017.

# FATIGUE OF OPTICAL RESISTANCE IN DIELECTRIC COATINGS: INVESTIGATION OF SINGLE PULSE CONTRIBUTION USING DIGITAL HOLOGRAPHY WITH HIGH TEMPORAL RESOLUTION

Evelina Drobužaitė, Linas Smalakys, Balys Momgaudis, Andrius Melninkaitis

Laser Research Center, Department of Physics, Vilnius University, Lithuania
evelina.drobuzaite@ff.stud.vu.lt

Laser Induced Damage Threshold (LIDT) is a physical characteristic of optical component which defines a critical power or peak fluence of laser irradiation causing irreversible changes in materials structure. Optical materials exhibit LIDT fatigue effect: LIDT of dielectric materials for multiple pulse exposures is lower compared to single-pulse illumination [1]. It is essential to understand mechanisms that create optical fatigue in order to precisely predict multiple pulse damage threshold. Knowledge on damage threshold dependence on pulse quantity would lead to faster, less expensive and guaranteed way of predicting optical components fatigue behaviour which is necessary in order to create reliable optical systems.

In this work we did an investigation of optical fatigue effect using digital holography experimental setup which provides high spatial and temporal resolution phase and amplitude contrast pictures [2]. Also, defect pictures were taken with a Nomarski microscope. Optical fatigue effect was seen as a red spot appearing in Nomarski microscope pictures and as negative phase shift in phase contrast image. This experiment was done with a zirconium dioxide thin film on silicon dioxide substrate ($ZrO_2/SiO_2$). Sample was exposed to different pulse fluences from $0,19\,J/cm^2$ to $1,24\,J/cm^2$ and to different pulse quantities from $10^2$ to $10^6$. Experiments were carried out using 316 fs 1030 nm pump and 26 fs 539 nm probe pulses. We compared signals from phase contrast images with signals from Nomarski microscope reflectance pictures Fig. 1.

As can be seen in Fig. 1 (a) the negative phase shift is decreasing with increasing number of pulses. Different dependence on number of pulses is seen in Fig. 1 (b), signal is increasing with increasing number of pulses. These dependencies Fig. 1 indicate existence of two defect states: long-lived and short-lived. Short-lived defect states create negative phase shift and are generated with each pulse but through relaxation process between pulses turn into long-lived states. Long-lived states create positive phase shift but there is no relaxation, so, these states accumulate in a material. Long-lived defect state accumulation in Nomarski pictures is seen as brighter red spot formation and as negative phase shift decrease in phase contrast images Fig. 1.

According to Lorentz model for bound electrons short-lived state resonance frequency is higher and long-lived state resonance frequency is lower than probe frequency (2,3 eV). It is known that defect states in zirconium dioxide ($ZrO_2$) are created by oxygen vacancies and their resonance frequencies are in agreement with our results [3]. In conclusion, optical fatigue in zirconium dioxide ($ZrO_2$) is caused by accumulation of long-lived oxygen vacancy states.

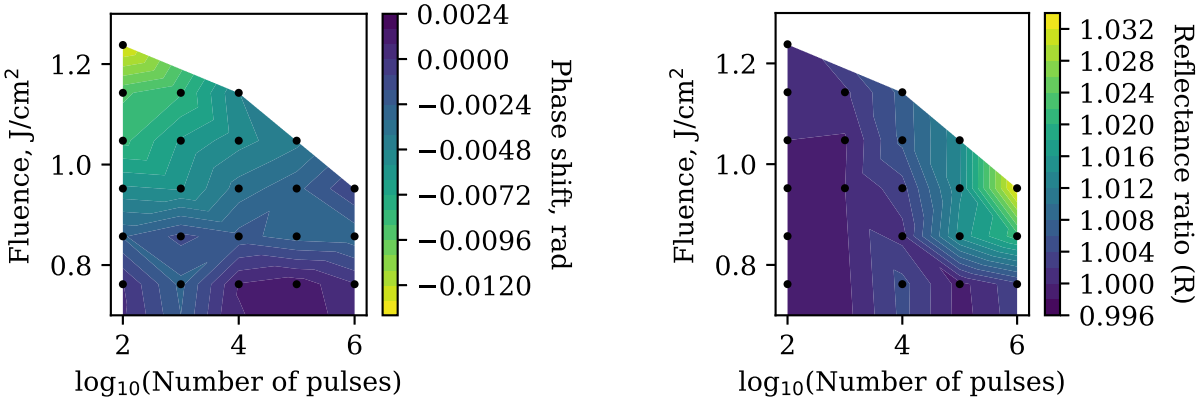


(a) Phase shift dependence on pulse energy and number of pulses.

(b) Nomarski microscope reflectance picture R chanel dependence on pulse fluence and number of pulses.

Fig. 1. Signals from phase contrast images and from Nomarski reflectance pictures.

[1] A. E. Chmel, Fatigue laser-induced damage in transparent material, Materials Science and Engineering B, **49**(3), 175-190 (1900).
[2] N. Šiaulys, L. Gallais, A. Melninkaitis, Direct holographic imaging of ultrafast laser damage process in thin films, Optics Letters, **39**(2), 2164- 2167 (2014).
[3] T. V. Perevalov, D. V. Gulyaev, V. S. Aliev et al., The origin of 2,7 eV blue luminescence band in zirconium oxide, Journal of Applied Physics, **116**(24), 2-6 (2014).

# VISUALISATION OF FEMTOSECOND LASER ABLATED MICROSTRUCTURES IN DLC:AG NANOCOMPOSITE THIN FILMS VIA MAPPING WITH SPECTROSCOPIC ELLIPSOMETRY

Justas Deveikis[1], Aušrinė Jurkevičiūtė[2], Tomas Tamulevičius[1,2], Sigitas Tamulevičius[1,2]

[1] Department of Physics, Faculty of Mathematics and Natural Sciences, Kaunas University of Technology, Studentų st. 50, LT-51368 Kaunas, Lithuania
[2] Institute of Materials Science of Kaunas University of Technology, K. Baršausko st. 59, LT-51423 Kaunas, Lithuania
justas.deveikis@ktu.edu

Diamond-like carbon (DLC) thin films are well known of their distinctive mechanical, optical, electrical and chemical properties [1]. Introducing free electron metal nanoparticles into DLC can be used to tailor the properties of films even further and opens up new possibilities in plasmonics. In this work, we investigated nanocomposite DLC films with embedded silver nanoparticles (DLC:Ag), irradiated by femtosecond laser. The analyzed films on the quartz substrate were deposited employing reactive magnetron sputtering of silver target in direct current mode under hydrocarbon atmosphere [2]. It was determined that the silver content in 60 nm thickness film was 12.6 at %.

Spectroscopic ellipsometry (SE) is a powerful optical measurement technique which is used to determine the change in polarized light upon reflection or transmission on a sample. This technique basically measures two parameters: amplitude ratio Ψ and phase difference Δ between *s* and *p* polarized waves [3]. Using these parameters, it is possible to calculate refractive index and the thickness of the film, deeper analysis provides information about surface roughness, etc.

Direct laser interference patterning (DLIP) was employed to impose periodic patterns in DLC:Ag films. A matrix of points varying applied number of pulses (1000-125000 pulses) and laser fluence (1-17 mJ/cm$^2$) was imposed. Total irradiated area was 300 × 300 μm$^2$. Data for preparing the SE map was acquired using spectroscopic ellipsometer GES5-E (Semilab). The angle of incidence was 75° and the step along *x* and *y* axis was 30 μm. Ψ parameter map was plotted at the wavelength of 690 nm and Δ was plotted at the wavelength of 640 nm (Fig. 1 a and b respectively). The wavelengths for different parameters Ψ and Δ map were chosen with highest differences in parameter values at different areas of the sample (Fig. 1c).

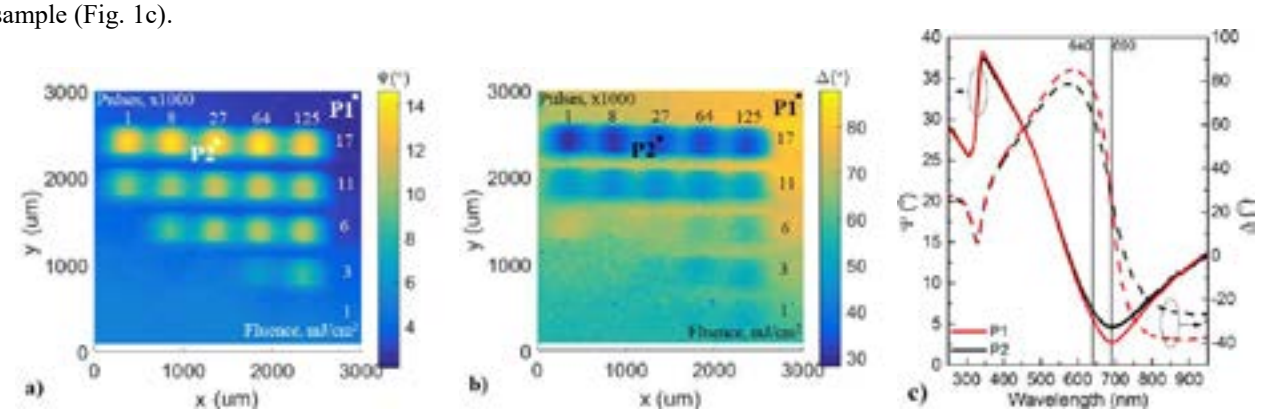


Fig. 1. Map of SE parameters of DLC:Ag nanocomposite film on quartz substrate: a) Ψ parameter at 690 nm wavelength; b) Δ parameter at 640 nm wavelength; DLIP fluence increases from bottom to top and number of pulses from left to right. c) Ψ and Δ dependencies on wavelength at two different sample locations identified (P1, P2) on the SE maps.

From the obtained SE maps, it is clear that increasing laser fluence provides highest differences in ellipsometric parameters. At fluences 6 mJ/cm$^2$ and lower, number of pulses becomes an important parameter. The further data analysis would lead to thickness decrease and refractive index modifications depending on applied number of pulses and laser fluence.

[1] J. Robertson, Diamond-like amorphous carbon, Master. Sci. Eng. R. Reports. **37**, 129-281 (2002).
[2] Sigitas Tamulevičius, Šarūnas Meškinis,Tomas Tamulevičius. Diamond like carbon nanocomposites with embedded metallic nanoparticles, Rep. Prog. Phys. **81**, 024501 (2018).
[3] H. Fujiwara. Spectroscopic Ellipsometry: Principles and Applications. 2007 John Wiley & Sons, Ltd. ISBN: 978-0-470-01608-4.

# PROPERTIES OF TERAHERTZ WAVE GENERATED BY LASER INDUCED AIR PLASMA

Danas Buožius[1], Maksym Ivanov[1], Illia Thiele[2]

[1] Vilnius University Laser Research Center, 10 Sauletekio avenue, LT-10223 Vilnius, Lithuania
[2] Chalmers University of Technology, 2B Fysikgarden, SE-41296 Gothenburg, Sweden
danas.buozius@ff.stud.vu.lt

Currently due to many applications in imaging and spectroscopy, terahertz (THz) radiation is a subject of great interest. One of the most efficient methods of creating very strong electric fields of THz radiation is using bichromatic femtosecond laser pulses consisting of the first and second harmonics (FH and SH, respectively) to create a plasma filament where THz pulses are emitted[1, 2]. In this research we examine polarization of THz wave as a function of polarizations of FH and SH and found conditions for the most efficient THz radiation generation. In addition, we have also conducted experiments studying properties of THz signal (modulation of intensity and azimuthal phase), emitted from laser induced plasma in air, when the SH pump was carrying an optical vortex charge. For the experiments we have used a Ti:sapphire laser system (Legend elite duo HE+, Coherent Inc.), delivering pulses with duration of 40fs (FWHM), central wavelenght of 800nm and a repetition rate of 1 kHz.

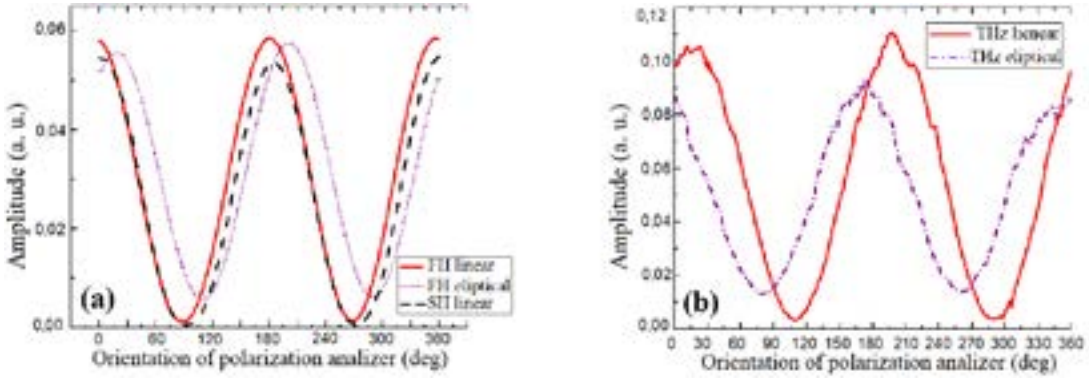


Fig. 1. (a) - FH and SH wave signal dependencies on orientation of analyzer; (b) - THz wave signal versus orientation of the analyzer for different ellipticies of the THz wave.

In the first experiment we used a Glan prism as an analizer to monitor polarizations of FH and SH, and a quarter-wave plate to change elipticity of these waves. By measuring amplitude ratios between the peak and minimum points (fig. 1(b)) it was found that THz frequency radiation has a higher elipticity of polarization than that of the pump (fig. 1(a)). We deduced that THz wave polarization depends on angle between lineary polarized pump beams as well as elipticities of FH and SH beams. Making pump polarizations parallel to each other not only increased THz signal but also decreased elipticity of THz wave. When polarizations of FH and SH were slightly eliptical (1:10 and 1:122 for the FH and SH, respectively), THz elipticity was higher, 1:7. This ratio increased to 1:25 after changing elipticities of FH and SH to 1:58 and 1:122.

In the second experiment we used s-waveplate in order to generate an optical vortex in the SH beam. FH beam remained Gaussian. Using method of THz wave generation from air plasma, radiation is being generated in a conical shape [3] thus, no significant change in beam shape is being observed when changing shape of a pump beam. We used a thermographic camera to observe THz signal spatial distribution. To estimate azimuthal phase distribution of the THz wave we used a Mickelson interferometer or a cilindrical mirror. We have compared THz beam profiles obtained under two different generation conditions: when there was an optical vortex charge in one of the excitation beams; and when both pump beams were Gaussian. We have found that when SH is an optical vortex, THz radiation also carries some properties of optical vortex which was found by examining its intensity distributions in focal plane of the cilindrical mirror, as well as by observing shifts of fringes in the THz interferogram.

Therefore we investigated THz wave polarization dependence on pump wave polarizations; and THz signal when there is an azimuthal phase modulation one of pump beams. We believe that the presented investigations will open new routes towards an active control of ultra-broadband THz beam properties.

[1] Mark D. Thomson, Markus Kreß, Torsten L¨offler, and Hartmut G. Roskos, Broadband THz emission from gas plasmas induced by femtosecond optical pulses: From fundamentals to applications, Laser and photonics reviews vol. 1, no **4**, 349-368 (2007).
[2] Mark D. Thomson, Volker Blank, and Hartmut G. Roskos, Terahertz white-light pulses from an air plasma photo-induced by incommensurate two color optical fields, Optics express, vol. **18**, no. 22, 23173-23182 (2010).
[3] Pernille Klarskov, Andrew C Strikwerda, Krzysztof Iwaszczuk and Peter Uhd Jepsen, Experimental three-dimensional beam profiling and modeling of a terahertz beam generated from a two-color air plasma, New journal of physics, vol. **15**, no. 7, 75012-75026 (2013).

# HIGHLY FOCUSED VECTOR COMPLEX SOURCE BEAMS AND THEIR INTERACTION WITH CLUSTERS OF NANOPARTICLES

Justas Berškys[1,2], Sergejus Orlovas[1]

[1] Center for Physical Sciences and Technology, Sauletekio av. 3, Vilnius, Lithuania
[2] Faculty of Physics, Vilnius University, Sauletekio av. 9, Vilnius, Lithuania
justas.berskys@ftmc.lt

Among the active fields of research in nanosciences are nanoparticles and their properties. The Mie theory was the very first description of light interaction with a particle and it was extended for describing the interaction with highly focused beams. The polarization properties of highly focused electromagnetic beams strongly influence the size and shape of the focal spot of the beams. Analytical vectorial solutions of Maxwell's equations describing highly focused and variously polarized vector complex source vortex beams [1] are used to investigate interaction with nanoparticles. In recent publications, the interaction between such beams and nanoparticles has been investigated [2,3]. Creation of artificial structures, where chirality is controlled via shape and geometry, is enabled by modern micro- and nano-fabrication techniques. A similar optical behavior can result also from purely geometrical properties of a three-dimensional arrangement of nanoobjects without chirality, such as nanospheres

In this work, the so-called T-matrix and MSM (multiple scattering matrix) methods are used to calculate fields scattered from a chiral cluster of nanoparticles. The incoming fields are calculated from a scalar wave equation using the complex source beam (CSB). From a scalar solution we can derive vectorial solutions using classical technique, which is described in [4]. The electric field can be expressed in terms of multipole functions Eq. (1) as

$$\mathbf{E}_{inc}(\mathbf{r}) = \sum_{n=1}^{\infty}\sum_{m=-n}^{n} A_{mn}\mathbf{M}_{mn}(\mathbf{r}) + B_{mn}\mathbf{N}_{mn}(\mathbf{r}). \tag{1}$$

Here coefficients $A_{mn}$ and $B_{mn}$ describe the incident field, which is related to the scattered field via a T-matrix. The T-matrix depends on the geometry of the particles configuration [5], so the scattered field is

$$\mathbf{E}_{sca} = \mathbf{T} \times \mathbf{E}_{inc} \tag{2}$$

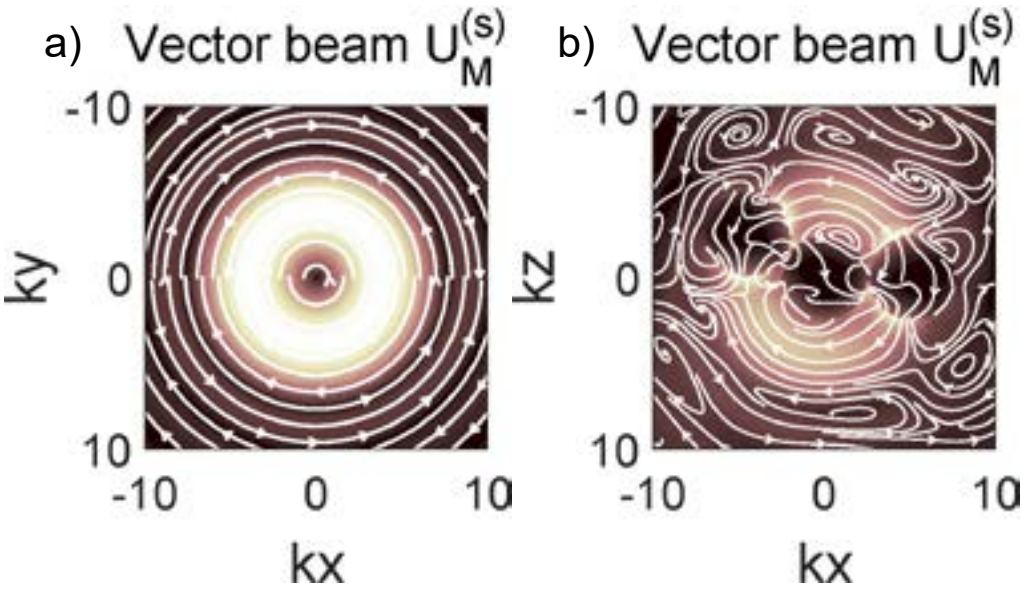


Fig. 1. Incoming beam (a) and the nanoparticles response after scattering (b).

Furthermore, we investigate different polarization states of the incident beam and their interaction with nanoclusters, see Fig. 1.

[1] S. Orlov and P. Banzer, Phys. Rev. A. **90**, 023832 (2014).
[2] P. Banzer, U. Peschel, S. Quabis, and G. Leuchs, Opt. Express, **18**, 10905 (2010).
[3] S. Orlov, U. Peschel, T. Bauer, and P. Banzer, Phys. Rev. A **85**, 063825 (2012)
[4] J. Stratton, Electromagnetic Theory, An IEEE Press classic reissue (Wiley, 2007).
[5] B. Peterson and S. Strom, Phys. Rev. D 8, 3661 (1973).

# MAGNETIC FIELD IMAGING FOR DESCRIPTION OF MAGNETIC THIN FILMS USING NITROGEN VACANCY CENTERS IN DIAMOND CRYSTAL

Andris Berzins[1], Janis Smits[1], Arturs Smiltnieks[1], Marcis Auzinsh[1], Ruvin Ferber[1], Andrejs Cebers[2]

[1] Laser Centre, University of Latvia, Latvia
[2] Laboratory of Magnetic Soft Materials, University of Latvia, Latvia
andris.berzins@lu.lv

Nitrogen-vacancy (NV) centers in diamonds have proven to be useful for the imaging of magnetic fields created by various magnetic structures [1-3]. When a thin layer of NV centers is located close to the surface of a diamond, magnetic field distributions at the position of the NV layer can be imaged. We have constructed a magnetic field microscope and are using it to study field distributions created by magnetic structures in (and on) thin films made from different materials.

As an example of the measurements in Fig. 1. an optical image in combination with magnetic image can be seen. In the pictures one can see a surface of a thin film made from $(Cr_{0,5}Mn_{0,5})_2GaC$ with some defects on the surface. The strongly magnetic defects are $Mn_5Ga_8$ or $Cr_5Ga_8$, but the nonmagnetic defects are pure Gallium.

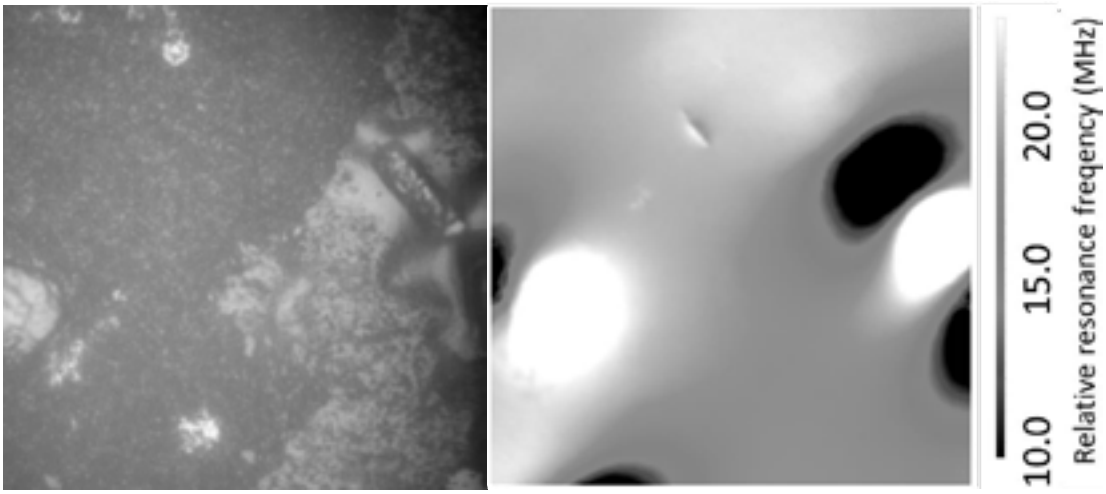


Fig. 1. On the left side – optical image, on the right – magnetic image. The color scale shows the relative resonance frequency of the optically detected magnetic resonance. The field of view is ~30x30 µm.

In perspective similar measurements will be done for imaging of magnetic phase transitions of thin films near liquid nitrogen temperatures. As the diamond is chemically, mechanically and temperature resistant the NV centers in diamond crystal has a great potential for characterization of magnetic thin film properties at different production phases.

A. Berzins acknowledges support from PostDoc Latvia project 1.1.1.2/VIAA/1/16/024 "Two-way research of thin-films and NV centres in diamond crystal" and LLC "MikroTik" donation, administered by the UoL foundation, for opportunity to improve experimental set-up. The Laser Centre group gratefully acknowledges support from Base/ Performance funding projects Y5-AZ27 and Y9-B013.

[1] J. Smits *et al*, Eur. Phys. J. Appl. Phys **73** 20701 (2016).
[2] L. M. Pham *et al*, New Journal of Physics **13** 045021 (2011).
[3] D. Le Sage *et al*, Nature **496** 486 (2013).

# VECTOR BESSEL BEAMS FOR ULTRASHORT PULSE INDUCED MODIFICATIONS IN TRANSPARENT MATERIALS

Justas Baltrukonis[1], Vytautas Jukna[1], Sergej Orlov[1]

[1] Center for Physical Sciences and Technology, Industrial Laboratory for Photonic Technologies, Saulėtekio al. 3, LT-10257 Vilnius, Lithuania
justas.baltrukonis@ftmc.lt

Over the years, Bessel beams gain popularity in laser microprocessing of transparent materials due to unique properties: nondiffractive propagation, extended focus, easy control of beam size, which makes them perfect for applications like high aspect ratio micro void formations [1] and transparent material cutting using induced micro crack propagation techniques [2, 3]. It is noticed, that asymmetric beam profile is the key for crack propagation direction control, which allows ultra-fast glass cutting over non-straight lines [3]. The glass modifications using variations of nondiffracting beams with asymmetric profiles and/or different polarizations are highly investigated to enhance the quality of current process or to find new applications in glass processing industry.

In this work we use an s-plate [4] (Workshop of Photonics) to generate azimuthally or radially polarized beam and with introduction of an axicon we produce vector Bessel beams. These beams are exceptional due to their complex spatial distribution of polarization and symmetric doughnut shaped profile. Polarizer is used to separate single polarization component constituting vector Bessel beam. Intensity distribution of single polarization component shows two peaks that do not diffract over a long distances and the rotation of intensity peaks is dependent on polarizer rotation (Fig. 1). Due to ability of s-plate to withstand high-energy pulses this approach to generate vector Bessel beams is applicable to high-energy beam systems and allows us to investigate volume modification and microcrack formation in various transparent materials.

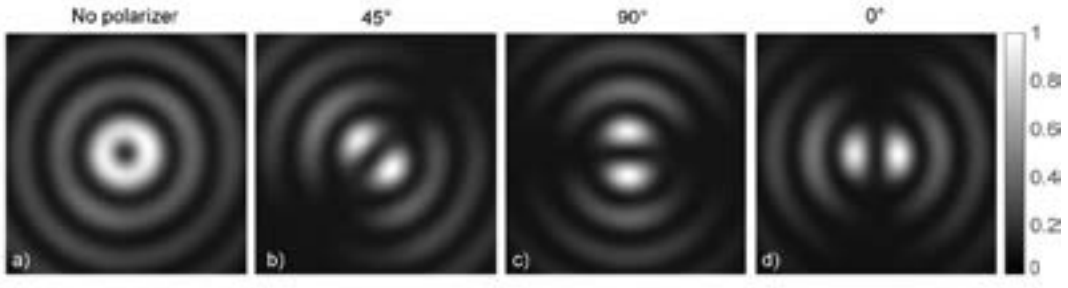


Fig. 1. Transverse intensity profiles of experimentally generated radially polarized vector Bessel beam (a) at the center of the Bessel zone and its single polarization component at different polarizer rotation angles (b, c, d).

**Acknowledgement:** The research has been supported by the grant 09.3.3-LMT-K-712-10-0193 of Research Council of Lithuania.

[1] M. K. Bhuyan, P. K. Velpula, J. P. Colombier, T. Olivier, N. Faure, and R. Stoian, "Single-shot high aspect ratio bulk nanostructuring of fused silica using chirp-controlled ultrafast laser Bessel beams", Appl. Phys. Lett. **104**, 021107 (2014).
[2] K. Mishchik, R. Beuton, O. Dematteo Caulier, Stefan Skupin, B. Chimier, et al. "Improved laser glass cutting by spatio-temporal control of energy deposition using bursts of femtosecond pulses", Opt. Express, **25**, 33271-33282 (2017)
[3] J. Dudutis, P. Gečys, and G. Račiukaitis, "Non-ideal axicon-generated Bessel beam application for intra-volume glass modification", Opt. Express, **24**, 28433-28443 (2016).[4] M. Beresna, M. Gecevičius, P. G. Kazansky and T. Gertus, "Radially polarized optical vortex converter created by femtosecond laser nanostructuring of glass", Appl. Phys. Lett. **98**, 201101 (2011).

# GOLD NANORODS VERSUS NANOSPHERES IN SURFACE-ENHANCED RAMAN SCATTERING

Liudmila Trotsiuk, Hanna Matsukovich

B.I. Stepanov Institute of Physics, National Academy of Sciences of Belarus, Belarus
mila_tro@yahoo,com

Since the moment of discovery the effect of surface-enhanced Raman scattering (SERS) in 1974, it has found wide application: in biosensors for detection of different types of cancer as well as Alzheimer's and Parkinson's diseases, for the gas phase detection of chemical warfare agents, in electrochemistry and catalysis, in the detection of single molecules etc [1]. Continuously, investigations are underway to improve the method and search for new directions of its application. The last decade, the attention of researchers is focused on anisotropic nanoparticles. Because of the presence of a second (morphological) localized surface plasmon resonance, that is much more sensitive to the environment, than the usual one, it is possible to increase significantly a detection limit of this method of analysis.

Gold nanorods are one of the most popular types of anisotropic nanoparticles with a well-known and relatively simple method of synthesis [2,3]. Due to the longitudinal (morphological) plasmon resonance that can be tuned in visible and near-IR region of the spectrum by controlling the aspect ratio of nanorods, they are a promising tool for SERS obtaining.

In this work, we compared the efficiency in SERS analysis the gold nanorod and nanospheres substrates at the different wavelength excitations (532 and 785 nm).

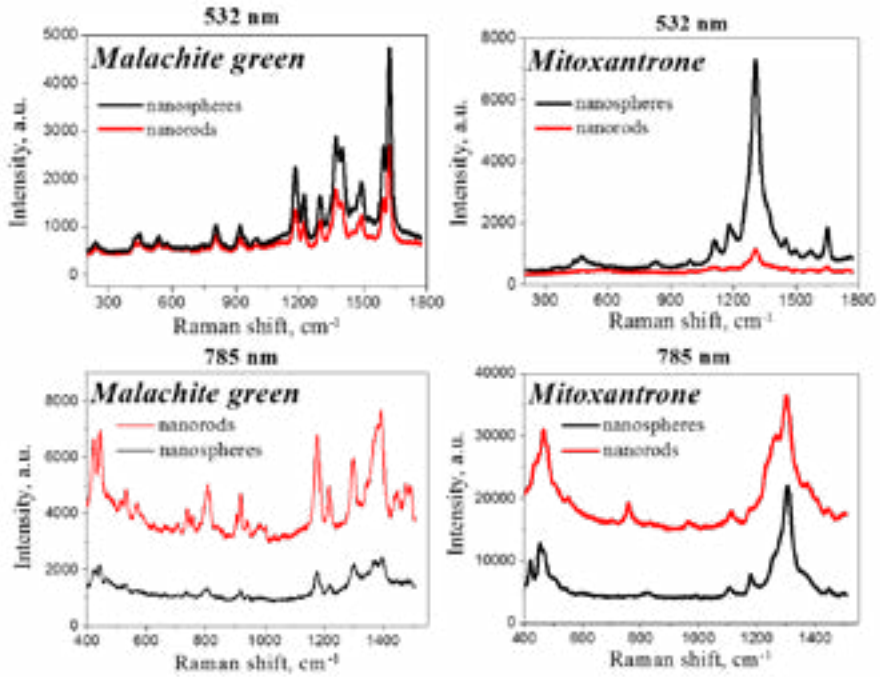


Fig. 1. SERS spectra of organic dyes on gold nanorod and nanosphere substrates.

We found that at 532 nm excitation wavelength gold nanospheres are more effective in SERS than gold nanorods. SERS intensity in the case of malachite green was 1.6-1.8 times higher on the nanosphere substrate than on the nanorod one. In the case of mitoxantrone, nanospheres were 6-8 times sensitive than nanorods. The using of more long-wave excitation (785 nm) increases significantly the SERS efficiency of gold nanorods, compared with nanospheres. SERS intensity of malachite green on nanorods was 3-3.5 times stronger than on nanospheres, for mitoxantrone the difference in intensities was nearly 2 times. Thereby, gold nanorod substrates are prospective materials for obtaining strong SERS signals at the excitation in near-IR region, which has some advantages over excitation in visible range like reduced fluorescence and photochemical processes in a sample.

[1] B. Sharma, R. R.Frontiera, A. I. Henry, E. Ringe, R. P. Van Duyne, SERS: Materials, applications, and the future, Materials today **15**, 16-25 (2012).
[2] N. R. Jana, L. Gearheart, C. J.Murphy, Seed- mediated growth approach for shape- controlled synthesis of spheroidal and rod- like gold nanoparticles using a surfactant template, Advanced Materials **13**, 1389-1393 (2001).
[3] B. Nikoobakht, M. A. El-Sayed, Preparation and growth mechanism of gold nanorods (NRs) using seed-mediated growth method. Chemistry of Materials **15**, 1957-1962 (2003).

# THERMOPHYSICAL LIMITATIONS FOR FIBER-OPTIC PHOTOACOUSTIC TRANSDUSERS BASED ON NANOSTRUCTURES

Alena Mikitchuk, Konstantin Kozadaev

Department of Radiophysics and Computer Technology, Belarusian State University, Belarus
m.helenay@yandex.by

Wideband ultrasound is a powerful diagnostic tool for advanced applications such as biomedical high-resolution high-contrast imaging and non-destructive analysis [1,2]. Number of studies of ultrasonic transducers have been conducted because ultrasonics offers very high-resolution diagnostics due to the relatively small speed of sound within the most part of liquids and solids. But, there are some limitations for effective ultrasound generation. Conventional piezoelectric are quite bulky, low-speed and unreliable. Furthermore, the attenuation of ultrasound is very high even at the sub-gigahertz frequencies [2,3]. Thus, the minimal thickness of the active layer within the ultrasound generator is required. However, wideband ultrasound can be generated by irradiating the optical absorber with a modulated optical signal in order to create, by conversion of optical power into heat, a rapid and localized temperature fluctuations [1-3]. These fluctuations in turn produces mechanical oscillations with ultrasound frequencies by thermal expansion. Fiber-optic generators based on the photoacoustic effect are very small, flexible and movable. Moreover, they are characterized by high electromagnetic immunity, dielectric design and chemical durability [4]. Nanostructures on the surface of an optical fiber edge are able provide very high absorbtion (up to 90%) within the thickness of nanoparticle (NP) monolayer. In our previous papers [4,5], it is shown that absorbed optical power can be higher than 50 mW for surface Au and Ag nanostructures. Due to very high absorbtion of modulated laser radiation, nanostructure thermal failure can occur. Moreover, in the case of water surrounding, boiling as well as cavitation processes are takes place near the nanostructure, limiting the performance of the fiber-optic photoacoustic transduser. In this paper we present theoretical investigation of thermophysical limitations for fiber-optic photoacoustic transdusers based on nanostructures.

It is assumed that absorbtion of laser radiation by the monolayer of noble metal nanoparticles takes place in water surrounding. Au and Ag NPs are deposited on the surface of the optical fiber edge. The simulation of the nanostructure temperature variation is performed in time by means the CST Microwave Studio Student Edition. The unit cell of the NP monolayer contains two infinite osculating parallelepipeds, one of them is optical fiber edge and another is water surrounding. NP is placed within the interface region between the surface and surrounding on the surface of the substrate. The contact between the NP and fiber core is located only in surface plane, assuming the NP volume to be wholly placed into the water. Spatial optical power density is assumed to be constant. Fig. 1. shows maximal temperature within the nanostructure on the optical fiber edge under illumination with laser vs NP radius and surface occupation density for Ag and Au based nanostructure. One can see that increasing of surface occupation density results in decreasing of the maximal temperature, at the same time radius increasing in turn leads to temperature increasing. Thus, in the worst case of 50 mW absorbed power, thermal effects do not limit the performance of the fiber-optic photoacoustic transduser based on Ag NPs with radius less than 25 nm and Ag NPs with radius less than 20 nm.

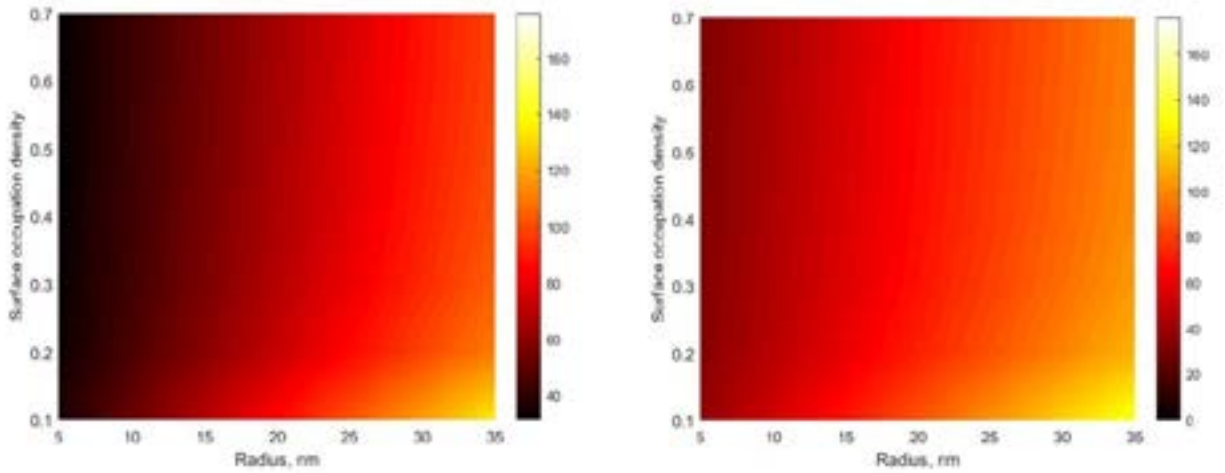


Fig. 1. Maximal temperature within the nanostructure on the optical fiber edge under illumination with laser versus NP radius and surface occupation density (absorbed power is assumed to be of 50 mW, optical signal is meander with period of 1000 ns, duty circle is 50%) for Ag (left) and Au (right) NPs based nanostructure

[1] R. Smith, A. Arca, X. Chen, et al, J. of Phys.: Conf. Ser. 278, 012035 (2011).

[2] H.Yang, K. Jin-Sung,A. Shai, et al, Appl. Phys. Lett. 91, 073507 (2007).

[3] Z. Xiaotian, W. Nan, T. Ye, et al, J. Acoust. Soc. Am. 137(1), 219 (2015).

[4] A.P. Mikitchuk, K.V Kozadaev, Quantum Electronics, 48(7), 630 (2018).

[5] A.P. Mikitchuk, K.V Kozadaev, Semiconductors.52 (14).1839 (2018).

# SEIRA FOR ADAMANTANE-CONTAINING MOLECULE

Anna Matsukovich, Darya Burak, Liudmila Trotsiuk

B.I. Stepanov Institute of Physics, National Academy of Sciences of Belarus, Belarus
a_matsukovich@tut.by

Infrared spectroscopy is a powerful tool widely used in research and industry for an identification of molecules. Its application to spectroscopic analysis of minute amounts of matter in sensing applications is hampered by the low infrared (IR) absorption cross-sections. Surface-enhanced infrared absorption (SEIRA) spectroscopy using resonant metal nanoantennas, or short resonant SEIRA, overcomes this limitation. SEIRA was found to be strongly dependent on the metal surface morphology that is the result of specific preparation conditions, such as substrate temperature, deposition rate, substrate material, and surface morphology [1]. In the present work, gold nanoparticles of different morphology have been synthesized and their impact was studied on IR absorption of 3-(adamantan-1-yl)-4-ethyl-1-[(4-phenyl-piperazine-1-yl)methyl]-1H-1,2,4-triazole-5(4H)-thione.

Infrared spectra (IR) were studied for 2 types of samples: the layer of molecules on the aluminum foil and that on the same foil with a layer of gold nanoparticles on top. IR spectra have been measured using a FT-IR spectrometer Nexus (Thermo Nicolet, USA) supplied with an IR microscope setup Continuum (Thermo Fisher Scientific, USA) with a 15x-objective.

Gold nanorods and nanospheres were synthesized by a seed-mediated growth method [2]. According to this procedure, at first, the seed solution was prepared by reduction of chloroauric acid ($HAuCl_4$) with sodium borohydride in the presence of cetyltrimethylammonium bromide (CTAB) as a stabilizer. Next, the growth solution was separately prepared, in which $Au^{3+}$ ions were reduced to $Au^{+}$ ions by ascorbic acid in the presence of CTAB and silver nitrate to facilitate the nanorod formation. The nanoparticle size and shape were controlled by amount of seeds that were added to the growth solution and the concentration of ascorbic acid. The resulting nanoparticles were covered with a 3.2 nm thick CTAB bilayer [3]. The optical density spectrum of gold nanorods has two broad plasmon peaks at 532 and 750 nm. Gold nanospheres coated with citrate-ion were prepared via standard Turkevich method [4] by the reduction of $HAuCl_4$ with sodium citrate at reflux. Citrate-ion played the role of both the stabilizer and the reducing agent. The optical density spectra of gold nanospheres stabilized with citrate-ion and CTAB have the plasmon peaks at 526 nm and 532 nm respectively.

It was shown (Fig.1a) that in the presence of gold nanospheres, the IR absorption of the molecule is increased up to 1.5 times. The presence of gold nanorods does not significantly affect the IR absorption of the molecules (Fig. 1b). Gold nanospheres stabilized with citrate-ion showed greater enhancement than gold nanoparticles stabilized by CTAB. This may be due to the smaller thickness of the stabilizer shell.

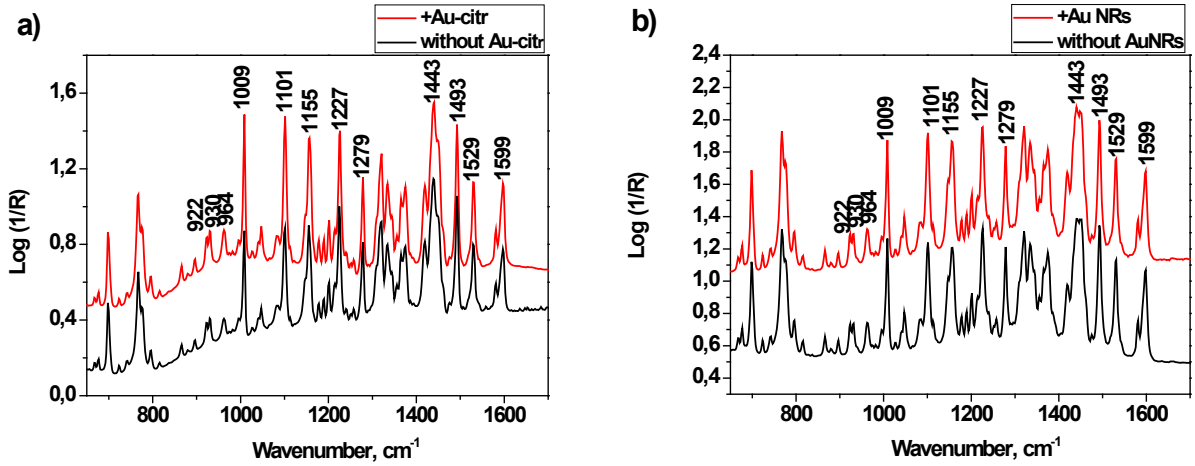


Fig.1 – Infrared absorption of 3-(adamantan-1-yl)-4-ethyl-1-[(4-phenyl-piperazine-1-yl)methyl]-1H-1,2,4-triazole-5(4H)-thione in the presence of a) Au nanospheres coated with citrate-ion and b) Au nanorods.

[1] Neubrech, F. et al., Surface-Enhanced Infrared Spectroscopy Using Resonant Nanoantennas, Chem. Rev. **117**, 5110-5145 (2017)
[2] Nikoobakht, B. et al., Surface-Enhanced Raman Scattering Studies on Aggregated Gold Nanorods, J. Phys. Chem. A **107**, 3372 (2003)
[3] Gómez-Graña, S. et al., Surfactant (Bi)Layers on Gold Nanorods, Langmuir **28**, 1453-1459 (2011)
[4] J. Turkevich et al., A study of the nucleation and growth processes in the synthesis of colloidal gold, Discuss. Faraday Soc. **11**, 55–57 (1951).

# SHELL-ISOLATED NANOPARTICLE-ENHANCED RAMAN SPECTROSCOPY OF RIBOFLAVIN MONOLAYER ADSORBED AT GRAPHENE

Agnė Zdaniauskienė, Tatjana Charkova, Ilja Ignatjev, Gvidas Astromskas, Rasa Pauliukaitė, Gediminas Niaura

Center for Physical Sciences and Technology, Lithuania
agne.zdaniauskiene@ftmc.lt

Electronic properties and function of graphene depend on the surface structure, origin of defects and adsorption of molecules at surface. Riboflavin can be employed in electrochemistry for different purposes as well as it can be detected electrochemically due to its aromatic nature. Riboflavin has been used as an electrode modifier in sensor construction for other important compounds such as iodate, hydrogen peroxide, persulphate [1].

Graphene science and development of graphene-based technologies requires to control adsorption processes and obtain molecular level knowledge of surface. To understand surface and interfacial chemistry, sensitive spectroscopic technique is needed. Surface-enhanced Raman spectroscopy (SERS) is one of the most sensitive surface analysis technique and fulfils such requirements. Unfortunately, SERS is limited by certain substrates (mostly Ag, Au, and Cu) and requirement to use roughened/nanostructured surface restrict the applicability of this method. Consequently, Tian et al. approached a novel SERS technique named ‘‘shell-isolated nanoparticle-enhanced Raman spectroscopy’’ (SHINERS). The method is based on enhancement of Raman signal by strong electromagnetic field provided by gold core nanoparticles surrounded by a few nanometer thick inert silica shell (Au@$SiO_2$) [2]. Recently, we employed SHINERS for analysis of monolayer at smooth gold Au in situ at controlled potential [3]. In this study, SHINERS was used to probe the structure of adsorbed riboflavin at graphene layers at molecular level.

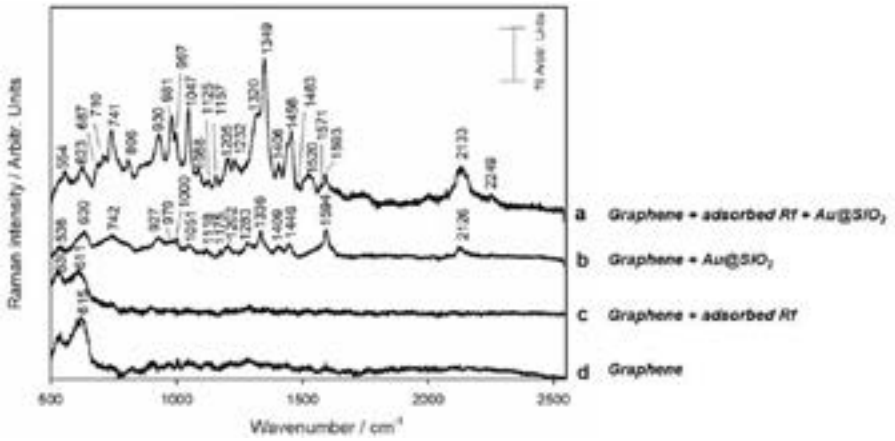


Fig. 1. Raman and SHINERS spectra of: a) adsorbed riboflavin onto graphene with Au@$SiO_2$; b) graphene substrate with Au@$SiO_2$; c) adsorbed riboflavin onto graphene; d) graphene substrate. Excitation wavelength is 785 nm.

It has been determined that bands from copper oxide, carbon network, defect sites and adsorbed riboflavin (Rf) are visible in SHINERS spectra. It allowed us to obtain all riboflavin characterized vibrational modes. To conclude, by adsorbing riboflavin molecules at surfaces of graphene, we have shown that SHINERS spectroscopy provides possibility to probe any adsorbed molecules at graphene.

[1] A. Radzevič, G. Niaura, I. Ignatjev, T. Rakickas, R. Celiešiūtė, R. Pauliukaitė, Electropolymerisation of the natural monomer riboflavin and its characterisation. Electrochimica Acta **222**, 1818–1830 (2016).

[2] J. F. Li, Y. F. Huang, Y. Ding, S. B. Li, Z. L. Yang, X. S. Zhou, F. R. Fan, W. Zhang, Z. Y. Zhou, D. Y. Wu, B. Ren, Z. L. Wang, Z. Q. Tian, Shelled-isolated nanoparticle-enhanced Raman spectroscopy. Nature, **464** (2010).

[3] A. Zdaniauskienė, T. Charkova, I. Matulaitienė, O. Eicher-Lorka, A. Matijoška, M. Skapas, A. Selskis, G. Niaura, Electrochemical shell-isolated nanoparticle-enhanced Raman spectroscopy: Bonding, structure, and ion-pairing of the positive charge bearing pyridinium ring terminated monolayer at smooth gold electrode. J. Phys Chem. C **122**, 1234−1242 (2018).

# NANO-COATING OF SEMICONDUCTING $C_{60}$ FULLERENE ON THE SURFACE OF A SUBSTRATE

Urol Makhmanov[1,2], Shukur Gofurov[1], Abdulmutallib Kokhkharov[1], Sagdilla Bakhramov[1], Donats Erts[2]

[1] Institute of Ion-Plasma and Laser Technologies, Uzbekistan Academy of Sciences, Uzbekistan
[2] Institute of Chemical Physics, University of Latvia, Latvia
urol_m@mail.ru

One of the most important tasks of modern nanotechnologies is the development of relatively inexpensive selective methods for the synthesis of new nanoscale structures and nanomaterials with new physical properties, as well as the generation of various functional devices based on them [1-2].

In this work, we obtained nanocoating based on semiconducting $C_{60}$ fullerene in the volume of the evaporating droplet on the surface of the mica substrate, for the first time.

A new accelerated method for the synthesis of $nC_{60}$ aggregates of a spherical shape from fullerene $C_{60}$ molecules has been developed and implemented (where n is the number of fullerene $C_{60}$ molecules in the synthesized aggregate). The method is based on the self-organization of $C_{60}$ molecules in the volume of the evaporating drop of the fullerene solution in N-methylpyrrolidone at room temperature. On the basis of the proposed method, a thin semiconductor fullerene $C_{60}$ (with a band gap of ~1.6 eV) coating with a thickness of ~800÷1000 nm was obtained, for the first time (see. Fig.1). In the experiment, the initial concentration of $C_{60}$ in the molecular solution in N-methylpyrrolidone was ~1.04 mol/m$^3$. It has been established that the most likely motive force for the self-organization of $C_{60}$ molecules in an evaporating droplet volume of solution due to the thermal action is the presence of strong temperature gradients both in the volume and in the near-surface layers of the evaporating drop. The physical mechanism of self-organization of fullerene molecules and formation of large nanoaggregates, so-called Ostwald ripening, according to which relatively large structures grow at the expense of smaller ones, has been proposed [3].

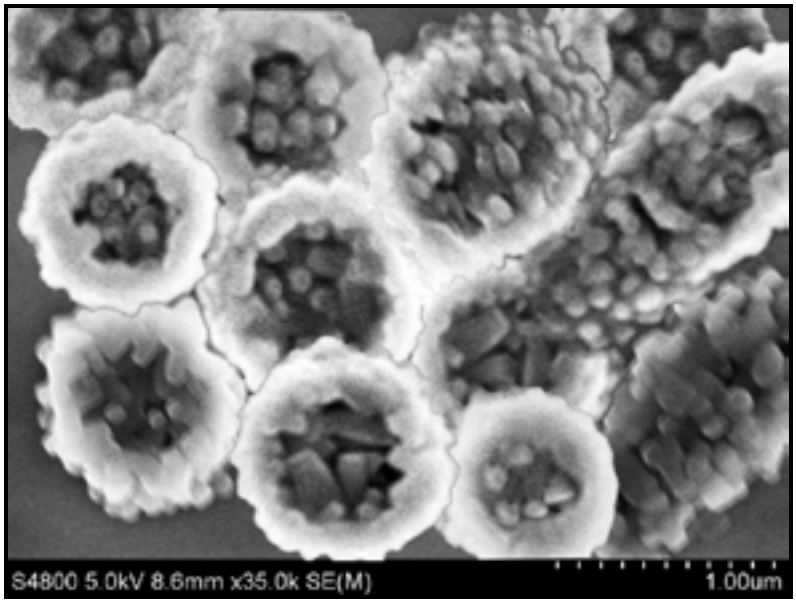


Fig. 1. SEM-image of the nanocoatings' consisting of one layer of large nanostructured porous fractal aggregates $nC_{60}$. The image was obtained on the surface of the mica substrate after complete evaporation of the solvent.

The most important factor determining the ordering of $C_{60}$ molecules and the formation of $nC_{60}$ nanoaggregates in the volume of evaporating droplets is the velocity of the contact line along the substrate, depending on the type of organic solvent used in the preparation of the initial $C_{60}$ solution. Prolonged microscopic observations of self-aggregation processes of $C_{60}$ in the experiments have allowed establishing that synthesized thin nanocoating of aggregates were stable to external mechanical and thermal influences. The proposed method can be used for the synthesis of nanosized thin two-dimensional (2-D) films based on $C_{60}$ molecules on the substrate surface in solar energy as a photoactive layer for high-efficiency solar cells, in optics as a photosensitive sensor, in nonlinear optics as an effective optical limiters of laser radiation and others.

[1] J. Son, J. Yu, S. Kwon et al., Colloidal Synthesis of Ultrathin Two-Dimensional Semiconductor Nanocrystals, Adv. Mater. **23**, 3214– 3219 (2011).
[2] U.K. Makhmanov, O.B. Ismailova, A.M. Kokhkharov et al., Features of self-aggregation of $C_{60}$ molecules in toluene prepared by different methods, Phys. Lett. A **380**, 2081–2084 (2016).
[3] S.A. Bakhramov, A.M. Kokhkharov, U.K. Makhmanov, Thin semiconductor films of fullerene $C_{70}$ nanoaggregates on the surface of a plane glass substrat, Applied Solar Energy **54**, 164–167 (2018).

# SYNTHESIS OF LANTHANIDE DOPED $NaGdF_4$ AND $NaYF_4$ NANOPARTICLES, CORE-SHELL MODIFICATION AND CHARACTERIZATION

Rokas Vargalis, Dovilė Baziulytė-Paulavičienė, Simas Šakirzanovas

Institute of Chemistry, Faculty of Chemistry and Geosciences, Vilnius University, Lithuania
rokas.vargalis@chgf.vu.lt

Lanthanide ions exhibit unique luminescent and magnetic properties. The presence of Yb and Er ion pair causes process of radiation upconversion. Such ion pair have the ability to convert near infrared long-wavelength excitation, via two or more photon process, into shorter visible wavelength light [1]. Various salts of gadolinium have outstanding paramagnetic properties, which provides opportunity for application in magnetic resonance imagining. Lanthanide doped $NaGdF_4$ and $NaYF_4$ can be used for different applications varying from magnetic resonance and biological imagining to targeted drug delivery. $NaGdF_4$: $Yb^{3+}$, $Er^{3+}$ exhibits upconversion fluorescence peaks in blue, green and red spectral areas under 980 nm IR laser excitation [2] while $Gd^{3+}$ ions provides necessary paramagnetic properties [2].

The main purpose of this work was to synthesize single phase monodisperse core $NaGdF_4$ and $NaYF_4$ (figure 1.) nanoparticles using thermal decomposition method. Subsequent step was core-shell particle preparation with the aim to find out optimum synthesis conditions for monodispersed core-shell nanoparticles. We investigated the main thermal decomposition synthesis parameters: temperature, time and ratio of solvents (oleic acid and octadecene).

Scanning electron microscopy (SEM), powder X-ray diffraction (XRD), and photoluminescence (PL) technique have been used to characterize the size, crystal structure and emission intensity of the samples.

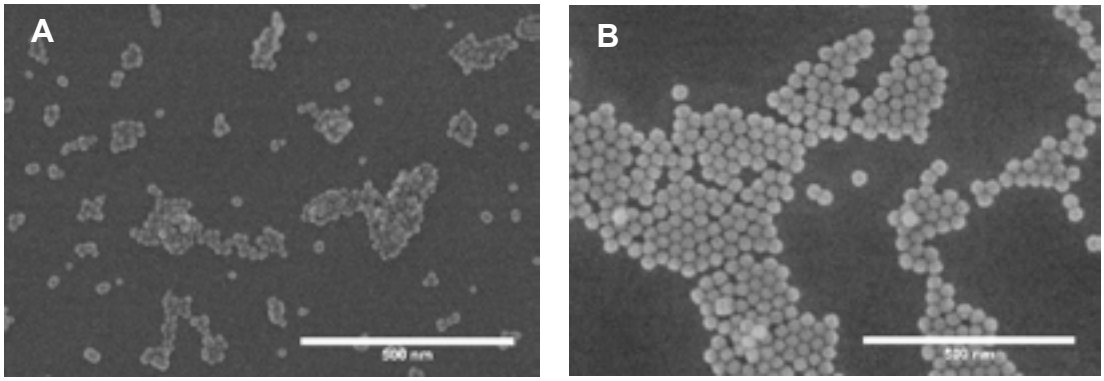


Figure 1. SEM images of $NaGdF_4$:$Yb^{3+}$,$Er^{3+}$ (A) and $NaYF_4$:$Yb^{3+}$ (B) nanoparticles, synthesis temperature 300 °C and synthesis time 60 minutes.

[1] Wang, F. and X. Liu, *Recent advances in the chemistry of lanthanide-doped upconversion nanocrystals.* Chemical Society Reviews, 2009. **38**(4): p. 976-989.

[2] Zhou, J., et al., *Dual-modality in vivo imaging using rare-earth nanocrystals with near-infrared to near-infrared (NIR-to-NIR) upconversion luminescence and magnetic resonance properties.* Biomaterials, 2010. **31**(12): p. 3287-3295.

# SYNTHESIS AND LUMINESCENCE PROPERTIES OF $NaGdF_4:Yb^{3+},Er^{3+}@NaGdF_4$ AND $NaGdF_4:Yb^{3+},Er^{3+}@NaYbF_4$ UPCONVERTING NANOPARTICLES

Rugile Zilenaite[1], Dovile Baziulyte-Paulaviciene[1], Simas Sakirzanovas[1]

[1] Institute of Chemistry, Faculty of Chemistry and Geosciences, Vilnius University, Lithuania
rugile.zilenaite@chf.stud.vu.lt

Rare earth metal (lanthanide) upconverting nanoparticles (UCNPs) have been extensively investigated because they possess unique optical properties. Depending on their size, crystal structure and composition, UCNPs are known to exhibit down-conversion luminescence or efficient upconversion luminescence. During upconversion process low-energy near-infrared (NIR) radiation photon is converted into higher energy (visible light) photon by multi-photon process [1]. UCNPs have shown their potential to be used in bioimaging, biosensors, noncontact fluoresce thermometers and drug delivery systems [2-3].

The main focus of this research was to synthesize $NaGdF_4:Yb^{3+},Er^{3+}@NaGdF_4$ and $NaGdF_4:Yb^{3+},Er^{3+}@NaYbF_4$ nanoparticles using thermal decomposition method and determine how UCNPs size and core-shell structure effect photoluminescence (PL) properties.

The obtained results show that synthesis temperature and core-shell composition influence UCNPs size, agglomeration and upconversion luminescence. The PL spectra (Fig. 1) of $NaGdF_4:Yb^{3+},Er^{3+}@NaGdF_4$ and $NaGdF_4:Yb^{3+},Er^{3+}@NaYbF_4$ nanoparticles (synthesized at 310 °C, 90 min) proves that inert $NaGdF_4$ shell increase emission intensity while active $NaYbF_4$ shell decrease it when compared to $NaGdF_4:Yb^{3+},Er^{3+}$ core nanoparticles. Powder X-ray diffraction (XRD), scanning electron microscopy (SEM) and photoluminescence (PL) spectra have been recorded to characterize the size, crystal structure and emission intensity of the synthesized samples.

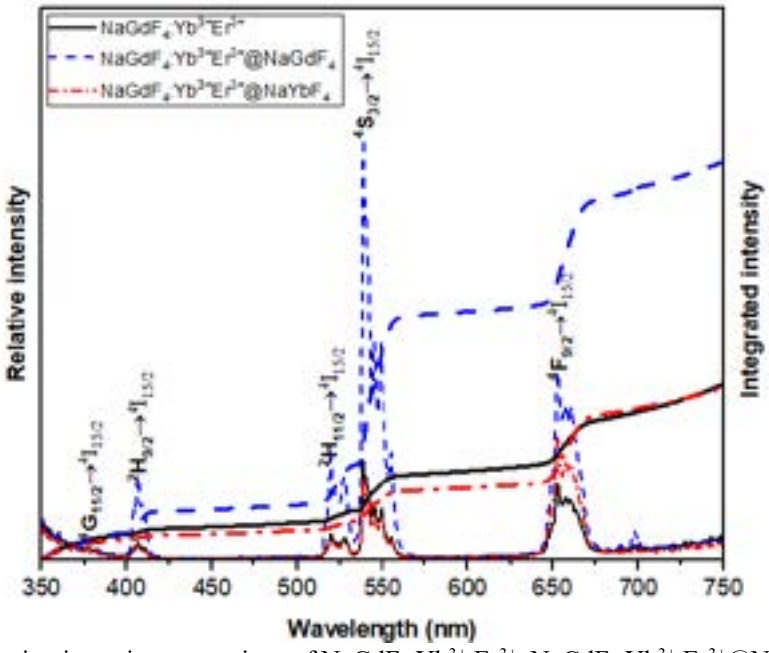


Fig. 1. Emission intensity comparison of $NaGdF_4:Yb^{3+},Er^{3+}$, $NaGdF_4:Yb^{3+},Er^{3+}@NaGdF_4$ and $NaGdF_4:Yb^{3+},Er^{3+}@NaYbF_4$ nanoparticles. Core-shell nanoparticles were synthesized at 310 °C, 90 min.

[1] Mader, H. S., Kele, P., Saleh, S. M. and Wolfbeis, O. S. (2010). Upconverting luminescent nanoparticles for use in bioconjugation and bioimaging. *Current Opinion in Chemical Biology*, *14*(5), 582–596.

[2] Yao L., Xu D., Li Y., Lin H., Yang S. and Zhang Y. (2019). Applied Surface Science upconversion nanoparticles by hydrothermal method and their dual-mode thermometric properties. *Applied Surface Science*, *466*(May 2018), 320–327.

[3] Baziulyte-Paulaviciene, D., Karabanovas, V., Stasys, M., Jarockyte, G., Poderys, V., Sakirzanovas, S. and Rotomskis, R. (2017). Synthesis and functionalization of NaGdF4: Yb, Er@NaGdF4core-shell nanoparticles for possible application as multimodal contrast agents. *Beilstein Journal of Nanotechnology*, *8*(1), 1815–1824.

# PHASE TRANSITION IN A HIGH ENTROPY AlCoFeCrVNi ALLOY UNDER MECHANICALL ALLOYING AND SINTERING

Kushnir V.V. [(1)], Cherniavsky V.V. [(1)], Yurkova A.I. [(1)], Burchenya A.V. [(2)]

[(1)] Igor Sikorskiy Kiev Polytechnic Institute", 37 Peremohy Ave., Kiev, 03056, Ukraine;
[(2)] National Academy of Sciences of Ukraine V. Bakul Institute for Superhard Materials, 2, Avtozavodska St., Kyiv, 04074, Ukraine
vlad987321@gmail.com; vadikv13@gmail.com; yurkova@iff.kpi.ua

High-entropy alloys (HEAs) are presently of growing attention for researches employed both in scientific and engineering fields of activities.High-entropy alloys (HEAs) are promising new class of materials and candidates for many potential applications with high solid-solution strengthening, high strength properties, excellent resistance to high-temperature softening, good ductility, high wear and corrosion resistance at room temperature as well as at high temperature [1, 2]. High homogeneity of HEAs and nanocrystalline structure allows to improve physical and mechanical characteristics. It can be achieved by use mechanical alloying (MA) for synthesis and next sintering under pressure at the low temperatures to maintain the initial HEAs structural state [3].

The present study describes the synthesis of nanocrystalline equiatomic AlCoFeCrVNi high-entropy alloy from elemental materials to solid solution phases by mechanical alloying (MA) with following sintering under high pressure and characterized by XRD (X-ray diffractometer Ultima-IV, Rigaku with Cu Kα radiation), SEM and mechanical testing. The elemental powders were milled in a planetary ball mill with tungsten carbide grinding media in petroleum. In order to confirm the alloy formation during milling, powder samples were taken out atthe intervals of 0.5, 1, 2, 5 and 10 hours. After the successful MA synthesis of equiatomic nanocrystalline AlCoFeCrVNi HEA powders, the consolidation was carried out at 1200 °C for 60 min in vacuum and at 800 °C for 30 min at a pressure of 5 GPa using hydraulic press DO 044. XRD pattern shown in Fig. 1 reveals the phase formation in AlCoFeCrVNi HEA with milling time. From the XRD results it is clear that the alloy formation is completed after 10 h with the formation of BCC solid solution (β-phase) along with small volume fraction of the FCC solid solution (α-phase).

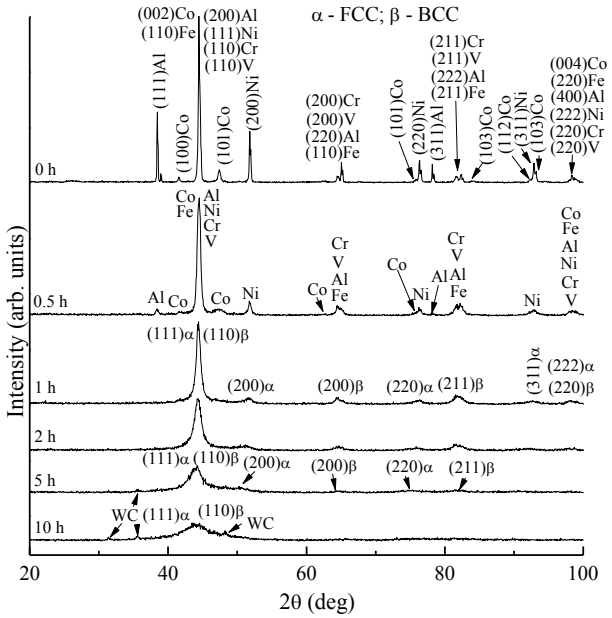


Fig. 1. XRD patterns of AlCoFeCrVNi HEA with varying milling time

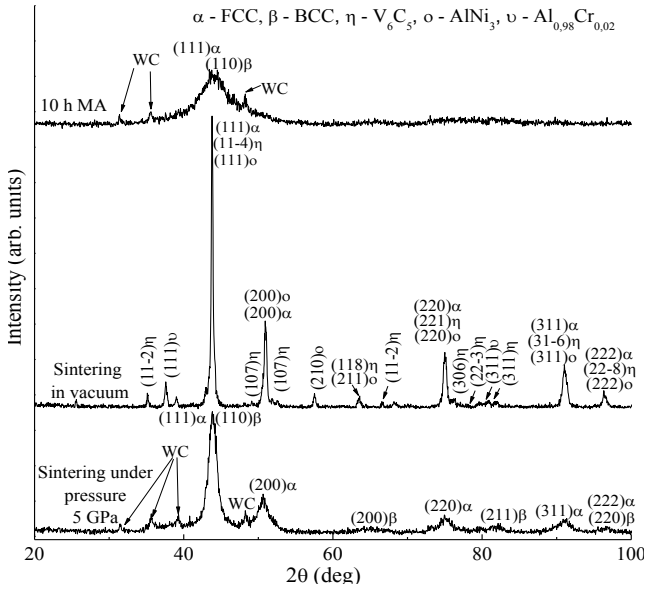


Fig. 2. XRD patterns of AlCoFeCrVNi HEA after 10h of MA and after sintering

The XRD patterns of the MA powder consolidated by sintering in vacuum and under pressure 5 GPa at 800 °C confirms that the BCC and FCC solid-solutions are metastable. After sintering under pressure the alloy is composed of two solid solutions with FCC and BCC structure and the small volume fraction of tungsten carbide. After sintering under pressure, the AlCoFeCrVNi alloy remains in a nanocrystalline state with a crystallite size about 50 nm, and the porosity of the sample doesn't exceed 1 vol. % and have high microhardness, HV = 11.7±1 GPa After sintering in vacuum the AlCoFeCrVNi HEA is composed of major FCC phase and intermetallic $V_6C_5$, $AlNi_3$, and $Al_{0,98}Cr_{0,02}$ phases. It was found that its microhardness HV = 3.7 ± 0.3 GPa. Such low microhardness of the alloys is a result of the high porosity of the samples after sintering in vacuum.

[1]. Yeh J.-W., Chen S.-K., Lin S.-J., Gan J.-Y., Chin T.-S., Shun T.-T., Tsau C.-H., Chang S.-Y. // Advanced Engineering Materials – 2004. – V 6. P. 299-303.
[2]. Miracle D.B., Senkov O.N. // Acta Materialia – 2017. – V 122. P. 448–511.
[3]. Yurkova A.I. Chernyavsky V.V., Gorban V.F. // Powder Metallurgy and Metal Ceramics – 2016. – V 55, № 3-4. – P.152-163.

# POLYETHYLENE FILM COATING OF ZINC OXIDE, TITANIUM DIOXIDE NANOPARTICLES AND NANOCOMPOSITE FILM ANTIMICROBIAL ACTIVITY

Vytautas Žutautas[1], Ingrida Bružaitė[1]

[1] Department of Chemistry and Bioengineering, Faculty of Fundamental Sciences, Vilnius Gediminas Technical University, Lithuania
vytautas.zutautas@stud.vgtu.lt

Focus on the new materials used in the packaging of foodstuffs and their coverage of the surface processes research. Some nanoparticles such as titanium dioxide ($TiO_2$) and zinc oxide (ZnO) nanoparticles are nontoxic. The photocatalytic reaction of $TiO_2$ nanoparticles has been to inactivate a wide spectrum of microorganisms [1].

The aim of this work is to cover the surface of the polyethylene (PE) films with nanoparticles of zinc oxide and titanium dioxide and to investigate their antimicrobial properties. The antimicrobial agents such as the $TiO_2$ or ZnO nanoparticles-coated PE films also help extend the shelf life of foods by extending the lag period of microorganisms [2].

The polyethylene films were coated with synthetic and commercial zinc oxide (ZnO) and titanium dioxide ($TiO_2$) nanoparticles. Antibacterial effects of $TiO_2$ and ZnO nanoparticle-coated PE films on *E. coli*, *B. megaterium*, *B. sphaericus* were investigated. The inhibitory activity of the coated and uncoated PE films was tested under UV (wavelength 365 nm, 6W power) lamp. The growth of cells cultures was monitored every two hours by the optical absorption and was expressed in the cell colony-forming units.

The antimicrobial activity of the ZnO nanoparticle-coated PE films had little influence compared to the control (uncoated PE films). $TiO_2$ nanoparticle-coated PE films were identified to inhibit cell growth (Fig. 1). Depending on the bacteria used, the growth may be as low as 37% (*E. coli*), 50% (*B. sphaericus*), 61% (*B. megaterium*) compared to the control. It is also evident that the use ZnO nanoparticle-coated PE films has resulted in more colony forming units than using $TiO_2$ nanoparticle-coated PE films.

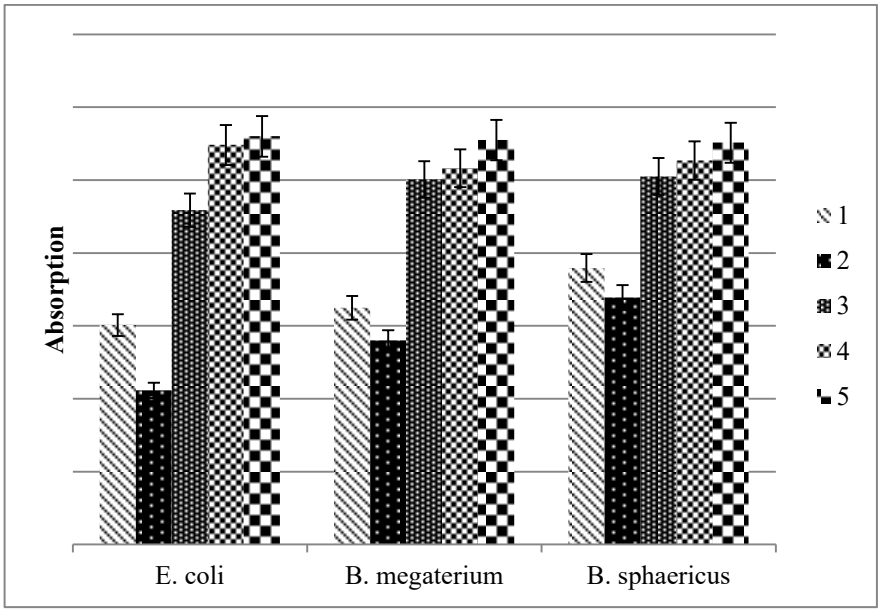


Fig. 1. A comparison of the optical absorption of bacteria cultures. Bacterial cultures have been treated nanoparticle-coated PE films and UV light for 11 h. *1* - coated films with synthetic $TiO_2$ nanoparticles; *2* - coated films with commercial $TiO_2$ nanoparticles; *3* - coated films with synthetic ZnO nanoparticles; *4* - coated films with commercial ZnO nanoparticles; *5* – uncoated films.

This study demonstrated that both synthetic and commercial $TiO_2$ nanoparticle-coated PE films inhibit cell development by 39-63%. It was also found that PE films coated with titanium dioxide nanoparticles and exposed under UV light reduces the growth of bacteria on foods better than just UV light.

[1] R. D. Joerger, Antimicrobial films for food applications: a quantitative analysis of their effectiveness, Packaging Technology and Science vol. 20, 231-273 (2007).

[2] A. Marcous, S. Rasouli, F. Ardestani, Low-density polyethylene films loaded by titanium dioxide and zinc oxide nanoparticles as a new active packaging System against *Escherichia coli* O157:H7 in fresh calf minced meat, Packaging Technology and Science vol. 30, no. 11, 693-701 (2017).

# SYNTHESIS, CHARACTERISATION AND SELF-ASSEMBLY OF SMALL CARBON QUANTUM DOTS FOR A BINARY SYSTEMS APPLICATIONS

Barbara Śliwa[1], Kacper Ornat[1], Agnieszka Jędrych[1], Michał Wójcik[1]

[1]Department of Chemistry, University of Warsaw, Poland
b.sliwa2@student.uw.edu.pl

Carbon quantum dots (CQDs) are carbon-based fluorescent nanomaterials with a size-dependent optical properties and have attracted attention in many applications such as light-emitting diodes, solar cells, sensing and bioimaging [1-3]. It has been shown that spherical nanoparticles can organize into many diverse soft structures when substituted by mesogenic ligands, due to the self-segregation of chemically non-compatible units [4]. Condensed aggregates of periodically organized nanoparticles are one of the most important research topics for the development of electronics, plasmonics and remote-control hybrid nanomaterials [5]. The range of application could be wide if the elements making these arrays formed large-scale and well-defined structures. The type of structure can be controlled by composition of organic layer and temperature as well as by the metal core size and density of grafting layer [6].

Carbon quantum dots incorporated hybrid nanomaterials (binary systems with plasmonic nanoparticles) possessing liquid crystalline properties have been proposed. To prepare the binary system the synthesis of small and monodispersed carbon quantum dots has been carried out. During the research several synthetic approaches have been applied to obtain purified quantum dots for future doping of liquid-crystalline hybrid binary system. CQDs have been characterized with SAXRD, TEM, UV_VIS and IR spectroscopy techniques. In this presentation, we will focus on a novel approach for synthesis and X-ray (SAXRD) characterization of carbon quantum dots suitable for self-organizing materials.

[1] H. T. Li, X. D. He, Z. H. Kang, H. Huang, Y. Liu, J. L. Liu, S. Y. Lian, C. H. A. Tsang, X. B. Yang and S. T. Lee, Angew. Chem., Int. Ed., 2010, 49, 4430–4434.

[2] S. T. Yang, Li Cao, P. G. Luo, F. S. Lu, X. Wang, H. F. Wang, M. J. Meziani, Y. F. Liu, G. Qi and Y. P. Sun, J. Am. Chem. Soc., 2009, 131, 11308–11309

[3] Y. Z. Yang, X. F. Lin, W. L. Li, J. M. Ou, Z. K. Yuan, F. Y. Xie, W. Hong, D. S. Yu, Y. G. Ma, Z. G. Chi and X. D. Chen, ACS Appl. Mater. Interfaces, 2017, 9, 14953–14959.

[4] M. Wojcik, W. Lewandowski, J. Matraszek, J. Mieczkowski, J. Borysiuk, D. Pociecha, E. Gorecka; Angew. Chem. Int. Ed. Engl., 2009, 48, 28, pp. 5167–9

[5] W. Lewandowski, M. Fruhnert, J. Mieczkowski, C. Rockstuhl, E. Górecka; Nat. Commun. 2015; 6:6590

[6] A. Zep, M. Wojcik, W. Lewandowski, K. Sitkowska, A. Prominski,J. Mieczkowski, D. Pociecha, E. Gorecka; Angew. Chem. Int. Ed. 2014, 53, 13725 –137

# SYNTHESIS OF CARBON SUPPORTED GOLD NANOPARTICLES FOR ETHANOL ELECTRO-OXIDATION

Daina Upskuvienė, Aldona Balčiūnaitė, Algirdas Selskis, Loreta Tamašauskaitė-Tamašiūnaitė, Eugenijus Norkus

Department of Catalysis, Center for Physical Sciences and Technology
Saulėtekio Ave. 3, LT-10257, Vilnius, Lithuania
e-mail.: daina.upskuviene@ftmc.lt

The development and investigation of various materials used in fuel cells is a major challenge in the scientific community. Literature describes many various supports, metals, methods, wich are able to enhance the electrocatalytic activity of the new created catalysts. The nano-sized gold nanoparticles (GNPs') have been known from the very beginning of human civilization, but systematic scientific investigations were performed much later. The methods to synthesize, efficiently, metallic nanoparticles are becoming more widespread. In this area, the challenges are to use low-cost methods with low-toxicity substances as well as novel techniques to control nanoparticles size and shape. Recently, formation of new composites by adsorption of gold nanoparticles on carbon has attracted interest due to their physical properties and applications in catalysis, electrochemical energy storage or electrochemical sensors.

This work is focused on the preparation of gold nanoparticles (GNPs) using various halides, such a KCl, KBr, and KI as additives with the aim to use them as electrocatalysts towards the electro-oxidation of ethanol. GNPs were reduced from $Au^{3+}$ ($HAuCl_4$) to $Au^0$ in an aqueous solution using glucose ($C_6H_{12}O_6$) as a reducing agent. Further, the obtained GNPs were deposited on the surface of carbon powder using the adsorbtion method. The size, shape and composition of the prepared gold nanoparticles were detected by means of Field Emission Scanning Electron Microscopy (FESEM) and Inductively Coupled Plasma Optical Emission Spectroscopy (ICP-OES).

It has been determined that, depending on the halides (KCl, KBr and KI), GNPs of ca. 20-90 nm in size were successively synthesized. The shape and size of the obtained Au nanoparticles are affected by halide ions. The electrocatalytical properties of the prepared GNPs, using various halides, towards the electro-oxidation of ethanol in an alkaline medium are compared and discussed on the basis of electrochemical data.

# SYNTHESIS OF N-DOPED CARBON SUPPORTED Au-Cu NANOPARTICLES USING MICROWAVE HEATING METHOD

Rūta Kaminskaitė, Aldona Balčiūnaitė, Daina Upskuvienė, Loreta Tamašauskaitė-Tamašiūnaitė, Eugenijus Norkus

Department of Catalysis, Center for Physical Sciences and Technology, Saulėtekio Ave. 3, LT-10257, Vilnius, Lithuania
aldona.balciunaite@ftmc.lt

One of the most commonly used renewable energy sources is fuel cells that directly convert the chemical reaction energy into electricity. In this work, the N-doped carbon materials derived from biological waste, such as alder wood chips and black liquor, were used as a substrate for deposition of gold-copper nanoparticles (Au-CuNPs) using the microwave heating method. The wood-based carbon powders were doped with nitrogen at a temperature of 800 ° C using dicyandiamide (DCDA) as a nitrogen precursor. For synthesis of catalysts, a reaction mixture of the same composition consisting of 1.3 mM $HAuCl_4$, 0.06 M $CuCl_2$, 0.05 M NaOH, ethylene glycol, and different N-doped carbon materials was put into a microwave reactor Monowave 300 (Anton Paar). Synthesis of Au-CuNPs and N-doped carbon composites was carried out at a temperature of 150°C for 30 min. After preparation, the synthesized catalysts were washed with acetone, then filtered and dried in an oven at a temperature of 80°C for 2 h.

The surface morphology and structure of the synthesized Au-CuNPs/N-doped carbon composites were investigated using transmission electron microscopy (TEM), X-ray photoelectron spectroscopy (XPS), scanning electron microscopy (SEM), and Inductively Coupled Plasma Optical Emission Spectroscopy (ICP-OES).

It was found that the size of Au-CuNPS were in the range of 5-50 nm in the prepared composites. Moreover, the Au loadings were in range from 71 to 90 $\mu g_{Au}$ $cm^{-2}$ and particles size were in the range 5-50 nm. The highest nitrogen content was found to be 7.44 at. % in the N-doped carbon powder obtained from cellulose waste.

# POLYOL SYNTHESIS OF SILVER NANOSTRUCTURES

Simona Vyčaitė[1], Asta Tamulevičienė[1,2]

[1] Department of Physics, Kaunas University of Technology, Lithuania
[2] Institute of Materials Science, Kaunas University of Technology, Lithuania
simona.vycaite@ktu.edu

Metal nanocrystals have excellent applications in the biomedical, electronic, catalytic, and sensing fields. Silver nanoparticles (AgNPs) have been one of the most important nanostructural materials due to their fascinating properties and potential applications in many fields. Due to extensive research performed in this field, it is well known that the properties of metal nanoparticles are closely related with their size, shape, composition and crystallinity. Therefore, the properties of the AgNPs could be controlled and adjusted by tailoring their particle shape and size [1]. And these can be adjusted by choosing the synthesis method and appropriate precursors. Up to now, AgNPs have been successfully synthesized with a variety of shapes, including spheres, spheroids, disks, rods, wires, stars, prisms, cuboctahedrons, right bipyramids, cubes etc [1].

The polyol synthesis designates the liquid-phase synthesis in high-boiling, multivalent alcohols [2]. The advantages of this synthesis route are the variety of polyols that can be used, good solubility of most metal salts, most polyols become reductive in high temperature, and according to the synthesis conditions one can obtain nanoparticles of different size and shape.

In this research, the polyol process is used for synthesis of silver nanocubes and synthesis kinetics is analysed. The precursor silver nitrate and copper chloride were dissolved in 1,5-pentanediol in a glass vial. In another glas vial polyvinylpyrrolidone was dissolved in 1,5-pentanediol. Two precursor solutions were injected repeatedly in hot reaction flask with 1,5-pentanediol (heated in oil bath) and reaction took for about 12 minutes after which the reaction media became opaque. Final colloidal solution was left to cool down at room temperature. More synthesis details can be found in [3]. Every two minutes the samples from reaction media were taken out to check the kinetics of the reaction. As silver nanostructures have size dependent surface plasmon resonance in visible light region, the UV-VIS spectroscopy (Avantes, measurement range 190 – 1100 nm, resolution 1.4 nm) was employed to check the reaction kinetics. For this purpose, silver colloid was dispersed in ethanol and measured. Corresponding spectra during different periods of reaction is shown in Fig. 1.

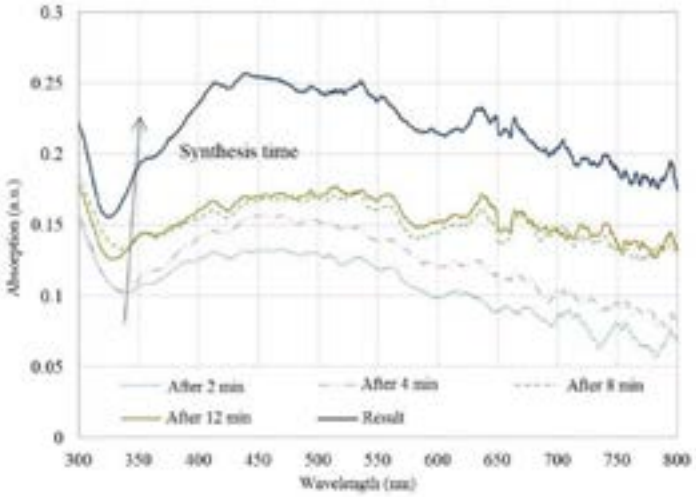


Fig. 1. UV-VIS absorption spectra after different duration of synthesis of silver nanoparticles

From the UV-VIS absorption spectra it was found that silver nanoparticles of different sizes were formed. It should be emphasized that the small absorption peak at 350 nm is responsible for the one of cube resonance modes (at the edges) [4]. The synthesis kinetics study revealed that the intensity of absorption peak increases with longer synthesis time, which shows that the number of nanoparticles was increasing in the solution but the position of the peak remained the same indicating retained size distribution.

[1] J. Zhang, Q. Wang, X. Zhang, et. al. Carbamide promoted polyol synthesis and transmittance properties of silver nanocubes, Inorg. Chem. Front., **3**, 547 (2016).
[2] H. Dong, Y.-C. Chen, C. Feldmann, Polyol synthesis of nanoparticles: status and options regarding metals, oxides, chalcogenides, and non-metal elements, Green Chem., **17**, 4107 (2015).
[3] A. Tao, P. Sinsermsuksakul, P. Yang, Polyhedral silver nanocrystals with distinct scattering signatures, Angew. Chem. Int. Ed. **45**, 4597-4601 (2006).
[4] M. B. Cortie, F. Liu, M.D. Arnold, et al., Multimode Resonances in Silver Nanocuboids, Langmuir, **28**, 9103-9112 (2012).

# NEW APPROACH TO ANTIBACTERIAL ACTIVITY AND SAFETY EVALUATION OF NANOSIEZED SILICON-SUBSTITUTED HYDROXYAPATITE CO-DOPED WITH $Zn^{2+}$ AND $Sr^{2+}$ IONS

Justyna Rewak-Soroczynska[1], Nicole Nowak[2],Sara Targonska[2], Agata Piecuch[1] and Rafal J. Wiglusz[2]

[1] Institute of Genetics and Microbiology, Uniwersity of Wroclaw, Przybyszewskiego 63/77, 51-148 Wroclaw, Poland
[2] Institute of Low Temperature and Structure Research, Polish Academy of Sciences, Okolna 2, 50-422 Wroclaw, Poland
justyna.rewak@uwr.edu.pl

Nanotechnology is the most intensively developing a multidisciplinary field of research combining various disciplines of science achievement. Nanomaterials show unexpected and interesting chemical and physical properties different from those of the original in the micro-sized scale.

Hydroxyapatite($Ca_{10}(PO_4)_6(OH)_2$ (HAp)) naturally occurs in human body as a component of teeth and bones. The HAp can be synthesizedand structurally modified as the product that is similar to natural one. Moreover, calcium hydroxyapatiteis considered non-toxic for human cells (*in vitro* and *in vivo*)andis being used as bone substitute as well as in implant coatings, dermal fillers and drug delivery systems.

The hexagonal structure in apatites belongs to $P6_3/m$ space group and allows the cations to localize in the 4(f) and 6(h) positions and are able to accommodate a variety of cations as substituents.Furthermore, metals like silver, gold or zinc are well-known for their antimicrobial effects therefore the metal-doped hydroxyapatites could be used in a bacterial infection prevention, in particular as concerns implant insertion procedure.

Zinc and strontium ions co-doped silicon-substituted hydroxyapatite were synthesized using a hydrothermal method.The concentrations of $Zn^{2+}$and $Sr^{2+}$ ions were set on 2, 5 and 10 mol% in a ratio to entire calcium ions molar content (please see Table 1).

Table 1 Formulas of tested hydroxyapatites

| **Dopants** | **Hydroxyapatite formula** |
|---|---|
| 5 mol% $Sr^{2+}$ | $Ca_{9,5}Sr_{0,5}(PO_4)_2(SiO_4)_4(OH)_2$ |
| 5 mol% $Sr^{2+}$, 2 mol% $Zn^{2+}$ | $Ca_{9,3}Sr_{0,5}Zn_{0,2}(PO_4)_2(SiO_4)_4(OH)_2$ |
| 5 mol% $Sr^{2+}$, 5 mol% $Zn^{2+}$ | $Ca_{9,0}Sr_{0,5}Zn_{0,5}(PO_4)_2(SiO_4)_4(OH)_2$ |
| 5 mol% $Sr^{2+}$, 10 mol% $Zn^{2+}$ | $Ca_{8,5}Sr_{0,5}Zn_{1,0}(PO_4)_2(SiO_4)_4(OH)_2$ |

XRD (X-ray diffraction) was performed in order to confirm their apatite structure. Their antibacterial activity was checked in the spot test using Gram-negative bacteria: *Pseudomonas aeruginosa, Klebsiella pneumoniae* and *Escherichia coli* strains. Moreover some safety tests were performed: cytotoxicity test (MTT), Ames test (to check mutagenic potential) and hemolysis (to check their effect on erythrocytes extracted from blood samples).

The obtained results suggest that tested compounds are potentially non-harmful for human, moreover these doped with strontium and 5-10% of zinc have antimicrobial activity against *K. pneumoniae* and *E. coli* cells. Pure strontium-doped hydroxyapatite (with no zinc additive) promoted the growth of these strains. Regarding *P. aeruginosa* strain no antimicrobial activity was observed for tested materials.

# STUDIES AND EVALUATION OF ANTICANCER PROPERTIES OF POLY(L-LACTIDE)/ $Sr^{2+}$, $Eu^{3+}$ AND $Cu^{2+}$ IONS CO-DOPED HYDROXYAPATITE POROUS SPONGE SCAFFOLDS

Nicole Nowak[1], Justyna Rewak-Soroczynska [2], Agata Piecuch[2], Konrad Szustakiewicz[3], Piotr Kuropka[4], Maciej Dobrzynski[5] and Rafal Jakub Wiglusz[1]

[1] Institute of Low Temperature and Structure Research, Polish Academy of Sciences, Okolna 2, 50-422 Wroclaw, Poland

[2] Institute of Genetics and Microbiology, Uniwersity of Wroclaw, Przybyszewskiego 63/77, 51-148 Wroclaw, Poland

[3]Polymer Engineering and Technology Division, Wrocław University of Science and Technology, Wyb. Wyspiańskiego 27, 50-370 Wrocław, Poland

[4]Department of Histology and Embriology, Wroclaw University of Environmental and Life Sciences, Norwida 31, 50-375 Wroclaw, Poland

[5]Department of Conservative Dentistry and Pedodontics, Wroclaw Medical University, Krakowska 26, 50-425 Wroclaw, Poland

n.nowak@intibs.pl

A success of nanotechnology in field of physical, chemical, and medical sciences, it has now started revolutionizing the drug delivery sciences and bio-detection. The specific advantages include superior pharmacodynamics, pharmacokinetics, reduced toxicity, and targeting capability.

It is well-known that hydroxyapatite ($Ca_{10}(PO_4)_6(OH)_2$) is a form of bioceramics material and is widely used as a bone substitute due to its adequate mechanical properties and the similar composition to bone mineral. Due to the bioactivity, biocompatibility, stability, nontoxic properties, hydroxyapatite with porous surface structure and $OH^-$ groups may serve as an ideal candidate drug carrier for the delivery of a variety of pharmaceutical molecules.

Metals such as gold, copper, europium or even ionic compounds of selenium are well-known for their potential anticancer properties. The synergy of such metals could bring promising effect by complete cancer cells eradication from healthy tissue.

The hexagonal structure in apatites belongs to $P6_3/m$ space group and allows the cations to localize in two different crystallographic positions and are able to accommodate a variety of cations as substituents and could find perfect application in bone cancer therapy.

In the research there have been obtained porous scaffolds based on poly(L-lactide) (PLLA) and synthetic hydroxyapatite (HAp) co-doped with $Sr^{2+}$, $Eu^{3+}$ and $Cu^{2+}$ ions using thermal induced phase separation technique (TIPS) supported by salt leaching process (SL). The obtained series of composite sponges consist of 50 wt.% of the hydroxyapatite in PLLA/HAp systems. The structural and morphological properties of the obtained samples were determined by using XRD (X-ray powder diffraction), TEM (transmission electron microscopy) and SEM (scanning electron microscopy) techniques (Fig. 1). In the present study, experimental *in vitro* anticancer tests concerning sponge scaffolds, which may substitute bone tissue, were discussed in detail.

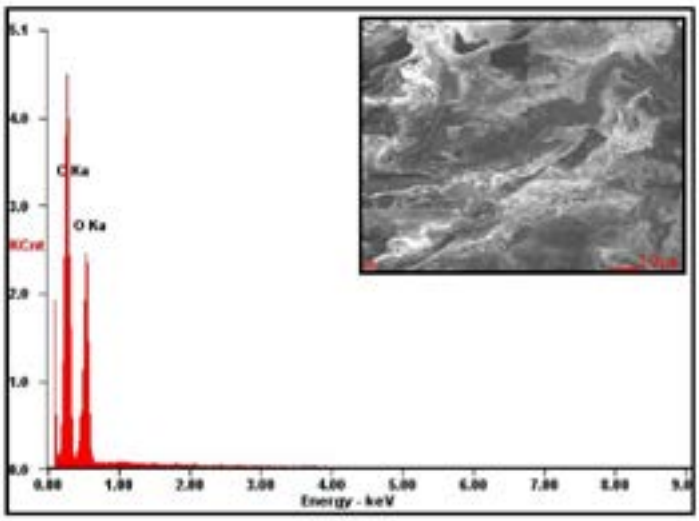


Fig. 1. Representative EDAX diagram for PLLA scaffold.

# CUSTOMIZED THERMOTHERAPY PACKS FOR ASTRONAUTS

Gintarė Plečkaitytė[1,2], Dong-il Moon[2], Jin Woo-Han[2], Meyya Meyyappan[2]

[1] Faculty of Chemistry and Geosciences, Vilnius University, Lithuania
[2] Center for Nanotechnology, Ames Research Center, National Aeronautics and Space Administration, United States of America
gintare.pleckaityte@chf.stud.vu.lt

As humans are not designed for the space environment, a medical suit is essential to support astronauts' life, safety and health. While focusing on life support so far, efforts are needed to improve the quality of life when astronauts stay in space for a long time. Accordingly, future exploration missions need further considerations for preventive care, regular wellness and treating medical conditions directly in space [1]. Until now, medical kits have been supplied from Earth to space, but they could be made in space on-demand in the future. On the other hand, heat therapy is effective, less expensive, safe and quick mode of treatment yielding relief. Preference for non-pharmacological treatment for pain especially in space is the key driver for the development. However, most heat packs are bulky, heavy and inconvenient to use because they are not custom-designed for individuals [2].

On this background, we have demonstrated a heat pack using nanotechnology and printed electronics: an office printer, nano-inks and medical tape without special equipment and toxic materials. Digital printing makes it possible to produce customized heaters on-demand, and chemical sintering is applied to eliminate the need for subsequent processing at high temperature [3]. The proposed healthcare system provides a thermotherapy to promote healing, decrease inflammation, ease headaches, reduce joint and muscle pain for astronauts. The heat pack can be designed for low energy consumption and therapeutic effect by optimizing the heat transfer with the pack sticking to the body, which is especially important in zero gravity. These results can be aligned with the aim of In Space Manufacturing and utilized to humans for long-term space exploration.

**Acknowledgments**: Internship was supported by Science, Innovations and Technologies Agency (MITA, Lithuania).

[1] https://www.nasa.gov/feature/nasas-exploration-campaign-back-to-the-moon-and-on-to-mars
[2] A. Stier, E. Halekote, A. Mark, S. Qiao, S. Yang, K. Diller, N. Lu, "Stretchable Tattoo-Like Heater with On-Site Temperature Feedback Control", Micromachines, 9, 170, 2018
[3] J. Perelaer et al., "Printed electronics: the challenges involved in printing devices, interconnects, and contacts based on inorganic materials," J. Mater. Chem., vol. 20, pp. 8446-8453, 2010

# FABRICATION OF LARGE-AREA PLASMONIC NANOSTRUCTURES FOR BIOSENSING APPLICATIONS

Mihai Suster[1], Piotr Wróbel[1]

[1] Department of Physics, University of Warsaw, Poland
mcsuster@gmail.com

In recent years plasmonic nanostructures have attracted a lot of attention allowing studies on enhanced light-matter interactions. Those are manifested in subwavelength light confinement and electromagnetic field enhancement, both associated with excitation of surface plasmons (SP). This opened up new applications including subdiffraction imaging, plasmon-enhanced photovoltaics and plasmonic sensing[1-2]. In case of the nanosensors, electromagnetic field localization in the vicinity of nanoobjects leads to high sensitivity to surface binding events and high resolution reaching up the single molecule detection capabilities[3]. Various designs have been used, such as nanohemispheres, nanorods[4] and nanohelices[5]. Silver nanoparticle (nAg) nanohelices are especially suitable because of their chiroptical properties and relatively high resonance quality factors with low losses at optical frequencies.

Performance of a SP-based biosensor depends on the quality factor of surface plasmon resonance (SPR) which in turn requires well-defined nanostructures achievable mostly by expensive and inefficient techniques like electron-beam or focused ion-beam lithography. Those commonly used nanotechnological tools allow for an up to nanometer resolution, but they tend to be time-consuming and limited to a micrometer-scale operation area.

In this study our focus is to master the manufacturing process of large-area metallic nanostructures in form of nanoparticles, nanopillars and nanohelices by means of Physical Vapor Deposition (PVD) technique combined with thermal annealing. In order to achieve anisotropic nanoparticles, Glancing Angle Deposition approach is used. To optimize the nanostructures and quality factor of SPR we systematically characterized several fabrication conditions including the type of substrate, the temperature and time of annealing and the rate and angle of deposition. Prepared samples are measured using UV-VIS reflectometry, spectrophotometry and scanning electron microscopy. Sensitivity of the final products is investigated using salt solutions at different concentrations. This whole procedure makes it possible to prepare uniform, a few centimeter square substrates of different plasmonic responses (Fig. 1-2) which can be controlled by adjusting only a handful of settings.

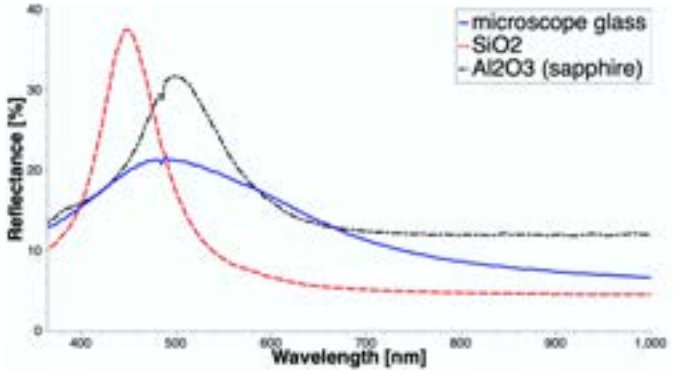


Fig. 1. Reflectance of a 5 nm thick Ag layer deposited on various substrates: microscope glass (continuous line), fused silica (dashed line) and sapphire (dashdotted), all annealed at 300°C for 20 minutes.

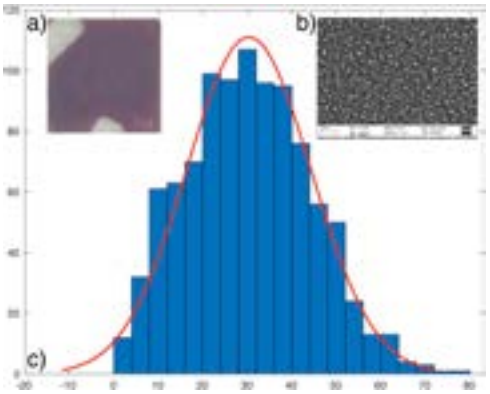


Fig. 2. a) 5nm Ag on a microscope glass substrate; b) SEM image after annealing; c) nAg size distribution histogram.

[1] J.N. Anker et al., Biosensing with plasmonic nanosensors, Nature Materials **7(6)**, 442-453 (JUN 2008).

[2] A. Fratalocchi et al., Nano-optics gets practical, Nature Nanotechnology **10**, 11–15 (2015).

[3] B. Spackova, et al., Optical Biosensors Based on Plasmonic Nanostructures: A Review. Proceedings of the IEE **104**, 2380-2408 (2016).

[4] CX Yu et al., Multiplex biosensor using gold nanorods, Analytical Chemistry **79(2)**, 572-579 (JAN 2007)

[5] M Ghasemi et al., Nanoengineered thin films of copper for the optical monitoring of urine – a comparative study of the helical and columnar nanostructures, Journal of Electromagnetic Waves and Applications **29(17)**, 2321-2329 (NOV 2015)

# INVESTIGATION OF SILVER NANOPARTICLES FOR RAMAN SIGNAL ENHANCEMENT

Mantas Mikalkevičius[1], Tomas Tamulevičius[1,2], Asta Tamulevičienė[1,2]

[1]Department of physics, Kaunas University of Technology, Lithuania
[2]Institute of Materials Science, Kaunas University of Technology, Lithuania
mantas.mikalkevicius@ktu.edu

Nanotechnology is rapidly growing by producing nanoproducts and nanoparticles (NPs) that can have novel and size-related physico-chemical properties differing significantly from larger matter. This open up new horizons for application of such nanosized objects. Among all investigated nanoparticles (Au, Al, Cu, etc.), silver nanoparticles (AgNPs) have attracted increasing interest due to their unique physical, chemical and biological properties compared to their macro-scaled counterparts [1]. Nowadays AgNPs show great potential for application as antimicrobial material, in sensor chips for Raman signal enhancement, medicine, optics, etc.

The purpose of this work was to synthesize silver nanoparticles using polyol method and use these particles for signal enhancement in Raman scattering spectroscopy. The synthesis was performed in heated 1,5-Pentanediol for 8-12 min. Silver nitrate $AgNO_3$ was used as precursor and polyvinylpyrrolidone was used as stabilizing agent to prevent particle agglomeration [2]. In the first (I) synthesis, 6 ml of $AgNO_3$ solution was added to the synthesis medium, and 4 ml of $AgNO_3$ – for the second (II) synthesis.

Optical properties of synthesized colloidal solutions were examined using UV-VIS spectrometry. Since the synthesized solutions are highly concentrated, the optical spectra are measured in ethanol by adding 50 µl of the test solution. Since ethanol is characterized by absorption at ~ 200 nm, the effect of ethanol could be avoided when assessing the absorption of colloidal solution, because usually silver nanoparticles have an absorption peak in a range of 350 – 800 nm depending on particle size and geometry. The measured absorption spectra and SEM micrograph of particles synthesized in II synthesis are presented in Fig. 1. and Fig. 2 respectively.

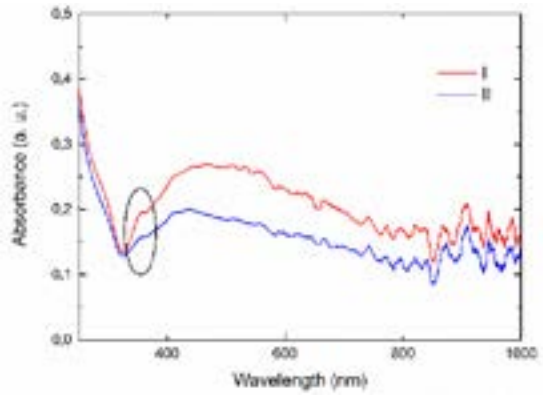


Fig. 1. Absorbance spectra of silver nanoparticles synthesized for different time I – 12 min, II – 8 min

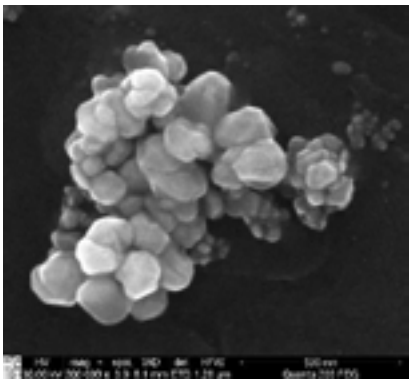

Fig. 2. SEM micrograph of AgNP synthesized via II route

The existence of cube silver nanoparticles was confirmed by appearance of the absorbance peak around 354 nm for both synthesis (resonance due to the polarizability of the charge at the edges of the cubes [3]). Even though, the characteristic absorption peak for cube nanoparticles appeared in spectrum, microscopic analysis has shown that particle geometry varies and no predominant shape can be distinguished (Fig. 2).

Further synthesized particles were tested for SERS using 2-naphthalene thiol as analyte material. The analysis of obtained results have shown that synthesized particles can be successfully applied for SERS as the concentration of analyte molecules up to $10^{-4}$ M was detected.

This research was funded by the European Social Fund under the No. 09.3.3-LMT-K-712 “Development of Competences of Scientists, other Researchers and Students through Practical Research Activities” measure.

[1] Q. H. Tran, V. Q. Nguyen, A.-T. Le, Silver nanoparticles: synthesis, properties, toxicology, applications and perspectives, Adv. Nat. Sci.: Nanosci. Nanotechnol. **4**, 033001 (2013).
[2] A. Tao, P. Sinsermsuksakul, P. Yang, Polyhedral silver nanocrystals with distinct scattering signatures, Angew. Chem. Int. Ed. **45**, 4597-4601 (2006).
[3] M. B. Cortie, F. Liu, M.D. Arnold, et al., Multimode Resonances in Silver Nanocuboids, Langmuir, 28, 9103-9112 (2012).

# APPLICATION OF NANOTECHNOLOGY IN THE TREATMENT AND PREVENTION OF MASTITIS IN DAIRY COWS*

Daniel Radzikowski[1], Aleksandra Kalińska[1], Brygida Kruzińska[1], Jan Slósarz[1], Marcin Gołębiewski[1], Urszula Ostaszewska[2]

[1] Department of Animal Breeding and Production, Warsaw University of Life Sciences, Poland
[2] Department of Cattle Breeding and Milk Evaluation, Siedlce University of Natural Sciences and Humanities, Poland
daniel18-1994@wp.pl

Mastitis is one of the most common and most expensive diseases of dairy cows. It can be caused by a broad spectrum of bacteria, both Gram- positive and Gram- negative, as well as pathogenic, fungi and algae. The effect of the mastitis in cow herds is the increase in the number of somatic cells, which cause losses for both producers and milk processors. Microorganisms involved in inflammation process in cows udder are often resistant for antibiotics, which are available with the most commonly used drug. These issues forced scientists to looking for new solutions in udder inflammations treatment.

Nanotechnology is currently one of the fastest growing fields of science, and the properties of nanoparticles are increasingly used in medicine, veterinary and pharmaceutical industries. Unique chemical and physical properties, as well as large surface area in relation to its volume, make nanomaterials an alternative in combating pathogens, including those causing mastitis in dairy cows. Literature data indicate more than 20 different nanoparticles of elements, whose properties allow their use in medicine and veterinary medicine, however, silver, gold and copper nanoparticles are most often used to fight pathogenic microorganisms. Moreover, nanoparticles do not effect on bacteria resistance which is currently the most crucial problem in mastitis treatment.

Nanoparticles also have toxic effect on bacteria because of formation reactive oxygen species, DNA degradation and lipids and proteins peroxidation. Gram-positive bacteria have thick peptidoglycan layer that makes them less susceptible on toxicity of silver nanoparticles comparing to Gram-negative bacteria. Gold nanoparticles change the membrane potential and activity of adenosine triphosphate synthesis (ATP) in the pathogen cell, which leads to inhibition of metabolism in pathogenic bacterial strains. Copper nanoparticles are more toxic for Gram-positive bacteria what results in damaging their cells membranes. It is connected with high amount of amine and carboxyl groups that are part of cell membranes in Gram-positive bacteria.

Currently, studies are being conducted to develop synergistic combinations of nanoparticles in mixtures that will be most effective in the treatment of various pathogens.

*The study was funded by National Centre for Research and Development

# GREEN SYNTHESIS OF STABILISED GOLD NANOPARTICLES

Aleksandra Wosztyl[1], Agnieszka Jędrych[1], Michał Wójcik[1]

1 Laboratory of Organic Nanomaterials and Biomolecules, Faculty of Chemistry, University of Warsaw, Poland
aleksandra.wosztyl24@gmail,com

Nanoparticles are emerging as a promising class of therapeutics for cancer. Clinical results suggest that therapeutics based on nanoparticles can show enhanced efficacy, while simultaneously reducing side effects arising from its properties, such as more targeted localization in tumours.

The aim of the project is to obtain peptides-capped nanoparticles, which act as an intracellular delivery of anticancer agents to tumor tissues. There are many publications, which indicate glutathione-stabilized gold nanoparticles, making them properly examined. Glutathione-stabilized gold nanoparticles synthesis distinguish from its stability. Moreover glutathione occurs in human body. It is needed to transform reactive oxygen species into harmless form, what stands out for good assimilability of glutathione-stabilized gold nanoparticles. Furthermore, glutathione has an amino group (-NH2), a thiol group (-SH) and carboxyl groups (-COOH), which set it as a perfect component to assemble with the therapeutic entities.

The synthesis features use of yeast extract instead of pure glutathione. Yeast extract contains from 5 up to 7% of glutathione, what gives the opportunity to optimize synthesis and make it more economical and eco-friendly. Usage of gold nanoparticles also provides entire removability from the organism[1].

Results show that changing parameters of the synthesis, such as reducing quantity of yeast extract or using buffer solutions influence on physical and chemical properties of gold nanoparticles.

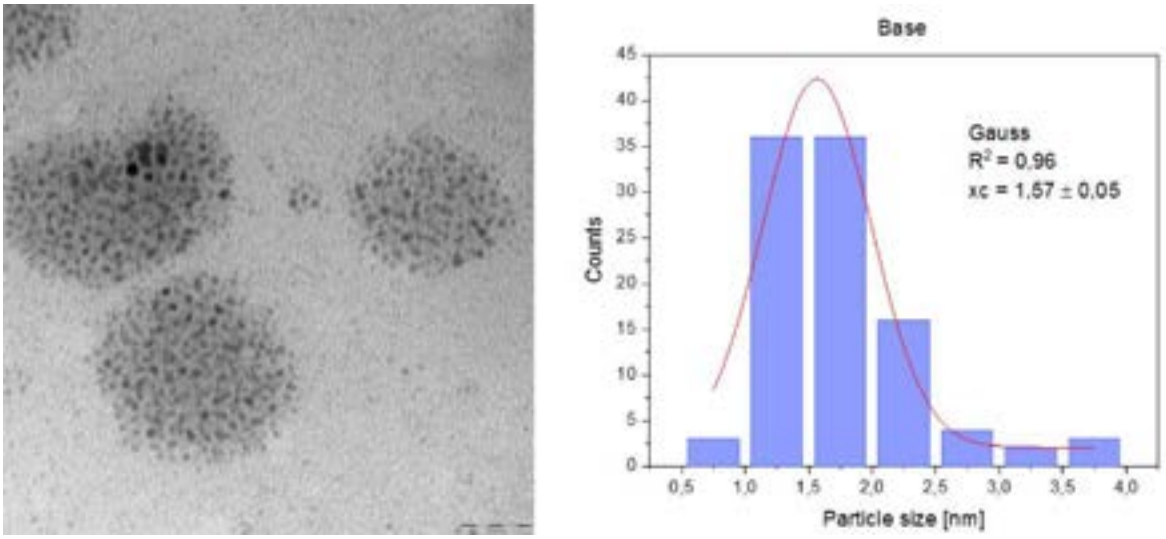


Fig. 1. Base synthesis using yeast extract. a) TEM image [scale: 20 nm]. b) Histogram of size distribution 1.57±0.05 nm.

Received nanoparticles have been characterized by SAXS, TEM, and UV-Vis analysis. In the future, further analyzation with SEM and MTT assay is planned.

[1] C.A.Simpson, In vivo toxicity, biodistribution, and clearance of glutathione-coated gold nanoparticles, Nanomedicine, 257–263(2013).

# ELECTROCHEMICAL PROPERTIES OF LIVBO$_3$F GLASS AND NANOMATERIAL

Przemysław P. Michalski[1], Jędrzej Doliński[1], Tomasz K. Pietrzak[1] and Jerzy E. Garbarczyk[1]

[1]Faculty of Physics, Warsaw University of Technology, Koszykowa 75, 00-662 Warsaw, Poland
michalski@if.pw.edu.pl

Lithium-vanadium fluorophosphate (so-called tavorite $LiVPO_4F$) is a cathode material for Li-ion batteries. Due to a high voltage value close to 4.2 V, it can be used in electric cars and other high-power mobile devices. On the other hand, its theoretical gravimetric capacity is modest and close to 156 mAh/g [1].

One of the possibilities to improve this value is the exchange of the heavy phosphate group to other lighter anionic group. In this work, the $PO_4^{3-}$ group was exchanged by the $BO_3^{3-}$, leading to synthesis of nominal composition $LiVBO_3F$. The material was obtained in a glassy form using melt-quenching method. After the melting, the glass was subjected to thermal nanocrystallization in order to obtain highly-conductive nanocomposite material.

The initial material was amorphous, which was confirmed by XRD method. Also, in the DTA thermograms, a glass transition and a few crystallization peaks were visible. After nanocrystallization, the electrochemically active $LiV_2O_5$ and $LiVO_3$ phases were present, with some addition of $B_2O_3$ phase. Nanocrystallization also led to improvement of electrical properties – in case of the glass, the total conductivity in RT (room temperature) was equal to $5 \cdot 10^{-9}$ S/cm, while after nanocrystallization in 400 °C and cooling down to RT – $1.2 \cdot 10^{-3}$ S/cm. The results of transference numbers measurement are also encouraging – in case of the glass, the ionic transference number $t_i$ was equal to 0.65, while for nanocomposite $t_i \approx 0.01$ (Fig. 1).

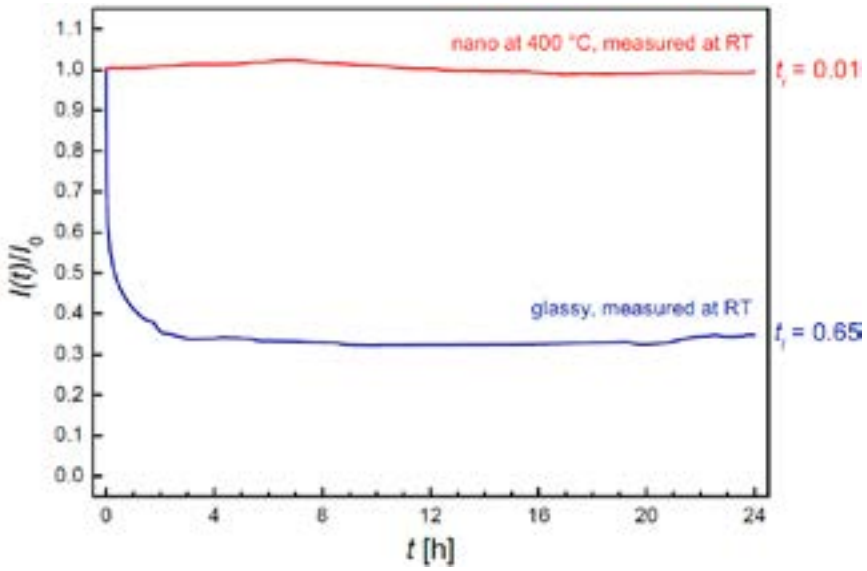


Fig. 1. The result of transference numbers measurement for a glass (blue line) and for nanocomposite (red line).

[1] M.V. Reddy, G.V. Subba Rao, B.V.R. Chowdari, Journal of Power Sources **195** (2010) 5768–5774.

# OPTIMIZATION OF ELECTRICAL PROPERTIES OF NANOCRYSTALLIZED VANADIUM-DOPED LITHIUM-MANGANESE-BORATE GLASSES

Agata Gołębiewska, Tomasz K. Pietrzak, Przemysław P. Michalski, Marek Wasiucionek

Faculty of Physics, Warsaw University of Technology, Koszykowa 75, 00-662 Warsaw, Poland
agata.golebiewska@fizyka.pw.edu.pl

Energy storage field is becoming more crucial nowadays, especially when it comes to ecological energy sources or electric cars industries. Therefore, it is worth to focus on studies towards new potential cathode materials in order to improve batteries parameters, especially when demand on electrochemical cells is rising.

Lithium manganese borate has found high interest in nowadays research on cathode materials for Li-ion batteries mostly due to its high theoretical gravimetric capacity of 222 mAh/g [1], which is even greater than for the widely studied phosphates. A glassy sample with nominal composition $LiMnBO_3$ was successfully synthesized using melt-quenching method and exhibited promising glass-forming properties. Therefore, thermal nanocrystallization method was applied then to obtain nanocrystalline material and study its properties [2]. However, our research on this compound showed that final electrical conductivity after nanocrystallization was still not sufficient enough. Basing on the studies [3] on vanadium-doped $LiFePO_4$ compound and on conclusion that even small amount of vanadium can significantly improve electrical and electrochemical properties of material, we attempted to dope aforementioned $LiMnBO_3$ with vanadium.

Glassy $LiMn_{0.925}V_{0.05}BO_3$ was successfully synthesized with use of melt-quenching process. Then, the samples were nanocrystallized in different temperatures and characterized with structural (XRD, SEM), thermal (DTA), and electrical (IS, TEP) methods.

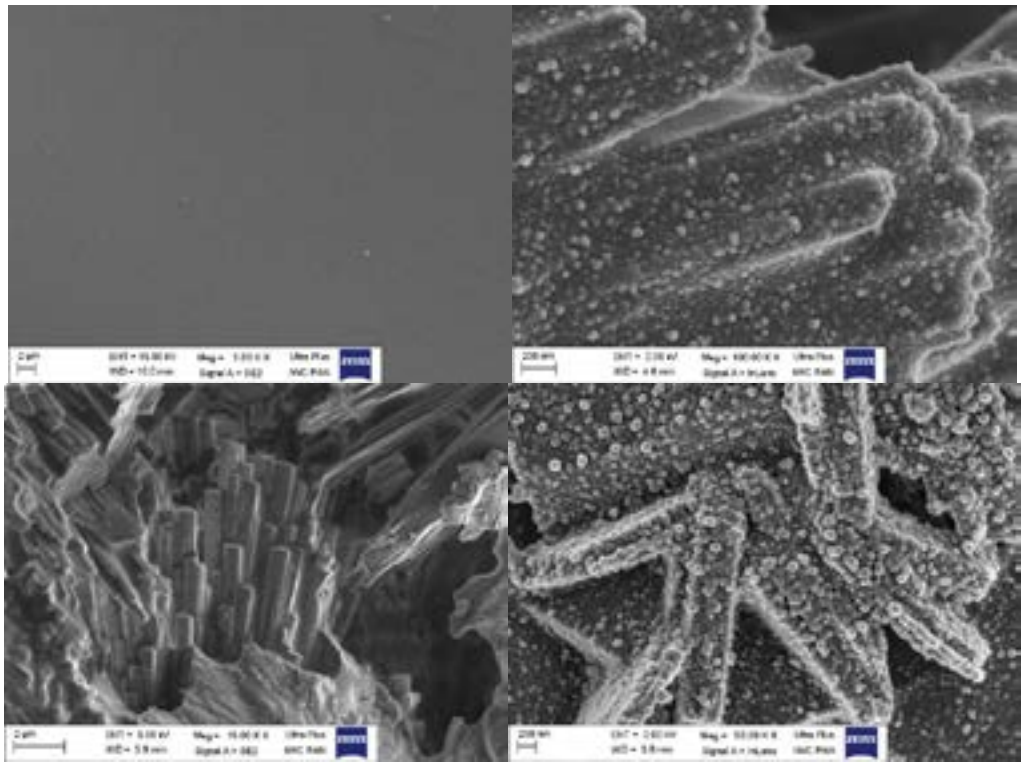

Fig. 1. SEM images for samples: upper left – amorphous, upper right – nanocrystallized at 600 °C, bottom left – nanocrystallized at 625 °C, bottom right – nanocrystallized at 675 °C.

[1] V. Legagneur, Y. An, A. Mosbah, R. Portal, A. Le Gal La Salle, A. Verbaere, D. Guyomard, Y. Piffard. Solid State Ionics 139 (2001) 37–46.
[2] A. Gołębiewska, Bachelor Thesis, Warsaw University of Technology (2017).
[3] F. Omenya, N.A. Chernova, S. Upreti, P.Y. Zavalij, K.-W. Nam, X.-Q. Yang, M.S. Whittingham, Chemistry of Materials 23 (2011) 4733-4740.

# THE INFLUENCE OF POLYMERIZATION USING GLUCOSE BIOSENSOR BASED ON INSOLUBLE MEDIATOR

Erika Putincevaite[1], Almira Ramanaviciene[2], Natalija German[1,2]

[1] Department of Chemistry and Bioengineering, Faculty of Fundamental Sciences, Vilnius Gediminas Technical University, Sauletekio ave.11, LT-10223, Vilnius, Lithuania
[2] Division of Immunology, State Research Institute Center for Innovative Medicine, Santariskių g. 5, LT-08406, Vilnius, Lithuania

erika.putincevaite@stud.vgtu.lt

The integration of nanotechnology with biology and electrochemistry produce major advantages in the field of electrochemical sensors. Nanotechnology is rapidly evolving to open new materials (nanoparticles, nanostructures) to solve bioanalytical problems, including specificity, stability and sensitivity [1,2]. Last decades biosensors have found promising applications in biotechnology, diagnostic technology, food and agriculture product processing, clinical analysis, medicine and pollution monitoring [2,3,4]. Main request for electrochemical biosensors are rapidity, simplicity to operate, long-term stability, miniaturization, elimination of oxygen dependency, high selectivity and sensitivity, easy fabrication and easy in application, the suitability to use in turbid media [3,4,5]. Conducting polymers improve the key performance characteristics of glucose sensors and are used to enhance rapidity, sensitivity and versatility of biosensors in diagnostics of analytes [3,6].

The main aim of this research was to evaluate the influence of polyaniline and polypyrrole on the sensitivity of glucose biosensors based on electrochemically synthesized gold nanostructures and immobilized insoluble mediator and glucose oxidase on carbon rod electrode. Gold nanostructures in a combination with glucose oxidase offered some advantages for the design of electrochemical biosensors. Gold compounds have got influence on the electrochemical signals of glucose oxidase and 1,10-phenanthroline-5,6 dione based electrodes. The optimal polymer, conditions of enzymatic polymerization were chosen to achieve the highest current responses of glucose. It was evaluated the sensitivity of determination, analytical characteristics and stability of glucose biosensor modified by pyrrole.

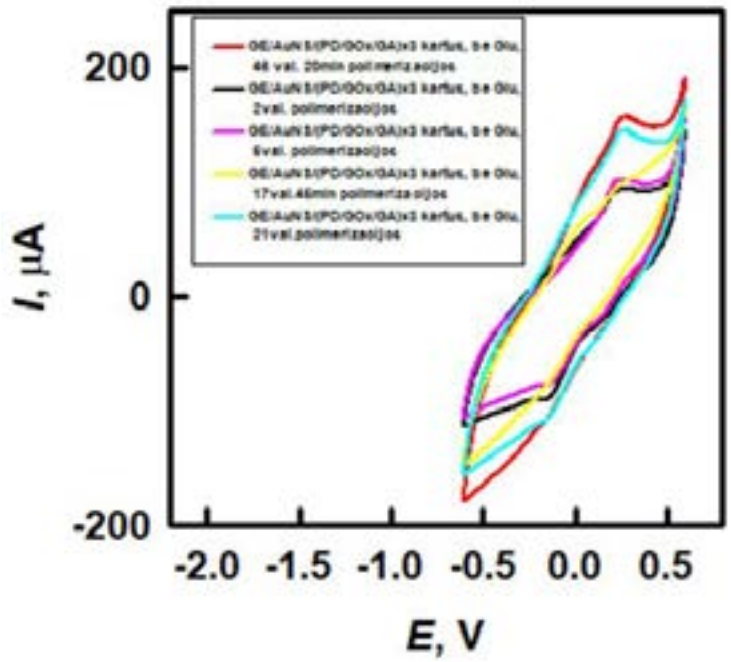


Fig.1. Cyclic voltamperograms of glucose biosensor modified by gold nanoparticles and pyrrole during different enzymatic polymerization time.

Gold nanostructures could be apply as novel transducer in the design of electrochemical glucose biosensors and could be important in most diagnostic and biocatalytic applications.

[1] M. Pumera, S. Sánchez, I. Ichinose, J. Tang, Electrochemical nanobiosensors, Sensors and Actuators B **123**, 1195-1205(2007).
[2] F. Wang, S. Hu, Electrochemical sensors based on metal and semiconductor nanoparticles, Microchim Acta **165**, 1-22 (2009).
[3] M. Gerard, A. Chaubey, B.D. Malhotra, Application of conducting polymers to biosensors, Biosens. Bioelectron. **17**, 345-359 (2002).
[4] P. D'Orazio, Biosensors in clinical chemistry, Clin. Chim. Acta **334**, 41-69 (2003).
[5] E. Bakker, Y. Qin, Electrochemical Sensors, Anal. Chem. **78**, 3965-3983(2006).
[6] Y. Wang, H. Xu, J. Zhang, G. Li, Electrochemical sensors for clinic analysis, Sensors **8**, 2043-2081(2008).

# THE CREATION OF GLUCOSE BIOSENSOR MODIFIED BY GOLD NANOSTRUCTURES AND POLYMER

Roberta Butkute[1], Rokas Jonaitis[1], Almira Ramanaviciene[2], Natalija German[1,2]

[1] Department of Chemistry and Bioengineering, Faculty of Fundamental Sciences, Vilnius Gediminas Technical University, Sauletekio ave.11, LT-10223, Vilnius, Lithuania
[2] Division of Immunology, State Research Institute Center for Innovative Medicine, Santariskių g. 5, LT-08406, Vilnius, Lithuania

roberta.butkute@stud.vgtu.lt

Nanotechnology has recently become one of the most exciting forefront fields in analytical chemistry and now is rapidly evolving to open new combination of electrochemical biosensors constructions and methods, resolve challenging bioanalytical problems, including specificity, stability and sensitivity [1,2]. Biosensors with immobilized enzymes and gold compounds are characterized by highly selectivity, sensitivity, rapidity, reversibility, reproducibility, practical application and excellent catalytic activities [3,4]. Characterized important properties, such as electrical conductivity, nonlinear optical and luminiscence properties, versatility conducting polymers are used as information storage materials and chemical sensors [5,6,7].

The main aim of this research was to create glucose biosensors using electrochemically synthesized gold nanostructures, immobilized by glucose oxidase and modified by polyaniline and/or polypyrrole on the surface of carbon rod electrode. Electrochemically synthesized gold nanostructures in a combination with enzyme offered some advantages for the design of electrochemical biosensors. The gold compounds facilitated indirect electron transfer, via phenazine methosulfate as the redox mediator and showed the positive effect on the electrochemical signals of glucose oxidase-based electrodes. It was chosen the optimal conditions of electrochemically synthesis and concentration of gold nanostructures, medium of analyze, registration's method, conditions of enzymatic polymerization to achieve the highest current responses of glucose. It was evaluated the sensitivity of determination, analytical characteristics and stability of created analytical system. Obtained results were compared with modified by polymer biosensor immobilized only by enzyme. The research of electrochemical glucose biosensor based on gold nanostructures and polypyrrole was characterized by high sensitivity, good reproducibility (9.83 %), lower detection of limit (0.07 mmol $L^{-1)}$ and great application in real objects.

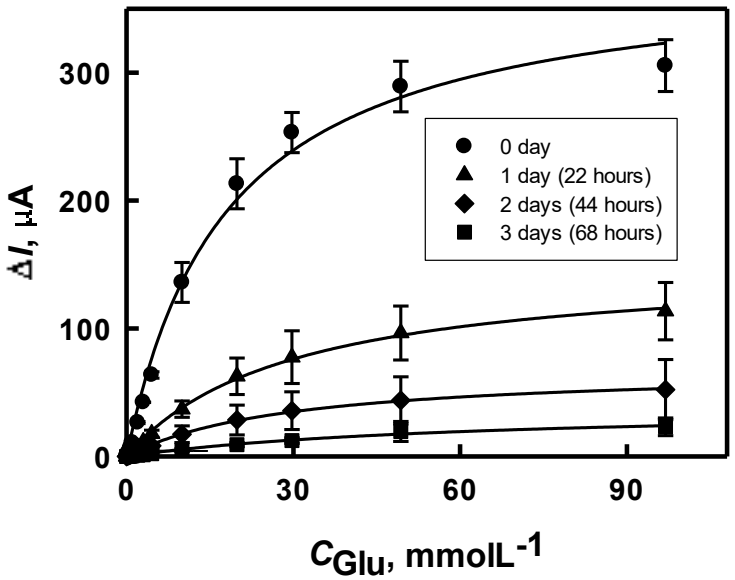


Fig.1. Calibration plots of modified by polypyrrole GOx/AuNS/GR electrodes.

Furthermore, the higher sensitivity of the biosensors also offers the possibility of using ultramicroelectrode designing for in vivo measurements.

[1] M. Pumera, S. Sánchez, I. Ichinose, J. Tang, Electrochemical nanobiosensors, Sensors and Actuators B **123**, 1195-1205(2007).
[2] F. Wang, S. Hu, Electrochemical sensors based on metal and semiconductor nanoparticles, Microchim Acta **165**, 1-22 (2009).
[3] P. Yáñez-Sedeño, J.M. Pingarrón, Gold nanoparticle-based electrochemical biosensors, Anal. Bioanal. Chem. 382 884-886 (2005).
[4] N. German, A. Ramanavicius, A. Ramanaviciene, Electrochemical deposition of gold nanoparticles on graphite rod for glucose biosensing, Sens. Actuators B 203 25-34 (2014).
[5] M.S. Freund, B.A. Deore, *Self-Doped Conducting Polymers* 1-74 *(*John Wiley & Sons, Ltd. 2007).
[6] S.C. Luo, Conducting polymers as biointerfaces and biomaterials: A perspective for a special issue of polymer reviews, Polymer Reviews **53** 303-310 (2013).
[7] J. Heinze, B.A. Frontana-Uribe, S. Ludwigs, Electrochemistry of conducting polymers - persistent models and new concepts, Chem. Rev. **110** 4724-4771(2010).

# DISINFECTANT PRE-DIPPING PREPARATIONS FOR DAIRY COWS WITH SILVER-COPPER NANOPARTICLES ADDITION*

Brygida Kruzińska[1], Aleksandra Kalińska[1], Daniel Radzikowski[1], Jan Slósarz[1], Marcin Gołębiewski[1]

[1] Department of Animal Breeding and Production, Warsaw University of Life Sciences, Poland
brygida_kruzińska@sggw.pl

Udder inflammations are one of the most crucial issues in dairy herds. Pathogens involved in inflammation process in cows udder (mastitis) are often resistant for conventional antibiotics. Because of that, scientists are still looking for new solutions in mastitis treatment and prevention. Metal nanoparticles can be one of the most promising agents. Unique properties of nanoparticles and lack of possibility of occurring resistant strains are only some of their best advantages. Moreover, metal nanoparticles are already used in human or veterinary medicine.

The main goal of the experiment was preliminary *in vitro* evaluation of *Staphylococcus aureus* and *Escherichia coli* viability using pre-dipping mixture of commercially available cosmetic substrates and silver-copper (AgCu) nanoparticles addition.

Two experimental mixtures containing common cosmetic substrates and silver- copper nanoparticles addition were prepared. Glass flasks containing only nutrient broth medium (Biomaxima, Poland) for control group (C), experimental groups with 1 ppm nanoparticles addition (Ag, Cu, AgCu), and experimental groups containing mixture of cosmetic substrates and 1 ppm nanoparticles addition (D1, D2) were prepared. Two bacteria species: *S. aureus* and *E. coli* isolated from cow's milk were used in the experiment to estimate pathogens viability, according to control group. Flasks were incubated for 24 hours in 37°C and 5% $CO_2$. Each group for each pathogen was prepared in three repetitions. Bacteria viability was calculated using absorbance measurement (570 nm) in PrestoBlue test (ThermoFisher, Poland).

Obtained results revealed that viability of *S. aureus* in P1 and P2 was 90,64% and 91,41%. Results for *E. coli* group were P1=48,13% and P2=42,50%. Viability of bacteria cells in flasks with only nanoparticles addition were: 67,35%, 57,38%, 49,90%, respectively for Ag, Cu, AgCu.

Observed changes in *in vitro* experiment suggest that prepared pre-dipping mixtures could be used in mastitis pathogens prevention. However, nanoparticles influence on bacteria viability requires further analysis.

*The study was funded by National Centre for Research and Development

# DISINFECTANT PREPARAIONS (DIPPING) FOR DAIRY COWS WITH SILVER AND COPPER NANOPARTICLES ADDITION*

Aleksandra Kalińska[1], Daniel Radzikowski[1], Brygida Kruzińska[1], Jan Slósarz[1], Marcin Gołębiewski[1]

[1] Department of Animal Breeding and Production, Warsaw University of Life Sciences, Poland
aleksandra_kalinska@sggw.pl

Udder inflammations, usually called mastitis, are one of the most crucial issues in dairy herds. Pathogens involved in inflammation process in cows udder are often resistant for conventional antibiotics. Therefore, scientists are looking for new and innovative solutions in mastitis treatment and prevention. Nanoparticles are becoming one of the most promising agents. Their unique properties and lack of possibility of occurring resistant strains are only some of their best advantages.

The aim of the study was preliminary *in vitro* evaluation of *Staphylococcus aureus* and *Escherichia coli* viability using dipping mixture of commercially available cosmetic substrates and silver (Ag), copper (Cu) nanoparticles addition.

Two experimental mixtures containing common cosmetic substrates and silver and copper nanoparticles addition were prepared. Glass flasks containing nutrient broth (Biomaxima, Poland) were prepared for control group (C), experimental groups with 1 ppm nanoparticles addition (Ag, Cu, AgCu), and experimental groups containing mixture of cosmetic substrates and nanoparticles (D1, D2). Two bacteria species: *S. aureus* and *E. coli* isolated from cow's milk were used in the study to estimate pathogens viability, according to control group. Flasks were incubated for 24 hours in 37°C and 5% $CO_2$. Each group for each pathogen was prepared in three repetitions. Bacteria viability were calculated using absorbance measurement (570 nm) in PrestoBlue test (ThermoFisher, Poland).

Obtained results revealed that viability of *S. aureus* in D1 and D2 was 47,23% and 44,31%. Similar results were obtained for *E. coli* group (D1=51,43% and D2=57,86%). Viability of bacteria cells in flasks with only nanoparticles addition were: 67,35%, 57,38%, 49,90%, respectively for Ag, Cu, AgCu.

Observed changes in *in vitro* experiment suggest that prepared mixtures could be useful in mastitis pathogens prevention. However, nanoparticles influence on bacteria viability require further analysis.

*The study was funded by National Centre for Research and Development

# THE EFFECT OF THE USE OF TISSUES WITH THE ADDITON OF SILVER AND COPPER NANOPARTICLES APPLIED TO HYGIENE UDDER OF DAIRY COWS BEFORE MILKING *

Daniel Radzikowski[1], Aleksandra Kalińska[1], Brygida Kruzińska[1], Jan Slósarz[1], Marcin Gołębiewski[1], Urszula Ostaszewska[2]

[1] Department of Animal Breeding and Production, Warsaw University of Life Sciences, Poland
[2] Department of Cattle Breeding and Milk Evaluation, Siedlce University of Natural Sciences and Humanities, Poland
daniel18-1994@wp.pl

Mastitis is caused by various strains of bacteria, fungi, and algae. Pathogens that cause mastitis in dairy cows are more and more often resistant to treatment with conventional methods (antibiotics), which is why scientists are looking for new solutions for the treatment of mastitis. The main form of treatment and prophylaxis of mastitis is antibiotic therapy, the effectiveness of which decreases due to the increase in bacterial resistance to the drugs used. The cause of this phenomenon is the excessive use of antibiotics in the treatment of animals, contributing to the emergence of strains resistant to therapies. One of the ways to eliminate microorganisms is the use of nanoparticles. The aim of the research was to determine the bactericidal properties of silver and copper nanoparticles as an addition to cow udder hygiene tissues.

Disposable udder hygiene wipes have been impregnated with silver and copper nanoparticles. The research was carried out in a herd of dairy cows, which was located in south-eastern Poland. The experiment used 10 Polish Holstein-Friesian cows. In each cow, 2 control tees and 2 test teats were selected. The control teats were cleaned using wipes without the addition of nanoparticles, and the test teats were cleaned using wipes impregnated with silver and copper nanoparticles. After testing, all tissues were placed in sterile cups. Each sterile cup used in the experiment contained 40 ml of 0,1 NaCl. After 12 hours, microbiological analysis was carried out to determine the pathogens found on the tissues.

The results showed that 98% of tissues were pathogens causing mastitis (*Streptococcus uberis, Streptococcus dysgalactiae, Escherichia Coli*). The cultures made of nanoparticle tissues were characterized by a smaller number of microorganisms. The experiment showed the bactericidal properties of silver and copper nanoparticles. The research results indicate a further need to carry out scientific work to develop new products with nanoparticles used in the treatment and prophylaxis of mastitis in dairy herds.

*The study was funded by Warsaw University of Life Sciences as grant for young scientists.

# ZnO TETRAPODS: SYNTHESIS AND APPLICATION AS UV SENSORS

Rasa Mardosaitė[1,2], Agnė Šulčiūtė[1,2], Simas Račkauskas[1,3*]

[1] Department of Physics, Kaunas University of Technology, Lithuania
[2] Department of Physical and Inorganic Chemistry, Kaunas University of Technology, Lithuania
[3] Institute of Materials Science, Kaunas University of Technology, Lithuania
Rasa.Mardosaite@ktu.lt

ZnO nanowires (NWs) have attracted a great deal of interest due to their exceptional properties and application for various electronic, photonic, biological, and energy related usage [1-2]. ZnO tetrapods (Ts), as more sophisticated forms of NWs, can be grown by simply controlling the crystal grow direction of ZnO. Among others (hydrothermal processes or chemical vapor deposition), a direct growth of ZnO Ts from Zn vapor is a highly attractive synthesis method with advantages of being a simple and high yield process. However, the control of concentration for uniform structures is still challenging.

Applicability of the ZnO Ts can be used as efficient UV sensors. ZnO NW sensing application is interesting by its high surface ratio which provides an enhancement of the surface effects. The main principle of sensing is to get a measurable response (mostly electrical) from the added substance. High sensitivity (response to extremely small amounts), selectivity (ability to differentiate between various substances) and linearity (for instance, response is linear amount of substance measured) are the main parameters for efficient sensors [3]. UV sensor response is associated with the depletion layer width. When illuminating ZnO Ts with a wavelength, higher than the ZnO bandgap (3.37 eV for ZnO), photogenerated holes combine with the negative $O_2$ ions, inducing desorption and increasing the conductivity.

In this work, ZnO Ts were synthesized in a continuous flow reactor by a gas phase oxidation of Zn metal vapor in an air atmosphere. No catalysts were used at any stage of synthesis. To produce ZnO T structure of nanometer size, a few experimental parameters had to be carefully controlled: Zn vapor at relatively high concentration must be quickly mixed with $O_2$, whereas the growth time should be kept minimal to avoid the thickening of the ZnO T legs. Thereby, the synthesis reactor was based on the combustion of Zn micron-sized particles in an open reactor in the air atmosphere. These allowed to rapidly evaporate Zn, to oxidize Zn vapor by surrounding air oxygen, and to form ZnO Ts by supersaturated ZnO vapor condensation. It was shown that morphology of ZnO Ts can be adjusted by Zn vapor pressure in the reactor by changing the evaporation temperature. The highest aspect ratio of single crystal ZnO T structure was obtained at 700 °C.

Finally, ZnO tetrapods showed high current increase under UV irradiation thus demonstrating potential application possibilities for transparent and flexible UV sensors.


Fig. 1. Principle of ZnO nanowire chemoresistive sensing based on the depletion layer width change with absorption-desorption of oxygen

[1] S. Rackauskas, K. Mustonen, T. Jarvinen et al., Synthesis of ZnO tetrapods for flexible and transparent UV sensors, Nanotechnology 23, 095502 (2012).
[2] S. Rackauskas, O. Klimova, H. Jiang et al., A Novel Method for Continuous Synthesis of ZnO Tetrapods, J. Phys. Chem. C 119, 16366 (2015).
[3] S. Rackauskas, N. Barbero, C. Barolo, G. Viscardi, ZnO Nanowire Application in Chemoresistive Sensing: A Review, Nanomaterials **7**, 381 (2017).

# NANOCRYSTALLIZATION OF GLASSY ANALOGS OF ALLUAUDITES WITH NOMINAL COMPOSITION OF $Na_2M_3(PO_4)_3$ (M = Fe, V, Mn)

Maciej Nowagiel, Adrianna Chamryga, Tomasz K. Pietrzak

Faculty of Physics, Warsaw University of Technology, Poland
m.nowagiel@gmail.com

The very first description of the alluaudite structure was given by Fisher in 1955 [1], and the investigation was carried out on natural minerals. The ideal composition of alluaudite $-K_xM_3(PO_4)_3$, where K = Na, Li, Ca etc., M = Fe, Mn etc., $0 \le x \le 4$ — was established by Moore [2]. Present knowledge of alluaudite structure comes from Hatert [3]. An alluaudite material of composition $Na_xMnFe_2(PO_4)_3$ attracted much interest of Trad and co-workers [4], since its theoretical gravimetric capacity could be close to 170 mAh/g if reversibly cycled between $x = 0$ and 2. Because electrochemical performance in polycrystalline materials was not spectacular, it was concluded that to improve its performance, nanomaterials are demanded.

Therefore we decided to synthesize amorphous analogs of alluaudites and apply properly planned heat-treatment. In previous studies on amorphous analogs of cathode materials for Li-ion batteries [5], a significant increase of electrical conductivity was observed as a result of this approach. It was suggested to be correlative with developing 10 nm size nanograins, which provide convenient conditions to polaron hopping mechanism of conduction.

In this work, we have proven the possibility of preparation of glassy alluaudites and that their crystallization is consistent with foregoing works [2-3]. We successfully synthesized glasses of nominal composition $Na_2M_3(PO_4)_3$, where $M_3 = Fe_3$, $Fe_2V$, FeMnV. Their thermal nanocrystallization led to nanomaterials isostructural with $Na_2MnFe_2(PO_4)_3$ reference pattern (PDF no. 04-012-0978, Fig. 1). As expected, in preliminary measurements, a significant (7 orders of magnitude) and irreversible increase of the conductivity was observed as a result of this process.

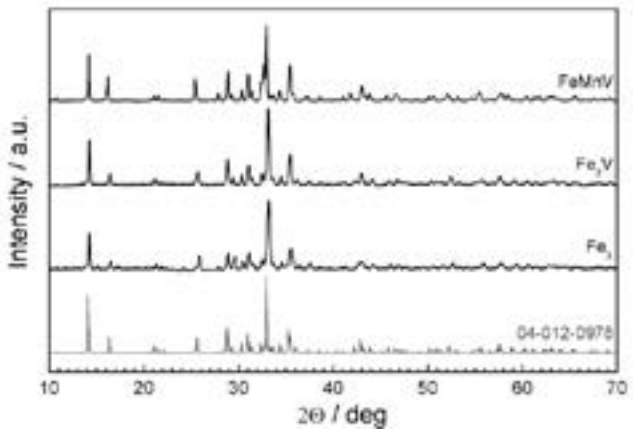


Fig. 1. XRD patterns of nanocrystallized $Na_2M_3(PO_4)_3$ glasses with $M_3 = Fe_3$, $Fe_2V$, FeMnV. A reference pattern is given for comparison.

[1] D.J. Fisher, American Mineralogist **40** (1955) 1100–1109.
[2] P.B. Moore, American Mineralogist **56** (1971) 1955–1975.
[3] F. Hatert et al., European Journal of Mineralogy **12** (2000) 847–857.
[4] K. Trad et al., Chemistry of Materials **22** (2010) 5554–5562.
[5] T.K. Pietrzak et al., Materials Science and Engineering **B 213** (2016) 140–147.

# SYNTHESIS, CHARACTERIZATION AND INVESTIGATION OF N-DOPED CARBON SUPPORTED Au-Co AND Au-Ni NANOCOMPOSITES

Danielė Kurlenskaitė, Aldona Balčiūnaitė, Daina Upskuvienė, Loreta Tamašauskaitė-Tamašiūnaitė, Eugenijus Norkus

Department of Catalysis, Center for Physical Sciences and Technology, Saulėtekio Ave. 3, LT-10257, Vilnius, Lithuania
daniele1kurlenskaite@gmail.com

The search and application of new efficient catalyst compositions for practical low temperature proton exchange membrane fuel elements (PEMFC), replacing well-known and expensive Pt or its alloy catalysts with base metals or reducing the amount of precious metals in catalysts, is a relevant research direction to improve and and reduce the price of fuel cells.

In this work, new nanocarbon material synthesized from bio-waste-alder chips was used to form an effective catalysts. Carbon powder from alder chips was chemically activated with NaOH at higher temperatures and then doped with nitrogen at a temperature of 800°C using dicyanodiamide (DCDA) as a nitrogen precursor. Then, gold-cobalt (Au-Co) and gold-nickel (Au-Ni) nanoparticles were precipitated on the nitrogen-doped carbon (N-doped carbon) using the microwave synthesis method.

For the synthesis, a reaction mixture consisting of N-doped carbon powder, 1.3 mM $HAuCl_4$, 0.06 M $CoCl_2$ or $NiCl_2$, 0.05 M NaOH and ethylene glycol was used. Microwave synthesis was performed using a Monowave 300 (Anton Paar) at a temperature of 150°C for 30 min. Synthesized Au-Co/N-doped carbon and Au-Ni/N-doped carbon nanocomposites were washed with acetone, distilled water and dried in a vacuum oven at a temperature of 80°C for 2 hours.

The surface morphology, structure, and composition of synthesized Au-Ni/N-doped carbon and Au-Co/N-doped carbon catalysts have been extensively investigated using transmission electron microscopy (TEM), X-ray photoelectron spectroscopy (XPS), scanning electron microscopy (SEM), Inductively Coupled Plasma Optical Emission Spectroscopy (ICP-OES), and Raman Spectroscopy.

TEM and Raman analysis data confirmed that the carbon powder derived from alder chips and nitrogen doped has a graphene structure. It has been found that the N-doped carbon powder consists of 92.68 at.% carbon, 0.74 at. % of nitrogen and 6.59 at. % of oxygen.

The use of the N-doped carbon as a substrate for the deposition of Au-Co and Au-Ni nanoparticles allows to develop an efficient catalysts for fuel cells.

# NANOCRYSTALLIZATION OF GLASSES IN LITHIUM-BORATE SYSTEM

Przemysław P. Michalski[1], Agata Gołębiewska[1], Jakub S. Otrębski[1], Olivier Lafon[2,3], Julien Trébosc[2], Tomasz K. Pietrzak[1] and Jerzy E. Garbarczyk[1]

[1]Faculty of Physics, Warsaw University of Technology, Koszykowa 75, 00-662 Warsaw, Poland
[2]University of Lille, CNRS, UMR 8181, UCCS-Unité de Catalyse et de Chimie du Solide, F-59000 Lille, France
[3]Institute Universitaire de France (IUF), 1 rue Descartes, 75231 Paris, France
michalski@if.pw.edu.pl

In the electrochemical energy storage field nanomaterials have established their position as a common solution to gravimetric capacity and cyclability of a cell related problems. There is a diversity of synthesis routes to produce nanostructured materials with desirable structure and properties. Most of them usually require sophisticated devices and preparation which cannot be easily scaled to industrial needs (e.g. MBE, MOCVD) or require many time-consuming steps of synthesis in various conditions (like sol-gel method).

Some time ago, interesting compounds with the composition $LiMBO_3$ (M = Fe, Mn) have emerged as potential cathode materials for Li-ion batteries [1]. The polycrystalline samples of those have exhibited low electronic and ionic conductivity which has led to insufficient gravimetric capacity and cyclability. Herein, we present our recent results of studies on selected physical properties of compounds obtained by thermal nanocrystallization of $LiMBO_3$ glasses. Previously, we have successfully applied this method e.g. in case of $LiFePO_4$-like system: $Li_2O$–$FeO$–$V_2O_5$–$P_2O_5$. The heat-treated materials exhibited an advantageous microstructure and significantly enhanced electric conductivity (up to 10 orders of magnitude!) [2].

In this work, $LiFe_xMn_{1x}BO_3$ ($x$ = 0, 0.25, 0.5, 0.75, 1) glasses were successfully synthesized and subsequently nanocrystallized. Glasses were obtained using melt-quenching method and characterized with thermal (DTA), structural (XRD, SEM) and electrical (IS) methods. Also nuclear magnetic resonance (NMR) was used to study the local environment of lithium ions. Manganese-rich samples exhibited better glass-forming properties, but the increase of electric conductivity after nanocrystallization was modest and the final conductivity was quite low. Addition of iron led to better conductivity and higher increases after nanocrystallization, but caused worse glass-forming properties. The dependencies of log(conductivity) and the activation energy on composition were linear (Fig. 1). These interesting results may be explained on the basis of Mott's theory of electron hopping. Also, by NMR and SEM methods, the presence of two lithium environments were proposed.

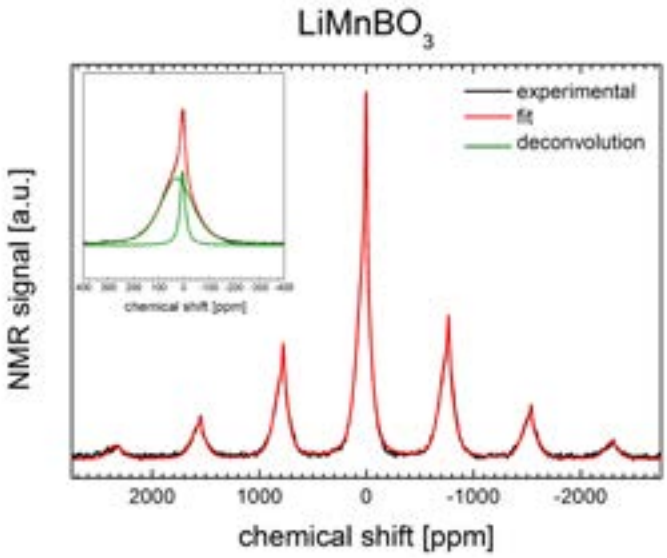


Fig. 1. Experimental (black line) and best-fit simulated (red line) 1D $^7$Li MAS NMR spectrum of the initial glass (black line) at 1.9 T with a MAS frequency of 30 kHz. The inset shows an expansion of the central transition. The simulated $^7$Li spectrum is the sum of two distinct lineshapes (displayed as olive lines in the inset).

**Acknowledgements**
This project has received funding from the European Union's Horizon 2020 research and innovation program under grant agreement No 731019 (EUSMI).

[1] V. Legagneur, Y. An, A. Mosbah, R. Portal, A. Le Gal La Salle, A. Verbaere, D. Guyomard, Y. Piffard, Solid State Ionics **139** (2001) 37–46.
[2] T.K. Pietrzak, M. Wasiucionek, P.P. Michalski, A. Kaleta, J.E. Garbarczyk, Materials Science and Engineering B **213** (2016) 140–147.

# BIOCOMPATIBLE AND HEAVY METAL FREE $CuInS_2$/ZnS QUANTUM DOTS FOR CANCER DIAGNOSTICS

Viktoras Mažeika[1,2], Dominyka Dapkutė[1,2], Artiom Skripka[3], Riccardo Marin[3], Fiorenzo Vetrone[3], Patrizia Canton[4], Ričardas Rotomskis[2,5], Vitalijus Karabanovas[2,6]

[1] Life Sciences Center, Vilnius University, Saulėtekio av. 7, LT-10257, Vilnius, Lithuania
[2] Biomedical Physics Laboratory, National Cancer Institute, P. Baublio 3B, LT-08406, Vilnius, Lithuania
[3] Institut National de la Recherche Scientifique, Centre Énergie, Matériaux et Télécommunications, Université du Québec, 1650 Boulevard Lionel-Boulet, Varennes, Quebec, Canada
[4] Department of Molecular Sciences and Nanosystems, Ca' Foscari University of Venice, Via Torino 155/b, I-30170, Venezia-Mestre, Italy
[5] Biophotonics group of Laser Research Centre, Vilnius University, Saulėtekio av. 9, LT-10222, Vilnius, Lithuania
[6] Department of Chemistry and Bioengineering, Vilnius Gediminas Technical University, Saulėtekio av. 11, LT-10223 Vilnius, Lithuania
viktoras.mazeika@gmc.stud.vu.lt

Quantum dots (QDs) have long been considered for various biomedical and therapeutic applications, for example, as drug delivery carriers or medical imaging agents. Possibly the most widely studied QDs for these purposes are CdSe and CdTe QDs because of their well-established and standardized synthesis methods, and good optical properties [1]. Another type of QDs that are currently under intense investigation are lead chalcogenide (namely PbS, PbSe and PbTe) QDs. These QDs exhibit photoluminescence (PL) in near-infrared (NIR) spectral region which coincides with human tissue transparency window; this property is important for deep-tissue imaging applications [2]. Even though Cd and Pb based QDs have very appealing PL properties over a wide range of emission wavelengths (from ultraviolet (UV) to NIR), both types of QDs are intrinsically toxic, which renders them unsuitable for therapeutic use [3]. This calls for research on QDs better suited for biomedical purposes, as such, these QDs would have to be composed of non-toxic materials and should still emit in the NIR region of tissue transparency window.

Heavy metal free $CuInS_2$ QDs are known to be less toxic, and emit bright PL reaching the tissue transparency window. In addition, core/shell structured $CuInS_2$/ZnS QDs can be obtained, further improving their PL quantum yield [4]. In spite of rapid advances made on the material science front, these structures are rather poorly researched from the biomedical standpoint. In order to make a move from material research to biomedical use, the nano-bio interface of these structures is ought to be thoroughly characterized and understood.

In this work, optical properties of $CuInS_2$/ZnS core/shell QDs and their stability in various media were investigated using steady-state and lifetime fluorescence spectroscopy. The size of the QDs was evaluated using atomic force microscopy and dynamic light scattering methods. The colloidal stability of the QDs in solution was assessed by measuring their zeta potential. The accumulation of QDs in cancer cells was investigated as well. Results of these experiments will help to assess the potential of using $CuInS_2$/ZnS QDs for cancer diagnostics, as well as their possible therapeutic use.

[1] D. Mo, L. Hu, G. Zeng et al., Cadmium-containing quantum dots: properties, applications and toxicity, Applied Microbiology and Biotechnology, **101(7)**, 2713–2733 (2017).
[2] F. C. J. M. van Veggel, Near-Infrared Quantum Dots and Their Delicate Synthesis, Challenging Characterization and Exciting Potential Applications, Chemistry of Materials, **26**, 111-122, 2014.
[3] R. Hardman, A Toxicologic Review of Quantum Dots: Toxicity Depends on Physicochemical and Environmental Factors, Environmental Health Perspectives, **114(2)**, 165–172, 2006.
[4] T. Pons, E. Pic, N. Lequeux et al., Cadmium-Free $CuInS_2$/ZnS Quantum Dots for Sentinel Lymph Node Imaging with Reduced Toxicity, ACS Nano, **4(5)**, 2531–2538, 2010.

# FABRICATION AND CHARACTERIZATION OF ELECTRICALLY TUNABLE MULTILAYER HYPERBOLIC METAMATERIAL

Alexander Korneluk[1], Julia Szymczak[1], Tomasz Stefaniuk[1]

[1] Faculty of Physics, University of Warsaw, Poland
a.korneluk3@student.uw.edu.pl

We report on development and characterization of electrically tunable metamaterial exhibiting elliptic, epsilon-near-zero and hyperbolic dispersion regimes [1,2]. The structure under study consists out of stacks of alternating layers of silver, fused silica and indium-tin-oxide (ITO), and is covered with $SiO_2$ antireflective coatings. To provide high transparency of the metamaterial the thicknesses of particular subwavelength layers were chosen after initial numerical modelling. To actively tune the optical response of this metal-oxide-semiconductor heterostructure we exploit the fact that the refractive index of ITO depends locally from the strength of the applied external electric field [3]. ITO is a degenerately doped semiconductor with optical properties governed mainly by the free electrons. The amount of free electrons in ITO depends mainly on Sn doping levels and the oxygen vacancy concentration. Both factors can be changed by selection of different fabrication procedures.

Here, we discuss the details of the fabrication method and describe the encountered difficulties. In particular we concentrate on the properties of ITO layers, which strongly depend on experimental conditions. In our investigations the subsequent films were evaporated using physical vapour deposition process (PVD). Afterwards, the samples were characterised using Scanning Electron Microscope (SEM) with Energy Dispersive Spectroscopy module (EDS), Atomic Force Microscopy (AFM), Hall Effect measurement system and optical microscopy. We study how the i) thermal annealing, ii) presence of oxygen, iii) ion assistance deposition and iv) substrate roughness affects the electric, optical and morphological properties of individual thin films and the entire structure. Some of these procedures have a contrary influence on the performance of the metadevice, improving one feature and decreasing the other. For example, post-annealing lead to higher transparency, but at the expense of homogeneity of the structure (see Fig. 1).

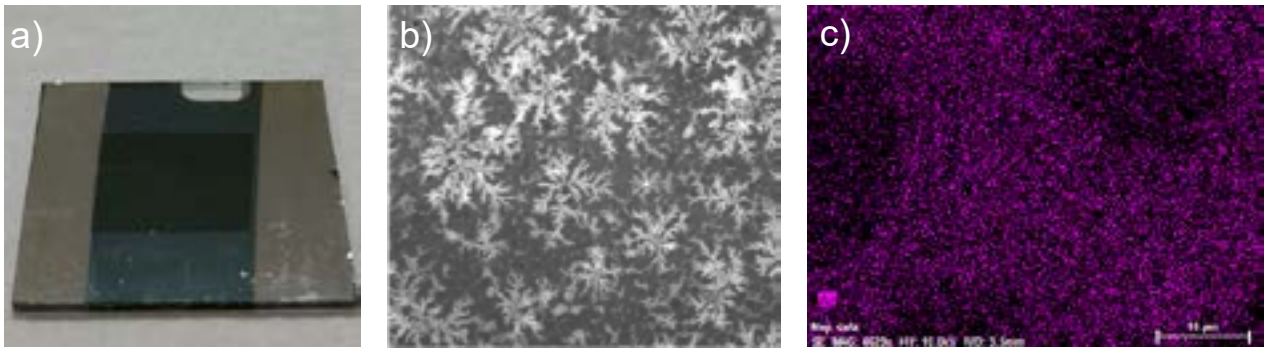


Fig. 1. (a) Photograph of the multilayer metamaterial structure. (b) Image from the optical microscopy, of the sample after post-annealing in 500 °C for 2 hours. It reveals star-like shapes. (c) Silver concentration map of the annealed sample obtained via EDS technique.

Overcoming these obstacles can possibly lead to development of electrically tuneable multilayer metamaterial, which unique optical properties like e.g.: spatial and temporal frequency filtering, hyperbolic dispersion, superresolving imaging, perfect absorption or enhanced nonlinear response can be modified across the VIS and NIR spectrum ranges simply by the applied voltage.

[1] Shekhar, Prashant & Atkinson, Jonathan & Jacob, Zubin. (2014). Hyperbolic metamaterials: Fundamentals and applications. Nano Convergence. 1. 10.1186/s40580-014-0014-6.

[2] Kotyński, Rafał & Stefaniuk, Tomasz. (2008). Comparison of imaging with sub-wavelength resolution in the canalization and resonant tunnelling regimes. Journal of Optics A Pure and Applied Optics. 11. 10.1088/1464-4258/11/1/015001.

[3] Feigenbaum, Eyal & Diest, Kenneth & Atwater, Harry. (2010). Unity-Order Index Change in Transparent Conducting Oxides at Visible Frequencies. Nano letters. 10. 2111-6. 10.1021/nl1006307.

# ELECTROSPUN NANOFIBROUS WEBS AND DISTRIBUTIONS OF NANOFIBERS POROSITY

Virginija Kleivaitė[1], Rimvydas Milašius[1]

Kaunas University of Technology, Faculty of Mechanical Engineering and Design, Lithuania, Studentu 56, LT-51424 Kaunas
e-mail: virginija.kleivaite@ktu.edu;

Different structures of nanofiber, such as coreshell, bicomponent, hollow and porous structures, could be produced by using special designs of spinnerets. Functionalizing nanofibers with super active surface properties can be produced by controlling nanofiber body size, mass and content. Special nanofiber morphologies and textures can be utilized in advanced applications, such as nanofluidics, catalysis, drug delivery and release, nano supports, energy storage and gas sensors.

One of parameter which characterises the structure of nanofibrous web is porosity. A very important parameter for describing porosity is the maximum value of the pore diameter in the surface of electrospun web. Such evaluation is especially important for nanofibrous webs of barrier application, which are used, for example, for antimicrobial protection. Preliminary analysis of webs shows a very big inequality of pore diameters in different places of nanowebs. There are a few methods for measuring the porosity such as conventional methods using apparent density and bulk density, image analysis and mercury porometer. On the other hand, the analysis of webs show a very big inequality of pore diameters in different places of nanowebs, but this inequality has not been fully investigated yet [1,3].

Porosity is also very important if the electrically spiked nano-formed cells are used for cell growth or barrier properties. In these cases, not only the maximum size of the pore, but also all the distribution of pores size are important. Many authors describe in their work the porosity of the structure of the nanoweb, but the papers do not provide porosity estimation methods [2]. The high porosity and microstructure of bio-aggregates are fundamental to their physical properties. Typically they have a low density and a complex pore structure. This has two principal effects. In the first instance, low density is associated with low strength, but also with low thermal conductivity. For this reason most bio-aggregates are not suitable for use as structural materials, but are eminently suited to act as a low density filler in composite materials conferring low thermal conductivity on the resulting bio-composite.

[1] Malašauskiene J., Milašius R., Mathematical Analysis of the Diameter Distribution of Electrospun Nanofibres. Fibres & Textiles in Eastern Europe, Vol. 18, No. 6 (83) p. 45-48, 2010.
[2] Kleivaitė V., Milašius R., Electrospinning – 100 Years of investigations and still open questions of web structure estimination. Autex Reasearch Journal, Vol. 18, No 4, December 2018.
[3] Brochocka A., Efficiency of electret polycarbonate nonwovens in respiratory protection against nanoparticles. Autex Reasearch Journal, Vol. 17, No 2. 2017.

# PRELIMINARY EVALUATION OF THE MOST FREQUENT MASTITIS PATHOGENS OCCURRING IN POLISH DAIRY HERDS*

Aleksandra Kalińska[1], Daniel Radzikowski[1], Brygida Kruzińska[1], Jan Slósarz[1], Marcin Gołębiewski[1]

[1] Department of Animal Breeding and Production, Warsaw University of Life Sciences, Poland
aleksandra_kalinska@sggw.pl

Udder inflammations in dairy cows (mastitis) are one of the most common issues for milk producers. Mastitis generates additional cost for producers and decreases milk quality. In Poland mastitis is the 2nd reason of cow culling (after infertility) in dairy herds. Most of the clinical udder inflammations have environmental source and are mainly caused by different bacteria species (about 90%). Excessive antibiotics use in the past in dairy cows treatment influenced on the increased antibiotic resistance of mastitis pathogens.

The aim of the study was preliminary evaluation of mastitis pathogens occurrence in Polish dairy herds.

Milk samples (n=419) were taken from herds (n=23) in which occurred mastitis cases. Milk was placed in sterile cups during evening milking and delivered to Cattle Breeding Division laboratory. Samples were store for 12 hours in the fridge (4°C). After 12 hours milk was used in microbiological analysis. Several specific mediums were used to diagnose bacterial and fungi pathogens species. In the experiment were used several mediums: Mannitol Salt Lab Agar, Edwards Lab Agar, Rose Bengal, Enterococcus Confirmatory Lab Agar, Pseudomonas CN Lab Agar Base, Eijkman Lactose Medium, Salmonella Shigella Lab Agar (Biocorp, Poland). Inoculations were stored for 24-48 hours (37°C, 5% $CO_2$) to properly diagnose mastitis pathogens.

At least one pathogen species was diagnosed in over 90% of milk samples. The most frequently isolated pathogens were: *Escherichia coli* (76,61%) *Staphylococcus aureus* (41,29%), *Streptococcus dysgalactiae* (40,81%), *Enterococcus* sp. (40,57%) and *Staphylococcus epidermidids* (28,16%). In 7,88% samples were diagnosed fungi from *Aspergillus* sp. genera and yeasts from *Candida* sp. genera.

Obtained data suggest that most frequent species involved in udder inflammation process are staphylococci and streptococci. It is also important to point out that different species from *Enterobacteriaceae* family (e.g., *E. coli*) were diagnosed in large amount of sample which may be the reason of not appropriate environmental conditions in dairy herds the effect in higher mastitis cases frequency.

*The study was funded by Warsaw University of Life Sciences as grant for young scientists..

# STUDY OF GRAPHITE COMPOSITES FOR DIFFRACTIVE TERAHERTZ OPTICS NEEDS

Rusnė Ivaškevičiūtė[1], Jonas Zinkevičius[1], Lukas Laurinavičius[1], Rasa Pauliukaitė[1], Jan Macutkevič[1], Gintaras Valušis[1]

[1] Center for Physical Sciences and Technology, Lithuania
rusne.ivaskeviciute@ftmc.lt

One of the important topics in terahertz (THz) science and technology is to reveal routes for convenient-in-use THz imaging systems and find new ways to control THz radiation using planar solutions [1]. In particular, these issues become essential designing imaging systems using on-chip approach, because metal diffusion cannot be further used as suitable tool to fabricate THz diffractive optics components [2].

In this communication, we consider graphite composites as a possible solution for diffractive THz optics components. Graphite composites with different concentrations of graphite (1%, 2,5%, 5% and 10%) and different number of layers (1, 3 and 9) were fabricated and investigated. Broadband dielectric spectroscopy and electrical techniques (I-V and RLC measurements) were employed to evaluate parameters of graphite composites, such as permittivity and electric conductivity. These results showed that one layer of 2,5% concentration graphite composite is the most promising candidate for creating diffractive THz optic components, because of its highest permittivity.

Moreover, effect of fluctuating potential barriers on carrier transport in graphite composites were considered, theoretical estimates are discussed as well.

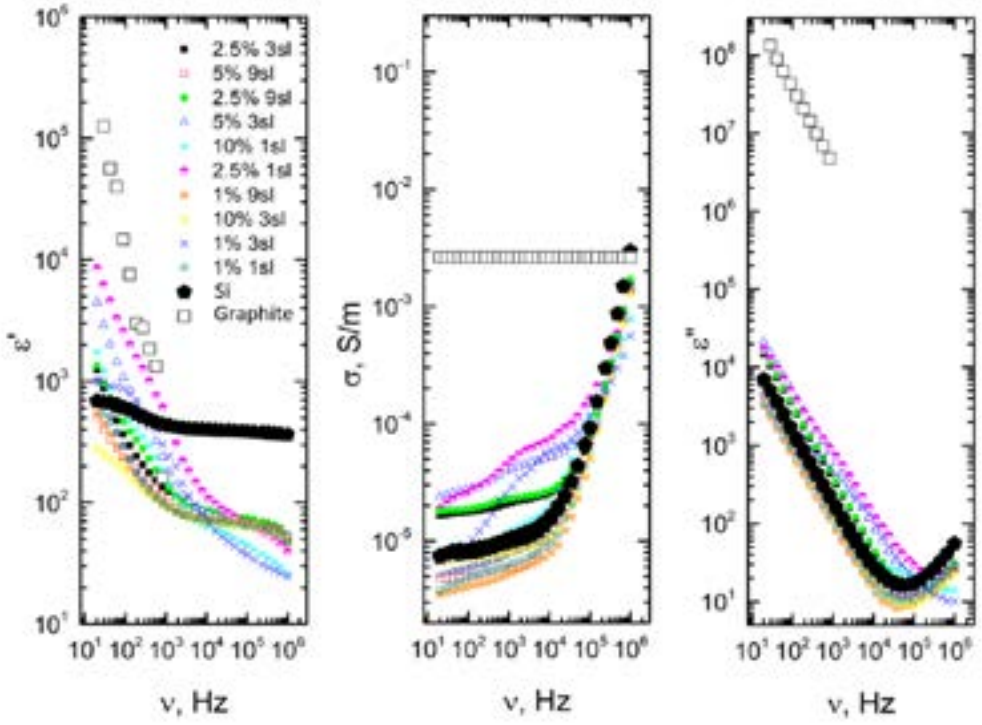


Fig. 1. Permittivity and conductivity of graphite composites with different concentrations

[1] S S Dhillon et al, J. Phys. D.: Appl. Phys. **50** (4), 043001 (2017).
[2] L. Minkevičius et al, JIMT **35** (9), 699-702 (2014).

# GRAPHENE FORMATION BY CARBON PRECIPITATION OF CARBON-NICKEL THIN FILMS

Paulius Dolmantas[1], Andrius Vasiliauskas[2], Šarūnas Meškinis[2]

[1] Department of Physics, Kaunas University of Technology, Studentų St. 50, LT-51368, Kaunas, Lithuania
[2] Institute of Materials Science of Kaunas University of Technology, K. Baršausko Str. 59, Kaunas LT-51423, Lithuania
Paulius.Dolmantas@ktu.edu

Graphene is 2D nanostructure consisting of one or few graphitic layers. In plane each carbon atom is bound to three neighbors by $sp^2$ hybridized σ bonds, while fourth electron orbital is normal to the structure and is delocalized. Graphene exhibits exceptional electronic (charge mobility up to $2.5 \cdot 10^5$ $cm^2V^{-1}s^{-1}$)[1], mechanical (Young's modulus ~ 1 TPa)[2], optical (transmittance more than 95 %)[3] and thermal (thermal conductivity ~ 5000 $Wm^{-1}K^{-1}$)[4] properties. Such combination of physical properties would improve characteristics of various semiconductor devices, such as touch screens, photodetectors, transistors, bendable electronics and more[5]. However, mentioned exceptional physical properties are only exhibited in highly ordered, contamination and defect free graphene. This is only achievable using mechanical exfoliation of highly ordered pyrolytic graphite (HOPG), while synthesis steps include complicated and time-consuming substrate-to substrate transferring. Graphene contamination and wrinkles formation problems arise. Therefore, direct synthesis of graphene on silicon substrate is favorable. One way of achieving this by chemical vapor deposition (CVD). In this case, growth mechanism involves dissociation of carbon precursor at high temperature on catalyst surface, carbon in catalyst (Cu, Ni, Co) and graphene precipitation at the surface of catalyst as sample cools down[6]. This relatively expensive process could be substituted by magnetron sputtered carbon-catalyst film annealing.

In present work, nickel and carbon composite films were deposited on monocrystalline silicon using direct current (DC) magnetron sputtering. Deposited films were annealed for 15 minutes at 800 °C in quartz cylinder using pulsed lamp. Argon gas was used to reduce oxidizing atmosphere. Films phase was investigated using Raman scattering spectroscopy (532 nm, inVia, Renishaw, UK). As seen from fig. 1. a) initial (before annealing) films did not exhibit sharp peaks, associated with carbon phase, which indicates that carbon was distributed in the bulk of the film. After annealing (fig. 1. b)) spectrum indicates characteristic carbon peaks typical for graphene: D peak (1346 $cm^{-1}$), G peak (1588 $cm^{-1}$) and 2D peak (2693 $cm^{-1}$). Analysis of these peaks revealed formation on the surface of the nickel film of the defected few-layer graphene.

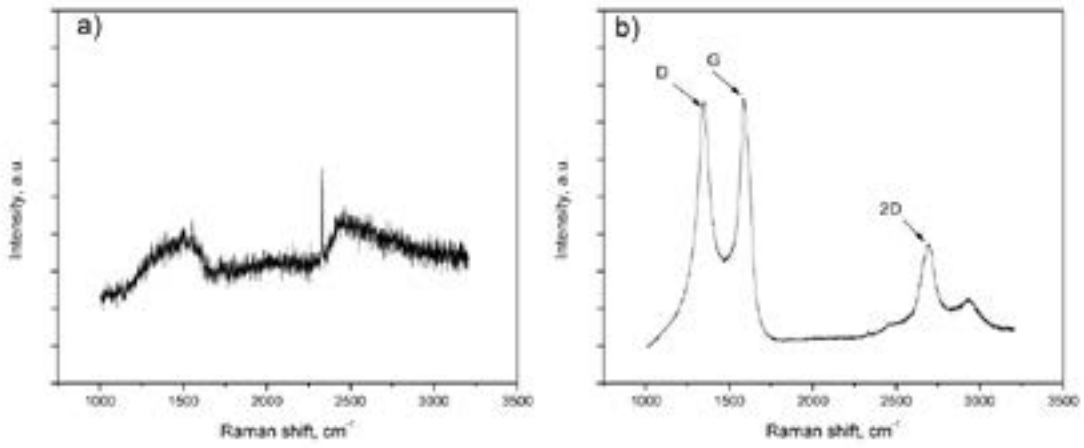


Fig. 1 Raman spectrum of nickel-carbon composite film produced by magnetron sputtering a) as deposited and b) after annealing at 800 °C for 15 minutes

[1] A. S. Mayorov, R. V. Gorbachev, S. V. Morozov, L. Britnell, R. Jalil, L. A. Ponomarenko, P. Blake, K. S. Novoselov, K. Watanabe, T. Taniguchi, and A. K. Geim, "Micrometer-scale ballistic transport in encapsulated graphene at room temperature," *Nano Lett.*, 2011.

[2] C. Lee, X. Wei, J. W. Kysar, and J. Hone, "Measurement of the Elastic Properties and Intrinsic Strength of Monolayer Graphene," *Science (80-. ).*, vol. 321, no. 5887, pp. 385–388, Jul. 2008.

[3] R. R. Nair, P. Blake, A. N. Grigorenko, K. S. Novoselov, T. J. Booth, T. Stauber, N. M. R. Peres, and A. K. Geim, "Fine Structure Constant Defines Visual Transparency of Graphene," *Science (80-. ).*, 2008.

[4] A. A. Balandin, S. Ghosh, W. Bao, I. Calizo, D. Teweldebrhan, F. Miao, and C. N. Lau, "Superior thermal conductivity of single-layer graphene," *Nano Lett.*, vol. 8, pp. 902–907, 2008.

[5] K. S. Novoselov, V. I. Fal′ko, L. Colombo, P. R. Gellert, M. G. Schwab, and K. Kim, "A roadmap for graphene," *Nature*, vol. 490, no. 7419, pp. 192–200, Oct. 2012.

[6] L. Baraton, Z. He, C. S. Lee, J. L. Maurice, C. S. Cojocaru, Y. H. Lee, and D. Pribat, "Study of graphene growth mechanism on nickel thin films," in *Carbon Nanostructures*, 2012.

# MODULATION OF EFFICIENCY OF NANOSTRUCTURED NISIN

Milda Babonaitė[1], Vitalij Novickij[2], Ramunė Stanevičienė[1], Jolanta Sereikaitė[3], Rūta Gruškienė[3], Elena Servienė[1], Juliana Lukša[1]

[1] Laboratory of Genetics, Institute of Botany, Nature Research Centre, Akademijos g. 2, 08412, Vilnius, Lithuania
[2] Institute of High Magnetic Fields, Vilnius Gediminas Technical University, Naugarduko g. 41, 03227, Vilnius, Lithuania
[3] Department of Chemistry and Bioengineering, Vilnius Gediminas Technical University, Saulėtekio av. 11, 10223, Vilnius, Lithuania
milda.babonaite@gmail.com

Nisin is a widely known lantibiotic often used in food processing as a natural preservative. Nisin exhibits a wide spectrum of antimicrobial activity against Gram-positive bacteria, however, many Gram-negative bacteria are nisin-resistant, so cell wall-permeabilization is required [1,2]. Nisin is sensitive to proteolytic degradation; it is known, that nano-encapsulation of bacteriocins protects them from degradation and can also increase their stability [3]. In this study, we used nisin-loaded pectin nanoparticles (NPs) in combination with nanosecond and microsecond pulsed electric fields (PEFs) to inhibit the growth of two strains of Gram-negative bacteria (*Eschericia coli*, *Salmonella enterica*) and one strain of Gram-positive bacteria (*Listeria innocua*). Also, we investigated the activity of magnetic nisin-loaded iron oxide NPs capped with citric, ascorbic and gallic acid, which were activated by high pulsed electric and electromagnetic fields against Gram-positive *Bacillus subtilis* and Gram-negative *E. coli*.

First of all, the minimum inhibitory concentration of nisin-loaded pectin NPs and free nisin samples was estimated. The encapsulated form of nisin has a better antimicrobial effect against both, Gram-positive and Gram-negative bacteria strains, in comparison to free nisin sample.

Secondly, we have applied a combination of NPs and 10-30 kV $cm^{-1}$ electric field with different electric pulse duration (500 ns-100 μs) for inactivation of *E. coli*. It was determined that the 20-30 kV $cm^{-1}$ electric field with pulses from 500 to 900 ns is efficient for permeabilization of *E. coli* and triggers synergistic response with nisin-loaded pectin NPs treatment [2]. For *Salmonella enterica* and *Listeria innocua* inactivation, 30 kV $cm^{-1}$ electric field in a broad range of pulse parameters (200 ns-500 μs) was used. Increasing the duration of electric pulses leads to better antimicrobial effects of NPs – 300 and 500 μs pulses demonstrates the highest antimicrobial effect against both bacteria strains.

For experiments with magnetic NPs, 10 and 30 kV $cm^{-1}$ electric field pulses (100 μs × 8) were applied separately and in combination with two pulsed magnetic field protocols: high dB/dt 3.3 T × 50 and 10 mT, 100 kHz, 2 min protocol to induce additional permeabilization and local magnetic hyperthermia. We have shown that the high pulsed magnetic fields increase the antimicrobial efficiency of nisin NPs similar to electroporation or magnetic hyperthermia methods, while synergistic treatment is also possible [4,5].

The results of our study are promising for the development of new methods for the treatment of the drug-resistant foodborne pathogens to minimize the risk of invasive infections.

This research was funded by the European Social Fund under the number No 09.3.3.-LMT-K-712-10-0100 “Development of Competences of Scientists, other Researches and Students through Practical Research Activities” measure.

[1] M. P. Zacharof, R. W. Lovitt, Bacteriocins produced by lactic acid bacteria: a review article. APBC Proc. 2, 50-56 (2012).
[2] V. Novickij, A. Zinkevičienė et al., Inactivation of Escherichia coli using nanosecond electric fields and nisin nanoparticles: a kinetics study. Front. Microbiol. 9:3006 (2018).
[3] H. A. Fahim, A. S. Khairalla et al., Nanotechnology: a valuable strategy to improve bacteriocin formulations. Front. Microbiol. 7:1385 (2016).
[4] V. Novickij, R. Stanevičienė et al., Overcoming antimicrobial resistance in bacteria using bioactive magnetic nanoparticles and pulsed electromagnetic fields. Front. Microbiol. 8:2678 (2018).
[5] V. Novickij, R. Stanevičienė, Overcoming antimicrobial resistance in bacteria using bioactive magnetic nanoparticles and pulsed electromagnetic fields, 15th international conference of the Lithuanian Biochemical Society 2018, ISBN 978-609-96030-0-1, Lietuvos biochemikų draugija, 45 (2018).

# THE INTERNAL STRUCTURAL ORGANIZATION OF POLYVINYLPYRROLIDON-DAUNOMYCIN-SELENIUM NANOPARTICLES NANOCOMPLEXES

Ilya Yakovlev[1], Lyudmila Borovikova[2], Albert Kipper[2], Oleg Pisarev[1,2]

[1]Department of Medical Physics, Peter the Great St. Petersburg polytechnic University, Saint Petersburg, Russia
[2]Laboratory of Polymeric Nanosystems and Biotechnology products, Institute of Macromolecular Compounds, Saint Petersburg, Russia
yakovlev.iliya@gmail.com

In order to create water-soluble non-toxic derivatives of the antitumor antibiotic daunomycin (DM), two methods have been developed for the synthesis of organic-inorganic nanocomplexes based on DM, polyvinylpyrrolidone (PVP) and selenium nanoparticles (Se NPs). PVP was used as an "additional" stabilizer, since Se NPs are aggregatively unstable in the presence of only DM [1]. It was previously shown that DM forms complexes with PVP due to hydrophobic interactions of anthraquinone aglycone of daunorubicinone with PVP [2].

The first method of synthesis is concluded in the preliminary stabilization of Se NPs (nanoparticles as a result of the redox reaction between selenous and ascorbic acids) with PVP followed by the addition of DM. The second method is implemented as a result of synthesis of the DM and PVP complex with the subsequent synthesis of NPs as a result of the redox reaction. The hydrodynamic radius (Rh) of the synthesized nanocomplexes were studied using dynamic light scattering.

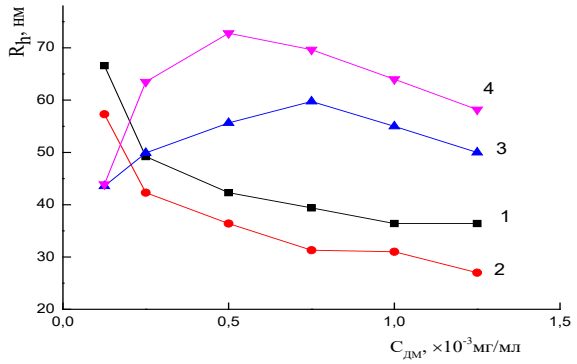


Fig.1. Dependence of the nanocomplexes hydrodynamic radius Rh on the concentration of DM: 1 – $C_{Se}$ =0,05 mg/ml (the first method of synthesis); 2- $C_{Se}$ =0,05 mg/ml (second method of synthesis); 3- $C_{Se}$ =0,025 mg/ml (the first method of synthesis); 4 - $C_{Se}$ =0,025 mg/ml (second method of synthesis).

Figure 1 presents data on the effect of the concentration of DM on the Rh values of nanocomplexes with $C_{Se}$ =0,05 mg/ml and $C_{Se}$ =0,025 mg/ml, which were synthesized by the described methods. For $C_{Se}$ =0,05 mg / ml, the value of Rh decreases with increasing $C_{DM}$, and the radius of the composites obtained by the first method are larger than the second. Probably, in the first case, Se NPs are first stabilized by PVP, and the introduced DM molecule, which is small compared to PVP, is "embedded" in the preformed PVP – Se composite (Rh = 40 nm). This embedding was carried out on the outer layer of the PVP-Se nanocomposite envelope and led to an increase in the Rh of nanoparticles obtained by the first method of synthesis at $C_{Se}$ =0,05 mg/ml.

For $C_{Se}$ =0,025 mg/ml, the dependence $R$h=f($C_{DM}$) has a maximum, and the radius of nanocomplexes obtained by the second method are larger than the first. Apparently, this is due to the influence of the concentration ratio of the components. In this case, due to the "reduction" of the Se NPs concentration, the previously formed PVP – DM complex (according to the second synthesis method) is relatively weakly bound to the NPs and the nanocomplex is a "loose" particle with a large size.

The appearance of a maximum in dependencies (curve 3, 4) with increasing DM concentration may be due to a change in the internal structure of a nanocomposite forming in solution: as a result of an increase in DM concentration, after the maximum loose structure is achieved and compaction of the forming nanocomplex begins.

Thus, the method of synthesis and the concentration ratio between PVP and DM determine the morphology and dimensional properties of nanocomplexes.

[1] Borovikova L.N., Kipper A.I., Titova A.V., Pisarev O.A. // Journal of Physical Chemistry. 2017.T. 91. № 9. C.1548-1552.
[2] Borovikova L.N., Titova A.V., Kipper A.I., Pisarev O.A. // Journal of General Chemistry. 2017. T.87. issue 5. C. 844-850.

# MATLAB BASED STUDY OF PHOTOVOLTAIC CELLS AND ARRAY IN DIFFERENT OPERATING REGIMES

Azem Hysa

Department of Applied and Natural Sciences, "Aleksandër Moisiu" University, Durrës, Albania
azemhysa@gmail.com

Solar radiant energy accounts for most of the usable renewable energy on this earth. Photovoltaic cell is a method of generating electrical power by converting solar radiation into direct current electricity using semiconductor that exhibit the photovoltaic effect [1]. In this research, MATLAB used to get the power-versus-voltage characteristics curves for photovoltaic cells. These curves used to calculate the specifications of a photovoltaic cell system such as short circuit current, open circuit voltage, power and maximum power [2]. Equivalent circuit of photovoltaic cell and mathematical model for photovoltaic cell and array are examined in this research [3].

Nevertheless, the current-voltage equation is a transcendental expression. It has no explicit analytical solution. The analytical methods give exact solutions by means of algebraic equations. However, due to implicit nature and nonlinearity of photovoltaic cell or module characteristics, it is hard to find out the analytical solution of all unknown parameters. Analytical methods have also some limitations and could not give exact solutions when the functions are not given. Thus numerical methods preferred in this case. It is because of the fact that numerical methods give approximate solution of the nonlinear problems without searching for exact solutions [4].

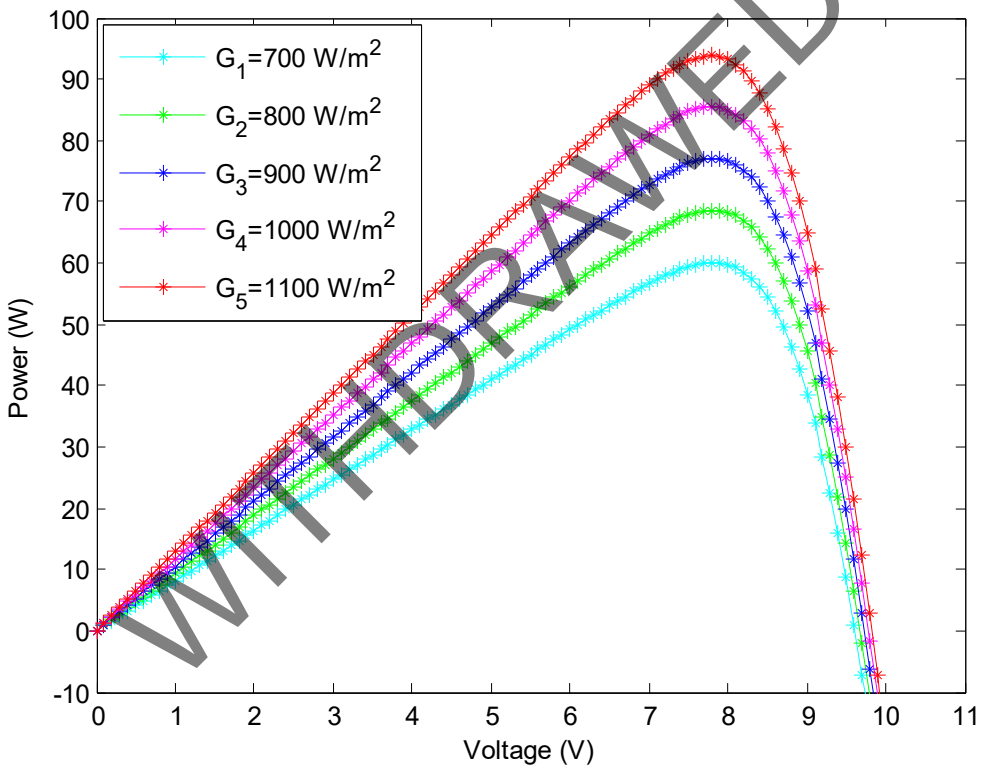




Fig.1. P-V characteristic curves of photovoltaic cells for various irradiance and constant temperature.

Figure 1 show the P-V curves for different irradiance. The effect of increasing irradiance while temperature was fixed is increasing the output and short circuit current, the output voltage almost not affected very much.

[1] M. W .Shah, Robert L. Biate, Design and simulation of solar PV model using mat lab/simulink, International Journal of Scientific & Engineering Research, Volume 7, Issue 3, March-2016 ISSN 2229-5518.

[2] R. Tariq Ahmad H, "Solar cell system simulation using matlab-simulink, Kurdistan Journal for Applied Research kjar.spu.edu.iq Volume 2, Issue 1, June 2017 P-ISSN: 2411-7684 – E-ISSN: 2411-7706.

[3] Ravi Prakash, Sanded Singh, Designing and Modeling of Solar Photovoltaic Cell and Array, IOSR Journal of Electrical and Electronics Engineering (IOSR-JEEE) e-ISSN: 2278-1676,p-ISSN: 2320-3331, Volume 11, Issue 2 Ver. III (Mar. – Apr. 2016), PP 35-40 www.iosrjournals.org.

[4] Abdul Qayoom Jakhrani, Salem Raza Samo,1 Shakeel Ahmed Kamboh, Jane Labadin, and Andrew Ragai Henry Rigit, An Improved Mathematical Model for Computing Power Output of Solar Photovoltaic Modules. Hindawi Publishing Corporation International Journal of Photoenergy Volume 2014, Article ID 346704, 9 pages http://dx.doi.org/10.1155/2014/346704.

# SYNTHES OF NANOSTRUCTURES OF GOLD IN THE PORES OF A $SIO_2$ TEMPLATE

Victoria Bundyukova[1], Dzmitry Yakimchuk[1], Egor Kaniukov[2]

[1] Cryogenic Research Division, Scientific-Practical Materials Research Center NAS of Belarus, Minsk, Belarus
[2] Institute of Chemistry of New Materials of National Academy of Sciences of Belarus, Minsk, Belarus
victoria.bundyukova@gmail.com

Controlling the morphology of gold nanostructures duaring the formation process is a very important aspect since their optoelectronic and physicochemical properties critically depend on the shape. Man-age the morphology of nanostructures is possible by using of template synthesis method. In this regard, ion-track technology, which allows to form nanostructures with a predetermined geometry is very promising. In this work an ion-track $SiO_2$/Si template was used to form gold nanostructures in pores of silica layer by electroless wet-chemical method. A detailed study of growth mechanisms and factors affecting on the structural and morphological features of gold nanostructures in the pores of the $SiO_2$/Si template was carried out. The influence of pores characteristics (diameters and their surface density), electrolyte composition and deposition modes (time, temperature and acidity) was studied and dependence of crystals morphology on these parameters was demonstrated. Choosing the optimal shape allows to use gold nanostructures for different applications, for example for Surface-enhanced Raman spectroscopy [1-4].

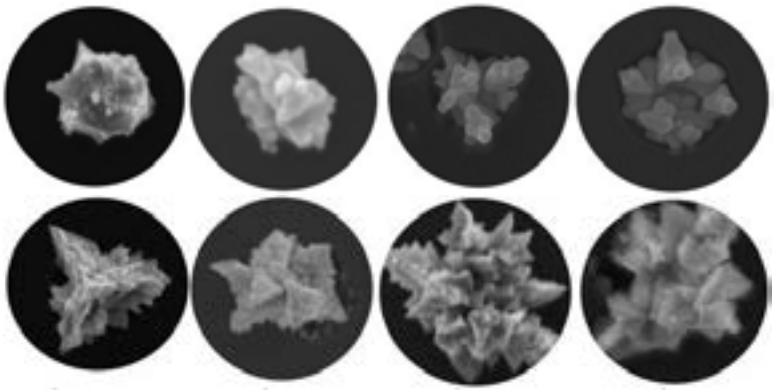

Fig.1: SEM image of self – organized nanostructures of gold grown in porous $SiO_2$/Si template with different deposition time and pore
diameters.

[1]. K. Kneipp, “Surface-enhanced raman scatter-ing,” Phys. Today, vol. 60, no. 11, pp. 40–46, 2007.
[2]. S. Uluok, B. Guven, H. Eksi, Z. Ustundag, U. Tamer, and I. H. Boyaci, “Designing multi-layered nanoplatforms for SERS-based detec-tion of genetically modified organisms,” J. Na-noparticle Res., vol. 17, no. 1, p. 43, Jan. 2015.
[3]. M. J. Natan, “Concluding Remarks : Surface enhanced Raman scattering,” Faraday Discuss., vol. 132, p. 321, 2006.
[4]. M. Moskovits, “Surface-Enhanced spectrosco-py,” Rev. Mod. Phys., vol. 57, no. 3, pp. 783–826, 1985.

# LUMINESCENT QUANTUM DOTS ENCAPSULATED BY ZWITTERIONIC AMPHIPHILIC POLYMER: CALCIUM-DEPENDENT INTERACTION WITH CELLS

Aliaksandra Radchanka[1], Tatiana Terpinskaya[2], Tatiana Balashevich[2], Tatsiana Yanchanka[2], Mikhail Artemyev[1*]

[1] Research Institute for Physical Chemical Problems, Belarusian State University, Belarus
[2] Institute of Physiology, National Academy of Science, Belarus
m_artemyev@yahoo.com

Luminescent semiconductor nanocrystals known as quantum dots (QDs) are found applications in various biological assays: bioimaging, cell functioning, and intercellular interactions [1]. Unlike organic dyes QDs possess high photostability and photoluminescence (PL) quantum yield (QY), broad absorption range and narrow emission peaks. These parameters make QDs as perspective alternative for traditional organic fluorophores. Monodisperse colloidal QDs with proper optical characteristics are made by high-temperature organic synthesis resulting in QDs with a hydrophobic surface ligand layer. For biological environments, post-synthetical treatment is needed. Modification of surface with an amphiphilic polymer (poly(maleic anhydride alt-1-tetradecene), PMAT) leads to NCs with small hydrodynamic size and preserved QY [2]. Derivatization of anhydride group of PMAT with different ionic groups improves biocompatibility and changes physical-chemical characteristics: zeta-potential and size. Surface charge influences the effectiveness and selectivity of interactions of QDs with cell cultures because the initial contact NCs and cells is determined by attractive forces such as electrostatic, hydrophilic, hydrophobic, etc. [3]

The aim of this work was to study the impact of zeta-potential and $Ca^{2+}$-ions on the effectiveness of cell labeling. $Ca^{2+}$-ions were selected due to their importance in a number of cell processes (signal transduction pathways, blood-clotting) and influence on zeta-potential QDs markers.

Chemical modification of PMAT was performed according to the procedure that involved a reaction of PMAT in organic solution with (2-aminoethyl)trimethylammonium chloride. The ratio of quaternary ammonium and carboxylic groups determines the surface charge of encapsulated nanoparticles. After chemical modification of PMAT hydrophobic CdSe/ZnS core-shell QDs were encapsulated by modified PMAT according to the standard protocol. Encapsulated QDs in a dry solid form were dissolved in phosphate buffer solution, zeta potential and hydrodynamic size of water-soluble QDs were measured with the dynamic light scattering analyzer Malvern Zetasizer NanoZS90. The labeling procedure was performed by mixing the suspension of cell culture and NCs solution at fixed pH, buffer and $Ca^{2+}$-ion concentration. Then cells were washed with phosphate buffer and labeled cells were explored with BD FACSCanto II Flow Cytometer and analyzed by fluorescence microscopy.

It was found that cells are labeled the most effective with NCs of low positive zeta-potential. However, the addition of $Ca^{2+}$-ions leads to decrease in PL intensity by a factor of two. This effect can be explained by the increase of zeta-potential and less intense cell binding, as well as the ability of $Ca^{2+}$-ions to quench the PL.

**Table 1.** Dependence of PL intensity of labeled cellular culture rat C6 glioma versus NCs zeta-potential and $Ca^{2+}$-ions presence.

| Sample | Zeta-potential, mV | PL intensity, a.u. | Zeta-potential after $Ca^{2+}$ adding, mV | PL intensity after $Ca^{2+}$ adding, a.u. |
|---|---|---|---|---|
| 1 (0% modified) | -33 | 0.3 | -15 | 1.6 |
| 2 (50% modified) | +13 | 2.3 | +27 | 1.1 |
| 3 (100% modified) | +23 | 1.6 | +27 | 1.7 |

The presence of $Ca^{2+}$- ions increases the fluorescence of cells if negatively-charged NCs are used. As shown by microscopic analysis, in the presence of $Ca^{2+}$- ions the nanoparticles are deposited on the cell membrane, forming large agglomerates. This phenomenon can be explained binding of carboxylic groups and calcium ions on the cell membrane. It is also possible that the shift of zeta potential to the positive side also plays a role in enhancing cell labeling.

Labeling with positively-charged NCs are not influenced by calcium addition due to electrostatic repulsion of quaternary ammonia groups and $Ca^{2+}$-ions.

We acknowledge the financial support from Chemreagents Program. M.A. acknowledges partial financial support from BRFFI grant X18P-173.

[1] N. Tomczak, R. Liu, J. G. Vansco, Nanoscale **5**, 12018 (2013).
[2] Pellegrino, T.; Manna, L.; Kudera, S.; Liedl, T.; Koktysh, D.; Rogach, A. L.; Keller, S.; Rädler, J.; Natile, G.; Parak, W. J. Nano Lett. **4**, 703 (2004).
[3] E. A. Petrova, T. I. Terpinskaya, A. A. Fedosyuk, A. V. Radchanka, A. V. Antanovich, A. V. Prudnikau, M. V. Artemyev, Journal of Belarusian State University 2, 3 (2018).

# ULTRAFAST RECOMBINATION AND DIFFUSION PROCESSES IN LEAD FREE MASNI3 PEROVSKITES

Džiugas Litvinas[1], Patrik Ščajev[1], Paulius Baronas[1], Ramūnas Aleksiejūnas[1], Saulius Juršėnas[1], Marek Kolenda[1], Chuanjiang Qin[2], Takashi Fujihara[2], Toshinori Matsushima[2], Chihaya Adachi[2].

[1] Institute of Photonics and Nanotechnology, Vilnius University, Saulėtekio al. 3, LT-10257 Vilnius, Lithuania
[2] Center for Organic Photonics and Electronics Research (OPERA), Kyushu University, 744 Motooka, Nishi, Fukuoka 819-0395, Japan
dziugas.litvinas@ff.stud.vu.lt

Lead-halide perovskites are attractive materials for wet-cast photonic applications, but their toxicity raises serious environmental and health concerns. Therefore, the lead-free perovskites are extensively studied as a possible nontoxic substitution of similar or even superior performance.

Here, we investigate the ultrafast processes of carrier thermalisation, recombination, and diffusion in a set of $MASnI_3$ layers, grown from solution by using different precursors [1]. We employ a unique light-induced transient grating technique (LITG) together with the photoluminescence (PL) and differential transmission (pump-probe) measurements.

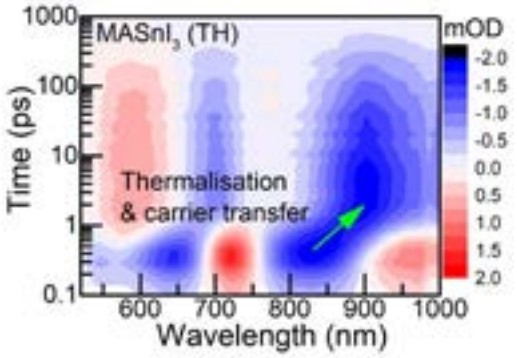


Fig. 1. Time-resolved differential transmission spectrum in $MASnI_3$ layer under pulsed 200 fs laser excitation at 515 nm.

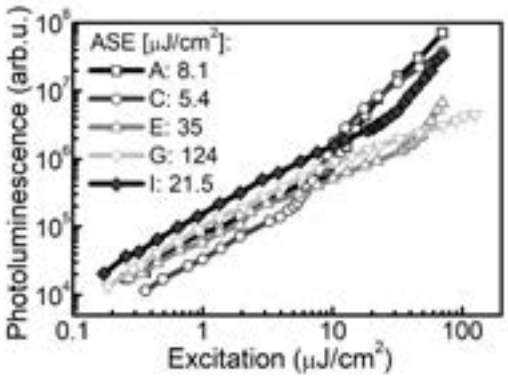


Fig. 2. Integrated photoluminescence vs. 532 nm laser excitation intensity across various $MASnI_3$ samples.

We demonstrate that highly excited Sn perovskite layers exhibit very promising electrical properties: the measured carrier diffusion coefficient and lifetime reach 0.5 – 1.6 $cm^2/s$ and 100 – 140 ps, respectively, resulting in the diffusion lengths of 100-150 nm. These values are comparable to those of vapour-deposited lead-halide perovskites [2]. We observe the fast (within 2 – 4 ps) carrier thermalisation in the layers (Fig. 1). We show that amplified stimulated emission (ASE) can be readily obtained in Sn perovskites, yet the ASE threshold strongly depends on layer quality; in our case it varied in the 5 - 120 $\mu J/cm^2$ range (Fig. 2). It's notable that the lowest ASE threshold value of 5.4 $\mu J/cm^2$ is considerably lower than that reported in $MAPbI_3$ samples with additives [3]. These results suggest that Sn perovskites can be an effective active material for photonic devices like lasers and high power LEDs.

[1] T. Fujihara et. al., J. Mater. Chem. C 5 (2017) pp. 1121.
[2] P. Ščajev et. al., J. Phys. Chem. C 121 (2017) pp. 21600.
[3] P. Ščajev et. al., J. Phys. Chem. Lett. 9 (2018), pp. 3167.

# PHOTODEGRADATION PROCESSES IN ORGANIC-INORGANIC PEROVSKITE SOLAR CELLS

Natallia Mahon, Olga Korolik, Alexander Mazanik

Energy Physics Department, Belarusian State University, Republic of Belarus
natalimahon@gmail.com

Hybrid organic-inorganic perovskites (HOIPs) are promising photoabsorbing material for solar cells (SCs) due to high light absorption coefficient, band gap energy close to the optimal value, long lifetime of charge carriers (up to microsecond range) and possibility of low temperature (not more than 100 ºC) synthesis from solutions [1–3]. Nowadays, perovskite SCs demonstrate more than 23% efficiency in laboratory conditions [4], however, we can't use them in mass SC production because they are easily degraded under influence of heat, oxygen, moisture, light soaking [5,6]. The main problem today is photodegradation, the mechanisms of which are not completely clear.

In this work, we analyzed photostability of the HOIP SCs with different chemical composition of perovskite layer: (1) $MAPbI_3$, (2) $Cs_{0.15}FA_{0.85}PbI_{2.7}Br_{0.3}$, (3) $Cs_{0.05}(MA_{0.15}FA_{0.85})_{0.95}PbI_{2.55}Br_{0.45}$, where MA is methylammonium ($CH_3NH_3^+$), and FA is formamidine ($NH_2CH{=}NH_2^+$). We used a Proscan MS122 UV-Vis-NIR spectrometer for measurement of transmission spectra, Nanofinder HE (LOTIS-TII) confocal spectrometer for recording photoluminescence (PL) and electroluminescence (EL) spectra, as well as PL kinetics and PL mapping. A Keythley 2400 source-meter was used for registration of I-V characteristics of SCs. White LED (5700 K, 1000 W/m$^2$ was applied as a source of photodegradation.

Studies show that photostability of perovskite SCs depends on the complexity of the lattice. So, for all samples a red-shift of PL mass center under continuous laser illumination was observed and it depends on the composition of perovskite layer (the more ions lead to the greater red-shift), which is due to ions migration in complex perovskites. Also it was found strong influence of back Au-contact on photoinduced processes in perovskite SCs, which manifested in stabilization of perovskite ions due to the formation of random potential relief forming ionic traps in the gold regions.

Obtained PL and EL spectra for fresh, degraded and restored in the dark perovskite SCs demonstrate the formation of defects at the interfaces between the perovskite and transport layers, which prevent the extraction of photogenerated charge carriers and increase the photoluminescence intensity, and formation of nonradiative recombination centers during photodegradation with white LED, the rate of elimination of which in the dark is insufficient to restore the original parameters in actual operation. Last conclusion is also confirmed by measured I-V characteristics. Besides, measured kinetics of short-circuit current and open-circuit voltage for different sample sites show that photodegradation occurs spatially inhomogeneously, which may be due to the defective perovskite lattice structure.

Results are useful for further study of photostability of organic-inorganic perovskite solar cells.

[1] T. A. Berhe, W.-N. Su, Ch.-H. Chen et al., Organometal halide perovskite solar cells: degradation and stability, Energy Environ. Sci. 9, 323–356 (2016).
[2] D. Zhou, T. Zhou, Y. Tian et al., Perovskite-Based Solar Cells: Materials, Methods, and Future Perspectives, J. of Nanomaterials 2018, 8148072 (2018).
[3] R. Gottesman, A. Zaban, Perovskites for Photovoltaics in the Spotlight: Photoinduced Physical Changes and Their Implications, Acc. Chem. Res. 49, 320–329 (2016).
[4] W. S. Yang, B.-W. Park, E. H. Jung et al., Iodide management in formamidinium-lead-halide-based perovskite layers for efficient solar cells, Science 356, 1376–1379 (2017).
[5] Y. Reyna, A. Pérez-Tomás, A. Mingorance et al. *Molecular Devices for Solar Energy Conversion and Storage* (Green Chemistry and Sustainable Technology, Springer, Singapore, 2017).
[6] M.I. Asghar, J. Zhang, H. Wang, P.D. Lund, Device stability of perovskite solar cells, Renew. Sust. Energ. Rev. 77, 131–146 (2017).

# PHOTOLUMINESCENCE OF GADOLINIUM GARNET GLASS-CERAMIC SCINTILATORS

Augustas Vaitkevičius[1], Vaida Marčiulionytė[1], Darius Dobrovolskas[1], George Dosovitsky[3], Mikhail Korjik[2], Gintautas Tamulaitis[1]

[1]Institute of Photonics and Nanotechnology, Faculty of Physics, Vilnius University, Vilnius, Lithuania.
[2]National Research Center "Kurchatov Institute", Moscow, Russia
[3] Research Institute for Nuclear Problems, Belarusian State University, Minsk, Belarus

Augustas.vaitkevicius@ff.vu.lt

Scintillating detectors are popular as a means of detecting and measuring ionizing radiation. Due to their high stopping power, high light yield and impressive signal dynamic time inorganic scintillators have allowed for rapid progress in nuclear instrumentation in the last two decades. In recent times production of scintillation materials has become a limiting factor for future development in this field. While growing crystals from a melt allow for high crystal quality this method is limited by the maximum size of the crystal and variety of compositions.

Using glass and glass ceramic production methods allows for a more flexibility of crystal compositions and geometries. However, glass based scintillators have low light yields when excited with ionizing radiation. Using polycrystalline, glass-ceramic, materials would allow for advantages of crystalline materials to be combined with the flexibility of glass scintillators.

In out study we investigate three samples of scintillating grass-ceramics. Compostion of the investigated samples was $Gd_{1,485}Y_{1,485}Ce_{0,03}Al_2Ga_3O_{12}$ (GYAGG:Ce). Samples were sintered in identical temperature of 1650 °C. Two methods of pressing were used, ultrasonic and uniaxial. Sintering was performed with and without bed powders. After sintering hydrostatic density measurements revealed densities of 98.4%, 98.8% and 99,2% compared to the monocrystaline form. The samples were produced in National Research Center "Kurchatov Institute", Moscow, Russia.

The study was performed by using confocal photoluminescence (PL) spectroscopy. A WITec Alpha300 S microscopic system coupled to a spectrometer with a thermally cooled CCD camera was used. A CW laser diode emitting at 405 nm was used for excitation. The spatial resolution of 250 nm in plane and 1 µm perpendicularly to the sample surface was achieved.

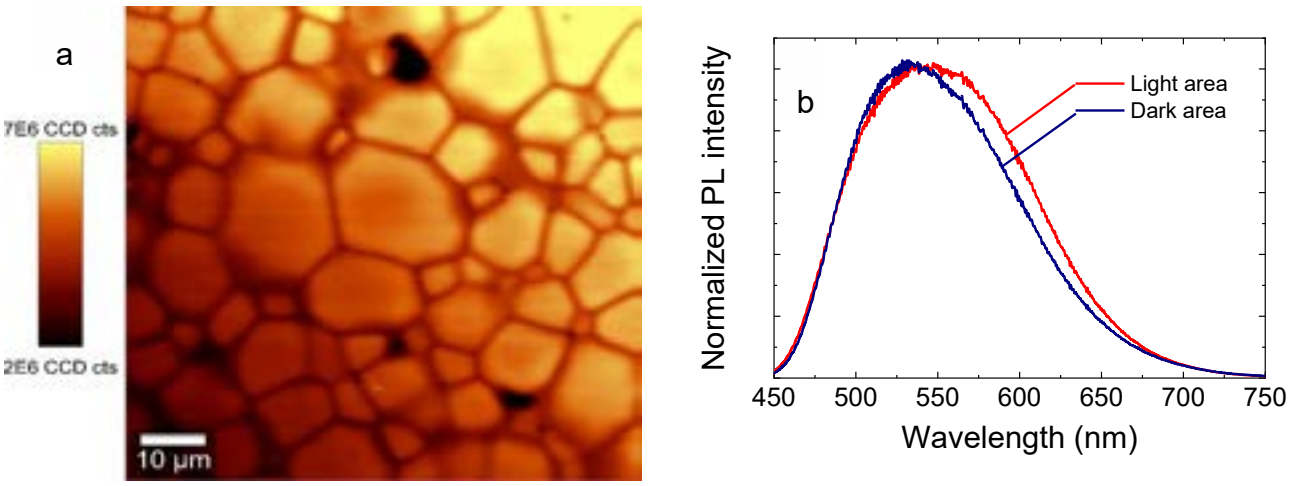


Fig. 1. Spatial distribution of spectrally integrated luminescence intensity of GYAGG:Ce over an 80×80 µm$^2$ area (a) and spatially integrated spectral photoluminescence intensity distribution from light and dark areas (b).

Our investigation revealed that GYAGG:Ce glass-ceramics samples all have a well-defined structure with clear boundries between crystallites (fig. 1). We also observed that between the aforementioned crystallites areas of reduced luminescence were present. These areas were roughly equivalent in size to the smallest observed crystallites and the luminescence measured from within those areas was less intense by a factor of 2. Spectroscopic measurements revealed that the shape of the photoluminescence spectra in the light and dark areas was similar, however the peak and the long-wavelength edge of the dark area spectra are blue-shifted by approximately 20 nm.

Similar distributions of photoluminescence parameters were observed in all samples. The density and shapes of the crystallites and dark spots are different. Density of dark spots increases with increased sample density. The results of this study will be usefull for determination of optimal production technology for GYGAGG:Ce glass-ceramics

# LINEAR AND NON-LINEAR PROPERTIES OF TERNARY CHALCOPYRITE SEMICONDUCTORS

Vijeta Jha

Patent Scientist, Samvad Partners, Chennai, India
dr_vjha@rediffmail.com

Chalcopyrite semiconductors are an important class of materials, which are having potential applications in new cutting-edge classes of electronic, photovoltaic and optoelectronic devices. The $A^{I}B^{III}C_2^{VI}$ and $A^{II}B^{IV}C_2^{V}$ groups of semiconductors crystallize in the chalcopyrite structure, which is a superlattice of the zinc blende structure obtained by doubling its unit cube along the z-axis that becomes the c-axis of the chalcopyrite structure. A considerable amount of experimental and theoretical work has been done on the synthesis and growth of $A^{I}B^{III}C_2^{VI}$ (A = Cu, Ag; B =Al, Ga, In; C = S, Se, Te) and $A^{II}B^{IV}C_2^{V}$ ($A^{II}$= Zn, Cd; $B^{IV}$= Si, Ge, Sn; $C_2^{V}$= P, As) groups of chalcopyrite semiconductors [1]. New chalcopyrite compounds of $A^{II}B^{IV}C_2^{V}$ group have been developed by replacing $A^{II}$ type atom with Be [2], Mn [3] and Mg [4] atoms. These new chalcopyrite materials are also having potential applications in the areas of magnetically controllable NLO devices and spintronics, which are less studied and only few papers are available on these materials. Recently, defect chalcopyrites of $A^{II}B_2^{III}C_4^{VI}$ family have been reported in the literature, which are obtained from their parent chalcopyrites I-III-$VI_2$ and their grandparent II-VI compounds, and having huge applications in frequency conversion and phase matching. This is because of their large birefringence, high second harmonic generation coefficients and better figure of merit. The models proposed by earlier workers for the calculation of various properties of ternary chalcopyrites are complex in nature and require experimental values of number of parameters, which are not known for some of these materials, especially the new chalcopyrites of $A^{II}B^{IV}C_2^{V}$ family and defect chalcopyrites of $A^{II}B_2^{III}C_4^{VI}$ family. In the present research work, various linear properties such as homopolar energy gap, heteropolar energy gap, average energy gap, ionicity and dielectric constant have been studied for these materials using plasma oscillation theory of solids. The refractive index and electronic polarizability have been calculated for these chalcopyrites, 13 new magnetic materials of $A^{II}B^{IV}C_2^{V}$ family, and $A^{II}B_2^{III}C_4^{VI}$ group of defect chalcopyrite semiconductors. Further, the nonlinear optical properties have been investigated for $A^{I}B^{III}C_2^{VI}$ semiconductors and second order NLO tensor coefficients ($d_{36}$) of whole family have been calculated. In almost all cases, our calculated values are in better agreement with the experimental values than the values reported by earlier workers which in turn demonstrate the soundness of the present calculations.

[1] Shay J L and Wernick J H, Ternary Chalcopyrite Semiconductors: Growth, Electronic Properties and Applications, Pergamon Press, New York, (1975).
[2] Shaposhnikov V L, Krivosheeva A V and Borisenko V E, Phys. Rev. B 85 205201(2012)
[3] Medvedkin G A and Voevodin V G, J. Opt. Soc. Am. B 22 1884(2005)
[4] Shaposhnikov V L, Krivosheeva A V, Borisenko V E, Lazzari J L, and d'Avitaya F A, Phys. Rev. B 85 205201(2012)

# PHOTOACOUSTIC SPECTROSCOPY OF SnS FILMS

Ekaterina Venhlinskaya[1], Leszek Bychto[2], Kaipakam Saritha[3], Mikhail Tivanov[1]

[1] Faculty of Physics, Belarusian State University, Belarus
[2] Department of Electronics & Computer Sciences, Koszalin University of Technology, Poland
[3]Department of Physics, Sri Venkateswara University, India
venglinskaya.e@gmail.com

SnS is attractive material for solar cells application because of its interesting physical and photovoltaic properties [1]. In this work the optical properties of SnS films were studied by photoacoustic spectroscopy. The bandgaps of SnS thin films were calculated from their photoacoustic spectra as well as spectral dependencies of absorption coefficients.

Photoacoustic spectroscopy is a sensitive method for investigating optical properties of semiconductors [2] both amorphous and crystalline. The method is also non-destructive [3].

SnS films were obtained by chemical bath deposition. The photoacoustic spectra were measured in the range of wavelengths of 500-1500 nm using Halogen Lamp (240W) at a constant frequency of modulation (770 Hz). The electrets microphone with a low noise preamplifier was used for detection of the photoacoustic signal. The obtained photoacoustic signal was calibrated using spectrum of glassy carbon.

The normalized photoacoustic amplitude was considered as:

$$q = \frac{P}{P_{sat}}, \tag{1}$$

where P – is gas pressure inside of photoacoustic cell, $P_{sat}$ – is gas pressure inside of photoacoustic cell for the big value of optical absorption coefficient [4].

Calculated spectra of normalized photoacoustic amplitude are presented on figure 1.

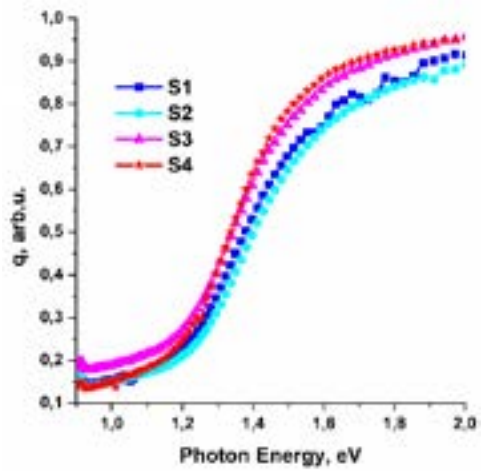


Fig. 1. Normalized photoacoustic amplitude spectra for SnS films.

The values of optical absorption coefficients α were obtained according to the formula below [4]:

$$-\ln(1-q) = \alpha d, \tag{2}$$

where d – is thickness of SnS film.

The values of bandgap (Eg) were obtained graphically. SnS – direct gap semiconductor [1] that means Eg values can be obtained by linear range extrapolation of $(\alpha h\nu)^2$ spectral dependency to the intersection with the x-axis. The calculated Eg values are 1.34 eV, 1.52 eV, 1.30 eV, 1.42 eV for S1, S2, S3 and S4 samples respectively.

This paper shows the photoacoustic spectroscopy is well appliable for SnS films investigation and can be useful for their further research.

[1] S.S. Hegde, A.G. Kunjomana, P. Murahari et al., Vacuum annealed tin sulfide (SnS) thin films for solar cell applications, JSIM **10**, 78-84 (2018).
[2] L. Bychto, M. Maliński, Determination of the optical absorption coefficient spectra of thin semiconductor layers from their photoacoustic spectra, Int J Thermophys **39**, 103 (2018).
[3] S. Rasool, K. Saritha, K.T. Ramakrishna Reddy et al., Optical properties of thermally evaporated $In_2S_3$ thin films measured using photoacoustic spectroscopy, Mat Sci Semicon Proc **72**, 4-8 (2017).
[4] L. Bychto, M. Maliński, A. Patryn et al., Determination of the optical absorption spectra of thin layers from their photoacoustic spectra, Opt Mater **79**, 196-199 (2018)

# NUMERICAL MODELING OF MAGNETIC FIELD EFFECT ON CYLINDRICALLY SYMMETRIC NEAR-SURFACE QUANTUM DOTS

Liliya Adanets[1], Elena Levchuk[1]

[1] Department of Applied Mathematics and Computer Science, Belarusian State University, Independence Ave. 4, 220030 Minsk, Belarus
*mashcovcheva@gmail.com*

Arrays of quantum dots (QDs) can be used in a vast variety of nanoelectronic devices such as quantum computer [1] and others [2]. The use of quantum dots requires understanding of their electronic structure and effect of external fields on it. Confinement potential of a QD can be created both with inhomogeneity of semiconductor material or with the electric field of nanosized gate [3–4] (electrically defined quantum dot – EDQD). In this paper, we study theoretically both types of QDs. Since these systems do not allow analytical solution, this paper also covers the applicability of a three-dimensional anisotropic harmonic oscillator model for describing the magnetic field effect on the electronic structure of cylindrical quantum dot with piecewise constant potential and electrically defined QD, which confinement potential is created by the electric field of the gate in the form of a thin metallic disk [5].

We consider electronic states in three types of QDs: the first type is QD with anisotropic parabolic confinement potential, the second type is EDQD, and the third type is cylindrical QD with piecewise constant potential. These dots are located near the surface of a semiconductor with permittivity $\varepsilon_s$ and electron effective mass $m^*$ in the area $z > 0$. In XOY plane there is a dielectric layer which creates an infinitely high potential barrier. Uniform magnetic field $B$ is directed along the OZ axis. Within the framework of effective mass approximation, this system is described by the stationary Schrödinger equation for the envelope function $\Psi$ and energy $E$:

$$\left(-\nabla^2 - i\mu\frac{\partial}{\partial\varphi} + \frac{\mu^2\rho^2}{4} + \hat{V}\right)\Psi = E\Psi, \qquad z > 0, \tag{1}$$

$$\Psi\big|_{z=0} = 0; \qquad \Psi \to 0 \ \text{ as } \ \rho \to \infty, z \to \infty, \tag{2}$$

where $(\rho,z,\varphi)$ are cylindrical coordinates. Effective Bohr radius $a^* = 4\pi\varepsilon_0\varepsilon_s\hbar^2/m^*e^2$ for length and effective Rydberg $Ry^* = m^*e^4/2\hbar^2\varepsilon_s^2$ for energies are used as nondimensionalization parameters. In Eq. (1), $\mu$ is dimensionless value of the magnetic field, defined by the expression $\mu = \left(a^*\right)^2/\lambda_B^2$, where $\lambda_B = (\hbar/Be)^{1/2}$. The operator $\hat{V}$ is the localization potential.

For quantum dots with anisotropic parabolic confinement potential an analytical solution has been obtained. Solutions for EDQD and QD with piecewise constant potential have been obtained numerically. Energy spectrum and wave functions of the ground and excited states have been calculated for different values of magnetic field and geometrical parameters of the system. The qualitative effect of the magnetic field value on the electron energy spectrum for three types of QDs is also described.

It has been found that a series of anticrossing points for electronic levels takes place at relatively small magnetic fields (e.g. points *A* and *B* at Fig. 1). It has been also shown that the model of the near-surface parabolic QD makes it possible to predict the number and position of anticrossing points and quasi-degeneracy of states.

We have also found that the structure of wave functions changes at anticrossing points. Classification of the states of cylindrically symmetric QD based on the model of an anisotropic near-surface parabolic QD is proposed.

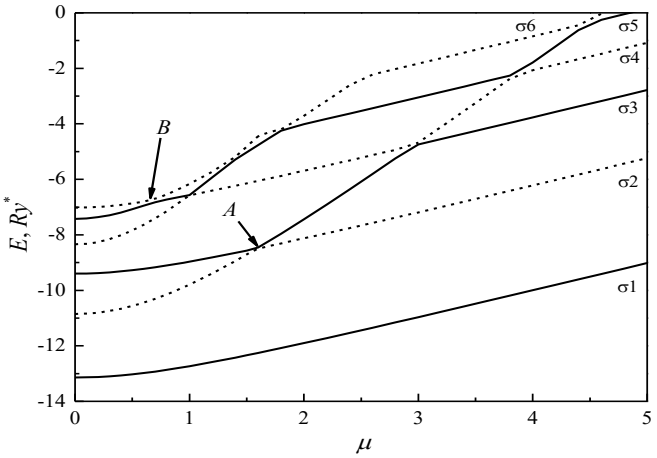


Fig. 1. Ground and lowest excited state energies of electrically defined quantum dot as functions of magnetic field value. The calculation was carried out for gate diameter $d = 6a^*$ and gate potential $\Phi_0 = 20\ Ry^*/e$.

The results of this work can be used in development new nanoelectronic devices.

[1] D. Loss, D. P. DiVincenzo, Quantum computation with quantum dots, Phys. Rev. A. **57**(1), 120-126 (1998).
[2] F. A. Zwanenburg [et al.], Silicon quantum electronics, Rev. Mod. Phys. **85**(3), 961 (2013).
[3] B. E. Kane, A silicon-based nuclear spin quantum computer, Nature (London) **393**, 133-137 (1998).
[4] M. Feuchsle [et al.], Single-atom transistor, Nature nanotechnology **7**(4), 242-246 (2012).
[5] G. D. J. Smit [et al.], Gate-induced ionization of single dopant atoms, Phys. Rev. B. **68**, 193302 (2003).

# HRTEM CHARACTERISATION OF Bi QD'S IN ANNEALED GaAsBi/AlAs MQW STRUCTURE

Martynas Skapas[1], Renata Butkutė[1]

[1] Center for Physical Science and Technology, Lithuania
Martynas.skapas@ftmc.lt

High Resolution Transmission Electron Microscopy (HRTEM) is the premier tool for understanding of the internal microstructure of materials at nanometer level. This method allows to distinguish real-space nano-scale peculiarities in material, and simultaneously from Fast Fourier Transform (FFT) diffraction patterns obtain the information about crystalline lattice of the investigated specific regions in the nanostructures, such us, nanoparticles, quantum dots, etc.

In this work, MBE grown and thermally treated GaAsBi/AlAs quantum wells were studied by structural (High-Resolution Transmission Electron Microscopy, HRTEM) characterization. The analysis of profile of GaAsBi/AlAs QWs containing Bi-nanoparticles measured by HRTEM and Scanning Transmission Electron Microscopy in High-Angle Annular Dark-Field (STEM HAADF) mode were performed to evaluate the influence of annealing on orientation of nanoparticles and strain distribution in whole quantum structure. Fast Fourier transform (FFT) analysis of HRTEM micrographs confirmed that Bi Quantum dots consist of pure rh-Bi phase, distributed in random orientation in zinc blende GaAsBi phase. EDX mapping and STEM HAADF further confirmed that these QD‘s consist of pure Bi. Furthermore, Geometric phase analysis also showed that GaAsBi layers are strained with respect to AlAs, while Bi Quantum dots are fully relaxed.

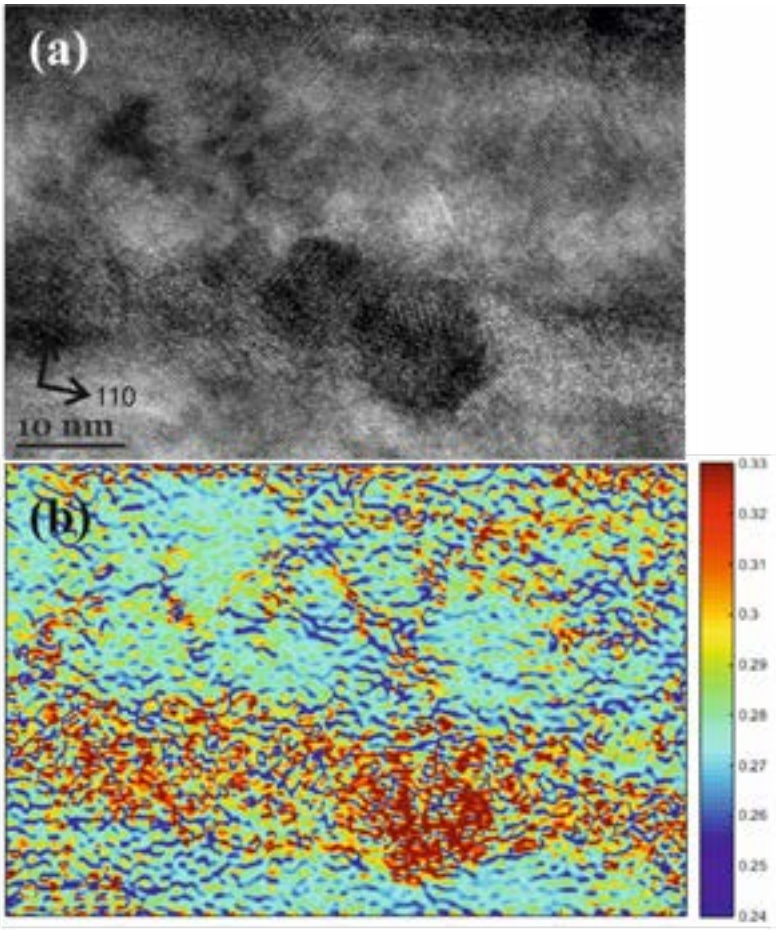


Fig. 1 HRTEM micrograph of Bi QD (a), and corresponding $d_{002}$ interplanar spacing map

[1] M. Skapas, S. Stanionytė, T. Paulauskas, R. Butkutė, Phys. Status Solidi B. doi:10.1002/pssb.201800365

# NON-EQUILIBRIUM CARRIER RECOMBINATION IN NITRIDE STRUCTURES REVEALED BY INTERFERENCE SPECTRA DYNAMICS

Martynas Riauka[1], Kazimieras Nomeika[1], Saulius Nargelas[1], Mikas Vengris[2], Ramūnas Aleksiejūnas[1]

[1]Institute of Photonics and Nanotechnology, Faculty of Physics, Vilnius University, Saulėtekis Avenue 3, Vilnius 10222, Lithuania

[2]Laser Research Centre, Faculty of Physics, Vilnius University, Saulėtekis Avenue 10, Vilnius 10223, Lithuania

martynas.riauka@ff.vu.lt

Recombination processes of excess carriers play a key role in optoelectronic device operation and thus must be well understood. A very attractive tool for this task is optical pump-probe technique, because it provides means for direct observation of carrier relaxation processes in a semiconductor on ultrafast time scales. Pump-probe measurements in thin semiconductor layers have to deal with the light interference effects due to multiple reflections from the layer surfaces. These effects are known to distort the carrier relaxation kinetics tremendously which is particularly noticeable in two-color pump-probe experiments (Fig. 1.).

In this work, the excess carrier temporal evolution in GaN and InGaN layers as well as GaN/InGaN quantum wells was investigated. In order to eliminate the negative light interference effects, a pump-probe setup with spectrally resolved broadband probing was used for recording the differential transmission interference spectra in the transparency region at various probe delay times. The density of excess carriers at each delay time was obtained by modelling the experimental data. The model was based on the transfer matrix method and took into account the geometrical properties of the layer, its wavelength-dependent refractive index as well as the carrier-induced refractive index change. The change in refractive index depends solely on the concentration of excess carriers, making it the only variable parameter in the model.

Calculations performed using the aforementioned method resulted in carrier relaxation kinetics, unaffected by the negative effects of light interference. These kinetics were compared with the kinetics obtained by other methods, namely, the light-induced transient grating (LITG) and differential transmission (DT) performed near the absorption edge, and were found out to be in close agreement with each other (Fig. 2.).

The model also allowed evaluating the initial excess charge density generated by the pump beam of different intensities at the surface of the investigated GaN and InGaN structures, as well as the excess carrier lifetime dependence on the excitation intensity and layer thickness.

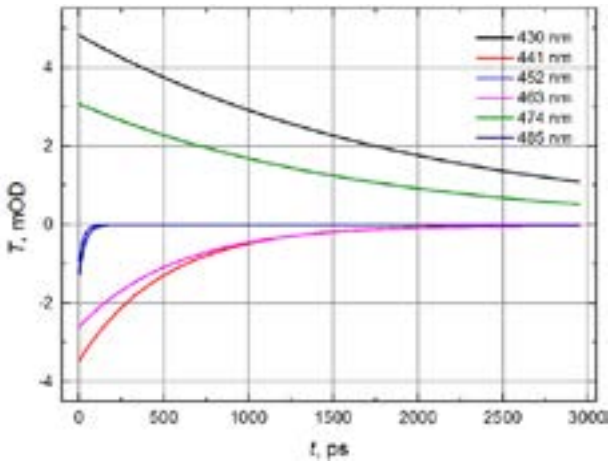


Fig. 1. Differential transmission (DT) kinetics in the sample 056 at different probing wavelengths.

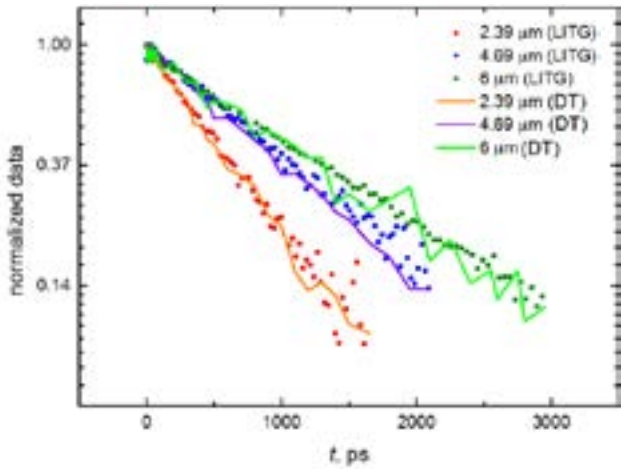


Fig. 2. Comparison of the excess carrier recombination kinetics obtained by the differential transmission (DT) and the light-induced transient grating (LITG) method.

# EPR STUDY OF STRUCTURAL PHASE TRANSITIONS IN VARIOUS HYBRID PEROVSKITES

Gediminas Usevičius[1], Mirosław Mączka[2], Magdalena Rok[3], Jūras Banys[1], Mantas Šimėnas[1]

[1] Physics Faculty, Vilnius University, Lithuania
[2] Polish Academy of Sciences, Poland
[3] Faculty of Chemistry, University of Wroclaw, Poland
gediminas.usevicius@ff.stud.vu.lt

Hybrid materials, crystallizing into perovskite-like structures with general formula $AMX_3$ (where A is an organic orinorganic cation, M is a metal center and X is anionic linker connecting A and M), have gained a lot of attention in recent years [1]. The desirable physical and chemical properties include gas adsorption and storage, efficient solar cells, multiferroicity and others [2-4].

Herein we report continuous-wave (CW) EPR study of structural phase transitions in different hybrid perovskite systems. X-band CW EPR experiments of $[(CH_3)_2NH_2]_2KCr(CN)_6$ and $[(CH_3)_3NH]_2KCr(CN)_6$ reveal one and two structural phase transitions, respectively. The phase transition temperature are 207 K for $[(CH_3)_2NH_2]_2KCr(CN)_6$ and 261 and 179 K for $[[(CH_3)_3NH]_2KCr(CN)_6$. Our research of [TPrA][Cd(dca)3]:$Mn^{2+}$ revealed two structural phase transitions at 230 and 212 K. From the Arrhenius analysis of the temperature dependence of the EPR linewidth (Fig. 1), we obtain the activation energy of 0.12(2) eV, which was assigned to dynamics of the dicyanamide framework.

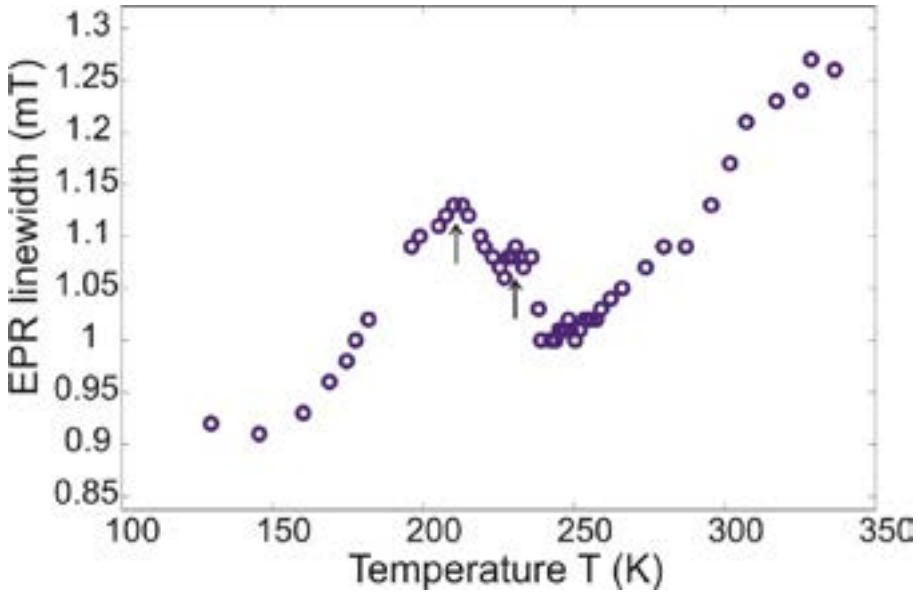


Fig. 1. Temperature dependence of the CW EPR peak-to-peak linewidth of $Mn^{2+}$ centers in [TPrA][Cd(dca)3]. The arrows indicate linewidth anomalies due to the structural phase transitions.

[1] W. Li, Z. Wang, F. Deschler, S. Gao, R. H. Friend and A. K. Cheetham, Nat. Rev. Mater., **2**, 16099, (2017).
[2] Saliba, M.; Matsui, T.; Seo, J.-Y.; Domanski, K.; Correa-Baena, J.- P.; Nazeeruddin, M. K.; Zakeeruddin, S. M.; Tress, W.; Abate, A.; Hagfeldt, A.; Gratzel, M. *Cesium-Containing Triple Cation Perovskite¨Solar Cells: Improved Stability, Reproducibility and High Efficiency*. Energy Environ. Sci. **9**, 1989−1997 (2016)
[3] H.-C. Zhou, J.R. Long, O.M. Yaghi, Chem. Rev. **112**, 673–674 (2012)
[4] R. Ramesh, N. A. Spadin, *Multiferroics: progress and prospects in thin films*, Nature Materials **6**, 21–29 (2007).

# CARRIER DYNAMICS IN PEROVSKITE SOLAR CELLS STUDIED BY LIGHT INDUCED TRANSIENT GRATING TECHNIQUE

Vaiva Soriūtė[1], Patrik Ščajev[1]

[1] Institute of Photonics and Nanotechnology, Vilnius University, Sauletekio Ave. 3, LT 10257 Vilnius, Lithuania
vaiva.soriute@ff.stud.vu.lt

Organic-inorganic perovskites recently emerged as a promising class of materials for low-cost photovoltaic technology. A major breakthrough in the efficiency of small area solar cells has been achieved within less than a decade [1]. However, commercialization of perovskite solar cells faces many challenges, including poor long-term stability and scaling-up of manufacturing. Therefore, perovskite materials require thorough scientific investigation and research.

The main goal of this work was to study $MAPbI_3$, $Cs_{0.15}FA_{0.85}PbI_{2.7}Br_{0.3}$ and $Cs_{0.05}(MA_{0.15}FA_{0.85})_{0.95}PbI_{2.55}Br_{0.45}$ layers using light-induced transient grating (LITG) technique. Carrier transport was analyzed in samples of different chemical composition by determining diffusion and recombination coefficients.

The samples were excited by the laser pulses at 527 nm. For probing, the pulses at 1053 nm with variable time delay were used. Optical attenuator was employed to change the excitation energy fluence, allowing to analyze photoelectric properties of perovskite samples within the wide range of excess carrier density ($10^{17}$ – $10^{19}$ $cm^{-3}$). Diffraction efficiency η transients at different grating periods (Fig. 1 (a)) provided the carrier lifetime $\tau_R$ and diffusion coefficient D and their dependencies on excess carrier density $\Delta N_{av}$.

The measured diffusion coefficient increased with the excitation (Fig. 1 (b)), which was attributed to either carrier delocalization, when the relatively smaller part of carriers remains localized as carrier density increases, or carrier plasma degeneracy [2]. On the other hand, carrier lifetimes reduced with the increasing excess carrier density (Fig. 1 (b)) due to Auger recombination, which was determined from the slope of this dependence. Using the determined values of carrier diffusion coefficient and lifetime, the diffusion length was calculated and yielded the values decreasing with excitation from 0.54 μm to 0.18 μm. Furthermore, comparing the diffusion lengths with thickness of perovskite layers allowed to conclude that the studied perovskite materials were suitable for producing solar cells because values of diffusion length were comparable to active perovskite layer thickness. Finally, the coefficients of radiative recombination and Auger recombination were calculated and compared to those reported in literature [3].

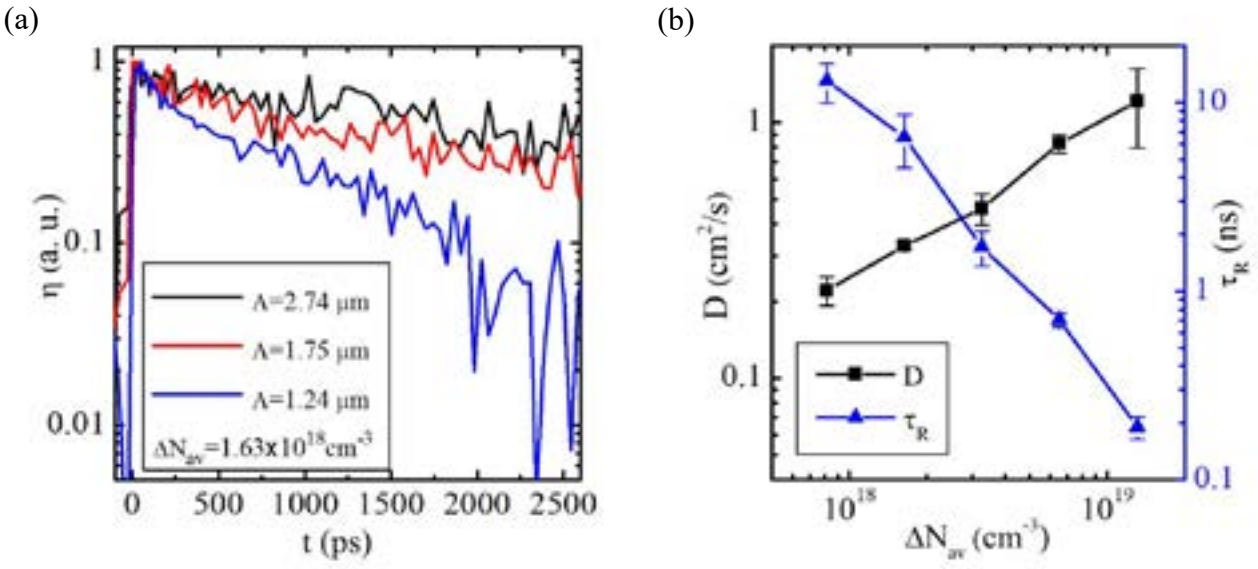


Fig. 1. (a) LITG transients recorded at three different grating periods Λ. (b) Diffusion coefficient D and lifetime $\tau_R$ as functions of excess carrier density.

[1] Y. Rong, Y. Hu, A. Mei, H. Tan, M. I. Saidaminov, S. I. Seok, M. D. McGehee, E. H. Sargent, H. Han, Challenges for commercializing perovskite solar cells. Science **361**, 1214 (2018).

[2] P. Ščajev, R. Aleksiejūnas, S. Miasojedovas, S. Nargelas, M. Inoue, C. Qin, T. Matsushima, C. Adachi, S. Juršėnas, Two regimes of carrier diffusion in vapor deposited lead-halide perovskites. J. Phys. Chem. C **121**, 21600-21609 (2017)

[3] Y. Shen, X. Zhang, S. Das, E. Kioupakis, C. G. Van de Walle, Unexpectedly strong Auger recombination in halide perovskites. Adv. Energy Mater. 1801027 (2018).

# EXCESS CONDUCTIVITY IN FeAs-BASED SUPERCONDUCTOR $EuFeAsO_{0.85}F_{0.15}$

Lyudmila Omelchenko, Andrei Solovjov, Eugene Petrenko, Andrei Terekhov
[1]B.Verkin Institute for Low Temperature Physics and Engineering of NAS of Ukraine,
Nauky Ave., 47, Kharkiv 61103, Ukraine
omelchenko@ilt.kharkov.ua

The discovery of high-$T_c$ superconductivity in FeAs-based compounds (Fe-pnictides) [1] has stimulated a great burst of research activity . Following the discovery in LaFeAs(O,F) with $T_c$=26 K[1], superconductivity was found in many materials with related crystal structures, that commonly possess iron-pnictide or iron-chalcogenide layers. Actually the various members of the iron containing FePn's can be divided into three main family of materials, which show superconducting (SC) transition upon substitution by a dopant or upon applying external pressure[1].

The study of excess conductivity $\sigma'(T)$ in the textured polycrystalline FeAs-based superconductor $EuFeAsO_{0.85}F_{0.15}$ ($T$c = 11 K) prepared by the solid state synthesis is reported for the first time. The $\sigma'(T)$ analysis has been performed within the local pair (LP) model based on the assumption of the LPs formation in cuprate high-Tc superconductors (cuprates) below the pseudogap (PG) temperature $T^* >> T$c [2]. Similarly to the cuprates, near $T$c $\sigma'(T)$ is adequately described by the 3D term of the Aslamasov–Larkin (AL) theory but the range of the 3D-AL fluctuations, $\Delta T_{3D}$, is relatively short. Above the crossover temperature $T_0$ =11.7 K $\sigma'(T)$ is described by the 2D Maki–Thompson (MT) fluctuation term of the Hikami–Larkin theory. But enhanced 2D-MT fluctuation contribution being typical for the magnetic superconductors is observed. Within the LP model the PG parameter, $\Delta^*(T)$, was determined for the first time. It is shown that $\Delta^*(T)$ demonstrates the narrow maximum at $Ts$ » 160 K followed by the descending linear length down to $T_{SDW}=T_{NFe}$=133 K [2]. Observed small $\Delta T_{3D}$, enlarged 2D $\sigma'(T)$ and linear $\Delta^*(T)$are considered to be the evidence of the enhanced magnetic interaction in $EuFeAsO_{0.85}F_{0.15}$. Importantly, the slop of the linear $\Delta^*(T)$ and its length are found to be the same as it is revealed for $SmFeAsO_{0.85}$. The results suggest both the similarity of the magnetic interaction processes in different Fe-pnictides and applicability of the LP model to the $\sigma'(T)$ analysis even in magnetic superconductors.

[1] M V Sadovskii, High-temperature superconductivity in iron-based layered iron compounds, Phys.—Usp. 51 1201-1227.
[2] A. L. Solovjov Superconductors - Materials, Properties and Applications. Chapter 7: Pseudogap and local pairs in high-$T_c$ superconductors, Rijeka.,137 (2012).

# PROFILING OF CURRENT TRANSIENTS IN LGAD AND PIN PARTICLE DETECTORS

Kornelijus Pūkas, Eugenijus Gaubas

Vilnius University, Faculty of Physics, Institute of Photonics and Nanotechnology, Lithuania
kornelijus.pukas@ff.stud.vu.lt

Silicon sensors with charge multiplication layer, known as Low Gain Avalanche Detectors (LGAD), are anticipated to be the functional particle detectors after heavy irradiations by hadrons. The concept of internal gain due to charge multiplication is addressed to an enhancement of the signal-to-noise ratio (SNR). The LGAD detectors become the most promising devices for applications in high energy physics experiments where harsh radiation environments, such as the inner detectors of Large Hadron Collider (LHC), are met.

Conventional a P-type LGAD consists of $N^+PP^-P^+$ layers with P-well formed by deep diffusion of boron (B) into $P^-$ layer. However, it was shown that an effect of the "acceptor removal" occurs in irradiated LGAD sensors which causes the loss of internal gain [1]. Radiation damage partially removes a boron from the multiplication layer, thereby reducing the effective doping concentration. This detrimental effect might be partially suppressed by forming the N-well ($P^+NN^-N^+$) Si structure with the phosphorus doped an epitaxial (N-well) layer. PIN structure ($N^+P^-P^+$) was formed from P-type LGAD structure by skipping the P-layer. In this work, the results of simulations of the operation characteristics for the P-type, N-type LGAD and PIN devices are reported.

A functionality of LGAD device has been validated by digital experiments performed using of Technology Computer-Aided Design (TCAD) algorithms and the Drift-Diffusion (DD) approach. Simulations have been carried out employing a Sentaurus Device software platform. It has been obtained that the breakdown voltages are approximately 8 times higher for the PIN structure than for the LGAD structures. One of the possible reasons is the absent P-layer in PIN structure compared with P-type LGAD structure. To evaluate those voltage differences the profiling of current transients for P- and N-type LGAD (Fig. 1 a) and PIN (Fig. 1 a) structures have been performed. Moreover, the shape and duration of current pulses is quite different in N- and P-type Si LGAD's mainly due to the difference of the ionization coefficients. These coefficients are approximately 10 times greater for electrons than for holes ($\alpha_e \cong 10 \cdot \alpha_h$). Nevertheless, the collected charge is almost the same for P-type and N-type Si devices if radiation traps are ignored in simulations.

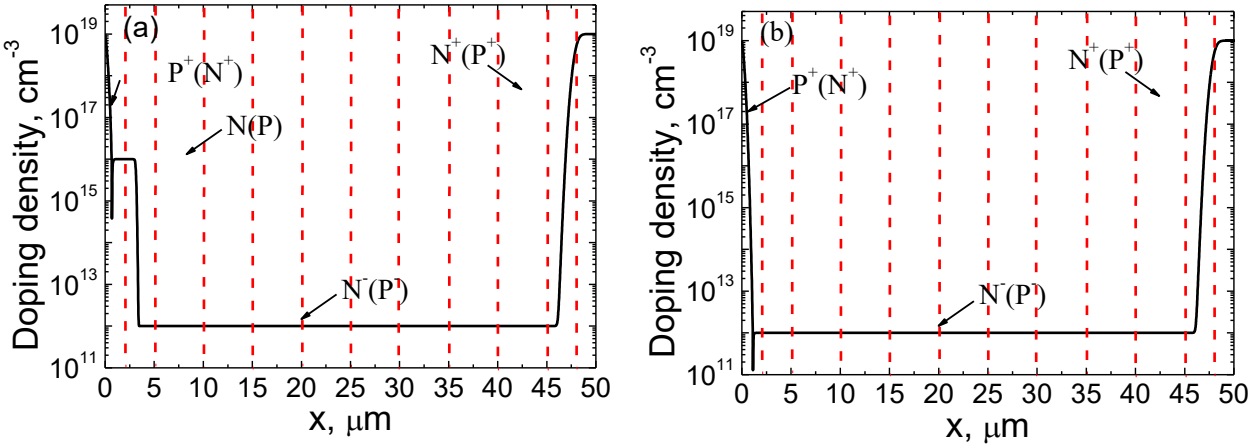


Fig. 1. Doping profiles (solid curves) in P as well as N type LGAD (a) and PIN (b) structures. The dashed lines represent the initial localizations of the photo-injected carrier domain.

It was assumed in simulations that a probability of carrier trapping during their drift increases with irradiation fluence. It has been shown that the thickness of the active layer within a sensor plays an important role in charge collection. Nevertheless, it has been demonstrated that even a rather thin (~50 μm) LGAD sensor can be functional with proper charge collection efficiency (CCE). The persistent CCE results from the carrier density increase through the internal amplification, proportional to a density of the radiation injected secondary carrier pairs. It has been demonstrated that the rather low bias voltage, applied to LGAD, is sufficient to get proper charge collection. Comparative analysis of the simulated and recorded current transients in the epitaxial LGAD structures will be presented. The impact of the radiation induced traps on detector current and charge collection efficiency, results of the detector current profiling in LGAD and PIN structures will be discussed.

[1] G. Kramberger, et al, Radiation effects in Low Gain Avalanche Detectors after hadron irradiations, Journal of Instrumentation **10**, P07006 (2015).

# BOSE-EINSTEIN CONDENSATES ILLUSTRATED BY THE EXAMPLE OF EXCITON-POLARITONS IN SEMIMAGNETIC AND NON-MAGNETIC MICROCAVITIES

Sara Piotrowska*, Mateusz Król, Rafał Mirek, Katarzyna Lekenta, Jean-Guy Rousset, Bartłomiej Seredyński, Wojciech Pacuski, Jacek Szczytko and Barbara Piętka

Institute of Experimental Physics, Faculty of Physics, University of Warsaw, Poland
*e-mail: s.piotrowska5@student.uw.edu.pl

Bose-Einstein condensate (BEC) is an extremely interesting state of matter. BECs occur when atoms or quasi-particles enter same quantum state. There are many types of BECs, depending on what particles are being condensated and by which mechanism they do so. For example, cooling gases to temperature near to absolute zero leads to Bose-Einstein condensation of its' atoms. However, condensation occurs also in small mass particles, like exciton-polaritons. Phenomena occuring in cavity exciton-polaritons are relatively new field of scientific research. Exciton-polaritons are quasi-particles, which emerge in strong coupling regime between photons and excitons. Exciton-polariton condensates can be observed in higher – and therefore easier to achieve – temperatures than atomic BECs, that's why there's a significant interest in studying those mixed light-matter quasiparticles in various systems. The most studied structures are semiconductor microcavities, in which cavity photons interact with excitons confined in quantum wells. Microcavity consists of two distributed Bragg reflectors grown using molecular beam epitaxy method. Exciton-polaritons present unique set of properties – bosonic nature and low effective mass in particular – which have enabled to localise them in micrometer size traps and observe BEC in solid-state system [1].

In this work, we present the formation of exciton-polariton condensates and discuss differences between them and their most remarkable properties in two types of microcavities. We examine microcavities with quantum wells containing magnetic manganese ions [2] as well as analogical but non-magnetic cavities. Detailed description of our microcavities structure will be given. Figure below shows difference between exciton-polaritons before and after condensation threshold. We describe the relation between changes of power of the laser excitation and localised condensates. Finally, we demonstrate an observation of circularly polarized condensates in semimagnetic microcavities and linearly polarized in non-magnetic ones.

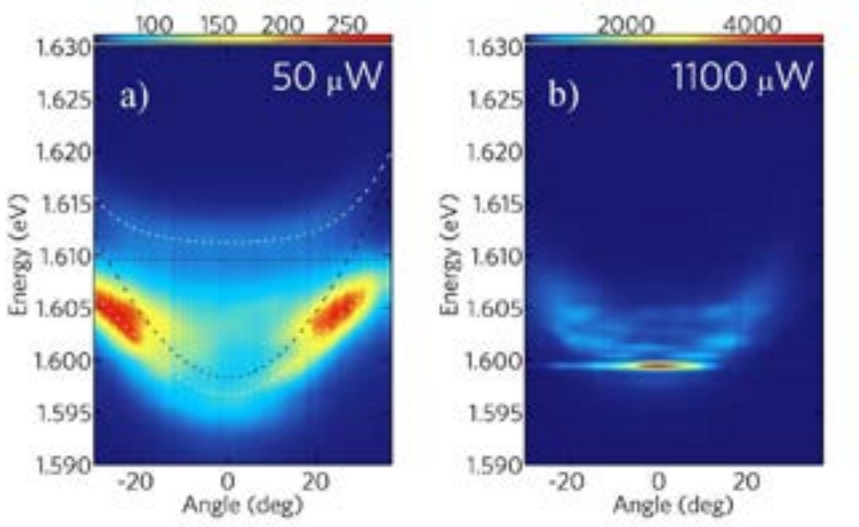


Figure. Exciton-polaritons below (a) and above (b) the condensation threshold.

[1] J. Kasprzak, et al., Bose-Einstein condensation of exciton polaritons, *Nature* **443**, 409–414 (2006).
[2] M. Król, et al., Spin polarized semimagnetic exciton-polariton condensate in magnetic field, *Scientific Reports* **8** 6694 (2018).

# FREE CARRIER ABSORPTION STUDIED BY PUMP-PROBE TECHNIQUE IN SEMICONDUCTORS AND SCINTILLATORS

Mariamija Nikitina, Ramūnas Aleksiejūnas

Institute of Photonics and Nanotechnology, Vilnius University, Lithuania
mariamija.nikitina@ff.stud.vu.lt

Upon irradiation of a semiconductor with high energy particles, a number of processes take place in the material, including generation of vast number of non-equilibrium carriers. These carriers alter material optical and electrical properties even on very short timescales; therefore, this process can be important in a number of applications, particularly in radiation detectors operating under strong irradiation [1]. Therefore, there is a demand for fast and sensitive ways to observe the dynamics of free carriers in semiconductors and scintillating materials that can be used in devices operating under irradiation. One of the parameters characterizing the optical response of a material to free carriers is the cross-section of free carrier absorption $\sigma_{FCA}$.

In this presentation, we demonstrate the determination of free carrier absorption cross-section in radiation hard materials GaN, SiC, and GAGG:Ce. For the measurements, we used a pump-probe technique based on YAG:Nd laser emitting 25 ps duration pulses. The nonequilibrium carriers were photoexcited using pulses at 355 nm and probed by the pulses at 1064 nm, which were delivered to the sample via 5 m fiber. The density of the excess carriers was varied within the $10^{18}$–$10^{20}$ $cm^{-3}$ range by using the optical attenuator.

Figure 1 shows the dependence of differential transmission signal on photoexcited carrier density in the investigated samples. The cross-section of free carrier absorption $\sigma_{FCA}$ is a material-specific parameter strongly depending on the wavelength. We determined the $\sigma_{FCA}$ values at 1064 nm in the investigated materials by fitting the data in Figure 1; the values are presented in Table 1.

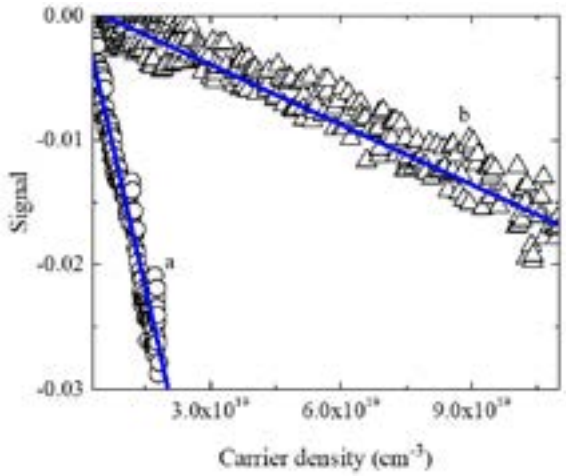


**Fig. 1**. The dependence of differential transmission signal on photoexcited carrier density in SiC (a) and GaN (b).

**Table 1**. Measured free carrier absorption cross-section coefficients $\sigma_{FCA}$.

| GaN | SiC | GAGG:Ce |
|---|---|---|
| $3 \cdot 10^{-17}$ $cm^2$ | $1.4 \cdot 10^{-17}$ $cm^2$ | $5.2 \cdot 10^{-18}$ $cm^2$ |

The other important parameters influencing the amount of free carrier absorption include the free carrier lifetime and the availability of thick crystals. Carrier lifetimes were determined from the pump-probe signal transients and varied from 2 ns for SiC to 79 ns for GAGG:Ce. Taking into account these factors, we conclude that thick GAGG crystals may be advantageous if high free carrier absorption coefficient is required.

[1] G. F. Knoll, "Radiation Detection and Measurement", pp. 223-235, 519-569. 2010.

# SYNTHESIS AND INVESTIGATION OF AMBIPOLAR 1,8-NAPHTHALIMIDE-BASED DERIVATIVES

Naveen Masimukku[1], Dalius Gudeika[1], Dmytro Volyniuk[1], Juozas Vidas Grazulevicius[1]

[1] Kaunas University of Technology, Department of Polymer Chemistry and technology
Radvilenu plentas 19, LT-50254, Kaunas, Lithuania
naveen.masimukku@ktu.edu

Organic materials exhibiting thermally activated delayed fluorescence (TADF) have attracted much attention due to their enhanced efficiency in organic light emitting diodes (OLEDs) which is possible due to harvesting triplet excitons. TADF occurs due to reverse intersystem crossing. It is possible when the energy difference between excited singlet ($S_1$) and triplet ($T_1$) energy levels is very low [1].

External quantum effiencies (EQEs) of TADF OLEDs have been rapidly boosting in past few years [2]. So far, considerable progress has been achieved in EQEs of blue and green TADF OLEDs. In contrast, the development of high-efficiency orange-to-red TADF OLEDs with electroluminescence peak wavelength longer than 580 nm remains far behind. Up to now, there are only few reports of relatively efficient orange–red TADF emitters [3]. For example, Orange–red TADF emitter, based on triphenylamine units and heptazine core enabled to achieve EQE of 17.5% with an emission peak of 610 nm [4]. However, the highest EQEs of orange–red TADF OLEDs are significantly less compared to those of blue and green TADF OLEDs. Consequently, new efficient orange–red TADF emitters are highly demanded to fill in the gap. The slow development of efficient orange-to-red TADF emitters is associated with numerous strict molecular design considerations and corresponding difficulties. Naphthalimide acceptor-donor molecular design is suitable for development of orange-red TADF emitters.

In this work we synthesized bipolar compounds containing 1,8-naphthalimide fragments linked to donor moieties such as phenoxazine, phenothiazine and acridine. The glass transition temperatures of synthesized compounds observed in the range of 51-94°C. The optical and photoelectrical properties of the synthesized materials were also investigated. Emission maxima of solid films of naphthalimide-based compounds observed in the range of 632-693 nm (Fig. 1).

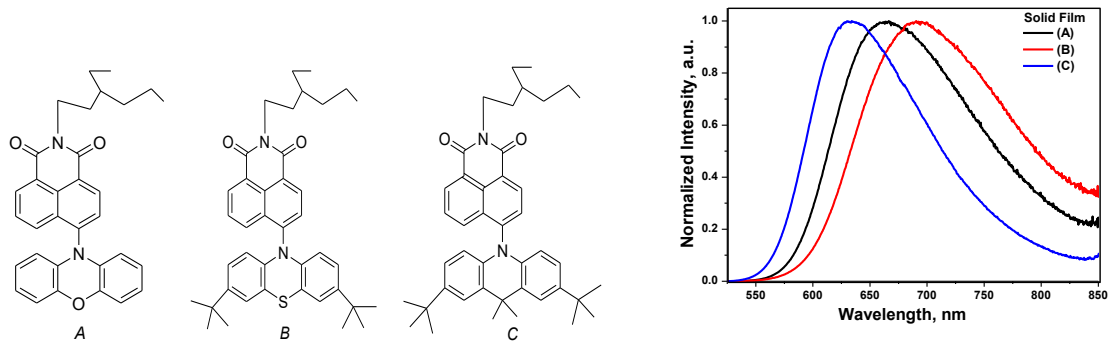


(a) (b)

Fig. 1. (a) structures (A, B, C); (b) fluoroscence spectra of naphthalimide-based derivatives in solid films

[1] T. J. Penfold, F. B. Dias, A. B. Monkman, The theory of thermally activated delayed fluoroscence for organic emitting diodes, Chem. Commun **58**, 3925 (2018).

[2] T. Miwa, S. Kubo, K. Shizu et al., Blue organic light-emitting diodes realizing external quantum efficiency over 25% using thermally activated delayed fluorescence emitters, Nature **7**, 1-2 (2017).

[3] S. Luo, J. Lin, J. Zhou et al., Novel 1,8-naphthalimide derivatives for standard-red organic light-emitting device applications, J. Mater. Chem. C **3**, 5259-5261 (2015).

[4 J. Li, T. Nakagawa, J. Macdonald et al., High efficient organic light-emitting diode based on a hidden thermally activated delayed fluorescence channel in a heptazine derivative, Adv. Mater **25**, 3319-3320 (2013).

# PHOTOLUMINESCENCE PROPERTIES OF DOPED AND UNDOPED BISMUTH GERMANATE SCINTILLATION CRYSTALS

Vaida Marčiulionytė[1], Augustas Vaitkevičius[1], Mikhail Korjik[2], Gintautas Tamulaitis[1]

[1] Institute of Photonics and Nanotechnology, Faculty of Physics, Vilnius University, Lithuania
[2] Research Institute for Nuclear Problems, Belarusian State University, Belarus
vaida.marciulionyte@ff.stud.vu.lt

Fast inorganic crystalline scintillators are on increasing demand for medical imaging and detectors for high energy physics experiments. Bismuth germanate (BGO) is one of the most extensively used oxide scintillation crystals. Self-activated BGO scintillator is already exploited in positron emission tomography (PET). For a long time, the main scintillator characteristics have been the light yield, radiation hardness, and luminescence decay time. Now, there is an increasing demand for fast scintillator detectors to be used in high-luminosity experiments at particle accelerators and for medical imaging applications with improved spatial resolution.

To have an insight into the processes limiting the luminescence response time of BGO scintillators in general and to reveal the capabilities of BGO doping to influence the emission properties, we investigated BGO ($Bi_4Ge_3O_{12}$) scintillation crystals doped with different ions: by 600 ppm Ca (BGO:Ca), 600 ppm Mg (BGO:Mg), 600 ppm Ti (BGO:Ti), 600 ppm La and Y (BGO:La,Y). Undoped BGO crystal was also investigated for reference. The samples under study with dimensions 1x1x0.2 $cm^2$ were grown by the Czochralski technique at the Nikolaev Institute of Inorganic Chemistry, Siberian Branch of Academy of Science.

The light emission properties of the samples under study were investigated by measuring their photoluminescence (PL) spectra at different excitation intensities and temperatures. The measurements were performed using luminescence spectroscopy under excitation by nanosecond pulses, which were substantially shorter than the free carrier lifetime in BGO. The PL spectra were recorded using a double monochromator (*HRD-1*) coupled with a photomultiplier tube (*Hamamatsu R1463P*). Tunable-wavelength laser (*Ekspla NT34B*) emitting at 257 nm (4.824 eV), having a pulse duration of 4 ns and a repetition rate of 10 Hz was exploited for excitation. The excitation beam was focused on the sample surface into a spot of ~600 µm in diameter. The measurements were performed in a wide temperature range from 10 to 300 K and under excitation intensities ranging from 0.012 MW/$cm^2$ to 3.64 MW/$cm^2$.

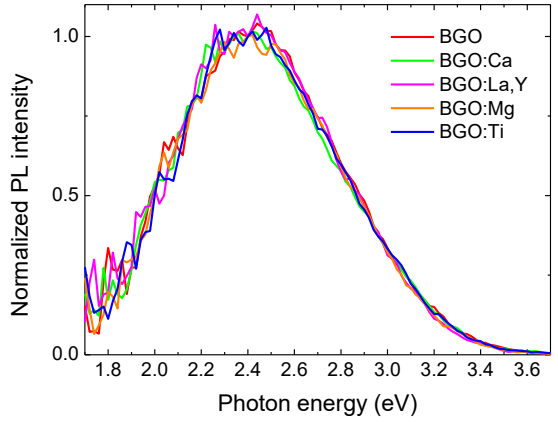


Fig. 1 Photoluminescence spectra of undoped BGO and BGO doped with Ca, Mg, Ti, La,Y (as indicated).

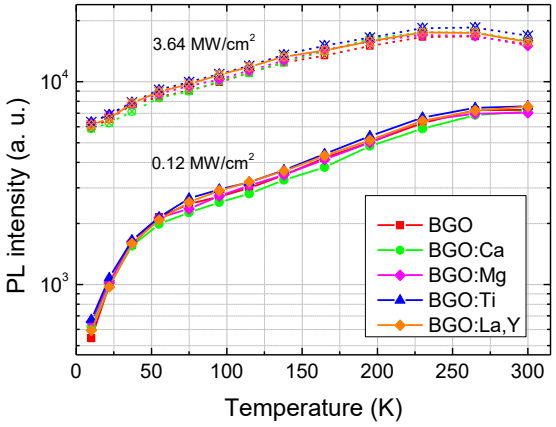


Fig. 2. Temperature dependence of spectrally-integrated photoluminescence intensity in undoped and doped (as indicated) BGO crystals at 0.12 MW/$cm^2$ and 3.64 MW/$cm^2$ excitation intensities (indicated).

It was observed that the absorption edge of BGO does not depend on doping with Mg, Ti, La, Y, while an additional absorption band at 312 nm is introduced by doping with Ca. As seen in Fig. 1, where the PL spectra of all the samples under study are presented, doping of BGO crystals has no influence on the form and intensity of photoluminescence spectra. No changes in the shape of PL band were observed when excitation power density was varied. Meanwhile, the PL bands in all samples under investigation become broader with increasing temperature. We also observed sub-linear dependence of PL intensity on excitation intensity tending to saturation at elevated excitation intensities. This process is more pronounced at higher temperatures. The origin of the dependence is discussed. Our results show that the PL intensity increases with the temperature increase (Fig. 2). The increase is stronger at lower excitation intensities. This behavior is explained by thermally activated carrier transfer to radiative centers.

# ELECTRON MOMENTUM RELAXATION TIME INFLUENCE ON THE TERAHERTZ EMISSION ENHANCEMENT IN MAGNETIC FIELD

Mingaudas Karevičius[1], Ieva Beleckaitė[1], Andrejus Geižutis[1], Ramūnas Adomavičius[1]

[1] Center for Physical Sciences and Technology, Vilnius, Lithuania
mingaudas.karevicius@ftmc.lt

In 1993 it was discovered [1], that terahertz (THz) emission varies greatly by applying external magnetic field close to semiconductor surface. It was suggested [2] that THz emission enhancement depends on the effective mass of electrons in a semiconductor, thus different materials have varying enhancement coefficients. Research in our laboratory suggests that this coefficient also depend on electron momentum relaxation time, given different enhancement coefficients in same type of semiconductor.

A novel method for determination of the terahertz pulse emitting dipole orientation by terahertz emission was developed. The method is based on the measurements of THz emission in reflection geometry, allowing for the determination of electric dipole tilt angle, $\theta$. In small magnetic fields, photoexcited electrons move perpendicular and parallel to the surface, where the forces responsible for the movement are due to electric field force and Lorentz force, respectively. Thus, the magnetic field induced change of dipole tilt angle, $\mathrm{d}\theta$:

$$\frac{\mathrm{d}\theta}{\mathrm{d}B} \approx \frac{F_{\parallel}}{F_{\perp}} \approx \frac{\mathrm{e}v_{\perp}B}{\mathrm{e}E} = \frac{\mathrm{e}\tau B}{m} \tag{1}$$

Since majority of THz energy is emitted during ballistic movement of electrons [3], $\tau$ is electron momentum relaxation time, and equation (1) can be simplified:

$$\frac{\mathrm{d}\theta}{\mathrm{d}B} = \mu B \tag{2}$$

A series of high-resistance semiconductor substrates were measured to determine this relationship. The determinated values were compared with electron mobility values obtained by already established Optical Pump – THz Probe (OPTP) method. A strong correlation was found between both methods. There are two advantages to the determination of THz pulse emitting dipole orientation by THz emission method compared to OPTP method. First, a fast and easier to implement measurement of samples was achieved. Second, greater stability to fluctuations in laser radiation was observed. We conclude, that determination of THz pulse emitting dipole orientation by THz emission method is a viable tool for the investigation of electron mobility in semiconductor substrates and epitaxial layers on top of them.

---

[1] X.-C. Zhang, Y. Jin, T. D. Hewitt et al., Magnetic switching of THz beams, Appl. Phys. Lett. **62**, 2003 (1993).
[2] C. Weiss, R. Wallenstein, R. Beigang, Magnetic-field-enhanced generation of terahertz radiation in semiconductor surfaces, Appl. Phys. Lett. **77**, 4160 (2000).
[3] R.O. Grondin, P Lugli, David Ferry, Ballistic Transport in Semiconductors. Electron Device Letters, IEEE. **3(12)**: 373 – 375 (1982)

# OPTICAL PROPERTIES OF (Pb, Cd) IODIDE FILMS

Olena Bondar[1], Igor V. Fesich[1], Vasyl V. Lendel[1], Anatolii P. Bukivskii[2], Petro M. Bukivskii[2]

[1]Taras Shevchenko National University of Kyiv, Ukraine

[2]Institute of Physics of NASU, Kyiv, Ukraine
e-mail: alionka-15@ukr.net

The obtained $Pb_{1-x}Cd_xI_2$ thick films may be considered as novel promising semiconductor materials for elaboration on their base effective low-cost scintillator detectors for biomedical and industrial applications. It was found that the films show intense photo- and cathodoluminescence at room temperature [1].

The $Pb_{0.3}Cd_{0.7}I_2$films were prepared by the conventional one-step deposition method from absolute N,N-Dimethylformamide (DMF). The thickness of the films was about 5–10 μm. It should be noted that all procedures were performed under open-air conditions at room temperature.

It was shown that these films have very complex crystal structure where $PbI_2$ microcrystallites of micron and submicron sizes as well as small nanoclusters (NCLs) are randomly formed in $CdI_2$ crystal matrix [1].

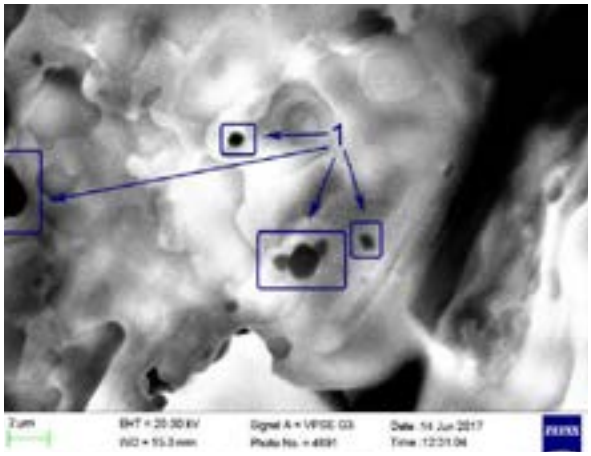


Fig. 1. SEM images of $Pb_{0.3}Cd_{0.7}I_2$ thick films.

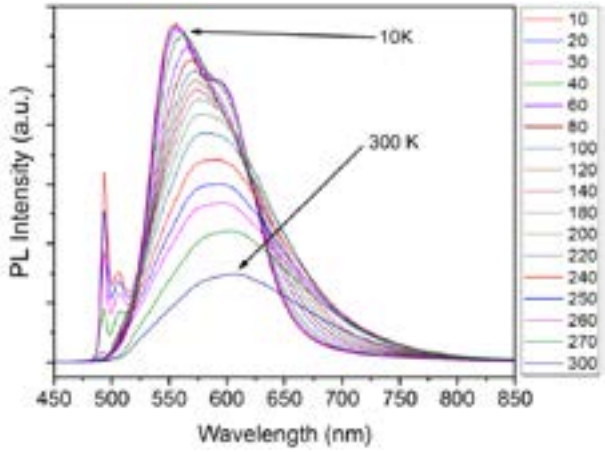


Fig. 2. Temperature dependence of PL spectrum of $Pb_{0.3}Cd_{0.7}I_2$ thick films.

At Fig. 1., the brightness of the areas corresponds to the intensity of their cathodoluminescence. Dark hexagon areas correspond to $PbI_2$ microcrystallites embedded in the CdI2 matrix that show no cathodoluminescence at room temperature [2].

As can be seen from photoluminescence (PL) spectra (Fig. 2.), there is an intense broad band with a maximum at $\lambda$ = 594 nm; the complex structure changes significantly with temperature (from 4.5 to 300 K). And it should be noted that PL intensity decreases mostly in the temperature range from 250 to 300 K. The analysis of the PL data of the films showed that analogous bands are observed in the spectrum, as in the case of bulk crystals of the composition $Pb_{0.3}Cd_{0.7}I_2$ [3].

[1] A. P. Bukivskii, Y. P. Gnatenko, Y. P. Piryatinski, I. V. Fesych, V. V. Lendel, V. M. Tkach, P. M. Bukivskij, "Nature of Radiative Recombination Processes in Layered Heterogeneous (Pb,Cd)$I_2$ Thick Films: Promising Scintillator Materials", *Journal Hindawi - Advances in Condensed Matter Physics*, Vol. 2018, p. 5, (2018).

[2] A.P. Bukivskii, Yu.P. Gnatenko, Yu.P. Piryatinski, R.V. Gamernyk, *Journal of Luminescence*, 185, pp. 83-91, (2017).

[3] F. V. Levy, A. K. Mercier, J.P. Voitchovsky, "Band-edge photoluminescence of $PbI_2$," *Solid State Communications*, vol. 15, no. 5, pp. 819–822, (1974).

# INVESTIGATION OF LUMINESCENCE QUANTUM YIELD IN GAGG:CE AND LYSO:CE SCINTILLATION CRYSTALS

Tomas Jurgutis[1], Saulius Nargelas[1]

[1] Falculty of Physics, Vilnius University, Lithuania
Tomas.jurgutis@ff.stud.vu.lt

Since their discovery scintillators have been used to detect high energy particles. Throughout last few decades the research and development was mainly driven by demand of scintillator with higher light yield and faster luminescence rise and decay times. These two qualities affect energy resolution and maximum number of measurable events, both of which are important for high energy physics experiments and medical applications such as positron emission tomography.

In this work the influence of co-doping on quantum yield of GAGG:Ce and LYSO:Ce scintillators‘ was investigated. Photoluminescence excited by various energy photons was measured and quantum yield value was evaluated using an integrating sphere method. It was evidenced that quantum yield of GAGG:Ce scintillator is affected by Mg co-doping only when photoexcited carries can escape to the conduction band of host matrix (fig. 1). The increased amount of $Ce^{4+}$ luminescence centers after co-doping LYSO:Ce with calcium resulted in a two-fold decrease of quantum yield value.

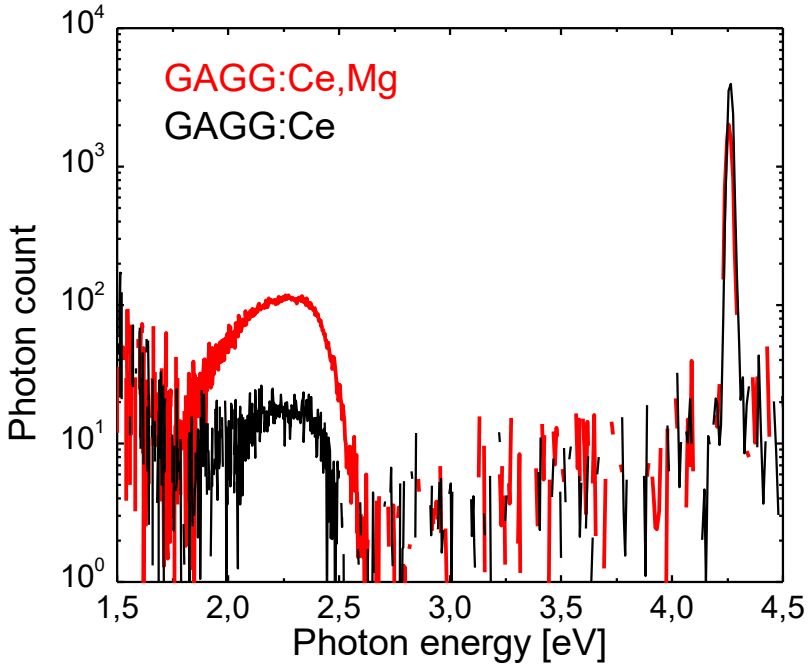


Fig. 1. Photoluminescence spectra of GAGG:Ce (black) and GAGG:Ce co-doped with Mg (red)

# SPECTRAL CHARACTERISATION OF GALLIUM NITRIDE MATERIALS APPLICABLE FOR RADIATION DETECTORS

Laimonas Deveikis, Tomas Čeponis, Eugenijus Gaubas

Institute of Photonics and Nanotechnology, Vilnius University, Saulėtekio av. 3, LT-10257, Vilnius, Lithuania
laimonas.deveikis@tmi.vu.lt

GaN is a promising wide band-gap material for fabrication of light-emitting diodes (LED), high-electron-mobility transistors (HEMT), high-frequency and high-power electronic devices, solar-blind photo-sensors and radiation tolerant particle detectors applied in high energy physics, radiation monitoring and other fields [1]. Wide band-gap of GaN determines a low leakage current and the proper radiation hardness of devices made of GaN. High luminescence efficiency is also an attractive characteristic of GaN in order to make the double response radiation sensors. Semi-insulating GaN bulk crystals of relevant thickness (~400 μm) and high resistivity (≥$10^6$ Ωcm) can also be used for manufacturing of the capacitor and Schottky diode type sensors with enhanced sensitivity. Such crystals are usually synthesised by the hydride vapour phase epitaxy (HVPE) and ammono-thermal (AT) techniques. Additionally, acceptor type dopants are intentionally introduced during growth of GaN to reach high resistivity of the material. However, the inevitable defects and impurities introduced during crystal growth affect functional characteristics of devices made of HVPE/AT GaN materials, despite these crystals contain significantly lowered densities of dislocations. Therefore, it is important to characterise these materials by identifying the prevailing defects and by evaluating their concentrations in order to produce devices of high quality and to predict their operational characteristics. The spectroscopic techniques are highly efficient tools for the investigation of defects and impurities in the materials.

In this work contactless pulsed-photo-ionization spectroscopy (PPIS) and steady-state photoluminescence (SS-PL) spectral measurements were applied for characterisation of defects and impurities introduced in bulk (~400 μm) GaN samples, grown by HVPE technology on AT-GaN seeds, and containing different carbon dopant ($N_C$ = 2×$10^{17}$ $cm^{-3}$ – $10^{18}$ $cm^{-3}$) concentrations.

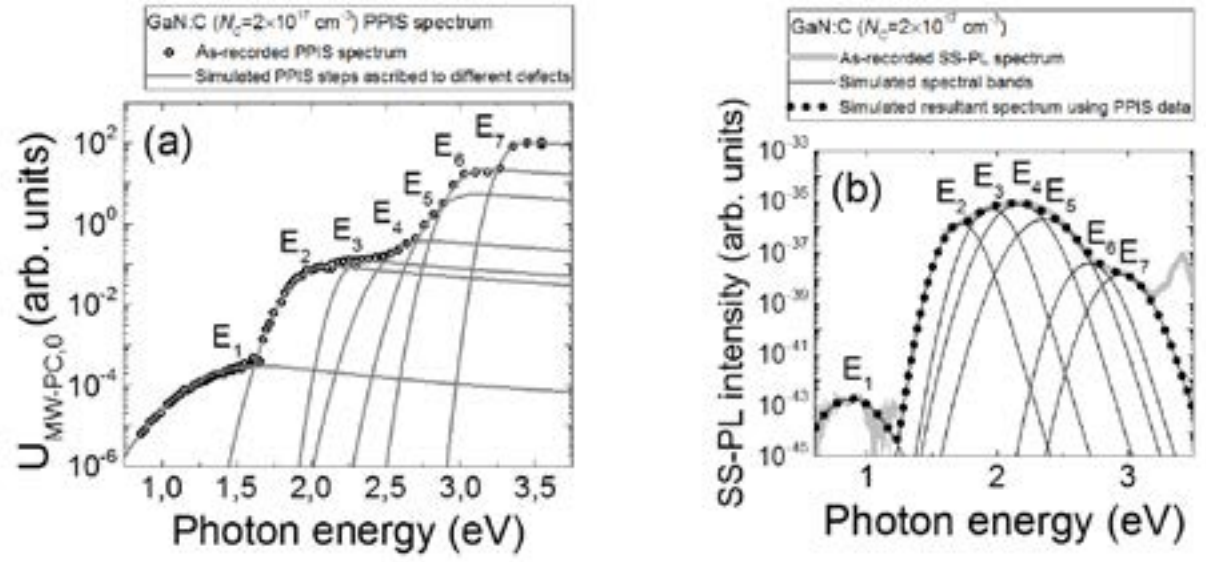


Fig. 1. (a) – Comparison of the as-recorded PPIS spectrum in lightly doped ($N_C$=2×$10^{17}$ $cm^{-3}$) GaN:C sample (circles) with simulated (using Kopylov and Pikhtin model [2]) photon-electron coupling cross-section spectral variations attributed to different energy levels (thin solid curves), and (b) –SS-PL spectrum obtained for lightly doped ($N_C$=2×$10^{17}$ $cm^{-3}$) GaN:C sample (grey line) compared with simulated energy levels (black dots and thin solid curves).

Combined consideration of the PPIS and SS-PL spectra allowed us to identify the dominant defects in GaN samples as well as their concentrations. The dominant defects have been identified to be the carbon interstitials ($C_I$), gallium vacancies ($V_{Ga}$), carbon substitutional atoms ($C_N$), carbon and oxygen complexes ($C_NO_N$) and two other unidentified, nevertheless carbon-related centres. The comparative analysis of the PPIS and SS-PL spectra as well as the procedure for identification of defects, impurities and calculation of their concentrations in carbon doped GaN samples grown by HVPE technique will be discussed. Operational characteristics of radiation detectors made of these materials will be demonstrated.

[1] S. J. Pearton, *GaN and related materials II*, (Gordon and Breach Science Publishers, Amsterdam, 2000).
[2] A. A. Kopylov and A. N. Pikhtin, Profiles of absorption and luminescence spectra of deep centres in semiconductors (oxygen in gallium-phosphide), Sov. Phys. Solid State **16**, 1200 (1975).

# MEASUREMENTS OF HIGH FREQUENCY PARAMETERS OF MICROWAVE DIODES IN $K_A$ FREQUENCY RANGE USING AUTOMATED PROBE STATION SETUP

Maksimas Anbinderis[1,2,3], Algirdas Sužiedėlis[1,2]

[1] Department of Electronics, Center for Physical Sciences and Technology, Lithuania
[2] Vilnius Gediminas Technical University, Lithuania
[3] Elmika Ltd, Lithuania
maksimas.anbinderis@ftmc.lt

In order to use microwaves, we need to have electromagnetic radiation detectors, which can sense high frequency signals even at lowpower levels. The detection of microwave radiation is obtained using non-linear elements, mainly diodes - two-terminal electronic components that can conduct current in one direction better than in another. Today semiconductor diode structures are most commonly used for electromagnetic detection. Most widespread Schottky junction-based [1] or planar doped-barrier diodes (PDB) [2] have found applications for microwave measurements. However, complexity of these electronic devices encourages scientific and engineering community to pursue new original design of microwave diodes sensing short pulses of microwave radiation and being cost effective at the same time [3]. Microwave and millimeter wavelength range requires certain specifications for electromagnetic detectors: the voltage sensitivity (thus the detected voltage also) should not depend on frequency, the detectors must be both reliable and sensitive to the impact of electromagnetic radiation. Investigation of high frequency detection properties of different semiconductor structures and design of electromagnetic radiation detectors are two inseparable subjects that are quite a hot issue in modern microwave electronics area. High frequency parameters of the microwave diodes, such as detected voltage, are usually investigated by mounting single diode into microwave waveguide transmission line [4]. However, that is rather complicated and time-consuming process. These measurements can be achieved using high frequency probe station, which allows to perform detected voltage and voltage sensitivity measurements. This measurement approach can both save time and exclude the possibility of diode damaging during the diode mounting process, because the measurements are made right onto semiconductor substrate, without dividing it into single diodes. In this paper, we present the developed automated high frequency probe station measurement setup for obtaining voltage-power characteristics of microwave diodes.

In order to test the measurement setup and determine the quality of the results, the detection properties of GaAs/AlGaAs heterojunction diodes were measured using the developed setup and also by mounting them into a waveguide head's micro-strip line where TEM wave propagates (fin-line adapter connects it to a waveguide transmission line). The results showed that the diodes are capable to detect electromagnetic radiation in the measured frequency range. The comparison of experimental results, obtained by using different measurement methods, showed that using the developed high frequency probe station setup while measuring detection sensitivity of microwave diode on a polyimide film in Ka frequency range gives truly reliable results, although further improvements can be made for better quality of the experiment.

---

[1] P .H. Siegel, Terahertz technology, IEEE Transactions on Microwwave Theory and Techniques, Vol. 50, No. 3, 910–928 (2002).
[2] R. J. Malik, , T. R. Aucoin, R. L. Ross, K. Board, C. E. C. Wood, L. F. Eastman, Planar-doped barriers in GaAs by molecular beam epitaxy, Electronic Letters, Vol. 16, No. 22, 836–838 (1980).
[3] A. Suziedelis, S. Asmontas, J. Gradauskas, A. Silenas, A. Lucun, A. Cerskus, C. Paskevic, M. Anbinderis, Pulsed microwave sensor on heavily doped semiconductor substrate, IEEE, PIERS 2017 Proceedings (2018).
[4] A. Suziedėlis, S. Asmontas, J. Gradauskas, A. Lucun, A. Cerskus, C. Paskevic, T. Anbinderis, Investigation of microwave properties of planar heterojunction diodes in Ka frequency range using probe station, IEEE, PIERS 2016 Proceedings (2016).

# EFFECT OF ANNEALING ON A PSEUDOGAP STATE IN UNTWINNED $YBa_2Cu_3O_{7-\delta}$ SINGLE CRYSTALS

Eugene Petrenko[1], Andrei Solovjov[1], Lyudmila Omelchenko[1], Ruslan Vovk[2]

[1] B. I. Verkin Institute for Low Temperature Physics and Engineering of National Academy of Science of Ukraine, 47 Nauki ave., 61103 Kharkov, Ukraine

[2] Physics Department, V. Karazin Kharkiv National University, Svobody Sq. 4, 61077 Kharkiv, Ukraine

petrenko@ilt.kharkov.ua

The effect of annealing both in the oxygen atmosphere and at room temperatures on the excess conductivity σ′(T) and pseudogap (PG), Δ*(T), of untwined $YBa_2Cu_3O_{7-\delta}$ (YBCO) single crystal with a small deviation from oxygen stoichiometry is studied. It was revealed that as the charge carrier density, nf, increases, $T_c$ also slightly increases, whereas T* decreases noticeably, which is consistent with the phase diagram (PD) of cuprates. The excess conductivity in the vicinity of $T_c$ is well described by the Aslamazov-Larkin and Hikami-Larkin fluctuation theories, demonstrating the 3D-2D crossover with an increase in temperature. The crossover temperature T0 determines the coherence length along the c axis, $\xi_c(0) = 0.86$ Å, which is 2.6 times larger than for optimally doped YBCO single crystals with defects. Taking into account the short coherence length in high-temperature superconductors, in the model of free charge carriers the phase relaxation time of fluctuation Cooper pairs is determined, $\tau_\varphi$ (100 K) = 4.42 ± 0.4 s, which is slightly (1.3 times) large than in well-structured YBCO films, and, as in films, in fact does not depend on nf. It is shown that Δ*(T) at different annealing stages practically does not change its shape. As in the well-structured YBCO films, Δ*(T) demonstrates maximum at $T_{pair}$ ~ 124 K which depends weakly on $n_f$. However, the maximum value of Δ*(Tpair) increases with increasing $n_f$, as it follows from the PD of cuprates. Comparing the experimental data with the Peters-Bauer theory we estimated the density of local pairs $\langle n_\uparrow n_\downarrow \rangle \approx 0.3$ near $T_c$, which can be a universal value for high-temperature superconductors.

We take advantage of single crystals to study fluctuation conductivity (FLC) and PG in untwined YBCO single crystal with $n_f$ close to optimal doping ($T_c$ = 91.6 K), when $n_f$ changes upon annealing in an oxygen atmosphere. We have studied three samples with different $n_f$. For a short notation, we name these samples A1, A2 and A3. The fluctuation contributions to σ′(T) were derived from the dc resistivity ρ(T) measurements, and temperature dependences of PG [1,2] Δ*(T), as a function of $n_f$ were calculated.



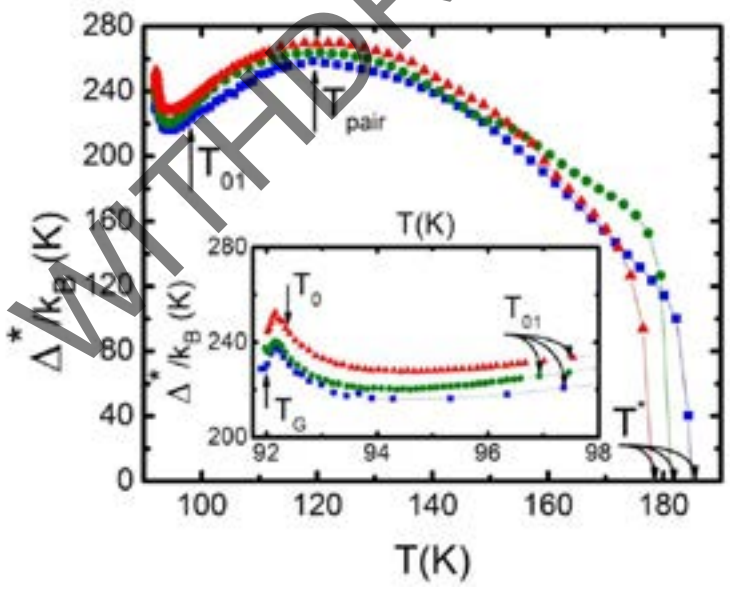


Fig. 1. Temperature dependences of the pseudogap Δ*(T) of the untwined $YBa_2Cu_3O_{7-\delta}$, single crystal for all annealing stages: A1 - blue squares, A2 - green points, A3 - red triangles. Insert: The same dependence for the temperature interval $T_G < T < T_{01}$. The arrows show all characteristic temperatures. Solid lines are to guide the eye.

[1] A. L. Solovjov, in *Superconductors - Materials, Properties and Applications*, edited by A. Gabovich (InTech, Rijeka, 2012), Chap. 7, p. 137.
[2] A. L. Solovjov and V. M. Dmitriev, Low Temp. Phys. **32**, 99 (2006).

# SYNTHESIS AND OPTICAL INVESTIGATIONS OF CARBON QUANTUM DOTS

Ignatij Mackevic[1], Arturas Katelnikovas[1]

[1] Faculty of Chemistry and Geosciences, Vilnius University, Naugarduko 24, LT-03225 Vilnius, Lithuania
ignatij.mackevic@chf.stud.vu.lt

The aim of this scientific work is synthesis and investigation of optical properties of carbon quantum dots (CQDs). Since accidental discovery of these nanomaterials during purification of single walled carbon nanotubes, the attention and interest to them has grown tremendously and keeps attracting many scientists and scientific groups. As a result of many investigation works carried out after their discovery, these formations proved to have unique and exceptionally useful properties that are often found in such nano scale sized materials.

Currently, the main focus concerning CQDs is directed towards the search and development of the most efficient and optimal synthesis methods that could provide their massive scale productions. Such particular attention to CQDs is deserved due to their physicochemical and luminescent properties. Especially worth mentioning are their good water solubility, easy surface modification, chemical inertness and photostability comparing to the traditional semiconductors quantum dots, all of which have a great practical potential. Additionally, such extremely useful and rarely found properties in material sciences as biocompatibility and low toxicity, render their application in white-LED production, bioimaging, biosensors and the field of theranostics that proves itself to be a very valuable and important branch of medicine currently being intensively developed. Nonetheless, important are electronic and photocatalytic properties that carbon quantum dots possess and can find their use in optical devices as well as catalytic systems [1].

As for now, there is no unambiguous model as to what physical processes make photoluminescence mechanism possible in CQDs [2]. However, it is evident, that it can be controlled upon changing size of these nano scale formations and modifying their surface by various organic functional groups or inserting heteroatoms into their structure which can be achieved using different synthesis methods and their variations. The graphitic like structure creates band gap between HOMO (highest occupied molecular orbital) and LUMO (lowest unoccupied molecular orbital) that take part in electron transition process between them and thus causing light emission. This suggested model predicts the energy/wavelength of light emitted upon excitation, i.e. with increasing size of quantum and level of condensation, band gap energy between HOMO and LUMO levels is getting more narrow and thus a red shift in emission spectrum takes place. Analogically, with decreasing size of QDS emission peak moves towards blue part of the visible spectrum.

Currently, the largest issues that have raised from synthesis of these nanomaterials are aggregation of formed CQDs, poor size reproducibility and monodispersity, and unsatisfactory precision in surface modification, all of which have motivated us to the idea of initiation of such project which might at least slightly contribute to the search and development of the most optimal synthesis method of these exceptionally useful nanomaterials. Factors like time, temperature, pH, solvent or presence of different oxidators and reductors during synthesis, that have impact on CQDs formed, will be considered to predict the best possible synthesis conditions.

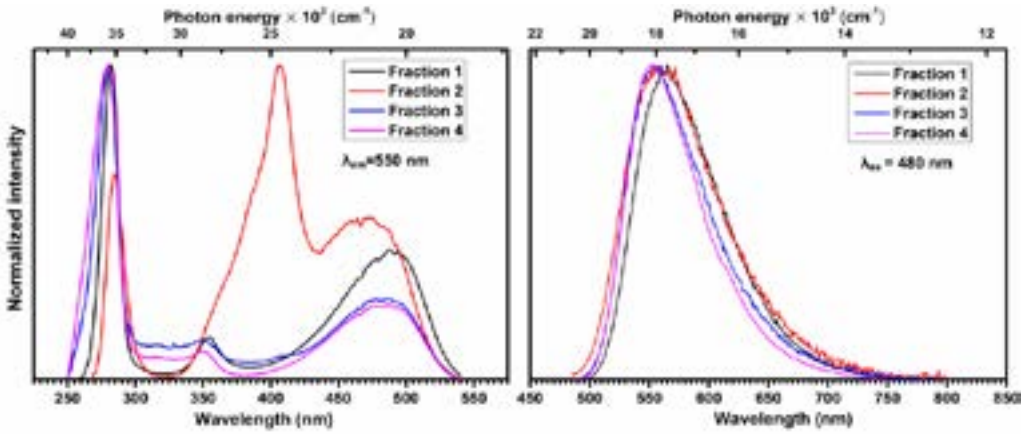


Fig. 1. Excitation ($\lambda_{em}$=550 nm) and emission ($\lambda_{ex}$=480 nm) spectra of 4 different fractions gathered during purification process using column chromatography (immobile phase: silica gel; mobile phase: ethyl acetate). The number written next to fraction corresponds to the succession of it's exit from chromatography column.

**Acknowledgements:** This research was funded by the European Social Fund under the No 09.3.3.-LMT-K-712-10-0120 "Development of Competences of Scientists, other Researchers and Students through Practical Research Activities" measure.

[1] Y. Wang, A. Hu, Carbon quantum dots: synthesis, properties and applications, J. Mater. Chem. C, 2014, 2, 6921.
[2] S. Zhu, Y. Song, X. Zhao, J. Shao, J. Zhang, B. Yang, The photoluminescence mechanism in carbon dots (graphene quantum dots, carbon nanodots, and polymer dots): Current state and future perspective, Nano Research 2015, 8(2): 355–381.

# LATTICE DISTORTION MODEL. MODELING OF ELASTIC CONSTANTS ON CRYSTALLINE MATERIALS OF BCC-LATTICES

Tomas Vaitkūnas[1], Audrius Jutas[1*]

[1] Department of Mechanical Engineering, Kaunas University of Technology, Lithuania
tomas.vaitkunas@ktu.edu

As the standpoint of this study is a creation of method based on the multi-scale modelling that was chosen as a way to collect and, in the case of high probability comparable with the experimental results or methods, to share all possible natural phenomena as some evidence of physical reality in crystalline materials. This method describes the complex behavior of atomic systems aligned by different spatial angles in neighbor microstructures. Virtually this allows us analyzing wave properties in discrete lattice/microstructure as the result of complex multi-directional neighbor impact. Firstly, the modeling of BBC-lattice deformation is presented according to the theory on computation of elastic constant like Poisson's ratio from the atomic perspective in close connection with experiment data obtained at macro-scale (Fig. 1). Poisson's ratio is expressed as:

$$\nu_i = -\frac{\varepsilon_{yi}}{\varepsilon_{xi}}; \tag{1}$$

where $\varepsilon_{xi}(d_{xi}, \alpha_{xi}, C)$ and $\varepsilon_{yi}(d_{yi}, \alpha_{yi})$ – longitudinal and transverse deformation, $C$ – coefficient of deformation intensity $1/\xi \le C \le 1/\xi^2$ while $\xi$ - parameter which show one atom inertia to another according to the movement direction and depends on deformation level ( $0 < \xi \le 1$ ).

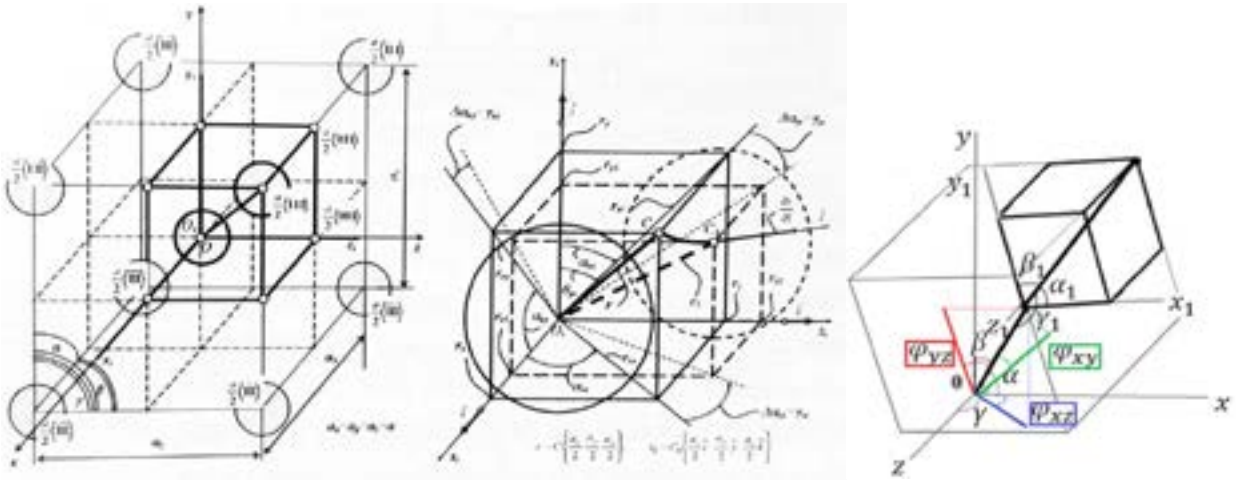


(A) (B) (C)

**Fig. 1. Lattice distortion model. A** is BCC-lattice. The one eight of the lattice is taken in order to model relation between the nearest neighbor atoms in system Center-Edge. Axes XYZ represent the global coordinate system according to direction of impact. **B** is geometrical representation on physical model of lattice deformation in the local spatial coordinate system $X_1Y_1Z_1$. An edge atom draws path $CC_1$ explaining the spatial change in atomic distance and volume. **C** is the aligned BBC-lattice in both global and local coordinate systems. The angles α, β, γ are used in equations of tangent plane going at any single point of the outside surface of the unit sphere and for an evaluation of Burger's vectors <XYZ> [1]

Parallel to development in statistical mechanics, atomistic modeling is shown as a maturing and perspective tool in solid state physics and materials science and for the fine investigations of bulk characteristics and their elastic limits in crystalline materials.

[1] D. Raabe, M. Sachtleber, Z. Zhao, F. Roters, S. Zaefferer, Micromechanical and macromechanical effects in grain scale polycrystal plasticity experimentation and simulation Acta Materialia 17, pp. 3433-3441 (2001)

# NEW BENZOYLPYRIDINE COMPOUNDS FOR APPLICATION IN TADF OLEDs

Domantas Berenis, Virginijus Ruibys, Ona Adomėnienė, Povilas Adomėnas, Gediminas Kreiza, Saulius Juršėnas, Karolis Kazlauskas

Institute of Photonics and Nanotechnology, Vilnius University, Lithuania
domantas.berenis@ff.stud.vu.lt

Organic light-emitting devices (OLEDs) are an attractive technology for commercial displays and lighting because of their high luminous efficiency, flexibility and adaptability to large areas as well as relatively easy color tuning. Currently, emitters exhibiting thermally activated delayed fluorescence (TADF) properties are considered as the most promising for next generation OLEDs. TADF allows harvesting of non-radiative triplet excitons through their conversion to radiative singlet states via reverse intersystem crossing (RISC) using thermal energy of the environment [1]. It was demonstrated that by careful design and optimization of donor-acceptor based molecular structure conversion, and thus, photoluminescence quantum yield (PLQY) as high as 100% can be achieved at room temperature [2].

In this work a series of new donor-acceptor-donor molecules containing benzoylpyridine acceptor and two carbazole donor moieties were investigated as potential TADF emitters. The studied molecules (see Fig. 1) had different linking positions of the carbazole moieties on a phenyl ring (para and meta linkage) as well as a different location of nitrogen atom in the pyridine moiety (3 and 4 position). Additionally, the impact of solubility-enhancing non-conjugated tert-butyl groups on the photophysical properties of the compounds were studied.

To determine the most efficient benzoylpyridine-based TADF compound for OLED application, absorption, PL, PLQY and PL transients of the compounds were measured in ambient and oxygen-free environments. Good correlation between PLQY values of solution and thin film samples (Fig. 1. right) was found for different emitters. Significantly higher PLQY values for the emitters doped in neutral PMMA films as compared to those of solutions indicated reduced non-radiative decay due to suppressed vibrational/rotational relaxation. Compounds possessing para- linked donors exhibited higher PLQY yet smaller delayed to prompt emission ratio as compared to their meta-substituted counterparts. Moreover, PLQY was found to be higher for compounds with a nitrogen atom in the 3rd position of the pyridine moiety as well as for compounds containing peripheral tert-butyl groups. The obtained results suggest that the compound U04 is the most promising option for fabrication of vacuum- and solution-processed TADF OLEDs.

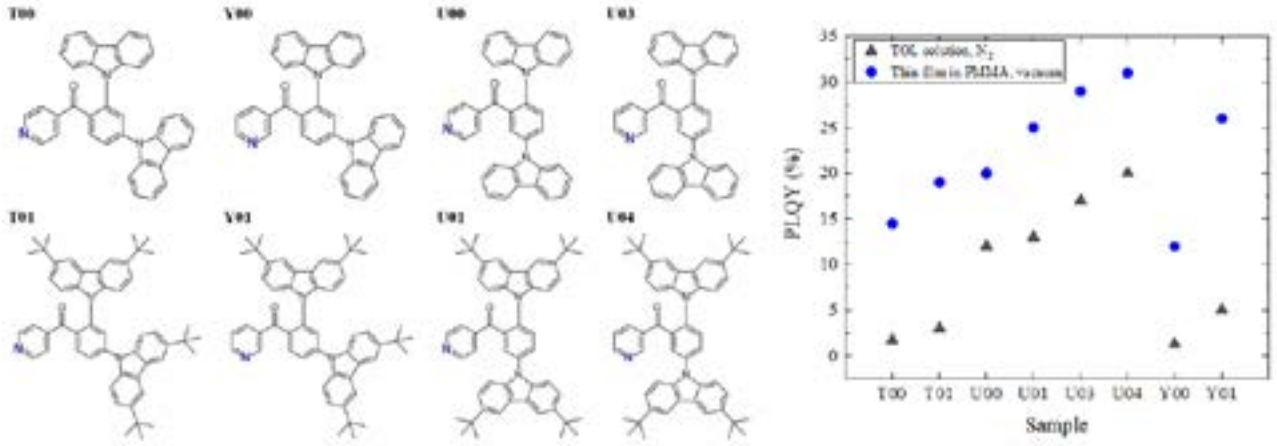


Fig. 1. Chemical structures of eight studied molecules (left) and determined PLQY values (right).

[1] H. Uoyama, K. Goushi, K. Shizu, H. Nomura, C. Adachi, Highly efficient organic light-emitting diodes from delayed fluorescence, Nature. 492 (2012) 234–238. doi:10.1038/nature11687.
[2] C. Adachi, Third-generation organic electroluminescence materials, Jpn. J. Appl. Phys. 53 (2014) 1–11. doi:10.7567/JJAP.53.060101.

# Co-DOPED MANGANITE/GRAPHENE AS NEW PROTOTYPE FOR MAGNETIC FIELD SENSOR APPLICATION

Eleonora Bolli[1], Alessio Mezzi[1], Saulius Kaciulis[1] , Rasuole Lukose[2], Nerija Zurauskiene[2,5], Voitech Stankevic[2,5], Milita Vagner[2,3], Valentina Plausinaitiene[2,3], Skirmantas Kersulis[2], Gediminas Niaura[4], Saulius Balevicius[2,5]

[1] Institute for the Study of Nanostructured Materials, ISMN-CNR, 00015 Rome, Italy
[2]Department of Material Science and Electrical Engineering, Center for Physical Sciences and Technology, LT-10257 Vilnius, Lithuania
[3]Institute of Chemistry, Faculty of Chemistry and Geosciences, Vilnius University, LT- 03225 Vilnius, Lithuania.
[4]Department of Organic Chemistry, Center for Physical Sciences and Technology, LT-10257 Vilnius, Lithuania
[5]Department of Electrical Engineering, Vilnius Gediminas Technical University, LT- 10223 Vilnius, Lithuania.
eleonora.bolli@ismn.cnr.it

Co-doped $La_{1-x}Sr_xMn_yO_3$ manganite with single or few layer graphene is a novel system designed for magnetic sensor application at room temperature. Manganite/graphene structure combines the properties of manganite with negative magnetoresistance (MR) and two-dimensional graphene with positive MR in order to increase the sensitivity of sensor based on magnetoresistence also in the presence of low magnetic field, in the range 0.1-21 T.

The properties of Co-doped $La_{1-x}Sr_xMn_yO_3$ with single layer graphene SLG, three-layer 3LG or five layer 5LG, were characterized by using X-ray photoemission spectroscopy (XPS) and Auger electron spectroscopy (XAES). XPS studies were focused on the analysis of photoemission C1s spectra of graphene layer, whereas the Auger spectra of C KVV region were used for determination of the D parameter [1].

Because this prototype of new device was prepared by exfoliating commercial high-quality monolayer graphene on Cu previously passivated with polymethylmethacrylate PMMA, from the component analysis of C1s spectra was possible to identify also the presence of polymer residues which could negatively affect the sensitivity to the magnetic field.

Magnetoresistance measurements of the sensors assembled with single and few layer graphene in permanent and pulsed magnetic fields have shown that the best sensitivity response is obtained for 3LG samples. This result was in accordance with XPS and XAES data, which revealed a better quality of 3L graphene with lower content of residues due to exfoliation process.

[1] S. Kaciulis, A. Mezzi, P.Calvani, D.M. Trucchi, Electron spectroscopy of the main allotropes of carbon. Surf. Interface Anal. 46 (2014) 966-969.

# MONTE CARLO METHOD APPLICATION FOR NEUTRON TRANSPORT CALCULATIONS IN IFMIF-DONES NUCLEAR SAFETY ASSESSMENT

Simona Breidokaite[1], Gediminas Stankunas[1], Andrius Tidikas[1]

[1]Laboratory of Nuclear Installation Safety, Lithuanian Energy Institute,
simona.breidokaite@lei.lt

The International Fusion Material Irradiation Facility DEMO-Oriented Neutron Source (IFMIF-DONES) is an accelerator based d-Li neutron source which aims at the qualification of materials at the fusion irradiation conditions. IFMIF-DONES is a complex nuclear facility. In order to assure safe operation and exploitation, Monte Carlo method based codes are used for safety analyses. Monte Carlo method allows simulation of physical experiments in realistic objects. Distribution function is used to repeatedly take random samples in order to obtain numerical results and the method is based on the law of large numbers and the central boundary theorem. This paper presents neutron transport equations and the application of Monte Carlo method as well as subsequent activation analysis.

The neutron-induced activities and dose rates at shutdown were calculated by the means of FISPACT-2010 code with data from JEFF-3.1.2 nuclear data library. Neutron fluxes and spectra were obtained with MCNP neutron transport calculations. The activities and the dose rates were calculated at the end of the irradiation and for further cooling times of 0s, 1s, 5 min., 30 min., 1 h., 3 h., 5 h., 10 h., 1 day, 3 days, 1 days, 2 weeks, 4 weeks, 8 weeks, 181 days, 1 year, 10 years, 100 years, 300 and 1000 year. In addition, radionuclides with contribution for at least 0.5% to the total value of activation characteristics at previously mentioned cooling times were identified.

# PREPARATION OF SnS FILMS ON THE FTO GLASS BY SILAR METHOD

Asta Bronušienė, Ingrida Ancutienė

*Department of Physical and Inorganic Chemistry, Kaunas University of Technology, Lithuania*
*E-mail: astbak@ktu.lt*

Tin sulfide presents good optical quality, electronic characteristics (band gap varying between 1-2.3 eV in the visible range, high charge carrier mobility and etc.), physicochemical properties [1]. One of the merits of SnS is that it's abundant in nature, cheap and nontroxic [2]. Other merit is that tin sulfide can be adapted to the fabrication of solar cells because of good electronic characteristics.

Thin SnS films can be deposited using a lot of technics, such as chemical bath deposition, spray pyrolysis, electrodeposition and etc [2]. In this work tin sulfide films were fabricated by using SILAR method. The main advantage of SILAR method is that it offers simple fabrication methodology [3]. Thin films can be made almost at standard conditions.

For the fabrication of SnS thin films we used FTO glass. The ultra-sonic cleaning of glass slides was carried out by dipping the glass slide into acetone at 40 °C for 10min, then rinsed with distilled water and dried. As the cationic precursor were used 40 °C 0.1M $SnCl_2$ solution and as the anionic precursor – 40 °C 0.1 M $Na_2S$ The precleaned substrate firstly immersed in the cationic precursor for 30 s and tin ions were adsorbed on the surface of the substrate [4]. Then the glass slide immersed in the anionic precursor solution for 30 s. Sulfide ions reacted with tin ions which were adsorbed on the substrate. Twenty such deposition cycles were repeated in order to get adherent film. For all samples the last step was immersing these in the cationic precursor. The XRD studies on a DRON-6 diffractometer operating with Cu $K_\alpha$ radiation (Ni filter) at 30 kV and 20 mA were performed.

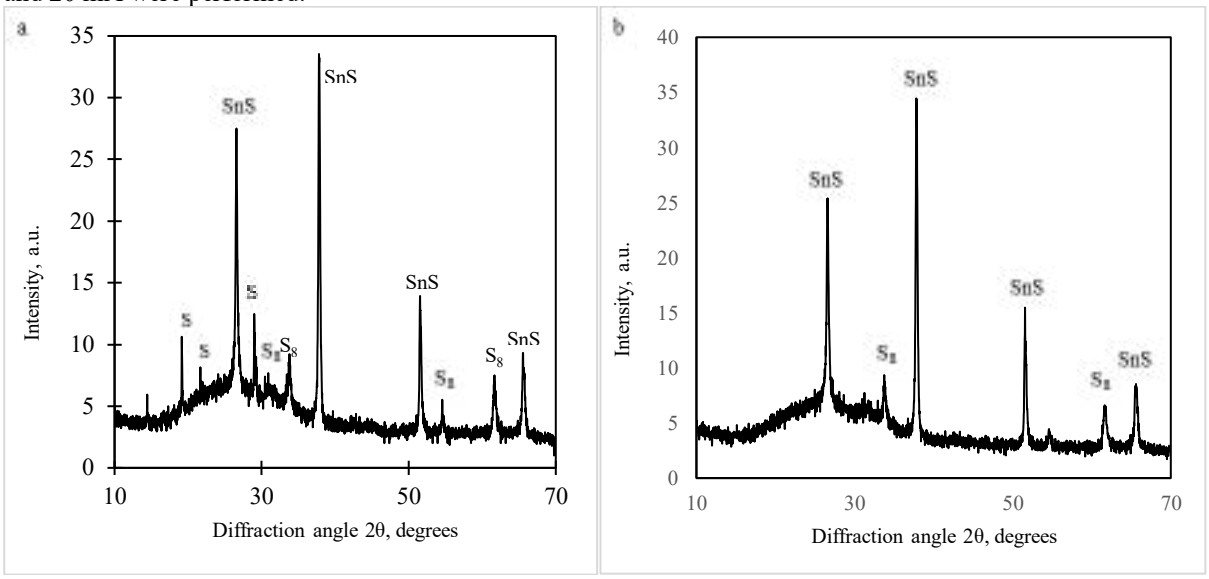


Fig. 1. X-ray diffractograms of formed layers: a – as deposited, b – after annealing.

The phase composition of the formed layers was determined by contrasting their X-ray diffraction pattern with those of known minerals. These formed layers consist of SnS (83-47), S (76-183), $S_8$ (74-1465). In both pictures the most intensive peak is assigned to SnS (2θ=37.8°). Other intensive peaks assigned to SnS, at 2θ=26.6; 51.6 and 65.6°. The sample was annealed in an inert (nitrogen) atmosphere at 100 °C for 24 h. This process stimulates the formation of tin sulfide. It means that elemental sulfur reacts with adsorbed tin ions to form SnS at higher temperature. SnS peaks are higher than before (Fig. 1 b).

[1] M. Mnari, N. Kamoun, J. Bonnet, and M. Dachraoui, "Chemical Bath Deposition of tin sulphide thin films in acid solution," *Comptes Rendus Chim.*, vol. 12, no. 6–7, pp. 824–827, 2009.

[2] B. Ghosh, M. Das, P. Banerjee, and S. Das, "Fabrication and optical properties of SnS thin films by SILAR method," *Appl. Surf. Sci.*, vol. 254, no. 20, pp. 6436–6440, 2008.

[3] B. Ghosh, S. Chowdhury, P. Banerjee, and S. Das, "Fabrication of CdS/SnS heterostructured device using successive ionic layer adsorption and reaction deposited SnS," *Thin Solid Films*, vol. 519, no. 10, pp. 3368–3372, 2011.

[4] N. G. Deshpande, A. A. Sagade, Y. G. Gudage, C. D. Lokhande, and R. Sharma, "Growth and characterization of tin disulfide (SnS2) thin film deposited by successive ionic layer adsorption and reaction (SILAR) technique," *J. Alloys Compd.*, vol. 436, no. 1–2, pp. 421–426, 2007.

# SELECTIVE COBALT (II) SALT ADSORPTION TO THIN FILMS OF POLYMER BLENDS - OBTAINING MAGNETIC DOMAINS IN NON-MAGNETIC MEDIUM

Michał Janik[1] , Paweł Dąbczyński[1] , Olaf Stefańczyk[2] , Anna M. Majcher[1]
[1]Faculty of Physics, Astronomy and Applied Computer Science, Jagiellonian University, Łojasiewicza 11, 30-348 Krakow, Poland
[2]Department of Chemistry, School of Science, The University of Tokyo, 7-3-1 Hongo, Bunkyo-ku, Tokyo 113-0033, Japan
michal.247.janik@student.uj.edu.pl

Investigation of using new magnetic materials in high-density memory storage or in molecular spintronics has gained great interest among material scientists. The presented research concerns using a recently reported exciting new material[1] that joins the features of Single Ion Magnets displaying slow magnetic relaxations[2] and polymers that are easy and cheap to process for creating magnetic domains of controllable size in a nonmagnetic medium. The mentioned material is a matrix of poly(4-vinylpyridine) (P4VP) cross-linked by Co (II) salt adsorbed to the polymer from solution - in which slow relaxations of magnetization (that is a certain delay of spin reorientation with respect to changes of external magnetic field useful for e.g. storing bytes of information) are preserved. Using phase separation of P4VP and polystyrene (PS) that has no groups to chemically bind the cobalt salt, through selective adsorption of cobalt bromide $CoBr_2$, magnetic domains of controllable sizes were obtained and investigated. Thin films of this polymer blend were prepared in varying mass ratios from solutions using the spin-casting method. Cobalt bromide adsorption was executed using its solution in a solvent orthogonal for both used polymers (that is, dissolving the salt but not the polymer). Changes in topography observed using Atomic Force Microscopy strongly indicate obtaining paramagnetic domains dispersed in diamagnetic medium, or vice versa, depending on the PS:P4VP mass ratio (see Fig. 1). This is a pioneering step towards applying Single Ion Magnets (till now usually studied in crystal form) in e.g. high-density memory storage using the ease of polymer processing.

This research was financed by the Polish National Science Centre within the SONATA Project UMO2015/19/D/ST5/01936.



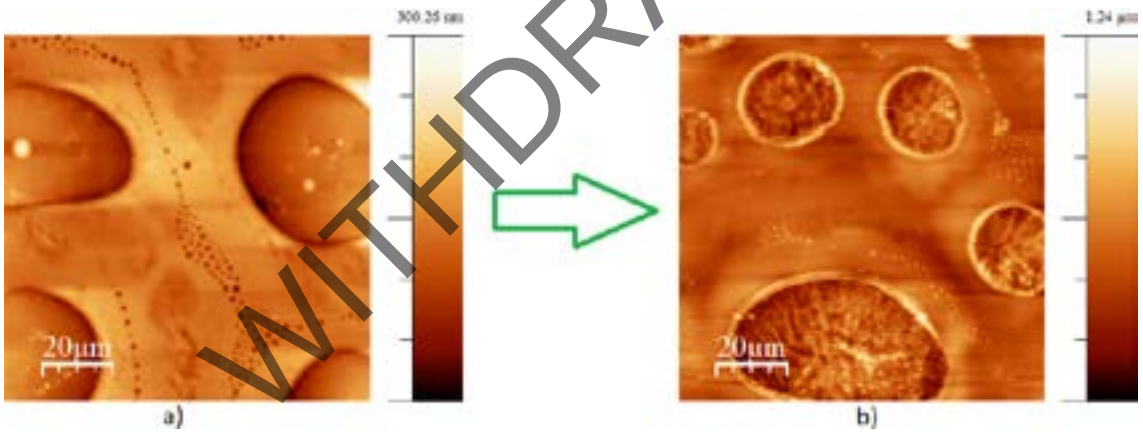


Fig. 1. AFM topography images of a thin film of polystyrene - poly(4-vinylpyridine) in 2:1 respective mass ratio a) before and b) after modification with solution of CoBr2 in solvent orthogonal to both polymers. Increase in roughness indicates adsorption of CoBr2 to polymer domain.

[1] A. M. Majcher, P. Dąbczyński, Mateusz M. Marzec et al., Between single ion magnets and macromolecules: a polymer/transition metal-based semi-solid solution, Chem. Sci.9, 7277-7286 (2018).
[2] G. A. Craig and M. Murrie, 3d single-ion magnets, Chem. Soc. Rev., 44, 2135-2147 (2015).

# FOCK'S QUASI-STATIONARY STATES THEOREM FOR A BINOMIAL DISTRIBUTION DERIVATION TO DESCRIBE REACTOR CORE NUCLEI RADIOACTIVE DECAY

Maksim Kravchenko[1], Tamara Korbut[1], Eduard Rudak[1], Andrey Petrovski[1]

[1] Laboratory of Nuclear Reactor Physics, Scientific institution «JIPNR – Sosny», Minsk, Belarus
m.kravch@sosny.bas-net.by

Classical experimental nuclear physics determines radioactive decay for a close to infinite number of nuclei as process described with a continuous differential function. Such an assumption is valid until one meets a finite amount of a radioactive nuclei in a system. In that case a binomial distribution must be applied instead of Poisson as well as the intensity of radioactive decay must depend on number of particles in a system.

Started in [1,2] the research direction in field of nuclear reactor physics aims to achieve common mathematical apparatus for simple analytic description of reactor's breeding medium parameters. These studies are based primarily on the theory of Markov processes [3] having a well-developed mathematical apparatus. The description of the reactor operation within the framework of this theory makes it possible to consider it as an analog of an oscillatory system with events of nuclei-emitters emergence and decay occur in time.

Current work is aimed at deriving mathematical apparatus for binomial distribution by the means of Fock's quasi-stationary states theorem. First implementation of such a mathematical apparatus was made in development of sub-Poisson distribution in [4,5]. Present work includes description of reactor core nuclei radioactive decay in terms of binomial distribution. Nuclei radioactive decay kinetics equations and asymptotical function form for an average nuclei number in a system has been have been derived by the means of probability analysis [6]. Main result of the work is to be an Eq. (1) for an average number of radioactive nuclei by moment of time $t$.

$$n(t)_{\mathrm{b}} = n \cdot \mathrm{e}^{n \cdot \ln(1-\lambda t/n)} \tag{1}$$

[1] Rudak Ed A and Yachnik O I 2012 Bulletin of the BAS. Phys. no. 4 pp 84–88
[2] Korbut T N, A.V. Kuz'min, E.A. Rudak 2015 Thermal Nuclear Reactor as an Analog of ADS Systems with Internal Sources of Neutrons Bulletin of the RAS. Phys. 79
[3] Kendall D G 1948 Ann. Math. Statist. no. 1 19 pp 1–15
[4] Korbut T N, Rudak Ed A and Piatrouski A M 2018 Bulletin of the Russian Academy of Sciences: Physics 82 pp 80–86
[5] Rudak Ed A, Korbut N N, Kuzmin A V and Kravchenko M O 2018 "Molodezh v nauke - 2.0'17 NAS of Belarus" no. 2 pp 285–291
[6] Whittle P 2000 Probability via Expectation Springer 369

# THREE-DIMENSIONAL PHOTOSTRUCTURING OF ACRYLATED EPOXIDIZED SOYBEAN OIL

Edvinas Skliutas[1], Miglė Lebedevaitė[2], Jolita Ostrauskaitė[2], Mangirdas Malinauskas[1]

[1] Laser Research Center, Vilnius University, Sauletekis Ave. 10, 10223 Vilnius, Lithuania
[2] Department of Polymer Chemistry and Technology, Kaunas University of Technology, Radvilenu Rd. 19, LT-50254 Kaunas, Lithuania
edvinas.skliutas@ff.stud.vu.lt

Optical three-dimensional printing (O3DP) has emerged as an additive manufacturing technology out of photosensitive materials employing light [1]. Light induced photopolymerization reaction is the key process to make liquid resin to solid objects. Most materials absorb ultraviolet (UV) or deep-UV light, thus relevant light sources common in scientific laboratories must be used. To operate in visible (VIS) light range, photoinitiators (PI) must be added [2]. On the other hand, PI are undesired because of their toxic properties. An approach enabling to avoid both of limitations, UV light and PI, is a two-photon polymerization (2PP) technique. 2PP is based on non-linear absorption, occurring due to high irradiation intensities within a confined small volume. It can be achieved with tightly focused ultrashort pulsed laser beam. Positioning the focused beam through the material it is possible to create various 3D objects in mesoscale with up to 100 nm spatial resolution [3]. This technology is a branch of so called direct laser writing (DLW) 3D lithography.

O3DP and DLW are based on light-matter interaction, which induces photoreaction in monomers, crosslinking them into polymers. Although technologies are implemented differently, a proper material selection remains a common task for both techniques. Most of the photosensitive resins are petroleum-derived even though alternative materials obtained from renewable resources can be used instead [4]. In the recent decade interest in plant-derived products has increased dramatically [5].

In this work we examine an acrylated epoxidized soybean oil (AESO), which is attractive due to the high amount of various functional groups such as the acrylic, epoxy and hydroxy groups. The aim of the work was to investigate if AESO as a plant-based renewable resin can be suitable for both technologies: O3DP, employing non-laser UV and visible light (385 nm and 405 nm wavelengths) digital light processing (DLP), and DLW using 515 nm wavelength (fundamental 1030 nm), 300 fs pulsed laser irradiation with high pulse repetition rate (200 kHz). There were used three different photoinitiators (BAPO, TPO and TPO-L) to absorb aforementioned irradiation and induce efficient radical photopolymerization. Three diluents (n-butanol, ethyl-lactate, Genomer 1122) were applied to dilute PI and reduce monomers viscosity. In DLP case, penetration depth $h_a$ to the resin and critical duration $T_c$, required to reach critical does to fully polymerize the resin, were assessed using Beer-Lamber law. In DLW case, irradiation power $P$, beam scanning velocity $v$ and distance between adjacent beam scans $d_{xy}$ were modified. It allowed finding the fabrication window in the AESO based resins.

In this research it was shown, that AESO monomers can be selectively polymerized employing 385 nm and 405 nm wavelengths light. Measured $h_a$ and $T_c$ were: 260 μm and 0.4 s for the 385 nm light; 400 μm and 0.8 s for the 405 nm light. O3DP was demonstrated using DLP (Fig. 1 (a)). It was assessed, that pure AESO monomers can be photostructurized employing DLW (Fig. 1 (b) and (c)). Evaluated fabrication parameters were: $P$=0.6-0.8 mW (2-2.7 TW/cm$^2$), when $v$=2.5-5 mm/s and $P$=0.9-1.2 mW (3-4 TW/cm$^2$), when $v$=5-10 mm/s. In both cases it is appropriate to set $d_{xy}$ between 0.25 μm and 1 μm.

In this paper photostructuring of AESO monomers was demonstrated at *mesoscale* – merging macro- and micro-objects. Evaluated parameters showed great perspectives for versatile applications of AESO in O3DP and DLW technologies [6] as a resin derived from natural resources.

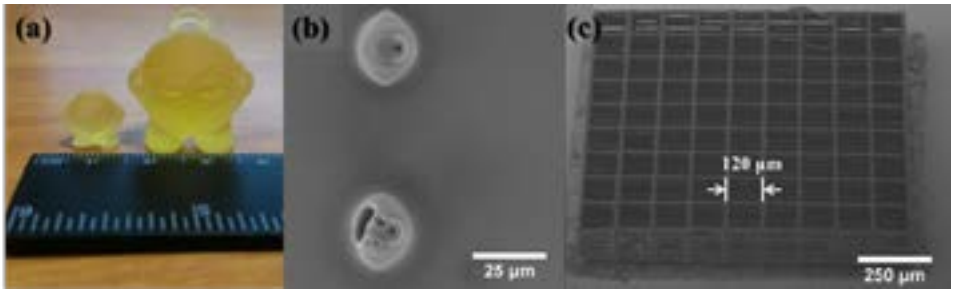


Fig. 1. (a) – 3D printed models of „Marvin" out of photosensitized AESO resin, employing DLP. From left to right: 2 times downscaled and original size; (b) – formed „Marvin" in pure AESO monomer using DLW. View from top; (c) – 1065x1065 μm$^2$ size 3D microporous scaffold. Pore size 120 μm. View at the angle of 45 degrees. (b) and (c) are scanning electron microscope (SEM) images.

[1] S. C. Ligon, et. al, Polymers for 3D Printing and Customized Additive Manufacturing, Chem. Rev. **117**, 10212–10290 (2017)
[2] E. Skliutas, et. al, M. Photosensitive Naturally Derived Resins Toward Optical 3-D Printing. Opt. Eng., **57**(4), 041412 (2018).
[3] L. Jonušauskas, et. al, Mesoscale Laser 3D Printing, Preprints, 10.20944/PREPRINTS201810.0384.V1 (2018).
[4] H. Pelletier, et. al, Acrylated vegetable oils as photocrosslinkable materials, J. Appl. Polym. Sci. **99**(6), 3218–3221 (2006).
[5] V. Sharma, et. al, Condensation polymers from natural oils, Prog. Polym. Sci. **33**(12), 1199-1215 (2008).
[6] M. Lebedevaite, et. al, Photoinitiator Free Resins Composed of Plant-Derived Monomers for the Optical μ-3D Printing of Thermosets, Polymers **11**(1), 116 (2019).

# FEMTOSECOND LASER 3D MICROFABRICATION OF ELASTOMERIC RESIN

Giedrė Grigalevičiūtė[1], Linas Jonušauskas[1,2], Mangirdas Malinauskas[1]

[1] Laser Research Center, Faculty of Physics, Vilnius University, Lithuania
[2] Femtika Ltd., Vilnius, Lithuania
giedre.grigaleviciute@gmail.com

The polymerization initiated by light is already successfully used and applied in such areas as laboratories research as well as industry. The main idea of 3D direct laser writing is simple and rapid way to fabricate 3D solid polymeric objects out of liquid prepolymer, consisting monomers, oligomers and photoinitiators. Employing femtosecond laser lithography true 3D, with intricate internal geometry, micro- or nano-scaled structures in high quality can be manufactured [1]. The applications of photopolymerization are shown in such fields as medicine, micro- and fiber optics, photonics, micro-mechanics. [2]

Despite the fact, that 3D laser lithography can be used as a versatile tool, there is a lack of elastomeric photosensitive materials that could be polymerized for specific applications. In this work femtosecond laser lithography experiments were performed with elastomeric resin UV-PDMS (manufacturer *ShinEtsu Japan*). During the experiments the goal was to determine the optimal parameters for the micro-fabrication of the aforementioned material. The 3D structures shown in the Figure 1 were fabricated with varied parameters and dosages by the change of laser beam average power, scanning (velocity, number and direction). The optimal parameters for achievements of quality results were while using the objective of 63x magnification and 1.4 numerical aperture, the power from 0.4 mW to 0.6 mW and the fabrication velocity up to 3000 μm/s. Also there was noticed, that the scanning in different directions (opposite and the same) results in different symmetry of the fabricated object (Fig. 2). This can be explained by the diffusion of generated radicals and heat [3].

Based on the optimized fabrication parameters, the sample microporous 3D scaffold structures for cell growth will be presented validating the applicability of the chosen material and fabrication technology.

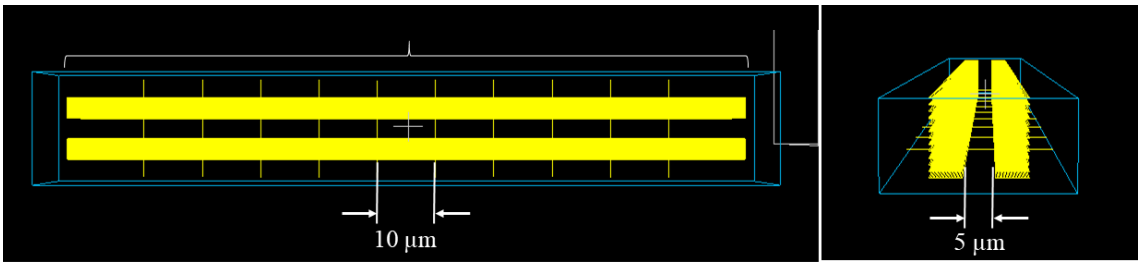


Fig. 1. The CAD model of fabricated structures during the experiment, on the left: the view from the top; on the right – the view from the side.

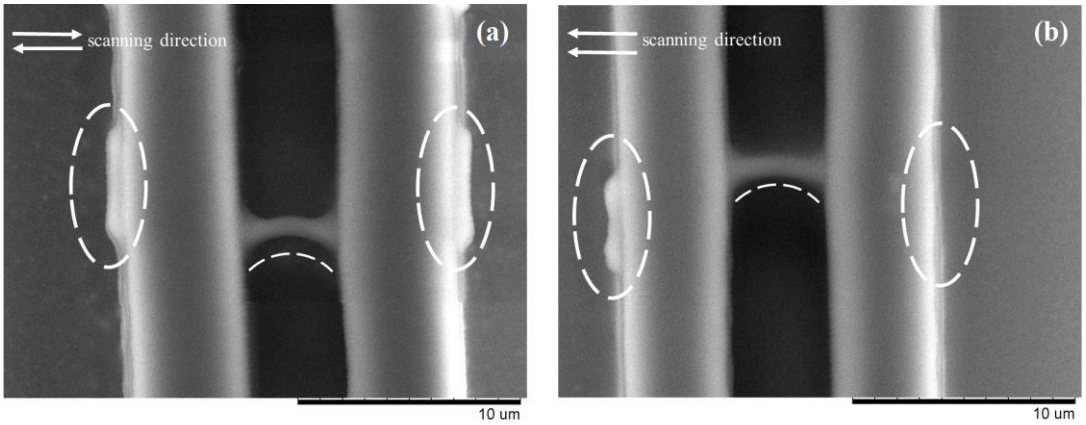


Fig. 2. The structures fabricated of UV-PDMS elastomer in different conditions: (a) the scanning directions are opposite, (b) the scanning directions are the same.

[1] M. Malinauskas et al, Ultrafast laser processing of materials: from science to industry, Light. Sci. Appl. **5**(e16133) (2016).
[2] A. Ovsianikov et al, Photonic and Biomedical Applications of the Two-Photon Polymerization Technique, Stereolithography Materials, Processes and Applications, 257-299, Springer, New York (2011).
[3] Y. Li et al, Uniform suspended nanorods fabricated by bididirectional scanning via two-photon photopolymerization, Nanotechnology **19** 375304 (2008).

# PEEL BEHAVIOUR OF HOT MELT PRESSURE SENSITIVE ADHESIVES

Nijolė Buškuvienė, Vaidas Bivainis, Indrė Danisevičienė

Department of Manufacturing Engineering, Kaunas University of Technology, Kaunas, Lithuania
nijole.buskuviene@ktu.lt

Hot melt pressure sensitive adhesives (HMPSA) are 100% solid thermoplastic materials. They do not contain any volatile organic compounds. Therefore, they are safe during production, transportation, storage, and application. Most importantly, they are environmentally friendly and are not harmful to human health. Because of the fast set feature, HMPSA are used for high speed production lines. The application is various - such as packaging, tapes, labels, wood-working, hygiene, automobile, medical, electronic, construction, etc. [1]

Generally, HMPSAs are composed from high molecular weight thermoplastic, tackifier, mineral oil, antioxidant, and other special additives – such as filler, colorant, and low molecular weight polymer if needed [2]. Most of these ingredients are thermoplastic materials and require a heated environment to mix them together. While offering aggressive bonds at room temperature HMPSAs most unique and defining feature is that it is capable of cold flow under a light finger pressure. These adhesives require no activation by water, solvent or heat in order to exert a strong adhesive holding force with substrates such as paper, plastic, glass, wood, cement and metal. They have sufficient cohesive holding power and elastic nature so that, despite their aggressive tackiness, they can be handled with fingers and removed from smooth surfaces without leaving a trace. [1-3]

The tack and peel behaviour of three types of HMPSA based on styrene block copolymers were compared and the results discussed in this study.

[1] Verma, A. K., Ajit, S., & Karanki, D. R. (2016). Applications of PSA. In Reliability and Safety Engineering (pp. 393-455). Springer, London.
[2] Zhao, Z., Liu, P., Zhang, C., Liu, W., Ding, Y., Zhang, Y., ... & Tang, T. (2017). Synthesis and structure–property relationships of SIS-g-PB copolymers and their application in hot-melt pressure-sensitive adhesives. RSC Advances, 7(70), 44068-44075.
[3] Sotoodeh Nia, Z., Hohmann, A., Buss, A., Williams, R. C., & Cochran, E. W. (2018). Rheological and physical characterization of pressure sensitive adhesives from bio-derived block copolymers. Journal of Applied Polymer Science, 135(34), 46618.

# SYNTHESIS IN PICKERING EMULSIONS OF BISMUTH-CONTAINING SORBENTS

Korotkith Ekaterina[1], Polyakova Irina[2], Borovikova Ludmila[2], Kipper Albert[2], Pisarev Oleg[1,2]

[1] Department of Medical Physics, Peter the Great Saint-Petersburg Polytechnical University, Russia
[2] Institute of Macromolecular Compounds, Russian Academy of Sciences, Saint-Petersburg, Russia
kkorotkith@mail.ru

The use of nanobiotechnologies for creating sorption materials for the treatment of wound infections is aimed at overcoming the antibiotic resistance of microorganisms. In this connection, sorption materials, contained an agent endowed with their own antibacterial activity, are in demand [1]. Bismuth (Bi) and its compounds are the most promising antibacterial agents. Moreover, Bi belongs to the "green" elements and widely used in medicine [2]. By introducing Bi nanoparticles (Bi-NPs) in the sorbent matrices and exploiting its specific properties, it is possible to achieve the necessary therapeutic effects of new composite sorbent materials.

In order to preserve the functionality of lipophilic Bi-NPs, previously a method for their synthesis in the medium of the β-cyclodextrin with polyvinylpyrrolidone (β-CD-PVP) stabilizing system in the process of redox reaction of bismuth nitrate with sodium borohydride was developed. β-CD was chosen as a stabilizer since its presence in the sorbent matrix will allow to improve the sorption efficiency due to β-CD is able to form inclusive "guest-host" complexes with biologically active substances [3].

Using UV- and visible spectroscopy and dynamic light scattering, it was shown the formation of Bi-β-CD-PVP ternary complexes. By varying the concentration ratio of β-CD / PVP (wt% / wt%), the optimal conditions for the formation of the most stable complexes were determined at β-CD / PVP = 10 / 90 and 90 / 10 . Depending on the β-CD / PVP, the stabilization on Bi-NPs occurred by different mechanisms. The steric stabilization with the distribution of PVP molecules on the surface of nanoparticles was occurred at β-CD / PVP = 10 / 90; the inclusion of nanoparticles in the hydrophobic cavities of oligosaccharide molecules was occurred at β-CD / PVP = 90 / 10 (Fig. 1).



a) b)

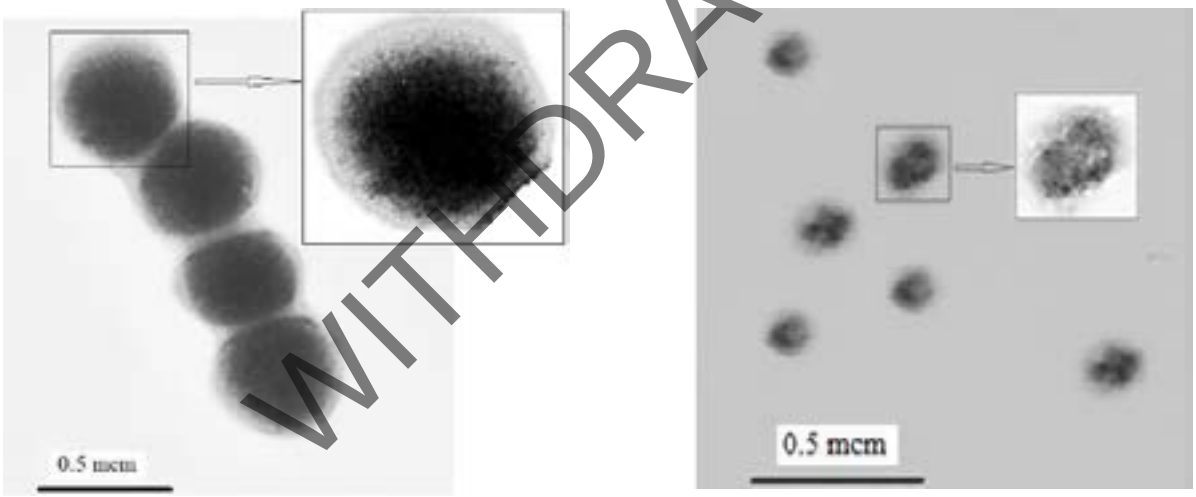


Fig. 1. The Bi-β-CD-PVP complexes synthesized at β-CD / PVP = 10 / 90 (a) and at β-CD / PVP = 10 / 90 90 /1 0 wt% / wt%.

For the synthesis of hybrid organic-inorganic sorbents, a method of radical copolymerization in Pickering emulsions of such monomers as methacrylic acid, hydroxyethyl methacrylate, ethylene glycol dimethacrylate was developed. Both simple (oil / water) and complex (oil / water / oil) Pickering emulsions were formed directly in colloidal solution of the Bi-β-CD-PVP complexes. The radical copolymerization of monomers proceeded in aqueous medium in which stabilization of the emulsion phases was carried out with an excess of the Bi-β-CD-PVP complexes. At the same time, the complexes were covalently attached in the polymer matrix. IR spectroscopy showed the presence of β-CD ligand and X-ray analysis showed the presence of Bi and bismuth oxide in the hybrid matrices.

This work was supported by the Russian Foundation for Basic Research (project code No. 18-03-00835).

[1] R. Jayakumar, M. Prabaharan, S. Kumar et al., Biomaterials based on chitin and chitosan in wound dressing applications, Biotechnology Advances **29**, 322–337 (2011).
[2] T. Kotani, D. Nagai, K. Asahi et al., Antibacterial properties of some cyclic organobismuth (III) compounds, Antimicrobial Agents Chemotherapy **49**, 2729-2734 (2005).
[3] T. Sikdera, M. Rahmand, Jakariya et al., Remediation of water pollution with native cyclodextrins and modified cyclodextrins: A comparative overview and perspectives, Journal of Chemical Engineering **335**, 920–941 (2019).

# EXCITATION OF BLOCH SURFACE WAVES IN PERIODIC STRUCTURES USING SPECTROSCOPIC ELLIPSOMETRY

Ernesta Buzavaite-Verteliene[1], Tomas Tolenis[2], Audrius Valavicius[2], Marija Narkauskaite[1], Zigmas Balevicius[1]

[1] Department of Material Science and Electrical Engineering, Center for Physical Sciences and Technology, Lithuania
[2] Department of Laser Technologies, Center for Physical Sciences and Technology, Lithuania
ernesta.verteliene@ftmc.lt

Electromagnetic surface waves have been used for various optical sensing such as protein interaction determination [1] or gas adsorption [2]. Depending on a structure of a sample, different surface waves can be generated. At a metal dielectric boundary a surface plasmon-polariton (SPP) wave can appear while a Bloch surface wave (BSW) can be generated on a periodic dielectric structure with semi-infinite dielectric media.

Bloch surface waves are confined on the photonic crystal surface and surrounding material interface [3]. Due to low losses in the dielectrics the BSW can propagate long distances. Another advantage of BSW is that it can be excited in both TE and TM polarization modes, thus it allows us to investigate changes of polarization states if measuring technique allows us to do so. To determine these polarization states and phase changes, we use spectroscopic ellipsometry measuring technique. In order to excite BSW a glass prism as a coupler to achieve conditions of total internal reflection (TIR) is commonly used. Ellipsometer configuration with prism coupler shown in Fig. 1 is called total internal reflection ellipsometry (TIRE). High sensitivity to changes of the polarization in TIRE method allows us to analyze small alterations in structure of a sample. Thus, depending on materials used and their periodicity, BSW shift can be measured. It is important to highlight that due to low energy losses in dielectrics, BSW has a narrow half-width dip in amplitude ($\Psi$ ellipsometric parameter) and in some cases even almost disappear, meanwhile changes in ellipsometric parameter $\Delta$ are always presented due to interference effect of the BSW. The sensitivity features of ellipsometric parameter $\Delta$ for angles larger than the critical angle is the main advantage of TIRE method over the standard ellipsometry and intensity measurements.

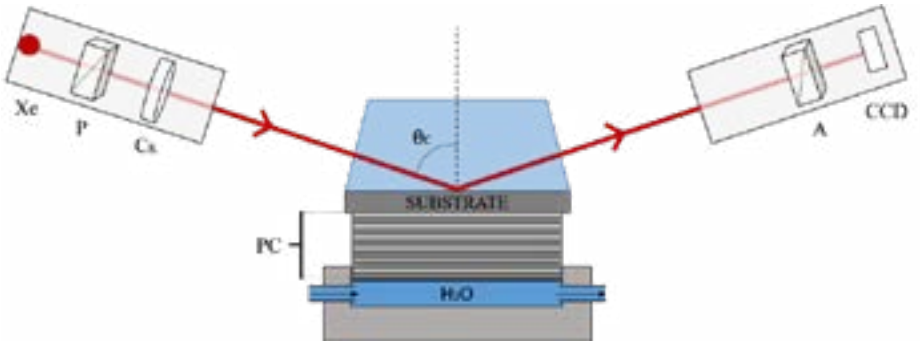


Fig. 1. TIRE schematic used for BSW generating. Components of ellipsometer: LS – light source, P – polarizer, CR – rotating compensator, A – analyzer, CCD detector.

In this study TIRE were carried out on a one dimensional photonic crystal (1D PC) in order to analyze optical response of such structures. PC was made of 6 pairs of periodic layers of $TiO_2$ (~60 nm) and $SiO_2$ (~110 nm) was used as a sample. For TIRE configuration a 70° prism and J. A. Woolam M-2000X ellipsometer were used. TIRE measurements were conducted cuvette filled with liquids with different refractive index dispersion in order to analyze the sensitivity properties of BSW.

[1] I. Baleviciute, Z. Balevicius, A. Makaraviciute et. al., Study of antibody/antigen binding kinetics by total internal reflection ellipsometry, *Biosensors and Bioelectronics* **39**, 170-176 (2013).
[2] A. Paulauskas, S. Tumenas, A. Selskis et al., Hybrid Tamm-surface plasmon polaritons mode for detection of mercury adsorption on 1D photonic crystal/gold nanostructures by total internal reflection ellipsometry, *Optics Express* **26**, 30400-30408 (2018).
[3] P. Yeh, A. Yariv, and C.-S. Hong, Electromagnetic propagation in periodic stratified media I General theory*, *Journal of the Optical Society of America* **67**, 423-438 (1977).

# DIELECTRIC PROPERTIES OF LEAD-FREE $BaTiO_3$-$Bi(Mg_{1/2}Ti_{1/2})O_3$-$BiFeO_3$ CERAMICS

Paulius Časas[1], Sergejus Balčiūnas[1], Jūras Banys[1], Satoshi Wada[2]

[1] Faculty of Physics, Vilnius University, Sauletekio 9/3, LT10222 Vilnius, Lithuania.
[2] Interdisciplinary Graduate School of Medical and Engineering, University of Yamanashi, Kofu, Yamanashi 400-8510, Japan
paulius.casas@ff.stud.vu.lt

In 2006 RoHS directive was accepted in European Union. It declared the need to diminish the use of lead-containing materials in electronic components due to harmful effects on health and environment. Therefore, the need to search for new lead-free compounds appeared. Options for such materials can be $BaTiO_3$ (BT) or Bi based perovskites such as $Bi(Mg_{1/2}Ti_{1/2})O_3$ (BMT), $BiScO_3$ and $BiFeO_3$ (BF). These compounds have high Curie temperature and simple $ABO_3$ perovskite structure. [1] Based on the requirements of RoHS and the mentioned properties of these materials measurements of dielectric properties of lead-free $BaTiO_3$-$Bi(Mg_{1/2}Ti_{1/2})O_3$-$BiFeO_3$ ceramic were carried out. .

BT BMT BF samples were polished down. Then contacts were applied with silver pasta on both surfaces. Later samples were calcined at 300K-573K temperature range on heating at 2 K/min rate. Dielectric measurements were made in 130-500K temperature range and 20 Hz – 1 GHz frequency range on cooling at 1 K/min rate. Measurements from 20 Hz to 1 MHz were made with LCR meter HP-4284A. With this device capacity and loss tangent were measured. From 10 MHz to 1 GHz measurements were made using vector analyzer Agilent 8714ET in coaxial line. Ferroelectric properties were measured using analyzer AixaCCt TF 2000.

Fig 1 shows polarization and current dependence of electric field. Graph on the left shows measured hysteresis loops, which explain that compound is ferroelectric. On the right graph watching two peaks of current. The wider may be related to the polarization switch. The other can be related to back switching, which can be explain by bismuth ferrite or bismuth magnesium titanate defects. Domain wall can hook up to defect and in material appears stress, which turns domain wall in previous position.

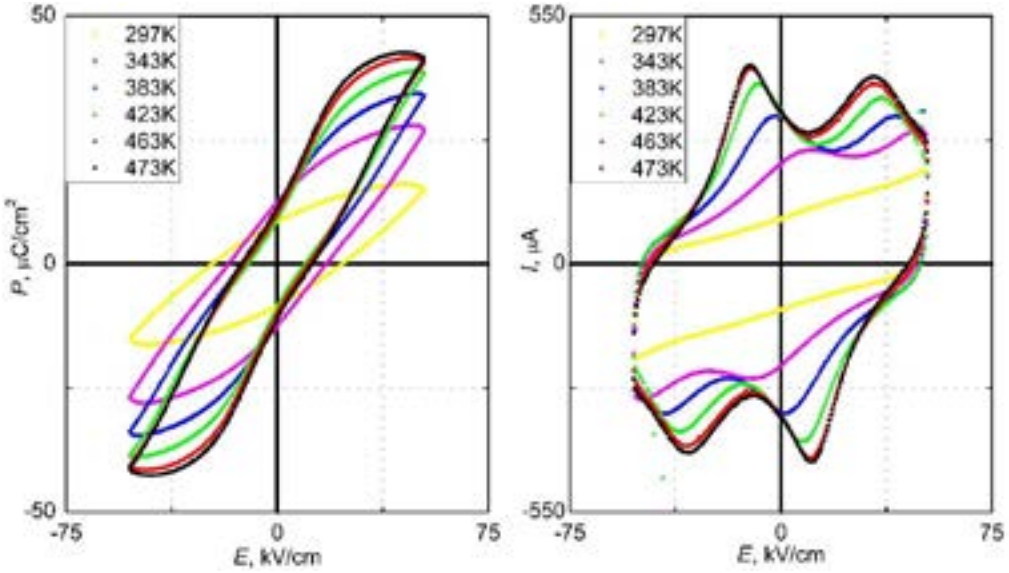


Fig 1. Polarization and current dependence of electric field

[1] H. Yabuta *et al.*, "Microstructure of BaTiO3–Bi(Mg1/2Ti1/2)O3–BiFeO3 Piezoelectric Ceramics," *Jpn. J. Appl. Phys.*, vol. 51, no. 9S1, p. 09LD04, Sep. 2012.

# MULTISTANDARD POWER-LINE COMMUNICATION MODULE PROTOTYPE CREATION FOR SMART LIGHTING APPLICATIONS

Vladislovas Čižas, Pranciškus Vitta

[1] Institute of Photonics and Nanotechnology, Vilnius University, Lithuania
vladislovas.cizas@gmail.com

In today's modern technology era, all developed countries understand the importance of nature preservation and undoubted technological achievement contribution to this process. One of the most obvious solutions to improve ecological situation is to try to reduce electrical energy consumption. Luckily, advances in control systems give huge possibilities to optimize electrical devices, thus reducing electricity consumption without refusing any conveniences, provided by these devices.

Nowadays, PLC (power-line communication) technology is being "reinvented" and becoming more and more popular for different solutions as safe and low noise-dependent technology, which can transfer small data packages using existing power line cables. Despite many advantages, PLC, being unpopular for a long time, wasn't properly standardized. As a result, several alliances were created and each of them developed their own PLC standard, which of course is unique and not supported by other standards. Therefore, there is a demand for cheap and simple solution to act as an intermediary for different standard-based PLC systems.

During this study, we tried to develop a concept for such device. According to our previous PLC standard analysis, we managed to create a simple phase modulation based hardware concept, which theoretically can manage connection between different standard PLC systems or act as an independent system. The concept was tested by Multisim simulation and circuit design software and after being confirmed, two prototypes were created. It is strongly believed that created prototypes would be able to solve existing Smart City PLC communication problems and create possibilities to add new features.

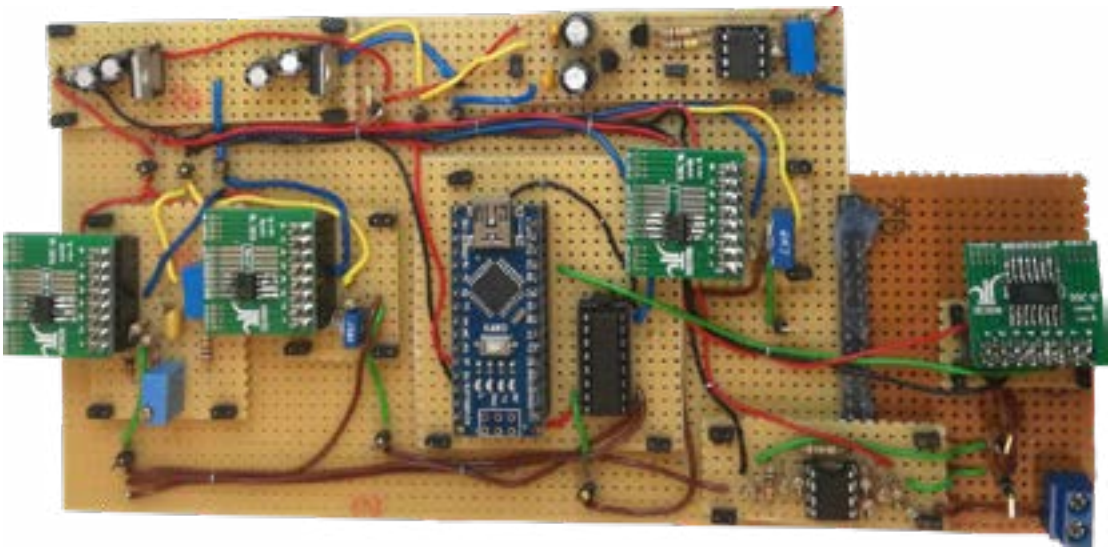

Fig. 1. Created PLC module prototype.

[1] H.C. Ferreira et al., Power Line Communications: Theory and Applications for Narrowband and Broadband Communications over Power Lines, Wiley & Sons, 528 (2010).

[2] K. Sharma, L. Saini, Power-Line Communication for Smart Grid: Progress, Challenges, Opportunities and Status, Renewable and Sustainable Energy Reviews **67**, 704-751 (2017).

# STATISTICAL LOS/NLOS CHANNEL MODEL FOR SIMULATIONS OF NEXT GENERATION 3GPP NETWORKS

Rimvydas Aleksiejunas[1], Albert Cesiul[1], Kestutis Svirskas[1]

[1] Institute of Applied Electrodynamics and Telecommunications, Vilnius University, Lithuania
albert.cesiul@ff.vu.lt

Line-of-sight or non-line-of-sight (LOS/NLOS) visibility conditions are required for radio wave propagation modeling to properly select empirical path loss model. For Monte Carlo statistical simulations a random generator of visibility states should be design according to a given spatial probability density. The methods of LOS state simulation are essential part in system level simulators such as SEAMCAT software tool [1] used by spectrum regulators. Statistical LOS probability function over distance can be derived from measurements and simulations using digital building height data. Various LOS probability approximations have been used to date, including ITU [2] and 3GPP [3] models. Such models apply the same LOS probability dependence on distance for a whole area of analysis. However, real urban territories represent city blocks with different building density and heights. Thus, taking into account inhomogeneity of propagation environment would increase accuracy of LOS probability approximations. In the paper, a dual environment LOS probability model is proposed which approximates probability by splitting all area into two environments depending on the building heights: one which allows LOS propagation with higher probability and another environment – represented by lower LOS probability.

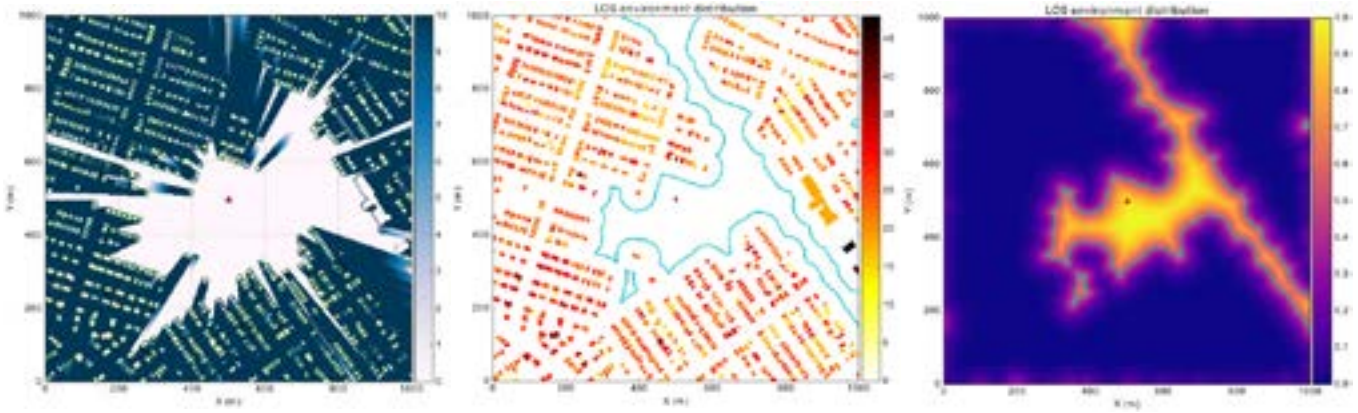

Fig. 1 Dual LOS environment separation for Manhattan city digital building model. The three images represent area with open circular region mentioned in the text as case 1. The right image represents line-of-sight visibility for each case, the numerical values express height in meters below visibility line, visible areas shown in white. The middle image represents building heights in meters and boundary zones around buildings lower than 3 m with buffer zone of 40 m. The left image shows us the continuous distribution function for the two LOS environments.

Three typical LOS conditions for different Manhattan city locations are illustrated in the Figure 1. Each set of images includes line-of-sight visibility around base station, building heights with buffer zones around them and the continuous distribution function (1) separating two LOS environments on each side of the buffer line

$$f(x) = 1 - \frac{1}{2}\left[1 - erf\left(\frac{h(x) - \mu_h}{\sqrt{2}\sigma_h}\right)\right] \tag{1}$$

A statistical line-of-sight visibility state model is proposed involving dual environments characterized by different obstacle heights. The method allows to combine two probability functions similar to those used by ITU and 3GPP models. This improves approximation accuracy with respect to deterministic LOS estimation using digital building model. From the comparison of 3GPP and dual environment model approximations applied to Manhattan city building data it is evident that dual environment model is more accurate for areas enclosing LOS visibility areas around base station. Advantages of dual environment LOS model is especially obvious for base station locations at the boundary of LOS and NLOS regions when antenna is placed on the rooftop of the buildings at the edge of city blocks. The only disadvantage of the proposed LOS model is increased complexity when at least two LOS probabilities are combined thus increasing the number of pLOS(d) coefficients. Dual environment approximation could be applied to other types of known LOS probability functions and more tests against diverse urban and suburban environments would enable reaching more quantitative results.

[1] "SEAMCAT – Spectrum Engineering Advanced Monte Carlo Analysis Tool". Available: http://www.seamcat.org/, accessed: 2017-05-19.
[2] ITU, "Guidelines for evaluation of radio interface technologies for IMT-Advanced", Report ITU, vol. M.2135, no. 1, p. 72, 2009.
[3] 3GPP TR 36.814, "Evolved Universal Terrestrial Radio Access (E-UTRA); Further advancements for E-UTRA physical layer aspects", 3GPP, Tech. Rep. Version 9.2.0, 2017. [Online]. Available: http://www.3gpp.org/dynareport/36814.htm.

# WHY DO WE NEED SHOTTKY DIODES BASED ON SILICON CARBIDE?

Adrianna Chamryga[1,2], Tymoteusz Ciuk[1], Wawrzyniec Kaszub[1], Kinga Kościewicz[1], Paweł Piotr Michałowski[1], Artur Dobrowolski[1,3], Jakub Jagiełło[1,3], Paweł Ciepielewski[1], Dominika Teklińska[1], Małgorzata Możdżonek[1], Paweł Kamiński[1]

[1]Institute of Electronic Materials Technology, Wólczynska 133, Warsaw, 01-919, Poland
[2]Faculty of Physics, Warsaw University of Technology, Koszykowa 75, Warsaw, 00-662, Poland
[3]Faculty of Physics, University of Warsaw, Pasteura 5, Warsaw, 02-093, Poland

adrianna.chamryga@itme.edu.pl

Electronic market is nowadays one of the fastest-growing branches of industry. No less than 30% of generated electricity is currently converted from AC to DC by a semiconductor power devices. With great probability, this number should rise up to 80% by the end of year 2030. In this light, looking for a new energy and cost efficient devices seems to be not only challenging, but also desired.

An interesting candidate for building high power and high frequency devices is silicon carbide [1]. However, quality of the samples is crucial for potential applications of this compound [2, 3]. Although, epitaxial SiC is widely used, there is still room for improvement, especially when it comes to reducing defects in epi-layers structures. Therefore, we would like to present the results of our work on unintentionally-doped and low-doped n-type ($N_2$) epi-layers.

The epitaxial growth is conducted at temperatures exceeding 1550-1600˚C and rates of 5-10 μm/h on up to 4-in 4H-SiC(0001) wafers in an R&D Aixtron VP508 and production type reactor Aixtron G5 WW.

The samples are tested by various method. Nitrogen concentration is monitored with SIMS (Secondary Ion Mass Spectroscopy) and low-temperature Raman spectroscopy. Charge carrier concentration is investigated with room-temperature Raman spectroscopy. SEM (Scanning Electron Microscopy), AFM (Atomic Force Microscopy), defect etching and photo-assisted DLTS (Deep Level Transient Spectroscopy) gives information about surface and crystal quality.

The last step planned is to build Shottky diodes for 1,9 and 3,3kV using homoepitaxial SiC layers.

[1] W. Strupinski, K. Kościewicz, J. Weyher, A. Olszyna, Effect of Substrates Thermal Etching on CVD Growth of Epitaxial Silicon Carbide Layers, Mater. Sci. Forum Vols. 600-603 (2009) pp 155-158

[2] K. Kościewicz, W. Strupiński, D. Teklińska, K. Mazur, A. Olszyna, Epitaxial growth on 4H-SiC on-axis, 0.5°, 1.25°, 2°, 4°, 8° off-axis substrates – defects analysis and reduction, Mater. Sci. Forum 679-680 (2011) 95-98.

[3] K. Kościewicz, R. Bożek, W. Strupiński, A. Olszyna, Microscopic investigation of SiC epitaxial layers on on-axis 4H-SiC substrates using Kelvin Probe Force Microscopy, Acta Physica Polonica A, Vol. 116 (2009), 69-71

# INVESTIGATION OF DIMETHILDIHYDROPYRENES PHOTOPHYSICAL PROPERTIES

Ignas Čiplys[1], Irena Kulszewicz-Bajer[2], Renata Karpicz[1]

[1]Center for Physical Science and Technology, Lithuania
[2]Warsaw University of Technology, Poland
*Ignas.Ciplys@gmail.com*

Dimethildihydropyrenes (DHP, closed ring form) are one of the most popular photochromic compounds that could be reversibly converted into cyclophanediene (CPD, opened ring form) when exposed to visible light. This kind of photochemical reaction leads to changes in physical properties such as absorption and fluorescence of DHP (Fig. 1). DHP substances could be applied in wide range of areas such as organic electronics, for example single molecule memory elements, and biology – diagnostics, control of metabolic reactions. To achieve even more suitable physical properties for different applications, DHP molecules could be modified by adding substitutes. However, the most common problem of these modified compounds is stability. To solve this problem, there is a need of deeper understanding of processes appearing during photochemical reactions [1].

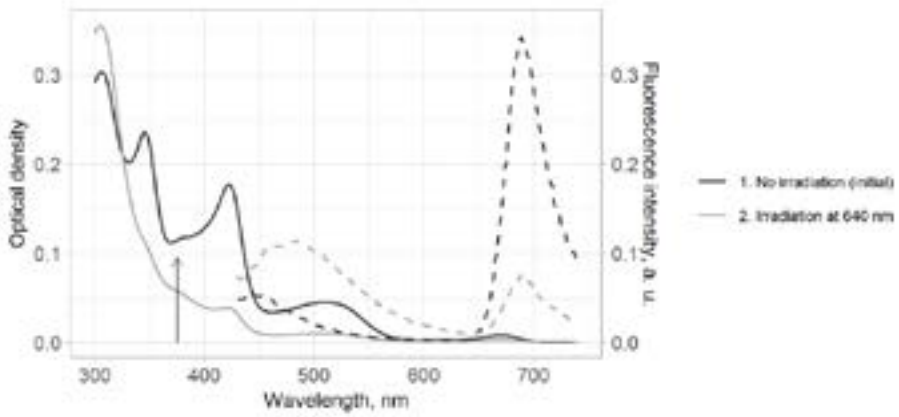


Fig. 1. Dimethildihydropyrenes (in toluene) absorption (continiuos line) and fluorescence (dashed line) spectra before and after exposition to red light (640 nm). Arrow indicates absorption band which was used for excitation (375 nm).

In our study, two derivatives of DHP were synthesized and its physical properties were measured. Several methods such as stationary absorption, transient absorption, fluorescence and fluorescence life time spectrometry techniques were used in sequential way for both DHP and CPD states. Control of photochromic form conversion were performed using additional UV (340 nm) and red light (640 nm) exposition. We found out, that the ring opening could be detected by measuring fluorescence life time (the fluorescence life time of DHP and CPD are respectively >3 ns and 0.2 ns). In addition, transient absorption measurements data gave supplement information about changes in DHP during photochemical reactions.

[1] Bohne, Cornelia, and Reginald H. Mitchell. "Characterization of the photochromism of dihydropyrenes with photophysical techniques." *Journal of Photochemistry and Photobiology C: Photochemistry Reviews* 12.2 (2011): 126-137.

# LUMINESCENCE OF $K_2(Cs/Rb)Y(VO_4)_2:Eu^{3+}$ PHOSPHORS WITH TRIGONAL CRYSTAL STRUCTURE

Egle Ezerskyte, Arturas Katelnikovas

Faculty of Chemistry and Geosciences, Vilnius University, Naugarduko 24, LT-03225 Vilnius, Lithuania
eglezerskyte@gmail.com

The purpose of this research was to synthesize new and efficient red light emitting phosphors which possess narrow emission spectrum assuming these luminofors could be used in the production of white LEDs. Therefore, phosphors containing $Eu^{3+}$ ions are ideal candidates in fulfilling this task due to the fact that their emission spectra consists of few narrow emission lines at approximately 610 nm (see Fig. 1. (b) and (d)). Thus, we decided to investigate the little studied $K_2(Cs/Rb)Y(VO_4)_2:Eu^{3+}$ phosphors assuming that by changing their chemical composition the emission of $Eu^{3+}$ ions will be easily manipulated.

Samples of $K_2RbY(VO_4)_2:Eu^{3+}$ and $K_2CsY(VO_4)_2:Eu^{3+}$ with trigonal (P-3m1, #164) structure were synthesized via conventional high temperature solid-state reaction. The stoichiometric amounts of precursors ($Y_2O_3$, $Eu_2O_3$, $K_2CO_3$, $NH_4VO_3$, $Rb_2CO_3$, $Cs_2CO_3$) were blended in the agate mortar employing acetone as the grinding media. The obtained powders were transferred to the porcelain crucibles and annealed at 800 °C for 10 h in air [1].

The investigation of structural, morphological and optical properties of the synthesized phosphors was carried out by powder X-ray diffraction (XRD), scanning electron microscope (SEM) analysis, Fourier-transform infrared (FTIR) spectroscopy and UV-Visible spectroscopy.

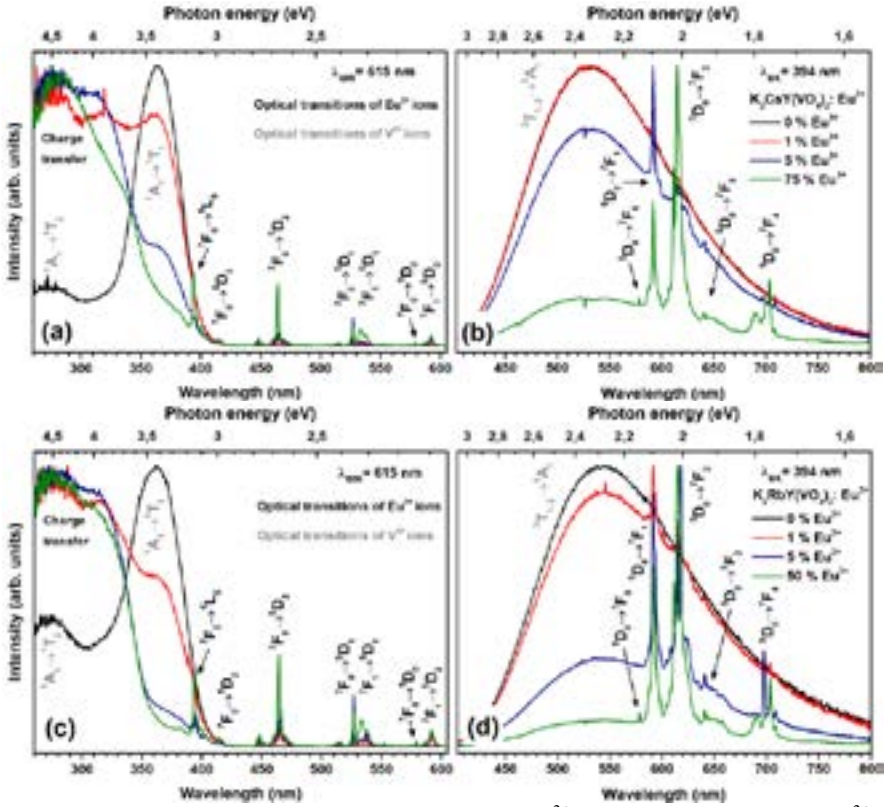


Fig. 1. Excitation (a) and emission (b) spectra of $K_2CsY(VO_4)_2:Eu^{3+}$ samples with different $Eu^{3+}$ concentrations; excitation (c) and emission (d) spectra of $K_2RbY(VO_4)_2:Eu^{3+}$ samples with different $Eu^{3+}$ concentrations.

XRD patterns, SEM images and FTIR spectra confirming crystal structure, showing the distribution of crystallites and revealing impurities of samples will be discussed in this work. Moreover, reflection spectra, excitation spectra ($\lambda_{em}$ = 615 nm), emission spectra ($\lambda_{ex}$ = 330, 394, 464.5 nm), temperature dependent emission spectra in 77 – 100 K temperature interval, decay curves, photoluminescence lifetime values, external quantum efficiencies, colour coordinates of $K_2RbY(VO_4)_2:Eu^{3+}$ and $K_2CsY(VO_4)_2:Eu^{3+}$ phosphors will be discussed.

**Acknowledgements:** This research was funded by the European Social Fund under the No 09.3.3.-LMT-K-712-09-0159 "Development of Competences of Scientists, other Researchers and Students through Practical Research Activities" measure.

[1] David, A.D.J., G.S. Muhammad, and V. Sivakumar, *Synthesis and optical properties of $Eu^{3+}$-substituted glaserite-type orthovanadates $CsK_2Y[VO_4]_2$.* Luminescence, 2017. **32**(5): p. 735-744.

# DIELECTRIC INVESTIGATIONS OF THE $BIFE_{1-x}CR_xO_3$ CERAMICS

Vaiva Gribauskaitė[1], Edita Palaimienė[1], Jūras Banys[1], Anatoli V. Pushkarev[2], Yury V. Radyush[2], Nikolai M. Olekhnovich[2]

[1] Institute of Applied Electrodynamics and Telecommunications, Vilnius University, Sauletekio 3, LT- 10257 Vilnius, Lithuania

[2] Scientific-Practical Materials Research Centre of NAS of Belarus, P. Brovka str. 19, 22072 Minsk, Belarus

vaiva.gribauskaite@ff.stud.vu.lt

Multiferroic materials attract scientific interest because they exhibit ferroelectric and magnetic ordering in a single phase. Bismuth ferrite, $BiFeO_3$ (BFO), shows ferroelectric (FE) and ferromagnetic (FM) ordering above room temperature [1]. In order to extend studies and investigate multiferroic materials BFO is doped with various elements (La, Nd, Sm, Gd and Cr). The following work is aimed to investigate the dielectric properties of chromium substituted bismuth ferrite ceramic ($BiFe_{1-x}Cr_xO_3$) by the impedance spectroscopy.

The electrical conductivity $\sigma^*$ is calculated using equation $\sigma^* = i\varepsilon^*\varepsilon_0\omega$. Fig 1(a) shows the frequency dependence of conductivity at different temperatures for the $BiFe_{1-x}Cr_xO_3$ ceramics (x = 0.5). The conductivity follows the Almond-West law [2] from which it is possible to determine DC conductivity. With decreasing Cr content the DC conductivity can be determined at lower temperatures in our measurements frequency range. For example, DC conductivity can be determined at 200 K for x = 0.5 and at 250 K for x = 0.85. From the $\sigma_{DC}$ values obtained at different temperatures the activation energy ($E_A$) was calculated using the Arrhenius law $\sigma_{DC} = \sigma_0 \exp(-E_A/kT)$ (Fig. 1(b)). Obtained values are $E_A = 0.29 \pm 0.01$ eV (for x = 0.5), $E_A = 0.33 \pm 0.01$ eV and $E_A = 0.27 \pm 0.01$ eV (for x = 0.85). Sudden change of activation energy for x = 0.85 at 385 K is attributed to the phase transitions that occur near room temperature for the compositional range of $0.6 < x \leq 0.9$ [3].

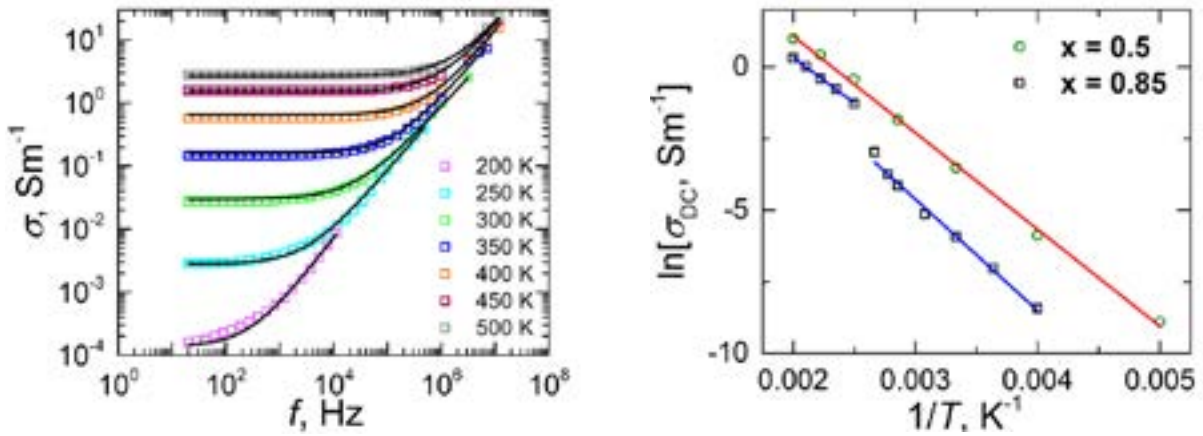


**a)** **b)**

Fig. 1. (a) Frequency dependencies of DC conductivity at different temperatures for $BiFe_{0.5}Cr_{0.5}O_3$ ceramics. (b) The 1/T dependence for $BiFe_{1-x}Cr_xO_3$ ceramics.

[1] H. Shima, H. Naganuma, S. Okamura. Optical Properties of Multiferroic $BiFeO_3$ Films. Materials Science: Advanced Topics. DOI: 10.5772 / 54908 (2012).

[2] M. R. Panda. Investigations on Structural and Electrical Properties of $Li_2NiSiO_4$. International Journal of ChemTech Research v. 6, p. 1962-1964 (2014).

[3] I. P. Raevski, S. P. Kubrin, A. V. Pushkarev, N. M. Olekhnovich, Y. V. Radyush, V. V. Titov, M. A. Malitskaya, S. I. Raevskaya, H. Chen. The effect of Cr substitution for Fe on the structure and magnetic properties of $BiFeO_3$ multiferroic. Ferroelectrics v. 525, p 1-10 (2018).

# RARE-EARTH IONS DOPED PHOSPHORS FOR SECURITY PIGMENTS APPLICATIONS

Julija Grigorjevaite[1], Arturas Katelnikovas[1]

[1] Institute of Chemistry, Faculty of Chemistry and Geosciences, Vilnius University, Naugarduko 24, LT-03225 Vilnius, Lithuania

julija.grigorjevaite@chf.vu.lt

One of the most serious worldwide problems is counterfeiting. The forgery of currency, goods or important documents is a huge problem for everyone, including government bodies and big companies. The modern achievements in science and technology create new ways to overcome this serious problem [1]. One of many techniques is security printing.

Luminescence materials emitting in the visible range upon ultraviolet light excitation are used for security printing, holograms, luminescence markers and security labels. All of anti-counterfeiting techniques have advantages and limitations. From this point of view, luminescent materials improved security pigments industry due to their unique optical properties. Usually lanthanides-rich materials are used as luminescent pigments in the security printing. Among them, europium ions doped phosphors have received the great attention, because of strong visible light emission.

In this work, $Rb_2Bi(PO_4)(MoO_4):Eu^{3+}$ and $K_2Bi(PO_4)(MoO_4):Sm^{3+}$ were investigated as the potential phosphors for luminescent security pigments. These materials showed good color saturation, high luminous efficacies, and good quantum efficiencies.

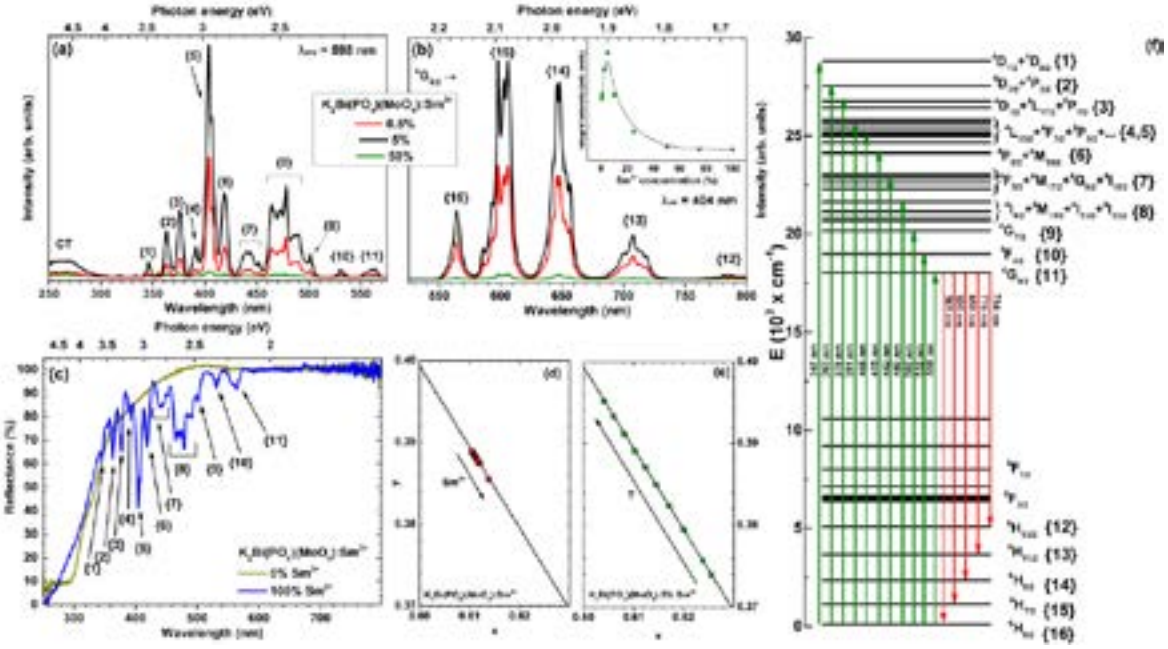

Fig. 1. (a) Excitation ($\lambda_{em}$ = 598 nm) and (b) emission ($\lambda_{ex}$ = 404 nm) spectra of $K_2Bi(PO_4)(MoO_4):Sm^{3+}$, inset shows emission integral intensity as a function of $Sm^{3+}$ concentration, (c) reflection spectra of $K_2Bi(PO_4)(MoO_4)$ and $K_2Sm(PO_4)(MoO_4)$. Fragments of the CIE 1931 color space diagrams with color points of (d) $K_2Bi(PO_4)(MoO_4):Sm^{3+}$ as a function of $Sm^{3+}$ concentration and as a function of temperature of (e) 5% $Sm^{3+}$ doped sample, (f) intraconfigurational $Sm^{3+}$ f-f transitions.

Rare earth doped materials have received a huge attention for security applications because of characteristic sharp emission lines due to the intraconfigurational f-f transitions (see Fig. 1f). These materials also demonstrate long lifetimes, excellent thermal stability, high quantum yields, etc.

The structural, morphological and optical characteristics of the synthesized compounds were investigated by powder X-ray diffraction (XRD), scanning electron microscopy (SEM) analysis and UV-Visible spectroscopy. The reflection, excitation and emission spectra of the single phase compounds were measured and analyzed. The temperature dependent emission spectra and decay curves in 77 – 500 K temperature interval were also recorded and will be discussed.

Moreover, color points, luminous efficacies (LE) and photoluminescence (PL) lifetime values were also calculated. $Eu^{3+}$ doped samples were red emitting and showed quantum efficiencies close to unity, whereas their $Sm^{3+}$ counterparts possessed ca. 55% efficiency. Differences between synthesized series as a function of $Eu^{3+}$ or $Sm^{3+}$ concentration will be presented and discussed.

[1] P. Kumar, K. Nagpal, B.K. Gupta, ACS Appl Mater Inter, 9 (2017), 14301-14308.

# $GaAs_{1-x}Bi_x$ MQW STRUCTURES AS AN ACTIVE REGION FOR NIR LASERS

Algirdas Jasinskas, Renata Butkutė, Sandra Stanionytė, Bronislovas Čechavičius, Martynas Skapas, Evelina Pozingytė

Center for physical sciences and technology, Saulėtekio al. 3, LT-10257, Vilnius, Lithuania
algirdas.jasinskas@ftmc.lt

The increasing need for efficient light sources emitting at different wavelengths forces engineering of novel compounds and progress in material science. One of the main problems of modern semiconductor lasers – bandgap sensitivity to the temperature deviations, makes such laser systems require additional cooling, reducing their efficiency, compactness and affordability. It was shows previously, that incorporation of 1% of Bi to the GaAs lattice reduces bandgap by up to 88 meV [1]. Moreover, spin-orbit splitting increases at higher Bi fractions, which opens up a possibility to suppress Auger and other non radiative losses [2]. Finally, dilute bismide alloys were shown to have unusually low bandgap temperature dependence compared to widely used III-V compounds [3]. These three properties make GaAsBi and other bismides attractive for various optoelectronics device applications, including lasers [4].

This study focuses on research of GaAsBi alloy as an active region of NIR lasers, emitting at around (1-1.2) μm. The aim of this work is to optimize technological growth conditions of GaAsBi Multiple Quantum Well (MQW) structures in order to achieve high intensity Photoluminescence (PL) signal. The influence of different element ratios, growth rate and temperature, QW and barrier layer thickness, Be dopant concentration to the optical and structural properties was investigated.

GaAsBi MQW structures were grown by molecular beam epitaxy (MBE) on semi-insulating GaAS (100) substrates. High resolution X-Ray Diffraction (HR-XRD) and Transmission Electron Microscopy (TEM) were employed to evaluate crystalline structure and content of bismuth (Fig 1). Atomic Force Microscopy (AFM) was used to determine surface quality, while PL measurements were performed to investigate optical properties (Fig 2).

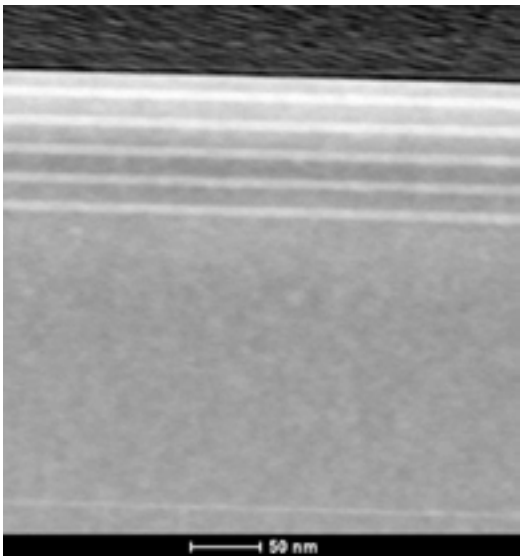


Fig. 1. TEM cross-section of a sample consisting of 5 QWs. Bright stripes correspond to GaAsBi QW layers, while darker zones are GaAs layers.

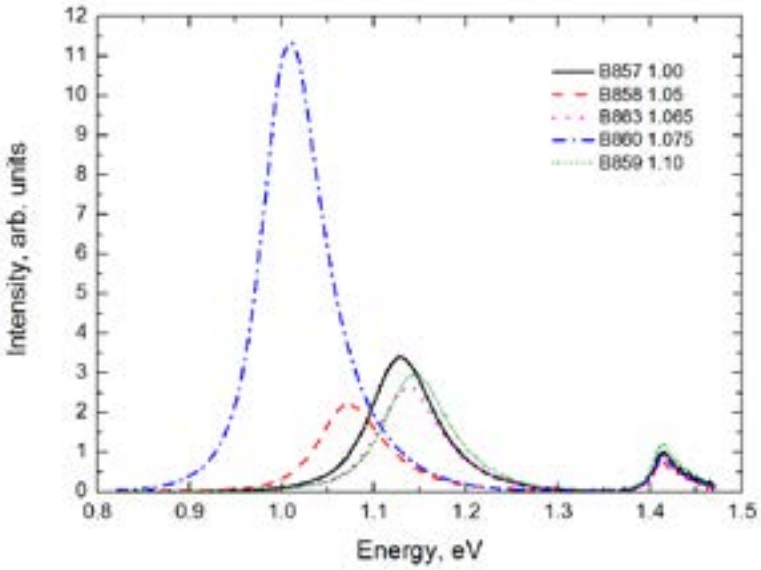


Fig 2. PL spectra of GaAsBi QW structures grown at different As/Ga BEP ratios. Peaks around (1 - 1.15) eV correspond to emission from GaAsBi QWs and 1.42 eV is emission from GaAs substrates.

Acknowledgement: this work was supported by the Research Council of Lithuania (project No. 09.3.3-LMT-K-712-10-0045).

[1] S. Francoeur et al., Band Gap of $GaAs_{1-x}Bi_x$, $0<x<3.6\%$, Appl. Phys. Lett. **82**, 3874 (2003).
[2] B. Fluegel et al., Giant Spin-Orbit Bowing in $GaAs_{1-x}Bi_x$, *Phys. Rev. Lett.* ***97,*** 067205 (2006).
[3] W. M. Linhart and R. Kudrawiec, Temperature dependence of band gaps in dilute bismides Semicond. *Sci. Technol.,* ***33(7),*** 073001 (2018).
[4] L. Wang et al., Novel Dilute Bismide, Epitaxy, Physical Properties and Device Applications, *Crystals* ***7(3),*** *63* (2017).

# DIELECTRIC PROPERTIES OF BT-BT AND BF-BT COMPOSITES

Augustas Karpavičius[1], Sergėjus Balčiūnas[1], Maksim Ivanov[1], Satoshi Wada[2], Jūras Banys[1]

[1] Faculty of Physics, Vilnius University, Sauletekio 9/3, LT10222 Vilnius, Lithuania.
[2] Interdisciplinary Graduate School of Medical and Engineering, University of Yamanashi,Kofu, Yamanashi 400-8510, Japan.
e-mail: augustas98@gmail.com

Concern of environmental welfare lead to search of lead free piezoelectric materials in the last few decades. European Union released Restriction of Hazardous Substances directive which has limited the use of lead in certain fields. For the past 40-50 years, lead base perovskite Pb(ZrxTi1-x)O3 (PZT) piezoelectric ceramics have dominated the commercial market of piezoelectric devices due to their remarkable dielectric and piezoelectric properties and ability to operate in wide temperature range. Replacing PZT solid solutions is a difficult task, due to poor dielectric and piezoelectric properties of its replacement contenders (BT, KNN, BZT, NBT and etc). In our study we investigate dielectric properties of core-shell-like structure of barium tinate (shell) - bismuth ferrite (core) (BT-BF) and barium titanate (shell) - barium titanate (core) (BT-BT), with molar ratios of 1:3.

BT or BF nanoparticles and TiO2 were combined with the ball mill technology, afterwards organic binder poly was added. The mixture was compressed and dried at 600 ˚C ,for BT and 400 ˚C for BF temperature and kept under these conditions for 10 h. Later, disk-shape pellets were submerged into barium hydroxide solution at 175 ˚C temperature for solvothermal solidification. As the result we obtained core-shell like structure with BT or BF as a core and BT, obtained by solvothermal reaction, as a shell.

In this presentation we can see the results of BT-BF temperature dependence of dielectric permittivity. The first thing we notice is the absence of anomalies in BT-BF composite. We can notice the gradual increase of real permittivity with increase of temperature. Overall, we can see that BT – BF exhibited large values of dielectric permittivity. Other, more particular results will be displayed in the poster presentation.

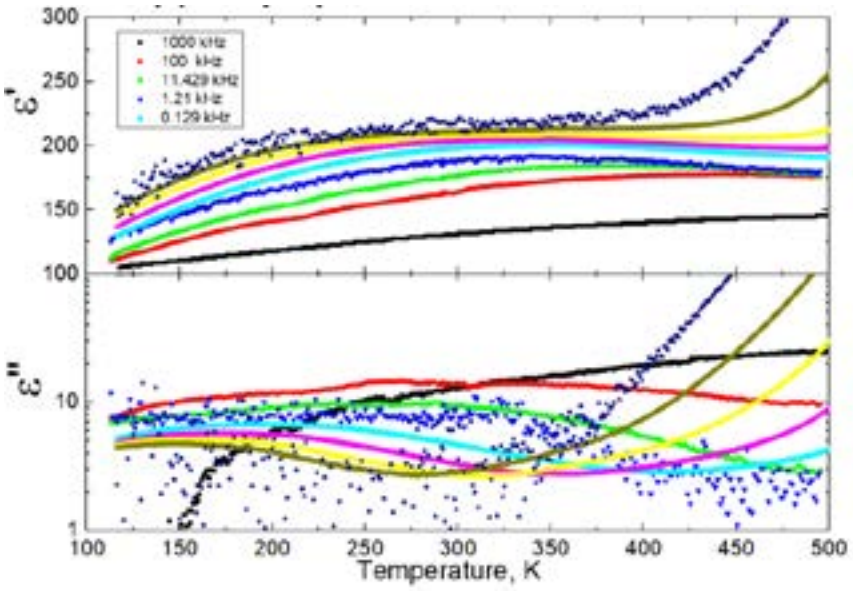


Fig. 1. BT-BF Temperature dependence of real and imaginary part of dielectric permittivity with different frequencies

[1] D. Berlincourt, C. Cmolik, and H. Jaffe, "Piezoelectric properties of polycrystalline lead titanate zirconate compositions," *Proc. IRE*, vol. 48, no. 2, pp. 220–229, 1960.
[2] Y. Qin, S. Zhang, Y. Wu, C. Lu, and J. Zhang, "Impacts of acceptor doping on the piezoelectric properties and domain structure in NBT-based lead-free ceramics," *J. Eur. Ceram. Soc.*, vol. 37, no. 11, pp. 3493–3500, 2017.
[3] S. Wada *et al.*, "Preparation of barium titanate–potassium niobate nanostructured ceramics with artificial morphotropic phase boundary structure by solvothermal method," *Jpn. J. Appl. Phys.*, vol. 50, no. 9S2, p. 09NC08, 2011.
[4] C. Chen, J. Cheng, S. Yu, L. Che, and Z. Meng, "Hydrothermal synthesis of perovskite bismuth ferrite crystallites," *J. Cryst. Growth*, vol. 291, no. 1, pp. 135–139, 2006.

# INVESTIGATION OF THE FREQUENCY-DOMAIN TECHNIQUE FOR RESEARCH OF ORGANIC SOLAR CELLS

Saulė Kemėraitė[1], Pranciškus Vitta[1]

[1] Institute of Photonics and Nanotechnology, Faculty of Physics, Vilnius University, Lithuania

saule.kemeraite@ff.stud.vu.lt

Organic solar cells are a promising type of modern optoelectronic devices with unique possibilities. In particular, lightness, flexibility, semi-transparency and potentially lower cost than silicon based solar cells, makes them competitive in photovoltaic market. However, organic photovoltaics is still a not mature technology with a lot of challenges like short lifespan and low efficiency, which is determined by carrier generation, separation, recombination and other internal physical processes. Investigation techniques for the research of transient characteristics of charge carriers in disordered materials are of high demand for fundamental and applied science. Currently time-resolved research methods are applied most frequently. Notably, Time of Flight (TOF) and Charge Extraction by Linearly Increasing Voltage (CELIV) and number of their variations are the reference techniques for the charge carrier transit time measurements and material investigation. Both of those methods rely on short-pulse photo (electron beam, x-ray etc.) excitation and further observation of the current propagation at constant or linearly increasing bias voltage. Due to the sophisticated structure of disordered materials, the results of investigation strongly depend on measurement conditions and different techniques may provide slightly different results. Therefore, various measurement technique upgrades, modifications and intercombinations are being developed by scientist and material engineers for deeper understanding of undergoing processes.

On the other hand, the principle of Fourier transform states, that time-dependent characteristics can be studied in frequency space and measured characteristics should be the same as in time-domain. Frequency-domain based investigation techniques are widely employed in radioelectronics, photoluminescence decay time and photoconductivity investigation but are not very popular. In this work we present the frequency-domain technique for the research of the transient characteristics of light excited charge carrier in disordered material. The experimental sample of poli(3-hexylthiophene) (P3HT) was made by drop casting method on the glass with fluorine-doped tin oxide (FTO) and silver contacts and zinc-oxide as hole blocking layer. The sample was investigated by frequency-domain technique, which setup and example data are shown in Fig.1. To analyse experimental data a mathematical model was developed, which combines exponential decay of carriers due to recombination and photocurrent in dispersive transport mode (power functions). Mathematical fit was accurate at lower frequencies but not so much at higher ones. The reason is not clear at the moment but probably the Fourier transformation of such a wide frequency (time) range and non-analytical (digital) functions was not accurate enough and can be improved. Nevertheless, the results obtained (e.g. transit times, dispersive coefficient α) were in line with the ones obtained by TOF for the same samples.

In conclusion we want to emphasize, that frequency-domain investigation methods of charge-carrier transient characteristics has a potential to supplement the traditional time-domain techniques, but appropriate methods and mathematical descriptions have to be developed and validated.

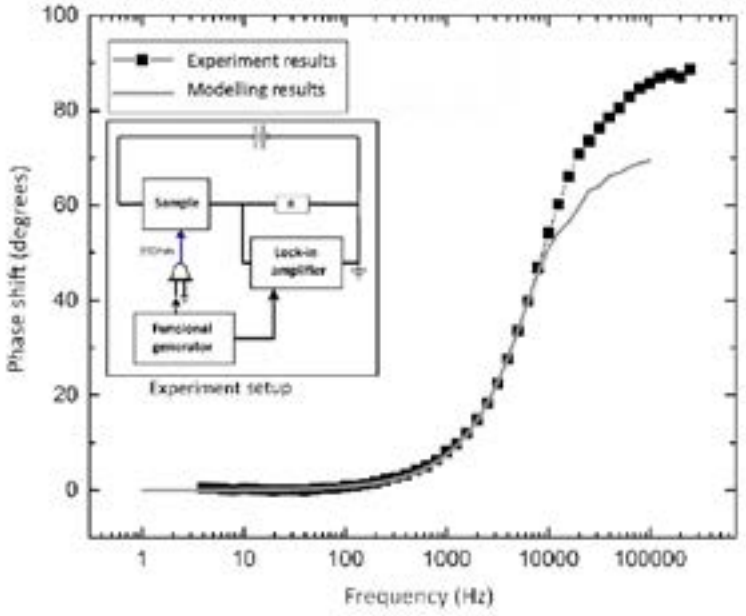


Fig. 1. Experiment results comparison with modelling results and the experiment setup (inset).

# ANALYSIS OF THE CHANGES IN AVERAGE AREA OF SILVER NANOPARTICLES EMBEDED IN DIAMOND-LIKE CARBON THIN FILMS UPON FEMTOSECOND LASER IRRADIATION

Gerda Klimaitė[1], Aušrinė Jurkevičiūtė[2], Tomas Tamulevičius[1,2], Sigitas Tamulevičius[1,2]

[1]Department of Physics, Kaunas University of Technology, Studentų St. 50, LT-51368 Kaunas, Lithuania
[2]Institute of Materials Science, Kaunas University of Technology, K. Baršausko St. 59, LT-51423 Kaunas, Lithuania
gerda.klimaite@ktu.edu

Size distribution of noble metal nanoparticles strongly influences their optical properties [1]. In most of the cases linear dimensions and shape of the nanoparticles is determined by the applied synthesis method and after synthesis it no longer can be varied. However, irradiation with ultrashort laser pulses can be employed to tailor the size distribution of nanoparticles even after their fabrication [2]. In this work we have investigated how the morphology and size distribution of silver (Ag) nanoparticles embedded in diamond-like carbon (DLC) matrix – DLC:Ag nanocomposite thin films – deposited on silicon substrate [3] is altered after irradiation with the interference field of two Yb:KWG femtosecond laser beams (290 fs pulse duration, 2H 515 nm wavelength, 40 kHz repetition rate) [4]. Pristine and laser processed samples were investigated employing scanning electron microscopy (SEM). The size and distribution of silver nanoparticles in thin film was determined from SEM micrographs with "ImageJ" software. Since the micrographs depicts micrometer range periodic patterns in films, further data filtering was applied to extract changes only in the laser affected areas. From the energy dispersive X-ray spectroscopy measurements it was determined that the investigated sample has 7.8 at.% silver content.

From the image analysis of the laser affected samples, average roundness of the nanoparticles was obtained to be 0.72 (perfect roundness is 1), thus in this particular case it was chosen to analyze area but not the diameter of nanoparticles. From the SEM micrographs of unaffected DLC:Ag films it was determined that an average area of nanoparticles was 530 nm$^2$. Upon irradiation with fluence of 6 mJ/cm$^2$ and 27k, 64k, 125k pulses, Ag nanoparticles with an average area of 1484, 854, 802 nm$^2$ were obtained, respectively. From 600 to 1200 nanoparticles were uses in the analysis of the single SEM micrograph. Nanoparticles size distribution histogram in Fig. 1 depicts the particles area size distribution prior and after laser irradiation under different laser processing conditions

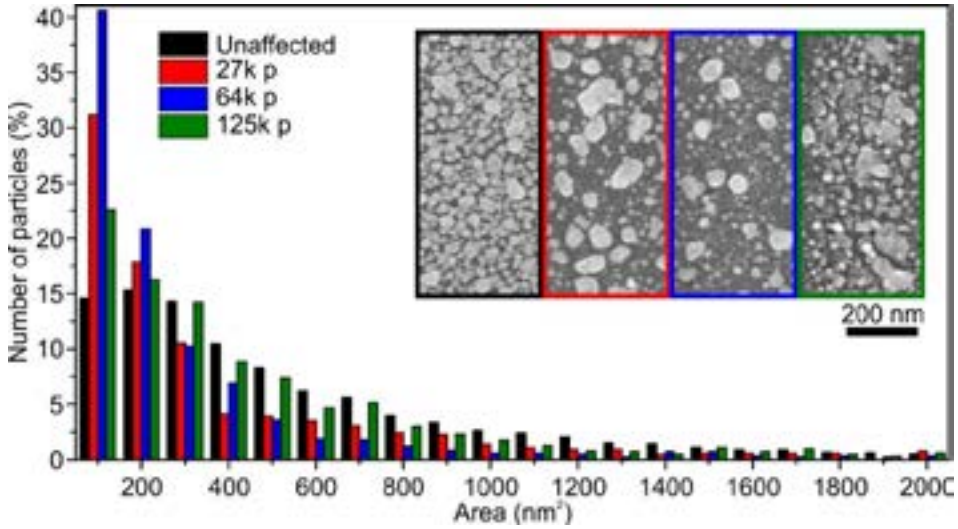


Fig. 1. Size distribution of Ag nanoparticles in DLC:Ag films before (unaffected – black) and after laser irradiation with 6 mJ/cm$^2$ fluence and different number of pulses: 27000 (red), 64000 (blue), 125000 (green). Small fraction of particles larger than 2000 nm$^2$ is not shown. The inset shows parts of SEM micrographs used for analysis.

The image analysis revealed that increasing number of applied laser pulses affects on the average nanoparticle area which tends to decrease and at the same time increases the total number of nanoparticles. The later indicates fragmentation of Ag nanoparticles that results in increasing number of smallest particles after laser irradiation. Acknowledgements: this research was funded by the European Social Fund under the No. 09.3.3-LMT-K-712 "Development of Competences of Scientists, other Researchers and Students through Practical Research Activities" measure, grant No. 09.3.3-LMT-K-712-10-0217.

[1] H. Xu, M. Käll, Modeling the optical response of nanoparticle-based surface plasmon resonance sensors, Sensors and Actuators B **87**, 244-249 (2002).
[2] F. Stietz, Laser manipulation of the size and shape of supported nanoparticles, Applied Physics A: Materials Science and Processing **72**, 381-394 (2001).
[3] S. Tamulevičius, Š. Meškinis, T. Tamulevičius, H.-G. Rubahn, Diamond like carbon nanocomposites with embedded metallic nanoparticles, Reports on Progress in Physics **81**, 024501, 2018.
[4] T. Tamulevičius, M. Juodėnas, T. Klinavičius, et al., Dot-Matrix Hologram Rendering Algorithm and its Validation through Direct Laser Interference Patterning, Scientific Reports **8**, 14245, 2018.

# DIELECTRIC SPECTROSCOPY AND PIEZOELECTRIC PROPERTIES OF LEAD-FREE (1-x)(0.8NBT-0.2BT)-xNN SOLID SOLUTIONS

Tomas Kudrevičius[1], Šarūnas Svirskas[1], Marija Dunce[2], Eriks Birks[2], Jūras Banys[1]

[1]Faculty of Physics, Vilnius University, Sauletekio 9/3, LT10222 Vilnius, Lithuania.
[2]Institute of Solid State Physics, University of Latvia, Kengaraga st. 8, 1063, Riga, Latvia
tomas.kudrevicius@ff.stud.vu.lt

Because of environmental regulations against high amounts of lead used in piezoelectric materials (RoHS directive in EU) there have been made a lot of studies trying to find the best lead-free alternatives. Morphotropic phase boundary (MPB) compositions in $Na_{0.5}Bi_{0.5}TiO_3$-$BaTiO_3$ (NBT-BT) offers high electromechanical strain [1]. In this work $NaNbO_3$ (NN) was used as a secondary material for 0.8NBT-0.2BT ceramic. This material changes dielectric spectrum and phase of ceramic. There have not been many publications about this composition except for M. Dunce *et al.* [2] and Y. Wu *et al.* [3] studies but they were investigating MPB composition of NBT-BT with NN impurities.

In this work five different concentrations were investigated: x = 0, 0.04, 0.05, 0.06 and 0.08. Dielectric properties were measured at a temperature range 250 K - 500 K on cooling with a rate of 1 K/min. Piezoelectric properties were measured using commercial aixaCCT TF 2000 analyzer.

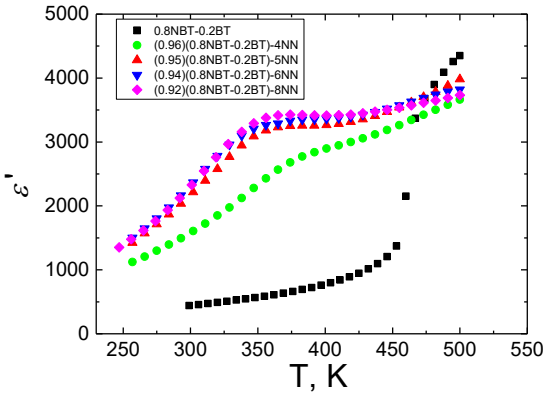


Fig 1. Temperature dependence of dielectric permittivity of all tested concentrations at 0.5 kHz frequency

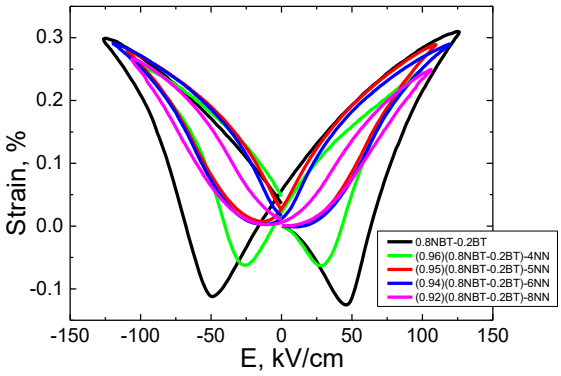


Fig 2. Electromechanical properties of all tested concentrations at room temperature

Fig. 1 shows temperature dependence of dielectric permittivity of all tested concentrations at 0.5 kHz frequency. Concentrations containing $NaNbO_3$ have dielectric anomaly occurring at a temperature interval 330 K – 370 K and there is no sign of phase transition which is monitored in 0.8NBT-0.2BT ceramic. Fig. 2 shows electromechanical properties of all tested compositions at a room temperature. Electromechanical stress in x = 0 and 0.04 concentrations are caused because of piezoelectricity and stress in x = 0.05, 0.06 and 0.08 concentrations occur because of antiferroelectricity.

[1] V. V. Shvartsman and D. C. Lupascu, "Lead-Free Relaxor Ferroelectrics," *Journal of the American Ceramic Society*, vol. 95, no. 1, pp. 1–26, Jan. 2012.
[2] M. Dunce *et al.*, "Dielectric and Polarization Properties of Na $_{0.5}$ Bi $_{0.5}$ TiO $_3$ -BaTiO $_3$ Solid Solutions with Na and K Niobates," *Ferroelectrics*, vol. 485, no. 1, pp. 80–88, Aug. 2015.
[3] Y. Wu, H. Zhang, Y. Zhang, J. Ma, and D. Xie, "Lead-free piezoelectric ceramics with composition of (0.97−x )Na1/2Bi1/2TiO3-0.03NaNbO3-x BaTiO3," p. 8.

# EFFECT OF BORON ON THE MICROSTRUCTURE AND MECHANICAL PROPERTIES OF HIGH-ENTROPY AlNiCoFeCrTiB$_x$ COATINGS

Vadim Cherniavsky, Alexandr Matveev, Alexandr Kremenchutskyy, Alexandra Yurkova

Igor Sikorskiy Kiev Polytechnic Institute", 37 Peremohy Ave., Kiev, 03056, Ukraine;
vadikv13@gmail.com;

Modern technology develops new requirements for the parts of machines and mechanisms operating in extreme conditions of exploitation. One of the effective methods for improving the physical, mechanical and operational properties of traditional materials (steels and alloys) is the application of protective reinforcement coatings from new materials. These materials include high-enthropy alloys (HEA) [1, 2]. Multi-component high-entropy alloys related to the newest class of metal composite materials Complex Metallic Alloys (CMAs) with complex crystallographic structure [2]. The high entropy of mixing various metal elements with a concentration close to equiatomic can significantly reduce the free energy of Gibbs and stabilize solid solutions with a simple crystalline structure and a good combination of properties. [1,2]. By controlling the composition at certain combinations of elements and their concentration, it is possible to achieve high hardness, wear resistance, corrosion resistance, resistance to oxidation, other characteristics [1]. Considering HEA's tendency to form simple structures, fabricating HEA coating by electron beam cladding process is of great significance and potential for extensive use. Until now this novel method for preparing HEA coatings has just been reported by any organizations.

The purpose of this work was to study the effect of boron content on the phase composition, structure and microhardness of multicomponent high-entropy AlCoNiFeCrTiBx coatings obtained by the method of electron-beam surfacing on a steel substrate.

Coatings with a nominal composition of AlCoNiFeCrTiBx (x = 0; 0.25; 0.5 and 1.0 mol) were prepared from a mixture of the starting components of Al, Co, Ni, Fe, Cr, Ti and B with a purity greater than 99.9% by weight . and the particle size about 50 microns. All the elements except B are equiatomic. The microstructure, chemical composition, and constituent phases of the synthesized coatings were characterized by SEM, EDX, and X-ray diffraction (XRD) analysis. Microhardness HV was also evaluated.

Experimental results demonstrate that the AlCoNiFeCrTi, AlCoNiFeCrTiB$_{0,25}$, AlCoNiFeCrTiB$_{0,5}$ coatings consist of 2 solid solutions with the BCC structure, which contain all components of the initial powder mixtures and differ in periods of crystalline lattices. As the content of boron increases to x = 1, the phase composition changes and in AlCoNiFeCrTiB coatings formation of one BCC solid solution and $Cr_2B$; $TiB_2$; $BCr_{0,2}Fe_{1,8}$ borides is observed due to the excess of boron atoms that do not dissolve in interstitial position of BCC solid solution.

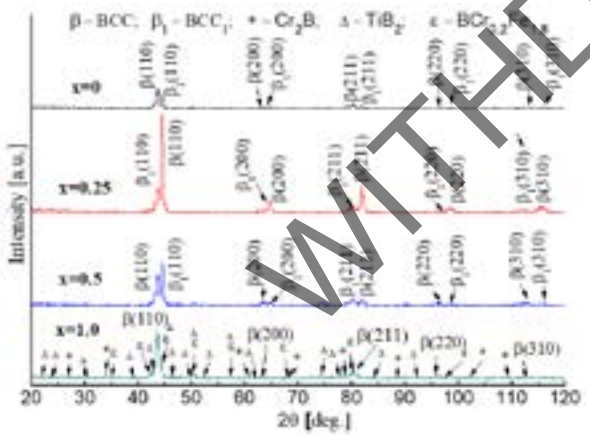


Fig. 1. XRD patterns of AlNiCoFeCrTiB$_x$ HEA coatings resulted from electron beam cladding.

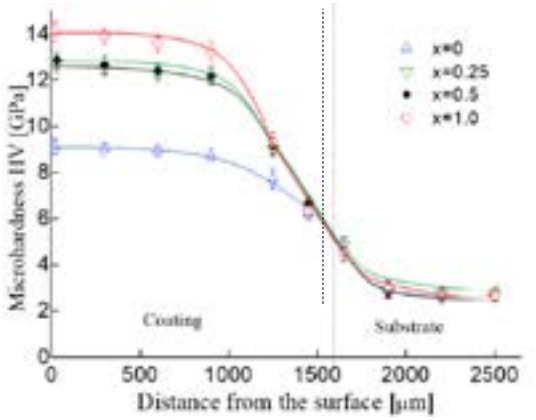


Fig. 2. Hardness of AlNiCoFeCrTiB$_x$ HEA coatings received from electron beam cladding.

The addition of boron (0,25; 0,5; 1) to original mixture AlNiCoFeCrTi leads to distortion of the crystal lattice and increase in hardness from 8,7 GPa to 12.8 GPa and then with a maximum content in AlNiCoFeCrTiB coating due to appearance of borides. Boron in solid solution as an interstitial atom, distorts the crystal lattice of BCC solid solution. Also we can indicate that increasing the proportion of boron to one mole leads to the formation of borides, which greatly increases the microhardness of the coatings. The hardness of high entropy AlNiCoFeCrTiB$_X$ coatings is much higher than that of the initial components and than the one of the steel substrate, and is much higher than that of the similar alloys prepared by laser cladding. It is shown that yield strength increases from 2,94 GPa to 4,54 GPa due to boron addition. Testing of coatings on the fracture toughness by loading on the indenter from 2 N to 10 N shows no cracks. That indicates the ability of the coating to counteract brittle fracture, namely, to inhibit the development of fragile cracks.

[1] *Yeh J.-W., Chen Y.-L., Lin S.-J., Chen S.-K.* // Materials Science Forum. – 2007. – V. **560**. – P.1- 9.
[2] *Yurkova A.I., Chernyavskii V.V., Gorban V.F.* Powder Metallurgy and Metal Ceramics. – July 2016. – Vol. 55. – Issue 3. – P. 152–163.

# RESEARCH ON SCANNING ELECTROCHEMICAL MICROSCOPY POSITIONING ACCURACY

Andrius Dzedzickis, Domantas Bartušis, Viktor Kovalevskyi, Mantas Makulavičius, Marius Šumanas, Algirdas Petronis, Vytautas Bučinskas, Justė Rožėnė, Aušra Liucija Konstantinavičiūtė, and Inga Morkvėnaitė-Vilkončienė

Department of Mechatronics, Robotics and Digital Manufacturing, Faculty of Mechanics, Vilnius Gediminas Technical University, J. Basanaviciaus g. 28,LT-03224 Vilnius, Lithuania
inga.morkvenaite-vilkonciene@vgtu.lt

Scanning electrochemical microscopy (SECM) is a technique, using which the local electrochemical activity of surfaces can be visualized. The advantage of SECM is that the technique can be applied for in-situ study without any damage to the biological system. We developed new 3-axis microelectromechanical positioning system, which will be used for positioning of SECM probe positioning at micrometers scale. Such a system can be called micro-electromechanical, since it ensures micrometric positioning accuracy at any point in the workspace [1]. Such systems are widely used in various fields of industry and science, ranging from numerically controlled machining centers to scanning probe microscopes [2,3]. The positioning accuracy of probe directly depends on dynamic characteristics of the system [4].

The design of this system was created in our laboratory. It was determined that the amplitudes of the table vibration acceleration are proportional to the speed of the table movement. When the speed of the table movement is 0.5 mm/min, the amplitude of the vibration acceleration is 0.015 G, increasing the speed of the table movement to 150 mm/min the amplitude of the vibration acceleration increases to 0.075 G, increasing the speed of the table up to 200 mm/s the amplitude of vibration acceleration increases significantly (0.22 G). Evaluating the oscillations generated by the stepper motor, it was found that they can be assessed with sufficient precision by analytical methods, especially when it comes to higher frequencies. The difference between the measured and calculated frequencies of 16.5% was obtained, when the table speed was 0.5 mm/min, and when the speed increases the difference between the calculated and measured excitation frequency does not exceed 1%. Significant differences (about 30%) between the excitation and the system response rate as soon as the speed of the table movement increases are explained by the high frictional forces in the system.

After additional measurements, the main frequencies of the system components are determined: the casing is about 250 Hz, the intermediate table between the X and Y axes is about 140 Hz, the working table is about 100 Hz. It has been found that the frequency of the system frequencies of the system components during work is not high compared to the vibrations of other frequencies. The system awakens itself while working, but it is rigid enough and well suppressed so that it does not affect its smooth functioning. Stand of experimental research consist: the micro-electromechanical positioning system and vibrations measuring equipment. The micro-electromechanical positioning system with marked places where sensors are mounted is shown in fig. 1.

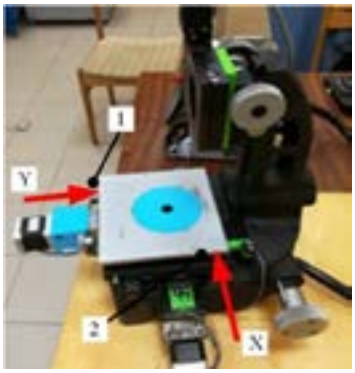


Fig. 1 Micro-electromechanical positioning system: 1, 2 – sensors mounting places

It was determined that general level of acceleration of the of the vibrations of the table is proportional to the table movement speed. When the table movement speed is 0.5 mm/min, the amplitude of vibration's acceleration is 0.015 G, increasing the speed of the table to 200 mm/s, the amplitude of vibration's acceleration increases up to 0.22 G.

**Acknowledgements**

This research is/was funded by the European Social Fund under the No 09.3.3-LMT-K-712 "Development of Competences of Scientists, other Researchers and Students through Practical Research Activities" measure.

[1] Carden, E. Peter, and Paul Fanning, (2004). Vibration based condition monitoring: a review. Structural health monitoring 3.4, 355-377.
[2] Dzedzickis, A., Bučinskas, V., Viržonis, D., Šešok, N., Ulcinas, A., Iljin, I., Morkvėnaitė-Vilkončienė, I. (2018). Modification of the AFM sensor by a precisely regulated air stream to increase imaging speed and accuracy in the contact mode. Sensors, 18(8), 2694.
[3] Dzedzickis, A., Bučinskas, V., Šešok, N., Iljin, I. (2016). Modelling of Mechanical Structure of Atomic Force Microscope. Solid State Phenomena, 251.
[4] Farrar, C.R., Doebling, S.W. and Nix, D.A., 2001. Vibration–based structural damage identification. Philosophical Transactions of the Royal Society of London A: Mathematical, Physical and Engineering Sciences, 359(1778), 131-149 p.

# INVESTIGATION OF THE QUALITY OF ADHESIVE BONDS OF PLAIN JERSEY KNITTED MATERIALS

Gerda Mikalauskaitė, Virginija Daukantienė

Department of Production Engineering, Kaunas University of Technology, Lithuania
gerda.mikalauskaite@ktu.edu

Plain jersey knitted fabrics and adhesive bonds are widely used in functional or leisure garments manufacture due to their excellent performance properties [1, 2]. The quality of adhesive bond depends on textile properties, on the technological parameters of bonding, on seam construction, etc. [3]. Thus, the aim of this research was to determine the influence of bonding duration on textile bonds peeling strength.

Investigation was performed with five commercially available knitted fabrics with a plain jersey knit type and one polyurethane (PU) adhesive film of 0.175 mm thickness (melting – 90-100°C temperature). The characteristics of the investigated materials are presented in Table 1. Bonds were laminated by applying PU adhesive film on pairs of lengthwise textile samples ensuring 8x50 $mm^2$ bond areas using the pressing device GTK DEA 25R. Bond was created by heat at 5.6 kPa pressure in three stages: 1st – the PU film was carried onto the face side of knitted material sample at 110 °C temperature for 5 s; 2nd – silicon paper was peeled off from PU adhesive film in 5 min; 3rd – the other side of knitted material sample was laid on the sample with the PU film and was bonded at 140°C temperature for 10 s, 20 s, 30 s and 40 s.

Table 1. Characteristics of investigated plain jersey knitted materials

| Material code | Fibre content | Density, $cm^{-1}$ | | Surface density, $g/m^2$ | Thickness, mm |
|---|---|---|---|---|---|
| | | Course count | Wale count | | |
| Ks2 | 84 % polyester, 16 % elastane | 21.0 ± 0.5 | 33.0 ± 0.5 | 218.8 ± 2.0 | 0.69 ± 0.02 |
| Ks3 | 90 % polyester, 10 % elastane | 14.0 ± 0.5 | 28.0 ± 0.5 | 235.5 ± 1.8 | 0.59 ± 0.01 |
| Ks6 | 81 % polyester, 19 % elastane | 19.0 ± 0.5 | 20.0 ± 0.5 | 207.1 ± 4.9 | 0.93 ± 0.01 |
| Ks7 | 80 % polyester, 20 % elastane | 20.0 ± 0.5 | 23.0 ± 0.5 | 262.3 ± 2.5 | 0.70 ± 0.02 |
| Ks8 | 82 % polyester, 18 % elastane | 20.0 ± 0.5 | 26.0 ± 0.5 | 195.0 ± 5.0 | 0.60 ± 0.01 |

Bond peeling strength testing was performed using the computerized CRE type tension machine H10 KT (Tinius Olsen, UK) at 50 mm/min peeling velocity. Five specimens were tested for each set of samples. The summary of the bond peeling strength values is presented in Figure 1.

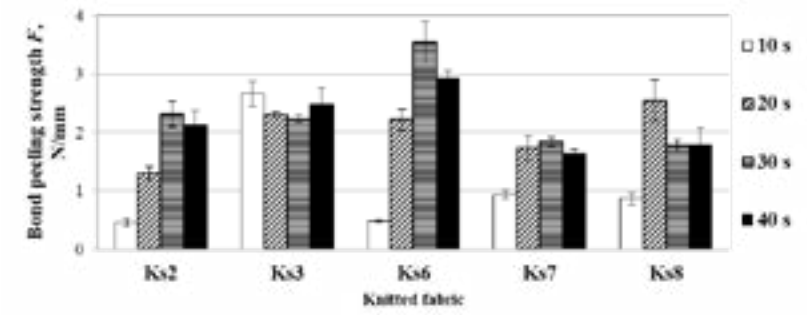


Fig. 1. Dependencies between bond peeling strength and bonding duration

The highest value of bond peeling strength was determined for the bonds which were laminated for 30 s duration for the thickest (0.93 ± 0.01 mm) knitted fabric Ks6 (3.55 ± 0.35 N/mm) and the lowest – for Ks2 (0.69 ± 0.02 mm) bond when bonding duration was 10 s (0.46 ± 0.22 N/mm). The higher peeling strength is also seen for the bonds of knitted fabrics Ks2 (2.32 ± 0.22 N/mm) and Ks7 (1.85 ± 0.07 N/mm) which were bonded for 30 s. For Ks3 bonded system the highest value was determined when the bonding duration was 10 s (2.67 ± 0.21 N/mm) and for Ks8 – 20 s duration (2.55 ± 0.36 N/mm). The lowest values almost for all the cases are determined when the duration is 10 s.

When the amount of the elastane fibre increases in knitted fabrics from 10 % up to 20 % results show that bond peeling strength does not increase evenly, so there are no relevant dependencies in bond peeling strength.

The investigation of the influence of bonding duration on textile bonds peeling strength has shown that almost in all cases (Ks2, Ks6, Ks7 and Ks8) the bond peeling strength increases from 97.8 % up to 642.7 % when the bonding duration increases from 10 s up to 30 s. Bond peeling strength decreases from 22.4 % up to 129.3 % when the bonding duration from 30 s rises up to 40 s. It could be concluded that the bond peeling strength depends on bonding duration.

[1] Seram, N. & Nandasiri, T. A. A Comparison Between Bonding and Sewing: Application in Sports Performance Wear. Journal of Academia and Industrial Research, 2015, vol. 3, no. 8. pp. 343-345.
[2] Busilienė, G., Strazdienė, E., Urbelis, V., & Krauledas, S. The Effect of Bonded Seams Upon Spatial Behaviour of Knitted Materials Systems. Materials Science (Medžiagotyra), 2015, vol. 21, no. 2. pp. 271-275.
[3] Jakubčionienė, Ž., et al. Investigation of the Strength of Textile Bonded Seams. Materials Science (Medžiagotyra), 2012, vol. 18, no. 2. pp. 172-176

# ACRYLATED VANILLIN-BASED PHOTOCROSS-LINKED POLYMERS

Auksė Navaruckienė[1], Jolita Ostrauskaitė[1]

[1]Department of Polymer Chemistry and Technology, Kaunas University of Technology, Radvilenu Rd. 19, LT-50254 Kaunas, Lithuania
aukse.ligeikaite@ktu.edu

Photopolymerization engendered high interest both in academia and in industry due to the considerable practical and economic benefits. Photopolymerization have the advantages of rapid cure, low energy consumption, high efficiency, low volatile organic compound emission, and the large number of applications in not only conventional areas such as coatings, inks, and adhesives, but also in high-tech domains, such as microelectronics, optoelectronics, laser imaging, stereolithography, and nanotechnology [1]. The renewable feedstock use in materials production using photopolymerization processes reveals the great potential of renewable raw molecules and their ability to replace petroleum-based materials. Recently, vanillin and its derivatives have attracted much attention as renewable building blocks for high performance polymers mainly because of their rigid aromatic structures. Synthetic vanillin from lignin or guaiacol is more commonly available, however it can be extracted from natural sources as well. With its functionalities and large-scale availability, vanillin is an ideal scaffold for monomer synthesis [2].

In this study, the cross-linked polymers were obtained by photopolymerization of vanillin diacrylate or vanillin dimethacrylate with 1,3-benzenedithiol using ethyl (2,4,6-trimethylbenzoyl) phenyl phosphinate as photoinitiator. The chemical structure of the photocross-linked polymers was confirmed by IR spectroscopy. The yield of the insoluble fraction of the photocross-linked polymers obtained after Soxhlet extraction with acetone for 24 h was in the range of (87-95) %. Thermal and mechanical properties of vanillin diacrylate- and vanillin dimethacrylate-based photocross-linked polymer films were investigated and compared.

It was established by differential scanning calorimetry that the photocross-linked polymers of vanillin diacrylate and vanillin dimethacrylate were amorphous materials with the glass transition temperature of -5 ºC. Their thermal degradation temperatures at the weight loss of 10 %, determined by thermogravimetric analysis, were 270 ºC and 240 ºC, respectively.

Mechanical testing of the photocross-linked polymers was performed by tensile test on a BDO-FB0.5TH (Zwick/Roell) testing machine. The mechanical characteristics of obtained vanillin diacrylate and vanillin dimethacrylate-based photocross-linked polymer films were following: tensile strength was 5 MPa and 25 MPa, the elongation at break was 31.4% and 0.5%, the Young modulus was 16 MPa and 2953 MPa, respectively.

It was determined that vanillin diacrylate-based photocross-linked polymer film is more rigid and mechanicaly stronger, whereas vanillin dimethacrylate-based photocross-linked polymer film is more soft and flexible.

**Acknowledgements.** This research was funded by the European Social Fund under the measure No. 09.3.3-LMT-K-712 “Development of Competences of Scientists, other Researchers and Students through Practical Research Activities”.

[1] Yagci Y., Jockusch S., Turro N.J. Macromolecules 2010, 43(15), 6245–6260.
[2] Zhang C., Madbouly S.A., Kessler M.R. Macromol. Chem. Phys. 2015, 216, 1816-1822.

# PHOTOINITIATOR-FREE PLANT-DERIVED RESINS FOR THE OPTICAL 3D μ-PRINTING

Miglė Lebedevaitė[1], Jolita Ostrauskaitė[1], Edvinas Skliutas[2], Mangirdas Malinauskas[2]

[1] Department of Polymer Chemistry and Technology, Kaunas University of Technology, Radvilenu Rd. 19, LT-50254 Kaunas, Lithuania

[2] Laser Research Center, Vilnius University, Sauletekis Ave. 10, 10223 Vilnius, Lithuania

migle.lebedevaite@ktu.lt

Most of the photosensitive resins for optical 3D printing are made from acrylic oligomers, acrylic monomers and/or reactive diluents, photoinitiators and UV stabilizators/blockers [1]. Petroleum-derived acrylic resins such as polyesters, polyether oligomers or diglicidylether bisphenol A acrylates are those that are mostly used for optical 3D printing [2]. Since petroleum recourses are decreaasing, it became crucial to search for alternative materials such as renewable resources Due to natural oils richness in double bonds which can be polymerized or converted to other functional groups, biodegradability and renewability, natural oils became a popular target of researchers [3].

Soybean oil is one of the most promising materials to replace petroleum-derived resins [4]. Due to the high amount of various functional groups such as the acrylic, epoxy and hydroxy groups, acrylated epoxidized soybean oil (AESO) is widely used in industry. AESO can be polymerized by UV/VIS light using appropriate photoinitiators and can form a cross-linked polymer network while the cross-linking of pure AESO is still considerable.

Vanillin dimethacrylate (VDM) or methacrylated vanillin alcohol is produced from lignin, one of the most abundant natural polymers. The bio-based thermosets made from VDM and maleinated AESO showed good thermal and mechanical properties, yet very long reaction time was also observed [5]. Vanillin diacrylate (VDA) is a bifunctional aromatic compound which can also be produced from lignin. It has two acrylic groups which can be polymerized via free-radical polymerization, yet no data was found of its usage in polymerization.

In this study, the plant-derived AESO, VDM and VDA were used as photosensitive monomers for the optical 3D printing. Chemical structure of the cross-linked polymers was confirmed by IR spectroscopy. The insoluble fraction of the cross-linked polymers was determined by Soxhlet extraction. Mechanical testing of the cross-linked polymer specimen was performed by compression test on a BDO-FB0.5TH (Zwick/Roell) testing machine. Thermogravimetrical analysis was conducted on a Perkin Elmer TGA 4000 instrument. Differential scanning calorimetry analysis was performed on TA Universal DSC Q2000 V24.10 Build 122 instrument. Direct Laser Writing (DLW) 3D lithography experiments were conducted employing a Pharos laser (515 nm, 300 fs, 200 kHz, Light Conversion Ltd). The fabricated structures were characterized using a scanning electron microscope (SEM, Hitachi TM-1000).

It was determined that the addition of VDM reduced the rate of photocross-linking and the values of the glass transition temperature, thermal decomposition temperature and compressive modulus. The formation of more linear and/or branched macromolecules considered the VDM effect as a plasticizer for AESO in photocross-linking without a photoinitiator. It was experimentally demonstrated that the homopolymer of AESO and the copolymer AESO/VDM are suitable materials for rapid 3D microstructuring by the DLW lithography technique, shown in Fig. 1. [6]

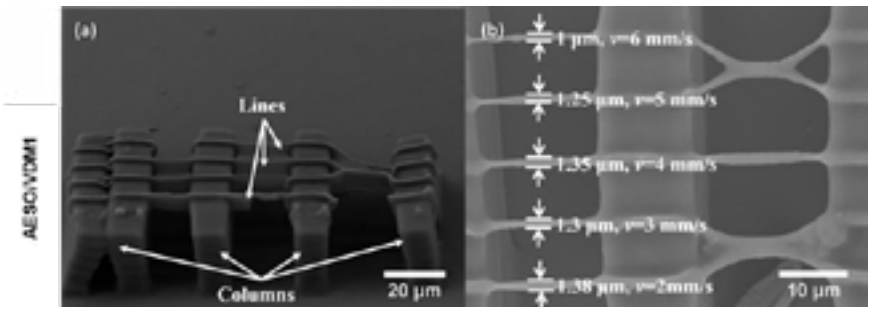


Fig. 1. The SEM images of resolution bridges (RB): (a) a side view of RB at the angle of 45 degrees and 1800 magnification. The applied power P to produce bridges was 0.6 mW (2 TW/cm$^2$), scan velocity v varied from 0.1 mm/s to 0.5 mm/s every 0.1 mm/s; (b) a top view of the other RB at 4000 magnification. P = 0.6 mW (2 TW/cm$^2$), v = 2–6 mm/s every 1 mm/s;

**Acknowledgments:** Financial support from the Research Council of Lithuania (project No. S-LAT-17-2) and EU ERDF, through the INTERREG BSR Programme (ECOLABNET project #R077) are gratefully acknowledged.

[1] Skliutas, E., et al., Photosensitive Naturally Derived Resins Toward Optical 3-D Printing. Opt. Engin. 57, 041412 (2018).

[2] Ligon-Auer, S.C., et al., Toughening of Photo-Curable Polymer Networks: A Review. Polym. Chem., 7, 257-286 (2016).

[3] Reddy, M.M., et al., Biobased Plastics and Bionanocomposites: Current Status and Future Opportunities. Progr. in Polym. Sci., 38, 1653-1689 (2013).

[4] Yang, Y., et al., Synthesis and Performance of a Thermosetting Resin: Acrylated Epoxidized Soybean Oil Curing with a Rosin-based Acrylamide. J Appl Polym Sci, 134 (2017)

[5] Zhang, Y., et al., Soybean-Oil-Based Thermosetting Resins with Methacrylated Vanillyl Alcohol as Bio-Based, Low-Viscosity Comonomer. Macrom. Mater. and Engin., 303, 1700278 (2018).

[6] Lebedevaite, M., et al. Photoinitiator Free Resins Composed of Plant-Derived Monomers for the Optical μ-3D Printing of Thermosets. Polymers, 2019, 11.1: 116.

# PIEZOELECTRIC COEFFICIENT AND DISPLACEMENT FACTOR OF BONE MEASURED BY LASER INTERFEROMETER

Ugnė Norkutė, Virgilijus Minialga

Department of Physics, Kaunas University of Technology
ugne.norkute@ktu.edu

Piezo materials are characterized by direct piezoelectric effect: pressure generates charges on the surface of piezoelectric materials. It will also work in reverse, the inverse piezoelectric effect causes a change in length in this type of materials when an electrical voltage is applied. Examples of piezoelectric materials are: quartz, Rochelle salt, lead titanate zirconate ceramics and bones. Piezoelectricity is good feature for bones because it can repair and heal bones. Also, bones can be remodeled with help of piezoelectricity [1].

We used Michelson interferometer with He-Ne laser in this work to measure displacement factor $\Delta h$ Eq. (1) and piezoelectric coefficient $d_{33}$ Eq. (2), due to inverse piezoelectric effect of pig rib and ox bone.

$$\Delta h = \frac{\lambda}{4} * N \quad (1)$$

$$d_{33} = \frac{\Delta h}{U}. \quad (2)$$

Here $\lambda$ = 632,8 nm is wavelength of laser light, $N$ is number of light intensity changes when thickness of specimen changes, $U$ is value of applied voltage.

Pig rib (9 mm x 5 mm x 7 mm) and ox bone (8 mm x 5 mm x 17 mm) specimens were placed in the attachment unit. Thin mirror which moved depending on the piezo material motion was on the front surface of unit. Voltage 500V was connected to both samples and has created electric field. Signal of exiting voltage (upper curve) and signal from the photodiode (lover curve) are presented in Fig. 1. The signals of photodiode show bones thickness change. $\Delta h$ = 16 nm was obtained for the pig rib, using this parameter was calculated $d_{33}$ = 32 pC/N and $\Delta h$ = 41 nm was obtained for ox bone, $d_{33}$ = 82 pC/N.

In comparison with the first bone measured $d_{33}$ = 2 pC/N (Japanese scientists: E. Fukada and I. Yasuda) [2], we received a little bit bigger coefficient. This difference can be explained that no charges leakage was in our experiments with inverse piezoelectric effect.

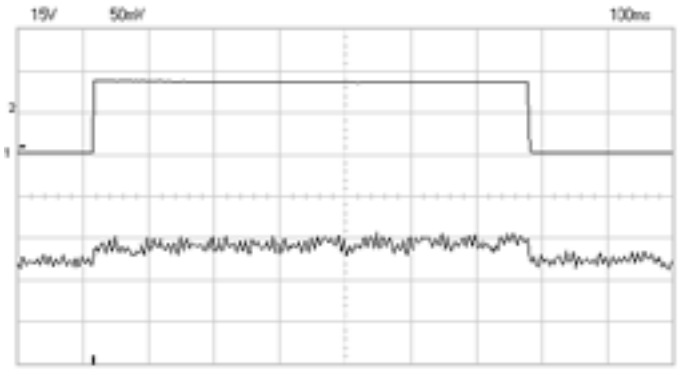


Fig. 1. Ox bone. Signals obtained from laser interferometer: upper – exiting high voltage signal; lover – signal from photodiode

[1] Bassett, C. A. L., and Becker, R. O., Generation of electric potentials in bone in response to mechanical stress, *Science*, 137, 1063-1064, 1962.
[2] E. Fukada and I. Yasuda, Piezoelectric effects in collagen, Japanese Journal of Applied Physics, 117-121, 1964.

# LOCALITY-SENSITIVE HASHING FOR MARKET SEGMENTATION

Paul Drozd[1]

[1]Department of Intelligent Systems, Belarussian State University, Belarus
drozdps@gmail.com

Customer (or market) segmentation is the process of dividing customers into groups based on common characteristics so that any business can market to each group effectively and appropriately. This research suggests new method for customer segmentation which have demonstrated great results on real business examples.

Our approach eliminates the instability of machine learning for customer segmentation using Locality-Sensitive Hashing algorithm (abbreviated as LSH), which is commonly used as the nearest neighbor search (NNS) [1]. LSH utilizes a specific set of bad hash-functions. The main feature of these hash functions is that they generate collisions on similar objects so neighboring points are tend to lie in the same hash bucket, which is strictly forbidden for regular applications of hash functions, such as cryptography (Fig. 1).

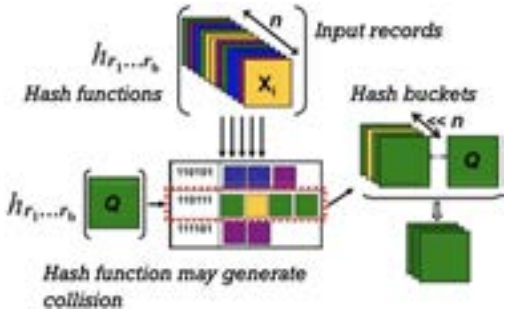


Fig. 1. Locality-Sensitive Hashing algorithm

Then Bisecting K-means algorithm (abbreviated as BSK) is used for processing the values of the hash functions in a metric space. This technique significantly increases machine learning stability and demonstrates better performance than other clustering algorithms [2].

The program implementation of the suggested LSH+BSK approach was developed using Apache PredictionIO technology stack. The sample use-case scenario of our market segmentation system is given below (Fig. 2).

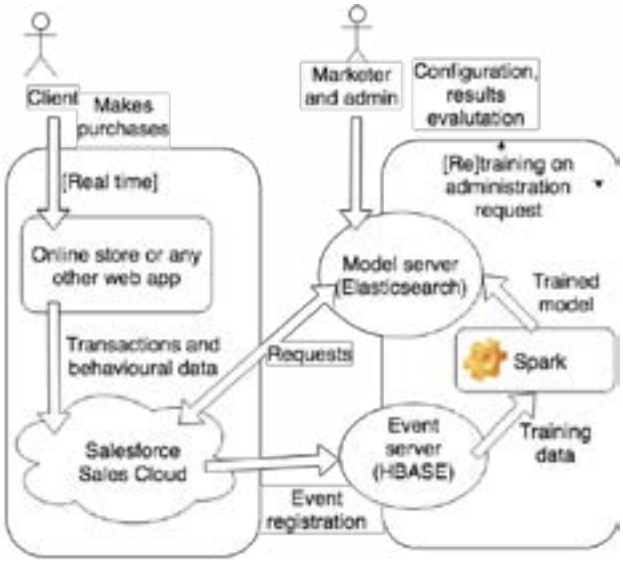


Fig. 2. Customer segmentation system use-case scenario

The system is able to handle both behavioural data (for example, the average session time a customer spends surfing your e-commerce website) and transactional records (for example, the most expensive transaction amount for a customer within a specified period of time). Our machine learning algorithms are completely automated, so the system can be used by marketers, financial analysts, product managers and other non-technical specialists.

[1] Fern, X.Z., Clustering ensembles for high dimensional data clustering / X.Z. Fern, C.E. Brodley // In Proc. International Conference on Machine Learning / ed. T. Fawcett. Washington DC, 2003. P.178-185.

[2] Drozd P. Kohonen's neural networks for Customer Segmention / P. Drozd // Open Readings 2018 / ed. E. Skliutas. Vilnius, 2018. P.93.

# NUMERICAL MODELLING OF ULTRASONIC WAVE PROPAGATION IN CARBON FIBRE MATERIAL

Mastan Raja Papanaboina[1], Dr. Elena Jasiūnienė[2,3], Dr. Egidijus Zukauskas[2]

[1]Kaunas University of Technology, Studentų 56, Kaunas, Lithuania, mastan.papanaboina@ktu.edu
[2]Prof. K. Baršauskas Ultrasound Research Institute, Kaunas University of Technology, K. Barsausko St. 59, LT-51423 Kaunas, Lithuania
[3]Department of Electronics Engineering, Kaunas University of Technology, Studentu St. 48, LT-51367 Kaunas, Lithuania.

The composite materials which have superior qualities such as high strength and light weight. There are different types of composite material combinations such as carbon fibre, glass fibre and many other kind of materials. Where high strength and light weight is required the composite materials are playing key role in the area of aeronautics and other engineering fields [1]. The carbon fiber sandwich materials are very stiff and have low bending properties. The attachment of two carbon fiber skins to the honeycomb core make carbon fibre honeycomb panel.

The 2D model of carbon fibre reinforced plate with delamination type defects was prepared using abaqus explicit finite element software. The thickness of the modelled plate was 1 mm. Investigations were carried-out using 5MHz frequency bulk ultrasonic waves in pulse-echo mode.

The ultrasonic waves excitation zone was placed on top of the plate at different positions-above defect free and defective zones. Ultrasonic waves reflected at different position where detected and investigation of ultrasonic waves interaction with defects was carried-out.

The delamination type defects between the composite layer have been created artificially and the ultrasonic scan results are obtained in CIVA simulation software which uses phased array transducer at a frequency of 3.5MHz and 5MHz. The transducer uses 128 elements. The longitudinal wave modes have been modelled. The sensitivity zone is enabled concerns defects and the depth direction of sensitivity zone is along local normal. The defect depth and size have been obtained.

The results conclude that the finite element software analysis used for testing with 5MHz gives better results compared to 3.5MHz for both with defect and without defect of carbon fibre material. The finite element software is used to see the wave interaction with the defect. Further the same was analyzed using CIVA software to identify the position and depth of the defects.

[1] **Seth S Kessler**, **S Mark Spearing**, **Constantinos Soutis,** Damage detection in composite materials using Lamb wave methods, 5 April 2002, Seth S Kessler et al 2002 Smart Mater. Struct. 11 269

[2] **Mastan Raja Papanaboina**, **Naga Manikanta Kommanaboina**, **Hari Prasanna Manimaran**, **Dr. elena Jasiuniene**, Inspection of the Honeycomb sandwich panel using Phased arrays, Proceedings of 22nd International Scientific Conference, Transport Means 2018.

# DIELECTRIC SPECTROSCOPY OF $BiCrO_3$ AND $BiCr_{0.9}Sc_{0.1}O_3$ MULTIFERROIC PEROVSKITES

Vaidotas Paukšta[1], Robertas Grigalaitis[1], Jūras Banys[1], Andrei Salak[2], Davide Delmonte[3], Edmondo Gilioli[3]

[1] Faculty of Physics, Vilnius University, Sauletekio av. 9, Vilnius, LT-10222 Lithuania
[2] Department of Materials and Ceramics Engineering and CICECO - Aveiro Institute of Materials, 3810-193 Aveiro, Portugal
[3] IMEM-CNR, Parco Area delle Scienze 37/a, 43124 Parma, Italy
vaidaspauksta@gmail.com

*Multiferroics* are materials in which two or all three of the properties, namely ferroelectricity, ferromagnetism, and ferroelasticity occur in the same phase. This means that they have a spontaneous magnetization that can be reoriented by an applied magnetic field, a spontaneous polarization that can be reoriented by an applied electric field, and a spontaneous deformation that can be reoriented by an applied stress [1]. The recent interest in magnetoelectric materials has been stimulated by their great potential for future multifunctional device applications and fascinating physics. Bi-containing perovskite-type transition-metal oxide systems are of special interest, since they are considered as the most promising multiferroic materials. In these systems, the ferroelectricity is known to originate from a relative Bi–O displacement resulting from the stereochemical activity of the lone-pair Bi cations [2]. Many of such systems can be synthesized only at special conditions (e.g., under high-pressure). Nevertheless, they are of great interest because of their possible practical applications (e.g., as multiple-state memory elements, field sensors and tuneable magnets).

$BiCrO_3$ was first synthesized by Sugawara et al. in 1968 and reported to be antiferromagnetic below 123 K with a weak parasitic ferromagnetic moment [3]. Despite enormous research efforts, physical properties of this material have not fully been understood and the peculiarities of magnetism and ferroelectricity of $BiCrO_3$ are still debated.

Dielectric response of the high-pressure synthesized $BiCrO_3$ and $BiCr_{0.9}Sc_{0.1}O_3$ ceramics was studied in a temperature range of 40-530 K. The dielectric permittivity was measured in a cooling mode with a rate of 1 K/min. The measurements were performed in two frequency ranges. Between 20 Hz and 1 MHz, capacity and loss tangent were measured using an LCR meter HP-4284A. In the 2 MHz - 3 GHz range, a vector network analyzer Agilent 8714ET in a coaxial line was used.

Broad dispersions and considerable dielectric losses were observed for both compositions. Therefore, we decided to investigate their direct current (DC) electrical conductivity. The calculated electrical conductivity was fitted with the Almond – West law, which describes the conductivity behavious rather well. Fig. 1 shows a dependence of DC conductivity on inverse temperature. From these data, using the Arrhenius law we got the activation energy (1):

$$\sigma_{\mathrm{DC}} = \sigma_0 \exp\left(\frac{-E_{\mathrm{A}}}{kT}\right) \qquad (1)$$

Activation energy before phase transition in both compounds are comparable ≈0.23 eV, but in paraelectric phase its value increases to 0.27 eV in $BiCrO_3$ and to 0.34 eV in $BiCr_{0.9}Sc_{0.1}O_3$

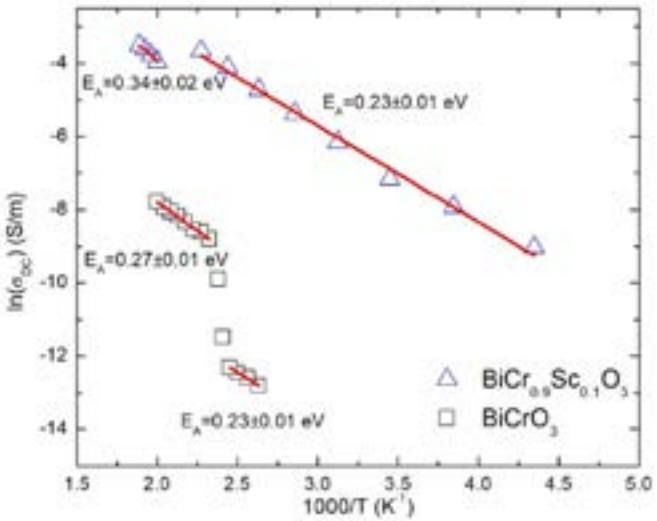


Fig. 1 DC electrical conductivity of $BiCrO_3$ and $BiCr_{0.9}Sc_{0.1}O_3$ as a function of inverse temperature.

[1] N. A. Hill, "Why Are There so Few Magnetic Ferroelectrics?," *The Journal of Physical Chemistry B*, vol. 104, no. 29, pp. 6694–6709, Jul. 2000.
[2] Y. Xu, X. Hao, J. Meng, D. Zhou, and F. Gao, "Electronic and magnetic properties of the monoclinic phase $BiCrO_3$ from first-principles studies," *Journal of Physics: Condensed Matter*, vol. 21, no. 23, p. 236006, Jun. 2009.
[3] N. Izyumskaya, Y. Alivov, and H. Morkoç, "Oxides, Oxides, and More Oxides: High-κ Oxides, Ferroelectrics, Ferromagnetics, and Multiferroics," *Critical Reviews in Solid State and Materials Sciences*, vol. 34, no. 3–4, pp. 89–179, Nov. 2009.

# DAMAGEABILITY IN CONTACT AREA OF TIRE AND ASPHALT CONCRETE UNDER VARIOUS LOADS

Gleb Gribovskii

Department of Theoretical and Applied Mechanics, Belarusian State University, Belarus
mmf.gribovskiy@gmail.com

Finite-element models for describing three-dimensional stress-strain state of a multielement system "car tire–asphalt concrete" have great practical importance in car and road industry for determination assessment of volume damageability and wear of tire and the asphalt concrete pavement, which work in conditions of contact, mechanical and sliding fatigue.

In this work simultaneous contact interactions of the full multielement system "car tire–asphalt concrete", loaded by the various tire inner pressure $P_S$ (from 0.65 to 0.85 MPa) and radial load $F_H$ (from 6 to 10 kN) on rim were modelled using finite-element method [1,2]. The main goal of this work is determine 3D stress-strain state of the whole system and the state of volumetric damageability in contact interaction area of tire and asphalt concrete, where maximum stresses occur: 1) asphalt concrete, 2) tire tread and 3) rubber under radial ply (fig. 1-a).

Calculation of damageability $\Psi_{int}$ is based on the model of deformable solid mechanics with dangerous volume [3]. According to this model dangerous volume $V_{int}$ is the volume where acting stresses $\sigma_{int}$ are greater than limiting stress $\sigma_{int}^{(lim)}$. Allowable limit stress by stress intensity for friction fatigue in contact zone of tire and asphalt is 0.5 MPa and for others rubber parts of tire is 1 MPa which work in conditions of mechanical fatigue.

$$\psi_{int} = \sigma_{int} / \sigma_{int}^{(lim)}, \tag{1}$$

$$V_{int} = \iiint\limits_{\psi_{int}(V)\geq 1} dV, \tag{2}$$

$$\Psi_{int} = \iiint\limits_{\psi_{int}(V)\geq 1} \psi_{int}(V)\, dV. \tag{3}$$

Damageability in tire tread and asphalt concrete (fig. 1-b and 1-c) increased 3.3–3.6 and 6.6–8.2 times when the radial load on rim is increased from 6 to 10 kN. However, damageability in rubber under radial ply (fig. 1-d) decreased by 17–34%, which may be due to the complex nature of the stress redistribution in this area. Damageability in tire tread and asphalt concrete increased by 1–3% and 3–30% when the tire inner pressure is increased from 0.65 to 0.85 MPa, except the rubber under radial ply where damageability increased 2.7–3.4 times, because this zone experiences large bending loads with a radial load on the rim in the condition of interaction with the radial ply and steel breaker. Maximum value of damageability in rubber under ply is 8412 mm$^3$ ($P_S$ = 0.85 MPa, $F_H$ = 6 kN) and minimal is 2022 mm$^3$ ($P_S$ = 0.65 MPa, $F_H$ = 10 kN). Minimal and maximum value of damageability for tire tread and asphalt concrete can be found in [2].

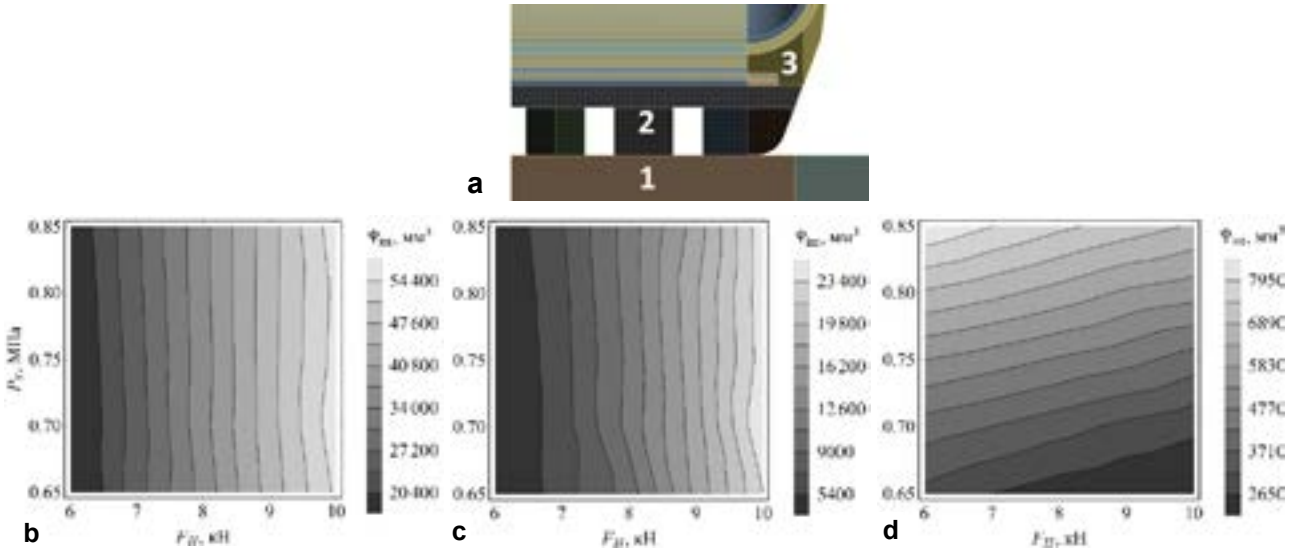


Fig. 1. Zones for analysis of damageability (a) in tire tread (b), asphalt concrete (c) and rubber under radial ply (d)

[1] G. V. Gribovskiy, S. S. Sherbakov, Volume damageability of rim–multicomponent tire–asphalt-concrete tribo-fatigue system, International Scientific and Technical Collection Theoretical and Applied Mechanics 32, 277 – 282 (2017).
[2] G. V. Gribovskii, Volumetric damageability of tire–asphalt contact pair under various loads, 60th scientific conference for young students of physics and natural sciences Open Readings 2018, Vilnius University, 117 (2018).
[3] L.A. Sosnovskiy, S.S. Sherbakov, Mechanothermodynamics (Springer, 2016).

# METHOXY-SUBSTITUTED (CARBAZOLYLMETHYL)BENZENE HOSTS FOR ORGANIC LIGHT-EMITTING DIODES

Edgaras Narbutaitis[1], Jonas Keruckas[1], Rasa Keruckienė[1], Dmytro Volyniuk[1], Juozas Vidas Gražulevičius[1]

[1] Department of Polymer Chemistry and Technology, Kaunas University of Technology, Lithuania
edgaras.narbutaitis@ktu.edu

Through the last two decades, much effort has been concentrated on the development of organic light-emitting devices (OLEDs) based on heavy metal organic complexes which produce both singlet and triplet excitons and allow to attain high quantum efficiencies [1]. However, heavy metal-based phosphorescent dyes are expensive and environmentally non-friendly materials which make them less attractive for wide applications. In recent years, a possibility to fabricate highly-efficient OLEDs employing thermally-activated delayed fluorescence (TADF) emitters was demonstrated by Adachi et al. [2]. Since both singlet and triplet excitons take part in generation of light in such devices, host materials possessing high singlet and triplet (at least 2.8 eV) levels are required in order to efficiently produce blue light. Triplet energy levels of electronically isolated carbazole fragments are known to be as high as 3.0 eV. Therefore we have designed and synthesized molecules comprised of carbazole moieties attached to the benzene core through methylene spacers in order to block π-electron conjugation between them and thus to preserve high triplet energy levels.

Four new methoxy-substituted (carbazolylmethyl)benzene compounds were designed and successfully prepared by a simple one-step nucleophilic substitution reaction of 3,6-dimethoxy-9*H*-carbazole and respective (halomethyl)benzenes. Photophysical, thermal and electrochemical properties of the materials were investigated. They show high triplet energy of 2.81 eV, glass-transition temperatures up to 99 °C and reversible electrochemical oxidation. The device obtained from 1,2-bis[(3,6-dimethoxy-9-carbazolyl)methyl]benzene doped with green DACT-II emitter and displayed high external quantum efficiency of 11.6%.

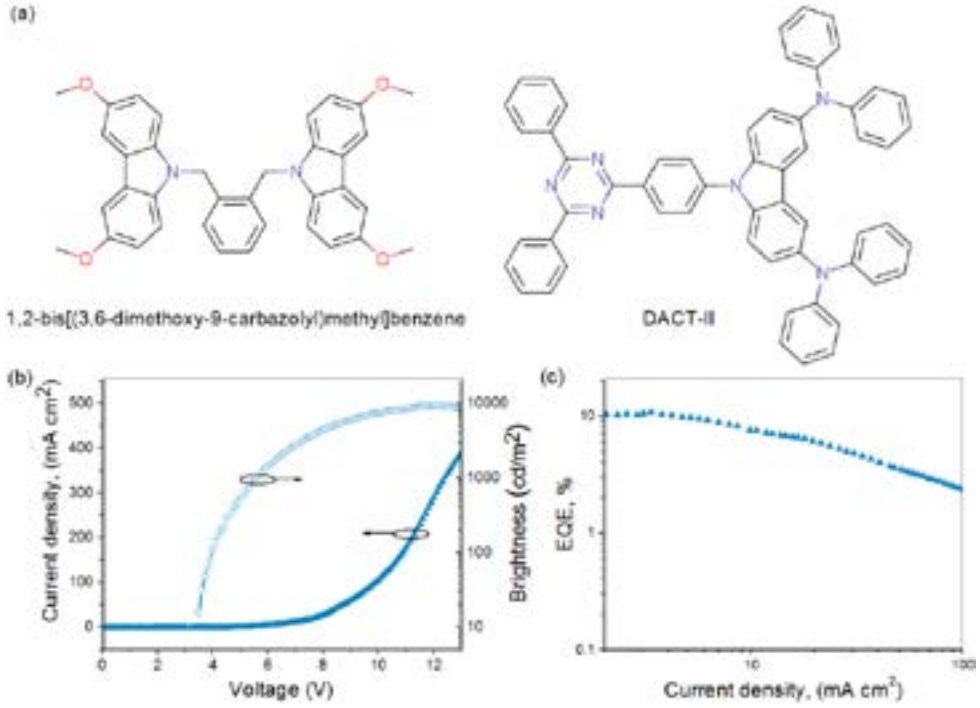


Fig. 1. The structures of host and emitter compounds (a), current density-voltage-luminance characteristics (b) and EQE-current density characteristics (c) of the device with doping concentration of 10 wt% DACT-II in 1,2-bis[(3,6-dimethoxy-9-carbazolyl)methyl]benzene host.

**Acknowledgement.** This research was funded by the European Social Fund under the No. 09.3.3-LMT-K-712 "Development of Competences of Scientists, other Researchers and Students through Practical Research Activities" measure.

[1] L. Xiao, Z. Chen, B. Qu, J. Luo, S. Kong, Q. Gong, J. Kido, Recent Progresses on Materials for Electrophosphorescent Organic Light-Emitting Devices. Adv. Mater. **23**, 926−952 (2011).

[2] H. Uoyama, K. Goushi, K. Shizu, H. Nomura, C. Adachi, Highly Efficient Organic Light-Emitting Diodes from Delayed Fluorescence. Nature **492**, 234−238 (2012).

# BROADBAND DIELECTRIC SPECTROSCOPY OF NANOCOMPOSITE MATERIALS

Rytis Šalaševičius[1], Sergejus Balčiūnas[1], Juras Banys[1], Satoshi Wada[2]

[1] Faculty of Physics, Vilnius University, Sauletekio 9, Vilnius, Lithuania
[2] Interdisciplinary Graduate School of Medical and Engineering, University of Yamanashi, Kofu,Yamanashi 400-8510, Japan
rytis.salasevicius@ff.stud.vu.lt

For the last few decades there has been a growing interest in applicable lead free materials [1]. Due to environmental concerns the lead free piezoelectric material research has grown significantly. As most commercially viable piezoelectric materials with lead have great piezoelectric constant and can in a broad temperature range, the aim of this research is to improve dielectric and piezoelectric properties in lead free solid solutions.

Nanocomposite ceramics have been making a breakthrough in search for piezoelectric materials. In this case the material is a "core-shell" type nanocomposite ceramic that consists of a BT-BMT crystallites cores which are coated in a BT shell.

BT-BMT/BT "core/shell" composites were prepared in two steps: the BT-BMT solid solution core was mixed with $TiO_2$ crystallites in a high pressure compressor into cylindrical shape pellets [2], [3] and then submerged into barium hydroxide solution at 175 ˚C for solvothermal solidification [4], [5].

In this presentation dielectric properties of 0,6BT-0,4BMT "core-shell" will be presented. From figure 1 we can observe an increase of dielectric permittivity between 150K and 380K temperatures. At 380K the real part of the dielectric permittivity reaches a peak point from which the dielectric permittivity drops. This sudden decrease could be interpreted as a structural transition since the composite consists of BT-BMT and BT crystallites.

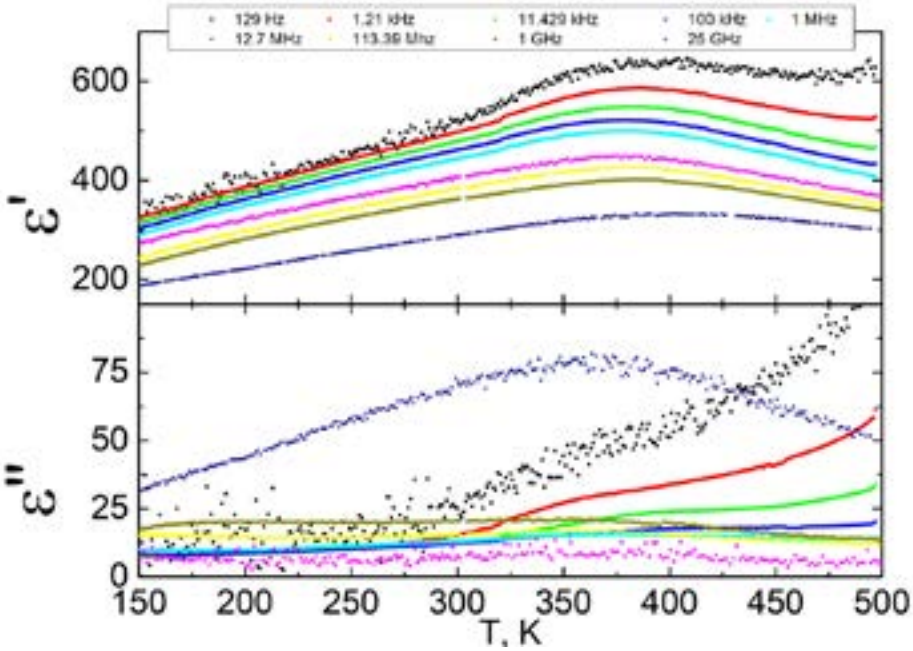


Fig. 1. Temperature dependence of real (indicated by $\varepsilon'$) and imaginary (indicated by $\varepsilon''$) parts of dielectric permittivity for 0,6BT-0,4BMT "core-shell".

In the poster presentation further investigation would be presented as the 0,6BT-0,4BMT composite would be compared to 0,7BT-0,3BMT composite.

[1] E. U. Council, "Directive 2002/95/EC of the European parliament and of the council." eur-lex.europa.eu, 2003.
[2] C. Chen, J. Cheng, S. Yu, L. Che, and Z. Meng, "Hydrothermal synthesis of perovskite bismuth ferrite crystallites," J. Cryst. Growth, vol. 291, no. 1, pp. 135–139, 2006.
[3] Y. Wang et al., "Mineralizer-Assisted Hydrothermal Synthesis and Characterization of BiFeO3 Nanoparticles," J. Am. Ceram. Soc., vol. 90, no. 8, pp. 2615–2617, 2007. [4] Y. Hirose, S. Ueno, K. Nakashima, and S. Wada, "Fabrication of BaTiO3/BiFeO3
Nano-complex Ceramics by Hydrothermal Method," Trans. Mater. Res. Soc. Jpn., vol.
39, no. 2, pp. 105–108, 2014.
[5] Y. Hirose, S. Ueno, K. Nakashima, and S. Wada, "Preparation of BaTiO3 Nanostructured Ceramics by Solvothermal Solidification Method," Trans. Mater. Res. Soc. Jpn., vol. 40, no. 3, pp. 239–242, 2015.

# COMPREHENSIVE STUDY OF STRUCTURAL AND OPTICAL PROPERTIES OF ZnO THIN FILMS GROWN IN VARIABLE CONDITIONS

Ewelina Nowak[1], Mirosław Szybowicz[1], Alicja Stachowiak[1], Edyta Chłopocka[1]

[1] Faculty of Techical Physics, Poznań University of Technology, Poland

ewelina.k.nowak@doctorate.put.poznan.pl

The research correlated with finding the most affordable materials for modern electronics seems to be one of the main goals for material science nowadays. Due to their wide, direct bang gap, II-IV compounds seem to be applicable in innovative electronics [1]. One of them is zinc oxide (ZnO). ZnO monocrystal exhibits wide band gap around 3.3 eV (which occurs at crystallization to wurtzite-type structure), high transparency and relatively low optical absorbance [2]. As grown, ZnO shows n-type conductivity; nevertheless thin film deposition techniques allow p- and n-type doping [3].

The most popular way to achieve material for an electronic purpose is thin layer's growing. In most cases, thin layers of ZnO crystallize to zinc blend or wurtzite structure from amorphous film in high temperature. The sol-gel technique, due to an ease low cost of production and deposition, is one of the most popular methods of obtaining a functional films for optoelectronics. However, besides of numerous research focused on properties of acquired layers [4], the universal method of achieving repeatable samples is still not developed. What is more, the process does not enable to acquire high quality layer during the process. However, this can be achieved by post-processing, where the recrystallization of films can be used [4].

Understanding the course of the recrystallization process – with a special consideration of the influence of the crystal growth kinetics on the substrate's orientation and the presence of defects – seems to be one of the main goal in development of methods for sol-gel synthesis of thin films on amorphous substrates [2].

The main goal of the presentation is to establish the influence of different conditions of annealing on thin films of ZnO produced with spin coating method from sol on their structure and properties. Therefore, the main element of the work was to assess the structure of the obtained samples using microscopic methods. Besides of micrographs, the quality of crystal can be successfully determined using Raman microscopy investigations. Our purpose, besides of evaluation of crystal structure, was to observe localized vibrational modes connected with changes in structure, which can occur with growing of a thin layer process. For complementary information UV-VIS absorption and photoluminescence measurements were conducted.

Presented work has been financed by the Ministry of Science & Higher Education in Poland in 2018 year under Project No 06/65/DSMK/0010.

[1] H.E. Ruda, Widegap II-VI compounds for opto-electronic applications, (1992)
[2] Ü. Özgür, Y.I. Alivov, C. Liu, A. Teke, M.A. Reshchikov, S. Doğan, V. Avrutin, S.-J. Cho, H. Morkoç, A comprehensive review of ZnO materials and devices, J. Appl. Phys. 98 (2005) 041301-041403
[3] O. Schmidt, P. Kiesel, C.G. Van de Walle, N.M. Johnson, J. Nause, G.H. Döhler, Effects of an electrically conducting layer at the zinc oxide surface, Jpn. J. Appl. Phys. 44 (2005) 7271–7274
[4] L. Znaidi, Sol-gel-deposited ZnO thin films: A review, Mater. Sci. Eng. B Solid-State Mater. Adv. Technol. 174 (2010) 18–30.
[5] J.S.Williams, R.G. Elliman , Role of Electronic Processes in Epitaxial Recrystallization of Amorphous Semiconductors, Phys. Rev. Lett., 51 (1983) 1069–1072

# DELAMINATION DETECTION IN ADHESIVELY BONDED DISSIMILAR MATERIALS USING ULTRASOUND

Damira Smagulova[1], Elena Jasiuniene[12]

[1] prof. K. Baršauskas Ultrasound Research Institute, Kaunas University of Technology, Lithuania
[2] Department of Electronics Engineering, Kaunas University of Technology, Lithuania
damira.smagulova@ktu.lt

Adhesively bonded joints of dissimilar materials such as carbon fibre reinforced plastic (CFRP) bonded to steel have a great interest of use in aerospace, automobile, marine, wind turbine industries. The main advantages in using such joints are because they are lightweight, have increased mechanical performance, corrosion resistance, high fatigue strength, uniform stress distribution, better damage tolerance, impact resistance [1], [2]. Delaminations between two dissimilar materials are the most common defects that affect the integrity of entire structure and can cause a great harm for human safety. Therefore, such structures have to be checked regularly in order to detect defects, assess the risk the defects can cause and the possibility of further use or repair of the structure [3].

The aim of this work was to investigate possibilities to detect delaminations in adhesively bonded steel to CFRP joints. The scope of work is as follows: analysis of sample characteristics, simulation of ultrasonic inspection, experimental inspections. There are three main methods to detect delaminations in dissimilar material joints: amplitude change of interface reflections, back wall reflection loss, and phase reversal [2]. Firstly, characteristics of the sample and artificial delaminations were analysed. The sample under inspection has a simple planar geometry. Bulk waves were selected according to the thickness of dissimilar materials. Delaminations are artificial and made of Teflon with oil to prevent bonding of layers.

Simulations of inspection of the sample in contact pulse echo mode using 5 MHz transducer were performed for all three existing delaminations in the sample using CIVA software. Inspection from metal side was selected since CFRP is 3 times more attenuating material than steel. Amplitudes of signals reflected from the interface with good bonding and with delamination were compared. It was determined, that the difference is only 0.6 dB. From this, it follows that in practice it will be hard to detect delaminations. In this case, multiple reflections from the interface were analysed to increase probability of defect detection. From results of simulation, the difference of subsequent reflected signal, amplitudes are growing from 3 dB and more so, the defects can be located more easily in practice. The next step was an experimental sample inspection in contact pulse echo mode using 5MHz phased array transducer. To detect delaminations from the first reflection from the interface was hard in A-scan, but analysing subsequent reflections the difference was more obvious in amplitude scale. Inspection in immersion pulse echo mode was performed as well using 10 MHz focused transducer to increase the accuracy of the results on sample interface. It was determined that 2nd reflection from the interface is the most appropriate to analyse, since the difference in amplitude from good and defected bond is higher comparing to 1st and subsequent reflections. In this case, C-scan of the inspection of delaminations was obtained and shown in Fig. 1.

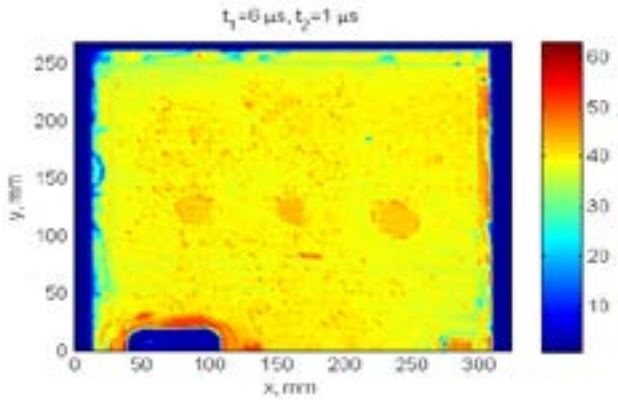


Fig. 1. C-scan of the inspection of dissimilar material joints in immersion pulse echo mode.

As a result, three artificial delaminations were detected using contact and immersion pulse echo mode inspection. It was determined that 2nd reflection from the interface should be analysed when inspecting joints of dissimilar materials.

[1] Huaqing Tang, Longquan Liu, "A novel metal-composite joint and its structural performance". Shanghai Jiao Tong University, China. Elsevier Ltd, Composite Structures 206, 2018, pp. 33-41. https://doi.org/10.1016/j.compstruct.2018.07.111.

[2] T.E.A. Ribeiro, R.D.S.G. Campilho, L.F.M. da Silva, L. Goglio, "Damage analysis of composite–aluminium adhesively-bonded single-lap joints". Department of Mechanical and Aerospace Engineering, Torino, Italy. Elsevier Ltd, Composite Structures 136, 2016, pp. 25-33. http://dx.doi.org/10.1016/j.compstruct.2015.09.054).

[3] B. S. WONG, "Non-destructive evaluation (NDE) of composites: detecting delamination defects using mechanical impedance, ultrasonic and infrared thermographic techniques". Nanyang Technological University, Singapore. Woodhead Publishing Limited, 2013, pp. 279-308. DOI: 10.1533/9780857093554.2.279.

# PHTHALOCYANINE-SENSITIZED RUBRENE FILMS FOR IR-to-VISIBLE UPCONVERSION

Edvinas Radiunas[1], Steponas Raišys[1], Saulius Juršėnas[1], Augustina Jozeliūnaitė[2], Tomas Javorskis[2], Ugnė Šinkevičiūtė[2], Edvinas Orentas[2], Karolis Kazlauskas[1]

[1]Institute of Photonics and Nanotechnology, Vilnius University, Lithuania
[2]Department of Organic Chemistry, Vilnius University, Lithuania
edvinas.radiunas@ff.vu.lt

Triplet-triplet annihilation (TTA) mediated light upconversion (UC) achieved in organic compounds under incoherent low-power excitation are of particular interest as it offers numerous applications, e.g. in bioimaging, anti-counterfeiting, fingerprint detection, photocatalysis and photovoltaics [1]. In many instances, efficient TTA-UC is realized only in organic solutions, meanwhile the most applications including photovoltaics demand solid-state architecture. The additional UC layer in a solar cell can be employed to recover sub-bandgap photons that are beyond the absorption range of the cell thus improving its efficiency. Lack of efficient IR-to-visible rigid UC devices could be attributed to limited number of efficient triplet sensitizers in the IR range, which experience severe non-radiative losses as a result of small energy gaps [2].

The current work focuses on TTA-UC performance of solution-processed polymer films containing conventional and modified rubrene emitters and (Pd,Pt)phthalocyanine sensitizers. Expressing excellent photostability, efficient intersystem crossing and long triplet-state lifetimes [1] the novel phthalocyanines are shown to exhibit strong Q-band absorption (up to 2.5 $10^5$ M/cm) at about 720 nm and broad transparency window at 450 - 630 nm (see inset of Fig. 1) suitable for the UC emission. These properties along with the determined triplet energies (1.12 - 1.18 eV) of the phthalocyanine sensitizers ensure their suitable combination with rubrene emitters for UC application. Rubrene was modified with tert-butyl side groups to preserve high emission quantum yield ($\Phi_{FL}$) at high concentrations, which are required for efficient triplet diffusion and thus TTA. Since the UC system is sensitive to oxygen, UC polymer films were fabricated by spin-coating on pre-cleaned glass substrates in nitrogen glovebox (with $O_2$ and $H_2O$ level < 0.1 ppm) and encapsulated with epoxy resin. Additional lower-energy DBP emitter introduced into the UC films (at a concentration of 0.5 wt%) served as a singlet exciton sink allowing to reduce detrimental singlet fission effects in the emitter. The achieved UC quantum yields (Fig. 1) are rather promising and encourages further development of rigid IR-to-VIS upconverting films.

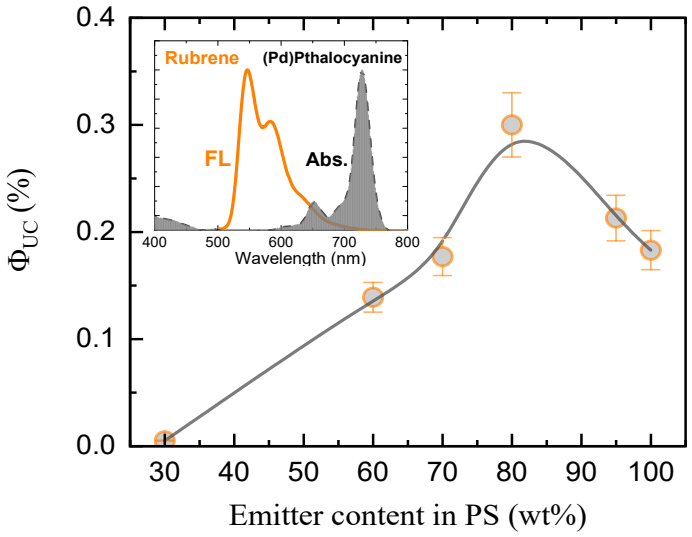


Fig. 1. UC quantum yield of (tert-butyl)rubrene/(Pd)phthalocianyne/DBP/PS film as a function of emitter concentration. Inset: (tert-butyl)rubrene fluorescence overlaid with (Pd)phthalocianyne absorption.

[1] J. Zhou, Q. Liu, W. Feng et al., Upconversion luminescent materials: advances and applications, Chemical Reviews **115**, 395-465 (2015).
[2] R. Englman, J. Jortner, The energy gap law for radiationless transitions in large molecules, Molecular Physics, **18**, 145-164 (1970).

# BROADBAND DIELECTRIC SPECTROSCOPY OF $Ag_{1-x}Li_xNbO_3$ (x = 0.05) CERAMICS

Arnas Vilmantas[1], Edita Palaimienė[1], Jan Macutkevič[1], Jūras Banys[1], Antoni Kania[2]

[1]Vilnius University, Faculty of Physics, Sauletekio av. 9, III b., LT-10222 Vilnius, Lithuania
[2] A. Chełkowski Institute of Physics, University of Silesia, Uniwersytecka av. 4, 40-007 Katowice, Poland
*arnas.vilmantas@ff.stud.vu.lt*

Nowadays ferroelectric materials are a widely investigated topic due to their wide array of uses. Currently, lead based ceramics are dominant in regard to their excellent piezoelectric properties. However, due to their pollutive nature, alternative materials are necessary [1]. One of the possibilities is Ag1-xLixNbO3. Its excellent piezoelectric properties, high polarization and phase transition temperatures spark an interest in further research of this material. The present work is aimed towards investigating Ag1-xLixNbO3 via dielectric spectroscopy on a wide frequency scale. Ceramics were prepared by solid-state reaction method [2]. The investigation was carried out for a sample of x = 0.05 in wide temperature (120 K – 500 K) and frequency (100 kHz – 750 GHz) ranges. The obtained results show a weak dielectric anomaly close to ferroelectric phase transition temperature T = 300 K and a much stronger dielectric anomaly close to antiferroelectric phase transition temperature T = 400 K (Fig. 1). The value of the dielectric permittivity is quite high, while losses are quite low in wide frequency and temperature ranges, indicating that the ceramics are suitable for microwave applications.

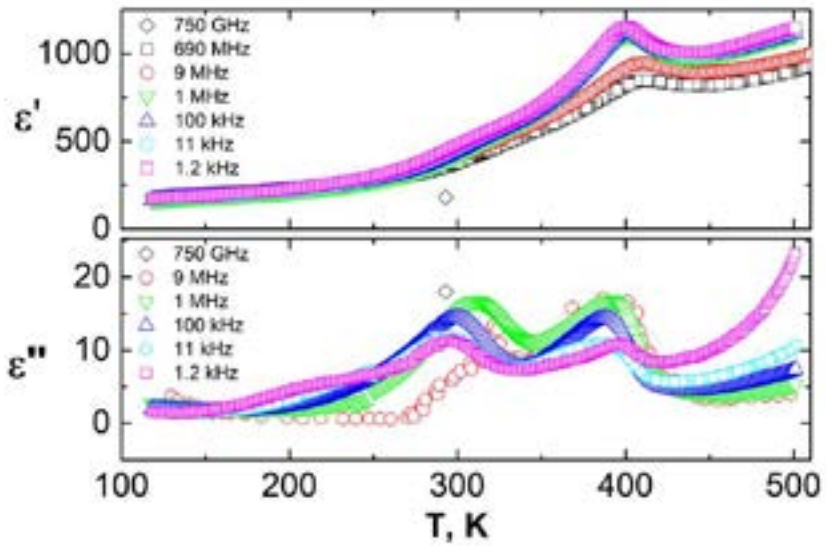


**Fig. 1.** Temperature dependence of real (*ε'*) and imaginary (*ε''*) parts of complex dielectric permittivity of $Ag_{0.95}Li_{0.05}NbO_3$ ceramics at varying frequencies.

1. A. Saito, S. Uraki, H. Kakemoto, T. Tsurumi, S. Wada, Growth of lithium doped silver niobate single crystals and their piezoelectric properties, Materials Science and Engineering B 120 (2005).
2. A. Niewiadomski, D. Kajewski, A. Kania, K. Balin, S. Miga, M. Pawlik, J. Koperski, *Microstructure and characterization of $Ag_{1-x}Li_xNbO_3$ ceramics*, Ceramics International 42, 4445-4451 (2016).

# PROPERTIES OF GLASSY AND NANOCRYSTALLINE LITHIUM IRON BORATE

Agata Romanowska[1], Przemysław P. Michalski[1], Jerzy E. Garbarczyk[1]

[1]Faculty of Physics, Warsaw University of Technology, Poland
romanowskagata@o2.pl

There is a huge demand for low cost, non-toxic and efficient energy sources. Such need is represented by vehicle and mobile devices markets. Increasing popularity of hybrid and electric cars as well as governments' actions are the reasons to develop more and more capacious energy storage systems. Lithium-ion batteries are now major sources and are still promising technology sector. One of the most important challenge in engineering of such systems is the choice of proper cathode material. Considering required properties: conductivity, energy storage capability, safety, costs and operating potential we have chosen lithium iron borate $LiFeBO_3$ to be examined for this application.

Investigated material has theoretical gravimetric capacity of 220 mAh/g. Moreover, it is known that electrochemical charging/discharging of this material leads to a little change of volume ca. 2%. Also its conductivity value reaches $10^{-7}$ S/cm, what makes lithium iron borates a competitive material to those in common use [1, 2].

The conductivity of the material may be further improved by electrochemically non-active additives, like carbon. In our case, an innovative method of synthesis was acquired - firstly, the glass was obtained by quenching of a melt. In the next step, the obtained glass was subjected to thermal nanocrystallisation, when the nanocomposite containing small (50–60 nm) grains of $LiFeBO_3$ was prepared. It has been reported, that nanocrystallisation of glassy material leads to improvement of its electrical properties, such as conductivity, even a few orders of magnitude [3, 4]. Taking into account good glass-forming properties of borates, it may result in promising cathode material.

Since the investigated material has not only a theoretical gravimetric capacity ca. 220 mAh/g [2], but also is safer and easier to obtain than popular $LiFePO_4$ and $LiCoO_2$ compounds [1], it has been characterised for suitability as a cathode material for Li-ion batteries. Samples were prepared with melt-quenching synthesis method and then tested with X-ray diffraction (XRD), differential thermal analysis (DTA) and impedance spectroscopy (IS) methods. Afterwards, cathode material was obtained in both glassy and nanocrystalline form and has undergone electrochemical cycling performance tests, of which results we present hereby.

XRD diffractograms obtained for room temperature and temperatures between 375–700°C revealed that initially material was glassy. During the heating of the sample, there occured crystalline phases of $Fe_3BO_5$, $LiFeBO_3$ and $LiB_3O_5$. DTA for 10°C/min served us in determining the temperature of glass transition (ca. 420°C) as well as three crystallisation peaks (458°C, 546°C, 647°C). Impedance spectroscopy examination showed, that heating has given rise to the conductivity value, lasting even after cooling the sample back to the room temperature – the biggest improvement was obtained for heating to 475 °C, where final value of conductivity was $1.4 \cdot 10^{-5}$ S/cm. However, electrochemical tests on this material showed that the gravimetric capacity is only modest.

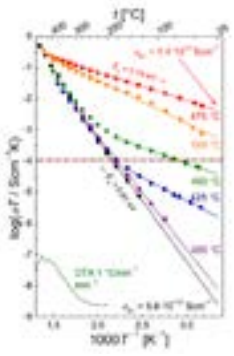

Fig. 1. Conductivity in function of temperature [3]. Black colour refers to data obtained during heating, whereas coloured marks represent values obtained in cooling after heating to various temperatures. Brown line stands for conductivity of crystalline material and the green one represents DTA curve for 1°C/min for comparison.

[1] A. Yamada et al., Adv. Mater., 22 (2010), 3583–3587
[2] P. Barpanda et al., J. Electrochem. Soc., 160 (2013), A3095–A3099
[3] P. P. Michalski et al., Solid State Ion., 302 (2017), 40–44
[4] T.K. Pietrzak et al., Solid State Ion., 98 (2014), 28–35

# INVESTIGATION OF MAGNETORESISTIVE PROPERTIES OF La-Sr-Mn-Co-O FILMS AT CRYOGENIC TEMPERATURES IN HIGH PULSED MAGNETIC FIELDS

Vakaris Rudokas, Nerija Žurauskienė

Center for Physical Sciences and Technology, Department of Material Science and Electrical Engineering, Vilnius, Lithuania
vakaris.rudokas@gmail.com

The renewed interest in thin manganite films of the type $La_{1-x}A_xBO_3$ (where A is a divalent alkaline-earth element like Ca, Sr, B-site element Mn) during last two decades has been motivated by fundamental understanding of colossal magnetoresistance phenomenon (CMR) as well as potential device applications [1]. It has been demonstrated that the CMR phenomenon in nanostructured (polycrystalline with nanosize grains) manganite films can be successfully used for the development of CMR-B-scalar sensors, which can measure the magnitude of pulsed magnetic fields in very small volumes independently on magnetic field orientation [2]. Such sensors based on La-Sr-Mn-O films have been successfully used at room temperatures to measure the distribution of magnetic fields in electromagnetic launchers and non-destructive pulsed-field magnets [3,4]. However, for specific applications in condensed matter physics or plasma science, sensors operating at cryogenic temperatures and measuring high magnetic field magnitude are required. It was found that substitution of Co for Mn in La-Sr-Mn-O films decreases the paramagnetic-ferromagnetic phase transition temperature and increases the resistivity of the material [5]. This is mostly related with Co which replacing Mn in the lattice destroys the long-range ferromagnetic ordering of the Mn network, resulting in changes of magnetic and electrical properties of the films. Therefore, the doping of manganite films with higher Co concentration could result in increase of low temperature magnetoresistance and can increase the sensitivity of manganite films to magnetic field at cryogenic temperatures.

The magnetoresistance (*MR*) of nanostructured $La_{1-x}Sr_x(Mn_{1-y}Co_y)_zO_{3\pm\delta}$ (La-Sr-Mn-Co-O) films with substitution of Co for Mn with amount of Co/(La+Sr)=0.12 and 0.14 was investigated at temperatures 4-150 K in pulsed magnetic fields up to 20 T. It was found that manganite-cobaltite films exhibit larger magnetoresistance in comparison with manganite films without Co doping. The manganite-cobaltite films with different Mn concentration Mn/(La+Sr)=1.05, 1.07, 1.11 were investigated. The magnetoresistance of the films with 0.12 and 0.14 amount of Co were found similar, however, the Mn excess slightly decreased the *MR* values. The largest magnetoresistance values and sensitivity to magnetic field were obtained for La-Sr-Mn-Co-O films having Mn content close to the stoichiometric ratio for manganites: Mn/(La+Sr)=1.05. It was found that magnetoresistance at high fields (20 T) has a minimum at (50-80 K) and increases with decrease of temperature. The possibility to use these films for the development of magnetic field sensors operating at cryogenic temperatures is demonstrated.

[1] C. Israel, M. J. Calderón, and N. D. Mathur, The current spin on manganites, Materials Today, **10**, 24-32 (2007).
[2] T. Stankevič, L. Medišauskas, V. Stankevič, S. Balevičius, N. Žurauskienė, O. Liebfried and M. Schneider, Pulsed magnetic field measurement system based on colossal magnetoresistance-B-scalar sensors for railgun investigation, Rev. Sci. Instrum., **85** 044704-1–044704-5 (2014).
[3] T. L. Haran, R. B. Hoffman, S. E. Lane, Diagnostic capabilities for electromagnetic railguns, IEEE Trans. Plasma Sci., **41**, 1526-1532 (2013).
[4] S. Balevičius, N. Žurauskienė, V. Stankevič, S. Keršulis, V. Plaušinaitienė, A. Abrutis, S. Zherlitsyn, T. Herrmannsdörfer, J. Wosnitza and F.Wolff-Fabris, Nanostructured thin manganite films in megagauss magnetic field, Appl. Phys. Lett., **101** 092407-1–092407-4 (2012).
[5] J. Hu, H. Qin, J. Chen and R. K. Zheng, Room temperature magnetoresistance in La0.67Sr0.33Mn1−xCoxO3, J. Appl. Phys., **91**, 8912-8914 (2002).

# EVALUATION OF BONDING QUALITY WITH DIFFERENT NONDESTRUCTIVE TESTING TECHNIQUES

Bengisu Yilmaz[1], Elena Jasiuniene[1,2]

[1] Prof. K. Baršauskas Ultrasound Research Institute, Kaunas University of Technology, K. Barsausko St. 59, LT-51423 Kaunas, Lithuania

[2] Department of Electronics Engineering, Kaunas University of Technology, Studentu St. 48, LT-51367 Kaunas, Lithuania

bengisu.yilmaz@ktu.lt

The rise in usage of highly developed engineering materials such as composites increased the research interest in joining technologies. Compared to traditional methods such as mechanical fasteners; adhesive bonding is a well-known and advantageous joining technique. Adhesive joints offer to bond dissimilar materials, preserves joint material integrity (no fibre discontinuity unlike with rivets and bolts), and homogenous load distribution through the joint with high strength to weight ratio. However, there is still a huge concern regarding the reliability of adhesive bonding due to lack of knowledge obtained from non-destructive testing techniques. Therefore, this project focuses on the evaluation of bonding quality with different non-destructive testing (NDT) techniques.

The goal of the project is to determine the bonding quality with easy to access and verified NDT techniques with the integration of information from different methods. The work builds on three main steps: numerical investigation, experimental investigation, and statistical validation. Both numerical and experimental investigations had taken a place to analyse different quality, material type/stage, thickness and geometry of bonding. NDT methodologies namely ultrasonic, electromagnetic and thermography would be compared and integrated where possible.

This work objectifies to compare before mentioned NDT techniques quantitatively based on the probability of detection curves obtained from variety in bonding quality, material, and geometry. In addition to comparison, the information obtained from different NDT techniques would be integrated (data fusion). In the end, the project aims to optimize an overall technique to evaluate bonding quality.

The single lap joint with specific dimensions had been selected to analyse different bonding quality responses. Three different bonding quality had been investigated: perfect bond, disbond, and kissing bond (where adhesive and adherend is completely in contact with no shear force). For ultrasonic NDT, numerical simulation results agree with experimental investigations. They suggest that the parameters such as amplitude, frequency and phase change obtained from ultrasonic response curves are relatable with bonding quality. On the other hand, as a combination of two different NDT methods - eddy current and thermography- induction thermography results suggest that the temperature evaluation curve had been affected by the quality of bonding.


Fig. 1. Schematic of single lap joint on the left. Different bonding (interface) quality schematics at the centre. The A-scan ultrasonic inspection of different interface qualities (semi analytical finite-element numerical study results- first interface time window) on the right.

The parameters related to bonding can be identified with NDT techniques such as ultrasonic and electromagnetic. As a result, the bonding quality of the adhesive joints can be obtained. The reliability studies and validation of techniques with statistical methods such probability of detection (PoD) has been planned. In addition, quantitative comparison of different ultrasonic and electromagnetic techniques will be reported based on PoD curves. Where possible, the data fusion will be applied, in other words the responses from different NDT techniques will be integrated.

This research is funded by NDTonAIR project from the European Union's Horizon 2020 research and innovation program under the Marie Sklodowska-Curie grant No. 722134.

# OPTICAL PROPERTIES OF CERIUM DOPED ZINC OXIDE STRUCTURES ON THE MOLYBDENUM SURFACE OF OBTAINED BY MICROVAWE ASSISTED METHOD

Aleksandra Shulga[1], Leonid Butusov[2,3], Galina Chudinova[2,3], Tatiana Sheshko[1]

[1] Peoples' Friendship University of Russia (RUDN University), Miklukho-Maklaya str. 6, Moscow, Russia, 117198
[2] A. Prokhorov Institute of General Physics. RAS,
Vavilov str. 38, Moscow, Russia, 119991
[3] National Research Nuclear University "MEPhI",
Kashirskoye sh., 31, Moscow, Russia, 115409
aleksandra-box@mail.ru

Research devoted to the study of the optical properties and morphology of the composite material based on cerium-doped zinc oxide on the surface of the molybdenum oxide film. The colloid solution was treated with microwave irradiation, sonicated and applied to the metal surface by the method of spincoating. The obtained samples were dried with a systematic increase in temperature to the temperature at which the growth of the molybdenum oxide film began, then further maintained for several hours and studied by electron microscopy and fluorescence. The obtained samples were dried with a systematic temperature increase until the beginning of the growth of the oxide film of molybdenum, with the aim of activating the growth of germinal grains, further maintained for several hours and studied by electron microscopy and fluorescence spectroscopy.

**Acknowledgements.**
This publication was prepared with the support of the “RUDN University Program 5-100”.

# DIELECTRIC PROPERTIES OF LA DOPED PMN-10PT CERAMIC

Erikas Šilobritas[1], Šarūnas Svirskas[1], Marko Vrabelj[2], Barbara Malič[2], Jūras Banys[1]

[1] Faculty of Physics, Vilnius University, Sauletekio 9/3, LT10222 Vilnius, Lithuania.
[2] Ceramics Department, Jožef Stefan Institute, Jamova cesta 39, 1000 Ljubljana, Slovenia
erikas.silobritas@ff.stud.vu.lt

Even though ferroelectric relaxors were discovered over 60 years ago the physics of their unusual characteristics remain not completely understood which leads to an ongoing investigation of their dielectric properties. Such materials have a high value of dielectric constant and a wide dielectric anomaly as well as dispersion in a wide range of frequencies. In contribution to all the research on relaxor ferroelectric materials, the dielectric spectroscopy of lanthanum doped PMN-10PT was carried out.

Silver paste electrodes were applied on both surfaces of a ceramic sample after polishing it. Then the sample was heated up to 750 K. Measurements were performed on a cooling cycle at the rate of 1 K/min in 120 – 500 K temperature range and 20 Hz – 1 GHz frequency range. Capacity and loss tangent were measured using HP-4284A impedance analyzer while the vector analyzer Agilent 8714ET was used to measure complex reflection coefficient. For measurements in temperatures below 300 K liquid nitrogen was used. The temperature was registered by either T-type thermocouple or platinum 100 Ω resistor.

Fig. 1 shows the temperature dependence of the real part of dielectric permittivity of PMN-10PT 2% La sample. The characteristics of the relaxor ferroelectric are clearly seen. The dielectric anomaly is wide and the maximum of dielectric constant shifts to higher temperature as the frequency increases. Such behavior of the dielectric constant is believed to be characterized by small (a few nanometers in size) polarized islands called the polar nanoregions (PNR), that appear upon cooling as the material transforms into the ergodic relaxor (ER) from the non-polar paraelectric (PE) phase.

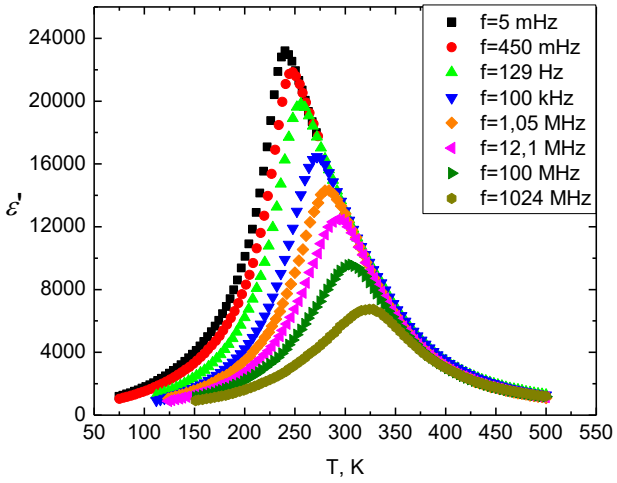


Fig. 1 Temperature dependence of the dielectric constant of PMN-10PT:2% La ceramic

# CHARACTERIZATION AND PERFORMANCE OF CoCrMo POWDER FOR ADDITIVE MANUFACTURING

Ada Steponavičiūtė[1], Andrius Šlivinskas[1], Genrik Mordas[1], Gediminas Račiukaitis[1]

[1] Department of Laser Technologies, Center for Physical Sciences and Technology, Lithuania
ada.steponaviciute@ftmc.lt

New manufacturing technologies, such as Direct Metal Laser Sintering (DMLS), allow the production of high-quality metal tools and prototypes of extremely complex geometries, but in order to achieve consistent and predictable properties and ensure high quality of 3D printed objects, the materials have to possess certain characteristics.

In this study, we analyze the characteristics of a cobalt-chrome-molybdenum-based super alloy powder by using standardized measurement methods such as scanning electron microscopy (SEM) with an energy dispersive X-ray spectrometer (EDS) (powder pictures shown in Fig. 1), X-ray diffraction (XRD), X-ray photoelectron spectroscopy (XPS), Auger electron spectroscopy and particle induced X-ray emission (PIXE).

The results of these analyses meet the powder chemical composition provided by the powder manufacturer, however individual particle chemical composition shows significant differences. The CoCrMo powder has a wide particle size distribution, most of the particles have a spherical shape with a grainy surface, but agglomerates with a smoother surface are present as well.

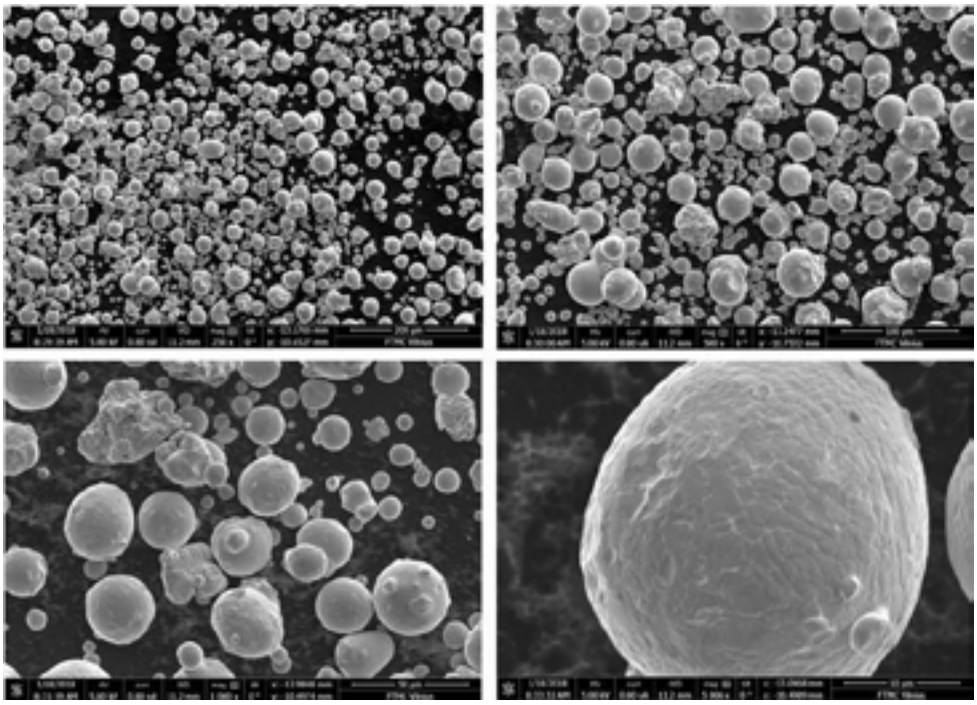

Fig. 1. SEM pictures of the CoCrMo powder

# ANALYSIS OF TRANSIENT CAVITATION ALTERATION IN SONOCHEMICALLY TREATED MG AQUEOUS SUSPENSIONS

Nadzeya Brezhneva[1,2*], Nikolai V. Dezhkunov[3], Ekaterina V. Skorb[2]

[1] Chemistry Faculty, Belarusian State University, Minsk, Belarus
[2] SCAMT Laboratory, ITMO University, Saint-Petersburg, Russia
[3] Department of Research and Development, Belarusian State University of Informatics and Radioelectronics, Minsk, Belarus

brezhNY@bsu.by

Herein, we investigated transient cavitation activity alteration in aqueous suspensions of Mg particles. The increase in the cavitation intensity can be attributed to the formation of small bubbles. The following decrease can be related with the formation of big bubbles by the coalescence of the small ones or the diffusion of the hydrogen gas that is produced during the chemical reaction of magnesium with water (Fig. 1a).

In the case of suspensions with lower concentration of Mg particles after the decrease of cavitation activity the plateau value was observed. This can be explained by the equilibrium of the formation rates of small and big bubbles. In the case of higher concentrations the cycles of enhancement/reduction in the cavitation activity were observed. Hydrogen gas – one of the products of the chemical reaction between water and magnesium – influences the formation and collapse of the cavitation bubbles. Various amounts of the released hydrogen can affect the cavitation intensity in a different way. The schematic illustration of the bubble evolution is presented in Fig. 1b. The initial bubbles of small size can grow as the result of the coalescence or rectified diffusion leading to the formation of the active size bubbles that can further either collapse and produce local areas of non-equilibrium conditions or the bigger ones that can diffuse into air [1]. The cycles of the decrease in cavitation activity can describe the process of the fragmentation of the big bubbles into the smaller ones. Due to a high diffusivity hydrogen can influence the bubble size by the possible diffusion of gas molecules into the bubbles, leading to their enlargement and the growth of the partial pressure of the gas inside the bubble making it more difficult to be collapsed by the external pressure [2].

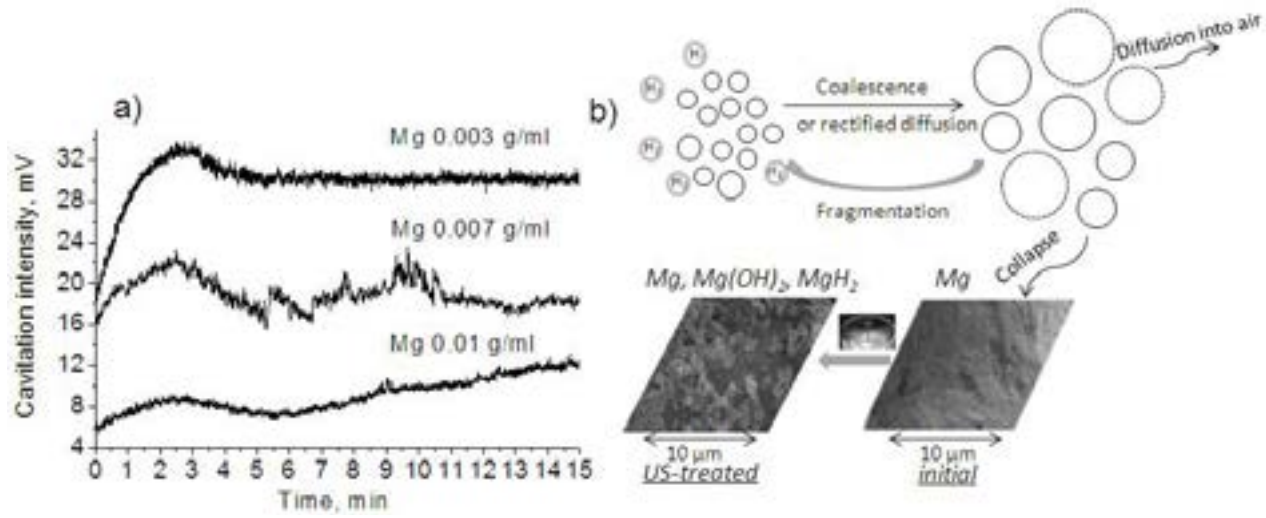


Fig. 1. Transient cavitation alteration during sonochemical treatment of Mg aqueous suspensions of different concentrations (a), scheme of the cavitation bubble evolution with the illustration of the initial particle surface and after ultrasonic (US) treatment (b).

The sonochemically treated particles are characterized by the production of porous structure on the surface of the particles and the presence of the new phases – $Mg(OH)_2$ (brucite) and $MgH_2$ which resulted from both chemical impact of water and released hydrogen and sonomechanical impact of the collapsed bubbles near the metal surface.

[1] B.-K. Kang, M.-S. Kim, S.-H. Lee et al., Effect of acoustic cavitation on dissolved gases and their characterization during megasonic cleaning, ECS Transactions **41 (5)**, 101-107 (2011).
[2] B.-K. Kang, M.-S. Kim and J.-G. Park, Effect of dissolved gases in water on acoustic cavitation and bubble growth rate in 0.83 MHz megasonic of interest to wafer cleaning, Ultrason. Sonochem. **21**, 1496-1503 (2014).

# THE INFLUENCE OF THE MAGNETIC FIELD ON THE STRUCTURE AND PHYSICAL PROPERTIES OF EPOXY COMPOSITE MATERIALS

Yuliia Bardadym [1], Edward Sporyagin [2], Oleksandr Naumenko[3]

[1] Institute of Macromolecular Chemistry of NAS of Ukraine
[2] Oles Honchar Dnipro National University
[3] Ukrainian State University of Chemical Technology
yuliia.bardadym@gmail.com

Polymer modifications are intended to impute different, typically desired properties to the new modified material properties such as enhanced thermal stability, strength, ductility, compatibility or degradability, flexibility, rigidity, melting and glass-transition temperatures etc. Physical modification is a directed change in the physical properties of polymers carried out by the transformation of their supramolecular structure under the influence of physical influences.

Physical modification is a simpler and more economical method of obtaining new materials than the synthesis of new polymers [1]. Physical modification of polymers is divided into chemical, physico-chemical and physical methods. The molecular structure of polymers change in physico-chemical modification. And only when using the physical modification the chemical composition and molecular structure are stable [2, 3]. Physical modification of polymers arises under the influence of various force fields (mechanical, electrical, magnetic, etc.) or as a result of thermal effects. The important role in the influence of magnetic field is the processes of orientation of macromolecules [4, 5].

This work is devoted to the study of the effect of external permanent magnetic field on the structure, thermophysical, dielectric properties of epoxy polymers and their composites containing metal oxides.

Samples of nanocomposites were formed from epoxy resin ED-20 and triethylenetetramine. Stoichiometric ratio was 1 mole of epoxy resin to 0,18 mole triethylenetetramine. Powder CdO, PbO and $Cr_2O_3$ were used as fillers. The content of metal oxide was 3 vol. %. Samples of nanocomposites were subjected to curing with different conditions. The influence of constant magnetic field was 2·105 A/m. All curing processes were done at 293 – 297 K for 24 hours. Then all polymeric samples were carried out temperature stabilization at 333 ± 2 K for 24 hours.

System studies of structure, thermophysical, thermomechanical and dielectric properties of composites filled with diamagnetic or paramagnetic metal oxides formed under the influence of external constant physical field were carried out for the first time. Patterns of connection between the structure and the physical and mechanical properties of epoxy composites were first established.

The introduction of inorganic filler causes the epoxy polymer to dissolution of the structure and reduces the glass transition temperature of the epoxy composite. The estimation of the influence of constant physical fields on the tangent angle of the dielectric losses of the filled composites shows that the orientation effect of constant physical fields increases the free volume of molecular chains of the chemical network of the epoxy polymer. As a result of the directed action of constant physical fields an orientation effect is observed that causes the structure and compaction of macromolecules and inorganic filler in epoxy composites to be streamlined. Also, the gel fraction of the epoxy polymer and its composites was calculated. The values are constant and range from 99,2 % to 97,98 % while the gel fraction of the polyepoxide matrix is 99,97 % to 99,3 %.

The obtained research results can be used as a scientific basis for finding optimal conditions for the formation of the structure of polymer composites filled with dispersed fillers, which will allow obtaining materials with the necessary pre-determined physical, mechanical, electrophysical and thermophysical properties.

[1] Yu. Golovin, S. Gribanovsky, D. Golovin, N. Klyachko, Towards nanomedicines of the future: remote magneto-mechanical actuation of nanomedicines by alternating magnetic fields, Journal of Controlled resease, **219**, 43 – 60 (2015).
[2] F. Cardone, G. Ferrotti, F. Frigio, Influence of polymer modification on asphalt binder dynamic and steady flow viscosities, Construction and Building Materials, **71**, 435 – 443 (2014).
[3] G. M. Su, E. Lim, A. R. Jacobs, Polymer side chain modification alters separation in ferroelectric-semiconductor polymer blends for organic memory, ACS Macro Letters, **3** (12), 1244 – 1248 (2014).
[4] J. Szajnar, M. Stawarz, T. Wrobel, Influence of electromagnetic field on pure metals and alloys structure, Journal of Achievements in Materials and Manufacturing Engineering, **34**, 95 – 102 (2009).
[5] Yu. Bardadym, E. Sporyagin, The influence of the constant physical fields on structure of polymer composites with cadmium oxide and polyaniline, 7th International Conference Nanomaterials: Application and Properties, ISBN 978-1-5386-2810-2, Ukraine, 03NNSA13-1 – 03NNSA13-4 (2017).

# INTERACTIONS OF A TWO-PHASE PLASMA FLOW WITH HEAT-SHIELDING MATERIALS

Dzmitry Nestsiarovich

A.V.Luikov Heat and Mass Transfer Institute, National Academy of Sciences of Belarus, Republic of Belarus
dmitry.nesterovith@gmail.com

It is known that heterogeneous flows affect the ablation of heat-shielding materials which strongly depends on the parameters of the dispersed phase. This is especially relevant when assessing the performance of thermal protection of rocket and space technology products both when landing descent objects on other planets, such as Mars, and when flying in the Earth's atmosphere [1]. In this regard, one of the main issues is the experimental study of the ablation of heat-shielding materials in conditions close to real. To do this, it is necessary to create heterogeneous high-temperature flows specified by thermal and aerodynamic parameters and careful control of parameters such as heat flow, deceleration pressure, velocity of gas flow and dispersed phase (particles), their size, temperature, etc.

The aim of the work is an experimental study of the interaction of a two-phase plasma flow with heat-shielding materials: fluoroplast, textolite, asbestos-textolite. We used a high enthalpy two-phase flow formed by an electric arc gas heater of a linear scheme with gas-dynamic and magnetic stabilization of an arc discharge, which makes it possible to obtain thermal and velocity flows comparable to real in laboratory conditions. As the dispersed phase, $SiO_2$ powder with a particle size of not more than 50 μm was used. The heat flux in various sections of the plasma jet was measured using uncooled regular mode sensors with an accuracy of ± 10%. Copper calorimeters of tablet type were used as heat-receiving elements, in which the temperature of the protected end was measured with a chromel-copel thermocouple. The velocity of the dispersed phase in the plasma flow was measured by the Particle Image Velocimetry (PIV) method, which allows to record «instant» spatial velocity distributions. The scheme of the experiment is shown on Fig.1.

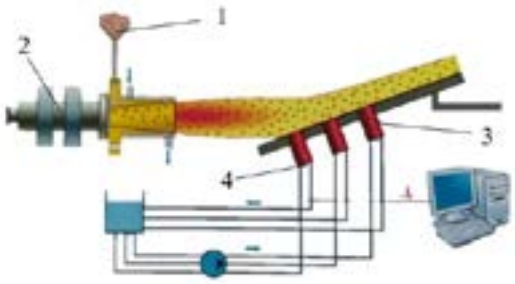


Fig.1 The scheme of the experiment, where 1 is a particle metering device, 2 is a plasma torch, 3 is a calorimeter, 4 is a thermocouple

During the experiment, for a steady subsonic mode of operation of an electric arc gas heater, the magnitude of the heat flux was obtained in different sections of the plasma homogeneous jet. The value of the heat flux on the axis of the plasma jet near its end is 200 W/cm$^2$ and monotonously decreases to 20 W/cm$^2$ at 280 mm. It is shown that the obtained value of the linear rate of destruction along the sample axis for all materials increases significantly with the introduction of dispersed $SiO_2$ particles into the homogeneous flow.

The results obtained can be used in solving practical problems related to the simulation of the phase of the entrance of a spacecraft into the atmosphere and the creation of advanced thermal insulation materials.

[1] Sauvage N., Tran P., Montois I. et al., CEA/CESTA and EADS ST Common Approach of Particles Impact Effect on Ablative Material Application to Mars Reentries, Proceedings of the 5th European Workshop on Thermal Protection Systems and Hot Structures, Noordwijk, The Netherlands, (2006).

# MONTE CARLO SIMULATIONS OF EQUILIBRIUM PHASE DIAGRAM OF FE-PT SYSTEM

Dominika Wieczorek[1], Rafał Abdank-Kozubski[1]

[1] Department of Solid State Physics, Faculty of Physisc, Astronomy and Applied Computer Science, Jagiellonian University in Cracow, Poland
dominika.wieczorek@student.uj.edu.pl

The iron - platinum system is characterized by high magnetic anisotropy, thanks to which it became the object of special interest of the technology industry as a candidate for applications in the technology of high density magnetic recording media. [1] The high surface activity and strength of Fe-Pt nanoparticles enables their potential applications in the domain of catalysis. [2] The source of these properties is the internal structure of the alloy - the existence of the $L1_0$ superstructure from low to moderately high temperatures and the presence of the "order - disorder" transition during which the superstructure is lost to a structurally disordered face centered cubic structure. [3]

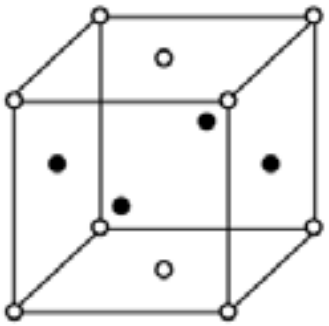

Fig. 1. $L1_0$ superstructure

Computer simulations of the atomic ordering process were carried out in the Fe-Pt system using the Monte Carlo method. The applicability of existing pair interaction parameters in this system for its modeling in a wide range of concentration has been verified by determining the order-disorder transition temperatures for three stoichiometric intermetallic compounds: $FePt_3$, FePt and $Fe_3Pt$ by simulation in a closed system using the “direct exchange” Monte Carlo algorithm. The obtained results were compared with experimental data. The moment of order – disorder transition was identified on the basis of temperature changes of the long range atomic order parameter. Then simulations of the same alloy were performed in a semi-open system using the SGCMC (Semi-Grand Canonical Monte Carlo) method to determine the stability ranges of the superstructures and to create a partial Fe-Pt equilibrium phase diagram. By determining the equilibrium configurations for systems with different platinum concentration at several given temperatures and calculating the long-range atomic order parameter for them the order - disorder transition temperatures were obtained. The results were consistent with the literature data within the limits of uncertainty of calculation.

[1] M. Muller, K. Albe, *Phys. Rev. B*, 2005, **72**, 094203.
[2] T.E. Fan, T.D. Liu, J.W. Sheng, G.F. Shao, Y.H. Wen, *J Alloy Compd*., 2016, **685**, 1008-1015.
[3] S. Brodacka, M. Kozłowski, R. Kozubski, Ch. Goyhenex, G.E. Murch, *Phys. Chem. Chem. Phys*., 2015, **17**, 28394.

# MASS TRANSFER OF T15K6 BY ELECTRIC-SPARK ALLOYNG ON TITAN ROTATION BODY

Zagonenco Vitali, Bulan Igor

JS VC plant "TOPAZ", MD-2069 Chisinau, D.Cantemir Square 1
zagonenco@topaz.md

Electric-spark alloying (ESA) is a process by which it is possible to achieve hard alloy coatings on the surface of a workpiece by transferring small portions of material from anode to cathode when plasma discharges occur. ESA is an economically advantageous process that is capable of widely changing mechanical, electrical, thermal and other properties of the workpiece depending on the selected alloying material, processing environment, pulse characteristics, electrode shape and type of tool electrode (TE).

One of the important indicators of ESA process is the transfer of material from electrode to the substrate, evaluation of the material transfer from anode to cathode is change in mass after ESA occurs. In this work we analyze changes in mass of a cylindrical shape billet of titanium alloy (GOST VT1-0) after applying on a surface hard alloy of T15K6, using two types of TE (vibrating, rotating). According to previously published papers related to the mass transfer problem between anode and cathode, it was established a relationship at which the cathode weight gain is clearly visible depending of the TE type on a flat stationary part [1]. Also, one of the problems of alloying titanium is that at the beginning of the process there is an erosion of the material occurs which disappears with increasing surface treatment time [2,3]. At the same time, the issue of applying hard alloys on rotating bodies made of titanium has not yet been reflected in scientific papers. This work was performed on the installation "TOPAZ-ESA" a lathe-like ESA machine with a system for holding the average current between the electrode and the workpiece by adjusting the interelectrode gap, when performing the work, different rotation modes of chuck with workpiece were considered, the angle at which the TE touches the workpiece as well as the speed of rotation of TE an vibrating amplitude for vibrating TE. Titanium workpiece was processed using pulse modes from 25 to 200μs with a frequency of 100,200,300 Hz.

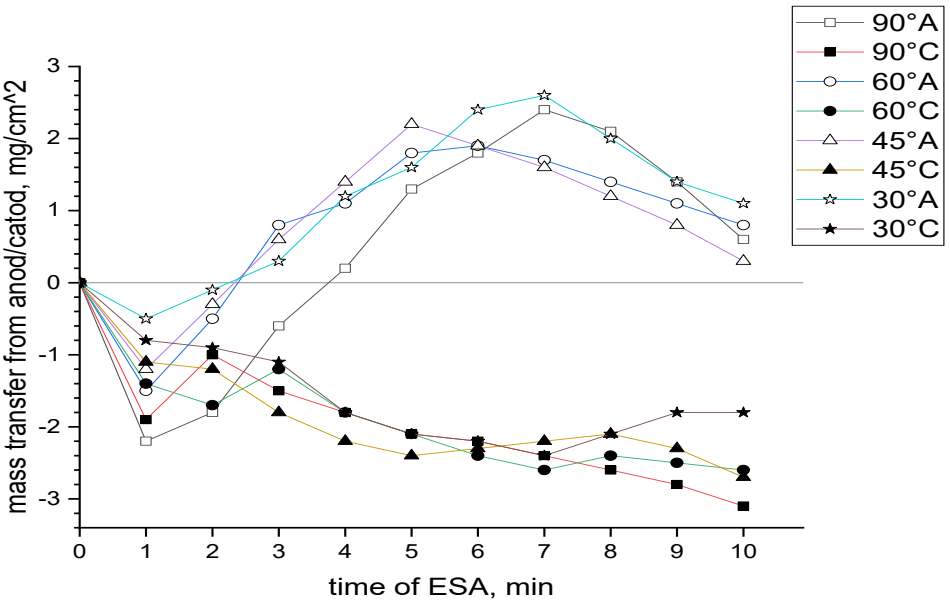


Fig.1 Mass transfer from anode/cathode at 25 μs pulse with a 100 Hz for rotating TE at different angles to the body of rotation. °

**Acknowledgments.** Authors acknowledge funding from H2020 project SMARTELECTRODES (No.778357)

[1] V.V.Mikhailov et al. Electrospark Alloying of Titanium and Its Alloys:The Physical, Technological, and Practical Aspects.Part I, Surf.Eng. & Apl.Electroch,vol.49 pp.375-395 (2013). DOI: 10.3103/S1068375513050074

[2] A.E.Kudryashov et al. On Application of Carbon-Containing Electrode Materials in Technology of Electrospark Alloying: Part 1, Surf.Eng. & Apl.Electroch,vol.54 pp.437-445 (2018). DOI: 10.3103/S1068375518050083

[3] I.V.Galinov, R.B.Luban Mass transfer trends during electrospark alloying, Surface and Coatings Technology vol 79 issue 1-3 pp 9-18 (1996)

# STRUCTURE AND MICROHARDNESS OF AlCuNiFeCr HIGH ENTROPY ALLOY REZULTED FROM MECHANICAL ALOYING AND ANNEALING

Vadim Cherniyavsky, Dmytro Hushchyk, Sergey Nakonechnyy, Alexandra Yurkova, Ihor Bilyk

National Technical University of Ukraine «Igor Sikorsky Kiev Polytechnic Institute»,
vadikv13@gmail.com; Dima94g@ukr.net; sergeynuts@gmail.com; yurkova@iff.kpi.ua; ii_bilyk@ukr.net;

Alloys traditionally have been based on a solvent element to which various solute atoms are added for improving specific properties. As a new focus on materials research and a novel alloy design concept, high entropy alloys (HEAs) have been achieved successfully and have attracted great attentions of material researchers since it was proposed in 2004 [1,2]. HEAs exhibit promising future for engineering applications due to their good thermal stability, high hardness and high strength, excellent wear resistance, as well as many other outstanding properties [1-3]. Most of multi-component HEAs were designed as equi-atomic or near equi-atomic and were mainly prepared by vacuum arc melting.

This study reports the structural evolution of equiatomic high-entropy AlNiCoFeCrTi alloy from elemental materials to metastable solid solution during mechanical alloying (MA), and further, to equilibrium phases during subsequent thermal annealing. Hardened steel vial and balls were used as a grinding media and gasoline was used as a process controlling agent. The effects of milling duration and subsequent annealing at temperature 1200 °C on the structure and phase transformation were investigated by means of Rigaku Ultima IV X-ray diffractometer (XRD) with Cu Kα radiation. A scanning electron microscope with an energy dispersive spectrometer (EDS) was used to observe microstructures and measure the elemental composition of powder alloy. Microhardness measurements were performed using a conventional microhardness machine equipped by standard Vickers' pyramid. Microhardness numbers were determined under indentation loads not higher than 1.0 N.

It was justified experimentally that MA of Al-Ni-Co-Fe-Cr-Ti powder mixture during 3 hours resulted in a single-phase nanocrystalline HEA with a structure of BCC-solid solution (Fig. 1). BCC solid solutions appear when the blended powder is ball milled for 1h. The 3h ball milled alloy powder shows excellent chemical homogeneity and refined morphology with mean particle size of less than 50 μm. The 3h ball milled microscaled particles are actually hard agglomerations of nanoscaled crystallites with crystal size of about 35 nm. The phase composition transforms to BCC and FCC solid solutions when the mechanically alloyed powder was annealed at 1200 °C for 1h, as can be seen in Fig. 2. The results of XRD analysis identify that during thermal annealing precipitation of TiC and grain growth of equilibrium phases occur. The formation of TiC is associated with the high activity of Ti, which is not completely dissolved in BCC solid solution during MA, and as a result, during annealing, Ti also reacts with carbon, which is a component of petrol, used as a process controlling agent. Simple equilibrium phases obtained in the annealed state of MA powders confirm that the high-entropy effect enhances the formation of simple solid solution phases instead of complex compound phases.



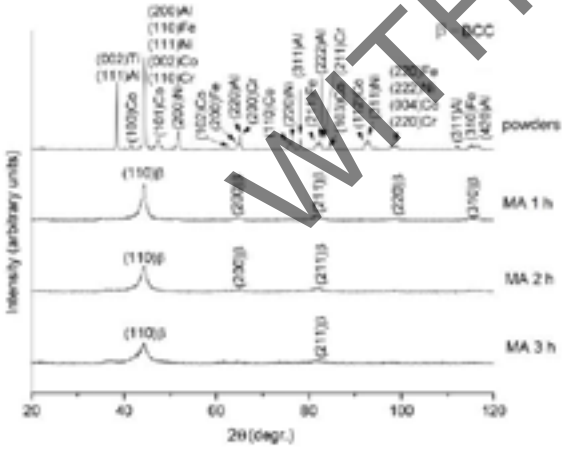


Fig. 1. XRD patterns of MA AlNiCoFeCrTi powders with different milling times

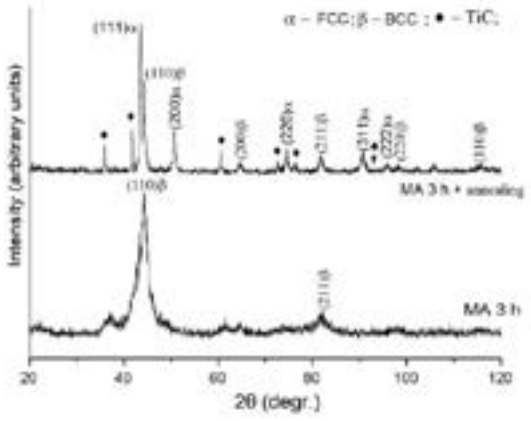


Fig. 2. XRD patterns of MA AlNiCoFeCrTi HEA powders after thermal annealing at temperatures 1200°C during 1 h

The Vickers microhardness of powder AlNiCoFeCrTi alloy after 3h of MA is 7.1±0.25 GPa.. The microhardness, HV, of 3h milled alloy powder after annealing in vacuum at 1200 °C for 1h increases and is 10.4±0.29 GPa. The high hardness could be attributed to the nanocrystalline nature of the alloy, the solid solution strengthening equiatomic nature of the phases and the presence of hard particles of carbides TiC. The very high hardness of 10 GPa prove the promising future of the alloy.

[1] High-Entropy Alloys. Fundamentals and Applications. Editors M. C. Gao , J.-W. Yeh, P. K. Liaw, Y. Zhang. Elsevier, 2015, 516 p.
[2] B.S. Murty, J.W. Yeh and S. Ranganathan. High-Entropy Alloys. Elsevier, 2014, 218 p.
[3] D.B. Miracle, O.N. Senkov. A critical review of high entropy alloys and related concepts // Acta Materialia. 122 (2017) 448-511.

# SIMULATION OF THE NEUTRON-PHYSICAL CHARACTERISTICS OF THE SUBCRITICAL ASSEMBLY YALINA-BOOSTER WITH LOW ENRICHMENT URANIUM FUEL

Valeryia Beresneva[1], Sergey Korneev[1], Tamara Korbut[1],
Maksim Kravchenko[1], Alexandr Dubrovskii[2]

[1] Scientific institution «JIPNR – Sosny», Minsk, Belarus
[2] ISEI BSU, Minsk, Belarus
vaberesneva93@gmail.com

The non-proliferation issues caused by the civilian use of highly enriched uranium (HEU) were solved by using of several international agreements, for example, Reduced Enrichment for Research and Test Reactors (RERTR) program [1], supported by the International Atomic Energy Agency (IAEA). Accordingly, efforts were made to reconstruct existing research reactors for using of low enriched uranium (LEU) and to encourage the usage of LEU in the development of new research reactors and other nuclear facilities, such as subcritical systems driving by external source (Accelerator driven system or ADS). ADS systems are considered as promising for energy production and transmutation of long-lived fission products and minor actinides. The study of the processes occurring in ADS systems with low enrichment uranium fuel is of high interest in the development of projects for innovative installations.

The controlled by external sources subcritical assembly Yalina-Booster [2] (Scientific Institution JIPNR-Sosny) makes it possible to study the neutron-physical characteristics and parameters of breeding media with fast and thermal neutron spectra with subcriticality levels of keff $\leq$ 0.975. Neutron-physical characteristics that can be measured in the ADS system can also be calculated by using modern simulation programs based on the Monte Carlo method.

In this paper a methodology for simulation of the neutron-physical characteristics of the subcritical assembly Yalina-Booster with low enrichment uranium fuel is developed by using the MCNP4B program implementing the Monte-Carlo method. The following characteristics of the Yalina-Booster with low enrichment uranium fuel and controlled by a neutron generator were calculated: an effective neutron multiplication factor at different stages of assembly loading, neutron spectra in experimental channels, reaction rates on a set of neutron activation detectors of various sizes, reaction rates of radiation capture of neutron on $Np^{237}$, $Am^{243}$ and $I^{129}$.

It was conducted a comparison of characteristics that were both calculated and obtained experimentally.

It is planned a further refine of the model and determination of the influencing factors in order to reduce the difference between the calculated and experimental values, which will improve the experiment planning procedure.

[1] The Reduced Enrichment for Research and Test Reactors (RERTR) Program [Electronic resource]. – Mode of access: https://www.rertr.anl.gov/. – Date of access: 30.01.2019.

[2] Gohar, Y. Smith, D. L. et al., YALINA Facility A Sub-Critical Accelerator-Driven System (ADS) for Nuclear-Energy Research Facility Description and an Overview of the Research Program (1997-2008), Report of Argonne National Laboratory (United States). Funding organisation: USDOE Office of Nuclear Energy, Science and Technology (United States).

# THEORETICAL INSIGHTS INTO GEOMETRIC STRUCTURES AND SPECTRAL PROPERTIES OF SOME ADAMANTANE DERIVATIVES

Darya Meniailava[1], Ulada Vysotskaya[1], Anna Matsukovich[2], Maksim Shundalau[1]

[1] Faculty of Physics, Belarusian State University, Belarus
[2] B.I. Stepanov Institute of Physics, National Academy of Science of Belarus, Belarus
meniailava@bsu.by

The adamantyl moiety was recognized as an essential fragment in various pharmacologically-active drugs. Adamantane derivatives possess antiviral activity against Influenza A virus and HIV, as well as, anti-microbial, anti-inflammatory and anti-proliferative activities. It is also known that adamantyl group changes the properties of known drugs or provides an important pharmacophore for the design of new drugs [1].

Nowadays, the modern quantum-chemical methods are high-reliable tools to establish the molecular structure of organic compounds. In its turn a high accuracy of the structural predictions is a prerequisite for the adequate simulation of the chemical and physical (i.e. optical) properties.

In this study, the structures (Fig. 1) and spectral properties (IR, Raman, UV/Vis and circular dichroism spectra) of four adamantane-based derivatives, namely ethyl 4-{[3-(adamantan-1-yl)-4-phenyl-5-sulfanylidene-4,5-dihydro-1*H*-1,2,4-triazol-1-yl]methyl}piperazine-1-carboxylate (compound **I**), (*Z*)-3-(adamantan-1-yl)-1-(3-chlorophenyl)-*S*-benzyl-isothiourea (compound **II**), *N*-(adamantan-1-yl)-4-phenylpiperazine-1-carbothioamide (compound **III**), 1-(adamantan-1-yl)-3-(3-chlorophenyl)thiourea (compound **IV**) have been obtained at the DFT (B3LYP/cc-pVTZ) and Multi-Reference Perturbation Theory (SA-CASSCF/XMCQDPT2 [2]) levels of theory calculations.

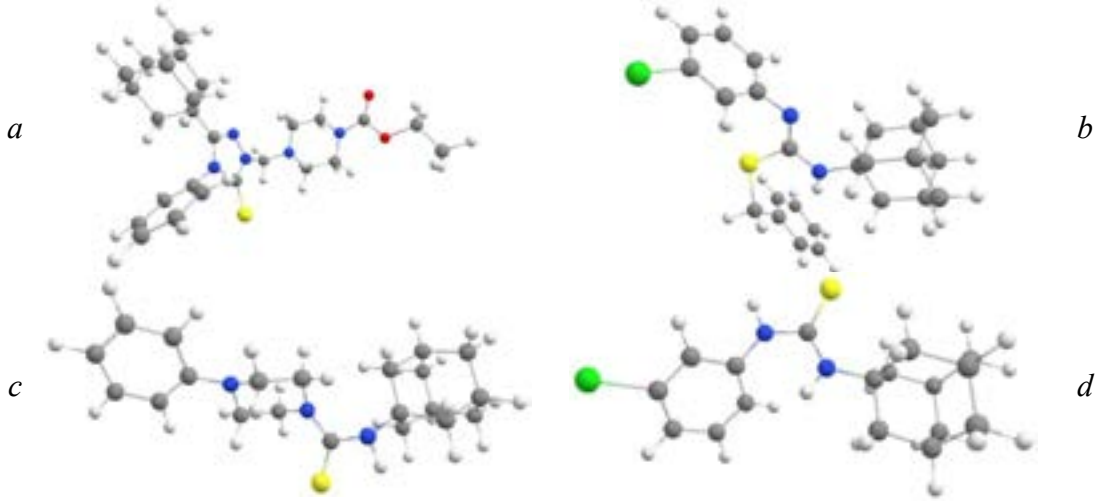


Fig. 1. Equilibrium structures of the compounds under consideration: **I** (*a*), **II** (*b*), **III** (*c*), **IV** (*d*).

Firstly, conformation analysis has been carried out for the all compounds. We found two (compound **I**), three (**II**), two (**III**) and four (**IV**) stable conformers.

The FT-IR spectra of the compounds for the crystalline phase have been measured in the range of 3200–650 $cm^{-1}$ in the reflection mode. The Raman scattering spectra of the compounds also for the crystalline phase have been measured in the range of 3200–150 $cm^{-1}$ using a compact solid-state Nd:YAG laser (second harmonic, 532 nm wavelength). Then the vibrational IR and Raman spectra were calculated and the experimental spectra were interpreted using the results of our calculations.

The UV/Vis spectra of solution of the compounds in ethanol were measured in the range of 450–200 nm. The UV/Vis spectra simulations at the Time-Dependent DFT and Multi-Reference Perturbation Theory levels of theory demonstrate unsuitability of the TDDFT for description of the experimental spectra of the compounds. It is highly probable that this is a consequence of the intramolecular charge transfer (ICT). In contrast, the MRPT results are in a good agreement with the experimental spectra.

The functional groups of the compounds having donor and acceptor properties and taking part in ITC have been determined on the basis of Mulliken and Löwdin atomic populations analysis.

This work was supported by Belarusian Republican Foundation for Fundamental Research (project No. F18MS-046).

[1] G. Ali Mansoori, P.L. Barros de Araujo, E. Silvano de Araujo. Diamondoid Molecules: With Applications in Biomedicine, Materials Science, Nanotechnology & Petroleum Science, Hackensack, World Scientific Publishing, 2012.
[2] A.A. Granovsky. Extended multi-configuration quasi-degenerate perturbation theory: the new approach to multi-state multi-reference perturbation theory. J. Chem. Phys. **134**, 214113 (2011).

# *AB INITIO* MULTI-REFERENCE PERTURBATION THEORY STUDY ON THE LiRb MOLECULE

Pavel Chareichyk, Darya Meniailava, Maksim Shundalau

Faculty of Physics, Belarusian State University, Belarus
pavel.gromov.1998@mail.ru

Cold and ultracold polar molecules offer prospects for the realization of new forms of quantum matter with possible applications to quantum information and to precision measurements [1]. One of the possibilities of obtaining of molecular quantum matter with controlled properties is the transferring of the polar diatomic molecules to the ground rovibronic state by initial optical excitation into the overlying rovibronic states with specific forms of electronic terms. In this case for the high efficiency of excitation and subsequent relaxation of the molecular system it is required knowledge of the exact forms of the potential energy curves (PECs) of the combining electronic states. The construction of exact empirical terms is performed on the basis of the analysis and interpretation of high-resolution rovibronic spectra, and may be based on *ab initio* potential curves. The knowledge of the exact PECs also allows to define the important spectra-energetic characteristics of molecules and the macroscopic physical properties of rarefied gases. So within the framework of the Chapman-Enskog kinetic theory of gases [2], it is possible to obtain important transport properties, for example, coefficients of diffusion, viscosity, thermal conductivity, etc., of gases and liquids.

The diatomic polar molecule LiRb is a typical example of the above-mentioned compounds. In this study, the SA-CASSCF(4,10)/XMCQDPT2 [3] calculations of the low-lying singlet and triplet states of the LiRb molecule performed (Fig. 1). The calculations were carried out in two stages in the wide range of internuclear distances taking into account static and dynamic part of correlation energy. The TZ-basis sets and Stuttgart RSC ECP (for Rb atom) have been used in calculations. The results of our calculations of the spectroscopic parameters of the LiRb's ground state $X^1\Sigma^+$ ($R_e$ = 3.4508 Å, $D_e$ = 5926.7 cm$^{-1}$,) very well agree with experimental data ($R_e$ = 3.4661 Å, $D_e$ = 5927.9 cm$^{-1}$ [4]). This is the best agreement among all previously performed for LiRb molecule *ab initio* calculations.

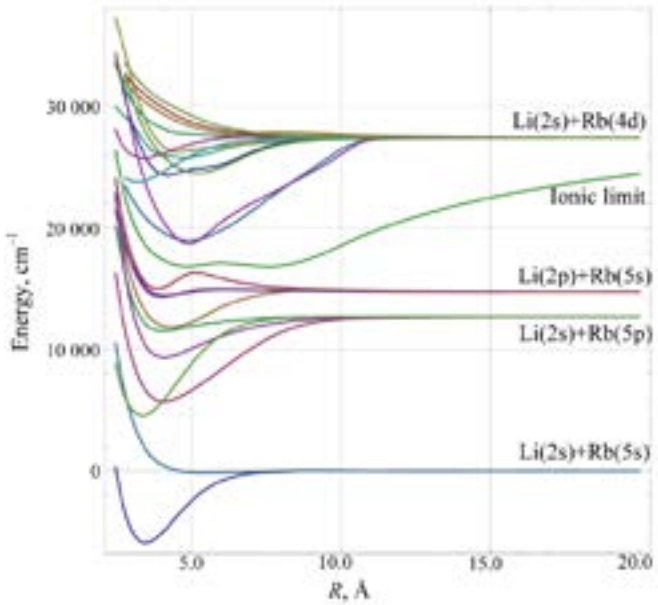


Fig. 1. The low-lying singlet and triplet states of the LiRb at the CASSCF(4,10)/XMCQDPT2 level of theory.

On the basis of the kinetic theory of gases and calculated potential for the ground state the transport properties of a diluted two-component Li-Rb gas were defined. At first stage the extrapolation of PEC into the region of small internuclear distances was made. Then consequent calculations of distance of the closest approach, the angle of deflection and the collisional cross-section were performed to evaluate the reduced collision integrals, through which coefficients of diffusion, viscosity and thermal conductivity are determined. These transport properties are obtained as functions of pressure and temperature.

This work was supported by State Committee on Science and Technology of the Republic of Belarus.

[1] O. Dulieu, C. Gabbanini, The formation and interactions of cold and ultracold molecules: new challenges for interdisciplinary physics, Rep. Prog. Phys. **72**, 086401 (2009).
[2] O. Hirschfelder, C.F. Curtiss, R.B. Bird, *Molecular theory of gases and liquids* (Wiley, New York; Chapman Hall, London, 1954).
[3] A.A. Granovsky, Extended multi-configuration quasi-degenerate perturbation theory: the new approach to multi-state multi-reference perturbation theory, J. Chem. Phys. **134**, 214113 (2011).
[4] M. Ivanova, A. Stein, A. Pashov, H. Knöckel, E. Tiemann, The $X^1\Sigma^+$ state of LiRb studied by Fourier-transform spectroscopy, J. Chem. Phys. **134**, 024321 (2011).

# THE LOW-LYING ELECTRONIC STATES OF KCs MOLECULE AND TRANSPORT PROPERTIES OF K AND Cs MEDIA

Tatsiana Puliak, Darya Meniailava, Maksim Shundalau

Faculty of Physics, Belarusian State University, Belarus
pulyak.tanya@gmail.com

The production of ultracold assemblies of alkali metal atoms and diatomic molecules containing such atoms has become a topical and rapidly developing direction in molecular and optical physics. Unlike atoms, molecules have more degrees of freedom, which gives the unique properties and the ability to manipulate them for using in various fields: creation of a Bose-Einstein condensate and subsequent studying of a new type of matter; quantum information processing by capturing such molecules into optical and magnetic traps, testing fundamental laws of physics by precision spectroscopy measurements; in controlled chemical reactions; investigating dynamics of low-energy collisions and etc. [1]. For the applications mentioned one needs to produce such molecules in the absolute ground state. So the knowledge about the ground and low-lying electronic states, spectral and other properties of ultracold diatomic molecules are crucial for potential use, which can be obtained by series of experiments or by performing *ab initio* quantum-chemical calculations and applying appropriate molecular theories. The diatomic polar KCs molecule is a typical example of ulracold molecules under comprehensive study.

The main goals of this study are prediction of the ground state potential energy curve (PEC) of the KCs molecule within spectroscopic accuracy (i) and calculation of the transport properties (coefficients of diffusion, viscosity, thermal conductivity) of the rarefied potassium and cesium gas media on the basis of calculated PEC (ii).

In this study, the SA-CASSCF(6,8)/XMCQDPT2 [2] calculations of the ground $X^1\Sigma^+$ and first triplet $a^3\Sigma^+$ states of the KCs molecule are performed (Fig. 1). The TZ-basis sets and Stuttgart RSC ECPs have been used in calculations. The results of our calculations of the spectroscopic parameters of the KCs's ground state $X^1\Sigma^+$ ($R_e$ = 4.2781 Å, $D_e$= 4070.3 cm$^{-1}$) very well coincide with experimental data ($R_e$ = 4.2838 Å, $D_e$=4069.2 cm$^{-1}$ [3]). This is the best agreement among all previously performed for KCs molecule *ab initio* calculations.

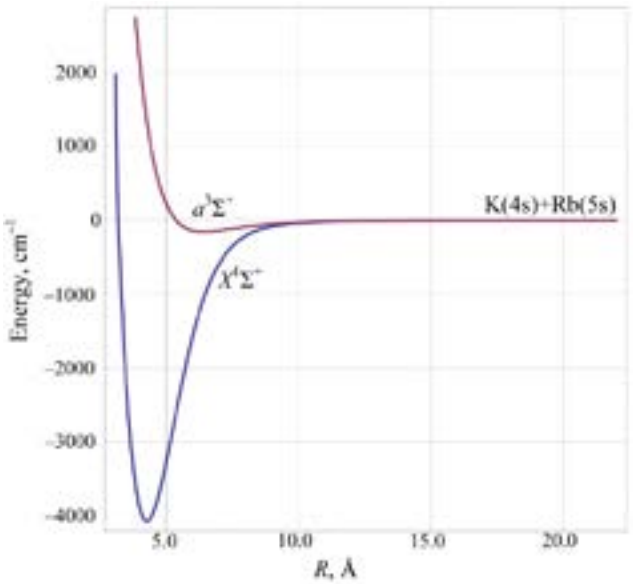


Fig. 1. The PECs of the ground $X^1\Sigma^+$ and first triplet $a^3\Sigma^+$ states of the KCs molecule at the CASSCF(6,8)/XMCQDPT2 level of theory.

On the basis of the kinetic theory of gases [4] the transport properties of a rarefied two-component K-Cs gas were calculated. These properties are uniquely related to the reduced collision integrals, which were obtained by calculating the distance of the closest approach of the particles involved in the collision, the angle of deflection and the collisional cross-section. Since the integration is carried out in the region of positive values of the potential, thus an extrapolation by the corresponding function into the region of small internuclear distances was carried out. The obtained coefficients depending on temperature and pressure are being planned to compare with experimental values.

This work was supported by State Committee on Science and Technology of the Republic of Belarus.

[1] L. D. Carr, D. DeMille, R.V. Krems, J. Ye, Cold and ultracold molecules: science, technology and applications, New J. Phys. **11**, 055049 (2009).
[2] A.A. Granovsky, Extended multi-configuration quasi-degenerate perturbation theory: the new approach to multi-state multi-reference perturbation theory, J. Chem. Phys. **134**, 214113 (2011).
[3] R. Ferber, I. Klincare, O. Nikolayeva, M. Tamanis, H. Knöckel, E. Tiemann, A. Pashov, $X^1\Sigma^+$ and $a^3\Sigma^+$ states of the atom pair K+Cs studied by Fourier-transform spectroscopy, Phys. Rev. A **80**, 062501 (2009).
[4] O. Hirschfelder, C.F. Curtiss, R.B. Bird, *Molecular theory of gases and liquids* (Wiley, New York; Chapman Hall, London, 1954).

# CONFORMATIONAL ANALYSIS AND ELECTRONIC STRUCTURE OF *N*'-(ADAMANTAN-2-YLIDENE)-LINKED CARBOHYDRAZIDES: DFT AND *AB INITIO* MULTI-REFERENCE STUDIES

Darya Meniailava[1], Aliaksandr Ruskikh[1], Anna Matsukovich[2], Maksim Shundalau[1]

[1] Faculty of Physics, Belarusian State University, Belarus
[2] B.I. Stepanov Institute of Physics, National Academy of Science of Belarus, Belarus
sash.rus787@gmail.com

The compounds from the diamondoids family (including adamantane as a simple diamondoid) and their derivatives have long been known as the good candidates for drug design, drug delivery and drug targeting. The incorporation of an adamantyl moiety into organic compounds modulates their biological activities due to increase of the lipophilicity, which is promoting transport through biological membranes [1].

In this study, the structures of four adamantane-based derivatives, namely *N*'-(adamantan-2-ylidene)-R-hydrazides (where R = thiophene-2-carbo-, adamantan-1-, benzo-, and pyridine-5-) have been obtained at the DFT level of theory (B3LYP/cc-pVTZ) calculations. All of them demonstrate existence of four stable conformers (Fig. 1): two "regular" *trans*- and *cis*-conformers (for C=O and N–H bonds) and two "side" *trans*-conformers, which correspond to left and right positions of the adamantyl moiety relatively molecular "frame" (i.e. rotation around N–N bond). It is assumed that for the crystalline phase an "open" configuration of the chain of the "regular" *trans*-isomers is more favorable. In this case each of the *trans*-isomers connects with two (or more) of its neighbors. Note that in crystalline phase "side" conformers do not exist due to steric distortions. In contrast, for solutions all above-mentioned conformers can exist. It is also worth mentioning that "side" conformers are typical only for adamantane-containing compounds, because calculations of the model structures without adamantyl group did not confirm the stability of the "side" conformers.

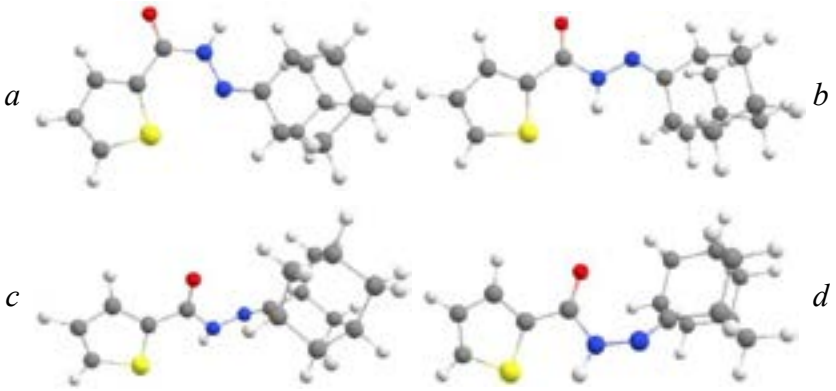


Fig. 1. *Cis*- (*a*), *trans*- (*b*), *trans*-left- (*c*), and *trans*-right- (*d*) conformers of *N*'-(adamantan-2-ylidene)-thiophene-2-carbohydrazide.

The structure of the title molecules allows one to classify their as molecular systems that may exhibit the intramolecular charge transfer (ICT). Then *ab initio* multi-reference SA-CASSCF/XMCQDPT2 [2] calculations for all conformers of all compounds were performed using cc-pVTZ basis set. Firstly the CASSCF calculations with state-averaged procedure were done for singlets and triplets. The active space comprises 4 electrons and 6-8 orbitals. Finally the calculations for singlets were performed at the XMCQDPT2 [2] level of theory.

The "side" conformers exhibit the more long-wave $S_1 \leftarrow S_0$ transitions than "central" ones. The differences in the values of the excitation energy for the "side" and "central" conformers may be caused by different positions of the adamantyl moiety relative to the molecular "frame", leading to the differences in the values of the transition moments and their orientations relative to the molecular coordinate axes. Such regularities find confirmation in the UV/Vis spectra of the solutions of compounds under consideration in ethanol. Analysis of the Mulliken and Löwdin populations shows that long-wave transitions are related with partial charge transfer. For example, in *N*'-(adamantan-2-ylidene)-pyridine-5-hydrazide ITC occurs from N atom to neighbor C atom in pyridine ring.

In continuation to our interest in the pharmacological and structural properties of the adamantane derivatives, the coexistence of all conformers should be taken into consideration when studying the pharmaceutical properties of such compounds and it may be useful in medicinal chemistry and for a drugs design.

This work was supported by Belarusian Republican Foundation for Fundamental Research (project No. F18MS-046).

[1] G. Ali Mansoori, P.L. Barros de Araujo, E. Silvano de Araujo. Diamondoid Molecules: With Applications in Biomedicine, Materials Science, Nanotechnology & Petroleum Science, Hackensack, World Scientific Publishing, 2012.
[2] A.A. Granovsky. Extended multi-configuration quasi-degenerate perturbation theory: the new approach to multi-state multi-reference perturbation theory. J. Chem. Phys. **134**, 214113 (2011).

# TEMPERATURE DEPENDENCE OF THE ETHANOL TORSIONAL SPECTRUM

Victoria Zheltok[1], Ekaterina Kozlovskaya[1], Alex Malevich[1], Goerge Pitsevich[1], Valdas Sablinskas[2]

[1] Belarusian State University, Minsk, Belarus
[2]Vilnius University, Vilnius, Lithuania
zheltokvika@gmail.com

Ethanol molecules are interesting objects to be investigated. In particular, because of the formation of the intermolecular hydrogen bonds, they are forming clusters, they exist in the form of two conformers and their energy is only 40 $cm^{-1}$ apart. Besides, there are two internal rotors in the ethanol molecule. Ethanol molecule torsion spectra were registered both at the room temperature and at the low temperature in the matrix isolation. Thus, it is of interest to calculate the ethanol molecule torsion spectra at the different temperatures. The energy of torsion states was calculated at the B3LYP-D3/acc-pVQZ level of theory. Simultaneously, 2D surface of the dipole momentum and partition function for different temperatures were calculated. Lorentz contours with the half-width equals to 1 $cm^{-1}$ were used for the modeling of the torsion IR spectra. Fig. 1 and 2 are presenting the calculated torsion IR spectra of the ethanol at T= 300 K (Fig.1) and T=20 K (Fig.2).

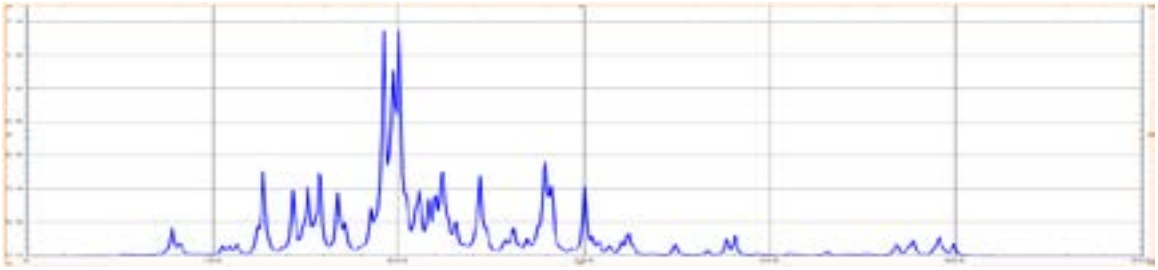

Fig.1. Calculated torsion spectrum of the ethanol molecule at T=300 K.

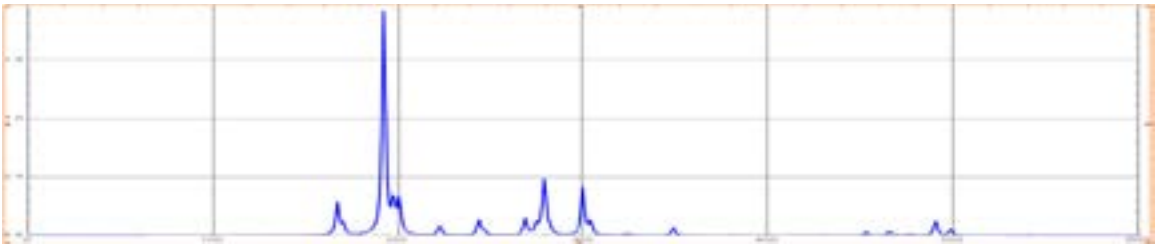

Fig.2. Calculated torsion spectrum of the ethanol molecule at T=20 K.

During the calculations of the ethanol low temperature torsion spectrum, the fact that gosh- and trans- conformers of the molecule are separated with significant potential barriers and, therefore, even at low temperatures the number of gosh-conformers are twice as big as the number of trans- conformers, was taken into account. Comparison of the Fig. 1 and 2 leads to the conclusion that with the decreasing of the temperature, torsion spectrum of the ethanol molecule become significantly less complicated. It is obvious that torsion spectrum of the ethanol molecule in matrix isolation should be compared to the spectrum, presented in the Fig. 2, and gas phase spectrum – with the spectrum from the Fig. 1.

# THE DEVELOPMENT OF ULTRASONIC ADAPTIVE METHOD FOR INSPECTION OF OBJECTS WITH COMPLEX GEOMETRY

Tautvydas Fyleris, Elena Jasiūnienė

Kaunas University of Technology, Kaunas, Lithuania
tautvydas.fyleris@ktu.edu

When various objects go through operating conditions such as stress, temperature changes, vibrations sooner or later defects such as cracks develop which will eventually cause structural failure. For the avoidance of catastrophe, objects have to be inspected periodically. It can be achieved with various inspection methods such as x-rays or ultrasonic inspection[1]. The examination method usually depends on budget and how critical structure is. Relative cheap method is ultrasonic inspection with phased arrays, because of transducer array structure is possible to change focus point electronically or in physical terms is a sound energy accumulation for chosen area with purpose to listen to stronger echo, it is an actual problem with bent object because of refraction it can form areas where very little energy is delivered. With the processing of echo signals is possible to decide the structure condition and even to map its interior.

The main aim of ultrasonic inspection is to effective transfer energy into the designated point for the purpose to be reflected in order to interpret it correctly. For this reason, acoustic paths must be modeled or calculated explicitly, when a surface structure is known beforehand there are readily prepared methods, but if there no such information then the surface needs to be determined and is an active research problem. It can be solved using the similar ultrasonic methods as for inspection, albeit usually, algorithms assumes defects are point scatters. After surface determination, collected information need to be used for further processing. It can be done by aligning (delaying) signals[2] and doing some mathematical operation for example summing, correlation or other, this operation commonly is called synthetic aperture focusing (SAFT) classical focusing in the time domain can be expressed following:

$$y(k) = \sum_{i=1}^{M} x_i(\delta_{k,i}) \tag{1}$$

Here $y(k)$ – region intensity, $M$ – active aperture (recorded elements), $x_i$ – recorded signal, $\delta_{k,i}$ – a signal model for point $k$. The focusing work by assumption if there is a response from object boundary or defect signals will make constructive interference if there no response they will create noise or cancel each other. There are already done much research for path calculation when there are direct visibility, or object surface boundary is a straight line, but solving imaging problem with curved surfaces is not a trivial problem[3]. Primary, the constraint is storage space and time, for example using 128 channel transducer with 10000 samples of data and firing element sequentially; then collecting data can reach in gigabytes storage space, of course, it can be reduced using plane wave imaging. Plane wave imaging is technique when all transducer element is firing same time; it reduces collected data. The secondary goal is to reduce processing time, even using powerful GPU it will take minutes to make a complete inspection image. For example graphically problem and solution can be shown in the following figure:

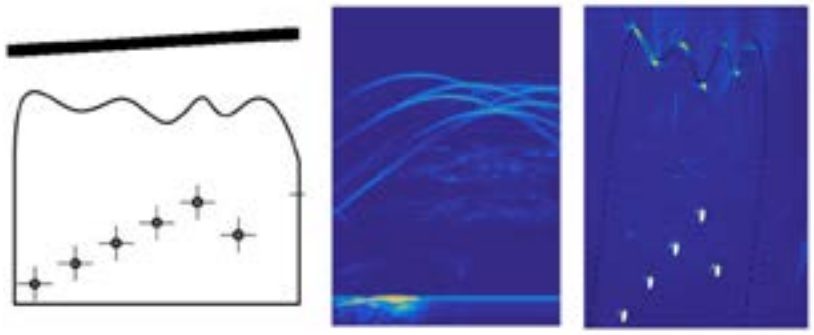

Fig. 1. Adaptive inspection method graphical representation: left image: imersed object with defects and transducer above , with bent surfaces; middle, shows a surface response and internal echoes, right showing developed method with reconstructed defects (dash line is the theoretical model)

In this work, we develop an effective methodology for inspection curved objects in various conditions such as noisy environment or not ideal transducer and object position knowledge.

[1] B. W. Drinkwater a/ac P. D. Wilcox, 'Ultrasonic arrays for non-destructive evaluation: A review', *NDT & E International*, rhif. 39, rhif. 7, tt. 525–541, Hyd. 2006.

[2] G. Matrone, A. S. Savoia, G. Caliano, a/ac G. Magenes, 'Ultrasound plane-wave imaging with delay multiply and sum beamforming and coherent compounding', yn *2016 38th Annual International Conference of the IEEE Engineering in Medicine and Biology Society (EMBC)*, 2016, tt. 3223–3226.

[3] E. Hoyle, M. Sutcliffe, P. Charlton, a/ac J. Rees, 'Virtual source aperture imaging with auto-focusing of unknown complex geometry through dual layered media', *NDT & E International*, rhif. 98, tt. 55–62, Med. 2018.

# MICRO-LITER LIQUID HANDLING SYSTEM DESIGN AND APPLICATIONS

Tomas Drevinskas[1], Audrius Maruška[1], Mihkel Kaljurand[2,1]

[1]Instrumental Analysis Open Access Centre, Faculty of Natural Sciences, Vytautas Magnus University, Vileikos 8, LT44404 Kaunas, Lithuania
[2]Department of Chemistry, Faculty of Sciences, Tallinn University of Technology, Akadeemia tee 15, 12618 Tallinn, Estonia
tomas.drevinskas@vdu.lt

Current trend in analytical chemistry is miniaturization and integration. Miniaturized instruments are not as interesting and important as their possibility to integrate them into autonomous vehicles and rovers. Autonomized systems provide numerous advantages over conventional stationary laboratory analytical instrumentation. Greatest advantage is that on the site sampling and analysis reduces errors due to sample transportation and makes analytical process faster. What is more important, if hazardous sites, such as chemical warfare usage cases, or remote savage areas are investigated, the threat to human researcher is not posed.

In this work we present micro-liter handling system that precisely supplies required liquid using silica capillary from the required bottle of reagent. The system can be operated from the battery (or AC power supply for laboratory operations). The system is intended for use with autonomous capillary electrophoresis, miniaturized colorimeters, or digital-droplet microfluidic systems [1–3].

The system was tested with various inner diameter capillaries for supplying different volumes of required chemical reagents. Design and application issues will be presented and discussed during the conference.

Acknowledgement. This research was funded by a grant (Nr. 09.3.3-LMT-K-712-02-0202) from the Research Council of Lithuania.

[1] T. Drevinskas, L. Telksnys, A. Maruška, J. Gorbatsova, M. Kaljurand, Compensation of the baseline temperature fluctuations for autonomous CE-C4D instrument working in harsh environments, Electrophoresis. (2018). doi:10.1002/elps.201800132.

[2] T. Drevinskas, A. Maruška, E. Gladkauskas, L. Telksnys, V. Girdauskas, J. Gorbatsova, M. Kaljurand, O. Ragažinskienė, Design and Applications of Miniaturized, Portable LED Based Colorimeter, Chemija. 4 (2018) 1–8 Accepted for publication.

[3] J. Gorbatsova, M. Jaanus, M. Vaher, M. Kaljurand, Digital microfluidics platform for interfacing solid-liquid extraction column with portable capillary electropherograph for analysis of soil amino acids, Electrophoresis. 37 (2016) 472–475. doi:10.1002/elps.201500284.

# LED-BASED MICRO COLORIMETER FOR DETERMINATION OF PHENOLIC COMPOUNDS

Kotryna Drungilaitė[1], Tomas Drevinskas[1,2], Audrius Maruška[1], Gorbatsova[2], Mihkel Kaljurand[2]

[1]Instrumental Analysis Open Access Centre, Faculty of Natural Sciences, Vytautas Magnus University, Vileikos 8, LT44404 Kaunas, Lithuania

[2]Department of Chemistry, Faculty of Sciences, Tallinn University of Technology, Akadeemia tee 15, 12618 Tallinn, Estonia

Kotryna.drungilaite@stud.vdu.lt

Autonomous and miniaturized analytical instruments are very important in today's science. Though, this approach has several obstacles, therefore the design of such instrumentation and applications are difficult. In this work we propose an improved micro colorimetry system that provides comparable results to the existing on the market instrumentation, except the fact that proposed system can measure micro-liter volume samples. By shaping initial micro colorimeter design, several novelties have been introduced that autonomize the operation of the device: upgraded LED's holder with a current controller for wide range measurements and system upgraded, so that absorbance values are provided.

The determination of total phenolic compounds was performed using Folin - Ciocalteu method. Rutin standard solution in the range of 0.01 and 1 mg/ml were used for the calibration and for comparing measurement results with Milton Roy Spectronic 1001 (USA) spectrophotometer. The obtained data proves that linear dependency between concentration of measured samples and absorbance can be obtained using different modes of operation.

The device was optimized for the determination of TPC in a 15 µl droplet and the LED light intensity was adjusted for optimal operation. In the further investigation, this technology will be integrated into the digital-droplet microfluidics platform. During this presentation, obtained results and the obstacles associated with design of the instrument will be discussed.

Acknowledgement. This research was funded by a grant (Nr. 09.3.3-LMT-K-712-02-0202) from the Research Council of Lithuania.

# MODERN METHOD BY NMR $^1$H SPECTROSCOPY FOR THE IDENTIFICATION OF FATTY ACIDS IN TEKHNOKONTROL INOPERATIVE PRODUCTION

Inna Hutsalo[1], Julia Korobka[1], Maksim Pashkevich[1]

National University of Food Technologies, Kyiv, Ukraine
hutsaloiv@ukr.net

The most important condition of production high-quality peanut butter is conducting fundamental research properties of raw materials and products from it. Production of high-quality oil products are possible on a strict basis compliance with technical and technological regulations, recipes, sanitary hygiene norms and rules and implementation multi-parametric monitoring of indicators of quality of raw materials and finished products. The technological and nutritional value of sunflower oil is determined by esters of oleic (Omega-9) and linoleic (Omega-6) acids. Sunflower oil with a high content of oleic acid (Omega-9) and a sufficiently low content of polyunsaturated lenoleic acid (Omega-6) is characterized by a lower nutritional value but greater chemical stability at high temperatures and in the presence of oxidizing agents. Therefore, that type of oil, especially refined, is more suitable for high temperature processing of food and can be stored longer saving its properties. The purpose of this work was to study the TAG composition of sunflower oil samples by $^1$H-NMR spectroscopy [1, 2]. The interpretation of the spectral data by the different authors' reports is different, so there are no valid reliable characteristics that could be relied on.

This method based on estimation and comparison the proton integral intensities of allyl and diallyl $CH_2$ groups with intensity of glycerol protons in $^1$H-NMR spectra that allows determining the amounts of each of these unsaturated fatty acids.

Integral intensities hydrogens can be compared with intensity of the tertiary hydrogen in the glycerin moiety ($H_g$). That allows making a conclusion about fatty acids composition of the oil samples.

The oil samples were solved in deuterated chloroform. The spectra of prepared solutions were recorded on a Varian VXR-300 spectrometr (300 MHz). Despite the fact that the data obtained do not allow the exact integration of the tertiary hydrogen of the Hg of the glycerol moiety, it is possible to determine the quantitive ratio of oleic and linoleic esters based on the comparison of integral intensities of typical signals. The proton resonances of the TAG acyl chains were assigned according to the literature data [3, 4].

Data on the content of oleic (Omega-9) and linoleic (Omega-6) acids in sunflower oil of domestic brands and, for comparison, data on fatty acids composition of olive oil and High-oleic oil obtained as a result of analysis of their spectra, are represented in Table 1.



| | | Oleic/linoleic acids ratio | Percentage, % | |
|---|---|---|---|---|
| | | | Oleic acid | Linoleic acid |
| 1 | Chumak | 1:2 | 32.06 | 63.64 |
| 2 | Maslinka | 5:7 | 40.05 | 55.65 |
| 3 | Shchedriy Dar | 5:7 | 40.05 | 55.65 |
| 4 | Oleyna | 1:1 | 48.03 | 47.67 |
| 5 | Olive oil | 9:1 | 86.19 | 9.51 |
| 6 | High-oleic oil | 200:1 | 95.23 | 0.47 |

Table 1. Data on the content of fatty acids in the sunflower oil samples

The method can be used to determine the wanted components over a wide range of concentrations for the analysis of numerous samples. It is shown the highest content of oleic acid and the lowest content of linoleic acid among the oil sample of domestic brand are found in the oil «Oleyna». Therefore, that oil is the most suitable to be used for high temperature processing of food.

[1] G. Vlahov, Application of NMR to the Study of Olive Oils. Prog. Nucl. Magn. Reson. Spectrosc. 1999, 35, 341–357.
[2] L. Mannina, C. Luchinat, M. Patumi, M. Emanuele, E. Rossi, A. Segre, Concentration. Dependence of 13C-NMR Spectra of Triglycerides: Implications for the NMR Analysis of Olive Oil. Magn. Reson. Chem. 2000, 38, 886–890.
[3] F. Soriguer, I. Esteva, G. RojoMartínez, Oleic and from cooking oils is associated with lower insulin resistance in the general population (Pizarra study). Eur. J. Endocrinol. (КЭ). – 2004. – 150, № 1. – P. 33–39.
[4] M. Lee, S. Lin, Dietary fat and breast cancer. Annu. Rev. Nutr. – 2000. – V. 20. – P. 221–248.

# COMPARATIVE ANALYSIS OF INFRARED REFLECTED SPECTRUM OF BULK FOOD PRODUCTS

Svitlana Litvynchuk, Oleksandra Lukiyanik

Department of Physics, National University of Food Technologies, Kyiv, Ukraine
litvynchuk@nuft.edu.ua

Recently, various physical methods have become widely used to determine the qualitative and quantitative composition of food and agricultural products. In particular, the method of infrared spectroscopy in the near field of the spectrum is a non-destructive, fast and environmentally safe method of identification of samples. This method allows you to determine the content and concentration of substances, including in foods [1, 2]. Therefore, this work is devoted to the use of infrared reflection spectra for the analysis of some bulk food products.

For experimental research, food samples that used in everyday life were selected: sugar sand, rock salt and baking soda. It was also interesting to study the flower pollen – a complex, concentrated plant-bee product with unique consumer and therapeutic qualities. According to scientific data [3], it has antiphlogistic and antioxidant properties its use does not cause allergic or other side effects.

Measurement of reflection spectra was carried on the analyzer "Infrapid-61" in the wavelength range 1330-2370 nm with a step 10 nm. For this purpose the experimental samples were successively loaded into the cuvette compartment and measured the intensity of the diffuse reflection in the above spectral region. The light flux which diffuse reflected from the object fell on the diffraction grating and then - on the photodetector. The resulting signal was then processed and analyzed using an electronic system. It should be noted that due to weak absorption in the near field and the use of diffuse reflection from the experimental sample, it is possible to direct analysis of the product which excludes complex sample preparation. The reliability of the registration system is quite high and provides a high level of repeatability and accuracy of the result. In this case the recording of the spectrum takes only in a few minutes.

Undertaken studies have shown that the largest number of extremums has a spectrum of sugar sand since it is a complex compound. A simpler view of the spectrum with one obvious extremum has baking soda. The rock salt spectrum is located much higher than other samples (that is the intensity of reflection is greatest). Spectrum of flower pollen is most closely related to sugar sand but its character is clearly different.

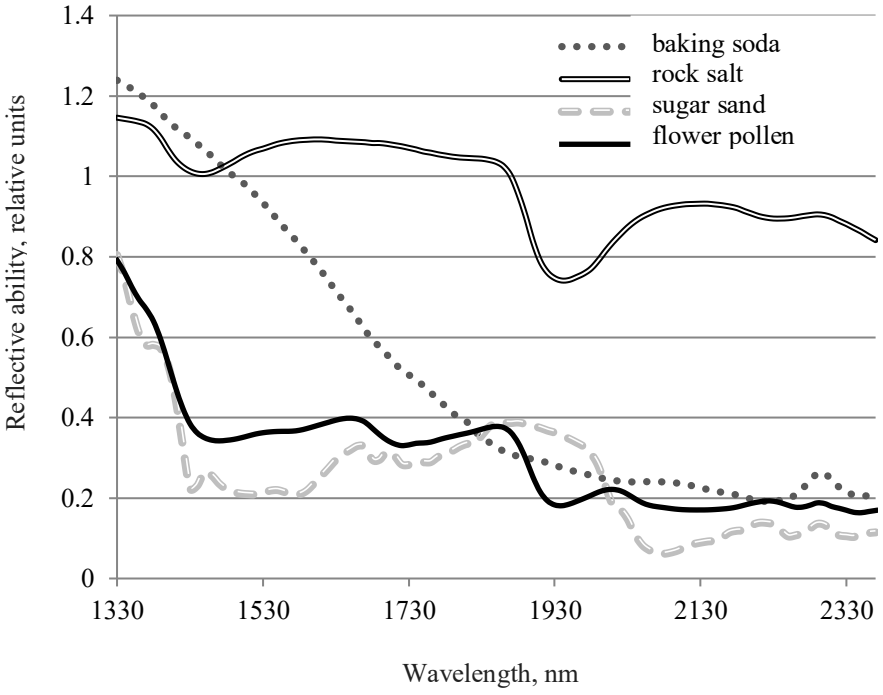


Fig. 1. Infrared spectra of reflection of some bulk food products.

So using the method of near-infrared spectroscopy can identify bulk foods products: baking soda, rock salt, sugar sand and flower pollen. Also by changing the nature and intensity of the corresponding reflection spectra it will be possible in the future to determine the presence in the samples of impurities.

[1] P. J. Larkin, Infrared and raman spectroscopy: principles and spectral interpretation, Elsevier, 230 p. (2011).
[2] Y. I. Posudin, Practical spectroscopy in agriculture and food science, Science Publishers, 188 p. (2006).
[3] V. Brovarskij, J. Brindza, Včelí obnôžkový peľ, Kyjev-Nitra: FOP I. S. Maidachenko, 288 p. (2010).

# VIBRATIONAL SPECTROSCOPY OF HUMAN GALLSTONES

Gerda Mickūnaitė[1], Rimantė Bandzevičiūtė[1]

[1]Chemical Physics Institute, Faculty of Physics, Vilnius University, Saulėtekio Ave. 3, LT-10257 Vilnius, Lithuania
mickunaitegerda@gmail.com

Gallstone disease is one of the major health problems which can cause cancer. Thus it is very important to remove gallstones in the early stages [1]. Currently used surgical gallbladder removal causes damage and complications but the use of non–surgical methods causes recurrence of gallstones [2]. In order to find new ways for the treatment of gallstone disease it is very important to know the composition and mechanisms of gallstone formation.

In this work Raman spectra of gallstones removed from different age men and women were analyzed. After spectral analysis it was established that cholesterol, phospholipids, fatty acids, proteins, calcium carbonate, calcium oxalate, calcium bilirubinate, bilirubin, biliverdin can be found in all types of gallstones. The gallstones were classified based on qualitative analysis of Raman spectra. The intensities of characteristic bands of cholesterol and bilirubin were compared and gallstones were classified into two major groups – cholesterol gallstones and pigment gallstones. The group of cholesterol gallstones included stones with the most intense spectral bands in the 3036 – 2850 $cm^{-1}$ spectral range. Pigment gallstones were identified according to the spectral band at 1618 $cm^{-1}$, which is assigned to bilirubin and calcium bilirubinate. One cholesterol gallstone had high intensity bands at 1087 $cm^{-1}$, 205 $cm^{-1}$, 153 $cm^{-1}$ which show a high content of calcium carbonate in the composition. According to this difference, cholesterol-carbonate gallstones were classified into a separate group. Spectral differences between pigment stones were also observed. Pigment gallstones were divided into two smaller groups: brown and black stones. Black gallstones had high intensity bands at 1087 $cm^{-1}$, 282 $cm^{-1}$, 153 $cm^{-1}$ that are attributed to calcium carbonate. These bands were not observed in brown gallstones. After classification of gallstones it was determined that 82 % of samples were identified as cholesterol gallstones.

While the reason and mechanism of the formation of cholesterol monohydrate crystals are still unclear, it is proposed that this process is influenced by the presence of glycoproteins (mucin), calcium bilirubinate and bilirubin [3]. Calcium bilirubinate promotes formation of the gallstone crystal; mucin influences the balance of bile salts, leading bilirubin to bind with lipids and form cholesterol monohydrate crystals. After visual examination of cholesterol gallstone samples, it was observed that cholesterol gallstones have specific layered structure (Fig 1b). The differences of chemical composition between different gallstone layers were observed in Raman spectra (Fig 1a). The spectrum of the central part of the gallstone has high intensity bands that are attributed to bilirubin (1618 $cm^{-1}$, 1497 $cm^{-1}$, 1192 $cm^{-1}$, 1338 $cm^{-1}$) and calcium bilirubinate (1618 $cm^{-1}$, 1581 $cm^{-1}$, 1497 $cm^{-1}$, 1192 $cm^{-1}$). The intensity of bands at 1270 $cm^{-1}$ and 1254 $cm^{-1}$ may increase due to increased amount of the calcium bilirubinate or bilirubin. However, increased intensity of the band at 1270 $cm^{-1}$ may be attributed to a higher amount of phospholipids, while increased intensity value of the band at 1254 $cm^{-1}$ may be attributed to a higher amount of proteins. The decrease of intensity of all these bands is observed in Raman spectra from the inner and outer parts of the cholesterol gallstone (the bands are marked with arrows in Fig 1a). The high intensity bands of bilirubin, calcium bilirubinate, phospholipids and proteins observed in the Raman spectra of the central part of the samples show that these substances affect the formation of the crystal of the stone and formation of the cholesterol monohydrate.

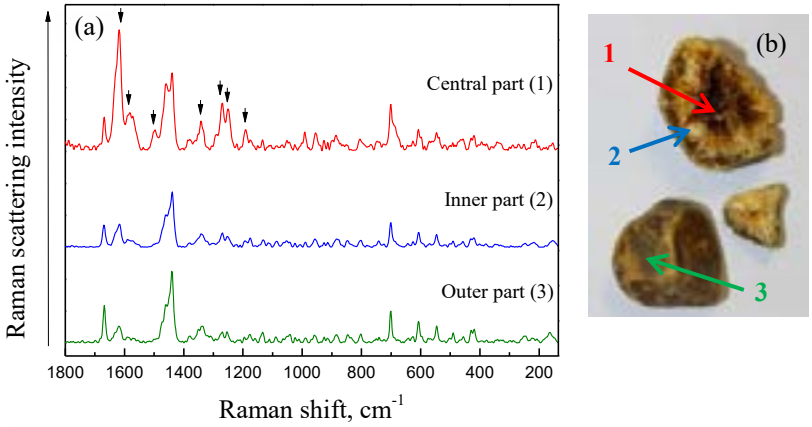


Fig 1. (a) typical spectra of cholesterol gallstone, (b) cholesterol gallstone sample.

[1] A. Y. Bhatti et al., A cross sectional study on the risk factors of gallbladder stone, Int J Res Med Sci **4**(11), 5041-5046 (2016)
[2] I. J. Beckingham, ABC of diseases of liver, pancreas, and biliary system. Gallstone disease, BMJ **322**(7278), 91-94 (2001)
[3] I. AD. Bouchier, The Formation of Gallstones, Keio J Med **41**(1), 1-5 (1992)

# DETECTION OF CAFFEINE TRACES IN SALIVA USING ELECTROCHEMICAL SERS METHOD

Edvinas Zacharovas, Martynas Velička, Valdas Šablinskas

Faculty of Physics, Institute of Chemical Physics, Vilnius University, Lithuania
edvinas.zacharovas@ff.stud.vu.lt

Detecting addictive and potentially dangerous psychoactive substances in the human body is an important area of medical research. Chemical compounds, most often of plant origin and belonging to the group of psychoactive substances, are called alkaloids. This group includes caffeine which is widely used and easily available worldwide. It is used in small amounts as a central nervous system stimulant that inhibits sleepiness and improves reaction, concentration and coordination. However, high doses of caffeine can cause serious health disorders, and in case of people with health problems, caffeine overdose can even lead to death [1-2]. This is especially important nowadays, as manufacturers often hide or misrepresent the true composition of the product.

The aim of this work is to identify and improve a sensitive and accurate methodology for detecting caffeine and other alkaloids in the human body by studying human biological fluids, and more specifically, saliva. The main advantage of saliva is that no special extraction devices and preparation methods are required. During the study, the main goal is to determine the minimum caffeine concentration (< 1 mM) that can be detected by Raman scattering spectroscopy methods (Fig. 1). To achieve this goal, a non-destructive electrochemical surface enhanced Raman scattering (E-SERS) spectroscopy method was used. As electrochemical processes can accurately control the strengthening of the SERS signal, the areas of use of E-SERS in medicine are expanding rapidly [3].

In order to strengthen the Raman scattering signal of the studied molecule, solutions of several noble metals (Ag and Au) nanoparticles, different ways of forming nanoparticle layers on the electrode surface and different electrode electric potential values are used. Nanoparticles of various sizes and shapes are prepared using steric (polymers) and electric (citrate molecules) stabilization. The dependence of enhancement factor on nanoparticle concentration is also investigated. The concentration is changed by centrifuging the colloidal solutions. The most effective method is used to investigate model saliva and caffeine solutions. Creating the optimum methodology will allow us to detect relatively quickly not only the amount of caffeine in the body, but also to identify the potentially toxic narcotic alkaloids contained in the human body.

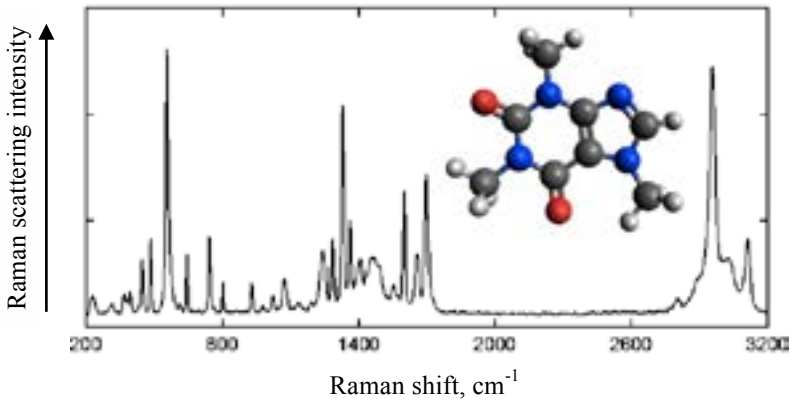


Fig. 1. Raman scattering spectra of caffeine.

Computations were performed on resources at the High Performance Computing Center „HPC Sauletekis“ in Vilnius University Faculty of Physics.

This research is funded by the European Social Fund under the No 09.3.3-LMT-K-712 “Development of Competences of Scientists, other Researchers and Students through Practical Research Activities” measure.

[1] S. Cappelletti, P. Daria, G. Sani, M. Aromatario, Caffeine: cognitive and physical performance enhancer or psychoactive drug?, Curr Neuropharmacol., 13, 71-72 (2015);
[2] D. Echeverri, F.R. Montes, M. Cabrera, A. Galan, A. Prieto, Caffeine’s vascular mechanisms of actions, Int. J. Vasc. Med., 1-2 (2010);
[3] R. A. Karaballi, S. Merchant, S. R. Power, C. L. Brosseau, Electrochemical surface-enhanced Raman spectroscopy (EC-SERS) study of the interaction between protein aggregates and biomimetic membranes, Phys. Chem. Chem. Phys. 20, 4513 (2018).

# AAA CLASS SOLAR SIMULATOR BASED ON HIGH-POWER LIGHT-EMITTING DIODES WITH MIRROR SYSTEM

Klemensas Laurinavičius, Algirdas Novičkovas, Vincas Tamošiūnas

Faculty of Physics, Vilnius University, Lithuania
klemensas.laurinavicius@ff.stud.vu.lt

Solar simulator is an artificial device that closely resembles the Solar irradiance for the purpose of testing photovoltaic devices in a controlled environment. Solar simulators are usually made using Xenon arc lamps. Considering the inefficiency of Xenon arc lamps [1], light emitting-diodes (LEDs) have recently been used in research laboratories to construct solar simulators, and offer promise in the future for energy-efficient production of spectrally tailored artificial sunlight [2]. There are three main aspects that a Solar simulator should comply with, defined in the IEC 60904-9 Ed. 2.0 [3] international standard.

The IEC 60904-9 Ed. 2.0 international standard defines the classifications of solar simulators for use in indoor measurements of terrestrial photovoltaic devices; solar simulators are classified as corresponding to A, B or C class for each of the three categories based on criteria of spectral distribution match, irradiance non-uniformity on the test plane and temporal instability. It also provides the required methodologies for determining the rating achieved by a solar simulator in each of these categories.

The purpose of this work was to design a Solar simulator, that would satisfy AAA class requirements of IEC 60904-9 Ed. 2.0 for at least 13×13 $cm^2$ illuminated area, using high-power light-emitting diodes with a square tubular mirror system. Such uniformly illuminated area would be sufficient for testing solar cells of several standard industrial sizes, based on wafers of up to five inches dimensions. Computer simulations of irradiance from the solar simulators were performed to optimize the design of the simulator using complex LED placement patterns and various optical solutions. Several designs were simulated: one with individual reflectors on white LED arrays, one with external mirrors reflection coefficient of 0.8 and one employing individual reflectors on color LEDs and external mirrors with reflection coefficient of 0.9. One of the best results is presented in (Fig 1 (a)). A prototype solar simulator was built and its specifications were measured (Fig. 1 (b)).

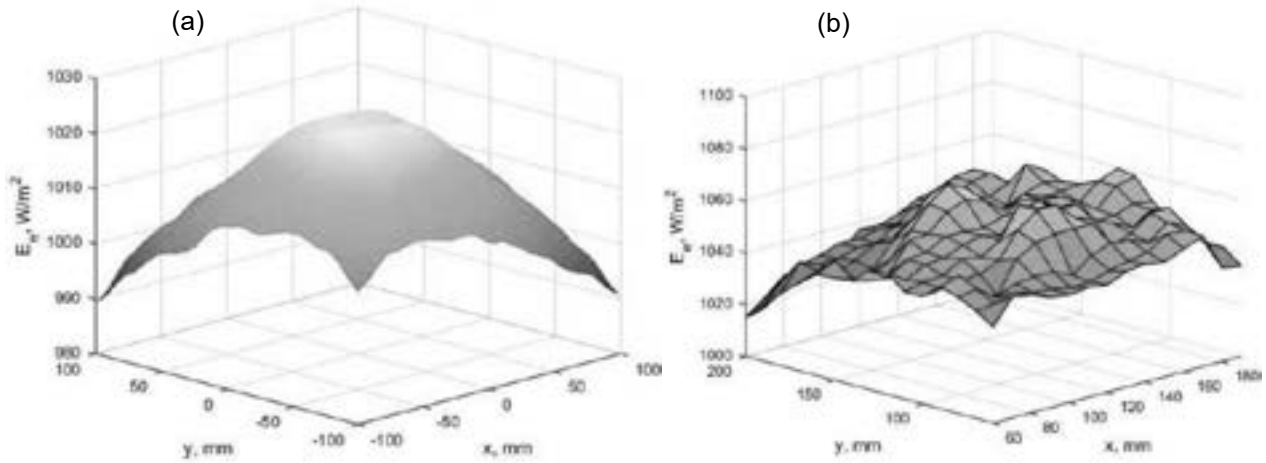


Fig. 1. Simulated irradiance of Solar simulator (a); Measured irradiance of prototype Solar simulator (b).

The developed Solar simulator satisfies A class irradiance uniformity requirements according to IEC 60904-9 Ed. 2.0 standard for 14×15 $cm^2$ area. Only 22 light-emitting diodes were used to achieve this result: 2 units of Bridgelux high-power white LEDs, in conjunction with LedEngin series 2 units of 450 nanometer LEDs, 2 units of 660 nanometer LEDs, 6 units of 740 nanometer LEDs, 4 units of 850 nanometer LEDs and 6 units of 940 nanometer LEDs. In addition, A class spectrum requirements are also satisfied in all points of the investigated area as will be demonstrated during the presentation. Inherent properties and long lifetime of LED arrays also ensures A class requirements for irradiance stability, thus completing the set of properties of AAA class solar simulator.

[1] Xue Dong, Zhiwei Sun, Graham J. Nathan, Peter J. Ashman, Dahe Gu, Time-resolved spectra of solar simulators employing metal halide and xenon arc lamps, *Solar Energy*, 115, pp. 613-620, 2015.
[2] A. Novičkovas, A. Baguckis, A. Mekys and V. Tamošiūnas, "Compact Light-Emitting Diode-Based AAA Class Solar Simulator: Design and Application Peculiarities, *IEEE Journal of Photovoltaics*, vol. 5, no. 4, pp. 1137-1142, 2015.
[3] *Photovoltaic Devices–Part 9: Solar Simulator Performance Requirements*,IEC 60904-9 Ed.2.0, 2007.

# ESTIMATION OF THE CONTRIBUTION OF DISSIPATED AND REFLECTED GAMMA-QUANTA TO THE VALUE OF THE DAP DEPENDING ON THE PARAMETERS OF THE X-RAY PROCEDURE

Dzmitry Kacharhin[1]

[1] Department of Nuclear Physics, Belarussian State University, Belarus
dmitriyrbu@gmail.com

In modern life, X-ray diagnostic procedures have a big role. We use it in epidemiology, traumatology and oncology for the diagnosis and visual presentation of the picture of the disease. So, in order to minimize harmful affection on patients it's necessary to most accurately account contribution of X-rays dose received during medical procedures to annual dose of radiation.

DAP – Dose Area Product, that show how much energy transported to square by particle.

$$DAP = \int_S D_{air}(\mathrm{S})\,\mathrm{dS} \tag{1}$$

This is a main parameter to control the X-ray medicine diagnostic procedures. The problem is to subtract from DAP value the contribution of dissipated and reflected gamma-quanta which was obtained from the detector. DAP detectors are established in the collimation system. They measure passing and dissipated, reflected radiation. Initially, a point source radiates into a cone with a given angle solution. The real X-ray machine have a collimation system, that transform a source radiation by cutting down some beams. It's known that gamma-quanta have strong penetrating power, and have reflections and dissipations in collimation system. Further it's also registered by DAP detector.

In this research the X-ray diagnostic procedure of rib thorax with DAP changes depending on different parameters of the X-ray machine is observed.

In this work Monte-Carlo modelling is used as most suitable and accurate method. In this approach we used a model of static X-ray machine. In MCNP (Monte-Carlo N-Particle Transport Code) [1] used two functionals – functional of transferred energy (f6) and functional of absorbed energy (f8*) [2]. We can use both this functionals, because we have an electron equal in air.

The model of X-ray machine consists of collimation system and X-ray source.

This model includes changeable parameters, that can influence on DAP value.

List of main parameters that was changing in research:

- Voltage of X-ray tube (in kV)
- Focal spot radius at anode (in mm)
- Voltage ripple (in %)
- DAP detector position (in mm)
- Filter depth (in mm)

In this approach data for X-ray energy spectra was taking from TASMIP [3], and include dependents from aluminum filter, voltage and voltage ripple. MCNP used for computation energy, that was delivered to detector by gamma-quanta.

Geometrically such simulated experiment is represented as a source of variable sizes that placed in front of water column. This water column is one of admissions in this model, because, as you can see later, reflected gamma-quanta don't make huge influence on DAP value. This water column has a parameters of averaged human body. In this model there are some detectors, located in front of source per each 10 cm, and 5 of them took place in collimator system per each 1 mm of lead curtains.

1. Results obtained from both functionals (f6 and f8*) have the same order, and their maximum discrepancy is 7%. In addition, the dependence obtained with F6 has a smoother appearance than its analogue obtained with F8 *. Also F6 has a smaller mistake (1% vs 3.5%). F6 faster than F8* in $10^3$ but needs an additional processing.
2. DAP value in collimation system has only 0.05% reflected gamma-quanta. Value of reflected gamma-quanta fall in 35 times at 40 cm distance.
3. Contribution of dissipated gamma-quanta to the value of DAP in the collimation system varies from 0.02% to 0.1% and it's depend on radius of source.
4. Changes in voltage lead to changes in DAP for 15%
5. Filters have a strong influence on DAP value – 5 mm of aluminum change DAP in 2 times.

According to the obtained results, location of the detector satisfy requirement for accuracy of the DAP value [4]. This results can apply only for systems that satisfy this research model. The optimal position for the detector placement was found, excluding consideration of reflected and dissipated gamma quanta.

[1] MCNP-A General Monte Carlo N-Particle Transport Code. Version 4B. / Los Alamos National Laboratory, editor J.F. Briesmeister. – Los Alamos NM, 1997. – 736 p.
[2] Denise B. Pelowitz MCNPXTM USER'S MANUAL USA, 2008. -551p
[3] John M. Boone J. Anthony Seibert TASMIP USA, 1997.
[4] ICRP Publication 103

# APPLICATION OF WIDE-BAND HYPERBOLICALLY FREQUENCY-MODULATED TECHNOLOGIES IN SURFACE ACOUSTIC WAVE SENSORS

Dmitrij Smirnov[1], Andrius Bartašiūnas[1], Rimantas Miškinis[1], Emilis Urba[1*], Victor Plessky[2]

[1] Department of Metrology, Center for Physical Sciences and Technology, Lithuania
[2] GVR Trade SA, Switzerland
emilis.urba@ftmc.lt

Developing the technology had been prompted by the fact that hyperbolically frequency-modulated signals are used in nature, e. g., by some of the species of dolphins and bats who use such a modulation for echo-location. Application of the technology in surface acoustic wave (SAW) sensors allows achieving their operation in a wide range of temperatures, which would be difficult to achieve by using other wide-band frequency modulations, e. g., linear [1]. To demonstrate that, a surface acoustic wave temperature sensor with the SAW reflecting gratings designed for operation with HFM signals was fabricated. The operating principle of the sensor is illustrated in Fig. 1.

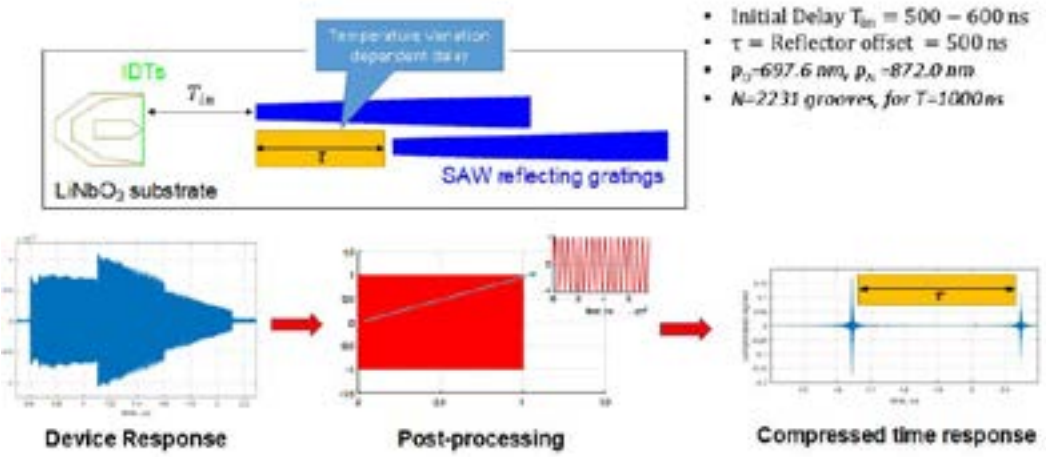


Fig. 1. Operating principle of the SAW sensor. IDTs – interdigital SAW transducers

The temperature response is obtained from the times of the SAW propagation in the sensors. The device was fabricated by forming two pairs of identical aluminum interdigital transducers and etched-groove reflectors in parallel acoustic channels on a YZ-cut lithium niobate ($LiNbO_3$) substrate. The sensors were remotely (via antennas) interrogated by a reader ("Hybrid SAW Reader" by RSSI GmbH) in the frequency range of (2 – 2.5) GHz. Echo-responses were post-processed using a numerical matched-to-signal filter to obtain the compressed time responses. The difference $\tau$ between the peaks of the time response was proportional to the deviation of the sensor temperature; the proportionality was determined by thermal properties of $LiNbO_3$.

The results obtained imply that the sensor properly operated remotely in the temperature range from -150 $^{o}$C to +140 $^{o}$C, allowing determining the temperature with the uncertainty of 50 mK (0.05 $^{o}$C) [2].

This work was carried out in the frame of the Swiss-Lithuanian Eurostars Project No. E!10640 UWB_SENS.

[1] V. Plessky, M. Lamothe, Hyperbolically frequency modulated transducer in SAW sensors and tags, Electronics Letters **49** (24), 1503-1504 (2013).
[2] S. Yandrapalli, R. Miskinis, D. Smirnov, V. Plessky, A. Shimko, Ultra-Wide-Band SAW Sensor with HFM Etched Reflectors, 2018 IEEE International Ultrasonics Symposium, DOI: 10.1109/ULTSYM.2018.8580225.

# GENERATION OF X-RAY EMISSION IN ALKALI METAL HALIDE SALTS VIA FEMTOSECOND LASER PULSES

Karolina Varsockaja[1,3], Anton Koroliov [2], Jonas Reklaitis [1]

[1]Center for Physical Sciences and Technology, Savanoriu av. 231, Vilnius LT-02300, Lithuania
[2]Center for Physical Sciences and Technology, Sauletekio av. 3, Vilnius LT-10257, Lithuania
[3]Faculty of Physics, Vilnius University, Sauletekio av. 9, Bld. III, Vilnius, Lithuania
*karolina.varsockaja@ff.stud.vu.lt*

X-Rays generation with ultrashort, high energy laser pulses is an attractive technique in ultrafast technology field. X-Ray emission obtained with this technique showcase unique characteristics [1] and could be used for numerous industrial, medicine and material science applications. Brilliance of X-rays generated by femtosecond laser pulses is comparable to that of synchrotrons, but a laser system is cheaper and more compact than a synchrotron.

One of the main goals of this study is to achieve a high emission yield and spectral light emittance at average X-Rays range (1 keV–20 keV). Previous experiment with metal targets in this area has shown that the X-Ray emission yield in the energy range mentioned before, is not sufficient [2].

For this experiment as targets we chose alkali metal halide salts — NaCl, KBr, KI, CsI. These compounds have a big energy band gap and are transparent in a wide range. Thus Plasma could be generated in the volume of the target rather then on the surface. This allows us to expect for better X-Ray emission yield than that of metal targets. More complex and non traditional laser beam geometries could be applied because of the target transperancy. "Pharos" femtosecond laser system (Light Conversion Ltd., central wavelength $\lambda$=1028 nm, pulse energy $E_p = 90\,\mu J - 1500\,\mu J$, pulse duration $\tau_p = 190$ fs, average output power 6 W, pulse repetition rate was changed from 1 kHz to 10 kHz) was used for X-Ray excitation in the targets. For detection of X-Rays "Amptek X-123" detector was used, positioned at 45° angle prior to the target ant the laser beam.

The plasma X-Ray source was generated in the KBr target, as seen in the Fig. 1. There are clearly distinguishable bromide $K_\alpha$ and $K_\beta$ X-Ray lines at 11.92 keV and 13.29 keV respectively as identified by NIST database [3].

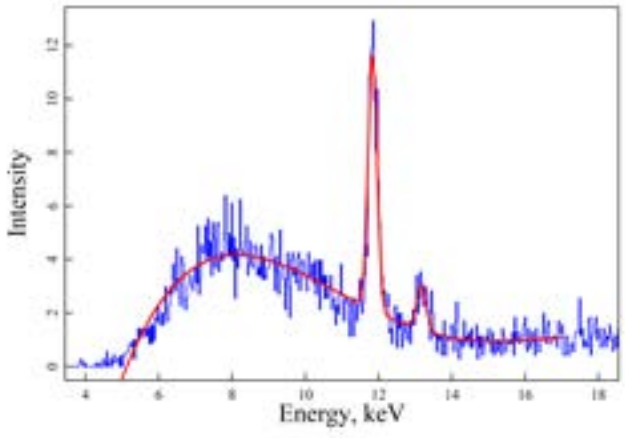


Fig. 1. X-Ray emission spectra of KBr compound excited with femtosecond laser pulses. Intensity is given by detected X-Ray photon count per second.

**Acknowledgements.** This research is funded by the European Social Fund under the No. 09.3.3-LMT-K-712 "Developement of Competences of Scientists, other Researchers and Students through Practical Research Activities" measure.

[1] S. Corde, K. Ta Phuoc, G. Lambert, R. Fitour, V. Malka, A. Rousse, A. Beck, and E. Lefebvre. Femtosecond x-rays from laser-plasma accelerators. *Reviews of Modern Physics*, 85:1–48, 2013.

[2] Artūras Baguckis, Artūras Plukis, Jonas Reklaitis, Vidmantas Remeikis, Linas Giniūnas, and Mikas Vengris. Generation of plasma x-ray sources via high repetition rate femtosecond laser pulses. *Applied Physics B*, 123(12):290, 2017.

[3] Siderius D.W. Krekelberg W.P. Shen, V.K. and Eds. Hatch, H.W. Nist standard reference simulation website. *NIST Standard Reference Database Number 173*, National Institute of Standards and Technology, Gaithersburg MD:20899. (retrieved 2019.01.30).

# HEAVY MINERAL CONCENTRATION AS A PROXY FOR HIGH-ENERGY EVENT TRACING ON SANDY BEACHES

Kristina Viršilaitė[1], Donatas Pupienis[1]

[1] Vilnius University, Faculty of Chemistry and Geosciences, Vilnius, Lithuania
kristina.virsilaite@chgf.stud.vu.lt

Sandy beaches fronting the Lithuanian coast of the Baltic Sea are composed mainly of quartz sands with a locally important increase in accessory minerals – heavy mineral concentrations (HMCs). The distribution of HMCs are determined by the swash flow, which upper limit varies accordingly to the extent of a high-energy event, and it helps to reconstruct paleo-hydrometeorological conditions. The heavy mineral deposits are distributed from the foreshore or berm crest on relatively calm conditions up to the middle part of the beach or foot of the foredune after severe storms. Our study has shown that higher HMCs are a proxy of hydrodynamic energy extent since the largest deposits are found at the upper boundary of storm surge [1, 2]. The aim of this study was to demonstrate that high-energy events may be traced by measuring HMCs on the sandy beaches.

To identify the high-energy event, a low-field magnetic susceptibility (MS) was measured on 11 cross-shore profiles at every 1 m with 0.565 kHz Bartington MS3 field scanning system with MS2K sensor. The beach topographic data was collected using a Topcon's HiPer SR receiver at 1 m interval. Measuring tape was used to measure the distance between topographic points along the cross-shore profile. The measurements were made three days after each of two subsequent storms. Profiles were analysed using the gathered topographic and MS data with Sequential Regime Shift Detection Software using the regime shift index where the cut-off length is 3 and the significance level $p = 0.1$. Analysis revealed that anomaly lag deposit of heavy minerals was found at the upper boundary of storm surge. It has proved that the measurement of HMCs show the extent of hydrodynamic energy.

This research was funded by the European Social Fund under the No 09.3.3-LMTK-712 “Development of Competences of Scientists, other Researchers and Students through Practical Research Activities” measure.

[1] D. Pupienis,, I. V. Buynevich, A. Bitinas, Distribution and significance of heavy-mineral concentrations along the southeast Baltic Sea coast. Journal of Coastal Research **64**, 1984–1988 (2011).

[2] R. Jagodziński, B. Sternal, W. Szczuciński, et al., Heavy minerals in 2004 tsunami deposits on Kho Khao Island, Thailand. Polish Journal of Environmental Studies **18**, 103–110 (2009).

# DETERMINATION OF OLIVE OIL QUALITY BY MEANS OF VIBRATIONAL SPECTROSCOPY

Elzė Saldžiūnaitė, Martynas Velička

Vilnius University, Faculty of Physics, Institute of chemical physics, Vilnius, Lithuania
*elze.saldziunaite@gmail.com*

Due to the value of extra virgin olive oil (EVOO), adulteration has become an important issue in the food industry. EVOO, being the highest quality olive oil is the most prone to be fraud. Typical adulterants would likely include edible oils that are much cheaper than EVOO, as there will be a greater profit for the producer [1]. Mostly three adulterants of different nature are used - sunflower oil, rapeseed oil, and soybean oil, and can be present in the range 5–95 %.

Near-infrared spectroscopy and principal components analysis were already employed to develop a discriminant analysis equation that could identify correctly the type of seed oil present in extra virgin olive oil in 90 % of cases [2]. Unfortunately, more accurate analysis is needed when EVOO is mixed with other types of olive oils. Fluorescence spectroscopy combined with second-order chemometric methods was previously used for the detection of extra virgin olive oil adulteration with lower quality olive oils [3], however this method cannot give the precise chemical information of the sample. In this work vibrational spectroscopy methods FTIR-ATR and FT-Raman are employed to analyze different qualities of olive oils. Vibrational spectroscopy was chosen since every molecule has its distinct vibrational spectra in the infrared region [4]. Furthermore, chemical information can be taken from the spectra which makes vibrational spectroscopy more precise than fluorescence measurements. By analyzing the registered spectra spectral markers which allow the discrimination of EVOO from lower quality olive oils were identified. Comparison between the FTIR-ATR spectra of EVOO and olive pomace oils are shown in fig. 1.

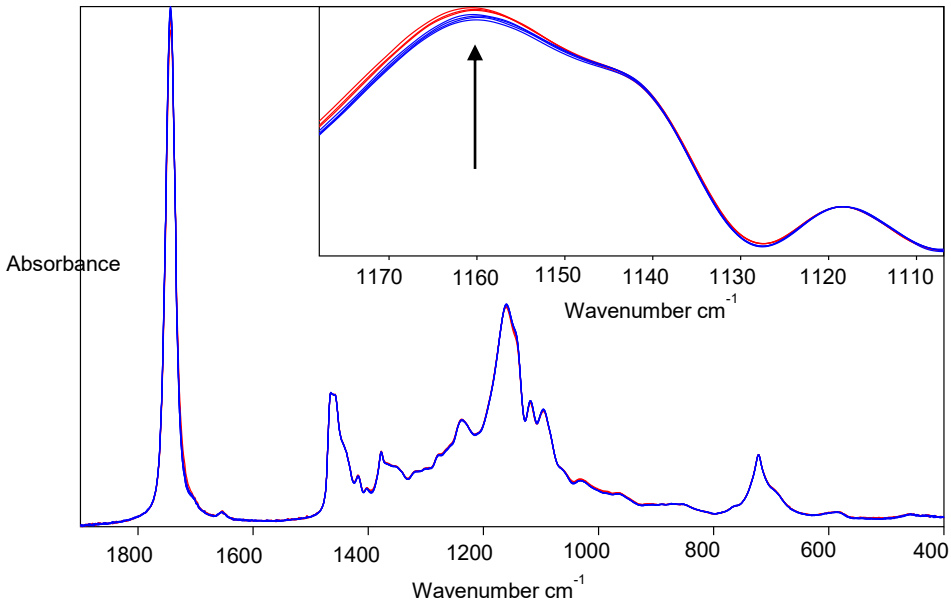


Fig. 1. FTIR-ATR spectra of EVOO (blue) and olive pomace oil (red) presented in the fingerprint region.

In conclusion, the analysis of the FTIR-ATR and FT-Raman spectra of various qualities of olive oils have shown that vibrational spectroscopy can be used identify EVOO adulterated with olive pomace oil. More research is needed in order to find the spectral markers which would allow to distinguish olive oils of similar quality.

[1] Nick Vanstone Andrew Moore Perry Martos Suresh Neethirajan, Detection of the adulteration of extra virgin olive oil by near-infrared spectroscopy and chemometric techniques Food Quality and Safety, 2(4), 2018, 189–198.
[2] I. J. Wesley, F. Pacheco, A. E. J. McGill, Identification of adulterants in olive oils, Journal of the American Oil Chemists' Society, 73(4), 1996, 515–518.
[3] Isabel Durán Merás, Jaime Domínguez Manzano, DiegoAirado Rodríguez, ArsenioMuñoz de la Peña, Detection and quantification of extra virgin olive oil adulteration by means of autofluorescence excitation-emission profiles combined with multi-way classification, Talanta 178, 2018, 751-762.
[4] Valdas Šablinskas ir Justinas Čeponkus. Modernioji molekulių virpesinė spektrometrija, Vilnius 2014, 150-174.

# TRANSIENT ABSORPTION SPECTROSCOPY AS A PROMISING TOOL FOR DEFECTS CHARACTERIZATION OF GRAPHENE LAYERS

Erika Rajackaitė[1], Domantas Peckus[1], Rimantas Gudaitis[1], Mindaugas Andrulevičius[1], Tomas Tamulevičius[1,2], Šarūnas Meškinis[1], Sigitas Tamulevičius[1,2]

[1]Institute of Materials Science of Kaunas University of Technology, K. Baršausko Str. 59, Kaunas LT-51423, Lithuania
[2]Department of Physics, Kaunas University of Technology, Studentų Str. 50, Kaunas LT-51368, Lithuania
erika.rajackaite@ktu.edu

Graphene is the best-known 2D material because of its extraordinary structural, physical, and chemical properties, and the industrial interest in investigating graphene applications in many different areas, such as electrooptics, photonics, plasmonics, optoelectronics [1], grew rapidly over the last decade. Simultaneously, different routes of production and synthesis of graphene are available with varying level of successfulness. Nevertheless, the development of graphene applications is fairly slow process, and possibly the main cause for this is not optimal, rather poor quality of the graphene produced by many companies in the world, which is an indisputable fact [2]. Therefore, it is very important to evolve and improve tools and methods for graphene quality exploration with regard to present defects and disorder.

At a moment, one of the best developed methods to characterize graphene films is Raman scattering spectroscopy for being nondestructive, fast, of high resolution, and so far providing the maximum structural and electronic information about graphene layers [3]. One the other hand, ultrafast spectroscopy method widely used in other fields, until now was not sufficiently explored for thorough systematic defects and disorder analysis of graphene. In our research we present ultrafast transient absorption spectroscopy (TAS) technique as an efficient tool to evaluate the quality of graphene layers. Understanding the influence of such defects on the charge carrier dynamics and excited state relaxation pathways is a key to modifying the optoelectronic properties of graphene-based devices.

Employing a widespread microwave plasma enhanced chemical vapor deposition (PECVD) technique, large area graphene layers were synthesized in two ways – directly on insulating substrates (fused silica) initiating the formation of vertical graphene nanosheets (VNGs), and on metallic catalyst (Cu foil) for production of continuous films possessing an intrinsic planar structure. These structural differences were identified by Raman scattering spectroscopy measurements, additionally revealing different prevailing types of defects within the analyzed graphene films, which are edges and boundaries for VGNs and vacancy-like defects for transferred planar graphene layers (Fig. 1). The detailed analysis and comparison of structural, electrical, optical, morphological, compositional and electro-optical properties of graphene layers depending on preparation method was carried out by utilizing transmission line method, UV-VIS spectroscopy, AFM, SEM, XPS.

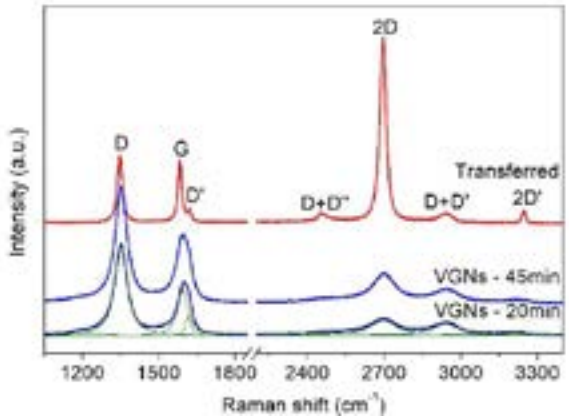


Fig. 1. Raman spectra of planar graphene transferred on quartz substrate and vertical graphene nanosheets directly grown on quartz for 20 min (and its deconvolution with Lorentzian line shape) and for 45 min by PECVD.

We used TAS technique to analyze excited state relaxation dynamics (typical relaxation times, absorbance spectral dependences) in graphene, and how the excitation phonon energy influences these dynamics. The analysis has shown that TAS relaxation kinetics for the measured samples is fastest under excitation with wavelength of 700 nm. We basically measured hot electron cooling dynamics, that originates from electron-optical phonon interaction, leading to phonon-phonon interaction. These relaxation durations have given the information about the defects as well. The better understanding of how defects influence excited state dynamics in graphene might lead to the creation of methodology based on TAS for defects investigation compatible with Raman scattering spectroscopy.

[1] K. C. Lin, M. Y. Li, L. J. Li et al., Ultrafast Dynamics of Hot Electrons and Phonons in Chemical Vapor Deposited Graphene, Journal of Applied Physics **113**, 133511 (2013).
[2] A. P. Kauling, A. T. Seefeldt, D. P. Pisoni et al., The Worldwide Graphene Flake Production, Adv. Mater. **30** (44), 1-6 (2018).
[3] L. M. Malard, M. A. Pimenta, G. Dresselhaus et al., Raman Spectroscopy in Graphene, Phys. Rep. **473** (5–6), 51-87 (2009).

# TRACES OF PARACETAMOL IN BLOOD AS STUDIED BY MEANS OF COLLOIDAL SERS

Sonata Adomavičiūtė, Martynas Velička, Valdas Šablinskas

Vilnius University, Institute of Chemical Physics, Vilnius, Lithuania
sonata.adomaviciute@ff.vu.lt

The most used over-the-counter (OTC) drug in European Union countries is paracetamol, also known as N-acetyl-para-aminophenol (APAP). Wide usage of this drug leads to high rate of accidents due to its missuse. Pharmacokinetics of 4 g of APAP dose after oral ingestion reveals that peak level of it in blood serum reaches 0.4 mM [1] after 40 minutes. Toxicity of APAP is stated when concentration of it in blood exceeds 1 mM when measured 4 hours after acute overdose. Nevertheless, the results of a blood test in clinical trial may take 6 hours or more to obtain, resulting delay in the treatment [2]. Application of colloidal SERS for detection of APAP traces in blood proposed by us is fast, simple and clean method which is capable to reduce the amount of blood needed for diagnosis down to a few drops. The extremely high sensitivity of the surface enhanced Raman scattering (SERS) method takes advantages of both molecular specificity of the Raman scattering and enhanced signal from the nanoparticles (NPs). Such spectroscopic approach allows identification of the molecules in micromole or even lower concentrations.

This work covers SERS based detection of APAP drug in blood samples. Spectral markers and possibility of APAP to be detected by means of SERS spectroscopy was set by examining SERS spectra with different concentration of APAP solutions in water: 1 mM, 100 μM; 75 μM, 50 μM, 25 μM, 10 μM, 1 μM. The spectra of APAP solutions in human blood or blood serum at different concentrations: 10 mM, 5 mM, 2.5 mM, 1 mM, 0.5 mM, 0.25 mM, 0.13 mM were measured to find appropriate preparation procedure of the samples. Possibility of APAP detection in real conditions was checked by measuring SERS spectra of blood serum after consumption of bolus dose of 4 g APAP.

The spectra of 10 mM and 1 mM of APAP solutions mixed with 10 times diluted blood serum are presented in figure 1. APAP molecule consists of benzene ring to which one amide and one hydroxyl group are attached in para conformation. In accordance with SERS spectral features of APAP solution in water, the orientation of APAP molecule changes from facing the nanoparticle with amide group to being oriented parallel to the NP surface. Such structural change is reasoning the changes in intensity of APAP vibrational spectral bands at 1168 $cm^{-1}$ (phenyl – N bending) and 863 $cm^{-1}$, 836 $cm^{-1}$, 805 $cm^{-1}$ (out of plane skeletal deformation) (Fig 1.). APAP can be identified from 1168 $cm^{-1}$ and 863 $cm^{-1}$ spectral bands in both blood and serum samples. Blood sample contains amino acids, fibers and other blood constituents which makes detection of APAP in blood difficult. SERS spectra of serum promises better results of drug detection and is composed mainly of spectral bands of uric acid. Our experiments of APAP detection after consumption of 4 g of APAP reveals that our proposed SERS method is not suitable for detection of traces of APAP in blood at such low concentrations. Sensitivity of the detection can be increased up to 1.3 mM concentration by using serum instead of whole blood.

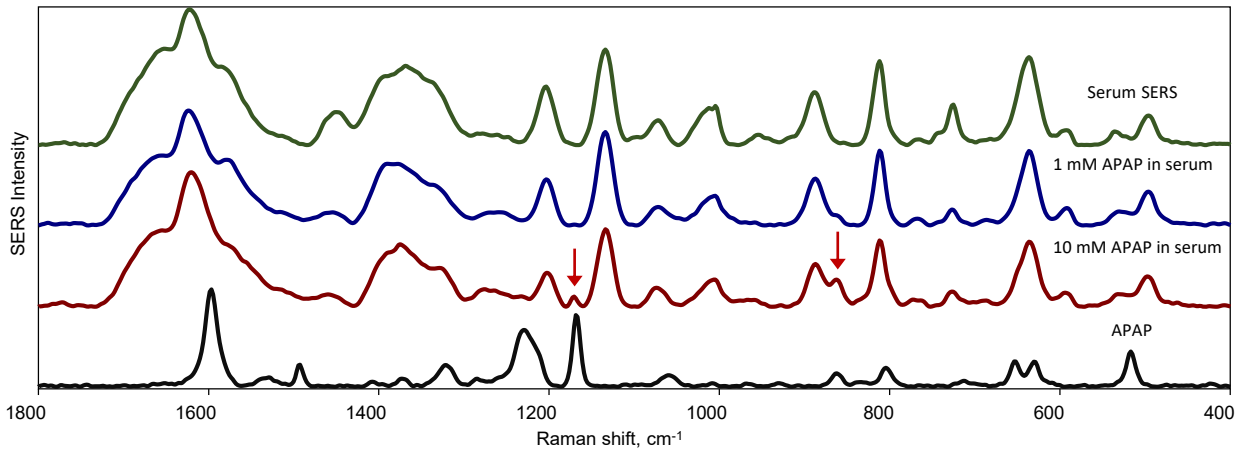


Fig. 1. SERS spectra of 1 mM APAP and blood serum mixture with different concentrations of APAP: 10 mM; 1 mM.

In conclusion, the concentration of APAP molecules in blood serum after consumption of 4 g should be about 0.4 mM [1] which is too low to detect with our current method by means of SERS. The lowest possible concentration of detection of APAP molecules is 1.3 mM in blood serum which indicates toxic and seriously toxic concentration.

[1] R. D. Fannin, M. Russo, T. M. O'connell, K. Gerrish, J. H. Winnike, J. Macdonald, J. Newton, S. Malik, S. O. Sieber, J. Parker, et al., Acetaminophen dosing of humans results in blood transcriptome and metabolome changes consistent with impaired oxidative phosphorylation, Hepatology **51**(1), 227–236 (2010).

[2] C. Dale, A. Aulaqi, J. Baker, R. Hobbs, M. Tan, C. Tovey, I. Walker, J. Henry, Assessment of a point-of-care test for paracetamol and salicylate in blood, Qjm **98**(2), 113–118 (2005).

# DRELL-YAN PROCESS ANALYSIS USING 2016 CERN CMS PROTON-PROTON COLLISION DATA

Marijus Ambrozas, Andrius Juodagalvis

Institute of Theoretical Physics and Astronomy, Faculty of Physics, Vilnius University, Lithuania
marijus.ambrozas@ff.stud.vu.lt

High-energy proton-proton collisions, performed using the Large Hadron Collider (LHC) at CERN, help us to look into the smallest building blocks of the Universe and search for the answers to yet unanswered questions. The proton-proton collision rate is getting increased every year in order to register more of the very rarely occurring events. This is challenging for scientists who have to decide where to store the data and how to reduce the time of the analysis.

Interactions between proton constituents, named "partons" (quarks and gluons), are happening during the high-energy proton-proton collisions. The probabilities of parton-parton interactions depend on the parton distribution functions (PDFs), which describe the inner structure of the proton. The precise knowledge of PDFs is required when calculating the probabilities of very rare events.

The Drell-Yan process is a quark-antiquark annihilation resulting in a lepton-antilepton pair. High-precision measurements of the differential Drell-Yan cross section are useful for constraining the PDFs, as well as for testing the perturbative framework of the Standard Model [1]. They are also important for many other experimental measurements, for example, the Higgs boson measurement, where the Drell-Yan process is a significant background [2].

The measurements of the differential Drell-Yan cross section are carried out at various $pp$ center-of-mass energies (7, 8, and 13 TeV) by ATLAS and CMS collaborations [1, 3, 4, 5, 6]. The CMS measurement with the 2015 data is submitted for publication [arxiv:1812.10529]. In 2016, the CMS experiment has registered more then 10 times the number of proton-proton collisions, registered in 2015. This helps to achieve higher measurement precision, but makes the time of the analysis a lot longer. In order to reduce the time of the analysis, additional event pre-selection can be made to create new data files containing only significant events for the further analysis procedures.

Some measurement uncertainties are related to simulation of distinct background processes. They can be reduced by estimating the number of background events using data-driven techniques. The number of background events in the signal region is determined from the observed yield in the background-dominated control region. Background processes which can independently produce different or same type of leptons are estimated using the $e\mu$ method. The event selection, background estimation and uncertainty calculation will be discussed during the presentation.

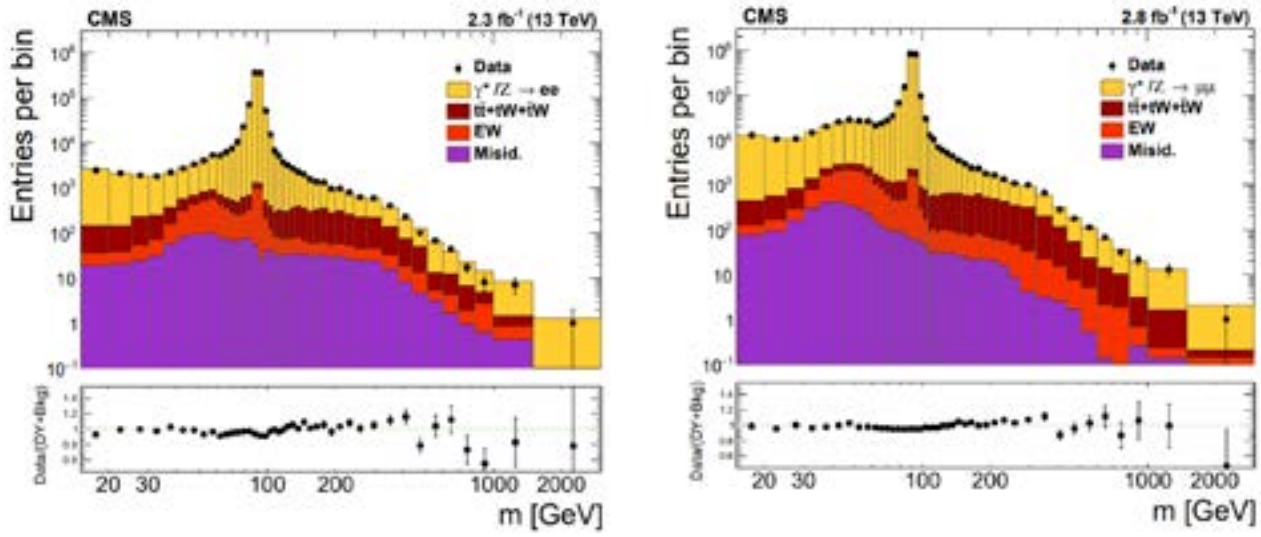


Fig. 1. Dielectron (left) and dimuon (right) invariant mass spectra at the proton-proton collision energy of 13 TeV [1]. The black dots represent the number of events measured with the CMS detector. The colors represent contribution of different processes. Yellow color marks the signal – the Drell-Yan process events. "EW" denotes diboson and DY $\to \tau\tau$ processes. "Misid." corresponds to $W$+Jets and *QCD* processes. The black vertical lines represent statistical uncertainties.

[1] CMS Collaboration, Measurement of the differential Drell-Yan cross section in proton-proton collisions at $\sqrt{s} = 13$ TeV, CMS-SMP-17-001 (2018).
[2] M. B. Kiani, Measurement of properties of the Higgs boson decaying to pairs of W and Z bosons at 13 TeV with the CMS experiment, CMS-CR-2017-267 (2017).
[3] CMS Collaboration, Measurement of the differential and double-differential Drell-Yan cross sections in proton-proton collisions at $\sqrt{s} = 7$ TeV, JHEP **12**, 030 (2013).
[4] ATLAS Collaboration, Measurement of the high-mass Drell-Yan differential cross-section in pp collisions at $\sqrt{s} = 7$ TeV with the ATLAS detector, Phys. Lett. B **725** 223 (2013).
[5] CMS Collaboration, Measurements of differential and double-differential Drell-Yan cross sections in proton-proton collisions at $\sqrt{s} = 8$ TeV, Eur. Phys. J. C **75** 147 (2015).
[6] ATLAS Collaboration, Measurement of the triple-differential Drell-Yan cross section in $pp$ collisions at $\sqrt{s} = 8$ TeV, JHEP **12**, 059 (2017).

# CALCULATING THE INFLUENCE OF 13C INTERACTION TO NITROGEN - VACANCY CENTER LEVEL ANTI-CROSSING OPTICALLY DETECTABLE MAGNETIC RESONANCE SIGNALS

Laima Busaite, Marcis Auzinsh, Andris Berzins, Ruvin Ferber, Florian Gahbauer, Reinis Lazda

Laser Centre, University of Latvia, 19 Rainis Boulevard, Riga, Latvia, LV-1586

laima.busaite@lu.lv

Nitrogen - Vacancy (NV) centers in diamond crystals are used in wide range of applications, such as quantum information, magnetometry and nanoscale sensing [1]. It is important to know the level structure of the NV center, including its hyperfine structure, which arises from interaction of the electron spin and the nuclear spin of $^{14}$N atom, which is part of NV center.

NV centers are defects in diamond crystal consisting of paired nitrogen (N) and vacancy (V). The NV center has a triplet ground state with a zero-field splitting between the $m_s = 0$ and $m_s = \pm 1$ ground state sublevels of 2.87 GHz (Fig. 1a). Due to nonradiative decay path from the excited state via singlet state that preferentially populates the $m_s = 0$ ground-state sublevel, the NV center can be polarized optically, and the fluorescence from exciting $m_s = 0$ sublevel is more intense than the fluorescence from exciting the $m_s = \pm 1$ sublevels. In presence of microwave field population of $m_s = 0$ can be transferred to $m = \pm 1$ levels, decreasing the total detected fluorescence.

In this study, we used a straight froward method of optically detected magnetic resonance (ODMR), to investigate the ground state $m_s = 0 \longrightarrow m_s = \pm 1$ electron spin transitions (Fig. 1b) and to study the hyperfine level structure of NV-center ensembles in the vicinity of the ground state level anti-crossing (GSLAC) (Fig. 1c).

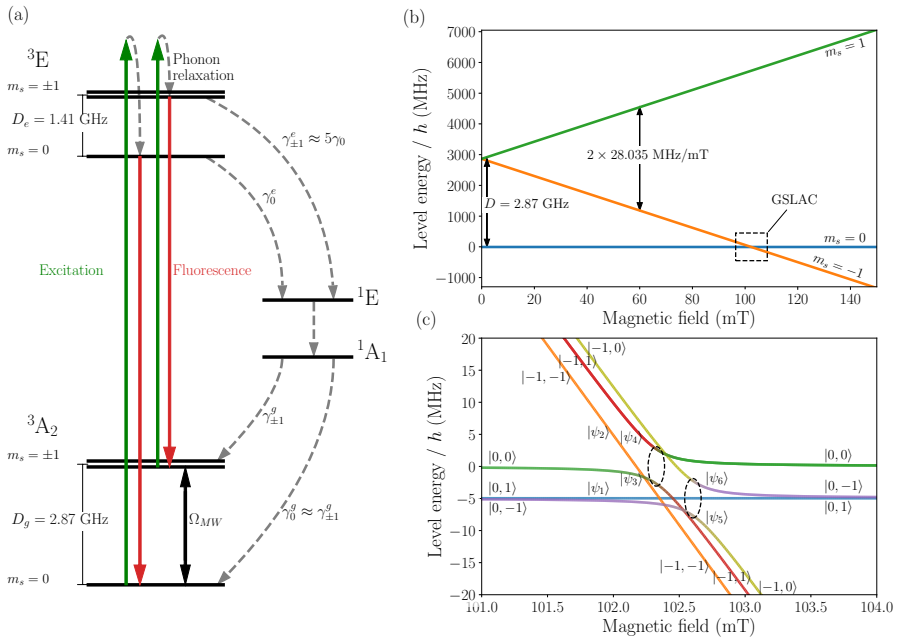


Fig. 1. (a) Energy levels scheme for an NV center. (b) Ground state levels in magnetic field. (c) Hyperfine level anticrossing at GSLAC.

As an addition to hyperfine interaction, we considered interaction with nearby $^{13}$C atoms for diamond crystals with natural $^{13}$C abundance 1.1% [3]. We calculated superhyperfine interaction between NV center $^{13}$C atoms in a lattice consisting $3 \times 3 \times 3$ unit cells. The full Hamiltonian of the system can be written as

$$\hat{H} = \hat{H}_{el} + \hat{H}_N + \hat{H}_C + \hat{H}_{N+el} + \hat{H}_{NV+C}, \tag{1}$$

where $\hat{H}_{el} = D_g \hat{S}_z^2 + \gamma_e \mathbf{B} \cdot \hat{\mathbf{S}}$ describes the ground state of the NV center with electron spin $\mathbf{S}$, $\hat{H}_N = Q\hat{I}_z^2 - \gamma_N \mathbf{B} \cdot \hat{\mathbf{I}}$ describes the $^{14}$N nucleus with spin $\mathbf{I}$, $\hat{H}_C = \Sigma_j \gamma_C \mathbf{B} \cdot \hat{\mathbf{J}}_j$ describes $^{13}$C nuclei with nuclear spin $\mathbf{J}_j$ in the external magnetic field, $\hat{H}_{N+el} = \hat{\mathbf{S}} \cdot \hat{A} \cdot \hat{\mathbf{I}}$ describes the hyperfine interaction of the NV center with the $^{14}$N nucleus and $H_{NV+C} = \Sigma_j \hat{\mathbf{S}} \cdot A'_{C13,j} \cdot \hat{\mathbf{J}}_j$ describes NV center interaction with nearby $^{13}$C atoms.

The results show, NV center interaction with $^{13}$C atoms alter the calculated ODMR signals slightly.

[1] L. Rondin et al., *Magnetometry with nitrogen-vacancy defects in diamond, Reports on Progress in Physics*, **77**, 056503 (2014), arXiv:1311.5214

[2] A. Nizovtsev et al., *Quantum registers based on single NV + $n^{13}C$ centers in diamond: I. The spin Hamiltonian method*, Optics and Spectroscopy, **108**, 230-238 (2010)

# ACTIVATION LEVELS AND PROBABILITIES OF ELECTROMAGNETIC γ- TRANSITIONS IN THE REACTION $(\gamma,\gamma')^m$ ON AVERAGES AND HEAVY NUCLEI

Eduard Gohman[1], Viktor Zhaba[1]

[1] Department of Theoretical Physics, Uzhgorod National University, Uzhgorod, Ukraine
viktorzh@meta.ua

In the experimental determination of the outputs of reactions (γ,γ') in the small interval of 5-9 MeV with a step up to 0.5 MeV there are points of deviation of the energy dependence of absolute outputs from a monotonically increasing curve [1]. This effect allows you to determine the values of individual or group of activation levels, through which the isomers of the nucleus are populated. In paper [1], the energy dependences of the outputs for reactions $(\gamma,\gamma')^m$ on the $^{77}$Se, $^{79}$Br, $^{89}$Y, $^{103}$Rh and $^{111}$Cd nuclei were analyzed for the presence of fractures.

Also, the dependences of the absolute output from energies [2-4] for the reactions $(\gamma,\gamma')^m$ on heavy nuclei $^{137}$Ba, $^{179}$Hf, $^{197}$Au and $^{199}$Hg are analyzed. The number of detected activation levels in each of these $(\gamma,\gamma')^m$- reactions ranges from one to three values.

The probabilities for γ- transitions can be approximately calculated from the formulas [5]:

$$W(EJ) \approx \frac{1}{\lambda}\left(\frac{R}{\lambda}\right)^{2J}; \qquad W(MJ) \approx \frac{1}{\lambda}\left(\frac{R}{\lambda}\right)^{2J+2}; \tag{1}$$

where $\lambda = \hbar c / E_\gamma$ - the wavelength for the emitted or absorbed γ- quanta's; $J$ - multipolarity; $EJ$ and $MJ$ - the electric and magnetic γ- radiations with parity $P=(-1)^J$ and $P=(-1)^{J+1}$ accordingly; $R$ - the radius of the emitted core.

For the selenium nucleus, the transitions from metastable levels to the isomeric level $^{77m}$Se are shown in Table 1, where the ratio of the γ transitions is indicated

$$\alpha = \frac{W(EJ)}{W(MJ)}. \tag{2}$$

Table 1. Transitions to the isomeric level $^{77m}$Se

| $\lambda$, m | $E_\gamma$, keV | $J$ | $W(EJ)$, m$^{-1}$ | $W(MJ)$, m$^{-1}$ | α |
|---|---|---|---|---|---|
| 1.48E-11 | 13.38 | 8 | 1.02E-44 | 1.44E-51 | 7.12E+06 |
| 2.25E-12 | 87.86 | 6 | 2.19E-20 | 1.33E-25 | 1.65E+05 |
| 1.42E-12 | 139.22 | 6 | 8.70E-18 | 1.32E-22 | 6.58E+04 |
| 7.12E-13 | 277.53 | 6 | 6.83E-14 | 4.12E-18 | 1.66E+04 |
| 3.81E-13 | 518.18 | 6 | 2.29E-10 | 4.82E-14 | 4.75E+03 |
| 2.98E-13 | 662.51 | 6 | 5.58E-09 | 1.92E-12 | 2.91E+03 |

Similar calculations of the probability ratio of electromagnetic γ- transitions can be made for nuclides $^{89m}$Y, $^{103m}$Rh, $^{179m}$Hf and others.

[1] V.S. Bohinyuk, V.I. Zhaba, A.M. Parlag et al., Investigation of isomeric states in the reaction $(\gamma,\gamma')^m$ on nuclei $^{77}$Se, $^{79}$Br, $^{89}$Y, $^{103}$Rh and $^{111}$Cd. Uzhhorod Univ. Scien. Herald. Ser. Phys. **37**, 161 (2015).

[2] V.I. Zhaba, I.V. Holovchak, Investigation of activation levels in the reaction $(\gamma,\gamma')^m$ on medium and heavy nuclei, Proceedings of International conference of young scientists and post-graduates "IEP-2017", Institute of electron physics, Uzhhorod, Ukraine, p. 135 (2017).

[3] V.S. Bohinyuk, V.I. Zhaba, A.M. Parlag, Investigation of isomeric states in the reaction $(\gamma,\gamma')^m$ on nuclei $^{77}$Se, $^{79}$Br, $^{89}$Y, $^{103}$Rh, $^{111}$Cd, $^{137}$Ba, $^{179}$Hf, $^{197}$Au and $^{199}$Hg, Abstracts of the reports of XXII Annual Scientific Conference of Institute for Nuclear Research of the National Academy of Sciences of Ukraine, Kiev, Ukraine, p. 24-25 (2015).

[4] V.I. Zhaba, E.V. Gohman, Activation levels in the reaction $(\gamma,\gamma')^m$ on medium and heavy nuclei, Abstracts of the XVI Conference on High Energy Physics, Nuclear Physics and Accelerators, Kharkov, Ukraine, p. 31 (2018).

[5] V.V. Varlamov, N.G. Goncharova, B.S. Ishhanov, *Physics of nuclei and nuclear data banks: the Manual* (Univ. Book, Moscow, 2010), 246 p.

# CALCULATION OF CHARACTERISTICS OF A BROWNIAN PHOTOMOTOR WITH A THREE-LEVEL ELECTRONIC SUBSYSTEM

Yuliya A. Kamysh, Irina V. Shapochkina

Department of Physics, Belarusian State University, Belarus
juliak1995@mail.ru

We present the results which are further development of the research of functioning mechanisms and operating modes of Brownian photomotors (ratchets) with a three-level electronic subsystem [1, 2]. Brownian photomotors move directionally due to changes in electronic density of a nanoparticle, in an asymmetric environment, under the action of cyclically acting laser pulses. We simulated the behavior (time changes) of populations of energy levels, including the dynamics of establishment of a stationary mode in the system.

Within the three-level model with a long duration of intervals with the laser turned off, it has been shown that the maximal motor effect is achieved with intensities and lifetimes of the states reducing the system to a two-level one. We investigated the kinetics of the three-level model of the electronic subsystem with arbitrary transition rate constants as well as the mechanism of optimization of functioning of a photomotor due to the contribution of an impurity non-resonant level, at time intervals with the laser turned off. The possibility of controlling the moment of occurrence of the motor effect is demonstrated, and it is concluded that with a certain choice of the system parameters, the main motor effect may occur when the laser is turned off.

The calculation of Brownian photomotor average velocity itself required specification of the potential energy of interaction of a nanoparticle with a substrate along which it moves. In the dipole approximation and under the assumption of one-dimensionality of the motion, this energy can be written as:

$$U(x,t) = -\sum_{j=1}^{3} n_j(t)\mu_j E(x)\,,$$

where $\mu_j$ is the dipole moment of the $j$ th level, $n_j(t)$ is the probability of finding an electron in the $j$ th state, and $E(x)$ is the strength the electric field of the substrate. For $\mu_1 = \mu_2 = 0$, $\mu_3 = \mu$, the function $U(x,t)$ is a special case of the additive-multiplicative representation $U(x,t) = u(x) + \sigma(t)w(x)$ with $\sigma(t) = n_3(t) - 1$ and $u(x) = w(x) = \mu E(x)$. This fact made it possible to use the high-temperature results of work [3] (Eq. (10)), specified for a periodic deterministic process (Eq. (15)), to calculate the average velocity of a Brownian photomotor and to study its dependence on frequency and geometric parameters of the system.

This work was partially supported by Belarusian Republican Foundation for Fundamental Research (Grant No. Ф18Р-022).

[1] Yu.A. Kamysh, I.V. Shapochkina. The theory of photomotors: stochastic process with deterministically changing transition rates. Book of abstracts of Ukrainian conference with international participation "Chemistry, physics and technology of surface" (Kiev, 23-24 May,2018. 190 p.), p. 77.

[2] V.M. Rozenbaum, M.L. Dekhtyar, Sh.H. Lin et.al, Photoinduced diffusion molecular transport. J.Chem.Phys. 145, 0641101-12 (2016).

[3] V. M. Rozenbaum, I. V. Shapochkina, Y. Teranishi, and L. I. Trakhtenberg High-temperature ratchets driven by deterministic and stochastic fluctuations // Phys. Rev. E 99, 012103 (2019).

# OPTIMAL COHERENCE WIDTH FOR IMAGING WITH PSEUDO-THERMAL LIGHT

Ilya Karuseichyk, Alexander Mikhalychev, Anton Sakovich, Dmitri Mogilevtsev

B. I. Stepanov Institute of Physics, National Academy of Sciences of Belarus, Belarus
ilkarusei@gmail.com

It is a well-known fact that imaging resolution defined by Rayleigh criterion is $\sqrt{2}$ times better for thermal light than for coherent light [1]. However, imaging resolution description in terms of Rayleigh criterion is suitable for direct image observation, but does not provide any understanding of the amount of information contained in the image, that can be gained by image post-processing. Development of resolution criteria based on informational approach is a rather popular topic today [2,3]. Yet, major researches in this field are aimed at studying imaging of uncorrelated (incoherent) sources in the subdiffraction limit (when the size of the whole imaged object is much smaller than Raleigh resolution).

In this study, we analyze imaging problem conditioning for the scheme shown in Fig. 1 (a). We make no assumption about size of the object, which is described by transmissions of its parts (pixels) $0 \le x_n \le 1$. Rotating ground glass disk, that generates pseudo-thermal light with varied coherence width $w_c$ is used as a source in the scheme. SPAD array detector is used to measure probabilities of the coincidence counts $p_{ij}$ of different detector pairs.

Using Fisher information matrix (FIM)

$$F_{mn} = \sum_{i,j} \frac{1}{p_{ij}} \frac{\partial p_{ij}}{x_m} \frac{\partial p_{ij}}{x_n} \tag{1}$$

one can predict minimal error of extracting $x_n$ values from measured probabilities $p_{ij}$ on the basis of Cramer-Rao bound

$$\Delta^2(x_n) \ge [F^{-1}]_{nn} / N, \tag{2}$$

where N is total number of joint detection events. Thus the total infidelity of object parameters $x_n$ estimation can be predicted as trace of inverse FIM $\sum_n \Delta^2(x_n) \ge \mathrm{Tr}\, F^{-1} / N$.

This approach allows to analyze imaging problem conditioning from informational point of view. Such an analysis is presented in Fig. 2 (b) (see description for details) and compared to results of experiment (Fig. 2 (c)). Theoretical analysis shows that for super-resolution regime there is an optimal coherence width $w_c$ that provides even better resolution than fully incoherent light ($w_c \to 0$), but for classical-resolution regimes incoherent source gives the best result. Value of the optimal coherence width was found to be about 1.5 size of the object pixel and being almost independent on the object shape. This prediction is in a good agreement with experimental data obtained for the same object and resolution regime.

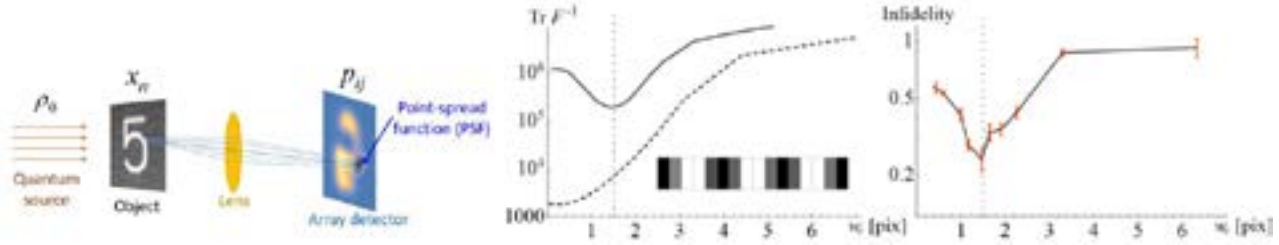


(a) (b) (c)

Fig. 1. (a) Scheme of the measurement setup. Quasi-thermal light with varied coherence width $w_c$ generated by rotating ground glass disk impinges on the object described by the transmissions $x_n$, passes through the imaging system and propagates to the array detector. (b) Prediction of the total imaging error dependence on coherence width $w_c$ for imaging of 1D object (in the inset) with quasi-thermal light. The solid and dashed lines correspond to super-resolution and classical-resolution regime respectively. Vertical dotted lines correspond to $w_c$ = 1.5 pix (the value of the minimum). (c) Experimentally measured infidelity for the same object and super-resolution regime as in (b). Red bars show the variance of the reconstruction results of 12 independent 1D data sets taken from a single 2D experiment.

Existence of optimal coherence width $w_c$ is an interesting example of tradeoff between "quantumness" of the source and additional information obtained from interference effects, that exists only for finite $w_c$. Knowledge of this optimal coherence width allows us to perform more efficient imaging beyond Raleigh limit with limited measurement statistics.

**Aknowledgments:** authors acknowledge Baenz Bessire, Manuel Unternahrer and Andre Stefanov from Institute of Applied Physics, University of Bern, for providing experimental data for this research.

[1] D'Angelo, M., & Shih, Y. H. (2005). Quantum imaging. Laser Physics Letters, 2(12), 567.
[2] Zhou, S., & Jiang, L. Modern description of Rayleigh's criterion. Physical Review A, 99(1), 013808 (2019).
[3] Tsang, M.. Quantum limit to subdiffraction incoherent optical imaging. Physical Review A, 99(1), 012305 (2019).

# SEVERE STORM FELIX: FORECASTING AND USAGE OF ECMWF AND HIRLAM MODELS

Izolda Marcinonienė

Faculty of Chemistry and Geosciences, Vilnius University
Research and Development Department, Lithuanian Hydrometeorology Service (LHMS)
izolda.marcinoniene@chgf.vu.lt

The Atlantic cyclones have the highest influence on the most episodes of severe weather in the Baltic region. In Lithuania, the maximum intensity of wind gusts is reached when the trajectory of cyclone is a bit further to the north, moving from the ocean towards Scandinavia and Russia. The cold period (late autumn-early spring) is the most preferable time this type of phenomena to occur.

The presentation demonstrates the case of 11 January, 2015. The severe weather event was selected to illustrate the prediction and development of the very powerful cyclone, called "Felix" which brought to Lithuania very strong wind (28–31 m/s), sleet, snow, freezing rain and even thunderstorm in the western part of the country (Fig. 1).

Forecasters at Lithuanian HMS mainly use global numerical weather prediction (NWP) model from European Center for Medium-Range Weather Forecasts (ECMWF), local model HIRLAM and global model ICON13 from German Weather Service (DWD). In this situation models were very successful (especially 10 m wind speed extreme forecast index, probability of wind gusts >25m/s). As a result, high wind gusts warning was issued 36 hours in advance.

The presence of the jet stream, temperature advection, cross sections of isentrops, the advection of positive upper level potencial vorticity anomaly downward to the mid-troposhere and tropopause dynamic anomaly were investigated using of the ECMWF and HIRLAM models.

| T (°C) 850 hPa | T (°C) 500 hPa | Jet stream (m/s) at 300 hPa height | CAPE (J/kg) | Indexes of instability (Lifted and Showalter) | PV=1 height (hPa) | Positive vorticity advection PVA | Condensation level LCL (hPa) | Free convection level LFC (hPa) |
|---|---|---|---|---|---|---|---|---|
| -5 | -35 | 50–60 | 100 | LI=1; SSI=3 | ~500 | ~1 | 896 | 833 |

Fig. 1. Atmospheric parameters over Lithuania at night on 11 January.

This paper focuses on the case study where very strong wind and other phenomena were used to demonstrate usefullness not only NWP models but also satellite data for analysis of pre-storm conditions, characterization of atmospheric layers and nowcasting future storm behaviour.

Different MSG satellite products, such as Water Vapour (WV6.2), Air Mass RGB, Infrared (IR10.8), pseudo satellite images including the layers of the atmospheric physical parameters (Fig. 2) helped to predict extremly dangerous phenomena precisely. The analysis of situation is widely illustrated in the presentation.

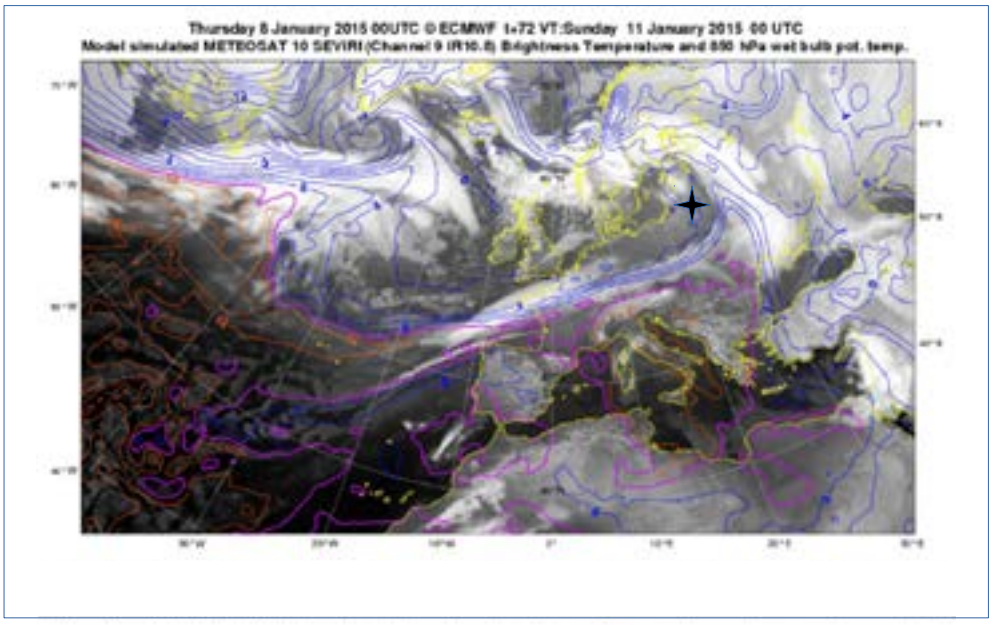


Fig. 1. Pseudo IR image and potencial temperature (isolines), forecast for 11 January 2.00 local time (ECMWF model run on 8 January).

# MEMORY EFFECTS IN EXCITATION DYNAMICS OF MOLECULAR AGREGATES

Svajūnas Korsakas[1], Darius Abramavičius[1]

[1]Institute of Chemical Physics, Vilnius University, Sauletekio ave. 9, Build. 3, LT-10222 Vilnius, Lithuania
svajunas.korsakas@ff.stud.vu.lt

Photosynthesis starts with the harvesting of sunlight energy by antena pigments from which molecular excitations are transfered to the reaction center [1]. Systems absorption spectra and energy transfer is dependent on pigments arrangement in photosynthetic complex and their interactions with surrounding environment. Even in systems where chlorophylls are the main light harvesters, antenna's composition and arrangement varies widely in nature. This wide variety lets photosynthesis to operate in fluctuating environment conditions.

There is many models to simulate dynamics for energy transfer from light harvesting antenna to reaction center. One of the most used is Redfield relaxation equation [2]. In this equation the energy transfer-relaxation enters via the correlation function of system - bath interaction operators. Correlation function gives us the dynamics of the system in time and defines the memory range in the system - bath feedback process.

In this work we study the memory effect in excitation dynamics by using the non-Markovian Redfield equation for „long memory" correlation functions that we obtain from fractional Langevin equation [3] .We take a look at Fenna-Matthews-Olson complex dynamics influenced by memory effects. By increasing the memory range, fluctuations become like classical, then the influence of coherence on population dynamics increases (fig. 1). Comparing fractional correlation function and the traditional long memory Drude model, the fractional model gives bigger influence of cohrerences on population dynamics.

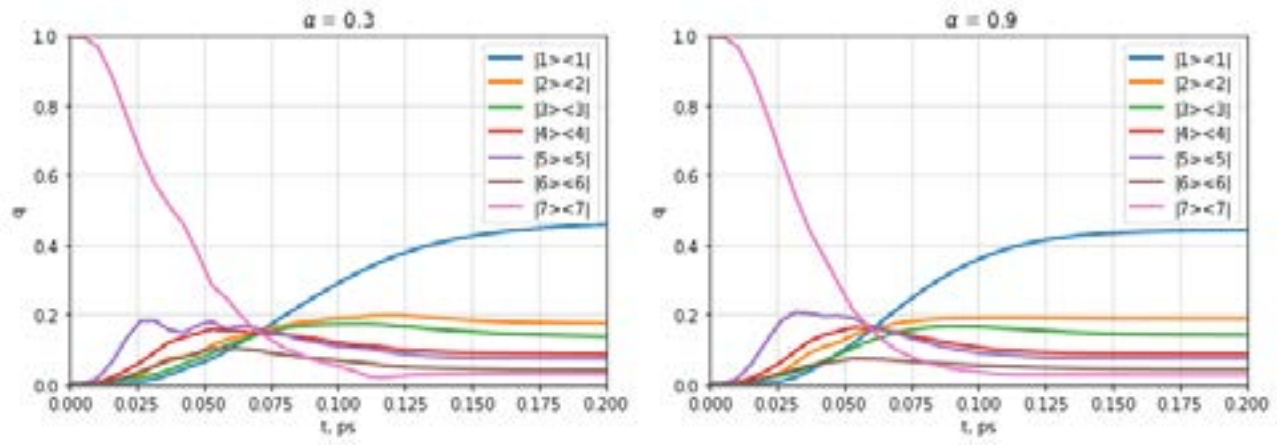


Fig. 1. FMO complex dynamics obtained by using fractional correlation function ($C(t) \sim t^{-\alpha}$), reorganization energy $20cm^{-1}$ ($\alpha \to 1$- no memory, $\alpha \to 0$- full memory).

[1] D. Abramavičius and S. Mukamel, Exciton dynamics in chromophore aggregates with correlated environment fluctuations, The Journal of Chemical Physics, **134** (2011).

[2] L. Valkūnas, D. Abramavičius, and T. Mančal, *Molecular Excitation Dynamics and Relaxation: Quantum Theory and Spectroscopy* (Wiley-VCH, Weinheim, 2013).

[3] J. Klafter, S. Lim, and R. Metzler, *Fractional Dynamics: Recent Advances*. (World Scientific Publishing CO. Pte. Ltd., 2011).

# QUARK-ANTIQUARK ANNIHILATION STUDY USING CMS 2011 DATA FROM OPENDATA PROJECT

Donatas Liupševičius, Andrius Juodagalvis

Institute of Theoretical Physics and Astronomy, Vilnius University, Lithuania
donatas.liupsevicius@ff.stud.vu.lt

In 1964 M. Gell-Mann and G. Zweig offered an idea [1] that hadrons are made of more elementary constituents, called quarks. Later it was found that hadrons are actually made of sea quarks and valence-quarks, which are held by gluons. Although quarks have a charge, they cannot be simply measured as electrons, due to their confinement in hadrons. This does not mean that they cannot be observed using experiments.

Quark-antiquark annihilation can be observed indirectly during high energy hadron collisions. Quark pair annihilation may produce a virtual Z boson, which decays into a lepton-antilepton pair. The Drell-Yan [2] process is a mechanism when quark-antiquark annihilates and lepton-antilepton is produced. This process can be observed experimentally and provides useful information about parton distribution functions, which describe the inner structure of hadrons. The Compact Muon Solenoid (CMS) [3] is one of the big CERN LHC particle accelerator detectors. The CMS detector is made of several layers. Each layer is designed to stop, track or measure different particles obtained from proton-proton or heavy ions collisions. Since most of the produced particles are unstable, they rapidly transform into the stable ones, which can be detected by the CMS. Some of the registered data can be publicly obtained from the OpenData [4] portal. The portal also provides a software and instructions of how to use data. Data analysis is done using CMS software, which is pre-installed in the CMS Virtual Machine (VM). Before starting the analysis it is useful to get acquainted with the CMS VM environment and example exercises. Therefore, a CMS Virtual Machine configuration manual [5] in the Lithuanian language was created.

This contribution presents results of the CMS 2011 collisions at $\sqrt{s} = 7$ TeV data analysis, that show a properly configured and working CMS VM. Results were obtained by modifying the example exercise to search for a process where the Z boson decays into a muon-antimuon pair. Fig. 1 shows a Z candidate invariant mass distribution, obtained analyzing data sets in CMS VM. Histogram's mean value within the error matches the known Z boson mass $-91.19$ GeV. Also, the histograms of energy, transverse momentum, and momentum components were obtained.

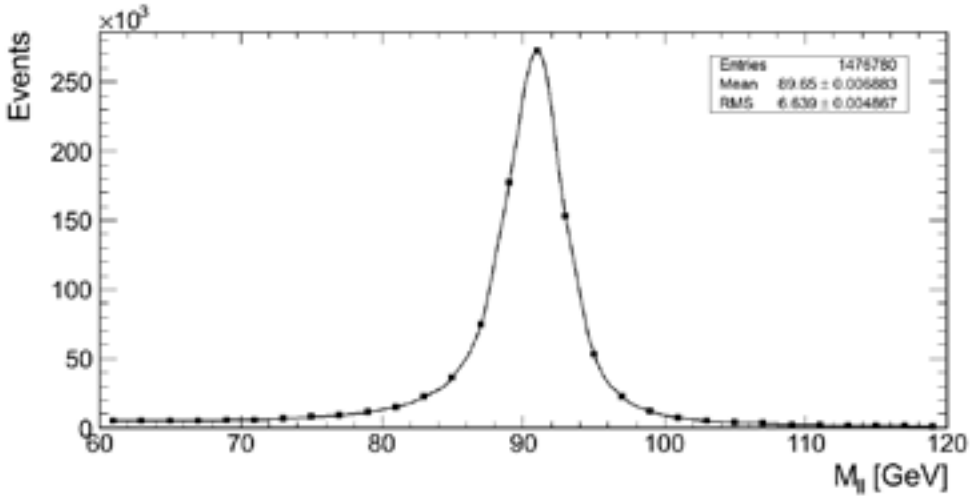


Fig. 1. A histogram shows Z candidate invariant mass distribution, obtained analyzing CMS 2011 collision data using CMS VM.

[1] D. J. Griffiths, Introduction to Elementary Particles, Wiley (2004).
[2] S. D. Drell, T. M. Yan, Massive Lepton-Pair Production in Hadron-Hadron Collisions at High Energies, Physical Review Letters, 1970, 25, 902.
[3] The CMS Experiment at CERN, About CMS, http://cms.cern/detector (Checked on 2019-02-01).
[4] Open Data Portal, About, http://opendata.cern.ch/docs/about (Checked on 2019-02-01).
[5] D. Liupševičius, A. Juodagalvis, CMS OpenData 2011 m. virtualiosios mašinos aplinkos diegimas ir konfigūravimas.

# MANIFESTATIONS OF WEYL DISPERSION FOR COLD ATOMS

Povilas Račkauskas[1], Gediminas Juzeliūnas[1]

[1]Vilnius University, Institute of Theoretical Physics and Astronomy, Lithuania
racpovilas@gmail.com

Recently a considerable amount of interest has been drawn to quasi-particles exhibiting a three-dimensional dispersion of the Weyl type. In such a dispersion there is a linear dependence of the energy on the momentum together with a Weyl singularity at zero-momentum [1]. The Weyl particles are massless fermions. As of today, no such elementary particles have been discovered in Nature. Yet the Weyl fermions can be simulated in condensed matter [2, 3, 4] and various metamaterials [5, 6], as well as using ultracold atoms [7, 8, 9].

Of significant interest is the behaviour of a Weyl particle in a magnetic field. In that case the zero-energy Landau level becomes chiral, and the particle exhibits a unidirectional motion parallel to the magnetic field. This produces what is called the chiral anomaly [1]. Up to now chiral anomalies have not been studied for cold atoms. In this work we show how a Weyl-like behaviour can be created using cold atoms within an optical lattice. We show that with an appropriate choice of complex tunnelling amplitudes the Weyl Hamiltonian can be derived from the Harper-Hofstadter Hamiltonian, the realization of which is well within experimental reach.

[1] N. P. Armitage, E. J. Mele, and A. Vishwanath, Weyl and dirac semimetals in threedimensional solids, Rev. Mod. Phys., Jan 2018, **90**, 015001.
[2] S.-Y. Xu, I. Belopolski, N. Alidoust, et al., Discovery of a weyl fermion semimetal and topological fermi arcs, Science, 2015, **349**, 613–617.
[3] B. Q. Lv, H. M.Weng, B. B. Fu, et al., Experimental discovery of weyl semimetal taas, Phys. Rev. X, Jul 2015, **5**, 031013.
[4] M. Hasan, S. Xu, I. Belopolski, and S. Huang, Discovery of weyl fermion semimetals and topological fermi arc states, Annual Review of Condensed Matter Physics, 3 2017, **8**, 289– 309.
[5] L. Lu, Z. Wang, D. Ye, L. Ran, L. Fu, J. D. Joannopoulos, and M. Soljacic, Experimental observation of weyl points, Science, 2015, **349**, 622–624.
[6] J. Noh, S. Huang, D. Leykam, Y. D. Chong, K. P. Chen, and M. C. Rechtsman, Experimental observation of optical Weyl points and Fermi arc-like surface states, Nature Physics, June 2017, **13**, 611–617.
[7] B. M. Anderson, G. Juzeliunas, V. M. Galitski, and I. B. Spielman, Synthetic 3d spin-orbit coupling, Phys. Rev. Lett., Jun 2012, **108**, 235301.
[8] B. M. Anderson, I. B. Spielman, and G. Juzeliunas, Magnetically generated spin-orbit coupling for ultracold atoms, Phys. Rev. Lett., Sep 2013, **111**, 125301.
[9] T. Dubcek, C. J. Kennedy, L. Lu, W. Ketterle, M. Soljacic, and H. Buljan, Weyl points in three-dimensional optical lattices: Synthetic magnetic monopoles in momentum space, Phys. Rev. Lett., Jun 2015, **114**, 225301.

# SIMULATION OF FUNCTIONING OF AN ADIABATIC BROWNIAN RATCHET DRIVEN BY SMALL SINUSOIDAL FLUCTUATIONS OF THE NANOPARTICLE POTENTIAL ENERGY

Ulada Vysotskaya[1], Viachaslau Dzianisau[1], Helena Shakel[2], Irina Shapochkina[1]

[1] Department of Physics, Belarusian State University, Belarus

[2]National Institute for Higher Education, Belarus

vladavysockaya@mail.ru

We present some new results in modeling of Brownian ratchets, i.e. systems that can demonstrate a directional motion as a result of rectification of unbiased nonequilibrium fluctuations under the broken reflection symmetry [1]. In the theory of Brownian ratchets, the development of various approximations is a promising and fruitful method of obtaining analytical results and formulating generalized conclusions [2]. Among them is the approximation of small fluctuations of potential energy of a nanoparticle. Under the assumption, justified for many artificial ratchet systems, of separation of the potential energy into a stationary spatially periodic ($L$ is a period) contribution, $u(x)$, and a small time-dependent perturbation, $\sigma(x)w(x)$, $U(x,t) = u(x) + \sigma(t)w(x)$, it turned out to be possible an elegant generalized integral representation of the average velocity of Brownian ratchets valid for arbitrary time laws $\sigma(x)$ [2,3]:

$$\langle v\rangle = L(\beta D)^2 \int_0^L dx \rho^{(+)}(x) w'(x) \int_0^L dy S(x,y) \frac{\partial}{\partial y} w'(x) \rho^{(-)}(y) \qquad (1)$$

$D$ is the diffusion coefficient, $\beta$ is the inverse thermal energy, $\rho^{(\pm)}(x)$ is the Boltzmann distribution in the potential $\pm u(x)$. This representation is based on the subtask of finding the Green's function of the equation of diffusion in the stationary profile $u(x)$ which, together with the second-order autocorrelation correlation function of $\sigma(t)$, determines $S(x,y)$ [2,3].

Obtaining quantitative characteristics of a ratchet requires specification of the spatial-temporal dependencies of the potential energy. As $w(x)$-function, a sinusoidal (spatially harmonic) signal has been chosen, relevant for practical applications. If the shape of $u(x)$-function is not extremely asymmetric (a saw-tooth potential, a two-well potential of the hindered rotation, a potential of the two first harmonics, etc.), a construction of the Fourier analogue of the integral result becomes an effective strategy in modeling. We were interested in studying changes in behavior of stopping points and the multiplicativity (in terms of frequency-geometric parameters) of the structure of the velocity of ratchets with varying temperature and frequency of the perturbing signal. The adiabatic approximation and the choice of dichotomous time dependence of fluctuations allowed us to simplify the model to a one-dimensional sum over the Fourier components of controlling functions of the problem. We discuss a strategy of a choice of a phase shift of the perturbing signal, frequency and temperature, which are nonlinear mixed, for the control of the direction of Brownian ratchet motion. Graphic interpretations of the results obtained and recommendations on the organization of optimal modes of a ratchet have been given.

This work was partially supported by Belarusian Republican Foundation for Fundamental Research (Grant No. Ф18Р-022).

---

[1] P. Reimann, Brownian motors: noisy transport far from equilibrium, Phys. Rep. **361,** 57 – 265 (1990).

[2] V.M.Rozenbaum, I.V.Shapochkina, L.I.Trakhtenberg, Green's function method in the theory of Brownian motors, Physics Uspekhi (Progress in Physical Science), accepted (2019).

[3] U. A. Vysotskaya, I. V. Shapochkina, V. M. Rozenbaum et al, Diffusion of Brownian particles in a spatially periodic potential with a finite life-time, Journal of the Belarusian State University. Physics **3**, 33-40 (2017).

# NON-LINEAR EXCITON DYNAMICS IN 1D MOLECULAR LATTICE

Aurimas Vitkus[1], Jevgenij Chmeliov[1]

[1]Institute of Chemical Physics, Faculty of Physics, Vilnius University, Lithuania
aurimas.vitkus@ff.stud.vu.lt

One-dimensional (1D) lattices are structures where particles (e.g. molecules) are placed in such a way that they can only communicate with two neighbours (e.g. single-walled carbon nanotubes [1]). In these lattices particles can be optically excited and molecular excitons can be generated. The dynamics and relaxation of these excitons can be modelled using multiple methods (Monte Carlo, kinetic equations, etc.).

However, in real experiments on molecular aggregates, sometimes several excitons per aggregate are simultaneously generated, especially at higher excitation intensities. When that happens exciton–exciton annihilation becomes very important. During this process, two or more excitons reach the same molecule, the resulting approximately doubly excited state relatively fast relaxes to a single excitation state, while the lost electronic energy is dissipated as heat. In small molecular system, when excitation migration through the aggregate can be neglected, the singlet–singlet annihilation can be modelled by solving the corresponding kinetic equations [1,2]. However, for larger aggregates, excitation diffusion must be taken into accounts, which significantly complicates modelling of the exciton dynamics.

In this work, we performed Monte Carlo simulations on the dynamics of multiple excitons in a 1D lattice. To produce the random walk of each exciton at each time step we generated random numbers between zero and one. We then compared these numbers to the probabilities of as single exciton's movement (move to the left; move to the right or stay in the previous position). After the random walk of a time step, we then checked if any molecule had more than one exxciton. If it did, then it had it's exciton number reduced to one and another time step began. Using this model, we generated multiple systems with varying numbers of excitons and eveluated the mean excitation lifetimes of each system. The obtained result is shown in Fig. 1.

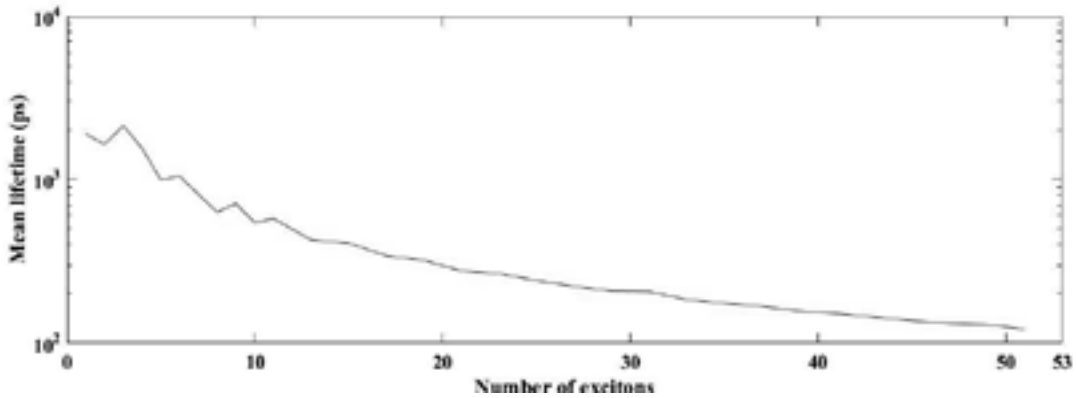


Fig. 1. The calculated relationship between the mean excitation lifetime and the number of the initially generated excitons per 1D aggregate.

[1]. Leonas Valkunas, Ying-Zhong Ma, Graham R. Fleming et al., Exciton-Exciton annihilation in single-walled carbon nanotubes, Phys Rev.**73**, 115432 (2006).

[2] A V Barzykin, M Tachiya et al., Stochastic models of charge carrier dynamics in semiconducting nanosystems, Phys Rev. **19**, 0953-8984 (2007)

# CAPABILITIES OF THE ELECTRONIC ENERGY STRUCTURE CALCULATION SOFTWARE

Sebastian Wilman[1], Magdalena Elantkowska[1], Jaroslaw Ruczkowski[2], Andrzej Sikorski[2]

[1]Faculty of Technical Physics, Poznan University of Technology, Poland
[2]Faculty of Electrical Engineering, Poznan University of Technology, Poland
sebastian.b.wilman@doctorate.put.poznan.pl

Due to the insufficient amount of data to perform accurate calculations of the energy structure of arsenic, antimony and bismuth atoms, the investigation of the analogous radial parameter values shift within the 15-th group of the periodic table will be performed. As the first step of this research the fine structure and hyperfine structure calculations of the even-parity configuration of the atomic nitrogen were carried out. The system of even configurations of the nitrogen has a similar structure, therefore it is purposeful to determine the two-body contributions to the fine and the hyperfine structures, resulting from the excitations from electronic closed shells to open shells and from closed shells to empty shells for this element first.

On the basis of experimental data [1, 2], a multi-configuration fit of 170 even configurations ($2s2p^4$, $2p^43d$, $2p^45g$, $2s2p^23s^2$, $2s2p^23d^2$, $\sum_{n=3}^{80} 2s^22p^2ns$, $\sum_{n=4}^{80} 2s^22p^2nd$, $\sum_{n=5}^{14} 2s^22p^2ng$) was carried out. The present report is the application of our many-body parametrization method allowing the analysis of a complex electronic system composed of a configuration of up to four open shells, presented in general terms in the first work of the series under the common title *Construction of the energy matrix for complex atoms* [3]. The contributions from the second-order perturbation theory originating from electrostatically correlated spin-orbit interactions in the fine structure, as well as electrostatically correlated hyperfine interactions (core polarization effects) in the hyperfine structure, were considered. Calculations of the nitrogen system was performed on personal computer (PC) due to the sufficiently low number of matrix elements describing the system.

The calculations of the enormous fine- and hyperfine structure matrices required high-performance computing (HPC), concerning both CPU (Central Processing Unit) speed and memory allocation. For the purpose of the huge matrix diagonalization in the case of terbium atom, the methods utilizing the personal computer clusters and, alternatively, the Microsoft Azure cloud computing, have been proposed by us in the papers [4]. Recently our program package was launched in Poznan Supercomputing and Networking Center (PSNC) and calculations of holmium atom are carried out using the resources of the Poznan Supercomputing and Networking Center.

For unknown electronic levels predicted values of the level energies and hfs constants are given, which can facilitate further experimental investigations.

The research within this work was financially supported by the Ministry of Science and Higher Education within the project realized at Faculty of Technical Physics, Poznan University of Technology (formerly: 06/65/DSPB/5183).

[1] J. E. Sansonetti, W. C. Martin, Handbook of Basic Atomic Spectroscopic Data, Journal of Physical and Chemical Reference Data **34(4)** , 1559-2259 (2015)
[2] M. A. Heald, R. Beringer, Hyperfine Structure of Nitrogenl Physical Review **96(3)**, 645-648 (1954)
[3] M. Elantkowska, J. Ruczkowski, A. Sikorski, J. Dembczyski, Construction of the energy matrix for complex atoms, The European Physical Journal Plus, 132(11) (2017) *(and previous papers)*
[4] M. Elantkowska, A. Sikorski, J. Ruczkowski, J. Dembczyski, Construction of the energy matrix for complex atoms, The European Physical Journal Plus, 132(3) (2017) .

# INTERACTION BETWEEN GRAPHENE AND SURFACE OF SILICON CARBIDE: QUANTUM-MECHANICAL SIMULATION

Dzmitry Hvazdousky, Maryia Baranava

Lab "CAD in Micro- and Nanoelectronics", Micro- & Nanoelectronics Department,
Belarusian State University of Informatics and Radioelectronics, Minsk, Belarus
gvozdovsky@bsuir.by

Graphene is a promising material with high charge mobility [1-3]. The substrate material has a significant negative influence on the charge carriers mobility. Silicon carbide well established as substrate in graphene technology. However, the mobility of charge carriers in such systems is worse than the theoretical calculations of a pure graphene sheet [2, 3]. The space charge inhomogeneity (so-called charge puddle) leads to degradation of the graphene electronic properties [4]. Physical characteristics leading to the occurrence of electron-hole puddles not identified uniquely [1, 5].

Silicon carbide (SiC) has unique electrical properties, due to which SiC is used in micro- and nanoelectronics. Silicon carbide has in the manufacture of high-power rectifier diodes, microwave diodes, thermistors, field-effect transistors with good frequency properties, as well as high-energy particle counters that are capable of operating in chemically aggressive environments.

Calculations were performed by quantum-mechanical simulation without taking into account of Van der Waals forces which are significant in layered structures. Calculations were performed based on the density functional theory (DFT) [6]. All of calculations have been carried out using VASP (Vienna Ab initio Simulation Package). The projector-augmented wave (PAW) potentials [7] and Perdew-Burke-Ernzerhof (PBE) functional [8] have been used. A cutoff energy of 520 eV. The atomic structures were relaxed until the forces on all unconstrained atoms were smaller than 0.01 eV/Å. A vacuum layer of 17.5 Å along z direction was constructed to eliminate the interaction with spurious replica images. The calculations were carried out without spin polarization. Integration in reverse energy space was carried on the 7×7×7 k-points grid determined by a fine grid of gamma-centered method. Static self-consistent calculations were performed using the tetrahedron method and Bloch corrections. The DFT-D3 method of Grimme [9] demonstrated the smallest difference between the calculated and experimental magnitude of lattice constants and have been used for further calculation. Fig. 1 shows charge distribution in graphene on silicon carbide substrate.

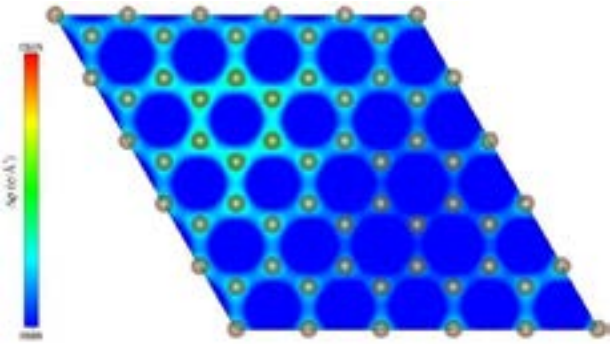

Fig. 1. Charge distribution in graphene on silicon carbide substrate.

Interlayer distances and adsorption energy were calculated. The absorption of graphene on the surface of silicon carbide with silicon dangling bonds is most energetically favorable ($E_{ads}$ = -7.2 kJ/mol). The distances between the graphene layer and the surface of the substrate range from 3.23 to 3.35 Å, which corresponds to physical adsorption with a strong influence of the Van der Waals forces.

The band structures were calculated for the graphene on silicon carbide surface. Changes in the states of graphene under the action of a substrate are observed in the immediate vicinity of the Fermi level. The Fermi level is shifted toward to the valence band, which indicates a small redistribution of charge on the substrate. Overflow of charge occurs on the near-surface silicon atoms. Energy gap arises width 86 meV between the bonding and antibonding π-zones of graphene. Electronic structure of adsorbed graphene has no changes.

Acknowlegments: This work was supported by the grant 3.02 Belarusian National Scientific Research Program "Convergence 2020".

[1] K. Geim, K. S. Novoselov, The rise of graphene, Nat. Mater. **6,** 183 (2007).
[2] F. Schwierz, Graphene transistors, Nat. Nanotechnol. **5**, 487 (2010).
[3] H. Castro Neto, F. Guinea, N. M. Peres et al., The electronic properties of graphene, Rev. Mod. Phys. **81**, 109 (2009).
[4] Y. Zhang, V. W. Brar, C. Girit et al., Origin of spatial charge inhomogeneity in graphene, Nat. Phys. **5,** 722 (2009).
[5] E. H. Hwang, S. Adam, S. Das Sarma, Carrier transport in two-dimensional graphene layers, Phys. Rev. Lett. **98**, 186806 (2007).
[6] R. G. Parr, W. Yang, Density-Functional Theory of Atoms and Molecules (Oxford University Press, 1989).
[7] P. E. Blöchl, Projector augmented-wave method, Phys. Rev. B: Mater. Phys. **50**, 17953 (1994).
[8] G. Kresse, D. Joubert, From ultrasoft pseudopotentials to the projector augmented-wave method, Phys. Rev. B: Mater. Phys. **59**, 1758 (1999).
[9] S. Grimme, Semiempirical GGA-type density functional constructed with a long-range dispersion correction, J. Comp. Chem. **27**, 1787 (2006).

# Deriving star cluster parameters with convolutional neural networks

Jonas Bialopetravičius[1,2], Donatas Narbutis[1,2], Vladas Vansevičius[1,2]

[1]Vilnius University Observatory, Saulėtekio av. 3, LT-10257 Vilnius, Lithuania
[2]Center for Physical Sciences and Technology, Saulėtekio av. 3, LT-10257 Vilnius, Lithuania
jonas.bialopetravicius@ff.vu.lt

Convolutional neural networks (CNNs) have been proven to perform fast object classification and detection on natural images and have the potential to infer astrophysical parameters on the exponentially increasing amount of sky-survey imaging data. The inference pipeline can be trained either from real human-annotated data or simulated mock observations. Until now, star cluster analysis was based on integral or resolved stellar photometry. This limits the amount of information that can be extracted from cluster images.

We aim to develop a CNN-based algorithm capable of simultaneously deriving ages, masses, and sizes of star clusters directly from multi-band images. We also aim to demonstrate CNN capabilities on low-mass semi-resolved star clusters in a low-signal-to-noise-ratio regime.

In this study a CNN was constructed based on the deep residual network (ResNet) architecture [1] and trained on simulated images of star clusters with various ages, masses, and sizes. To provide realistic backgrounds, star fields of M31 galaxy taken from The Panchromatic Hubble Andromeda Treasury (PHAT) survey [2] were added to the mock cluster images. Examples of generated clusters can be seen in Fig. 1.

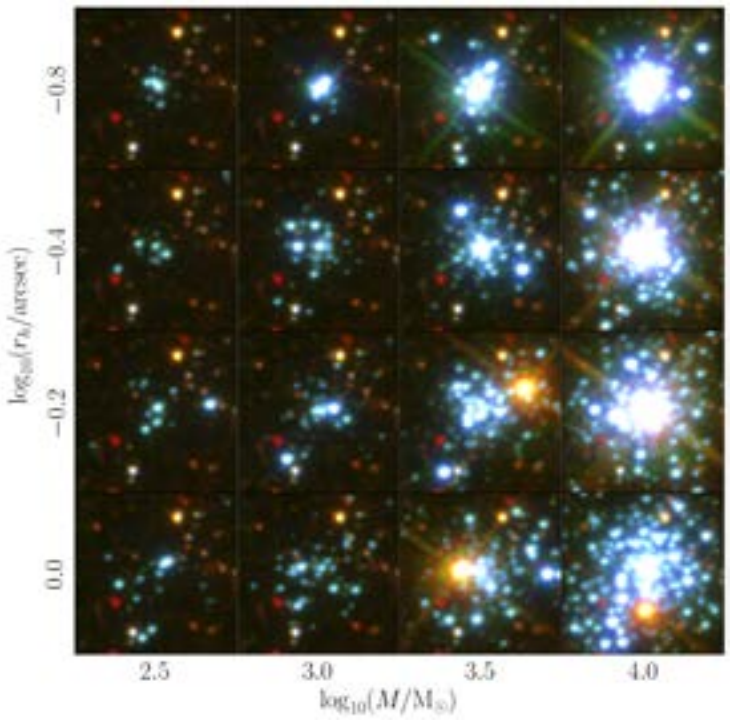


Fig. 1. Examples of generated clusters on the same real background image. The ages of all displayed clusters are 10 Myr. The mass and $r_h$ (radius that encloses half the number of stars) values are varied as shown on the axes. The intensity scale of the images was normalized with the arcsinh function.

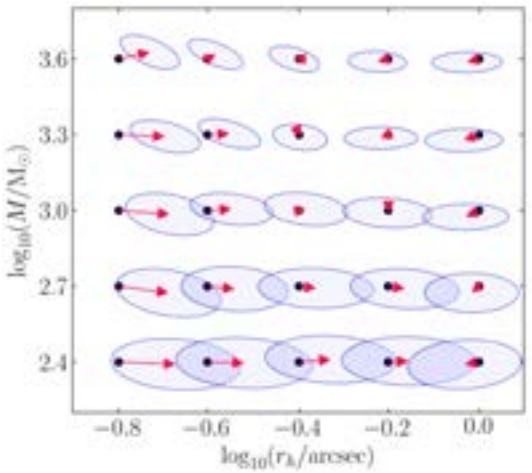


Fig. 2. Test results of CNN performance of clusters with age 10 Myr. Each black dot corresponds to the true parameters of 200 artificial clusters. Ellipses enclose one $\sigma$ (39% of 2D distribution) of their inferred values (precision), with the red arrows pointing to the means of the distributions (bias).

The proposed CNN was verified on mock images of artificial clusters and has demonstrated high precision and no significant bias (Fig. 2) for clusters of ages less than 3 Gyr, masses between 250 and 4000 $M_\odot$, and sizes ($r_h$) between 0.15 and 10 arcsec. The CNN-based cluster analysis pipeline is end-to-end, starting from input images all the way to the inferred parameters; no hand-coded steps have to be performed: estimates of parameters are provided by the neural network in one inferential step from raw images [3].

This allows both unresolved and semi-resolved cluster cases to be dealt with homogeneously, and multiple photometric passbands to be used in an integrated manner.

[1] K. He, X. Zhang, S. Ren, J. Sun, Deep Residual Learning for Image Recognition, 2016 IEEE Conference on Computer Vision and Pattern Recognition (CVPR).
[2] PHAT survey data: https://archive.stsci.edu/prepds/phat/.
[3] J. Bialopetravičius, D. Narbutis, V. Vansevičius, Deriving star cluster parameters with convolutional neural networks. I. Age, mass, and size, Astronomy & Astrophysics, doi:10.1051/0004-6361/201833833.

# SOIL MOISTURE AND PRECIPITATION CONDITIONS IN 2017

Viktorija Mačiulytė

Institute of Geosciences, Vilnius University, Vilnius, Lithuania
viktorija.maciulyte@chgf.vu.lt

In 2017 warm season eastern part of Baltic Sea region got huge precipitation amount. It was calculated that Lithuania in June-October got 50 % more precipitation than normal. In some Lithuania parts there were 2-3 times more monthly precipitation than usual. Long term precipitation in many Lithuanian municipalities has caused high damage to crops, and some of the crops have not been harvested. Autumn sowing was heavily aggravated by soaked soil and low air temperatures [1]. Because of this situation about 22 % of agriculture harvest was lost and about 88 % of winter agricultural plants were not seeded, so farmers have lost over 246 million of euros income.

The goal of this research – to estimate the soil moisture and precipitation patterns in the eastern part of Baltic Sea region (53–60°N and 20–30°E) covering warm season (May–October) of the 2017.

Remote sensing soil moisture data were derived from Copernicus Sentinel SWI (Soil Water Index, % ) product which was created from METOP/ASCAT sensor with 0.1° spatial and daily temporal resolution. It was also used daily precipitation amount from E-OBS database with 25 km spatial resolution. It was calculated daily SWI anomalies from 2007–2016 average and clustered using k-means method to separate spatial differences of anomalies.

Analyzed Sentinel SWI showed, that start of June SWI was normal (almost no anomalies comparing with 2007–2016 period). After heavy rainfalls (not shown) soil moisture anomaly increased. All the season soil moisture was higher than usual and soil moisture anomalies variation were determined by long term high precipitation amount.

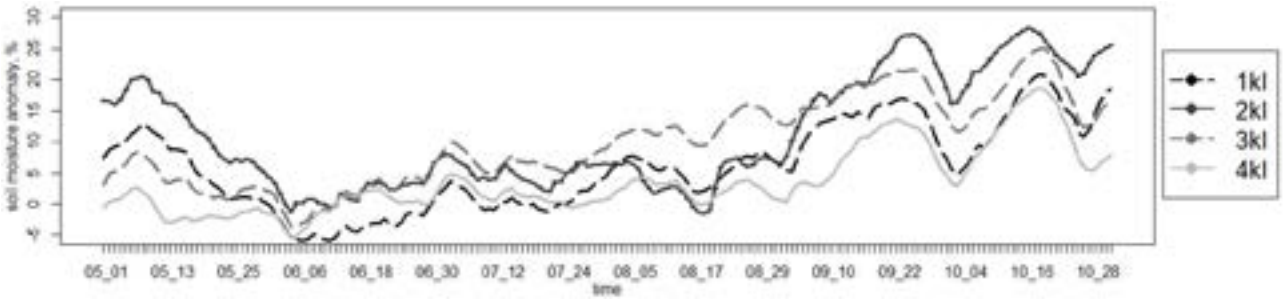


Fig. 1. Clusters of soil moisture anomalies means in %.

In September 23–October 2 there was almost no precipitation, that leads soil moisture anomaly decreasing (Fig. 1). After this period smaller amounts of precipitation than previously leads increasing soil moisture anomaly at the same level than before non-rainy period. It is believed that this anomaly increase determined of less precipitation is related with soil saturation by water.

Almost all territory got more precipitation than usual, but highest soil moisture anomalies were in eastern Latvia and eastern–southwestern Lithuania parts (2th and 3th clusters in Fig. 1 and Fig. 2). Not all territories react to precipitation amount at the same way. It mostly depends on land use, soil type and texture, so further analysis is needed.

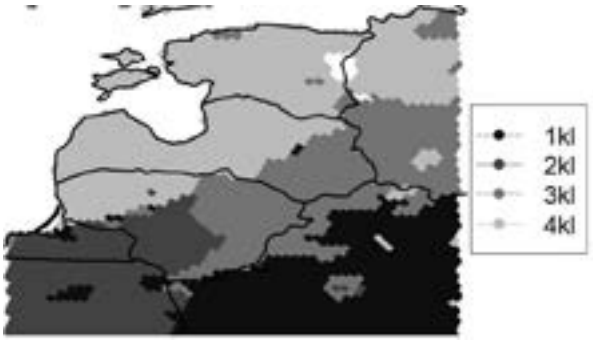


Fig. 2. Clusters of soil moisture anomalies in 2017 June-October.

On climate change precipitation amount and distribution in time and space is changing. Mostly soil moisture studies are focused on drought analysis. But heavy and long-term rainfalls periods are also important. Especially, if it is not usual events. Remote sensing information allows to analyze spatial distribution on droughts and floods to appreciate damage on spatial and temporal scales.

[1] Lietuvos Respublikos Žemės ūkio ministerija. 2017. 2017 metų veiklos ataskaita, Nr. 8D-108 (16.12). Vilnius.

# SEARCH AND IDENTIFICATION OF EXTRATERRESTRIAL PARTICLES (MICROMETEORITES)

Anastasiya Martynava[1], Anastasiya Huryna[1], Natallja Arekhava[1],
Anatoli Zajogin[2], Maksim Shundalau[2]

[1] Secondary School No. 64, Minsk, Belarus
[2] Faculty of Physics, Belarusian State University, Minsk, Belarus
nastzmart2002@mail.ru

Micrometeorites are small (usually < 0.5 mm) extraterrestrial particles of dust that have mainly asteroid and comet origin. It is estimated that approximately 7 tons of extraterrestrial dust daily reach the Earth surface [1]. In contrast of rare large meteorites, micrometeorites fall to the Earth daily and accumulate on its surface. They can be found on flat roofs in the warm dry season. Micrometeorites contain important information of state of interplanetary matter and its evolution. The classification of micrometeorites one can find in [2].

In this study, at the first time in Belarus micrometeorites were found and their chemical composition was established by laser-induced breakdown spectroscopy.

Firstly we have collected dust from the part (10×5 m) of the roof of apartment building by mobile electric vacuum cleaner before and after Earth's passing through Arietids, Southern Delta Aquariids, and Perseids meteor showers. Then we have sifted samples and separated small particles from large ones. After that light particles were removed by flushing out with water and sediment has been dried. Particles with magnetic properties have been separated by a magnet. Then we viewed them through the Delta Optical BioLight 300 microscope (up to 400× power) and took samples, which are similar to spherules, particles with unusual structure and color and particles looking as melted. Using Larsen's classification [3] we have pre-selected samples of terrestrial origin and extraterrestrial particles supposed. All of them were from 0,3 to 3 mm.

The chemical composition of 82 particles was determined using double-pulse atomic-emission spectrometry. The analysis has been carried out using multichannel laser LSS-1 spectrometer, which has the following characteristics: wavelength is 1064 nm (first harmonic of Nd:YAG laser), pulse duration is around 15 ns, pulse energy is 35 mJ, pulse-to-pulse time interval is 8 μs. The thickness of the layer evaporating by laser ablation is 5 μm, which makes it possible to perform a layer-by-layer analysis of the largest particles.

The spectra of the iron and stony parts of the Brahin meteorite (pallasite) [4] were used as reference spectra. Fig. 1*a* presents emission spectra of the iron part of Brahin meteorite and one of the samples (surface and subsurface layers). One can see that this particle has the similar chemical composition as the iron part of Brahin pallasite. The presence of such elements as iron, magnesium, calcium, and titanium (the only one particle) has been established in the collected samples. Totally, 19 iron micrometeorites have been identified by laser spectral analysis. One of the iron meteorites is shown in Fig. 1*b*.

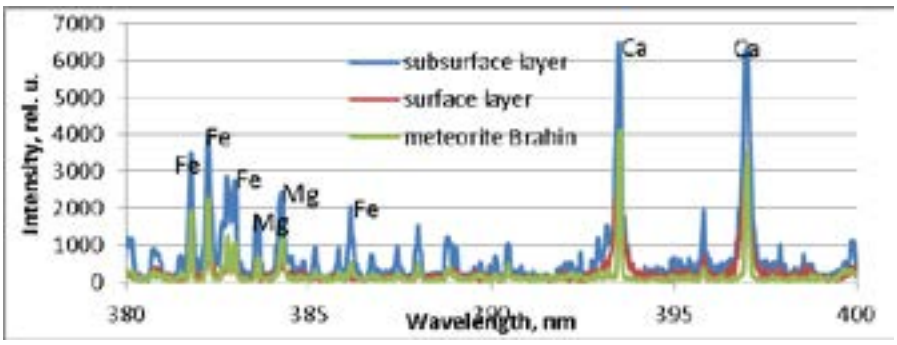


*a*

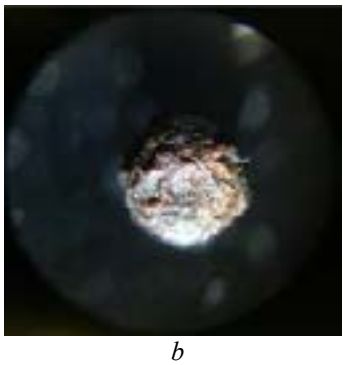

*b*

Fig. 1. Emission spectra of iron part of Brahin meteorite and one of the iron micrometeorites (*a*). Microscope image of one of the iron micrometeorites (*b*).

Similar studies were carried out for stony samples (one chondrite including). Using layer-by-layer analysis of the particles collected after passing of the Perseids shower it is determined that the samples contain magnesium only in internal layers. This fact indicates an extraterrestrial origin of the particles, because magnesium was evaporated from surface when micrometeorites passed through the Earth's atmosphere. Totally, 7 stony micrometeorites have been found using laser spectral analysis.

[1] S. Taylor, J.H. Lever, R.P. Harvey. Accretion rate of cosmic spherules measured at the South Pole. Nature 392, 899 (1998).
[2] M.J. Genge, C. Engrand, M. Gounelle, S. Taylor. The classification of micrometeorites. Meteorit. Planet. Sci. 43, 497 (2008).
[3] J. Larsen. In Search of Stardust: Amazing Micrometeorites and Their Terrestrial Imposters, Voyageur Press, 2017.
[4] The Meteoritical Society. Database. Meteorite Brahin. https://www.lpi.usra.edu/meteor/metbull.php?code=5130

# THE INFLUENCE OF GALACTIC COSMIC RAYS FLUX ON THE CLOUD COVERAGE AND POSSIBLE CLIMATE CHANGE

Porchkhidze Natia[1], Didebulidze Goderdzi[2], Todua Maya[3]

1Faculty of Natural sciences and engineering, Ilia State University, Georgia
2Faculty of Natural sciences and engineering, Abastumani Astrophysical Observatory, Ilia State University, Georgia
3Faculty of Natural sciences and engineering, Abastumani Astrophysical Observatory,Ilia State University, Georgia
natia.forchkhidze.1@iliauni.edu.ge

Climate change is one of the most important problems of modern society, which have natural and anthropogenic causes. The cosmic factor is natural one (like the Sun, Solar wind and etc.) Galactic Cosmic rays (GCRs) possible indirect influence on the Earth's climate has been under increased interest since the end of last century. The galactic cosmic rays, which are modulated by the solar wind, interact with atmosphere molecules and create cloud condensation nucleus and have effect on cloud covering process. In general, cloud covering influences on radiative balance on the earth surface.[1] In my presentation will be shown, the long-term trends of GCRs flux seasonal changes for whole seasons and cloudless days and cloudless nights and for Solar Radio Flux $F_{.10.7}$ index seasonal changes too. It is known that different levels of clouds have dissimilar sensitivity on GCRs.[1] Therefore using cloudless days and cloudless nights are suggested to the current investigation, is important for revealing influence of cosmic factors on cloud coverage. Solar Radio Flux $F_{.10.7}$ index is chosen, because it correlates well with the solar activity.[2] Solar Radio Flux $F_{.10.7}$ trends are monotonous, but on the other hand, the behaviors of the GCRs trends are not the same. The opposite GCR flux trends for the different season support that GCRs have an influence on climate change.
The results are got according to the GCR flux data of Rome "SVIRCO NM' and the data of cloudless days and nights of Abastumani Astrophysical Observatory (41.75N ;42.82E). The GCRs data of Rome is considered because the cut-off rigidity of Rome is close to the region near from Abastumani. (Approximately 6-7Gev)

[1] Didebulidze G.G. Todua M. "The inter-annual distribution of cloudless days and nights in Abastumani: Coupling with cosmic factors and climate change. " "Journal of Atmospheric and Solar-Terrestrial physics'', 2015
[2] https://www.swpc.noaa.gov/phenomena/f107-cm-radio-emissions

# FIRST EARTH-SCALE QUANTUM SENSOR NETWORK: DARK MATTER SEARCHES WITH THE USE OF OPTICAL ATOMIC CLOCKS

Beata Zjawin[1], Piotr Ablewski[1], Kyle Beloy[2], Sławomir Bilicki[1,3], Marcin Bober[1], Roger Brown[2], Roman Ciuryło[1], Robert Fasano[2], Hidekazu Hachisu[4], Tetsuya Ido[4], Jerome Lodewyck[3], Andrew Ludlow[2], William McGrew[2], Piotr Morzyński[1,4], Daniele Nicolodi[2], Marco Schioppo[2], Mamoru Sekido[4], Rodolphe Le Targat[3], Piotr Wcisło[1], Peter Wolf[3], Xibo Zhang[2] and Michał Zawada[1]

[1]Institute of Physics, Faculty of Physics, Astronomy and Informatics, Nicolaus Copernicus University, Grudziadzka 5, 87-100 Torun, Poland
[2]National Institute of Standards and Technology, 325 Broadway, Boulder, CO 80305, USA
[3]SYRTE, Observatoire de Paris, PSL Research University, CNRS, Sorbonne Universités, UPMC Univ. Paris 06, LNE, 61 avenue de l'Observatoire, 75014 Paris, France
[4]National Institute of Information and Communications Technology
4-2-1 Nukuikitamachi, Koganei, 184-8795 Tokyo, Japan
Email: beatazjawin@wp.pl

Observations at astronomical scales provide a strong evidence for the existence of dark matter. It is responsible for the structures that we see in the Universe, however we do not know what it consists of. We can only observe the gravitational interactions of our matter with dark matter, for example the impact that it have on stars and galaxies. Examining dark matter structure requires fine models that explain its composition in both macro and micro scales. Searches for dark matter in form of topological defects or oscillating massive scalar fields must be executed in the best laboratories in the world that enable examining the fundamentals of physics.

We established the first Earth-scale quantum sensor network based on optical atomic clocks [1]. It is aimed at dark matter detection. We provide a new bounds on dark matter-standard model coupling for the cases of both topological-defect dark matter and oscillating massive scalar fields. We use the archival data (see Fig. 1) to constrain existing dark matter models. With the use of Yb and Sr optical atomic clocks placed at three continents to improve the previous results by two orders of magnitude.

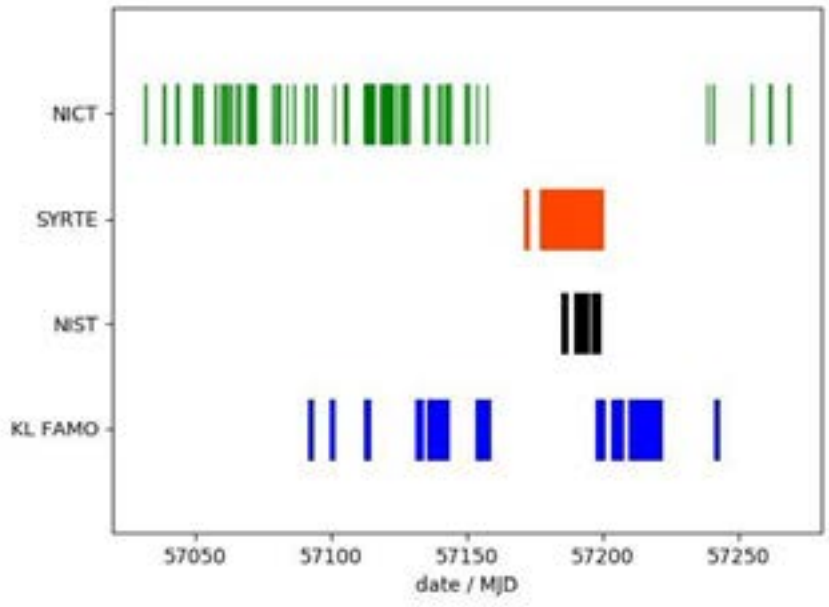


Fig. 1. Data availability from four operating optical atomic clocks: National Institute of Information and Communications Technology (NICT) in Tokyo, Observatoire de Paris (SYRTE) in Paris, National Institute of Standards and Technology (NIST) in Boulder and National Laboratory of Atomic, Molecular and Optical Physics (KL FAMO) in Toruń.

[1] P. Wcisło et al., Sci. Adv. 2018;**4**: eaau4869

# MODERN TECHNOLOGIES IN DAIRY FARMING AND MILK PRODUCTION

Karolina Grzymała[1], Daniel Radzikowski[2], Aleksandra Kalińska[2], Brygida Kruzińska[2], Urszula Ostaszewska[3]

[1] Faculty of Production Engineering, Warsaw University of Life Sciences, Poland
[2]Department of Animal Breeding and Production, Warsaw University of Life Sciences, Poland
[3] Department of Cattle Breeding and Milk Evaluation, Siedlce University of Natural Sciences and Humanities, Poland
grzymkarolina@gmail.com

In recent years, in our country we have to deal with the rapid development of technology related to the breeding of dairy cattle. The main objectives of the improvement of production methods to improve animal performance and the creation of the cows comfortable residence conditions to housing.

In his speech, I would like to introduce modern technologies, which for several years, are introduced into the breeding and dairy cows. One of the key elements of the culture is adequate genetic value of the herd. Thanks to modern breeding programs, we can choose the suitable breeding individuals, thus improving their herd. Over the years, the production of milk are introduced newer technical solutions to improve animal welfare and, above all, the increase in production economics.

The use of modern barns milking robots, robots for feeding and devices that detect estrus in cows, contribute significantly to reducing the demand for labor-intensive at the farm, thereby increasing their profitability. Recently, especially on farms with high concentration of herds, advanced electronic systems have been introduced to help producers oversee technological milking, feeding and other processes. The herd management system is a tool enabling to take everyday decisions important for production results, among which the analysis of animal behavior in the herd and their current productivity is mentioned, which facilitates the planning of long-term activities related to animal service. This allows you to increase milk yield while reducing the cost of feeding and handling the flock. In addition to the increase in milk yield, there are additional benefits associated with frequent infestation of small portions of concentrate feed, which helps maintain optimal rumen pH. As a consequence, the occurrence of potential metabolic problems in cows is reduced. It also has a positive effect on the condition of cows and reproduction rates, as well as reduces the risk of health problems associated with excessive fatness of cows before calving.

Analyzing the changes that are taking place for several years in the Polish dairy industry, only decisive changes in herd management and investments, to improve production efficiency, they can have a significant bearing on the future profitability of milk production.

# EXPRESSION OF *MDM2* GENE IN NEUROBLASTOMA PRIMARY TUMORS

Kseniia Mazan[1,3], Mariia Inomistova[1,3], Oksana Skachkova[1], Oleksandr Gorbach[1], Irina Prikhodko[2], Grygoriy Klymniuk[2], Natalia Khranovska[1]

[1] Laboratory of Experimental Oncology, National Cancer Institute, Ukraine
[2] Department of Pediatric Oncology, National Cancer Institute, Ukraine
[3] ESC "Institute of Biology and Medicine", Taras Shevchenko National University of Kyiv, Ukraine
ksusamazan@gmail.com

Neuroblastoma (NB) is an aggressive pediatric malignancy that is mostly common diagnosed during the first year of life. NB arises as ganglioneuroma or ganglioneuroblastoma from ganglion cells of the nerve crest [1]. Despite the fact that mutations in TP53 gene arise very rarely in NB, deregulation of p53-pathway often occurs and MDM2 protein involved in this process. MDM2 protein helps to target p53 for degradation through its ubiquitin activity decreasing its tumor suppressing activity [2]. In fact, MYCN is known to be one of the *MDM2* gene expression regulators. On the other hand, hyperexpression of the MDM2 protein in the cytoplasm amplifies the stabilization and translation of the *MYCN* mRNA [3]. The aim of our study is to investigate changes in *MDM2* gene expression in NB and the association with disease outcome.

We have investigated tissue samples of 80 patients with verified diagnosis of NB. The age of patients verified from 1 month to 17 years with mean age 39.45 ± 4.81 month. For total RNA isolation was used «NucleoSpin miRNA» (Macherey-Nagel, Germany) kit. To detect the level of expression of *MDM2* gene, specific TaqMan primers and probes were used; amplification was performed on 7500 Real-Time PCR System (Applied BioSystems, USA). The real-time recording of the results was carried out in accordance with the manufacturer's recommendations. Calculations were performed using the ΔΔCt relative quantification method. To detect the *MYCN* amplification FISH analysis was performed using dual-color Vysis LSI® N-MYC Spectrum Green/CEP 2 Spectrum Orange™ (Abbott, USA). Prognostic significance of markers was verified with the ROC-curve (Receiver Operating Characteristic curve). Event free survival was evaluated by Kaplan-Meier estimator, statistical significance of parameters differences was determined using F-Cox criterion.

*MDM2* expression was higher in patients with recurrent and metastatic tumors compared to primary NB. In primary tumors, the *MDM2* mRNA expression was statistically lower in 32 and 2.6 times in comparison with recurrent and metastatic tumors respectively, $p < 0.001$. Moreover, the expression level of the mRNA *MDM2* gene varied in a quite wide range and in particular depending on the stage of the disease in the primary NB tumors. The level of *MDM2* gene expression was in 28 times higher in tumor samples obtained from patients with stage IV compared to early stages, $p < 0.001$. In additional, *MDM2* expression level was significantly lower in primary tumors without *MYCN* amplification. The *MDM2* mRNA expression was in 2.9 times higher in patient group with *MYCN* amplification in comparison with *MYCN*-negative group, $p < 0.03$. The obtained data may indicate that inactivation of p53 / MDM2 pathway in NB occurs most often during treatment and is involved in the progression of the disease and the relapse occurrence.

For the distribution of patients in two groups with high or low risk according to the level of expression of the mRNA of the *MDM2* gene, the progression free survival rate as a criterion for clinical efficacy was used. For determining of the groups to high and low *MDM2* expression levels, an optimal criterion 0.0822 a.u. was obtained. According to the ROC analysis, high expression of *MDM2* mRNA was determined as a marker for a poor outcome in NB and a risk of disease recurrence. This marker is of sufficient sensitivity (> 70%) and specificity (> 65%) and can serve as an independent marker for predicting the NB outcome and stratification of patients by risk groups.

It has been established that high expression of *MDM2* gene is associated with a decrease in the rates of progression free survival in patients with NB, regardless of the *MYCN* gene status and disease stage ($p < 0.001$). Accordingly, the 3-year-old progression free survival rate in patients with high *MDM2* mRNA expression was only 12%, whereas in patients with low expression levels reached 66%.

Such a significant difference indicates that this marker plays an essential role in the pathogenesis and progression of the NB and the disruption of MDM2 / p53 pathway leads to a poor outcome in NB patients.

[1] R. Luksch, M.R. Castellani, P. Collini et al., Neuroblastoma (Peripheral neuroblastic tumours), Crit Rev Oncol Hematol 107, 163-181 (2016).
[2] G. Barone, D. Tweddle, J.M. Shohet et al., MDM2-p53 interaction in paediatric solid tumours: preclinical rationale, biomarkers and resistance, Current drug targets 15(1), 114-123 (2014).
[3] H. Zhang, L. Gu, J. Li et al., MDM2 regulates *MYCN* mRNA stabilization and translation in human neuroblastoma cells, Oncogene 31(11), 1342-1353 (2012).

# GENETIC POLYMORPHISMS OF TOLL-LIKE RECEPTORS AT TRIPLE-NEGATIVE BREAST CANCER

Olena Ripa [1,3], Maria Inomistova[1,3], Oksana Skachkova[1], Oleksandr Gorbach[1], Sergey Lyalkin[2], Natalia Khranovska[1]

[1]Laboratory of Experimental Oncology, National Cancer Institute, Ukraine
[2]Research Department of Solid Tumors Chemotherapy, National Cancer Institute, Ukraine
[3] ESC "Institute of Biology and Medicine" of Taras Shevchenko National University of Kyiv, Ukraine
alionaripa31@gmail.com

Breast cancer is the most common cancer among women in Ukraine [1]. Approximately from 8% to 20% are categorized as triple-negative breast cancer (TNBC) that does not overexpress a human epidermal growth factor receptor 2 (HER-2/neu), estrogen receptor (ER) and progesterone receptor (PR) [2]. Recent experiments have shown that toll-like receptors (TLRs) can enhance cancer cell progression, induce evasion of immune surveillance, and induce chemotherapeutic and metastasis [3]. TLRs polymorphisms may be involved in the process of breast carcinogenesis and play an important role in cancer development and treatment.

The aim of this study was to investigate *TLR2*(G753A), *TLR4*(C399T), *TLR9*(G2848A) polymorphisms and analyze their association with TNBC development.

In the present study, samples of peripheral blood of 63 patients with TNBC from age 24 to 76 years (52 ± 3.5 years) were used as a biological material to investigate polymorphisms of *TLR2, 4* and *9* genes. After DNA extraction, we used polymerase chain reaction (PCR) method to make many copies of the *TLR* 2, 4 and 9 genes with specific primers. The PCR products of *TLR2* were digested by restriction endonuclease SsiI (AciI) at 37 ºC overnight and then analyzed by 3% agarose gel electrophoresis. Bands of 228, 75 and 40 bp corresponded to TLR2 G/G; 268, 228, 75, 40 bp bands were designated as heterozygous G/A individuals; a band of 268, 75 bp corresponded to the homozygous A/A genotype. The PCR products of *TLR4* were digested by restriction endonuclease Hinf I. It was incubated overnight at 37ºC and electrophoresed in 3% agarose gel to identify the TLR4 alleles on the basis of the respective allele size. Bands of 406 bp corresponded to *TLR4* C/C; 406, 377, 29 bp bands were designated as heterozygous C/T individuals; a band of 377, 29 bp corresponded to the homozygous T/T genotype. The PCR products of *TLR9* were digested by restriction endonuclease Bsh 1236 I (BstU I) at 37 ºC overnight and then analyzed by 3% agarose gel electrophoresis. Bands of 135, 42 bp corresponded to *TLR9* G/G; 177, 135, 42 bp bands were designated as heterozygous G/A individuals; a band of 177 bp corresponded to the homozygous A/A genotype.

According to the results, in the group of 56 patients with TNBC, were found 76.8% (43/56 patients) – with homozygous genotype of the wild type *TLR2* allele (genotype G/G), 5.4% (3/56 patients) – with homozygous genotype of the mutant type allele (genotype A/A) and 17.9% (10/56 patients) with heterozygous genotype (genotype A/G). Patients with the A/A genotype of the *TLR2* gene have significant increased risk (in 13.15 times) of TNBC development compared to the control ($\chi 2 = 11.49$; $p = 0.003$).

Our results indicated that *TLR4*(C399T) is not associated with risk of TNBC development, as all of the 60 patients had CC genotype - homozygous genotype of the wild type allele of the *TLR4* gene.

According to the results, in the group of 59 patients with TNBC, were found 33.9% (9/59 patients) – with homozygous genotype of the wild type *TLR9* allele (genotype G/G), 15.3% (20/59 patients) – with homozygous genotype of the mutant type allele (genotype A/A) and 30.5% (30/59 patients) with heterozygous genotype (genotype A/G). Patients with the A/A genotype of the *TLR9* gene have significant increased risk (in 9.77 times) of TNBC development compared to the control ($\chi 2 = 95.94$; $p = \leq 0.0001$).

We established that presence of *TLR2*(G753A) and *TLR9*(G2848A) polymorphisms have an increased risk of TNBC development and may be recommended to the diagnostic marker in the primary screening of BC. Our results showed that *TLR4*(C399T) is not associated with the TNBC development.

1. Ukrainian cancer registry (National Cancer Institute, Ukraine, 2017).
2. G. Palma, G. Frasci, A. Chirico. Triple negative breast cancer: looking for the missing link between biology and treatments, Oncotarget 6(29), 26560 - 26574 (2015).
3. L. Sun, Q. Jiang, Y. Zhang. Toll-like receptors and breast cancer, Integrative Cancer Science and Therapeutics 3(2), 432 - 436 (2016).

# REVERSIBLE, ELECTRIC-FIELD INDUCED MAGNETO-IONIC CONTROL OF MAGNETISM IN MESOPOROUS COBALT FERRITE THIN FILMS

Shauna Robbennolt[1], Pau Mercier-Fernández[1], Aliona Nicolenco[1*], Eva Pellicer[1], Jordi Sort[1,2]

[1] Departament de Física, Universitat Autònoma de Barcelona, E-08193 Cerdanyola del Vallès, Spain
[2]Institució Catalana de Recerca i Estudis Avançats (ICREA), Pg. Lluís Companys 23, E-08010 Barcelona, Spain
Aliona.Nicolenco@uab.cat

Magnetic materials overall are a very useful class of materials that have been used in many applications affecting our everyday lives. Nanoporous, magnetic materials in particular are of interest in areas such as spintronics where surface and interface effects are hugely important. Traditionally in devices, magnetism has been controlled by the use of external magnetic fields created by passing current through a conducting wire. However, as devices become smaller, resistive heating in the conducting wire (or Joule heating) has led to much lower energy efficiencies. Therefore, there has been a significant research effort to control micro- and nano-scale magnetic materials directly with electric fields, thereby minimizing the electric currents involved. [1] A number of mechanisms for controlling magnetism with applied voltage have been investigated including direct voltage application, multiferroic coupling, and cation intercalation. Recently, another mechanism has been popularized called the magneto-ionic effect ion which ionic migration (often of oxygen anions) is used to induce changes in magnetism.[2]

Here we present the synthesis of nanoporous cobalt ferrite ($CoFe_2O_4$, CFO) and demonstrate magnetoionically-controlled, reversible changes in its magnetic properties. Thin films of CFO are prepared using sol-gel chemistry and made nanoporous by introducing a sacrificial block copolymer templating agent. The films are deposited via dip coating onto a Pt-coated Si and then annealed to crystallize the CFO and remove the polymer template. The final porous films are then assembled into an electrochemical cell with a Pt wire counter electrode and a propylene carbonate-based liquid electrolyte. By applying a negative voltage, the cobalt ferrite becomes partially reduced, leading to an increase in saturation magnetization of 15% ($M_S$) and a reduction in coercivity ($H_C$) as high as 28%, depending on the voltage applied (from –10 V to –50 V). Upon removal of the negative voltage, the effects are found to largely remain (*e.g.,* after removal of –10 V, $M_S$ remains 12% higher than in the pristine sample). Interestingly, with the application of a positive voltage, all changes can be completely reversed and thus the initial properties are recovered. The samples were characterized by SEM, XRD, XPS and magnetometry in order to better understand the underlying mechanism which we determine is the magneto-ionic effect where oxygen ions migrate in and out of the CFO in respond to the applied electric field.

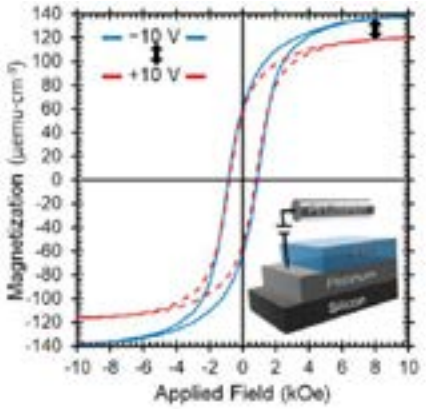


Fig. 1. Room temperature, magnetic hysteresis loops of porous cobalt ferrite (CFO) under -10 V (blue, solid curve) and +10 V (red, dashed curve) applied voltages. Inset diagram shows the sample structure (CFO on top of a Pt on Si substrate) and the Pt wire counter electrode. The voltage was applied in an electrochemical cell using a liquid electrolyte.

[1] Song, C.; Cui, B.; Li, F.; Zhou, X.; Pan, F., Recent progress in voltage control of magnetism: Materials, mechanisms, and performance. *Prog. Mater. Sci.* **2017**, 87, 33-82.
[2] Gilbert, D. A.; Grutter, A. J.; Arenholz, E.; Liu, K.; Kirby, B. J.; Borchers, J. A.; Maranville, B. B., Structural and magnetic depth profiles of magneto-ionic heterostructures beyond the interface limit. *Nat. Commun*. **2016**, 7, 12264.

# VACANCY ANALYSIS FOR THE REGIONAL LABOUR MARKET RESEARCH

Andrei Kryshtapovich[1]

[1]Department of Intelligent Systems, Belarussian State University, Belarus
krisht96@gmail.com

The labour market is the most important and complex segment of the aggregate market. In addition, the amount of information about vacancies and job applicants is constantly growing. Applicants are ready to change their place of residence in order to meet their professional goals associated with career growth, possibility of new projects, higher salaries and qualifications. The need for an automated labour market analysis system is obvious. In this research an attempt was made to create a system for collecting and analyzing information about vacancies.

Nowadays employers are interested not only in professional knowledge and skills of specialists, but also in other skills (such as fluency in foreign languages, ability to work with people and solve problems independently, etc.). For effective recruitment, staff competency matrices are developed. It is a set of requirements for company employees which displays a set of competencies and their level for specific positions. However, it is difficult for a potential job seeker to quickly cover the whole range of requirements imposed by various employers. The developed system allows you to identify the most common requests for a particular city or region, which will increase the effectiveness of preparation for the interviews and as a result will contribute to successful employment. Data is collected from open Internet recruitment agencies using Web Mining technology, accumulated and analyzed [1]. The results are provided in the form of text reports and charts. The system is implemented in Python as it is a high-level programming language focused on improving developer productivity and readability of the code [2].

The created system was tested on such job posting platforms as indeed.com (Seattle) and jobs.tut.by (Moscow, Minsk and Brest). The results are displayed as bar charts. The histogram below is the result of using the system for Minsk city (Fig. 1).

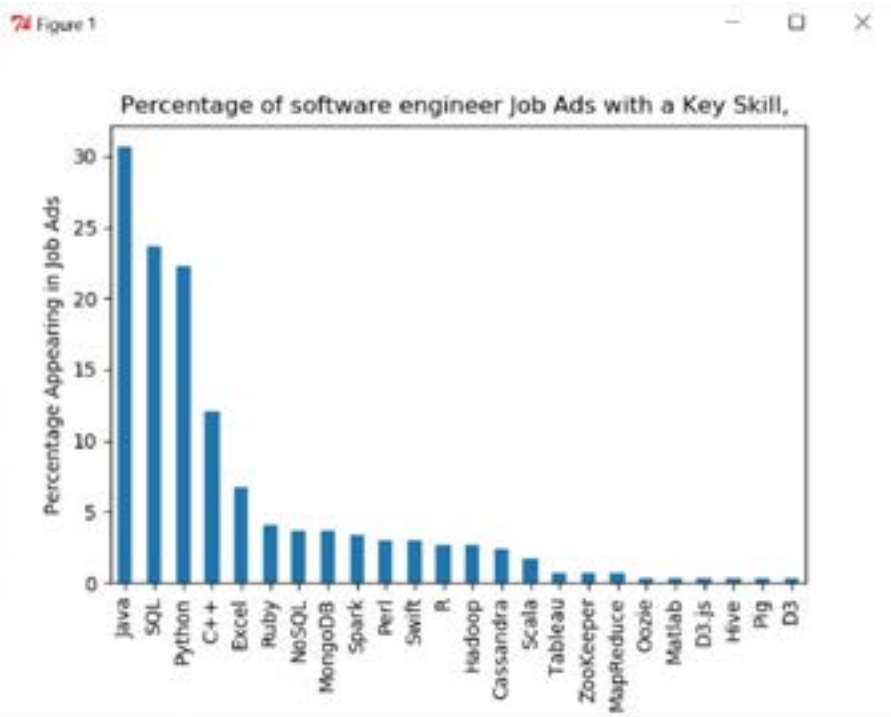


Fig. 1. Results of job market analysis (Minsk)

It can be seen that the leading positions among the most demanded skills in Minsk are held by knowledge of the Java programming language and knowledge of relational databases and SQL. There are plans to completely automate the system so it can be used by personnel specialists and other non-technical people.

[1] Mitchel, R. Web Scrapping with Python./ R.Mitchel New-York: John Wiley & Sons Inc, 2008.
[2] Lubanovic, B. Introducing Python./ B. Lubanovic. New-York; PACKT, 2017.

# STRUCTURAL CHARACTERIZATION OF SAMARIA DOPED CERIA PREPARED BY COMBUSTION AND CO-PRECIPITATION SYNTHESES

Olzhas Shalkhar[1], Fariza Kalyk[1*], Brigita Abakevičienė[1]

[1]Department of Physics, Kaunas University of Technology, K. Donelaičio 73, Kaunas, Lithuania
*fariza.kalyk@ktu.lt

Solid oxide fuel cells (SOFCs) is one of the most efficient and environmentally friendly device which transforms chemical energy of fuel into electrical energy. Due to these properties SOFCs systems are being developed for transportation, military and industrial applications. In SOFCs, Samarium doped ceria (SDC), Gadolinium doped ceria (GDC) and Yttria stabilized zirconia (YSZ) are utilized as solid electrolyte materials. Samarium-doped ceria electrolyte is known as most usable as it possesses high ionic conductivity as well as chemical and structural stability. Ceramic powders can be produced by variety of different synthesis methods such as combustion, sol-gel, colloidal, hydrothermal, Pechini and co-precipitation. Since glycine-nitrate precursor (GNP) combustion synthesis saves time and has better stoichiometric control and co-precipitation (CP) synthesis offers low cost and simplicity, these methods were used in this study to form Samarium doped ceria powders, $Sm_xCe_{1-x}O_{2-\delta/2}$ (with samarium content x = 0.26 (26 SDC)). After obtaining ceria based electrolytes they were calcined at different temperature ranges (200, 400, 600, 800 and 1000 $^{o}$C) for 5 h. X-ray powder diffractometer (XRD) is a widely employed tool which can investigate chemical, physical and mechanical properties of material. XRD analysis was performed at room temperature and diffraction patterns were recorded in the 2θ angle range of 5-100$^{o}$. The results showed that 26 SDC prepared by both synthesis routes have pure phase cubic fluorite structure with Fm-3m space group. The crystallite size and lattice parameter were calculated.

[1] Arnab Choudhury, H. Chandra, A. Arora., *Application of solid oxide fuel cell technology for power generation—A review,* (2012)
[2] Worawat Wattanathana, Chatchai Veranitisagul, Suttipong Wannapaiboon, Wantana Klysubun, Nattamon Koonsaengd, Apirat Laobuthee., *Samarium doped ceria (SDC) synthesized by a metal triethanolamine complex decomposition method: Characterization and an ionic conductivity study,* (2017)
[3] Bora Timurkutluk, Cigdem Timurkutluk, Mahmut D.Mat, Yuksel Kaplan*., A review on cell/stack designs for high performance solid oxide fuel cells.,* (2015)
[4] A. Kopp Alves., *Novel Synthesis and Characterization of Nanostructured Materials, Chapter 2.,* (2013)
[5] J. Ian Langford, D. Louer., *Powder diffraction*, 131-135 (1996)

# EVALUATION OF DNA DAMAGE AFTER BLEOMYCIN ELECTROTRANSFER TO CHO AND MX-1 CELL LINES BY USING COMET ASSAY

Aistė Rimgailaitė, Paulius Ruzgys, Saulius Šatkauskas

Faculty of natural sciences, Vytautas Magnus university, Lithuania
aiste.rimgailaite@stud.vdu.lt

Electroporation is a process, when applied electric field is a cause for an increased cell membrane permeability, leading to increased uptake of exogenous molecules such as anticancer drugs. Therefore, this method was applied to cancer treatment, as anticancer drugs can be easier transported into electroporated tumour cells. Currently, the combination of anticancer drug (mainly bleomycin) and the method of electroporation is used in clinics and termed as electrochemotherapy. Electroporation enables to reduce working concentration by 3 orders of magnitude, yet at constant cancer treatment effect.

Once inside the cell, the anticancer drug bleomycin induces the cellular DNA cleavage, that in turn leads to cell death. To the best of our knowledge, there is no published research that present cellular DNA damage after BLM transfer to electroporated cells. Consequently, it is unknown, whether the BLM has the same effect in healthy cells as compared to tumour cells and vice versa. Therefore, in this *in vitro* study, the evaluation of DNA damage after bleomycin electrotransfer to breast cancer tumour (MX-1) and chinese hamster ovary (CHO) cell lines was done by using comet assay (a single cell gel electrophoresis (SCGE)) technique.

CHO and MX-1 cell lines were used for bleomycin electrotransfer experiments. The anticancer drug bleomycin was used for electrotransfer experiments in the concentrations ranging from 0.2 to 20000 ng/ml. Cells with bleomycin were suspended in electroporation medium (conductivity 0.1 S/m, osmolarity 270 mOsm, pH 7.1). Then electroporation was performed by using combination of 8 electric pulses that induced electric fields at the amplitude of 1400 V/cm for the duration of 100 µs. Afterwards, comet assay was performed to evaluate DNA damage. In addition, clonogenic assay was done to evaluate cell viability.

Electroporated cells were resuspended in low melting agarose (0.5 %), was put on objective glass and covered with cover slip, 70 min after electroporation. Afterwards, cells were kept in lysis buffer for 24 hours. Thereafter, electrophoresis for 30 min in alkaline buffer (pH 13) was performed with voltage at 0.74 V/cm and 300 mA current. Fluorophore ethidium bromide (1 µg/ml) that binds to DNA was used to obtain visualization of the DNA damage under fluorescent microscope. Obtained cell DNA\Ethidium bromide complex fluorescence images were processed with open access software ImageJ plugin OpenComet v1.3.1.

Obtained results indicate a significant DNA damage caused by BLM electrotransfer in both used cell lines, as compared to incubation with BLM without effect by electric field. Notable, that significantly higher DNA damage as a result of BLM electrotransfer was done in MX-1 cell line when comparing to incubation with BLM without effect by electric field. Nevertheless, the tendency of dealt DNA damage was observed to be higher in CHO cell line as compared to MX-1, when using same BLM concentrations were used. As compared to MX-1, a higher DNA damage was observed in CHO cell line, which lead to decreased cell viability, approximated by evaluating cell ability to form a colony.

# FRACTIONATED IONIZING RADIATION IMPACT ON BREAST CANCER CELLS MCF-7

Akvilė Gasiūnaitė[1], Greta Jarockytė[1], Jonas Venius[1], Vitalijus Karabanovas[1,2], Ričardas Rotomskis[1,3]

[1] Biomedical Physics Laboratory of National Cancer Institute, Baublio 3B, LT-08406, Vilnius, Lithuania;
[2]Department of Chemistry and Bioengineering, Vilnius Gediminas Technical University, LT-10223, Vilnius, Lithuania;
[3]Biophotonics group of Laser Research Centre, Vilnius University, Saulėtekio 9, c.3, LT-10222, Vilnius, Lithuania
akvile.gasiunaite@nvi.lt

Cancer is one of the leading causes of death globally. Various methods are used to cure oncological diseases and radiation therapy is among the most frequently applied treatments. However, in some cases the treatment fails and cancer recurrence takes place. One of the theories states that cancerous tissue renewal after radiation therapy is due to the activity of cancer stem cells (CSC's). [1] These cells are thought to be radioresistant because of their slow cell cycle, rapid DNA repair mechanisms, ROS scavenging, ability to detoxify or exclude cytotoxic agents. [2] One of the cell surface markers used to identify CSC's is a transmembrane glycoprotein CD44 – a hyaluronic acid receptor, which is responsible for cell adhesion, proliferation and migration. [3] It is well known that the expression of CD44 is increased in CSC's. [4]

The main purpose of this research is to determine the response of cancer cells to fractionated ionizing radiation. In this study we investigate changes of morphological properties such as cell size and granularity, differences in autofluorescence, CD44 expression levels and accumulation of quantum dots (QD's) in breast cancer cells MCF-7 after treatment with ionizing radiation. In our work MCF-7 cells were treated with fractionated ionizing radiation (3x4 Gy) using linear accelerator. The expression of CD44 was assessed using monoclonal antibody conjugated with FITC and as model nanoparticles carboxylated CdSe/ZnS QD's were employed. Quantitative measurements were obtained by flow cytometer and for qualitative evaluation confocal fluorescence microscope was used. CD44 expression allows the estimation of CSC's proportion in radioresistant cells' population produced by fractionated ionizing radiation, autofluorescence may evince the changes in molecular mechanisms caused by radiation therapy and intracellular accumulation of QD's can let us gain insight into the effect of ionizing radiation on the internalization of substances as well as to evaluate a possible usage of QD's in diagnostics and therapy of radioresistant cells.

Such researches could provide a better comprehension of fractionated radiation therapy impact on cancer cells and give a deeper understanding of optimizing radiation therapy or combining several treatment methods with respect to elimination of radioresistant CSC's so that the cancer treatment would be improved and patients' survival rates increased.

[1] Rycaj, K., & Tang, D. G. (2014). Cancer stem cells and radioresistance. *International journal of radiation biology*, *90*(8), 615-21.
[2] Yoshida, G. J., & Saya, H. (2015). Therapeutic strategies targeting cancer stem cells. *Cancer science*, *107*(1), 5-11.
[3] Senbanjo, L. T., & Chellaiah, M. A. (2017). CD44: A Multifunctional Cell Surface Adhesion Receptor Is a Regulator of Progression and Metastasis of Cancer Cells. *Frontiers in cell and developmental biology*, *5*, 18. doi:10.3389/fcell.2017.00018
[4] Chen, C., Zhao, S., Karnad, A., & Freeman, J. W. (2018). The biology and role of CD44 in cancer progression: therapeutic implications. *Journal of hematology & oncology*, *11*(1), 64. doi:10.1186/s13045-018-0605-5

# INFLUENCE OF CARBOXYLATED MULTIWALLED CARBON NANOTUBES ON PROPERTIES OF RED BLOOD CELLS

Alena Kavalenka, Alexandra Zayko

Department of Biophysics, Faculty of Physics, Belarusian State University, Belarus
ai0628k@gmail.com

Carbon nanotubes (CNTs) are thought can be perspective systems for delivery of therapeutical agents and destructing of tumor cells. Nevertheless, CNTs can influence negatively on normal cells of organism [1-3]. It was shown that cytotoxic effect of CNTs on cells is strongly depends on their length and diameter, physical and chemical surface properties, method of CNTs synthesis and contamination by catalysts [4-6]. The purpose of our study was to investigate the influence of carboxylated multiwalled CNTs (CMWCNTs) and covered by polyethylene glycol (PEG) CMWCNTs on properties of red blood cells (RBC).

RBC were isolated from blood of healthy donors by washing in 0.15 M NaCl and suspended in Earl's balanced saline solution (pH 7.3). CMWCNTs were mixed with PEG 400/4000 or 0.15 M NaCl in amount of 4 mg per 1 ml and sonicated at frequency of 44 kHz during 30 min. Then, CMWCNTs were added into RBC suspension samples up to the final concentrations of 0.001, 0.01 or 0.1 mg/ml and incubated at 37 $^0$C for 20 h. After that, the cells were transferred to sediment by centrifugation and resuspended in fresh medium, and the obtained supernatants were collected to determine of hemoglobin release from RBC. The levels and type of hemoglobin in the samples of RBC extracellular medium were determined by analysis of absorption spectra at 380-700 nm. The sizes of RBC were estimated using light microscopy and nephelometry methods.

It has been revealed that under action of CMWCNTs the levels of free hemoglobin in RBC extracellular medium are decreased, particularly after addition of 0.1 mg/ml CMWCNTs (fig.1). PEG-treated CMWCNTs induce more significant changes of hemoglobin levels, but PEG without CMWCNTs is not influence on this parameter (fig.1). The decrease of free hemoglobin concentration is shown to be caused by sorption of hemoglobin molecules by CMWCNTs that it doesn't allow to characterize the RBC lysis or safety of the cells. The partial small transformation of oxy-form of hemoglobin to met-form has been detected.

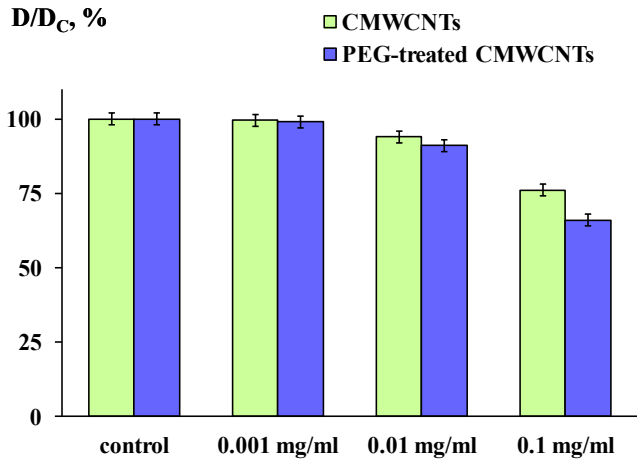


Fig. 1. The levels of free hemoglobin in extracellular medium after incubation of RBC for 20 h in the absence (control) and in the presence of 0.001, 0.01, 0.1 mg/ml CMWCNTs without or with PEG.
D and $D_C$ – optical density at 410 nm in experimental and control samples

In the result of RBC properties investigation by microscopy and light scattering (nephelometry) methods the modification of RBC is established. It has been obtained that diameter of the cells rises significantly, but the count of the cells is decreased after incubation of RBC in the presence of CMWCNTs and especially PEG-treated CMWCNTs.

[1] W. Wu, X.J. Jiang, A practical strategy for constructing nanodrugs using carbon nanotubes as carriers, Methods Mol Biol. **751**, 565–582 (2011).
[2] M.S. Ladeira, et al. Highly efficient siRNA delivery system into human and murine cells using single-wall carbon nanotubes, Nanotechnology. **21**, 385101 (2010).
[3] C. Sacchett et al., In vivo targeting of intratumor regulatory T cells using PEG-modified single-walled carbon nanotubes, Bioconjugate Chem. **24**, 852-860 (2013).
[4] V. Yuvaraj, et al. Toxicity assessment of carbon nanotubes on erythrocyte morphology and lymphocytes in vitro, Asian J. Pharm. Clin. Res. **9**, 278-280 (2016).
[5] D. Cavallo et al., Multi-walled carbon nanotubes induce cytotoxicity and genotoxicity in human lung epithelial cells, J. Appl. Toxicol. **32**, 454–464 (2012).
[6] A.M. Gaffney et al., Blood biocompatibility of surface-bound multi-walled carbon nanotubes, Nanomed. Nanotech. Biol. Med.. **11**, 39-46 (2015).

# STUDYING OF PLATELET ACTIVATION USING PATCH-CLAMP

Anatoly Kokhan[1], Ekaterina Shamova[1], Daria Grigorieva[1], Irina Gorudko[1]

[1] Department of Biophysics, Belarusian State University, Belarus
rrchypp@gmail.com

Platelets are the smallest cellular fragments circulating in bloodstream, with an average size of around 2.5 × 0.5 μm. They play a pivotal role in the blood coagulation cascade, forming a clot in the location a blood vessel rupture. This provides the functioning of the normal hemostasis (that is, stopping of the bleeding), as well as pathological thrombosis (the overlapping of the vessel). Besides, platelets are also involved in inflammatory response and perform the angiotrophic function. Platelet activation in response to various stimuli involves complex multiple ways of intracellular signaling, among which changes in plasma membrane ion channel permeability play a pivotal role. But still the mechanisms of platelet membrane ion channel functioning in response to various stimuli are pure and further investigations are needed [1].

The best method of studying the ion channels on various cells is patch-clamp (PC). Because the small size of platelets made the use of this method rather difficult, megakaryocytes are widely used to represent the properties of platelets in patch-clamp studies [2]. But still, one cannot be sure that this applies to all of the platelet properties, and important data from the recordings of activation can be lost. In this work we represent the method of platelet function investigation by patch-clamp technique in which we emphasize it various peculiarities with regard to platelets.

Venous blood samples from healthy donors was collected in tubes containing 3.8% (w/v) trisodium citrate as anticoagulant at 9:1 ratio and Prostaglandin $I_2$ at final concentration of 0.5 μM was added to avoid spontaneous platelet activation. Platelet-rich plasma (PRP) was prepared by centrifugation of blood at 200 *g* for 10 min. Washed platelets were prepared by additional two-step centrifugation of PRP at 400 *g* for 30 s at 20°C, and the cell pellet was resuspended in a NaCl HEPES solution (140 mM NaCl, 10 mM HEPES, 10 mM D-glucose, 5 mM KCl, 1 mM $MgCl_2$, pH 7.4), with final cell concentration of $10^6$ cells/ml.

Prior to the experiment, 5 to 7 μl of washed platelets was carefully placed in the bottom of a Petri dish containing 3 ml of NaCl HEPES solution with 1 mM $CaCl_2$. Patch pipettes were prepared from the borosilicate glass on a puller Sutter P-97 (HEKA Elektronik GmbH). For whole cell (WC) configuration measurements fire polished glass pipettes with resistance of 5–10 MΩ were used to reach a tight contact between platelet plasma membrane and pipette surface and to avoid patch resealing. For cell-attach (CA) configuration measurements pipette resistance of 14–18 MΩ was required to prevent spontaneous switching to WC. Using a micromanipulator (MP-225, Sutter Instrument), the pipette filled with KCl HEPES solution (5 mM NaCl, 10 mM HEPES, 145 mM KCl, 1 mM $MgCl_2$, 0.3 mM $CaCl_2$, 3 mM EGTA, pH 7.2) was brought close to a single cell and a small negative pressure was applied to the pipette, leading to tight seal formation (5 to 60 GΩ). To monitor the dynamic changes in cell membrane potential, CA and WC patch-clamp recordings were carried out in current-clamp (CC) or voltage clamp (VC) mode using an amplifier HEKA EPC 8 (HEKA Elektronik GmbH), filtered at 0.7 kHz.

Switching to WC from CA was spontaneous after about 10–15 min, when using pipettes with small resistance, while using pipettes with high resistance made CA stable for more than 30 min. It should be noted that CA with seal resistance >5GΩ can be used to measure the kinetics of membrane potential in CC mode (but only with the internal solution closely representing the intracellular one) [3]. According to this in our experiments the kinetics of membrane potential in WC and CA were identical.

When using fire polished pipettes, a short hyperpolarization to values of -100 – -120 mV occurred after gigaseal formation. This can be linked to platelet activation after adhesion to the glass of the patch pipette. And without fire polishing there was no hyperpolarization, most likely because the area of contact with glass was much lower. The average membrane potential was -40±4 mV.

Addition of physiological agonist ADP (10μM) and calcium ionophore ionomycin (1μM) led to the hyperpolarization of plasma membrane for 15±4 mV and 10±3 mV respectively and was due to inwardly-rectifying currents. This is consistent with previous results, obtained for megakaryocytes [4]. Furthermore, PC technique can be used to investigate intracellular signaling mechanisms initiated by various regulatory proteins the effect of which measured by traditional methods (turbidimetric aggregometry, fluorescent microscopy, flow cytometry, etc.) is rather weak.

Thus, PC of platelets may serve as a very sensitive method to study the effects of various signaling molecules on platelet activity, despite of platelet small size.

[1] M. Mahaut-Smith, The unique contribution of ion channels to platelet and megakaryocyte function, Journal of Thrombosis and Haemostasis **10 (9)**, 1722-1732 (2012).

[2] G. Tolhurst, C. Vial, C. Leon, C. Gachet et al., Interplay between P2Y1, P2Y12, and P2X1 receptors in the activation of megakaryocyte cation influx currents by ADP: evidence that the primary megakaryocyte represents a fully functional model of platelet P2 receptor signaling, Blood **106**, 1644-1651 (2005).

[3] M. Mason, A. Simpson, M. Mahaut-Smith, H. Robinson, The interpretation of current-clamp recordings in the cell-attached patch-clamp configuration, Biophysical Journal **88**, 739-750 (2005).

[4] K. Kawa, ADP-induced inward currents through $Ca^{2+}$-permeable cation channels in mouse, rat and guinea-pig megakaryocyites: a patch-clamp study, Journal of Physiology **495(2)**, 339-352 (1996).

# INFLUENCE OF EPIGALLOCATECHIN-3-GALLATE ON INSULIN FIBRIL FORMATION

Sakalauskas Andrius[1], Smirnovas Vytautas[1]

[1]Institute of Biotechnology, Life Sciences Center, Vilnius University, Vilnius, Lithuania
sakalauskas.and@gmail.com

Amyloid protein aggregation into fibrils has been known to cause neurodegenerative diseases, such as Alzheimer‘s, Parkinson‘s and prion diseases [1]. For a long time there has been a search to find compounds that could inhibit such aggregation into amyloid fibrils and prevent the onset or progression of these diseases. A polyphenol from green tea-known as epigallocatechin-3-gallate (EGCG) was shown on multiple occasions to inhibit fibril formation [2]. A model protein used to study amyloid aggregation is insulin and it has been documented that EGCG is capable of inhibiting it‘s fibrilization [3].

In this work we examine the inhibition effect of insulin aggregation dependence on the oxidation time of EGCG. We found that the EGCG autooxidation process time is one of the key parameters to increase the inhibition of insulin aggregation. The inhibition mainly affect the nucleation stage, suggesting that the inhibition pathway is towards biding the native state of insulin and/or primary nucleation complexes.

[1] Choi M.L., Gandhi S. 2018. Crucial role of protein oligomerization in the pathogenesis of Alzheimer ’ s and Parkinson ’ s diseases, 285: 3631–3644.
[2] Doig A.J., Derreumaux P. 2015. ScienceDirect Inhibition of protein aggregation and amyloid formation by small molecules, Current Opinion in Structural Biology 30: 50–56.
[3] Wang S., Dong X., Sun Y. 2012. Effect of - (-) epigallocatechin-3-gallate on human insulin fibrillation / aggregation kinetics, Biochemical Engineering Journal 63: 38–49.

# APPLICATION OF SCANNING ELECTROCHEMICAL MICROSCOPE FOR THE EVALUATION OF ANTIBODY IMMOBILIZATION EFFICIENCY

Antanas Zinovicius[1], Vilius Aukscionis[1], Aura Kisieliute[1], Inga Morkvenaite-Vilkonciene[2,3], Vytautas Zutautas[2], Almira Ramanaviciene[3], Arunas Ramanavicius[1, 4]

[1] Department of Physical Chemistry, Faculty of Chemistry and Geosciences, Vilnius University, Naugarduko 24, Vilnius, Lithuania
[2] Vilnius Gediminas Technical University, Faculty of Mechanics, J. Basanavičiaus g. 28, 03224 Vilnius, Lithuania
[3] Nanotechnas – Center of Nanotechnology and Materials Science, Faculty of Chemistry and Geosciences, Vilnius University, Naugarduko 24, Vilnius, Lithuania
[4]Center for Physical Sciences and Technology, Saulėtekio 3, 10257 Vilnius, Lithuania
antanas.zinovicius@chgf.vu.lt

Biologically modified surfaces, which employ a biomaterial, permit the development of biosensors. This analytical device consists of two main components: a biorecognition element and a transducer [1]. Human body has one of the most advanced recognition systems – an immune system. Immunosensor is a biosensor, in which an antibody or an antigen serves as the biorecognition element [2]. One of the biggest problems in creating immunosensors is the immobilization of the biomolecules [3]. Not all immobilization methods provide stability of biomolecules on the surface and site-directed positioning.

In order to evaluate the efficiency of the antibody-enzyme conjugate immobilization on the surface, scanning electrochemical microscopy (SECM) was employed. SECM is a non-invasive technique and can be used in an optimal medium for the biorecognition element. The aforementioned method provides the possibility to detect antibodies at localized surface areas and to determine the changes in electrochemical activity, by adjusting substrate and mediator concentrations in medium (fig. 1).

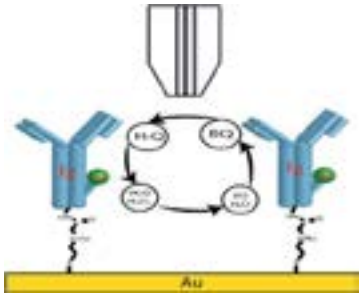


Fig. 1. Immobilization of antibodies conjugated with horseradish peroxidase on gold coated sensor disk.

This study was conducted by using horseradish peroxidase labeled antibodies as biorecognition element, the red-ox mediator hydroquinone ($H_2Q$) and hydrogen peroxide. Experiments were performed with three different mediators: ferrocene methanol, ferrocene carboxylic acid and hydroquinone, which proved to be the most effective red-ox mediator for the SECM surface imaging. The current measured with $H_2Q$ was about 3 times higher than with ferrocene carboxylic acid.

Therefore, SECM proved to be a suitable technique for validating the quality of the antibody immobilization and the enzyme's activity.

**Acknowledgements**

This research was funded by the European Social Fund according to the activity "Development of Competences of Scientists, other Researchers and Students through Practical Research Activities" measure No.: 09.3.3.- LMT-K-712- 10-0169.

[1] Bhalla, N., Jolly, P., Formisano, N., Estrela, P. Introduction to biosensors. Essays in Biochemistry 2016, 60(1), 1–8.
[2] B. Byrne, E. Stack, N. Gilmartin and R. O'Kennedy, Antibody-Based Sensors: Principles, Problems and Potential for Detection of Pathogens and Associated Toxins. Sensors 2009, 9, 4407-4445.
[3] Makaraviciute A., Ramanaviciene A. Site-directed antibody immobilization techniques for immunosensors. Biosensors and Bioelectronics 2013, 50, 460–471.

# INFLUENCE OF DIFFERENT LIGHTING SPECTRUM AND *BOTRYTIS CINEREA* ON TOTAL PHENOLIC CONTENT IN GREEN-LEAF LETTUCE

Asta Bylaitė, Aušra Brazaitytė, Neringa Rasiukevičiūtė, Alma Valiuškaitė, Viktorija Vaštakaitė-Kairienė

Institute of Horticulture, Lithuanian Research Centre for Agriculture and Forestry. Kaunas str. 30, Babtai, LT-54333, Kaunas dist. Lithuania.
a.bylaite@lsdi.lt

Nowadays artificial lighting is widely used at closed environment systems. That innovative growing method is safe because of its opportunities to use less of fertilizers. In the same way red (650–660 nm) and blue (450–460 nm) light emitting diodes (LED) lighting induce growth and development of vegetables. Also spectrum of chlorophyll absorbtion appropriate blue and red lights suppress most of pathogenic fungus such as *Botrytis cinerea* (BC). This fungus has great adaptability under broad environmental conditions and is well known to rapidly develop fungicide resistance lines [1]. Plants response to pathogens by activating phenolics that can expressed locally at the site of pathogen invasion as well as systematically in the uninfected tissue [2]. Phenolics are biological active components which possess antioxidant and plant defence mechanism properties. Furthermore, the commercial development of plants as sources of antioxidants that can be used to enhance the properties of foods, for both nutritional purposes and for preservation, is currently of major interest [3].

The aim of the research was to determine hight pressure sodium (HPS) and led emitting diodes (LED) lighting influence for total phenolic content in lettuces (*Lactuca sativus* L.) after its inoculation with *B. cinerea*.

The objects were: 'Little Gem' green-leaf lettuces and *B. cinerea* LT13B_FRA_76 (BC). Lettuces were grown in the growth chambers for 4 weeks. Day/night temperatures of 21 / 17 ±2 ˚C and relative humidity 70–85 %. The experiment conducted under different lighting conditions – high pressure sodium (HPS) and light emitting diodes (LED's). Photosynthetic photon flux density was set on 200 $m^{-2}s^{-1}$ and selected 16-h photoperiod. The BC isolate was maintained on Potato Dextrose Agar (PDA) at 22±2 ˚C in the dark for 7 days. Plants were inoculated with the 50 mm diameter isolate. After experiment was made biochemical analysis. 1/4 millilitre of extract was diluted with 1/4 ml Folin–Ciocalteau reagent (Folin reagent diluted with bi-distilled water 1:8) and with 1/2 ml 7.5% $Na_2CO_3$ solution. The absorbance was measured after 20 min at 765 nm with Genesys 6 spectrophotometer (Thermospectronic, USA) against water as a blank [4]. The total phenolic content (TPC) was measured spectrophotometricaly of inoculated and healthy lettuces (control) lettuces every day till 7 days after inoculation (DAI).

Results showed that 1 and 2 DAI the TPC concentration of infected lettuces under both lighting conditions were higher than non-infected lettuces. 3 and 4 DAI the TPC of infected lettuces under HPS was lower, but higher under LED light than non-infected plants. Results of 5–7 DAI the TPC of infected plants decreased respectively. On the contrary, infected lettuces under HPS revealed that increased of TPC on 5 and 7 DAI.

As a result, phenolic compounds had tendency to increase on first and second days after inoculation independent from different lighting conditions. Other days TPC varied subject from BC progress and lighting spectrum. Supposedly that with the TPC increased other antioxidants such as enzymes, but further researches are needed.

[1] K. Kim, H. S. Kook, Y. J. Jang1, W. H. Lee, S. Kamala-Kannan, J. C. Chae1, K. J. Leel, The effect of blue-light-emitting diodes on antioxidant properties and resistance to *Botrytis cinerea* in tomato, J Plant Pathol Microb Volume 4 Isse 9, 1000203, 1–5 (2013).
[2] V. Lattanzio, V. M. T. Lattanzio, A. Cardinali, Role of phenolics in the resistance mechanisms of plants against fungal pathogens and insects, Phytochemistry: Advances in Research, 23–67 (2006).
[3] C. A. Rice-Evans, N. J. Miller, G. Paganga, Antioxidant properties of phenolic compounds, April 1997, VoL 2, No. 4, 152–159 (1997).
[4] G. Samuolienė, R. Sirtautas, A. Brazaityte, P. Duchovskis, LED lighting and seasonality effects antioxidant properties of baby leaf lettuce, Food Chemistry Volume 134 Issue 3, 1494–1499 (2012).

# Effects of Light Intensity on the Photosynthetic system Response in vegetables

Lukas Simanavičius [1,2], Giedrė Samuolienė[1]

[1] Institute of Horticulture, Lithuanian Research Centre for Agriculture and Forestry. Kaunas str. 30, Babtai, LT-54333, Kaunas dist. Lithuania.

[2] Vytautas Magnus University. K. Donelaičio str. 58, Kaunas LT-44248 Lithuania

simlukass@gmail.com

Light is one of the most important environmental factors that regulates plant photosynthetic system growth and development [1]. At high and low light intensities, photosynthetic carbon fixation increases, but the excess light is a stressor and therefore causes depression of photosynthetic efficiency [2]. Photosynthetic systems are also exposed by the spectrum of light. The effects of blue radiation on photosynthesis are the consequences of the specific absorption spectrum of photosynthetic pigments (chlorophylls, carotenoids) [3].

Photosynthetic rate is one of non-intrusive tools for rapidly inferring several functionally important leaf and plant properties. Photochemical reflectance index (PRI) is related with photosystem II (PSII) via the xanthophyll cycle and could be used as a proxy for light use efficiency (LUE). PRI can track minor LUE changes in an environment with changing light, or it can serve as a proxy for physiological variables of light-dependent photosynthetic reactions. Long-term research showed that the main source of variation in the PRI–LUE relationship is changes of chlorophylls and carotenoids ratio under changing temperature [4]. However, it is not yet well known, how different combinations of light intensity affects vegetables photosynthetic systems response.

In this study we present how different light intensity produced by light emitting diodes (LEDs) influence the response of photosynthetic system in different vegetables, cultivated in the closed environment. Red leaf lettuces (*Lactuca sativa* L., 'Lobjoits Red Cos') and radish (*Raphanus sativus* L., 'Cherry Belle') were cultivated under combinations of red (660nm) and blue (445 nm) LED lighting under different photosynthetic photon flux density (PPFD) of 150 and 250 µmol $m^{-2}s^{-1}$ for three weeks. Before the technical maturity stage, plants were treated as follows: (1) 150 µmol $m^{-2}s^{-1}$ (2) 150 µmol $m^{-2}s^{-1}$ to 250 µmol $m^{-2}s^{-1}$ (3) 250 µmol $m^{-2}s^{-1}$ and (4) 250 µmol $m^{-2}s^{-1}$ to 150 µmol $m^{-2}s^{-1}$. At the technical maturity stage, photosynthesis rate, PRI, LUE, chlorophyll a and b and xanthophyll's (zexanthin+lutein) contents were evaluated.

Results has shown that light intensity differently affects photosynthetic response of different growth strategy vegetables (Table 1). In contrast to radish, red leaf lettuce was less sensitive to changes of PPFD during vegetation period. The common tendency for both plants was found only for LUE – significantly lower values were found under 250 µmol $m^{-2}s^{-1}$ , whereas significant increase was observed when seedlings of both plants were treated with 250 µmol $m^{-2}s^{-1}$ and during maturity stage were treated with 150 µmol $m^{-2}s^{-1}$. In contrast to radish, grown only under 250 µmol $m^{-2}s^{-1}$ PPFD and illuminated by lower PPFD during maturity stage, the significant increase of photosynthetic rate followed by significant decrease of chlorophyll's and xanthophylls accumulation was observed in radish grown only under 250 µmol $m^{-2}s^{-1}$ PPFD.

Table 1. Influence of PPFD on photosynthesis rate, PRI, LUE, chlorophyll a, b and xanthophyll's contents

| Light intensity µmol $m^{-2}s^{-1}$ | PRI | | Photosynthetic rate | | Light usage efficiency | | Chl-b µg/$g^{-1}$ | | Chl-a µg/$g^{-1}$ | | Zexsanthin + Lutein µg/$g^{-1}$ | |
|---|---|---|---|---|---|---|---|---|---|---|---|---|
| | Red leaf lettuce | Radich | Red leaf lettuce | Radich | Red leaf lettuce | Radich | Red leaf lettuce | Radich | Red leaf lettuce | Radich | Red leaf lettuce | Radich |
| 150 | -0,075 | **0,090**** | 8,715* | 20,831 | 0,058 | **0,139** | 118,644 | 94,211 | 455,208 | 319,783 | 1,974 | 2,204 |
| 150→250 | -0,085 | 0,069 | 13,097 | 18,408* | 0,052 | 0,074* | 111,937 | 84,717 | 416,909 | 321,882 | 1,936 | 2,031* |
| 250 | -0,086 | 0,054* | 11,253 | **25,013**** | 0,045* | 0,100* | 114,804 | 54,160* | 393,281 | 199,549* | 2,084 | 1,361* |
| 250→150 | -0,069* | 0,073 | 13,037 | 17,177* | **0,087**** | 0,115* | 130,307 | **176,521**** | 428,769 | **657,410**** | 2,183 | **5,115**** |
| $LSD_{0,05}$ | 0,008 | 0,007 | 1,616 | 1,156 | 0,010 | 0,006 | 25,695 | 39,108 | 87,680 | 138,924 | 0,366 | 0,594 |
| $LSD_{0,01}$ | 0,012 | 0,011 | 2,448 | 1,752 | 0,016 | 0,009 | 38,932 | 59,254 | 132,848 | 210,490 | 0,554 | 0,900 |

* Significant at P <0.05; ** Significant at P <0.01, according to Fisher's criteria

Concluding remark. The photosynthetic behaviour of different life strategies vegetables varies depending on solid-state lighting intensity. The most favorable conditions for red leaf lettuce photosynthetic system is cultivation only under 250 µmol m-2s-1 PPFD and illumination by lower PPFD during maturity stage. Whereas, the significantly lower amount of photosynthetic pigments resulted in increase of photosynthetic rate in radish cultivated only under 250 µmol $m^{-2}s^{-1}$ PPFD.

Acknowledgements: This research was funded by a grant (No. 09.3.3.-LMT-K-712-10-0188) from the Research Council of Lithuania.

[1] L. Simanavičius, A.Viršilė. THE EFFECTS OF LED LIGHTING ON NITRATES, NITRITES AND ORGANIC ACIDS IN TATSOI 24th Annual International Scientific Conference "Research for Rural Development 2018" ISSN 1691-4031, Latvia University of Life Sciences and Technologies Volume 2, 95-99 (2018).

[2] H.C, Nguyen, K –H. Lin, T.-C. Hsiung et al., Biochemical and Physiological Characteristics of Photosynthesis in Plants of Two Calathea Species Int. J. Mol. Sci., **19**, 704 (2018).

[3] L. Huché-Thélier, L. Crespel, J. Le Gourrierec et al.,Light signaling and plant responses to blue and UV radiations — Perspectives for applications in horticulture Environmental and Experimental Botany **121**, 22–38 (2016).

[4] J.A. Gamon, J.S. Surfus. Assessing Leaf Pigment Content and Activity with a Reflectometer. New Phytologist **143** (1): 105–117. (1999).

# THE EFFECT OF LED LIGHTING ON STRAWBERRY PHOTOSYNTHESIS SYSTEM RESPOND IN *B. CINEREA* PATHOGENESIS

Mantas Kačiušis[1,2], Viktorija Vaštakaitė-Kairienė[1]

[1] Institute of Horticulture, Lithuanian Research Centre for Agriculture and Forestry. Kaunas str. 30, Babtai, LT-54333, Kaunas dist. Lithuania
[2] Kaunas University of Technology. K. Donelaičio str. 73, LT-44249, Kaunas
mantas14kaunas@gmail.com

Plants are usually affected by many biotic stress factors which can reduce plant photosynthesis system e.g. plants diseases. Normally, intensive growing systems are based on using pesticides to control diseases spreading. However, it has toxic and harmful effect on environment. Besides, pathogens can become resistant to different chemicals. Due to this reason, it promotes to search and implement new control strategies and technologies in horticulture

Light is essential factor which has impact on whole plant photosynthesis and development. Light emitting diodes (LEDs) lighting has a wide range of technological possibilities to control main plants physiological processes [1]. This type of lighting can provide a possibility to apply a corresponding wavelength, change light intensity or to save up energy costs [2]. The experiments with LEDs have claimed a positive effect on photosynthesis intensity and growth [3] [4].

Grey mould (*Botrytis cinerea*) can infect many horticultural plants. It is necrotrophic and one of the most pathogenic fungi in horticulture [5]. Strawberry (*Fragaria x annanasa*) cv. 'Deluxe' are important commercial crop, which characterized by high antioxidants and mineral content [6]. There is no many researchers and evaluations how LEDs can affect photosynthesis respond and optical properties in plants.

The aim of this study was to establish light conditions effect on strawberry cv. 'Deluxe' photosynthesis system and optical properties respond in grey mould (*Botrytis cinerea*) pathogenicity/ effect. The experiment was conducted in Institute of Horticulture, Lithuanian Research Centre for Agricultural and Forestry. All plants were grown in closed environment chamber under LED lighting modules 'Heliospectra RX30' (HelioSpectra) and high-pressure sodium lamps 'SON-T Agro' (Phillips). Day and night temperatures 21/17 °C, relative humidity ~80-85 %. Plants were inoculated by *B. cinerea* isolates discs on the leaves. In order to evaluate strawberry cv. 'Deluxe' photosynthesis system respond (instantaneous photosynthesis (Pn)) to infection by pathogens in light effect all non-destructive measurements (chlorophyll fluorescence ratios, leaf pigments and optical indices) were done 1, 3, and 5 days after inoculation.

It was determined, instantaneous photosynthesis intensity (Pn) has decreased 27 % after first day inoculation by *B. cinerea* comparing with non-inoculated plants under LED lighting. After third day, Pn decreased more than previous day – 23%. Thus, after five days was measured higher photosynthesis intensity, comparing with first and third-day measurements. The same trend was determined under HPS lights. In first and third day after inoculation Pn was reduced 20% and 11% respectively, comparing with non-inoculated plants. After five days Pn increased. Chlorophyll fluorescence results showed, that after first day inoculation under LED maximum quantum yield (Fm/Fv) was decreased ~3,7%. However, under HPS this ratio was higher ~6,3% comparing with non-inoculated. The same trends were measured in next days. Comparing II photosystem efficiency ($Y_{(II)}$) and electron transport rate (ETR) after first day and five-day results showed soft suppression of ratios, though in third day were measured intensive photochemistry. Leaf pigments measurements under LED light first day after inoculation showed reduction of Chl index (~4,6%), respectively. The same results measured in other indexes. Not significant increasement fixed in third day after inoculation, thus in five-day indices slightly decreased again. Under HPS light were measured 7,1% Chl increasement after first day inoculation by *B.cinerea*, comparing with non-inoculated. Leaf optical properties measurements showed slight increasement comparing all experiments days. Photochemical reflectance index (PRI) and photochemical senescence reflectance indexes under HPS light showed more intensive respond.

In conclusion, *B. cinerea* had significant effect on Pn intensity suppression and reduced it after inoculation. In 5 days Pn increased more than initial Pn in first days. Strawberry leaf pigments and optical indices did not show significant differences comparing both illuminations. Under HPS light strawberry indexes respond was slightly higher than LED.

Acknowledgements. This research was funded by a grant No. 09.3.3-LMT-K-712-10-0216 from the Research Council of Lithuania.

[1] C.M. Bourget, An Introduction to Light-emmiting Diodes, HortScience 43:7, 1944-1946 (2008).
[2] D. Singh, C. Basu, M. Meinhardt-Wollweber et al., LEDs for energy efficient greenhouse lighting, Renewable and Sustainable Energy Reviews 49, 139-147 (2015).
[3] J. H. Kang, S. KrishnaKumar, S. L. S. Atulba et al., Light intensity and photoperiod influence the growth and development of hydroponically grown leaf lettuce in a closed-type plant factory system, Horticulture, Environment and Biotechnology 54:6, 501-509 (2013)
[4] X. X. Fan, Z. G. Xu, X. Y. Liu et al., Effects of light intensity on the growth and leaf development of young tomato plants grown under a combination of red and blue light, Scientia Horticulturae 153, 50-55 (2013).
[5] Y. Elad, D. Shtienberg,. Botrytis cinerea in greenhouse vegetables: chemical, cultural, physiological and biological controls and their…, Integrated Pest Management Reviews 1, 15-29 (1995).
[6] F. Giampieri, J.M. Alvarez-Suarez, M. Battino, Strawberry and Human Health: effects beyond antioxidant activity, Journal of Agriculture Food Chemistry 62:18, 3867-3876.

# THE MECHANISMS OF REACTIVE OXYGEN SPECIES GENERATION IN PHAGOCYTES UNDER ACTION OF LOW STRENGTH ELECTRIC FIELDS

Elizaveta Kavalenka, Artsemi Yushkevich, Alena Kavalenka

Department of Biophysics, Faculty of Physics, Belarusian State University
ai0628k@gmail.com

The endogenous electric fields are found to be generated in organism tissues at damages [1,2]. These are non-uniform fields characterized by low strength values do not exceed 2 V/cm. The stimulating effects of such electric fields on migration and proliferation of the cells which play an important role in reparative regeneration have been demonstrated in vitro [3-6]. However, alterations of other functional properties of the cells under the low strength electric fields have not yet been investigated. Immune cells such as phagocytes participate in reparative processes ingesting and utilizing abnormal materials by the use of reactive oxygen species (ROS). So, the aim of our work is to study the mechanisms of activation of phagocytes to ROS formation under impact of the low strength electric fields.

**Methods.** Human blood phagocyte suspensions in Earle's solution were placed in glass cuvettes, and stainless steel electrodes located at a distance of 1 cm apart were submerged in the samples. The electrodes were connected to electrical signal generator with shielded twisted pair. The voltage values of 0.1, 0.25, 0.5 or 1 V were applied to electrodes for experimental samples, and value of 0 V was set for control samples. The processes of ROS formation were studied by luminol-amplified chemiluminescence method. Luminol emits visible light after oxidation by ROS such as $\cdot O_2^-$, $H_2O_2$, $\cdot OH$, $OCl^-$, $ONOO^-$. The samples with electrodes were located inside completely darkened metal cuvette compartment of biochemiluminometer during the measurements. The values of chemiluminescence integral intensity which characterize the total ROS generation in the experimental and control samples were determined for 20 min. The inhibitors of enzymes were added 30 min prior to the onset of electric stimulation.

**Results.** It has been established that low strength electric fields induce the increase of ROS generation in phagocytes when the cells are activated by addition of phagocytosis stimulator latex. The most significant effects have been detected at the voltage on the electrodes of 0.25 and 0.5 V. The differences of inhibitory effects on ROS yields ($\Delta I_{inh.}$) in experimental and control phagocyte samples are represented in fig.1. The involvement of redox-enzymes in ROS generation has been studied using DPI (NADPH-oxidase inhibitor), $NaN_3$ (myeloperoxidase inhibitor), AET (NO-synthase inhibitor) and PTIO (NO scavenger) and illustrated in fig.1, a. Our data indicate contribution of NADPH-oxidase and myeloperoxidase, but not NO-synthase in the increase of ROS formation in phagocytes under electric field exposure.

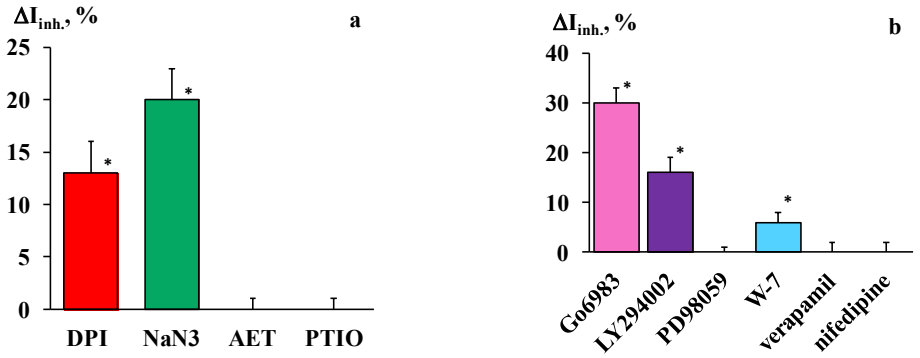


Fig. 1. The alteration of inhibitory effects on ROS generation in phagocytes under exposure to electric field

Activation of phagocytes are known to include signal transduction ways coupled with $Ca^{2+}$-dependent processes and phosphorylation by kinases which can be protein kinase C (PKC), phosphatidylinositol-3 kinase (PI-3K) or mitogen-activating protein kinases (MAPK) [7]. In the present research the inhibitors Go6983, LY294002, PD98059, W-7, verapamil, nifedipine of PKC, PI-3K, MAPK, calmodulin and L-type of $Ca^{2+}$-channels have been tested, and the results are shown in fig.1, b. The obtained findings allow to conclude that low strength electric field causes amplification of ROS generation in phagocytes by NADPH-oxidase and myeloperoxidase via modulation of signal transduction associated with PKC, PI-3K and calmodulin.

[1] R. Nuccitelli et al., Imaging the electric field associated with mouse and human skin wounds, Wound Repair Regen. **16**, 432–441 (2008).
[2] R.H.W. Funk, Endogenous electric fields as guiding cue for cell migration, Front. Physiol. **6**, ArtID 143 (2015).
[3] C.R. Keese et al., Electrical wound-healing assay for cells in vitro, Proc. Natl Acad. Sci. USA **101**, 1554–1559 (2004).
[4] A. Guo et al., Effects of physiological electric fields on migration of human dermal fibroblasts, J. Invest. Dermatol. **130**, 2320–2327 (2010).
[5] S.N. Iwasa et al., Environmental factors that influence stem cell migration: an "Electric field", Stem Cells Int. ArtID 4276927 (2017).
[6] M. Zhao et al., Electrical signals control wound healing through phosphatidylinositol-3-OH kinase-γ and PTEN, Nature. **442**, 457–460 (2006).
[7] S. Volmering, et al., The neutrophil Btk signalosome regulates integrin activation during sterile inflammation, Immunity. **44**, 73-87 (2016).

# NANOMECHANICS OF TETHERED LIPID BILAYER MEMBRANES

Auksė Rapnikaitė[1], Marija Jankunec[2]

[1] Department of Physics Chemistry, Vilnius University, Lithuania
[2]Institute of Biochemistry, Life Science Center, Vilnius University, Lithuania
aukse.rapnikaite@chgf.stud.vu.lt

Biological membranes are a base in biology of the living cell. Membranes are the hydrophobic barrier which separates two water soluble compartments and a supra-molecular entity that has vital structural functions. Notably, they are involved in many exchange processes between the outside and inside cellular spaces [1]. The profile of interaction between protein and lipid is highly dependable on the physical properties of lipid bilayer. That is why very important to investigate nanomechanical stability of a membrane. It is interrelated to phase state behaviour and various other influencing aspects such as temperature, cholesterol [2, 3] and membrane proteins. Due to the complexity of cell membranes, biomimetic models are needed to acquire current knowledge of the molecular processes occurring in membrane. To simplify the investigation of phospholipid and cholesterol interactions, the use of artificial membranes is an approach that allows manipulation of the lipid composition by choosing the desired ratio of the lipids [2].

Tethered bilayer lipid membranes (tBLM) – a platform for a rapid artificial bilayer formation. To investigate the effect of cholesterol on DOPC (dioleoylphosphocholine) tBLM, various lipid mixtures of DOPC/cholesterol (1/0, 8/2, 7/3, 6/4, 1/1) were prepared. Simultaneously, Atomic Force Microscopy (AFM) imaging and Force spectroscopy studies were carried out. Fig. 1 shows a schematic image of tBLM structure in the presence of cholesterol molecules.

Force curves (force (nN)-versus distance (nm) curve) show the deflection of cantilever during scanner movement (z-displacement) towards the surface and backwards. The profile of the curve highly depends on the nature of interaction between the AFM tip and analysed surface. Through applying contact models from force curve nanomechanical properties as adhesive force, Young modulus (elasticity) etc. are calculated.

In order to determine the mechanical strength of the DOPC bilayer as a function of cholesterol, experiment was carried out using force curves over 3 μm×3 μm area at the places of interest. The breakthrough force ($F_B$) is an appropriate indicator to gauge the mechanical stability of the membrane. Average roughness values were measured in 3 independent experiments. This let us know about arrangement and distribution of cholesterol in lipid bilayer. Cholesterol pulls the lipid closer and fills the gap between the head group in small concentration. This result higher mechanical stiffness in fluid phase membranes and smaller values of surface roughness. However, at higher additions of cholesterol, surface roughness increases as increases the gap between the head groups [3].

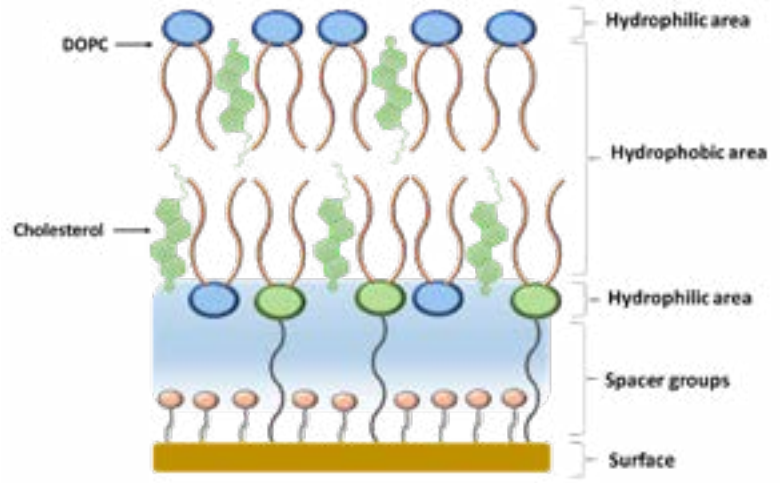


*Figure 1. Schematic view of tBLM with incorporated cholesterol molecules*

[1] S. Rebaud, O. Maniti, and A. P. Girard-Egrot, "Tethered bilayer lipid membranes (tBLMs): Interest and applications for biological membrane investigations," Biochimie, vol. 107, pp. 135–142, 2014.
[2] R. M. A. Sullan, J. K. Li, C. Hao, G. C. Walker, and S. Zou, "Cholesterol-dependent nanomechanical stability of phase-segregated multicomponent lipid bilayers.," Biophys. J., vol. 99, no. 2, pp. 507–16, 2010.
[3] P. R. Adhyapak, S. V. Panchal, and A. V. R. Murthy, "Cholesterol induced asymmetry in DOPC bilayers probed by AFM force spectroscopy," Biochim. Biophys. Acta - Biomembr., vol. 1860, no. 5, pp. 953–959, 2018.

# UREA GRANULATION USING ALGAE ADDITIVE

Mikolaitienė Austėja, Šlinkšienė Rasa

Department of Physical and Inorganic Chemistry, Kaunas University of Technolgy, Kaunas, Lithuania
austeja.eimontaite@ktu.edu

One of main sources of nitrogen, which is very important for plant, is soil. The lowest nitrogen amount is in the sand, and higher in the black soil and peat. Humus is the main nitrogen store and holder, it can hold up to 5 % nitrogen. There is only a small part of the soil nitrogen is absorbed by the plant, before the soil organisms have to mineralize the organic nitrogen [1]. Nitrogen fertilizers are very important for plants, especially when fertilizing plants in spring. They provide plants with nutrients, affect plant growth, are important for protein formation, and regulate soil pH. However, there are even three forms of nitrogen (ammonia, nitrate and amide) and they assimilation on plants is distinct. Urea is a high concentrate nitrogen fertilizers (nitrogen concentration is 46%) where the nitrogen is in the form of an amide group. Nitrogen in this group dissolves much more slowly, are slower compared to other forms of nitrogen, not so strongly washed out of the soil. The amide form of the soil eventually migrates to the ammonia form. Urea is suitable for fertilization both through the leaves and through the roots and is often used [2].

However, urea is very hygroscopic and this makes it difficult to store it. Furthermore nitrogen from simple urea granules is lost in leaching, denitrification, nitrous emission processes. Many scientists are exploring ways to reduce the increase its efficiency of use and reduce nitrogen pollution. One of this research is manufacturing granular urea fertilizer encapsulated with biodegradable film to obtain controlled release coated urea [3].

In this research, to slow down urea solubility another bioactive component – Chlorella Vulgaris algae, is used. Chlorella Vulgaris algae are widely used bioactive substances containing many chemical elements (K, P, Ca, S, Fe, Cu, Na, Mg, Mn, Si). However, the amount of chemical elements in the algae depends on the algae cultivation medium. Scanning electronic microscope (SEM) Phenom World ProX (G5) image shows the concentration of the elements (Fig. 1 a) and that the particles are spherical regular form and the surface of the particles is slightly uneven (Fig. 1 b).

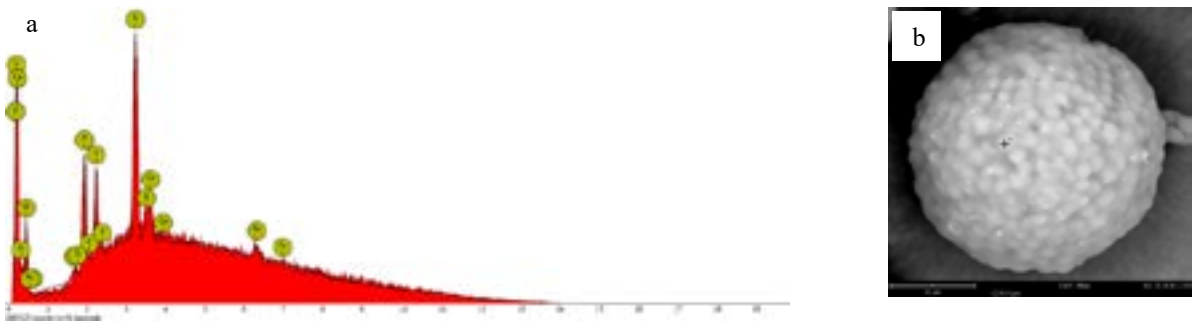


Fig. 1. SEM of Chlorella Vulgaris algae: a – concentration, b – surface

In this research together urea and bioactive component granulation method was used. Granulation is the process by which pellets from small particles are formed. In this case, also distilled water as granulating material (binder) was used. Granulation process was carried out on a laboratory drum granulator-dryer [4]. Pelletizing of fertilizers using liquid phase for irrigation of the material consists of four stages: powdered irrigation of raw materials, granulation of wetted material, drying of pellets, granule analysis.

For granulation, urea samples with 5–20 % algae addition were prepared and moisture content in the mixture from 5–20 % ranged. Granulator rotation speed was 24 rpm, inclination angle 3 degrees, air flow temperature for pellet drying 55–65 ºC. The got granules were dried, fractionated and the static strength of granules and hygroscopicity of the marketable fraction were determined.

[1] Agrozinios. Azoto trąšos, available at: http://www.agrozinios.lt/portal/categories/109/1/0/1/article/12883/azoto-trasos (accessed on 2019 01 27)
[2] Mano ūkis. Azoto trąšos ir dirvos rūgštingumas, available at: http://www.manoukis.lt/mano-ukis-zurnalas/2012/03/azoto-trasos-ir-dirvos-rugstumas/ (accessed on 2019 01 27)
[3] Uzoh, Ch. F; O. D. Onukwuli, I. H. Ozofor, R. S. Odera. Encapsulation of urea with alkyd resin-starch membranes for controlled $N_2$ release: Synthesis, characterization, morphology and optimum $N_2$ release. Elsevier. https://doi.org/10.1016/j.psep.2018.10.015. 2018, Vol. 121, p. 133-142.
[4] Paleckienė, R.; A. M. Sviklas, R. Šlinkšienė, V. Štreimikis. Processing of rape straw ash into compound fertilizers using sugar factory waste. Polish journal of environmental studies. Olsztyn: HARD Publishing Company. ISSN 1230-1485. 2012, Vol. 21, No. 4, p. 993-999.

# INDIUM TIN OXIDE COATED GLASS ELECTRODE WITH GOLD NANOSTRUCTURES FOR IMMUNOSENSOR DESIGN

Benediktas Brasiūnas[1,2], Anton Popov[1,2], Almira Ramanavičienė[1,2]

[1] Department of Analytical and Environmental Chemistry, Vilnius University, Vilnius
[2] NanoTechnas – Center of Nanotechnology and Materials Science, Vilnius University, Vilnius
benas.brasiunas@gmail.com

Immunosensors are biosensors predominantly based on antibodies immobilized on the signal transducer that converts the affinity interaction with the analyte to a signal proportional to analyte concentration. Many different types of signal transducers can be used for immunosensor design, such as electrochemical, piezoelectric and optical [1]. Electrochemical signal transducers are advantageous because they can be easily miniaturized and are versatile – a change in current, voltage or resistance can be measured [2]. Nanotechnology and nanoscience have a significant impact on analytical chemistry and is still growing every year. Gold nanostructures are one of the most widely used metal nanoobjects due to their desirable physical and optical properties [3]. Application of gold nanostructures in immunosensor design result in a bigger surface density of antibodies which yield a higher analytical signal [4]. Human growth hormone (hGH) also known as somatotropin is a polypeptide hormone secreted by the anterior pituitary gland. hGH is essential for normal human growth and development as it is involved in several biological processes, including activation of macrophages, lactation, somatogenesis and more, which is why quantitative detection of hGH is essential [5].

The main aim of this study was to investigate an immunosensor for human growth hormone detection based on indium tin oxide (ITO) coated glass electrode with gold nanostructures and covalently coupled antibodies against human growth hormone (anti-hGH). In this work ITO coated glass electrode was electrochemically modified with gold nanostructures and was characterized using scanning electron microscopy, cyclic voltammetry and X-ray diffraction methods. In addition, nanostructured electrode was covalently modified with anti-hGH through self-assembled monolayer. Developed immunosensor was used to directly detect hGH employing various electrochemical methods such as cyclic voltammetry, differential pulse voltammetry and square wave voltammetry. Furthermore, analytical parameters of this immunosensor were investigated.

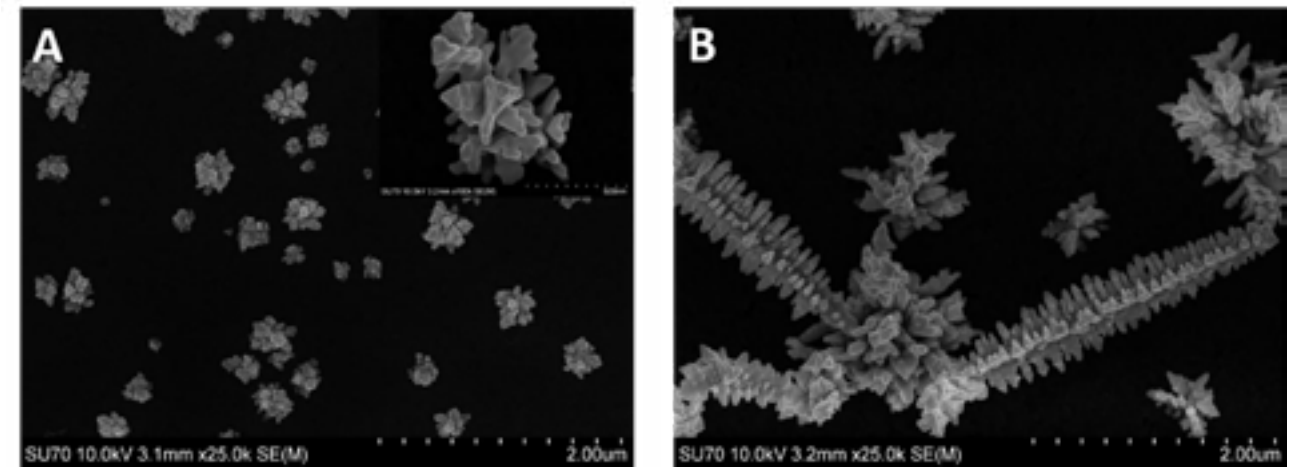


Fig. 1. Gold nanostructures electrochemically formed on ITO-glass electrode using different synthesis conditions (A-B).

**Acknowledgements**

This research is/was funded by the European Social Fund under the No 09.3.3.-LMT-K-712-10-0168 "Development of Competences of Scientists, other Researchers and Students through Practical Research Activities" measure.

[1] A. Ramanavicius, Y. Oztekin, A. Ramanaviciene. Electrochemical formation of polypyrrole-based layer for immunosensor design, Sensors and Actuators B Chemical **197**, 237-243 (2014).
[2] A. Ramanaviciene, N. German, A. Kausaite-Minkstimiene et. al., Comparative study of surface plasmon resonance, electrochemical andelectroassisted chemiluminescence methods based immunosensor for thedetermination of antibodies against human growth hormone, Biosensors and Bioelectronics **36**, 48-55 (2012).
[3] A. Ramanaviciene, J. Voronovic, A. Popov et. al., Investigation of biocatalytic enlargement of gold nanoparticles using dynamic light scattering and atomic force microscopy, A. Colloids Surf. A Physicochem Eng Asp **510**, 183–189 (2016).
[4] A. Makaraviciute, T. Ruzgas, A. Ramanavicius, A. Ramanaviciene, Antibody fragment immobilization on planar gold and gold nanoparticle modified quartz crystal microbalance with dissipation sensor surfaces for immunosensor applications, Anal. Methods **6**, 2134 – 2140 (2014)..
[5] A. Kausaite-Minkstimiene, A. Ramanavicius, J. Ruksnaite, A. Ramanaviciene, A surface plasmon resonance immunosensor for human growth hormone based on fragmented antibodies, Anal. Methods **5**, 4757-4763 (2013).

# *BOTRYTIS CINEREA* INHIBITION BY PHOTOACTIVATED ZNO NANOPARTICLES

Bernadeta Žudytė[1], Vilmantas Pupkis[2], Vilma Kisnierienė[2], Živilė Lukšienė[1]

[1] Institute of Photonics and Nanotechnology, Vilnius University, Lithuania
[2]Department of Neurobiology and Biophysics, Vilnius University, Lithuania

bernadetazud@gmail.com

*Botrytis cinerea* is the gray mold pathogen, which causes diseases for pre- and post-harvest fruits [1]. It is the most important postharvest decay pathogen [2] and the second most economically significant plant pathogen [3]. In order to control *B. cinerea*, it is necessary to find effective antifungal method.

In recent years, a rapid development of nanotechnology opens up whole universe of new possibilities for agriculture. ZnO nanoparticles have high specific toxicity against bacteria and only minimal effects were observed on human cells. The aim of this study was to evaluate the antifungal efficiency of ZnO nanoparticles in suspension after photoactivation with visible light against harmful fungi *B. cinerea* in vitro.

The absorption spectrum of ZnO nanoparticles suspension ($1\times10^{-3}$ M) is presented in Fig. 1. It is obvious, that absorption maximum at 375 nm. No other peaks were observed in the spectrum, what confirms the high purity of ZnO nanoparticles.

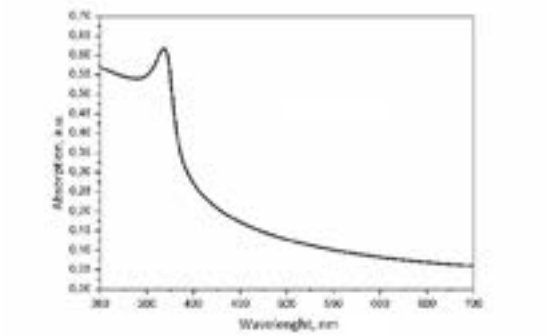

Fig. 1 Absorption spectrum of $1\times10^{-3}$ M ZnO nanoparticles

Radial growth of *B. cinerea* was examinated in control and treated samples in vitro. As seen in Fig. 2 photoactivated ZnO nanoparticles significantly (~80 %) inhibited the radial growth of *B. cinerea* compared to the control.

Membrane potential (MP) is useful parameter to measure because it reflects physiological status of the cell and integrity of plasma membrane. Cells in treated group exhibited less negative MP (-24.8±1.4 mV) compared to MP of untreated cells (-35.5±1.5 mV). These results are in agreement with other studies, which showed that photoactivated ZnO nanoparticles increases permeability of plasma membrane.

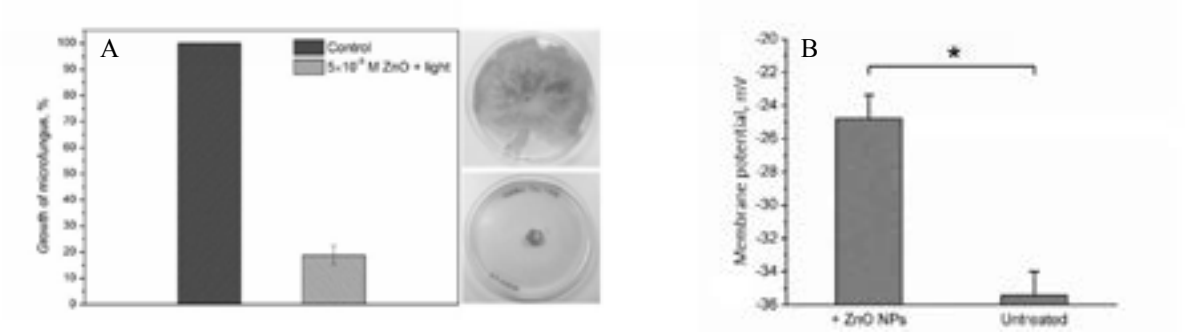


Fig. 2 A – *B. cinerea* growth inhibition by $5\times10^{-3}$ M photoactivated ZnO nanoparticles; B - Effect of ZnO nanoparticles on *B. cinerea* cell membrane potential

Obtained results confirms the idea, that photoactivated ZnO nanoparticles can be used as effective antifungal treatment against *B. cinerea.*

[1] Stockwell, V. O., Shaffer, B. T., Jones, L. A., & Pscheidt, J. W. (2018, July). Fungicide resistance profiles of Botrytis cinerea isolated from berry crops in Oregon. In International Congress of Plant Pathology Abstracts and Proceedings.
[2] Romanazzi, G., & Feliziani, E. (2014). Botrytis cinerea (Gray Mold). In Postharvest decay (pp. 131-146).
[3] Dean, R., Van Kan, J. A., Pretorius, Z. A., Hammond□Kosack, K. E., Di Pietro, A., Spanu, P. D., ... & Foster, G. D. (2012). The Top 10 fungal pathogens in molecular plant pathology. Molecular plant pathology, 13(4), 414-430.

# UNDERSTANDING *E. COLI* DAMAGES AFTER CHLOROPHYLLIN-BASED PHOTOSENSITIZATION USING SERS

Bernadeta Žudytė[1], Martynas Velička[2], Živilė Lukšienė[1], Valdas Šablinskas[2]

[1] Institute of Photonics and Nanotechnology, Vilnius University, Lithuania
[2]Institute of Chemical Physics, Vilnius University, Lithuania
bernadetazud@gmail.com

Every year Centers for Disease Control and Prevention and World Health Organization reports numerous cases of illnesses and even deaths, which are related with food, contaminated with pathogens [1,2]. Chlorophyllin-based photosensitization is one of the most promising innovative approaches for decontamination of fresh produce [3]. However, main disadvantage of this method is limited susceptibility of Gram-negative bacteria [4]. In order to find ways for the optimization of this technology, it is necessary to find out precise mechanism how does it destroy bacterial cell. For this reason, surface enhanced Raman scattering (SERS) was used.

The collected SERS spectra of pure *E. coli*, aqueous 1 mM chlorophylin solution and bacteria treated by chlorophyllin-based photosensitization are presented in the Fig. 1.

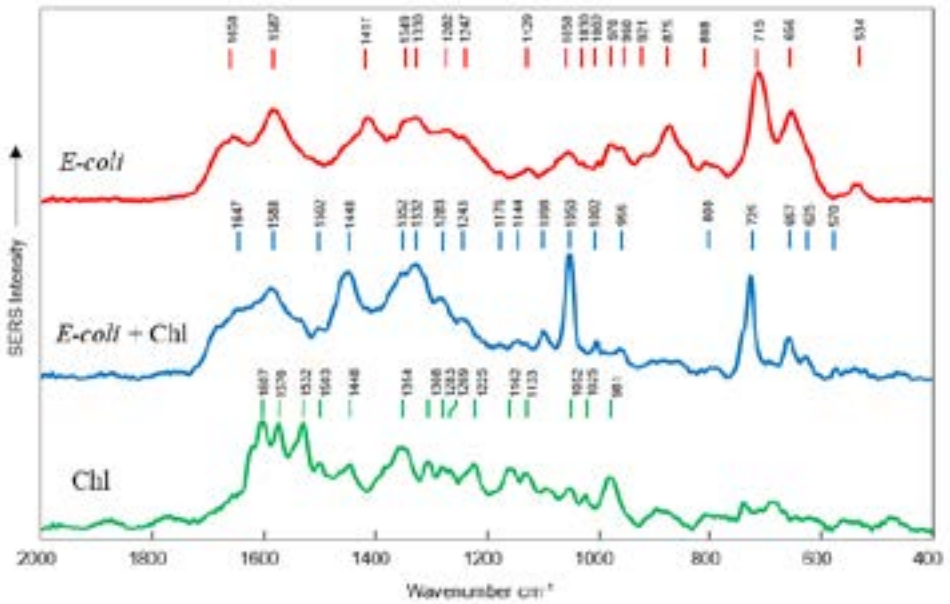


Fig. 1 SERS spectra of *E. coli* in the buffer solution (red), bacteria affected by chlorophyllin-based photosensitization (blue) and chlorophyllin (green)

Noticeable differences in the spectra of bacteria after the treatment with chlorophyllin-based photosensitization can be seen. The major differences are the appearance of an intense spectral bands located at 1050 $cm^{-1}$, 1448 $cm^{-1}$ and 1098 $cm^{1}$. These bands can be attributed to the vibrations of carbohydrate fragments, δ(CH2) and ν(C-C) normal vibrational modes of the lipids [5]. This finding can be associated with bacteria cell membrane.

SERS spectra of these molecules are weak in the unaffected bacteria, since due to the close packing of molecules in the membrane of undamaged cells the carbohydrate molecules cannot appear in close neighbourhood with metal nanoparticles of the colloidal solution, used for Raman signal enhancement. The situation is different when the membrane is damaged - fragments of molecules from the membrane can get closer to the nanoparticles what in turn can reason strong SERS spectral bands.

These spectral features indicate that some changes related to the lipid molecules, proteins and carbohydrates are taking place due to the bacteria treatment with chlorophyllin-based photosensitization. These changes are induced by ROS [6] which lead us to believe that in fact the disruption of the integrity of the membrane is the key effect of the chlorophyllin-based photosensitization treatment.

[1] CDC (2011). https://www.cdc.gov/VitalSigns/foodsafety/ (Retrieved on date: 10/01/2019).
[2] WHO (2017). http://www.who.int/mediacentre/factsheets/fs399/en/ (Retrieved on date 10/01/2019).
[3] Paskeviciute, E., Zudyte, B., & Luksiene, Z. (2018). Towards better microbial safety of fresh produce: Chlorophyllin-based photosensitization for microbial control of foodborne pathogens on cherry tomatoes. Journal of Photochemistry and Photobiology B: Biology, 182, 130-136.
[4] Buchovec, I., Lukseviciūtė, V., Kokstaite, R., Labeikyte, D., Kaziukonyte, L., & Luksiene, Z. (2017). Inactivation of Gram (−) bacteria Salmonella enterica by chlorophyllin-based photosensitization: Mechanism of action and new strategies to enhance the inactivation efficiency. Journal of Photochemistry and Photobiology B: Biology, 172, 1-10.
[5] Colniță, A., Dina, N. E., Leopold, N., Vodnar, D. C., Bogdan, D., Porav, S. A., & David, L. (2017). Characterization and discrimination of gram-positive bacteria using Raman spectroscopy with the aid of principal component analysis. Nanomaterials, 7(9), 248.
[6] Kashmiri, Z. N., & Mankar, S. A. (2014). Free radicals and oxidative stress in bacteria. Int J Curr Microbiol App Sci, 3(9), 34-40.

# GENETICAL IDENTIFICATION OF ANTIBACTERIAL AGENTS PRODUCING MICROORGANISMS AND ANALYSIS OF BACTERIOCINS AND KILLER TOXINS PRODUCED BY THEM

Domantas Armonavičius, Audrius Maruška, Tomas Drevinskas

Instumental Analysis Open Access Centre, Department of Biology, Vytautas Magnus University, Lithuania
*domantas.armonavicius@stud.vdu.lt*

Research on naturally occurring antibacterial agents has attracted considerable scientific attention worldwide over the last twenty years. Instead of chemical food additives, it is possible to use natural antimicrobials released by lactic acid bacteria and yeast. The pure antimicrobials produced by microorganisms or the microorganisms that produce these substances can be used for food bio-preservation or as antibiotics in medicine and veterinary medicine. Searching for lactic acid bacteria and yeast in natural foods and researching their application possibilities are relevant worldwide. Depending on the environment, microorganisms adapt, resulting in different strains that can produce antibacterial substances with different properties. Such substances are bacteriocins, produced by lactic acid bacteria and killer toxins, produced by yeast [1, 2].

The aim of this work is genotyping of microorganisms, isolated from cottage cheese, which shows antibacterial activity against S. aureus, E. coli, M. luteus and P. vulgaris strains. MALDI-TOF MS method was used for this task [3]. Leuconostoc mesenteroides lactic acid bacteria and Kluyveromyces marxianus, Debaromyces hansenii, Candida zeylanoides, Candida inconspicua yeasts were identified during this work. To analyse what kind of bacteriocins and killer toxins were produced, capillary electroforesis was used [4]. Detailed results of the work will be presented during the conference.

**Acknowledgements:**
This project was financed by Research Council of Lithuania, grant No. 09.3.3-LMT-K-712-10-0235

[1] Kaškonienė V., Stankevičius M., Bimbiraitė-Survilienė K., Naujokaitytė G., Šernienė L., Mulkytė K., Malakauskas M., Maruška A., Current State of Purification, Isolation and Analysis of Bacteriocins Produced by Lactic Acid Bacteria, Applied Microbiology and Biotechnology 101, 1323-1335 (2017).
[2] Buyuksirit T., Kuleasan H., Antimicrobial Agents Produced by Yeasts, *Int*ernational Journal of Biological, Biomolecular, Agricultural, Food and Biotechnological Engineering 8, 1114-1117 (2014).
[3] Singhal N., Kumar M., Kanaujia P. K., Virdi J. S., MALDI-TOF mass spectrometry: An emerging technology for microbial identification and diagnosis, Frontiers in Microbiology, 6, 1-16 (2015).
[4] Drevinskas T., Stankevičius M., Bimbiraitė-Survilienė K., Naujokaitytė G., Šernienė L., Kornyšova O., Malakauskas M., Maruška A., Optimiation of capillary zone electrophoresis-contactless conductivity detection method for the determination of nisin, Electrophoresis 39, 2425-2430 (2018).

# BIOTECHNOLOGICAL POTENTIAL OF SECONDARY METABOLITES PRODUCED BY CYANOBACTERIA FROM CURONIAN LAGOON

D. Overlinge[1], M. Cegłowska[2], A. Toruńska-Sitarz[3], K. Szubert[3], R. Pilkaityte[1], H. Mazur-Marzec[2,3]

[1]Marine Research Institute, Klaipeda University, Klaipeda, Lithuania
[2]Institute of Oceanology, Polish Academy of Sciences, Poland
[3]Division of Marine Biotechnology, Faculty of Oceanography and Geography, University of Gdańsk, Gdynia, Poland
donata.overlinge@apc.ku.lt

The Curonian Lagoon is the largest and one of the most severely impacted by harmful cyanobacteria blooms in Europe. In summer, cyanobacterial biomass reaches over 100 mg/l [1,2] and is dominated by *Aphanizomenon flosaquae*, *Planktothrix agardhii*, *Microcystis* and *Dolichospermum* spp. [3]. The goal of this study was to examine the activity of metabolites produced by cyanobacteria from the Curonian Lagoon. Bloom samples collected in 2018 over the season differed in species composition and cyanobacterial biomass. The extracts prepared in 75% methanol were preliminary fractionated, and the obtained material was tested using enzymatic, antibacterial and cytotoxicity assays. The content of the samples was determined using LC-MS/MS. All tested samples inhibited the activity of trypsin and thrombin (mean relative inhibition of 81,5%), however, the strongest activity was observed in samples dominated by Aph. flosaquae. In antibacterial assays, samples dominated by *Dolichospermum* and *Microcystis* showed strong (>70%) inhibition of *Staphylococcus aureus*, *Enterococcus faecium* and *Pseudomonas aeruginosa* antibiotic resistant strains. Cytotoxic effects against human breast adenocarcinoma cell line were also observed. LC-MS/MS analysis of active fractions revealed presence of several classes of cyanopeptides, including aeruginosamids, microginins, anabaenopeptins and cyanopeptolins. Preliminary studies indicated that apart from the known toxins, cyanobacteria from Curonian Lagoon produce many bioactive metabolites of potential pharmacological application.

[1] Bartoli M. et al., (2018) Drivers of Cyanobacterial Blooms in a Hypertrophic Lagoon. Frontiers in Marine Science 434:1–12.
[2] Olenina I. (2012) Identification of algae species in the Curonian Lagoon. SUBMARINE report 17A:1–14.
[3] Pilkaityte R., Razinkovas A. (2007) Seasonal changes in phytoplankton composition and nutrient limitation in a shallow Baltic lagoon. Boreal Environment Research 12:551–559.

**Acknowledgements:**
This study was partially financially supported by the COST Action ES1408: European Network for Algal Bioproducts (EUALGAE).

# EVALUATION OF ANTIMICROBIAL AND ALLELOPATHIC PROPERTIES OF *ARTEMISIA DUBIA* WALL.

Dovilė Jurevičiūtė[1], Audrius Sigitas Maruška[1],Vita Tilvikienė[2], Renata Žvirdauskienė[2], Aušra Bakšinskaitė[2]

[1]Instrumental Analysis Open access center, Faculty of Natural Sciences, Vytautas Magnus University, Kaunas, Lithuania
[2] Lithuanian Research Centre for Agriculture and Forestry, Akademija, Kėdainiai distr., Lithuania
dovile.jureviciute@vdu.lt

Plant biotechnology is one of the most dynamically developing fields of plant biology that modifies the most important patterns of food and raw material production. This area of biotechnology also includes energy crops. These plants produce a lot of biomass [1]. This is one of the fastest growing areas of alternative energy. In Lithuania, one of these plants investigated as potential plant for biomass, is from the *Artemisia* tribe - *Artemisia dubia* Wall. [2].

The aim of the study is to evaluate the antimicrobial and allelopathic properties of this energy plant *Artemisia dubia* Wall., in order to maximize the plant's potential for use.

*A. dubia* was collected from three different experimental areas with fertilization type: non-fertilized and fertilized with two mineral nitrogen fertilizers of different nitrogen amount - $N_{90}$ fertilizer and $N_{180}$ fertilizer, during different period of vegetation [2]. Samples were obtained from two different regions of Lithuania: Akademija, Kedainiai district. (55.3896° N, 23.8624° E) and Trakų Vokė, Vilnius district. (54.6238° N, 25.1113° E). Collected raw material was air-dried in Lithuanian Research Centre for Agriculture and Forestry.

According to the latest results on *A. dubia* grown in Lithuania, exceptionally high productivity of this energy plant was obtained, however, in order to make full use of this valuable renewable source rich in phenolic compounds and essential oils it is necessary to investigate the antimicrobial, allelopathic and other properties of volatile and non-volatile compounds extracts. Preliminary data from previous studies [3] demonstrated the potential of this raw material for the accumulation of polyphenols and essential oils.

In this research, the antimicrobial activity of different extracts were evaluated by using modified antimicrobial analysis methods [4]. Different bacteria, such as Gram-positive *Staphylococcus aureus* and Gram-negative *Escherichia coli,* were selected for this study. For the evaluation of allelopathic properties [5], the commonly used plant, sedative salad (*Lactuca sativa* L.) was chosen.

The report will include an evaluation of the antimicrobial and allelopathic properties of the *Artemisia dubia* Wall., the conditions of the experiments (bacterial strains and media, concentrations, methods, etc.) and a statistical analysis.

**Acknowledgements:**
This project was financed by Research Council of Lithuania project No. 09.3.3-LMT-K-712-10-0236.

[1] E Masarovičová, K Kráľová, M Peško, Energetic plants – cost and benefits, Ecological Chemistry and Engineering S , Vol. 16, No. 3 (2009).
[2] A. Kryževičienė, Šarūnaitė, L., Stukonis, V. And Z. Dabkevičius, Daugiamečių kiečių (*Artemisia vulgaris* L. ir *Artemisia dubia* Wall.) potencialo biokuro gamybai įvertinimas.. No. 1, p. 32–40 (2010).
[3] D. Jurevičiūtė, A. Maruška, M. Stankevičius, V. Tilvikienė, Ž. Kadžiulienė, J. Titova, Phytochemical Analysis of Biologically Active Compounds of *Artemisia dubia* Wall. Using Spectrophotometric and Gas Chromatography - Mass Spectrometry (GC-MS) Analytical Methods, The International Vital Nature Sign 2018, Kaunas (2018).
[4] W. Andrews, Manuals of food quality control, Chapter 4 - Microbiological analysis. Washington, DC, USA (1992).
[5] K. Piechowski, D. Mathees, R. Reese, Identification of Potentially Allelopathic Isobutylamides in *Echinacea angustifolia* D.C. Roots, USA (2006).

# UPTAKE OF VISCOSITY SENSITIVE BODIPY-H MOLECULAR ROTOR IN BREAST CANCER CELLS

Džiugas Jurgutis[1], Greta Jarockytė[1], Aurimas Vyšniauskas[2], Vitalijus Karabanovas[1, 3], Ričardas Rotomskis[1, 4]

[1] Biomedical Physics Laboratory of National Cancer Institute, Baublio 3B, LT08406, Vilnius, Lithuania;
[2] Center for Physical Sciences and Technology, Saulėtekio Av 3, LT-10257, Vilnius, Lithuania;
[3] Department of Chemistry and Bioengineering, Vilnius Gediminas Technical University, LT-10223, Vilnius, Lithuania;
[4] Biophotonics group of Laser Research Centre, Vilnius University, Saulėtekio 9, c.3, LT-10222, Vilnius, Lithuania
*dziugas.jurgutis@nvi.lt*

Viscosity is cell's fundamental mechanical property, which plays a major role in determining mobility and diffusion rates of different molecules. Abnormal viscosity changes might trigger cellular malfunctions causing cancer, atherosclerosis, diabetes and Alzheimer's disease [1]. Greater understanding and imaging of viscosity changes within cells during the course of these diseases is required to achieve earlier diagnosis and increased survival rate.

BODIPY (boron-dipyrromethene) is a fluorescent dye and its peripheral substitutions of the core are used to create unique modified forms such as BODIPY-h. These forms are termed 'molecular rotors' and can be utilized for the detection of changes in viscosity [2]. During the process of normal cells becoming cancer cells a wide range of mutations occur, including abnormal viscosity changes within cell. Therefore, breast cancer cells are used in the experiment with BODIPY-h, which has the potential to detect the following changes.

The aim of our study was to find absorption and fluorescence spectra of newly synthesized dye in different solutions as well as accumulation and distribution of BODIPY-h using living breast cancer cells.

Absorption and fluorescence spectra of BODIPY-h were measured in different solutions: phosphate-buffered saline (PBS), distilled water and cell growth media - Dulbecco's Modified Eagle Medium (DMEM). For uptake evaluation breast cancer cell lines MDA-MB-231 and MCF-7 were used. Cells were seeded in 8-well microscopy plates at density of $3 \cdot 10^4$ cells/well and cultivated in 37 °C incubator. After 24 h of cultivation, the old medium in each well was replaced with 9 nM BODIPY-h solution diluted with DMEM (1:1000) (Gibco, US) and incubated for 60 min, 30 min, 15 min respectively. After incubation with the dye, the nuclei of the cell were stained with Hoechst 33258 (Sigma, Germany). The accumulation of BODIPY-h was observed using Nikon Eclipse Te2000-U0, confocal microscope (Nikon, Japan).

Results revealed that the BODIPY-h absorption and fluorescence spectra depend on solvent, as well as that BODIPY-h is a cell membrane permeable fluorescent dye. Further research is compulsory before viable application of BODIPY-h as a viscosity indicator within cells.

[1] M. K. Kuimova, "Mapping viscosity in cells using molecular rotors," *Phys. Chem. Chem. Phys.*, vol. 14, no. 37, p. 12671, 2012.
[2] A. Vyšniauskas *et al.*, "Exploring viscosity, polarity and temperature sensitivity of BODIPY-based molecular rotors," *Phys. Chem. Chem. Phys.*, vol. 19, no. 37, pp. 25252–25259, 2017.

# SPECIFICITY OF THE ARGONAUTE PROTEIN FROM ARCHAEOGLOBUS FULGIDUS TO THE 5‘-END OF THE GUIDE

Mindaugas Zaremba, Elena Manakova, Edvardas Golovinas, Saulius Gražulis, Virginijus Šikšnys

Vilnius University, Life Sciences Center, Institute of Biotechnology, Vilnius, LT-10257, Lithuania
edvardas.golovinas@gmc.vu.lt

Argonaute proteins (Agos) are widespread in all three domains of life (bacteria, archaea and eukaryotes), and are structurally highly conserved [1]. In eukaryotic organisms, eAgos constitute the functional core of the RNA-silencing machinery, which is critical for regulation of gene expression, silencing of mobile genome elements, and defence against viruses. According to the latest experimental data prokaryotic Agos (pAgos) constitute an additional defence system with high versatility against invading nucleic acids [1].

The structural organization of full-length pAgos, as well as eAgos is bilobal, composed of four domains. The N-terminal and the PIWI/Argonaute/Zwille (PAZ) domains together with the L1 and L2 linker regions constitute the N-terminal lobe, whereas the C-terminal lobe is composed of the MID and the P-element-induced wimpy testis (PIWI) domains, the latter harbouring the catalytic site of cleavage-active Agos (Figure 1).


Fig. 1. Domain architecture comparison of full-length Argonautes and AfAgo. Full-length Argonautes (eg. TtAgo from Thermus thermophilus) are composed of four structural domains (N-terminal (blue), PAZ (cyan), MID (orange) and PIWI (green)) and linker regions (L1 and L2 (grey)). Red bars show the inactivated catalytic sites of PIWI domain within AfAgo. Numbers represent amino acid positions of domain boundaries within AfAgo.

pAgos are further divided into two major groups termed long (full-length, as above) and short pAgos that lack the PAZ domain, the N-terminal domain and consequently the L1 linker region. The short Argonaute protein from an archaeon *Archaeoglobus fulgidus* (AfAgo) is composed of only the L2 linker region and the MID and PIWI domains and therefore corresponds to the “MID/PIWI” lobe of full-length Agos (Figure 1). Its PIWI domain is inactivated by mutations of active site residues. AfAgo is well crystallographically characterized with solved crystal structures of the apo protein and its complexes with RNA and DNA duplexes providing initial information on the molecular mechanism of RNA interference (RNAi) in eukaryotes [2-5].

Target recognition by Agos is realized via complementarity between the Ago-bound guide and the target strands (RNA or DNA). The 5’-end of the guide strand is anchored in the evolutionarily conserved pocked of the MID domain. Eukaryotic and prokaryotic Agos usually show a preference for a specific 5’-nucleotide of the guide strand (e.g. human Ago2 for a 5’-U, while bacterial TtAgo for a 5’-dC). Here we present biochemical and structural studies of AfAgo specificity for the 5’-end of the guide strand.

[1] Willkomm S, Makarova KS, Grohmann D. DNA silencing by prokaryotic Argonaute proteins adds a new layer of defense against invading nucleic acids. FEMS Microbiol Rev. 2018 May 1;42(3):376-387.

[2] Parker JS, Roe SM, Barford D. Crystal structure of a PIWI protein suggests mechanisms for siRNA recognition and slicer activity. EMBO J. 2004 Dec 8;23(24):4727-37.

[3] Ma JB, Yuan YR, Meister G, Pei Y, Tuschl T, Patel DJ. Structural basis for 5'-end-specific recognition of guide RNA by the A. fulgidus Piwi protein. Nature. 2005 Mar 31;434(7033):666-70.

[4] Parker JS, Roe SM, Barford D. Structural insights into mRNA recognition from a PIWI domain-siRNA guide complex. Nature. 2005 Mar 31;434(7033):663-6.

[5] Parker JS, Parizotto EA, Wang M, Roe SM, Barford D. Enhancement of the seed-target recognition step in RNA silencing by a PIWI/MID domain protein. Mol Cell. 2009 Jan 30;33(2):204-14.

# STRUCTURE DETERMINATION OF PROTEIN AGGREGATES ADSORBED AT PHOSPHOLIPID MONOLAYER BY USING SUM FREQUENCY GENERATION SPECTROSCOPY

Edvinas Navakauskas[1], Simona Strazdaitė[1], Gediminas Niaura[1]

[1]Center for Physical Sciences and Technology, Saulėtekis ave. 3, LT-10257 Vilnius
Edvinas.Navakauskas@ftmc.lt

Formation of amyloid fibrils in cells and an intercellular net is associated with more than 40 different clinical conditions: Alzheimer's disease, Parkinson's disease, Huntington's disease, type II diabetes, and others. Each of these diseases caused by an aggregation of a different protein, which is a normal product of cellular metabolism. Protein elimination processes operating in parallel usually counterbalance production of the protein [1]. Nevertheless, when these production and elimination processes are disbalanced, protein starts to form different aggregates: small soluble oligomers and insoluble polymeric fibrils. All these aggregates are accumulating in tissues, causing inflammatory processes, tissue degradation and cell death.

The aim of our work is fully understand the protein aggregation process on a molecular level, to identify secondary structures of the aggregates and to investigate the interaction with phospholipid monolayer. It is believed that the interaction between protein and phospholipid layer greatly affects the aggregation process, therefore, it is important to understand how the molecular structure of the protein and its aggregates changes due to interaction with the lipid membrane. For this, a surface-sensitive spectroscopic method is needed. Vibrational sum-frequency generation spectroscopy is one of the most suited techniques to study protein aggregation and its interaction with phospholipid layer.

Vibrational sum-frequency generation (VSFG) spectroscopy is a surface sensitive and molecular specific technique. It is a widely used non-linear second order optical spectroscopic tool to study the conformation and orientation of proteins at various interfaces. Two pulsed laser beams, one of fixed visible frequency and the other of tunable infrared frequency overlap spatially and temporally at an interface to generate SFG signal (schematics shown in Fig.1.). The frequency of the generated SFG signal is the sum of the two incident field frequencies.

We applied the VSFG technique to study the structure of hen egg white lysozyme (HEWL) aggregates adsorbed at phospholipid monolayer. HEWL is an ideal model protein to study the mechanism of amyloid fibril formation. It has been studied extensively with other techniques and is closely related to human lysozyme, which also forms fibrils and causes hereditary systemic amyloidosis [2]. HEWL starts to form aggregates when the native structure of the protein is disrupted. This can be achieved by lowering the pH of the protein solution and elevating the temperature close to the protein´s denaturation temperature. The protein aggregates adsorbed at the phospholipid monolayer due to a strong electrostatic interaction: negatively charged phospholipid monolayer attracted positively charged lysozyme aggregates. Whereas at the water/air interface only non-aggregated protein could be adsorbed. VSFG spectra were recorded in the Amide I region. The secondary structures of the aggregates were identified from the position and shape of this Amide I band.

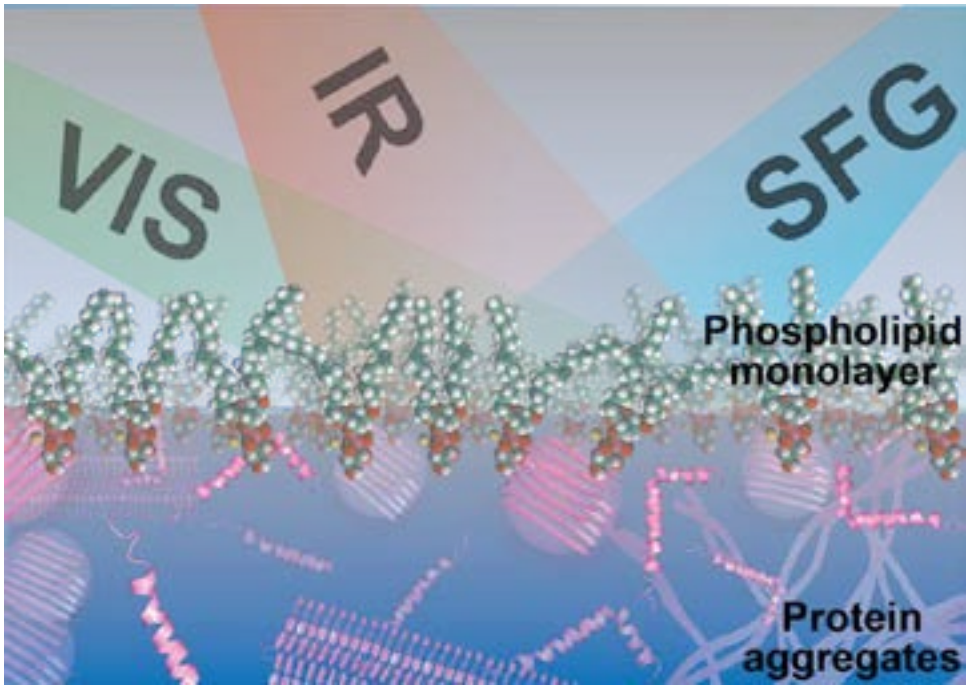


Fig. 1. Schematics showing adsorption of protein aggregates at phospholipid monolayer and an application of sum-frequency generation spectroscopy to study it.

[1] T. Saido , M. A. Leissring. Proteolytic Degradation of Amyloid β-Protein, Cold Spring Harb Perspect Med **2(6)**: a006379 (2012).
[2] Y. Yonezawa, S. Tanaka, S. Fujiwara, et al, An Insight into the Pathway of the Amyloid Fibril Formation of Hen Egg White Lysozyme Obtained from a Small-angle X-ray and Neutron Scattering Study, Journal of Molecular Biology **323(2)**, 237–251 (2002).

# INTEGRATIVE PROTEOMIC, BIOINFORMATIC AND PRIMARY CELL CULTURE APPROACH FACILITATES THE PREDICTION OF ANTICANCER DRUGS

Egle Zalyte[1], Marija Ger[1], Algirdas Kaupinis[1], Benediktas Kurlinkus[2], Marius Petrulionis[2], Audrius Sileikis[2], Kęstutis Strupas[2], Mindaugas Valius[1]

[1] Institute of Biochemistry, Proteomics Center, Vilnius University Life Sciences Center, Vilnius, Lithuania;
[2] Institute of Clinical Medicine, Clinic of Gastroenterology, Nephrourology and Surgery, Faculty of Medicine, Vilnius University, Vilnius, Lithuania
egle.zalyte@gmail.com

Pancreatic ductal adenocarcinoma (PDAC), the most common type of pancreatic cancer, is basically resistant to all mainstream cancer treatment modalities, such as chemotherapy and radiotherapy, and a surgical resection is effective for only 15-25% of patients [1]. Together with an unclear tumor subtyping system and the absence of treatment individualization strategies it makes PDAC one of the most hardly curable forms of cancer, bearing an average 5-year survival of patients, diagnosed with this disease [2]. The key to PDAC treatment could be targeting not only mutant malignant cells but the whole tumor as a system, consisting of cancerous cells in complex relationship with extensive stroma. On the other hand, almost no molecular signatures for individualized treatment for pancreatic cancer have been provided so far.

The present study combines proteomic analysis of PDAC surgical specimens and drug testing in patient derived primary cell culture in search for effective PDAC treatment. We performed high-throughput differential proteomic analysis of tissue samples taken during operations of patients with PDAC, chronic pancreatitis (CP) and those without these diseases. Differentially expressed PDAC-specific proteins (DEPs) enabled us to identify a set of proteins specific to pancreatic cancer but not pancreatitis patients. By comparing proteomic data to the databases of gene expression perturbation with small molecules we extrapolated a shortlist of chemotherapeutic compounds for evaluation as potential drugs for PDAC treatment: sorafenib, BGJ398, ASP2215, afatinib, 17AAG, ABT737. The efficiency of the drugs was assayed using primary patient-derived PDAC cell cultures. All of the drugs except for ABT737 significantly slowed down proliferation of primary cells in most PDAC cell cultures, and the combination of BGJ398 and ASP2215 was distinguished by exceptional efficiency. Most of the drugs also inhibited cell dissemination from spheroids and cell cycle to a various extent. Our results show a promising potential of this integrative pipeline for anticancer drug discovery and evaluation.

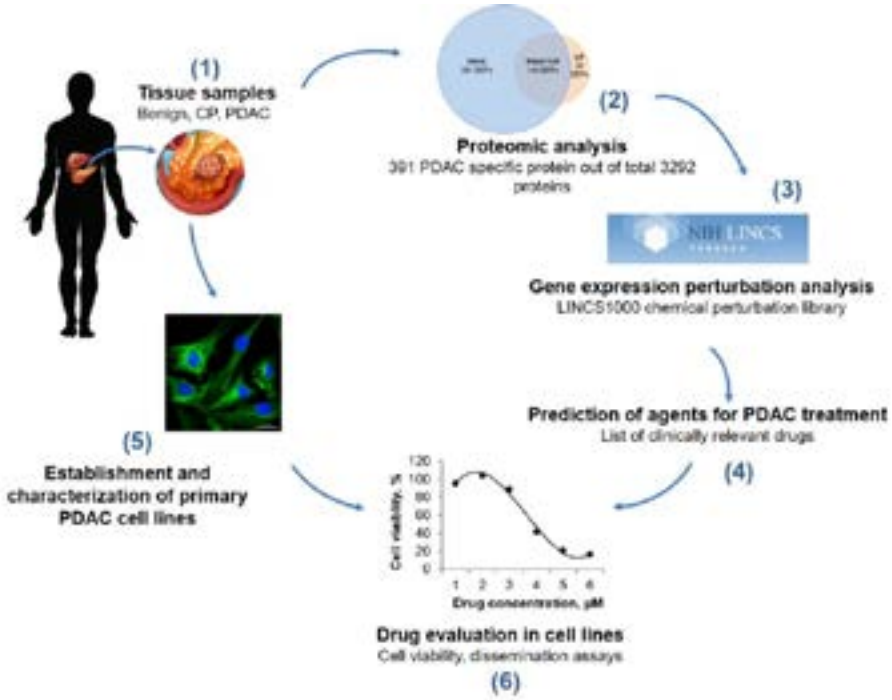


Fig. 1. Experimental workflow of an integrated proteomic, bioinformatic and cell culture approach for PDAC drug discovery and evaluation.

[1] Goodman MD, Saif MW. Adjuvant therapy for pancreatic cancer. JOP : Journal of the pancreas. 2014; 15: 87-90.
[2] Gall TM, Tsakok M, Wasan H, Jiao LR. Pancreatic cancer: current management and treatment strategies. Postgraduate medical journal. 2015; 91: 601-7.

# FUNCTIONAL CHARACTERIZATION OF SEPTICOLYSIN FROM THE OPPORTUNISTIC PATHOGEN *ACINETOBACTER BAUMANNII*

Gabija Lauciūtė[1], Jūratė Skerniškytė[1], Edita Sužiedėlienė[1*]

[1] Institute of Biosciences, Life Sciences Center, Vilnius University, Lithuania
gabija.lauciute@chf.stud.vu.lt

One of the biggest threats in health care settings is the Gram negative opportunistic pathogen *Acinetobacter baumannii* which causes a variety of infections in immunosuppressed patients. Its ability to persist in clinical environment and multidrug resistance profile makes *A. baumannii* one of the most challenging nocosomial pathogens [1]. Therefore, identification of the virulent features is for understanding of the pathogenesis mechanisms displayed by *A. baumannii*.

Frequently virulence genes are acquired during horizontal gene transfer, e.g. plasmids or transposable elements [2]. *spl* gene is located in *A. baumannii* plasmid pAB120 [3] and possibly could be described as one of the putative virulence genes, since the product of this gene -septicolysin- has homology to the pore-forming toxins in other pathogenic bacteria [4]. The aim of this work was to assess the importance of septicolysin in *A. baumannii* pathogenesis.

In order to determine, whether septicolysin could be a pore-forming virulence factor, *spl* gene from plasmid pAB120 was cloned into pUC_gm_AcORI and pUC_gm_AcORI_Ptac vectors. These constructs were further transformed into septicolysin-lacking *A. baumannii* strain. Resulting strains were tested for the hemolytic activity. Cytotoxicity on the mice lung epithelial cells LLC1 was determined by measuring cell viability by trypan blue uptake. *C. elegans* fertility assay was performed to identify if septicolysin increases *A. baumannii* virulence *in vivo*.

According to our results, we did not observe any differences in hemolysis and cytotoxicity comparing *A. baumannii* wild type strain and the strain with introduced *spl* gene. Also, *spl* gene did not have an impact on nematodes fertility.

In conclusion, septicolysin didn't demonstrate the expected properties of pore-forming toxins in the tested models. However, further investigations using purified septicolysin are needed in order to determine its virulence.

[1] D. M. Sengstock et al., Multidrug-Resistant Acinetobacter baumannii: An Emerging Pathogen among Older Adults in Community Hospitals and Nursing Homes, Clinical Infectious Diseases 2010:50 (15 June), 1611-1616 (2010).

[2] R. W. Jackson et al., The influence of the accessory genome on bacterial pathogen evolution, Mobile Genetic Elements 1:1, 55-65; May/June (2011).

[3] J. Povilionis et al., Spread of carbapenem-resistant Acinetobacter baumannii carrying a plasmid with two genes encoding OXA-72 carbapenemase in Lithuanian hospitals, J Antimicrob Chemother 2013 May, 68(5):1000-6 (2013).

[4] S. K. B. Cassidy et al., More Than a Pore: The Cellular Response to Cholesterol-Dependent Cytolysins, Toxins 2013, 5, 618-636 (2013).

# ANALYSIS OF POLYCYCLIC AROMATIC HYDROCARBONS DEGRADING ENZYMES USING CAPILLARY ZONE ELECTROPHORESIS METHOD

Gediminas Dūda[1], Tomas Drevinskas[1], Audrius Maruška[1]

[1] Instrumental Analysis Open Access Center , Vytautas Magnus University, Lithuania
Corresponding author: tomas.drevinskas@vdu.lt

Capillary electrophoresis is powerful technique for separating chemical compounds in aqueous solutions. Capillary electrophoresis method is capable of effectively separating such chemicals as inorganic compounds, amino acids, vitamins, organic acids and proteins. The aim of this study is to adapt capillary electrophoresis analysis conditions for effective analysis of polycyclic aromatic hydrocarbons degrading enzymes produce by white root fungi. This study consists of two major parts. First part of the study is optimization of enzyme extraction method from white root fungi. Second part is optimization of capillary electrophoresis analysis conditions for effective separation.

First part is enzyme extraction. It was decided to start experiments with most simple extration solution – bidistilated water. Samples were prepared using 10 ml of bidistilated water as extraction solvent. Extration was conducted in ultrasonic bath for 1 hour. Second part is analysis of extracts using capillary zone electrophoresis method, analysis results are show in Fig 1.

Analysis conditions were: 0.5 M acetic acids was used as background electrolyte, 50 µm inner diameter fussed silica capillary (total length - 59 cm, length to the detector – 49 cm), sample injection – hydrodynamic 50 mbar * 30 s, analysis voltage 14 kV, analysis time - 35 minutes, detector type – contactless conductivity detector. Analysis results show promising trends for capillary electrophoresis as effective protein separation method.

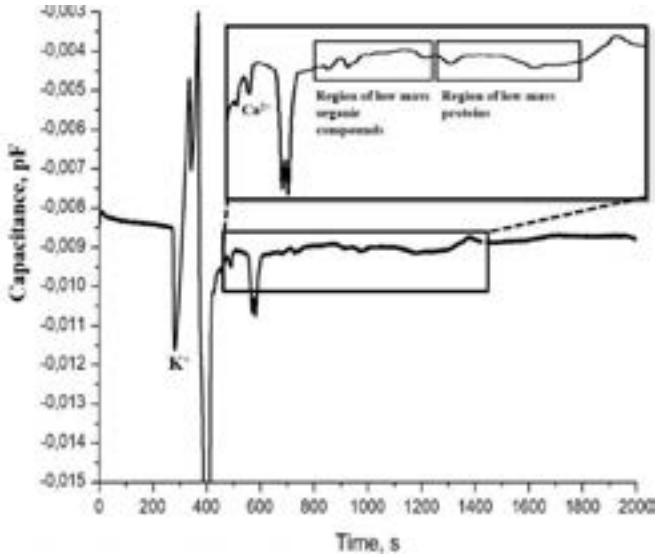


Fig. 1. Electopherogram of white root fungi extract after extraction using bidistilated water.

**Acknowledgements:**
The research was granted by Research Council of Lithuania, project No. 09.3.3-LMT-K-712-10-0223.

# SUB-MICROSECOND RISE TIME MAGNETIC FIELD PULSER FOR BIOLOGICAL MAGNETOTRANSFER EXPERIMENTS

Gediminas Staigvila[1,2], Vitalij Novickij[1,2]

[1] Department of Electrical Engineering, Vilnius Gediminas Technical University, Lithuania
[2] Institute of High Magnetic Fields, , Vilnius Gediminas Technical University, Lithuania
gediminas.staigvila@vgtu.lt

The emerging contactless cell membrane permeabilization methodology (magnetoporation), which is based on high pulsed magnetic field (PMF) is highly dependent on the applied pulse parameters. In order to trigger PMF induced cell permeabilization, magnetic field in the range of 3-6 T and the induced electric field in the range of 5-10 V/cm are required [1,2]. As a result, high *dB/dt* systems are advantageous [3,4].

In this work, a high *dB/dt* generator, which is applicable for magnetoporation or study of the biological effects of PMF has been developed and is presented. The generator is based on an ignitron switch (20 kV, up to 100 kA) and an array of silicon controlled rectifiers (SCR). The SCRs, as the main pulse forming switches (typical in PMF generation technology) are no longer suitable for the task due to the *dI/dt* and *dV/dt* ratings of the setup, therefore, ignitron is used for the output pulse forming.

The photograph of the generator and the output waveform are shown in Fig. 1.

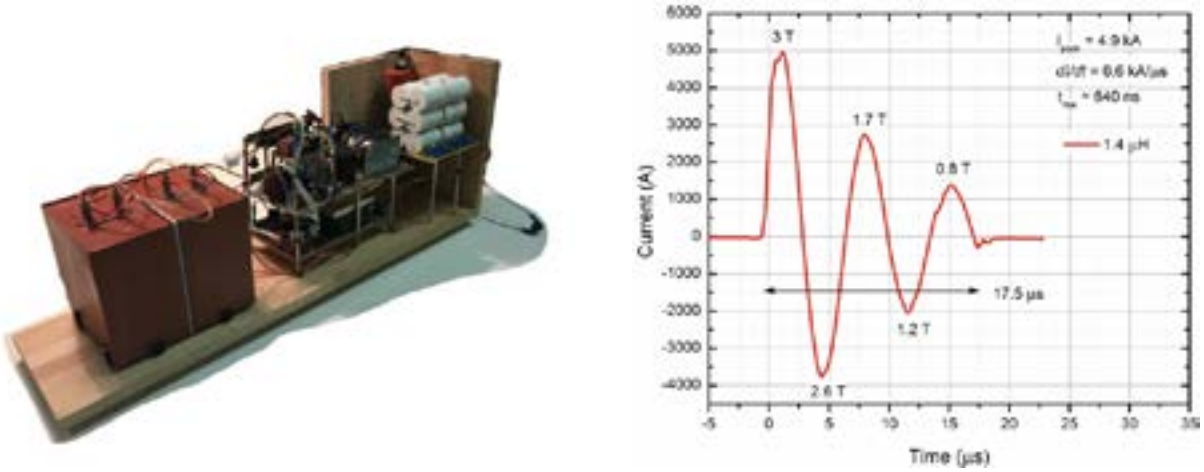


Fig. 1. The photo of the generator and the output waveform

The ignitron switch due its superb current handling capability allowed using both the nearly short-circuit and highly inductive loads. To present the concept we have used merely 5% of the current handling capability of the generator. The structure, the waveforms and the step by step development process will be presented in the conference, while the results may find direct application as a platform for basic magnetoporation experiments.

[1] S. Kranjc, M. Kranjc, J. Scancar, J. Jelenc, G. Sersa, and D. Miklavcic, "Electrochemotherapy by pulsed electromagnetic field treatment (PEMF) in mouse melanoma B16F10 in vivo," Radiol. Oncol., **50**, 39–48 (2016).
[2] V. Novickij, J. Dermol, A. Grainys, M. Kranjc, and D. Miklavčič, "Membrane permeabilization of mammalian cells using bursts of high magnetic field pulses," PeerJ, **5**, e3267 (2017).
[3] J. W. M. Van Bree, J. J. G. Geysen, E. J. M. Van Heesch, and A. J. M. Pemen, "Novel nanosecond pulsed electric field device for noncontact treatment of cells in native culture conditions," IEEE Trans. Plasma Sci., **41**, 2654–2658 (2013).
[4] V. Novickij et al., "Membrane Permeabilization of Pathogenic Yeast in Alternating Sub-microsecond Electromagnetic Fields in Combination with Conventional Electroporation," J. Membr. Biol., **251**, 189-195 (2017).

# DESIGNING FUSED MUTANT LIPOLYTIC ENZYMES FOR BETTER UNDERSTANDING OF STRUCTURE-FUNCTION RELATIONSHIP IN CHIMERIC PROTEINS

Gytis Druteika, Renata Gudiukaitė

Department of Microbiology and Biotechnology, Institute of Biosciences, Life Sciences Center, Vilnius University, Sauletekio avenue 7, LT-10257 Vilnius, Lithuania
*gytis.druteika@gf.stud.vu.lt*

Lipases and esterases from *Geobacillus* bacteria are enzymes possesing industrially attractive characteristics such as activity in wide temperature, pH, substrate range, stability in organic solvents [1,2]. These enzymes are involved in organic chemistry, food, pharmaceutic and many other industries. Obtaining highly active, stable and, most importantly, low-cost lipolytic enzymes is one of the principal research objects.

Protein engineering is probably the main strategy, allowing us to develope enzymes which have ideal properties for certain bioprocess [3]. One of the most rapidly evolving fields is the design of multifunctional chimeric proteins [4]. Fusing two or more protein domains may lead to increased bioactivities or produced new functional combinations with an expanded range of biotechnological and (bio)pharmaceutical applications [5]. However, the remaining question is whether both fused domains retain their activity. The answer would help to model the structure of novel bifunctional proteins as biocatalyzers for cascade reactions.

In order to find the solution, we re-designed in previous studies characterised GDEst-lip and LipGD95-GD66 chimeric proteins [2,6]. *Geobacillus* lipases (GD-95 and GD-66) together with esterase (GDEst-95) were chosen as fusion partners and alanine mutagenesis for knocking-out amino acids in the active sites was applied in order to create chimeric protein variants with only one functional active site (Fig. 1). Later the fused genes were cloned into pET-21c(+) vector, expressed in *E*. coli BL21 (DE3) cells, purified using IMAC methodology and analyzed via SDS-PAGE and zymography methods.

These results may open on to better understanding of the relationship between the structure of chimeric enzymes and their functionality, as well as expanding the knowlegde about genotype and phenotype space of lipolytic enzymes from *Geobacillus.*

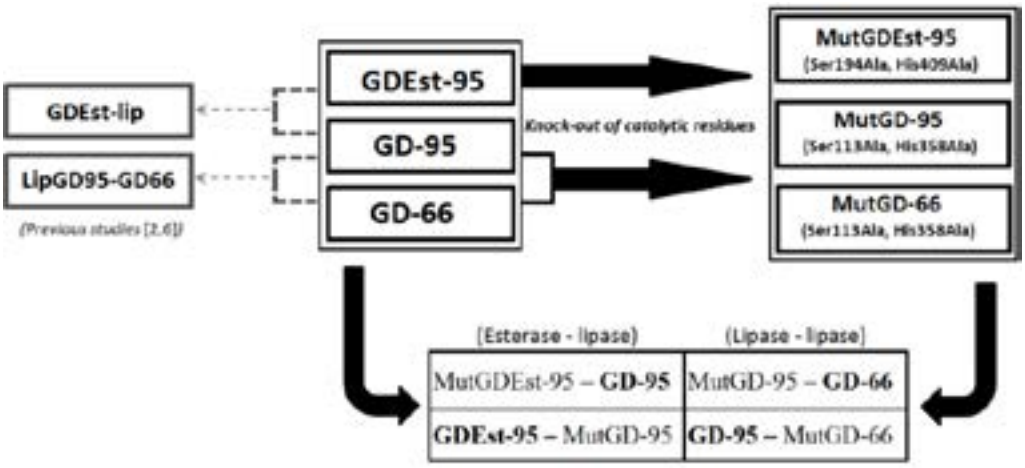


Fig. 1. The principle of this study: first, catalytic residues in lipolytic enzymes were mutated into alanine in order to knock-out their activity. Then mutated genes were fused with non-mutated genes of lipolytic proteins to create four new chimeric enzyme variants, where only one domain has retained functionality (active domains are in bold).

1. N. Gurung, S. Ray, S. Bose, and V. Rai, Biomed Res Int **2013**, 329121 (2013).
2. R. Gudiukaite, M. Sadauskas, A. Gegeckas, V. Malunavicius, and D. Citavicius, J. Ind. Microbiol. Biotechnol. **44**, 799 (2017).
3. C. D. Anobom, A. S. Pinheiro, R. A. De-Andrade, E. C. G. Aguieiras, G. C. Andrade, M. V. Moura, R. V. Almeida, and D. M. Freire, BioMed Research International (2014).
4. R. A. George and J. Heringa, Protein Eng. **15**, 871 (2002).
5. K. Yu, C. Liu, B.-G. Kim, and D.-Y. Lee, Biotechnol. Adv. **33**, 155 (2015).
6. V. Malunavicius, G. Druteika, M. Sadauskas, A. Veteikyte, I. Matijosyte, E. Lastauskiene, A. Gegeckas, and R. Gudiukaite, International Journal of Biological Macromolecules **118**, 1594 (2018).

# LACCASE II PROTEIN DISPLAY WITH THE YSD SYSTEM AGA1-AGA2

Hanna Yeliseyeva[1,2], Eivydas Andriukonis[1], Arūnas Stirkė[1]

[1] Department of Material Science and Electrical Engineering, Center for Physical Sciences and Technology, Bioelectrochemistry laboratory, Lithuania
[2] Department of Microbiology and Biotechnology, Vilnius University's Life Sciences Centre, Lithuania
hanna.yeliseyeva@gf.stud.vu.lt

Yeast surface display (YSD) is a technology for displaying recombinant proteins on the surface of *Saccharomyces cerevisiae* via anchoring them to a native cell agglutination wall protein AGA1- AGA2 complex. YSD is commonly used as a protein engineering and library screening tool. Though, YSD can also be used to arm yeast cell with industrially important enzymes localized on the surface of cells.

In the current work we are aiming to produce *S.cerevisiae* whole cell surface biocatalysts using the recombinant protein technique by fusing Laccase II enzyme with AGA2 protein from the AGA1-AGA2 cell wall two-protein complex. (Fig. 1) Yeast Laccase II is a copper-containing oxidase enzyme that catalytic reaction via one-electron oxidation leads to aromatic compound oxidation. This enzymatic reaction can be implemented for oxidation of aromatic monomers which consequently undergo polymerization. (1) Thus bio assisted synthesis of polymers can be achieved. As main target, such conductive polymers as polyaniline (PANI) and polypyrrole (Ppy) could be produced. They are widely applied in the development of fuel cells [1], "artificial muscles" technology [2], printed circuit board and other smart material manufacturing. Implementing Laccase II specific activity, these novel YSD based biocatalysts can be applicable in bio assisted conductive polymers production. [3]

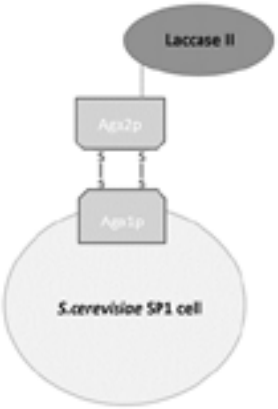


Fig. 1. YSD based on AGA1-AGA2 schematic view.

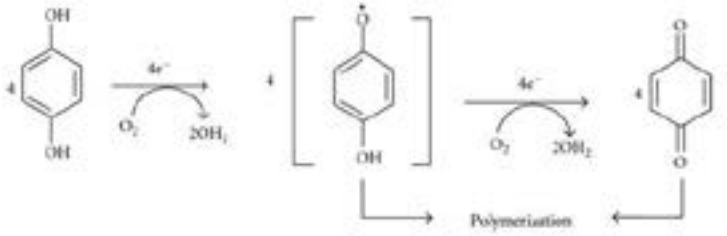


(1)

[1] Unni, Sreekuttan M.; Dhavale, Vishal M.; Pillai, Vijayamohanan K.; Kurungot, Sreekumar (2010). "High Pt Utilization Electrodes for Polymer Electrolyte Membrane Fuel Cells by Dispersing Pt Particles Formed by a Preprecipitation Method on Carbon "Polished" with Polypyrrole". *The Journal of Physical Chemistry C*. **114** (34): 14654–14661

[2] Hara, S., Zama, T., Takashima, W. & Kaneto, K. Artificial Muscles Based on Polypyrrole Actuators with Large Strain and Stress Induced Electrically. *Polymer Journal* **36**, 151 (2004).

[3] B. Dedeyan, A. Klonowska, S. Tagger et al., "Biochemical and molecular characterization of a laccase from Marasmius quercophilus," Applied and Environmental Microbiology, vol. 66, no. 3, pp. 925–929, 2000.

# EFFECTS OF HEAVY METAL IONS AND QUANTUM DOTS ON THE AUTOFLUORESCENCE OF FRESHWATER MICROALGAE

Ieva Austėja Jakaitytė*, Agnė Kalnaitytė, Saulius Bagdonas

Laser Research Center, Vilnius University, Saulėtekio av. 10, LT-10223, Vilnius, Lithuania
ieva.a.jakaityte@gmail.com

The fluorescence spectroscopy of chlorophylls in plants and algae is an effective non-invasive technique to assess their physiological state and photosynthetic activity. Changes of the fluorescence yield and kinetics indicate the disruption of photosynthesis and metabolic processes. Thus, autofluorescence measurements can be used for toxicity assessment[1]. Heavy metal-containing quantum dots (QDs) represent nanoparticles that are also useful as luminescent markers for biological imaging owing to the enhanced photostability, bright tuneable photoluminescence (PL) and wide possibilities for surface modification.

In this work the fluorescence spectroscopy and microscopy methods were applied to evaluate the effects of different concentrations of copper ions ($Cu^{2+}$) and water soluble CdTe-MSA quantum dots (a peak of photoluminescence at 550 nm) on the green freshwater *Chlorella* sp. and *Scenedesmus* sp. microalgae. When exposed to blue light, chlorophylls of healthy microalgae cells fluoresce brightly in the red spectral region as detected by measuring autofluorescence spectra by means of a spectrophotometer Perkin Elmer LS 55. Samples were kept under natural daylight conditions and remained in the dark overnight for adaptation before measuring the slow part of autofluorescence kinetics (at 683 nm, the peak of the main fluorescence band) using Ocean Optics USB 2000+ spectrometer (excitation wavelength – 405 nm).

Changes in both intensity and form of the microalgae fluorescence spectra were observed when being affected by various concentrations of copper ions, in comparison to the control samples. The autofluorescence decreased depending on the ion concentration and the exposure time, indicating damage to the photosynthetic apparatus of microalgae. Regarding the changes in the spectral shape, the intensity of the longer-wavelength slope has decreased (Fig. 1).

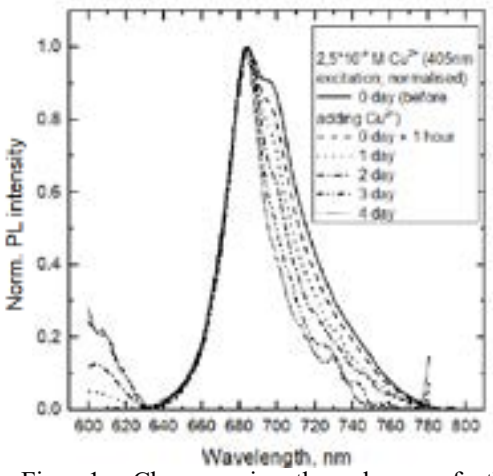


Fig. 1. Changes in the shape of the normalized fluorescence spectra of *Chlorella sp.* during 4 days of exposure to $2.5*10^{-4}$ M $Cu^{2+}$

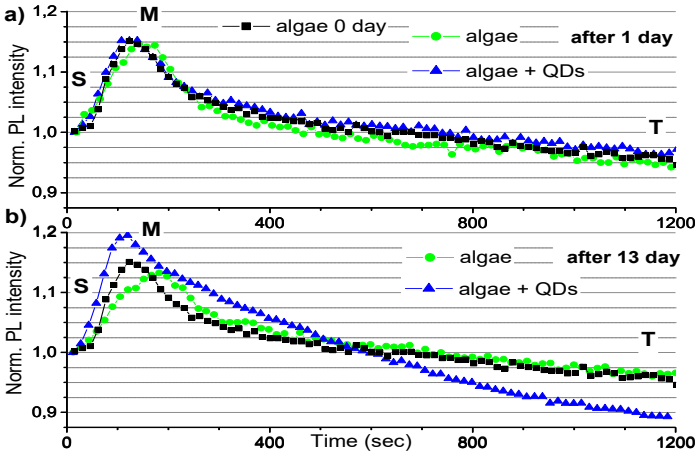


Fig. 2. Kinetics of the photoinduced changes in peak fluorescence intensity recorded before (black squares) as well as after one (a) and thirteen (b) days of incubation with QDs. The spectral data values were normalised at the beginning of kinetics.

The pattern of the photoinduced fluorescence kinetics in microalgae consisted of the steady-state level "S", the maximum level "M" and the terminal level "T" (Fig. 2). The influence of QDs on the autofluorescence of algae cells became more pronounced on later days, and the biggest changes in the kinetics curve were observed after 13 days incubation with QDs, which included relative enhancement and further shift of the maximum "M" position as well as steeper FL intensity reduction from the level "M" to "T".

The microscopic measurements were done by means of a fluorescence microscope (Nikon eclipse 80i). There were no obvious changes seen in algae cells using a phase contrast mode after 24 hours of incubation with copper ions or QDs. However, fluorescence images, taken using UV or violet spectral excitation, showed some of round-shaped *Chlorella* sp. algae starting to photoluminesce in yellow in the samples with QDs, and the red fluorescence intensity in green algae cells was disappearing in a non-uniform manner in the presence of copper ions in comparison with those in the samples of microalgae kept without heavy metals. The contact with QDs resulted in decrease of the autofluorescence starting from the second day of incubation, which seems to be related with the reduced quantum yield of chlorophylls and does not involve the direct inactivation of algae cells during the first week of incubation.

[1] K. S. Kumar, H.-U. Dahms, J.-S. Lee, H. C. Kim, W. C. Lee, &K.-H. Shin. Algal photosynthetic responses to toxic metals and herbicides assessed by chlorophyll a fluorescence, Ecotoxicology and Environmental Safety**104**, 51-71 (2014)

# PICOMOLAR INHIBITORS OF CARBONIC ANHYDRASE: IMPORTANCE OF INHIBITION AND BINDING ASSAYS

Joana Smirnovienė and Daumantas Matulis

Department of Biothermodynamics and Drug Design, Institute of Biotechnology, Life Sciences Center, Vilnius University
joana.smirnoviene@gmc.vu.lt

Human carbonic anhydrases (CAs) are targets for drug design due to their role in numerous diseases such as glaucoma, epilepsy, and cancer. Clinically used CA inhibitors–drugs are relatively weak and non-selective for human CA isoforms thus exhibiting toxic side effects. Further drug development should lead to compounds with picomolar affinities and significant selectivities. Currently, the $K_i$ of CA inhibitors is usually determined by the stopped-flow $CO_2$ hydration assay, the method that directly follows inhibition of CA enzymatic activity. However, the assay has limitations, such as largely unknown concentration of $CO_2$ and the inability to determine the $K_i$ below several nM. The widely used direct binding assay, isothermal titration calorimetry, also does not determine the $K_d$ below several nM. In contrast, the thermal shift assay can accurately determine picomolar affinities.

The inhibitor dose-response curves were analyzed using Hill and Morrison equations demonstrating that only the Morrison model is applicable for the determination of tight-binding inhibitor $K_i$. The measurements of interactions between ten inhibitors and seven CA isoforms showed the limitations and advantages of all three techniques. Inhibitor **6**[1] exhibited the $K_d$ of 50 pM and was highly selective towards human CA IX, an isoform which is nearly absent in healthy human, but highly overexpressed in numerous cancers. Combination of inhibition and binding techniques is necessary for precise determination of CA–high-affinity inhibitor (such as **6**) interactions and future drug design[2].

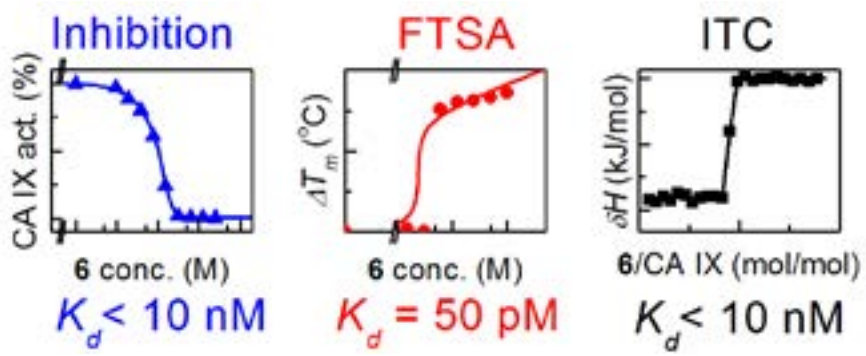


Fig. 1. Comparison of enzymatic activity inhibition assay, fluorescent thermal shift assay and isothermal titration calorimetry.

[1] Dudutienė, V. et al.. Discovery and characterization of novel selective CAIX inhibitors. J. Med. Chem 9435–9446 (2014).
[2] Smirnovienė, J., Smirnovas, V., and Matulis, D. Picomolar inhibitors of carbonic anhydrase: Importance of inhibition and binding assays. Anal. Biochem. **522** 61-72 (2017).

# CHANGING OF LACTOFERRIN IRON-BINDING CAPACITY IN INFLAMMATION

Maria Terekhova[1], Daria Grigorieva[1], Irina Gorudko[1], Alexey Sokolov[2,3]

[1] Department of Physics, Belarussian State University, Belarus
[2] Institute of Experimental Medicine, Saint-Petersburg, Russia
[3] Federal Research and Clinical Center of Physical-Chemical Medicine, Moscow, Russia
autumn_frost@mail.ru

In accordance with the program of World Health Organization new drug development, aimed to prevention of infectious diseases and increasing humans' lifespan and level of living, is underway around the world. Lactoferrin (Lf), non-hemic iron-binding protein of the transferrin family, is the promising protein for this aim because of its many physiological functions, including regulation of iron absorption and immune responses; it also exhibits antioxidant activity and has both anticarcinogenic and anti-inflammatory properties. The antimicrobial activity of Lf, most widely studied function, is driven generally by two mechanisms: 1) direct interaction positively charged amino acids in Lf with anionic molecules on certain microorganism surface causing cell lysis and 2) iron sequestration in site of infection, which deprives microorganisms of this nutrient and causes a bacteriostatic effect [1].

Ceruloplasmin (CP) is a serum ferroxidase that contains greater than 95 % of the copper found in plasma, this protein is an acute phase reactant part of the organism's defense in inflammation. Lf concentration highly increases in inflammation focuses because of neutrophil degranulation. Due to this fact it was found the complexes Lf-CP in blood serum of patients with pleuritis of different etiology [2]. As is known, complexes creation can influence on biological properties of the composing proteins. It already has been revealed [3, 4] that ferroxidase activity of Cp can be stimulated by Lf. But it's still unknown whether iron-binding property of Lf will be changed in case of CP influence by complexes formation in inflammation focuses or not. ROS and RHS formed in inflammatory focuses are high reactivity oxidants modifying biomolecules (lipids, proteins, nucleic acids) and resulting in changing of their properties. Thus in the previous work [5] we showed the reduction of iron-binding capacity of Lf in case of modification by HOBr and HOCl. The present work is aimed to study modification of iron-binding capacity of Lf, which is crucial and necessary for antibacterial property, in case of formation complexes Lf-CP in inflammatory foci.

Lf-CP complex formation was performed by mixing and incubation Lf and CP in equal concentration (i.e. molar ratio 1:1) for 30 min at 37 °C. CP was modified by HOCl in a molar ratio CP:HOCl 1:50, modification lasted for an hour. Iron-binding capacity of Lf was investigated using spectrophotometric analysis. Addition of $Fe^{3+}$ (salt – ($NH_4$ $Fe(SO_4)_2$)) to Lf solution leads to change in absorption at λ=465 nm due to transition of apo-state of Lf (i.e. iron-unbound form) to holo-state of Lf (i.e. iron-bound form).

It was found that formation of Lf-CP complexes causes reduction of 30 % of iron-binding capacity of Lf. Lf has two iron-binding sites per one molecule, which comprise four protein sidechains (2 Tyr, 1 Asp, and 1 His), side chain of an Arg residue, balanced the negative charge of a $CO_3^{2-}$ anion. Moreover iron binding is cooperative process, at first $Fe^{3+}$ fits into N-lobe of Lf, after that due to conformational reorganization C-lobe becomes open and let $Fe^{3+}$ fits into lobe. It's necessary to mention that when the N-lobe site was knocked out, the C-lobe site behaved as normal (closed form) [6]. Formerly it was showed that cationic N-lobe of Lf is responsible for interaction between Lf and CP [4,7]. Due to complexes formation iron-binding site becomes partially inaccessible because of interruption of conformation alteration, those processes lead to decreasing of number binding ions (10 molecules of Lf bind 14 ions of $Fe^{3+}$). Nevertheless the modification of CP by HOCl, which leads to structure and activity modification of CP [8], causes formation of slightly remodeled complexes (Lf-CP-Cl). This results in decrease of 39 % of iron-binding capacity of Lf.

Thus it was showed that creation of the complexes Lf with native CP (Lf-CP) and CP under halogenative stress (Lf-CP-Cl) in inflammation focuses leads to decrease Lf iron-binding capacity, which can influence on antibacterial property of Lf.

This study was supported by Russian Foundation for Basic Research (18-515-00004) and Belarusian Republican Foundation for Fundamental Research (B18R-058).

[1] T. J. Ochoa, T. G. Clear, Effect of lactoferrin on enteric pathogens, Biochemie. **91(1)**, 30-34 (2009).
[2] A. V. Sokolov, M. O. Pulina et al., Interaction of ceruloplasmin, lactoferrin and myeloperoxidase, Biochem. (Mosc), **72(4)**, 409-415 (2007).
[3] A. V. Sokolov, M. O. Pulina et al., Effect of lactoferrin on the ferroxidase activity of ceruloplasmin, Biochem. (Mosc), **70(9)**, 1015-1019 (2005).
[4] A. V. Sokolov, K. V. Ageeva et al., Effect of lactoferrin on oxidative features of ceruloplasmin, Biometals., **22(3)**, 521-529 (2009).
[5] M. S. Terekhova, I. V. Gorudko et al., Iron-binding property of lactoferrin in the case of inflammation, Doklady BGUIR, **117 (7)**, 80-84 (2018).
[6] E. N. Baker, H. M. Baker, Molecular structure, binding properties and dynamics of lactoferrin, Cel. and Mol. Life Sci., **62**, 2531-2539 (2005).
[7] A. Sabatucci, P. Vachette et al., Structural characterization of the ceruloplasmin: lactoferrin complex in solution, J. Mol. Biol., **371**, 1038–1046 (2007).
[8] A. V. Sokolov, V. A. Kostevich et al., Capacity of ceruloplasmin to scavenge products of the respiratory burst of neutrophils is not altered by the products of reactions catalyzed by myeloperoxidase, Biochem. and Cell Biol. **96(1)**, 457-467 (2018).

# THE USE OF ALTERNATIVE PROTEIN FEED IN ANIMAL NUTRITION

Karol Radzikowski[1], Daniel Radzikowski[2] Aleksandra Kalińska[2], Urszula Ostaszewska[1]

[1] Department of Natural Sciences, Siedlce University of Natural Sciences and Humanities, Poland
[2]Department of Animal Breeding and Production, Warsaw University of Life Sciences, Poland
kradzikowski93@wp.pl

In light of the constantly rising prices of soy meal, it is worth looking at other sources of protein in compound feed. Post-extraction soy meal is today the basic high-protein feed used in feeding pigs and poultry.

The aim of the presentation is to present alternative fodder and protein crops that we can use in animal nutrition in order to be able to partially become independent of post-extraction soy meal.

A chance for partial replacement of post-extraction soy meal is also legume seeds. In the climate of our country, the cultivation of pea, horse bean and lupins should be taken into account. Of the listed plants, peas may potentially be of greatest importance. It is characterized by a relatively low protein content, but it is a protein with a favorable amino acid composition. Bean seed is characterized by a higher content of protein (28-30%), its composition is slightly worse than peas. They contain, however, certain amounts of pyrimidine glycosides, worsening increments, feed intake, and laying hens, egg size. Therefore, its participation in the mixture should be limited. Of the listed legumes, the richest in protein are yellow (43%) and white (40%) lupine seeds. Narrow-leaved lupine contains about 32% of protein. However, this is a protein deficient in essential amino acids, especially lysine and tryptophan. The basic limiting factor in the use of lupine in compound feed is the presence of toxic alkaloids. In addition, carbohydrates contained in lupine seeds are not digested by poultry. Soy protein can be partially replaced by means of dried distillers (DDGS), a by-product in the process of obtaining spirit. The most common are corn and rye decoctions. The protein content in DDGS is quite high, and is about 34% for rye decoction and 29% for maize decoction. Pigs of animal origin are an excellent but expensive source of protein. Most often, raw materials such as fish meal, blood meal and dried blood plasma are used. These are high protein feeds with excellent amino acid composition. In addition, blood meal and dried blood plasma contains immunoglobulins, stimulating the immunity of young animals.

In conclusion, it should be noted that the alternative protein sources on the domestic market are able to partially replace the extracted soy meal. However, we are not able to completely eliminate it from the nutritional doses used in animal nutrition.

# INNOVATION IN THE PRODUCTION OF FEED AND FEEDING OF DAIRY COWS

Karolina Grzymała[1], Daniel Radzikowski[2], Aleksandra Kalińska[2], Brygida Kruzińska[2], Urszula Ostaszewska[3]

[1] Faculty of Production Engineering, Warsaw University of Life Sciences, Poland
[2]Department of Animal Breeding and Production, Warsaw University of Life Sciences, Poland
[3] Department of Cattle Breeding and Milk Evaluation, Siedlce University of Natural Sciences and Humanities, Poland
grzymkarolina@gmail.com



Intensive use of dairy cattle and the need to maintain high quality standards of the obtained raw material, requires constant modernization of the production of feed and cow feeding.

The most important role in modernizing and improving the efficiency of feeding dairy cattle is to obtain high quality feed adapted to the cow's dietary needs. The introduction of new technologies (TMR / PMR) in cow nutrition contributed to a large extent to the increase in milk yield of cows, improved feed utilization and increased commerciality of farms specializing in milk production. The specialization of farms in milk production and the observed increase in the number of herds is conducive not only to the introduction of innovations in cow nutrition, but also to mechanization and automation, and even robotisation of the entire milk production cycle. The use of biotechnology achievements, including new generation products obtained through biotechnology, in the production of feed and cow nutrition, is one of the determinants of progress in balancing the specific nutritional needs of dairy cattle. The use of these products in the nutrition of dairy cattle, contributes, among others to stimulate the milk yield of cows, a beneficial effect on the uptake of dry matter and rumen metabolism, as well as on the health condition of animals. The introduction of TMR / PMR technology in the nutrition of cows has also contributed to the development of automatic feeding and feeding systems. In feeding the cows in PMR technology, automatic feed dosing stations have been additionally introduced. Also in the case of milking robotics, a system of automatic dosing of concentrate feed or feed additives in milking robots was used.

The observed constant increase in the number of herds in farms rearing dairy cattle and the need to increase the efficiency of this branch of animal production will encourage the introduction of new solutions, which will have a positive impact on the effectiveness of milk production in our country.

# ELECTROPHYSIOLOGICAL STUDIES OF PRIMARY CULTURES OF CEREBELLAR GRANULE NEURONS FROM THE RAT USING THE PATCH-CLAMP METHOD

Kristina Majauskaite[1], Silvija Jankeviciute[2]

[1]Institute of Biochemistry, Life Sciences Center, Vilnius University, Lithuania
[2]Neuroscience Institute, Lithuanian University of Health Sciences, Lithuania
kristina.majauskaite@bchi.vu.lt

Electrical signal transmission mechanisms in cholinergic synapses are widely studied, but many important questions remain unanswered. There is the enzyme acetylcholinesterase in cholinergic synapse, that catalyses the hydrolysis of acetylcholine into the metabolites choline and acetic acid, the latter dissociates into the acetate and proton. Are there any proton channels in cholinergic synapse and whether the protons affect the postsynaptic potential?
Trying to find the answers to these scientific questions, we combined two excellent techniques – primary cultures of cerebellar granule neurons (CGN) from the rat cerebellum and the Patch-clamp. CGN cultured *in vitro* maintain the same features displayed *in vivo* by mature cerebellar granule cells.

Combining primary cultures of cerebellum granule neurons from the rat and patch-clamp technique we succeeded in recording the action potentials in cerebellum granule neurons. This means that neurons are alive and responsive to stimuli. This provides a means to administer and study how analytes (for example, ion channels blocking or opening compounds) can affect neurons or ion channels in real time. Combining this both techniques we can investigate not only proton channels in cholinergic neurons and synapses, but also apply for other scientific purposes. These techniques enable researchers to understand how neurons (or ion channels in neurons) behave and how different drugs, toxins, ions, or other analytes can modify normal conditions.

# A STUDY ON THE INFLUENCE OF WATER ON THE L-LEUCINE FRAGMENTATION

Laura Baliulytė[1], Jelena Tamulienė[2]

[1]Institute of Biosciences, Life sciences center, Vilnius University, Vilnius, Lithuania
[2]Institute of Theoretical Physics and Astronomy, Vilnius University, Vilnius, Lithuania
baliulyte.laura@gmail.com

All living organisms are constantly affected by ionizing radiation emitted by natural sources such as cosmic rays and radionuclides contained in rocks from the Earth, food, water, air, etc. Moreover, ionizing radiation exposures also occurs during medical procedures. Low-energy electrons are produced due to ionizing radiation. These low-energy electrons cause damage of biomolecules, including amino acids, e.g., leucine. Data on fragmentation of amino acids in water under impact of ionizing radiation are scarce, although they are relevant to the analysis of processes in living organisms.

Hence, the aim of our research is to determine whether the appearance energies of fragments differ between conditions with and without the influence of water included.

The fragmentation of the L-leucine molecule was theoretically studied by using Becke's three-parameter hybrid functional applying the non-local correlation provided by Lee, Yang and Parr (B3LYP) with the correlation consistent triple zeta basis (cc-pVTZ). The polarized continuum model (PCM) method was used to evaluate the presence of water. We applied Gaussian 03 Rev D.01/09 Rev D.01 program. Fragments for the research were selected on the basis of the experimental data of mass spectrometry.

We determined that cation with mass 86 a.m.u. is $C_5H_{12}N^+$, cation with mass 44 a.m.u. is $C_2H_6N^+$ and cation with mass 30 a.m.u.- $CH_4N^+$. The results of our research with and without the influence of water indicate that more energy is needed for the formation of same cations in water.

**Acknowledgment**
The authors are thankful for the high performance computing resources provided by the Information Technology Open Access Center of Vilnius University.

# IDENTIFICATION OF THE TOXIN-ANTITOXIN SYSTEMS IN THE OPPORTUNISTIC PATHOGEN *STENOTROPHOMONAS MALTOPHILIA*

Laurita Klimkaitė, Julija Armalytė, Edita Sužiedėlienė

Institute of Biosciences, Life Sciences Center, Vilnius University, Vilnius, Lithuania
lauritaklimkaite@gmail.com

Bacterial toxin-antitoxin (TA) systems are small genetic elements, coding a stable protein toxin and an unstable molecule, neutralizing its toxic effect – antitoxin. In stress conditions (e.g. starvation, antibiotic pressure, host immune system attack) the unstable antitoxin molecule is degraded and the toxin inhibits the main cellular processes – DNA replication or protein, cell wall, ATP synthesis [1]. TA systems are potentially associated with the virulence traits of pathogenic bacteria, such as persistence, biofilm formation, host colonization [2]. Furthermore, TA systems are proposed as new targets for antimicrobial therapy especially important for the multidrug-resistant pathogen treatment [3].

*Stenotrophomonas maltophilia* is an environmental bacterium found in aqueous habitats, the rhizosphere of plants, on animals, in foods. In clinical settings *S. maltophilia* is known as an opportunistic multidrug-resistant nosocomial pathogen causing respiratory tract, bloodstream, urinary tract infections [4]. At present there is no information about the TA systems of this pathogen, thus our goal is to identify and characterize the TA systems of *S. maltophilia.*

Bioinformatic analysis was performed on 21 *S. maltophilia* genome sequences available to this date and 50 putative TA systems were predicted. 7 genes pairs best matching TA systems criteria were selected for further analysis. All selected TA systems were detected in clinical or environmental *S. maltophilia* isolates from laboratory collection. Interestingly, the frequency and spread of detected TA systems differed from bioinformatic analysis predictions. Detection results showed that several selected TA systems are present only in clinical *S. maltophilia* bacteria and are not found in environmental *S. maltophilia* isolates.

[1] Yamaguchi, Y., Park, J.-H. & Inouye, M. Toxin-Antitoxin Systems in Bacteria and Archaea. *Annu. Rev. Genet.* 45, 61–79 (2011).
[2] Fernández-García, L. *et al.* Toxin-Antitoxin Systems in Clinical Pathogens. *Toxins* 8, 227 (2016).
[3] Williams, J. J. & Hergenrother, P. J. Artificial activation of toxin–antitoxin systems as an antibacterial strategy. *Trends Microbiol.* 20, 291–298 (2012).
[4] Brooke, J. S. Stenotrophomonas maltophilia: an Emerging Global Opportunistic Pathogen. *Clin. Microbiol. Rev.* 25, 2–41 (2012).

# ANDROGEN-DERIVED COMPOUNDS REGULATE C6 GLIOMA CELLS GROWTH

Valeryia Klopava[1], Jan Panada[2,3], Alexandra Falchevskaya[2], Tatsiana Kulahava[1], Yaroslav Faletrov[2,3], Vladimir Shkumatov[2,3]

[1] Department of Biophysics, Physics faculty, Belarusian State University
[2] Chemistry faculty, Belarusian State University
[3]Research Institute for Physical Chemical Problems, Belarusian State University
fiz.klopova@bsu.by

Steroid hormones may influence the development and control of glioma growth by interacting with their receptors and regulating the transcription of target genes. C6 glioma cells and many types of glioblastomas were shown to express two types of the classical androgen receptors. Dihydrotestosterone in a concentration-dependent manner could regulate signaling pathways in C6 glioma cells [1]. One of perspective antitumor androgen-derivative drugs is abiraterone acetate (AA). To the best of our knowledge, in spite of the ability of AA to penetrate blood-brain barrier [2], effects of the compound on glioma cells have not been reported.

The aim of this work was to investigate the effects of steroidal and indole derivatives on C6 glioma cells proliferation. Two steroids, N-(indol-3-ylethyl)-3β-hydroxyandrost-5-en-17β-amine (DTPA) and N-methyl-3β-hydroxyandrost-5-en-17β-amine (DAM) were obtained by reductive amination of dehydroepiandrosterone (DHEA) with tryptamine (TRPA) and methylamine hydrochloride, respectively, according to [3]. The structures were confirmed by mass, infrared and nuclear magnetic resonance spectroscopy. C6 glioma cells in monolayer on the 2nd day of growth were exposed to compounds for 24 h and then the number of cells was counted.

Treatment with DTPA, DAM and TRPA for 30-60 min did not affect cell viability. In contrast our study we demonstrated that AA and compound DTPA at $1 \cdot 10^{-5}$ M concentration can inhibit glioma cells proliferation by 55±5% and 45±6%, respectively. At the same time, steroid DAM, being a structural moiety of DTPA, did not cause such pronounced effect, implying the importance of the N-heterocycle in the steroids' side chains. TRPA, another part of DTPA, led to 25 % decrease of glioma cells proliferation.

The effect of DTPA could be due to influence on steroidal signaling, including potentially competing membrane-associated and nuclear androgen receptors, which are confirmed in C6 glioma cells [1]. It was published that DHEA promotes survival of glioma cells [4], whereas its biosynthetic precursor pregnenolone induces their apoptosis [5]. Thus, inhibition of CYP17, which catalyzes pregnenolone-to-DHEA conversion, could be a new therapeutic strategy against this type of cancer. Depending on the specificity of steroid biosynthesis, tranport and reception, the outcome of androgen treatment of glioma might be different. In general, enzymes of steroidogenesis are known to be promising targets for anti-cancer drug developing [6]. Therefore, synthesis of androgen-containing molecules with designed properties is of current interest.

In summary, ability of AA and a newly synthesized DTPA demonstrated glioma growth inhibition, providing opportunity to develop steroidal derivatives as potential drug candidates agains the cancer.

---

[1] J. W. Gatson, P. Kaur, M. Singh, Dihydrotestosterone differentially modulates the mitogen-activated protein kinase and the phosphoinositide 3-kinase/Akt pathways through the nuclear and novel membrane androgen receptor in C6 cells, Endocrinology **149**, 2028-2034 (2008).
[2] https://www.ema.europa.eu/documents/assessment-report/zytiga-epar-public-assessment-report_en.pdf
[3] E. O. J. Porta, P. B. Carvalho, A. M. Avery et al., Click chemistry decoration of amino sterols as promising strategy to developed new leishmanicidal drugs, Steroids **79**, 28-36 (2014).
[4] J. Y. Chuang, W. L. Lo, C. Y. Ko et al., Upregulation of CYP17A1 by Sp1-mediated DNA demethylation confers temozolomide resistance through DHEA-mediated protection in glioma, Oncogenesis **6**, e339 (2017). doi: 10.1038/oncsis.2017.31.
[5] X. Xiao, L. Chen, Y. Ouyang et al., Pregnenolone, a cholesterol metabolite, induces glioma cell apoptosis via activating extrinsic and intrinsic apoptotic pathways, Oncol. Lett. **8**, 645-650 (2014).
[6] L. A. Novikova, Y. V. Faletrov, I. E. Kovaleva et al., From structure and functions of steroidogenic enzymes to new technologies of gene engineering, Biochemistry (Moscow) **74**, 1482-1504 (2009).

# GALLOCYANINE-BASED SCREENING METHOD FOR SUPEROXIDE DISMUTASE-LIKE AGENTS

Veronika Lutsenko[1], Daria Grigorieva[1], Irina Gorudko[1], Alexey Sokolov[2,3,4]

[1] Department of Physics, Belarusian State University, Belarus
[2] Department of Molecular Genetics, Research Institute of Experimental Medicine, Saint-Petersburg, Russia
[3] Department of Biophysics, Research Institute of Physico-Chemical Medicine, Moscow, Russia
[4] Department of Fundamental Problems of Medicine and Medical Technology, Saint-Petersburg State University, Saint-Petersburg, Russia
nika.lutsenko@tut.by

One of the most relevant areas in medical biophysics is screening of compounds capable to correct the development of oxidative/halogenative stress that accompanies many significant diseases. An important source of reactive oxygen species (ROS) and halogens (RHS), initiating the development of oxidative/halogenative stress, are neutrophils – the most abundant leukocytes in the blood which are constitute the first line of host defense against numerous infectious pathogens [1]. ROS have a crucial role in human physiological and pathophysiological processes. However, prolonged exposure to high ROS concentrations may lead to diseases (e.g., cardiovascular and neurodegenerative diseases), for which screening of selective antioxidant drags is required [2].

In the field of antioxidant therapeutics, ongoing researches are conducted to better understand the mechanism of action of known antioxidant agents and to design and test novel therapeutic agents [3]. So, problem of searching for specific and sensitive probes for ROS detection is being actively studied. Recently the fluorescence method of measuring the kinetics of superoxide ($^{\bullet}O_2^-$) production by monitoring of the gallocyanine – C.I.51030 (GC) dye bleaching, which is accompanied by an increase in the fluorescence intensity of the dye solution in cell suspensions has been proposed [4]. Using this method, the effect of well-known agents, such as superoxide dismutase (SOD), ceruloplasmin (CP), cysteine (Cys), N-acetylcysteine (NAC), taurine (Tau) and acetaminophen (APAP) on $^{\bullet}O_2^-$ neutrophil production has been tested.

Sodium citrate, phorbol 12-myristate 13-acetate (PMA), GC, SOD, CP, Tau, Cys, NAC, APAP were obtained from "Sigma", USA; dextran T70 – from "Roth", Germany; histopaque – from "Nycomed", Norway; others – from "Reachem", Russia and "Belmedpreparaty", Belarus. Neutrophils were isolated from venous blood of healthy donors as described elsewhere [5]. Cells were suspended in a phosphate buffered saline (PBS) containing 10 mM $Na_2HPO_4/KH_2PO_4$, 137 mM NaCl, 2.7 mM KCl, 0.9 mM $CaCl_2$, 0.5 mM $MgCl_2$, 5 mM D-glucose (pH 7.4) and stored at 4 ºC. Fluorescent characteristics of GC (5 μM in PBS) bleaching were registered on a spectrofluorimeter CM 2203 "Solar" (Minsk, Belarus), $\lambda_{ex.}$=360 nm, $\lambda_{em.}$=490 nm. Oxidation rate ($v$), defined as the slope of the initial linear portion of the fluorescence intensity curve, and reaction amplitude ($h$), defined as changes in fluorescence intensity of the solution compared to the background level at 7 min, were used to describe this process.

Data obtained in the study of SOD, CP, Tau, Cys, NAC, APAP effect on the fluorescent properties changes of GC in suspensions of 50 nM PMA-activated neutrophils ($1\times10^6$ cells/ml) are given in the table 1.

Table 1. Anti-inflammatory effects of test substances (% of the PMA effect, *$p < 0.05$ compared to PMA effect).

| | Control | SOD, 50 mg/l | CP, 150 mg/l | Tau, 3.2 mM | Cys, 3.3 mM | NAC, 500 μM | APAP, 100 nM |
|---|---|---|---|---|---|---|---|
| $v$, % | 100 | 10±7* | 11±10* | 105±15 | 19±18* | 60±3* | 101±13 |
| $h$, % | 100 | 15±10* | 40±25 | 104±17 | 44±32 | 62±9* | 96±22 |

The results presented in table 1 indicate that SOD and CP, which has superoxide dismutase-like activity, inhibit the production of $^{\bullet}O_2^-$ compared to the control (PMA only). Tau, a hypochlorite interceptor, did not affect the changes in the fluorescence parameters of the solution. Cys and NAC containing sulfhydryl groups are quite good scavengers for ROS, as can be seen from table 1. It is known that APAP has antipyretic (cyclooxygenase-3 and myeloperoxidase inhibitor), but not anti-inflammatory effect [6], which is also confirmed by our research (see table 1). Given together, the data obtained in the study has been showed that GC is a promising dye for screening SOD-like activity of drugs and for better understanding the mechanism of their action. This study was supported by Russian Foundation for Basic Research (18-515-00004) and Belarusian Republican Foundation for Fundamental Research (B18R-058).

[1] C. Rosales, N. Demaurex, C. A. Lowell et al., Neutrophils: Their Role in Innate and Adaptive Immunity, Journal of Immunology Research **2016**, 1-2 (2016).
[2] K. Brieger, S. Schiavone, F. J. Miller et al., Reactive oxygen species: from health to disease, Swiss medical weekly **142**, w13659 (2012).
[3] A. A. Alfadda, R. M. Sallam, Reactive oxygen species in health and disease, Journal of Biomedicine and Biotechnology **2012**, 1-14 (2012).
[4] V. E. Lutsenko, D. V. Grigorieva, S. N. Cherenkevich et al., Fluorescent method for estiment neutrophils functional activity, Russian journal of biological physics and chemistry **3** (3), 612-618 (2018).
[5] I. V. Gorudko, A. V. Mukhortava, B. Caraher et al., Lectin-induced activation of plasma membrane NADPH oxidase in cholesterol-depleted human neutrophils, Archives of biochemistry and biophysics, **516**, 173-181 (2011).
[6] M. H. Pillinger, C. Capodici, P. Rosenthal et al., Modes of action of aspirin-like drugs: salicylates inhibit erk activation and integrin-dependent neutrophil adhesion, Proceedings of the National Academy of Sciences, **95** (24), 14540-14545 (1998).

# FEMTOSECOND LASER 3D MICROFABRICATION OF ELASTOMERIC RESIN

Giedrė Grigalevičiūtė[1], Linas Jonušauskas[1,2], Mangirdas Malinauskas[1]

[1] Laser Research Center, Faculty of Physics, Vilnius University, Lithuania
[2] Femtika Ltd., Vilnius, Lithuania
giedre.grigaleviciute@gmail.com

The polymerization initiated by light is already successfully used and applied in such areas as laboratories research as well as industry. The main idea of 3D direct laser writing is simple and rapid way to fabricate 3D solid polymeric objects out of liquid prepolymer, consisting monomers, oligomers and photoinitiators. Employing femtosecond laser lithography true 3D, with intricate internal geometry, micro- or nano-scaled structures in high quality can be manufactured [1]. The applications of photopolymerization are shown in such fields as medicine, micro- and fiber optics, photonics, micro-mechanics. [2]

Despite the fact, that 3D laser lithography can be used as a versatile tool, there is a lack of elastomeric photosensitive materials that could be polymerized for specific applications. In this work femtosecond laser lithography experiments were performed with elastomeric resin UV-PDMS (manufacturer *ShinEtsu Japan*). During the experiments the goal was to determine the optimal parameters for the micro-fabrication of the aforementioned material. The 3D structures shown in the Figure 1 were fabricated with varied parameters and dosages by the change of laser beam average power, scanning (velocity, number and direction). The optimal parameters for achievements of quality results were while using the objective of 63x magnification and 1.4 numerical aperture, the power from 0.4 mW to 0.6 mW and the fabrication velocity up to 3000 μm/s. Also there was noticed, that the scanning in different directions (opposite and the same) results in different symmetry of the fabricated object (Fig. 2). This can be explained by the diffusion of generated radicals and heat [3].

Based on the optimized fabrication parameters, the sample microporous 3D scaffold structures for cell growth will be presented validating the applicability of the chosen material and fabrication technology.

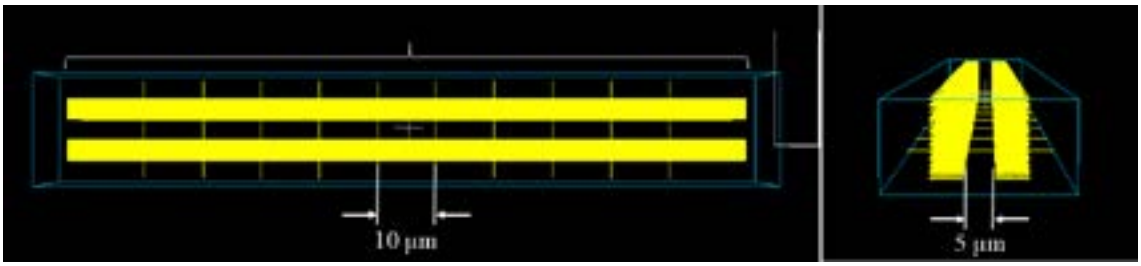


Fig. 1. The CAD model of fabricated structures during the experiment, on the left: the view from the top; on the right – the view from the side.

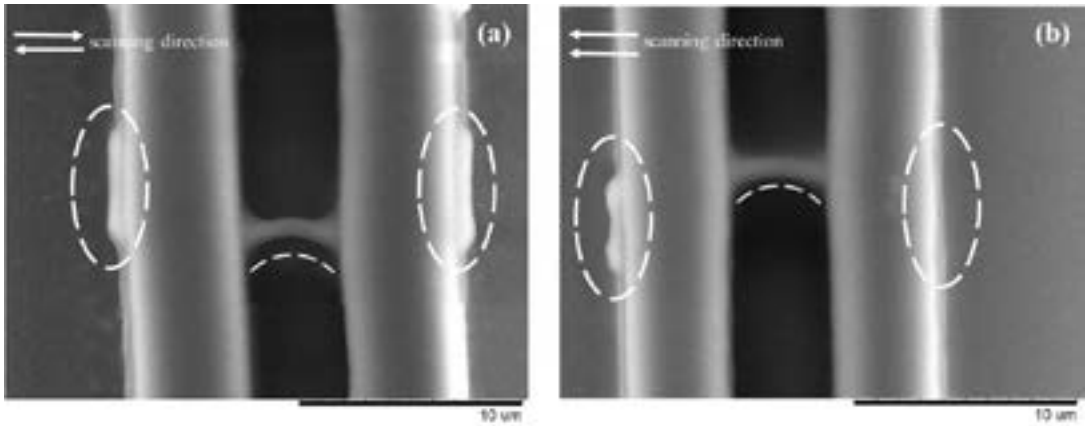


Fig. 2. The structures fabricated of UV-PDMS elastomer in different conditions: (a) the scanning directions are opposite, (b) the scanning directions are the same.

[1] M. Malinauskas et al, Ultrafast laser processing of materials: from science to industry, Light. Sci. Appl. **5**(e16133) (2016).
[2] A. Ovsianikov et al, Photonic and Biomedical Applications of the Two-Photon Polymerization Technique, Stereolithography Materials, Processes and Applications, 257-299, Springer, New York (2011).
[3] Y. Li et al, Uniform suspended nanorods fabricated by bididirectional scanning via two-photon photopolymerization, Nanotechnology **19** 375304 (2008).

# MAGNETIC NANOPARTICLES DECORATED WITH GOLD NANOCLUSTERS – NEW THERANOSTIC NANOPLATFORM

Marijus Pleckaitis[1], Vitalijus Karabanovas[1,2], Greta Jarockyte[1], Agne Mikalauskaite[3], Arunas Jagminas[3], Ricardas Rotomskis[1,4]

[1]Biomedical Physics Laboratory, National Cancer Institute, Vilnius, Lithuania
[2]Department of Chemistry and Bioengineering, Vilnius Gediminas Technical University, Vilnius, Lithuania
[3]State Research Institute Centre for Physical Sciences and Technology, Vilnius, Lithuania
[4]Biophotonics group of Laser Research Center, Faculty of Physics, Vilnius University, Vilnius, Lithuania
marijus.pleckaitis@nvi.lt

Efficient nanoprobes for multimodal bioimaging and therapeutic applications are in high demand. Therefore, nanomaterials exhibiting both magnetic and optical properties have been in the spotlight because of high potential for promising biomedical applications. In our study, we show that magnetic nanoparticles decorated with gold nanoclusters have a high applicability promise in the fields that are in need for multifunctional nanoprobes, e.g. for cancer diagnostics and therapy (theranostics). To evaluate the implementation possibilities of such multimodal nanoplatforms, we performed a variety of experiments assessing photophysical, photochemical characteristics and *in vitro* biocompatibility of magnetic nanoparticles decorated with gold nanoclusters. The experiments proved nanoparticles to have good optical properties and colloidal stability in various solutions (distilled water, PBS, cells growing media). Moreover, this nanoplatform demonstrated the reversible photoquenching effect – the ability to restore photoluminescence in the dark after irradiation with various wavelengths that induced photoquenching effect. During before mentioned process, additionally we noticed the formation of photoproducts. Further experimentations showed the generation of singlet oxygen species. Biodistribution of magnetic nanoparticles decorated with gold nanoclusters was evaluated at subcellular level using confocal laser scanning microscope. After assessing uptake dynamics of nanoparticles we performed cell viability assays with different cell lines and showed that at tested concentrations (from 0.25 to 2.5 mg/ml) nanoparticles had no cytotoxic effects. Therefore, the results of this study highlight the promising potential of magnetic nanoparticles decorated with gold nanoclusters for future bimodal bioimaging and cancer therapy purposes.

# THE EFFECT OF EXOGENOUS ORGANIC SUBSTANCES ON SPIRULINA GROWTH

Kotynskiy Andriy[1], Salyuk Anatoliy[1], Tobilko Volodymyr[1], Shapovalov Yevgen[1]

Faculty of Biotechnology and Environmental Control, National University of Food Technologies, Ukraine
moinbergofficial@gmail.com

When exogenous organic substances are added in the light, the growth of blue-green algae greatly improves as a result of the transition from photoautotrophic to photoheterotrophic cultivation regime [1-3]. Accordingly, it can lead to a change in the pigment composition of microalgae. Therefore, it is advisable to carry out investigations to determine the effect of various concentrations of organic carbon sources on the increased productivity of the culture by biomass and pigments.

The influence of various concentrations of exogenous organic carbon sources on the productivity of the culture of cyanobacterium Spirulina platensis and its photosynthetic activity has been determined. The culture of cyanobacterium *Spirulina platensis (Gom.) Geitl*, culture LSU-603, taken from the collection of cultures of the M.G. Kholodny Institute of Botany, NAS of Ukraine, has been used for the research

The cultivation process was carried out in the nutritional medium Zaruka in a vertical tubular plant with diameter of 8 cm and volume of 2 $dm^3$, the culture medium was constantly stirred by air. The illumination of the culture on the surface of the plant was maintained at the level of 8 klx, the duration of the photoperiod was 12 hours per day. The temperature of the culture medium was maintained in the range from 30 to 32 ° C.

The growth of biomass was determined by photometric method by change in the optical density of the suspension at a wavelength of 750 nm. The conversion of units of optical density into dry biomass was carried out according to the calibration graph. The choice of samples for determination of culture was carried out every day when the light was switched off, after the dark phase of cultivation.

In the process of the research, absolutely dry biomass (ADB) and moisture content of the product were determined by the weight method, the mass fraction of protein in the biomass of spirulina - by the biuret reaction, the content of phycocyanin and chlorophyll - by spectrophotometric methods.

The dependency of the influence of exogenous organic substances on the growth of culture and the biosynthesis of phycocyanin, chlorophyll and carotenoids in the biomass of spirulina has been established. The optimum ratios of concentrations of sodium acetate, saccharose, succinate and glycine (when maximum accumulation of pigments in spirulina biomass and maximum culture productivity is observed) have been also determined.

It has been found out that the highest productivity of a culture by biomass, the yield of phycocyanin and chlorophyll can be obtained using succinate in a concentration of 0.03%. At the same time there is an increase in the productivity of the culture by biomass by 25%, the yield of phycocyanin - by 46%, and chlorophyll - by 34%, compared with the photoautotrophic cultivation regime without the addition of succinate.

It has been determined that the addition of sodium acetate to the culture medium at a concentration of 0.02% leads to an increase in the yield of carotenes by 54% compared with autotrophic cultivation regime without adding sodium acetate.

An increase in the concentration of saccharose by more than 0.02% leads to the rapid death of most of the spirulina culture, due to its inhibition by a foreign microflora and the occurrence of fermentation processes.

The study showed that the use of glycine at concentrations greater than 0.01% during the first five days of cultivation leads to inhibition of the culture growth due to the destruction of trichomes of microalgae. However, further cultivation leads to a significant increase in the productivity of culture (more than twice) compared with the control.

It has been determined that spirulina is able to use such exogenous sources of organic carbon as succinate, saccharose, sodium acetate, glycine for the intensification of biosynthesis processes and, thus, can switch from photoautotrophic to photoheterotrophic cultivation.

The obtained results can be used to increase the productivity of the culture by biomass and phycocyanin.

---

[1] *Marquez Facundo J., Nishio Naomichi, Nagai Shiro* Enhancement of biomass and pigment production during growth of *Spirulina platensis* in mixotriphic culture. *J. Chem. Technol. and Biotechnol*. 1995, 62 (2), P. 159–164.

[2] *Скороход Т.Ф., Тупик Н.Д., Черня В.Ф.* Зависимость липидного состава *Spirulina platensis (Nordst.) Geitl.* от способа энергетического существования культуры. От фотоавтотрофии к фотогетеротрофии. *Альгология*. 1996, 6 (2), С. 133–141.

[3] Шнюкова Є.І. Фотоорганотрофний і гетеротрофний ріст гормогонієвих синьозелених водоростей. *Укр. бот. журн*. 1984, №4, т.41, С.49-54.

# CAN MACROPHYTES FROM THE BALTIC SEA BE A NEW SOURCE OF NOVEL ANTIBACTERIAL COMPOUNDS?

Marlena Szeligowska, Ilona Złoch, Anna Toruńska-Sitarz

Department of Oceanography and Geography, University of Gdańsk, Poland
marlenaszeligowska@gmail.com

Marine organisms are a rich and still unexplored source of compounds with novel molecular structures and activities. In recent years many secondary metabolites from macrophytes were shown to possess different bioactivities such as antimicrobial, antiviral and antifungal [1] and thus they are promising agents for drug discovery and development. Some of the marine-derived compounds are either in preclinical or clinical trials [2].

Currently, emergence of microbial resistance to antibiotics has become a global problem and macrophytes might be a potential source of new therapeutics. Some promising results have already been obtained for organisms collected in tropical and subtropical ecosystems. However, there is still no information about the antibacterial activity of the macrophytes form the Baltic Sea. The aim of our work was to screen crude extracts from the Baltic macrophytes against antibiotic-resistant strains of Gram-positive and Gram-negative bacteria. Individuals from *Chara*, *Cladophora*, *Myriophyllum* and *Ulva* genera were collected in the Puck Bay (Gulf of Gdańsk). In order to extract a wide range of metabolites different solvents were used: 90% ethanol, water and isopropanol/hexane (1:1). Agar disc diffusion method was applied in search for antibacterial activity of the obtained crude extracts.

[1] R. De Felício, S. De Albuquerque, M. C. M. Young, et al., Trypanocidal, leishmanicidal and antifungal potential from marine red alga Bostrychia tenella J. Agardh (Rhodomelaceae, Ceramiales), Journal of Pharmaceutical and Biomedical Analysis, **52**, 763–769 (2010).

[2] D. J. Newman, M. C. Gordon, Marine natural products and related compounds in clinical and advanced preclinical trials, Journal of natural products **67**, 1216-1238, (2004).

# UV RADIATION INDUCED SYNTHESIS OF SILVER NANOPARTICLES IN BIOGEL

Matas Damonskis[1], Judita Puišo[1]

[1] Department of Physics, Kaunas University of Technology, Lithuania
matas.damonskis@ktu.edu

Silver nanoparticles (AgNPs) have remarkable antimicrobial and localized surface plasmon resonance (LSPR) properties. These AgNPs properties are reported to be dependent on the size, shape and surrounding medium. The unique properties of NPs opened broad prospects for the applications in various fields including medicine and biology [1-2]. Despite AgNPs inhibitory behavior towards few hundred species of microbes, including antibiotic resistant bacterials, AgNPs also have gained interest in gel dosimetry to enhance the dose deposited in the tumor while using low radiation as well as for better imaging purposes [3].

Most commonly used method for synthesis of silver nanoparticles is the chemical reduction of silver salts in aqueous medium (Lee-Meisel method). In certain areas of application, such as medicine, there is a need of pure AgNPs without any toxic byproducts and impurities. In such cases, mostly chemical and physical methods of AgNPs synthesis are not suitable. Then AgNPs could be produced by using irradiation of electromagnetic radiation (UV, X-ray etc.). Such techniques have several advantages over convention chemical methods, such as: i) reduction of silver ions can be carried out without excessive reducing agents or producing undesired byproducts of the reductant; ii) reducing agent is uniformly distributed in the solution; iii) radiation-induced reduction is done at ambient temperature [1-3].

In this study AgNPs in 10% gelatin medium were synthesized by UV irradiation. As silver precursor has been used silver nitrate, which concentration varied up to considerably high – 50 mM.

All materials used for AgNP synthesis were analytical grade and was used as received without any further purification. Silver nitrate ($AgNO_3$) (Sigma Aldrich, Poland, CAS No 7761-88-8), gelatin (Sigma Aldrich, Poland, CAS No. 9000-70-8) and sodium citrate dehydrate ($C_5H_5Na_3O_7 \cdot H_2O$) (Sigma Aldrich Reachem, Slovakia s.r.o., CAS No. 68-04-02) were used as silver precursor, main stabilizator, secondary stabilizator and reducing agent, respectively. There was prepared 6 samples, silver nitrate concentration varied from 1 mM to 50 mM, gelatin medium concentration was 10 %. Prepared samples were irradiated 60 min by UV light source (365 nm, 36 W for polymer gel curing). To eliminate the deep UV irradiation samples (<320 nm) were stored in the transparent 20 ml glass bottle. AgNPs formation, growth, and stability were analyzed by measuring UV-Vis spectrum. Spectra were measured by Ocean Optics USB4000 spectrometer at the range of 300-800 nm. AgNPs size was evaluated theoretically by applying Mie theory calculations (computer program MiePlot v4.6) [4].

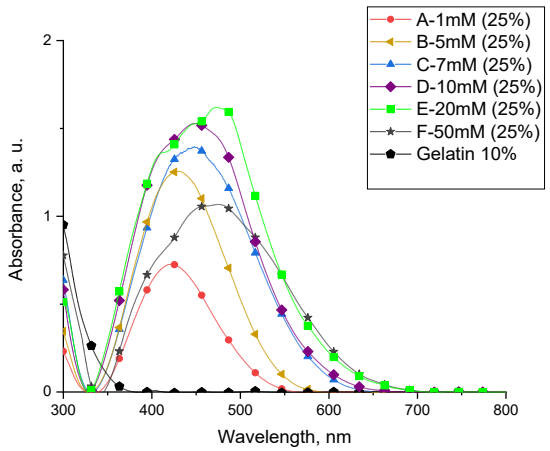


Fig. 1. UV-Vis spectra of samples

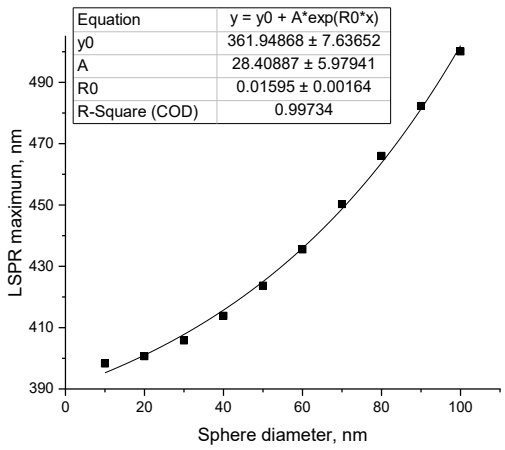


Fig. 1. LSPR maximum for extinction versus Ag nanosphere diameter

Colour of prepared silver nanoparticles solution varied from yellow to darkish brown. Synthesized samples showed very high absorption and in order to obtain visible spectrum of the LSPR samples were diluted to 25 % (fig. 1). It was measured that as silver nitrate concentration increases, peak location of the LSPR shifts towards red from 422,4 to 475,0 nm, while peak FWHM increases from 101,2 to 178,4 nm, peak height varies from 0,73 to 1,63 a. u. According to Mie calculations results, synthesized AgNPs size varied from 47,4 nm to 86,6 nm (fig. 2).

[1] PULIT-PROCIAK, Jolanta and Marcin BANACH. Silver nanoparticles – a material the future...? Open Chem 2016, 14(1), 76-91. https://doi.org/10.1515/chem-2016-0005 [Accessed 30 Jan. 2019].

[2] NATSUKI, Jun, Toshiaki NATSUKI and Yoshio HASHIMOTO. A Review of Silver Nanoparticles: Synthesis Methods, Properties and Applications. International Journal of Materials Science and Applications 2015, 4(5), 325-332. https://doi.org/10.11648/j.ijmsa.20150405.17 [Accessed 30 Jan. 2019].

[3] TITUS, D. et al. Current scenario of biomedical aspect of metal-based nanoparticles on gel dosimetry. Applied Microbiology and Biotechnology 2016. Vol. 100, no. 11, p. 4803–4816. https://doi.org/10.1007/s00253-016-7489-5 [Accessed 30 Jan. 2019].

[4] MiePlot. http://philiplaven.com/mieplot.htm [Accessed 30 Jan. 2019].

# CHANGES IN THE FUNCTIONAL STATE OF GLIOMA CELLS UNDER THE INFLUE NCE OF ETHANOL AND MELDONIUM

Elizaveta Kharkovskaya, Konstantin Kulagin

Department of biological chemistry, Smolensk State Medical University, Russia
adm@smolgmu.ru

Introduction:

Gliomas are one of the most malignant neoplasms in the human body.[1] Today there are several hypotheses of glial cell proliferation and glioma formation. One of the main is the theory that neuronal stem cells, which were under strict control, lost it,as a result the process of malignancy begin.

The danger of gliomas is due to the difficulty of their therapy, both medical and surgical. In this regard, a large number of scientific groups are focused on finding new ways and drug compounds that will allow targeted destruction of glioma cells without surgery.

Taking into account the presence of the blood-brain barrier among the considered drug candidates, the compounds whose chemical properties will allow to penetrate this barrier without hindrance have the greatest potential

The aim of our study was to study the effect of a number of BBB-permeable compounds on some metabolic characteristics of glioma cells.

At first, human glioma lines[2] were cultured in DMEM during the day, then Meldonium[3] was added at a concentration of 1 μg / ml and incubated for 24 hours (37°C, 5% CO2). To another group of glioma cells, ethyl alcohol was added at a concentration of 10% and also incubated for 24 hours with the same conditions

Mitochondrial membrane potential was detected by laser scanning confocal microscope. To do this, the mitochondria in cells stained with tetramethylrhodamine at a concentration of 40 nM incubated for 40 minutes (37°C, 5% CO2). TMRM-accumulated in mitochondria depending on their membrane potential and was excited at a wavelength of 543 nm, the potential was recorded at a wavelength in the range of 560 – 570 nm. On each Petri dish with the inhibitor substance (Meldonium) 5 zones with the brightest fluorescence were found. Then, using the Z-stacks method on the laser scanning confocal microscope LSM 780 (Carl ZEISS)[4], total fluorescence from mitochondrial membranes was obtained from these cells and the state of membrane potential was assessed. Statistical processing of the results was carried out by the method of non-parametric statistics with the calculation of the Mann-Whitney criterion.

Results:

Glioma cells after the addition of Mildronate increased mitochondrial membrane potential by approximately 5-10% without a statistically significant difference. When alcohol was added, the ethyl potential on the membrane decreased by 60% (statistically significant).

[1] Louis D. N. et al. The 2016 World Health organization classification of tumors of the central nervous system: a summary //Acta neuropathologica. - 2016. - Vol. 131. - no. 6. - P. 803-820

[2]Grobben b, De Deyn P., Slegers H. Rat C6 glioma as experimental model system for the study of glioblastoma growth and invasion //Cell and tissue research. - 2002. - Vol. 310. - no. 3. - P. 257-270.

[3]Dambrova M., Liepinsh E., Kalvinsh I. Mildronate: cardioprotective action through carnitine-lowering effect //Trends in cardiovascular medicine. - 2002. - Vol. 12. - no. 6. - P. 275-279 (мельдоний)

[4]Svishchev, G. M. Confocal microscopy and live cell ultramicroscopy //M.: Fizmatlit. - 2011.

# THE PLANAR ELECTRODES ELECTRIC FIELD DISTRIBUTION AND DIELECTROPHORESIS FORCE STUDY USING FINITE ELEMENT METHOD

Paulius Butkus[1], Sonata Tolvaišienė[1]

[1] Department of Electrical Engineering, Faculty of Electronics, Vilnius Gediminas technical university, Vilnius, Lithuania
paulius.butkus@vgtu.lt

The microfluidics-based electroporation technique is rapidly developing [1]. This technique is advanced with its unique characteristics of miniaturization and integration, but it is still difficult to study fast, nanoscale pore formation dynamics using real-time fluorescent microscopy. In order to perform such experiments, the electrode structures, which are capable of trapping cells with the usage of dielectrophoretic forces is required. Dielectrophoresis (DEP) is the phenomenon described by Pohl [2] as the creation of forces on neutral, but polarizable particles when they are exposed to nonuniform electric fields.

The DEP force is specified via an electric potential or the electric field and depends on the electric field gradient frequency and particle property. Under the proper geometry and electrical parameters set-up, the DEP force can be used for trapping single particles between electrodes, which would allow to observe electroporation phenomena dynamics using real-time fluorescent microscopy.

In this work we study the configuration of planar electrodes and electric field distribution using finite element method (FEM) analysis (see Fig. 1). It is aimed to determine the proper electric field distribution for the effective DEP force application. A multiparametric investigation of the four electrodes topology is performed in COMSOL Multiphysics environment to define the configuration of electrodes and electric field distribution, which would ensure a proper DEP force exposure on the selected cells for the research.

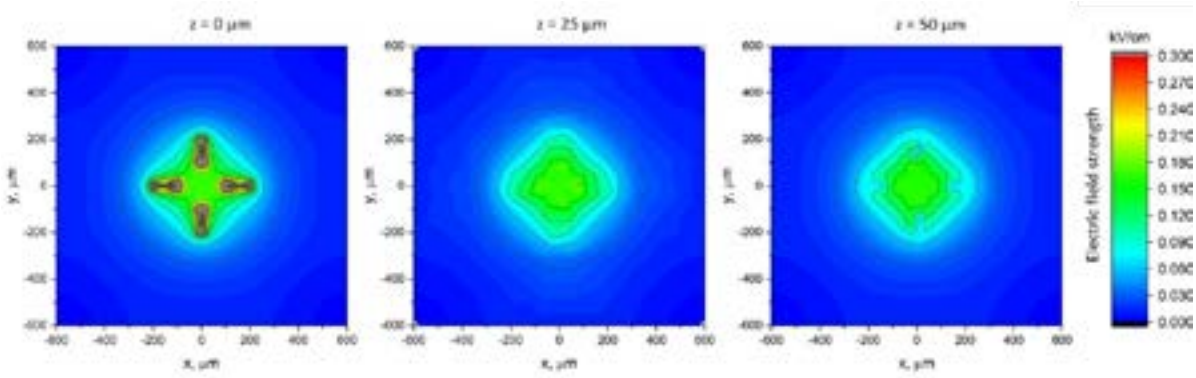


Fig. 1. Electric field distribution of two planar electrodes pairs in XY plane under different height from the electrodes.

The generated electric field intensity and homogeneity dependency on the electrodes configuration is evaluated and the optimal configuration is proposed, which would be further used to study the effectiveness of DEP force application in the real-time electroporation investigation.

[1] T. Geng and C. Lu, "Microfluidic electroporation for cellular analysis and delivery," Lab Chip, vol. 13, no. 19, pp. 3803–3821, 2013.
[2] H. A. Pohl, Dielectrophoresis. Cambridge, U.K.: Cambridge University Press, 1978.

# DESIGN OF A MICROFLUIDIC CHIPS WITH A DETERMINED CONFIGURATION OF THE MICROFLUIDIC NETWORKS

Alexandra Litvinova[1], Maxim Silkin[1], Vladislav Fomin[1], Alexey Shanturov[1], Andrey Demidov[1], Viktor Zhilkin[1], Vladimir Glotov[1]

[1]Department of Human Anatomy, Smolensk State Medical University, Russia
anatom@smolgmu.ru

**Introduction.** Modeling of hydrodynamic parameters of blood microflow and their distribution in real microvascular networks is one of the main tasks of Biomicrofluidics. It can be solved in experiments on artificial microfluidic (microvascular) networks. Model microfluidic chips (MMCs) were developed in our study and their suitability to be used in experimental platforms designed for the cultivation of self-developing functioning endothelial networks in vitro was evaluated.

The aim of the study was to develop a line of technological procedures for creation of simulation MMCs, suitable for further work as a part of the experimental platform to control and automation data processing of microcirculation modeling.

**Material and methods**. The study was carried out with the interaction of biotechnologists and engineering specialists in modern production. It made possible to produce variants of experimental samples of MMC directly in the course of the study and testing as a part of the experimental platform to control, automated analysis, evaluation and processing of microcirculation data and their completion. We designed biotechnical requirements for the structure of the MMCs. An electronic model was developed in the SolidWorks computer-aided design environment. The model was used for loading into one of the types of processing complexes with software control.

**Results.** The first technology (procedure) involved manufacturing topology with a milling cutter diameter 0.1-0.5 mm to a depth of 0.01-0.5 mm on a substrate of plasticized organic glass. The study was performed on precision automated processing centers "HAAS". Then the same solid organic glass was put on the substrate and the ports of the working fluid were formed.

The second technology (procedure) involved matrix topology MMCs with a method of laser cutting on the fiber machine of laser cutting ML-35 made of stainless steel 12X18H10T of thickness 0.01-0.5 mm. Then the matrix was placed on the flat surface of the cuvette and was filled with neutral silicone compound. After solidification of the compound, the silicone substrate with the printed topology was closed with solid organic glass and ports were formed.

The third technology (procedure) involved application of topology directly on the surface of organic glass on a laser plotter with an organic laser. The substrate was stacked with solid organic glass and ports working fluid were formed.

Each of the technologies has its own characteristics, which allow making the best choice for specific tasks.

Pilot control units of the generator of micro nutrient medium (micropump) using the microcontroller Arduino Due based on the processor Atmel SAM3X8E ARM Cortex-M3 based 32-bit microprocessor ARM core were designed using the demonstration microcomputer STM32F469N1 with micro-computer Raspberry Pi 3 Model B. Proper software was developed for each unit [1].

**Conclusion.** MMCs formed with any of the above mentioned technologies (procedures) have a unified port of the working fluid, installation dimensions and a transparent top. It allows them being installed in an experimental platform for control and automation of microcirculation modeling data processing. Flow of fluid is created with micropumps, working on gravitational, electromagnetic and micropulsation principles, and regulated with valve platform through software. Observation, analysis and registration of the experiment are carried out with an electronic USB microscope and a computer with software. Measurements and registration of primary parameters are performed: flow rate, volume and temperature of various working fluids. The software calculates and analyzes hemodynamic factors of microcirculation and structural parameters of artificial microfluidic (microvascular) networks, which ultimately allow forming the structure of the MMCs as much as possible corresponding to the required parameters of the initial biological object and studying its functioning under different microcirculation modes [2].

[1] Демидов А. Л., Жилкин В. В. Экспериментальная исследовательская платформа для управления и автоматизации обработки данных моделирования микроциркуляций // Смоленский медицинский альманах.– 2018. - №1. – С. 85-87.

[2] Глотов В. А. Структурный анализ микрососудистых бифуркаций (Микрососудистый узел и гемодинамический фактор). - Смоленск: Амипресс, 1995. – 255 с.

# ENZYMATIC SYNTHESIS OF NOVEL INDIGOID PIGMENTS

Roberta Statkevičiūtė*, Mikas Sadauskas, Justas Vaitekūnas, Renata Gasparavičiūtė, Rolandas Meškys

Department of Molecular Microbiology and Biotechnology, Institute of Biochemistry, Life Sciences Center, Vilnius University, Lithuania
*roberta.statkeviciute@gf.stud.vu.lt

Indigo is one of the oldest pigments used in the dyeing industry. With the rise of modern sciences, we gained the ability to modify the indigo molecule and create new pigments with novel applications, based on special semiconductor properties [1-3]. Compared to silicon semiconductors, indigoid pigments have the advantage of being biodegradable and also very stable when exposed to air and water [4]. In order to overcome the hazardous effects of chemical indigo modifications, enzymatic synthesis was used to obtain novel variants of indigo [5,6]. Nevertheless, the selection of indigoids with desirable chemical modifications is still insufficient.

Here, a set of new indigoid pigments synthesized by employing bacterial enzymes is presented. Screening of metagenomic libraries for indole-oxidizing activities revealed several oxygenase enzymes, capable of oxidizing indole derivatives to corresponding indigo derivatives. In total, seven different oxygenases capable of performing oxidation of 24 different indole derivatives to corresponding indigoid pigments were characterized. Indigoids synthesized by these enzymes were the following: different regioisomers of indigo dimethanol and indigo dicarboxaldehyde, 5,5'-diaminoindigo, 5,5'-di(aminoethyl)indigo, 5,5'-difluoroindigo, 5,5'-dihydroxyindigo, indigo-5,5'-dicarbonitrile, indigo-5,5'-dicarboxamide, 5,5'-dibrom-7,7'-diiodoindigo, 5,5'-dichloro-7,7'-diiodoindigo, 7,7'-dibromoindigo, 7,7'-diiodoindigo, 7,7'-dimethylindigo and 7,7'-dinitroindigo. Most of these pigments demonstrated different colors (Fig. 1) and different visible spectra absorbance patterns. Moreover, some indigoids, including indigo dimethanols and indigo-5,5'-dicarbonitrile, were produced without the formation of indirubin isomeric form.

To our knowledge, production of some of these pigments has not been reported neither by chemical nor enzymatic methods to date. Due to different spectral properties and additional chemical modifications, these indigoid pigments are potential nanomaterials for novel applications.


Fig. 1. Diversity of indigoid pigments obtained using oxygenases.

[1] K. Ramig, O. Lavinda, D. J. Szalda et al., The nature of thermochromic effects in dyeings with indigo, 6-bromoindigo, and 6,6′-dibromoindigo, components of Tyrian purple, Dyes and Pigments, **117**, 37–48 (2015).
[2] P. Deng, Y. Lei, X. Zheng et al., Polymer based on benzothiadiazole-bridged bis-isoindigo for organic field-effect transistor applications, Dyes and Pigments, **125**, 407–413 (2016).
[3] B.-Y. Ren, Q. Xu, M. Kolaczkowski et al., Bay-annulated indigo derivatives based on a core of spiro[fluorene-9,9′-xanthene]: Synthesis, photophysical, and electrochemical properties, Dyes and Pigments, **160**, 25–27 (2019).
[4] E. D. Glowacki, G. Voss, N. S. Sariciftci. 25th anniversary article: progress in chemistry and applications of functional indigos for organic electronics, Advanced Materials, **47**, 6783–6800 (2013).
[5] Frabel S, Wagner B, Krischke M, Schmidts V, Thiele CM, Staniek A, Warzecha H. Engineering of new-to-nature halogenated indigo precursors in plants. Metabolic Engineering, **46**, 20–27 (2018).
[6] Namgung S, Park HA, Kim J, Lee PG, Kim BG, Yang YH, Choi KY. Ecofriendly one-pot biosynthesis of indigo derivative dyes using CYP102G4 and PrnA halogenase. Dyes and Pigments, **162**, 80–88 (2019).

# THE EFFECTS OF ANTIOXIDANTS ON PULSED ELECTRIC FIELD TREATED YEAST CELLS

Rūta Cibulskaitė[1], Povilas Šimonis[1], Arūnas Stirkė[1]

[1] Laboratory of Bioelectrochemistry, State Research Institute, Center for Physical Sciences and Technology, Sauletekio ave. 3, LT-10257, Vilnius, Lithuania
ruta.cibulskaite@chf.stud.vu.lt

Pulsed electric field (PEF) technology is abiotic treatment usually used for permeabilization of various cells and tissues. Nowadays it is attracting attention as a non-thermal pasteurization method for liquid foods [1]. It is known that PEF is not only capable to induce permeabilization of yeast plasma membrane but also to trigger programmed cell death mechanism [2]. The mechanism by which microorganisms are killed is not validated yet.

High survival rate after PEF is very important for introducing biomolecules into the cell. One of the key components used for detoxification of reactive oxygen species in cells is glutathione system. Our goal was to reduce PEF induced stress response and increase viability of microorganisms by supplementing cells with antioxidants.

First of all, we evaluated effects to yeast cells viability using different electric field strength (E = 4, 5, 6, 8, 10 kV/cm) at the same 150 μs pulse duration. WT (Y10000) and Δgsh1 yeast cell lineages where examined. No significant differences in viability between cells from different strains was observed. Such effects were caused by cultivation in full growth medium which provides glutathione externally. For further experiments we chose 5 kV/cm electric field strength which decreases yeast cell viability by 50 % (Fig. 1).

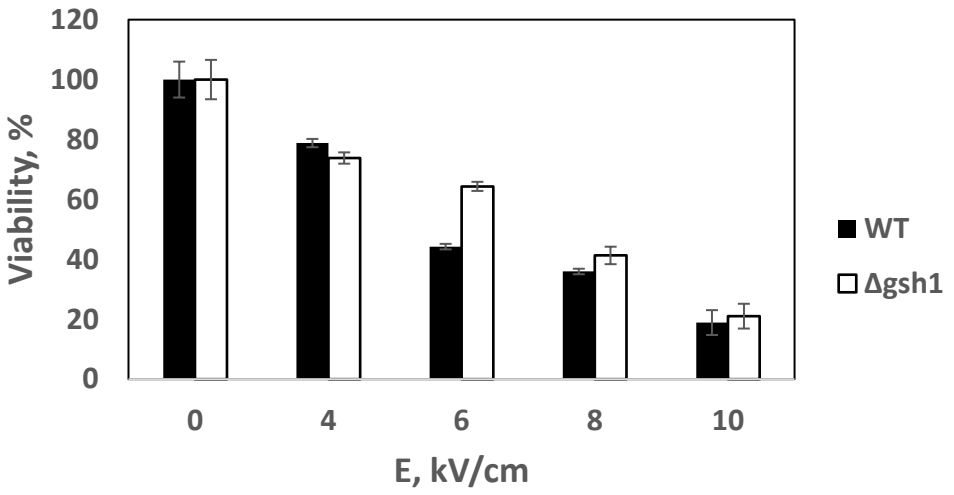


Fig. 1. Yeast cells viability dependence to PEF strength

We further investigated glutathione effects on yeast viability by adding it into solid growth media. Optimal glutathione concentration was 1 mM. WT yeast cells viability was not significant dependent to glutathione concentration. However Δgsh1 cells were more sensitive to external glutathione concentration fluctuations. This cell lineage showed increasing number of colony forming units as the glutathione concentration in solid medium increased. Moreover Δgsh1 cells formed colonies of different sizes. Number of small colonies decreased with raise in glutathione concentration. Decrease in colony size was compensated by adding 5 mM of glutathione in solid media. Worth to mention that smaller colonies did not showed respiratory deficient *petite* phenotype. This suggests that colony size dependence to GSH concentration in solid medium is unannotated phenomenon for Δgsh1 cells lineage.

Furthermore, we conducted experiments which investigated glutathione effects on PEF treated WT yeast cells. Yeast cells where incubated with various concentrations of glutathione before PEF treatment. Also, WT yeast cells were plated on solid minimal medium with different glutathione concentrations. Incubation of WT yeast cells in mediums with glutathione before and after treatment provide no significant effects suggesting that this strain can produce enough of glutathione itself.

We conclude that the viability of yeast decrease with raise in pulsed electric field strength. The roles of antioxidants such as glutathione and vitamin E during exposure to PEF treatment and recovery of cells remain to be investigated.

[1] Jarm T, Kramar P. 1st World Congress on Electroporation and Pulsed Electric Fields in Biology, Medicine and Food & Environmental Technologies: Portorož, Slovenia, September 6 –10, 2015.

[2] P. Simonis, S. Kersulis, V. Stankevich et al., Caspase dependent apoptosis induced in yeast cells by nanosecond pulsed electric fields, Bioelectrochemistry **115**, 19–25 (2017).

# N-TERMINAL DOMAINS OF NEUROCALCIN δ AND HIPPOCALCIN DETERMINE DIFFERENCE IN THEIR $Ca^{2+}$-DEPENDENT SIGNALING

Iryna Bilous[1,3], Alexander Dovgan[3], Jeffrey Viviano[2], Jingyi Zhang[2], Venkat Venkataraman[2], Pavel Belan[1,3]

[1] Kiev Academic University, Kyiv, Ukraine;
[2] Department of Cell Biology, Graduate School of Biomedical Sciences,
Rowan University School of Osteopathic Medicine, Stratford, NJ 08084, USA;
[3] Department of Molecular Biophysics, Bogomoletz Institute of Physiology, Kyiv, Ukraine;
dermenji48@gmail.com

Hippocalcin (HPCA) and Neurocalcin δ (NCALD) are the members of neuronal $Ca^{2+}$-sensor (NCS) protein family. In spite of minor distinctions in AA sequence between HPCA and NCALD, these proteins demonstrate a substantial difference in their $Ca^{2+}$-sensitivity and kinetic of translocation to the plasma membrane. Both proteins contain myristoilated N-terminal region responsible for interaction with cellular membrane and 3 EF-hand domains responsible for binding of $Ca^{2+}$. Here we compared translocation of wild type NCALD with NCALD-HPCA chimera protein, NCHC, consisting of the first N-terminal region of NCALD and three other domains from HPCA (three $Ca^{2+}$-binding EF-hands). We suggested that NCHC translocation to the plasma membrane would tend to be HPCA-like if cytosolic $Ca^{2+}$ affinity is important for protein signaling, and NCALD-like if stabilization of $Ca^{2+}$-bound form on the membrane plays a crucial role. NCALD and NCHC tagged by different fluorescent proteins were co-expressed in cultured rat hippocampal neurons. Protein translocation to the plasma membrane was induced by membrane depolarization resulting in fast $[Ca^{2+}]_i$ transients and was assayed by fluorescent measurements in dendrites of hippocampal neurons. We have demonstrated that NCALD and NCHC had very similar translocation kinetics and $Ca^{2+}$-sensitivity, whereas NCALD and HPCA had substantial difference in these biophysical parameters. We conclude that the difference in signaling between NCALD and HPCA may be attributed to the distinctions of their N-terminal domains.

# THE EVALUATION OF RELATIVE ROS GENERATION IN MEDIA AND CELLS TRIGGERED BY SCATTERED DOSE AFTER X-RAY IRRADIATION

Tadas Didvalis[1,2], Paulius Ruzgys[1], Saulius Šatkauskas[1], Diana Adlienė[3], Saulius Mickevičius[1]

[1]Vytautas Magnus University, K. Donelaičio 58, LT-44248, Kaunas, Lithuania
[2]Hospital of Lithuanian University of Health Sciences Kauno klinikos,Eivenių 2, LT-50161, Kaunas, Lithuania
[3]Kaunas University of Technology, K. Donelaičio 73, LT-44249, Kaunas, Lithuania
tadas.didvalis@fc.vdu.lt

Radiotherapy is conventional type of cancer treatment. However, a fundamental research on ionising radiation application to cells and tissues is still in need.. The rise of complex and multi-field radiotherapy techniques, such as IMRT, VMAT and SRS usage in patient treatment, suggests that the evaluation of low doses impact for healthy and malignant tissue is in need[1]. In this study we present a simulation of scattered radiation doses, and experimentally obtained relative ROS generation with and without side scattering effect in affected media and in cells.

Materials and methods. We compare obtained modeling results with ionizing radiation induced ROS generation by irradiating 96 well plate with and without water between plate wells. Water works as scattering material between individual wells and, in addition to the primary photons from the radiation source, increase the number of scattered and secondary photons in a medium. For this study black flat bottom 96 well plate (Thermo Fisher) was placed in a laboratory made PMMA phantom with 4 cm of build-up plastic below and above plate. We applied ionizing radiation dose of 8 Gy with a linear accelerator Varian Clinac DMX with 6 MeV energy X-ray photons and 4x4 $cm^2$ irradiation field. This field size allows to fully covers 36 wells. Linear accelerator gantry was positioned from the bottom of the phantom to reduce dose distribution distortions induced by air gaps above medium. Monitor unit calculation and dose distribution simulation were performed using AAA algorithm on Varian Eclipse treatment planning system on computed tomography scans of phantom withplate with scatter material and without scatter material. Obtained values for in-field and out-of-field doses were used for comparison with experimental results of this study. Chinese hamster ovary cells (CHO-K1) were used for this study. Our recent study [2] showed that one of the parameters that can be monitored and correlates to cell DNA damage and cell death is ROS generation during and after irradiation, therefore we used DCFDA dye method for ROS evaluation. Cells were incubated with 50 µM/ml of 2',7'-dichlorodihydrofluorescein diacetate ($H_2$DCF-DA) molecules for 60 min prior to the irradiation and then distributed in each well. 50 µl per well). After irradiation the amount of 50 µl of 96 % ethanol was put on cell suspension in order to equally disperse DCF dye. After 30 min incubation the DCF induced fluorescence was measured by using spectrophotometer (TECAN Genios Pro 96/384). For the experiments with additional scattering material 100 µl of water were added between each well.

Results: We found a significant ($p < 0.001$) increase of generated ROS in wells with scatter material in both in-field and out-of-field wells by 28.18 % for in-field and by 45.07 % for out-of-field wells. It is notable that scatter material increases relative in-field and out-of-field ROS concentration by 4.6 %, from 34.95 % to 39.56 %. The experimental results go with an agreement with dose distribution simulation.

Conclusions: Side scattering of an applied x-ray energy is significantly changing applied energy to affected cells in the in-field and out-of-field cells, thus in turn ROS generation is altered. It is known that cell death after X-Ray irradiation is a result of DNA damage generated by induction of ROS. Therefore, a ROS generation evaluation in out of irradiation field is crucial for out-of -field cell viability change estimations. Here we show a significant ROS generation in out-of -field for the viability change of the affected cells.

[1] G. Lazzari, A. Terlizzi, MG Leo, G. Silvano, VMAT radiation-induced nausea and vomiting in adjuvant breast cancer radiotherapy : The incidental effect of low-dose bath exposure, Clin Transl Radiat Oncol, 43–8 (2017).
[2] T. Didvalis, P. Ruzgys, S. Šatkauskas et al., Assessment of ROS production using DCFH-DA dye in CHO cells after application of ionizing radiation, 2nd International Conference SmartBio 3th – 5th May 2018, 34 (2018).

# THE IMPACT OF INTENSIVE DAIRY FARMING ON NATURAL ENVIRONMENT AND CLIMATE CHANGES

Urszula Ostaszewska[1], Daniel Radzikowski[2], Aleksandra Kalińska[2], Brygida Kruzińska[2]

[1] Department of Cattle Breeding and Milk Evaluation, Siedlce University of Natural Sciences and Humanities, Poland
[2] Department of Animal Breeding and Production, Warsaw University of Life Sciences, Poland
uostaszewska@onet.pl

Counteracting adverse climate change is becoming a more urgent problem to be solved by the international community. In efforts to stop climate change and extreme weather events, more and more attention is now paid to agriculture, and especially to animal husbandry, which plays a special role in the context of climate change.

Intensive livestock production has always been and continues to be a significant burden for the environment through the emission of air pollutants (dusts, gases, microorganisms) and animal excrements (mainly slurry) which, entering the soil and water environment, pose a significant threat to human health and animals. The most dangerous for the environment is ammonia due to its physical and chemical aggressiveness and emission to the atmosphere. Ammonia is colorless and affects the mucous membranes of the eyes, nose and mouth leading to their inflammation. The consequence is the reduction of local immunity that facilitates the penetration of pathogenic microorganisms into the blood and tissues. Hydrogen sulfide, which is formed from animal waste as a result of the bacterial breakdown of proteins containing sulfuric amino acids, is equally dangerous for animal and human health. Methane and hydrogen arise as a result of bacterial fermentation processes in the digestive tract of livestock, especially dairy cattle. Intestinal fermentation is a natural part of the digestion process. Of particular importance, due to the release of a dangerous greenhouse gas - methane, is the digestion of ruminants - cattle, sheep or goats.

In conclusion, it should be stated that the production of greenhouse gases is much lower than the emissions by people and machinery. In order to reduce the adverse impact of excess gases during intensive dairy production, rules must be respected regarding the way animal waste is collected and stored, and animals must be kept in line with welfare principles, without allowing too much compaction.

# THE INFLUENCE OF THE CONDITIONS OF THE PIG'S TRANSPORT ON THE BIOCHEMICAL CHANGES OCCURRING IN MEAT

Urszula Ostaszewska[1], Daniel Radzikowski[2], Aleksandra Kalińska[2], Brygida Kruzińska[2]

[1] Department of Cattle Breeding and Milk Evaluation, Siedlce University of Natural Sciences and Humanities, Poland
[2] Department of Animal Breeding and Production, Warsaw University of Life Sciences, Poland
uostaszewska@onet.pl

Meat quality is a set of all characteristics and properties of meat raw material, affecting its high sensory, technological, utility and culinary values.

High quality meat should be characterized by the absence of microorganisms, chemicals, physical contaminants dangerous for health, be free of quality defects and have a high nutritional value. The correct way of transporting live pigs has a significant impact on the quality of the meat. During loading, transport and unloading of animals there is the greatest probability of lowering the quality of the raw material through the occurrence of scratches, bruises, bloody bruises and leg fractures. We are able to obtain high quality pork meat only by caring for the welfare of animals. The driver is responsible for maintaining animal welfare during transport. That is why it is so important to train them and pass their exams and have certificates confirming their qualifications in the field of road transport of slaughter animals. Short-term action of stressors, up to 24 hours before slaughter, can cause animals to increase the rate of post-mortem glycolytic changes, i.e. defects aqueous meats (PSE). The stressors include: noise, improper driving of animals, too high temperature prevailing during transport and mixing litters, ie contact with foreign individuals. The most negative impact on the quality of meat is caused by improper loading and transport of animals, because at this point the animals are subjected to the greatest stress associated with the change of the environment. It is recommended to limit the use of electric drovers to plastic scouts and rattles.

The article presents transport as the main factor affecting the quality of pork. It includes aspects such as types and appropriate transport of live pigs, loading and unloading of animals and the causes of watery water defect.

# OPTIMIZATION OF BEE POLLEN FERMENTATION CONDITIONS USING CHEMOMETRIC ANALYSIS

Vaida Adaškevičiūtė[1], Vilma Kaškonienė[1], Paulius Kaškonas[1,2], Audrius Maruška[1]

[1] Instrumental Analysis Open Access Centre, Vytautas Magnus University, Vileikos str. 8, LT – 44404 Kaunas, Lithuania
[2] Kaunas University of Technology, Studentų str. 50, LT – 51368, Kaunas, Lithuania
vaida.adaskeviciute@stud.vdu.lt

Bee pollen is one of the most valuable natural products produced by bees (lot. *Apis mellifera)*. Bees are the insects that help transfering pollen between plants and also bring them to beehive. Bees mix collected pollen with saliva, nectar and honey and then place this mixture in the honeycomb for storage. The mixture changes over time because of the fermentation becoming a new product, known as bee bread. The fermentation of bee pollen contribute to increase of bioactive compounds content, nutritional value and antioxidant activity, which helps to preserve products against spoiling [1, 2]. The aim of this study was to optimize bee pollen fermentation conditions using chemometric analysis methods. Spontaneous fermentation and fermentation with *L. rhamnosus* was applied on bee pollen keeping prepared samples for 2, 4, 8, 12, 16 and 20 days, respectively. Total phenolic compound content, total flavonoid content and antioxidant activity were determined in the fermented bee pollen extracts by spectrophotometric methods in order to optimize fermentation process conditions [2, 3, 4]. The total content of phenolic compounds was measured using Folin–Ciocalteu reagent. The total flavonoid content analysis was carried out performing colorimetric reaction with aluminum chloride. Antiradical activity, characterized by the total radical scavenging activity, was measured using 2,2-diphenyl-1-picrylhydrazyl (DPPH) free radical. Results were evaluated employing chemometric analysis methods, which included principal component analysis (PCA), multidimensional scaling (MDS) and hierarchical clustering analysis (HCA). The spectrophotometric analysis of different bee pollen extracts showed that total content of phenolic compounds increased by 1.11-1.67 times and antiradical activity – 1.56-2.26 times in all fermented samples, but total flavonoid content – by 1.13-1.35 times after 4 and more days of fermentation. The optimal duration of fermentation was determined finding the highest observed total phenolic content, total flavonoid content compounds and antioxidant activity in the samples. According to the results, the optimal duration of fermentation are 8 days using *L. rhamnosus* and 12 days for spontaneous fermentation.

**Acknowledgements:**
This project was financed by Research Council of Lithuania project No. 09.3.3-LMT-K-712-10-0232.

[1] A. Gendrolis. *Žiedadulkės ir bičių duonelė. Kaip ilgai ir sveikai gyventi* (Kaunas, 2012, ISBN 9786094082832).
[2] V. Kaškonienė, A. Katilevičiūtė, P. Kaškonas, A. Maruška (2018). The impact of solid state fermentation on bee pollen phenolic compounds and radical scavenging capacity, *Chemical Papers*, 1-6. ISSN 2585-7290, (2018).
[3] V. Kaškonienė, G. Ruočkuvienė, P. Kaškonas, I. Akuneca, A. Maruška, Chemometric analysis of bee pollen based on volatile and phenolic compound compositions and antioxidant properties, *Food Analytical Methods*, 8(5), 1150-1163 (2015).
[4] M. Stankevičius, I. Akuneca, I. Jakobsone, A. Maruška, Comparative analysis of radical scavenging and antioxidant activity of phenolic compounds present in everyday use spice plants by means of spectrophotometric and chromatographic methods, *Journal of Separation Science*, 34 (11), 1261-1267 (2011).

# PROBLEMS OF DRY ANAEROBIC DIGESTION OF CHICKEN MANURE

Usenko Stanislav, Shapovalov Yevhen, Salyuk Anatoliy, Kotynsky Andrey.

Department of Ecology and Sustainable Nature Use, University of Food Technoligies, Ukraine
farkry17@gmail.com

According to the European trends of waste management[1], waste must be firstly be recycled, if it's possible, or be utilized with energy production. Such an approach can be achieved by methane fermentation. In addition, biogas plant effluent is a high-quality organomineral fertilizer. On the other hand, in case of the absence of government standards for this type of fertilizer and the seasonal functioning of the agrarian sector, there is a problem of the formation of an excess amount of wastewater[2]. Regulation of their amount is possible by conducting dry fermentation or recycling of liquid phase of effluent. However, providing both this methods for the poultry waste may cause nitrogen accumulation problems. The results of our previous studies indicated the possibility chicken manure dry fermentation providing, but it was characterized by significantly lower performance than liquid phase fermentation. Some repeats of dry fermentation were characterized by a significantly higher yield of biogas and methane compare the mean value, which may indicate the possibility of a methanogenic consortium to adaptation. Previous studies of organic waste dry fermentation prove a number of it's advantages. Thus, dry fermentation provide reducing the size of biogas plant, reducing the operational coast and higher volumetric methane output [3]. Dry fermentation of chicken manure is poorly understood and relevant to study it. According the literature the process was unstable both in thermophilic and mesophilic conditions, so we decided to study this phenomenon. Most of researchers were conducted in the mesophilic mode(30-55C), as in thermophilic it is especially unstable. Methane yield in previous researches was in range of 0 to 247 ml/g VS\. Theoretically it is possible to improve process by reduction influence of an ammonium nitrogen[4].

**Materials and methods**

The research was carried out in plastic reactors of a total volume of 50 ml in a thirteen repetitions. The substrate content was 20 g with 10% of inoculate content. Humidity of the substrate was 78%, 80%, 82% and 84%. For dilution to the required humidity, tap water was used. The reactors were placed in a thermostats. The reactors were operating in mesophilic (35 ° C) and thermophilic conditions (50 ° C). The experiment was conducted in batch mode for 160 days.
The biogas output was measured daily. The methane content was measured when the required for analysis amount of biogas was accumulated.$V = \frac{\sigma}{\bar{K}}$ -The coefficient of variation formula.

**Results and discussion**

The coefficient of variation of methane production in mesophilic and thermophilic mode was used to assess the stability of the process. The coefficient of variation of methane production was varied from 14.84% to 35.17% in mesophilic mode and from 14.4% to 78.21% in thermophilic mode. Thus, the process was unstable both in thermophilic and mesophilic conditions. In addition, the normal distribution of values was not typical for the methane and biogas production, which also indicates the low stability of the process. Consequently, providing of dry chicken manure fermentation is not appropriate to reduce water consumption in the utilization of poultry waste.

**Conclusions**

1. The process is unstable both in thermophilic and mesophilic conditions. The process in the thermophilic condition is more unstable than methopilic process. The research of stability of chicken manure methane fermentation process in solid-phase conditions was conducted for the first time.
2. Dry fermentation of chicken manure is not appropriate to reduce water consumption in the utilization of poultry waste.



[1] Directive 2008/98/EC [e-commerce recourses] // eur-lex. – 2008. –http://eur-lex.europa.eu/legal-content/En/TXT/?uri=celex:32008L0098.
[2] Nie H., Jacobi, F., Strach, K., et al., 2015. Mono-fermentation of chicken manure: Ammonia inhibition and recirculation of the digestate. Bioresource Technology, 178: 238-246.
[3] Karaalp D., Caliskan G., Azbar N. Performance evaluation of a biogas reactor processing chicken manure with high solids content: digital proceeding of the ICOEST Cappadocia 2013. Nevsehir, Turkey, June 18-21, 2013. P. 768-773.
[4] Methane fermentation of chicken manure at the lowered concentration of inhibitors in Ukraine/ . Salyuk, A., Zhadan, S., Shapovalov, Ye., Tarasenko, R.. // International Scientific Journal for Alternative Energy and Ecology (ISJAEE). – 2017. – №4. – С. 89–98

# SYNERGETIC EFFECT OF HETEROCYCLIC COMPOUND WITH ANTITUMOR DRUG

Tatsiana A. Gurinovich, Anastasia V. Kvachonak, Margarita O. Dosina, Svetlana G. Pashkevich

Institute of Physiology, National Academy of Sciences of Belarus, 28 Academicheskaya Str., 220072 Minsk, Belarus
gurinovich.tanya@gmail.com

Treatment of malignant neoplasms with cytotoxic drugs causes various side effects and fatal toxic complications. High resistance of malignant neoplasm cells to chemotherapy drugs, presence of multipotent chemo-and radio-resistant stem cells in neoplasm, metastasis and recurrence of tumors require the search for new approaches to increase the selective inhibition of tumor growth [1].

The purpose of the study was to assess the effectiveness of the combined application of heterocyclic compounds with chemotherapy drugs on the possibility of potentiating the effect of reduced dosage of a chemotherapy drug. Water soluble Li salts of comenic acid conjugates with isoxazole scaffold (4-oxo-5-((5-phenylisoxazol-3-yl)methoxy)-4H-pyran-2-carboxylate) were used for the study, which was synthesized in the Institute of Physical Organic Chemistry, the National Academy of Sciences of Belarus [2]. The use of water-soluble Li forms is due to preference for subsequent biotesting, as well as Li cations have a cytotoxic enhancing effect in contrast to other monovalent or divalent cations [3].

To evaluate the synergistic activity of the combined application of conjugate of the heterocyclic compounds with the antitumor drug Temobel® (Temozolomid), studies were carried out on C6 glioma cells in 96-well (in vitro) [2]. The initial concentration of C6 glioma cells was 5000 cells per well of the plate. The cells were cultured in F10 nutrient medium supplemented with 10% bovine fetal serum. The Vybrant MTT Cell Proliferation Assay Kit (Thermo Fisher Scientific, Lithuania) was used to determine the viability of cells [4]. The absorbance of the contents of the wells was measured on an automatic biochemical immuno-fermental analyzer ChemWell® 2910 (Combi) using ChemWell® software version 6.3 (Revision A), USA. An antitumor effect was evaluated for the recommended therapeutic dose of Temobel® 100 μg per 250 μl, as well as for a dose of 10 μg and 1,0 μg. Water soluble Li salts of comenic acid conjugates with isoxazole scaffold was used in the indifferent dosages which did not exhibited any cytotoxic effect.

With the application of Temobel® at a dose of 100 μg to C6 glioma cells, about 40% of the cells died within 28 h. While using a dose of 10 μg and 1.0 μg, there were no significant differences in the number of dead cells from their spontaneous death after 28 h (cell death of 5-8%). With a combined application of Temobel® at a dose of 10 μg and 1 μg with isoxazole conjugate at doses of 1.0 and 0.1 μg, a significant ($p < 0.05$) death of tumor cells (20 – 25%) was revealed, which indicates the manifestation conjugate of the synergistic effect. It is especially important that such an impressive cell death occurs only 28 h after the application of Temobel® in subthreshold concentrations with water soluble Li salts of comenic acid conjugates with isoxazole scaffold, which in the indifferent dosages used did not exhibited any cytotoxic effect.

The results obtained will be useful for further research in this area and for the development of new effective drugs and chemotherapy with reduced therapeutic doses.

[1] Li, Y. J. Autophagy and multidrug resistance in cancer / Y. J. Li, Y. H. Lei, N. Yao, C. R. Wang, N. Hu, W. C. Ye, D. M. Zhang, Z. S. Chen // Chinese Journal of Cancer. – 2017. – Vol.36, №1. – P.52-62.

[2] Kletskov, A. V.Synthesis and Biological Activity of Novel Comenic Acid Derivatives Containing Isoxazole and Isothiazole Moieties / A. V. Kletskov, V. I. Potkina, I. A. Kolesnika, S. K. Petkevicha, A. V. Kvachonakb, M. O. Dosinab, D. O. Loikob, M. V. Larchenkob, S. G. Pashkevich and Vladimir A. Kulchitsky// Natural Product Communications, Vol. 13 (11) 2018, 1507-1510

[3] R. Beyaert, C. De Potter, B. Vanhaesebroeck, F. Van Roy, and W. Fiers (1991) Induction of inflammatory cell infiltration and necrosis in normal mouse skin by the combined treatment of tumor necrosis factor and lithium chloride. The Americal Journal of Pathology. 1991 Mar; 138(3): 727–739.

[4] L. A. Quayle, P. D. Ottewell, I. Holen (2018) Chemotherapy resistance and stemness in mitotically quiescent human breast cancer cells identified by fluorescent dye retention. Clinical and Experemental Metastasis. 2018; 35(8): 831–846.

# THE BEHAVIOURS OF DIFFERENT ELECTRON TRANSFER MEDIATORS IN MEASURING THE REDOX ACTIVITY OF SACCHAROMYCES CEREVISIAE

Vilius Aukscionis[1], Antanas Zinovicius[1], Aura Kisieliute[1], Arunas Ramanavicius[1,2]

[1] Vilnius University, Faculty of Chemistry, Department of Physical Chemistry, Vilnius, Lithuania
[2] State Research Institute Centre for Physical Sciences and Technology, Laboratory of Bio-nanotechnology, Vilnius, Lithuania
vilius.aukscionis@chf.stud.vu.lt

Saccharomyces cerevisiae (S. cerevisiae) is a robust eukaryotic organism that has a fast metabolism and can survive in both aerobic and anaerobic conditions. Yeast cells can be used in biosensor and microbial fuel cell development but as all systems involving live cells, they are often less efficient than conventional energy generators i.e. fossil fuels etc., unstable and prone to breakdown overtime. To increase the efficacy of these microbial systems the cells can be immobilized in different matrices, chemically modified i.e. with polypyrrole [1] or operated without aeration and mixing.

In our study we focused on the electrochemical investigation of S. cerevisiae under varying conditions using different electron transfer mediators. Lipophilic mediators participate in redox reactions with intracellular reduced species in the respiratory pathway while the hydrophilic mediators shuttle the electrons to the electrode in the extracellular medium. Mediators compete with oxygen for the role of electron acceptor and their effectiveness may depend on the presence or absence of oxygen [2], [3].

We performed cyclic voltammetry, chronoamperometry and spectrophotometric measurements on the system of yeast cells, grown in aerobic and anaerobic conditions, modified with polypyrrole, and measured with different pairs of electron transfer mediators. The metabolic activity of S. cerevisiae is evaluated indirectly by electrochemical and optical methods which detect the reduced forms of mediators.

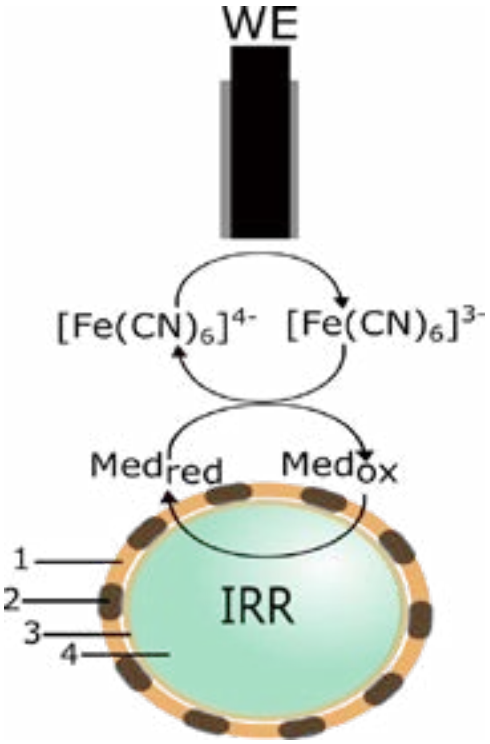


Fig.1. A representative scheme of the double redox mediator pair action in a polypyrrole modified cell. WE – working electrode; $Med_{ox}/Med_{red}$ – the oxidized/reduced form of the mediator; 1 – cell wall; 2 – polypyrrole; 3 – plasma membrane; 4 – cytoplasm; IRR – intracellular redox reactions;

[1] Andriukonis, E. et al. (2018) 'Yeast-assisted synthesis of polypyrrole: Quantification and influence on the mechanical properties of the cell wall', Colloids and Surfaces B: Biointerfaces. Elsevier B.V., 164, pp. 224–231. doi: 10.1016/j.colsurfb.2018.01.034.
[2] Rawson, F. J., Downard, A. J. and Baronian, K. H. (2014) 'Electrochemical detection of intracellular and cell membrane redox systems in Saccharomyces cerevisiae', Scientific Reports, 4, pp. 1–9. doi: 10.1038/srep05216.
[3] Ramanavicius, A. et al. (2017) 'Scanning electrochemical microscopy based evaluation of influence of pH on bioelectrochemical activity of yeast cells − Saccharomyces cerevisiae', Colloids and Surfaces B: Biointerfaces. Elsevier B.V., 149, pp. 1–6. doi: 10.1016/j.colsurfb.2016.09.039.

# YKL-40 EXPRESSION IN GLIOMAS PATIENTS BLOOD SERUM AND TUMOR TISSUE

Živilė Švėgždaitė[1]; Rūta Urbanavičiūtė[1], Indrė Valiulytė[1], Arimantas Tamašauskas[1], Daina Skiriutė[1]

[1]Laboratory of Molecular Neurooncology, Neuroscience Institute, Medical Academy, Lithuanian University of Health Sciences, Eiveniu str. 4, Kaunas, LT 50009, Lithuania
zivile.svegzdaite@gmail.com

Glioblastoma is the most common, very infiltrative and most agressive out of astrocytic tumors [1]. Because of its malignancy and high relapse possibility, average survival time is less than 15 months in patients, who are diagnosed with glioblastoma [2]. It is very important to find biomarkers for earlier glioblastoma detection, etter treatment and longer survival time [3]. YKL-40 – secreted protein which is associated with proliferation, migration, invasion, angiogenesis of cancer cells and it is considered as a potential glioblastoma marker in blood serum [4;5].

The aim of this study was to verify suitability of YKL-40 as astrocytomas detection biomarker in patients blood serum and postoperative tumor tissue.

In order to evaluate YKL-40 suitability for astrocytomas detection in blood serum ELISA method was used. Results showed that there is a significant difference ($p=0.033$) between healthy control and high grade astrocytoma blood serum specimens based on YKL-40 protein level means of each group. Western Blot method was used to measure a relative amount of YKL-40 protein in postoperative tumor tissue but while performing statistical analysis no significant differences were found between different malignancy grade. *YKL-40* gene expression in tumor tissue was evaluated by RT-PCR method. Results showed statistically significant difference ($p<0.0001$) between low and high grade astrocytoma based on *YKL-40* gene expression.

Results of this research also have shown that protein amount and gene expression is related with survival time. Long-term survival was significantly influenced by lower protein level in blood serum and lower gene expression in tumor tissue, while lower protein level in tumor tissue influenced shorter survival time. All values were also compared with individual patients characteristics: malignancy grade, age, gender and survival time. It was found significant connections of protein amount in blood serum with malignancy grade ($p=0.036$), age ($p=0.008$) and survival time ($p=0.016$). Significant gene expression connections with malignancy grade ($p=0.000013$), age ($p=0.0001$), gender ($p=0.015$) and survival time ($p=0.001$) were also noticed. It was also found statistically significant ($p=0.04$) weak positive correlation ($r=0.273$) between YKL-40 protein level in blood serum and *YKL-40* gene expression in tumor tissue.

Results of this study confirmed that YKL-40 is a potential glioblastoma marker. Protein and gene expression showed interfaces with astrocytoma malignancy grade and survival time and also correlation between each other.

[1] Davis ME. Glioblastoma: overview of disease and treatment. Clin J Oncol Nurs. 2016 Oct;20(5):S2-8.
[2] Paolillo M, Boselli C, Schinelli S. Glioblastoma under siege: an overview of current therapeutic strategies. Brain Sci. 2018 Jan;8(1):15
[3] Miyauchi E, Furuta T, Ohtsuki S, Tachikawa M, Uchida Y, Obuchi W. Identification of blood biomarkers in glioblastoma by SWATH mass spectrometry and quantitative targeted absolute proteomics. PloS One. 2018 Mar;13(3): e0193799.
[4] Iwamoto FM, Hormigo A. Unveiling YKL-40, from serum marker to target therapy in glioblastoma. Front Oncol. 2014 Apr;4:90.
[5] Schultz NA, Johansen JS. YKL-40—a protein in the field of translational medicine: a role as a biomarker in vancer patients? Cancers (Basel). 2010 Sep;2(3):1453-91.

# TEMPERATURE DEPENDENT CHANGES IN STRUCTURE AND SEEDING POTENTIAL OF AMYLOID FIBRILS

Mantas Žiaunys, Vytautas Smirnovas

Institute of Biotechnology, Life Sciences Center, Vilnius University, Lithuania
mantas.ziaunys@gmail.com

Amyloids are self-assembled and highly ordered peptide or protein aggregates, which are usually rich in beta-sheet structures. Their formation is linked to several neurodegenerative diseases, such as Alzheimer's, Parkinson's or prion diseases. Recently is has been shown that prolonged incubation may induce structural changes in amyloid fibrils [1][2].

Prion proteins (PrP) were incubated at 37 °C in a 2 M GuHCl, pH 6 buffer with a final concentration of 0.5 mg/ml for 3 days with constant sample rotation at 10 rpm. The generated fibril samples were additionally incubated at 60 °C for different amounts of time. Each sample was sonicated and their seeding potential, as well as Thioflavin T binding ability and fibril stability were tested at different denaturant concentrations.

PrP fibril incubation lead to an increased stability under higher denaturant concentrations, suggesting a change in their structure upon incubation at a higher temperature. There was also a noticeable difference in their ThT binding capacity, as incubation resulted in a sizable shift of ThT fluorescence emissions. Finally, the seeding potential was affected negatively at lower and positively at higher denaturant concentrations.

The results of PrP fibril incubation at an elevated temperature all point towards a restructurization into higher stability amyloid assemblies (Fig. 1), suggesting that temperature and time are an important factor not only during the initial aggregation of amyloid proteins, but also after the fibrils are already generated.

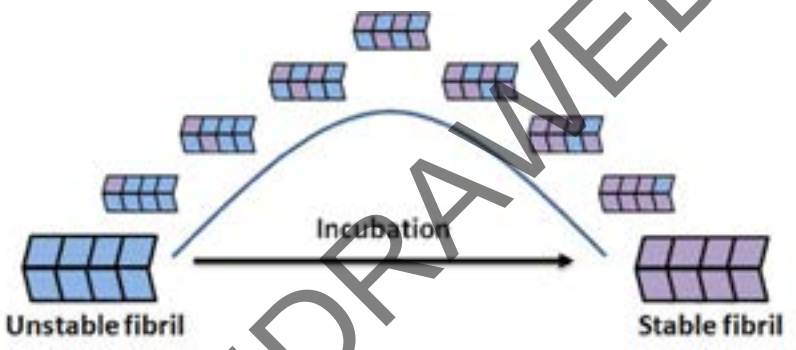


Fig. 1. Prion amyloid fibril restructurization into a higher stability assembly.



[1] K M. Zampieri, G. Legname, and C. Altafini, "Investigating the conformational stability of prion strains through a kinetic replication model," *PLoS Comput. Biol.*, vol. 5, no. 7, pp. 1–9, 2009.

[2] M N. J. Cobb, M. I. Apostol, S. Chen, V. Smirnovas, and W. K. Surewicz, "Conformational Stability of Mammalian Prion Protein Amyloid Fibrils Is Dictated by a Packing Polymorphism within the Core Region," *J. Biol. Chem.*, vol. 289, no. 5, pp. 2643–2650, Jan. 2014.

# POLIDIMETHYLSILOXANE AND MEDICAL PLANTS EXTRACTS COMPOSITES DEVELOPMENT AND INVESTIGATION

Akvilė Andziukevičiūtė-Jankūnienė[1], Birutė Sinkutė[2], Virginija Jankauskaitė[1]

[1] Department of Production Engineering, Kaunas University of Technology
[2] St. Ignatius Loyola College
akvilea@gmail. com

Scarring is an unfortunate and unavoidable consequence of cutaneous surgery [1]. Scar outcomes vary widely from a spectrum of fine and asymptomatic to unappealing keloids. Raised hypertrophic scars exist within this scar spectrum and occur by the over expression of extracellular matrix molecules during the proliferative and remodeling phases of wound healing [2]. Silicone gel sheeting has been shown to mitigate the development of post-operative scars. The use of silicone sheeting is generally considered as a first-line option for extenuating and treating hypertrophic scars [3, 4]. Medicinal plants are used for different therapeutic purposes or as precursors of drugs containing different phytochemicals. A large number of plants with medical properties have been studied for their effectiveness in the prevention of scarring [5, 6]. Observations in vitro and in vivo display extracts and compounds of medicinal plants with antiscar activity. Although many possibilities of scarring inhibitions using compounds from medical plants have been experimentally studied, but their action mechanism on scar healing is not well understood. Figure 1 summarizes the suggested mechanisms of antiscar activity of compounds obtained from medicinal plants [6].

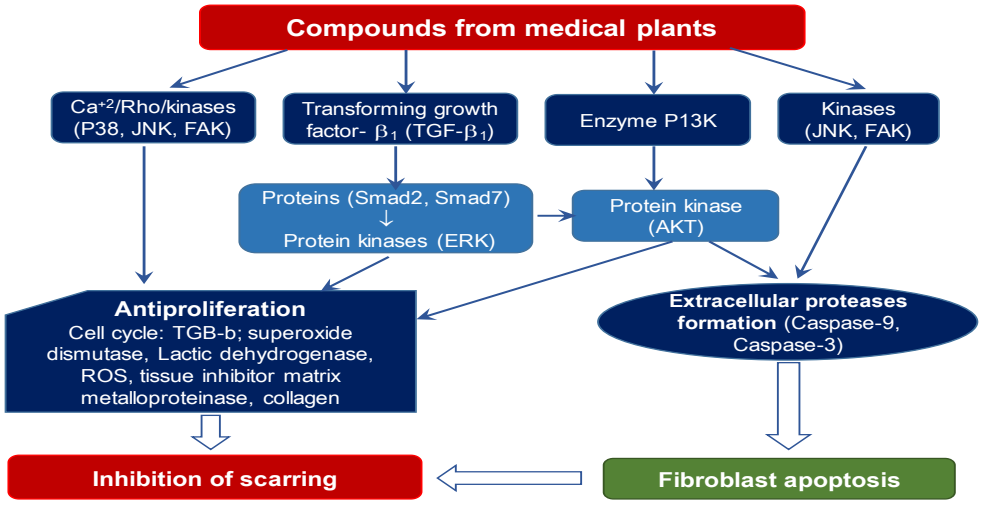


Fig. 1. The mechanism of antiscar activity displayed by compounds from medical plant extracts [5].

The goal of this investigation was to create compositions of elastic biosynthetic silicone rubber with medicinal herbal extract for scar treatment.

Highly biocompatible, room temperature vulcanized polydimethylsiloxane (PDMS) was used. This PDMS has low hardness and strength, is hydrophobic, viscoelastic, and repels dust. Extracts of red onions (*Allium cepa*) have been selected for PDMS modification. *Allium cepa* contains a lot of organic substances: phenolic acids, thiosulfinates, quercetin, flavonoids, cysteine, sulfoxides, selenium, and other compounds. It was determined that freeze-dried *Allium cepa* extract changes PDMS surface tension, reduces its hardness and slightly deteriorates properties at tension. Therefore, *Allium cepa* extract was encapsulated into a low-strength polymeric shell to protect it from contact with PDMS. This shell can easily break down after mechanical loading that allow the extract to leak out and increase PDMS ability for scar healing. The morphology of the surface, the tendency to aggregate and the average size of microcapsules with polystyrene shell and *Allium cepa* core depend on the method of production and ratio of shell/core materials.

[1] A.S. Clayton, T. Stasko. Surgical Complications and Optimizing Outcomes. In: Bolognia JL, Jorizzo JL, Schaffer JV, eds. Dermatology. Vol 3. Atlanta: Elsevier Inc; (2016).
[2] G.P. Sidgwick, D. McGeorge, A. Bayat. A comprehensive evidence-based review on the role of topicals and dressings in the management of skin scarring. Arch Dermatol Res. 2015;307:461-477 (2015).
[3] Kim JS, Hong JP, Choi JW, Seo DK, Lee ES, Lee HS. The efficacy of a silicone sheet in postoperative scar management. Adv Skin Wound Care. 2016;29:414-420, (2016).
[4] Medhi B, Sewal RK, Kaman L, Kadhe G, Mane A. Efficacy and safety of an advanced formula silicone gel for prevention of postoperative scars. Dermatol Ther (Heidelb). 2013;3:157-167 (2013).
[5] Ye Q., Wang S.-Y., Chen J.-Y., Rahman K. Xin H.- L., Zhang H.. Medicinal Plants for the Treatment of Hypertrophic Scars. Evidence-Based Complementary and Alternative Medicine. Article ID 101340 p.1-15 (2015).
[6] Mehta M., Branford O. A., Rolfe K. J.. The evidence for natural therapeutics as potential anti-scarring agents in burn related scarring. Burns & Trauma 4(15).. p. 1-12. (2016).

# AN EXPERIMENTAL RABBIT MODEL OF POSTOPERATIVE PERICARDIAL ADHESIONS

Anastasiya Kanunnikava, Yury Linnik

The Republican Scientific and Practical Center for Pediatric Surgery, Belarus
a.r.kanunnikova@gmail.com

The formation of postoperative adhesions is a serious clinical problem for the present-day cardiac and general surgery. It is characterized by a pronounced abnormal tissue growth caused by the proliferation of fibrous tissues that stick to the nearby normal organs, thus impairing their function and potentially leading to severe clinical complications. In particular, postoperative adhesive pericarditis is a development of abnormal fibrotic attachments between the heart and mediastinum. It significantly complicates multistage surgical corrections of heart conditions, since at each subsequent step the heart needs to be separated from the surrounding adhesions, what extends the duration of the operation as well as increases the risk of injury to the various heart structures during the separation. Also, aortocoronary bypasses are also involved in the process of adhesion formation, which leads to their luminal occlusion and total obstruction over time. In addition to that, adhesion pericarditis reduces myocardial contractility, since the heart becomes attached to mediastinal tissues and as a result the amplitude of its movement decreases [1].

The study of the adhesion formation and the elucidation of its mechanism require a procedure to reliably induce them in a controllable manner. Aside from the investigation of such adhesions, models are used for developing protocols for the treatment and prevention of these postoperative complications. Most experimental models of adhesion formation are based on the simulation of this process in the abdominal cavity [2]. However, the etiology and pathogenesis of the postoperative abdominal and pericardial adhesions are different.

The objective of this study was the development of the experimental animal model of postoperative adhesion pericarditis in order to further assess the efficacy of various strategies for preventing this pathological process.

Five rabbits of the same age weighing 3–4 kg were quarantined for 3 days in the vivarium. They were kept in a 12:12-h light-dark cycle. Food and water were available ad libitum. The rabbits were anesthetized by intramuscular injection of 55 mg/kg of Calypsol (Ketamine) and 5 mg/kg of Xylanit (Xylazine). Mechanical control of ventilation was not required. Chest hair was removed by shaving and the skin was scrubbed with Iodiskin. After left anterior thoracotomy the pericardium was opened longitudinally, an area 2×2 cm was excised and the epicardium of the heart was abraded with a sterile dry swab to develop punctuate bleeding. The pericardium was left open. A pleural drain with a low vacuum drainage system was placed in the thoracic cavity while closing the thoracotomy. Intercostal analgesia was induced by injecting bupivacaine. Postoperative wound was closed in layers of continuous sutures. To prevent infections prophylactic antibiotic (100 mg/kg cefazolin) was injected 1 h before the surgery. After the surgery, cefazolin was administered intramuscularly twice daily for 3 days. Until the rabbits were euthanized, they were observed every day and the wound was cleaned with Iodiskin postoperatively, if necessary. The rabbits were euthanized 4 weeks after the surgery with lethal doses of Thiopental. The heart was excised with its pericardium as a block.

The samples were examined macroscopically by a surgeon, who was blinded with respect to the animal groups. Adhesion formation was evaluated by a macroscopic inspection according to the adhesion rating scale from 0 to 3 proposed by Heydorn et al. [3]. Grade 0 of this scale corresponds to no adhesions, while grade 1 corresponds to adhesions that could be easily dissected by a finger. Moderate adhesions are assigned grade 2, while severe and difficult to dissect adhesions are classified as grade 3. After the implementation of the protocol described above four rabbits of the experimental group had severe grade 3 adhesions, while the remaining one had grade 2 adhesions. Obtained results demonstrate the applicability of this protocol to produce the experimental model of postoperative adhesion pericarditis, which can be used for the comparative assessment of various potential antiadhesive agents.

All experiments were carried in compliance with the recommendations of the European Convention on Humane Treatment of Laboratory Animals [4].

[1] Cannata, A. et al. Postsurgical Intrapericardial Adhesions: Mechanisms of Formation and Prevention. Ann. Thorac. Surg. 95, 1818–1826 (2013).
[2] Li, J. et al. Polymer materials for prevention of postoperative adhesion. Acta Biomater. 61, 21–40 (2017).
[3] Heydorn, W., Daniel, J. & Wade, C. A new look at pericardial substitutes. J. Thorac. Cardiovasc. Surg. 94, 291–296 (1987).
[4] European Convention for the protection of vertebrate animals used for experimental and other scientific purposes. Strasbourg: Europ. Treaty Series, 1986. № 123. P. 48.

# GEOCHEMICAL AND METAGENOMIC ANALYSIS OF URBAN RIVER SEDIMENTS FOR ANTHROPOGENIC CITY POLLUTION

Augustė-Ona Jančauskaitė[1], Dalius Butkauskas[1], Vytautas Samalavičius[2], Vesta Skrodenytė-Arbačiauskienė[1*]

[1] The Nature Research Centre, Vilnius, Lithuania
[2] Faculty of Chemistry and Geosciences, Vilnius University, Lithuania
auguste-ona.jancauskaite@gmc.stud.vu.lt

Human activities in the city area leads to greater pollution with significant impact on human health and damage to the natural or built environment [1]. Sediments cores are one of the most important tools for monitoring anthropogenic transformations in aquatic environments and some metals correlate as anthropogenic trace indicating that these elements had an identical origin [2]. Also, environmental pollution is an important factor to shape the microbial communities that eventually could lead into spread of pathogens and ecological functions disable and sediments is an active place with high abundance of microorganisms [3]. This study was conducted to investigate the shift in structure of sediment bacterial communities of river exposed to multiple anthropogenic contaminants and relate changes to chemical composition for potential of bioindication.

Neris river is a suitable model object to investigate the impact of pollution on the aquatic ecosystem, it crosses the capital Vilnius - one of the most urbanized cities in Lithuania. Three different anthropogenic sites were selected to sample Neris river sediments in two years row 2017-2018: before the city, city center and after wastewater treatment plant. Using the Inductively coupled plasma optical emission spectrometry, the chemical composition of heavy metals was analysed to uncover anthropogenic trace in river sediments samples. The microbiome was characterized on the basis of the V3 and V4 hypervariable regions of the 16S rRNA gene by using next generation sequencing platform Illumina MiSeq.

The chemical analysis of Neris river sediments uncovered anthropogenic trace in sampled sites. Comparison of Neris river bacterial communities revealed several uniquely found genera and pathogenic genera of Nostocales and Spirochaetales order as candidate bioindicators to monitor river pollution. Furthermore, potentially pathogenic bacterial genera Flavobacterium and Clostridium was dominant in anthropogenic impact sites. Overall, bacterial communities could provide a useful tool for monitoring and assessing ecological state in freshwater sediments while indicating anthropogenic city pollution.

[1] N. B. Grimm, S. H. Faeth, N. E. Golubiewski, C. L. Redman, J. Wu, X. Bai, J. M. Briggs, Global Change and the Ecology of Cities, Science 319(5864), 756-760 (2008).
[2] Z. Balogh, S. Harangi, I. Gyulai, M. Braun, K. Hubay, B. Tóthmérész, E. Simon, Exploring river pollution based on sediment analysis in the Upper Tisza region (Hungary), Environ Sci Pollut Res Int 24(5), 4851-4859 (2017).
[3] Z. Hou, W. C. Nelson, J. C. Stegen, C. J. Murray, E. Arntzen, A. R. Crump, D. W. Kennedy, M. C. Perkins, T. D. Scheibe, J. K. Fredrickson, J. M. Zachara, Geochemical and Microbial Community Attributes in Relation to Hyporheic Zone Geological Facies, Sci Rep 7(1):12006 (2017).

# PLANTS QUALITY AND ADAPTION TO THE PRODUCTION OF BIOPRODUCTS

Aušra Bakšinskaitė[1], Vita Tilvikienė[2]

[1] Vytautas Magnus University, Faculty of Agricultural Engineering, Studentų 15, Akademija, Kaunas distr.
[2] Lithuanian Research Centre for Agriculture and forestry, Instituto al. 1, Akademija, Kėdainiai distr.
Ausra.baksinskaite@lammc.*lt*

Plastic product production is very high in the world. Last year it was made about 448 million tons of plastic. This product is very useful in our daily life, but also makes may problems for the environment. Most of the products are not recyclable and usually discarded in landfills. Plastic pollution grow up it is very fest. Therefor it is important to find a solution to protect world and find a substitute. There few main solutions for reducing the damage of non-degradable materials: reduce the use of them, increase the recycling or make the bio-degradable materials which could change or at least reduce the quantity of plastics in the world. One of such bio-resources for different purposes could be biomass of agricultural crops.

The aim of this investigation is to evaluate the chemical composition, structure and suitability of herbaceous plants for the development of bio-products. The object of this study was *Artimisia dubia*, Virginia mallow (*Sida hermaphrodita L. Rusby*), Miscanthus (*Miscanthus ×giganteus*), and wheat straw. All energy crops and wheat were grown at the Institute of Agriculture in Akademija, Kėdainiai distric (55˚ 24'N) on an *Apicalcari – Endohypoglevic Cambisol,* light loam. Nitrogen (N) fertilization at one rates (90 kg ha $^{-1}$) was applied in spring. Grasses and wheat were fertilized with mineral fertilizer. The main parameters for analyzing crop biomass as source for bio-product is their structural composition. For the reason, according to the van Soest method, the samples were subjected to the fibers component analyses: acid detergent fiber (ADF), neutral detergent fiber (NDF) and acid detergent lignin (ADL). The content of cell wall structure carbohydrates hemicellulose and cellulose was calculated:

$$cellulose = ADF - ADL \quad (1)$$

$$hemicellulose = NDF - ADF \quad (2)$$

The highest cellulose content was in biomass of *Artimisia dubia* 54,43 % , which shows that this crop could be repository suitable for bio-plastic production, then others plants whose cellulose was lower. The content of hemicellulose is different in all plants. The highest quantity of hemicellulose had Virginia mallow 28,05 %, a little smaller miscanthus 24,07 %, *Artimisia dubia* had 15,95 % and least had wheat straw 8,86 %. However, lignin content in *Artimisia dubia* (10,25 %) was higher than Virginia mallow (7,38%), but lower in wheat straw (10,70%) which presented the highest lignin content. The lowest amount of lignin is better reduce the energy for braking the plant cell wall. Also was measured ash content in biomass. The results suggest that - miscanthus had the lowest – 2,18 % and wheat straw had the highest ash content – 5,39 %.

No less important is crop productivity, which guaranty the economic benefit of the processing technologies. In 2018 dray matter (DM) yield of five years harvesting miscanthus was 18,55 t ha$^{-1}$ – very high compared to Virginia mallow (3,99 t ha$^{-1}$), *Artimisia dubia* (3,82 t ha$^{-1}$) and wheat straw ( 1,79 t ha$^{-1}$).

The first results suggest that the most appropriate for bio-products is *Artimisia dubia*, which had high cellulose content, but on the other hand miscanthus had highest biomass yield which could play the significant role in economic benefit of biomass processing. Therefor more research will be conducted for the analysis of fiber content and fiber parameters as well as chemical composition of biomass.

# AIRWAY CELL EXOSOME UPTAKE IN MICROGLIA IS RELATED TO MITOCHONDRIAL SUPPRESSION AND ROS PRODUCTION

Deimantė Blažauskaitė[1], Aistė Jekabsone[1,2], Lina Jankauskaitė[2]

[1] Laboratory of Molecular Neurobiology, Neuroscience Institute, Lithuanian University of Health Sciences, Kaunas, Lithuania;
[2] Laboratory of Pharmaceutical Sciences, Institute of Pharmaceutical Technologies, Lithuanian University of Health Sciences, Kaunas, Lithuania
d.blazauskaite@gmail.com

Upper respiratory tract infections are the most common [1], and approximately 80% of them are caused by viruses [2]. The viruses do not spread far from the infection site, but an inflammatory signal can be transmitted through liquid and exosomal communication [3]. Previous studies have shown that the exosomes from virus-primed cells may have viral genetic material or other inflammatory factors [4]. Exosomes can pass membrane barriers, including the brain blood barrier, and transmit the inflammatory signal away from periphery to the brain [5]. It is known that immune cells including microglia respond to viral infection via mitochondrial antiviral signaling protein including changes in mitochondrial function and increased production of reactive oxygen species (ROS) [6]. However, it is not clear whether exosomes from virus-affected airway cells might induce similar immuno-metabolic changes. The aim of our study was to analyse the effect of exosomes from virus infection-mimicking polyinosinic polycytidylic acid (poly (I:C)) sequence-primed respiratory tract cells (RTC) on mitochondrial functions and on the formation of ROS in primary rat microglia.

Primary microglial cells were isolated from mixed glial culture that was prepared from the brain hemispheres of 5-7 days old Wistar rats. Exosomes were isolated from the culture medium of heterogeneous rat RTC culture by "Total Exosome Isolation Reagent" (Thermo Fisher Scientific) according to the manufacturer protocol. For simulation of viral infection, the RTC were stimulated with 1 μg/ml poly (I:C). The amount of exosomal protein was determined by spectrophotometric Bradford assay. Microglial cells were identified using fluorescence microscope after staining them with Isolectin GS-IB4-Alexa Fluor 488 conjugate, and RNA of exosomes was labeled by a specific die conjugated with Alexa Fluor 555 (BLOCK-iT Alexa Fluor Red Fluorescent Control, Thermo Fisher Scientific). Respiration of microglial mitochondria was evaluated by Oroboros Oxygraph-2k. ROS formation in microglial cells was determined by DCFDA fluorescence intensity calculated from fluorescent images by ImageJ software. Statistical data analysis was performed by SigmaPlot 12.5 software.

The study revealed that exosomes from both poly I:C-primed and not primed RTC enter microglia within 30 min by direct pathway (endocytosis, phagocytosis or micropinocytosis). After 16-18 hours of incubation both primed and unprimed exosomes significantly reduced the activity of oxidative phosphorylation of microglial mitochondria by suppressing the respiratory chain and increased ROS production. The level of ROS induced by exosomes was similar to that caused by 3 hour direct treatment of microglia with 1 μg/ml poly (I:C). The obtained data show that exosomes from both poly I:C-primed and not primed RTC similarly affect mitochondrial respiration and ROS production in microglia.

[1] A. Rohilla, V. Sharma, and S. Kumar, "Upper Respiratory Tract Infections: an Overview," *Int. J. Curr. Pharm. Res.*, vol. 5, no. 3, pp. 1–3, 2013.
[2] Y. Bin Seo *et al.*, "Etiology and clinical outcomes of acute respiratory virus infection in hospitalized adults," *Infect. Chemother.*, vol. 46, no. 2, pp. 67–76, 2014.
[3] H. S. Chahar, T. Corsello, A. S. Kudlicki, N. Komaravelli, and A. Casola, "Respiratory Syncytial Virus Infection Changes Cargo Composition of Exosome Released from Airway Epithelial Cells," *Sci. Rep.*, vol. 8, no. 387, pp. 1–18, 2018.
[4] J. S. Schorey, Y. Cheng, P. P. Singh, and V. L. Smith, "Exosomes and other extracellular vesicles in host-pathogen interactions," *EMBO Rep.*, vol. 16, no. 1, pp. 24–43, 2015.
[5] C. C. Chen *et al.*, "Elucidation of Exosome Migration Across the Blood – Brain Barrier Model In Vitro," *Cell. Mol. Bioeng.*, vol. 9, no. 4, pp. 509–529, 2016.
[6] A. P. West, G. S. Shadel, and S. Ghosh, "Mitochondria in innate immune responses," *Nat. Rev. Immunol.*, vol. 11, no. 6, pp. 389–402, 2011.

# *SEMA3A*, *SEMA3C*, *SEMA3F* AND *NRP1* GENES EXPRESSION ANALYSIS IN DIFFERENT GRADE ASTROCYTIC GLIOMA TUMORS

Deimantė Kardonaitė[1], Indrė Valiulytė[1], Arimantas Tamašauskas[1], Arūnas Kazlauskas[1]

[1] Neuroscience Institute, Lithuanian University of Health Sciences, Lithuania
deimkard@gmail.com

Glioma is the most common tumor in the central nervous system. The most aggressive form of glioma is glioblastoma (grade IV), which is characterized by increased cell proliferation, invasion and formation of new blood vessels around the tumor. Despite the complex treatment of glioblastoma (surgery, chemotherapy and radiation therapy), the survival time of patients is generally short (approximately 15 months) [1]. Therefore, scientists try to find a way to inhibit tumor development and identify potential biomarkers for an earlier glioma prognosis and also to discover tumor-specific molecules that could be used in target treatment therapies or which could help to predict the response to treatment. According to the latest studies, secreted class 3 semaphorins (Sema3) and their receptors play an important role in regulating cell viability, invasiveness, and angiogenesis in tumorous diseases [2-4]. However, not all SEMA3 proteins have the same effect on tumor diseases because, for example, increased SEMA3A expression in oral cancer cells significantly reduces tumor growth [5], increased SEMA3F expression inhibits cell invasiveness in breast cancer and melanoma [6] but increased SEMA3C expression promotes tumor progression in prostate, liver, stomach cancer and is associated with shorter patient lifespan [7]. Therefore, the aim of this study was to analyze the changes of *SEMA3A*, *SEMA3C*, *SEMA3F*, and *NRP1* gene expression in different grade astrocytic glioma tumors and to identify the association between gene expression and patients' clinical data.

To achieve this goal, total RNA was extracted from frozen tumor tissue and cDNA was synthesized by using reverse transcriptase. Before analyzing gene expression, *SEMA3A*, *SEMA3C*, *SEMA3F*, and *NRP1* gene quantitative real-time PCR (qRT-PCR) conditions were optimized by gradient PCR and the expression of these genes was determined by qRT–PCR analysis with SYBR Green fluorescent dye. During the study, beta-actin gene (ACTB) was selected for internal control and gene expression changes were compared to healthy brain tissue. The comparative $2^{-\Delta\Delta Ct}$ method was used for the calculations of genes mRNA expression. The obtained data was used to investigate associations between *SEMA3A*, *SEMA3C*, *SEMA3F*, and *NRP1* gene expression and the patients' clinical data (gender, age before surgery, tumor grade, and survival of patients). Also, the correlation between expression of *SEMA3A*, *SEMA3C*, *SEMA3F* and their receptor *NRP1* in gliomas was evaluated.

69 tumor samples taken from patients with the diagnosis of I – IV grade astrocytic glioma tumors were analyzed. Increased *NRP1* and *SEMA3F* gene expressions were observed in higher grade (III-IV) gliomas as compared with lower grade gliomas (*Mann-Whitney* test, $p = 0.001$ and $p = 0.01$, respectively). In contrast, increased *SEMA3C* gene expression was observed in lower grade (I-II) gliomas (*Mann-Whitney* test, $p < 0.05$). The upregulation of *SEMA3A* was associated with poor patient prognosis in higher grade astrocytoma (*Kaplan-Meier* test, $p < 0.01$). Increased *SEMA3F*, *SEMA3A* and *NRP1* gene expressions were observed in older patients (*Mann-Whitney* test, $p < 0.01$, $p < 0.05$ and $p < 0.01$, respectively). In addition, the correlation between *SEMA3F* and *NRP1* expressions was found (*Spearman's rank correlation coefficient*, $r_s = 0{,}644$ and $p < 0.001$). For all studied genes (*SEMA3A*, *SEMA3C*, *SEMA3F* and *NRP1*) statistical difference between genders was not observed. These findings suggest that *NRP1* and *SEMA3F* genes could be used as a prognostic biomarkers for determining the malignancy grade of glioma, whereas changes in *SEMA3A* and *SEMA3C* gene expression could be used to predict the survival of patients.

[1] Johnson DR, Ma DJ, Buckner JC, Hammack JE. Conditional probability of long-term survival in glioblastoma: A population-based analysis. Cancer. 2012;118(22):5608-13.
[2] Bussolino F, Giraudo E, Serini G. Class 3 semaphorin in angiogenesis and lymphangiogenesis. Chem Immunol Allergy. 2014;99:71-88.
[3] Mumblat Y, Kessler O, Ilan N, Neufeld G. Full-length semaphorin-3C is an inhibitor of tumor lymphangiogenesis and metastasis. Cancer Res. 2015;75(11):2177-86.
[4] Sabag AD, Bode J, Fink D, Kigel B, Kugler W, Neufeld G. Semaphorin-3D and semaphorin-3E inhibit the development of tumors from glioblastoma cells implanted in the cortex of the brain. PLoS One. 2012;7(8):e42912.
[5] Huang C, Wang Y, Huang JH, Liu W. Sema3A drastically suppresses tumor growth in oral cancer Xenograft model of mice. BMC Pharmacol Toxicol. 2017;18(1):55.
[6] Nasarre P, Kusy S, Constantin B, Castellani V, Drabkin HA, Bagnard D. Semaphorin SEMA3F has a repulsing activity on breast cancer cells and inhibits E-cadherin-mediated cell adhesion. Neoplasia. 2005;7(2):180-9.
[7] Hao J, Yu JS. Semaphorin 3C and Its Receptors in Cancer and Cancer Stem-Like Cells. Biomedicines. 2018;6(2).

# CHARACTERIZATION OF *XANTHOMONAS* SPP. ISOLATES OBTAINED FROM FABACEAE PLANTS

Dovilė Čepukoit[1*], Karolis Sivickis[1], Monika Kałużna[2], Daiva Burokienė[1]

[1]Nature Research Centre, Laboratory of Plant Pathology, Vilnius, Lithuania
[2]Research Institute of Horticulture, Department of Phytopathology, Laboratory of Bacteriology, Skierniewice, Poland
dovile.cepukoit@gamtc.lt

*Xanthomonas* genus bacteria are plant pathogens that can cause a variety of diseases, including necrosis, vascular or parenchymatous diseases on leaves, stems or fruits of many plants. Various species of these pathogenic bacteria are extensively studied due to their ability to cause economic, industrial and ecological losses. Recently, the classification, genetic diversity, and phylogenetic relationships are being studied more extensively. The aim of this study was to identify and to characterize the species of *Xanthomonas* genus using molecular methods and to estimate which species of these pathogenic bacteria may cause serious diseases on Fabaceae plants in Lithuania.

During the 2017-2018 plant material from different species of Fabaceae was collected. In this study more than 280 bacterial isolates were obtained. The yellowish bacterial colonies were tested for Gram stain and Gram-negative isolates were selected for further molecular studies. For genetic characterization DNA from bacterial isolates was extracted using CTAB method [1] and protocol of Aljanabi and Martinez [2]. *Xanthomonas*-like isolates were analyzed by PCR using genus specific primers. Phenotypic characterization of *Xanthomonas* isolates was confirmed using pathogenicity and hypersensitive reaction tests on potato, tomato and tabaco plants. Genetic diversity and phylogenetic analysis with four molecular methods was performed: three enzymes for PCR melting Profile (PCR MP) were used; repetitive PCR (rep-PCR) with primers for BOX, ERIC and REP were performed, dendrograms were constructed using FREETREE software; four housekeeping genes for multilocus sequence analysis (MLSA) of *Xanthomonas* spp. bacteria were used, sequences were analyzed using the SeqMan software package LASERGENE (DNASTAR, Madison, USA), following the results phylogenetic trees were constructed with the MEGA 7 software package; for detection of type three effector (T3E) genes, PCRs with 15 primers were performed. Furthermore, we completely investigated only a small part of the bacterial collection and the other part is still under investigation.

[1] Wilson, K., 2001: Preparation of genomic DNA from bacteria. Current protocols in molecular biology, 56(1): 2-4.
[2] Aljanabi S. M., Martinez I., 1997: Universal and rapid salt-extraction of high quality genomic DNA for PCR-based techniques. Nucleic acids research, 25(22): 4692–3.

# HAEMOTOLOGICAL AND BIOCHEMICAL INDICES IN RAINBOW TROUT (*ONCORHYNCHUS MYKISS*) AFTER 4, 7- AND 14-DAYS EXPOSURE WITH METALS MIXTURE

Eglė Stasiūnaitė[2]*, Brigita Čapukoitienė[1], Reda Eglinskaitė[1], Milda Stankevičiūtė[1], Tomas Makaras[1], Laura Butrimavičienė[1]

[1] Nature Research Centre, Institute of Ecology, Akademijos Str. 2, LT-08412 Vilnius, Lithuania
[2] Vilnius University, Life Sciences Center, Institute of Biosciences, Saulėtekio av. 7, LT-10257 Vilnius, Lithuania
egle.stasiunaite96@gmail.com

Chemical agents can able to induce changes in the various haematological components [1]. Estimation of haematology and biochemical parameters (determination of glucose concentration in blood) is used as an index of fish health status in a number of fish species to detect physiological changes following variety of stressors [2, 3, 4]. Furthermore, non-destructive haematological technique and changes in the proportion of blood parameters may be indicative and sensitive biomarker of the biological effects of metals in fish [5].

The aim of this study was to analyse the changes in haematological and biochemical parameters in Rainbow trout's (*Oncorhynchus mykiss*) peripheral blood after exposure with metals (Zn – 0.1, Cu – 0.01, Ni – 0.034, Cr – 0.01, Pb – 0.014 and Cd – 0.0015 mg/L (2013/39/EB; 2008/105/EB)) mixture at various time points (4, 7 and 14 days). Haematological biomarkers were assessed as differentiation of leukocytes and the relative abundance of thrombocytes and different types of leukocytes in fish blood and the measurement of blood haematocrit levels. Biochemical indices – assessed concentration of glucose in *O. mykiss* blood.

*O. mykiss* peripheral blood samples were taken from fish caudal vein with synergies (rinsed with 3.8% sodium citrate solution). The differential count of leukocytes and thrombocytes was performed by microscopy at a magnification of ×1,000 (Olympus BX51, Japan) in Giemsa-stained peripheral blood samples. Differentiation of leukocytes and the relative abundance of analysed cell types was determined by counting a total of 300 leukocytes on each slide [4]. Haematocrit levels were determined directly by microhematocrit centrifugation. Concentrations of glucose in fish blood were determined by using the automatic Glucose Analyser (EKSAN-Gm, ANALITA, Joint-Stock Company Ltd, LITHUANIA). The minimum detection limit of the blood glucose method is from 2 to 30 mmol/L and the error for repeated measurements (precision) is ≤5%. Minimal blood sample volume per measurement is 50 µL.

Statistically significant induction of thrombocytes was estimated in all exposure groups of treated *O. mykiss*. The number of thrombocytes in fish from 7-days group was 5 times higher, while after 14 days treatment there was found only 4 times higher induction in comparison to control. In all exposure groups there was observed two times higher elevation of neutrophils number. Moreover, induction in neutrophils (neutrophilia) and monocytes after 7 days exposure differed significantly in comparison to control. The levels of haematocrit and concentrations of glucose did not vary significantly between exposure groups and in comparison, to control.

Based on the presented results it can be concluded that chemical stress (exposure with six metals mixture) induces both thrombocytosis and neutrophilia in fish. The measuring of haematological parameters in fish is useful biomarker and was performed in wide range of fish species after exposure to different trace metals [5, 6, 7]. The understanding of toxicant uptake, behaviour and responses in fish may, therefore, have a high ecological relevance and pollution risk prediction.

[1] J.C. Bloom, J.T. Brandt, Toxic responses of the blood. In: Casarett, L.J., Klaassen, C.D. (Eds.), Casarett and Doull's, Toxicology: The Basic Science of Poisons, 7th ed. McGraw-Hill Medical, New York, 455–484 (2008).
[2] F. Ejraei, M. Ghiasi, H. Khara, Evaluation of hematological and plasma indices in grass carp, Ctenopharyngodon idella, with reference to age, sex, and hormonal treatment – Arch. Pol. Fish, 23, 163-170 (2015).
[3] P. Satheeshkumar & G. Ananthan & D. Senthil Kumar & L, Jagadeesan, Haematology and biochemical parameters of different feeding behaviour of teleost fishes from Vellar estuary, India, Comp Clin Pathol DOI 10.1007/s00580-011-1259-7, (2011).
[4] F. Fazio, V. Ferrantelli, G. Piccione, C. Saoca, M. Levanti, M. Mucciardi, Biochemical and hematological parameters in European sea bass. (Dicentrarchus labrax Linnaeus, 1758) and Gilthead sea bream (Sparus aurata Linnaeus, 1758) in relation to temperature, Vet. arhiv 88, 397-411, (2018).
[5] R. Maheswaran, A. Devapaul, S. Muralidharan, B.Velmurugan, S. Ignacimuthu, Haematological studies of fresh water fish, Clarias batrachus (L.) exposed to mercuric chloride, International Journal of Integrative Biology IJIB, Vol. 2, No. 1, 49 (2008).
[6] S. F. Alwan, A. A. Hadi, A. E. Shokr* Garyounis, Alterations in Hematological Parameters of Fresh Water Fish, Tilapia zillii , Exposed to Aluminum, University Press Journal of Science and Its Applications Vol. 3, No. 1, 12-19, April (2009).
[7] Sheeba Ali Siddiqui, C. M. Noorjahan, Toxicity of copper nanoparticle on haematology and biochemistry of fish, tilapia mossambica. International research journal of pharmacy, Int. Res. J. Pharm, 2018, 9 (10).

# ISOLATION AND CHARACTERIZATION OF OUTER-MEMBRANE VESICLES FROM OPPORTUNISTIC PATHOGEN *ACINETOBACTER BAUMANNII*

Emilija Karazijaitė[1], Jūratė Skerniškytė[1], Edita Sužiedėlienė[1]

[1] Institute of Biosciences, Life Sciences Center, Vilnius University, Saulėtekio av. 7, 10257, Vilnius, Lithuania
e.karazijaite@gmail.com

Gram-negative bacterium *Acinetobacter baumannii* is recognized among most dangerous microorganisms in health care settings worldwide. This opportunistic pathogen causes variety of nosocomial infections to immunocompromised patients. Due to its ability to acquire multidrug resistance and persist in clinical environment, infections caused by *A. baumannii* are difficult to cure. An inefficiency of antibiotics against this pathogen encourages the development of alternative treatments [1].

*A. baumannii* secretes nano-spherical structures called outer-membrane vesicles (OMV) which contain variety of bacterial molecules. Most abundant proteins found in OMVs are outer-membrane porin OmpA and β-lactamase AmpC [2]. OmpA acts as multivirulent factor and possibly influence OMVs biogenesis [3], while AmpC contributes to antimicrobial resistance of *A. baumannii*. Therefore outer-membrane vesicles are considered to play an important role in *A. baumannii* pathogenesis. Due to high prevalence of bacterial antigens on the surface, OMVs are one of the most promising vaccine candidates against *A. baumannii* [4].

The aim of this work was to isolate and characterize outer-membrane vesicles from clinical *A. baumannii* strain. For this purpose we isolated OMVs from *A.baumannii* clinical strain and *ompA* gene knockout mutant. OMVs were visualized using transmission electron microscopy (TEM). Quantity and protein content of OMVs were measured using Bradford assay and SDS-PAGE. Detection of OmpA was performed using Western blot. AmpC β-lactamase activity using nitrocefin assay was performed as well.

According to our results, *A. baumannii* Δ*ompA* mutant produced ~3 times more OMVs comparing with wild-type strain and showed differences in OMVs protein profiles. Also both OMVs from wild-type and *ompA* deletion mutant contained active β-lactamase AmpC. However absence of OmpA resulted in slower hydrolysis of nitrocefin.

In conclusion, we confirmed that OmpA plays an important role in biogenesis of outer-membrane vesicles secreted by clinical *A. baumannii* strain and possibly contributes to the bacterial resistance to β-lactam antibiotics.

[1] Peleg, A.Y., Seifert, H., and Paterson, D.L. (2008). Acinetobacter baumannii: Emergence of a Successful Pathogen. Clin. Microbiol. Rev. 21, 538–582.

[2] Jin, J.S., Kwon, S.-O., Moon, D.C., Gurung, M., Lee, J.H., Kim, S.I., and Lee, J.C. (2011). Acinetobacter baumannii Secretes Cytotoxic Outer Membrane Protein A via Outer Membrane Vesicles. PLoS ONE 6, e17027.

[3] Moon, D.C., Choi, C.H., Lee, J.H., Choi, C.-W., Kim, H.-Y., Park, J.S., Kim, S.I., and Lee, J.C. (2012). Acinetobacter baumannii outer membrane protein a modulates the biogenesis of outer membrane vesicles. J. Microbiol. 50, 155–160.

[4] Chen, W. (2015). Current advances and challenges in the development of Acinetobacter vaccines. Hum. Vaccines Immunother. 11, 2495–2500.

# MOLECULAR IDENTIFICATION OF *SARCOCYSTIS* SPECIES IN MUSCLES OF THE HERRING GULL (*LARUS ARGENTATUS*) IN LITHUANIA

Evelina Juozaitytė-Ngugu, Dalius Butkauskas, Petras Prakas

Institute of Ecology, Nature Research Centre, Akademijos St. 2, Vilnius, LT-08412, Lithuania

(juozaityt.evelina@gmail.com)

*Sarcocystis* are protozoan parasites characterised by an obligatory prey-predator two-host life cycle. Sarcocysts are formed mainly in muscles of intermediate hosts, while sporocysts develop in small intestine of definitive host. In the period of 2015-2018, having examined leg muscles of 46 herring gulls in Lithuania, sarcocysts were detected in 12 birds (20.1%). *Sarcocystis* spp. were characterized using light microscopy (LM) and first internal transcribed spacer (ITS1) region sequences analysis. By LM, one morphological type of sarcocyst was distinguished. Sarcocysts were microscopic, ribbon-shaped, had smooth and thin (about 1 μm) cyst wall, and contained banana-shaped bradyzoites. Based on molecular analysis, four *Sarcocystis* species, *S. wobeseri*, *S. lari*, *S. halieti* and *S. columbae* were identified. It should be noted that it was impossible to distinguish *Sarcocystis* species detected by LM. Species identified in the herring gull were previously found in birds of families Anatidae, Columbidae, Laridae and Phalacrocoracidae. Thus, *Sarcocsytis* species using the herring gull as intermediate host are not host specific. Furthermore, it was demonstrated that one infected bird can harbour morphologically indistinguishable *Sarcocsytis* species. In conclusion, we recommend examining several *Sarcocsytis* isolates from one bird of genus *Larus*.

# THE ANTIBACTERIAL ACTIVITY OF SILVER NANOPARTICLES

Gabija Šakalytė[1], Julija Armalytė[1], Robertas Galinis[2], Andrius Aukštuolis[2], Gediminas Galinis[2], Edita Sužiedėlienė[1]

[1] Institute of Biosciences, Life Sciences Center, Vilnius University, Vilnius, Lithuania
[2] "Rho nano" UAB, Vilnius, Lithuania
gabija.sakalyte@gf.stud.vu.lt

In recent years, multidrug resistant (MDR) microorganisms have become a major challenge towards successful treatment of various infectious diseases. Unresponsiveness of MDR microbes to various antimicrobial drugs often leads to increased time and cost of treatment and higher rates of morbidity and mortality. These problems have led to the growth of interest in research of alternative antimicrobial treatments free of resistance and high cost.

One of the most promising methods for managing resistant microorganisms is treatment with silver nanoparticles (AgNPs). It has been proved that interaction with AgNPs has lethal effect on both Gram-positive and Gram-negative microorganisms including multidrug resistant microorganisms [1]. There are four main modes of silver nanoparticles action against various microorganisms which include AgNPs adhesion to microbial cells and penetration inside the cells, modulation of transmembrane transport and generation of reactive oxygen species (ROS). Moreover, it was demonstrated that bactericidal efficiency of AgNPs highly depends on their size making 5-10 nm nanoparticles the most lethal to different microorganisms [2].

In this work, we have tested the antimicrobial effects of 7 nm silver nanoparticles, manufactured by "Rho nano", UAB. To assess the ability of AgNPs to inhibit the growth of the bacteria, minimum inhibitory concentrations (MIC) of the particles were determined by microdilution method [3]. The experiments were performed with *E. coli* DH5α strain bacteria. AgNPs used in these experiments were suspended in ethanol, $H_2O$ or polyvinylpyrrolidone (PVP) solution. We have observed that nanoparticles suspended in aqueous solutions tended to aggregate and this process decreased their ability to inhibit bacterial growth. In order to solve this problem AgNPs were suspended in PVP solution which reduces aggregation process. Results have shown that *E. coli* treatment with AgNPs was lethal to the bacteria. Furthermore, as expected AgNPs suspended in PVP solution demonstrated lower MIC values than AgNPs suspended in ethanol or aqueous solutions.

[1] Agnihotri S, Mukherji S and Mukherji S. Size-controlled silver nanoparticles synthesized over the range 5–100 nm using the same protocol and their antibacterial efficacy. RSC Adv., 2014, 4 , 3974 -3983.
[2] Dakal TC, Kumar A, Majumdar RS, Yadav V. Mechanistic Basis of Antimicrobial Actions of Silver Nanoparticles. Front Microbiol. 2016;7:1831. Published 2016 Nov 16. doi:10.3389/fmicb.2016.01831.
[3] Wiegand I, Hilpert K, Hancock RE. Agar and Broth dilution methods to determinate the minimal inhibitory concentration (MIC) of antimicrobial substances. Nat Protoc, 2008, 3: 163–175.

# HIPPOCAMPAL ASTROCYTES WITH TRIPLE ALZHEIMER'S DISEASE MUTATION HAVE ALTERED MITOCHONDRIAL FUNCTION AND RESPONSE TO POLY (I:C) SIGNAL

Gabrielė Vydmantaitė[1], Lina Jankauskaitė[2], Zbigniev Balion[2,3], Julius Liobikas[3], Dmitry Lim[4], Ramunė Morkūnienė[5], Aistė Jekabsone[1,2]

[1]Laboratory of Molecular Neurobiology, Neuroscience Institute, Lithuanian University of Health Sciences, Kaunas, Lithuania
[2]Laboratory of Pharmaceutical Sciences, Institute of Pharmaceutical Technologies, Lithuanian University of Health Sciences, Kaunas, Lithuania
[3]Department of Biochemistry, Faculty of Medicine, Medical Academy, Lithuanian University of Health Sciences, Kaunas, Lithuania
[4]Department of Pharmaceutical Sciences, Università del Piemonte Orientale, Novara, Italy
[5]Department of Drug Chemistry, Faculty of Pharmacy, Medical Academy, Lithuanian University of Health Sciences, Kaunas, Lithuania

Virus-induced inflammation is known to accelerate progression of the most prevalent neurodegenerative disorder – Alzheimer's disease (AD) [1]. Mitochondria are key players in immuno-metabolic responses and antiviral signaling via mitochondrial antiviral-signaling protein (MAVS) pathway [2]. In AD, neurodegeneration starts from hippocampus, and astrocytes are important mediators of neuronal dysfunction and death [3,4].

In our study, we investigated mitochondrial function and reactive oxygen species (ROS) production in response to virus signal-mimicking polyinosinic:polycytidylic (Poly (I:C) sequence in hippocampal astrocytes containing three AD-related mutations (APPswe/Tau-P301L/PS-1M146V, further referred to as TG). Immortalized hippocampal astrocyte TG and wild type (WT) lines were generated by means of retroviral transfection of SV40 [5], mitochondrial function was assessed by Oroboros oxygraph-2k system, mitochondrial superoxide production was determined by MitoSOX and fluorescence microscope, image processing was performed by ImageJ, and statistical analysis – by SigmaPlot v13 software.

TG astrocytes had suppressed mitochondrial respiration and higher ROS production compared to the WT cells. Moreover, they demonstrated no mitochondrial response to Poly (I:C) treatment, whereas WT cells reacted to the virus primer by decrease in mitochondrial respiration and burst in mitochondrial ROS.

These results suggest that TG astrocytes have mitochondrial dysfunction and therefore respond differently to virus infections comparing to normal astrocytes. Further investigation of the virus-induced mitochondrial changes in hippocampal astrocytes can shed light on the pathogenesis of neurodegeneration.

[1] Deleidi M, Isacson O., Viral and inflammatory triggers of neurodegenerative diseases. Sci Transl Med.; 4(121):121ps3 (2012)
[2] Loetsch C, Warren J, Laskowski A, Vazquez-Lombardi R, Jandl C, Langley DB, et al. Cytosolic Recognition of RNA Drives the Immune Response to Heterologous Erythrocytes. Cell Rep. 2017;21(6):1624–38.
[3] Mu Y, Gage FH. Adult hippocampal neurogenesis and its role in Alzheimer's disease. Mol Neurodegener. 2011;6(1):85.
[4] Sofroniew M V., Vinters H V. Astrocytes: Biology and pathology. Acta Neuropathol. 2010;119(1):7–35.
[5] Rocchio F, Tapella L, Manfredi M, Chisari M, Ronco F, Ruffinatti FA, Conte E, Canonico PL, Sortino MA, Grilli M, Marengo E, Genazzani AA, Lim D. Gene expression, proteome and calcium signaling alterations in immortalized hippocampal astrocytes from an Alzheimer's disease mouse model. Cell Death Dis. 2019 Jan 10;10(1):24.

# SINGLE NUCLEOTIDE POLYMORPHISM OF VARIOUS GENES AND MALE INFERTILITY

Giedrė Vidutytė[1, 2], Živilė Gudlevičienė[2, 3], Aušra Stumbrytė[2, 3]

[1 1]Institute of Biosciences, Vilnius University Life Sciences Center, LT-10257 Vilnius, Lithuania
[2]Fertility Center Santara, Vilnius university Hospital Santaros Clinics, LT-08661 Vilnius, Lithuania
[3]Biobank, National Cancer Institute, LT-08660 Vilnius, Lithuania
giedre.vidutyte@gf.stud.vu.lt

During the past decades infertility of various populations around the World is growing. Usually the risk factors for male's subfertility are unknown. However, genetic polymorphisms in methylenetetrahydrofolate reductase (*MTHFR*) and *TP53* are suspected to have a role in idiopathic male infertility. The purpose of this study was to analyze the distribution of *MTHFR* 677C>T and *TP53* 72Arg>Pro polymorphisms amongst idiopathic infertile Lithuanian men whose partners were undergoing *in vitro* fertilization (IVF) treatment and to find associations between these polymorphisms and various clinical data.

61 men from Fertility Center Santara were included and all of them signed Informed consent before the study (permission of Vilnius Regional Committee of Bioethics No 158200-14-743-260). After IVF, remaining sperm cells were collected and transported to the Biobank (Vilnius, Lithuania) for the future analysis. The sperm quality was evaluated according to the World Health Organization criteria and separated into four groups: normospermic, polyspermic, asthenospermic and oligoasthenospermic. The presence of *MTHFR* 677C>T and *TP53* 72Arg>Pro polymorphisms was analysed by PCR and PCR-RFLP after extracting genomic DNA from sperm cells. The frequency of polymorphic variants and their distribution according to sperm quality was calculated using statistical analysis.

After sperm evaluation from 61 men, 33 were normospermic, 8 polyspermic, 15 asthenospermic and 4 oligoasthenospermic. 8% of all men had *TP53* 72ProPro genotype, 89% - 72ProArg and 3% - 72ArgArg genotype. When only asthenospermic and oligoasthenospermic patients were taken into consideration, the distribution of genotypes was 10%, 85% and 5% respectively.

33% of all men had *MTHFR* 677CC genotype, 57% - 677CT and 10% - 677TT genotype. When only asthenospermic and oligoasthenospermic patients were taken into consideration, the distribution of genotypes was 35%, 59% and 6% respectively.

Statistical analysis showed that there were no significant differences in MTHFR 677C>T and TP53 72Arg>Pro polymorphism's distribution between patients with different sperm quality.

In our pilot study we did not find any statistical differences in the distribution of polymorphic variants *MTHFR* 677C>T and *TP53* 72Arg>Pro according to men sperm quality results. However, more clinical samples needed to be included in the analysis, especially men who are asthenospermic, oligospermic or oligoasthenospermic.

# DISTRIBUTION OF FOLLICLE-STIMULATING HORMONE RECEPTOR (*FSHR*) POLYMORPHISMS IN LITHUANIAN WOMEN

Indre Strauzaite[1, 2], Zivile Gudleviciene[2, 3], Ausra Stumbryte[2, 3]

[1]Institute of Biosciences, Vilnius University Life Sciences Center, LT-10257 Vilnius, Lithuania
[2]Fertility Center Santara, Vilnius university Hospital Santaros Clinics, LT-08661 Vilnius, Lithuania
[3]Biobank, National Cancer Institute, LT-08660 Vilnius, Lithuania
indre.strauzaite@gf.stud.vu.lt

**Objectives:** To our knowledge, this is the first study that observes FSHR Asn680Ser and Thr307Ala polymorphisms in Lithuanian women. The aim of this study is to investigate *FSHR* (follicle-stimulating hormone receptor) Asn680Ser and Thr307Ala polymorphisms and their association with clinical data in women undergoing assisted reproductive procedures at Fertility Center Santara. Ovarian stimulation is one of the most important steps in assisted reproductive procedures, amount and quality of retrieved oocytes often determines pregnancy success. FSHR polymorphisms could be biological markers for ovarian stimulation prediction and outcome prognosis.

**Keywords:** FSH receptor, DNA polymorphism, Ovarian stimulation, Asn680Ser, Thr680Ala, SNP, Assisted reproductive procedures.

**Materials and methods:** 66 women were included in this study. All women signed Informed consent (permission of Vilnius Regional Committee of Bioethics No 158200-14-743-260). Follicular fluid with remaining granulosa cells were collected after ultrasound controlled ovarian punction procedure and transported to Biobank (Vilnius, Lithuania), where DNA was extracted. Asn680Ser polymorphism was determined by PCR-RFLP and Thr307Ala – by nested PCR-RFLP. Age, amount and quality of retrieved oocytes, zygotes, embryos and procedure outcome (pregnancy) was registered in each woman.

**Results:** The frequency of Ser680Ser, Asn680Ser and Asn680Asn variants in women was 38, 45, and 17%, respectively, distribution of Thr307Thr, Thr307Ala and Ala307Ala variants was 30, 50 and 20%, respectively. Asn680Asn carriers provided more oocytes than other allelic variants – 12,60±8,49, Asn680Ser carriers provided 10,23±5,23 oocytes and Ser680Ser carriers provided less than other allelic varients – 9,36±5,70 oocytes, however differences were not statistically significant.

**Conclution:** Although Ser680Ser carriers provided less oocytes than other allelic variants, the differences were not statistically significant. Regardless statistically significance the further analysis of various SNP and their combination is needed to find the biological markers for the ovarian stimulation prediction.

# ENVIRONMENTAL GENOTOXICITY AND RISK ASSESSMENT IN THE GULF OF RIGA (BALTIC SEA) USING FISH, BIVALVES, AND CRUSTACEANS

Janina Pažusienė[1], Laura Butrimavičienė, Janina Baršienė, Milda Stankevičiūtė, Roberta Valskienė

Nature Research Centre, Akademijos str. 2, LT-08412 Vilnius, Lithuania
janina.pazusiene@gamtc.lt

The main objective of the present study was to assess the environmental genotoxicity using different bioindicators (Mollusca, Arthropoda, and Chordata phyla) collected at 14 study stations in the Gulf of Riga. The levels of nuclear abnormalities (micronuclei (MN) and nuclear buds (NB)) were evaluated in peripheral blood erythrocytes of flounder (*Platichthys flesus*), herring (*Clupea harengus*), and eelpout (*Zoarces viviparous*), in gill cells of the Baltic clam (*Macoma balthica*) and for the first time in gill cells of isopods *Saduria entomon*. Environmental genotoxicity risk in the Gulf of Riga was assessed using MN responses in three fish species and clams.

Blood samples were collected from 88 *P. flesus*, 89 *C. harengus*, and 22 *Z. viviparous* specimens caught during r/v "Walther Herwig" sampling cruise using standard bottom or pelagic trawls. Gills were dissected from 84 of *M. balthica* and 42 of *S. entomon* specimens sampled with the Van Veen grab (0.1 $m^2$) according to the HELCOM guidelines during r/v "Aranda" sampling campaign.

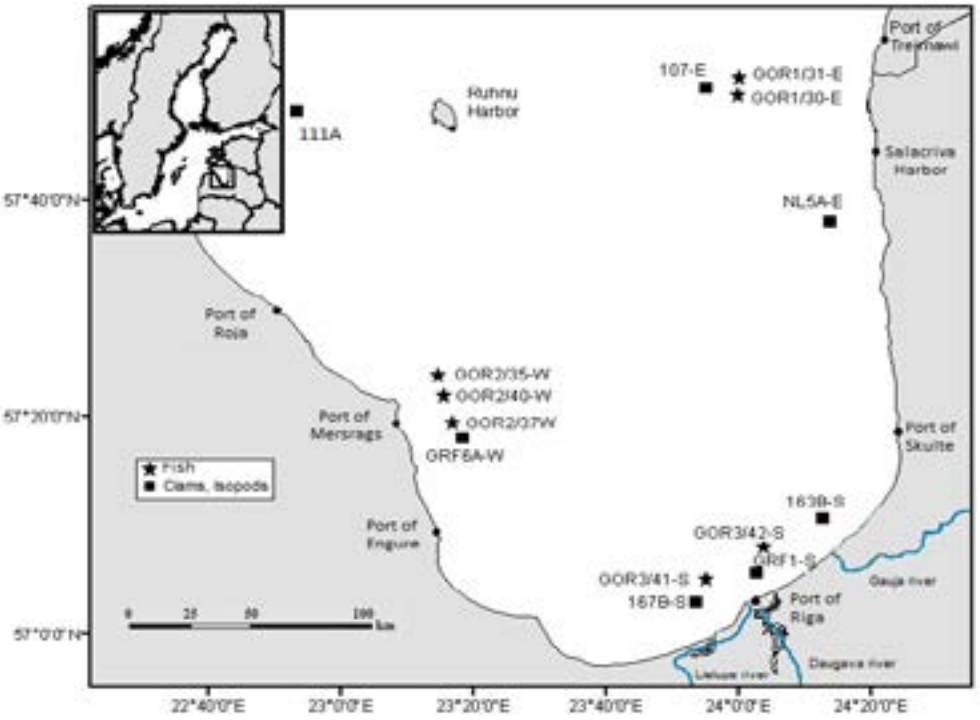


Fig. 1. Study stations in the Gulf of Riga

Increased frequency of MN and NB in organisms from investigated sites of the Gulf of Riga indicates the presence of pollution with genotoxic agents. The highest frequency of micronuclei (MN/1000 cells) was detected in eelpout caught at station GOR3/41-S and was equal to 0.68‰, in herring at GOR3/41-S station (0.38‰), in flounder at GOR2/37-W (0.61‰). In all three fish species caught at station GOR1/30-E, the highest induction of nuclear buds (NB) was determined with the gradient of NB responses in fish - eelpout (0.37‰) < herring (0.47‰) < flounder (0.84‰).

The highest induction of MN and NB in gill cells of *M. balthica* and *S. entomon* was recorded in specimens from station 111A, which is located on the open sea in Gulf of Riga (offshore sea zone). The frequency of MN in clams was equal to 6.1‰, in isopods, 4.59‰. Both species caught at the same station revealed the highest values of nuclear buds (4.69‰ in clams, 6.09‰ in isopods). The lowest MN incidences (0.94‰) were registered in isopods from station 107-E. Moreover, isopods from station 107-E revealed the lowest level of NB (0.72‰).

The environmental genotoxicity risk was assessed using four different bioindicators (three fish species and clams) collected in the Gulf of Riga. The highest genotoxicity risk was determined in 8 out of 14 study stations investigated in the Gulf of Riga Analysis of MN levels revealed an exceptionally high risk for flounder inhabiting four out of seven stations, for eelpout one out of three stations, and for clams collected from four out of seven study stations. Low genotoxicity risk level, according to four different bioindicators, was attributed for eelpout and only in one station.

According to elevated MN responses in fish (herring and eelpout) and the risk assessment (there were found exceptionally high risk levels for flounder, eelpout, and clams), southern coastal area of Gulf of Riga could be considered as the most affected by genotoxin's pollution. The highest induction of NB in all investigated fish species was at station GOR1/30-E (eastern coastal area).

# COMPARISON OF AUTOTOXIC EFFECTS OF SOLIDAGO SPECIES

Birutė KARPAVIČIENĖ[1,*], Julija DANILOVIENĖ[1], Roberta VYKERTAITĖ[2]

[1] Institute of Botany, Nature Research Centre, Vilnius, Lithuania
[2] Institute of Biosciences, Life Sciences Center, Vilnius Lithuania
daniloviene.julija@gmail.com

*Solidago canadensis* L. and *S. gigantea* Aiton. are highly invasive species which widely spread in Europe and threaten local plant communities. Distribution of natural hybrid of *S. canadensis* and local species S. *virgaurea* L., known as *S.* x *niederederi* Khek., also expands rapidly. One of reasons why invasive species are so successful is their allelopathic activity.

The aim of this work was to compare allelopathic effect of all *Solidago* species occurring in Lithuania on germination of *Solidago* seeds (autotoxicity). *Solidago canadensis* and *S. ×niederederi* were used as target species. The aqueous extracts of dried green leaves in six concentrations were used. Total percentage of germination, radicle and hypocotyl length of seedlings were measured and the response ratio to treatment was counted. A factorial ANOVA was used to analyze the effect of each factor. In case of significant interactions, a t-test was used to test differences between mean values of treatments.

The inhibitory effect of *Solidago* leaf extracts was target species specific. *S. canadensis* was much more sensible to *Solidago* leaf extracts than *S. ×niederederi* ($F=68.85$, $p< 0.001$). The inhibitory potential of all four tested *Solidago* species did not differ statistically ($F=1.40$, $p=0.251$). Therefore, stronger allelopathic effect in nature could be achieved only by higher biomass of invasive species.

# CASE REPORT: SKIN *CRYPTOCOCCAL* INFECTION IN RENAL-TRANSPLANT RECIPIENT

Justina Mackevičiūtė [1], Miglė Jarašūnienė [2,3], Emilija Šerpytienė [2,3], Jonas Lauraitis [2,3], Raimundas Meškauskas [4], Jūratė Grigaitienė [2,3]

[1]Vilnius University Faculty of Medicine
[2]Vilnius University Faculty of Medicine, Clinic of Infectious Diseases and Dermatovenereology, Vilnius, Lithuania
[3]Vilnius University Hospital Santaros Klinikos, Centre of Dermatovenereology, Vilnius, Lithuania
[4]National Centre of Pathology, Vilnius, Lithuania
jusma17@gmail.com

BACKGROUND: Cryptococcosis is the infection caused by the encapsulated yeast Cryptococcus neoformans, a dimorphic fungus. Although the primary site of infection is most often the lungs, the disease frequently manifests involving the skin in approximately 10-15% of cases. Dissemination occurs most often in the immunocompromised host, such as those with AIDS, lymphoreticular malignancy, those on long-term immunosuppression and others [1]. The prevalence in organ transplanted patients reportedly is 2.8%. The age of onset more common over the age of 40 years in male sex. Clinically, it may appear as painless papule, which then becomes nodule with surrounding erythema that may ulcerate and exude a liquid [2]. The distinct histopathologic patterns show - oval, thick-walled spherule surrounded by a polysaccharide capsule [3]. Special staining with methylene blue may be performed to demonstrate the capsule. We present a case of skin Cryptococcal infection in renal-transplant recipient.

CASE REPORT: A 69-year-old woman, cadaveric renal transplant recipient for 26 months presented with papular, nodular and ulcerative lesions on both hands and left cheek.
The patient had a significant past medical history of long standing renal failure and hemodialysis for 18 months. She received a related-donor kidney transplant when she was 67 years old. And therefore she had been treated with systemic tacrolimus, mycofenolatum mofetilum and methylprednisolone. Seven months later it had been noted a nodule on the right hand, which slowly enlarged and finally ruptured into a small ulcer. Histology showed epidermal and hair follicle epithelium proliferation and latent inflammatory infiltration with possible infection of Cryptococcus.
Initially treatment with fluconazole 200 mg PO a day resulted in only slight improvement and new lesions appeared.
Physical examination revealed a cyanotic nodule measuring 2 cm, surrounded by erythema with central ulceration and liquid exudation.
The second histological examination showed granulomatous inflammation, most possible infection - Cryptococcus.
Exudate from the lesion serology examination showed secondary infection of Curvularia sp., which did not require additional treatment.
The diagnosis of skin Cryptococcosis was made. Treatment with itraconazole 200 mg PO a day and topical therapy of Nizoral® washing liquid 2-3 times a week, Travocort® and clotrimazolum 2 times a day was started and after one month showed marked improvement.

CONCLUSION: Cryptococcus usually affect immunocompromised host. It is frequently localized in the lungs and rarely involves the skin. Cutaneous lesions often provide the opportunity for early diagnosis by lesional biopsy.

[1] Liapis K, Taussig D, Cotter FE, Gribben JG. Cutaneous cryptococcosis in Hodgkin lymphoma. Br J Haematol. 2014 Feb. 164(4):467.
[2] Minta DK, Traoré AM, Coulibaly I, et al. [Non-neuromeningeal cryptococcosis in patients with AIDS in Bamako, Mali: 2 case reports.]. J Mycol Med. 2013 Dec 30.
[3] Molina-Leyva A, Ruiz-Carrascosa JC, Leyva-Garcia A, Husein-Elahmed H. Cutaneous Cryptococcus laurentii infection in an immunocompetent child. Int J Infect Dis. 2013 Dec. 17(12):e1232-3. [Web]. [Read: 2018 11 30].

# ANTAGONISTIC MICROORGANISMS EFFICIENT FOR BIOLOGICAL CONTROL OF FUNGAL PATHOGEN OF *PINUS* SPP.

Dovilė Čepukoit[1], Julija Šepetovskaja[2], Karolis Sivickis[1*], Daiva Burokienė[1]

[1]Nature Research Centre, Laboratory of Plant Pathology, Vilnius, Lithuania
[2]Vilnius University, Life Science Centre, Institute of Biosciences, Vilnius, Lithuania
karolis.sivickis@gamtc.lt

Pine (*Pinus*) stands occupies the largest area in Lithuanian forests (34,6%). This genus of coniferous has tremendous economic importance, but emerging plant pathogens are posing serious threat to the forests. The latest observations of forest health indicated that 1,5% of pine trees were damaged by fungal diseases in Lithuania [1].

In 2017, the observation and evaluation of disease symptoms on *Pinus* spp. trees was done. Special attention was given to the pine needles, which showed tip dieback, red bands and small black fruit bodies. These disease symptoms are similar to Dothistroma Needle Blight (DNB), also commonly known as "red-band disease", "red spot" or "red-band needle blight" and is one of the most important foliage diseases of *Pinus* spp. worldwide [2][3][4]. Then, plant material (needles, buds and twigs) from native and introduced trees of seven species of *Pinus* (*P. sylvestris* 'Beuvronensis', *P. mugo* 'Frisia', *P. strobur*, *P. nigra*, *P. banksiana* xp *contorta*, *P. ponderosa* var. *scopulorum* and *P. parviflora* 'Glauca') was selected. During our research, 187 fungal isolates were obtained and a fungal pathogen *Dothistroma* spp. was detected and identified.

DNB affects over 80 species of *Pinus*, as well as other species in the Pinaceae [5]. Therefore, the second part of our work was to perform proof of the concept experiments with specific fungal antagonistic species in order to get better understanding on their biological control properties. In this study, 78 fungal isolates from 36 morphogroups obtained from *Pinus* spp. and 24 fungal isolates from Laboratory of Plant Pathology (Nature Research Centre, Vilnius) collection for antagonistic activity against *Dothistroma* spp. were investigated. As screening of potential biocontrol agents is essential for their further development and suitability to use them for biocontrol, further research will be followed with effects of the pathogen *in vivo*.

The research was performed by grant „InvazBio" (No. S-LU-18-10) from the Research Council of Lithuania within joint Lithuanian-Ukrainian Cooperation Programme in the Fields of Research and Technologies.

[1] Lithuanian Statistical Yearbook of Forestry 2017, Ministry of Environment and State Forest Service, 2017, ISSN 1648-8008, Kaunas, Lithuania.
[2] R. E. Bradshaw, Dothistroma (red-band) needle blight of pines and the dothistroma toxin: a review. Forest Pathology **34**, 163-185 (2004).
[3] R. Drenkhan, V. Tomešová-Haataja, S. Fraser et al., Global geographic distribution and host range of *Dothistroma* species: a comprehensive review, Forest Pathology **46**, 408-442 (2016).
[4] I. A. S. Gibson, Dothistroma blight of *Pinus radiata*, Annual Review of Phytopathology **10**, 51-72 (1972).
[5] M. S. Watt, D. J. Kriticos, S. Alcaraz et al., The hosts and potential geographic range of Dothistroma needle blight, Forest Ecology and Management **257**, 1505-1519 (2009).

# SYNTHESIS AND ANTIMICROBIAL ACTIVITIES OF CARBAZOLE DERIVATIVES AS POTENTIAL ANTIBACTERIAL AGENTS

Kestutis Dabrovolskas[1], Gintare Krucaite[1], Eigirdas Skuodis[1], Ilona Jonuskiene[2], Dalius Gudeika[1]

[1] Department of Polymer Chemistry and Technology, Kaunas University of Technology, Lithuania
[2] Department of Organic Chemistry, Kaunas University of Technology, Lithuania
kestutis.dabrovolskas@ktu.edu

Even though there are many antibacterial agents multidrug resistant bacteria poses a huge threat to public health and has become one of the biggest health problems in the last decade. Therefore, there is an urgent need to develop and provide novel and more potent antibacterial agents to overcome drug resistance [1].

Nitrogen containing heterocycles are widely spread in nature, they are found in various forms such as part of amino acid tryptophan, serotonin and they can be essential part of plant alkaloids [2]. That is exactly what carbazole is, a nitrogen containing aromatic heterocyclic compound, which can be found in nature as carbazole alkaloid that is isolated from various part of the plant. Since some carbazole derivatives show a good antioxidative activity they can be also found in some microorganisms [3]. Such carbazole ring containing alkaloids are carbomycins, that were first isolated from *Streptoverticillium ehimense* and showed good activity against various organisms, which made carbazoles a desirable target for further biological research [4]. Carbazole and its derivatives are extensively used in various chemistry fields such as photoelectrical materials, dyes, supramolecular recognition [5,6,7,8]. In medicinal chemistry they show potential activity against various organisms, tumor and they can be a multifunctional agent to help in the treatment of neurological disorders [9]. Therefore, carbazole and its derivatives are attractive target to develop and produce new antibacterial compounds that could help resolve drug resistance problem.

In this work a series of carbazole-based derivatives were synthesized, and their antibacterial activity was evaluated against *Bacillus subtilis* and *Escherichia coli* Various functional groups were introduced into carbazole-based compounds in order to investigate their biological activity. Synthesized compounds were screened for their *in vitro* antibacterial activity against Gram-positive *Bacillus subtilis* and Gram-negative *Escherichia coli* according to the disc diffusion method. The minimum inhibitory concentration (MIC) was determined by the serial dilution technique using dimethylsulphoxide (DMSO) as a solvent. All compounds were evaluated at the concentrations of the antibacterial agents ranging from 62.5 to 1000 μg/mL and compared against chloramphenicol, ciprofloxacin and furacin after overnight microorganisms growth. The results are displayed in Table 1.

**Table 1.** *Antimicrobial activity data of carbazole-based compounds.*

| | Compound | 1a | 1b | 2a | 2b | 3 | 4 | 5 | Chloramphenicol | Ciprofloxacin | Furacin |
|---|---|---|---|---|---|---|---|---|---|---|---|
| MIC (mg ml-1) | *B. subtilis* | 62.5 | 62.5 | 62.5 | 125.0 | 62.5 | 62.5 | >1000 | >512.0[5] | 6.0[10] | 12.5[11] |
| | *E.coli* | 250.0 | 250.0 | 125.0 | 125.0 | 125.0 | 125.0 | >1000 | 64.0[5] | 6.0[10] | 6.0[11] |

DMSO – negative control.

[1] D.Y. Aksoy, New antimicrobial agents for the treatment of Gram-positive bacterial infections, Clinical Microbiology and Infection **14**, 411-420 (2008).
[2] T. Indumathi,T. Brant, M. Zeller, K.J.R. Prasad, Synthesis and antibacterial evaluation of bromo phemyl substituted carbazoles, Indian Journal of Chemistry **52B**, 405-413 (2013).
[3] Y. Tachibana, H. Kikukazi, N. Lajis, N. Nakatani, Antioxidative Activity of Carbazoles from *Murraya koenigii* Leaves, Journal of Agricultural and Food Chemistry **49**, 5589-5594 (2001).
[4] S. Chakraborty, B. Chakraborty, A. Saha, C. Saha, T.K. Ghosh, I. Bhattacharyya, Evaluation of antimicrobial activity of synthesized fluorocarbazole derivatives based on SAR, Indian Journal of Chemistry **56B**, 701-708 (2017).
[5] F. Zhang, L. Gan, C. Zhou, Synthesis, antibacterial and antifungal activities of some carbazole derivatives, Bioorganic & Medicinal Chemistry Letters **20**, 1881-1884 (2010).
[6] J.F Morin, M. Leclerc, D. Adès, A.Siove, Polycarbazoles: 25 Years of Progress, Macromolecular Rapid Communications **26**, 761-778 (2005).
[7] D. Kim, J.K Lee, S.O Kang, J. Ko, Molecular engineering of organic dyes containing N-aryl carbazole moiety for solar cell, Tetrahedron **63**, 1913-1922 (2007).
[8] C. Zhou, L. Gan, Y. Zhang, F. Zhang, G. Wang, L. Jei, R. Geng, Review on supermolecules as chemical drugs, Science in China Series B: Chemistry **52**, 415-458 (2009).
[9] A. Głuszyńska, Biological potential of carbazole derivatives, European Journal of Medicinal Chemistry **94**, 405-426 (2015).
[10] A.E. Martin, K.J.R. Prasad, Synthesis and characterization of carbazole derivatives and their antimicrobial studies, Acta Pharmaceutica Sinica B **56**, 79–86 (2006).
[11] R. Balamurali, K.J.R. Prasad, Synthesis, characterization and pharmacological activities of 5,6,11,12-tetrahydroindolo[2,3-a]carbazole derivatives, IL Farmaco **56**, 229-232 (2001).

# *GEOBACILLUS SPP.* INDUCED BIOSYNTHESIS OF SILVER NANOPARTICLES AND THEIR ANTIFUNGAL PROPERTIES

Kotryna Čekuolytė[1], Renata Gudiukaitė[1], Vitalij Novickij[2,3], Audrius Maneikis[4], Eglė Lastauskienė[1]

[1]Vilnius University Life Sciences Center, Institute of Biosciences, Saulėtekio av. 7, LT-10257 Vilnius, Lithuania
[2]Institute of High Magnetic Fields, Vilnius Gediminas Technical University, Naugarduko st. 41, 03227, Vilnius, Lithuania
[3]Department of Electrical Engineering, Vilnius Gediminas Technical University, Naugarduko st. 41, 03227, Vilnius, Lithuania
[4]Faculty of Electronics, Vilnius Gediminas Technical University, Saulėtekio av. 11, LT-10223 Vilnius, Lithuania.
Presenting author: kotryna.cekuolyte@gf.stud.vu.lt

The growing number of yeast caused skin diseases and resistance to the antifungal therapy are the key problems that boost the research for the new antifungal materials. The antimicrobial effect of silver has long been known, thus nowadays antimicrobial properties of silver nanoparticles (AgNPs) are receiving more interest. The biological synthesis of nanoparticles is effective and environmentally friendly method compared to chemical or physical synthesis of this nanomaterial.

The present study reports the extracellular biosynthesis of AgNPs using secretomes of *Geobacillus spp*. strains 18, 25, 95 and 612 and 2 mM AgNO3. $Ag^+$ reduction and formation of AgNPs in all *Geobacillus spp*. secretomes were confirmed by UV-Visible (UV-vis) Spectroscopy and Scanning Electron Microscopy (SEM). Obtained AgNPs were tested for their antimicrobial activities against pathogenic yeast (*Candida lusitaniae*, *Candida guilliermondii*). The antifungal activity of the AgNPs was evaluated by growth inhibition (100 µg/ml concentration of each AgNPs for 2 days). Also, the synergistic effect of the AgNPs and electroporation was examined (concentration of AgNPs was 5 µg/ml, parameters of electroporation were single 100 µs impulse, 2,5; 5; 7,5; 10; 12,5; 15 kV/cm electric field). The results show that all tested AgNPs have antifungal effect against *Candida* yeast (the most effective results were obtained with *Geobacillus spp.* strain 25 AgNPs). Furthermore, the synergistic effect of AgNPs and electroporation was established.

The results obtained in this study suggests that *Geobacillus spp.* strains 18, 25, 95 and 612 are appreciable tool for preparation of AgNPs. Moreover, due to their antifungal activities, AgNPs have a potential to be used as biocontrol agents against pathogenic yeast.

# Cocaine induced myocardial infarction - myth or reality?

Lina Matuliauskaitė[1], Jolita Badarienė [2,3]

[1] Country Vilnius University Faculty of Medicine, Vilnius, Lithuania
[2] Clinic of Cardiac and Vascular Diseases, Institute of Clinical Medicine of the Faculty of Medicine, Vilnius University, Vilnius, Lithuania
[3] Vilnius University Hospital Santaros Klinikos, Vilnius, Lithuania
lina.matuliauskaite@gmail.com

Background: In 2018 more than 17 million European people (5.1 % of 15- to 64-year-olds) are reported to have used cocaine at least once in their life, and 3.5 million are estimated to have done so in the last year (1.1 % on average) [1]. In Lithuania during the five years from 2006–10 a total of 8.9 % (127 of 1 423) intoxications in drugs and psychotropic substances involved cocaine [2,3].

Case presentation: A 37-year-old male was brought to our emergency department with sudden onset of retrosternal chest pain radiating to the all chest cavity and lasting for 30 minutes. Paramedics had given him aspirin and diazepam tablets. On arrival to hospital patient blood pressure was 116/61 mmHg, heart rate 45 beats/minute and his lung sounds were normal. He had a body mass index 24.7 kg/m2 and smoked 6-7 cigarettes per day. There was no personal or family history of cardiac disease, he was neither diabetic nor hypertensive, but had an increased serum cholesterol level 6.08 mmol/l and low-density lipoprotein 4.22 mmol/l for which he was not on treatment. ECG demonstrated ST elevation in inferior and lateral leads (ST elevation above 0.5-1mm in II, III, aVF and V3-6, V7-9) and patient was admitted directly for cardiac catheterisation. The serum Troponin-I level was recorded at 1392.6 ng/L (normal range <14 ng/L on high-sensitivity Troponin-I), confirming the diagnosis of myocardial infarction. Coronary artery angiography was performed within 1 h of admission, but there were no residual stenosis, which could have represented mild coronary artery disease or persistent vasospasm. As there was no evidence of atherosclerotic disease percutaneous coronary intervention was not performed and patient was transferred to cardiology reanimation and intensive care unit for comprehensive examination. On further questioning patient confessed, that he had taken cocaine by inhalation a day ago. Blood tests, including haematology, biochemistry and gases were all within ranges. Radiological imaging revealed normal chest X-ray.

Conclusion: Myocardial infarction is rare, but possibly deadly consequence of cocaine consumption. Although it is difficult to determine incidence of cocaine associated MI because of lack of diagnostic algorithms, we hope that this case will contribute to raising public awareness about cocaine use and its impact to our health.

[1] European Monitoring Centre for Drugs and Drug Addiction (2018), European Drug Report 2018: Trends and Developments, Publications Office of the European Union, Luxembourg. pp. 17-96.
[2] EMCDDA (2014), Emergency health consequences of cocaine use in Europe. A review of the monitoring of drug-related acute emergencies in 30 European countries, Technical report, European Monitoring Centre for Drugs and Drug Addiction, Lisbon.
[3] de Millas, W, Haasen C, Reimer J, Eiroa-Orosa, F. J. and Schaefer I. (2010), 'Emergencies related to cocaine use: a European multicentre study of expert interviews', European Journal of Emergency Medicine, 17(1), pp. 33–36.

# A NOVEL HIGH MOLECULAR WEIGHT BACTERIOCIN PRODUCED BY A THERMOPHILIC BACTERIUM

Manta Vaičikauskaitė, Marija Ger, Mindaugas Valius, Eglė Lastauskienė, Lilija Kalėdienė, Arnoldas Kaunietis

Department of Life Sciences Center, Vilniaus University, Lithuania
manta.vaicikauskaite@gmc.stud.vu.lt

We have revealed that *G. stearothermophilus* 15 secretes a novel high molecular weight antibacterial protein geobacillin 26, which belongs to the III class of bacteriocins. We successfully purified native bacteriocin and determined its amino acid sequence and structural gene based on MS/MS analysis and genome mining. Geobacillin 26 has no sequence similarities to any known function proteins. This is the first report of high molecular weight bacteriocin produced by thermophilic bacteria. Usually, producers of III class bacteriocins encode proteins responsible for immunity to the bacteriocin [1, 2, 3, 4]. The genomic context of geo26 does not include any genes that might encode proteins related to the latter function. The cell wall lysis assay confirmed that geobacillin 26 is not a cell wall degrading enzyme, as some III class bacteriocins [5], most probably it is killing cells by non-lytic mode of action. Geobacillin 26 is the first bacteriocin of this class, which has activity against thermophilic bacteria. Moreover, it has narrow antibacterial spectrum against some thermophilic *(Para)Geobacillus* sp. strains. We determined the MIC value of geobacillin 26 inhibiting growth of thermophilic bacterium *P. genomospecies* 1 NUB36187 – 620 nM (16.3 µg/mL). It is thermo-labile bacteriocin, its antibacterial activity is reduced by 50% after incubation at 60˚C and completely lost after incubation at 90°C temperature.

This study revealed the function of hypothetical protein encoded in *G. stearothermophilus* 15. Geobacillin 26 does not contain any conservative amino acid sequences and domain structures characteristic to other bacteriocins. Hypothetical proteins sharing sequence similarity with this novel bacteriocin are encoded in other thermophilic *Geobacillus* sp., *Anoxybacillus* sp. or mesophilic *Bacillus* sp. bacteria. Geobacillin 26 is very interesting subject for research on novel antibacterial proteins, which potentially may have a new mode of action. Further studies could focus on the characterization of antibacterial activity mechanisms of the bacteriocin, its targets in the cell or receptors. Moreover, geobacillin 26 could be applied as antibacterial agent against other thermophilic bacteria, which are undesirable in some food or biotechnological industry.



[1] Kiss, A. *et al.* Cloning and characterization of the DNA region responsible for megacin A-216 production in Bacillus megaterium 216. *J. Bacteriol.* **190,** 6448–6457 (2008).
[2] Beukes, M., Bierbaum, G., Sahl, H. G. & Hastings, J. W. Purification and partial characterization of a murein hydrolase, millericin B, produced by Streptococcus milleri NMSCC 061. *Appl. Environ. Microbiol.* **66,** 23–28 (2000).
[3] Swe, P. M., Heng, N. C. K., Cook, G. M., Tagg, J. R. & Jack, R. W. Identification of DysI, the immunity factor of the streptococcal bacteriocin dysgalacticin. *Appl. Environ. Microbiol.* **76,** 7885–7889 (2010).
[4] DeHart, H. P., Heath, H. E., Heath, L. S., LeBlanc, P. A. & Sloan, G. L. The lysostaphin endopeptidase resistance gene (epr) specifies modification of peptidoglycan cross bridges in Staphylococcus simulans and Staphylococcus aureus. *Appl. Environ. Microbiol.* **61,** 1475–1479 (1995).
[5] Acedo, J. Z., Chiorean, S., Vederas, J. C. & Belkum, M. J. Van. The expanding structural variety among bacteriocins from Gram-positive bacteria. *FEMS Microbiol. Rev.* **42,** 805–828 (2018).

# LIVING UNDER A RAIN OF FAECES: MAMMALS IN THE COLONY OF CORMORANTS

Marius Jasiulionis, Laima Balčiauskienė, Linas Balčiauskas

Nature Research Centre, Akademijos 2, Vilnius, Lithuania
jasiulionis.m@gmail.com

In Lithuania, after 100 years of eradication, great cormorants (*Phalacrocorax carbo sinensis*) started to breed again in 1985. In 2015 the number of breeding pairs in the largest colony in Lithuania (located on the Curonian Spit near the Juodkrantė village) was estimated at about 3800 breeding pairs. Great cormorants are able extremely to change the ecosystem in territory of the breeding colony. A single bird consumes 400 g fish per day and depositing 20-50 g faeces. Great cormorants spent about 20 h daily in breeding colonies and about 80% of faeces are depositing there [1]. Deposited faeces overload the ecosystem with N and P by $10^4$ to $10^5$ times [2]. Exchanged chemical properties of soil affecting plants [3], lichens [4], insects and lizards [5]. There have been no investigations on how the cormorant colony influences mammals.

The aim of our study was to investigate small mammals biodiversity and abundance in the Juodkrantė great cormorant colony and estimate other mammals activities in the colony. Snap trap line method was used for small mammal research. The activities of other mammals was evaluated using camera traps (system with a trigger or a sensor that activates a camera to take a photograph when an animal is present) and snow transect counts (density of the footprints in the snow) methods.

Seven small mammal species were trapped in the different zones of the great cormorant colony and in the control zone. The dominant species was yellow necked mouse (*Apodemus flavicollis*), accounting for 70.5% of all trapped individuals, with bank vole (*Myodes glareolus*) subdominant (25.0%). The proportion of other species is very low. Reduction in biodiversity and abundance of small mammals was found in the most active parts of the colony. Snow transect count method shown in winter the area influenced by cormorants are attractive for the wild boar (*Sus scrofa*), roe deer (*Capreolus capreolus*), red fox (*Vulpes vulpes*). But there are no differences of use the territory of control and impacted zones for moose (*Alces alces*), European hare (*Lepus europaeus*), red squirrel (*Sciurus vulgaris*) and marten (*Martes* sp.). Using camera traps nine mammal species were registered in Juodkrantė cormorants colony. Most often colony was visited by roe deer, wild boar and moose. Two invasive species were also registered: common raccoon (*Procyon lotor*) and sika deer (*Cervus nippon*).

[1] P. Klimaszyk, P. Rzymsky, The complexity of ecological impacts by great cormorants, Hydrobiologia **771**, 13-30 (2016).
[2] L. V. Garcia, C. Ramo et al., Protected wading bird species threaten relict centenarian cork oaks in a Mediterranean biosphere reserve: a conservation management conflict, Biological Conservation **144**: 764–771 (2011).
[3] W. B. Anderson, G. A. Polis, Nutrient fluxes from water to land: seabirds affect plant nutrient status on Gulf of Californiaislands, Oecologia **118**: 324–332 (1999).
[4] K. Żółkóś, M. Kukwa, R. Afranowicz-Cieślak, Changes in the epiphytic lichen biota in the Scots pine (*Pinus sylvestris*) stands affected by a colony of grey heron (*Ardea cinerea*): a case study from northern Poland, Lichenologist **45**: 815–823 (2013).
[5] G. A. Polis, S. D. Hurd, Linking marine and terrestrial food webs: allochthonous input from the ocean supports high secondary productivity on small islands and coastal land communities, The American Naturalist **147**: 396–423 (1996).

# ROLE OF BIO-FERTILIZERS IN YIELD AND PRODUCTIVITY OF SPRING WHEAT CULTIVATION

Modupe Doyeni[1], Vita Tilvikiene[1], Skaidre Suproniene[1]

[1]Institute of Agriculture, Lithuanian Research Centre for Agriculture and Forestry.
modupe.doyeni@lammc.lt

The steady increase in global population has led to an increased demand for food supply however, with limited land resources. This has led to seeking for processes that would increase the productivity and quality of food crops while also ensuring that the soil and the environment at large are not put at risk from the demand placed on them. There is a gradual rise in the use of bio-fertilizers in the production of food crops and these are fast becoming alternatives to the use of chemical fertilizers in agriculture. Bio-fertilizers are produced from the anaerobic breakdown of different types of biomass including animal wastes, agricultural wastes and plant wastes. They are able to compete favourably in terms of yield, productivity, nutrient availability, cost effectiveness and reduced environmental risks. Digestate manures are good examples of bio-fertilizers. They contain a high level of nutrients, are relatively stable and affordable and have been effective in solving the challenges of waste management.

The aim of this on-going study is to compare the role of fertilization of different digestate manures (pig, chicken and cow manure) and mineral nitrogen fertilizers on the growth and productivity of spring wheat cultivation. The analysed digestate manures were composed of varying organic and mineral nutrients that are important in plant growth. Chicken manure digestate was found to be richer in nitrogen and potassium than other digestate manures. The experiment field was split fertilized with 90 and 80 kg N $ha^{-1}$ at wheat tillering and stem elongation stages. Parameters such as Chlorophyll index, soil moisture, leaf area index, grain quality (stalk length and spike length), grain yield and soil microbial activities were measured.

The results showed that Pig digestate manure had more influence on spring wheat productivity in comparison with other digestate manures in terms of chlorophyll content. There was a significant correlation between the chlorophyll content, Nitrogen use efficiency and yield in the plots treated with mineral nitrogen and pig manure. The baseline results from the first year of spring wheat cultivation using digestate manures suggest that their use as fertilizers in dry and warm weather conditions can lead to favourable productivity.

# ELECTRIC ACTIVITY OF ALPHA2-ADRENE REACTIVE POPULATIONS OF THE NUCLEAR SOLITARY TRACT IN THE ENDOTOXEMIA CONDITIONS

Zhanna Hladkova

Institute of Physiology of the National Academy of Sciences of Belarus, Minsk, Republic of Belarus;
gladkova_z@mail.ru

*Escherichia coli* endotoxins play a key role in the pathogenesis of various diseases of the central nervous system, such as Parkinson's disease, Alzheimer's disease, etc. It is believed that one of the triggers for the development of these pathologies is an increase in the endotoxin concentration in the blood, which is also observed during aging [1]. With age, the risk of developing hypertension increases. In this connection, studies of the central regulation of vital functions under conditions of endotoxemia modeling and the use of the antihypertensive first aid clonidine are promising.

The purpose of the study was an experimental analysis of the electrical activity of the neuronal populations of the solitary tract nucleus during changes of the functional status of alpha 2-adrenoreceptors under endotoxemia.

Acute experiments were performed on anesthetized (nembutal and urethane in the proportion of 30 and 500 mg / kg intraperitoneally) male Wistar rats weighing 280-320 g (n=32). Lipopolysaccharide of *Escherichia co*li was slowly injected into the right femoral vein (LPS; 1,10,100 μg/kg/ ml). After 2 minutes, clonidine was administered intranasally (50 μl, 0.01% of solution). An apyrogenic physiological solution was used as a solvent for LPS, and it was used as a control. The coordinates of the solitary tract nucleus were calculated using the brain atlas of Wistar rats: 13.3 - 13.5 mm caudal to Bregma, 1.0 mm lateral to the midline and 8.0 8.1 mm ventral to the surface of the skull [2]. Neural activity was recorded by a glass-insulated tungsten electrode (2-3 MΩ). An electrocardiogram was recorded in the II standard lead in order to control the functional state of the animals. Background activity was recorded for 15 minutes, then LPS was administered by intravenous injection for 1 minute and then clonidine was intranasally instilled. The total registration time was 120 minutes. All experiments were carried in compliance with the recommendations of the European Convention on Humane Treatment of Laboratory Animals [3].

Intranasal administration of apyrogenic physiological solution against endotoxemia (LPS 1 μg/kg/ml) at 60 minutes of the experiment was found to be accompanied by a decrease in the frequency of neuronal discharges compared with background activity (from 5.9 ± 1.4 pulses/s to 2.8 ± 0,7 pulses/s, $p < 0.05$, n=8). No significant effects were observed at doses of 10 and 100 μg/kg/ml. Heart rate (HR) increased by 50± beats per minute (bpm) with LPS infusion at a dose of 1 μg/kg/ml at the 40th minute of the experiment.

Intranasal application of clonidine after intravenous infusion of LPS at a dose of 1 μg/kg/ml by the 60th minute of the experiment was characterized by a decrease in the frequency of neuronal discharges compared with background activity (from 1.8 ± 0.5 pulses/s to 0.6 ± 0, 2 pulses/s, $p < 0.05$, n = 8), while the HR decreased 80 to 120 minutes from 400 ± 50 bpm to 235 ± 28 bpm ($p < 0.05$) compared to with background.

Intravenous infusion of LPS at a dose of 10 μg / kg / ml in combination with the intranasal administration of clonidine by the 120th minute of the experiment was accompanied by an increase in the frequency of neuronal discharges compared with background activity (from 2.9 ± 1.1 pulses/s to 5.2 ± 1.1 pulses/s, $p < 0.05$, n=8) and a decrease in heart rate also at the 120th minute of the experiment (from 370 ± 70 bpm to 260 ± 40 bpm, $p < 0.05$)

Intranasal administration of apyrogenic physiological solution with simultaneous intravenous administration of LPS at a dose of 100 μg / kg / ml by the 40th minute of the experiment caused a decrease in the frequency of neuronal discharges compared with background activity (from 3.8 ± 0.8 pulses/s to 2.1 ± 0.4 pulses/s, $p < 0.05$, n=8) with a subsequent increase in neural activity by the 120th minute of the experiment. The heart rate decreased from 389 ± 32 bpm to 300 ± 20 bpm ($p < 0.05$) by the 60th minute of observation.

The experiments have demonstrated that intranasal application of clonidine against endotoxemia is accompanied by a change of the heart rate and neuronal electrical activity of the solitary tract nucleus, indicating disruptions in the central and cardiovascular systems after injection of endotoxin Escherichia coli into the bloodstream. Therefore, it can be assumed that it is advisable to investigate the level of LPS in the blood before prescribing antihypertensive drugs.

---

[1] Zhao Y., Jaber V., Lukiw W.J. Secretory Products of the Human GI Tract Microbiome and Their Potential Impact on Alzheimer's Disease (AD): Detection of Lipopolysaccharide (LPS) in AD Hippocampus. Front Cell Infect Microbiol. 7, 1-9 (2017).
[2] Paxinos, Y., Watson C. The rat brain in stereotaxic coordinates. San Diego: Academic Press. 256 p.1998.
[3] European Convention for the protection of vertebrate animals used for experimental and other scientific purposes. Strasbourg: Europ. Treaty Series, 1986. № 123. P. 48.

# THE USE OF SUPERBRIGHT LIGHT EMITTING DIODES IN THE STUDY OF POPULATION DYNAMICS OF AQUATIC AND SEMI-AQUATIC BEETLES (INSECTA: COLEOPTERA)

Elena Rodionova[1,2], Alexey Sazhnev[3], Alexey Pachkin[4], Irina Balackhnina[5]

[1]Laboratoty of Chemical Communication and Mass Rearing of Insects, All-Russian Research Institute of Biological Plant Protection, Krasnodar, Russia
[2]Faculty of Biology, Kuban State University, Krasnodar, Russia
[3] Laboratory of Water Invertebrate Ecology, Papanin Institute for Biology of Inland Waters Russian Academy of Sciences, Borok, Russia
[4]Laboratory of Phytosanitary Monitoring, Instrumental and Technical Equipment, All-Russian Research Institute of Biological Plant Protection, Krasnodar, Russia
[5]Laboratory of pest regulation within agroecosystems, All-Russian Research Institute of Biological Plant Protection, Krasnodar, Russia
rigaey@gmail.com

Currently, about 12.600 Coleoptera species have aquatic (True Water Beetles) representatives and are to be considered as aquatic (False Water Beetles and Phytophilous Water Beetles). [1]. They form a combined ecological group that includes representatives of all Coleoptera suborders (Adephaga, Polyphaga, Myxophaga, Archostemata). Each year, new taxons are described within this order. Aquatic and semi-aquatic beetles can serve as bioindicators of water quality [2]. The use of light traps is one of efficient methods to study the insect fauna composition. As a rule, either mercury-vapour lamps or fluorescent lamps are used as a light source to attract insects. However, they are not quite feasible for collecting samples in remote places because of their power demands which limit their mobility. Conversely, the use of light-emitting diodes (LEDs) reduces power consumption by 50–60%; moreover, this light source is more environmentally friendly [3], portable and can be adapted to the trichromatic colour vision of insects. Considering these requirements, trap applicators with super bright LEDs were developed in the ARRIBPP (All-Russian Research Institute of Biological Plant Protection) to collect insect samples [4].

The sample collection was conducted in June-September 2018 in the ARRIBPP grounds located in Krasnodar boundaries (45°02'56.5"N 38°52'22.1"E). The trap was placed at a height of 1.7 m.

A trap applicator was used to attract insects. Its structure includes a lid with a solar battery that is attached to two mutually perpendicular plates fastened to a light emitter cone. A cylinder with an imago container for insects caught forms the lower part of this device. There are light sensors which contain photosensing elements on the backside of the lid. Strips with LEDs of ultraviolet light (365–400 nm) in the upper part and LEDs of white light in the lower part (colour temperature: 5000 K) were used as guides toward the imago container to make insects come down into it. The LEDs were automatically activated at dusk thanks to the photosensing elements. At dawn the samples were collected from the trap and the species richness (S) was evaluated by using the Menhinick's index D that is the number of species divided by the square root of the number of individuals in the sample: $D = S/\sqrt{N}$; where S – the number of different species и N – the total number of individuals [5]. In parallel, the Margalef's diversity index was used: $\alpha = (S - 1)/\ln N$; where S – the number of species, N – the total number of individuals in the sample [6]. In total, 1252 specimens of Coleoptera were collected.

Nearly a third of the species diversity (33.8%) and the greatest part of the material collected (85.3%) were aquatic and semi-aquatic beetles which shows a certain selectivity of the trap applicator. The presence of artificial bodies of water built in the 1960s at a distance of over 100 m and the Kuban river 1 km away could have played an important role in obtaining these data.

Research conducted to date showed that the potential of using insect traps with superbright LEDs to collect coleopterans is rather good and they can be used as an eco-friendly technique for attracting insects. An important role here plays the selection of locations where the traps will be placed because the area within the city limit has light pollution that may compete with our traps.

[1] M.A. Jäch, M. Balke, Global diversity of water beetles (Coleoptera) in freshwater, Hydrobiologia **595**, 419–442 (2008).
[2] D. Sánchez-Fernández, P. Abellán, A. Mellado, et al., Are water beetles good indicators of biodiversity in Mediterranean aquatic ecosystems? The case of the Sigura river basin (SE Spain), Biodiv. and Cons. **15**, 4507–4520 (2006).
[3] L. Cohnstaedt, J.I. Gillen, L.E. Munstermann, Light-emitting diode technology improves insect trapping, J. Am. Mosq. Control Assoc, V. 21, №2, 331-334 (2008).
[4] V.T. Sadkovski, Yu.G. Sokolov, A.A. Pachkin et al., Insect trap applicator. Patent for utility model № 152224. 2015 May 10.
[5] Yu. A. Pesenko, Principles and methods of quantitative analysis in faunistic studies, Moscow: Nauka, (1982).
[6] R. Margalef, Perspectives in ecological theory, University of Chicago Press, (1968).

# THE INVESTIGATION OF PERSPECTIVE SPICES (AROMATIC) PLANTS IN VYTAUTAS MAGNUS UNIVERSITY

Sandra Saunoriūtė[1], Ona Ragažinskienė[1], Audrius Maruška[2], Erika Šeinauskienė[1]

[1]Sector of Medicinal Plants, Kaunas Botanical Garden, Vytautas Magnus University, Ž.E. Žilibero str. 6, LT-46324 Kaunas, Lithuania
[2]Instrumental Analysis Open Access Center, Faculty of Natural Sciences, of Vytautas Magnus University, Vileikos str. 8, LT-44404 Kaunas, Lithuania
sandra.saunoriute@vdu.lt

Research on the preservation, enhancement and improvement of human health of biodiversity, investigations of medicinal, spice (aromatic) plants (MAPs) have a scientific and practical significance not only in Lithuania, but also in the whole world. These plants are grown in green spaces, decorated with landscapes, used in the food, cosmetics, pharmaceutical industry and medicine [8].

The aim of research − to investigate the introduction of perspective spice (aromatic) plants, their biologically active compounds in the part of overground. The investigation of perspective spices (aromatic) plants introduction carried out in the Botanical Garden at Vytautas Magnus University. Analysis of secondary metabolites and antioxidant activity of MAPs are carried out using integrated sample preparation, spectrophotometric, chromatographic and microanalysis techniques [3,8]. Ecological and biological characteristics of wild and cultivated varieties of MAPs and phenology studies [2,4,5].

1997-2018 years, promising medicinal, selected (aromatic) plants: *Salvia officinalis* L., *Origanum vulgare* L., *Perilla frutescens* (L.) Britton, *Satureja montana* L, *Desmodium canadense* (L.) DC, *Hyssopus officinalis* L. In the field of *ex situ* experimental areas of sector Medicinal and spice plants collections of Botanical Garden at Vytautas Magnus University in the experimental test areas, during the introduction, promising medicines. The introduction and their applicability and significance for cultivation in green spaces and their impact on human health have been investigated [1,5,6].

The introduction of perspective spice (aromatic) plants and their applicability and significance for cultivation in green spaces and their impact on human health have been investigated. These plants are recommended for multiplication, their diversity, growing in gardens, industrial plots and for the development of herbal medicine and for improving public health in Lithuania.

[1] European pharmacopoeia. 9 Edition. Strasbourg: Council of Europe, 2, 5145, 2017.
[2] Juknevičienė G., Juronis V. Medicinal plants (Collections of Kaunas Botanical Garden of Vytautas Magnus university), 2000.
[3] Maruška A., Kornyšova O. Continuous beds (monoliths): stationary phases for liquid chromatography formed using the hydrophobic interaction-based phase separation mechanism, 59 (1) 1-48, 2003.
[4] Penkauskienė E, Rimkienė S. Lietuvos laukinių ir sukultūrintų vaistinių augalų rūšių ekologinės ir biologinės savybės: monografija. Vilnius, 1991.
[5] Ragažinskienė O., Rimkienė S. Medicinal and aromatic plants: genetic resources and cultivation in Lithuanian. Journal of Medicinal and Spice Plants, 8 (4), 189-191, 2003.
[6] Ragažinskienė O., Šeinauskienė E., Janulis V., Jankauskaitė L., Milašius A.. The influence of meteorological factors on growth and vegetation process of *Perilla frutescens* (L.) Britton in Lithuania. Medicina, 42 (8), 2006.
[7] Ragažinskienė O., Maruška A. Perspektyvių vaistinių augalų cheminės sudėties mokslinių tyrimų raida Vytauto Didžiojo universitete. Vytauto Didžiojo universiteto Botanikos sodo raštai, 15, 82-94, 2011.
[8] Secretariat of the Convention on Biological Diversity (2011a) COP 10 Decision X/17. Consolidated update of the Global Strategy for Plant Conservation 2011-2020: http://www.cbd.int/decision/cop/?id=12283.
[9] Stankevičius M., Akuņeca I., Jākobsone I., Maruška A., Comparative analysis of radical scavenging and antioxidant activity of phenolic compounds present in everyday use spice plants by means of spectrophotometric and chromatographic methods, 34 (11), 1261-7, 2011.

# RELATIONS BETWEEN OIL-DEGRADING BACTERIA *ALCANIVORAX BORKUMENSIS* AND NEMATODE *TURBATRIX ACETI*

Sarbinaz Shayhulova, Gölnur Fakhrullina, Leysan Nigamatzyanova, Farida Akhatova, Rawil Fakhrullin

Department of Microbiology, Kazan (Volga region) Federal University, Russian Federation, Republic of Tatarstan
sarbinaz2016@gmail.com

*Alcanivorax borkumensis* belongs to an important group of hydrocarbon-degrading microorganisms. This bacterium is found in low quantities in all the oceans of the world and is the dominant specie living in oil-contaminated environments [1]. There are studies that demonstrate more effective biodegradation of petroleum products during the cooperation of primary oil destructors with a higher level organism in the food chain [2]. For example, it has been demonstrated that the nematode *Caenorhabditis elegans*, cousin of *Turbatrix aceti*, increases the degradation of oil in oil-contaminated soil by regulating the number of soil microorganisms [3].

The goal of this work was to study a non-trivial model of the mutual relations of oil-degrading marine bacteria *Alcanivorax borkumensis (A. borkumensis)* with free-living soil nematodes *Turbatrix aceti (T. aceti)*.

According to the results of nematode chemotaxis using the bacteria *A. borkumensis* ($2.2\times10^9$ CFU) and *Escherichia coli* ($2.2\times10^9$ CFU) as a control, it turned out that *A. borkumensis* is not a repellent (chemotaxis index was -0.2), and nematodes have approximately the same preference for both - control (52%) and experienced bacteria (48%).

Nematodes of the same age were cultivated in three different medium: in oil-contaminated standard nutrient medium NGM (nematode growth medium) with bacterial food and without bacterial food and in not oil-contaminated medium with bacterial food.

Observation of the growth and development of nematodes was carried out using stereo- and inverted microscopy. The distribution of oil in the digestive system of the nematodes was visualized using hyperspectral and inverted microscopy. During the microscopy, oil was detected along the entire length of the nematode's digestive system (Fig. 1).

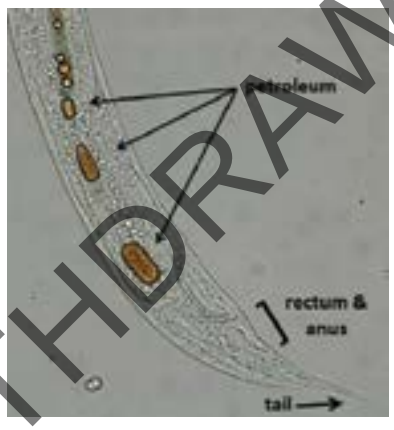


Fig. 1. The aboral part of *T. aceti* with petroleum in the digestive system.



It was found that nematodes, cultured in the absence of bacterial food in oil-contaminated medium passed through all stages of development, although they had a low reproductive potential. In oil-contaminated medium with oil-degrading bacteria nematodes developed in the same way as in a standard nutrient medium enriched with bacterial food.

Therefore, nematodes *T. aceti* can be cultivated in cooperating with the bacteria *A. borkumensis*, moreover, due to the *A. borkumensis*, reproductive potential of nematodes in oil-contaminated medium increases, which can be explained by the fact that nematodes move oil-degrading bacteria to the food source and influence their colonization.

This work was supported by RFBR Grant №18-34-00778 and by the subsidy allocated to Kazan Federal University for the state assignment in the sphere of scientific activities (project 16.2822.2017/4.6).

[1] P. N. Golyshin, V. A. P. Martins Dos Santos, M. Ferrer, Y. S. Sabirova, H. Lünsdorf, T. N. Chernikova, Olga V. Golyshina, K. N. Timmis et al., Genome sequence completed of *Alcanivorax borkumensis*, a hydrocarbon-degrading bacterium that plays a global role in oil removal from marine system, Journal of Biotechnology 106, 215-220 (2003).

[2] P. Cuny, G. Miralles, V. Cornet-Barthaux, M. Acquaviva, G. Stora , V. Grossi, F. Gilbert, Influence of bioturbation by the polychaete Nereis diversicolor on the structure of bacterial communities in oil contaminated coastal sediments, Marine Pollution Bulletin 54, 452-459 (2007).

[3] J. Zhou, D. Chen, R. Huang, G. Huang, Y. Yuan, H. Fan , Effects of bacterial-feeding nematodes on soil microbial activity and the microbial community in oil-contaminated soil, Journal of Environmental Management 234, 424-430 (2019).

# RESULTS OF ARTIFICIAL CROSSING EXPAND DATA ABOUT REPRODUCTION AND COMPOSITION OF UNUSUAL POPULATION SYSTEM (*PELOPHYLAX ESCULENTUS* COMPLEX)

Anna Fedorova[1], Eleonora Pustovalova[1]
[1]Department of Zoology and Animal Ecology, V. N. Karazin Kharkiv National University, Ukraine
annaph94@gmail.com

European water frogs from *Pelophylax esculentus* complex are an example of natural interspecies hybridization and polyploidization. Diploid and triploid hybrids *Pelophylax esculentus* (Linnaeus, 1758) can reproduce through crossing with parental species due to the phenomenon of hemiclonal inheritance. Siverskyi Donets center of diversity of water frogs (east of Ukraine) is characterized by various population systems, where hybrids (both di- and triploid) live and reproduce with only one parental species *P. ridibundus* (Pallas, 1771) (the other parental species *P. lessonae* (Camerano, 1882) is absent). In 2018 it was found that population system in floodplain lake (village Brusivka, Donetsk region) [1] consists of *P. ridibundus* individuals of both sexes and only of female triploid hybrids *P. esculentus* (R-Epf type). Such type of population system was first described by G. Lada in 2010 in lake Pidpesochne (Kreminna, Lugansk region) [1].

Previous research on reproduction of triploid hybrids showed that they appear due to diploid gametes (both male and female) produced by diploid hybrids [2]. In Brusivka neither male nor diploid hybrids were found. Therefore, we can distinguish two main problems: (i) the way of triploid appearance; (ii) absence of male hybrids.

In this study we focused on the second problem. We suggested three hypotheses: (i) genetically male individuals develop as females; (ii) male tadpoles eliminate on early stages of development (gonads are not differentiated); (iii) male tadpoles eliminate on late stages of development during metamorphosis or later (gonads are formed).

To check, which hypothesis is right, we studied 18 tadpoles produced by crossing between triploid *P. esculentus* female and *P. ridibundus* male collected in Brusivka. We got tadpoles from D. A. Shabanov, who had provided crossing. We identified tadpoles' stages of development according to Gösner [3], and then incubated tadpoles in 0.4 % colchicine for 12-18 hours. After anesthesia, sex was identified by gonad morphology [4]. The ploidy of individuals was determined by Ag-staining with addition of Giemsa-staining [5]. We estimated number of metaphase chromosomes and interphase nucleoli in cells of intestine epithelium.

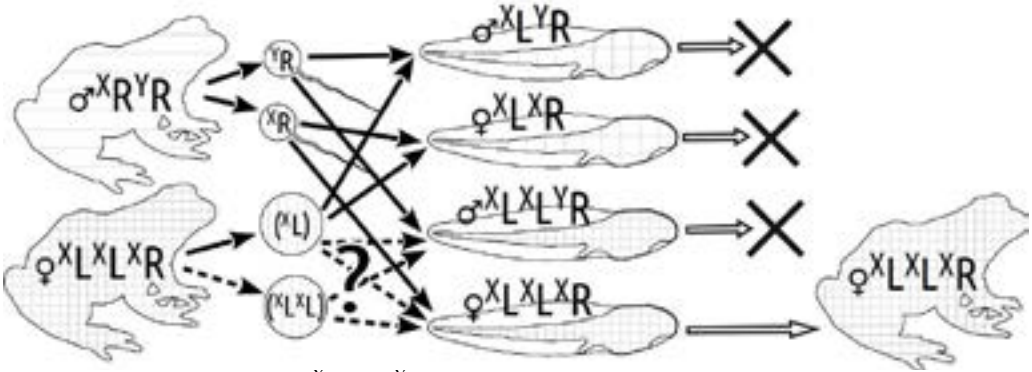


Fig. 1. Scheme of studied crossing. $^{X}$R and $^{Y}$R – female and male genomes of parental species *P. ridibundus*, $^{X}$L and $^{Y}$L – female and male genomes of parental species *P. lessonae*, ($^{X}$L) – clonal genome.

Our previous data shows that female have genotype composition LLR (2 genomes of *P. lessonae* and 1 genome of *P. ridibundus*) and can produce haploid gametes with L-genome (probably, reduplication takes place after fertilization) [1]. Based on the data of system composition we can assume that only triploid females can occur in artificial crossing. However, we found both triploid males (4 from 18 tadpoles) and diploid individuals (3 males and 7 females) (Fig. 1.). The presence of triploid males on late stage of development (from 28 and more) supports our third hypothesis (elimination takes place during metamorphosis or later). Presence of diploid individuals can be explained in 2 ways: (i) reduplication of L genome doesn't always happen; (ii) triploid females produce mix of L and R gametes. The latter is unlikely, because production of R-gametes by LLR females from various systems was never shown.

Our next steps are to repeat artificial crossings and analyze more quantity of progeny after metamorphosis, and to provide taxonomic identification of diploid and tadpoles.

[1] M. O. Drohvalenko, R. M. Makaryan, O. V. Biriuk, O. V. Korshunov, D. A. Shabanov, The paradox of the reproduction of triploid Pelophylax esculentus in the hemiclonal population systems in Brusivka (Donetsk region) and Kreminna (Lugansk region), The Journal of V. N. Karazin Kharkiv National University **29,** 142-150 (2017).
[2] D. Dedukh, S. Litvinchuk, J. Rosanov, G. Mazepa, A. Saifitdinova, D. Shabanov, A. Krasikova, Optional endoreplication and selective elimination of parental genomes during oogenesis in diploid and triploid hybrid European water frogs, Plos One **10**(4), 1–19 (2015).
[3] K. L. Gosner, A simplified table for staging anuran embryos and larvae with notes on identification. Herpetologica **16**(3), 183-190 (1960).
[4] M. Ogielska, *Reproduction of amphibians*. (Science Publishers, Enfield, New Hampshire, 2009).
[5] O. V. Biriuk, D. A. Shabanov, A. V. Korshunov, L. J. Borkin, G. A. Lada, R. A. Pasynkova, J. M. Rosanov, S. N. Litvinchuk, Gamete production patterns and mating systems in water frogs of the hybridogenetic *Pelophylax esculentus* complex in northeastern Ukraine, Journal of Zoological Systematics and Evolutionary Research **54**(2), 215-225 (2016).

# ARTIFICAL INFECTION OF THE LOBSTER COCKROACHES WITH THELASTOMID NEMATODES FROM THE MADAGASCAR HISSING COCKROACHES: A PRELIMINARY STUDY

Anna Yalova, Sofiia Shapoval, Anastasiia Tsymbaliuk, Nataliia Shliakhtova, Bohdan Yuriev, Natalia Matushkina

Educational and Scientific Center "Institute of Biology and Medicine", Taras Shevchenko National University of Kyiv, Ukraine
annnortis@knu.ua

The host specificity is an important characteristic of most parasitic species, which reflects the general evolutionary strategy of parasitism. Parasitic nematodes of the order Oxyurida (Nematoda: Oxyuroidea) comprise among other the family Thelastomatidae, which are the parasites of invertebrates. The oxyurid nematodes have a simple life cycle: eggs laid by the adult females are spread with feces of the host; ingestion of the eggs by new host individuals leads to their infection. The nematodes of the family Thelastomatidae parasitize more than 40 species of cockroaches that do not reflect their host/parasite co-speciation. In absence of genotypic characterizations, it is still unknown whether these nematodes present one species with a wide host range or several host-specific cryptic species. Here, we show preliminary results of an artificial infection of the nematode-free lobster cockroaches (*Nauphoeta cinerea*) with thelastomid nematodes collected from feces of infected Madagascar hissing cockroaches (*Gromphadorhina portentosa*). Our preliminary data indicate that eggs of thelastomid nematodes are able to infect unspecific hosts and develop until larval stages.

# REMOTE SENSING OF COASTAL UPWELLING IN THE SOUTH-EASTERN BALTIC SEA AND ITS EFFECT ON THE COASTAL ENVIRONMENT

Toma Dabulevičienė[1,2], Igor Kozlov[1,2,3], Diana Vaičiūtė[1,2]

[1]Marine Research Institute, Klaipeda University; Universiteto ave. 17, Klaipeda, Lithuania
[2]Natural Sciences Department, Klaipeda University; Herkaus Manto str. 84, Klaipeda, Lithuania
[3]Satellite Oceanography Laboratory, Russian State Hydrometeorological University, St. Petersburg, Russia
toma.dabuleviciene@adaptm.eu

Coastal upwelling, a phenomenon found in large stratified lakes, estuaries, and oceans [1] is an important process for ecologically sensitive regions of the global ocean, like the Baltic Sea. During the warm season (April-September) northerly winds are known to trigger intense occurrences of coastal upwellings in the SE Baltic Sea coast. Typically, there are about 4 upwelling events taking place per warm season each year in the study region, but their total duration might represent up to 30 % of the warm season. Wind-induced coastal upwelling is an important dynamical feature in the Baltic Sea region: it significantly changes hydro-meteorological conditions and ecosystem functioning in the SE Baltic Sea coastal zone and during rapid inflows to the Curonian Lagoon may strongly influence its environment.

In this study, we analyse the impact of coastal upwelling events on the sea surface temperature (SST) and chlorophyll-a (chl-a) concentration in the SE Baltic Sea and the Curonian Lagoon. Satellite Terra/Aqua Moderate Imaging Spectroradiometer (MODIS) SST maps for the period of 2000-2015 were used to characterize the coastal upwelling from the distribution and evolution of its surface thermal signatures. Spatial variability of chl-a induced by upwelling was assessed using MERIS/Envisat (Medium Resolution Imaging Spectrometer on board of Envisat satellite, European Space Agency) maps. For the estimation of chl-a concentration FUB processor (1.2.4 version, plug-in in BEAM/VISAT software) was applied in the coastal waters, as described and validated in [2]. In the Curonian Lagoon chl-a was estimated by semi-empirical band ratio algorithm applied to images after atmospheric correction with the 6SV. The algorithm is based on band ratio of the red and near-infrared spectral regions [3].

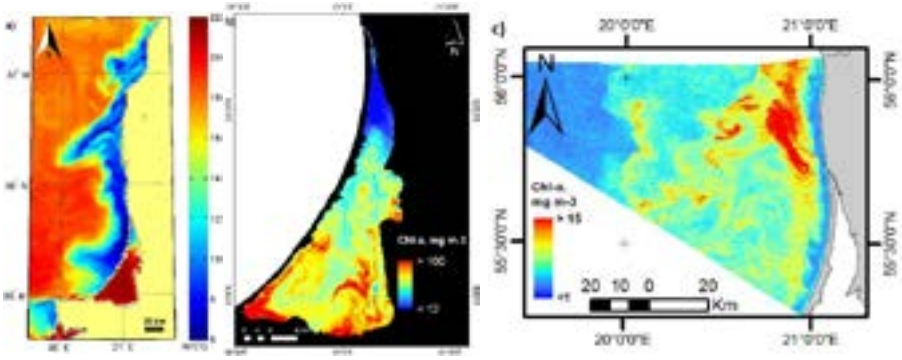


Fig. 1. Upwelling induced (a) SST and chlorophyll-a changes in the (b) Curonian Lagoon and (c) in the SE Baltic Sea.

Altogether, during April-September 2000 – 2015, 69 coastal upwelling events were registered in MODIS data from which 18 events had an influence to the pelagic environment of the Curonian Lagoon due to sea-lagoon interaction through the narrow Klaipeda Strait. A detailed analysis of coastal upwelling development, its main oceanographic characteristics together with an impact on the Curonian Lagoon and the coastal environment are presented.

We show that during extreme events cold upwelled waters with SST drop up to 15 °C are extending offshore in the form of transverse filaments of about 70 km in length (Fig. 1a). Our research evidently shows that coastal upwelling events has significant impact on the chl-a concentration changes in both the Curonian Lagoon (Fig. 1b) and the coastal area of the SE Baltic Sea (Fig. 1c).

Acknowledgments

The study was co-funded by the European Community's Seventh Framework Programme (FP7/2007-2013), grant agreement no. 606865, INFORM project and EOMORES project belonging to the EU Horizon 2020 research and innovation programme (grant agreement n°730066).

[1] Plattner, S.; Mason, D.M.; Leshkevich, G.A.; Schwab, D. J.; Rutherford, E. S. Classifying and Forecasting Coastal Upwellings in Lake Michigan Using Satellite Derived Temperature Images and Buoy Data. J. Great Lakes Res. 2006, **32**, 63–76, doi:https://doi.org/10.3394/0380-1330(2006)32[63:CAFCUI]2.0.CO;2.

[2] Vaičiūtė, D., Bresciani, M., Bučas, M., Validation of MERIS bio-optical products with *in situ* data in the turbid Lithuanian Baltic Sea coastal waters. J. Appl. Remote. Sens. 2012, 6(1), 1-20

[3] Bresciani, M., Adamo, M., De Carolis, G., Matta, E., Pasquariello, G., Vaičiūtė, D., Giardino, C., Monitoring blooms and surface accumulation of cyanobacteria in the Curonian Lagoon by combining MERIS and ASAR data. Remote Sens. Environ 2014, 146, 124-135

# *THYMUS PULEGIOIDES* α-TERPINYL ACETATE CHEMOTYPE: DISTRIBUTION IN LITHUANIA, ALLELOPATHIC AND AUTOALLELOPATHIC FEATURES

VaidaVaičiulytė [1], Kristina Ložienė [1]

[1]Institute of Botany, Nature Research Centre

vaiciulyte.vaida@gmail.com

Chemical polymorphism is characteristic of essential oil bearing medicinal and aromatic large thyme (*Thymus pulegioides*). α-Terpinyl acetate chemotype is one of six *T.pulegioides* chemotypes found in Lithuania; α-terpinyl acetate is the main chemical compound of essential oil accumulated in this chemotype [1;2]. This chemotype of *T. pulegiodes* is very rare in Europe; mean while it has not been investigated in Lithuania fully. α-Terpinyl acetate is oxygenated monoterpene. Monoterpenes are strong allelochemicals therefore can affect associated plants (i. e. to inhibit or stimulate their seeds germination and/or seedlings growth) and composition of plant communities [3;4]. The aim of study was:1) to establish prevalence of *T. pulegioides* α-terpinyl acetate chemotype in Lithuania; 2) to determine allelopathic and autoalelopathic potential of essential oil of this chemotype.

131 different habitats of *T. pulegioides* were investigated to evaluate the distribution of *T. pulegioides* α-terpinyl acetate chemotype in Lithuania. The essential oils of *T. pulegioides* were isolated by hydrodistillation in the Clevenger-type apparatus and analysed by GC/FID and GC/MS methods. Allopathic effects (through air and water) of essential oil of *T. pulegioides* α-terpinyl acetate chemotype on germination and radicles growth of *Trifolium pratense*, *Poa pratensis*, *Phleum pratense*, *Hypericum perforatum* and *T. pulegioides* were investigated in laboratory conditions.

Results showed that *T. pulegioides* α-terpinyl acetate chemotype is rare in Lithuania: α-terpinyl acetate was found only in 35 % of all investigated habitats. Amount of α-terpinyl acetate in essential oil was higher than 10 % in four investigated habitats only. The essential oil of α-terpinyl acetate chemotype differently affected on seeds germination and radicles growth of investigated species.The essential oil of this chemotype strongly inhibited seeds germination and radicles growth of *P. pratensis*; the effect through water was stronger than trough air. The inhibitory effect of α-terpinyl acetate on germination of monocotyledon *P.pratense* was weaker. The negative effect of α-terpinyl acetate chemotype on seeds germination of *T. pratense* was the lowest. The effect of the essential oil of α-terpinyl acetate chemotype on radicles growth of *H.perforatum* was stronger than on seeds germination of this species. Autoalelopathic effect of essential oil of *T. pulegioides* α-terpinyl acetate chemotype was low.

---

[1] D. Mockutė G. Bernotienė, The main citral-geranio and carvacrol chemotypes of essential lil of growing wild in Vilnius district (Lithuania), J. Agric. Food. Chem. **47**, 3787–3790 (1999)

[2] D. Mockutė G. Bernotienė, The α-terpinyl acetate chemotype of essential oil of *Thymus pulegioides* L., Biochem. Syst. Ecol. **29**, 69–73 (2001).

[3] B.K. Ehlers, A. Charpentier, E. Grendahl, 2014, An allelopathic plant facilitates species richness in the Mediterranean garrigue, J. Ecol. **102**, 176–185 (2014).

[4] Y.B. Linhart, P. Gauthier, K. Keefover-Ring, J.D. Thompson, Variable phytotoxin effects of *Thymus vulgaris* (Lamiaceae) terpenes on associated species, International journal of plant science **176 (10)**, 20–30 (2015).

# *CHARA CONTRARIA* GERMINATION FROM VARIOUS SEDIMENT BURIAL DEPTH

Vaiva Stragauskaitė, Martynas Bučas

Klaipėda University, Marine research institute, Klaipėda
vaiva.stragauskaite@jmtc.ku.lt

Charophytes are a part of littoral submerged vegetation which provide habitats, nursery, feeding grounds for various organisms and acts as sink and storage of nutrients. For many charophytes species, the dispersion, colonization and maintenance of populations depend entirely on the oospore bank. It is important to know, how environmental factors influences current status of the population and ensure success of establishment in the case of restoration.

Estuarine environment is exposed to high hydrological disturbance (resuspension and sedimentation), where oospores can be buried by sediments. Therefore, the aim of this study was to test the impact of different cover by sediments to germination of oospores from Chara *contraria,* which is a dominant charophyte in the Curonian lagoon. Charophyte oospores with sediments were collected in the lagoon at the end of the vegetation season in 2017 and stored at 4-5 $^{o}$C temperatures in the dark for month before experiment. Selected 50 viable calcified oospores were buried in the tubes with sediments at depths of 1, 5 and 10 cm (3 replicates for each depth). The experiment lasted 60 days.

Oospores germinated in the all experimental set ups, but different emergence time for germlings was observed. First germlings were observed in 1 cm sediment depth set up at the 12$^{th}$ day of the experiment, in 5 cm set up at the 21$^{th}$ day and germlings emerged from 10 cm sediment depth only on 49$^{th}$ day. Germlings developed only from 1 cm buried oospores, whereas shoots stopped growing after germination in other (5 and 10 cm) set ups. Results indicate that *C. contraria* oospores can germinate buried under 10 cm sediments, but germlings can delay in development and can be outcompeted by other macrophytes.

# PREVALENCE OF DEPRESSION AND ANXIETY AMONG PATIENTS WITH EPILEPSY

Viktorija Belogorceva[1], Irutė Zagorskienė, MD[2], Prof. Rūta Mameniškienė, MD, PhD[2]

[1] Vilnius University Faculty of Medicine
[2] Vilnius University, Faculty of Medicine, Institute of Clinical Medicine, Centre of Neurology
Viktorija.belogorceva@gmail.com

**Introduction:** Depression is the most frequent psychiatric comorbidity in epilepsy. [1] Indeed, some authors estimate the lifetime prevalence of depression in association with epilepsy to be as high as 55%. [2] Depression can lead to seizures by means of sleep deprivation, and seizures can lead to depression both through biological mechanisms and the psychosocial impact that epilepsy has. [3] Comorbid anxiety disorders have a major impact on the affected patients' quality of life and may increase the risk for suicidality. [4]

**Methods and materials:** Data for analysis were collected in a Lithuanian tertiary epilepsy center to assess the prevalence of depression and anxiety in epilepsy patients. We asked patients to complete several questionnaires which included Hospital Anxiety and Depression Scale (HADS). Demographic data and information about patients' type of seizures, epilepsy duration and instrumental findings was collected from the outpatient cards. Data were processed with Microsoft Excel 2016, and analyzed by IBM SPSS® (version 23.0). Difference was considered statistically significant if $p<0.05$.

**Results:** 167 cases (96 (57.5%) - women), mean age - 36.05±15.75 years, mean epilepsy duration– 14.35±11.82 years) were analyzed. According to Hospital Anxiety and Depression Scale, 92 patients (55.1%) experience no anxiety, 35 patients (21%) have borderline abnormal level of anxiety and 40 patients (24%) have abnormal level of anxiety. Concerning depression results, 118 patients (70.7%) have no depression, 26 patients (15.6%) have borderline abnormal level of depression and 23 patients (13.8%) resulted in having abnormal level of depression. When comparing men and women, 24 men (33.8%) vs 51 women (53.1%) had borderline abnormal and abnormal level of anxiety ($p=0.032$), whereas results of the depression evaluation, according to HADS, do not differ between genders. We observed a moderate positive correlation between higher level of anxiety (abnormal HADS result) and higher frequency of epileptic seizures ($r=0.464$, $p=0.001$) and a moderate positive correlation between depression and higher frequency of epileptic seizures ($r=0.443$, $p=0.003$). Less patients, who have seizures only during the day, had a borderline abnormal and abnormal HADS anxiety result in comparison with those, who experience seizures also in the nighttime (27 patients (31%) vs 42 patients (61.8%)) ($p=0.004$). We also found higher anxiety levels, according to HADS, in patients, whose marital status was widowed, divorced or single. In contrary, patients who are married or in a relationship expressed lower levels of anxiety ($p=0.016$). Marital status does not have a significant impact on the HADS depression evaluation result. We observed no significant differences in HADS depression and anxiety results when comparing groups, according to the type of epilepsy (generalized vs focal). HADS depression and anxiety results were not affected by epilepsy duration.

**Conclusions:** Depression and anxiety are common comorbidities among patients with epilepsy. The abnormal level of anxiety is more prevalent in women. Depression and anxiety in epilepsy patients are mostly related to higher frequency of seizures, nighttime seizures and marital status.

---

[1] Kanner, Andres M. "Depression and epilepsy: a new perspective on two closely related disorders" *Epilepsy currents* vol. 6,5 (2006): 141-6.
[2] Jackson MJ, Turkington D. "Depression and anxiety in epilepsy" *Journal of Neurology, Neurosurgery & Psychiatry* 2005;76:i45-i47.
[3] Gnanavel, Sundar. "Epilepsy and Depression: A Bidirectional Relationship" *Journal of neurosciences in rural practice* vol. 8, Suppl 1 (2017): S5-S6.
[4] Brandt, Christian et al. "Anxiety disorders in people with epilepsy" *Epilepsy & Behavior*, Volume 59, 87 – 91.

# SLEEP QUALITY EVALUATION IN PATIENTS WITH EPILEPSY

Viktorija Belogorceva[1], Irutė Zagorskienė, MD[2], Prof. Rūta Mameniškienė, MD, PhD[2]

[1] Vilnius University Faculty of Medicine
[2] Vilnius University, Faculty of Medicine, Institute of Clinical Medicine, Centre of Neurology
Viktorija.belogorceva@gmail.com

**Introduction:** Epilepsy is a neurological disorder that highly affects the quality of life. [1] Sleep disturbances are common in people with epilepsy. Therefore, patients are more likely to experience daily fatigue and pathological sleepiness, what can trigger epileptic seizures. [2]

**Materials and methods:** This study was developed in a Lithuanian tertiary epilepsy center to assess the sleep quality and daytime sleepiness in epilepsy patients. We asked patients to complete several questionnaires and collected information from outpatient cards on epilepsy etiology, type of seizures, instrumental findings, and information about patients' antiepileptic drugs. Sleep quality was assessed by Pittsburgh Sleep Quality Index (PSQI), Epworth Sleepiness Scale and Insomnia Severity Index (ISI).

Data were processed with Microsoft Excel 2016, and analyzed by IBM SPSS® (version 23.0). Difference was considered statistically significant if $p<0.05$.

**Results:** 167 cases (96 (57.5%) – women), mean age - 36.05±15.75 years, mean epilepsy duration – 14.35±11.82 years) were analyzed. Generalized epilepsy (GE) was diagnosed in 29 patients (25.66 %), 84 patients (74.34%) had focal epilepsy (FE) and we couldn't identify seizure type in 54 patients. Our results showed that 97 patients (58.1%) have poor sleep quality according to PSQI. According to Epworth Sleepiness Scale, 42 patients (25.1%) have pathological, 30 patients (18%) - average, and 95 patients (56.9%) - normal level of daytime sleepiness. According to Insomnia Severity Index, 36 patients (21.6%) have moderate severity or severe insomnia, 63 patients (37.7%) have subthreshold insomnia and 68 patients (40.7%) do not have clinically significant insomnia. 12 GE patients (41.4%) more often had an abnormal daytime sleepiness according to Epworth Sleepiness Scale ($p=0.05$) in comparison with 17 FE patients (20.2%), but more FE patients (23 FE patients (24.7%) vs 5 GE patients (17.2%)) were evaluated as having moderate or severe insomnia according to ISI ($p>0.05$). A poor sleep quality (according to PSQI) showed 16 GE patients (55.2%) vs 53 FE patients (63.1%) ($p>0.05$). Those who experience seizures during the night time (76.1%) had significantly worse sleep quality according to PSQI scale when comparing to 50.0% of patients, who experience seizures only during the day ($p<0.05$).

74.4% of patients with irregular sleep time and 52.8% of patients with regular sleep time had abnormal sleep quality according to PSQI ($p<0.05$). The same results were obtained according to ISI: 41.9% of patients with irregular sleep time vs 14.6% of those with regular sleep time were found to have moderate or severe insomnia ($p<0.05$). Abnormal sleep quality (according to PSQI) was found in 80.0% of patients, who felt sleepy and exhausted often, and in 88.2% of those, who experience sleepiness and fatigue always ($p<0.05$). 70% of patients who reported in difficulty to get up early had an abnormal PSQI result. Similar results were obtained according to Epworth Sleepiness Scale and ISI. Patients, who have abnormal PSQI and ISI scores, feel the highest fatigue in the morning and during the day. In comparison, those with tiredness in the evening, showed normal PSQI and ISI results. Patients with prolonged seizures (longer than 5 min) had clinically significant insomnia to compare with those with shorter seizures (duration up to 1 min), 90% vs 51.1% ($p<0.05$).

**Conclusions:** Many patients with epilepsy have poor sleep quality and experience daytime sleepiness. Every fifth patient with epilepsy suffers from moderate or severe insomnia. Worse sleep quality is related to irregular sleep time habits, nighttime and longer seizures. We didn't find significant sleep quality difference in patients with focal vs generalized epilepsy according to Epworth Sleepiness Scale, Insomnia Severity Index and Pittsburgh Sleep Quality Index.

[1] Ryan, Jamie L et al. "Quality of Life Changes and Health Care Charges Among Youth With Epilepsy" *Journal of pediatric psychology* vol. 41,8 (2015): 888-97.
[2] Wang, Yi-Qun et al. "The Mutual Interaction Between Sleep and Epilepsy on the Neurobiological Basis and Therapy" *Current neuropharmacology* vol. 16,1 (2018): 5-16.

# DEVELOPMENT OF BREEDING TECHNIQUES IN HERPETOCULTURE AS AN APPROACH TO LEAF-TAILED GECKOS' (GEKKONIDAE, UROPLATUS) CONSERVATION

Dubyna Anastasiia[1], Tkachev Dmitri[2], Neizhko Ivan[2], Nekrasova Oksana[3], Marushchak Oleksii[3]

[1] Educational and Scientific Center "Institute of Biology and Medicine", Taras Shevchenko National University of Kyiv, Kyiv, Ukraine
[2] BION Terrarium Center, Kyiv, Ukraine
[3] I. I. Schmalhausen Institute of Zoology, NAS of Ukraine, Kyiv, Ukraine
nastya.dubyna88@gmail.com

Today, Madagascar stands on the verge of ecological disaster due to the rapid deforestation, which leads to the disappearance of unique plant communities, the reduction and fragmentation of the endemic animals' natural habitats and, as a result, globally threatens the entire ecosystem of the island. Like many other narrow-ranged species, leaf-tailed geckos are dying out as a result of habitat loss, food resources' declining and poaching [1, 2]. Thanks to the island's isolation and unique climatic conditions that affected evolution of these reptiles, leaf-tailed geckos are endemic representatives of the world's herpetofauna showing exciting abilities to mimicry. For today the main reasons why leaf-tailed geckos have become popular in herpetoculture are as follows: availability, successful breeding experience, unusual appearence and collection-related value. 18 species of leaf-tailed geckos have been described so far. BION Terrarium Center (Kyiv, Ukraine) – a reptile breeding center – has a long lasting experience of successful breeding of these unique geckos. Breeding of reptile species in controlled environment (herpetoculture) plays important role in nature conservation. Observations and research in captivity give necessary information for establishing reserve reptile and amphibian populations' conservation. From another side, the herpetoculture as part of world zooculture and reptile trade is an important part of economics worldwide. Finally, captive breeding gives valuable data for herpetological studies and healthy animals for pet market thus reducing level of poaching and other presses on wild populations [3].

The purpose of this work is to highlight general statements of keeping and breeding approaches for geckos of the genus *Uroplatus* (CITES II), for sustainable keeping of further breeding stocks in order to save these species in future. 10 leaf-tailed geckos' species, that have been breeding at BION Terrarium Center for the last 10 years were selected as research objects: *Uroplatus alluaudi* Mocquard, 1894, *Uroplatus ebenaui* (Boettger, 1879) , *Uroplatus fimbriatus* Schneider, 1797, *Uroplatus giganteus* Glaw, Kosuch, Henkel, Sound & Böhme, 2006, *Uroplatus guentheri* Mocquard, 1908, *Uroplatus henkeli* Böhme & Ibisch, 1990, *Uroplatus phantasticus* Boulenger, 1888, *Uroplatus pietschmanni* Böhle & Schönecker, 2003, *Uroplatus sameiti* Böhme & Ibisch, 1990, Uroplatus sikorae Boettger, 1913 [3, 4].

Based on literary data and other informational resources and personal experience, the optimal conditions for keeping and breeding were selected: temperature and lighting regimes, humidity, optimal diet, incubation conditions. All the following statements have prooved to create generally the most preferable conditions for leaf-tailed geckos' keeping and breeding. Meanwhile each species has its own narrow figures of mentioned parameters. It was found out that, depending on the species, the optimum temperature for keeping Madagascar flat-tailed geckos ranges from +23 to +25 °C during the day and from +19 - +22 °C at night. Humidity level should stay between 60-90%. Lighting period is 12 hours per day. Diet consists of ckickets, cockroaches, locusts, wax moths and other variable food items that are accessable and free of parasites and are of appropriate size. For successful animals' breeding in captivity, it is necessary to simulate a brumation period yearly with a gradual decrease in temperature and humidity to +20 - +16 °C and 50-60%. Decrease in daylight to 4 hours, and a decrease in feeding intensity to 1 time per week are also obligatory. Females lay an average of 2 (1-3) eggs at a time. Eggs are incubated at a humidity of 80-90% and at a temperature of +20 - +25 °C, depending on the species. Vermiculite is used as a substrate. The incubation period lasts 120-160 days, thus juveniles may hatch earlier or later depending on temperature fluctuations. These conditions guarantee the maximum hatching of healthy individuals that later are able to give next generations. To exclude intraspecific competition, specimens of this genus (females and males) should be kept separately in individual terrariums with the interior decoration imitating their natural habitat as soon as possible. This minimizes the attacks of aggression towards their partners.

To summarize it should be mentioned that successful keeping and breeding experience of rare species according to statements of international species' protection documentation is one of the most promissing ways to wild populations' conservation. Joint efforts of breeders and herpetologists shows results in *Uroplatus* spp. breeding and can be used to support wild populations therefore saving wild biodiversity.

[1] Wright P. Lemur traits and Madagascar ecology: Coping with an island environment. American Journal of Physical Anthropology Suppl 29(S29):31-72, (1999).
[2] Rakotomavo A. The Mangroves of the East of Madagascar: Ecological Potentials and Pressures. Open Journal of Ecology 08(08):447-458 (2018).
[3] Glaw F., Vences M. *Field Guide to the Amphibians and Reptiles of Madagascar*. (Vences & Glaw Verlag GbR 3rd Edition, Germany, 2007).
[4] Svatek S., van Duin S. *Leaf-tailed geckos – the Genus Uroplatus*. (Brahmer-Verlag, Germany, 2001).

# EFFECTS OF GAMMA RADIATION ON MORTALITY OF PRUSSIAN CARP (*CARASSIUS GIBELIO*)

Uliana Karnaukhova[1, 2], Maxim Hutsaliuk[1]

[1]Educational and Scientific Center «Institute of Biology and Medicine», Taras Shevchenko National University of Kyiv, Ukraine
[2]Kyiv Regional Cancer Center, Ukraine
uliana033@gmail.com

All living creatures are exposed to ionizing radiation. Even though they are adapted to low doses, high doses of gamma radiation may predispose organisms to high risks of certain diseases' developing and lethality [1].

The growing dependence on nuclear power obliges us to predict possible harmful results caused by radiation. The adverse effects of acute radiation doses on mammals are fairly understood, however there is still lack of information about their impact on aquatic organisms.

Effects of low (5 Gy) and high (20 and 35 Gy) doses of gamma radiation were examined on the behavioral changes (including mortality, loss of balance etc.) of *Carassius gibelio* (n=112). Negative effects of gamma radiation on survival were observed as radiation level increased (Fig.1).

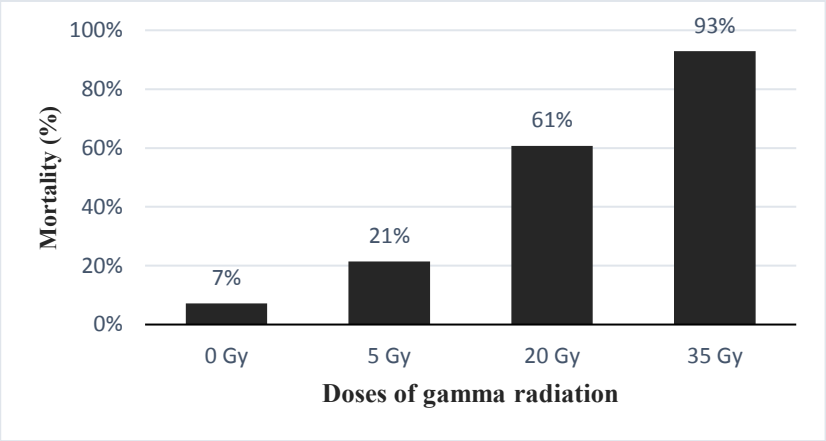


Fig. 1. Mortality of prussian carp irradiated at different levels.

Such symptoms as orientation loss, uncoordinated movements and hemorrhages were registered several hours after irradiation session. Control group demonstrated the lowest mortality rate ($P<0,05$) at the end of the experiment. Thus, consideration must be given to the level of gamma radiation and its influence on aquatic ecosystems.

[1] Effects of ionizing radiation on plants and animals at levels implied by current radiation protection standards. — Vienna : International Atomic Energy Agency, 1992.

# DETECTION OF OPHTHALMIC DISORDERS ON THE BASIS OF NEURAL NETWORK ANALYSIS OF MEDICAL RESEARCH DATA

Ilya Grigoryev, Katsiaryna Halavataya, Elena Kozlova

Department of Intelligent Systems, Belarusian State University, Belarus
ilyhryh@gmail.com

The volume and complexity of diagnostic imaging is increasing at a pace faster than the availability of human expertise to interpret it [1, 2]. Ophthalmic imaging provides a way to diagnose and objectively assess the progression of a number of pathologies. Automated diagnosis of a medical image, even for a single disease, faces two main challenges: technical variations in the imaging process, and patient-to-patient variability in pathological manifestations of disease. As far as we are aware, the state-of-the-art approaches tried to deal with combinations of these variations using an end-to-end black-box network, thus typically requiring quite a few of labeled samples. By contrast, our framework separates the two problems (technical variations in the imaging process and pathology variants) and deals with them independently. A segmentation network (uses modified U-Net architecture [3]) creates a detailed device-independent segmentation map. Subsequently, a deep classification network analyses this segmentation map and provides diagnoses and as the primary outcome one of four referral suggestions currently used in clinical practice.

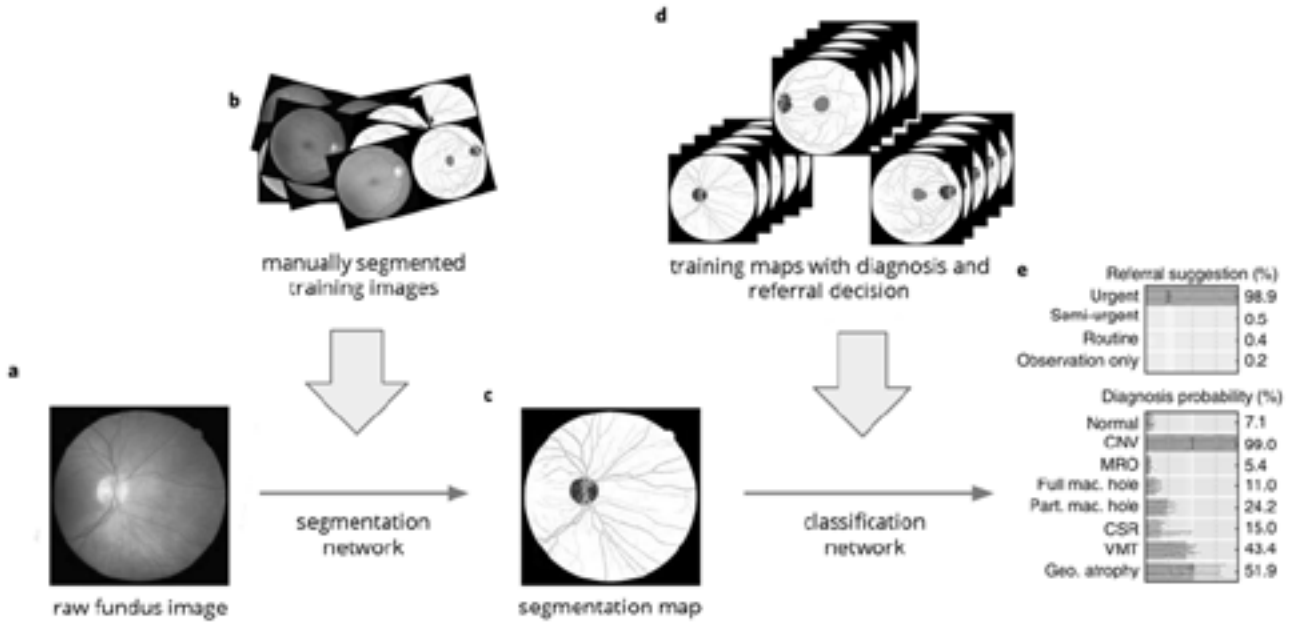


Fig. 1. Proposed AI framework. **a**, Raw fundus image. **b**, Deep segmentation network, trained with manually segmented fundus images. **c**, Resulting segmentation map. **d**, Deep classification network, trained with segmentation maps with confirmed diagnoses and referral decisions. **e**, Predicted diagnosis probabilities and referral suggestions.

This study is focused on Diabetic Retinopathy and Glaucoma diseases. Our key insight is the ability to analyse simple fundus images that can be obtained through phones equipped with special lenses or simple fundus cameras and not be far from state-of-the-art approaches [4]. The method was tested on Kaggle Diabetic Retinopathy challenge, ORIGA, SCES, EyePACS-1 datasets, which were laid out in free access.

In conclusion, we present a novel framework that analyses clinical fundus images and makes referral suggestions to a standard that is comparable to clinical experts. Although we focused on one common type of medical imaging, future work can address a much wider range of medical imaging techniques, and incorporate clinical diagnoses. For future work, we consider the exploration of possible performance gains in other downstream tasks such as image level recognition or grading of diabetic retinopathy. Our method can be applied for other medical images as well. We can use AI to predict adverse outcomes before they happen, better manage highly complex situations, and ultimately allow clinicians to spend less time analysing data and more time harnessing their experience and human touch in delivering care.

[1] Dinggang Shen, Guorong Wu, Heung-Il Suk, Deep Learning in Medical Image Analysis, Annual Review of Biomedical Engineering 19:1, 221-248 2017.
[2] De Fauw J, Ledsam JR, Romera-Paredes B, Nikolov S, Tomasev N, Blackwell S, et al. Clinically applicable deep learning for diagnosis and referral in retinal disease. Nat Med. 2018;24:134250
[3] Olaf Ronneberger, Philipp Fischer, Thomas Brox, U-Net: Convolutional Networks for Biomedical Image Segmentation, MICCAI 2015
[4] Litjens, Geert et al., A survey on deep learning in medical image analysis, Medical Image Analysis , Volume 42 , 60 - 88 2017

# FUZZY INFERENCE SYSTEM FOR AUTOMATED IMAGE-BASED KARYOTYPING

Aliaksandr Kurachkin[1], Vasiliy Sadau[1]

[1]Faculty of Radiophysics and Computer Technologies, Belarusian State University, Belarus
lawliet29@gmail.com

Karyotyping, or chromosome analysis, is a series of steps to produce karyotype information (i.e. the number of chromosomes and their structure), usually based on visual metaphase analysis. A normal human karyotype contains 22 diploid autosomes and 2 gender chromosomes for a total of 46 chromosomes, each of them with specific structure and size, the most common reference being International System for Human Cytogenic Nomenclature (ISCN). Chromosome aberrations - structure disordering, chromosome fragment displacement and abnormal number of chromosomes - usually indicate an error in cell division cycle, and can be detected by cytogeneticist by ground-truth reference comparison during karyotyping. Early detection of such abnormalties is extremely important in prenatal diagnostics, as well as cancer cell analysis and treatment planning [1].

Chromosome analysis is commonly performed by manual visual expert analysis, although there are several well-known algorithms that allow automated chromosome separation and classification from slide shots. The input images for such algorithms are captured using high-magnification electron microscope and contain an image of a glass slide with individual chromosome species extracted from cells arrested during metaphase.

The expected output of an automated chromosome analysis system is a karyogram - a set of separated, ordered and classified chromosomes extracted from the image, that can be examined individually. The reference comparison for each chromosome is usually based on chromosome length, the configuration of alternating brighter and darker stripes along the chromosome length and their brightness distribution, presence of sattelites, and centromere location.

The most challenging problems are chromosome separation and classification. Separation is a process of extracting parts of the slide image that are only relevant to a single chromosome, independently of the others present on the image. However, chomosome species present on the slide often overlap, requiring a precise boundary detection and cutout analysis. Even when boundaries of a single chromosome are detected correctly, some parts of the separated chromosome that belong to one of the other species (i.e. because of the overlap) can alter further analysis. Chromosome classification is the procedure of assigning a specific chromosome number to the separated chromosome.

Existing classification methods are usually performed via sequential analysis of an individual separated chromosome and expectation maximization techniques based on a specific encoding of brightness pattern alternations. However, these algorithms are usually very sensitive to individual non-structural chomosome deformations like bending, and generally perform worse when the observed species overlap percentage is significant.

The proposed solution to this problem is to enhance existing sequential analysis algorithms with the introduction of a fuzzy inference system for classification [2]. The basis of fuzzy inference analysis is higher-order Denver chromosome classification, which groups individual chromosomes into 7 classes based on their centromere position. Relative centromere detection can be performed by iterative chromosome species analysis and is far less sensitive to non-structural defromations. Chromosome brightness distribution and relative length can be used to further refine Denver class selection.

The input terms for fuzzy inference system are centromere position, brightness distribution as mean and standard deviation and relative length, calculated directly from separated chomosome. Centromere position fuzzy set values include sets for metacentric, submetacentric and acrocentric chromosomes with sigmoidal activation functions. Brightness input variable uses a regular triangular 7-level grid for mean and standard deviation. Finally, relative chromosome length is provided as a crisp, non-fuzzy value. Fuzzy inference rules bind input parameter values to their respective output Denver classification classes. For inference itself, Mamdani algorithm is used.

Resulting Denver classification projection can be used to enhance initial classification estimate of traditional algorithms and increase their accuracy, especially for cases of non-structural chromosome species deformations and overlap.

[1] A. P. Britto, G. Ravindran, A Review of Cytogenetics and its Automation, Journal of Medical Sciences, vol 7 (1), pp. 1-18 (2007).
[2] T. J. Ross, Fuzzy logic with engineering applications, 3rd ed. John Wiley & Sons, Ltd., 607p., (2010).

# ALGORITHM OF FACIAL METRIC FORMATION IN THE APPLICATION OF DETERMINING THE EMOTIONAL STATE OF A PERSON BY VIDEO SEQUENCE

Siarhei Sadau

Department of Radio Physics and Computer Technologies, Belarusian State University, Belarus
seregasadov@gmail.com

Most of the known computer systems which determine the emotional state of a person are based on obtaining data from an image. This approach assumes the availability of a sufficient amount of information about the object being analyzed. A more promising direction is based on the analysis of video sequences. The proposed algorithm allows to obtain all the necessary information about the object in real time.

The task of recognizing facial expressions in a video sequence includes the following main subtasks: search and tracing of individuals; selection and processing of informative facial characteristics; video segmentation; classification of facial expressions.

We give a brief description of the components of the facial expression recognition system for the video stream:

1. The module of sustainable search and face tracking. Such a module is the primary and most important part of the system. Its main tasks are deciding whether a person is in a video stream and narrowing the processing area in frames of a video sequence from the full space to the space containing the face.

2. Video segmentation module. Video segmentation methods allow to detect and calculate the movement characteristics of human facial muscles, and also to increase the efficiency of recognition of changes in facial expressions.

3. Classifier of the emotional state of a person. The input of the algorithm receives a set of sequences of facial expressions (of various durations) and a set of parameters characterizing emotional states. The task of the algorithm, in accordance with the proposed information model for describing the emotional state of a person, is to determine the form of the function F, which relates each sequence to one of the human states.

### Face Search and Tracking Module

The classical problem of finding a face is usually solved using such well-known methods as the Principal Component Analysis (PCA), Linear Discriminant Analysis (LDA), artificial neural networks, Haar cascades, etc. These approaches of solving the problem have a number of disadvantages: low recognition accuracy with changes in face position in front of the camera. For this emotion recognition system module, it was decided to apply a hybrid algorithm that combines several approaches, such as the Haar cascades and the AdaBoost algorithm, as well as the use of neural networks. The hybrid scheme is constructed as follows: the components of the adaptive gain algorithm decide whether there is a face in the frame of the video sequence and rejects frames without faces. This makes it possible to use it in real time.

### Video segmentation

The proposed video segmentation unit is a temporal segmentation of the entire video sequence into sections that contain frames of a single facial expression. This video segmentation algorithm contains the following steps: calculation of movements of pixels of a frame; building a time series; selection and presentation of the analyzed facial characteristics; application of the classification algorithm.

### Classification of the emotional state of a person

The state array of facial objects obtained at the previous step of the algorithm is the basis for searching in it the compositions of objects describing a certain emotional state. Such search can be carried out using the methods of fuzzy logic and using neural networks. This a task is not unambiguous, since a person does not experience only one specific emotional state in a period of time. The development and description of methods for analyzing the complex emotional state of a person is the task of further research.

[1] Sochman J. AdaBoost with totally corrective updates for fast face detection, URL: http://cmp.felk.cvut.cz sochmj1.

[2] Viola P., Jones J. Robust real-time object detection // Proc. of IEEE Workshop on Statistical and Computational Theories of Vision, 2001. P. 324 - 332.

# 3D RECONSTURCTION OF SMALL-SCALE INTERIOR SURFACES

Katsiaryna Halavataya[1], Vasiliy Sadau[1]

[1]Faculty of Radiophysics and Computer Technologies, Belarusian State University, Belarus
katerina-golovataya@yandex.ru

3D reconstruction is a problem of creating a representation of real-world objects and structures as point cloud, mesh or polygonal 3D models based on regular observation methods. The most common form of input data for 3D reconstruction is a set of photographs of an object of study, usually taken manually with several points of view, by single or multiple cameras, in order to capture the object from different angles. Another relatively common form of input is a video sequence.

A photographic representation of an object can be thought of geometrically as a central projection of the scene onto the image plane. Epipolar camera optics and projective transformations provide a sufficient model for tracing projections of the same point across several images to a single point in three-dimensional space. These problems are traditionally solved using photogrammetry structure from motion (SFM) methods and involve a number of steps: calibration, keypoint detection and matching, bundle adjustment, sparse and dense point cloud reconstruction, mesh estimation and texturing [1].

However, there are several limitations of existing structure from motion methods that prevent their use in several important applications. One of them is the 3D reconstruction of medical images, allowing to enhance diagnostic capabilities and help with optimal treatment planning. Specifically, 3D reconstruction from video endoscopic images has the following distinctions:

- Object size. Traditional structure from motion photogrammetry assumes specific physical size of the objects and scenes. Near and mobile photogrammetry methods are used to reconstruct the objects with sizes ranging from 0.5m to 200m across any of the dimensions, aerophotographic and sattelite photogrammetry work with larger sizes, while microscopic image photogrammetry works with electron microscope scans for nanoscale objects with high magnification factor. Videoendoscopic research usually works with objects 0.1-5 cm of size.
- Optical system. Structure from motion methods are very sensitive to various geometric transformations imposed by optical system of a camera, specifically distortion and fish-eye effects. To mitigate these effects, camera calibration is mandatory to adjust to optical system irregularities around the edges of the image. However, videoendoscopic systems typically use ultra-wide angle cameras with fields of view up to 140°, which create heavy non-linear distortion effects around the entire image.
- Interior scene acquisition. It is assumed that objects described with photogrammetry methods can be isolated and exterior image acquisition can be used to observe the object independently of the background. In videoendoscopic research, an interior image acquisition is performed, most of the objects that need to be analyzed cannot be separated from the background, and the relevant part of a 3D model should be based on interior surface organ area.
- Dynamic nature of the environment. Usually, structure from motion analysis is performed on a static object that doesn't move, and its geometry is assumed to be constant across different camera positions. Surface areas of interior organs, however, may expand and contract with time and generally have a dynamic geometry within specific constraints.
- Dynamic nature of lighting and surface reflections. Classic photogrammetry methods assume static lighting and non-reflective surfaces of the object to correlate object points across images based on their absolute brightness. In videoendoscopic research, however, the light source is rigidly connected to the camera and moves along with it. Moreover, inner organs are usually covered in liquids, resulting in abdundant reflections and glares that fluctuate with the light source movement.

All of the described problems prevent the direct usage of traditional photogrammetry methods for endoscopic research 3D reconstruction and mandate the need to create adjustments to existing models [2, 3]. The paper proposes several solutions to these problems. For object size limitation, it's necessary to use more precise keypoint detection methods that select points of interest based on smaller features of the endoscopic image (like blood vessels and formation edges), as well as adjusted higher-resolution point cloud reconstruction techniques. Optical system specifics mean that a combination of ultra-wide projections must be calculated and used for distortion correction. Interior scene acquisition requires a reworked bundle adjustment process with point correspondence estimation across the depth axis of the image. Environment motion can be compensated with the introduction of correction matrix to the fundamental and essential matrix recaltulation algorithms during bundle adjustment. Dynamic nature of lighting can be mitigated by using a brightness-invariant colorspace transform, for example, 2-nd order component of principle component analysis, while glares can be compensated based on surrounding video sequence frames. Reconstruction based on adjusted methods allows for accurate and detailed 3D model acquisition for these types of images and video sequences.

[1] T. Luhman, S. Robson, S. Kyle, J. Boehm, Close-Range Photogrammetry and 3D Imaging, De Gruyter; 2nd ed. edition, 702 p. (2013).
[2] K. Halavataya, A. Kurachkin, Realtime computer-aided object detection in endoscopic screening, International conference Open Semantic Technologies for Intelligent Systems (OSTIS-2018), Minsk, BSUIR, pp. 247-250 (2018).
[3] J. C. McGlone, Manual of Photogrammetry, ASPRS; 6th ed. 1372 p. (2013).

# BIOMETRIC AUTHENTICATION SYSTEM BASED ON NEURAL NETWORK PROCESSING FOR EEG DATA

Nastassya Horlova[1], Uladzislau Barayeu[2], Pavel Bulai[2*]

[1]Department of Mathematical Modeling and Data Analysis, Belarusian State University, Belarus
[2]Department of Biophysics, Belarusian State University, Belarus
g.nasta.work@gmail.com

In our research, a reliable biometric authentication system was proposed by means of features identification of human electroencephalograms (EEG) using neural networks.

We took EEG-data from "PhysioNet" database [1] (https://www.physionet.org/pn4/eegmmidb/). This dataset consists of EEG recordings of 109 subjects with 23 trials each with Motor Movement/Imagery tasks, performed with 64-channel BCI2000 EEG system. For authentication system development we used only "opening and closing right and left fist" tasks .

In order to preprocess raw data and extract features, we wrote MATLAB based program. First, we subtracted baseline, for which we used recording of 2-second relaxation before each trial. Then this data was filtered with zero phase delay filter from 1 to 50 Hz.

After that, Empirical Mode Decomposition (EMD) was calculated for each trial and only first 5 intrinsic mode functions (IMFs) were left as the most useful ones. For each IMF Shannon, Log, Sample and Approximate entropies were calculated. Values of these entropies were later used as features for the neural network. Moreover, Spectra were calculated from each trial by Multi-taper method (MTM) in "Chronux" toolbox. Intensity of different rhythms were used as features as well. Finally, for each trial and each subject all features were combined in 2D matrix 64*40 (64 - number of channels, 40 - number of features), and these matrices were later on used as input for the neural network. (Fig.1)

We build three authentication systems: in the first two systems, the input data was a record of one action (opening and closing left or right fist respectively). The input data for the third system was a sequence of two separate actions (opening and closing left and right fist consistently), so that a subject will be authenticated only if he or she will be authenticated by both of these actions.

To recognize each of the actions, a separate neural network with the same architecture was trained. For creation and training neural networks we used "Keras" framework in Python. To obtain the accuracy of each model, 5-fold cross-validation was used. Within each fold, the training sample was normalized within each feature, and accuracy was tested on a test sample, which was normalized using the minimum and maximum values of the training sample.

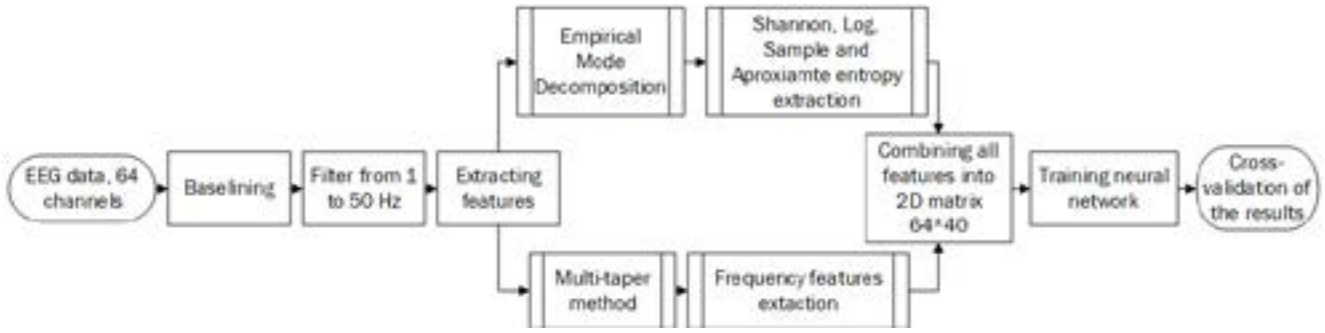


Fig.1 Discription of the Analysis.

We got accuracy around 93% for each task, and around 90% for both tasks, but the most interesting fact, that false positive (type II error) is zero for each task and for both tasks as well. (Table 1) Therefore this method is 100% authentication system.

Table 1: Errors for each authentication system.

| | **Right fist** | **Left fist** | **Combination of 2 fists** |
|---|---|---|---|
| **Type I error, %** | 0.15 | 0.13 | 0.2 |
| **Type II error, %** | 0.0 | 0.0 | 0.0 |

[1] Goldberger AL, Amaral LAN, Glass L, Hausdorff JM, Ivanov PCh, Mark RG, Mietus JE, Moody GB, Peng C-K, Stanley HE. PhysioBank, PhysioToolkit, and PhysioNet: Components of a New Research Resource for Complex Physiologic Signals. Circulation 101(23):e215-e220 [Circulation Electronic Pages; http://circ.ahajournals.org/cgi/content/full/101/23/e215]; 2000 (June 13).

# MACHINE LEARNING APPLICATIONS IN HUMAN LANDSCAPE PALAEOECOLOGY

Liudas Daumantas[1], Andrej Spiridonov[1,2], Lauras Balakauskas[1]

[1]Department of Geology and Mineralogy, Vilnius University, Lithuania.
[2]Institute of Geology and Geography, Nature Research Centre, Lithuania
liudasdau@gmail.com

Sensible applications of predictive modelling can profoundly enlighten the nature of prehistoric settlement distributional rules. This is especially useful for cultural heritage management, prediction of new archaeological sites and research of human-environment systems. Yet, current studies in the field are mostly of local scale and lack time-depth perspective. Thus, the global context needed for the interpretations is often missing. In addition, the field is still in the search for "the optimal" computational approach. To tackle these problems, we performed a predictive settlement modelling study in south-east Baltic, Lithuania. This study was of regional scale and had time-series study design. The settlement data used was obtained from archaeological-site dataset PROLIGIS, while regional explanatory variables (21 in total) were derived by GIS from various sources (DEM, geological, hydrological map and etc.). We analysed the data using a set of machine learning and statistical methods with thorough testing procedures. Random forest, for instance, was used for variable importance estimation, PCA – for the reduction of number of variables, k-means clustering – for classification of regional environment, Generalized Additive Models – for model performance estimation and creation of predictive landscapes. The problematic nature of archaeological and spatial data was approached by using dummy variables (simulated as random fields on the basis of original variables) for null hypothesis tests, as well as by performing repeated stratified cross-validation and parallel analyses that treated only settlements with specific (period-confined) dating. Thus, this strategy allowed us to quantitatively formalize and track changes in prehistoric human regional settlement behaviour from times of Palaeolithic to Iron Ages.

The results revealed that regions of higher settlement probability at all times were generally confined within one regional landscape type, characterized by rougher landscape, denser hydrography and more diverse soils. They also revealed that changes in Lithuanian settlement regional niche are best described by two stability periods (Stone Age and Metal Age), separated by a marked shift at Neolithic-Bronze Age boundary. Regions of Stone Age settlements were defined by amount of water, distance to flint mines and to the sea, landscape roughness, ratio of sand to moraine loam area and LS-factor. Whereas, regions of Metal Age settlements were defined by amount of water, landscape roughness, distance to the sea, slope steepness and elevation above channel network. Small scale, gradual and period-specific variations were also observed within these period groups. We argue that the observed grand settlement reorganization event may be associated with immigration of steppe people to the Baltics, 4.2 ka. climatic event and spread of agricultural practices. Other results showed continuously increasing complexity of regional settlement strategies in terms of 1) predictive landscape surface roughening, 2) decreasing performance of predictive models, 3) increasing spatial randomness and regional environment diversity of settlement locations. The results of this study, therefore, provides the preliminary, but essential global context for further, more detailed studies in the area and serves for hypotheses generation.
This research is funded by the European Social Fund under the No 09.3.3-LMT-K-712 "Development of Competences of Scientists, other Researchers and Students through Practical Research Activities" measure.

# THE SIMULATION MODEL OF THE "HELPERS" INFLUENCE ON THE POPULATION WITH LIMITED RESOURCES

Pavlo Otriazhyi[1]

[1]Department of Zoology and Animal Ecology, V. N. Karazin Kharkiv National University
paveloo108@gmail.com

The research of various population processes is an important stage in the understanding of different patterns of the group behavior inside the population. In our time, the society goes through a significant amount of thrills connected with unusual behavior models of individuals, such as homosexual behavior, abandonment of children, etc. Different scientific underpinnings can help in accepting of this kind of individuals by radical-minded people.

The simulation model of these processes allows evaluating them in different conditions and with a significant amount of cycles. This allows understanding the ways and under which conditions different behavioral models are the most efficient and are fixed in the population

The model simulates competitiveness for common resource between two groups. The first group (G1) consist of "parents" (individuals that are engaged in reproduction) and "helpers" (that are not engaged in reproduction, but potentially influence the intra-group process). The second group (G2) consist of "parents" individuals. We believe that conditions, in which the model group displaces the alternative group, may in the real biological evolution contribute to the alleles pinning, which foster the emergence of the "helper".

The most important part of the model is the competitive reduction. The competitive reduction was calculated with the algorithm [1] in which competitive reduction depends on resources, number of all groups after breeding and competitiveness of each group. You can find the model: http://dspace.univer.kharkov.ua/handle/123456789/14511.

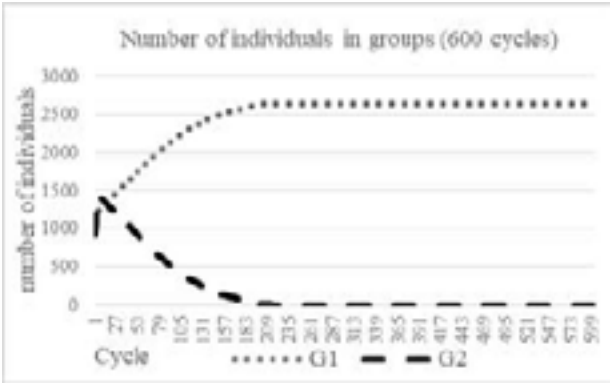


Fig. 1. Influence of 16% of "helpers" in G1 on the population. Fertility = 3, assistance of "helpers" = 85%, surviving of adult = 85%, surviving of progeny = 70%, competitiveness of adult = 78%, competitiveness of progeny = 50%

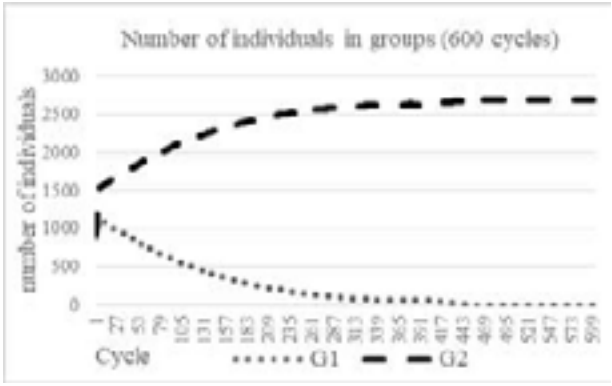


Fig. 2. Influence of 25% of "helpers" in G1 on the population. Fertility = 3, assistance of "helpers" = 85%, surviving of adult = 85%, surviving of progeny = 70%, competitiveness of adult = 78%, competitiveness of progeny = 50%

Influence of "helpers" on the population depends on many parameters: (i) number of "helpers"; (ii) fertility of parents; (iii) surviving of individuals; (iv) competitiveness of individuals; (v) assistance of "helpers". Fig. 1 shows positive influence of "helpers" optimal number on competitiveness of progeny. As a result, G1 displaces G2. Fig. 2 shows that big percent of "helpers" reduce their positive influence and G2 displaces G1. A similar process is observed when assistance of "helpers" from Fig.1 decreases to 50% (all another parameters stay the same). Therefore, G2 displaces G1. Relatively low decrease in adult survival in both groups (for example, to 80% on Fig. 1) also can lead to G2 expansion.

So, groups that include "helpers" (individuals that don't reproduce but influence the intra-group process through raising children etc) get huge evolutionary advantage in case of competition for resourses. Unfortunately, this advantage is possible only in relatively rare cases characterized by a combination of certain parameters that were discussed below. However, if groups develop with such parameters, discussed behavior patterns can spread.

[1] M.O.Kravchenko, D.A.Shabanov, Modeling the transformations of water frogs (*Pelophylax esculentus* complex; Amphibia, Ranidae) hemiclonal population systems by the use of recurrent difference equations, The Journal of V. N. Karazin Kharkiv National University **12**, 70-82 (2010).

# THE QUALITY USED FOR BIOENERGY OF ORGANIC RAW MATERIALS

Urtė Stulpinaitė [1,2], Vita Tilvikienė[2], Karolina Barčiauskaitė[2]

[1] Vytautas Magnus University, Agricultural Academic, Faculty of agricultural engineering, Lithuania
[2] Lithuanian Research Centre for Agriculture and Forestry, Lithuania
urte.stulpinaite@lammc.lt

Nowadays the highest problem in the world is climate changes. One of the most important challenge is to guaranty that the average global temperature change would not increase by more than 1,5 °C. Therefor we need to find some alternatives to help to stop this process and one of the ways is to use more bio products in everyday using. One of the sectors with the highest pollution and green-house gas emissions is heating and cooling sectors. Lithuania uses quite large amount of biomass for heating, but it is expected that the use of biomass residues could be even more profitable and environmentally friendly. On the other hand, some residues, such as oak sawdust have good heating value, but low stability while pelleted while others are not so good for heating purpose, but have adhesive properties which could improve the quality of pallets. Therefor the mixing of different biomass residues could be one of solutions while looking for materials to increase energy value as well as economic and environmental benefits.

The aim of this study was to evaluate the quality of diffrent organic raw materials - residues from industry processing and their mictures – used bioenergy.

In the present study, 5 organic raw materials (oak sawdust, lignin, potato peelings, linseed cake) and their mixtures were analyzed. This samples were collected from different places after processing. The main parameters describing the quality of biomass are moisture content, ash content, biomass chemical composition, energy value and chemical composition of smoke.

The results of study revealed differences in ash content of organic raw materials mixes (Fig. 1). The Ash content was the highest with oak sawdust 20 % and lignin 80 % it was 12.2 % of the ash then specificity reached 2 %. The least ash content was with oak sawdust 80 % potatoes waste 20%, oak sawdust 80 % linseed oil waste 20% and oak sawdust 80 % miscanthus 20%. In other treatments when oak sawdust concentration was the lowest and other materials - the highest ash content was highest too.

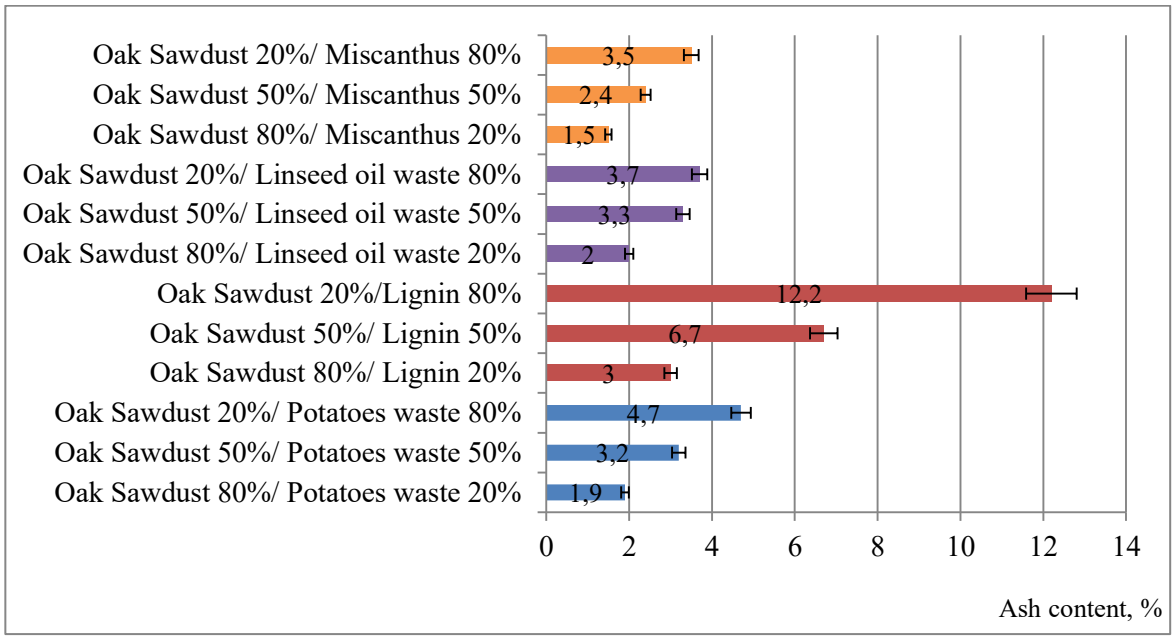


Fig. 1. Different concentration and mixes of organic raw materials ash content.

In conclusion this analysis revealed what is the concentration of ash content after burning into organic raw materials. Oak sawdust 80 % and other organic raw materials which is in the specificity stint can to solve a two problems. One is that it is can be new biofuel type. The second one is the help make a pallets from oak sawdust, because now oak sawdust is unstable. The energy value and quality of pallets produced from different biomass source are influenced by biomass quality.

# SCALE OF ILLEGAL MINERAL EXCAVATION IN LITHUANIA

Audrius Armanavicius[1], Jonas Satkunas[2]

[1] Nature research centre, Akademijos str. 2, 08412 Vilnius, Lithuania
[2] Lithuanian Geological Survey, S. Konarskio str. 35, 03123 Vilnius, Lithuania
audrius.armanavicius@gmail.com

Mineral resources state assets, the excavation of which is an engine of economic and social progress. There are 17 species of minerals found in Lithuania. In recent years, nine types of minerals have been used in Lithuania: dolomite, limestone, underground water, clay, sapropel, gravel, sand, peat and oil. Safe and rational use of useful resources is the maximum benefit for the state and society, and the minimum impact on our environment, while the mining processes are managed and maintained. Most of the resources used in Lithuania, like the rest of the world, are groundwater and building materials. According to the data of the Lithuanian Geological Survey, extraction of mineral resources for construction and road industry (dolomite, sand and gravel) has significantly increased over the past year [1]. Some have been exterminated and rehabilitated, and, of course, new ones have emerged. The emergence of new quarries and the closure of depleted plants are monitored by state institutions, but they collect information only on legally extracted minerals, but there are no accounts of other types of cadastral areas of damaged land, quarrying quantities, and such cask condition. The Lithuanian Geological Survey performed the State Damaged Land Management Plan 2014-2020 approved by the Minister of Environment and carried out an audit of all Lithuanian cadastral damaged areas of more than 0.3 ha - "Collection and systematization of information on damaged lands" [2]. The purpose of this project was to identify the sites and condition of the land damaged by any mining operation; to calculate excavated mineral resources; to accumulate and systematize information on damaged lands and based on the collected data to identify the damaged lands to be treated first. The results of this work showed that 3300 sites of more than 0.3 hectares are affected by casual damage (fig. 1).

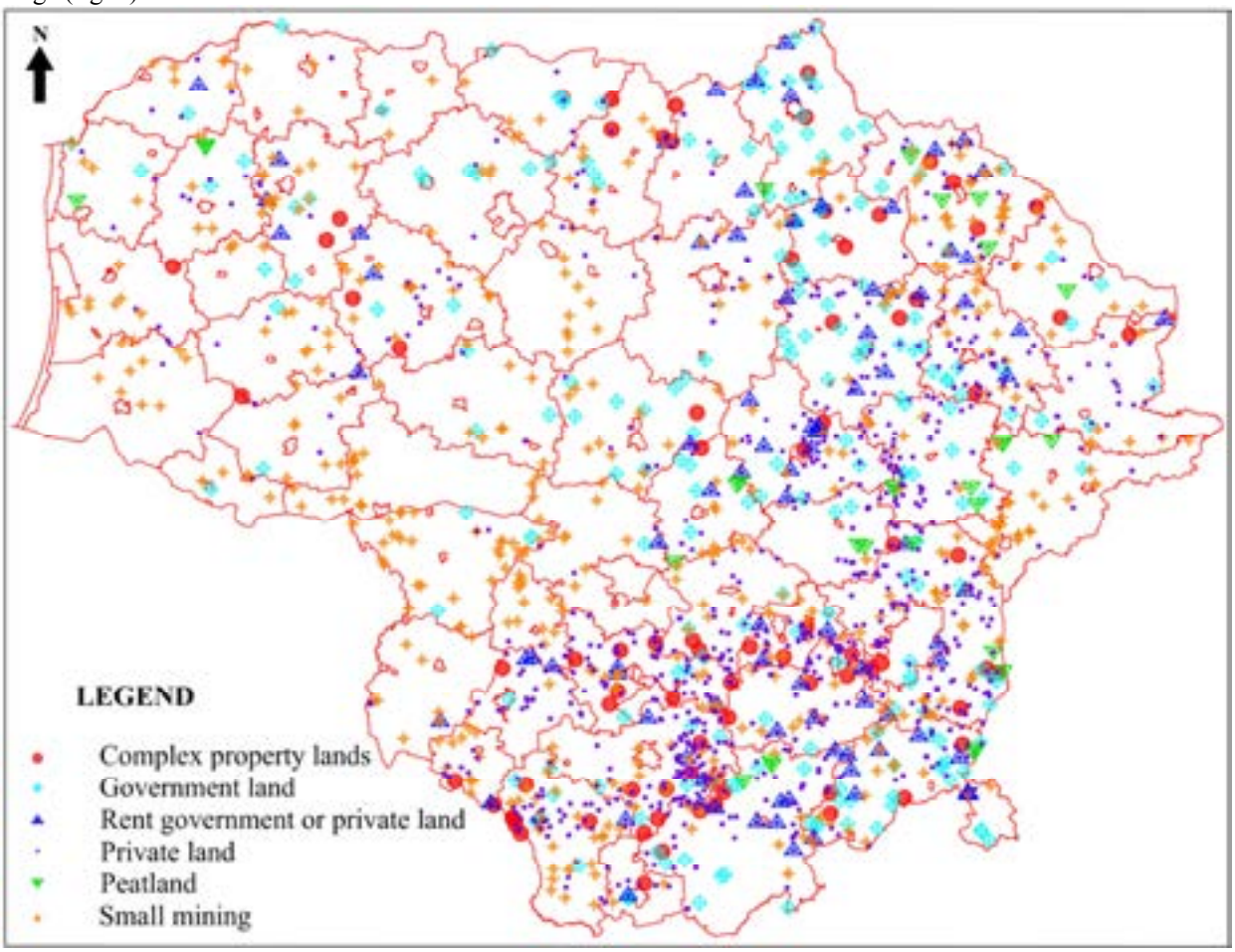


Fig. 1. Plan of damaged land area.

The amount of minerals likely to be illegally dumped, mainly gravel and sand, amounts to 15 million $m^3$, thus the state has lost about 6 million Euro taxes.

[1] Lithuanian Geological Survey, Annual report 2017, 140 Vilnius (2018).
[2] G. Juozapavicius, A. Armanavicius et al., Collection and systematization of information on damaged lands, Final report, 225, (Vilnius, 2015).

# CHEMICAL COMPOSITION AND STRUCTURE OF GRANULAR BIOFUEL ASHES AND ITS INFLUENCE ON SOIL

Kristina Bunevičienė[1], Romas Mažeika[2]

[1,2] Institute of Agriculture, Lithuanian Research Centre for Agriculture and Forestry, Lithuania
kristina.buneviciene@lammc.com

Constantly expanding the biofuel boiler network in Lithuania there are large amounts of ash from this fuel that are not rationally used and accumulate as waste. Biofuel ash is alkaline waste (pH ~ 13) [1]. It is therefore very useful to use it where there are acidic soils (pH <5.5). In ash contains a lot of nutrients (K, P, Ca, Mg), which are necessary for plants and soil.

Biofuel ash can be practiced by as agriculture fertilizer. The environment benefits when less waste ends up in landfill sites and nutrients are returned to the environment from which they came.

The objective of the present study was to produce granulated biofuel ashes. To investigate chemical composition, structure of granulated, strengths, to assess their quality and the impact the soil. For the experiment, we used three different ash variants of granulated biofuel, where the ash content in the granule was 30 %, 50 % and 70 %. The concentrations of heavy metals (Cd, Cr, Cu, Pb, Ni, and Zn) in the granules were sufficiently low not to prevent their use in agriculture fertilizer [2]. Overall, the concentrations of nutrients (Ca, Mg, K, and P) were reasonably high [3].

The XRD patterns attributed to calcium hidroxide, calcium carbonate and quartz were identified in all granulated biofuel ash samples. The main difference between the samples was the intensity of the calcium carbonate peaks, which decreased with increasing granule size (Fig. 1). Biofuel ash is generally used for fertilization because of its very long-lasting fertilizing effect. The granules should be hard enough to promote gradual and slow dissolution of nutrients to the forest soil during several years. On the other hand, too high compressive strength may also be problematic since it can retard and possibly prevent the leaching of nutrients [3]. Pellet strength increases as the ash content of the pellet increases.

Fertilization was carried out two weeks before sowing. During vegetation, the consumption of minerals was recorded, which confirmed that the growth of spring barley absorbed most of the nutrients from the soil. Meanwhile, the loss of material was reduced to the end of vegetation, and therefore the concentration of minerals increased again. After measuring the concentrations of Cd, Cr, Cu, Pb, Ni, and Zn, it became clear that the soil was not contaminated with heavy metals, proving that these materials did not damage plant vegetation.

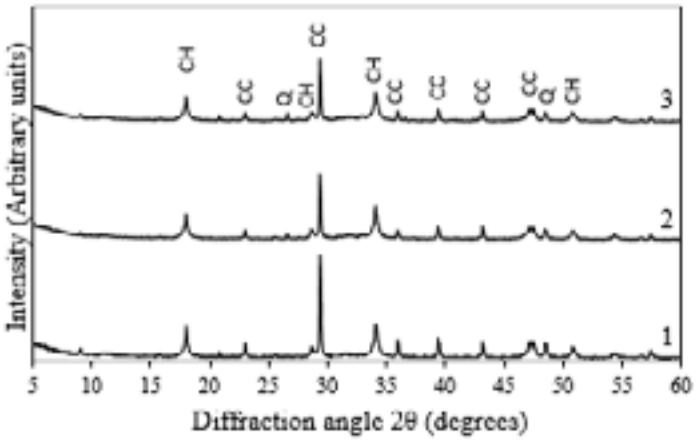


Fig. 1. X-ray pattern of granulated biofuel ash samples: 1 – 30 % ash in granule, 2 – 50 % ash in granule, 3 – 70 % ash in granule (abbreviations: CC – $CaCO_3$; CH – $Ca(OH)_2$; Q – $SiO_2$).

[1] J. Yliniemi, H. Nugteren, M. Illikainen, M. Tiainen, R. Weststrate, J. Niinimaki, Lightweight aggregates produced by granulation of peat – wood fly ash with alkali activator, International Journal of Mineral Processig, 42 – 49 (2016).

[2] R. Poykio, M. Makela, G. Watkins, H. urmesniemi, O. Dahl, Heavy metals leaching in bottom ash fly ash fractions from industrial – acale BFB – boiler for environmental risks assessment, Transactions of Nonferrous Metals Society of China, 256 – 264 (2016).

[3] J. Pesonen, V. Kuokkanen, T. Kuokkanen, M. Illikainen., Co-granulation of bio-ash with sewage sludge and lime for fertilizer use, Journal of Environmental Chemical Engineering, 4817 – 4821 (2016).

# THE INFLUENCE OF CLIMATE CHANGE ON MINERAL NITROGEN IN ORGANIC SOILS

Andrius Šarka
Lithuanian Agriculture and Forestry Sciences Center, Agrochemical Research Laboratory, Lithuania
a.sarka@inbox.lt

The productivity and competitiveness of agricultural production are highly dependent on the climate, which is changing faster than predicted. The challenges of adapting the agricultural sector to climate change include not only the growth of crop products, but also the conservation of soil and water resources [1]. Climate change in Lithuania in 2017 occurred with 1.5-1.9 times higher precipitation amount compared to perennial precipitation amount. The opposite result was in 2018 as the air temperature was $2^0$C higher than perennial air temperature and natural drought was recorded. Therefore, in order to predict the impact of the changing climate on agriculture and environment, the 2016, 2017 and 2018 climate conditions allowed to design two different scenarios and assess their impact on organic soils. This is very important because organic soils are rich in organic carbon (SOC) and organic nitrogen (SON) [2]. As a result, climate change can affect not only $CO_2$ emission from organic soils, but also increase $N_{min}$ (ammonium and nitrate nitrogen) amount [3].

To achieve the goal, 9 sites were selected in different places in Lithuania (3 locations: Vepriai - $54^0$02'59N,$61^0$26'36E; Perloja - $52^0$81'88N,$60^0$10'19E; Piktupėnai - $37^0$13'74N,$61^0$14'42). In each location, three platforms with a maximum of 10x10 meters were selected according to the exact GPS coordinates. Soil samples were taken from them, one soil sample from the probe was taken from 4 - 6 places.

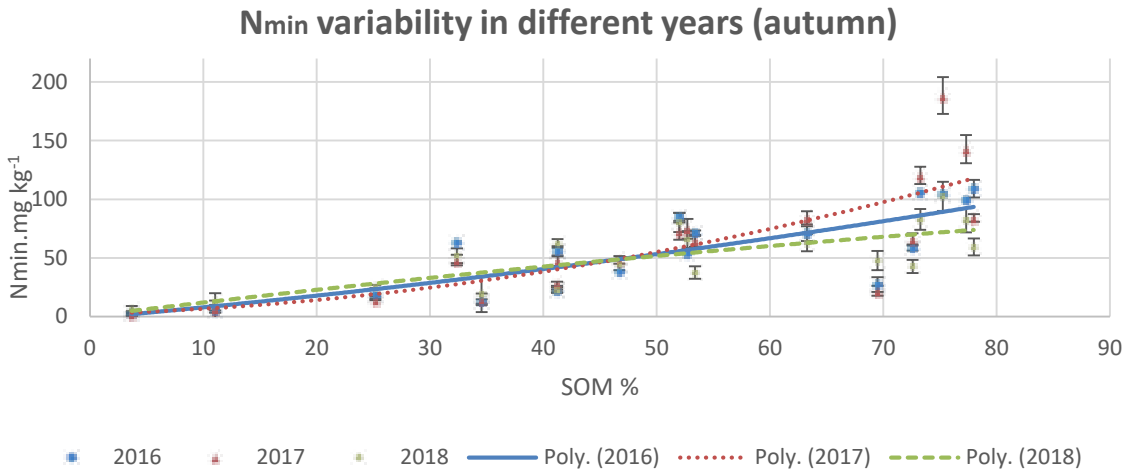


Fig. 1. $N_{min}$ dependency on SOM in different years (2016, 2017, 2018).

The assessment of the study results showed not only relationship between SOM and $N_{min}$ but also $N_{min}$ dependence on different climate conditions. These results showed that although in 2017 fixed $N_{min}$ amount was the lowest - 2.6 ± 0.9 at ≥ 40% SOC compared to other years, but at 60-80% SOM $N_{min}$ amount was the highest - 153 ± 18.3, and this was influenced by precipitation. The 2017 reliability curve is y = 0.0045x2 + 0.8651x - 1.309 for the $R^2$ = 0.649 reliability score. Conversely, high air temperatures were recorded in 2018 and low precipitation resulted in a higher $N_{min}$ amount - 4.2 ± 1.5 at ≥ 40% SOM but at 60-80% SOM $N_{min}$ amount was the lowest - 84 ± 14.6. The reliability curve is y = - 0.0029x2 + 1.1699x + 0.4988 for $R^2$ = 0.5883 reliability score. In 2016 $N_{min}$ amount was 3.2 ± 0.7 at ≥ 40% SOM, and at 60-80% SOM $N_{min}$ amount was 97.2 ± 12.9.

Therefore, when predicting $N_{min}$ change scenario in organic soils, the research results can provide that if the climate change increases precipitation but the air temperature will not increase, then $N_{min}$ amount will increase when SOM is 60-80%, the opposite result will be at high air temperatures with low precipitation amount.

[1] Karofeld, E., Jarašius, L., Priede, A., Sendžikaitė, J. On the after-use and restoration of abandoned extracted peatlands in the Baltic countries. Restoration Ecology. 25 (2): 293-300. (2017).
[2] Miguel S., Castillo., Alan L., Soil phosphorus pools for Histosols under sugarcane and pasture in the Everglades, USA Geoderma 145 130–135 (2008)
[3] Steffens M., Kohlpaintner M., Buddenbaum H. Fine spatial resolution mapping of soil organic matter quality in a Histosol profile Soil Science 827-839 (2014)

NOTES

NOTES

NOTES

NOTES

NOTES

NOTES

# Open Readings 2019

## Organizers

Faculty of Physics

CENTER FOR PHYSICAL SCIENCES AND TECHNOLOGY

SPIE. STUDENT CHAPTER VILNIUS UNIVERSITY

OSA Vilnius University Student Chapter

EPS Young Minds

LITHUANIAN LASER ASSOCIATION

## Sponsors

Research Council of Lithuania

EKSPLA

LIGHT CONVERSION

SCIENCE AND TECHNOLOGY PARK

EKSMA OPTICS

OPTOGAMA

Ruptela

Altechna

MONO SPEKTRA

TERAVIL

BROLIS SEMICONDUCTORS

Quantum Light Instruments

femtika

LIDARIS LIDT Service

OPTOMAN

THORLABS

Optoteka

HOLTIDA

STØP FAKE FOOD

RC cola

standa

Gudobelė

akvilė natural mineral water

Go Vilnius